16th INTERNATIONAL CONGRESS OF SPELEOLOGY

Proceedings

VOLUME 3




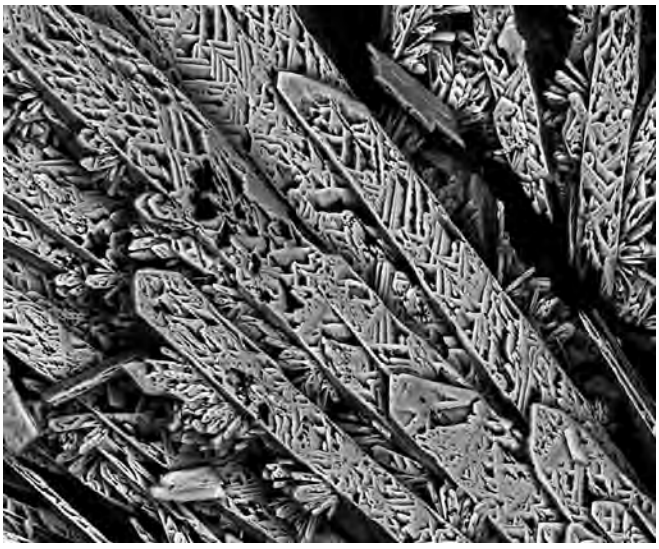

Edited by
Michal Filippi
Pavel Bosák

16th INTERNATIONAL CONGRESS OF SPELEOLOGY
BRNO 2013 CZECH REPUBLIC
WHERE HISTORY MEETS FUTURE

16th INTERNATIONAL CONGRESS OF SPELEOLOGY

Czech Republic, Brno

July 21–28, 2013

Proceedings

VOLUME 3

Edited by

Michal Filippi

Pavel Bosák

2013

16th INTERNATIONAL CONGRESS OF SPELEOLOGY
Czech Republic, Brno
July 21–28, 2013

Proceedings
VOLUME 3

Produced by the Organizing Committee of the 16th International Congress of Speleology.
Published by the Czech Speleological Society and the SPELEO2013 and in the co-operation with the International Union of Speleology.
Design by M. Filippi and SAVIO, s.r.o.
Layout by SAVIO, s.r.o.
Printed in the Czech Republic by H.R.G. spol. s r.o.

The contributions were not corrected from language point of view. Contributions express author(s) opinion.

Recommended form of citation for this volume:
Filippi M., Bosák P. (Eds), 2013. Proceedings of the 16th International Congress of Speleology, July 21–28, Brno. Volume 3, p. 499. Czech Speleological Society. Praha.

ISBN 978-80-87857-09-0

KATALOGIZACE V KNIZE - NÁRODNÍ KNIHOVNA ČR

International Congress of Speleology (16. : Brno, Česko)
16th International Congress of Speleology : Czech Republic, Brno July 21–28,2013 : proceedings. Volume 3 / edited by Michal Filippi, Pavel Bosák. -- [Prague] : Czech Speleological Society and the SPELEO2013 and in the co-operation with the International Union of Speleology, 2013
ISBN 978-80-87857-09-0 (brož.)

551.44 * 551.435.8 * 551.435.88-021.252 * 549
- speleology
- karstology
- karst
- pseudokarst
- mineralogy
- proceedings of conferences
- speleologie
- karsologie
- kras
- pseudokras
- mineralogie
- sborníky konferencí

551 - Geology, meteorology [7]
551 - Geologie. Meteorologie. Klimatologie [7]

Cover photos (some photos were adjusted/cropped)
Top left – Specific carbonate speleothem decorations in the Ghost Chamber, Sima de la Higuera Cave. Photo by V. Ferrer. For details see the paper by F. Cázquez and J.-M. Calaforra.
Top right – A challenging exploration in the Cueva de los Cristales. Mexico. Photo by La Venta Exploring Team and Speleoresearch & Films. For details see the paper by F. Cázquez et al.
Bottom left – An example of a microcrystalline grained halite speleothem, the Octopus formation in the 3N Cave, Qeshm Island, Iran. Photo by NAMAK team. For details see the paper by Filippi et al.
Bottom right – Internal skeleton structure of cryogenic gypsum crystals caused by the presence of partitions oriented parallel to the faces. For details see the paper by Kadebskaya and Tchaikovsky.

Scientific Committee

Chairman

Pavel Bosák	(Czech Republic) – Karst and Pseudokarst

Vice-Chairman

Michal Filippi	(Czech Republic) – Karst and Pseudokarst

Members

Jiří Adamovič	(Czech Republic) – Pseudokarst
Philippe Audra	(France) – Speleogenesis
Jean-Pierre Bartholeyns	(France) – Management and Protection
Aaron Bird	(USA) – Exploration
Didier Cailhol	(France) – Speleogenesis
Matt Covington	(USA) – Modelling in Karst and Caves
Robert Eavis	(USA) – Exploration
Anette S. Engel	(USA) – Geomicrobiology
Lukáš Faltejsek	(Czech Republic) – Biospeleology
Derek Ford	(Canada) – Climate and Paleoclimate
Franci Gabrovšek	(Slovenia) – Modelling
Mladen Garašič	(Croatia) – Survey, Mapping and Data Processing
Martin Golec	(Czech Republic) – Archeology and Paleontology
Christiane Grebe	(Germany) – Management and Protection
Nadja Zupan Hajna	(Slovenia) – Extraterrestrial Karst
Ivan Horáček	(Czech Republic) – Biospeleology
Stephan Kempe	(Germany) – History
Aleksander A. Klimchouk	(Ukraine) – Speleogenesis
Jiří Kyselák	(Czech Republic) – Exploration
Peter Matthews	(Australia) – Survey, Mapping and Data Processing
Iona Meleg	(France) – Management and Protection
Mario Parise	(Italy) – Artificial Underground
Bohdan P. Onac	(USA) – Mineralogy
Yavor Shopov	(Bulgaria) – Climate and Paleoclimate

The names of the Committee members are given along with their home countries and fields of research they represented as convenors.

Contents

Preface

Dear readers, the Proceedings volumes you are holding in your hands were issued within the 16th International Congress of Speleology (hereafter 16thICS) on July 21–28, 2013 in Brno, Czech Republic. Let us welcome you to its reading.
In total, over 320 contributions (over 250 oral presentations and over 70 posters) by more than 750 authors have been received to be included within the Congress Proceedings. This represents over 2,300 received e-mails and a similar number of responses during the last 6 months, approximately 4,300 electronic files and over 1,450 printed pages of the text. To put it simply, "really, really much interesting stuff concerned with cave and karst subject". The author's guidelines stipulated that the particular contributions should not exceed 6 pages of text and we were delighted to find that most authors prepared contributions close to this upper limit. Only very few contributions did not exceed one page of text. This illustrates a clear willingness of the cavers and karst scientist to share their discoveries and research conclusions.

The presented contributions (abstracts/papers) stand for both oral and poster presentations as indicated in the headings. Contributions in each session are arranged alphabetically by the last name of the first author. All contributions were reviewed from the viewpoint of technical quality and scientific content by members of the scientific committee and invited reviewers. The authors had the opportunity to revise their papers in response to reviewer's comments and we were pleased to see that the reviews have improved the clarity and readability of the contributions. However, profound improvement of the English language could not be arranged due to the shortage of time and insufficient human resources; the authors themselves are therefore responsible for the linguistic level of their contributions.

Thirteen thematically different sessions and six special sessions were scheduled within the call for your contributions to cover the whole range of subjects to be discussed within the wide scope of the 16thICS. The low number of contributions for some of these "detailed" sessions necessitated their merging with others. As a result, eleven original and three joint sessions are presented within the Proceedings. The contributions were grouped into three separate volumes. The purpose of this arrangement was that each particular Volume is filled with a certain logical hierarchy of topics, and that related topics are presented together. It was also the intention that the content of each Volume is topically balanced and contains both generally interesting (popular) topics with rich photographic documentation and hardcore scientific topics dominated by tables and plots.

Volume I starts with three plenary lectures representing three global topics related to 16thICS subject. Further it contains papers concerned with history of research (session "History of Speleology and Karst Research"), archeology and paleontology (sessions "Archaeology and Paleontology in Caves"), topics focused on management and preservation of caves and karst areas and other social-related aspects (sessions "Protection and Management of Karst, Education"; "Karst and Caves: Social Aspects and Other Topics"). In the last mentioned session you can also find a small part devoted to extraterrestrial karst. Volume I is ended by a relatively large portion of biology-oriented papers placed within the session "Biospeleology, Geomicrobiology and Ecology".

Volume II contains the traditionally heavily attended session "Exploration and Cave Techniques" and by the related session "Speleological Research and Activities in Artificial Underground". These exploration topics are, we believe, logically supplemented with contributions from the field of "Karst and Cave Survey, Mapping and Data Processing". The content of the second Volume is completed with a somewhat more specialized session "Modelling in Karst and Cave Environments" and with session "Cave Climate and Paleoclimate Record". The last mentioned session probably better fits to the end of Volume III, but it was placed into Volume II in order to reach balance in the extent of the individual volumes.

Volume III also starts with traditional, heavily attended topics organized in two sessions: "Karst and Caves in Carbonate Rocks, Salt and Cypsum" and "Karst and Caves in Other Rocks, Pseudokarst". These topics are supplemented by the related session "Speleogenesis". This last volume of the Proceedings is ended by the study of cave minerals, included in a specific session "Cave Minerals".

It is clear already from the previous ICS meetings that the range of the published topics becomes wider and wider, including localities in the whole world but also – owing to the access to high-quality spacecraft images – from other planets. The range of the instrumental, analytical and software methods employed in cave and karst research is remarkable and shows that the topic of "cave & karst exploration" attracts an ever increasing number of researchers even from already established scientific disciplines.

Let us also say a few words about the selection of the cover photos for the Proceedings volumes. The idea was to select such photos which would best represent all topics (especially those enjoying the highest interest) in each particular volume and be of high technical quality. Since we believe the cover page is a place for a serious presentation of the inner content, we made our selection from photos used in the presented papers. In one case the additional photo was requested to get a better representation of the topic. For our purpose, we decided to place several photos on the cover page of each volume. We hope that you enjoy them.

We wish to take this opportunity to apologize for the all mistakes which might have possibly originated within the operations with different versions of the manuscripts and other related files and e-mails which passed through our computers. We believe that everybody find their interesting reading in the Proceedings and we wish that the whole publication (Volumes I–III) becomes a valuable record of the 16th meeting of enthusiasts addicted to the fascination of the underground world.

Finally we wish to thank all the authors for their contributions. Enormous thanks belong to the reviewers and especially convenors (members of the scientific committee) of the particular sessions for their time and effort in the improvement of the overall message of the texts. We also wish to thank Michal Molhanec who significantly helped with the on-line form for the contribution submission, to Jiří Adamovič who repeatedly helped us with the improvement of our English, and to Jan Spružina, Zdeněk Motyčka, Jana Holubcová, and Renata Filippi who contributed to the preparation of the Proceedings.

After the few introductory words, let's now enjoy the papers from localities all over the world, presenting all forms of activities in karst, caves and other related surface and subsurface environments!

Michal Filippi and **Pavel Bosák**
Proceedings editors

Session:

Karst and Caves in Carbonate Rocks, Salt and Gypsum

KARST HYDROGEOLOGY OF THE HANEY LIMESTONE, SOUTH-CENTRAL KENTUCKY

Sarah M. Arpin, Christopher G. Groves
Hoffman Environmental Research Institute, Department of Geography and Geology, Western Kentucky University, Bowling Green, KY 42101, USA, sarah.arpin759@topper.wku.edu, chris.groves@wku.edu

South-central Kentucky has one of the world's most intensively studied karst areas, with most work focusing on the Mammoth Cave System and its aquifers. However, slightly higher in the stratigraphic section than Mammoth Cave, the Haney Limestone is an important but less well studied carbonate aquifer. This research provides the first comprehensive hydrogeologic description of the Haney Limestone, synthesizing patterns of the cave and karst features developed within. Joints are the most dominant control on passage development in the Haney Limestone within the study area; when considered together the orientation of these joints is consistent with the orientation of regional joint sets. There is evidence that the spaces along these joints in some cases may have been were enlarged by stress release fracturing. Bedding planes and the presence of insoluble rock at the base of the Haney also exert significant control on conduit development in the Haney Limestone. The strong influence of joints on conduit development in the Haney Limestone contrasts with the major caves of the St. Louis, Ste. Genevieve, and Girkin Limestones below, in which bedding planes are a dominant influence.

Most of the caves of the study area developed in the Haney Limestone are single-conduit caves that receive water through direct, allogenic sources. Cave entrances are frequently perennial spring resurgences; whereas the presence of active streams suggests that the caves are a function of the current landscape, acting as drains for localized recharge areas. The hydrology of the Haney Limestone plays an important, if localized, role in the regional hydrology of south-central Kentucky; integrated into the current system of surface and subsurface drainage of the regional karst landscape. Evidence supports the idea that caves of the Haney Limestone are, geologically, relatively recent phenomena. A majority of the caves in the study area are hydrologically active, the water resurging from the sampled springs is undersaturated with respect to limestone, and the caves are developed along potential stress release fractures associated with small, relatively young valleys. This suggests that caves in the Haney Limestone were not directly influenced by the incision of the Green River, like Mammoth Cave, but that cave development is a much more recent process.

AN INTRODUCTION TO KALAHROUD CAVE, NORTH OF ESFAHAN, IRAN

Shirin Bahadorinia[1], Sayed Hassen Hejazi[1], Alireza Nadimi[2], Derek Ford[3]
[1]Department of Geology, Islamic Azad University, Khorasgan Branch, Esfahan, Iran, sbahadorinia@gmail.com
[2]Department of Geology, Isfahan University, Esfahan, Iran
[3]School of Geography and Earth Sciences, McMaster University, Canada

Kalahroud Cave (Lat. 33˚22’ 21” N, Long. 51˚34’ 35” W, at 2,300 m a.s.l. near the village of Kalahroud, Esfahan Province, Iran) is an interesting and complex cave formed in Cretaceous limestones. It is located on the southwestern boundary of high mountains of the Urmiyeh-Dokhtar magmatic belt of Iran, which is a dramatically faulted, active tectonic area. The cave has formed in the foot wall of the Kalahroud Thrust. The limestones are thick to massively bedded but contain thinner shales, are locally tectonized, and are overlain (capped) by insoluble strata. Stratal dip is approximately 15°. The cave entrance is in cliffs ~25 m above the floor of a strike-aligned river valley with a channel active only in rare storms. The region is semi-arid, with only 51.8 mm average annual precipitation and a mean temperature of 22.1 °C.

The explored cave is ~200 m in length and has three morphologically distinct parts. From the entrance a steep breakdown passage extends broadly down dip to a depth of ~50 m. There the form changes to two large solution notch chambers beveling the dipping strata, with multiple notches, solution pockets and pendants, tapering ramiform extensions upwards and laterally, and blind pits in the floors. Two constricted joint-guided tributaries enter at the notching level that display irregular phreatic form, including slow flow scalloping, and terminations in blind pits. There were a-periodic pools many metres in diameter in the main chambers, indicated by stranded calcite raft debris and many conulites built up to precise paleo-water surfaces. On a visit shortly after rains in April 2012 one small pool with some raft accretion was found.

There is a variety of chemical and clastic sediments in the cave. Precipitates include the calcite rafts, widespread popcorn and cave coral on walls and pits, anthodites, frostwork associated with ferruginous shale bands, and dogtooth spar. Very significantly, cemented rinds of highly weathered bedrock overlain by dense layered calcite are the oldest chemical deposits, reminiscent of those in Wind Cave, South Dakota, USA. ICPMS U-Series dating (courtesy of the Department of Earth Sciences, Oxford University, UK) shows that the oldest rafts in the largest pool are ~ 9,000 y B.P. in age, and the uppermost are modern. Clastic sediments are limited to breakdown and colluvial debris flows in the entrance passage, abundant clay fines in the notch chambers and tributaries. There do not appear to be any vadose stream deposits.

From field observations, two main factors in cave development were tectonic uplift and deformation facilitating groundwater circulation, and dissolution with prominent rest levels (notching). Surface river entrenchment has drained and truncated the upper cave and there is only net deposition in the notch chambers. It appears that Kalahroud Cave is a hypogene cave, but further studies are required to prove this.

CAVE SYSTEM OF KITA GAĆEŠINA – DRAŽENOVA PUHALJKA THE LONGEST CAVE IN THE DINARIC KARST

Teo Barišić, Darko Bakšić, Dalibor Paar
The Speleological Committee of the Croatian Mountaineering Association, Kozarčeva 22, Zagreb, Croatia
teobarisic@gmail.com, baksic@sumfak.hr, dpaar@phy.hr

The Croatian cavers have continued to explore the Crnopac Massif, the most northern, the highest and the most karstified part of the south-eastern Velebit mountain ridge known thanks to its underground karst phenomena. In more than 8 years of intensive research Cave system of Kita Gaćešina – Drazenova puhaljka reached the length of 23,334 m, depth of 737 m and became the Croatian and Dinaric karst longest cave. Speleologists have done some geomorphological research, microclimatic and radon concentracion measurements, collecting and analysing some animal species. The whole area shows enormous speleological and tourism potential.

1. Introduction

The Dinaric karst form a mountain chain in the Southern Europe, spanning areas of Slovenia, Croatia, Bosnia and Herzegovina, Serbia, Albania and Montenegro. They extend for 645 km along the coast of the Adriatic Sea (northwest-southeast), from the Julian Alps in the northwest down to the Šar-Korab Massif. The highest mountain of the Dinaric Karst is Mount Prokletije, located on the border of eastern Montenegro and northern Albania (2,692 m a.s.l.).

The Dinaric Karst is the fifth most rugged and extensively mountainous area of Europe after the Caucasus Mountains, Alps, Pyrenees and Scandinavian Mountains.

The Dinarides are known as a place of origin of term karst, the German name for Kras, a region in Slovenia partially extending into Italy, where the first scientific research of karst topography was made. This includes use of Croatian karst phenomena terms such as ponor, dolina, polje, jama, etc., in international geological vocabulary.

Dinaric karst is also the top of hotspots of world's subterranean biodiversity. The Postojnska Cave, described for the first time in 17th century is one of the famous and oldest tourist caves in the World. Since that time it was also known as the longest Dinaric cave.

In last few decades, number of speleological explorations in whole area grows. Hundreds of cavers in each country have found new caving attractive zones with deep and long caves.

The Crnopac Massif in Croatia is the most northern, the highest and the most karstified part of the south-eastern Velebit mountain ridge (part of Dinaric coastal mountainous karst). Numerous surface and underground karst phenomena are characteristic, including Cave system of Kita Gaćešina – Draženova puhaljka, since 2011 – the Dinaric longest cave.

2. Crnopac Massif

The Crnopac Massif is situated between higher terrain of the Gračac Polje on the north and Zrmanja and Krupa river valleys on the South and East. The massif is built of thick upper Triassic, Jurassic and Cretaceous carbonate deposits. In higher parts of the massif, mentioned rocks are covered with Oligocene to Lower Miocene carbonate breccias, probably deposited on the flanks of tectonically uplifted areas during older tectonic phase (Korbar 2009).

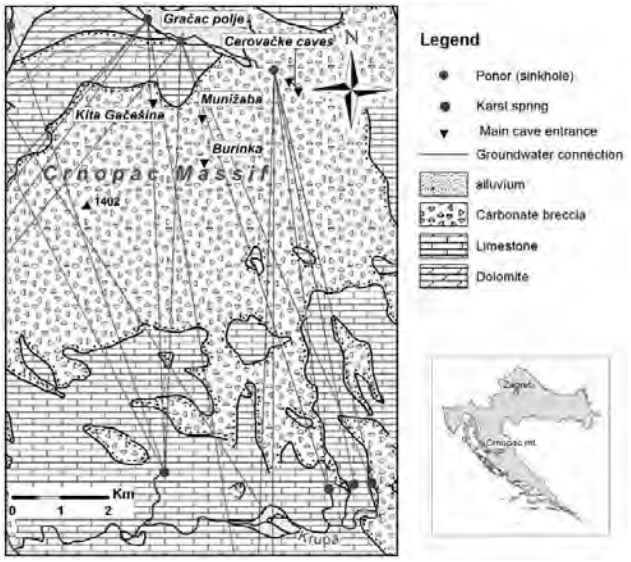

Figure 1. Geology of Crnopac Massif.

Due to dominantly carbonate structure of this part of Velebit, waters flow subterraneous through the Crnopac Massif generally southwards. Underground waters get water from sinking streams that come from karst polje in Lika and Gračac areas and appear in springs on right side of Zrmanja and Krupa river valleys.

In such conditions, polygenetic multilevel caves have developed. Speleogenesis of the caves in the Crnopac Massif probably have lasted continuously from the beginning of the massif uplift (Upper Miocene).

Mechanical properties of the Oligocene to Lower Miocene carbonate breccias (Jelar breccias) play a significant role in the cave morphology. Low frequency of cracks and joints in these massive breccias enables the preservation of underground passages and chambers of very large dimensions.

The most important caves of the Crnopac Massif are Munižaba (9,318 m, -510 m, volume 2.3 millions of m^3). Cave system Kita Gaćešina – Draženova puhaljka (23,334 m, -737 m, volume 1.3 millions of m^3), Burinka

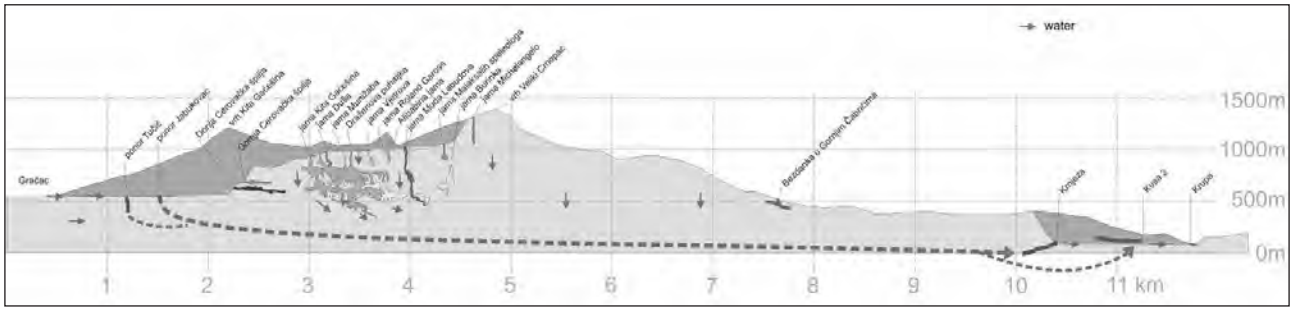

Figure 2. Projected section of large caves in Crnopac Massif: N–S.

(930 m, -290 m, volume 1.1 millions of m^3), Gornja (Upper Cave) (1,292 m) and Donja (Lower Cave) Cerovačka pećina (2,779 m), and Muda Labudova (2,490 m, -680 m).

3. History of explorations

While the Upper Cerovačka Cave entrance was known to local people, Lower cave entrance was found during the railway building in 1913. New found cave brought large quantities of archaeological findings, sites of the cave bear, cave lion and amazing speleothem forms. Both caves in a total length of 4 km become most popular tourist cave site in Croatia.

Modern cave explorations with rope techniques started in late seventies. Year after year just a few cavers succeeded to rich summit plateau. Members of Speleological section (SS) Željezničar (Zagreb) in cooperation with others clubs have found impressive chambers in Burinka (160 × 90 × 90 m), Munižaba (185 × 60 × 70 m) and Veliko Grotlo pit (100 × 85 × 130 m). War in Croatia stopped further caving activity.

Explorations continued few years after the end of the war. Members of SS Željezničar have found dozens of new pits and caves (Michelangelo pit -274 m, Alibabina jama -218 m, Muda Labudova pit -680 m). Today, there are more than 250 known caves on the Crnopac. The SS PDS Velebit (Zagreb) continued exploration of Munižaba channels with massive use of alpine techniques; drilling, bolting and spending a lot of time in underground camps what led to the total length of more than 9 km. Using the cave diving techniques, the DDISKF Dinaridi explored Kusa iI Cave (3,010 m) and Krnjeza spring (sump, -106 m) in Zrmanja and Krupa river valleys – the outputs of hydrologic system. In 2004, cavers from the SS St. Mihovil (Šibenik) found lower entrance of Cave system of Kita Gaćešina – Draženova puhaljka. Cavers from the SS PDS Velebit and SS Mosor (Split) join them and new cave rapidly grew up. Draženova puhaljka pit was found in 2005 (the SS Željezničar), and 2009 connected to Kita Gaćešina. In 2010, the system became the longest cave in Croatia and 2011 the longest in Dinarides. Eighty-one explorations conducted by cavers of the almost every caving club in Croatia brought the total length of 23,334 m and placed system on the list of 200 World longest caves. Caving accidents in 2011 and 2012 caused two most complex cave rescue operations in Croatia ever with two blissfully happy ends.

4. Cave system Kita Gaćešina – Draženova puhaljka (KG–DP)

Cave system of KG–DP is a network of multiphase cave passages, remnants of various levels of paleodrainage systems that conducted waters from the higher terrain to the base level springs on the south and south-east. Older phreatic and epiphreatic channels are frequently crossed by younger invasion vadose shafts, which provide entrances and also connections between different levels. These are three main levels in the system. The highest one approximately at 800 m is developed in Jelar breccias. The middle one is approximately at 600 m, similar to Cerovačke caves and the Munižaba Cave. Even not in breccias, this level also characteristics large passages, result of simultaneous collapsing and removing of collapsed material by big underground water flows during the hydrologically active phase of their development. The lowest level (250–400 m) is inclined according to carbonate layer inclination (-20 to -35°, SW).

Lower entrance (Kita Gaćešina) is at 920 m, and the higher one (Draženova puhaljka) at 985 m a.s.l. The lowest point (-737 m) is at 248 m a.s.l. what means almost 300 m lower than the Gračac Polje (545) and its sinkholes. All water in system is the rainwater or melted water from ice and snow caves in the Crnopac Massif. Permanent water stream – Gračac Polje drainage system haven't been found yet.

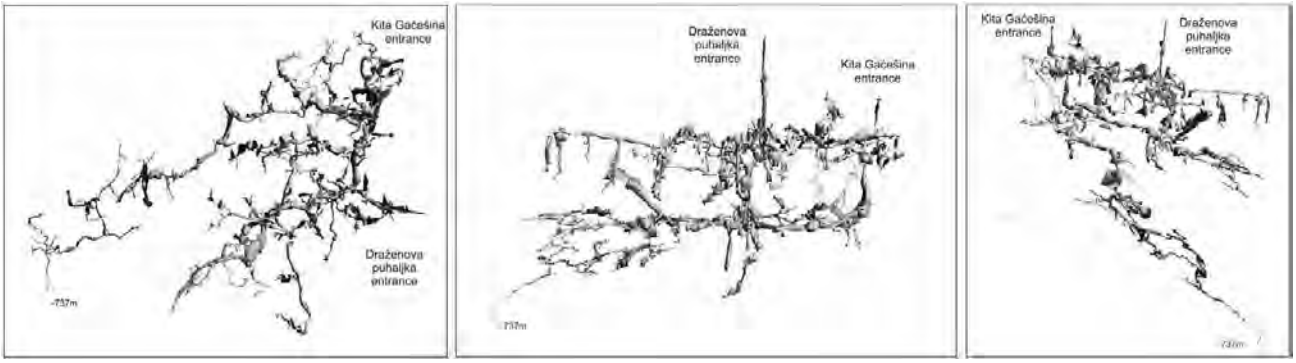

Figure 3. Cave system of Kita Gaćešina – Draženova puhaljka – 3D view.

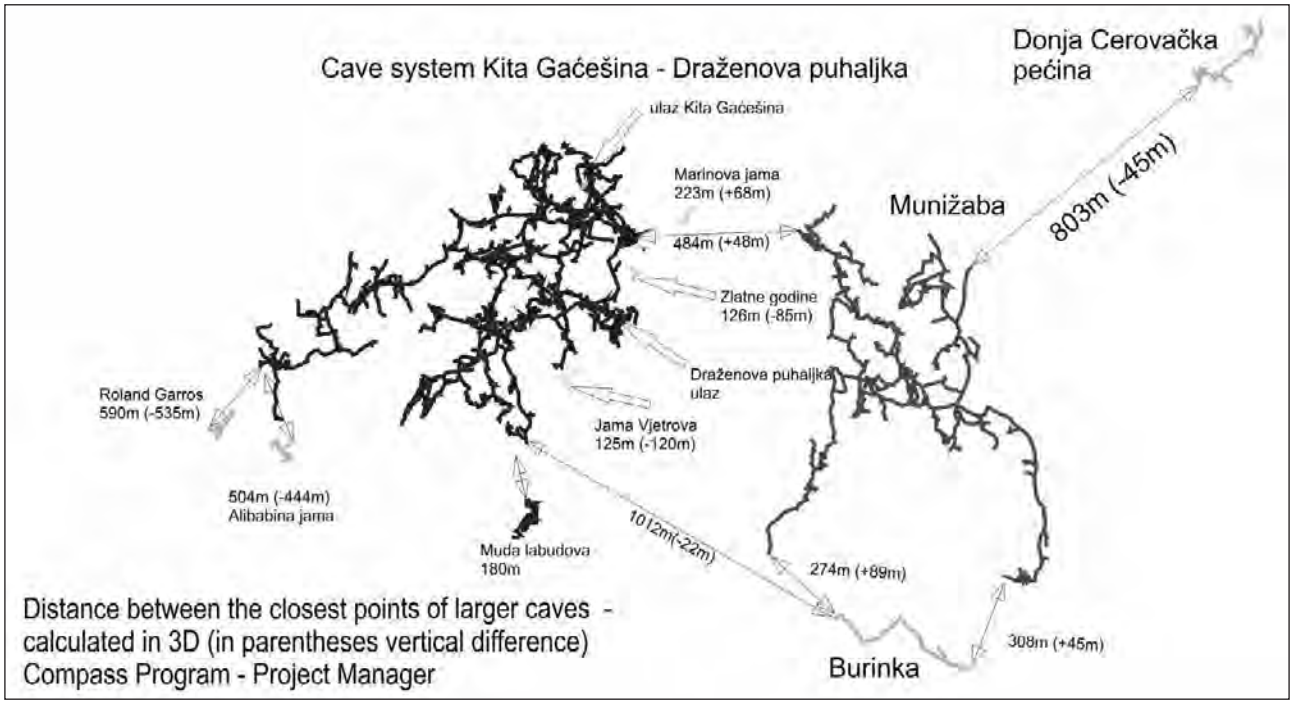

Figure 4. Plans of largest caves on Crnopac Mt.

The KG–DP cave system in almost all parts and many surrounding caves characteristics strong air flow. In permanent air pressure during the summer it tends to came out from the entrances and during the winter its changes the direction. Cold air flows lowers the temperature and create ice speleothemes in areas close to the entrances. There must be some higher entrances placed close to the top of the Crnopac Massif (1,402 m a.s.l.) and connected to the lowest parts of the system. Measured temperatures in system vary from 3.7 to 5.4 °C.

5. Biospeleological research

Biospeleologists collected KG–DP cave system fauna material only twice and collected 20 different species. First interpretation of results showed that organisms are similar to surrounding caves that were visited much more times by the biospeleologists. Some data still wait to be explained and there are some indications that there must be at least one new speciae.

Cavers were collecting remains of cave bats and it is confirmed that at least 8 different bats lived in the cave system.

6. Measurements of radon concentration

Measurements of radon concentration were performed during 6 months in the upper level of the system at 7 locations. Concentration range, between 514 and 1,220 Bq.m^{-3} and it is higher during summer. These values are comparable with the results of measurements in the deep pits of the northern Velebit (Paar et al. 2008) and significantly lower than the concentration of radon in Žumberak caves (Paar et al. 2005). In complex caves like Kita Gaćešina, there is no simple connection of radon concentration with ground surface climate conditions. Future investigations will try to connect radon dynamic with cave microclimate and geology.

7. Nature Protection and tourism potential

Existing known values, diversity of forest cover and extraordinary landscapes with existing near tourist centers makes exceptional tourism potential. Opening of the forest road construction has made the area more accessible but in karst areas hitherto untouched forests have been felled. Speleological research results presentation initiates idea of establishing a more nature protection zone – Speleological Park Crnopac what become one of the Zadar County goals (SPARC project). For now, cavers have succeed to stop intensive logging

8. Conclusion

Croatian cavers have found more than 250 caves, dozens kilometers of subterranean channels and impressive chambers showing Crnopac massif remarkable geomorphologic phenomena. In more than 8 years of intensive research Cave system of Kita Gaćešina – Drazenova puhaljka reached the length of 23,334 m, depth of -737 m and became longest cave in Croatia and Dinaric Karst. The whole area shows high speleological and tourism potential

Despite undertaken geomorphological research, microclimatic measurements, radon, physico-chemical analysis of water, the collection and analysis of animal species, we can say that the systematic scientific investigation of the whole area is still in its infancy.

Acknowledgments

We would like to thank to Velebit Nature Park, The Speleological Committee of the Croatian Mountaineering Association, Croatian Mountain Rescue Service.

References

Barišić T, Bakšić D, Paar D, Rnjak G, 2010. Kita Gaćešina – Draženova puhaljka Speleological Explorations 2004–2010 and Some Characteristics of Cave System, 1. Croatian speleological Congress, Poreč.

Bočić N, 2009. Cerovačke caves and other karst phenomena of the Crnopac Massif. International Interdisciplinary Scientific Conference "Sustainability of the Karst Environment – Dinaric karst and other karst regions", Plitvička jezera.

Kovač-Konrad P, Jalžić V, 2006. Prvi sifon špilje Kusa 1. Speleolog, Vol 54., 20–23, Zagreb (in Croatian).

Kovačević A, 2008. Kusa nad Manastirskim lukama – Kusa 2. Speleolog, Vol. 56, 61–65, Zagreb (in Croatian).

Kuhta M, Stroj A, 2005. The Speleogenesis of the caves in Crnopac Mt. Area. Proceedings of the 14th International Congress of Speleology, 46–48, Hellenic Speleological Society, Athens.

Kuhta M, Borovec M, Bosner N, 2002. Speleološka istraživanja Crnopca u 2002. i 2003. godini. Speleolog, Vol. 50–51, 48–55, Zagreb (in Croatian).

Lukić O, 1988. Speleološka istraživanja Crnopca na Velebitu. Speleolog, Vol. 36–37, 14–26, Zagreb (in Croatian).

Paar D, Ujević M, Bakšić D, Lacković D, Čop A., Radolić V, 2008. Physical and Chemical Research in Velebita pit (Croatia), Acta Carsologica 37/2–3, 273–278.

CAVES OF EL PEÑON, CORDILLERA ORIENTAL, COLOMBIA

Martin Bochud[1,2], Roman Hapka[1], Jean-Marc Jutzet[1]
[1]Spéléo Club des Préalpes fribourgeoises, 1700 Fribourg, Switzerland, info@scpf.info,
[2]GeoAzimut Sàrl, Rte de la Fonderie 8, 1700 Fribourg, Switzerland, martin.bochud@geoazimut.com

Abstract. In 2011, to celebrate their 40th anniversary, the Préalpes Fribourgeoises Caving Club (SCPF) of the Swiss Society of Speleology set out to explore the Colombian depths of South America. Following the discoveries made in 2011 in the El Peñon karstic field located in the state of Santander, a second expedition was launched in January–February 2012. The Colombia reveals a country with a rich speleological heritage. As proof 10 km of galleries were discovered in a few weeks by a Swiss-Colombian team: the labyrinthine karst found at over 2,500 m, pastures punctuated by thick forests, tropical mists, imposing verticals where cave-dwelling birds of prey circle, mysterious rumbling underground rivers and fossil galleries with beautiful concretions. This article summarizes the discoveries made in 2011–2012 and makes a first attempt to define the geological and hydrogeological context of the area.

Abstrait. En 2011, à l'occasion de ses 40 ans d'existence, le Spéléo-Club des Préalpes Fribourgeoises (SCPF) de la Société Suisse de Spéléologie s'est lancé à la conquête des abîmes sud-américains de Colombie. Suite aux découvertes réalisées en 2011 dans le massif karstique d'El Penon, situé dans l'état de Santander, une seconde expédition a vu le jour en janvier–février 2012. La Colombie se révèle un pays au riche patrimoine spéléologique. Pour preuves, 10 km de galeries ont été découvertes en quelques semaines par une équipe suisso-colombienne: karst labyrinthique à plus de 2,500 m d'altitude, pâturages entrecoupés d'une épaisse forêt, brumes tropicales, grandes verticales imposantes où tournoient les rapaces cavernicoles, rivières souterraines mystérieuses et grondantes et galeries fossiles magnifiquement concrétionnées. Cet article résume les découvertes faites en 2011–2012 et fait un premier essai d'interprétation géologique et hydrogéologique de la zone explorée.

1. Introduction

In 2011, the Préalpes fribourgeoises caving club (SCPF) decided to start an exploration of the Colombian karst. Together with Colombian cavers, they find the unexplored and interesting El Peñon karstic area. After a successful first expedition in February–March 2011 and the very friendly welcome of the local people, a second expedition was set-up at the beginning of 2012. During both expeditions, more than 10 km of galleries were discovered and documented by the Swiss-Colombian team.

The karst is located at an altitude of over than 2,500 m under pasture, thick forest and tropical mists. The climate of the area is humid to very humid. The high annual precipitations between 2.5 to 3 m combined to the favourable geology are ideal for the development of major cave systems. The anticline formed by the limestones of the Rosablanca Formation is drilled by imposing vertical pits and traversed by imposing decorated horizontal galleries. The speleological potential proves to be important and the two expeditions to date in this region have only scratched the surface.

2. Short history of caving in Colombia

The Colombian caves situated on the high central plateaux or in the low south-eastern forests were known to the Indian civilisations that used them as burial places and refuges. The first descriptions of caves, often picturesque made by foreign travellers, date from the mid-19th century. In 1878 Alexander von Humboldt published a work on the rifts and caves of the Cordillera. Various caves are mentioned in the first half of the 20th century but it was in 1940 that Luis Cuervo Marquez described the famous Hoyo del Aire (a pit cave of 120 m), remapped during Speleo Colombia in 2011 and various other caves. During the next 30 years various scientific authors became interested in Colombian karst but it was not until 1975 that a Polish caving expedition explored 24 caves using modern equipment.

In 1977 a single reconnaissance expedition of the Colombian karst was carried out by the Speleological Group of Nice (France; Hof 1977). Three months of on-site presence resulted in an impressive work of exploration and data compilation extending over almost the entire country. More than 100 caves and pit caves were visited, explored and mapped. The Hermosura region, close to El Penon, drew attention for the first time, and two large pit caves – including the Hoyo del Aguila (-149 m, 105 m pit) – were explored. Other French and American incursions, more or less related to mineral and oil research, were occasionally reported later, without it being possible to find published material. For example, the list of the largest caves in the world indicates that the longest Colombian cave is the Hermosura Sistema (4,926 m, -193 m). However, the bibliographic references, the geographical location and topography currently cannot be found.

3. Geography and geology

The El Peñon Massif (cities of El Peñon and Bolivar, see Fig. 1) is located in the Santander State in the Eastern Cordillera of the Andes in Colombia about 160 km North of Bogota city.

The area is sparsely populated and the few localities found here have only FWD cars or even no car access. The community of El Penon is only 50 years old and the access road is only a few decades old.

Figure 1. Location of El Peñon Massif and Santander Department in Colombia.

The studied area lies at altitudes between 3,000 m in the SW and lower than 1,000 m in the NE. The southern part is bounded by a huge cliff on the Panama deep incised valley. From the SW to NE, the massif dips slowly down. In the NW, it dips fast to 400 m and then reaches the Magdalena Plain at 100 m.

3.1. Climate

The climate is humid and annual precipitation is about 2.25 to 3 m. The mean annual temperature is about 22 °C (Pabón-Caicedo et al. 2001).

3.2. Hydrology – hydrogeology

The karstic hydrogeological systems of the area have been little studied at present.

Based on maps and satellite images, some watersprings seem to spread out along the W–NW cliff of the Massif but they were still not observed. No major karst spring has been found yet.

On the El Peñon Massif, small rivers are present. They flow out of cave and they generally rapidly disappear by infiltration in doline or directly in other cave. The El Peñon area is surrounded by the Rio Dorada to the S and W and by the Rio Horta to the NW and N. They seem to drain the main part of the water of the massif and they both join at an altitude of 385 m.

In caves, rivers, lakes or impenetrable siphons can be observed at different levels. The lack of flooding cue in caves despite the high precipitation indicates that the water flow is certainly rapidly spread over the whole massif.

3.3. Geology

Lithologically, the Cretaceous limestone extends over several hundred kilometers between cities of Bogota and Bucamaranga at altitudes between 50 and 3,000 m. The karst and all discovered caves of El Peñon and surrounding areas are located in the Lower Cretaceous Rosablanca Formation (Late Valanginian–Early Hauterivian). The thickness of the whole formation can reach 400 m (Guerrero 2002). As described on Figure 2, it is composed of a succession of grey dolomites, grey limestones, brown limestones, marls, sandstone and finally limestone on the top (Guerrero 2002; Mendoza-Parada et al. 2009; Toussaint 1996). Based on our observations in the Panama Valley, the caves of El Peñon area seem to be located in the lower-middle part of the Rosablanca Formation in the grey and brown limestones. In some area, the thickness of this lower part of the formation can reach 200 m (Guerrero 2002).

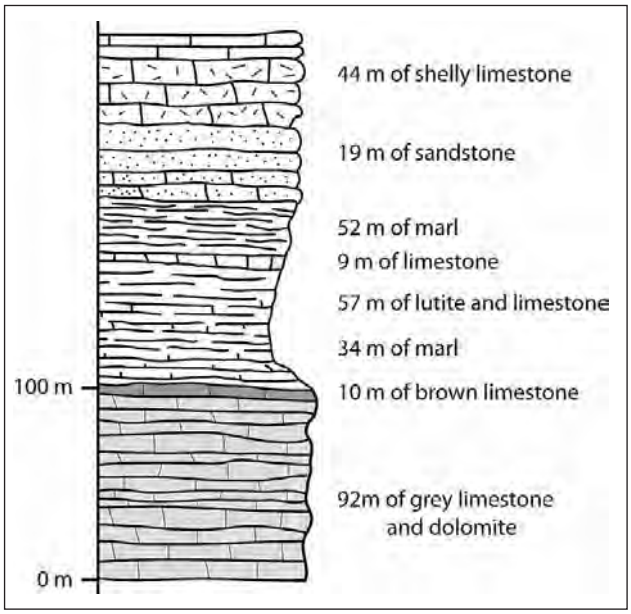

Figure 2. Rosablanca Formation in the Mesa de los Santos area (Toussaint 1996).

Structurally, the El Peñon area is located on a main anticline structure with secondary folds forming the plateau where the caves are located. The main fold axis is dipping slightly to the NNE. As described by Coletta et al. (1990). The Velez–El Peñon area is a large pop-up structure bordered by two opposite verging thrust fault involving Jurrassic and pre-Jurassic structure. The west verging thrusts are located to the West of the El Peñon Area. The Cretaceous-Jurassic deposits thrust over Tertiary deposits.

Geographical, hydrological and geological settings points on a speleological potential of more than 2,500 m. Indeed, the highest altitude in the SE of El Peñon is about 3,000 m and the limestone deposits almost reach the altitude of 385 m where the two rivers draining most of the massif join in the west of the massif.

4. Area surveys and exploration

The two expeditions in 2011 and 2012 are the first of this kind to be carried out in this region of Colombia. This is the first systematic exploration and survey of the predominantly vertical high altitude karst caves. After a few weeks of survey and exploration, the surface of the karst field has barely been scratched. The dead end sumps, the impenetrable squeezes or cave-ins at depths exceeding 200 m, did not take anything from the pleasure of caving. In fact, these discoveries have succeeded one another at a frantic pace of nearly one cave per day. Future expeditions, in connection with a better hydrogeological knowledge of the region and search for the access to a larger system, will take cavers deep into the depth of the Rosablanca Limestones.

Figure 3. Pit in the Tronera cave (Jutzet 2012).

Nine caves were explored and mapped in 2011, totalling 4,200 m of development. In 2012, 15 caves were mapped, totalling 4,500 m. About ten other important caves (pits of 100 m and more, areas of large cave entrances) were located and partially explored during area surveys. The Table 1 summarizes the discovered caves and their main characteristics.

5. Field observation and discussion

5.1. Cave morphology

There are predominately three types of caves: shallow pits 50 to 150 m deep, sometimes giving access to large rooms or horizontal galleries; horizontal caves sometimes with 2 levels; and more or less impressive hollow shelters in cliffs leading sometimes to underground streams.

With a depth of -219 m, the Hoyo de los Ocelotes is the deepest cave at present in the area whereas the Cueva de los Carracos is the cave with the most important development (1,500 m). The entrance pit of the Hoyo de la Neblina is the deepest of the area with its 147 m.

Figure 4. Horizontal gallery in the Cueva de los Carracos (Bochud 2012).

Based on cave survey data (statistics based on measures of more than 20 m), two main gallery directions were emphased: N50° and N140° (Figure A). It is interesting to note that they both correspond to morphologic lineaments visible on satellite images.

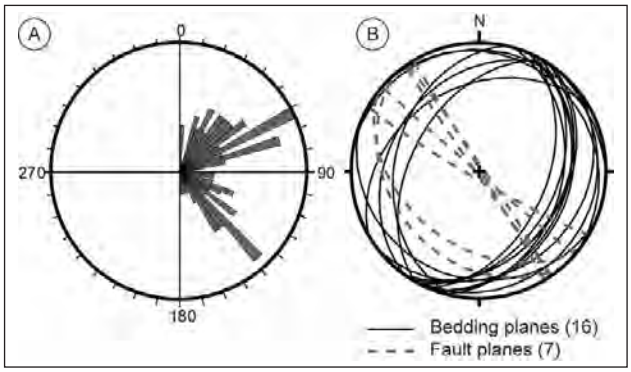

Figure 5. A) direction rosediagram of cave survey data of more than 20 m (150 measures); B) Lower hemispher equal area projection stereogram of faults and bedding great circles.

Numerous caves finish on a mud plug on a level corresponding to the base of the high pits. The mud level seems to correspond to the contact of limestone with a lower and less permeable geological layer at the base of the Rosablanca Formation that allows the accumulation of erosional products. In the Hoyo de los Ocelotes, two pits zones linked by a horizontal gallery were discovered and they both have a mud zone. These two levels could be explained by the presence of a vertical fault that moves down the Rosablanca Formation and allowed the formation of the second and deeper pits zone. The fault can be observed in a part of the gallery that link both zone. This part is a straight, high roofed and narrow (~2–3 m) gallery that follows directly the first mud zone.

5.2. Tectonic properties

Only few measures were made until now. They are represented on the steoreogram of Figure B.

Beddings are concordant with the main anticline structure that has an NNE–SSW fold axis. Faults can be separated in 2 groups: vertical faults dipping to the north at 58/89 and

to the south at 222/87 and inclined faults (probably inverse) dipping to the south at about 223/36. The N140° gallery direction can be related to the faulting. The second main gallery direction N50° is, as said before related to a surface geomorphologic lineation but presently cannot be linked neither with the bedding nor the measured faults. It is probably linked to a conjugate fault system.

Another observation can be made on the alignment of pits higher than 100 m on a vertical cross-section. On the Fig. 7, five caves are represented in a 3 dimensional cross-section on a W–E direction. High pits from 60 to 100 m can be linked with a synclinal structure that can be related to the structure of the limestones layer. Moreover, the high of the pit can be related to the thickness of the Lower–Middle part of the Rosablanca Formation that is estimated between 100 and 200 m.

5.3. Biospeleology and paleontology

To date, no systematic work has been done on the El Peñon area. Some interesting and punctual observations will be related.

In several caves, the typical cave bird Guácharo (*Steatornis caripensis*) can be observed. It is a night bird navigating by echolocation in the same way as bats. Some crabs were also observed until the bottom of the Hoyo de los Ocelotes at -219 m. Some bats and spiders were also seen.

An interesting discovery was made in the Hoyo de los Ocelotes: a cranium with two canines (Fig. 6). As a first assumption, it was identified as an ocelot and it gave the name of the cave. Afterwards, the picture was sent to the specialist Michel Blant at the Swiss Institute of Speleology and karst Research and he determined that it was a *Choloepus didactylus* (Southern two-toed sloth).

6. Conclusions

The two expeditions Colombia 2011 and 2012 were carried out in the El Peñon Massif in the Santander Department in Colombia.

The karst morphology is well developed in this humid area with more than 2.5 m of precipitations per year. The El Peñon area is structurally located on an anticline structure with a flattened hinge.

Twenty-four caves were explored and documented in a relatively small area during two expeditions totalizing about 10 km of galleries. Geologically they developed in the limestones of lower–middle part of the Lower Cretaceous Rosablanca Formation. The caves morphology seems to be closely related the structural deformation of the area. Although the deepest discovered caves stop presently at depth between 150–200 m, the speleological potential is estimated at 2,500 m.

In term of scientific observations, no systematic work has been done until now except the detailed survey of the caves. But the few observations indicate that the El Peñon area is very interesting in term of caves and karst morphology but also in term of biospeleology and paleontology.

Future expeditions, in connection with a better hydrogeological knowledge of the region and search for the access to a larger system, will take us certainly deeper into the depth of the Rosablanca Limestones.

Figure 7. 3-dimensional cross-sections with 5 caves. It emphazises the alignment of high pits along a syncline formed by the limestones of the lower and middle parts of the Rosablanca Formation.

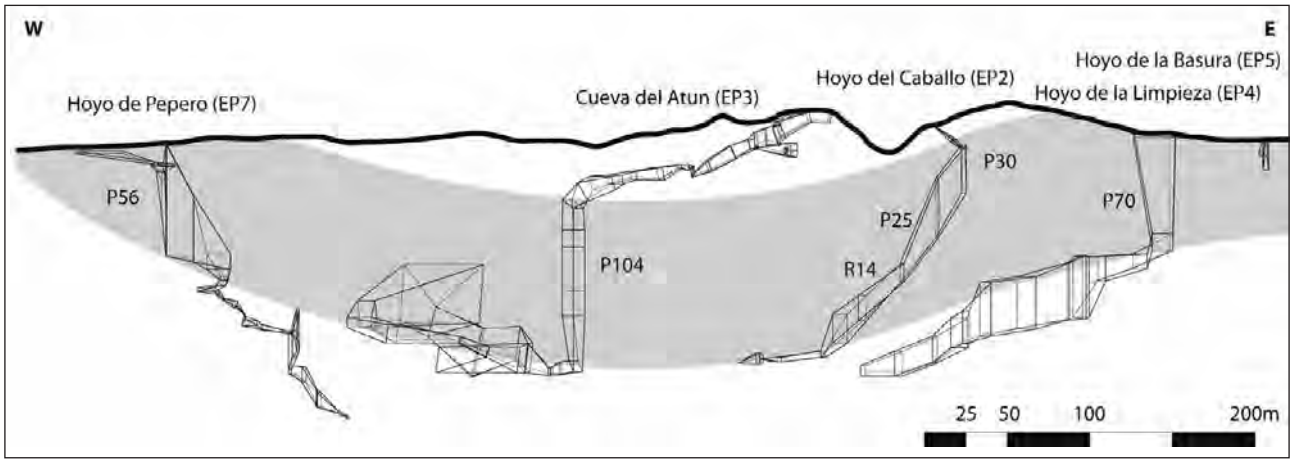

Figure 6. The cranium Choloepus didactylus (Southern two-toed sloth discovered in the Hoyo de los Ocelotes (Bochud 2012).

Acknowledgments

A great thank to the participants of the 2 expeditions for their motivation and the good ambiance. A special thanks to Jesus Fernandez for the organisation of the expedition.

References

Colletta B, Hebrard F, Letouzey J, Werner P, Rudkiewicz, J-L, 1990. Tectonic style and crustal structure of the Eastern Cordillera (Colombia) from a balanced cross-section, in: Letouzey, J. (Ed.), Petroleum and tectonics in Mobile Belts. Technip, Paris, 81–100.

Guerrero J, 2002. A proposal on the Classification of the Systmes Tracks: Application to the Allostratigraphy and Sequence Stratigraphy of the Cretaceous Colombian Basin. Part 1: Berriasian to Hauterivian. Geologia Colombiana 27, 3–25.

Hof B, 1977. Recherches spéléologiques en Colombie. Fédération Française de Spéléologie, G.S. Nice.

Mendoza-Parada JE, Moreno-Murillo JM, Rodriguez-Orjuela G, 2009. Rosablanca Formation Karstic Systems lower Cretaceous in Vélez, Santander Province, Colombia. Geologia Colombiana 34, 36–44.

Pabón-Caicedo JD, Eslava-Ramírez JA, Gómez-Torres RE, 2001. Generalidades de la distribución espacial y temporal de la temperatura del aire y de la precipitation en Colombia. Meteorologia Colombiana 4, 47–59.

Toussaint J-F, 1996. Evolución geológica de Colombia durante el Cretácico. Universidad Nacional de Colombia, Medellin.

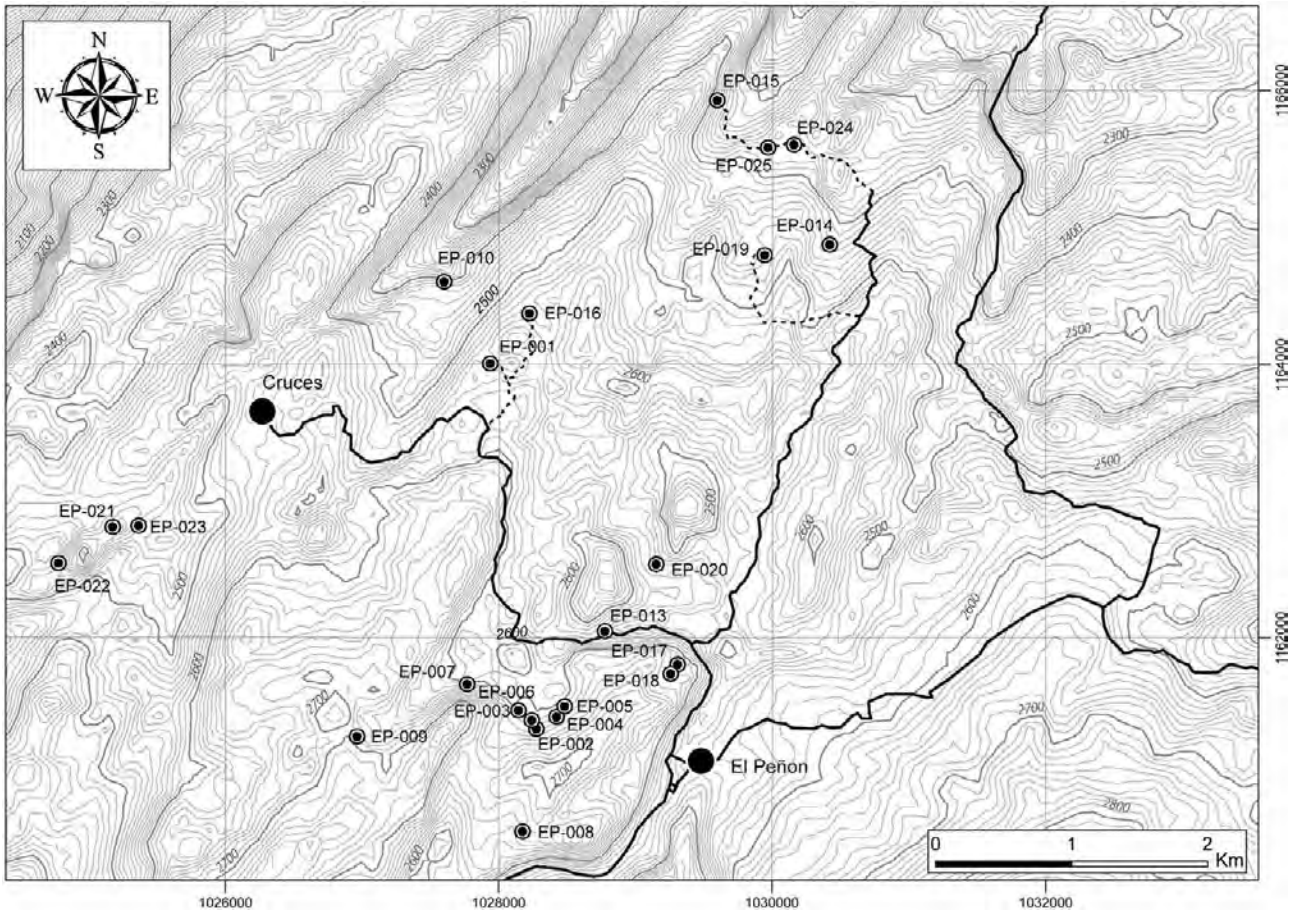

Figure 8. Map with the discovered caves in the El Peñon area. Numbers are related to the Table. Caves of the la Hermosura area are not represented on the map (B1, B2, B3, B4 and B5).

Table 1. List of discovered caves in El Peñon-Bolivar area (department of Santander, Colombia).

No	Name (place)	Length [m]	Depth [m]	Altitude [m a.s.l.]	Year	Comment
EP1	Cueva de los Carracos (El Peñon)	1,500	(-81, +4)	2,488	2011	Underground river with fossil gallery. Explored by local people.
EP2	Hoyo del Caballo (El Peñon)	267	(-149, +10)	2,593	2011	Swallow hole with river and sump.
EP3	Cueva del Atun (El Peñon)	764	-159	2,593	2011	Stops on a sump in a big room. Sinking river at the entrance.
EP4	Hoyo de la Limpieza (El Peñon)	343	-147	2,612	2011	Swallow hole with river and sump.
EP5	Hoyo de la Basura (El Peñon)	25	-15	2,617	2011	Swallow hole with river. Garbage.
EP6	Cueva de los Elechos (El Peñon)	50	-5	2,636	2011	Small horizontal cave.
EP7	Hoyo de Pepero (El Peñon)	321	-167	2,601	2011	Swallow hole with river.
EP8	Hoyo de la Neblina (El Peñon)	715	-217	2,686	2011	Swallow hole with river and big room.
EP9	Cueva del Hipocampo (El Peñon)	913	(-15, +28)	–	2011	Cave with a river. Numerous unexplored galleries.
EP10	Cueva del Caracol (El Peñon)	324	-36	2,410	2012	Collapsed sinkhole with river and sump.
EP11	Cueva del Krypton (El Peñon)	~ 40	~ -40	–	2011	Swallow hole (no survey).
EP12	Cueva sin Fin (El Peñon)	~ 50	~ -50	–	2011	Swallow hole (no survey).
EP13	Cueva de la Casa Virgen (El Peñon)	102	-78	2,553	2011	Swallow hole with river.
EP14	Hoyo de la Bollas de Oro (El Peñon)	159	-131	2,422	2012	Swallow hole with sinking river.
EP15	Cueva de las Escuillas (El Peñon)	310	-53	2,374	2011	Collapsed sinkhole.
EP16	Hoyo de los Ocelotes (El Peñon)	812	-219	2,544	2012	Swallow hole with 2 entrances and a river.
EP17	Hoyo de las Professoras 1 (El Peñon)	130	-92	2,633	2012	Swallow hole.
EP18	Hoyo de las Professoras 2 (El Peñon)	79	-40	2,636	2012	Swallow hole.
EP19	Cueva de la Tronera (El Peñon)	1203	-167	–	2011	Collapsed sinkhole - swallow hole with river
EP20	Cueva de las Gallinas (El Peñon)	179	30	–	2012	Cave with a river.
EP21	Cueva de las Golondrinas (Cruces, El Peñon)	50	0	2,412	2012	Huge entrance.
EP22	Cueva Grande (Cruces, El Peñon)	~400	~ -40	2,484	2012	Huge entrance.
EP23	Cueva de los Murcielagos (Cruces, El Peñon)	~ 300	~ -20	2,414	2012	Cave with a river.
EP24	Hoyo de los Golondrinas 1 (El Peñon)	77	-47	–	2012	Swallow hole on a fault.
EP25	Hoyo de los Golondrinas 2 (El Peñon)	94	-48	–	2012	Swallow hole on a fault.
B1	Hoyo del Campesino / del Aguila (La Hermosura, Bolivar)	~ 120	~ -120	–	1977?	Big pit, probably explored by Hof 1977.
B2	Hoyo de la Campesina (La Hermosura, Bolivar)	~ 100	~ -100	–	1977?	Big pit, probably explored by Hof 1977.
B3	Cueva de la Puerta de los Cerros (La Hermosura, Bolivar)	524	-205	1,835	2011	Cave with a large gallery.
B4	Hoyo Horrible (La Hermosura, Bolivar)	~ 100	~ -100	–	1977?	Big pit, probably explored by Hof 1977.
B5	Cueva de Los Ossos 1-2-3 (La Hermosura, Bolivar)	~ 1,000	~ -50	1,130	2012	Cave with 3 entrances and a river (not explored).

RECENT SURVEY AND EXPLORATION IN LECHUGUILLA CAVE, NEW MEXICO, USA

Peter Bosted[1], John Lyles[2]
[1]PO Box 6254, Ocean View HI 96737 USA, peter@cavepics.com
[2]PO Box 95, Los Alamos NM 87644 USA, jtml@vla.com

Since the last ICS in 2009, considerable progress has been made in the survey and exploration of Lechuguilla Cave, located in Carlsbad Caverns National Park, New Mexico, USA. The most important new discovery is an area called Oz, reached by a long aid climb from Emerald City, in the western portion of the cave. Many smaller discoveries were made as well, bringing the total length to over over 218 km. In addition, a big effort was put into improving the survey quality of passages explored in the early years (1988–1991). Most of the poor survey loop closures were fixed, and quadrangle maps were updated with improved detail.

1. Introduction

Lechuguilla Cave was known in the early 1900's as a relatively short cave with a 30 m entrance pit leading to a rich deposit of bat guano, which was mined for a time. After several unsuccessful attempts, cavers finally pushed through a breakdown choke in 1986 to discover a vast and beautiful cave (Reames, 1989). Over 100 km were explored and surveyed by the early 1990's, with the 200 km mark being passed in 2008. The cave is most famous not for it's great length and volume, but rather for the spectacular cave formations, such as the long selenite crystals in the Chandelier Ballroom, or the impressive flowstone columns in Tower Place (Widmer, 1998). The overall structure of this single-entrance cave is large long borehole trunk passages that connect extremely complex three-dimensional mazes together. In recent years, the number of week-long exploration and survey expeditions has been reduced in number to just one every two to four months. Nonetheless, new discoveries remain to be made, with about 4 to 6 km of newly discovered passages being mapped each year. In parallel, there has been an increased effort to improve the quality of early surveys done in the "frenzy" years of 1988–1991. This effort includes removing survey blunders, improving survey accuracy, and improving sketching quality. Since the beginning of 2009, there have been 26 week-long expeditions, with almost 18 km of new passage surveyed, and over 15 km of passage re-surveyed.

2. New discoveries

Most of the newly discovered passages in the past few years have been relatively small, and have resulted from pushing smaller passages than was the norm in the early days of exploration. This "mopping up" process was greatly facilitated by cartographers drawing up detailed maps of their sections of the cave, making it easier to identify which passages had been surveyed already. Some of the most productive areas included Southern Climes in the Far West, the Chandelier Maze and Voids in the South, and the Outback in the Far East. Some spectacular example of cave formations were found, such as the "Wasp's Nest" in the newly discovered Coral Sea area of the Far East, and individual gypsum flowers and selenite needles in Southern Climes each over 110 cm long.

A large effort went into climbing domes. One such example was the six-day effort to aid climb the Capitol Dome above Mt. Vernon, in the Far East branch of the cave. Unfortunately, the passages at the top ended after only a short distance.

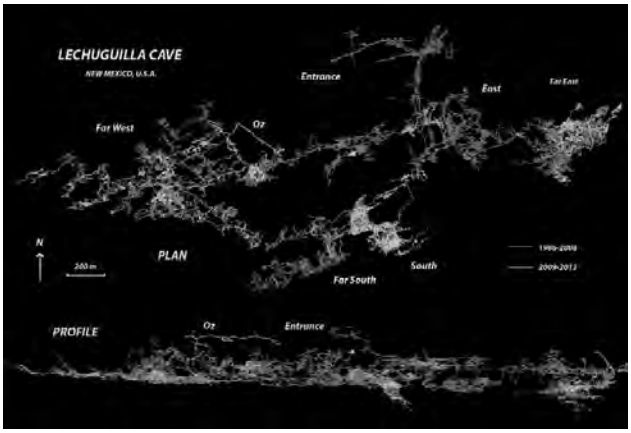

Figure 1. Plan and profile line plots of Lechuguilla Cave. Green lines show passages mapped prior to 2009, while red lines show new discoveries or passages that have been re-mapped since 2009.

More successful was the climb of the Kansas Twister, a 125-m-tall dome in Emerald City. The first 30 m were very difficult, and were finally conquered using a sling-shot to shoot a line over a bridge in 2010. The sling-shot technique proved un-successful for reaching the second bridge, so in 2012 a team climbed straight up the overhanging wall in very poor quality rock, reaching the summit five days later. On the last day of the expedition, a large new area was found, including big rooms, massive flowstone formations, and lakes. It was named "Oz", following the naming theme of Emerald City below. Many leads remain to be explored, as of this writing. As can be seen in Figure 1, the Oz area is very high up in the cave stratigraphy, nearly matching the elevation of the entrance. Maps and photographs of this new area will be shown in the oral presentation.

3. Blunder fixing

The method used for finding possible survey blunders used a computer code that simultaneously closes all the loops in a given section of the cave. The basic method is a least-squares fit that minimizes that total corrections (added

quadraticly, and called χ^2) to all of the segments, where a segment is defined as a sequence of survey shots that connect one junction to another. The corrections in each case are weighted by the "expected" errors based on station placement uncertainties of 5 cm, and compass and inclinometer readings with random errors of 2 degrees.

Once all the segments were closed simultaneously, a search for likely blunders was made by removing one segment at a time, and re-closing the remaining loops, starting with the one with the largest contribution to χ^2. Using the junction locations defined by all other segments, a search is done for the removed segment to see what could make it close with a contribution to χ^2 of less than two units. The following possibilities were examined: reversed inclinometer reading, reversed compass reading, both reversed, compass off by 100°, inclinometer read on percent scale instead of degree scale, digits on distance reversed, and either starting or ending station being different that the one noted in the survey book. If any of these possibilities was considered to be probable, an examination of the survey notes was made to see if there had been a data entry error, or if the notes contradicted the sketch. In about half of the cases, the blunder was found in this manner.

In the case where the problem could not be resolved by an examination of the survey notes, a report was generated for cavers to field check the problem.

Generally, we re-measured all the front and back-sight shots in each bad loop, using the Disto-X instrument. We used the Auriga program, running on a PDA using Palm OS, to enter the new loop data and make sure that it closed well. Sometimes, we found a major blunder early on, and didn't need to re-shoot the entire loop.

During 2008–2012, we were able to reduce the fraction of loops that almost certainly contained a blunder from over 6% to about 2%. The area of the cave that we have concentrated on the most, the Far West, currently has no "very bad" loop closures, with closures worse than four standard deviations.

The most common blunders were found to be (in order from most common to least common):

a) One or more stations with the wrong station number written on them (in this project, every station is labelled with flagging tape).

b) Front and back sights were reversed, and the sketcher used the reversed numbers to make the sketch.

c) Compass and/or inclinometer readings were off by more than 2° for many shots in a sequence.

d) Distance reading was wrong for one reason or another.

e) Shot simply didn't make any sense upon field checking (for example, shot goes through solid wall).

f) Station marker was moved from its original location.

4. Future prospects

A big effort is currently underway to produce high-quality, detailed quadrangle maps of the entire cave surveyed to date. In support of this effort, we will attempt to identify and remove most of the remaining survey blunders, and continue to re-sketch areas for which the original survey notes were poor. In parallel, exploration of new areas such as Oz will continue. With hundreds of leads remaining in the cave, prospects are good for eventually passing the 250 km mark for the overall surveyed length of Lechuguilla Cave.

Acknowledgments

We would like to acknowledge the efforts of the recent cave explorers and cartographers. Among the most active in the past four years are: Stan Allison, Andy Armstrong, Bonny Armstrong, Mark Andrich, Jeff Bartlett, Hazel Barton, Peter Bosted, Cathy Borer, Derek Bristol, Paul Burger, Daniel Chailloux, Andrea Croskley, Jen Foote, Art Fortini, James Hunter, Jean Krejka, Luc LeBlanc, Heather Levy, Vivian Loftin, John Lyles, Ron Miller, Annick Normandin, Carol Vesely, Simeon Warner, James Wells, and Max Wisshak.

We also are very grateful to the National Park Service for their support, which includes a place to stay while working in the Park, maintaining the gates and ropes in the cave, providing supplies, entering the data into the computer, and archiving all of the survey notes. We especially acknowledge the support of Stan Allison, Cave Resource Technician at the Park.

References

Reames S, Fish L, Burger P, Kambesis P, 1989. Deep Secrets: The Discovery and Exploration of Lechuguilla Cave. 412, Cave Books. ISBN-10: 0939748282.

Widmer U, 1998. Lechuguilla, Jewel of the Underground. 168, Speleo Projects. ISBN-10: 3908495016.

PLEISTOCENE SEA LEVEL CHANGES AS REVEALED BY FLANK MARGIN CAVES IN TELOGENETIC LIMESTONES IN SICILY AND SARDINIA (ITALY)

Ilenia Maria D'Angeli[1], Jo De Waele[1], Rosario Ruggieri [2], Laura Sanna [3]
[1]Department of Biological, Geological and Environmental Sciences, Bologna University, Via Zamboni 67, 40126 Bologna, Italy, ileniamaria.dangeli@studio.unibo.it; jo.dewaele@unibo.it
[2]Centro Ibleo di Ricerche Speleo-Idrogeologiche, Via Carducci 165, Ragusa, Italy – University of Nova Gorica, info@cirs-ragusa.org
[3]Department of Natural Sciences and Land, Sassari University, Via Piandanna 4, 07100 Sassari, Italy, speleokikers@tiscali.it

Coastal karst areas often host many indices of past sea level changes, such as marine terraces, fossiliferous sediments, tidal notches and coastal caves. Tectonic movements can then displace these ancient coastlines vertically. The interplay between rising or falling sea level and uplifting or subsidence can be very complex and difficult to unravel. The combination of a detailed knowledge of marine terraces and the study of some flank margin caves located at various altitudes have allowed to reconstruct the speleogenetic history of the coastal plain of Cornino-Custonaci (NW Sicily). Along the central-eastern coast of Sardinia, instead, the detailed study of the Fico Cave has allowed to recognise it as a flank margin cave developed on five levels, related to Pleistocene sea level highstands. These studies show that this type of mixing corrosion caves is much more widespread than previously thought also in telogenetic limestones. These caves, being excellent sea level markers, might help coastal geomorphologists to understand more on both sea level rise and fall and tectonic movements in coastal areas.

1. Introduction

Geomorphological evidences of past sea level changes are best preserved in coastal karst areas around the world. Carbonate shorelines exhibit some typical landforms created at or close to sea level, like tidal notches (Furlani et al. 2011), coastal caves (Mylroie and Carew 1988), biocorrosion (e.g., lithophaga borings) or bioconstruction (e.g., vermetid reefs) morphologies. These sea level markers, combined with other data derived from marine terraces and fossiliferous continental or marine sediments, have been used worldwide for sea level reconstructions (Dorale et al. 2010).

It is well-known that more or less horizontally developed solutional caves in coastal areas often indicate the position of sea level at the time of their formation (Mylroie and Carew 1988; Florea et al. 2007). Among the different types of coastal caves, flank margin caves are the most reliable sea level indicators. In fact, flank margin caves form at the top and the bottom of the freshwater lens in coastal karst areas by mixing dissolution (Mylroie and Carew 1990), showing clear evidence of widening at the fresh-salt water boundary, often very close to sea level.

Flank margin caves develop easily in young immature (eogenetic) limestones, where primary porosity facilitates the ingression of salt water and its mixing with seeping fresh water. Many of these caves have been reported from carbonate islands such as the Bahamas and Bermuda (Mylroie et al. 1995), Guam (Mylroie et al. 2001), Isla de Mona (Puerto Rico) (Frank et al. 1998), and the Mariana Islands (Jenson et al. 2006), or from eolian calcarenites such as the case of Kangaroo Island, Australia (Mylroie and Mylroie 2009). In more recent times flank margin caves have also been found in older and mature limestones, where mixing occurs along secondary permeability pathways such as fractures and bedding planes. Nice examples are described from New Zealand (Mylroie et al. 2008), and Croatia (Otonicar et al. 2010).

Where fresh water discharge on the carbonate coast is greater, caves with a ramiform pattern will form. When fresh water discharge largely overrules the salt water entering the rock mass, caves will have very extensive stream passages developing inland. In this case speleogenesis is mainly controlled by normal dissolution and erosion processes, and cave altitudes do not necessarily reflect sea levels. The influence of mixing processes is visible only in the cave passages closest to the sea, fading slowly going landwards.

Figure 1. Location of the study areas: 1) San Vito Lo Capo, Sicily; 2) Fico Cave, Sardinia.

Where fresh water discharge is slightly more important than salt water intrusion, ramiform caves develop, with passages modified by mixing corrosion processes also far inland. This type of caves, halfway between normal epigenic stream caves and flank margin caves, can be reliable sea level indicators only in their parts close to the coast (Smart et al. 2006).

In this paper we describe three interesting Pleistocene flank margin caves in telogenetic limestones: two are located respectively at 100 and 70 m a.s.l. on the border of the Cornino-Custonaci plain in W Sicily, the other is situated at 14 m a.s.l. in the Gulf of Orosei, E Sardinia (Fig. 1). The timing of formation of these caves is based on a series of correlations with dated marine terraces, geomorphological observations, and dated speleothems and their phreatic organic overgrowths.

2. Study areas

2.1. Cornino-Custonaci plain

The Cornino-Custonaci coastal plain is located on the western edge of the San Vito Lo Capo peninsula, halfway between Trapani and Palermo (W Sicily). The geology of the area is characterised by Mesozoic dolostones and limestones, and Eocene-Miocene limestones, marly limestones, marls and clays. Since Upper Pliocene the region is slowly uplifting (Nigro and Renda 2002). Extensive both continental, transitional, and marine Pleistocene deposits are present in the coastal plain, mostly composed of calcarenites (Di Maggio et al. 1999).

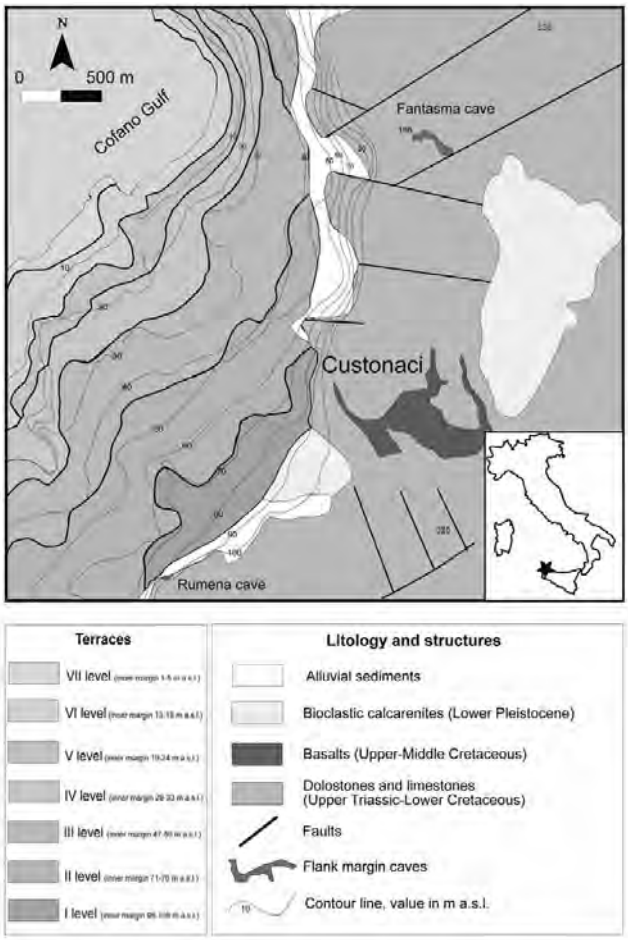

Figure 2. Geological map of the Cornino-Custonaci plain.

The Fantasma and Rocca Rumena I caves are located in the Cretaceous limestones that form cliffs surrounding the coastal plain (Fig. 2). Seven marine terraces are present between altitudes of 0 and 105 m a.s.l. (Di Maggio et al. 1999). The age of these terraces has been estimated based on stratigraphical and paleontological evidences. The marine terrace of VIth order, with upper boundary at 13–18 m a.s.l., contains the typical warm fauna with *Strombus bubonius* and can be attributed to MIS 5e. A speleothem sampled at 8 m a.s.l. in a notch related to this terrace at San Vito Lo Capo has given a U/Th age of 19,625 ± 5,300 years BP, confirming this terrace to be older than LGM (Antonioli et al. 1999). Based on these observations, terrace VII should thus be related to MIS 5a or 5c, terrace V to MIS 7, terrace IV to MIS 9, terrace III to MIS 11, terrace II to MIS 13, and finally the highest terrace to MIS 15 or older. The presence of *Elephas falconeri* in some continental deposits at elevations above 40 m a.s.l., roughly corresponding to terraces III or IV, confirms their age older than MIS 9. A speleothem that covered the notch at 42 m a.s.l. at San Vito Lo Capo is beyond the U/Th radiometric dating method and indicates terrace III to be older than 300 ka BP (Antonioli et al. 1999).

2.2. Gulf of Orosei

The Gulf of Orosei is characterised by the outcropping of Mesozoic dolostones and limestones that overly a Palaeozoic Variscan basement composed of granites and phyllites (Dieni and Massari 1985) (Fig. 3).

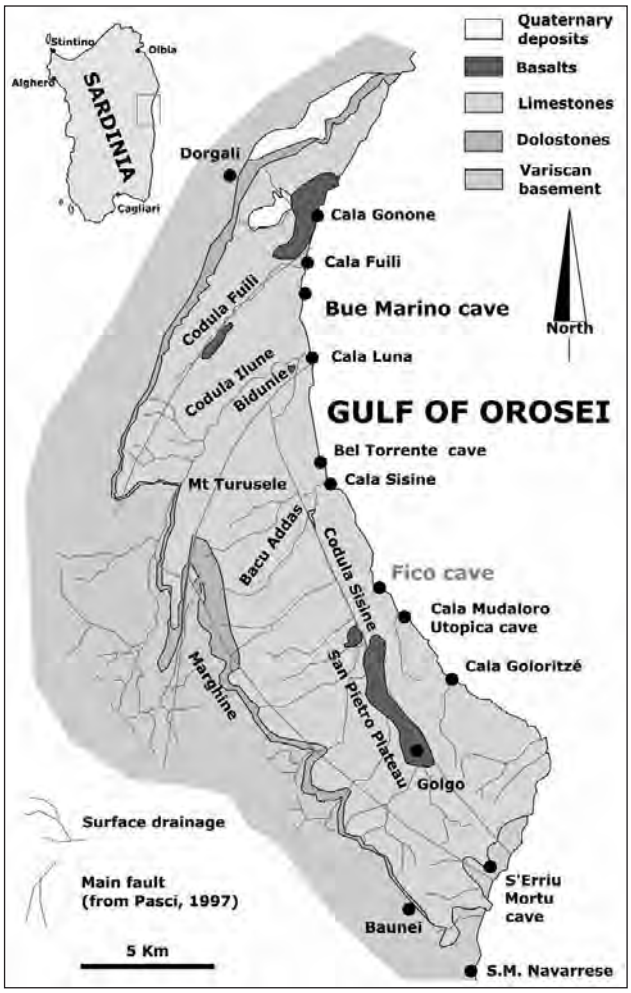

Figure 3. Geological map of the Gulf of Orosei.

This carbonate sequence forms a monocline ridge dipping gently eastwards to the centre of the Gulf, showing two transcurrent arcuate fault systems directed NNW-SSE and NNE-SSW (Pasci 1997). These Mesozoic rocks are locally covered with alluvial conglomerates and quartz sands, related to an intense erosion-deposition cycle caused by an uplifting phase of Middle Pliocene age (Massari and Dieni 1973). In the same period Pliocene basalts with K-Ar ages of 3.56 ±0.23 to 1.99 ±0.08 million years (Savelli and Pasini 1973) were put in place. Early Pleistocene alluvial sands and conglomerates are found upon these basalts (Dieni and Massari 1966). During Pleistocene stratified slope-waste deposits (éboulis ordonnées), and aeolian sands visible in karst pockets and coastal cave entrances have deposited.

The Fico Cave is located at 14 metres height along the coastal limestone cliffs, about 20 km N of Santa Maria Navarrese. Detailed geomorphological studies have been carried out along the coastline, and especially in the Bue Marino Cave located 8 km to the North. Pleistocene basalts filling phreatic conduits in Bue Marino Cave (Mahler 1979), the Golgo shaft and Su Molente Cave testify the start of speleogenesis to be pre-Quaternary (De Waele 2004). Several tidal notches are well developed along the entire carbonate coast of the Gulf and indicate present and past mean sea levels. Such tidal notches are well described from depths of 10 m below sea level to heights of 10.5 m above sea level (Antonioli et al. 1999; Carobene and Pasini 1982). The relict tidal notch, that has a decreasing height from North to South between 10.5 and 7.7 m a.s.l., is attributed to the isotopic stage 5e (125,000 B.P.) and its continuity along the 37 km of limestone coast testifies a relative tectonic stability since, exception given for the slight N-S tilting (Antonioli et al. 1999). At the Fico Cave, although not visible anymore, its height would have been 8.5 m a.s.l.

3. Cave morphology

3.1. Fantasma Cave

Fantasma (or Monte Cofano I) Cave opens at 198 m a.s.l. in the area of Contrada Marcato Gnarosa, close to marble quarries (Fig. 4) (Ruggieri and Messina Panfalone 2011). The cave follows two main fault systems, NE–SW with inclination of 75° toward the SE, on which the entire first part of the cave is developed, and the second with WNW–ESE direction and dipping 80º toward the SSW that influences the deepest part of the cave. The first part is developed along a rapidly descending low and wide fissure with many indices of recent tectonic activity (broken columns and deflected stalagmites). At 120 m depth (around 80 m a.s.l.) the cave changes its morphology, with rounded passages, cupola, and a large ellyptical room called "Sala del Fantasma", which centre is occupied by a large heap of old bat guano, while large white and corroded speleothems contrast the dark background. The northern part of this chamber is formed along a WNW–ESE fault with reddish mylonite creating a perfectly straight wall up to 10 m high. The roof and walls of this room have extremely well rounded shapes, and at around 70 m a.s.l. the walls are perforated by rounded tubes, forming a perfectly horizontal notch. Nowhere in the cave there are fluvial sediments, and the walls are always smooth and do not reveal any scallops or similar forms. The southern sector of the Fantasma room, however, hosts some evidences of phreatic (paragenetic) and vadose morphologies.

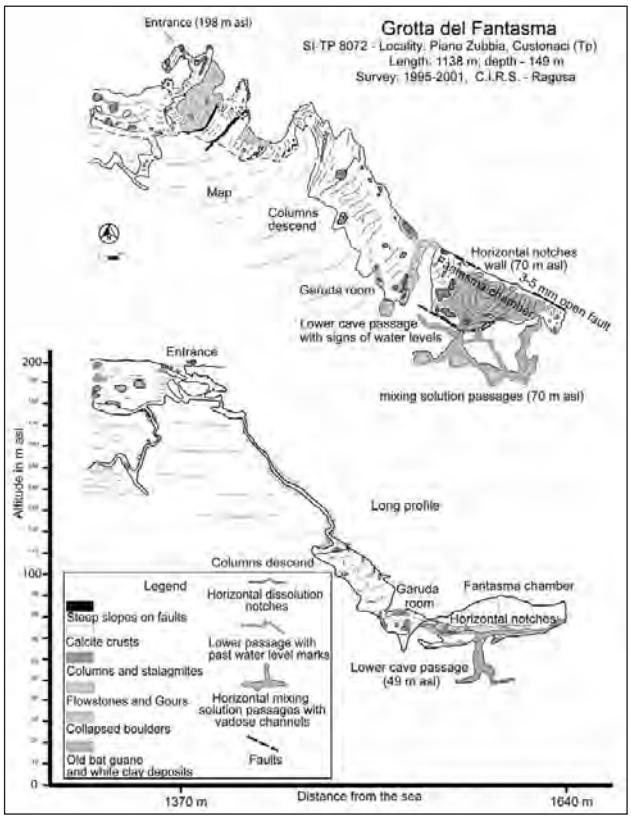

Figure 4. Map of the Fantasma Cave.

3.2. Rocca Rumena I Cave

Rocca Rumena I is a small mostly horizontally developed cave formed at the foot of the 20 m high Pleistocene coastal cliff (Ruggieri and Messina Panfalone 2011).

Figure 5. Map of the Rocca Rumena I Cave.

Its entrance opens at 100 m a.s.l. in correspondence of a not well-defined notch and a clear level of lithophaga borings. It is composed of a series of small chambers and passages with rounded forms, small tubes and pillars (Fig. 5). The passages develop parallel to the cliff wall, mostly along fractures and bedding planes, but tend to tighten gradually going away from the cliff. The roof and part of the walls are covered with organogenic crusts, mostly scleractinian corals that also fill part of the lithophaga holes. Also speleothems are covered with these corals and are perforated by lithophaga. One stalactite in particular shows three growth hiatuses, suggesting submersion at least three

times (Ruggieri et al. 2012). The corals have been dated using $^{87}Sr/^{86}Sr$ ratio and appear to be 1,100 ± 200 ka years old (Antonioli et al. 2012). $\delta^{18}O$ measurements on the continental stalactite layers and comparison with marine and continental records suggest this speleothem to be formed during MIS 27–31, around a million years ago (Antonioli et al. 2012).

3.3. Fico Cave

The Fico Cave has three entrances (respectively at -7, 0 and 14 m), and is characterised by a large passage running parallel to the coastline, and by a much smaller mostly submerged branch running perpendicular (Fig. 6).

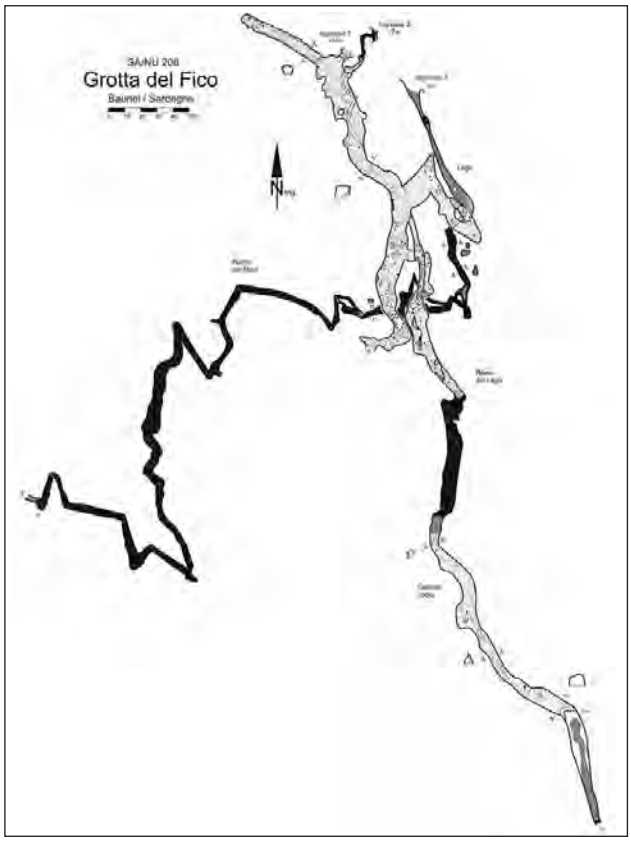

Figure 6. Map of the Fico Cave.

The development of most passages is clearly influenced by fractures directed NNW–SSE and NE–SW. Water flow is present only along the small submerged branch, containing sediments deriving from the weathering of granites and carbonatic rocks, while the main branch has only few sediments mostly of autigenic origin. Nowhere, except from the active submerged branch, signs of phreatic flow have been observed (e.g., scallops). Close to the entrance some sands of aeolian and marine origin have been found at altitudes up to 7 m a.s.l. Cave passages tend to diminish in size the farher they develop from the coastline, ending abruptly on blind walls. Five Cave levels can clearly be recognised: the main branch at 14 m a.s.l., three fossil levels at 22, 40 and 50 m a.s.l. respectively, and the active submerged branch below present sea level. The level at 22 m a.s.l. has a perfectly flat ceiling, no sediments except for residual clays, and a nice corrosion notch on its walls, all testifying a relatively stable sea level. A stalagmite at 8 m a.s.l. in the "Ramo del Lago" shows organic overgrowths, testifying a submersion during its growth.

4. Results and conclusions

4.1. Cornino-Custonaci plain

Palaeontological and geomorphological evidences, combined with absolute datings on speleothems and corals, allow for a relatively detailed reconstruction of the speleogenetic phases and relative sea level changes in the Cornino-Custonaci plain. Rocca Rumena I Cave formed during an interglacial period, with relatively high sea level, around MIS 29. The Fantasma Cave, instead, is an enlarged (Middle Pleistocene) fault intercepted by a flank margin cave at 80 m a.s.l., located at around 500 m of the Pleistocene coastline, with the main level of mixing corrosion, corresponding to the longest stable position of the sea level, located at 70 m a.s.l.. Based on tectonic uplift rates calcolated using the Rocca Rumena date and the MIS 5e (terrace VI) (0.1 m/ka) (Antonioli et al., 2012) and other geomorphological constraints (Di Maggio et al. 1999), the horizontal maze-like chamber and conduits of Fantasma Cave might thus have been created by the mixing corrosion of fresh and salt water probably around 800,000 years ago (ca. MIS 19) (Fig. 7).

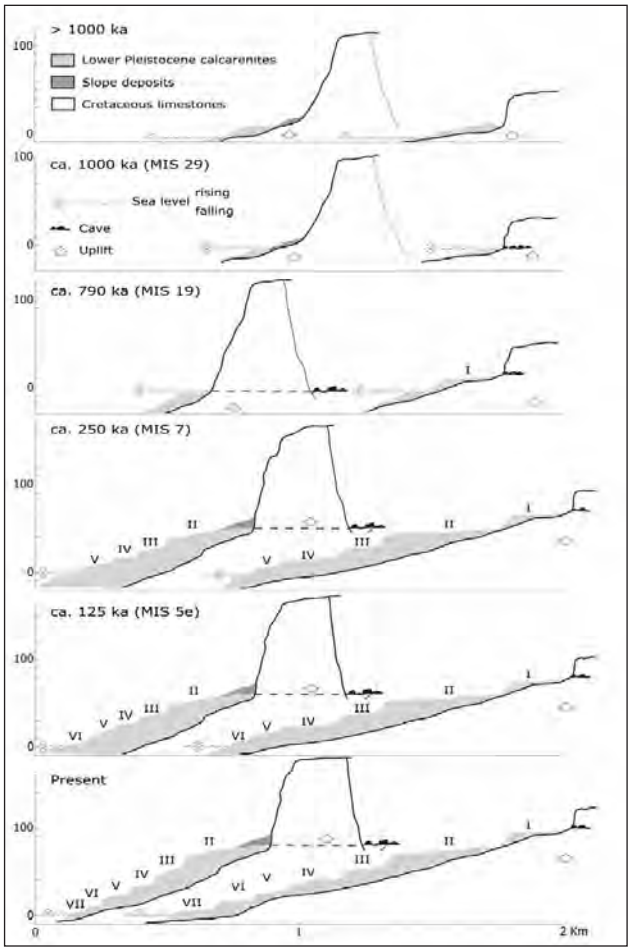

Figure 7. Evolution of the Cornino-Custonaci plain.

4.2. Gulf of Orosei

The horizontal levels of Fico Cave have been formed during high sea level stands prior to MIS 5e. Using estimated uplift rates somewhat higher than those revealed by the Tyrrhenian notch (0.02 m/ka) and those estimated by Carobene and Pasini (0.03 m/ka), and considering that

during MIS 7 the sea level highstand stayed around 10 m below present, the active submerged level would have formed during MIS 7 (ca. 250 ka), the main level at 15 m a.s.l. during MIS 9 (ca. 350 Ka), the 22 m a.s.l. one during MIS 11 (ca. 425 ka) and the upper levels would be older than MIS 21 (>865 Ka).

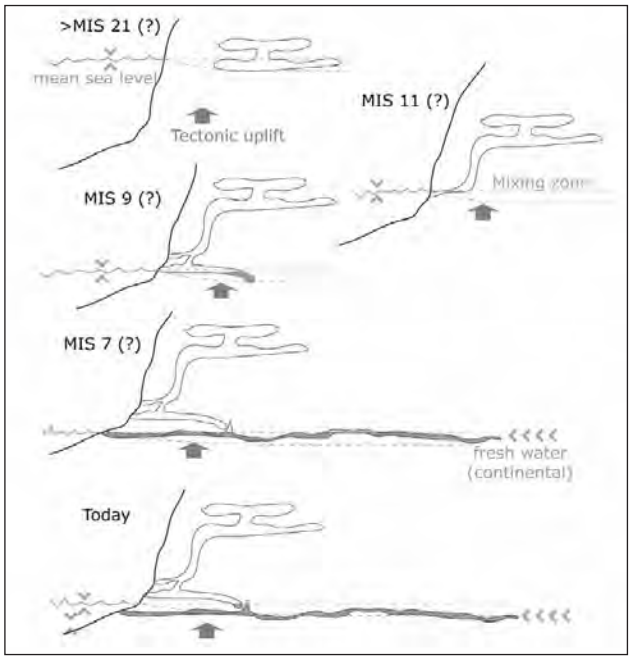

Figure 8. Evolution of the Fico Cave.

Acknowledgments

Field work at Custonaci was made comfortable thanks to Davide Vito Messina Panfalone, while access to Fico Cave was guaranteed by the cavers of the Società Speleologica Baunese.

References

Antonioli F, Montagna P, Caruso A, Ruggieri R, Lo Presti V, Silenzi S, Frank N, Douville E, Pierre C, 2012. Investigation of marine and continental layers in a stalactite older than 1 million years (Custonaci, north-western sector of Sicily), SLALOM 2012, Athens 19–22 March 2012, 57–58.

Antonioli F, Silenzi S, Vittori E, Villani C, 1999. Sea level changes and tectonic mobility: precise measurements in three coastlines of Italy considered stable during the last 125 ky. Physics and Chemistry of the Earth (A), 24, 337–342.

Carobene L, Pasini G, 1982. Contributo alla conoscenza del Pleistocene superiore e dell'Olocene del Golfo di Orosei (Sardegna orientale). Bollettino della Società Adriatica di Scienze, 64, 5–35.

De Waele J, 2004. Geomorphologic evolution of a coastal karst: the Gulf of Orosei (Central-East Sardinia, Italy). Acta Carsologica, 33, 37–54.

Di Maggio C, Incandela A, Masini F, Petruso D, Renda P, Simonelli C, Boschian G, 1999. Oscillazioni eustatiche, biocronologia dei depositi continentali quaternari e neotettonica nella Sicilia nord-occidentale (Penisola di San Vito Lo Capo – Trapani). Il Quaternario, 12, 25–50.

Dieni I, Massari F, 1966. Il neogene e il Quaternario dei dintorni di Orosei (Sardegna). Memorie della Società Italiana di Scienze Naturali e del Museo Civico di Storia Naturale di Milano, 15, 91–141.

Dieni I, Massari F, 1985. Mesozoic of Eastern Sardinia: 19th European Micropaleontological Colloquium-Guide Book, Cagliari, 1–10 October 1985, 66–78.

Dorale JA, Onac BP, Fornos JJ, Gines J, Gines A, Tuccimei P, Peate DW, 2010. Sea-Level Highstand 81,000 Years Ago in Mallorca. Science, 327, 860–863.

Florea LJ, Vacher HL, Donahue B., Naar D., 2007. Quaternary cave levels in peninsular Florida. Quaternary Science Reviews, 26, 1344–1361.

Frank EF, Mylroie JE, Troester J, Calvin Alexander E, Carew JL, 1998. Karst development and speleogenesis, Isla de Mona, Puerto Rico. Journal of Cave and Karst Studies, 60(2), 73–83.

Furlani S, Cucchi F, Biolchi S, Odorico R., 2011. Notches in the northern Adriatic Sea: genesis and development. Quaternary International, 232, 158–168.

Jenson JW, Keel TM, Mylroie JR, Mylroie JE, Stafford KW, Taborosi D, Wexel C, 2006. Karst of the Mariana Islands: The interaction of tectonics, glacio-eustasy, and freshwater/seawater mixing in island carbonates. In: RS Harmon and CM Wicks (eds.). Perspectives on Karst Geomorphology, Hydrology, and Geochemistry. Geological Society of America Special Paper, 404, 129–138.

Mahler A, 1979. Verkarstung der Karbonatgebiete am Golfo di Orosei (Sardinien). Geologischer Palaeontologischer Mitteilungen Innsbruck, 7, 1–49.

Massari F, Dieni I, 1973. La Formazione fluvio-lacustre di Nuraghe Casteddu ed i suoi rapporti con i basalti di Orosei-Dorgali (Sardegna). Memorie della Società Geologica Italiana, 12, 377–410.

Mylroie JE, Carew JL, 1988. Solution Conduits as Indicators of Late Quaternary Sea-Level Position. Quaternary Science Reviews, 7, 55–64.

Mylroie JE, Carew JL, 1990. The flank margin model for dissolution cave development in carbonate platforms. Earth Surface Processes and Landforms, 15, 413–424.

Mylroie JE, Mylroie JR, 2009. Caves as Sea Level and Uplift Indicators, Kangaroo Island, South Australia. Journal of Cave and Karst Studies, 71, 32–47.

Mylroie JE, Carew JL, Vacher HL, 1995. Karst development in the Bahamas and Bermuda. In: HA Curran and B White (eds.). Terrestrial and Shallow Marine Geology of the Bahamas and Bermuda. Geological Society of America Special Paper, 300, 251–267.

Mylroie JE, Jenson JW, Taborosi D, Jocson JMU, Vann DT, Wexel C, 2001. Karst features of Guam in terms of a general model of carbonate island karst. Journal of Cave and Karst Studies, 63, 9–22.

Mylroie JE, Mylroie JR, Nelson CS, 2008. Flank margin cave development in telogenetic limestones of New Zealand. Acta Carsologica, 37, 15–40.

Nigro F., Renda P., 2002. From Mesozoic extension to Tertiary collision: deformation patterns in the units of the North-Western Sicilian chain. Bollettino della Società Geologica Italiana, 121, 87–97.

Pasci S, 1997. Tertiary transcurrent tectonics of North-Central Sardinia. Bulletin de la Société Géologique de France, 168, 301–312.

Ruggieri R, Messina Panfalone D, 2011. Dentro e fuori la montagna. Priulla, Palermo 2011, 182.

Ruggieri R, Messina Panfalone D, Antonioli F, Rosso A, San

Filippo R, Maniscalco R, 2012. The Rumena Flank Margin cave and its implications in support of paleogeographic evolution of the Monti di Capo San Vito (north western Sicily). Rendiconti Online Società Geologica Italiana, 21, 632–633.

Savelli C, Pasini G, 1973. Preliminary results of K-Ar dating of basalts from Eastern Sardinia and the Gulf of Orosei. Giornale di Geologia, 39, 303–312.

Smart PL, Beddows PA, Coke J, Doerr S, Smith S, Whitaker FF, 2006. Cave development on the Caribbean coast of the Yucatan Peninsula, Quintana Roo, Mexico. In: RS Harmon and CM Wicks (eds.). Perspectives on Karst Geomorphology, Hydrology, and Geochemistry. Geological Society of America Special Paper, 404, 105–128.

SOME SCIENTIFIC FEATURES OF THE PUERTO PRINCESA UNDERGROUND RIVER: ONE OF THE NEW 7 WONDERS OF NATURE (PALAWAN, PHILIPPINES)

Antonio De Vivo[1], Leonardo Piccini[1,2], Paolo Forti[1], Giovanni Badino[1,3]
[1]La Venta Esplorazioni Geografiche – Via Priamo Tron, 35F – 31100, Treviso – Italy, t.devivo@laventa.it
[2]Department of Earth Science – Università di Firenze
[3]Nuclear Physic National Institute – Università di Torino

This paper describes some of the most significant scientific issues of interest of a cave system in the island of Palawan, Philippines. The Puerto Princesa Underground River and the surrounding protected area represent a unique karst environment under several points of view. Its geographical position in the tropical area and its closeness to the sea, making it a true underground estuary, create unique conditions in the fields of hydrology, meteorology, mineralogy and biology. These aspects are analyzed as elements contributing to the comprehension of the exceptionality of this karst phenomenon.

1. Introduction

Palawan covers an area of 12,000 km^2 and is located between 11°50' and 12°20' latitude N, and 117°00' and 120°20' longitude E, in the south-western part of the Philippines archipelago, not far from Borneo. The island is narrow, elongated and mostly mountainous. Two important N–S depressions, corresponding to valleys or lowlands, divide the island into three tectonic sectors. Along the depression which divides the northern from the central sector, we find the Saint Paul Dome karst ridge (Fig. 1).

Here, since 1991, the Puerto Princesa Subterranean River National Park was established in order to protect a unique underground system and the surrounding area. Originally covering only 3,900 ha, in 1999 the park was expanded to over 38,700 ha, and in the same year it was inscribed in the list of Unesco natural World Heritage Sites. Formerly managed by the Dept. for Environment and Natural Resources, since 1993 it falls under the rule of the City Government of Puerto Princesa.

The first recorded explorations in the underground River date back to 1930, witnessed by some writings on the walls of the outflow and the area called Rockpile. In 1973 a first sketch of the main gallery of the cave was carried out by the Hungarian geologist Balazs (Balazs 1976). In the early 80s two expeditions from Australia explored the whole main branch and some side tributaries, pushing the total development of the cave to over 8 km (Hayllar 1980, 1981). Between 1986 and 1992 several expeditions were organized by the Italian Speleological Society, leading to the discovery of giant fossil branches which brought the total development to over 20 km (Piccini and Rossi 1994). The first decade of the new millennium has seen a methodic research project carried out by the Association La Venta from Italy, also assisted by interesting explorations by the Gaia Exploring Club from the Philippines (De Vivo et al. 2009). The last La Venta expedition, in 2011, has brought the development of the cave to 32 km (Piccini and De Vivo 2012). In 2012 the PPUR has been elected on of the New 7 Wonders of Nature.

Figure 1. An aerial view of the Saint Paul Dome (1,028 m a.s.l.) from SE (photo L. Piccini, La Venta).

2. Geological and morphological overview

The St. Paul area is located east of Ulugan Bay, about 50 km NE of Puerto Princesa. The length of the ridge, placed between the Babuyan River valley to the E and the Cabayugan River Valley to the W, is about 10 km and its average width is 4 km (Fig. 2).

The carbonate rock covers an area of about 35 km^2 and is made of massive to roughly bedded, light to dark grey limestone showing levels rich in fossils. Such rock formation, more than 400 m thick, lays over sedimentary (mudstones, sandstones and marls) and volcanic rocks, dating back to Oligocene–Miocene and covering an older metamorphic basement (Hashimoto 1973).

The limestone outcrop is shaped as a NNE–SSW-elongated, asymmetric ridge sloping down to the west. From a structural point of view it consists of a multiple NW dipping homoclinal relief limited by NE–SW-oriented faults. Such lineaments have controlled both the general shape of the mountain and the karst landforms, determining the lining up of dolines and the development of the major caves.

The landscape of the area is a typical tropical karst consisting of towers, cones, pinnacles, and large depressions, occurring mainly in the northern and southern sectors of the ridge. Large closed depressions (cockpits and dolines) cover about 10 % of the total limestone surface. Major depressions occur in the form of elongated blind valleys on the east side of the northern zone, and are mainly developed on clastic rocks.

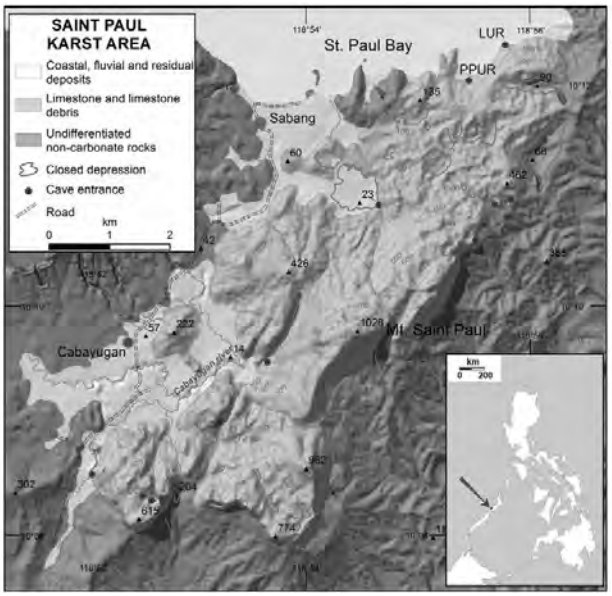

Figure 2. Geological sketch map of Saint Paul karst area.

Steep slopes and calcareous cliffs characterise the central part of the St. Paul Ridge, while to the north the landscape consists of an irregular plateau with several dolines. Large and deep depressions occur along the eastern limit of the limestone outcrop and can actually be considered as small blind valleys (Fig. 2). Some of the eastern sinking streams, located at 290 and 250 m a.s.l., feed two active Nagbituka caves), which consist of large tunnels, mainly vadose in origin, descending to the north along the contact between limestone and sandstone. At present, Nagbituka 1 is the deepest cave in the Philippines (Laumanns 2010).

The southern part of the St. Paul Ridge has a different morphology and is characterised by two mountains, which have plain summit surfaces gently descending toward the NW, intersected by large and deep elongated depressions and large sinkholes.

Along the coastline, a notch, located about 6–7 m above the present sea level, testifies the sea-level highstand which occurred about 120,000 years ago, when the mountain glaciers and polar ice-sheets had a much smaller extension than today. A similar notch can also be found inside the Underground River, up to 4 km from the entrance and at the same elevation (Piccini and Iandelli 2011).

3. Underground Hydrology

The Underground (or Subterranean) River is a cave stream about 8 km long which collects the water from a wide surface basin, diverting it to the sea through huge galleries flooded by water.

The main access to this cave is from the sea. On the side of a beach, a water stream carves a shallow canal through the coralline sand. Going upstream, after a few dozen metres you reach a small lagoon bounded by a calcareous cliff, at the foot of which a portal opens the way into the subterranean river. The main underground stream runs in a large tunnel, with lateral minor diverting passages and in some places upper old relict galleries joining with the active one through large chambers. This cave represents the main resurgence of the Cabayugan River, that disappears into the limestone 7 km upstream.

Another marine spring cave is located a few hundred metres further E and collects the water sinking in the closed basins occurring along the east side of the karst in its northern sector. This cave is named the Little Underground River. Based upon the known hydrologic setting of the area at least two drainage systems can be identified, one drained by the Underground River and one by the Little Underground River. However, the occurrence of submarine and presently unknown springs cannot be excluded.

As the entrance of the Underground River on the coast is at sea level, the tides affect a large part of the cave up to about 6 km inside the mountain (Forti et al. 1993). Along the whole navigable part, the salt water lies under a thin sheet of fresh water, just a few centimetres thick. This condition is only found during the dry season and in absence of rain. During the floods the cave is cleared of salt water, which later returns slowly once the flood has passed. Mixing phenomena between fresh and salt waters take place inside the cave causing particular processes of rock corrosion, which lead to the formation of water level notches (Mylroie and Carew 1988). In the past, sea level was often lower than now, so the PPUR has not always been a marine cave.

Figure 3. The Underground River just downstream the inflow, where the effect of tides does not occur. The lower limit of flowstone on the left wall indicates the water level during flood (photo by R. De Luca, La Venta).

Indeed, despite the occurrence of corrosion produced by the mixing of fresh water with saline water, the speleogenesis of the PPUR is mainly due to solution by continental water and to mechanical erosion by suspended load during floods (Fig. 3). Only in its downstream part, mixing corrosion has produced typical forms of coastal caves, such as waterline notches, spongework and lateral conduits. From this perspective, the system may be considered a classic example of an underground estuary.

This cave with its numerous branches houses, in fact, one of the world's largest and most important underground ecosystems. There are hundreds of thousands of swiftlets (*salangane*) nests, and almost as many bats. Seemingly, the *salangane* and bats have reached an agreement about the timing of their entry and exit from the cave, in general, when the bats begin to exit, almost all the swallows are back on their nests. Because of the great amount of organic matter that swallows and bats bring daily into the cave, there are many other animals present, made up of reptiles (snakes), fishes, crustaceans, and insects (Piccini and Rossi 1994).

A fact that has always been surprising is that the cave runs all along the north-western side of the Saint Paul ridge, this means that most of the karst surface lies on the right-hand (eastern) side of the cave; despite this the Underground River has no consistent tributary from the right side. Why? Where does the water infiltrated all over the karst area flow to? How does it reach the sea?

The first part of the cave, close to the seaward exit, presents a very complex pattern. Several branches divert from the main gallery. One of these lateral branches, just 150 m upstream of the outlet, was explored by the Filipino cavers of the Gaia Exploring Club in 2003. A large gallery, which they reached after a narrow flooded corridor, goes towards the E and closes at a huge stalagmite formation, 15 m high.

Beyond this obstacle, which stopped the exploration of the Gaia Club, a second dry and huge system of galleries exists: it is like entering another cave, a parallel system of new amazing galleries that are flooded only during very rainy seasons (Fig. 4).

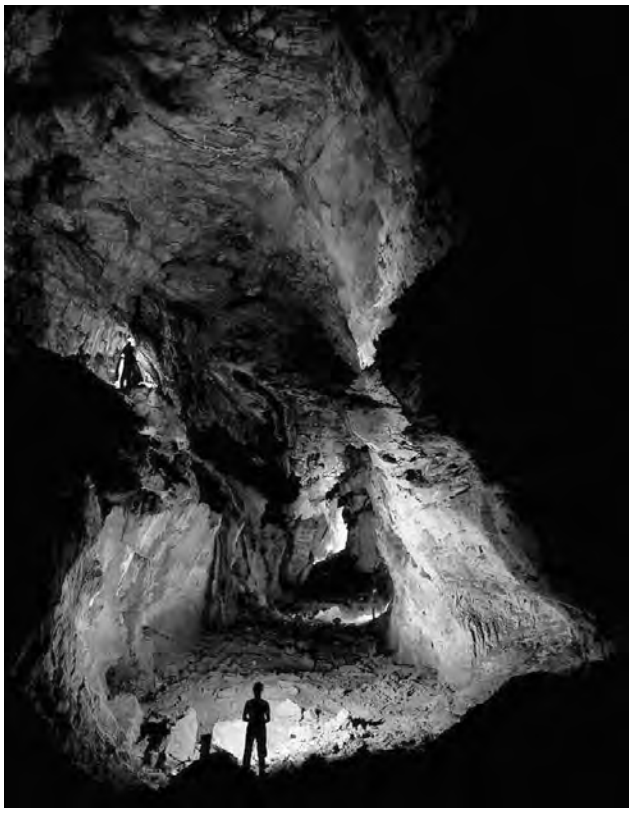

Figure 4. The huge canyon of 150 Years Gallery formed by downcutting of a large epi-phreatic tube (photo by A. Romeo, La Venta).

The first part consists of a high gallery, about 10 m wide and 40–50 m high. The floor is formed by a sand deposit. On the right an upper sector hosts a hall with very nice helictites. On the left we reach a part of the passage where the floor is covered by extraordinary calcite crystals.

This branch probably represents the high inactive level of the main drainage pathway of the cave (Fig. 5).

In several points it is possible to descend in little branches that have typical epiphreatic morphologies until you reach a network of small horizontal often waterfilled tunnels, which lay at sea level. We can argue that the main tunnels collecting the infiltration water of the karst area lay now below the sea level, due to the present high-stand condition and that a new epiphreatic system is now developing. During the rainy season, the water level rises and inundates the upper galleries.

4. Geomorphology

The Underground River has a long and multiphase evolution history which is strictly linked with the sea level fluctuation and with the uplift phases (Piccini and Iandelli 2011). Features that indicate former water levels are present along the PPUR up to 5 or 6 km upstream from the coastal spring. In the last sector of the navigable path, where the ceiling of the main tunnel rises up to 20 m or more, there are two evident old corrosion notches carved by persistent levels of water. The upper notch is at 11–12 m above present mean sea level (pmsl). The second notch is at 7–8 m above the pmsl. Some of the lateral branches contain alluvial terraces consisting of sands and gravels, which are related to this second high-stand notch. This circumstance allows us to correlate the lower notch to the marine one, visible on the coastal cliff at about 7 m above sea level (Maeda et al. 2004; Omura et al. 2004), which dates back to the last interglacial phase (MIS 5e, about 125,000 years before the present time; Linsley 1996).

The morphology of the active level of the PPUR is clearly adjusted to the current sea level, but we have to consider that in the last 500,000 years, the sea was most of the time lower than now (mainly 50–60 m lower; Haq and Hardenbol 1987). This implies that the PPUR has functioned as a vadose through-cave affected by fresh water flow, with a substantial load of insoluble material, forming a subterranean canyon that is buried by the alluvial sediments that form the current riverbed.

The PPUR profile also shows several large passages at an elevation of mainly 50–80 m above the pmsl. This level consists of large inactive tunnels parallel to the current river containing thick alluvial deposits covered by flowstones, which in places almost completely fill the conduits.

In the upstream sector of the cave, erosion forms may be found, indicating a long phase of vadose entrenchment. This ancient "underground river" could reasonably be dated back to the Early Pleistocene, as suggested by the extrapolation of the recent low uplift rate of the coastal zone (Piccini and Iandelli 2011).

Several morphologic features, such as the presence of corrosion notches at 12.4 m above the pmsl, and the huge

speleothems corroded and interbedded with alluvial deposits, suggest that this lower and presently active level experienced more than two sea level highstands and could have formed during most of the Middle-Late Pleistocene.

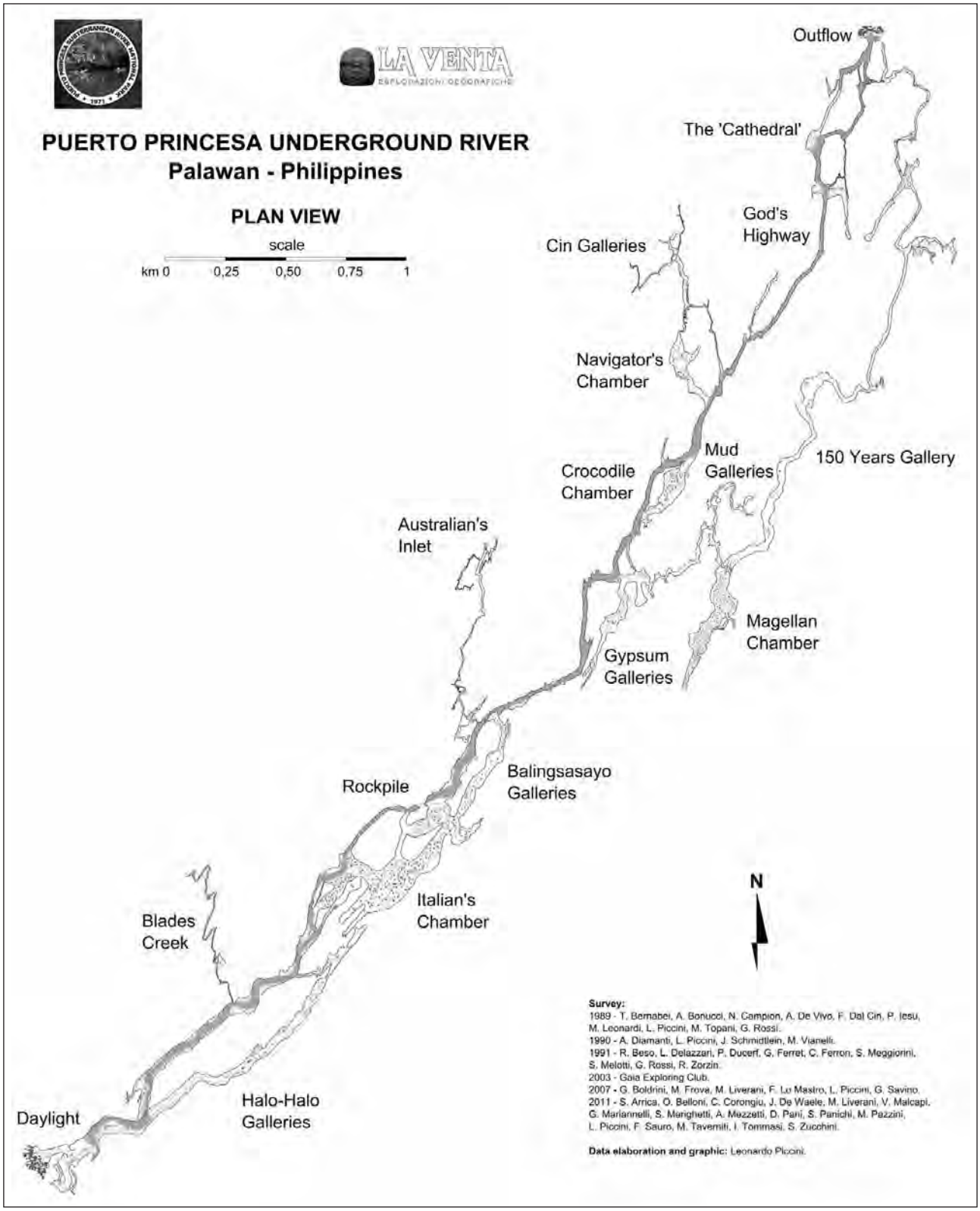

Figure 5. Survey of the PPUR in plan view.

5. Speleothems and cave minerals

Huge stalagmites and flowstones are abundant in several parts of the cave together with some rare speleothems. One of these speleothems is "calcite grass", an extremely rare kind of helictite, consisting of bended and twisted calcite monocrystals growing from the cave floor and covering several tens of square metres of the 150 Years Gallery (Fig. 6).

From the mineralogical point of view, recent and still ongoing investigations are evidencing that the number of cave minerals is much higher than supposed. Most of the minerals of the system are concentrated within the "black crusts", which are widespread along the main galleries of the PPUR. These crusts, often completely detached from the cave wall, are related to periods of strong biogenic reactions induced by the mineralization of guano in water filled conditions. The same process was active in all the

other caves of the St. Paul karst: in two of these cavities the process also allowed peculiar black cave pearls to develop (Forti et al. 1991). In general, the crusts consist of several very thin layers of different colour: beside the far more dominant black ones, other layers are present from black to reddish and from yellow to white. Each colour corresponds to one or more compounds. In the black layers most of the minerals are manganese compounds, the reddish are characterised by iron-manganese minerals, while the white and yellow ones consist of gypsum and phosphates, many of which are amorphous.

Up to now eleven different minerals have been detected in the PPUR: calcite ($CaCO_3$), gypsum ($CaSO_4 \cdot 2H_2O$), apatite [$Ca_5(PO_4)_3$ (C,F,Cl,O,OH)], variscite [$AlPO_4 \cdot 2H_2O$)], strengite [(Fe, Al)$PO_4 \cdot 2H_2O$)], manganite [MnO(OH)], rhodochrosite ($MnCO_3$) pyrolusite (MnO_2), robertsite [$Ca_6Mn_9(PO_4)_9O_6(H_2O)_6 \cdot 3(H_2O)$], janggunite [$Mn_{5-x}(Mn,Fe)_{1-x}O_8(OH)_6$] and serrabrancaite [$MnPO_4 \cdot 2H_2O$)]. The first 8 minerals were already known from the cavern environment while the last three (robertsite, janggunite and serrabrancaite) are new cave minerals, being restricted to the single St. Paul karst: in particular serrabrancaite is very rare even outside caves, being found before only once in Brazil.

6. The Sirenian fossil

During the scientific explorations carried out by La Venta Esplorazioni Geografiche inside the Puerto Princesa Underground River (February–March 2011), several partially articulated bones (ribs and dorsal vertebrae) exposed for approximately 10 cm of their length, were observed about 3 m above the river (Fig. 7). The bones emerge from the rock wall due to the differential dissolution of the limestone with respect to bones and were not extracted to preserve this rare paleontological site.

Figure 6. The crystallized pavement in the 150 Years Gallery (photo by A. Romeo – La Venta).

A detailed comparison of the bones with several available photos of closely related taxa, and with the fossil specimens present in many museums all over the world, has allowed us to state that they belong to a sirenid. The specimen discovered on the Island of Palawan represents the first from the Philippines and the easternmost occurrence in the region. The partially articulated thoracic elements include a well preserved vertebra with exposed neural spine and processes, partial centrum and complete articulation with the head of the ribs. Several bone fragments are well preserved in situ, showing broad and re-curved ribs typical of sirenians. The specimen is approximately 60 cm wide, whereas the vertebra is 10 cm wide and 15 cm high including the centrum. It is therefore possible to estimate a total length for the individual of 180 cm. This sirenid is obviously coeval with the hosting rock, the St. Paul Limestone, which is Oligo-Miocene in age.

Figure 7. The bones of a Sirenian fossil along the main active gallery of PPUR (photo N. Russo – La Venta).

7. Underground meteorology

The Underground River is a cave into which an external river flows and which transports all the meteorological events from the outside deep into the rocks: precipitation peaks, large biological load and temperature jumps. The peculiarity which makes this cave so unique is that it reaches the sea level already within the mountain, in the core of Mt. Saint Paul.

The flows of fresh water from upstream and salt water from downstream are not connected to each other and, on the contrary, for long distances they don't mix, the former flowing on top of the latter. This creates pockets of cooler air in contact with the water and, seasonally, generates flows of relatively warm and humid air which fills the galleries. Micro-meteorological niches and extremely complicated ecosystems are thus created, each having their own seasons, which at the moment we have only barely glimpsed. The island of Palawan lies directly on the thermal equator, therefore the UR cave is at the maximum temperature possible for a cave created by external water flows.

Then there is the wind, which is very noticeable when you pass through the portal to visit the cave on the *bancas*. The galleries are crossed by an important airflow, with peaks of up to 150 $m^2.s^{-1}$. The origin of air circulation within caves is usually the temperature difference between inside and outside. But, unique also in this, the PPUR is affected by a subtle factor which is insignificant elsewhere: the variations in the humidity of the outside air.

The cave has a very peculiar characteristic. On one hand it is very hot, as it opens in an area where the average temperature is especially high – in fact the highest possible – on the other, it opens in an area where the climate is "super-oceanic", that is characterised by a small – in fact, the smallest possible – thermal excursion between day and night and summer and winter. The result is therefore that the temperature difference between inside and outside is always small, just a few degrees difference, and it is very ineffective in creating an underground air circulation. In these conditions, a variation in the outside air density due to humidity variations can assume a decisive role. So, one of the powers of the "underground storm" is the humidity of the outside air, which in other places doesn't manage to move anything.

8. Final notes

The Puerto Princesa Underground River represents a unique karst environment under several points of view.

To start with, being an underground estuary, the PPUR hydrology is strongly affected by the sea tides, that reach up to 6 km inside the cave, with salt/fresh water mixture effects heavily influencing the cave genesis.

On the mineralogical front, the huge fossil levels above the main gallery, particularly the recently explored 150 Years Gallery, contain extremely interesting and rare cave minerals and speleothems, some of which new to science and still under study.

Absolutely unique is the presence of a sirenid fossil englobed in the wall of God's Highway, along the cave's main active branch. The paleontological specimen may supply interesting information on the geological history of the area and the cave genesis.

Among others, the biological aspect is also extremely significant. The presence of huge colonies of bats and swallows and their guano production, together with the biological mass carried inside the cave by the underground river, has allowed the development of a complex and rich trophic network. From the ecological point of view, the cave presents three distinct ecosystems, each characterised by the different nature and abundance of the trophic resources.

These features make the PPUR system an extraordinary natural laboratory to study the evolutionary processes and the ecology of hypogean environments. At present, the PPUR has become the most important show cave of the Philippines, with over 150,000 visitors per year. Its inscription in the New 7 Wonders of Nature will unavoidably increase the anthropic pressure on this cave. If the presence of the tides inside the cave is sufficient to guarantee the stability of its microclimate, the same cannot be guaranteed regarding its ecosystem, which might undergo serious alterations.

It is thus absolutely necessary that the cave managing authorities pay particular attention to the problems that might arise from its tourist overexploitation.

Acknowledgements

Partners: Società Speleologica Italiana, Club Alpino Italiano, City of Puerto Princesa, Puerto Princesa Subterranean River National Park. Sponsor: Ferrino, Dolomite, Chelab, GT Line, Allemano Metrology, Intermatica, Amphibious, New Foods. Special thanks to: Mayor Edward Hagedorn, Rebecca Labit, Anthony Russell Abaya, Jamas Mendoza and the PPSRNP Staff.

References

Balazs D, 1976. Karst Types in the Philippines. Proc. 6th International Congress of Speleology, vol. 2, Praha (1973): 13–38.

De Vivo A, Piccini L, Mecchia M, 2009. Recent explorations in the St. Paul karst (Palawan, Philippines). Proc. XVth International Congress of Speleology, Kerrville, Texas (USA), July 19–26 2009, vol. 3: 1786–1792.

Forti P, Gorgoni C, Piccini L, Rossi A, 1991. Studio mineralogico e genetico delle pisoliti nere della Lyon Cave (Palawan – Filippine). Le Grotte d'Italia, 4(15), 59–71.

Forti P, Piccini L, Rossi G, Zorzin R, 1993. Note preliminari sull'idrodinamica del sistema carsico di St. Paul (Palawan, Filippine). Bulletin Societé Geographique de Liege 29: 37–44.

Haq BU, Hardenbol J, Vail PR, 1987. Chronology of fluctuating sea level since the Triassic. Science, 235, 1156–1167.

Hashimoto ST, 1973. Geologic Structure of North Palawan and its bearing on the Geological History of the Philippines. Geology and Paleontology of Southeast Asia, 13, 145–161.

Hayllar T, 1980. A description of the St Paul Cave, Palawan, Philippines. The Journal of the Sydney Speleological Society, 24 (7), 153–158.

Hayllar T, 1981. Caving on Palawan. The Journal of the Sydney Speleological Society, 25 (12), 215–231.

Laumanns M, 2010. Philippines. In: Laumanns M, Prize L, Atlas of the Great Caves and the Karst of Southeast Asia. Berliner Höhlenkundliche Berichte (BHB) 40–41: 203–237.

Linsley BK, 1996. Oxygen isotope evidence of sea level and climatic variations in the Sulu Sea over the past 150,000 years. Nature, 380, 234–237.

Maeda Y, Siringana F, Omurab A, Berdina R, Hosonob Y, Atsumib S, Nakamurac T, 2004. Higher-than-present Holocene mean sea levels in Ilocos, Palawan and Samar, Philippines. Quaternary International, 115–116, 15–26.

Mylroie JE, Carew JL, 1988. Solution conduits as indicators of Late Quaternary sea level position. Quaternary Science Reviews, 7, 55–64.

Omura A, Maeda Y, Kawana T, Siringan FP, Berdi RD, 2004. U-series dates of Pleistocene corals and their implications to the paleo-sea levels and the vertical displacement in the Central Philippines. Quaternary International, 115–116, 3–13.

Piccini L, Rossi G, (Eds.), 1994. Le esplorazioni speleologiche italiane nell'Isola di Palawan, Filippine – Italian caving exploration in the island of Palawan, Philippines. Speleologia, 31, 5–61 (Italian–English).

Piccini L, De Vivo A, 2012. Il carso del Monte Saint Paul (Palawan – Filippine). Speleologia, 66, 46–59.

Piccini L, Iandelli N, 2011. Tectonic uplift, sea level changes and evolution of a coastal karst: the Saint Paul Mountan (Palawan, Philippines). Earth Surface Processes and Landforms, 36, 594–609.

SUBTERRANEAN GLACIAL SPILLWAYS: AN EXAMPLE FROM THE KARST OF SOUTH WALES, UK

Andrew R Farrant[1], Michael J Simms[2], Steven R Noble[1]
[1]British Geological Survey, Keyworth, Nottingham, NG12 5GG, UK, arf@bgs.ac.uk
[2]Department of Geology, National Museums Northern Ireland, Cultra, Holywood, Co. Down, BT18 0EU, Northern Ireland, michael.simms@nmni.com

Many karst areas in the UK have been glaciated one or more times during the last 0.5 Ma, yet there are few documented examples of caves in these regions being affected by glacial processes other than erosion. The karst of South Wales is one area where sub or pro-glacial modification of pre-existing caves is thought to occur. Evidence from the Ogof Draenen cave system suggests that caves can sometimes act as subterranean glacial "underspill" channels for melt-water. This cave, one of the longest in Britain with a surveyed length of over 70 km, underlies the interfluve between two glaciated valleys. Sediment fills and speleo-morphological observations indicate that melt-water from a high level glacier in the Afon Lwyd valley (>340 m a.s.l.) filled part of the cave and over-spilled into the neighbouring Usk valley, temporarily reversing non-glacial groundwater flow directions in the cave. It is suggested that this may have occurred during a Middle Pleistocene glaciation.

(Note: Welsh terms used in this paper: Ogof = Cave, Afon = River, Cwm = Valley, Mynydd = Mountain).

1. Introduction

Most of the upland karst areas in the north and west of the UK have been glaciated several times during the past 0.5 Ma, particularly during the Marine Isotope Stage (MIS) 12 Anglian glaciation (equivalent to the Elsterian of northwest Europe) and the MIS 2-4 Devensian glaciation (equivalent to the Weichselian), but also during Middle Pleistocene glaciations. Glaciations can have profound and complex effects upon karst landforms and their underlying aquifers, and may destroy, inhibit, preserve, or stimulate karst development (Ford 1987). Sub-glacial water flow can be considerable, especially in active, warm based glaciers, and at the margins of glaciers and ice sheets. Where these are in contact with karstified aquifers, there is scope for significant input of allogenic melt water into pre-existing cave systems (Lauritzen 1984, 1986).

The impact of glaciations on caves in the UK is poorly understood, with few documented examples of caves being affected by glacial activity except through valley incision and erosion. One example of a cave system being affected by glacial activity is Dale Barn Cave in the Yorkshire Dales karst of northwest England, which is thought to have been reactivated by sub glacial melt waters (Murphy et al. 2001). This largely phreatic system connects two adjacent glacial valleys, Chapel-le-Dale and Kingsdale near Ingleton, Yorkshire. Speleothems dated to 343.4 (+86.0/-47.7) ka within the Illusion Pot section of the cave suggest that the conduit was drained during or prior to Marine Isotope Stage 10. However, scalloping on these speleothems suggest it underwent a second, later phreatic episode, with water forced uphill from Chapel-le-Dale to Kingsdale, a distance of approximately 1.5 km. Sediments preserved within the conduit contain distinctive lithologies derived from the Chapel-le-Dale end of the cave, and resemble those described from sub-glacial eskers. The reactivation of the conduit is most plausibly explained by sub-glacial drainage near the snout of the Chapel-le-Dale glacier flowing through to the higher, but unglaciated Kingsdale valley.

In the karst of South Wales, there is further evidence for glacial modification of pre-existing cave systems through melt water recharge. Copious amounts of sediment have been introduced into some caves by glacial melt-water, notably those under Mynydd Llangattock (Smart and Gardner 1988). This has led to ponding and localized paragenesis; blocking some passages, reactivating others and in some cases, facilitating the development of new conduits (Farrant and Smart 2011). In Ogof Agen Allwedd, Simms and Hunt (2007) provide evidence of sediment influx, glacial flooding and impoundment and suggest that glacial damming and recharge from melt-water might have been a significant factor in its development. The discovery of a major new cave system Ogof Draenen in 1994 (Farrant and Simms 2011) a few kilometers to the southeast of Mynydd Llangattock has provided additional evidence for the utilization of caves by glacial melt water.

2. Ogof Draenen

Ogof Draenen [National Grid Reference SO 24631 1179] is a complex multiphase intrastratal cave system located six kilometres south-west of Abergavenny, South Wales (Figure 1). It is currently one of the longest cave systems in the UK at more than 70 km in length and spanning over 150 m in elevation (Chelsea Speleological Society and Stevens 1997; Waltham et al. 1997). The cave is developed within Lower Carboniferous limestones on the north-eastern margin of the South Wales coalfield. The limestones are overlain by Upper Carboniferous siliciclastics including the Twrch Sandstone Formation ("Millstone Grit") and the "Coal Measures", a cyclical sequence of sandstones and mudstones with some coal seams (Barclay 1989). The geological structure is relatively simple, with dips to the south-west at between 5° and 20°. Ogof Draenen underlies the interfluve between the deeply incised Usk valley and its tributaries to the north and east, and the smaller Afon Lwyd valley to the west.

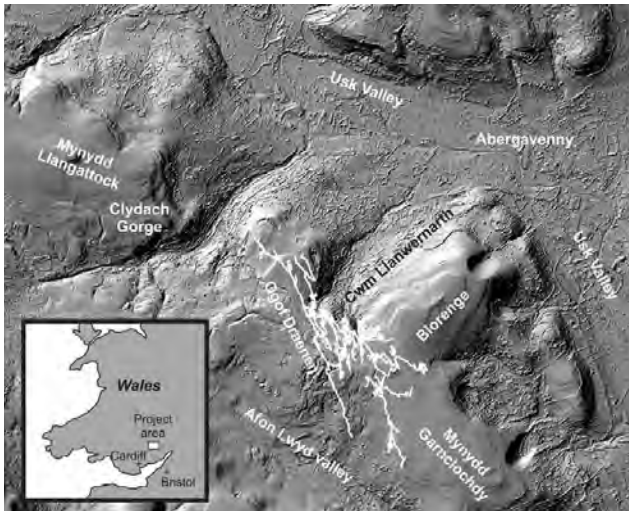

Figure 1. Nextmap hill-shaded surface model image of the north-eastern part of the South Wales coalfield and the Usk valley, showing the location of Ogof Draenen.

The cave has had a long and complex evolutionary history (Farrant and Simms 2011; Simms and Farrant 2011). It essentially comprises three vertically stacked, genetically separate, cave systems linked by phreatic under-captures, shaft drains, chance passage intersections and invasive vadose inlets.

The present autogenic catchment is very small as the limestone forms only a relatively narrow outcrop along the steep scarp of the Usk valley. Consequently, recharge throughout the cave's history has been predominantly allogenic, derived largely from numerous small streams draining the Upper Carboniferous clastics that cap the escarpment above the cave.

The higher level passages in the cave system (those that lie up dip to the east of the Score-Gilwern Passage conduit) are considered to have drained south, initially to resurgences at c. 360 m above sea-level (asl) in the Usk valley (Farrant and Simms 2011), and then to progressively lower resurgences in the Afon Lwyd valley at 360–320 m a.s.l. Subsequent cave development occurred in response to valley incision in the Clydach Gorge to the north, effectively reversing the hydraulic gradient. This change facilitated the development of a lower level series of passages (the Score-Gilwern Passage conduit) that flowed northwest to a former resurgence in the Clydach Gorge at 320–300 m a.s.l. (Figure 2). Subsequent valley incision in the Afon Lwyd valley caused a second reversal in flow direction, this time to the south, creating the present Beyond a Choke stream-way, which resurges 10 km to the south near Pontypool at 120 m a.s.l. This streamway is fed by a series of small inlets and stream sinks along the margin of the overlying sandstone cover.

3. Cave sediments

Observation of the sediment fills in and around the northern end of the main streamway and its tributaries (Gilwern Passage, Upstream Passage, The Score and Pen-y-Galchen Passages; Figure 2) suggested that two distinct sediment

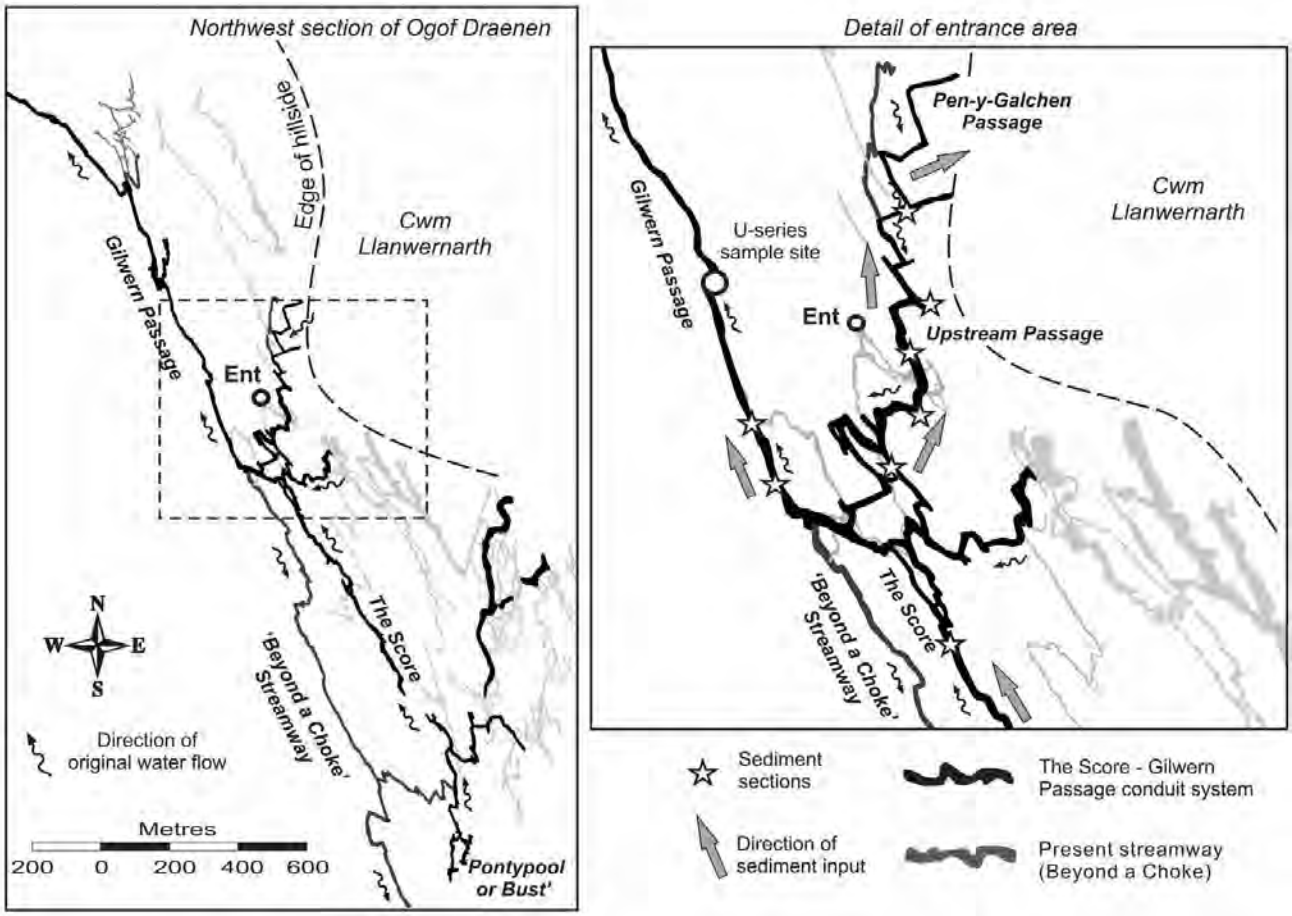

Figure 2. Outline centre-line survey of Ogof Draenen, adapted from surveys by Chelsea Speleological Society and Stevens (1997). A. The northwestern part of the cave. B. Inset of area around the cave entrance. The black passages are those developed during the Score-Gilwern Passage conduit phase of development, whilst the Beyond a Choke streamway (dark grey) represents the final phase of cave development. Directions of water flow are those when the passage was formed. The rest of the cave is shaded pale grey.

facies occur in this area. These comprise coarse, poorly sorted sands and gravels in the active streamway; and relict, finer-grained, silt, sand and sandy gravel preserved at higher levels. To characterize these sediments, samples were collected from over 30 sites and subjected to clast size, lithology and facies analyses (Pash 2003; Trowbridge 2003). Clast lithology data, together with two surface streams for comparison is shown in Table 1, and particle size cumulative frequency graphs in Figure 3.

Table 1. Clast lithologies for the 2,000–3,350 mm particle size range (Mean %) for the present streamway, Gilwern Passage and two surface sites. The "Total Sandstone" is a combination of "Millstone Grit" and Sandstone. The glacial till samples were collected from Forgeside, near Blaenavon [NGR SO 2471 0876], whilst the Coal Measures sample was taken from a tributary feeding the River Clydach at [NGR SO 2156 1254]. Data from Pash, (2003).

Lithology (Mean %)	Beyond a Choke Stream-	Gilwern Passage	Glacial Till (surface)	Coal Measures (surface)
Mudstone (Shale)	67.4	58.9	28	100
Sandstone	16.2	20.7	38.4	0
"Millstone Grit"	7.1	11.5	25.1	0
Quartz	6.7	7.5	6.5	0
Limestone	1.1	0.7	0	0
Total Sandstone	*23.3*	*32.2*	*63.5*	*0*
Carbonaceous clasts	1.4	0.7	2	0

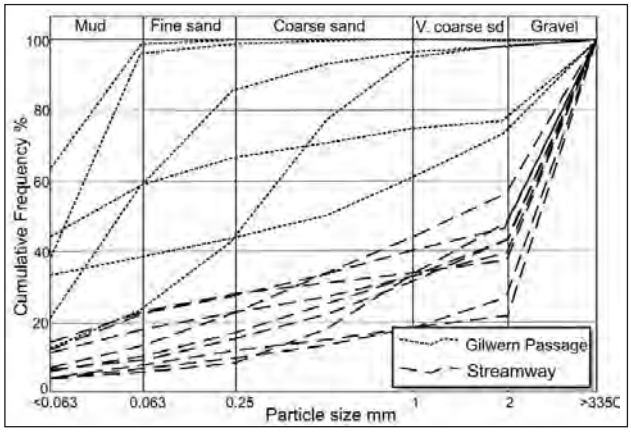

Figure 3. Cumulative frequency plots for the streamway and Gilwern Passage sediments.

Sediments in the active streamway are dominated by poorly sorted, sandy gravels comprising mostly allogenic mudstone and sandstone clasts, often with a dark grey manganese patina. Most of the clasts are angular to sub rounded. Angular clasts of limestone, derived from passage collapse and breakdown (largely caused by vadose incision and secondary gypsum growth in fractures) are common, but not appear to be undergoing significant transport. These are typical of the thalweg facies of Bosch and White (2007). A second distinct facies occurs as sediment banks and remnant fills preserved up to 22 m above the present stream-way and in neighbouring relict passages. This consists of fine- to medium-grained, moderately sorted, pale grey, brown and black, cross-bedded sand, silty sand and laminated clays. Minor amounts of coarse sand and gravel comprising mudstone and quartz occur in places, but few large clasts are present. Remnants of this once extensive fill can be observed throughout the upper reaches of the streamway (Upstream Passage) and surrounding passages. Sedimentary structures are often picked out by conspicuous, very distinctive, dark grey or black laminae, comprised of coal, carbonaceous or manganese stained material. These cross-bedded sands are more typical of the channel deposits of Bosch and White (2007), but locally are capped by laminated sediments of the slack-water facies.

Excellent exposures occur in Gilwern, Upstream and Pen-y-Galchen passages. At the southern end of Gilwern Passage (307 m a.s.l.), >2 m of fine- to medium-, locally coarse-grained, cross-bedded sand with coal-rich laminae overlain by a few centimetres of fine grained, laminated silts can be seen. Cross bedding here and ripple marks 200 m farther downstream indicate northward flow. Significantly, no other deposits are known in the rest of Gilwern Passage and its northerly continuation. A similar sequence can be seen in Upstream Passage, 50 m north of Cairn Junction at 321 m a.s.l. Here up to two metres of fine- to medium-grained dark grey sands overlying boulders are capped by 1 m of laminated silts (Figure 4).

Figure 4. Desiccated, cracked laminated silts overlying fine-grained silty sand, draped over breakdown, Upstream Passage (photo M J Simms).

Another 100 m upstream at the same elevation, plaques of cross bedded sands (Figure 5) can be seen high up on the walls, at least 4–5 m above the current floor and within a couple of metres of the roof. The 0.5 m high northerly dipping foresets are picked out by the dark grey and black carbonaceous or manganiferous laminae.

A short distance further on the large passage ends in a sediment choke, again comprised of fine-grained dark grey sands with ripple cross-lamination showing northward flow. Remnants of similar, but coarser sand again with northerly dipping cross beds, and sometimes cemented by calcite can be seen on the walls of Pen-y-Galchen Passage. Similar coal-rich sediments occur further south in "The Score", an inlet passage off White Arch Passage, at 313 m asl. This passage is the upstream continuation of the Gilwern Passage conduit (Farrant and Simms 2011), and contains an abundant sandy fill throughout, as does its southerly continuation ("Crystal Mole" passage and "Pontypool or Bust"). In the Entrance Series, a conspicuous tide-mark is present on the passage walls up to an elevation of c. 325 m, indicating the maximum sediment fill level.

Figure 5. Cemented remnants of cross-bedded coaly sands preserved several metres above the floor of Upstream Passage. Cross bedding indicates flow to the left ("upstream"). Height of face shown is about three metres. Photo M J. Simms.

It is clear that these passages were largely filled with sediment in the past. The sedimentary structures preserved in the deposits within Upstream Passage and its tributaries indicate flow "upstream" into progressively smaller vadose inlet passages. This is in the opposite direction to the present stream and the regional hydraulic gradient. Moreover, these sediments overlie extensive breakdown indicating they were deposited after considerable vadose incision and collapse. The sands bear no resemblance to the poorly sorted, manganese stained, fine-medium grained fluvial sand and gravel currently in transport. Today, even in extreme flood conditions, water levels in Upstream Passage rarely exceed a metre in depth, barely enough for the stream to be visible above the boulder floor and 4–6 m below the relict cross bedded sands observed on the passage walls. Very little sediment is transported during these floods; indeed, many of the gravel banks in the inlet streams are cemented with a manganese and iron oxide coating.

Significantly, no relict sediment deposits occur in the southerly continuation of the streamway downstream of the junction with Gilwern Passage. This part of the streamway ("Beyond a Choke") is a late-stage under-capture off the relict MS&D-Score-Gilwern Passage conduit (Farrant and Simms 2011), and only carries a small amount of sandy gravel in the active stream. Unlike Upstream Passage, no sediments are preserved above stream level. The point of capture is clearly marked at the southern end of Gilwern Passage where the stream that flows down Upstream Passage swings south into a smaller, lower level passage, whilst the roof tube swings north into Gilwern Passage.

It is clear that these finer grained, carbonaceous and manganiferous sands seen in Gilwern Passage, The Score and Upstream Passage are genetically distinct from those currently in transport in the active stream. Although both are fluvial sediments, there is a striking difference between them in composition, fabric and volume of sediment in transport. As such they must have been brought into the cave system under very different hydrological conditions. The presence of fine fragments of sandstone and mudstone, together with abundant quartz clearly indicates an allogenic source, most probably from the overlying Upper Carboniferous Coal Measure sandstones and the Twrch Sandstone Formation. The cross bedding preserved within these relict sediments indicate that when they were emplaced, hydraulic gradients were locally reversed to that of the stream that formed the passage. This must have been a temporary reversal, as these sediments have since been largely flushed out and the former hydraulic gradients restored. Moreover, the time during which the sediment was emplaced must have been short lived as there is no significant evidence for dissolution, scalloping or paragenetic modification of the passage morphology (Farrant and Smart 2011). No pendants, notches, wall anastomoses or half tubes have been identified in Upstream Passage or in Gilwern Passage. Clearly, fluvial transport under present climatic conditions cannot account for these anomalous sediments. An alternative explanation is that the sediments were emplaced during glacial or pro-glacial conditions when glacial melt water was able to transport significant amounts of sediment into the cave. This hypothesis has been invoked for the extensive sediment fills in the Mynydd Llangattock caves, notably Ogof Agen Allwedd (Smart and Gardner 1989; Simms and Hunt 2007), a few km to the north across the Clydach Gorge (Figure 1).

4. Discussion

4.1. Age of the sediments

Although these relict cave sediments have not been dated directly, two strands of evidence suggest that they are of considerable antiquity and predate the last Devensian (MIS 2-4) glaciation. Firstly, the lack of fine-grained relict sediments in the "Beyond a Choke" streamway is in marked contrast to the abundant sediment fills in the passages associated with the relict MS&D-Score-Gilwern Passage conduit. This suggests that the finer grained sediments were deposited prior to the development of the streamway. This passage, which is up to 30 m high in places, is too large to have developed since the end of the last glaciation. It currently flows south to resurgences in the Afon Lwyd valley and probably developed during and subsequent to the last interglacial (MIS 5). Secondly, much of the sediment fill has been flushed out, leaving remnants preserved up to 6 m above the floor. Whilst sediment removal can be a very efficacious process, it is hard to imagine this amount of sediment being removed since the end of the last glaciation.

A speleothem in Gilwern Passage was taken for Uranium series dating at the NERC Isotope Geosciences laboratory, at the British Geological Survey, Keyworth. The sample (OD-07-96E) was dissolved in hydrochloric acid, and the uranium and thorium were co-precipitated with Fe-hydroxide and separated by ion exchange (AG1x8 and UTEVA). Uranium isotopes were measured by TIMS (Triton) and Thorium by MC-ICP-MS (Nu HR). The sample yielded an age of 302.9 ± 2.8 ka (Table 2) which suggests the passage was vadose by this time. However, it is not clear whether the sediment fill predates speleothem deposition or represents a later stage reactivation of the passage. Either way, it is probable that the sediments predate the last interglacial (the most likely period when the present streamway developed), and possibly as old as the Anglian (Elsterian) glaciation (MIS 12). Further U-series dating work is currently in progress to constrain the age better.

Table 2. U-series data. U and Th total procedural blanks were <26 pg and <8 pg, respectively. Data reduced using an in-house spreadsheet and Isoplot with decay constants from Cheng et al. (2000).

Sample	U ppm	^{232}Th ppm	[^{230}Th/^{232}Th]
OD-07-96E	25.9	0.0014	9.088E+04
[^{230}Th/^{238}U]	**2σ%**	**[^{234}U/^{238}U]**	**2σ%**
1.637	0.22	1.566	0.04
ρ 08-48	**Age (ka)**		**[^{234}U/^{238}U]$_{initial}$**
0.000	302.9±2.8		2.335±0.010

4.2. Glacial geomorphology

Mid and South Wales was glaciated on at least two occasions during the Pleistocene; during the Anglian (Elsterian) and more recently during the Devensian (Weichselian) glaciation (Barclay 1989). A further three Middle Pleistocene glaciations have been postulated, during MIS 16, 10 and 6 (Saalian glaciations) (Lee et al. 2012). Whilst the extent of some of these Middle Pleistocene glaciations across Britain may be controversial, it seems likely that upland parts of Wales would have been at least partially glaciated during these events. During any of these glaciations, it is probable that Ogof Draenen would have lain at or close to the southern margin of the ice sheet at various times (Ehlers and Gibbard 2004).

These ice caps probably had several spreading centres, principally in mid and north Wales, but a local dispersion centre was also likely over the Brecon Beacons. These reconstructions are supported by the presence of till up to elevations of 445 m asl on the flanks of the Usk valley and its tributaries (Barclay 1989), and glacial striae on the Llangattock plateau. The uplands of Mynydd Llangattock, Gilwern Hill and Mynydd Garnclochdy were probably occupied by ice caps (as they were during the Late Glacial Maximum where glacial till forms an extensive sheet at c. 350–400 m around Brynmawr). To the south the ice was funneled into a series of valley glaciers, including the Afon Lwyd glacier. Locally derived gravelly till (of presumed Devensian (MIS 2-4) age) over 10 m thick is present in the Forgeside borehole [SO 2504 0828; 345 m asl], and thin pre-Devensian tills extend south as far as Pontypool. To the north, the major glacier in the Usk valley was largely confined to the present valley (Barclay 1989). During the Devensian, the ice surface was not much above 250 m in the Abergavenny area, terminating in a complex series of moraines around Kemys Commander [SO 340 040] south of Abergavenny. Patches of morainic material demonstrate that the small north-east facing cirques on The Blorenge contained small glaciers or snow patches, but there is little evidence for a major glacier in Cwm Llanwernarth during this time. We suggest that during either the Anglian (Elsterian) glaciation, or possibly during MIS 10 and 6, similar conditions prevailed (Figure 6). It is possible that a comparable glacial setting may have occurred during the early Devensian (MIS 4), but the size and maturity of the Beyond a Choke streamway suggests that the sediments were deposited prior to this time.

The presence of a glacier in the Afon Lwyd valley at elevations above 350 m, and an ice surface less than 250 m in the lower Usk valley, coupled with open, relict cave

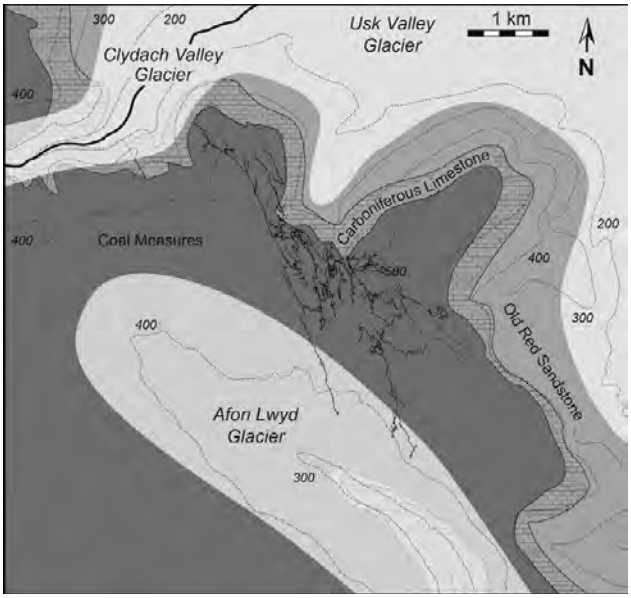

Figure 6. Proposed glacial setting during periods of subterranean glacial under-spill through Ogof Draenen. Contours at 100 m intervals. Glaciated areas are pale grey.

passages extending through the intervening mountain provided suitable conditions for the reactivation of these passages by glacial melt-water. Sediment laden melt water flowed into the cave via inlets along the eastern margin of the Afon Lwyd valley around Blaenavon (>320 m a.s.l.). From these and other inlets, water flowed north via a currently sediment choked passage ("Pontypool or Bust") into "The Score" and then into the start of Gilwern Passage and the surrounding area. In doing so, it deposited fine-grained sand and silt up to an elevation of c. 320–325 m asl. With outlets to the north (the Clydach Gorge) blocked by glacial ice, sediment or collapse, and the present streamway not yet in existence, the only available outlet was into Cwm Llanwernarth, a small tributary valley to the Usk.

Although this valley probably contained a small cirque glacier, the glacier surface was considerably lower than the Afon Lwyd (Figure 7). Consequently, the water then flowed out "upstream", via a series of passages at the eastern end of Upstream Passage, including Pen-y-Galchen Passage. These former inlet passages had previously been truncated by valley incision at the head of Cwm Llanwernarth, but because they form the lowest overspill point in the cave system, they were subsequently reactivated as series of temporary resurgences.

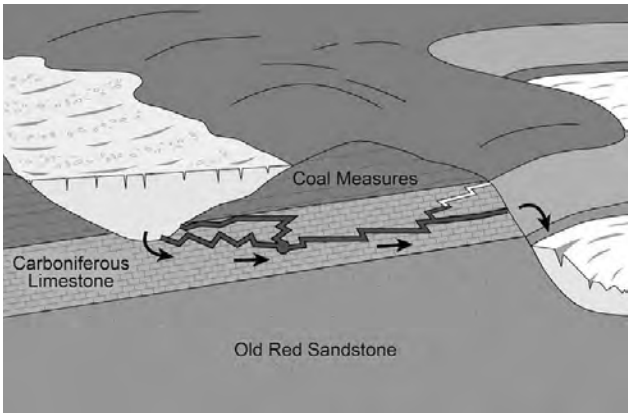

Figure 7. Schematic cross section between the Afon Lwyd valley to the west (left) and the Cwm Llanwernarth valley to the east.

5. Conclusions

Within Ogof Draenen, several distinct sediment facies can be observed in the network of passages around Gilwern Passage, Upstream Passage, The Score and the present streamway. In particular, the deposition of a distinctive suite of fine grained sediments that infilled parts of the cave to depths of over 20 m is ascribed to the influx of sediment laden glacial melt water, either during the Anglian (Elsterian) glaciation or possibly during MIS 10 or 6. This melt water, derived from the base of a glacier in the Afon Lwyd valley flowed into the lower part of Ogof Draenen via many pre-existing inlets. As the level of glacial ice in the neighbouring Usk valley was significantly lower, this melt-water was able to flow north through the cave (in the opposite direction to normal interglacial drainage), over spilling through various truncated inlet passages in the headwall of the Cwm Llanwernarth cirque to form a series of temporary springs at c. 320 m. The cave thus acted as a subterranean glacial spillway, transferring water from one catchment to another.

Acknowledgements

We would like to thank the many people who have contributed, in particular Laura Trowbridge and Jon Pash who did the sedimentological analyses, John Hunt, John Stevens, members of the University of Bristol and Chelsea Spelaeological Societies and Oxford University Caving Club, all the cave surveyors and the Pwll Ddu Cave Management Committee. Farrant and Noble publish with the approval of the Executive Director, of the British Geological Survey (NERC).

References

Barclay WJ, 1989. Geology of the South Wales Coalfield, Part II, the country around Abergavenny. Memoir for 1:50,000 geological sheet 232. British Geological Survey, HMSO, London.

Bosch R, White WB, 2007. Lithofacies and transport of clastic sediments in karstic aquifers. In: ID Sasowsky, J Mylroie, R, Bosch and WB White (Eds.). Studies of Cave Sediments. Springer, Netherlands, 1–22.

Chelsea Spelaeological Society, Stevens, J, 1997. Ogof Draenen. Chelsea Spelaeological Society Cave Survey (3 Sheets).

Cheng H, Edwards RL, Hoff J, Gallup, CD, Richards, DA, Asmerom, Y. The half-lives of uranium-234 and thorium-23. Chemical Geology, 169(1–2), 17–33.

Ehlers J, Gibbard PL, (Eds.), 2004. Quaternary Glaciations – Extent and Chronology, Part I: Europe. Elsevier, Amsterdam, 488.

Farrant AR, Simms MJ, 2011. Ogof Draenen: speleogenesis of a hydrological see-saw from the karst of South Wales. Cave and Karst Science, 38(1), 31–52.

Farrant AR, Smart, PL, 2011. Role of sediment in speleogenesis: sedimentation and paragenesis. Geomorphology, 134 (1–2) 79–93.

Ford DC, 1987. Effects of glaciations and permafrost upon the development of karst in Canada. Earth Surface Processes and Landforms, 12(5), 507–21.

Lee JR, Busschers FS, Sejrup HP, 2012. Pre-Weichselian Quaternary glaciations of the British Isles, The Netherlands, Norway and adjacent marine areas south of 68°N: implications for long-term ice sheet development in northern Europe. Quaternary Science Reviews, 44, 213–228.

Lauritzen S-E, 1984. Evidence of subglacial karstification in Glomdal, Svartisen, Norway. Norsk Geografisk Tidsskrift, 38, 169–170.

Lauritzen S-E, 1986. Kvithole at Fauske, northern Norway: an example of ice contact speleogenesis. Norsk Geografisk Tidsskrift, 66, 153–161.

Murphy PJ, Smallshire R, Midgley C, 2001. The sediments of Illusion Pot, Kingsdale, UK: Evidence for sub-glacial utilisation of a karst conduit in the Yorkshire Dales? Cave and Karst Science, 28, 29–34.

Pash J, 2003. Sediment dynamics in Ogof Draenen (South Wales) – An assessment of past flow regimes. BSc (Hons) dissertation, Department of Geographical Science, University of Bristol.

Simms MJ, Hunt JB, 2008. Flow capture and reversal in the Agen Allwedd Entrance Series, South Wales: evidence for glacial flooding and impoundment. Cave and Karst Science, 34(2), 69–76.

Simms MJ, Farrant AR, 2011. Landscape evolution in southeast Wales: evidence from aquifer geometry and surface topography associated with the Ogof Draenen cave system. Cave and Karst Science, 38(1), 7–16.

Smart PL, Gardener CG, 1989. The Mynydd Llangattwg cave systems. In TD Ford (Ed.). Limestones and Caves of Wales. Cambridge Univrsity Press, Cambridge, 124–151.

Trowbridge L, 2003. Ogof Draenen: the sedimentary dynamics and development stages. BSc (Hons) dissertation, Department of Geography, Aberystwyth University.

Waltham AC, Simms MJ, Farrant AR, Goldie HS, 1997. Karst and caves of Great Britain. Geological Conservation Review Series 12. Joint Nature Conservancy Council, Peterborough.

PROJECT NAMAK: SOME OF THE MOST SPECTACULAR FINDINGS IN THE IRANIAN SALT KARST

Michal Filippi[1], Jiří Bruthans[2], Ondřej Jager[3], Mohammad Zare[4], Naser Asadi[5]
[1]Institute of Geology ASCR, v. v. i., Rozvojová 269, 165 00 Prague 6, Czech Republic, filippi@gli.cas.cz
[2]Charles University in Prague, Albertov 6, 128 43 Prague, Czech Republic, bruthans@natur.cuni.cz
[3]AQH s. r. o., Frýdlanstká 1310/23, 182 00 Prague, Czech Republic
[4]Departmnet of Earth Sciences, Shiraz University, Shiraz, Iran
[5]Department of Geology, Faculty of Science, Sistan and Baluchestan University, Zahedan, Iran

NAMAK Project ("namak" means salt in Persian language) is an informal association of geologists and speleologists who cooperate on exploration and scientific research of the salt karst in southern and southwestern Iran. During the Project (from 1998 until 2013) about 16 salt diapirs were visited and more than 60 caves were discovered, 30 of which were mapped. The most exciting scientific and speleological discoveries were made in the Namakdan, Hormoz and Jahani salt diapirs; however, many other remarkable discoveries have been made on other several Iranian salt diapirs. This contribution summarizes the most interesting findings achieved during the ten expeditions carried out by the NAMAK team.

1. Introduction

The NAMAK team studies Iranian salt karst since 1998. Up to now the 10 full-scale expeditions and several shorter trips were carried out between 1998 and 2010. Members of the NAMAK team assisted during film documentaries made by the BBC, Iranian TV and the Czech TV. The discovery and documentation of the 3N Cave by the NAMAK team positively influenced declaring a part of Qeshm Island as a National Geopark, which was also recognized as part of the UNESCO Network of Geoparks in the year 2006.

The southern and southwestern part of the Zagros Mts. in Islamic Republic of Iran (provinces Hormozgan, Fars and Bushehr) represents an area with the largest number of piercing salt diapirs in the world. Numerous diapirs teem with a variability of well-developed karst phenomena, including countless salt caves with brine springs and rich secondary halite deposits. However, the area was not previously subjected to some systematic geological research, except the tectonic and structural studies (see references in Talbot and Alavi, 1996). New knowledge from other geological fields has been obtained within the last circa 10 years. Characterization of the karst phenomena and notes to the speleogenesis in this area were presented by Bosák et al. (2002). Evolution of the surface morphology in relation to the karstification on some coastal salt diapirs was described by Bruthans et al. (2008, 2009, 2010). Overview of the various types of secondary cave deposits was presented by Filippi et al. (2011). Also the speleological findings will be summarized in detail soon (Filippi et al. in prep.). The presented contribution extracts some of the most spectacular findings made by the NAMAK team.

2. Geography and geology of the area

Four salt diapirs were studied in detail during the NAMAK expeditions: Hormoz and Namakdan diapirs on islands in the Persian Gulf (Hormozgan Province), Kuh-e Jahani diapir near Firuzabad (Fars Province) and Namak diapir (Busher Province) in the Zagros Range. However some other salt diapirs (e.g., Namak, Gach, Saadad Abad, Mesijune have been visited (for location see the Fig. 1 in Bruthans et al. 2009). The climate in the visited areas is arid or semi-arid. Main precipitation occurs from November–April. The annual average temperature is 27 °C in the Persian Gulf region and 20 °C at mountainous diapirs. Temperature can reach 50 °C in the summer. During our expeditions (usually in the period from January to May), temperatures varied between 15 and 40 °C. The humidity on the surface varied from 50 % to 98 %. Strong precipitation events occur sporadically every several years, usually during the winter season.

Geologically salt karst areas are situated in the eastern part of the Zagros Mountain Range and the Persian Gulf Platform, which is composed of elongated whaleback or box-shaped anticlinal mountains, generally NW–SE-trending (Bosák et al. 1998). The relief is young; the principal folding started only in Middle Pliocene. Rock salt composing the diapirs belongs to the Hormoz Complex, which was deposited during Upper Precambrian to Middle Cambrian times, i.e. more than half a billion years ago (Bosák et al. 1998). The salt deposits have been covered by other sedimentary rocks, which attained a thickness of several kilometers. Due to high pressure in such depths, tectonic factors, and due to the high plasticity and low density of salt, the deposits started to rise towards the surface in form of salt diapirs (plugs, domes).

Salt diapirs in Iran are represented by more or less circular, cylindrical, etc. bodies with diameter between ca. 1 to 18 km. The rock salt is folded into tight to isoclinal folds, with alternating white to grayish and reddish salt with varicolored carbonate, siliciclastic, iron oxides and volcano-sedimentary rocks and rarely anhydrite and gypsum. Blocks of exotic (igneous and sedimentary rocks) transported by halokinesis from depth reach diameters up to 2 km across in many diapirs.

3. Methods

Topographical maps (1:25,000 and 1:50,000), satellite images (presented by the Google Earth utility), and aerial

photographs were used as a basis for morphological and geological surveys. Global positioning system (GPS) instruments, with a horizontal accuracy of ±5 m, were used for field orientation and identification of sampling sites. Altitudes of the important points were determined using precise barometric altimeters (BARIGO 43, GARMIN eTrex Summit) with accuracy better than ±2 m. Some points with small elevation differences were measured using a total station (Leica). Cave passages were mapped by compass, clinometer, and a tape or a laser rangefinder. Polished sections were prepared for the mineralogical study of the speleothems followed by the scanning electron microscope (SEM) and X-ray diffraction spectroscopy (XRD).

4. Karstology of the Iranian salt karst

Iranian salt karst is very a dynamic landscape, especially during and after heavy rains. In such time intense transport of sediments and abundant rock falls occur on the surface and also in caves. One would expect that salt caves will originate on salt diapirs with large areas of exposed rock salt, but that's not the case. Caves usually do not occur in bare salt diapirs. Runoff water reaches very rapidly saturation with respect to halite and looses ability to dissolve rock salt. Runoff water leaves the bare salt diapirs via dense net of surface streambeds and canyons in lower reaches. Fortunately for cavers, surfaces of the salt diapirs in Zagros Mountains are mostly covered by various types of surficial (residual) deposits (detail see in Bruthans et al. 2009). Regardless of the type of surficial deposit, its thickness and areal extent, its presence is the key factor governing the degree of karstification and cave development on salt diapirs in Iran (Bruthans et al. 2000). Thickness of surficial deposits above cave does not influence the cave itself; more important is the thickness of surficial deposit in recharge area of the cave. The surficial deposits act as impermeable cover that enables accumulation of large amount of fresh water. Also large blocks of exotic rocks act similarly as impermeable surficial deposits. Thickness of overburden above the cave usually influences intensity of breakdowns when caves in shallow subsurface are less stable compared to those in greater depth. The two very important geomorphological and/or karstological features affected by thickness of the surficial deposits (overburden of halite) are as follows (for details see Bruthans et al. 2000, 2009 and Filippi et al. in prep.):

- Density (and character) of recharge points, which has a negative correlation with thickness of overburden. Surface of diapirs with no surficial deposits is typical by presence of steep canyons and gullies, sharp Rillenkarren on rock exposures. Thin overburden is permeable for water at numerous places and therefore prevents development of extensive drainage networks that transmit and concentrate fresh water. As a result, dense fields of small dolines and ponors develop. On the contrary, thick impermeable overburden enables evolution of landscape with well developed drainage network terminated in valleys and deep canyons with scarcely distributed large ponors (followed by large caves) and also with large dolines.
- The rate of lowering the surface of salt karst. There is relatively very low denudation rate of surface in case of the thick overburden; salt dissolution is concentrated into cave passages. On the contrary, the denudation rate of ground surface in case of bare salt surfaces is very fast (centimeters per year) and could simply exceed the rate of halokinesis (Bruthans et al. 2008).

5. Speleological finds

5.1. The longest/largest salt cave

Absolute majority of caves discovered in the Iranian salt karst reach first tens to few hundreds of meters in their lengths. So far, there are only three caves exceeding one kilometer: the White Foam Cave (1,262 m) on Jahani diapir, the Ghar-e Daneshyu (Students' Cave; 1,909 m) on Hormoz diapir and finally the 3N Cave (6,580 m) on Namakdan diapir. The 3N Cave is probably the most impressive and remarkable salt cave in Iran. The 3N Cave is located in the southeastern part of the Namakdan diapir in the western part of the Qeshm Island (Persian Gulf). Since the detailed description of the cave was presented in English and in French by Bruthans et al. (2006) and Filippi et al. (2006), respectively, we present here only general description and underline some most important knowledge about this unique cave.

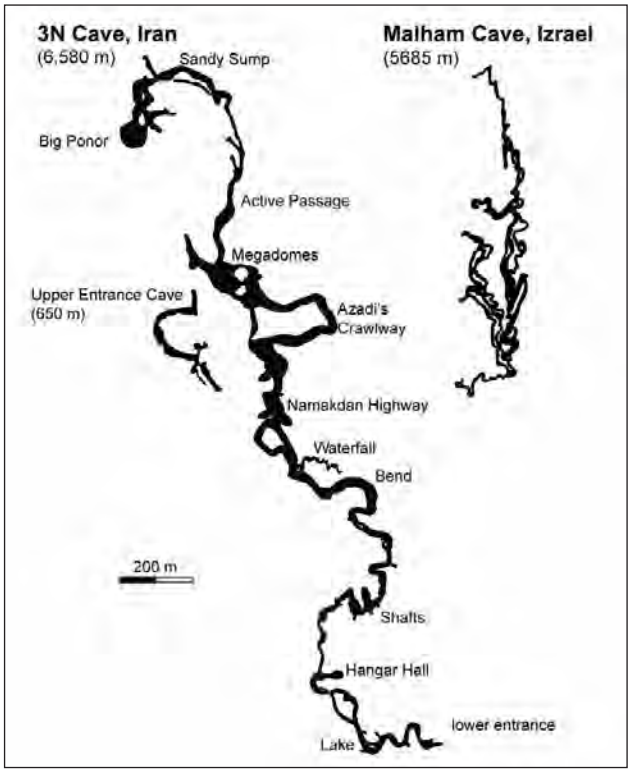

Figure 1. Comparison of the first and the second world's longest salt caves.

Generally, the 3N Cave consists of a singular large meandering passage (Fig. 1) opened to a valley, via lower entrance (resurgence partly filled by brine) 8 m wide and 2 m high. A large salt lake, usually 100–300 m long (changing based on presence/absence of natural dams formed by salt precipitates) and up to 1 m deep, is at intervals forming approximately 160 m from this entrance. The roof is lowered here to only 20–60 cm above the water level. Very high salt concentration (up to approximately 330 $g.l^{-1}$ of dissolved salt) made it easy to swim because of

similar buoyancy effect to that of the Dead Sea. However, the oversaturation with salt is badly etching to skin scratches and open cuts, which are unavoidable when exploring caves. About 700 m from the southern entrance, the "Hangar" chamber (35 × 20 × 16 m) is situated. Behind this point, the width of the mostly muddy and collapse-prone passage decreases from 10–15 m to only 6 m. One kilometer from the entrance, several collapse domes occur. Three shafts connecting the cave with the surface are situated behind them, all about 40 m in height. Since the year 2000 the NAMAK Project has used one of these shafts as a main entrance to the cave. North of the shaft mounts the draught inside the cave dies out and makes progress extremely uncomfortable with a temperature of 28 °C, high humidity and no air draught. Also, the general character of the cave changes: the common arched cross-sections caused by breakdown occurring south of the shafts turn into passages with flat ceiling without any breakdown – resembling to a large underground garage. This is probably related with a larger depth of this part of the cave below surface. 150 m long low crawl named the "Bend" is very uncomfortable part of the cave. After it, the passage increases in size. On the right side a small inlet creates a permanent brine shower called "Waterfall", the 10 m high vertical chimney with a window into approximately 170 m long narrow meandering passage ending in dangerous narrow collapsed space. However, in 2010, this inlet was hidden by a rock fall, so its recent accessibility is questionable. The main passage named the "Namakdan Highway" is 40 m wide and up to 6 m high. The most challenging and endless long "Azadi´s Crawlway" starts after this large sapces. After approximately 800 m creeping over fine mud one reaches "Megadomes" (see the next chapter). Fortunately, a bypass of "Azadi´s Crawlway" was discovered in 2004 providing a shortcut dug through an older +6 m higher level. This shortcut was named "Motashakkeram", what means "Thanks a lot" in Farsi. Behind the Megadomes, the main passage changes into a sandy to gravelly crawlway called "Active Passage". The Big Ponor Cave entrance is the main inflow into the cave (for details see next section).

5.2. The largest underground spaces

Width and height of accessible parts in most of the visited caves usually range from one to several meters. However, sometimes a large corridors and underground halls may develop. The Big Ponor is one of the largest natural semi-underground spaces in the rock salt. This cave (actually part of the 3N Cave – the main ponor of this cave) contain an incredibly large entrance hall consisting of a huge portal (35 × 15 m) and an entrance hall (approximately 50 m by 50 m, 15 m high). The hall continues by dozens of low manholes in sedimentary infill leading in different directions and getting (with one exception) inaccessibly low after several tens of meters. Besides the mapped parts, there are many more inlets leading in westerly direction. This makes sense as Big Ponor is actually developed in a 200 m (probably more) wide underground alluvial fan where sheet floods model the cave. It actually represents an underground alluvial of a meandering underground river channel. Bottom of this great hall changes very significantly in time because of large a volume of incoming water during heavy rains. Collapses from the ceiling are very often and may endanger possible visitors.

One of the largest underground spaces was documented also in the 3N Cave. The space called as the Megadomes consists of two connected relatively low halls (from 2 up to 8 m in the height), which together occupy an area of 200 m by 100 m (Fig. 3A). In general, these halls have flat ceilings only locally interrupted by fallen rocks; the walls often consist of fluvial sedimentary infill which points at their possible larger extent. The Megadomes are situated at a confluence of streams from two main sinkholes. The main stream is coming from the Big Ponor part and the second from other important tributary, the neighboring Upper Entrance Cave. Unfortunately, the connection with this cave is impossible due to a complete sedimentary infill.

The Coffee Bar Hall in Eugen's Cup of Coffee Cave on the Mesijune salt diapir is the largest and most impressive cave hall found in the Iranian salt karst and probably also worldwide (Figs. 2A, 3B). It has an extent of 70 × 30 × 35 m (length, width and height). The Eugen's Cup of Coffee Cave is situated close to the northern margin of the diapir and is developed in apparently unstable environment – in a rock salt covered by relatively thin surficial sedimentary overburden. The relatively short cave (the length 235 m) consists of a large meander passage with common width of 5 to 10 m and the similar height and already mentioned large hall. The cave has a flat bottom which is periodically flooded by rain water coming from the surficial valley. The large volume of sweet water coming quickly into the cave after the heavy rains is the main reason for development of such a large underground space located close to the cave inlet. Fallen rocks from the ceiling are quickly dissolved and thus the space remains partly empty (from the bottom to the ceiling). The inactive part of the passage is progress towards the surface. The lack of fresh water causes successive infilling of the space by rock fragments and fluvial sediments in many other documented underground spaces.

5.3. The deepest shaft

Based on vertical cross-section, there are two general groups of caves in the Iranian salt karst: (i) more or less sub-horizontal caves, and (ii) vertical shafts. The first group of caves is typically situated as endings of larger elongated valleys with intermittent streams. Shafts are typical for short circular valleys and dolines, commonly without a significant water supply. Important factor for the shaft development seems to be sub-surficial subrosion, especially in the early stadium of their development. One of the one of the largest and deepest shafts was found in the western part of the Jahani salt diapir and was named the Goat's Shaft, according to numerous goats grazing all around. The shaft has a typical morphology for such environment – a short streambed on the bottom of circular funnel-shaped doline ends in a vertical shaft (Figs. 2B, 3D). The doline and first meters of the shaft are created in unstable only partly consolidated surficial sediment with large blocks of exotic rocks. The shaft with an oval crosscut and a flask vertical profile is mostly developed in rock salt. Narrow

terrace composed of large blocks of rocks that are cemented by halite and gypsum occur 30 meters below the shaft mouth. Shaft bottom covered by rock boulders can be reached after another 40 m. The shaft continued by a sloping cave starting with relatively extensive dome with an unstable ceiling. After approximately 120 m the cave terminates in inaccessible riverbeds in sediment and debris.

5.4. Caves formed in two different rocks

Rare examples of caves may develop in areas where salt glaciers (overflow) cover the surroundings country rocks (mostly limestone). Bottoms of such caves and partly also walls are formed in limestone and ceilings consist of rock salt. Cave of Deliverance in western part of the Khurgu salt diapir (about 2 km SEE from the south portal of the road tunnel situated on the main road from Bandar-e Abbas to Yazd) is one of the best developed examples of such caves (for cave map see Bosák et al. 2002). The cave drains a huge blind canyon, which is developed on the border of salt diapir and a limestone anticline. The small southern cave branch drains a funnel-shaped doline developed on contact between limestone and salt. Originally, the cave was exclusively developed in salt on the contact with limestone bedrock. After having been enlarged enough to enable the transport of a clastic load, the vadose canyon entrenched into the limestone. An inclined (35°) contact between salt and limestone is visible in the small southern branch of cave.

5.5. The most remarkable doline/canyon

Iranian salt karst is rich in various types of blind valleys, shafts, abysses and dolines. Mostly they are represented by funnel-shaped depression with gentle slopes. Sometimes these depressions are followed by vertical shafts continued by relatively short steeply inclined inlet cave. For unusual morphology and complex genesis, the Puzzle Canyon on the Jahani salt diapir is quite different and unique. The branched labyrinth-type canyon with up to 13 m high, but only 0.5–1.5 m wide walls is situated on a flat bottom of the doline 100 × 200 m wide (Fig. 3C). The bottom of the doline is formed by fine deposits which settled there by numerous floods after heavy rains before the swallow hole in the bottom of doline was activated. The canyon developed due to headword erosion of sediment during heavy rains when streams enter the doline from several sides and rapidly carve several canyon branches and sink into the Puzzle Canyon Cave (Fig. 2C). The cave starts with a 15 m deep vertical step followed by relatively high and apparently unstable underground space formed in sediment. Fallen blocks of the sediments and rock fragments are common there. Gradually decreasing height of passages ends the passability of the cave on a distance 128 m from the entrance.

5.6. The highest “waterfall”

Majority of the visited caves are more or less sub-horizontal. However, few caves located on margins of salt diapirs with significant positive morphology are

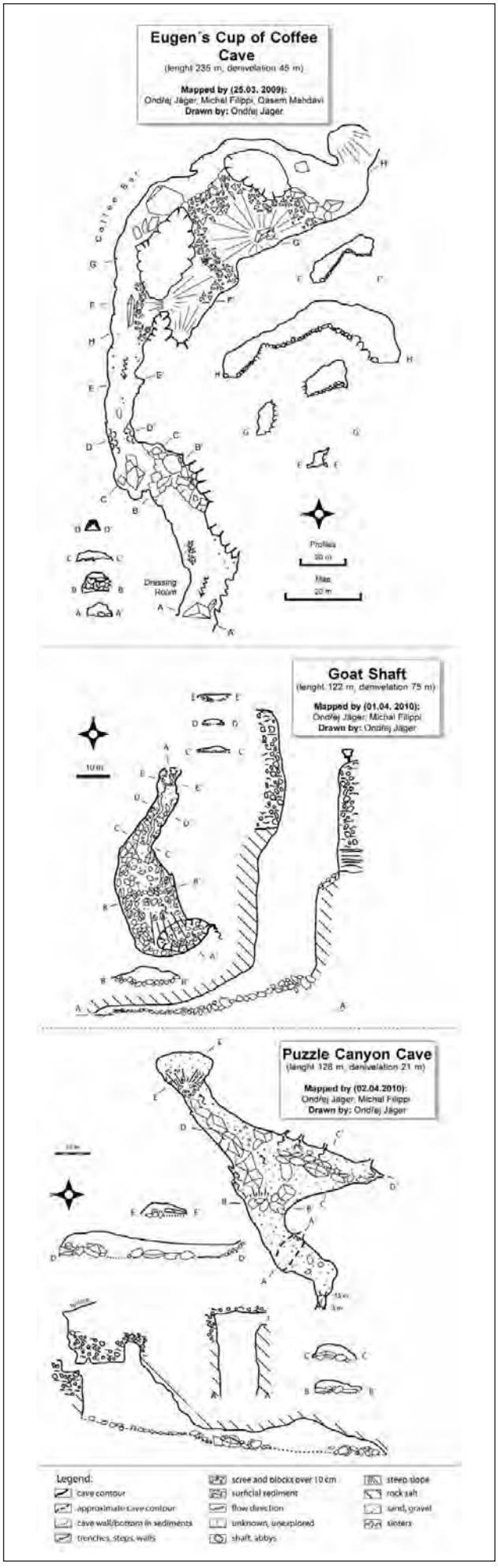

Figure 2. Maps of the selected speleological objects.

characteristic by a relatively steep slope and/or sharp vertical steps. Waterfall Cave on the southeastern margin of the Jahani salt diapir is the most interesting locality from this point of view. This cave is situated in an area consisting of a valley interrupted by several caves and drained by relatively permanent stream of brine. The cave is usually entered from the lower entrance (resurgence),

that is accessible from the valley on the south-eastern margin of the diapir. The 15 m high step occurs at the hinder part of the cave, approximately 30 m from the inlet entrance. The flow rate is usually small up to several liters per second; however, during heavy rains it rises significantly. Splashing and aerosol brine causes precipitation of interesting halite speleothems on the walls around the waterfall (see Filippi et al. 2011).

5.7. The greatest speleothems

Speleothems consisting of a microcrystalline to grained porous halite matter are the absolutely prevailing type of secondary precipitates in the Iranian salt karst. The initial microcrystalline deposits start to form on halite-/rocks-saturated sites. The microcrystalline halite matter is able to create quite a large speleothems like sinters, stalactites and stalagmites (Fig. 3E). Their initial formation is primarily related to the presence of dripping water; however, evaporation of capillary water is the key factor governing their growth. Usually, the microcrystalline stalactites form only when the water feed decreases so that capillary transport prevails over gravitational dripping. This is the stage when the "primary" forms finish their development. In fact, microcrystalline stalactites are mostly the second stage in the secondary halite deposition (for details see Filippi et al. 2011). The largest microcrystalline stalactites and stalagmites reach up to approximately 4 m in length and up to approximately 30 cm in width. The stalactites are usually not vertical but are wildly curved or zigzag shaped. This is caused by the shape of the original form and by successive development, i.e. periodic changes in the shape at the tip of the stalactite, and by outer factors, such as the air draft direction or spatial distribution of the atmospheric humidity.

Straw stalactites are another common speleothem type, which may reach notable proportions. Straw stalactites grow directly from rock salt or from older and destroyed secondary halite precipitates. This is caused by reopening of the central channels inside the grained stalactites after the rains. Straw stalactites display more or less uniform diameter usually of 0.5 up to 1 cm and a smooth surface composed of compact glazy halite. In ideal cases, the halite straws are straight and regular, like in carbonate caves. More often, they are irregular, slightly curved and combined with microcrystalline (grained) growths or rarely with filamentary helictites. Straw stalactites commonly have a length of 0.1 up to 1 m, but can reach up to approx. 3.5 m, as was documented in the White Foam Cave.

5.8. The most unusual speleothem

A variety of secondary halite deposits (speleothems) was distinguished in the Iranian salt karst. The speleothems were classified into several groups, on the basis of the site and mechanism of their origin (Filippi et al. 2011). Some speleothems are similar to those known from carbonate karst, others are different. Macrocrystalline skeletal speleothem is surely one of the most interesting and most unusual halite forms (Fig. 3F).

Halite macrocrystalline stalactites have been documented earlier (see references in Filippi et al. 2011). However, even the discovery of rich occurrences of macrocrystalline forms in the Iranian salt karst helped to understand their formation. Macrocrystalline skeletal forms (stalactites, stalagmites and wall/bottom crusts) are connected to irregularly splashing brine around waterfalls and on cave ceilings with strong dripping. Rich but more or less random water supply, accompanied by gravity- and capillary-induced water movement are the main prerequisites for growth of these forms. Compared to some other forms, macrocrystalline speleothems exhibit no internal feeding tube and the brine is distributed on their surface. Euhedral to skeletal, mostly irregular and sometimes hopper-shaped crystals are clustered into "twigs" forming the whole tree-like formations. Macrocrystalline speleothems consist of a central columns and side "twigs". The side twigs typically occur in groups of three, mutually forming an angle of 120°, with an angle of ~70° to the central column. The directions of the central and side columns thus correspond to the four body diagonals of a cube. Each twig is terminated with a cube when all the cubes are equally oriented, again documenting that the whole form is actually a single crystal, albeit with a fractal appearance (a "fractal cube"). As the form grows more and more, the central column and the twigs can be completely buried under the growing cubes. For other details about this unusual form see Filippi et al. (2011).

6. Important notes

We ask all possible visitors of the Iranian salt karst to be considerate and protect them. Project NAMAK has its own website where you can find other information: http://home.gli.cas.cz/namak/. All important speleological findings are summarized in the work of Filippi et al. (in prep.).

Acknowledgments

Many thanks to the Heads of Shiraz University and Head of the Qeshm Free Zone Organization. The authors thank to participants of the NAMAK Project: M. Audy, R. Bouda, M. Geršl, E. Janoušek, J. Kamas, M. Kolčava, J. Kukačka, M. Novák, Š. Mikeš, T. Svoboda, S. Šlechta, J. Šmíd, M. Vašíček and Z. Vilhelm. Research was supported by projects no. KJB315040801, RVO67985831, MSM00216220855, and MZP0002579801.

References

Bosák P, Jaroš J, Spudil J, Sulovský P, Václavek V, 1998. Salt plugs in the Eastern Zagros, Iran: results of regional geological reconnaissance. GeoLines 7, 1–174.

Bosák P, Filippi M, Bruthans J, Svoboda T, Šmíd J, 2002. Karstogenesis and speleogenesis in salt plugs: Case study from the SE Zagros Mts., Iran. Proc. of the Middle-East Speleology Symposium, April 20.–21. 2001, Lebanon, 62–79.

Bruthans J, Filippi M, Zare M, Asadi N, Vilhelm Z, 2006. 3N Cave (6580 m): longest salt cave in the world – the NSS news. National Speleological Society 64, 10–18.

Bruthans J, Asadi N, Filippi M, Vilhelm Z, Zare M, 2008. Erosion rates of salt diapirs surfaces: An important factor for development of morphology of salt diapirs and environmental consequences (Zagros Mts., SE Iran). Environmental Geology, 53(5), 1091–1098.

Bruthans J, Filippi M, Asadi N, Zare M, Šlechta S, Churáčková Z, 2009. Surficial deposits on salt diapirs (Zagros Mts. and Persian Gulf Platform, Iran): Characterization, evolution, erosion and influence on landscape morphology. Geomorphology. 107, 195–209.

Bruthans J, Filippi M, Zare M, Churáčková Z, Asadi N, Fuchs M, Adamovič J, 2010. Evolution of salt diapir and karst morphology during the last glacial cycle: effects of sea-level oscillation, diapir and regional uplift, and erosion (Persian Gulf, Iran). Geomorphology. 121, 291–304.

Filippi M, Bruthans J, Vilhelm Z, Zare M, Asadi N, 2006. La grotte 3N, Iran (6 580 m): le nouveau record du monde de la plus longue cavité dans le sel. Spelunka, 104, 15–18.

Filippi M, Bruthans J, Palatinus L, Zare M, Asadi N, 2011. Secondary halite deposits in the Iranian salt karst: general description and origin. International Journal of Speleology. 40(2), 141–162.

Filippi et al. (in preparation). Project NAMAK. (working title).

Talbot CJ, Alavi M, 1996. The past of a future syntaxis across the Zagros, in Alsop. In: Alsop GI, Blundell DJ, Davison I (eds) Salt Tectonics, Geol. Soc. Amer. Spec. Paper, 100, 89–109.

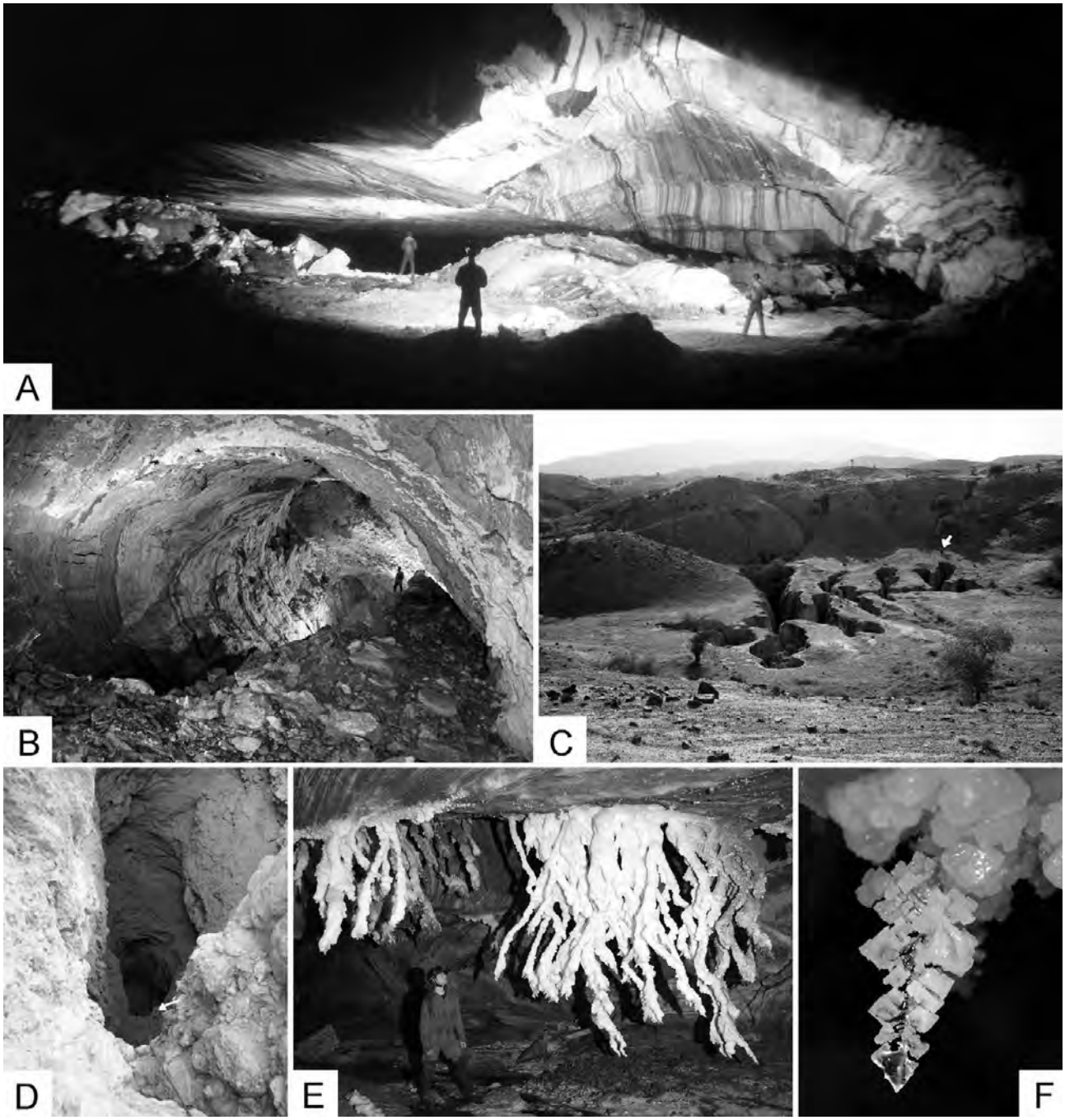

Figure 3. A) The Megadomes in the 3N Cave; B) Upper part of the Coffee Bar Hall in the Eugen's Cup of Coffee Cave; C) The Puzzle Canyon; D) Goat Shaft and a caver on a step in -30 m; E) An example of a microcrystalline grained halite speleothem, the Octopus formation in the 3N Cave; F) An example of a macrocrystalline skeletal halite speleothem; narrows point at persons in the photos.

KARST DEVELOPMENT IN THE GLACIATED AND PERMAFROSTREGIONS OF THE NORTHWEST TERRITORIES, CANADA

Derek Ford
School of Geography and Earth Sciences, McMaster University, Canada dford@mcmaster.ca

The Northwest Territories of Canada are ~1.2 million km^2 in area and appear to contain a greater extent and diversity of karst landforms than has been described in any other region of the Arctic or sub-Arctic. The Mackenzie River drains most of the area. West of the River, the Mackenzie Mountains contain spectacular highland karsts such as Nahanni (Lat. 62° N) and Canol Road (Lat. 65° N) that the author has described at previous International Speleological Congresses. This paper summarizes samples of the mountain and lowland karst between Lats. 64–67° N that are located east of the River. The Franklin Mountains there are east-facing cuestas created by over-thrusting from the west. Maximum elevations are ~1,000 m a.s.l., diminishing eastwards where the cuestas are replaced by undeformed plateaus of dolomite at 300–400 m asl that overlook Great Bear Lake. In contrast to the Mackenzie Mountains (which are generally higher) all of this terrain was covered repeatedly by Laurentide Continental glacier ice flowing from the east and southeast. The thickness of the last ice sheet was >1,200 m. It receded c.10,000 years ago. Today permafrost is mapped as "widespread but discontinuous" below 350 m a.s.l. throughout the region, and "continuous" above that elevation. The vegetation is mixed taiga and wetlands at lower elevations, becoming tundra higher up. Access is via Norman Wells (population 1,200), a river port at 65° 37'N, 126° 48'W, 67 m a.s.l.: its mean annual temperature is -6.4 °C (January mean -20 °C, July +14 °C) and average precipitation is ~330 mm.y^{-1}, 40 % falling as snow.

In the eastern extremities a glacial spillway divides the largest dolomite plateau into "Mahony Dome" and "Tunago Dome". The former (~800 km^2) has a central alvar draining peripherally into lakes with overflow sinkholes, turloughs, dessicated turloughs, and stream sinks, all developed post-glacially in regular karst hydrologic sequences. Tunago Dome is similar in extent but was reduced to scablands by a sub-glacial mega-flood from the Great Bear basin; it is a mixture of remnant mesas with epikarst, and wetlands with turloughs in flood scours. Both domes are largely holokarstic, draining chiefly to springs at 160–180 m a.s.l. in the spillway.

The eastern limit of overthrusting is marked by narrow ridges created by late-glacial hydration of anhydrite at shallow depth in interbedded dolostones and sulphate rocks. Individual ridges are up to 60 km long, 500–1,000 m wide, 50–250 m in height. They impound Lac Belot (300 km^2), Tunago Lake (120 km^2) and many lesser lakes, all of which are drained underground through them. In the main overthrust structures, the Norman Range (Franklin Mountains) is oriented parallel with the direction of Laurentide ice flow. It displays strongly scoured morphology with elongate sinkholes on its carbonate benches. In contrast, the Bear Rock Range is oriented across the ice flow, has multiple cuestas, is deeply furrowed and holokarstic but preserves pinnacle karst on higher ground due to karst-induced polar thermal (frozen-down) conditions at the glacier base there.

LITTLE LIMESTONE LAKE: A BEAUTIFUL MARL LAKE IN MANITOBA, CANADA

Derek Ford
School of Geography and Earth Sciences, McMaster University, Canada, dford@mcmaster.ca

Marl lakes are those accumulating fine-grained bottom sediments that include at least 15 % $CaCO_3$. They are found worldwide. The most visually attractive, however, have higher proportions of $CaCO_3$, with crystallites precipitating in the water to give it a rich and opaque duck-egg blue colouration. From the literature, such lakes are largely limited to recently glaciated carbonate rock terrains. Most are also shallow, with much or all of the water column being in the photic zone.

Little Limestone Lake, (Lat. 53°47'N, Long. 99°19'W in the province of Manitoba) is the finest example that the author has seen. It stands out sharply from neighbouring lakes in summertime colour satellite imagery due to the intensity and uniformity of its colour. The lake occupies a shallow glacial trough scoured in a plain of flat-lying cyclothem dolomites. It is ~12 km long, 1–5 km wide, rarely >7 m deep. Including bordering wetlands, it occupies ~45 % of the area of an elongated, narrow topographic basin. Recharge is through impoverished boreal forest with little soil cover; it discharges chiefly as springs and seeps along and below the shore. Mean annual temperature is ~0 °C, and precipitation is ~475 $mm.y^{1}$.

Previous studies of springs in the surrounding region showed ground waters to be simple bicarbonate composition, with TDS = 230–300 $mg.l^{-1}$ (Ca 40–60 $mg.l^{-1}$, Mg 30–40 $mg.l^{-1}$). Grab sampling at 27 sites throughout the lake found the waters de-gassed to 125–135 $mg.l^{-1}$, placing them in the mid-range of one hundred marl lakes investigated in more detail in the British Isles. Ca was reduced to 25–30 $mg.l^{-1}$, while Mg was stable at 30–40 $mg.l^{-1}$. There were 2–3 $mg.l^{-1}$ of free CO_3 in two fully analysed samples, indicating that plankton photosynthesis might be occurring. However, samples of the bottom marl were predominantly inorganic in their composition.

Little Limestone Lake is visually spectacular because it is almost entirely groundwater-fed, with a ratio of recharge area to lake area that is low. It has no large, chemically equilibrated, surface streams entering it. In contrast, the dozens of nearby lakes (similar, larger or smaller in size) are regularly flushed by channelled storm water and, although they also produce some carbonate marl, cannot maintain high densities of crystallites in suspension. Little Limestone Lake was placed under legislated protection as a provincial park in June 2011.

1. Marl lakes

Sediments accumulating on lake floors may be divided into: (1) *clastics*, which are fragments of insoluble rocks carried into the lakes by rivers or the wind; (2) *organics*, consisting of animal or vegetal material carried in by air or water currents from surrounding land, and the remains of fish, molluscs, plankton, etc. created in the water body itself; (3) *precipitates and evaporites*, crystalline or micro-crystalline minerals created by organic or inorganic chemical processes along the lake shore, on the bottom, or in the water column and mechanically settled out of it. At the global scale, mixtures of clastic and organic sediments in varying proportions are overwhelmingly predominant in the world's lakes. Amongst the chemical class evaporite lakes and ponds are more numerous than precipitate lakes (including marl lakes), and probably quantitatively predominant in bulk terms because much greater tonnages are being deposited in them each year. Lakes in which carbonate precipitates make up a significant proportion of the sediment accumulating on the floors are thus comparatively rare. In a popular sedimentological classification of them mixtures of 25–75 % calcium carbonate with clay or silt or non-carbonate organic debris are considered to be "marl" (Schurrenberger et al. 2003). They have the feel and appearance of soft mud or ooze. Some authorities would extend "marl" to include sediments with up to 95 % calcium carbonate provided that they remain soft, i.e. unconsolidated. An essential feature of the most attractive marl lakes everywhere is that there are also calcium carbonate micro-crystals ("crystallites") in suspension in sufficient concentration in the water column to scatter sunlight and create strong and opaque blue colouration.

Lakes where marl contributes between 5 % and 95 % of the bottom sediments (marl lakes *sensu lato)* are found in every region of the world where there are large quantities of limestone and/or dolomite to contribute the essential calcium ions, and the climate is humid enough to maintain the lakes and keep the concentrations of dissolved solids in them well below the levels where evaporite deposition begins. Most climatically humid regions and the wetter fringes of the sub-humid/semi-arid regions qualify. However, it is recognised that a disproportionately large number of marl lakes are to be found in the glaciated regions, including perhaps a majority of the visually very attractive. Most marl lakes that have been described in the scientific literature are located in the glaciated regions of northern Europe and North America.

Following Pentecost (2005, 2009) there are two different paths to the creation and deposition of the marl, *biogenic* and *abiogenic* (inorganic). Processes in a given lake may be completely dominated by one of them, or be a mixture of both that may differ in its proportions as the seasons progress. The abiogenic is the simple process of limestone or dolomite inorganic dissolution, with crystallite precipitation following when CO_2 degasses from the Ca, Mg, HCO_3 solution due to warming or loss of pressure or both.

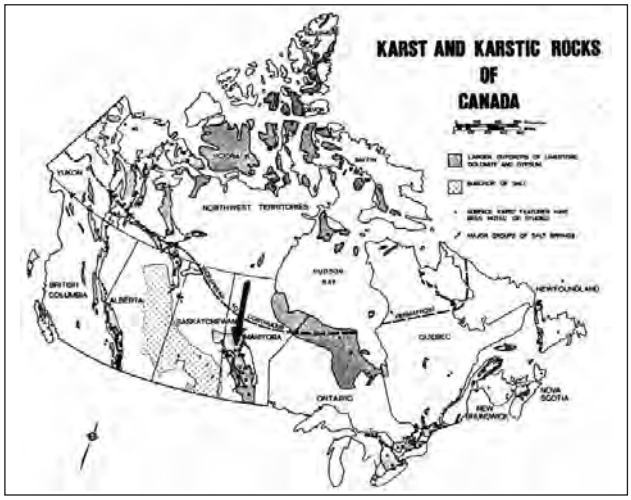

Figure 1. Location of Little Limestone Lake, Manitoba.

Wholly biogenic deposits may arise because photosynthesis in fresh waters creates many species of microscopic algae and bacteria. Pentecost (2009) focuses on the common green alga *Chara* but there are a host of alternatives. In the first step: $2HCO_3^- \rightarrow CH_2O_{(photosynthesis)} + O_2 + CO_3^{2-}$. There is abundant HCO_3^- in karst lake waters, e.g., McConnaughey et al. (1994) found that macrophytes, chiefly *Chara*, extracted ~23 grams C/m^2 during the growth season in a Minnesota marl lake. With abundant Ca^{2+} also being present via the inorganic path, step 2 proceeds: $Ca^{2+} + CO_3^{2-} \rightarrow CaCO_{3\,(calcite)}$. "calcite begins to form in strongly alkaline surface regions of the internodal *Chara* cells and subsequently envelops almost the entire plant. During the later stages of calcification additional inorganic precipitation may be taking place but this has been little studied" (Pentecost 2009). The inorganic calcite probably accretes to the outer surface of the alga in the manner that it accretes to larger plants to form *tufa* deposits in many streams and lakes around the world. The algae remain very tiny, however, suspended in the water and scattering incident light, settling slowly downwards only if conditions become very calm.

2. Little Limestone Lake and its setting

Little Limestone Lake (Figs. 1, 2; Lat. 53°47'N, Long. 99° 19'W in the province of Manitoba, Canada) is the finest example of a marl lake that the author has seen in many years spent in glaciated karst regions. It stands out sharply from the neighbouring lakes in summertime colour satellite imagery due to the intensity and uniformity of its duck-egg blue colour. Viewed from the shore or in a boat it is equally colourful. For these reasons the Manitoba chapter of the Canadian Parks and Wilderness Society, a national conservation body, argued for its protection for many years. The Conservation Branch of the provincial government requested an independent evaluation by a specialist (Ford 2010), which resulted in a park protection area being proclaimed in 2011.

Little Limestone Lake is one amongst hundreds of small lakes in the Interior Lowlands geologic region of North America. It is located a few kms northwest of the much larger Lake Winnipeg, and drains to Hudson Bay (Fig. 1). The bedrocks are platformal dolomites of Silurian age totalling approximately 80 m in thickness that dip very gently westwards (Bezys 1991; Bezys and Kobylecki 2003). Local relief upon them is never more than 70 m, created chiefly by glacial scour, or the deposition of glacial moraines during the recession of the last Laurentide Continental Icesheet ~11,000 years ago. A sample bedrock section exposed in a road cut a few km south of the lake is shown in Figure 3. The strata are a cyclic succession of regular beds varying from "medium" (10 cm) to "massive" (>100 cm) in thickness. The thicker beds are mechanically stronger and so survived glacier scour more readily. Clint-and-grike solutional pavement (epikarst) has developed on them in post-glacial times (Ford 1987; Ford and Williams 2007). They also have a high density of vugs, which can increase the matrix permeability of the rock and thus the quantities of dolomite taken into solution by groundwater permeating through it. Examples of the cliffs on massive dolomites and epikarst on thinner beds along the shores of Little Limestone Lake are shown in Figures 4 and 5.

In Figure 2 the boundaries of the Lake basin are drawn conventionally to follow the surface topographic divide because no karstic diversions of groundwater flow are known. The basin is ~20 km in length, 5–8 km wide. It has an area of ~91 km^2, of which 36 km^2 is occupied by the Lake itself. Pond A (~2 km^2; Fig. 2) is a former arm of the lake that is now separated by wetlands but still drains into it; it has negligible ground water supplies of its own and its water is clear, not opaque and blue. The dry land area that is believed to contribute to the lake is thus ~53 km^2. Wetlands at or very close to the lake level occupy ~3.5 km^2 of this and the balance consists of gentle side slopes and broad plateaus. The lake is at ~267 m above sea level and the highest ground is around 290 m a.s.l.

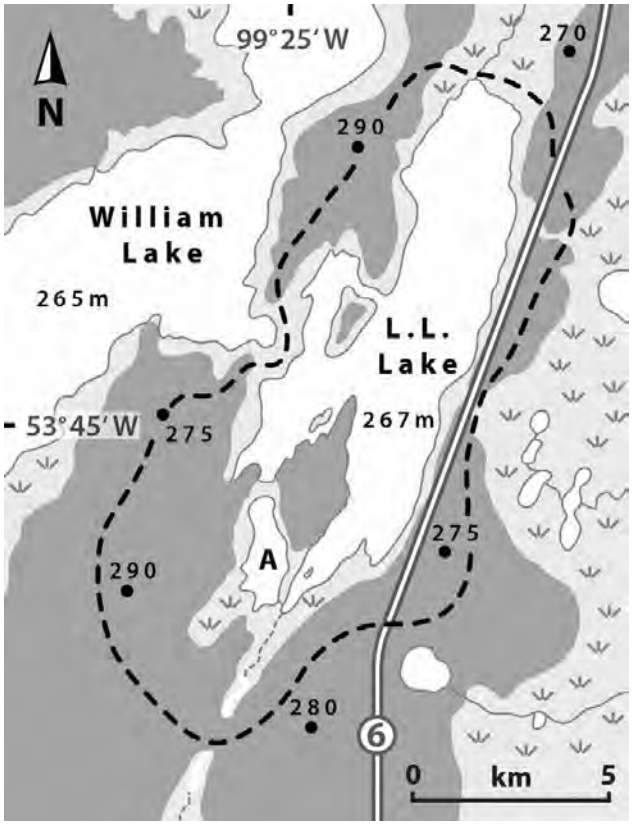

Figure 2. Sketch map of Little Limestone Lake. The watershed is shown by dashed line.

Figure 3. A typical section of the cyclic dolomite beds at Little Limestone Lake.

There is no bathymetric map of Little Limestone Lake and the bottom is always obscured by the suspended load in summer. The geologic and physiographic setting indicates that the lake is likely to be shallow everywhere. A few measured depths suggest that much of it has a flat floor at 7.0 to 7.5 m. This is comparatively deep for a marl lake but not as great as the deepest mentioned in Pentecost's 2009 sample of 100 such lakes in the British Isles. At 7.5 m the waters are fully in the photic zone. Sample cream-coloured carbonate oozes were dredged from the bottom there.

At its north end Little Limestone Lake is drained by a regular stream channel that passes through a wetland into a lake about one metre lower (266 m a.s.l.). A small spring-fed stream flows into the southern end. To the west William Lake, a much larger water body, is at 265 m a.s.l. To the east and south there are extensive wetlands and smaller dolomite plateaus draining 18–20 km eastwards into Lake Winnipeg at 217 m a.s.l. The important consequence is that the Little Limestone Lake basin, although it functions as a water-retaining shallow trough, can be envisioned as an elongated hydrological ridge or "high" perched between drainage to lower lake levels around it. The Lake plus Pond A and associated wetlands occupy nearly 46 % of the basin, a very large proportion. Recharge from the remaining ~54 % is almost entirely by groundwater that has passed through the dolomite. The basin is not prone to flushing by mud-laden flood waters from proportionally greater recharge areas, as the majority of other lakes in the region are. Under the natural conditions that have prevailed for at least some thousands of years here a delicate physical, chemical and (probably) biogenic balance has been able to build up and establish the remarkable marl blue colouration. The current climatic conditions are Cool Continental (Koppen type D). The mean annual temperature is ~1.0 °C and precipitation is 475 $mm.y^{-1}$. The natural vegetation is Boreal Forest (coniferous).

Nearly flat plateau and bench surfaces in bedrock are predominant in the recharge areas. There is thin and discontinuous glacial till cover on them due to erosion by over-wash immediately after the ice receded. There is a nearly 100 % cover of mosses, lichens, flowers, juniper and other low shrubs, and forest litter. The trees are widely

Figure 4. Cliffed shore with groundwater outlets at and below the waterline.

spaced, slow-growing or stunted in many places, reflecting the edaphic drought that occurs where the dolomite surfaces are efficiently drained by epikarst (Figure 6). Forest fires have broken up the karst on thinner beds, increasing the efficiency of groundwater recharge. The greatest straight-line distance that groundwater must flow from these uplands to the lake is no more than 3–4 kms, giving hydraulic gradients (depth/length gradients) of 5 $m.km^{-1}$ or more. There are some seepages in the cliffs and at the water line in the lake but most ground water discharge is below that, perhaps because industrious beavers have raised the lake level by ~0.5 m in recent decades.

3. Water chemistry

The water chemical characteristics of the Lake itself have not been studied in detail. However, McRitchie (1994, 1995) carried out systematic sampling at springs and seeps in the dolomite escarpment immediately south of it, plus two water samples from springs on William Lake. Seventy water samples were analysed for the standard water quality variables plus trace concentrations of economic minerals and of contaminants. All of the waters were simple calcium bicarbonate ground waters typical of clean dolomite terrains. Total hardness ranged between 230 and 300 $mg.l^{-1}$; Ca 40–60 $mg.l^{-1}$, Mg 30–40. The waters were saturated or supersaturated with respect to calcium carbonate under standard atmospheric conditions. Na, K, SO_4 and Cl were negligible in amount. At each site there was one-time sampling only and in most cases the water was taken from the spring itself before it had had any opportunity to de-gas its CO_2 content or make other adjustments to open air conditions.

McRitchie (1994) described what happened downstream, however – precipitates quickly appeared, as sand-sized particles at first but rapidly shrinking in size downstream and ceasing to form after 200–300 m of flow in the open channels. In the ponds at some springs there were organic-rich mats of material. Downstream there was only cream-grey carbonate ooze, very like that collected from the bottom of Little Limestone Lake. The oozes were almost entirely $CaCO_3$, chiefly of inorganic origin although one of four samples may have contained as much as 10 % organics (i.e. from photosynthesis, as described above).

Figure 5. Shoreline recharge directly from the epikarst.

Figure 6. Recently burned forest on medium-bedded dolomite. The epikarst surface has been broken up by the heat, by toppling and by frost.

In September 2010 the author took one near-shore bulk water sample from the surface of Little Limestone Lake and a second from -2.0 m in the centre. Comprehensive standard analyses (ALS Laboratory,Winnipeg) found the two samples nearly identical, indicating that at least the upper two metres of the lake are uniform in composition. Na, K, Cl and SO_4 were negligible in amount. Total hardness (as $CaCO_3$) was 200 $mg.l^{-1}$. This is significantly less than the values between 230 and 300 $mg.l^{-1}$ that Ritchie obtained at the springs and seeps from the dolomites. It suggests that the Lake waters have de-gassed CO_2 and precipitated large amounts of their dissolved load. This explanation is substantiated by the Ca: Mg ratios of 26: 33–34. In the large majority of published dolomite karst water compositions the ratio is the reverse of this (60: 40 to 70: 30 in favour of Ca^{2+} until vigorous precipitation begins). The detection of 2–3 $mg.l^{-1}$ of CO_3^{2-} also indicates de-gassing, at a pH above 8.3.

Determination of free CO_3 in the lake waters is a hint that photosynthesis was occurring.

Water temperature and electrical conductivity were measured at a depth of ~1.0 m at 27 different points in the Lake. The Krawczyk and Ford (2006) "best fit" equation for "clean" bicarbonate waters (salts + sulphates + nitrates + phosphates <10 %; electrical conductivity <600 µS) was used to calculate total hardness as $mg.l^{-1}$ $CaCO_3$:-

$$TH = 0.53\ EC - 1.6\ (R^2 = 0.93;\ n = 2300) \quad (1)$$

The principal finding was the uniformity of shallow water chemistry everywhere on the Lake proper. Despite a range of temperatures from 12.8 to 17.4 °C during the two days of sampling, EC was in the narrow range of 240–250 µS with one exception. From Equation 1, estimated $CaCO_3$ concentrations of 126–132 $mg.l^{-1}$ place the Lake waters comfortably in the mid-range that Pentecost (2009) has cited in his sample of more than one hundred marl lakes and ponds in the British Isles.

The one exception was the small spring-fed stream draining the southern epikarst. It entered the Lake at a temperature of 11 °C, EC = 296 µS, and was clear (no blue opacity). Twenty metres further out into the Lake sampling a few minutes later yielded T = 14.4 °C, EC = 247 µS. This suggested rapid warming with net precipitation of ~25 $mg.l^{-1}$ $CaCO_3$.

Concerning the stability of the density and hue of the colour, my previous visits to the Lake (1984, 2004) were of short duration during warm sunny afternoons which led me to wonder whether there might be a daily "blooming" of crystallites in response to solar warming, such as occurs in knee-deep water on the Bahamas Banks for example. It is now appreciated that this is not the case; the crystallites can have a duration of at least many weeks in suspension during the ice-free period on the Lake, giving sufficient time for winds to mix them thoroughly across the surface. Further, many authorities contend that lakes that are as shallow as typical marl lakes do not develop strong thermal or other stratification (Pentecost 2009); the physical and chemical conditions are broadly similar from surface to the bottom. From the physical chemistry some increase in the rate of precipitation is to be expected at the warmest times of the day: at Little Limestone Lake other observers have reported their qualitative impressions that there is some increase in density (opacity) then.

4. Conclusions and recommendations

Little Limestone Lake has outstanding blue ("marl lake-type") colouration because its elongated, small and shallow, basin is delicately perched between much larger basins draining to east and west respectively and thus is protected from flushing or clastic or organic detrital input by large surface streams during any strong thaw or rain flood events. The ratio of recharge area to lake area is low. Almost all annual recharge is from the combination of seasonal snowmelt and perennial groundwater flow directed through the enclosing dolomites. From current knowledge it appears that the water chemical behaviour that determines the striking blue colouration of the Lake during the summer is quite robust. The bulk of $CaCO_3$ crystallite precipitation appears to be of physical origin but the contribution of photosynthesis is not adequately understood at present.

The location is remote and the local population is very small. However, there are nickel exploration prospects in Canadian Shield rocks beneath the dolomites around William Lake that touch the western side of Little Limestone Lake. Physical threats to the lake could arise if

the volumes of water flowing into it were substantially increased or diminished by any exploration or other development. Both could impact the colouration and its chemical stability in ways that are difficult to forecast. Chemical hazards could include acidification or introduction of other contaminants that kill off the pertinent biota if biogenic activity is a crucial contributor to the carbonate precipitation. Heavy gasoline-powered boat traffic could also pose a threat. It is hoped that the creation of the provincial park will deal with these problems.

Acknowledgements

The author is indebted to Roger Turenne and Ron Thiessen (Manitoba chapter, Canadian Parks and Wilderness Society), Ken Schykulski (Manitoba Conservation) and Chief Buck of the Mosakahiken First Nation for thweir encouragement and support in the field.

References

Bezys RK, 1991. Stratigraphic mapping (NTS 63F, 63K) and corehole programme 1991. Manitoba Energy and Mines, Report of Activities 1991, 61–73.

Bezys RK, Kobylecki AJ, 2003. Preliminary karst inventory of areas north and south Grand Rapids, Manitoba (NTS 63B and 63G). Manitoba Energy and Mines, Report of Activities 2003, 213–223.

Ford DC, 1987. Effects of Glaciations and Permafrost upon the Development of Karst in Canada. Earth Surface Processes and Landforms, 12(5), 507–522.

Ford DC, 2010. Final Report upon Field Studies and Review at Little Limestone Lake Park Reserve. Parks, Natural Areas Branch, Manitoba Conservation. 48.

Ford DC, Williams PW, 2007. Karst Hydrogeology and Geomorphology. Chichester: John Wiley & Sons, Ltd. xiii, 563.

Krawczyk WE, Ford DC, 2006. Correlating Specific Conductivity with Total Hardness in Limestone and Dolomite Karst Waters. Earth Surface Processes and Landforms. 31, 221–234.

McConnaughey TA, Labaugh JW, Rosenberry DO, Striegl RG, Reddy MA, Schuster PF, Carter V, 1994. Carbon budget for a groundwater-fed lake: calcification supports summer photosynthesis. Limnology and Oceanography, 39, 1319–1332.

McRitchie WD 1994. GS-29. Spring water and marl geochemical investigations, Grand Rapids Uplands (NTS 63G). Manitoba Energy and Mines, Mineral Division, Report of Activities 1994, 148–162.

McRitchie WD, 1995. GS-22. Spring water and marl geochemical investigations, Grand Rapids Region, 1995 Status Report (NTS 63G). Manitoba Energy and Mines, Mineral Division, Report of Activities 1995, 109–119.

Pentecost A, 2009. The marl lakes of the British Isles. Freshwater Reviews, 2009(2), 167–197.

Schurrenberger D, Russell J, Kerry Kelts, 2003. Classification of lacustrine sediments based on sedimentary components. Journal of Paleolimnology, 29, 141–154.

CAVES AND KARST HYDROGEOLOGY OF JERUSALEM, ISRAEL

Amos Frumkin
Israel Cave Research Center, Geography Department, The Hebrew Universit of Jerusalem, Israel 91905, msamos@mscc.huji.ac.il

The city of Jerusalem, Israel, is growing for ~4,000 years on karst terrain. Lacking closed depressions, surface topography seems fluvial, but karst is well demonstrated by speleology and subsurface hydrology. Several caves in the city were truncated by construction works, including an 800 m long river cave (longest limestone river cave in Israel), and a 200 × 140 × 90 m isolated chamber cave (largest chamber cave in Israel). Caves are being discovered at a growing rate, as construction works dig deeper into the subsurface in the crowded city. Some of them are eventually destroyed by the construction works; only presently accessible caves are discussed here. The hydrogeology and hydrochemistry of the Gihon, Jerusalem's main karst spring, was studied in order to understand its behavior, as well as urbanization effects on karst groundwater resources. High-resolution monitoring of the spring discharge, temperature and electrical conductivity, as well as chemical and bacterial analysis demonstrate a rapid response of the spring to rainfall events and human impact. A complex karst system is inferred, including conduit flow, fissure flow and diffuse flow. Electrical conductivity is high compared to nearby springs located at the town margins, indicating considerable urban pollution in the Gihon area. The previously cited pulsating nature of the spring does not exist today. This phenomenon may have ceased due to additional water sources from urban leakage and irrigation feeding the spring. The urbanization of the recharge area thus affects the spring water dramatically, both chemically and hydrologically.

1. Introduction

Famous as a sacred city for the western world religions, it is rarely mentioned that Jerusalem is built on karst. The city was founded just above the Gihon karst spring. This paper briefly presents the karst underlying the city. In addition to the well-developed karst features, human impact on the karst is also discussed. The data comes from ongoing research by Israel Cave Research Center (ICRC) which monitors closely the new caves and karst phenomena found during urban development. The paper deals with presently accessible features, neglecting small isolated chambers and vadose shafts which have been destroyed or filled during construction works.

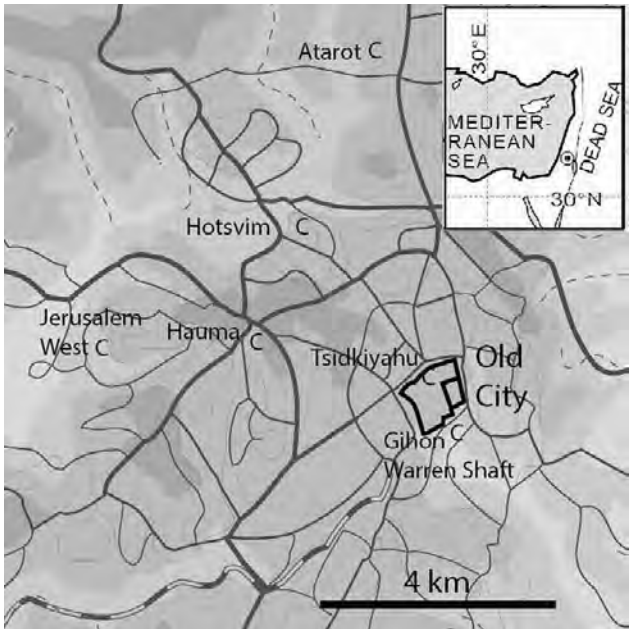

Figure 1. Location topographic map with roads and mentioned caves.

2. Setting

2.1. Topography

Jerusalem is located on hilly surface on both sides of the main water divide of Israel, ~600–800 m above sea level (Fig. 1). The Jerusalem Hills (20 km around Jerusalem) is a structural and topographic saddle within the plateau-like Judean Mountains, at the center of the Judea and Samaria Mountain range. The present topography demonstrates an uplifted Tertiary erosion surface entrenched by fluviokarstic wadies (rarely flowing streams) which drain westward to the Mediterranean and eastward to the Dead Sea. Closed depressions are not observed within the city, but do exist a few km to the north (Frumkin 1993).

2.2. Geology

Jerusalem is underlain by Late Cretaceous rocks. Most of the city is built on Judea Group, dominated by shallow, epiric marine carbonates, on which karst is well-developed (Gill 1997; Picard 1956, Sneh and Avni 2011). The eastern suburbs of the city were recently built on the overlying Mt. Scopus Group, dominated by chalk and some chert deposited in a deeper southern basin of the Neo-Tethys Sea.

The dominant rocks are well-bedded to massive limestones, dolomites and chalk, with smaller amounts of marl and chert. Stratal dip across Jerusalem ranges from 5 to 15° to the southeast, associated with several stages of uplift and folding. Jerusalem was last inundated by marine water probably during the early Eocene. Following regional regression and exposure during the late Eocene, an erosion surface has cut the dipping strata, exposing older layers to the west and younger to the east of the city. Periodic uplift and mild folding was accompanied by continuous karstification and erosion, truncating hundreds of meters of the bedrock (Frumkin 1993).

The section of Judea Group underlying Jerusalem is divided into six sub-units (Sneh and Avni 2011): (A) Cenomanian Kefar Shaul Formation (Dir Yasini, 10–80 m thick) – chalk and well-bedded limestone; (B) Cenomanian-Turonian Weradim Formation (Mizi Yahudi-Ahmar, 55 m thick) – karstified massive to bedded crystalline, dense dolomite; (C) Turonian Shivta Formation (Meleke, 20–40 m thick) – karstified massive, porous biosparitic limestone; (D) Nezer Formation (Mizi Hilu, 40–90 m thick) – well-bedded dense biomicritic limestone; (E) Santonian–Campanian Menuha Formation (60–150 m thick) – biomicritic chalk with some chert; (F) Campanian Mishash Formation (90 m thick) – mainly chalk and chert.

2.3. Climate

Jerusalem is located at the boundary between the temperate Mediterranean climatic belt to the west and the rain-shadow Judean Desert to the east. Mean annual temperature is 18 °C, and precipitation averages 550 mm.y^{-1}, falling during the cool winter (October–May), when potential evaporation is ~2 mm/day. The summer (June–September) is hot and dry with potential evaporation ~7 mm/day (Goldriech 1998). During December–January about 2/3 of the annual rainfall occurs, typically concentrated in rainfall events lasting from a few hours to several days. Less commonly, some precipitation falls as snow. August is the hottest month with an average temperature of 24 °C, while the winter average is 10 °C.

About 30 % of precipitation flows and infiltrates to the subsurface, and the rest is mostly evapotranspirated. Natural surface runoff amount to few %, but has increased due to urbanization (Benami-Amiel et al. 2010).

Speleothem stable isotopes indicate that glacial periods were wetter and cooler than interglacials (Frumkin et al. 1999; 2000). Increased dust input has contributed to local terra rossa soils, mainly during glacial periods (Frumkin and Stein 2004).

2.4. The urbanization of Jerusalem

During the 2nd millennium Before the Common Era (BCE), Jerusalem occupied ~0.04 km^2 on the hill above the Gihon Spring. The area increased to ~1 km^2 around 700 BCE, and to ~2 km^2 during the Roman period (1st century CE). Following the Arab conquest the city contracted to ~0.85 km^2, within the presently walled Old City (Ben-Aryeh 1977), covering only a small portion of the Gihon Spring catchment. This was followed by rapid growth outside the walls of the Old City, since the mid 19th century. Population has increased from 4,700 in 1525 CE, through 45,000 in 1896, to 933,000 in December 2011.

Today, Jerusalem covers ~130 km^2 (Kaplan et al. 2000). Open area accounts for 65 % of the land-use within the municipal area of the city. Land uses in the catchment include small industrial areas, archaeological parks, public administration buildings, religious compounds and mostly residential quarters. The main anthropogenic activities that pose threat to the quality of groundwater are small industry and human residence where sewage infrastructure is old.

Figure 2. Vadose shaft with a trace of meandering canyon at its ceiling. Tsidkiyahu Cave, view upward. Photo by author.

3. Caves in Jerusalem

Few small natural caves were known within the present city borders prior to human intervention. Most known karst caves were truncated by construction works since ancient times. Thousands of years ago, the City of David water systems have truncated some phreatic and vadose voids of local nature. Of these, Warren Shaft is the largest vadose cave, and the Gihon Spring Cave is the largest phreatic cave. Both caves are connected to (but not part of) the famous Siloam Tunnel (Frumkin et al. 2003). In general, most ancient water systems did not follow karst voids (Shimron and Frumkin 2011), but were artificially excavated (Frumkin and Shimron 2006). Underlying the Old City, the large ancient underground quarry dubbed "Tsidkiyahu Cave" (also called "King Solomon Quarry") truncated some karst voids, mostly vadose shafts (Fig. 2).

Modern construction has truncated many caves, some of which much larger than known before. The longest one is the 800 m long Hauma Cave (Figs. 3, 4), truncated by an artificial shaft 80 m below surface. It is the longest limestone river cave at the northern edge of the Sahara-Arabia desert belt in the Levant, and the 8th longest cave in Israel (Langford and Frumkin 2013). It was explored by the ICRC upstream until becoming a narrow tube-like conduit, and downstream down to a sump.

Figure 3. Vadose canyon in Hauma Cave. Photo by author.

The cave is mostly a low-gradient dip passage perched on Kefar Shaul Formation, with a ten m vertical segment. The cave is mostly a vadose canyon with remnants of an original phreatic tube. Some 16 vadose shafts are connected to the stream passage, forming "domepits" up to 32 m above stream level.

The largest volume chamber under Jerusalem (and in Israel) is Atarot Cave, at Atarot industrial zone (Fig. 5). It is a 200 × 140 m large isolated chamber cave (Frumkin and Fischhendler 2005), with 90 m maximal depth. It was formed in Shivta Formation probably under phreatic (hypogenic?) conditions, but large scale collapse features conceal the original solutional morphology. The chamber intersects some vadose shafts. The Atarot Cave is well-decorated with speleothems (Fig. 6), but unfortunately, it was partly rubble-filled by construction contractors before it was known to speleologists and authorities.

Hotsvim Cave (Fig. 7) is another chamber cave, truncated by a building at Har-Hotsvim industrial zone. This cave is a symbol of cave conservation in Jerusalem, as the building plan above it was altered in order to preserve the cave.

Among the vadose shafts truncated by construction works, the Jerusalem-West Cave is one of the most studied in the city. This small shaft system in the western suburb of Har-Nof was blasted by a contractor; consequently its speleothems were used for paleoclimatic reconstruction of the last 220,000 years (Frumkin et al. 1999; 2000). This exceptional, almost continuous record has shown that regional climate was much wetter and dustier during glacial periods (Frumkin and Stein 2004).

Relict karst features in Jerusalem include a wide range of dissolution voids filled with breccias of chert fragments, derived from collapse, erosion and disintegration of Menuha and Mishash Formations chert layers. Some of these voids reach deep into the Judea Group rocks. These voids are probably associated with deep karstification of the Tertiary Judean erosion surface. An age of at least early Pleistocene is indicated by archaeozoologic deposit in one such pit at nearby Bethlehem (Hooijer 1958). Their geology has been properly described following their discovery (Picard 1956; Shaw 1961), but unfortunately, they were misinterpreted in later publications (e.g., Horowitz 1970; Sass and Freund 1977).

4. Gihon Spring hydrology

Gihon is the largest karst spring in Jerusalem (Fig. 7), and the reason for its original location. Gihon recharge zone is within the older parts of Jerusalem, on Judea Group outcrops (Cenomanian–Turonian carbonates). The Spring emerges 635 m asl within a small phreatic cave, 3 m below the current Qidron Valley level, whose lower channel is filled with thick debris. The spring hydrology was studied by Benami-Amiel et al. (2010).

We cleared out the Gihon Spring cave from debris. It was found that the water emerges into the cave from an underwater (~130 cm below water surface) vertical fissure ~1.5 cm wide in Mizi Ahmar dolomite (Gill, 1997).

Discharge, temperature and electric conductivity (EC) were measured continuously during 2004/5. Discharge during the

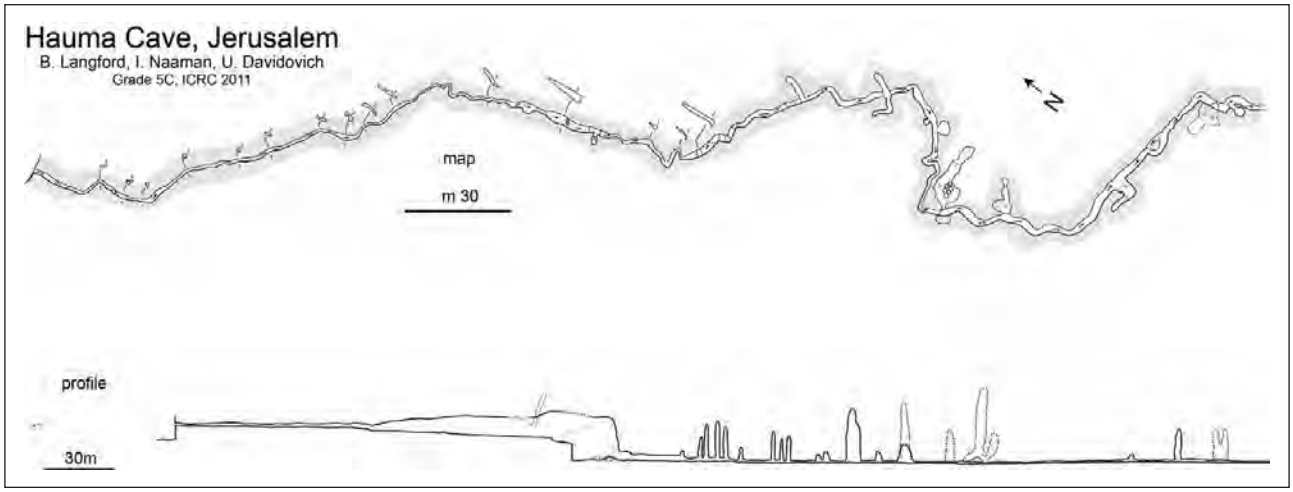

Figure 4. Hauma Cave – vadose river cave, survey by Boaz Langford.

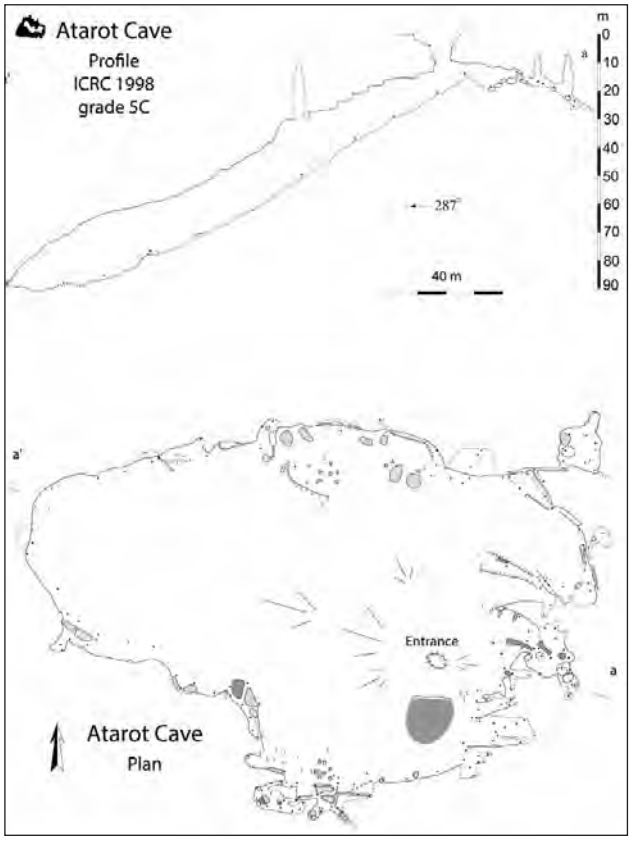

Figure 5. Atarot Cave survey – the largest chamber cave in Israel. In gray areas the fill reaches the ceiling.

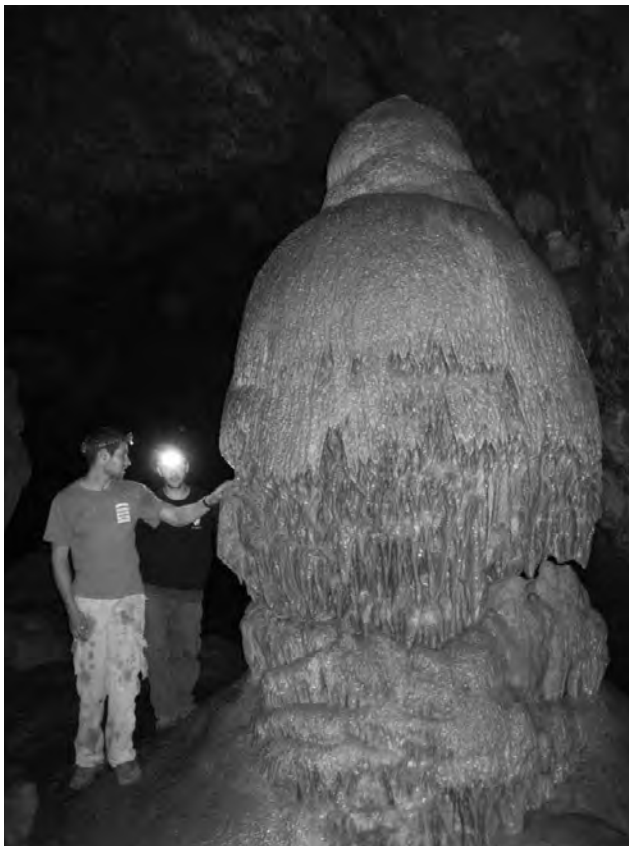

Figure 6. A stalagmite in Atarot Cave.

dry summer is relatively stable, ~0.01–0.03 $m^3.s^{-1}$. During the investigated hydrological year (2004/5; 564 mm precipitation) spring discharge started at 0.025 $m^3.s^{-1}$ (October), peaked at 0.164 $m^3.s^{-1}$ (February), and recovered by the end of the year (September) to 0.031 $m^3.s^{-1}$. During rainstorms and soon afterwards, quick-flow response time ranged from 3.5 to 89 hours, depending on rainstorm type, rainfall amount, and the previous saturation of the system with water. A century ago Vincent (1911) observed discharge pulses ("ebb and flow") in the Gihon Spring:

"… water emerges accompanied by loud echoing noise heard 1–2 min before the water rises and during the whole period of the strongest flow… water rushed out unexpectedly every two or three hours, running for twelve or fifteen minutes at a time."

Today the Gihon Spring is not pulsating any more, possibly due to anthropogenic impact. We suggest that water sources added to the recharge (from irrigation and pipe losses) within the city may continuously fill the underground "siphon" feeding the spring. External water import to Jerusalem has increased substantially overtime with the development and expansion of the city.

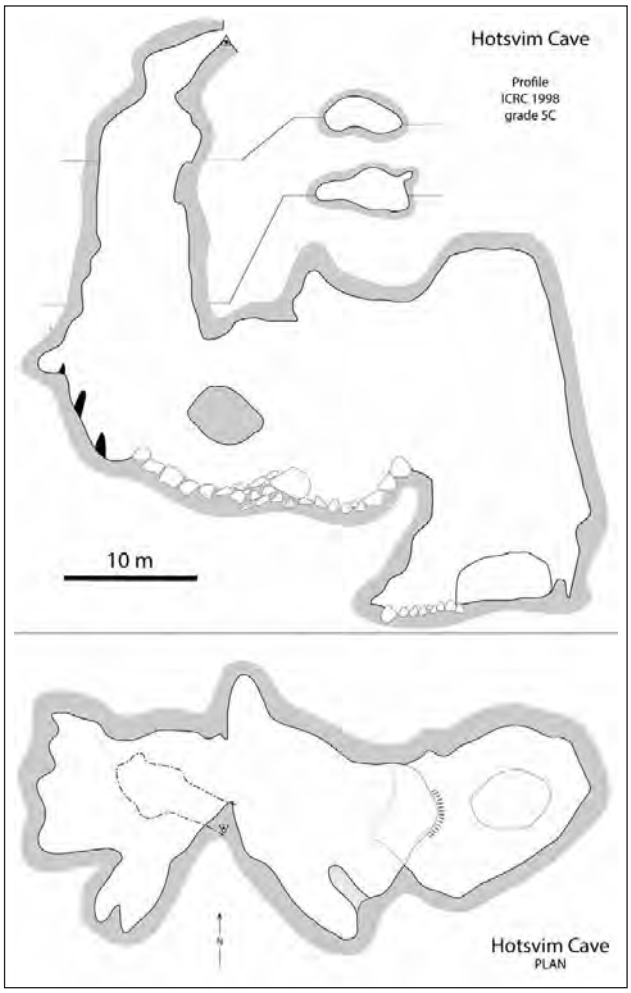

Figure 7. Hotsvim Cave survey.

The average EC is relatively high (1.54 $mS.cm^{-1}$) compared with other springs around Jerusalem, especially those in nearby natural open areas (~0.6 $mS.cm^{-1}$). The EC fluctuates considerately: Maximal EC (2.39 $mS.cm^{-1}$) was recorded at the end of the dry season and minimal EC (1.278 $mS.cm^{-1}$) on February at the peak of the rainy season. Temperature of the water is more stable – between 19.03 °C during wintertime (February) up to 19.42 °C at the end of the dry season (September).

Water temperature and EC minima are closely associated with rainfall peaks. The EC and temperature values began to decline 9–18 hours after rainfall began, and reached

minimum values 8–48 hours later. After about 8 days, both values recovered to their initial values.

Despite large air temperature variations, water temperature fluctuates only slightly, indicating the dominance of rock temperature on fissure water. Water temperature is higher than average air temperature, explained by the geothermal gradient of the Judea Group stratum and the water residence time in the host rock.

The Gihon Spring rather small temperature fluctuations correlate with the EC. As expected, arrival of fresh rainwater results in lower solute concentration, EC and temperature.

The saturation index (SI) of the water indicates that the water is always under-saturated with respect to dolomite (and evaporites). Super-saturation with respect to calcite was recorded in some samples, suggesting possible calcite precipitation. Historic calcite tufa deposits of the Gihon waters (Frumkin and Shimron 2006) indicate that super-saturation with respect to calcite is a recurring phenomenon. These results match the characteristics of the aquifer: the quick flow component of the water is often under-saturated, although baseflow waters can become super-saturated with respect to calcite, especially under free-flow conditions in the Siloam Tunnel downstream of the spring, where rapid CO_2 degassing occurs.

Figure 8. The study of Gihon Spring.

Due to the quick flow component of karst springs they are vulnerable to rapid pollution. Indeed, a major pollution event occurred on May 2002. This event occurred due to leakage from a sewage pipeline about 1.2 km north of the spring.

5. Conclusions

Although the topography of Jerusalem seems fluvial, its karstic nature is revealed by underground features and, to a minor extent, by subaerial morphology. The underground karst voids incloude a river cave, vadose shafts (Fig. 9) and ancient isolated chambers. The discussed caves were found due to truncation by anthropogenic construction works. The Gihon karst spring reflects typical karst hydrology with increasing human interference by pollution and modification of the flow regime. Modern infrastructure is increasingly moving to the subsurface; karst features are intercepted at an accelerated rate and should be closely monitored and preserved wherever possible; the ICRC is doing its best in both these respets.

Figure 9. Vadose shaft truncated by construction works. Close and similar to Jerusalem West Cave. Photo by author.

Acknowledgements

I thank Boaz Langford, Ronit Benami-Amiel, Shmulik Avidan, and other members and volunteers of the Israel Cave Research Center who took part in studying individual karst features.

References

Benami-Amiel R, Grodek T, Frumkin A, 2010. Characterization of the hydrogeology of the sacred Gihon Spring, Jerusalem: A deteriorating urban karst spring. Hydrogeology Journal 18, 1465–1479.

Ben-Aryeh Y, 1977. A City Reflected in its Times: Jerusalem in the Nineteenth Century, the Old City, Yad Ben-Zvi Press, Jerusalem (in Hebrew).

Frumkin A, 1993. Karst origin of the upper erosion surface in the Northern Judean Mountains, Israel. Israel Journal of Earth Sciences 41, 169–176.

Frumkin A, Ford DC, Schwarcz HP, 1999, Continental oxygen isotopic record of the last 170,000 years in Jerusalem: Quaternary Research, 51, 3, 317–327.

Frumkin A, Ford DC, Schwarcz HP, 2000, Paleoclimate and vegetation of the last glacial cycles in Jerusalem from a speleothem record: Global Biogeochemical Cycles, v. 14, 3, 863–870.

Frumkin, A. Stein M, 2004, The Sahara – East Mediterranean dust and climate connection revealed by strontium and uranium isotopes in a Jerusalem speleothem: Earth and Planetary Science Letters 217, 451–464.

Frumkin A, Fischhendler I, 2005. Morphometry and distribution of isolated caves as a guide for phreatic and confined paleohydrological conditions. Geomorphology 67, 457–471.

Frumkin A, Shimron A, Rosenbaum J, 2003. Radiometric Dating of the Siloam Tunnel, Jerusalem. Nature 425, 169–171.

Frumkin A, Shimron A 2006. Tunnel engineering in the Iron Age: geoArchaeology of the Siloam Tunnel, Jerusalem. Journal of Archaeological Science 33, 227–237.

Gill D, 1997. The Geology of the City of David and its Ancient Subterranean Waterworks, Qedem, 35, Monographs of Institution of Archaeology, Hebrew University of Jerusalem, IV, 1–28.

Goldreich Y, 1998. The Climate of Israel: Observations, Research and Applications, Bar Ilan University, Ramat Gan (in Hebrew).

Hooijer DA, 1958. An early Pleistocene mammalian fauna from Bethlehem. The Bulletin of the British Museum (natural history) 3(8), 26–292.

Horowitz A, 1970. Outrops of Hazeva and Taqiye formations in the Jerusalem area and their possible significance. Israel Journal of Earth Sciences 19, 35–39.

Kaplan M, Kimhi I, Choshen M, 2000. The Jerusalem Hills and the Judea Coastal Plain: Policy for Land Conservation and Sustainable Development, Keter Press, Jerusalem (in Hebrew).

Langford B, Frumkin A, 2013. The longest limestone caves of Israel. Proceedings of the 16th International Congress of Speleology, Brno.

Picard LA, 1956. Geology, The Book of Jerusalem: Jerusalem, its Natural Conditions, History and development from the Origins to the Present Day, Avi-Yonah (ed.) vol. 1, The Bialik Institute, Jerusalem, 35–44 (in Hebrew).

Sass E, Freund R, 1977. Deeply incised Senonian unconformity in Jerusalem and its implication on the early evolution of the Judean hills. Israel. Israel Journal of Earth Sciences 26, 108–111.

Shaw SH, 1961. Geological report on the elephant pit, Bethlehem. The Bulletin of the British Museum (natural history) 5, 4, 87–90.

Shimron AE, Frumkin A, 2011. The Why, How, and When of the Siloam Tunnel Reevaluated: A Reply to Sneh,Weinberger, and Shalev. BASOR 364, 53–60.

Sneh A, Avni Y, 2011. Geological map of Jerusalem, 1:50,000. Israel Geological Survey, Jerusalem.

Vincent LH, 1911. Underground Jerusalem: Discoveries on the Hill of Ophel (1909–11), Horace Cox, London.

CAVES UNDER DUBROVNIK AIRPORT IN CROATIA

Mladen Garašić
University of Zagreb, Faculty of Civil Engineering, Department of Geotechnics and Geolog., Kačićeva 26, HR-10000 Zagreb, Croatia, mgarasic@grad.hr
Croatian Speleological Federation, Society for the Research, Surveying and Filming on Karst Phenomena (DISKF) "Zagreb", Nova Ves 66, HR-10000 Zagreb, Croatia, dgarasic@lycos.com
Croatian Academy of Sciences and Arts (HAZU), Committee for Karst, Zrinjski trg 11, HR-10000 Zagreb, Croatia, mgarasic@zg.t-com.hr

Six speleological sites are known to exist at the premises of the Dubrovnik Airport in Croatia. This is a highly weathered area that has been in the focus of attention of speleologists ever since the airport was built in 1961/62. Two vertical caves with the depth of 31 m and 10.5 m were discovered at that time. Both are now situated right underneath the new control tower of the Dubrovnik Airport. A tunnel entrance to the cave that has been known to local population for a long time is situated in the immediate vicinity of the control tower. In late 1950s, the cave entrances were closed with concrete because of a military airport construction, but a tunnel was built to enable access to the cave. The cave is about 200 m long and it fully occupies the space underneath the concrete runways of the Dubrovnik Airport. Thanks to efforts made by speleologists in 2010 the cave was adapted to enable tourist visits, and it is now the world's only tourist cave underneath an operating airport. During apron extension activities in May 2012, three additional speleological sites were discovered and examined, together with other previously discovered caves, from the standpoint of geophysics, geology and speleology.

1. Detailed speleological investigation (research and exploration)

Three cavern systems were discovered at the site of the Dubrovnik Airport's future apron on May 2012. Out of these systems, only the cavern No. 1 (K-1) complies with size requirements for speleological sites according to classification proposed by the UIS (Union Internationale de Spéléologie – International Union of Speleology) where it is specified that speleological sites are only those sites that can be entered by humans. The entrance to the cavern K-1 was discovered during construction works conducted on March 2012. The original entrance measuring 0.30 × 0.30 m was subsequently widened to 1.09 × 0.82 m (Fig. 1). After the initial opening of the cavern, its depth was measured, according to the supervising engineer, by lowering the measurement rope (Garašić and Cvetković 2012).

Figure 1. Narrow passages in Cave 4 (or K-1) at Dubrovnik airport.

It was established that the cavern is about 22 m deep. The width of this vertical cavern (Fig. 3) was not established at that time. Former geophysical measurements by the GPR (ground penetrating radar) and exploratory drilling did not greatly point to the existence of cavern systems in this part of the Dubrovnik Airport. It should however be noted that during airport construction in early 1960 as many as three greater speleological sites were subjected to speleological study in the area presently occupied by the control tower and terminal building. Two speleological sites are vertical with the depths of 31 m and 10.50 m, while the remaining site is complex and measures about 200 m long, and about 30 m deep. All this, in addition to the discovery of new caves, level of weathering of Senonian limestones in this area, and intensive tectonic situation, has pointed to the need to study the newly discovered cavern systems in more detail, and to propose the best possible method for their improvement. The decision was made to conduct the speleological study and to investigate possibilities for penetrating into the deeper parts of the caverns, and also to prepare geophysical profiles so as to cover the surface weathering zone, and to present the area all the way down to compact rocks. To facilitate the analysis of geological situation, the cavern systems were marked with K-1 (cavern No. 4), K-2 (widened space around the opening measuring 0.57 x 0.33 m – Fig.1), and K-3 (area in which the material caved in, but the entrance to cavern was not found). The zones K-1, K-2 (Fig. 2) and K-3 were connected by geophysical profiles (Fig. 6) which were then analysed in form of a geophysical presentation. Three profiles were prepared. The speleologists descended into the K-1, while in K-2 the cavern system could not be penetrated even after the widening. No search of cave entrance was conducted in K-3.

The cavern was formed in Upper Cretaceous (Senonian) limestones and dolomites and the layer thickness varies from 20 to 50 cm. Limestones alternating with dolomites are quite frequent in this zone (Marković 1966, 1975).

Limestones are light to dark grey in colour, and brown intercalations of carbonate calcitic binder are locally found between the layers. In the speleological site, and in its immediate vicinity, the inclination of carbonate formations

Figure 2. Cave 5 (or K-2) at Dubrovnik airport.

varies between 10° and 15°, while the formations strike toward the northeast (from 55° to 58°). Joints observed in the cave and in its immediate vicinity are up to ten cm in width, they are planar and smooth, and are locally filled with very fine-grained clayey material and with carbonate calcitic binder, in crystalline or amorphous form (Garašić 1986, 1991). Intensive joint and fault zones varying from 3 to 4 m in width are situated in the area. Together with lithological and hydrogeological conditions, these zones have greatly influenced the genesis (formation) of the cavern. According to speleological survey, these are relatively young but presently inactive neotectonic faults, as locally proven by thin dripstone coatings that freely cover fault paraclases, especially in top parts of the cavern and, at that, they are neither fractured nor deformed. From the tectonic standpoint, the apron area is a part of the para-autochthon. The para-autochthon occurs in a coastal part, and is formed of Maastrichtian and Middle Eocene limestones and dolomites, preceded by Eocene and Lower Oligocene flysch deposition. Endogenetic movements during geological past, as well as exogenetic processes, have caused formation of the present day structure. Thus, orogenetic movements that occurred during the Helvetian phase resulted in thrusting of the geotectonic unit "High Karst" over the para-autochthon, from the northeast direction. Then the intensive faulting took place in the area under study, and significant faults of general NE–SW-trend (Slivnica Fault), and N–S-trend (Zubak Fault), were formed. Structure inclinations and further reverse overthrusting occurred along these formations. Such past movements caused formation of blocks on which, especially next to transverse faults, we even now experience movements, which results in a pronounced seismic activity in the area under study. The Konavle Zone, as well as its wider surroundings, is characterized by linear folds of northwest-southeast strike, but transverse deformations of secondary significance are not so frequent in this area. Strikes are of the NE–SW orientation and are manifested as transverse faults with frequent relative lowering of one of the blocks. From the engineering-geology standpoint, the following can be said about Upper Cretaceous limestones or dolomites: the uniaxial compressive strength of the substratum (limestones at cavern level) amounts to 100–170 MPa, the RQD value differs, but is mostly higher than 75 percent, on an average discontinuities are spaced at 50 to 200 cm intervals, and are locally filled with clay. Cave systems sometimes exceed 20 m in length, and are normally 10 m long. Joints vary from 0.1 to 1 mm in aperture. In top parts, joints are rough and undulating, while they are smooth in lower parts of the cavern.

2. Hydrogeology of caves

From the hydrogeological standpoint, it can be stated that a permanently active (but not primary) underground stream has not been found at this speleological site (caves), although the dripping water is probably present. The water flow in the cavern varies depending on climatic conditions on the ground surface. The water reaches the cavern via joints directly from the ground surface (to a lesser extent) or in deeper parts via joints and paraclases from other parts of Cretaceous carbonates (in most cases).

Figure 3. Vertical entrance in Cave 4 (or K-1) at Dubrovnik airport.

Even today, the dripping water exerts an intense mechanical and chemical action on the surrounding rocks (erosion and corrosion), thus creating speleothems (stalagmites, dripstone crusts – Figs. 4, 5) The weathering depth in the area of this speleological site, despite the fact that these are practically impermeable rocks, is estimated at 300 to 500 m, and the zone of vertical circulation varies from 50 to 150 m. It is followed by the zone of horizontal circulation in which the ground water is carried via Cretaceous limestones toward submarine springs in the Adriatic Sea (Cavtat Bay and Molunat, Ćilipi coast).

As the Upper Cretaceous (Senonian) and Paleocene (Danian) carbonate rocks are permeable from the hydrogeological standpoint, and this due to intensive

Figure 4. Cave 4 (or K-1) speleothems near bottom of the cave.

secondary (joint) porosity, it may be expected that several similar caverns that can not be accessed from the ground surface are situated in the continuation of this joint, or parallel to it in a zone with genetically correspondent joints formed in the area of the same or similar fault due to general subduction. These caves might even be connected with the mentioned hydrogeological system in deeper zones of this part of the Konavle Zone. They are probably situated more than 30 meters beneath the apron level.

3. Speleogenesis

This speleological site (cavern) has been formed by widening of the fault paraclase with the strike of 51–231° and 120–300°, and with a noticeable rotation of paraclase in intensely weathered Upper Cretaceous and Paleocene limestones and dolomites. The initial water that is significant in the speleogenesis of the cavern, has penetrated through surface joints, and has widened these joints through its corrosive and erosive action to the present day dimensions. The bottom part of the cavern was formed through regressive palaeo-influence of ground water. The processes occur even today, but only in the parts of the cavern that are at least some fifty meters below the apron level. A continuous water stream has not been noticed, i.e. only the speleothems were registered. Cavern dimensions may be even greater, but the narrowness of canals has prevented speleologists from advancing any further. This speleogenesis is related to the weathering processes that occurred after general uplift of the mountainous massif "Cukali Zone" or "High Karst Zone" starting at the end of Cretaceous and continuing to the present time.

Figure 5. Cave 4 (or K-1) – speleothems at the first step.

4. Geophysical investigations and surveying

The geophysical survey was conducted using the seismic refraction method (three profiles: Profile 1, Profile 2 and Profile 3, 385 m in total length – Fig. 7, Fig. 9): The physical disposition of profiles and test sites is presented in the following Figure 6. The test method was selected taking into account the geological structure of the terrain, and geotechnical nature of the problem with regard to design requirements. In this test method, the emphasis was placed on definition of longitudinal wave velocities. Based on seismic wave velocities and their spatial distribution, as determined during the testing, the following information relevant for geotechnical design can be determined and estimated: depth of layers, soil stiffness at small deformations, position of faults and fault zones, and ground water level.

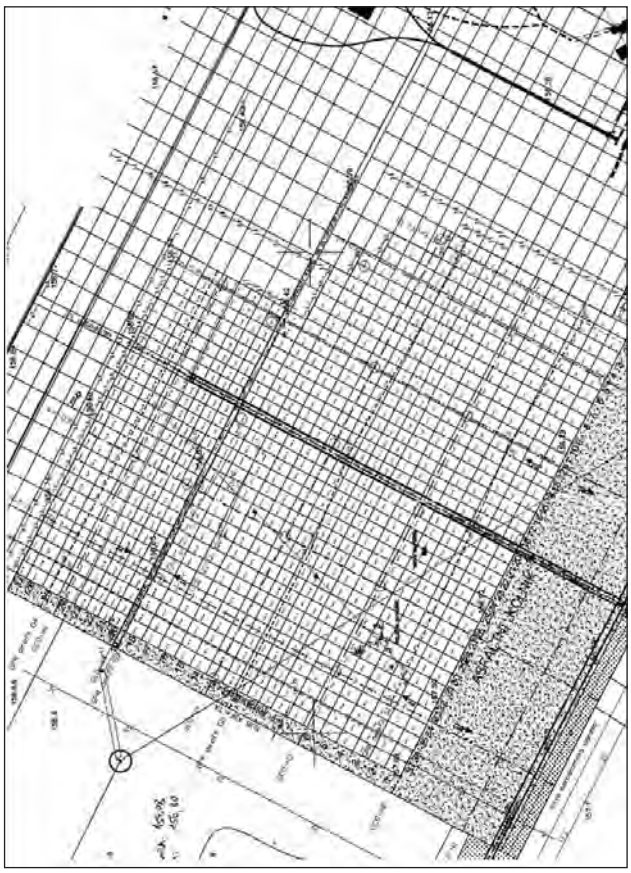

Figure 6. Situation of the Caves Nos. 4, 5, 6 (or K-1, K-2, K-3) at the Dubrovnik Airport.

Seismic tests are conducted in order to define velocity of elastic waves across the depth. Wave velocities are directly linked with elastic stiffness properties of materials they are passing through. Tests are conducted at the ground surface and they belong to the group of non-destructive tests. Seismic methods are based on the propagation of elastic waves through soil or rock. Waves are initiated at the ground surface through generation of impulses or controlled vibrations. At the contact between layers the waves are reflected or refracted, and then they travel back to the ground surface. The wave refraction or reflection is operated according to the Snell's law on propagation of light rays through a stratified medium known from optics. The wave coming from the top layer at an angle i1 from the vertical, and at speed v1, which arrives at the boundary with the bottom layer, is partly reflected at the same angle and

goes back to the surface at the speed of v1, and is partly refracted at an angle i2 and goes to the underground at the speed of v2. If v2>v1 the wave refracts at an angle greater than that of the incoming wave and, if v2<v1, the wave refracts at a smaller angle to the vertical. The ratio of the sine of angles of incoming and refracted wave is equal to the ratio of velocities at which the wave moves in the top and bottom layers. If a wave arrives at the boundary between layers at the so called critical angle ic, then it fully refracts and propagates along the boundary of the layers and, after some time, it returns to the surface at the same critical angle. This is valid only if the wave velocity in the bottom layer is higher that the velocity in the top layer. If the opposite is true, the wave refraction can not occur.

Figure 7. Geopysical profile K-3 at airport caves.

The arrival of waves to the ground surface is detected via sensors – geophones that are placed at previously defined points. The time the waves need to reach the geophone is measured. If a 2D profile of wave velocities is required, geophones are placed at equal intervals along a previously defined straight line. If a 3D profile of wave velocities is required, geophones are placed at predefined positions along the ground surface. The seismic refraction method is applied if refracted waves are used in the interpretation of results. However, the seismic reflection method is applied in if reflected waves are used in the analysis. The hybrid seismic method is used in case both refracted and reflected waves are used in the interpretation of results. As longitudinal P waves are used in these analyses, a presentation of longitudinal wave velocities, as related to the media traversed, is given in the following table.

Several methods are currently used for the determination of wave velocity profiles and for interpretation of measurement results. The following ones are most often used: Generalized Reciprocal Method (Palmer 1981), Delta-t-V Method (Gebrandl and Miller 1985), Amplitudes in Seismic Refraction Inversion (Palmer 2001) and the Diving-wave Tomography (Zu et al. 2000). A typical refraction profile obtained by the Diving-wave tomography method is shown in Figure 8.

5. Data processing

The program package Rayfract 3.14 was used for the processing of input data. At that, the tomographic inversion method was applied. The above software is used for modelling the refraction, passage and diffraction of seismic waves. A good model of initial velocities can be obtained from first untreated seismic waves using the so called Delta t-V turning ray method. When this model is used, a good correspondence is obtained between the model and first wave arrival times, even in case of reverse velocities (when velocity reduces with the depth).

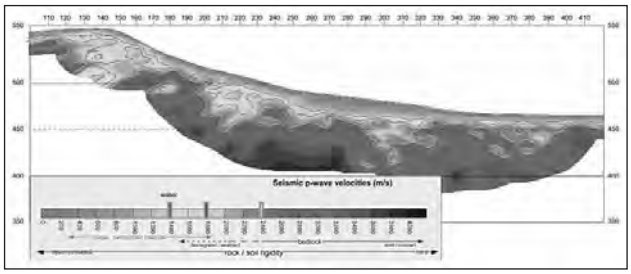

Figure 8. Geophysical profiles K-1 and K-2.

In this case, the model is automatically adjusted for the use of the Wavepath Eikonal Traveltime WET tomography inversion method. The velocities model is refreshed until the moment when the design arrival times coincide in an optimum way with the measured and selected values. The Rayfract 3.14 program supports extreme tomography and presents accurate geological situations (e.g., faults, lateral and vertical changes in velocity, local anomalies in velocity, soil intercalations, etc.).

Figure 9. Geopysical profiles K-2 and K-3.

The processing consists in the definition of geometry and in the entry or selection of the first wave arrival time.

6. Conclusion

The world's only international airport that has a visitable cave under its runway is the Dubrovnik Airport (Fig. 10), in Croatia. Speleologists have invested great efforts to adopt the cave for such visits in the length of 199 meters.

Đurovića Cave is located in the area of the Airport Dubrovnik (Kovačević 2006; Buzjak 2006), at its southern edge, near the control tower. Due to the intensive tourist traffic during the summer season and nearby tourist centres of Dubrovnik and Cavtat, airport management is interested in its use as a show cave.The wider area is characterized by karst proceses and forms, mainly dolines. The cave entrance is located on a small karst plateau developed in the Upper Cretaceous limestone and breccia where the Airport Dubrovnik was built 1960–1963.

Figure 10. Entrance of Cave under Dubrovnik Airport (Airport director and author of paper).

The depth of the cave is 25 m (129 m above sea level and 49 m above the Konavosko polje level). The cave volume is about 9,000 m^3. During the airport construction the cave's natural entrance was closed and a 37 m entrance artificial tunnel was built. Its entrance is closed by an iron door. It is located 154 m above sea-level. According to literature, the cave was first visited and explored by the researchers of the cave fauna in the first half of the 20th century. First detailed speleological research was performed in 2001.

The cave was formed in the Upper Cretaceous limestone and breccia beds along the fissures which controlled the passage directions (Kovačević et al. 2006).

Figure 12. Touristic part of Djurovica Cave in big channels.

As observed during recent researches the dripping water is abundant in wet seasons. It is very interesting because the passages are below the airport where the surface is covered with concrete and asphalt. It is proved by a very branched fissure water circulation in vadose zone where the cave is

Figure 11. Djurovica Cave under the Dubrovnik Airport after reparation for tourists visiting.

Figure 13. Touristic Stairways in Djurovica Cave under Dubrovnik Airport.

located today. Water temperature and pH were measured in two small cave pools. It can be concluded that Đurovića cave is very suitable for tourist use (Fig. 11, Fig. 12, Fig. 13).

In addition to this longest horizontal Đurovića Cave, five additional vertical speleological sites have also been found within the airport premises. Two of them, 31 m and 10.5 m deep, are situated under the control tower. Three more caves, one of which is 22 m deep, were discovered during apron extension works in May 2012. The most recent GPR methods and geoseismic and geoelectric methods were used in the survey and analysis of these speleological sites. According to speleological analyses, it is highly probable that several significant speleological sites (caves) are situated near the already discovered ones, and so future surveys will be oriented in that direction.

References

Buzjak N, 2006. Speleomorfološke i hidrološke značajke Đurovića špilje (Čilipi, južna Dalmacija). Hrvatski geografski glasnik, 68/2, 57–72, Zagreb.

COST project 620, 2004. Vulnerability and risk mapping for the protection of carbonate (karst) aquifers. EUR 20912 EN, Final report. Directorate-General Science, Research and Development, Brussels, Belgium.

Garašić M, 1986. Hidrogeologija i morfogeneza speleoloških objekata u hrvatskom kršu. Disertacija, 1–161, Sveučilište u Zagrebu, Zagreb.

Garašić M, 1991. Morphological and Hydrogeological Classification of Speleological structures (Caves and Pits) in the Croatian Karst area. Geološki vjesnik, vol. 44, 289–300, fot. 3, sl. 4, Zagreb.

Garašić M, Cvetković M, 2012. Izvješće o rezultatima speleološke prospekcije novootvorenih kaverni I rezultati geofizičkih ispitivanja stijenske mase u neposrednoj blizini kaverni. Faculty of Civil Engineering, University of Zagreb. 1–55, Zagreb.

Kovačević T, Brečak D, 2006. Elaborat o speleološkim, geomorfološkim, meteorološkim, paleontološkim, arheološkim I biospeleološkim istraživanjima, te geodetskom I fotografskom snimanju Đurovića jame-špilje ispod platforme Zračne luke Dubrovnik u Ćilipima. DISKF Zbornik radova, Proceedings, 177–182, Zagreb.

Marković B, 1966. Osnovna geološka karta OGK, list Dubrovnik, K34–39. Savezni geološki zavod, Beograd.

Marković B, 1975. Tumač za OGK, list Dubrovnik, K34–39, 1–44, Beograd.

SOME INFORMATION ABOUT THE DEEPEST CAVES KNOWN IN CROATIAN KARST AREA

Mladen Garašić [1, 2, 3], Davor Garašić [2]

[1]University of Zagreb, Faculty of Civil Engineering, Department of Geotechnics and Geolog., Kačićeva 26, HR-10000 Zagreb, Croatia, mgarasic@grad.hr

[2]Croatian Speleological Federation, Society for the Research, Surveying and Filming on Karst Phenomena (DISKF)"Zagreb", Nova Ves 66, HR-10000 Zagreb, Croatia. dgarasic@lycos.com

[3]Croatian Academy of Sciences and Arts (HAZU), Committee for Karst, Zrinjski trg 11, HR-10000 Zagreb, Croatia. mgarasic@zg.t-com.hr

The investigation of 3 caves explored more than 1,000 meters in depth in the Dinaric karst area in Croatia, has been in progress for a considerable period of time. These are complex speleological features situated in the longest mountain range of the Dinara karst, i.e. at the Northern Velebit mountain range. In fact, these caves have been studied for over two decades now. The first one is a cave system of Lukina jama (Luke's Cave) – Trojama cave, which has been investigated until the depth of 1,421 meters (Jalžić 2007; Šmída 1993). Its total length is 3,731 m and a new expedition will soon continue to investigate this pit through speleodiving in siphons. The second greatest cave by depth is Slovačka jama (Slovak Cave), 1,320 meters in depth, with cave chanals measuring 5,677 m in total length. The third greatest cave by depth is the Cave system of Velebita, reaching down to 1,026 m in depth, with the chanal length of 3,176 m (Bakšić 2006a, b). However, another 3 speleological sites, which can rightly be added to those deeper than 1,000 m, have recently been discovered. These are three caverns that were discovered during construction of the Sveti Ilija Tunnel that passes through Mt. Biokovo, in the Dinaric karst area. These caverns undoubtedly point to the link with the ground surface, while the rock overburden above the tunnel in the zone where the caverns were discovered ranges from 1,250 and 1,350 m. Bats from the ground surface were found in the caverns and, according to measurements, they are situated in the depth from 200 and 300 m below the tunnel level. This would mean that the depth of these newly found caves ranges from 1,450 and 1,650 m, when observed from the ground surface. There are several hundreds of known caves in Biokovo, and the deepest ones discovered so far are Jama Mokre noge (Wet Feet Cave) 831 m in depth, and Jama Amfora (Amphora Cave) 788 m in depth (Bockovac 1999; Bakšić et al. 2002; Lacković et al. 2001). The investigations and surveys have been still in progress.

1. Introduction

The speleological team formed of experts from the Faculty of Civil Engineering – University of Zagreb, and the Society for the Research, Surveying and Filming on Karst Phenomena (DISKF) from Zagreb, conducted a detailed speleological investigation of the newly opened caverns, vertical spelological sites (caves), situated in the so called service tube (tunnel) of the Sveti Ilija Tunnel at KM 1+415; KM 1+193, and KM 1+637 on the route of the Zagvozd – Baška Voda link road in Dalmatia (Garašić 2009a, b, c).

According to the request placed by the client, the objective of the investigation was to prepare a documentation that will contribute to better understanding and possible repair of the speleological site crossing the tunnel line.

Already at the time of discovery of the first cavern in tunnel, a good correspondence was noted with the results of statistical processing of tectonic elements and occurrences of speleological sites, which has been conducted since 1991 upon discovery of each speleological feature during tunnel construction in Croatia. Over one thousand of caverns studied in almost fifty tunnels in Croatian karst can statistically be approximated, through their morphology and geological parameters, to the prognosis that is dependent on tectonic, lithostratigraphic and hydrogeological conditions.

The Sveti Ilija Tunnel passing through the Biokovo Mountain in the so called External karst belt is characterized by the following features. The entrance to the tunnel at the north side of Biokovo starts at KM 3+971, and the south-side exit is located at KM 8+220. The main tunnel tube is 4,250 m long. The tunnel consists of the main tube and the service tube, which are connected to one another via cross-links destined for the passage of pedestrians and emergency vehicles. The service tube is destined for the rescue and evacuation of participants in traffic in emergency situations. That is why it is first of all destined for fire-fighting vehicles and ambulances, for which an undisturbed access and manoeuvring space must be ensured. It is also used as an evacuation route for pedestrians. The main tunnel tube is 4,249 m long, while the service tube in 4,255 m long.

The traffic will be operated (in 2013) via the main tunnel tube only, as the service tube must not be used for regular traffic. The driving speed will be limited to 80 $km.h^{-1}$. In the beginning, the tunnel tube is in the right-side curve (600 meters in radius, with transition curve 200 m in length).

The main tunnel tube has two driving lanes (each 3.25 m in width) and each of these lanes has two marginal strips (0.3 m). Thus, the total pavement width amounts to 7.7 m. When two elevated pedestrian sidewalks are added (each 0.75 m in width), the highest width of the tunnel tube is 9.81 m, while the overhead clearance in the mid-pavement is 6.85 m. The width of one driving lane in the service tube is dependent on the fire-fighting vehicle width, and amounts to 3 m. There are two footways for individual rescue of pedestrians (each 0.8 m wide). The maximum width is 6.06 m, and the overhead clearance in the mid-pavement is 5.26 m. The cross sectional profile of the footway totals

1.6 m, the greatest width is 3.5 m, and the overhead clearance is 3.75 m. As the pavement structure in tunnels can not be realized in phases, it is dimensioned for the twenty-year design life. Thus, in the main tube, the pavement structure is composed of the following layers: asphalt concrete 5 cm in thickness, bituminised base course 10 cm in thickness, and mechanically compacted base course 25 cm in thickness. This all rests on the subgrade or embankment formed of stone materials. In the service tube, the pavement structure is formed of the bituminised base course (wearing course) 6 cm in thickness, and of the mechanically compacted base course 30 cm in thickness. These layers also rest on the subgrade or embankment formed of stone materials. In zones where invert is planned, the pavement structure lies on concrete subgrade. The north-side portal of the tunnel is situated at 360 m a.s.l., and the south-side one is at 224 m a.s.l. It should be noted that this tunnel has the highest overburden when compared to other road tunnels in Croatia. It locally reaches 1,380 m above the tunnel line.

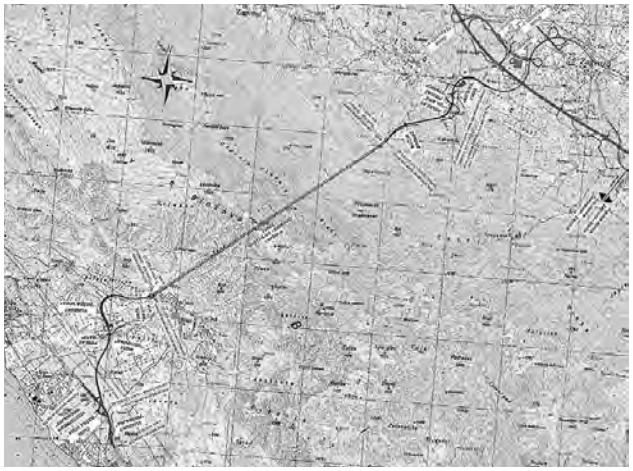

Figure 1. Map situation of tunnel "Sveti Ilija".

Interestingly, although no cavern was discovered during the works in the main tubes, as many as three vertical caverns were discovered in the main pressure and highest overburden zone of the service tube.

In addition, after discovery and study of the first cavern in the service tube of the Sveti Ilija Tunnel at KM 1+415, it was concluded that, considering the geological situation and former statistical study, an another cavern "should be located" about 200 to 250 m away from this one. The speleologists have made the corresponding note in the diary and thus warned the contractor about possible problems. Soon thereafter, the second cavern was found at KM 1+193, some 222 m away from the first one. By comparing geological parameters, tectonics and statistical processing data, the speleologists have once again predicted an another cavern which should be situated 200 to 250 m away. The corresponding note was also made in the technical diary and the speleological report. Several weeks later, a cavern was discovered at KM 1+637, i.e. precisely 222 m from the second cavern. Thus, something that no one could predict with absolute certainty has actually happened. The distance between each of the 3 caverns discovered in the service tube is 222 m, which is really amazing.

2. Geology

The rocks in which the caverns were formed belong to the Lower Cretaceous Baremian–Aptian limestones $K_1^{4,5}$, and these formations vary between 15 and 75 cm in layer thickness. The limestones are light to dark grey in colour, and brown intercalations of carbonate calcitic binder can locally be observed between the layers. In the immediate vicinity of the cave, and in the site itself, the inclination of carbonate formations varies between 45 ° and 55 °, and they strike toward the northeast (from 42 ° to 48 °). The fissures noted in the site and in its immediate vicinity are up to 10 cm wide, they are planar and smooth, very rarely filled with clayed material, and are very firm. They are more often filled with carbonate calcitic binder in crystalline or amorphous form.

Intensive joint and fault zones varying from 3 to 4 m wide are situated in each the area where the three speleological sites were discovered. Together with lithological and hydrogeological conditions, these zones have greatly influenced the genesis (formation) of the caverns under study. Mylonitic fault zones were not registered. According to speleogeological survey results, these are relatively young but presently inactive neotectonic faults, as locally proven by thin dripstone coatings that freely cover fault paraclases, especially in top parts of the cavern and, at that, they are neither fractured nor deformed (Marinčić et al. 1969a, b; Raić et al. 1968a, b; Marinčić et al. 1972a, b).

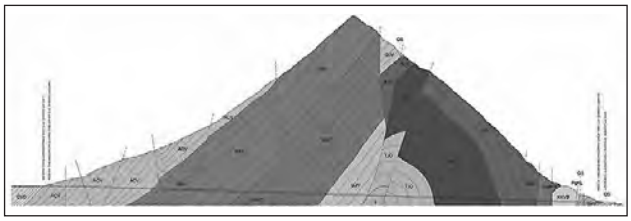

Figure 2. Geological cross section through Mt.Biokovo tunnel.

The strike of the dominant fault is 105–285°, and the paraclase is fully vertical. The corrosion of the surrounding rocks is highly intensive. In case of dolomitic limestones, it is however less pronounced than in case of pure limestones. In fact, it is most probable that dolomitic limestones are transformed, in their upper part, into calcareous dolomites. Pure limestones and dolomitic limestones could be expected closer to the reverse (thrust) contact with older formations.

These limestones, and also late-diagenetic dolomitic limestones, are crystalline, and are formed of dolomite grains distributed in form of a mosaic. Grains are filled with calcitic inclusions, and with some clay and limonite. Fossil remains have not been discovered in the cavern.

Lithologically, these sediments are Baremian-Aptian limestones and locally dolomitic limestones undergoing transition into younger Upper Cretaceous formations. Dolomites are less often found and, when found, they are in form of a continuous package in the upper and top parts of the sedimentary column, or in form of intercalations in limestones, or as the dominant member with limestone intercalations. They are mostly coarse grained, with many calcitic micro-grained inclusions of zonal distribution, and

their concentration reduces going from the centre toward periphery. They therefore correspond to metasomatic dolomites with the dolomitisation process completed, and so relicts of primary micritic structure are not visible. According to their type, these formations are calcitic dolomites (Blašković 1998).

Figure 3. Cavern at km 1+415 in Biokovo tunnel.

The tunnel runs through central lower parts of all three caverns. Thus, if viewed from the tunnel axis, the caverns spread vertically toward the ground surface, but also vertically downwards. Dolomitic intercalations locally appear as "shelves" in vertical cave segments.

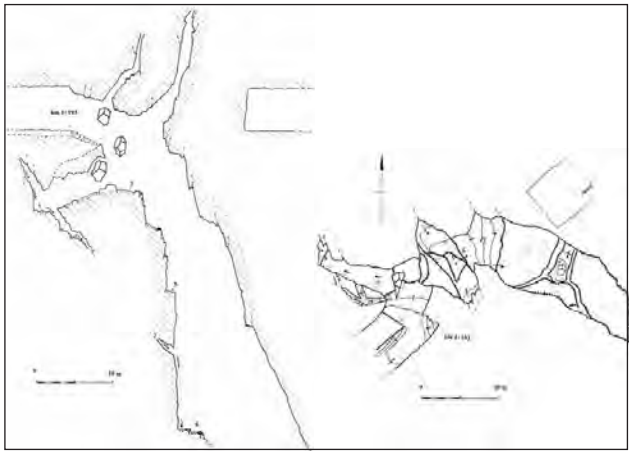

Figure 4. Cave profile and plan of cavern at km 1+193 in Biokovo tunnel.

Both the top and bottom parts of the cavern are of so called vertical or cave shape. They are characterized by generally large cross-sections, and follow the fault paraclase of E–W-trend (105–285°). The initial water, significant in the speleogenesis of these caves, had sunk through surface fissures (some of which were later on covered with clay) and has over time extended these caves to present dimensions through extensive corrosive and erosive action. These processes are still going on and, in this respect, it was noted that an intermittent stream runs through lower parts of the caverns. This steam enters the west part of the cavern through fissures and reaches the scree material at the cave bottom, and from there it continues to sink vertically further down into the underground.

These caverns show signs of karstification by gravity in their upper parts, while there are traces of regressive karstification, i.e. aggressive karstification towards the ground surface, in the bottom parts of the caverns. Rare corrosive forms were noted. The caves may be greater in size, but this could not have been determined as further passage was prevented by collapsed and unstable blocks through which the water passes intermittently. This undoubtedly points to the link with a (presently unknown) greater underground space. The difference in temperature between the discovered part of the cavern (+8.9 to +9.1 °C) and the undiscovered part of the cavern (+8.5 °C) points to the possible presence of a permanent ground water body.

From the engineering-geology standpoint, the following can be said about these Lower Cretaceous limestones or dolomitic limestones to possibly calcareous dolomites: uniaxial compressive strength of the substratum (cave-level limestones) amounts to 150 MPa, the RQD value differs, but is mostly higher than 70 percent, on an average discontinuities are spaced at 50 to 200 cm intervals, and are locally filled with clay. Cave systems sometimes exceed 20 m in length, and their usual length varies from 10 to 15 m. The joint aperture varies from 0.1 to 1 mm. In top parts joints are rough and undulating, while they are smooth in lower parts of the caverns.

According to the RMR classification, the rocks in the zone where the caves were discovered can be classified as a good rock mass (category III). This is a rock complex that was classified in the prognostic geological documentation as the second geotechnical unit.

Figure 5. Cavern at km 1+193 in Biokovo tunnel.

Figure 6. Deeper part in Cavern km 1+637 in Biokovo tunnel.

Figure 7. Cavern at km 1+415 in Biokovo tunnel.

3. Methods and Results

State of the art speleological methods were used for measuring vertical distances and geological parameters. A special attention was paid to the radon concentration measurement, and to chemical analyses of ground water.

According to current speleological site classifications (Garašić 1986, 1991), the caves discovered at KM 1+415, KM 1+193, and KM 1+637, are large-size vertical speleological sites (caves) of an elbow shaped morphological type, characterized by the occurrence of the so called "false bottoms", with heigh differences of about 297 m, 268 m and 203.5 m, respectively. This is the zone of the highest tunnel overburden (from 1,300 to 1,380 m). This means that the deepest parts of these caverns (accessed by bats from the ground surface rather than from the tunnel) sometimes extend to 200–250 m below the tunnel line. Therefore, from the standpoint of geology, these sites can be classified among the deepest speleological sites discovered so far in Dinara karst in Croatia (Garašić 1986, 1989, 1991, 1995). The depths from the ground surface range from 1,350 to possible 1,650 m.

Some speleologists will rightfully argue that no one has as yet descended into these caverns from the ground surface, and that their relative depth is smaller. Nevertheless, the objective geological depth established in this karst complex is certainly one of the greatest in Croatia. This has also been revealed by measurement of ground water properties and temperature, ^{222}Rn and ^{218}Po. It was established that these properties are comparable to those measured at other deepest speleological sites in Croatia. This will however be demonstrated during subsequent investigations.

From the hydrogeological standpoint, it can be stated that intermittent and maybe continuously active underground streams run through these speleological sites. The presence of dripping water has also been established. This dripping water exerts an intensive chemical action on the surrounding rocks (corrosion), which results in formation of underground karrens. Smaller parts of these caverns are covered with speleothems (dripstone formations). The palaeo-hydrogeological function of these caves is characterized by sinkholes on the ground surface (although their entrances are most probably now caved-in or yet undiscovered), and perhaps by a part of cave canals of a swallow hole (ponor) in the Biokovo hinterland (which is less probable because of intensive neotectonic uplift of this mountainous mass).

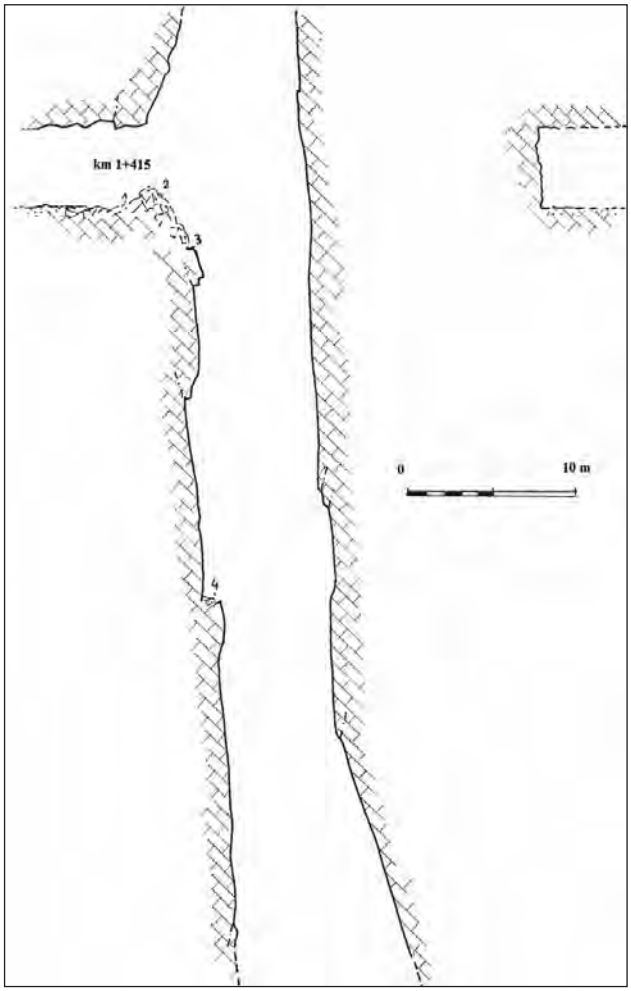

Figure 8. Cave profile of one part of cavern at km 1+415 in Biokovo tunnel.

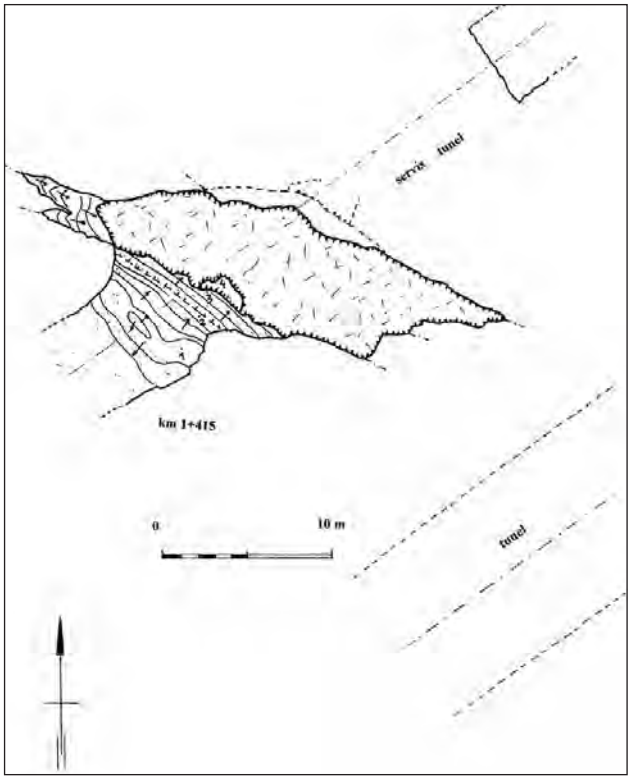

Figure 9. Cave plan of cavern at km 1+415 in Biokovo tunnel.

Inaccessible bottom, northern and eastern parts of the cavern might be linked with the speleological system of caverns passing through Biokovo and participating in

formation of submarine springs in the sea below Biokovo. In fact, the ground water found in these speleological sites has to pass either below or through the Sveti Ilija Tunnel, as it re-emerges from numerous submarine springs in the coastal area of the Makarska (from sites of Dubac to Podgora and Drašnica; Alfirević, 1969). The depth of karstification (weathering) in the zone of this speleological site is estimated at several hundreds meters, with an estimated maximum of 1,500 m, while the zone of vertical circulation ranges from 500 to 1,700 m. This is followed by the zone of inclined or horizontal circulation through which the water is carried toward the Adriatic Sea. Impermeable Triassic and maybe even Palaeozoic clastite or dolomite formations are situated in the substratum. As Triassic dolomites are from the hydrogeological standpoint permeable, due to intensive secondary porosity (jointing), it can reasonably be expected that several similar and genetically correspondent joints, formed in the anticline due to general subduction, are situated in continuation of these sites (or are parallel to them). These possible caves are not accessible from the surface and might be linked to the mentioned hydrogeological system in the lower parts of Biokovo. A note should also be made of the Pavlinovići cave situated some ten kilometres to the northeast of the tunnel, where the ground water oscillation of as many as 236 m has been registered. This information is particularly relevant for the tunnel zone approaching the impermeable substratum. In fact, such increase in the ground water level shows that sometimes in rainy season the capacity of underground chanals becomes insufficient to transport the water through Biokovo toward the sea, and so the water level rises enormously once this temporary hydrogeological barrier is reached.

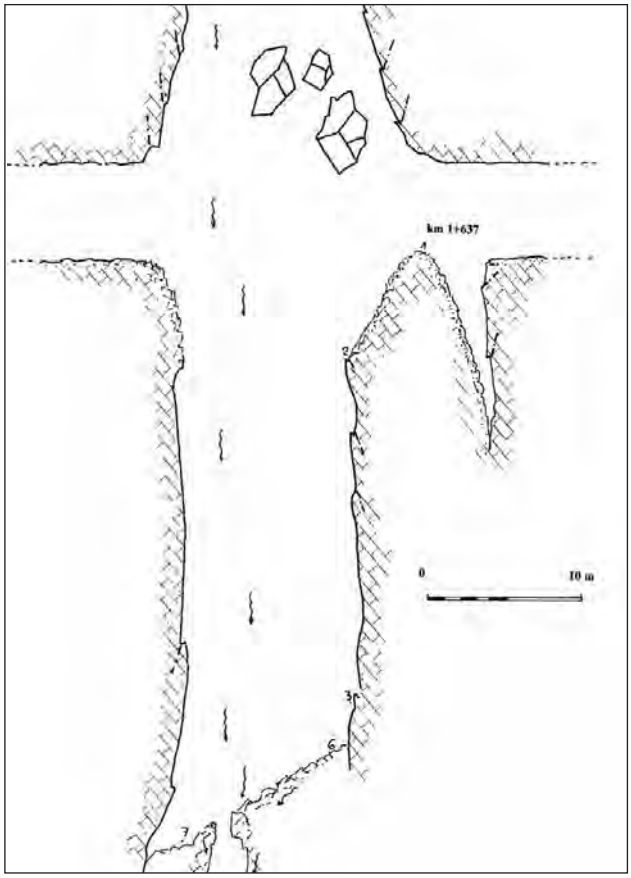

Figure 10. Cave profile and plan of cavern at km 1+637 in Biokovo tunnel.

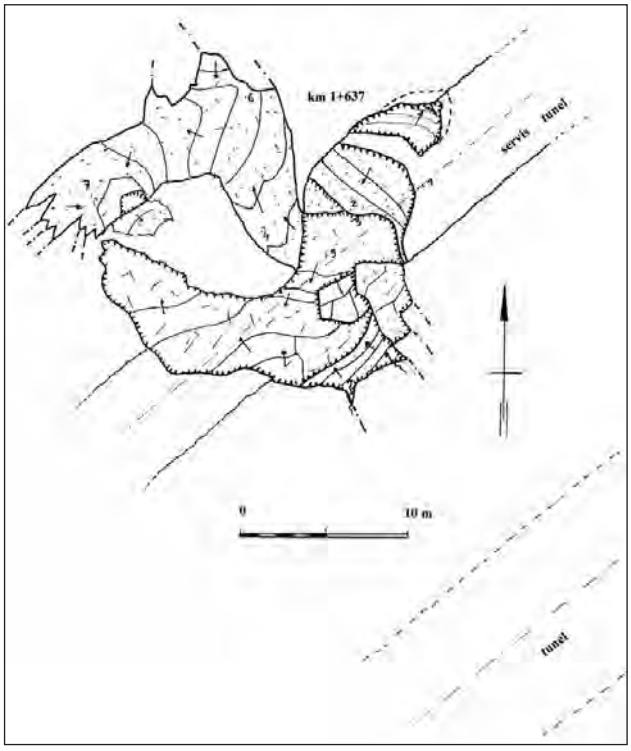

Figure 11. Cave plan of cavern at km 1+637 in Biokovo tunnel.

4. Conclusion

Based on the position, morphology and other geological characteristics of three newly-investigated vertical caves situated in the service tube of the Sveti Ilija Tunnel, it has been established that the speleogenesis of these caves can be compared with that of other deepest caves in Croatia. Although the caves were not accessed from the ground surface, i.e. their entrances are about 1,300 m below the ground surface, they have most certainly been formed under conditions of intensive weathering and can as such be analysed from the geological point as well. An excellent correspondence of their occurrence shows that statistical processing of caverns located in tunnels is finally giving some results in correlation with the tectonics. It should also be noted that a certain trace of karstification and dripstone formation has been found in Croatian karst in a deep borehole in the Adriatic Sea, where a speleothem was found at the depth of 3,125 m in a smaller cavern.

References

Alfirević S, 1969. Jadranske vrulje u vodnom režimu dinarskog primorskog krša i njihova problematika. Krš Jugoslavije 6, Zagreb.

Bakšić D, Lacković D, 2002. Jama Amfora, -614 m – najdublja jama Biokova. Velebiten 36, 16–22, Zagreb.

Bakšić D, Paar D, 2006a. Croatia and the Deep Caves of Northern Velebit. Alpine Karst, vol 2., ed. J. and T. Oliphant, 105–124, Cave books, Dayton, USA.

Bakšić D, 2006b. "Ekspedicija Velebita 2005". Velebiten 43, 2–21, SO PDS Velebit, Zagreb.

Blašković I, 1998. The two stages of structural formation of the coastal belt of the External Dinarides. Geologica Croatica, vol 51/1, Zagreb.

Bockovac Ž, 1999. Jama Amfora. Speleo'zin, 12, 7, 14–15, Karlovac.

Garašić M, 1986. Hydrogeology and Morphogenesis of the Caves in Croatin Karst. Ph.D. Thesis, 1–161, University of Zagreb, Faculty of Geology, Zagreb.

Garašić M, 1989. New conception of the morphogenesis and hydrogeology of the speleological objects in karst area in Croatia (Yugoslavia). 10. International Congress of Speleology, Procceedings, vol. 1, 234–236, s1. 8, Budapest, Hungary.

Garašić M, 1991. Morphological and Hydrogeological Classification of Speleological structures (Caves and Pits) in the Croatian Karst area. Geološki vjesnik, vol. 44, 289–300, Zagreb.

Garašić M, 1995. Speleogeneza u okviru hidrogeologije krša i procesa karstifikacije. 1. Hrvatski geološki kongres, Opatija, Zbornik radova, Proceedings, 177–182, Zagreb.

Garašić M, 2009a. Izvješće o speleološkom istraživanju, fotografskom i topografskom snimanju, te hidrogeološkim opservacijama u novootvorenoj jami (kaverni) u tunelu "Sveti Ilija" (servisna tunelska cijev), na stacionaži km 1+193, na trasi spojne ceste Zagvozd – Baška voda u Dalmaciji. University of Zagreb, 1–39, Zagreb.

Garašić M, 2009b. Izvješće o speleološkom istraživanju, fotografskom i topografskom snimanju, te hidrogeološkim opservacijama u novootvorenoj jami (kaverni) u tunelu "Sveti Ilija" (servisna tunelska cijev), na stacionaži km 1+415, na trasi spojne ceste Zagvozd – Baška voda u Dalmaciji. University of Zagreb, 1–43, Zagreb.

Garašić M, 2009c. Izvješće o speleološkom istraživanju, fotografskom i topografskom snimanju, te hidrogeološkim opservacijama u novootvorenoj jami (kaverni) u tunelu "Sveti Ilija" (servisna tunelska cijev), na stacionaži km 1+637, na trasi spojne ceste Zagvozd – Baška voda u Dalmaciji. University of Zagreb, 1–55, Zagreb.

Jalžić B, 2007. Jamski sustav "Lukina jama – Trojama". 1–156, HPS, Zagreb.

Lacković D, Bakšić D, 2001. Izvješće sa speleološkog istraživanja jame Amfora u Parku prirode Biokovo. 16, Park prirode Biokovo, Makarska.

Marinčić S, Magaš N, Benček Đ, 1972a. Osnovna geološka karta 1:100,000, list Ploče, K 33-35. Institut za geološka istraživanja Zagreb, Savezni geološki zavod Beograd.

Magaš N, Marinčić S, Benček Đ, 1972b. Osnovna geološka karta 1:100,000, tumač za list Ploèe, K 33-35. Institut za geološka istraživanja Zagreb, Savezni geološki zavod Beograd.

Marinčić S, Korolija Ž, Majcen Ž, 1969a. Osnovna geološka karta 1:100,000, list Omiš, K 33-22. Institut za geološka istraživanja Zagreb, Savezni geološki zavod Beograd.

Marinčić S, Korolija Ž, Majcen Ž, 1969b. Osnovna geološka karta 1:100,000, tumač za list Omiš, K 33-22. Institut za geološka istraživanja Zagreb, Savezni geološki zavod Beograd.

Raić V, Ahac A, Papeš J, 1968a. Osnovna geološka karta 1:100,000, list, Imotski K 33-23. Institut za geološka istraživanja Sarajevo, Savezni geološki zavod Beograd.

Raić V, Papeš J, 1968b. Osnovna geološka karta 1:100,000, tumač za list Imotski, K 33-23. Institut za geološka istraživanja Sarajevo, Savezni geološki zavod Beograd.

Šmída B, 1993. Velebit '92. Speleoforum '93, 51–52, Brno.

HYPOGENE SPELEOGENESIS AND SPELEOTHEMS OF SIMA DE LA HIGUERA CAVE (MURCIA, SOUTH-EASTERN SPAIN)

Fernando Gázquez[1,2], José-María Calaforra[1]

[1]Water Resources and Environmental Geology Research Group, Dept. of Hydrogeology and Analytical Chemistry – University of Almería, Crta.Sacramento s/n, 04120 La Cañada de San Urbano, Almería, Spain, f.gazquez@ual.es, jmcalaforra@ual.es

[2]Unidad Asociada UVA-CSIC al Centro de Astrobiología, University of Valladolid, Parque Tecnológico Boecillo, 47151, Valladolid (Spain)

Sima de la Higuera Cave (Pliego, south-eastern Spain) has been recently adapted for speleological use. Nevertheless, knowledge of the hypogenic origin of this cavity is still quite limited. The peculiar genetic mechanisms could provide added value if the cave is exploited for speleotourism. By studying geomorphological features and speleothem characteristics, it has been possible to deduce the predominant speleogenetic mechanism (whether hypogenic or epigenic) that controlled the evolution of this cave. The hypogenic mechanism that gave rise to this cavity was associated with upflow of CO_2-rich hydrothermal fluid from depth, and was unconnected to meteoric water seepage. In this paper we describe some of the geomorphological evidence and unusual speleothems in Sima de la Higuera Cave. Large scallops are found on the upper level (-74 m); these are related to the mechanism of hypogenic speleogenesis and generally indicate the direction of ascending flow. There are also corrosion crusts made of micritic calcite. In addition, bubble trails related to bubbles of rising CO_2 have been identified. Centimetric calcite spar speleothems frequently fill fractures in the host rock. Other typical hypogenic speleothems occur in this cave, including calcite raft cones, folia, cave clouds, tower coral and calcite raft deposits, all suggesting the influence of thermal water during the cave's formation. Furthermore, the first reported occurrence of calcite raft double-tower cones has been described in this cave; their origin is linked to water table oscillations in Paradise Chamber (-82 m). At the deepest level (-110 m), Mn-Fe oxyhydroxides occur as a black coating totally covering the cave walls, usually over subaerial "boxwork" formations. The wide variety of speleothems unconnected to meteoric water seepage make Sima de la Higuera Cave one of the most unusual hypogenic caves in Spain.

1. Introduction

Seepage of meteoric water in karstic terrains is the most common mechanism for cave development. However, besides this kind of cavity (epigenic caves), there is another type of genesis linked to rising hydrothermal fluids, usually rich in dissolved CO_2 and/or H_2S. These hypogenic caves form as a result of circulation of thermal water, usually from depth, and are unconnected with superficial flow (Palmer 2011). The term "hypogenic" does not refer specifically to extremely deep caves but rather to the origin of the fluids responsible for these caves' development (Klimchouk 2009). This kind of system is represented by around 5–10 % of the cavities worldwide (Forti 1996; Forti et al. 2002).

Geomorphological features and specific speleothems are the most useful tools for identifying whether the origin of a cave was hypogenic or epigenic (Audra et al. 2002). The morphologies generated by hypogene mechanisms depend on the characteristics of the host rock, the temperature at which dissolution occurs, and the nature of the gases in solution. For instance, H_2S-rich thermal water gives rise to acid attack that is more efficient than corrosion produced exclusively by CO_2 (Forti et al. 2002). Furthermore, in H_2S-rich systems, the water-rock interaction frequently results in gypsum precipitation (Palmer and Palmer, 2012).

Other morphological features typical of hypogenic conditions are bubble trails, bell-shaped condensation-corrosion domes, scallops and widespread corrosion pockets (Forti 1996).

On the other hand, the speleothems and cave minerals formed under subaqueous conditions from a solution highly saturated in calcium carbonate can provide the evidence to support a hypogenic origin of caves. For example, speleothems such as large bisphenoidal calcite crystals (Lundberg et al. 2000), calcite raft cones (Audra et al. 2002), cave clouds and folia (Audra et al. 2009; Davis 2012), tower coral and calcite raft deposits (Hill and Forti 1997) all commonly occur in hypogenic caves.

In the current paper, we describe and examine the hypogenic geomorphological features of Sima de la Higuera Cave (Murcia, South-eastern Spain), which has been recently adapted for speleological use. Together with the mineralogical and geochemical characteristics of some of its speleothems, these have enabled a preliminary model of the evolution of this cave to be established.

2. Geological setting

Sima de la Higuera (Fig Tree Cave) is located in the Sierra de Espuña, in the municipal district of Pliego (Murcia Region). Its entrance lies 485 m a.s.l. and its mouth is crowned by a large fig tree that gives the cave its name. Speleological exploration of the cave began in 1997, although there is evidence that it was discovered earlier than this date (Club Cuatro Picos and Club Pliego Espuña 2001; Ferrer 2010). Its surveyed length is 5,500 m and its deepest part is 156 m below the cave entrance (82 m below the base of the entrance sinkhole) (Fig. 1B).

The cave lies in Oligo-Miocene detrital and marly limestone (Fig. 1A). The carbonate sequence is quite fractured due to NW-SE pressure that has given rise to a series of joints and

faults that subsequently determined the cave's morphology, particularly its deeper levels. Significant hydrothermal springs currently arise in the vicinity of the cave, with temperatures ranging from 30 to 50 ºC.

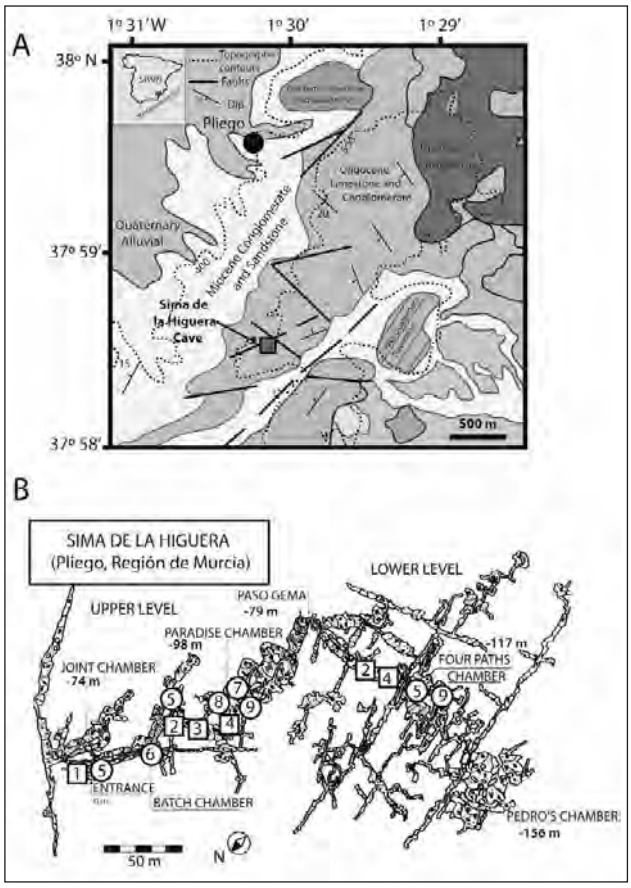

Figure 1. A. Location and geological setting of Sima de la Higuera Cave. Geological cartography modified from Kampschuur et al. (1972); B. Location of the main hypogenic geomorphological features (squares) and speleothem formations (circles) in Sima de la Higuera Cave (topography by the Cuatro Picos and Pliego-Espuña caving clubs (2001): 1. Scallops, corrosion domes and alteration crusts; 2. Bubble trails; 3. Bubble grooves on mammillary crusts; 4. Boxwork and ferromanganese coatings; 5. Calcite "spars" infilling fractures; 6. Tower coral; 7. Calcite raft cones; 8. Folia and cave clouds (mammillary crusts); 9. Piles of calcite rafts.

The cave contains strong evidence of a hypogenic origin. In this study, we use the term "hypogenic" as postulated by Palmer (2011), who suggested that hypogenic caves form due to the upward flow of deep-seated water, or by solutional aggressivity generated at depth below the ground surface. In Sima de la Higuera Cave the hypogene speleogenetic mechanisms are evidenced by the presence of different types of speleothems and geomorphological features typical of hypogenic caves, such as calcite raft cones, tower cones, cave clouds (mammillary crusts), folia, specific corrosion forms, cupola, condensation domes and scallops.

Further evidence comes from the fact the ambient cave temperature is higher than the annual mean outside temperature of 13.8 ºC. The current cave temperature oscillates between 18.6 ºC and 21.7 ºC, increasing slightly in the deeper parts, and this indicates a significant positive thermal anomaly. Relative humidity of the cave air is between 87.5 and 90 % (Club Cuatro Picos and Club Pliego Espuña 2001).

Although the evidence points to deep hydrothermal water flowing through the caves in the past, present-day water inflow is entirely from infiltration of meteoric water. There are only a few vadose speleothems generated from dripwater (stalactites, stalagmites, etc.) in the shallowest levels, around -74 m, and above the level of Bath Chamber.

3. Methodology

3.1. Inventory of speleological features and sampling

The speleothems and the speleogenetic forms of the Sima de la Higuera Cave were inventoried and photographed for classification and analysis. The locations of these features were included on the topographical map drawn by the Cuatro Picos and Pliego-Espuña caving clubs (2001).

The cave cones of the Paradise Chamber were inventoried and positioned relative to a topographic station located -85.2 m below the cave entrance. Distances were measured using a laser-distance meter Disto A3 of Leica Geosystems AG® and an upgrade kit (DistoX) which adds a 3-axis compass, clinometer and a Bluetooth connection. This wireless instrument was connected to a PDA device where data were stored. Calibration was performed using Palm OS software designed by Luc Leblanc and adapted for the topographical Auriga software.

A fragment of a dark-coloured "boxwork" blade (SHG) was taken from the roof of the Manganese Gallery, situated in one of the deeper levels of Sima de la Higuera Cave, at the -110 m level (Fig.2H, I). The sample comprised a mineral lamina, 5–10 mm thick with a sugary texture, whose outer surface was covered by dull greyish-blue deposits, rough in texture.

One sample of a calcite raft consisting of thin, brownish calcite laminae (CR-01) was collected from the Paradise Chamber (-85 m). Lastly, a sample of powdered raft calcite was taken from the Four Paths Chamber (-117 m) where the piles of white raft calcite reach up to 2 m high (CR-02) (Fig. 2E).

3.2. Analytical methodology

SEM microphotographs were taken using a HITACHI S-3500 instrument in high vacuum mode. The samples were previously dried and coated with graphite to increase electron transmissivity. The elemental chemistry was determined by EDX (Energy Dispersive X-ray Spectroscopy) microprobe at two points with different typology over the *boxwork* sample (Fig. 5).

Microanalyses employed the same instrument coupled to an Oxford INCA 7210 X-ray detector. The diameter of the beam was approximately 1 μm. (Table 1). Carbon concentration was not measured due to masking by the graphite coating. Quantitative chemical analysis of samples was done using X-ray fluorescence (wavelength dispersive XRF) with a BRUKER S4 Pioneer instrument.

A subsample of dark material of the boxwork from Manganese Gallery (CMN) was extracted using a needle for subsequent mineralogical analysis by XRD (X-Ray Diffraction). The mineralogy of the internal crystalline

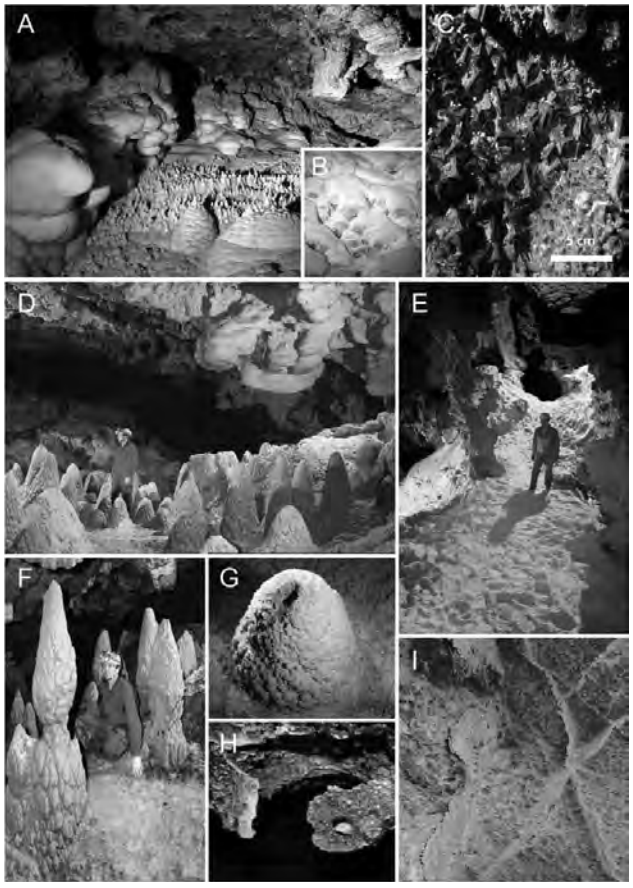

Figure 2. Speleothems linked to the hypogenic origin of Sima de la Higuera Cave. A. Tower coral (floor), cave clouds (wall) and folia (ceiling) in the Bath Chamber level; B. Folia; C. Calcite "spar" crystals coated with ferromanganese oxyhydroxides; D. Calcite raft cones and cave clouds in Ghost Chamber; E. Piles of calcite rafts in Four Paths Chamber; F. Double-tower raft cones in Paradise Chamber; G. "Volcano cone" in Ghost Chamber; H and I. Boxwork and ferromanganese coatings in Manganese Gallery (Photos: Víctor Ferrer).

laminae was also determined by XRD of a powdered sample. The calcite raft samples (CR-01 and CR-02) were crushed and analyzed by XRD. Mineral analysis using XRD used a BRUKER APEX CCD area detector. The geochemical and mineralogical analyses were performed in the Servicios Centrales de Investigation of the University of Almería (Spain).

4. Results

Observations led us to identify three zones with different morphological appearances in Sima de la Higuera Cave:

(1) The mouth of the cave gives access to a subvertical sinkhole 74 m deep, which is developed along the length of a diaclase running E-W, which finally opens out in Junction Chamber. This chamber and the galleries that communicate with it form one of the upper levels of the cave, which also run E-W. On this level appear several, small perched lakes (Coral Lake and Bath Chamber).

The temperature of the lake water is 19.8 ± 0.5 ºC, similar to the cave air (20.2 ±2.2 ºC), while pH (8.10), conductivity (550 µS/cm) and HCO_3^- concentration (220 mg/l) are typical of cave infiltration water. This fact suggests that the only water inflow to these lakes come from dripwater following infiltration of meteoric water through the carbonate rock overlying the cave. Dripstones like stalagmites and stalactites are scarce in this cave level; however, some examples can be observed around the lakes.

Typical features of phreatic speleogenesis such as scallops, cupolas and bell-shaped condensation domes appear in this area (Fig. 3A). Furthermore, dissolution forms like bubble trails (Fig. 3C) and alteration calcite crusts (Fig. 3B) are seen above the -85 m level.

(2) Beyond this point, the cave morphology changes considerably, with larger galleries and chambers, such as Ghost Chamber and Paradise Chamber, which occupy an intermediate level (-85 m).

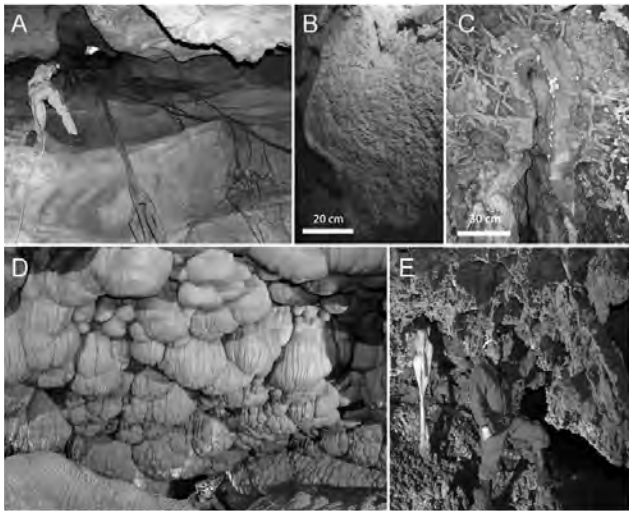

Figure 3. Features related to the hypogenic origin of Sima de la Higuera Cave: A. Scallop in the entrance shaft; B. Alteration calcite crusts; C. Bubble trails and boxwork; D. Bubble grooves on cave clouds in Ghost Chamber; E. Corrosion forms due to acid dissolution appear in several places inside the cave. (Photos: Víctor Ferrer).

This cave level accommodates speleothems such as calcite spars that fill fractures in the host rock, cave clouds, folia, tower coral and calcite raft cones (Fig. 2), all of them indicative of epiphreatic conditions during their precipitation.

Of particular note are the calcite raft cones present in Ghost Chamber. In Paradise Chamber, 92 cave cones have been inventoried (Fig. 5) displaying two different morphologies. Thirty-seven of them can be considered as tower cones (or simple-tower cones), whilst the remaining fifty-five cones have a notch in the middle and look like two cones, one superimposed over the other (Fig. 2F).

(3) Lastly, the deepest levels include labyrinthine galleries (three-dimensional "maze caves") that are smaller in size and typical of hypogenic caves (Klimchouk 2009). Features like *pendants*, related to phreatic dissolution-corrosion have been identified in this level. Boxwork formations and ferromanganesic deposits also appear, particularly in Manganese Gallery (-110 m level) (Gázquez et al. 2012) (Fig. 2H).

The SEM microphotographs enabled two visibly different zones to be identified (Fig. 4B). The first comprises sub-millimetric euhedral calcite crystals, some of which have a sphenoidal habit with well-defined faces and edges. The

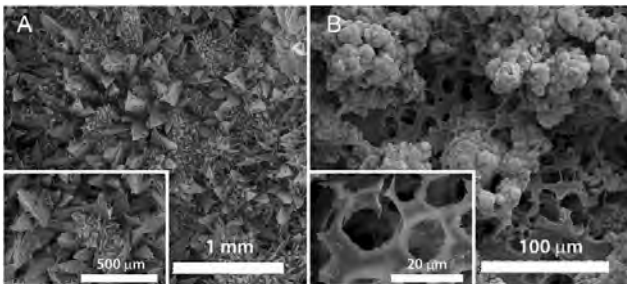

Figure 4. Secondary electron images of (A) calcite rafts from Four Paths Chamber and (B) ferromanganese coatings on the boxwork of Manganese Gallery.

Table 1. Elemental composition of the samples analyzed by X-ray fluorescence (XRF) and EDX microprobe. Analytical errors ranged from ±0.33‰ for oxygen to ±0.13‰ for aluminum. Errors for Fe and Mn were better than ±0.2‰ (n.a = not analyzed; n.d = non detected).

Elements (% wt)	CR-01^{XRF} (-117 m)	CR-02^{XRF} (-98 m)	CMNcal^{EDX} (-110 m)	CMNmn^{EDX} (-110 m)
Ca	52.8	51.8	38.1	2.3
O	22.2	22.4	50.8	34.8
C	n.a	n.a	n.a	n.a
Mg	0.111	0.110	n.d	0.7
Sr	0.0616	0.0603	n.d	n.d
Mn	0.0032	0.0051	2.1	38.2
Fe	0.0621	0.173	1.5	10.3
Si	0.324	0.778	0.7	2.4
Al	0.149	0.465	n.d	2.8
K	0.0341	0.104	n.d	n.d
P	0.261	0.0961	n.d	n.d
S	0.103	0.0918	n.d	n.d

calcite mineralogy of this lamina was confirmed using XRD. EDX analysis revealed traces of Mn, Fe and Si, in addition to Ca, C and O (CMNcal, Table 1).

Over this mineral lamina appear botryoidal structures. EDX analysis of their chemical composition indicated Mn concentrations of up to 38.2 % wt, and Fe of up to 10.3 % wt. Other elements like Na, Al and Si were present in quantities below 3 % wt.

The XRD analyses revealed that this patina is composed of todorokite ($NaMn_6O_{12}\cdot 3H_2O$) (22 %), pyrolusite (MnO_2) (16 %), in addition to the calcite (42 %) and amorphous phases (20 %), probably poorly crystalline Fe oxyhydroxides (CMNmn, Table 1).

Finally, the samples of calcite raft analyzed were composed exclusively of calcite, though the XRF analyses revealed traces of Si, Mg, P, S and other minor elements. The composition of samples taken from Paradise Chamber (CR-01) and Four Paths Chamber (CR-02) were similar (Table 1).

5. Discussion

5.1. Speleogenetic forms and dissolution-corrosion features

Sima de la Higuera Cave hosts a great number of morphological features and speleothems, indicating that its origin is not linked to seepage of meteoric water.

Typical features of hypogenic speleogenesis, such as white micritized rind and alteration crusts, appear in the upper levels and in the entrance sinkhole (Fig. 3B). The origin of these elements is usually connected to interactions between carbonate host rock and acid hydrothermal water (Palmer and Palmer 2012). Furthermore, forms typical of phreatic speleogenesis, such as the large scallop (Fig. 3A) identified along the diaclase that gives access to the main galleries, suggest slow upward flows during the speleogenetic stages. Besides, cupola and corrosion domes in the upper levels of the aquifer indicate interactions between the carbonate rock and the thermal water in its gaseous phase (due to lower hydrostatic pressure) here.

Bubble trails have been identified on the ceiling in the intermediate levels, for instance, around Bath Chamber (Fig. 3C). Such features also formed due to acid aggressivity of thermal water; however in this case, gases (CO_2 and/or H_2S) were released as bubbles that rose along preferential trails (Forti 1996) that eventually carved channels on the cave ceiling.

Other features related to rising CO_2 bubbles were observed on the ceiling of Ghost Chamber (-85 m). Grooves several centimeters deep appear on the mammillary crust (cave clouds) that covers the ceiling of this chamber (Fig. 3D). When this cave level was under water, CO_2 degassing caused bubble trails on the hemispherical surface of the cave clouds. The continuous trail of rising bubbles led to dissolution-corrosion of the calcite crusts.

Thermal water accessed the intermediate cave level mostly through a large fracture in the floor of Paradise Chamber (-98 m). This diaclase seems to have acted in the past as a feeder of deeper thermal water into this chamber.

The cave forms found below the level of Paradise Chamber differ substantially from those in the upper levels. The are no dissolution features due to CO_2 bubbles. Instead, “pendants”, a cave form typical of phreatic dissolution, indicate a different mechanism of carbonate dissolution. The difference was determined by the different hydrostatic pressure of the solution containing the dissolved CO_2. As the thermal water flowed toward the upper levels, the hydrostatic pressure fell and the volume of the gaseous phase increased. As a result, larger bubbles formed and these followed preferential trails that carved vertical dissolution grooves and channels.

Other dissolution-corrosion forms, in this case generated under vadose conditions, appear in the lower cave levels. Dissolution-corrosion mechanisms affected the cave walls when the water table dropped and left the cave exposed. Wet CO_2-rich air entered from lower levels and condensed on the slightly cooler cave walls and ceiling. Dissolution of the host rock by the condensed water increased as a result of the high CO_2 partial pressure in the cave atmosphere (Sarbu and Lascu 1997). Current CO_2 levels in the cave reach 2000 ppm and may have been even higher in the past due to degassing of hydrothermal water below the cave galleries.

Dissolution-corrosion forms are particularly striking in Manganese Gallery (-110 m). Boxwork and ferromanganese coatings on the cave walls have been described (Fig. 2H, I) whose origin lie in (1) the

precipitation of sparitic calcite veins in the fissures of the carbonate host rock when the cave was submerged in thermal water; and (2) the corrosion of carbonates by acid generated from CO_2 diffusion into the condensed water, and oxidation of reduced Fe-Mn under aerobic conditions. The acid attack preferentially dissolved the carbonate host rock (which has a microcrystalline structure), while the veins of sparitic calcite were more resistant to corrosion. As a result, the calcite blades now project into the cave in the form called *boxwork* (Gázquez et al. 2012).

On a microscopic scale, the Fe-Mn oxyhydroxides are botryoidal structures over a visibly altered sugary-textured calcite substrate (Fig. 4B). Oxidation of manganese and iron from the host rock gave rise to protons that acidified the medium, so lead to corrosion of the calcite beneath (Gázquez et al. 2012).

5.2. Hydrothermal speleothems

Sima de la Higuera Cave contains a wide variety of speleothems of subaqueous origin which were generated from a solution highly saturated in calcium carbonate. As a general rule, this type of speleothem precipitates out from hydrothermal solutions that have a high CO_2 content, frequently related to dissolution of the host rock during the genesis of the cave.

Nevertheless, some cases have been reported where subaqueous speleothems (calcite raft cones, folia, etc.) have been generated from cold water in epigenic caves (Davis 2012). Notwithstanding, the relatively high ambient temperature of Sima de la Higuera Cave (up to 6 ºC higher than the annual mean temperature outside the cave) clearly points to this cavity retaining residual heat from an earlier hypogenic stage.

Speleothems in Sima de la Higuera are not randomly distributed; rather, there is a gradation from the base of the cave towards shallower levels. This fact suggests that speleothem precipitation was controlled by the saturation state in calcite of the water, which in turn was conditioned by the hydrostatic pressure of the solution. Thus, crystallization of larger calcite crystals (Fig. 2C) was favoured in the lower cave levels, where slower CO_2 degassing caused low calcite supersaturation leading to slower calcite precipitation. As the hydrothermal fluid rose, CO_2 degassing intensified, resulting in other kinds of phreatic speleothems, such as cave clouds and folia (Fig. 2A, B) in the intermediate levels of Sima de la Higuera Cave. These type of speleothems usually form near the water surface (Audra et al. 2009; Davis 2012), where CO_2 degassing is more active and calcite precipitation faster than in the levels beneath. In some places, crusts of microcrystalline calcite cover the walls and ceiling of the intermediate levels (Fig. 2D).

More recently, the groundwater level gradually fell and the water table intercepted the intermediate cave levels. In such a situation, precipitation of calcite raft laminae was favoured on the water surface due to intense evaporation and CO_2 degassing. Significant temperature and pCO_2 differences between the thermal water and the cave atmosphere triggered rapid precipitation of calcite rafts.

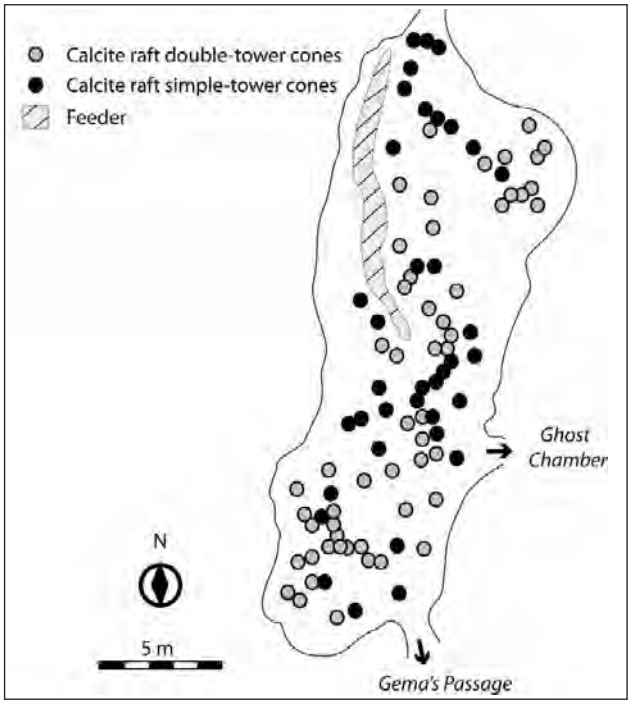

Figure 5. Spatial distribution of cave cones in Paradise Chamber of Sima de la Higuera Cave, distinguishing simple-tower cones (n =37, in black) and double-tower cones (n =55, in grey).

This process would have started in the upper levels; nowadays however, calcite raft deposits are scarce in this shallower level as they would have been eroded during subsequent vadose stages. By contrast, there are abundant calcite raft piles in deeper levels, like Paradise Chamber and Four Paths Chamber (Fig. 2E).

On a microscopic scale, the calcite rafts in Sima de la Higuera Cave display well-developed faceted crystals (Fig. 4A). This kind of *dogtooth* calcite crystal often precipitates at a low-medium temperature (Lundberg et al. 2000). A similar trace element composition of the calcite rafts at -82 and -110 m depth points to the precipitation of calcite laminae with similar characteristics.

When the weight of the crystalline laminae is greater than the surface tension can support, rafts of calcite sink and accumulate on the pool bottom. Since the drips fall consistently at one point over a long period, piles of rafts lamina accumulate on the pool bed forming a cone-shaped speleothem, dubbed cave cones (Hill and Forti 1997). In Sima de la Higuera Cave, cave cones are particularly significant in the Ghost and Paradise Chambers (Fig. 2D, F, G).

A new variety of cave raft cones has been recently discovered in Paradise Chamber, called “calcite raft double-tower cones” (Fig. 2F) (Gázquez and Calaforra 2012). They represent 60 % of the cave cones in this chamber (Fig. 5). The unusual shape of these speleothems is explained by an intermediate phase of rapid calcite precipitation of uncemented calcite rafts covering cave cones formed in previous stages. When conditions favouring slow calcite raft formation were restored, new cave cones were formed exactly on top of some of the earlier cones (Gázquez and Calaforra 2012).

The phreatic/epiphreatic conditions ceased when the water table definitively left the cave. Under the new vadose

conditions, condensation and corrosion processes took over as dripwater became the main source of water to the cave. In some cases, a subtype of cave cone was formed as the water dripping onto the cave cones, being subsaturated in calcite, gradually drilled a hole in the apex of the cone, giving rise to the so-called "volcano cones" (Fig. 2G).

Finally, tower coral speleothems appear near Bath Chamber (Fig. 2A). These subaqueous speleothems, less than 10 cm high, formed in a shallow pool where evaporation caused the near-surface water to be slightly more saturated with respect to calcite than the water nearer the pool bottom (Hill and Forti 2007). This mechanism favored the vertical cone-shaped structure of these speleothems.

6. Conclusions

The geomorphological characteristics and subaqueous speleothems of Sima de la Higuera Cave are related to rising hydrothermal water. Speleothems in Sima de la Higuera are not randomly distributed over the vertical cave profile but show a gradation from the base to the top of the cave, suggesting that calcite precipitation and dissolution-corrosion forms were determined by the hydrostatic pressure of the solution.

Acknowledgments

The authors are grateful for the support of Andrés Ros, Pepe Liza and the Speleoclub "G40" during the field work. Financial support was made available through the Spanish Science Grant AP-2007-02799, the Project "RLS Exomars Science" (AYA2011-30291-C02-02; Ministry of Science and Innovation, Spain and FEDER funds of EU). The authors thank Víctor Ferrer for his kind permission to use photographs to illustrate this paper. Sarah Steines is also acknowledged for improving our English.

References

Audra Ph, Bigot JY, Mocochain L, 2002. Hypogenic caves in Provence (France). Specific features and sediments. Acta Carsologica, 31(3), 33–50.

Audra Ph, Mocochain L, Bigot JY, Nobécourt, JC, 2009. The association between bubble trails and folia: a morphological and sedimentary indicator of hypogenic speleogenesis by degassing, example from Adaouste Cave (Provence, France). International Journal of Speleology, 38(2), 93–102.

Club Cuatro Pico, Club Pliego Espuña, 2001. Sima de la Higuera. El mayor complejo subterráneo topografiado de la Región de Murcia. Subterránea, 16, 35–41.

Davis DG, 2012. In defense of a fluctuating-interface, particle-accretion origin of folia. International Journal of Speleology, 41(2), 65–74.

Ferrer V, 2010. La Sima de la Higuera (Pliego-Murcia). 80.

Forti P, 1996. Thermal karst systems. Acta Carsologica, 25, 99–117.

Forti P, Galdenzi S, Sarbu SM, 2002. The hypogenic caves: a powerful tool for the study of seeps and their environmental effects. Continental shelf research, 22, 2373–2386.

Gázquez F, Calaforra JM, Rull F, 2012. Boxwork and ferromanganese coatings in hypogenic caves: an example from Sima de la Higuera Cave (Murcia, SE Spain). Geomorphology, 117–118, 158–166.

Gázquez F, Calaforra, JM, 2012. Origin of the double-tower raft cones in hypogenic caves. Earth Surface Processes and Landforms (accepted).

Hill CA, Forti P, 1997. Cave minerals of the World 2. National Speleological Society, Huntsville. 461.

Klimchouk AB, 2009. Morphogenesis of hypogenic caves. Geomorphology, 106, 100–117.

Kampschuur W, Langeberg CW, Montenat Ch, Pignatelli R, Egeler CG, 1972. Mapa Geológico de España 1:50,000, hoja nº 933 (Alcantarilla). IGME, Madrid.

Lundberg J, Ford DC, Hill CA, 2000. A preliminary U-Pb date on cave spar, Big Canyon, Guadalupe Mountains, New Mexico. Journal of Cave and Karst Studies, 62(2), 144–148.

Palmer AN, 2011. Distinction between epigenic and hypogenic maze caves. Geomorphology, 134, 9–22.

Palmer MV, Palmer AN, 2012. Petrographic and isotopic evidence for late-stage processes in sulfuric acid caves of the Guadalupe Mountains, New Mexico, USA. International Journal of Speleology, 41(2), 231–250.

Sarbu SM, Lascu C, 1997. Condensation corrosion in Movile Cave. Journal of Karst and Cave Studies, 59, 99–102.

THE APPLICATION OF GIS METHODS IN MORPHOMETRICAL ANALYSIS OF DOLINES ON LIMESTONE AND DOLOMITE BEDROCK

Petra Gostinčar
Karst Research Institute ZRC SAZU, Titov trg 2, SI-6230 Postojna, Slovenia, petra.gostincar@zrc-sazu.si

The dolines are considered to be a "diagnostic" karst landform. In this paper a GIS method, which was developed for the automatic delineation and classification of karst depressions (Obu 2010), was used for a study of morphometrical characteristics of dolines on limestone and dolomite bedrock. The spatial extent of auto-delineated dolines was compared to the manually delineated dolines from topographic maps. The analysis was conducted on three case study areas.

The morphometrical characteristics of auto-delineated dolines show that the dolines on dolomite are larger in area but shallower. Their slopes are not as steep as the slopes of the limestone dolines and they are less regular-shaped. On the other hand, the dolines on limestone are smaller in area but deeper and their slopes are steeper. Their shape is more circular.

This method, when used on DEM of higher resolution (e.g., LIDAR DEM) and a greater number of case study areas, could be used as an efficient tool for determining the characteristics of dolines on various bedrock and even as a part of computer-based detection of bedrock (geological mapping) in karst areas.

1. Introduction

Geomorphometry is the science of quantitative land surface analysis. It offers a modern and analytical approach to the geomorphological analysis of the landscape with the use of digital elevation model (DEM) data and parametrization software. With the rapid increase of sources of DEMs today the methods of geomorphometry are more and more attractive to conduct (Pike et al. 2009).

For the analysis of karst surface the methods of general geomorphometry alone (e.g., Wood's method (Wood 1996), method of Surface Specific points (Peucker and Douglas 1975), the use of supervised and unsupervised classification (MacMillan et al. 2000)) or methods of specific geomorphometry applicable to the fluvial or any other geomorphic system (MacMillan and Shary 2009) do not provide good results as they are not adjusted for detection of specific karst landforms.

The dolines are considered to be a "diagnostic" karst landform (Ford and Williams 2007). A number of attempts of auto-delineation of dolines and similar features (e.g., craters) with the use of DEMs and satellite images have been described in the literature (Portugal et al. 2004; Guimarães et al. 2005; Matsumoto et al. 2005; Krøgli et al. 2007; Siart et al. 2009; Suma et al. 2010; etc.).

In this paper a GIS method, which was developed for the automatic delineation and classification of karst depressions (Obu 2010), was used for a study of morphometrical characteristics of dolines on limestone and dolomite bedrock. The results of GIS auto-delineation using DEM and manual delineation of dolines on topographic maps were compared. Later on, a comparison of characteristics of dolines on dolomite and bedrock obtained by auto-delineation was made.

2. Characterisation of study area

In Slovenia karstic i.e. carbonate rocks (mainly limestones and dolomites) cover 43 % of the surface (Figure 1) – approximately 35 % of the surface is on limestone and about 8–12 % on dolomite (Gams 2003). Limestone and dolomite areas in Slovenia interchange on small distances as the area is fractured into numerous smaller segments due to sedimentary and tectonic modifications.

Because of chemical and physical characteristics of the two rock types, karst on limestone and dolomite is different. Dolines are a common surface karst feature of Slovenian (Dinaric) karst and are present on both, dolomite and limestone areas.

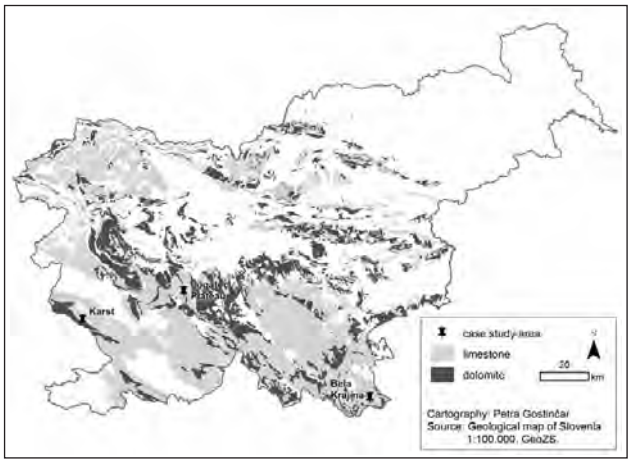

Figure 1. Distribution of limestone and dolomite in Slovenia with marked case study areas.

The analysis of morphological characteristics of dolines was conducted on tree case study areas: the Karst, the Logatec Plateau and Bela Krajina (Figure 1).

The Karst Plateau (the Classical Karst) is situated in western part of Slovenia on elevation 220–290 m a.s.l., with an average yearly temperature 10.9 °C and 1,399 mm of precipitation (1971–2000; ARSO 2011).The case study area is situated on bedded granular Cretaceous dolomite (2.4 sq km) and platy laminated Cretaceous limestone (1.9 sq km) (Figure 2).

The Logatec Plateau is situated in central part of Slovenia on elevation 530–640 m a.s.l., with an average yearly

temperature 8.7 °C and 1,587 mm of precipitation (1971–2000; ARSO 2011). The case study area is situated on Jurassic dolomite (0.7 sq km) and Jurassic limestone (0.6 sq km) (Figure 3).

Bela Krajina is situated in the south-eastern part of Slovenia on elevation 260–310 m a.s.l., with an average yearly temperature 10.4 °C and 1,257 mm of precipitation (1971–2000; ARSO 2011). The studied area is situated on Jurassic dolomite (1.4 sq km) and Cretaceous limestone (1.3 sq km) (Figure 4).

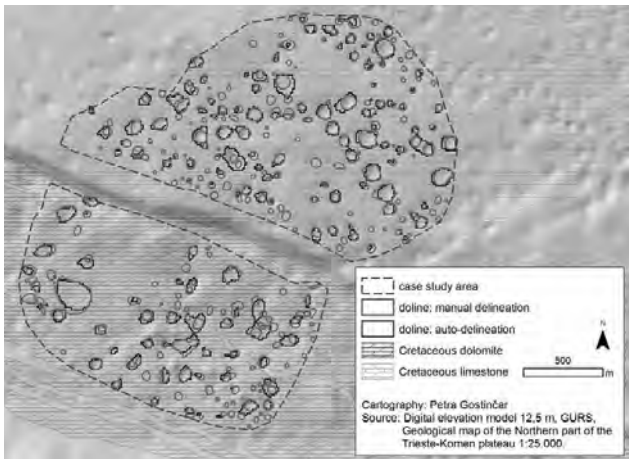

Figure 2. Case study area 1: Karst.

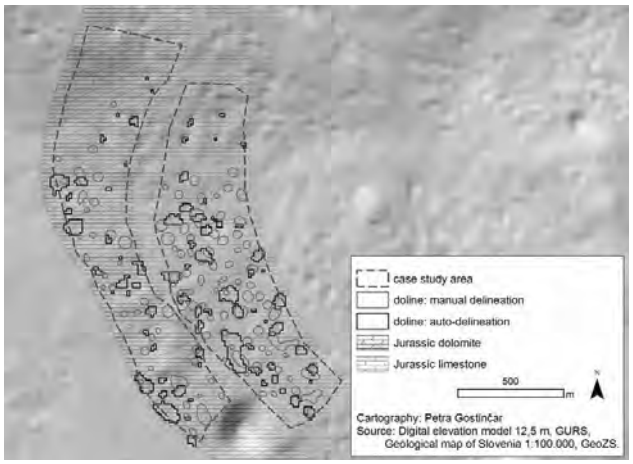

Figure 3. Case study area 2: Logatec Plateau.

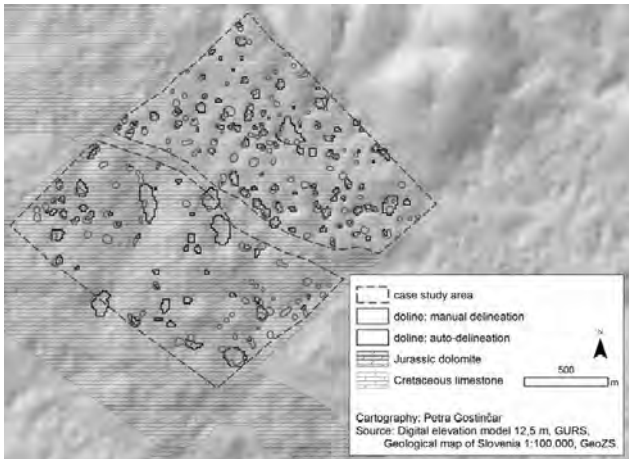

Figure 4. Case study area 3: Bela Krajina.

3. Method

3.1. Auto-delineation of depressions on karst (Obu 2010)

A GIS method for automatic delineation and classification of karst depressions has been developed by Obu (2010). The delineation of karst depressions is conducted on the basis of the lowest elevation of depression watershed border cells. This elevation represents the level on which water starts to flow out of the depression when it is theoretically filled with water. The method introduces the existence of karst depressions on different levels. In our research the depression detected on "level 1" were used for the morphological analysis. For the analysis ArcGIS software (the Spatial Analyst extension) was used, as it supports the Python programming language in which the script was written.

The second part of the developed method is karst depression classification based on a number of attributes calculated for each depression. These attributes (e.g., area, circumference, depth, volume, average diameter, the length of the shortest axis through the centroid of a doline, the length of the longest axis through the centroid of a doline, roundness, the highest elevation, the lowest elevation, mean elevation, lowest slope, highest slope, mean slope, mean curvature, area of flattened part of doline, percentage of flattened floor comparing to the area of doline etc.) are stored in a database. A database with morphological characteristics for each delineated doline was used for comparison of morphological characteristics of dolines on neighbouring dolomite and limestone areas.

Auto-delineation of dolines with GIS was conducted on DEM with a resolution 12.5 m (provided by Surveying and Mapping authority of Republic of Slovenia – GURS). It was produced in 2005 with a method of data integration. An average height accuracy of the DEM is 3.2 m (Podobnikar 2008).

3.2. Manual delineation

The dolines were also manually delineated (digitized) on topographic maps with a scale of 1:5,000 (provided by Surveying and Mapping authority of Republic of Slovenia – GURS). The contour interval of these topographic maps is 10 m.

With the manual delineation of the actual extent of dolines on case study areas the method of auto-delineation of depressions could be evaluated.

At the beginning the comparison between the manually delineated and auto-delineated depressions was made.

4. Results

When comparing the number of delineated dolines it was calculated that auto-delineation was able to detect from 45 % up to 87 % of dolines comparing to manual delineation (Figure 5). In most cases the smaller depressions were not

detected with GIS as the resolution of DEM 12.5 m is not suitable for their recognition. Details of the relief smaller than 12.5 m (cell size) cannot be detected as well as those up to 17.7 m (length of the diagonal of cells). This is especially visible at case study area of Logatec Plateau (Figure 3) where a large number of smaller depressions went undetected. Obu (2010) determined that only dolines with diameter greater than 30 to 50 meters are successfully recognised on a DEM 12.5 m. In many cases the spatial extent of manually delineated and auto-delineated dolines does not overlap entirely (see Figures 2, 3, and 4).

Table 1. Comparison of number of manually- and auto-delineated dolines.

	Manual delineation		Auto-delineation	
Case study area	**detected dolines**	**Dolines / km²**	**Detected dolines**	**Dolines / km²**
Dolomite	247	55	132	30
1 – dolomite	104	43	51	21
2 – dolomite	39	59	34	51
3 – dolomite	104	74	47	33
Limestone	431	113	243	64
1 – limestone	180	96	107	57
2 – limestone	71	111	46	72
3 – limestone	180	140	90	70

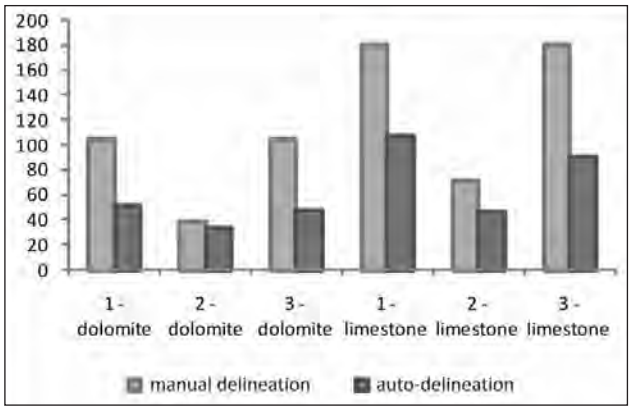

Figure 5. Number of detected dolines.

A number of attributes of auto-delineated depressions were calculated. The results of analysis show a great variation when comparing the three case study areas. There is more variation of the parameters when comparing individual case study areas than the dolines according to the rock type. However, some general characteristics of the dolines on limestone and dolomite were determined.

The mean volume of auto-delineated dolines on dolomite (3,375 m^3) is slightly bigger than of those on limestone (3,208 m^3); however the maximum volume is bigger on limestone (61,373 m^3) than on dolomite (53,683 m^3). On the other hand the average depth is smaller on dolines on dolomite bedrock (1.5 m; average depth of dolines on limestone is 1.8 m), and the mean circumference is much larger (213.3 m on dolomite; 180.8 m on limestone). The average slope of dolomite dolines (3.5°) is smaller than of those on limestone (4.2°). Additionally, the mean roundness of dolines on dolomite is slightly smaller (0.6 on limestone; 0.7 on dolomite). The mean area parameter shows that the dolines on dolomite cover an approximately 30 % larger area than dolines on limestone, and the percentage of flattened floor comparing to the area of doline is on average slightly bigger (dolomite: 3.4 %; limestone: 3.2 %).

The morphometrical characteristics of auto-delineated dolines show that the dolines on dolomite are larger in area but shallower. Their slopes are not as steep as the slopes of the limestone dolines and they are less regular-shaped. On the other hand, the dolines on limestone are smaller in area but deeper and their slopes are steeper. Their shape is more circular.

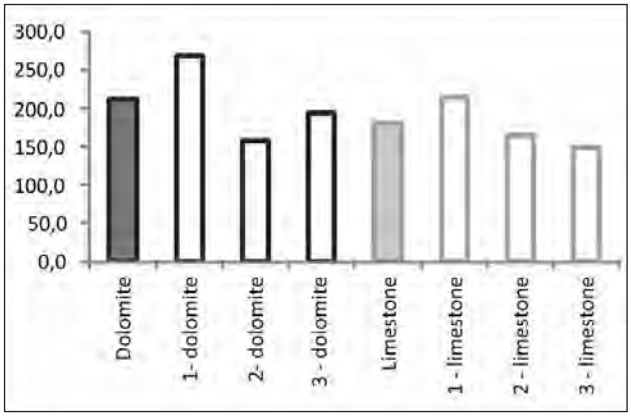

Figure 6. Circumference (mean, m) (auto-delineation).

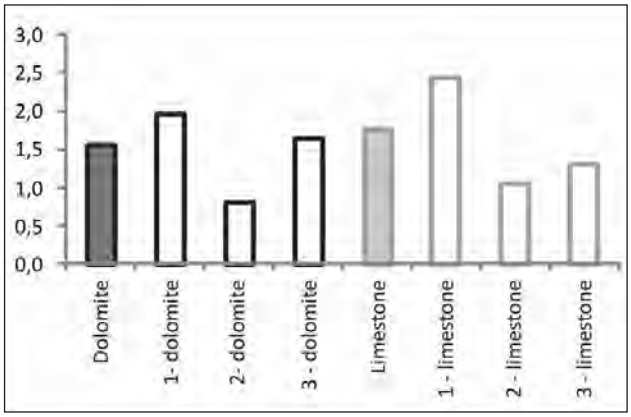

Figure 7. Depth (mean, m) (auto-delineation).

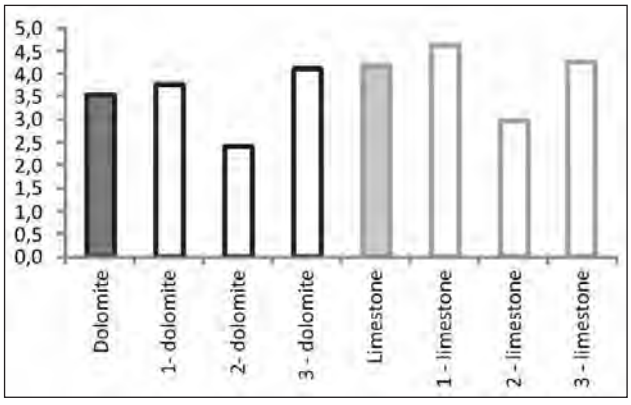

Figure 8. Slope (mean, °) (auto-delineation).

Table 2. Some morphometrical characteristics of auto-delineated dolines.

Study area	A	B	C	D	E	F	G	H	I
Dolomite	213.3	1.5	7.1	3,374	53,683	49.9	0.6	3.5	3.4
1 - dolomite	268.1	2.0	6.1	4,604	53,683	62.1	0.6	3.8	3.5
2 - dolomite	157.4	0.8	3.9	798.0	4,500	37.5	0.7	2.4	3.8
3 - dolomite	194.1	1.6	7.1	3,904	41,639	45.4	0.6	4.1	3.1
Limestone	180.8	1.8	10.6	3,208	61,373	43.1	0.7	4.2	3.2
1 - limestone	214.0	2.4	10.6	5,573	61,373	51.4	0.7	4.6	3.8
2 - limestone	164.1	1.1	4.2	1,156	11,953	38.5	0.6	3.0	2.7
3 - limestone	149.7	1.3	6.1	1,443	22,260	35.5	0.7	4.3	2.8

A: Circumference (m)
B: Depth (mean, m)
C: Depth (max, m)
D: Volume (mean, m^3)
E: Volume (max, m^3)
F: Diameter (mean, m)
G: Roundness (mean)
H: Slope (mean, °)
I: % of flattened floor comparing to the area of doline (mean)

5. Discussion and conclusions

Even though the GIS method for auto-delineation of dolines used for our research has a number of drawbacks, the general morphometrical characteristic of dolines on limestone and dolomite bedrock were calculated.

There is a problem of determining the extent of dolines which directly influences the results of morphometrical analysis. The results of auto-delineation were compared with the manual delineation. When analyzing a landscape with smaller dolines the auto-delineation recognizes less than a half of existing dolines. However, the method is much more reliable in case of larger dolines. The comparison clearly showed that when analyzing the morphometrical characteristic of auto-delineated dolines we must take into account that a large percentage of existing dolines could have been undetected.

When conducting a GIS analysis the results are limited by the quality of the data. For more accurate results LIDAR DEM should be used. For the doline study 12 points/m^2, vertical accuracy of few dm, and positional accuracy half a meter would be needed (Triglav Čekada 2011). The methodology also ignores the influence of the strong structural control which results in the morphology of the dolines – e.g., elongation, depth, slope, etc. For more accurate calculation of the morphometrical parameters of dolines on different bedrock more case study areas would be needed too.

Despite the presented drawbacks of the method, the proposed technique, when used on DEM of higher resolution and a greater number of case study areas, could be used as an efficient tool for determining the characteristics of dolines (or any other depressions, as a matter of fact) on various bedrock. Moreover, this data could be used for computer-based detection of the bedrock (geological mapping) in karst areas only with the analysis of the morphometrical analysis of the local dolines.

References

ARSO, 2011. Opazovalne postaje (Observation stations), http://meteo.arso.gov.si/met/sl/climate/observation-stations/

Čar J, 1986. Geološke osnove oblikovanja kraškega površja (Geological bases of karst surface formation). Acta Carsologica, 14/15, 31–38.

Digital Elevation model 12,5 × 12,5 m. Surveying and Mapping authority of Republic of Slovenia (GURS), Ljubljana, Slovenia.

Ford D, Williams P, 2007. Karst Hydrogeology and Geomorphology. John Wiley & Sons, Chichester.

Gams I, 2003. Kras v Sloveniji v prostoru in času (Karst in Slovenia in time and space). Založba ZRC, Ljubljana.

Geological map of SFRY: Črnomelj, 1984. 1:100,000. Federal Geological Survey, Beograd.

Geological map of SFRY: Postojna, 1967. 1:100,000. Federal Geological Survey, Beograd.

Geological map of Slovenia (digital map). 1:100,000. Geological Survey of Slovenia (GeoZS), Ljubljana, Slovenia.

Guimarães RF, de Carvalho Júnior OA, de Souza Martins E, Ferreira de Carvalho AP, Trancoso Gomes RA, 2005. Detection of karst depression by aster image in the Bambui Group, Brazil. Proc. SPIE 5983, Brugge, College of Europe Press, 328–339.

Jurkovšek B, 2008. Geological map of the Northern part of the Trieste-Komen plateau 1:25,000. Geological Survey of Slovenia, Ljubljana, Slovenia.

Krøgli SO, Dypvik H, Etzelmüller B, 2007. Automatic detection of circular depressions on digital elevation data in the search for potential Norwegian impact structures. Norwegian Journal of Geology, 87, 157–166.

MacMillan RA, Pettapiece WW, Nolan SC, Goddard TW, 2000. A generic procedure for automatically segmenting landforms into landform elements using DEM's heuristic rules and fuzzy logic. Fuzzy Sets and Systems, 113, 81–109.

MacMillan RA, Shary PA, 2009. Landforms and landform elements in geomorphometry. Geomorphometry – Concepts, Software, Applications. Elsevier, Oxford, 227–257.

Matsumoto N, Asada N, Demura H, 2005. Automatic Crater Recognition on Digital Terrain Model. Lunar and Planetary Science, 34, http://www.lpi.usra.edu/meetings/lpsc2005/pdf/1995.pdf

Obu J, 2010. Prepoznavanje kotanj na podlagi digitalnega modela višin (Recognition of karst depressions on basis of digital elevation model). B.Sc. Thesis. Faculty of Arts, Department of Geography, Ljubljana, Slovenia.

Peucker TK., Douglas DH, 1975. Detection of Surface-Specific Points by Local Parallel Processing of Discrete Terrain Elevation Data. Computer graphics and image processing 4, 4. New York.

Pike RJ, Evans I, Hengl T, 2009. Geomorphometry: a Brief Guide. In Geomorphometry – Concepts, Software, Applications. Elsevier, Oxford, 3–33.

Podobnikar T, 2008. Nadgradnja modela reliefa Slovenije z visokokakovostnimi podatki. Geodetski vestnik, 52/4, 834–843.

Portugal RS, De Souza Filho CR, Bland PA, 2004. Automatic Crater Detection Using DEM and Circular Coherency Analysis – A Case Study on South American Craters. 67th Annual Meteorological Society Meeting, www.lpi.usra.edu/meetings/metsoc2004/pdf/5096.pdf

Siart C, Bubenzer O, Eitel B, 2009. Combining digital elevation data (SRTM/ASTER), high resolution satellite imagery (Quicbird) and GIS for geomorphological mapping. A multi-component case study on Mediterranean karst in Central Crete. Geomorphology, 112, 1–2, 106–121.

Suma A, Prieto FJG, de Cosmo PD, 2010. Detection and mapping of karst depressions through remote sensing approach: an example from Sierra de Libar. "Classical karst"s, 18th karstological school, Postojna, Slovenia.

Triglav Čekada M., 2011. Možnost uporabe zračnega laserskega skeniranja (LIDAR) za geomorfološke študije (Possibilities of aerial laser scanning (LIDAR) usage for geomorphic studies). Geografski vestnik, 83/2, 81–93.

Wood JD, 1996. The Geomorphological Characterisation of Ditigal Elevation models: Ph.D. Thesis, University of Leicester, London, United Kingdom.

ORIGIN OF ATYPICAL CALCITE SPELEOTHEMS FILLING FISSURES IN SANDSTONES

Michał Gradziński[1], Marek Duliński[2], Helena Hercman[3], Andrzej Górny[4], Stanisław Przybyszowski[5]

[1]Institute of Geological Sciences, Jagiellonian University, Oleandry 2a, 30-063 Kraków, Poland, michal.gradzinski@uj.edu.pl

[2]Faculty of Physics and Applied Computer Science, AGH – University of Science and Technology, al. Mickiewicza 30, 30-059 Krakow, marek.dulinski@fis.agh.edu.pl

[3]Institute of Geological Sciences, Polish Academy of Sciences, Twarda 51/55, 00-818 Warszawa, Poland, hhercman@twarda.pan.pl

[4]Andrzej Górny, Geological Museum, Faculty of Geology, Geophysics and Environment Protection, AGH Academy of Science and Technology, Aleja Mickiewicza 30, 30-059 Kraków, Poland, a.gorn@op.pl

[5]Stanisław Przybyszowski, Kleczany Stone Resources Company Ltd, 33-394 Kleczany 176, Poland

Atypical calcite speleothems developed in fissures in the Cergowa sandstones were found in the Kleczany Quarry (Polish Western Carpathians). They represent flowstone and stalactites, rafts and various sparry crusts. Such speleothems, especially phreatic ones, are uncommon in the Outer Carpathians composed mainly of siliciclastic rocks of flysch type, with only limited content of calcium carbonate.

The analyzed speleothems grew in vadose and phreatic conditions as well as at the air-water interface. Phreatic speleothems and thin rafts comprise calcite crystals of eccentric morphology, as for example gothic-arch crystals, macrotrilate crystals, single- and multi-stepped crystals. They were formed due to disequilibrium conditions probably resulting from the presence of foreign ions in parent water. Flowstones were fed with thin film of seepage water flowing down the fissure walls. Based on their stable isotope composition, the majority of speleothems form two clusters. The first of them is characterized by $\delta^{18}O$ values between -9.8 and -8.5‰ and of $\delta^{13}C$ values between -5.7 and -0.6‰. The second cluster of samples yields $\delta^{18}O$ values between -9.4 and -7.3‰ and values of $\delta^{13}C$ from -11.5 to -9.7‰.

The speleothems originated between 230 +14, -13 ka and Holocene, mainly during warm periods. Phreatic speleothems, including massive rafts, precipitated from ascending water of deep circulation whereas vadose and water-table speleothems crystallized from local infiltration water charged with soil CO_2. Mixing of both waters in a shallow phreatic zone is plausible near the water-table. It affected the morphology of crystal composing the thin-rafts.

UPLIFT EVIDENCE FROM KARST MORPHOLOGY: PRELIMINARY EVIDENCE FROM BLAMBANGAN PENINSULA KARST, INDONESIA

Eko Haryono
Karst Research Group, Fac. of Geography, Gadjah Mada University, Yogyakarta, Indonesia, e.haryono@geo.ugm.ac.id

This paper aims at exploring morphological evidence of uplift history from karst morphology. Special interest is attributed to the relationship between phases of uplift on one hand and karst landform development on the other hand. Morphology variables involved in this research are karst hill distribution, karst hill density, karst valley drainage density, and valley width. Morphology data were acquired mainly from panchromatic aerial photograph (at the scale of 1: 50,000) incorporated with field survey. Field survey was conducted to collect cave entrance altitude. The result shows that karst hill dispersion, karst valley density, karst valley depth, and karst valley width were proven having been differentiated as a result of uplifting phases. The oldest terrace is characterized by scatter karst hills with no karst valley networks; middle terrace is recognized from deep incised valley with high valley density, whereas the younger terrace is characterized by nearly flat morphology with no karst valley and karst hills.

1. Introduction

Karst development in the convergence plate margin in many localities has been reported being governed by uplift history of karst host rock. Uplift attains its important roles in the karst development through the fact that karstification will take place only if the karst rocks have been uplifted to the sub-aerial environment. Uplift has been found having close association with speleogenesis (Mylroie and Carew 1995; Taboroši et al. 2003), epikarst development (Klimchouk 2004), dry valley terrace development (Sartono et al. 1978; Urushibara 1995; Urushibara 1997).

Being driven by uplift, karst landforms in vice versa record the uplift history through their morphology, the so-called morphological evidences. Multilevel cave systems associated with past sea water level were documented in many areas being resulted from uplift phases (Urhushibara 1997; Taboroši et al. 2003). The caves associated with sea water level still stands were developed through corrosion at the mixing zone either between descending meteoric water and phreatic water or between phreatic water and saline water near shoreline. Marine and river terraces are also ubiquities documented in association with uplift history (Brahmantyo et al. 1998; Urushibara and Yoshino 1997; Sutikno and Tanudirdjo 2006). Series of these terraces are found in Gunungsewu Karst of Java-Indonesia.

Evidences of uplift from cave levels and terraces have been much documented. However, uplift evidences from dry valley and karst hill morphology is less explored. Karst valley and karst hills in this case imprint the time that is consumed by karstification. It has been suggested by Lehman (1936) from his observation of Gunungsewu Karst that karstification is initiated by the development of dry valleys. As karst develops, dry valleys are disorganized to form conical karst morphology. Based on this theory the research documented herein tries to explore the morphological evidences of uplift from dry valley and karst hill morphometry.

2. The Study Area

Blambangan Peninsula is the eastern-most fragment of carbonate formation which is physiographically situated in the Southern Zone or Plateau Zone of Java Island (Fig. 1). The southern zone is bordered in the north by steep escarpment. Not like generally Southern Zone where north of the escarpment are occupied by fluvio-vulcanic material and volcanoes, the north escarpment of Blambangan Peninsula shares a border with Bali Strait. In the west, Blambangan Peninsula is separated from coastal-alluvial plain of Segara Anakan by escarpment. To the south, the plateau of Blambangan Peninsula gradually lowers with several terraces.

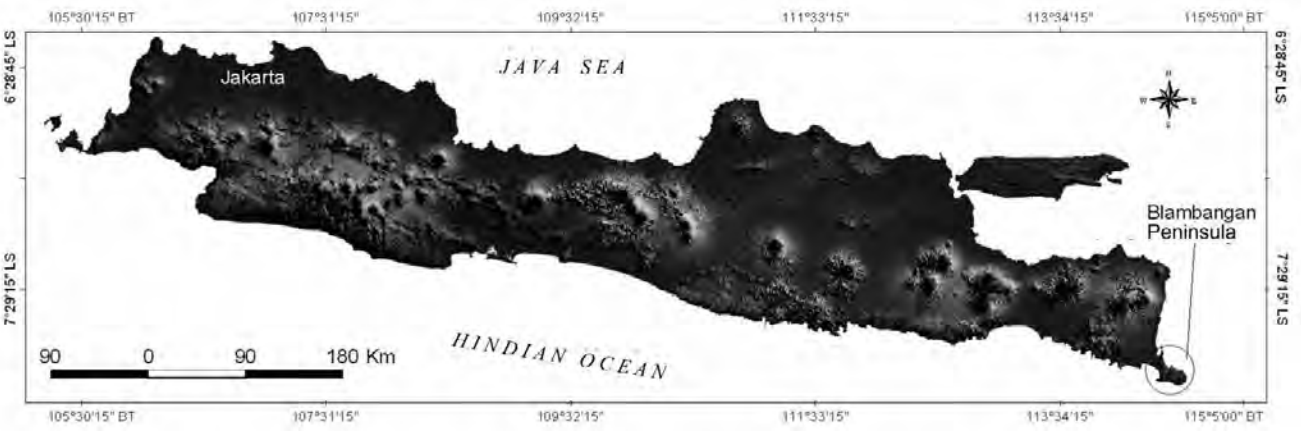

Figure 1. Blambangan Peninsula, the study area.

Blambangan Peninsula constitutes mainly coral limestone of Punung Formation (Achdan and Bachri 1993). The limestone underlies volcanic breccias and conglomerate of Wuni Formation. In general, the limestone is massive, composed mainly of packstone and rudstone. The limestone outcrop is uplifted between 0 and 325 meters above mean sea level with thew highest segment situated in the western part. The limestone of Blambangan Peninsula was deposited during late Miocene up to Middle Miocene (Achdan and Bachri 1993; Bemmelen 1977; Balazs 1968).

The prevailing contemporary climate in the Blambangan Peninsula is strongly influenced by the Northwest and Southeast monsoon, which result in wet season from October to April and a dry season between May and September. The average annual rainfall is 1,350 mm.

3. Methods

Karst morphology data were acquired mainly from 1:30,000 panchromatic aerial photograph interpretation incorporated with field survey. Interpretation was conducted complementary under Topcon Mirror Stereoscope and under computer (on screen interpretation). First, aerial photographs were examined under mirror stereoscope to get 3D view and then delineation was conducted directly on screen used in this over geometrically corrected aerial photograph. Geometric correction was employed in Arc View through polynomial procedure. Minimal of nine control points were employed to every single photographs. Field survey was conducted to collect data of caves entrance altitude and to observe the nature of karst morphology. Dip and strike of bedding plane were also measured during field survey.

4. Results and Discussion

Three difference pattern of karst morphology can be observed from aerial photographs of Blambangan Peninsula. From the higher to the lower part, pattern of karst morphology are described as follows:

- Upper terrace, characterized by scattered karst hills with extensive corrosion plain,
- The middle terrace, characterized by well organized deep incised dry valley,
- The lower terrace, characterized by shallow valley indicating less develop karst area (Figure 2).

Those three karst morphology differentiation must have resulted from three major uplifts. The phases of uplift took place in Blambangan Peninsula are confirmed by the occurrence three difference levels of caves (Table 1). Most of the caves found in the area are horizontal caves. Since there is no clear field evidence that cave occurrence is associated with bedding plane, the development of caves in the Blambangan Peninsula must have been associated with uplift through the formation of cave at former water levels. Development of horizontal cave close to water table have

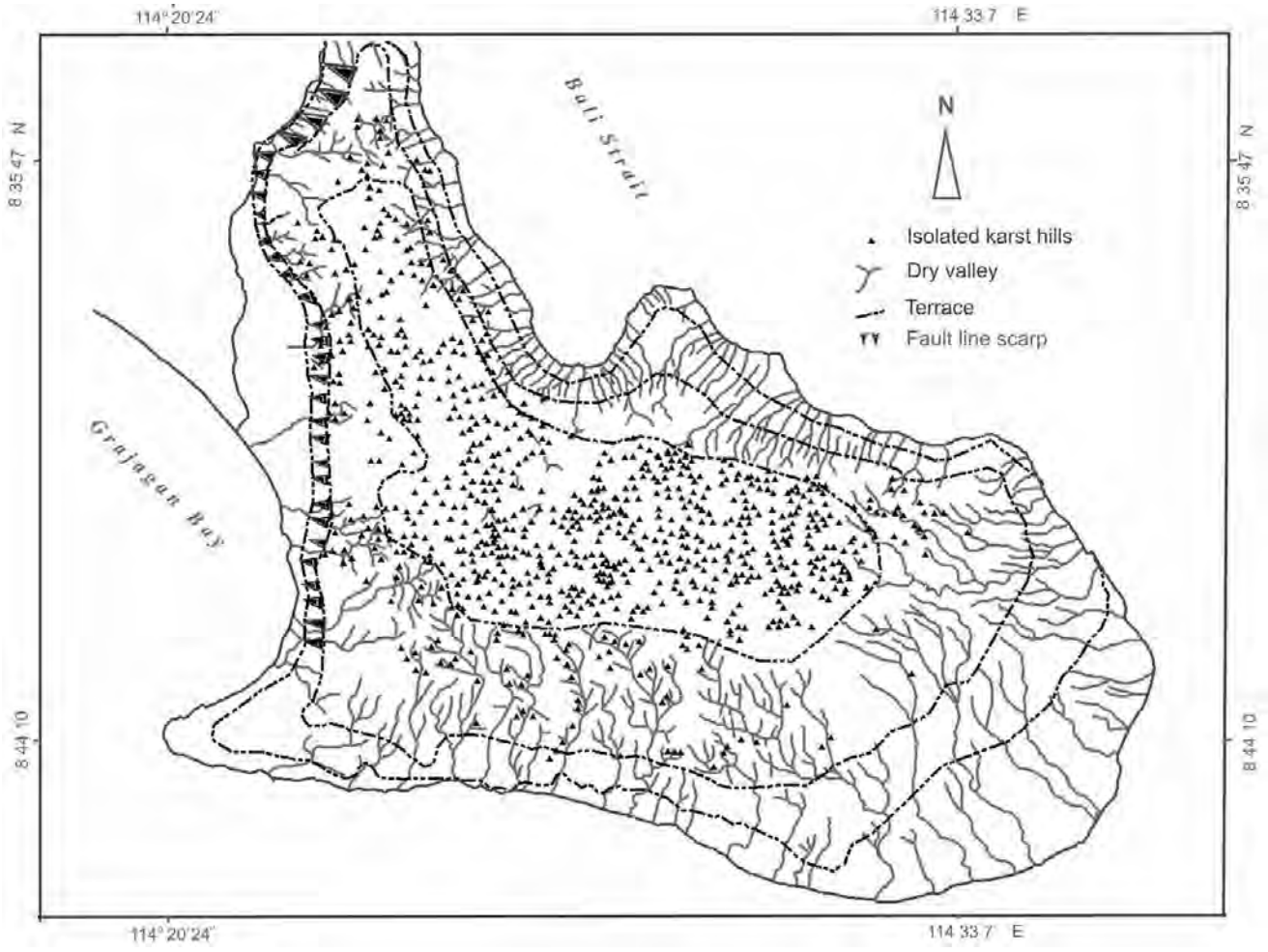

Figure 2. Morphological features of Blambangan Peninsula.

been observed in many karst areas by previous works Mylroie and Carew 1995; Taborosi et al, 2003) through a mixing water mechanism. This result echoes the previous works in Gunungsewu Karst (Urushibara 1995; Urushibara and Yoshino 1997) and in Karangbolong Karst (Brahmantyo 2005) suggesting that since Middle Pliocene, Southern Zone of Java Island have experienced three major uplifts. However karst morphology differentiation related to uplift history is more distinguishable in this area, compare to Gunungsewu Karst and Karangbolong Karst.

4.1. Morphology in the upper terrace

Karst morphology of upper terrace of Blambangan Peninsula is characterized by scattered karst hills with extensive corrosion plain. Scattered karst hills with extensive corrosion plain in the upper terrace indicate that karstification had taken place for much longer period than those during the lower terrace formation. Referring to karst development model (Grund 1914; Lehmann 1936; Aref et al. 1987), karst morphology of upper terrace is considered being in the stage of old karst landform development. The existence of corrosion plain in this area indicates that karstification must had took place intensively before the lower terraces were uplifted.

The other evidence of intensive karstification in the upper terrace is the occurrence of degraded caves in the highest terrace (third level caves). The caves found in the uppermost terraces are generally collapsed big chamber and shallow. Major speleothem found within the caves are column. In some localities like in Trisula Cave (242 m m.s.l.) huge column are situated in the outermost part of cave entrance.

4.2. Karst morphology in the middle terrace

Karst morphology of middle terrace in Blambangan Peninsula is characterized by well organized deep incised dry valley network. It indicates that karst morphology of the middle terrace is not developed yet. Referring to the karst development model of Lehmann (1936), karst morphology of middle terrace is considered in the stage of incipient karst. In this stage, fluvial processes are still prominent in sculpturing karst landform. It is confirmed by evidence that running water takes place during rainy season. No blind valley or pocket valley are found in the middle terrace.

4.3. Karst morphology in the lower terrace

Morphology of the lower terrace does not indicate any karst landform. The lower terrace is the latest parts of the carbonate formation in the area which was exposed to the sub aerial environment. No karst remnant is found indicating that the lower terrace is a newly uplifted limestone formation rather than a planation surface. The

Table 1. Major Caves in Blambangan Peninsula.

No	Caves	Altitude (meters from msl)	Cave Level	Water occurrence
1	Goa Istana	94	FIRST LEVEL CAVE	Static pool
2	Goa Basori	60		Underground river
3	Goa Lowo	46		Dry
4	Goa Baru	25		Dry
5	Goa Jengger	45		Dry
6	Goa L	40		Dry
7	Goa Dampit	38		Dry
8	Goa Dobol 3	48		Dry
9	Goa Dobol 2	31		Dry
10	Goa Dobol 1	23		Dry
11	Goa Kaji	72		Drip water
12	Goa Satrio	74		Drip water
13	Goa Gajah Mungkur	80		Dry
14	Goa Garuda	75		Drip water
15	Goa Mayangkara	109	SECOND LEVEL	Dry
16	Goa Padepokan	110		Dry
17	Goa Mangkleng	138		Drip water
18	Goa 45	144		Dry
19	Goa Rajawali	136		Dry
20	Goa Angkrik	152		Dry
21	Goa Trisula	242	THIRD LEVEL	Dry
22	Goa Putri	247		Dry
23	Goa Gentong	175		Dry

lower terrace is separated from the middle terrace by east-west direction structural terrace.

5. Concluding remarks

Uplift history of Java Island was documented very well in Blambangan Peninsula, either from morphological evidence as discuss here or structural evidence. Three major uplifts as describe from different part of the island are clearly documented in this area. Different evidence from cave sediment seems also very interesting topic for further research, especially for dating purpose, neo-tectonic, or paleo-climate reconstruction.

References

Aref El MM, Kadrah AMA, Lotfy ZH, 1987. Karst topography and karstification processes in the Eocene limestone plateau of El Bahariya, Z. Geomorphologie N.F, (31)1, 45–64.

Achdan A, Bachri S, 1993. Geologic Map of The Blambangan Quadrangle-East Java, Centre for Geological Research and Development, Bandung.

Balazs D, 1968. Karst Regions in Indonesia, Karszt es Barlangkutatas, Volume 5, Budapest.

Bemmelen RWVan, 1970. The Geology of Indonesia, Vol IA, Second edition, Martinus Nijhoff, The Hgue.

Brahmantyo B, Puradimaja DJ, Bandono, Sadisun IA, 1998. Interpretasi kelurusan dari citra SPOT dan hubungannya dengan pola pengaliran bawah tanah pada Perbukitan Karst Gunung Sewu, Jawa Tengah bagian selatan, Buletin Geologi, 28 (1), 37–49.

Brahmantyo B, 2005. Perkembangan bentangalam karst Gombong Selatan, dengan geologi sebagai faktor kendali, Disertasi, Tidak dipublikasikan, ITB, Bandung.

Gillieson D, 1996, Caves: Processes, Development, and Management, Blackwell, Oxford.

Grund A, 1914. Der geographische Zyklus im Karst, Z. Ges Erdkunde, 52, 621–40.

Mylroie JE, Carew JL, 1995. Karst Development on carbonate Islands, in Budd, D.A. Sallet A.H. dan Harris, P.A. (eds), Unvconfromity in Carbonat strata-Their Reconition and the significance of Associated Porosity, AAPG Meomoir, 63, 55–76.

Pannekoek AJ, 1949. Outline of The Geomorphology of Java, Leiden.

Taboroši D, Jenson JW, Mylroie JE, 2003. Zones of enhanced dissolution and associated cave morphology in an uplifted carbonate island karst aquifer, northern Guam, Mariana Islands, Speleogenesis and Evolution of Karst Aquifers. 1 (4), December 2003, 16.

Klimchouk A, 2004. Towards defining, delimiting and classifying epikarst: Its origin, processes and variants of geomorphic evolution, in Jones, WK, Culver, D.C. and Herman, J. (Eds.). 2004. Epikarst. Karst Water Institute special publication, 9, 23–35.

Lehmann H, 1936. Morphologiche Studien auf Java, Gogr, Abh, 3, Stutgart.

Sartono S, Hidayat S, Zaim J, Nababan UP, Djubiantono T, 1878. Undak Sungai Baksoko Berdasarkan Analisis Foto Udara, Proyek Pendendalian dan Penggalian Purbakala, Dep P dan K.

Sutikno, Tanudirdjo D, 2006. Kajian Georkeologi Kawasan Gunungsewu sebagai Dasar Model Pelestarian Lingkungan Karst, Laporan Penelitian, UGM, Yogyakarta.

Urushibara-Yoshino K, 1995. Environmental change in the karst areas on the Island of Java, Proceedings of The International Symposium on Paleoenvironmental Change in Tropical-Subtropical Monsoon Asia, Research Centre for Regioanal geography, Hiroshima University. Hiroshima.

Urushibara-Yoshino K, dan Yoshino M, 1997. Palaeoenvironmental change in Java Island and its surounding areas, Journal of Quarternary Science, 12 (5), 435–442.

VALLEY INCISION IN THE NÍZKE TATRY MTS. (SLOVAKIA) ESTIMATED BASED ON PALEOMAGNETIC AND RADIOMETRIC CAVE SEDIMENT DATINGS

Jaroslav Kadlec[1], Pavol Bella[2], Kristýna Čížková[1], Darryl E. Granger[3], Helena Hercman[4], Peter Holúbek[5], Martin Chadima[1,6], Monika Orvošová[5], Petr Pruner[1], Petr Schnabl[1], Stanislav Šlechta[1]

[1]Institute of Geology AS CR, v.v.i., Rozvojová 269, 165 00 Praha 6, kadlec@gli.cas.cz

[2]Správa slovenských jaskýň, Hodžova 11, 031 01 Liptovský Mikuláš

[3]Earth and Atmospheric Sciences, Purdue University, West Lafayette, Indiana 47907

[4]Institute of Geological Sciences PAS, Twarda 51/55, 00-818, Warsaw

[5]Slovenské múzeum ochrany prírody a jaskyniarstva, Školská 4, 031 01 Liptovský Mikuláš

[6]Agico spol. s r.o., Ječná 29a, 621 00 Brno

Up to eleven horizontal cave levels occur at different altitudes in Jánska, Demänovská and Mošnická karst valleys in the Nízke Tatry Mts. Most of the caves are filled with allochthonous sediments transported from the area formed mostly by granite. The cave levels were filled with fluvial sediments in dependence on the valleys incision caused by Neogene and Pleistocene uplift of the mountain range. The fluvial sediments are intercalated with, or capped, by flowstone layers in the caves. The paleomagnetic polarities measured both in clastic and chemogenic sediments indicate the age of deposition. Based on obtained polarity data we are able to distinguish cave sediments deposited during the Brunhes, Matuyama and Gauss chrons. The paleomagnetic interpretation was partly verified by U-series datings of flowstones preserved in the sedimentary sections. Except for the horizontal cave levels located in the karst valleys, additional large cave systems were found at extremely high altitudes in the Nízke Tatry Mts. 600–700 m above the lowest horizontal cave level.

1. Introduction

An estimation of deposition time of inner cave sediments is possible based on measurement of paleomagnetic polarity record preserved in fine clastic and chemogene deposits. The paleomagnetic interpretation can be verified by U-series dating of speleothems intercalated into the sedimentary sections (e.g., Bosák and Pruner 2011).

2. Geography and geology

Triassic carbonate rocks forming the northern slopes of the Nízke Tatry Mts. in Slovakia are hosting cave systems developed in eleven levels (Droppa 1966). Cave passages located in different altitudes were filled with fluvial, flood and chemogenic deposits during the Demänovská and Janská karst valleys incision. Except for the horizontal cave levels located in these karst valleys, additional cave systems were developed at high altitudes in the Nízke Tatry Mts. in Krakova Hoľa, Kozie Chrbty, and Ohniště Plateau.

3. Methods

Paleomagnetic polarities recorded in both fine clastic and chemogenic cave deposits were acquired by thermal or alternating field demagnetization. Directions of magnetization vector were measured using both spinner and superconducting rock magnetometers. Magnetostratigraphic inter-pretations were verified by U-series ($^{230}Th/^{234}U$ and $^{234}U/^{238}U$) dating of speleothems deposited in the sedimentary sections. The paleomagnetic age of sediments preserved in the high altitude cave systems was verified based on cosmogenic isotope activity (^{10}Be and ^{27}Al) measured in quartz pebbles.

4. Results and discussion

Based on obtained magnetostratigraphic pattern we are able to distinguish cave sediments deposited during the Gauss (2.588–3.58 Ma), Matuyama (0.781–2.588 Ma), and Brunhes (<0.781 Ma) paleomagnetic chrons. The paleomagnetic record extracted from the high altitude cave systems indicates deposition between 3.1 and 1.75 Ma ago. The sediments had to be deposited during a period of tectonic stability when only shallow valleys were developed on both sites of the mountain range. The tectonic uplift in this area was accelerated since 1.7 Ma. The valley incision rate can be estimated based on paleomagnetic polarity and elevation data as follows: 6 $cm.ka^{-1}$ during 1.7–1.1 Ma; 32 $cm.ka^{-1}$ during 1.1–0.78 Ma; and 4 $cm.ka^{-1}$ since 0.78 Ma. The remarkable increase of the valley incision during the latest Early Pleistocene corresponds with results of valley incision study performed in the Swiss Alps reaching twice to four times faster rate in comparison with ther Nizke Tatry Mts. (Haeuselmann et al. 2007). The periods of alluvial agradation in the caves were also correlated with terraces deposited by the Váh River running 10 km North from the karst area. Paleomagnetic polarity of the fluvial deposits filling the largest 4^{th} cave level show the age of sediments younger than 0.78 Ma which is in agreement with stratigraphic conclusion of the most extensive Váh River terrace to the early Mid-Pleistocene (Droppa 1966).

5. Conclusions

The cave levels in the Nízke Tatry Mts. were filled with fluvial sediments in dependence of Neogene and Pleistocene uplift of the mountain range. Sediments preserved in the large cave systems developed in extremely

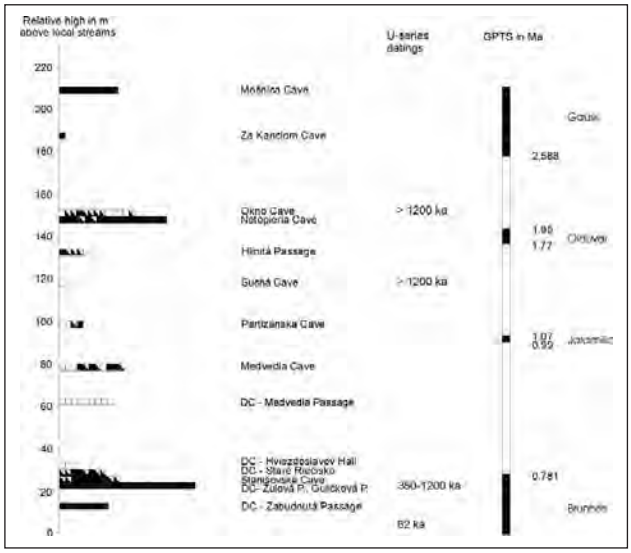

Figure 1. Magnetostratigraphic pattern of cave sediments in the Nízke Tatry Mts. karst valleys. Black (white) squares represent normal (reverse) magnetization of sample, black-and-white squares represent transitional character of sample. DC – Demänovská Jaskyňa Slobody Cave.

high altitudes in the Nízke Tatry Mts. Were deposited between 3.1 and 1.75 Ma ago (paleomagnetic chrons Gauss and Matuyama). Sediments deposited in cave levels developed in Demänovská, Jánská and Mošnica karst valleys in a relative elevation above 185 m are older than 2.588 Ma (Gauss chron). Fluvial sediments found in the cave levels in the relative elevations 30–185 m were deposited 2.588–0.781 Ma ago (Matuyama chron). Fluvial sediments deposited in lower elevation cave levels are younger than Brunhes/Matuyma paleomagnetic boundary (0.781 Ma). After relative tectonic stability period between 3.1 and 1.7 Ma the tectonic uplift was accelerated since 1.7 Ma. The valley incision rate can be estimated based on paleomagnetic polarity and elevation data as follows: 6 cm.ka^{-1} during 1.7–1.1 Ma; 32 cm.ka^{-1} during 1.1–0.78 Ma; and 4 cm.ka^{-1} since 0.78 Ma.

Acknowledgments

The research is supported by grants No. IAA3013201 and IAA30013001. The institutional funding is provided by the Institute of Geology AS CR, v. v. i. (AV0Z30130516).

References

Bosák P, Pruner P, 2011. Magnetic rekord in cave sediments. In Petrovský E, Herrero-Bervera E, Harinarayana T, Ivers D (Eds.) The Earth's magnetic interiér, 343–360.

Droppa A, 1966. The correlation of some horizontal caves with river terraces. Stud. Speleol., 1(4), 186–183.

Haeuselmann P, Granger DE, Jeannin P-Y, Lauritzen S-E, 2007. Abrupt glacial valley incision at 0.8 Ma dated from cave deposits in Switzerland. Geology, 35(2), 143–146.

MAGNETIC FABRIC AND MINERALOGY OF CAVE DEPOSITS IN BOTOVSKAYA CAVE (EASTERN SIBERIA, RUSSIAN FEDERATION)

Jaroslav Kadlec[1], Helena Herman[2], Martin Chadima[1,3], Lenka Lisá[1], Hedi Oberhänsli[4], Alexandr Osintsev[5]
[1]Institute of Geology AS CR, v.v.i., Rozvojova 269, CZ-165 00 Praha 6, Czech Republic, kadlec@gli.cas.cz
[2]Institute of Geological Sciences, PAN, Warszawa, Poland
[3]Agico spol. s r.o., Ječná 29a, 621 00 Brno
[4]GeoForschungsZentrum Potsdam, Germany
[5]Speleoclub Arabica, Irkutsk, Russia

The Botovskaya Cave is a typical example of a two-dimensional maze with a total length of explored passages exceeding 60 km, which represents the longest limestone cave system in the Russian Federation. The clastic cave sediments filling the cave passages differ in both mineral and mineral magnetic properties and were deposited under different hydrological conditions. The older portion of the clastic cave fills was derived from overlying sandstones, whereas the properties of younger cave sediments show closer affinity to the soils and weathering products originating on the sandstone plateau above the cave. The cave sediments underwent repeated periods of deposition and erosion during the Tertiary and Pleistocene.

1. Introduction

The aim of this project is an examination of the Botovskaya Cave deposits using methods operating with magnetic and heavy minerals and with quartz grain exoscopy. Obtained mineral characteristics were used for correlations from the point of view of sediment source and mode of transportation into the cave passages. Radiometric and paleomagnetic datings of the cave carbonate bed allowed us to estimate the age of both depositional and post-depositional processes.

2. Geography and geology

The Botovskaya Cave is located on the Angarsko-Lensky Plateau of the southern Siberian Craton about 500 km north of Irkutsk City. The area reaches altitudes of 1,100 m a.s.l., and belongs to the Zhigalovo District of the Irkutsk Area. The plateau is dissected by river valleys up to 400 m deep. Cave entrances lie at a relative elevation of 310 m above the Lena River level, in a valley of the Garevogo Creek, the left tributary of the Boty River, which joins the Lena River. The cave system, dipping gently to the north, has developed in an Early Ordovician limestone formation with a thickness of 6 to 12 m. The limestone bed is underlain by Middle and Late Cambrian sandstone, siltstone, marl and gypsum and overlain by Middle Ordovician sandstone, limestone and argillite. The cave system developed under confined (artesian karst) settings (Klimchouk 2000, 2003). The speleogenesis of the Botovskaya Cave system was interpreted by Filippov (2000) and is due to two different processes: (i) corrosion involving meteoric water, and (ii) ascending deep circulating artesian water (below groundwater level) spanning the time period between Late Mesozoic and Early Neogene.

3. Methods

The studied sections of the cave deposits were documented with special reference to lithology, sedimentary structures and aggradation and erosion event records. Mineral magnetic characteristics such as low field bulk magnetic susceptibility (MS) and anhysteretic remanent magnetization (ARM) together with anisotropy of magnetic susceptibility (AMS) help to find the source of the cave fills and estimate a mode of sediment transport to the cave passages. The character of quartz grain surfaces indicates transportation and post-depositional history of clastic sediments. Exoscopic observations were performed on quartz grains larger than 0.25 mm separated from either clastic cave deposits or from the Ordovician sandstone bedrock after wet sieving and boiling in HCl. Heavy minerals were separated after wet sieving from the grain-size fraction of 0.25–0.063 mm using tetrabromethane and observed in Canadian balsam. At least 300 grains of transparent heavy minerals were determined in each sample. The flowstone bed used for the paleomagnetic polarity measurements was also dated by the $^{230}Th/^{234}U$ radiometric method.

4. Results

4.1. Magnetic fabric and mineral magnetic characteristics

The MS values slightly increase from bottom sand sediment beds to the above lying clay dominating sediments (see Fig. 2). The highest MS values were measured in the modern topsoil collected above the Medeo Entrance. The ARM values show steep increase in the top beds. The AMS parameter is sensitive to presence of very fine superparamagnetic minerals originating during pedogenesis or forest fires. The magnetic fabric of the sediments is mostly oblate. The magnetic lineation directions in the top sedimentary beds show concentration in NW to SW directions with the mean direction tending to the WSW. The poles to magnetic foliation are usually concentrated around the center of the projection. The magnetic lineation directions measured in the bottom sedimentary beds show almost random distribution accompanied by large dispersion of poles to magnetic foliation.

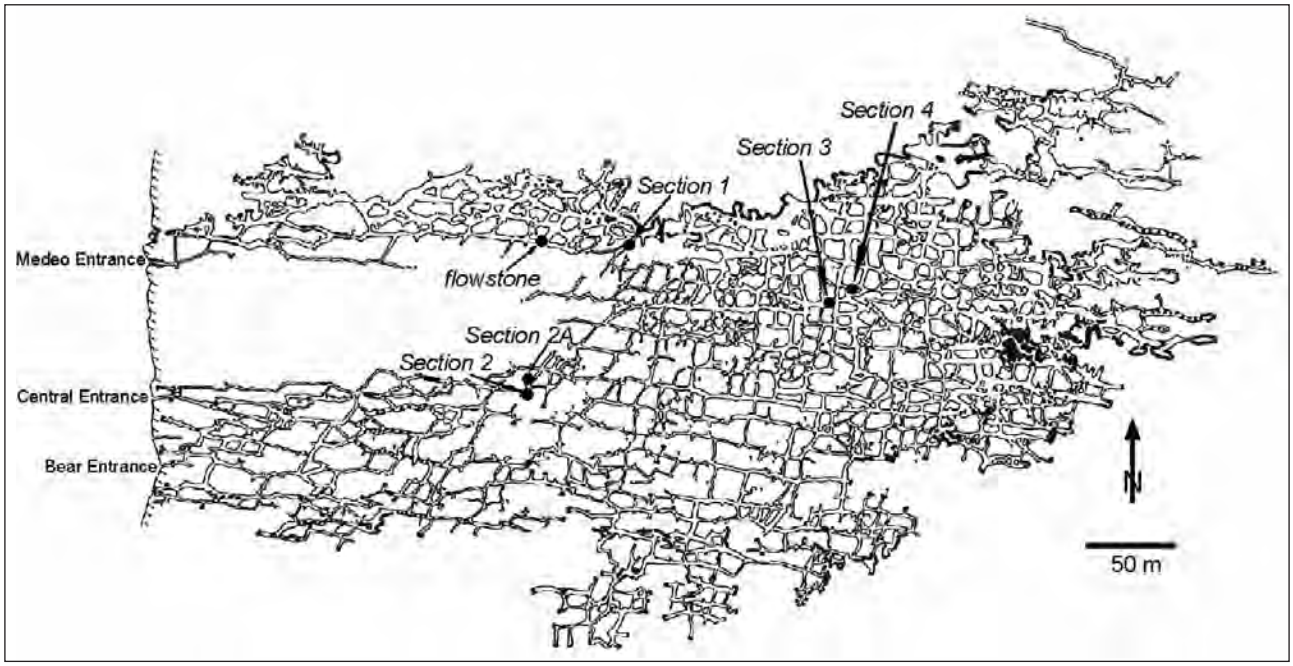

Figure 1. Botovskaya Cave (The Old World) map (adopted from Göbel and Breitenbach 2003) with indication of studied sections and dated flowstone.

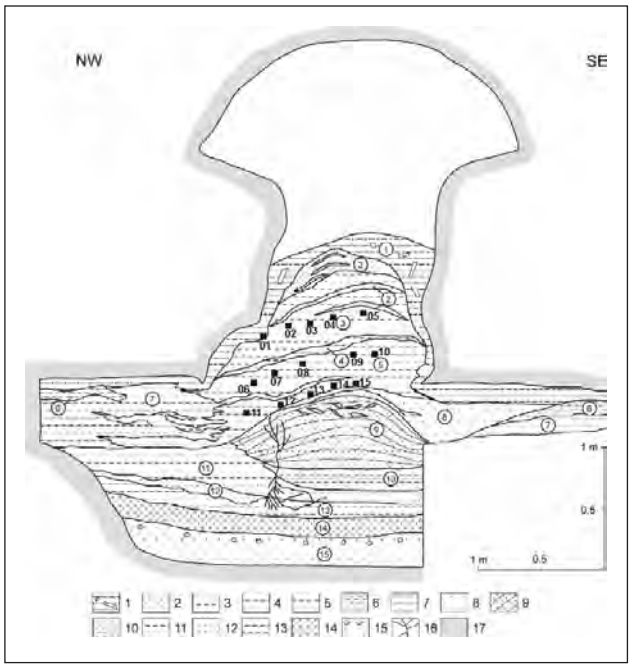

Figure 2. Section 1 – SW face
1 – clay, sporadic angular clasts of sandstone; 2 – sand; 3 – clay; 4 – sandy clay to clayey sand; 5 – clay; 6 – sandy clay; 7 – slightly sandy clay; 8 – sand; 9 – sand, fine-grained; 10 – clayey sand, laminated; 11 – clayey sand; 12 – sand; 13 – clayey sand; 14 – sand with sandy aggregates; 15 – sand; 16 – carbonate cementation along fissures; 17 – bedrock wall; black squares with numbers – collected samples.

4.2. Quartz surfaces and heavy mineral content

Three types of microstructures were observed on quartz grain surfaces: (i) precipitation of SiO_2 on the surface of grains in lace-like patterns; (ii) corrosive etched microstructures, and (iii) overgrowth with quartz crystals. The bedrock Ordovician sandstone forming the ceiling of the cave passage above Section 2 contains rounded quartz grains about quartz grains about 1 mm in diameter. The grain surfaces show weak dissolution and precipitation of SiO_2. The studied samples of the bedrock and cave deposits show monotonous association of stable heavy minerals. Grains of transparent heavy minerals are rounded, while the opaque mineral grains are mostly angular. Beds in the upper portions contain greater amounts of garnet, similar to modern soil.

4.3. Flowstone datings

Radiometric dating of the flowstone bed by $^{230}Th/^{234}U$ method reveals that the age of three dated samples exceeds 350 ka (see also Breitenbach et al. 2005). The flowstone age is probably higher than 1.2 Ma based on $^{234}U/^{238}U$ ratio. Based on the paleomagnetic data, it is evident that the flowstone records normal polarity of the Earth magnetic field from the time of the carbonate deposition.

5. Discussion

The bottom beds of the cave sequences reveal similar lithological, magnetic and heavy metal properties. Basal sand deposited on the bedrock bottom shows a lower MS, similar to the bedrock sandstone exposed in the cave. The exoscopic quartz grain characteristics are similar, too. The deposits filling the bottom part of cave corridors were derived from the local bedrock formed by Early Ordovician sandstones. The younger cross-bedded and laminated, mostly clayey sands (beds No. 1–7 in Fig. 2) were deposited after partial erosion of the basal deposits. The deposits reveal slightly higher MS values. The exoscopic observation shows cemented quartz grain aggregates indicating the source in the local cross-bedded sandstone. The inner structures of these laminated sediments show a frequent alternation between local aggradation and erosion events. The sediments were deposited during heavy precipitation events, when water penetrated into the cave corridors from the surface through the swallow holes and along open vertical cracks. The water escape structures

Figure 3. View on the Angara–Lena Plateau formed by Lower Paleozoic sedimentary sequences. A white strip marked by arrow represents the limestone bed intercalated between sandstones probably containing undiscovered cave systems.

were formed during the compaction of sediments. The combination of radiometric and paleomagnetic polarity datings suggests a likely age for the carbonate bed before 2.588 Ma (e.g., the boundary Matuyama and Gauss paleomagnetic chrons). In the time of the flowstone deposition the artesian aquifer regime was already disrupted due to surrounding valley incision and vadose conditions dominated in the cave system. The later intensive erosion removed clastic sediments from under the flowstone bed and destroyed the entire flowstone. This erosional event had to be triggered by unusually heavy precipitation, which entered the bedrock through vertical ruptures opened both in sandstone and limestone due to differential gravity-induced subsidence of the massif during the Pleistocene.

6. Conclusions

1. The sections in detrital cave sediments in Botovskaya Cave (in The Old World part) evidence periodical sediment deposition. Sediments of the cave fill are of two different types: the older, bottom sands are derived from weathered bedrock sandstones and were probably horizontally transported over a short distance probably not exceeding first hundreds of meters. The overlying sediments dominated by clay and clay/sand were transported vertically with precipitation waters from the surface above the cave.
2. If the bottom sand was transported horizontally through the cave by flowing water, it must have taken place before the incision of the present deep valleys, probably in the Late Tertiary

Acknowledgements

The project was supported by the INTAS Program No. 03-51-4152: Speleothems and other cave sediments from Siberia: An archive from the boreal climate zone with the potential for climate reconstruction on an annual to decadal basis (SPELEOARCH) and it is a part the research project of the Institute of Geology AS CR, v.v.i. No. AV0Z30130516.

References

Breitenbach S, Fernandez D, Adkins J. Mingram B, Oberhänsli H, Haug G 2005. Speleothem records older than 500 ka from Southern Siberia. Kalamos, Hellas, Hellenic Speleological Society, 614–618.

Filippov AG, 2000. Speleogenesis of Botovskaya Cave, Eastern Siberia, Russia. In: A.B. Klimchouk, D.C. Ford, A.N. Palmer and W. Dreybrodt (Eds.). Speleogenesis, Evolution of Karst Aquifers. Huntsville, Ala., National Speleological Society, 282–286.

Göbel E, Breitenbach S, 2003. Die Peschera Botovskaja, die längste Höhle Russlands. Mitteilungen des Verbandes der Deutchen Höhlen – und Karstforscher, 49(2), 42–45.

Klimchouk A 2000. Speleogenesis under deep-seated and confined settings. In: A.B. Klimchouk, D.C. Ford, A.N. Palmer and W. Dreybrodt (Eds.). Speleogenesis, Evolution of Karst Aquifers. Huntsville, Ala., National Speleological Society, 244–260.

Klimchouk A, 2003. Conceptualisation of speleogenesis in multi-storey artesian systems: a model of transverse speleogenesis, http://www.speleogenesis.info/archive/publication.php?PubID524&Type5publication&keyword5Klimchouk

CASE STUDIES OF FLUORESCENT GROUNDWATER TRACING IN RECENT CAVE RESEARCH

Benjamin V. Miller[1], Chris Groves[1], Jason S. Polk[1], Robert N. Lerch[2]
[1]*Western Kentucky University, Department of Geography and Geology, 1906 College Heights Blvd., Bowling Green, KY 42101, United States, benjamin.miller@wku.edu*
[2]*USDA-Agricultural Research Service, Cropping Systems & Water Quality Research Unit, Agricultural Engineering Building, University of Missouri, Columbia, MO 65211, United States*

Groundwater studies have utilized fluorescent dyes in order to map groundwater flow paths and confirm hydrologic connections amongst karst features. These techniques are now well established so that common dyes and common monitoring techniques can be used to apply these methods to a wide range of applications and in a variety of locations. This paper examines four case studies where groundwater tracing with fluorescent dyes to better understanding the hydrologic characterization of cave and karst systems. A five-year project delineated recharge areas for two significant cave systems; Onondaga Cave and Cathedral Cave; which are publicly owned and manage cave systems. Dye tracing was used to delineate recharge areas for streams located in Carroll Cave, a hydrologically complex and biologically significant cave system in central Missouri. P-Bar Cave, located in the Bighorn Mountains of Wyoming, is a large stream swallet draining approximately 104 km^2 into the main cave entrance. Groundwater tracing techniques were applied at P-Bar Cave to determine resurgences for the stream at springs located 9.6 kilometers down canyon. Crumps Cave, a large cave located on the Pennyroyal Sinkhole Plain of south-central Kentucky is a site where epikarstic research on contaminant transport is taking place. Tracing with fluorescent dyes has examined the extreme variances in travel times between flow from the surface into the epikarstic aquifer and travel from in-cave perennial waterfalls to the resurgence for the cave stream 35 kilometers away. Groundwater tracing continues to be a useful tool in understanding the complex flow systems found in karst areas and provides useful information for both researchers and agency land managers.

1. Common groundwater tracing methods

Fluorescent dyes have been used in groundwater tracing to delineate groundwater basins and to compliment hydrologic research in cave and karst regions. In conducting groundwater tracing in a karst area one of the initial tasks is to identify all recharge and discharge features during a Karst Hydrologic Inventory (KHI). This KHI helps to identify potential monitoring locations, at features draining the aquifer or in local surface streams, and potential dye injection locations, at features recharging the aquifer (Crawford Hydrology Lab 2010).

Once discharge features are identified, a monitoring method is chosen depending on given objectives for the trace. Charcoal receptors are the most common method for monitoring groundwater features and consist of a mesh packet containing 3–5 grams of crushed coconut charcoal (Crawford Hydrology Lab, 2010). These are attached to wire or nylon string and are placed directly in the flow of discharge features. Regular changing of these receptors at given time intervals aids in determining travel from injection location to recovery site. Grab samples can also be collected in glass vials for analysis of current concentrations of dye. Autosamplers can be used for the collection of these grab samples at specific time intervals and when combined with discharge data quantitative tracing can be used to examine the amount of dye recovered versus the amount of dye injected. Technological advances have also made portable field fluorometers, which can analyze concentrations of specific dyes and record this data to a memory device for later download (Meus et al. 2006).

Tracers used in groundwater tracing commonly use five common dyes; fluorescein, eosine oj, rhodamine wt, sulphorhodamine b, and tinopal ob (Aley and Fletcher 1976; Jones 1984). Picking a specific dye for trace must be determined by background levels in a study area and the type of features tracers are injected into. Injection methods also vary depending on the hydrologic conditions present at a given location. Dry streambeds or sinkholes may require the use of a dry-set where powdered dye is placed inside of a PVC pipe and then staked to the base of a stream channel to await injection of the tracer following a storm event. If road access is available fire tanker trucks may also be used to create a temporary stream into which dye can be injected. Finally if flowing streams are located at an injection site then the dye can be directly poured into the stream for an injection. However, in all cases extreme care must be taken to prevent any contamination of dyes amongst injection locations and specifically amongst monitoring sites.

Several examples of case studies from groundwater traces in various locations in the continental United States (Fig. 1) are presented below. Each of these examples utilized groundwater tracing to achieve different objectives and used different methods.

2. Case Studies of Groundwater Tracing in Cave Studies

2.1. Onondaga Cave and Cathedral Cave, Missouri, USA

Onondaga Cave and Cathedral Cave are two large cave systems located in central Missouri in the Ozarks ecoregion. Both caves are preserved by the Missouri Division of State Parks and are the centerpieces of Onondaga Cave State Park

(OCSP). The caves share many common aspects, including a high biodiversity of largely aquatic dominated biota, a large quantity of speleothems, and the fact that perennial streams flow through the caves, which drain losing streams in the surrounding area. A project was initiated in 2003 to begin delineation of recharge areas for both caves in order to guide cave management, future land acquisition, and to determine possible threats from land use. A total of 15 monitoring sites were established in surface and subsurface streams, as well as other groundwater discharge features, utilizing charcoal packets as the primary monitoring method. Over the next five years a total of 21 dye injections resulted in six positive traces to Onondaga Cave and three positive trace to Cathedral Cave (Fig. 2). This information was then used to delineate recharge areas using GIS (Fig. 3), resulting in a 24 km^2 recharge are for Onondaga Cave and a 2.9 km^2 recharge area for Cathedral Cave

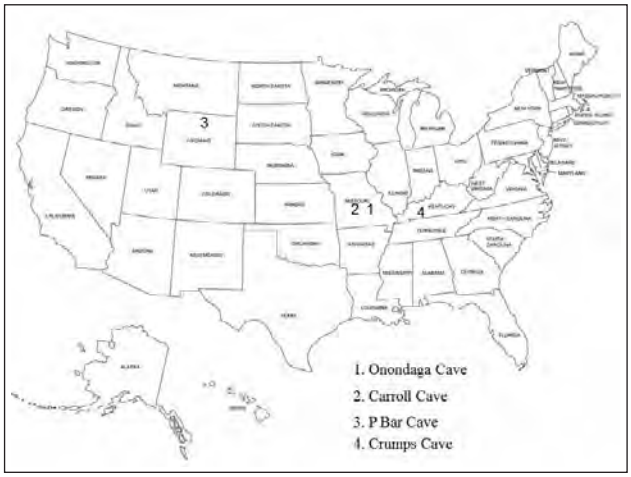

Figure 1. Map of USA showing location of case studies discussed in paper.

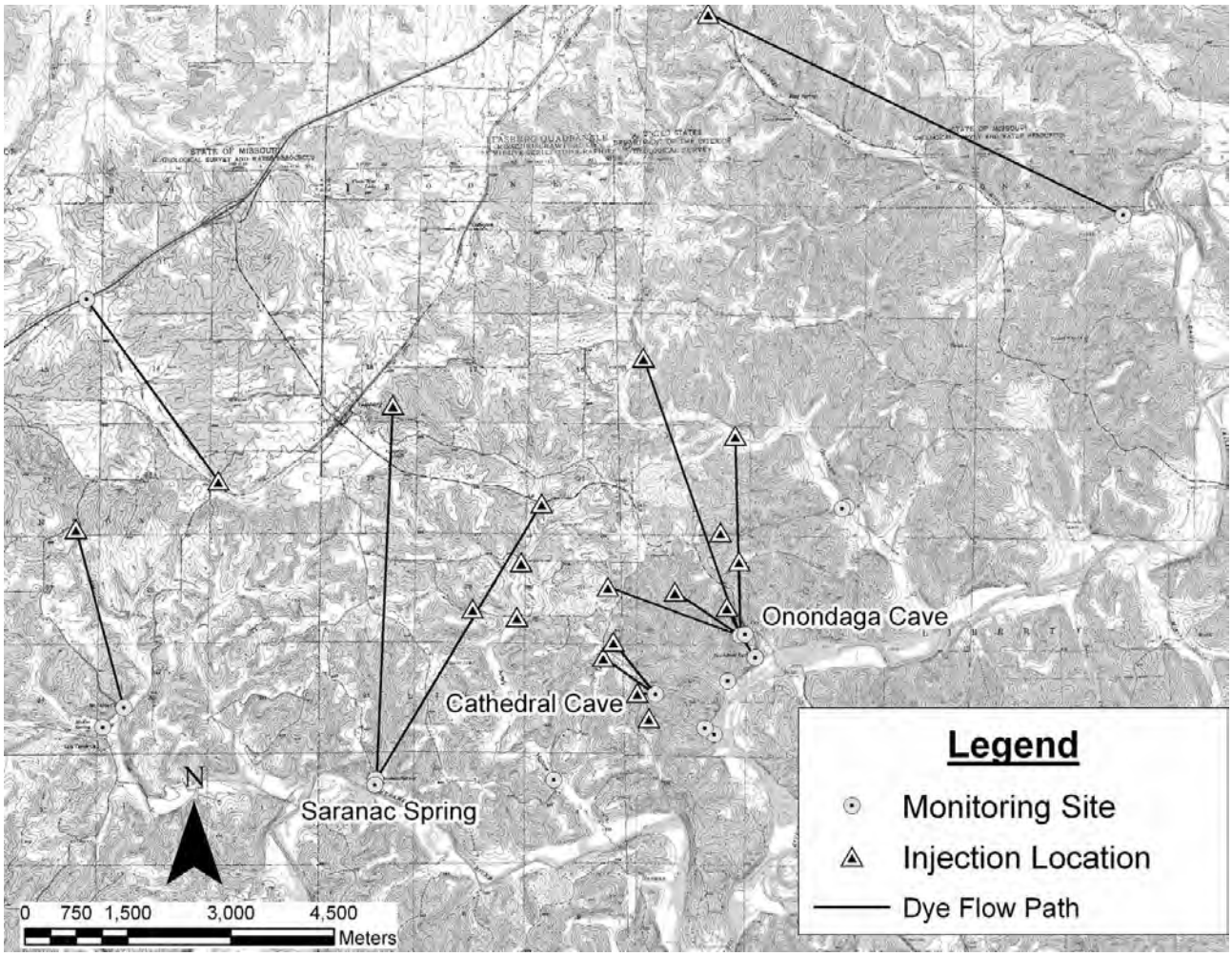

Figure 2. Map of positive groundwater traces conducted in the Onondaga Cave area.

(Miller and Lerch 2011). The majority of the recharge areas for both caves are located outside of the park, however current land use in the recharge areas is dominated by deciduous forest. Information from the traces has been applied to the Park's management in the form of a cave management plan and now gives agency land managers a target area for possible threats to water quality in the cave streams.

2.2. Carroll Cave, Missouri, USA

Carroll Cave is an extensive stream cave system, currently 28 km in length and still being explored. The cave is developed within the Ordovician Gasconade Dolomite and located in the northwest portion of the Wet Glaize Creek watershed. The cave is known to have dense populations of the Southern Cavefish (*Typhlichthys subterraneus*) and the Grotto Salamander (*Eurycea spelaea*) both stygobitic

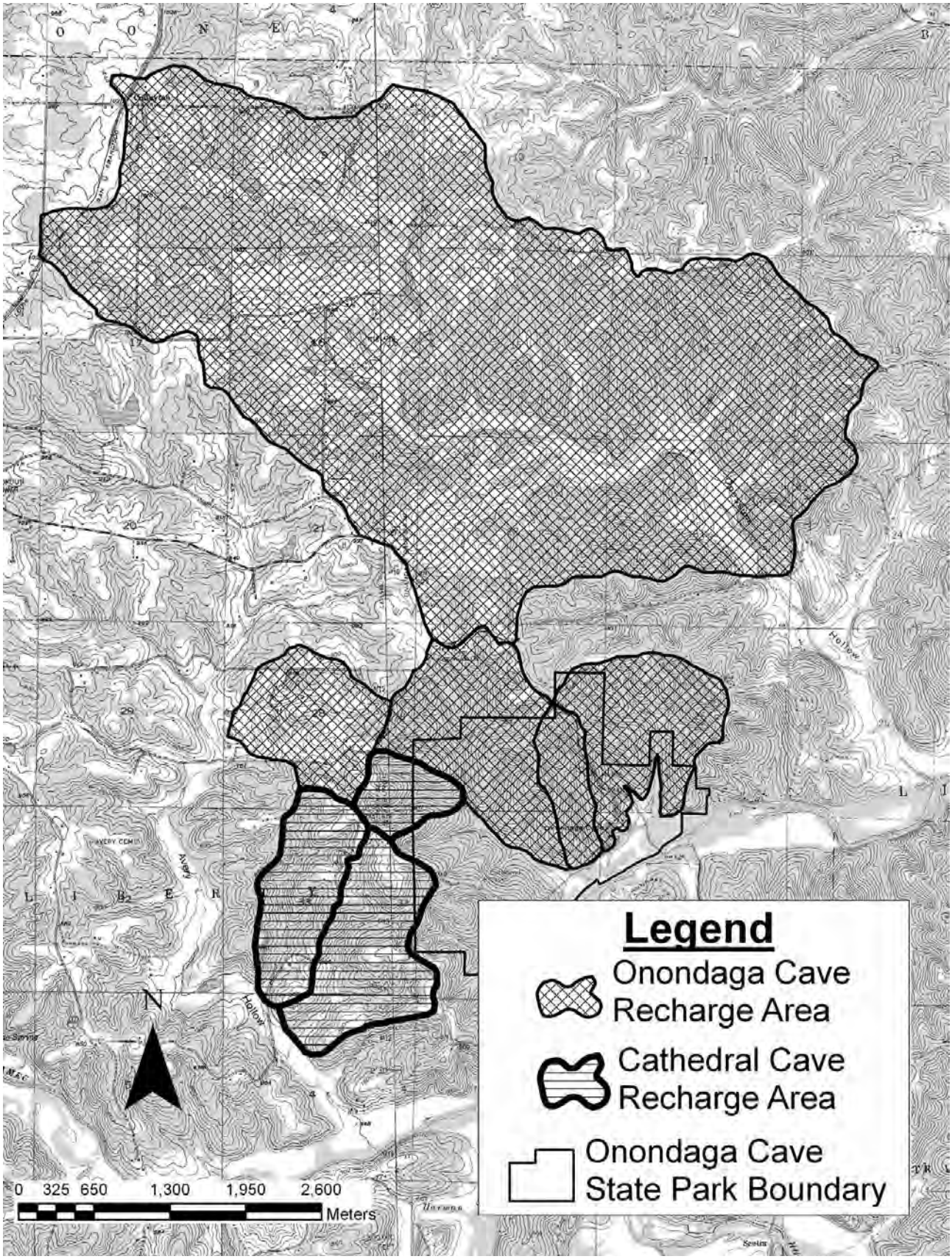

Figure 3. Recharge areas for Onondaga Cave and Cathedral Cave.

species of special concern within the state of Missouri. The hydrologic behavior of the cave is controlled by three independent cave streams; Carroll River, Thunder River, and Confusion Creek/New River. Thunder River, the largest of the cave streams, has an average daily flow of 150 L/s and contains multiple tributaries along the 11 km course of the cave stream. Dye tracing confirmed the resurgence for two of the cave streams is Toronto Springs, a multiple outlet alluviated springs system located 4 kilometers north of the cave (Figure 4). The dye tracing project which was took place from 2008–2010 delineated a recharge area of 18.4 km^2 for Carroll Cave (Fig. 5) and identified a total of eight resurgences for two of the cave streams; Thunder River and Confusion Creek; at Toronto Springs.

Additional traces in area losing streams indicated a mixing zone (of surface and subsurface streams) which recharge the 13 springs at Toronto Springs (Miller 2010). Use of the recharge area has allowed for land use analysis (Fig. 6) and indicates a land use dominated by deciduous forest and grasslands used as pasture for cattle.

2.3. P Bar Cave, Wyoming, USA

P Bar Cave is located in the western Bighorn Mountains in north-central Wyoming. The cave is co-owned and managed by the US Forest Service and the Bureau of Land Management. Formed in Ordovician Bighorn Dolomite, the cave is a large swallet located near the contact with igneous basement rocks, and is recharged by Wet Medicine Lodge Creek, which drains a 104 km^2 area consisting largely of granitic uplands. The cave was mapped in the 1970's to a total of 2.9 kilometers in length and additional hydrologic work identified a series of springs 9.6 kilometers down-canyon, which were speculated to be the resurgences for the cave system based on micaceous sands found downstream of the spring outlets (Huntoon 1985). A project to remap the cave was started in 2009 and in 2012 this work was combined with some groundwater tracing to confirm which springs and how many springs were hydrologically connected to the cave system. A KHI identified eight springs in lower Wet Medicine Lodge Canyon (Fig. 7) that were then monitored using charcoal receptors, two springs were also located immediately downstream of the main

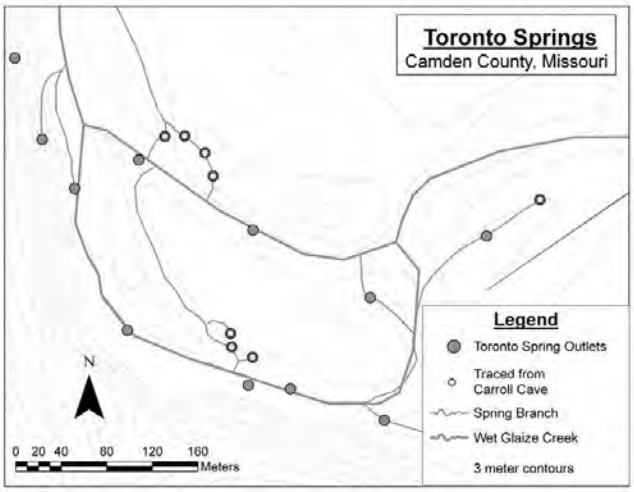

Figure 4. Map of Toronto Springs, showing springs hydrologically connected to Carroll Cave.

cave entrances which sank into the streambed after a few hundred meters. Rhodamine WT was injected into Wet Medicine Lodge immediately downstream of the upper springs yet above the stream sink and fluorescein was injected into the main cave entrance to see if the water flowing into the cave resurged at the same springs as the water sinking below the upper springs. The water which enters the main entrance was traced to the second spring, located immediately downstream of the cave entrances, but bypassed the uppermost spring. This indicates that the lower spring is fed by groundwater sources independent from the

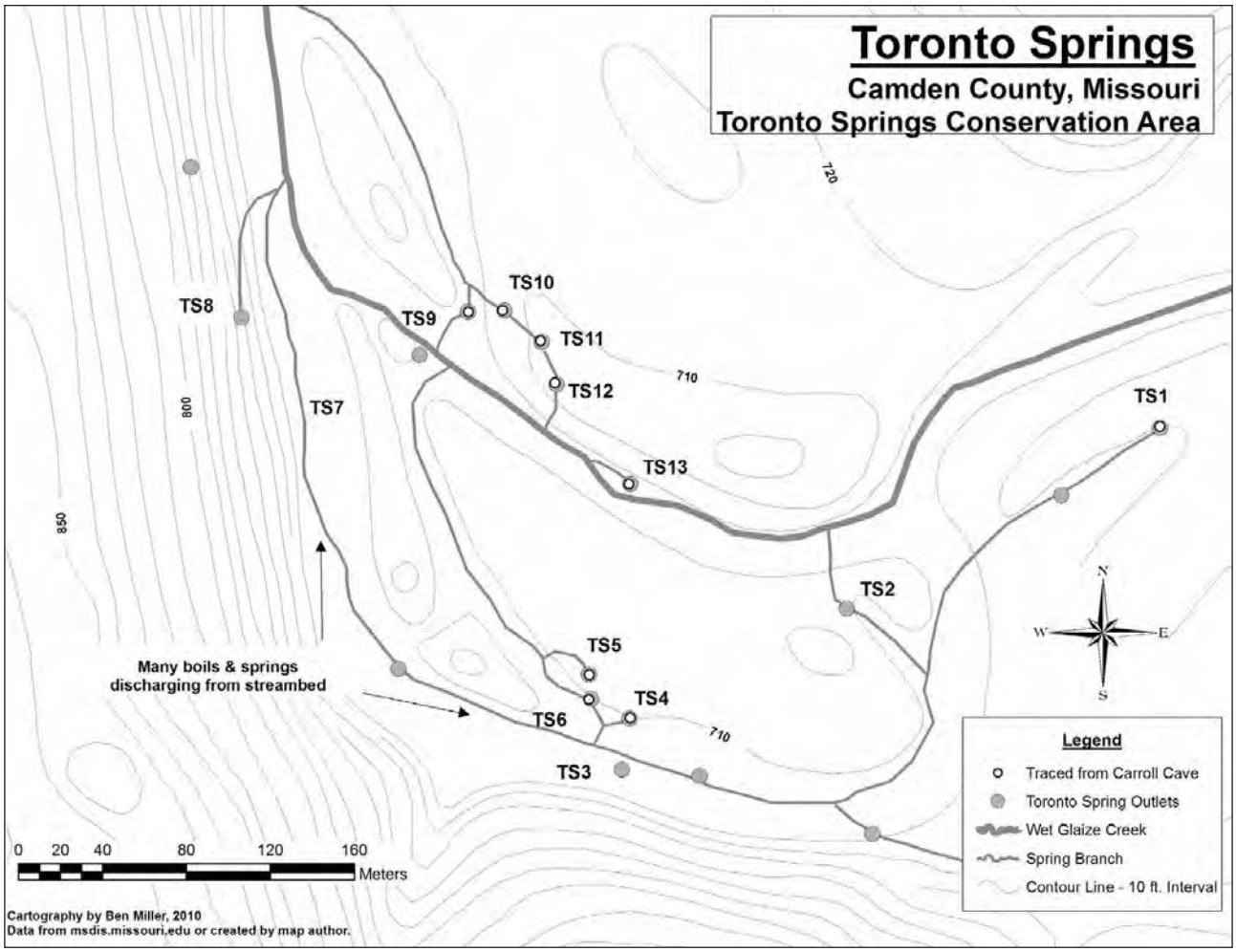

Figure 5. Recharge area for Carroll Cave showing positive groundwater traces.

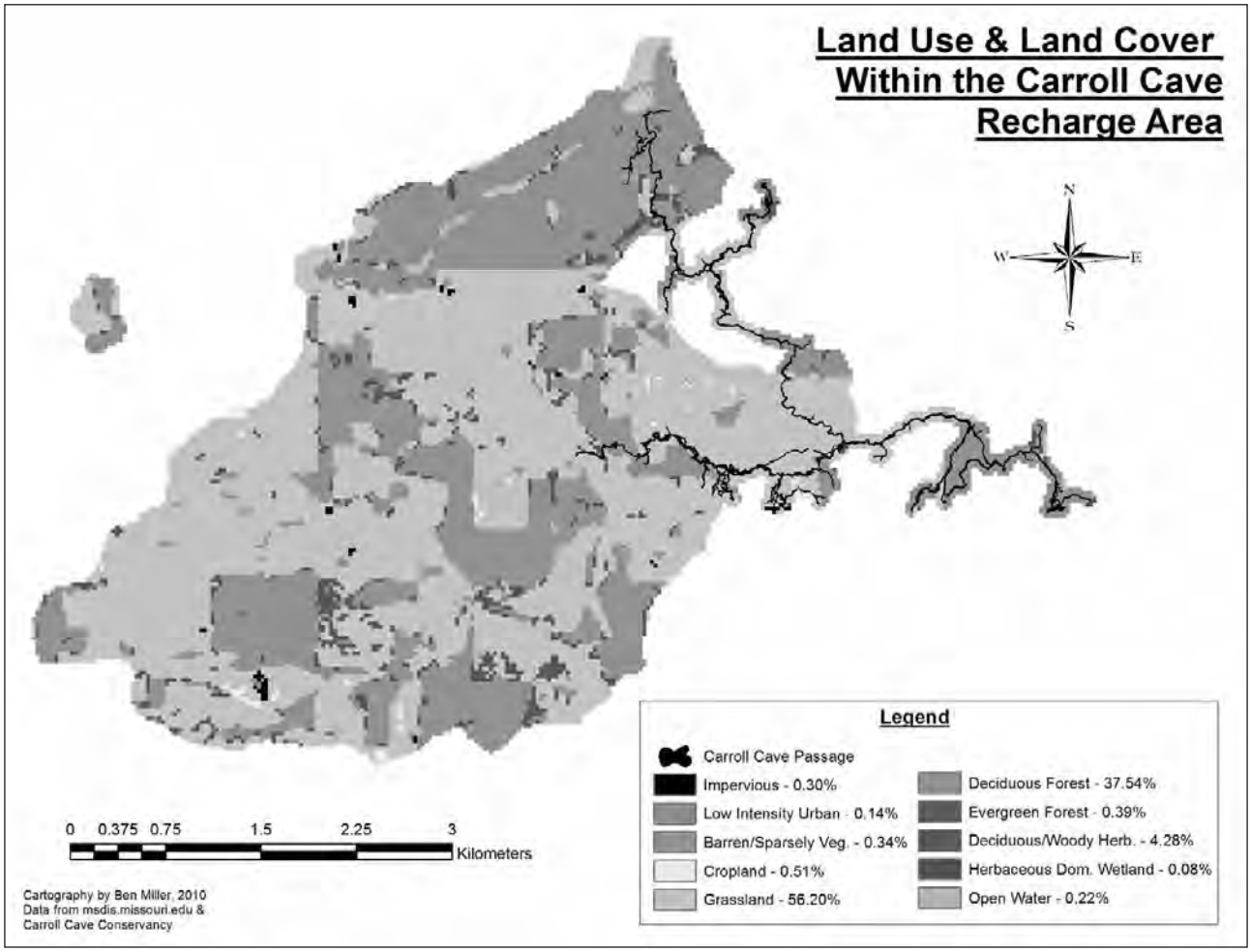

Figure 6. Land Use – Land Cover in the Carroll Cave recharge area.

main swallet. The water sinking downstream of the upper springs was positively traced to all eight of the springs located 9.6 kilometers down canyon. Travel time from injection site to resurgences took less than seven days and flow velocities in the area at least 56 m/hr but likely exceed this rate. This information was reported to agency personnel and will be incorporated into the management of the water resources of this area, especially since Wet Medicine Lodge Creek is utilized for irrigation a short distance downstream of the resurgences.

2.4. Crumps Cave, Kentucky, USA

Crumps Cave is a two-kilometer-long cave located in south-central Kentucky on the Pennyroyal Sinkhole Plain. The cave is formed in the Carboniferous St. Louis Limestone and is located in the headwaters of the Graham Springs recharge area, a 360 km^2 basin recharging one of the largest springs in Kentucky (Hess et al. 1989). The cave is owned and managed for karst research and education by the Hoffman Environmental Research Institute at Western Kentucky University.

Hydrologic research examining the characteristics of the epikarstic aquifer has used groundwater tracing to compliment geochemical analyses to aid in determining flow rates from the surface environment to monitored perennial waterfalls located throughout the cave. These injections have been conducted using augured holes into the soil column (Fig. 8) as well as artificial rainfall simulators. Additionally tracer tests have been conducted from the in-cave waterfalls to the final resurgences at Graham Springs located over 35 kilometers to the west. Variances in travel times of the epikarstic traces largely depend on the hydrologic conditions of the epikarstic aquifer influenced primarily by rain events and the storage capacity of the aquifer. Traces through the epikarst to the in-cave waterfall, a distance of less than 150 meters, may take as less than a few hours if aided by rainfall simulator or as much as several weeks if conducted during a drier period. Traces from the perennial waterfalls inside the cave to Graham Springs also vary, but traces conducted in base flow conditions took approximately six days to travel 35 kilometers. These traces highlight the variability in travel

Figure 7. Conducting a Karst hydrologic Inventory in Lower Wet Medicine Lodge Canyon, Wyoming.

Figure 8. Injecting fluorescein dye into drilled hole in the soil column.

times between the epikarstic aquifer and the conduit- flow aquifers feeding the large springs of the sinkhole plain. Traces continue to examine these variances and aid in understanding contaminant transport in a karst area where land use is dominated by row crop agriculture.

3. Conclusions

Groundwater tracing is a useful tool in understanding the hydrology of a cave system or karst area, which can be applied in a variety of different situations. By identifying recharge and discharge features in a karst area one can determine good monitoring locations and good dye injection locations. Monitoring for the traces typically use charcoal receptors, however other options exist which may work better depending on one's objectives and budgets. Case studies highlighted in this paper used groundwater tracing to delineate groundwater recharge areas for significant caves, determine resurgences for cave streams, and to compliment hydrologic research on contaminant transport in karst systems. Many other applications of groundwater tracing exist in cave studies and many karst areas still contain a large amount of work which can be done to better understand the ongoing hydrologic processes.

References

Aley T, Fletcher MW, 1976. Water tracers cookbook. Missouri Speleology, 3(16), 1–3.

Crawford Hydrology Laboratory, 2010., Karst Groundwater Investigation Procedures. Bowling Green, Kentucky. www.dyetracing.com

Hess JW, Wells SG, Quinlan JF, White WB, 1989. Hydrogeology of the south-central Kentucky karst. In: White, W.B. and White, E.L. (Eds.). Karst Hydrology. Concepts from the Mammoth Cave Area Van Nostrand Reinhold New York. P. 15–63.

Huntoon PW, 1985. Gradient Controlled Caves, Trapper Medicine Lodge Area, Bighorn Basin, Wyoming. Groundwater, 23(4), 443–448.

Jones WK, 1984. Dye tracer tests in karst areas. The NSS Bulletin, Vol. 46, 3–9.

Miller B, Lerch R, 2011. Delineating recharge areas for Onondaga and Cathedral Caves using groundwater tracing techniques. Missouri Speleology, 51(2), 1–36.

Miller BV, 2010. The Hydrology of the Carroll Cave-Toronto Springs System: Identifying and Examining Source Mixing through Dye Tracing, Geochemical Monitoring, Seepage Runs, and Statistical Methods. Master's Thesis, Western Kentucky Univ. Bowling Green, Kentucky.

Meus P, Käss W, Schnegg PA, 2006. Background and detection of fluorescent tracers in karst groundwater. Karst, climate change and groundwater. Hidrogeologia y Aguas Subterráneas, 18, 65–75.

THE JAJ PLATEAU (LEBANON): TYPICAL HIGH ALTITUDE MEDITERRANEAN KARST

Fadi H. Nader, Hughes Badaoui, Marc Metni, Chadi Chaker, Habib Helou, Johnny Tawk
Spéléo-Club du Liban, P.O. Box: 70-923 Antelias, Lebanon, fadi.nader@gmail.com

The high Plateau of Jaj in Mount Lebanon displays an excellent open-air museum for a typical Mediterranean Karst landscape (Fig. 1). It exposes the Jurassic carbonate rocks (limestone and hydrothermal dolomites), locally called the Kesrouane Formation over a relief ranging from about 1,300 to 1,955 m above sea level (Qornet el Alieh, being the highest point). Structurally speaking, this area is part of the Qartaba folded (asymmetrical) structure with relatively gentle dipping towards the west and steep limbs towards the east. The Jurassic rocks were covered by volcanic deposits that were eroded later on upon the emergence of Mount Lebanon. This could explain not finding deep caves – most of them are filled by volcanic weathered material.

Such a high elevated Jurassic landscape, with well evolved karstified weathered surface cannot be overlooked by speleologists and cave explorers! Even if, the plateau is bounded by major karst features like the Bala'a sinkholes (three potholes with average depth of 200 m), undertaking field search for caves at altitudes averaging 1,700 m, with no water sources or enough shades (except the few majestic cedars trees) and on rough terrain has proven to be less attractive (Fig. 2). Decades ago, cavers from the Spéléo-Club du Liban have discovered and documented around 20 caves on the plateau, mostly pitches; some of which hosted ice that was thought to remain from year to year. Recent systematic exploration has started again and was planned together with the 3rd Middle East Speleology Symposium (2011).

This presentation will expose some geomorphological peculiarities of the Jaj Plateau, and the exploration work that is undergoing with its first results. It will also highlight the need to protect this special karstic area.

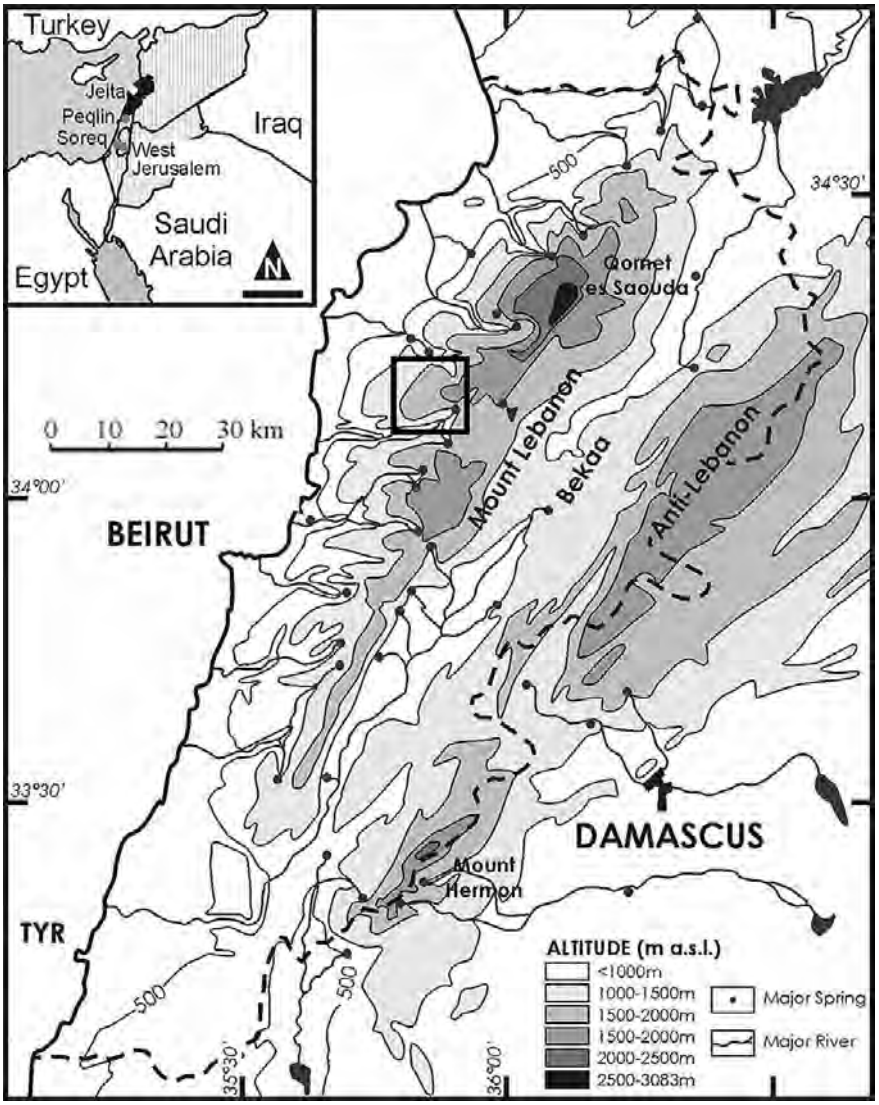

Figure 1. Simplified topographic map of Lebanon indicating the location of the Jaj Plateau (square). The index map shows the location of Lebanon in the Eastern Mediterranean region.

Figure 2. View from a cave on the Jaj Plateau showing the bare-karst landscape.

A CONCEPTUAL MODEL OF SPELEOGENESIS IN GREECE

Christos Pennos[1] Stein-Erik Lauritzen[2]
[1]School of Geology, Department of Physical Geography, Aristotle University of Thessaloniki, GR-54124, Greece, pennos@geo.auth.gr
[2]Department of Geology, University of Bergen, N-5007 Bergen, Norway, Stein.Lauritzen@geo.uib.no

Over 70 % of Greece's territory consists of carbonate rocks (limestone and marble). This almost homogenous geology in correlation with the special tectonic regime of the broader region of the east Mediterranean makes the region an ideal site for cave development. The exact number of Greek caves is still unknown since there is no formal cadastral. However, there is an estimation of more than 10,000 caves and rockshelters. Here, we attempt to make a correlation between the cave dimensions and their locality. First, a creation of a cadastral took place using data provided by cavers and caving clubs. Statistical analyses of depth, length and altitude of the caves were performed in order to define the key factor for the development of the caves and to create a general conceptual model about the speleogenesis in Greece. The combination of the above revealed a clear difference on the speleogenesis between the caves in the outer and the inner part of the Aegean orogeny.

1. Introduction

The lithological structure of Greece consists mainly of carbonate rocks in combination with the Mediterranean climate, favors the development of karst phenomena to a large extent. A rough estimation of the total number of karst caves in Greece includes more than 10,000 caves. During the last decades the development of cave exploration in Greece along with the increasing interest of many European cavers has led to numerous caving expeditions. However, little attention has been paid to the study of caves from a scientific point of view. In this work we attempt for the first time to create a general conceptual speleogenetic model for the Greek caves based on cave statistics of their characteristics, such as depth, width and length. A correlation between cave locality and the tectonic regime is tested.

2. Geological setting.

The Greek territory consists mainly by carbonate rocks (marbles and limestones). In general, northern Greece consists of Paleozoic marbles and metamorphic rocks since it is part of the old continental crust around which the closing of the Tethys Sea took place during the Alpine orogenesis. In contrast, the rest of the Greek mainland as well as most of the Greek islands are mainly built up of Mesozoic limestones that represent the shallow and deep marine deposits of the Tethys Sea. The general structure is characterized by a series of stacked nappes, ~ 5–10 km thick (composite), consisting of the upper crust that decoupled from the present subducted continental and oceanic lithosphere of the Adriatic–African Plate (van Hinsbergen et al.; 2005, 2010; Jolivet and Brun 2010). These nappes (or "mega-units") were thrusted and stacked in a north-to-south direction since the Cretaceous (Faccenna et al. 2003; van Hinsbergen et al. 2005; Jolivet and Brun 2010) and form a strongly shortened representation of the paleogeographical distribution of continental ribbons and deep basins that existed in the western Neo-Tethys (e.g., Dercourt et al. 1986; Barrier and Vrielynck 2008; Stampfli and Hochard 2009).

The Aegean Sea and the surrounding areas belong to the active continental boundary of the Alpine–Himalayan belt (Fig. 1) and as a result suffer a large-scale active deformation, stemming from the subduction of the eastern Mediterranean lithosphere under the Aegean Sea, along the Hellenic Arc (Papazachos and Comninakis 1969). Consequently, the continental and coastal parts of Greece share the common characteristics of the back–arc extensional tectonics, expressed by the presence of a strong deformational pattern, volcanic activity and the development of fault bounded grabens, lying in accordance with the dominant N–S extensional stress field. However, as illustrated in Figure 1, the northern part of Greece is additionally influenced by a subsidiary right–lateral shear because of the coexistence with the North Aegean Trough, a dextral strike-slip structure associated with a series of strong earthquakes (McKenzie 1972).

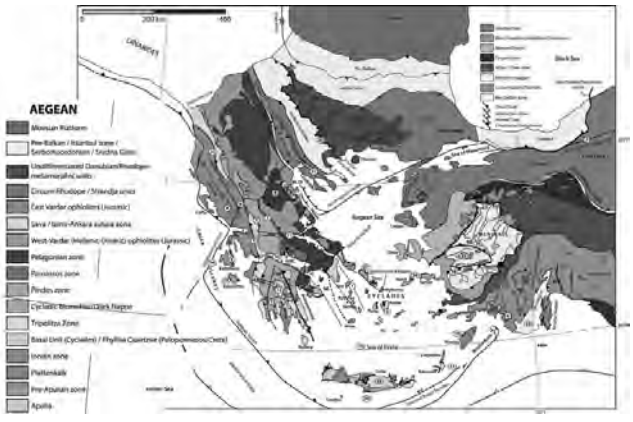

Figure 1. Geotectonic Regime of the Aegean (from van Hinsbergen and Schmid 2012).

3. Methodology

In order to investigate the key factors that influenced the development of Greek caves and to set up a general model concerning the speleogenesis in Greece, a proper cadastral was created. Parameters concerning cave dimensions such as depth, length and altitude, as well as the locality of almost 4,000 Greek caves are included. The cadastral is based on an enriched version of the SPELEO club cadastral (Theodosiadis 2011), while further data provided from the

Greek cavers K. Adamopoulos (SELAS caving club) and G. Sotiriadis (Proteas caving club). A statistical analysis of the relation between various speleometric parameters was conducted and explored through correlation plots. Moreover, ArcGIS software was used to create a thematic map with the position of the forty deepest caves in order to clarify the relation of the present tectonic regime and cave development.

4. Results and discussion

Statistical analysis revealed that there is no clear correlation between the altitude and the length of the studied caves (Fig. 2). This is probably due to the different geological and hydrological criteria that prevailing in the study area (Greece) and they are controlled by the regional geology, tectonic activity and the landscape.

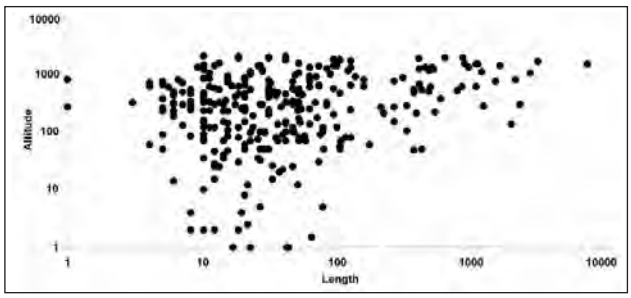

Figure 2. Altitude – length plot.

In contrast as it seen in the diagram between the depth and the length of caves (Fig. 3) there is appositive correlation between these two parameters. This is because the measured length of the cave is a function of the surveyed depth, deep caves tend to be long and *vice versa*.

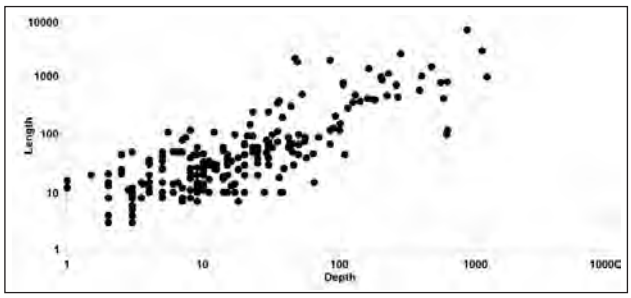

Figure 3. Length – depth plot.

Furthermore, the diagram created to investigate the relationship between the depth and the altitude at which the caves appear (Fig. 4) shows that the majority of the deeper caves occur at an altitude over 400 m. There is also an upper boundary of cave altitude, controlled by the topography. The lower boundary (slope 0.91) is connected to the internal relief; deep caves are found in terrain of great relief.

In order to further investigate the factors that influenced Greek cave development a map showing the positions of the studied caves and the tectonic setting of Greece with the main tectonic lines was created (Fig. 5). In this map, it becomes evident that the deepest caves tend to be located in areas adjacent to the subduction arc. This is explained by the fact that at these areas compressive stress results in constant uplift and in intense (tensional) fracturing of the bedrock at high altitudes. The continuous raising of these

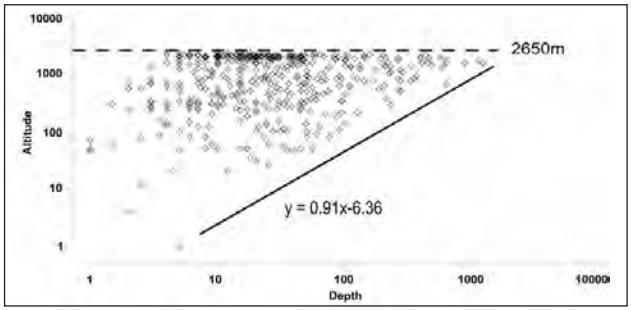

Figure 4. Altitude – depth plot.

regions (and erosion) lead to continuous lowering of the phreatic zone and, as a consequence, to the creation of a deep vadose zone. This fact, in combination with the strong fracturing favors the creation of deep caves.

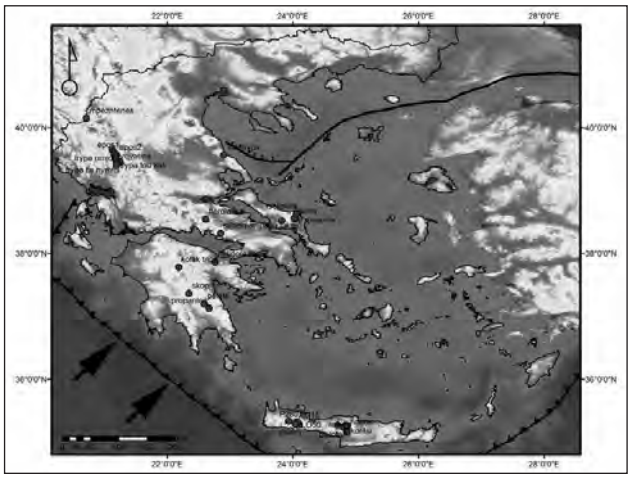

Figure 5. Map of the region with the main tectonic lines. The positions of the forty deepest Greek caves are depicted with dots.

5. Conclusions

The exploratory statistical analysis of the cave parameters in relation to the spatial distribution of the deep caves suggests that the major factor controlling the speleogenesis in the area is the tectonic activity of the region. The tectonic setting of the broader Greek territory results in the fracturing of the carbonate bedrock in accentuated topographic relief, creating ideal conditions for vadose speleogenesis (most deep caves of the World are essentially vadose). The high tectonic activity is responsible for the continuous lowering of the phreatic zone creating a high vadose zone in which the deep caves occurred.

Acknowledgments

The authors would like to thank the cavers Thomas Theodosiadis (SPELEO club), George Sotiriadis (Proteas club) for providing data from their personal archives and Kostas Adamopoulos (SELAS club) for providing us numerous unpublished data from his archive as well as for the discussions on the topic. Special thanks to Dr. Sofia Pechlivanidou and Charikleia Garlaouni for their valuable conversations during the preparation of the manuscript. Finally, the authors would like to express their gratitude to Pavel Bosak and Michal Filippi for their remarks and recommendations.

References

Adamopoulos K, 2005. The deepest and the longest caves in Greece, Proceedings of 14th International Congress of Speleology, 21–28 August, 2005, Athens, Kalamos, Greece.

Adamopoulos K, 2011. Lefka Ori, The biggest Greek caves in Crete island (in Greek). Proceedings of the 14th Panhellenic speleological meeting, Chania, Crete.

Barrier E, Vrielynck B, 2008. MEBE Atlas of Paleotectonic maps of the Middle East, Commission for the Geological Map of the World.

Dercourt J, Zonenshain LP, Ricou L-E, Kazmin VG, Le Pichon X, Knipper AL, Grandjacquet C, Sbortshikov IM, Geyssant J, Lepvrier C, Pechersky DH, Boulin J, Sibuet J-C, Savostin LA, Sorokhtin O, Westphal M, Bazhenov ML, Lauer JP, Biju-Duval B, 1986. Geological evolution of the tethys belt from the atlantic to the pamirs since the LIAS, Tectonophysics, Volume 123, Issues 1–4, Pages 241–315, ISSN 0040-1951, 10.1016/0040-1951(86)90199-X.

Faccenna C, Jolivet L, PiromalloC, Morelli A, 2003. Subduction and the depth of convection of the Mediterranean mantle, Journal of Geophysical Research, 108(B2), 2099.

Jolivet L, Brun J-P, 2010. Cenozoic geodynamic evolution of the Aegean, International Journal of Earth Sciences, 99, 109–138.

McKenzie D, 1972. Active Tectonics of the Mediterranean Region. Geophysical Journal of the Royal Astronomical Society, 30: 109–185. doi: 10.1111/j.1365-246X.1972.tb02351.x.

Papazachos B, Comninakis P, 1970. Geophysical features of the Greek island arc and eastern Mediterranean ridge, Com. Ren. Des Sceances de la Conference Reunie a Madrid, 1969, Vol. 16, 74–75.

Stampfli G, Hochard MC, 2009. Plate tectonics of the Alpine realm, in Ancient orogens and modern analogues. Geological Society, London, Special Publications, edited by J. B. Murphy, et al., 89–111.

Theodosiadis T, 2011. SPELEO cave cadastral, SPELEO club, Athens, Greece. http://arxeio.speleo.gr

van Hinsbergen, DJJ, Hafkenscheid E, Spakman W, Meulenkamp JE, Wortel MJR, 2005. Nappe stacking resulting from subduction of oceanic and continental lithosphere below Greece, Geology, 33(4), 325–328.

van Hinsbergen, DJJ, Kaymakci N, Spakman W, Torsvik TH, 2010. Reconciling the geological history of western Turkey with plate circuits and mantle tomography, Earth and Planetary Science Letters, 297, 674–686.

van Hinsbergen, DJJ, Schmid SM, 2012. Map view restoration of Aegean–West Anatolian accretion and extension since the Eocene, Tectonics, 31, TC5005, doi:10.1029/2012TC003132.

COMPLEX EPIKARST HYDROLOGEOLOGY AND CONTAMINANT TRANSPORT IN A SOUTH-CENTRAL KENTUCKY KARST LANDSCAPE

Jason S. Polk[1], Sean Vanderhoff[1], Chris Groves[1], Benjamin Miller[1], and Carl Bolster[2]
[1]Hoffman Environmental Research Institute, Western Kentucky University, Bowling Green, KY 42101 United States, jason.polk@wku.edu
[2]USDA-Agricultural Research Service, Bowling Green, KY, 42101 United States

The movement of autogenic recharge through the shallow epikarstic zone in soil-mantled karst aquifers is important in understanding recharge areas and rates, storage, and contaminant transport processes. The groundwater in agricultural karst areas, such as Kentucky's Pennyroyal Plateau, which is characterized by shallow epikarst and deeper conduits flow, is susceptible to contamination from organic soil amendments and pesticides. To understand the storage and flow of autogenic recharge and its effects on contaminant transport on water flowing to a single epikarst drain in Crump's Cave on Kentucky's Mississippian Plateau, we employed several techniques to characterize the nature and hydrogeology of the system. During 2010–2012, water samples and geochemical data were collected every four hours before, during, and between storm events from a waterfall in Crumps Cave to track the transport and residence time of epikarst water and organic soil amendments during variable flow conditions. Geochemical data consisting of pH, specific conductivity, temperature, and discharge were collected continuously at 10-minute intervals, along with rainfall amounts. In addition, stable isotope data from rainfall, soil water, and epikarst water were collected weekly and during storm events to examine storage and recharge behavior of the system. The changes in geochemistry indicate simultaneous storage and transport of meteoric water through epikarst pathways into the cave, with rapid transport of bacteria occurring through the conduits that bypass storage. The isotopic data indicate that recharge is rapidly homogenized in the epikarst, with storage varying throughout the year based on meteorological conditions. Results indicate current best management practices in agricultural karst areas need to be revisited to incorporate areas that do not have surface runoff, but where contaminants are transported by seepage into local aquifers.

1. Introduction

Kentucky's subtropical climate and fertile soil provide extensive agricultural lands for row crops. A common agricultural practice in the area is to apply animal waste as an organic soil amendment for soil nutrient enhancement. If these amendments are not completely exhausted through crop utilization, they can become pollutants and enter the groundwater system. In Kentucky, 55 % of the land area is characterized by highly soluble carbonate rocks within which karst landscapes form (Currens 2002). The resulting karst landscape/aquifer systems, typically with high permeability, are characterized by the development of features such as sinkholes, caves, and large springs. Because much of the recharge entering these systems moves rapidly under turbulent flow, and in many cases as sinking streams with little physical filtration, groundwater in these karst aquifers is often highly susceptible to contamination from agricultural practices, among other sources of pollution (White 1988; Drew and Holtzl 1999).

This research was designed to better understand the fate and transport of agricultural contaminants in the well-developed karst aquifer/landscape systems of south-central Kentucky by conducting field experiments associated with actual field-scale agriculture at the Crumps Cave Educational Preserve, and aimed to answer the following research questions: (1) if aquifer recharge influences manure transport at this representative site, is there significant retardation of flow and storage of water and/or fecal bacteria in the soil/epikarst zone before it enters the main part of the aquifer?; and, if so 2) what is the timing of flow through this shallow part of the epikarst flow system?; 3) how does that effect the introduction of fecal bacteria into the main part of the aquifer?; and 4) where is the primary storage for contaminants and bacteria in the soil-epikarst setting?

2. Study Area

Crumps Cave is located beneath a portion of the extensive sinkhole plain of the Pennyroyal Plateau within the Mississippian Plateaus Section of the Interior Low Plateaus Physiographic Province in Waren County, KY, USA (Figure 1) (Groves et al. 2005). There is about two km of horizontal cave passages beneath several agricultural fields, with the cave floor averaging 25 m below the surface. The recharge area lays within the Graham Springs groundwater basin (Ray and Currens 1998, 2000) which discharges at Wilkins Bluehole on the Barren River, 18 km southwest. It is the second largest spring in Kentucky (Ray and Blair 2005). The site is underlain by Crider silt loam, Pembroke silt loam and Baxter gravelly silt loam soils (Soil Survey Staff NRCS 2011). These soils are moderately permeable, well-drained soils, reddish in color with chert fragments in their lower portions. The thickness of the soils varies throughout the study area. Auger hole tests show the thickness before encountering chert fragments ranges from 0.3–4 meters.

The entrance to Crumps Cave is a collapse sinkhole that has partially collapsed. The cave passages have formed within the highest part of the Mississippian-aged St. Louis limestone, with a local dip of 1–2° to the west (Richards 1964). The bedded Lost River Chert lies between the ground surface and the cave below, and locally appears to operate as a leaky perching layer. Water tends to reach the

cave at distinct locations, mainly at perennial or intermittent waterfalls emerging from the cave ceiling through fractures, draining the epikarstic zone to the east of the cave and flowing westward down the dip of the rock (Bolster et al. 2005). Six perennial in-cave waterfalls are located within the entrance area of the cave. These waterfalls are focused on the east side of the cave, but some flow from different parts of the ceiling. Waterfall One (WF1) is approximately 4.5 m tall and is located 40 m from the entrance. It is the closest waterfall to the entrance and has perennial flow (Figure 2). It is the focus of the monitoring and research described herein.

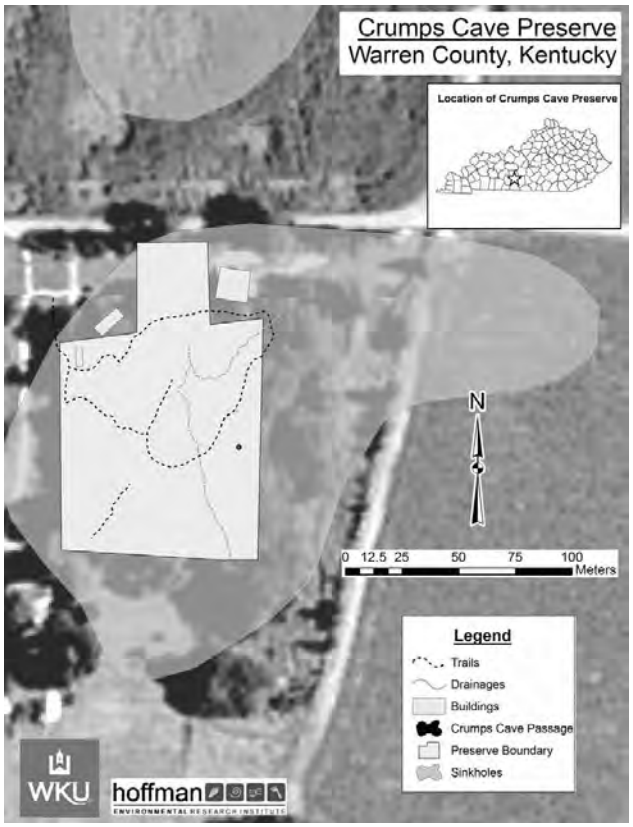

Figure 1. Location of Crumps Cave, Warren County, KY, USA.

The climate of Warren County is classified as a humid subtropical climate on the Köppen climate classification scale (*Cfa*). Its humid summers reach an average high temperature of 31 °C and its mild to cool winters average a high of 7 °C (NOAA 2011). The average annual total precipitation is around 1,294 millimeters. Of this, about 721 millimeters, or 56 percent, usually falls in April through October. May has the highest average rainfall with 136 millimeters (NOAA 2011). The growing season for most crops falls in the April through October range. Hess (1974) estimated that mean-annual potential evaporation is 800 mm, varying from near zero to over 100 mm/mo.

Land use above and surrounding Crumps Cave is dominated by agriculture (Figure 1). Row cropping, which usually rotates between corn, soy, and wheat, surrounds the Crumps Cave property to the east and north. West of the property is a residential property at which a bed and breakfast operation is run. Northeast of the property land is currently being used for cattle grazing.

3. Methods

The movement of autogenic recharge through the shallow epikarstic zone in soil-mantled karst aquifers is important in understanding recharge areas and rates, storage, and contaminant transport processes. To understand the storage and flow of autogenic recharge flowing to a single epikarst drain in Crump's Cave on Kentucky's Mississippian Plateau, we employed several methods to characterize the nature of the system.

3.1. Storm Event Contaminant Sampling

From 2010–2012, on the surface at Crumps Cave, 110 meters from the sink entrance, a HOBO U-30^{tm} weather station was used to collect weather data. A rain gauge tipping bucket collected rainfall amounts every ten minutes. The weather station also collected temperature, dew point, solar radiation, relative humidity, wind speed and direction, and soil moisture content with ten-minute resolution.

Inside the cave, a 208 liter barrel with circular holes drilled into its side to measure discharge was placed under WF1 and a conical tarp directs virtually all flow of the epikarst drain into the barrel (Figure 3). A procedure based on Bernoulli's law relates the WF1 discharge rate (L/s) to the water level (stage height) in the barrel (White 1988). The water level is measured by a pressure transducer inside a stilling well at ten-minute resolution. At WF1, two Campbell Scientific CR10x data loggers were used to collect geochemical and discharge data for the waterfall. Data Logger One (DL1) recorded data from one pH probe, one dual specific conductance and temperature probe, and a pressure transducer probe placed in the discharge barrel at WF1. Data Logger Two (DL2) recorded data from two pH probes and a duel specific conductivity probe. Both data loggers collected data every two minutes and recorded the average every ten minutes for temperature, specific conductance (SpC), and pH. Stage height from the pressure transducer was also recorded every ten minutes.

During the farming season of late winter through spring, three fluorescent dye traces (sulphorhodamine B, fluorescein, and eosine, respectively) took place to track transport and residence time of water from storm events and epikarstic waters. The dyes were chosen for their spectrum wavelength so as to be able to recognize each individual dye as it came through WF1 from the surface. The traces were performed in a location on the edge of the property in an area that has previously been established as having a hydrological surface connection to WF1.

ISCO 3700 portable water samplers were placed in the cave at WF1 to collect water samples to analyze for dye, bacteria, cations and anions. Samples were collected in 1000 mL polypropylene bottles every four hours during storm events occurring within the study period. During a portion of the winter and spring sampling period weekly samples of fecal coliform bacteria (FC) were taken. Samples were also collected weekly for the analysis of dye and collected within 24 hours of analysis time for total coliform, *E. coli*, cations and anions.

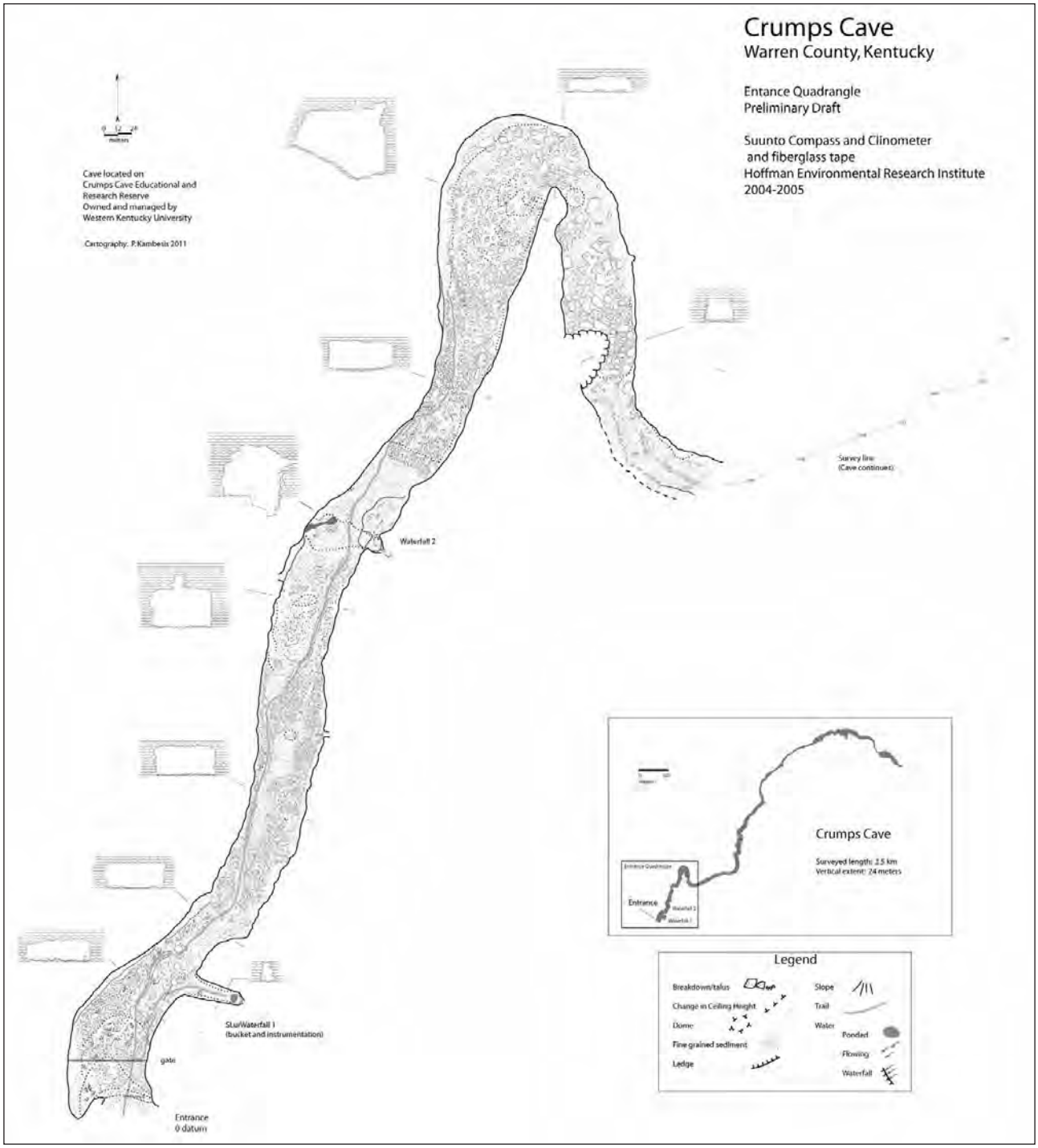

Figure 2. Map of Crumps Cave in south-central Kentucky.

3.2. Epikarst Storage and Recharge

First, we performed base flow separation of several discrete storms, where stormflow was integrated to measure individual storm volumes, and a nominal recharge area parameter, ζ, was calculated for each storm event by determining the measured amount of rainfall (thickness) and setting the drainage volume from the in-cave waterfall during the event to be equal to this recharge amount, and then dividing the resulting recharge volume by the presumably uniform measured rainfall depth. In this manner, we are taking the volume of discharge at the waterfall and dividing it by the amount of rainfall during the event (volume/thickness) to calculate an estimated area over which the rainfall presumably fell during the event, or in this case an average recharge area on the surface that contributes to the water flowing from the waterfall.

A second independent proxy of recharge and epikarst storage conditions from isotopic analysis of precipitation and epikarst water supports this finding. Rainfall amounts above the cave and discharge of the water flowing from the drain below were measured every ten minutes in 2010–12. Weekly precipitation and cave waterfall samples were collected for stable isotope (O and H) analysis, with higher resolution sampling of the waterfall during storm events.

A third measure of the character and response of the epikarst was the three dye-traces performed during the study period, which resulted in a breakthrough curve for each storm event that caused the dye to move through WF1, which provided an estimated threshold for epikarst storage to be flushed out and the travel time of surface water to WF1

under various antecedent storage conditions (Figure 4).

Figure 3. Discharge barrel and data logger setup at WF1 during storm event.

4. Results and Discussion

Identifying the hydrological characteristics of the soil-epikarst zone in response to storm events is an important task for understanding the fate of agricultural contaminants. Recognizing the mechanisms of movement and storage is central for determining the fate of these pollutants. The movement of fecal coliform bacteria through the soil-epikarst is dictated by the amount and intensity of storm events. During the study period, the majority of storm events provoked a response at WF1 indicated by the increased discharge. The data show contaminants that move through the epikarstic system correlate with significant rainfall events and rainfall amount. The dye traces and SpC data support this statement and further the understanding of soil-epikarst hydrology and contaminant transport.

The various storm event data and dye traces combined with fecal coliform analysis indicate rapid response of the epikarst drain to precipitation events (Figures 5, 6). High levels of contaminants, including *E. Coli*, were found during the peak of each storm event, with maximum numbers (greater than 200 colonies/100mL) being reached shortly after surface application, but lasting for many months.

For the epikarst storage data, values of ζ range from 843 m^2 to 11,200 m^2, with lower values likely resulting from water entering epikarst storage that does not reach the drain during that storm response. Values of ζ may thus provide way to quantify varying epikarst storage input. Data also suggest that the actual recharge area is on the order of 100 × 100 m. Using between-storm baseflow discharges and individual values of ζ for storm events, we calculated unit-baseflow (UBF – baseflow discharge per unit recharge area, calculated from dividing total discharge during baseflow conditions by calculated area from ζ), and show that calculated values for the epikarst drain are 2–3 orders of magnitude higher than published UBF values for regional springs (Worthington 2007). This gives quantitative evidence that storage is more concentrated in the epikarst than the regional aquifer as a whole.

Precipitation isotope $\delta^{18}O$ values ranged from -5.7 to -16‰, while the cave waterfall $\delta^{18}O$ values averaged -6.3‰ (ranging between -5.2 to -7.3‰), indicating that despite intense storm events with highly variable $\delta^{18}O$ values, a rapid homogenization of meteoric recharge water with epikarst storage water occurs in the system, further supporting that substantial storage occurs in the epikarst zone through diffuse flowpaths.

From the seasonal data, there are two conditions that occur in the soil that dictate the transport of fecal coliform and *E. coli*. First, there is a threshold for rain intensity and rain amount that push the bacteria (Pasquarell and Boyer 1995) and dye through the soil-epikarst system (Figure 6). Additionally, diffuse flow through conduits adds to the movement of bacteria through the soil-epikarst system. Significant storm events infiltrate the soils and create a high hydraulic head that rapidly pushes the bacteria through main conduits of the epikarst (WF1). This causes a quick drop in SpC and a rise in discharge simultaneously. After the head is lowered, discharge decreases, SpC will slowly rise back toward pre-storm levels and FC counts will decrease. Often, the SpC does not return to previous base flow levels, likely due to the dilution of storage water by rainfall. However, during periods of higher storage, it appears as though continuing recharge and hydraulic pressure pushes out additional storage waters after storm event recovery, and there is a rise in SpC during the falling limb of the discharge curve. During time in-between storms, waters percolate through diffuse conduits as evident by the lower fecal coliform and *E. coli* counts and steady rise of SpC, which indicates water that is in contact with the bedrock for a longer duration, thus dissolving more carbonate rock.

This information is vital to understanding and improving best management practices in agriculture on karst terrains, particularly with regard to water quality degredation from the application of organic soil amendments. The results indicate that rapid, continuous contamination can occur from the use of manure and fertilizers in karst areas, and this must be addressed through better policy creation.

Acknowledgments

We gratefully acknowledge USDA ARS for funding support for this project and Western Kentucky University for

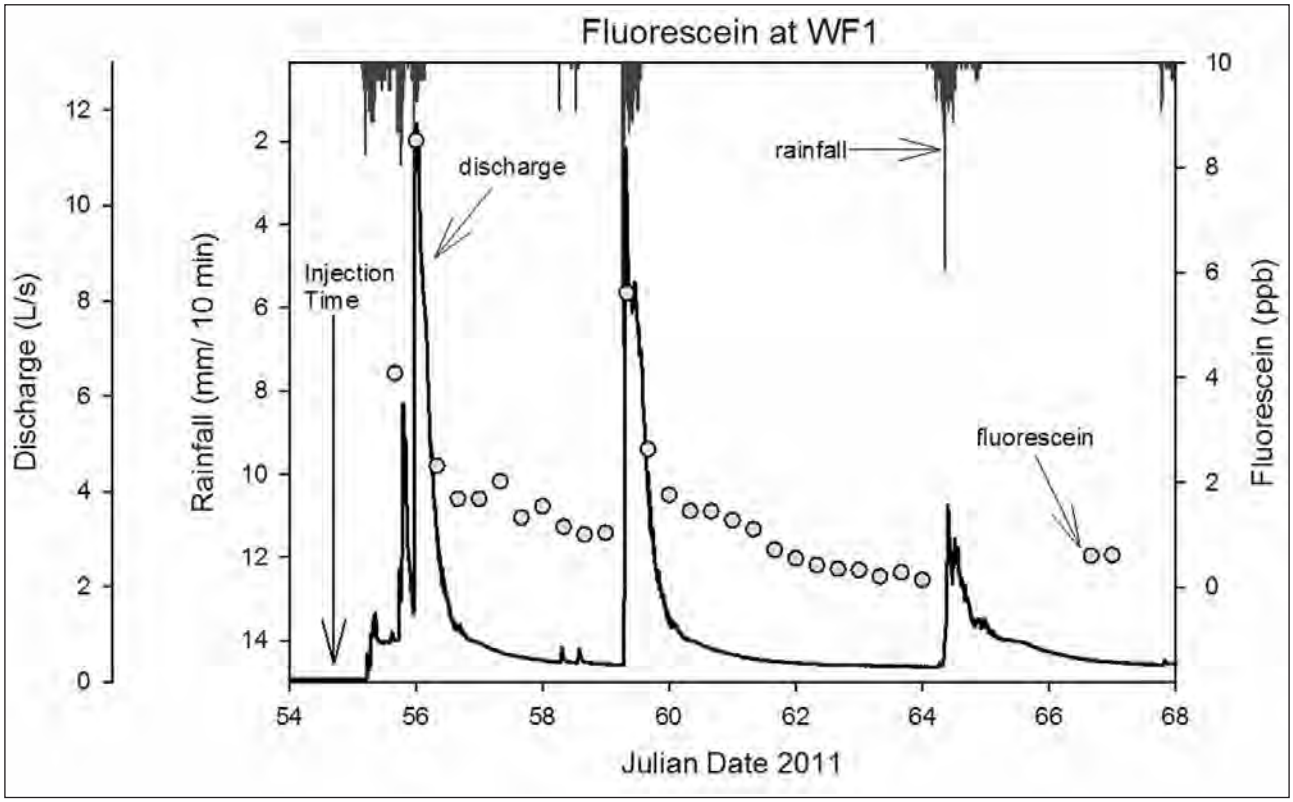

Figure 4. Dye trace 2 during the study period (dots), indicating the WF1 response to a storm event as shown by how the dye moved through with the storm pulses.

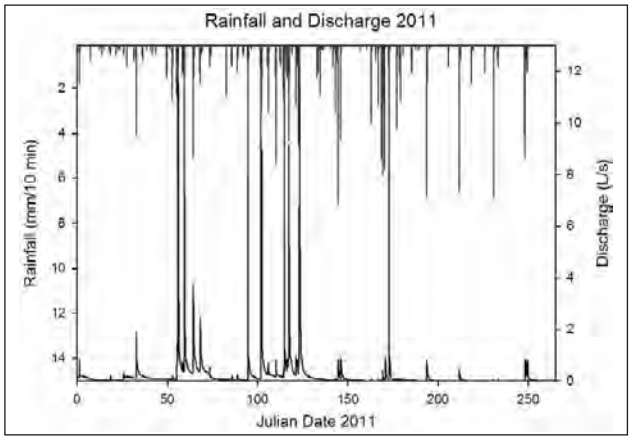

Figure 5. Example of discharge response in WF1 during storm events from 2011.

contributing resources to site management. Crumps Cave site purchased using a Kentucky Heritage Land Conservation Funds. Much thanks to WKU Hoffman Institute staff and students, Nick Lawhon, Sarah Arpin, Micah Ruth, Dan Nedvidek, Celia Davis, Lee Anne Bledsoe, Beth Tyrie, Kegan McClanahan, Laura Osterhoudt, Gabe Russell, and Dalene Smith for assistance in the field and lab.

References

Bolster C, Grover C, Meiman J, Fernandez-Cortez A, Carrie Crockett, 2006. Practical limits of high-resolution evaluation of carbonate chemistry within karst flow systems. Proceedings of the Conference on Limestone Hydrogeology.

Currens JS, 2002. Kentucky is Karst Country*:* What you should know about sinkholes and springs. Kentucky Geological Survey. Information Circular 004, Series 12.

Drew D, Holtzl H, 1999. Karst Hydrogeology and Human Activities. Impacts, Consequences and Implications. Rotterdam, Brookfield: Balkema.

Groves C, Bolster C, Meiman J, 2005. Spatial and temporal variations in epikarst storage andflow in south central Kentucky's Pennyroyal Plateau sinkhole plain. Proceedings of the USGS Karst Interest Group Conference.

Hess J, 1974. Hydrochemical Investigations of the central Kentucky Karst Aquifer System. PhD. thesis, Department of Geosciences, The Pennsylvania State University.

NOAA. National Climatic Data Center http://www.ncdc.noaa.gov/oa/ncdc.html. Accessed 11/23/2011.

Pasquarell GC, Boyer DG, 1995. Agricultural Impacts on Bacterial Water Quality in Karst Groundwater. Journal of Environmental Quality 24(5): 959–969.

Ray JA, Currens JC, 1998. Mapped karst groundwater basins in the Beaver Dam 30 × 60 Minute Quadrangle, Kentucky Geological Survey.

Ray JA, Currens JC, 2000. Mapped karst groundwater basins in the Campbellsville 30 × 60 Minute Quadrangle, Kentucky Geological Survey.

Ray JA, Blair RJ, 2005. Large perennial springs of Kentucky: Their identification, base flow, catchment, and classification. *in* Beck, B.F. (ed) Sinkholes and the Engineering and Environmental Impact of Karst. Geotechnical Special Publication 144. American Society of Civil Engineers, Reston, Virginia, 410–422.

Richards PW, 1964. Geologic map of the Smiths Grove quadrangle, Kentucky. US Geological Survey Geologic Quadrangle Map GQ 357.

Soil Survey Staff NRCS. 2011. United States Department of Agriculture. Web Soil Survey. http://websoilsurvey.nrcs.usda.gov/. Accessed (11/7/2011).

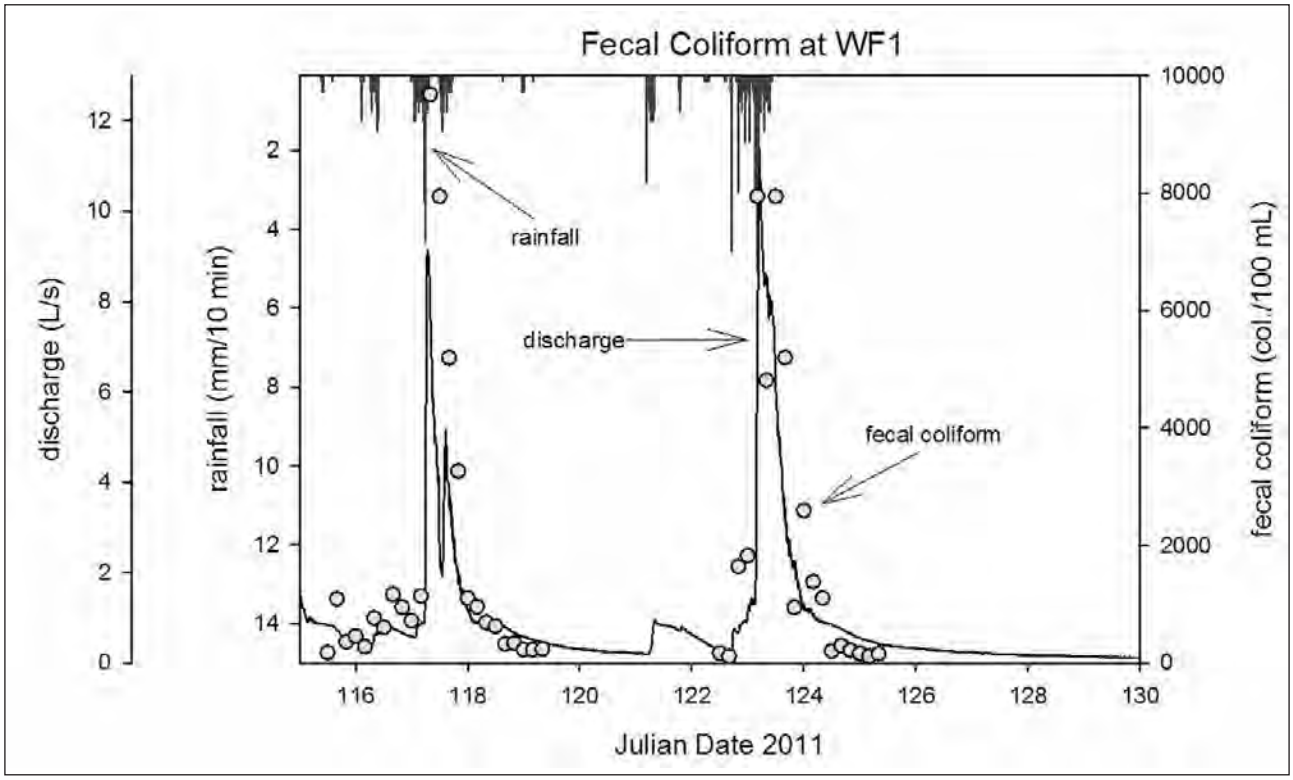

Figure 6. Fecal coliform (dots) counts at WF1 during a storm event from April 25 – May 10, 2011.

White WB, 1988. Geomorphology and Hydrology of Karst Terrains. Oxford University Press: New York.

Worthington S, 2007. Groundwater residence times in unconfined carbonate aquifers. Journal of Cave and Karst Studies 69(1): 94–102.

KARST HYDROGEOLOGICAL OBSERVATIONS IN CAO BANG PROVINCE (VIETNAM): THE TRA LINH-THANG HEN LAKE AREA

Gheorghe M. Ponta[1], Bogdan P. Onac[2], Nyguen Xuan Nam[3]
[1]PELA GeoEnvironmental, 1009 23rd Avenue, Tuscaloosa, AL 35401, USA, gponta@yahoo.com
[2]Department of Geology, University of South Florida, 4202 E. Fowler Ave., SCA 528, Tampa, FL 33620 USA, bonac@usf.edu
[3]Vietnam Institute of Geoscience and Mineral Resource, nam_nguyen_xuan@hotmail.com

In March 2012, the "Geokarst Adventure" Association under the auspices of the French Speleological Federation and the Romanian Speleological Federation along with the Vietnam Institute of Geoscience and Mineral Resource organized an expedition to explore the karst systems located in the Cao Bang Province, Northeastern Vietnam. The results include karst geological and hydrogeological observations and preliminary geochemical data based on 14 water samples. The values measured for the specific conductance are typical for caves waters (between 232.6 and 371 μS/cm). Total alkalinity as $CaCO_3$ ranges between 92.5 and 186 mg/l (gour 68), and the total hardness as $CaCO_3$ varies between 85 and 326 mg/l. The highest pH value (8.29), specific conductance (371 μS/cm) and concentration of calcium (97.93 mg/l) were recorded at Thang Hen Lake. The lowest temperature of 16.4 ºC, specific conductivity of 166.9 μS/cm, and total alkalinity as $CaCO_3$ of 68 mg/l were recorded in the water sample collected in the gour of Bang Ga T09 cave. The waters are calcium bicarbonate type. The local meteoric water line (LMWL) for the investigated region is $\delta D = 7.83\delta^{18}O + 14.694$ and shows a higher intercept and slope value than the global meteoric water line (GMWL), suggesting major changes in the origin of precipitation during the seasonal rain cycles.

1. Geographical Settings

The Socialist Republic of Vietnam is situated in the easternmost part of the Indochinese Peninsula (Fig. 1a). It covers a total area of 331,210 km^2 of which 40 % is represented by mountains, mostly forested. Carbonate rocks are exposed over 60,000 km^2, representing 18.12 % of countries' surface (Clements 2006).

The Province of Cao Bằng is located in the northeastern Vietnam, 270 kilometers from Hanoi, on the border with China. It has a surface of 6,724.6 km^2 and a population of 632,450 (Fig. 1a). The topography of the region is characterized by mountain ranges with elevation over 900 m above sea level (a.s.l.), and karstic plateaus developed between 500 and 700 m a.s.l. Tropical climate is characteristic to the area. The temperature varies from 5 °C in December and January to 37 °C in July and August.

The karst of northern Vietnam was extensively explored over the last 15 years and several cave exploration reports, karst geology and hydrology papers are available: Brouquisse (1998/1999), Holroyd and his team (2003, 2005, 2010), Limbert and his team (1999, 2007), Nyuyen Thi Thuy (2007) and Italian-French-Vietnamese Caving Project (2007).

2. Geology

The Cao Bang province is underlain by a variety of rocks ranging in age from Cambrian to Quaternary. The majority of the karst features identified in the field and water samples collected in March 2012 are hosted in the Bắc Sơn formation of Carboniferous–Permian age (C-P bs) which consists of siliceous shales, shaly limestones, and limestones. The limestone unit is up to 800 m thick. The Bac Son limestone is finely crystalline, light gray to dark gray. Bedding is generally 30 to 50 cm thick, oriented NW–SE, dipping 19º to 25º. Groundwater movement occurs along solutionally enlarged fractures, cavities, joints, and bedding planes. The area underlain by limestones is extensive. The topography consists of large poljes, surrounded by prominent limestones pinnacles and tower karst.

3. Karst hydrogeological observations in the Tra Linh – Thang Hen lake area

The Tra Linh – Thang Hen Lake area is formed by a sequence of poljes and karst windows developed along the Tran Linh River (Q ~400 l/s in March 2012). The limestone massifs are traverse by caves that carry rivers from one polje to the next. In some areas two levels of cave passages are developed, one as a stream passage at the present flood plain level, and a fossil one at 50 m relative altitude, marking a former flood plain level.

The Tra Linh River is collecting its waters a few kilometers north of the border with China. Fourteen km downstream, the river is disappearing underground at the base of a limestone massif, reappearing 500 m downstream in an underwater cave, which ends with a large spring. Hundred meters downstream from the cave entrance an 8 m high waterfall is formed. Downstream, the Tra Linh River is meandering through a large polje, covered with alluvial deposits, sinking for the second time in a cave/swallet, which is penetrable for about 100 m (Fig. 2). The end sump is clogged with alluvial deposits, trash and tree branches. The sump was not explored due concerns that flash flood waters moved unexploded ordinances from the Vietnam War era into the cave. One km north from the cave, a stream with a flow of about 10 l/s is disappearing underground through an impenetrable swallet.

The Tra Linh River continues the underground pathway, reappearing for about 100 m, in two separate karst windows (Karst Window 105 and Tra Linh Sinking Stream Ponor 107 on Fig. 1b), and later is recharging the Thang Hen Lake through a stream cave. The lake is a large swallet, located at the bottom of a polje, where the Tra Linh River is sinking underground for the fifth time, recharging the main spring located at 374 m elevation, 5 km away. In March 2012, the lake was about 300 m long and 150 wide. Around the lake several dry swallets were identified. The main spring, with a discharge of 200 l/s represents the partial outlet of the system. Along the river, additional groundwater sources recharge the stream. About 1 km downstream from the spring, the yield of the river reaches 1,000 l/s.

The type of the tower karst landscape develop along the Tra Linh River is "Residual Hills on a Planed Limestone Surface" (Ford and Williams 2007). During the raining season, the water level can rise up to 50 m in the area, the poljes mention above being flooded and interconnected, forming a large lake. A cross section along Tra Linh River, traversing tower karst landscape is shown in Figure 3.

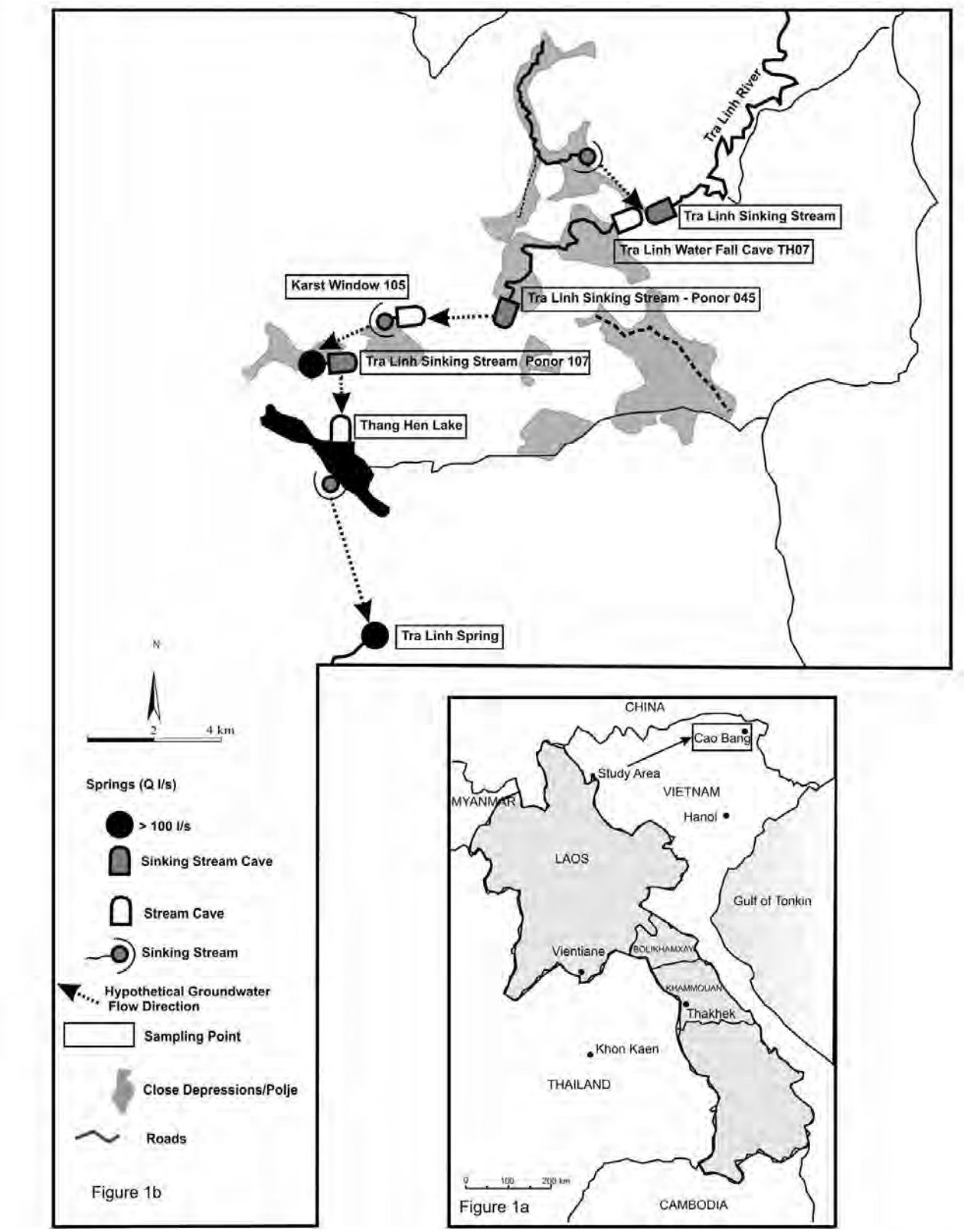

Figure 1. Location of the study area within the Cao Bang Province in the northern part of Vietnam.

Figure 2. Polje along the Tra Linh River with a fossil cave marking the former flood plain level (Photo Gheorghe Ponta with Geokarst Adventure).

4. Sampling and methods

Fourteen water samples were collected and analyzed from the following areas: Thang Hen Mountain Lake (7), Trung Han (2), Bao Lac (2), Bang Ga (2; one spring and one cave pool water), and one rain water sample. Only the seven sampling point in the Tra Linh – Thang Hen Lake area are shown on Figure 1b.

The water samples were analyzed for anions, metals, and stable isotopes. Field parameters, including temperature, pH, specific conductance, and salinity, were measured with an YSI 63 instrument. A digital titrator (Hach Model 16900) was used to determine alkalinity and total hardness as $CaCO_3$ and carbon dioxide in the field (Table 1).

Anion analyses were performed at the University of Alabama, whereas the metals and stable isotopes at the Department of Geology, University of South Florida. Anions were analyzed using a Dionex DX 600 Ion Chromatograph, trace metals analysis was achieved using a Perkin-Elmer Elan DRC II Quadrupole inductively coupled plasma mass spectrometer (ICP-MS) analytical instrument. Standards used were formulated stock standards with metals in concentrations from 1,000 mg/l to 10,000 mg/l. US EPA Test Methods 200.7 and 6010B were performed to complete the metals testing and analysis. The stable isotope analyses were conducted on a Thermo Fisher Scientific (Finnigan) Delta V Isotope Ratio Mass Spectrometer.

Table 1. Field parameter data. 1: Trung Han cave system; 2: Bao Lac; 3: Thang Hen cave system; mean sea level (MSL).

Sample Name	Date	Time	Elevation	Discharge (Q)	ph	Temperature (T)	Specific Conductance	Salinity	Alkalinity as $CACO_3$	Carbon Dioxide	Total Hardness as $CACO_3$
Units			m (MSL)	l/s		°C	µS/cm	ppt	mg/l	mg/l	mg/l
[1/] Trung Han Spring 1 HQ 31	3/13/2012	13:50	475	100	7.54	21.70	352.30	0.20	156.00	115.60	326.00
[1/] Trung Han Spring 2 HQ 32	3/13/2012	15:14	443	250	8.25	19.80	339.60	0.20	186.00	92.60	274.00
[2/] Bao Lac HQ14 Spring	3/15/2012	14:22	219	20	7.31	20.10	232.60	0.10	192.50	74.40	85.00
[2/] Bao Lac Sump in Hang Kanh Xuan BL14 Cave	3/15/2012	16:09	249	20	7.47	20.40	241.20	0.10	92.50	40.60	120.00
[3/] Tra Linh Sinking Stream	3/19/2012	15:45	643	400	7.76	23.50	279.40	0.10	119.00	32.40	147.00
[3/] Tra Linh Water Fall Cave TH 07	3/18/2012	14:02	635	250	7.11	18.60	300.50	0.10	118.00	48.80	163.00
[3/] Tra Linh Sinking Stream Ponor 045	3/18/2012	11:44	625	250	6.51	19.10	297.60	0.10	124.00	40.20	
[3/] Karst Window 105	3/21/2012	14:47	603	300	7.73	21.60	296.60	0.10	131.00	45.60	
[3/] Tra Linh Sinking Stream Ponor 107	3/21/2012	16:00	593	100	7.78	21.50	296.50	0.10	125.00	49.00	188.00
[3/] Thang Hen Lake	3/21/2012	11:11	590	400	8.29	20.60	371.00	0.20	168.00	42.60	151.00
[3/] Tra Linh Spring	3/19/2012	13:10	374	50	7.70	21.70	325.40	0.20	119.00	91.80	193.00
Bang Ga Gour Cave TR 09	3/20/2012	14:46	698	0.0001	7.88	16.40	166.90	0.10	68.00	45.40	123.00
Bang Ga 098 Spring TR 04	3/20/2012	17:24	602	5	7.20	20.40	318.70	0.20	136.00	74.00	273.00

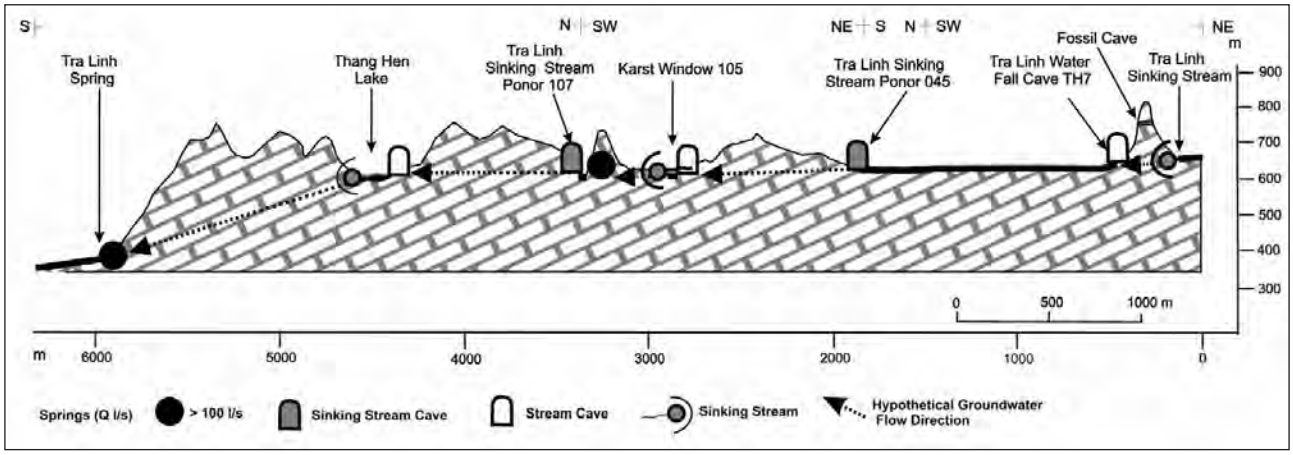

Figure 3. Cross section along Tra Linh River, traversing tower karst landscape.

5. Water quality data

Laboratory results for anions and cations are provided in Table 2. Sampling locations are shown on Figure 1b. The elevations of sampling points range between 219 m and 698 m. The estimated flow rates of the sampled springs range between 20 l/s and 400 l/s. The pH value ranges between 6.51 and 8.29, typical for karst waters. Temperatures ranged between 18.6 and 23.5 ºC, which correspond to mean annual air temperature in the area.

The values we measured for the specific conductance are typical for caves waters (between 232.6 and 371 µS/cm). Total alkalinity as $CaCO_3$ ranges between 92.5 and 186 mg/l (gour 68), and the total hardness as $CaCO_3$ varies between 85 and 326 mg/l.

Calcium concentration ranges between 48.60 and 97.94 mg/l, with the highest values at the Thang Hen Lake, whereas the magnesium concentration was found to fluctuate between 0.30 and 5.76 mg/l.

Carbon dioxide concentration ranges between 32.40 to 115.60 mg/l.

The highest pH value (8.29), specific conductance (371 µS/cm) and concentration of calcium (97.93 mg/l) were recorded at Thang Hen Lake.

The lowest temperature of 16.4 ºC, specific conductivity of 166.9 µS/cm, and Total Alkalinity as Ca CO_3 of 68 mg/l were recorded in the water sample collected in the gour of Bang Ga T09 Cave. The waters are bicarbonate calcium type.

6. Stable isotopes

Isotope fractionation accompanying evaporation from the ocean and condensation during atmospheric transport of water vapour causes spatial and temporal variations in the deuterium and ^{18}O composition of precipitation (Dansgaard 1964). Regional-scale processes such as water vapor transport patterns across landmasses and the average rainout history of the air masses precipitating at a given place controls the isotopic composition of local precipitation (Table 3).

Table 2. Summary of the water quality data. 1: Trung Han cave system; 2: Bao Lac; 3: Thang Hen cave system. As, Cd, Cr, Zn, F, and Br were not detected.

			CATIONS (METALS)						ANIONS			
Sample ID	**Date**	**Time**	**Total Calcium**	**Total Magnesium**	**Total Manganese**	**Total Potassium**	**Total Sodium**	**Total Strontium**	**Chloride**	**Nitrate**	**Phosphate**	**Sulfate**
Units			mg/l	mg/l	mg/l	mg/l	mg/l	mg/l	mg/l	mg/l	mg/l	mg/l
[1] Trung Han Spring 1 HQ 31	3/13/2012	13:50	95.42	2.45	0.02	0.55	1.80	0.05	1.27	3.54	0.18	4.40
[1] Trung Han Spring 2 HQ 32	3/13/2012	15:14	94.37	3.13	0.02	0.62	2.09	0.05	1.23	3.05	0.09	4.71
[2] Bao Lac HQ14 Spring	3/15/2012	14:22	57.02	4.25	0.00	0.59	2.98	0.08	0.73	3.64	0.02	4.92
[2] Bao Lac Sump in Hang Kanh Xuan BL14 Cave	3/15/2012	15:37	57.67	4.38	0.01	0.67	3.73	0.09	0.62	3.94	0.00	4.94
[3] Tra Linh Sinking Stream	3/19/2012	15:45	57.67	4.38	0.01	0.67	3.73	0.09	1.61	2.01	0.00	5.79
[3] Tra Linh Water Fall Cave TH 07	3/18/2012	14:02	82.23	5.77	0.05	0.91	3.51	0.07	1.60	2.06	0.01	5.76
[3] Tra Linh Sinking Stream Ponor 045	3/18/2012	11:44	75.31	5.35	0.05	0.97	3.28	0.07	1.61	2.79	0.01	5.76
[3] Karst Window 105	3/21/2012	14:47	75.31	5.35	0.05	0.97	3.28	0.07	1.67	2.28	0.05	5.77
[3] Tra Linh Sinking Stream Ponor 107	3/21/2012	16:00	48.60	0.30	0.00	0.18	1.70	0.02	1.64	2.56	0.01	5.82
[3] Thang Hen Lake	3/21/2012	11:11	97.94	1.15	0.01	0.42	1.89	0.06	1.70	2.77	0.03	5.88
[3] Tra Linh Spring	3/19/2012	13:10	86.87	5.76	0.37	1.07	3.78	0.08	1.48	3.21	0.00	5.61
Bang Ga Gour Cave TR 09	3/20/2012	14:46	84.78	5.68	0.20	1.15	3.98	0.08	0.65	1.33	0.00	8.30
Bang Ga 098 Spring TR 04	3/20/2012	17:08	0.00	0.00	0.00	0.00	0.00	0.00	0.78	3.76	0.11	5.60

The $\delta^{18}O$ values of the water samples collected over 8 days ranged from -9 to -7.62‰. The δD values in the cave waters, springs, and rivers ranged from -55 to -42‰. The only rainfall sample collected on March 13, 2012 stands out with its very positive values for both $\delta^{18}O$ and δD (see Table 3).

The relationship between ^{18}O and ^{2}H in world's fresh surface / cave waters is predicted by the GMWL defined by Craig (1961) as:

$$\delta D = 8\delta^{18}O + 10 \text{ (‰)}.$$

The local meteoric water line (LMWL) for the investigated region is δD = 7.8359x + 14.694 and shows a higher intercept and slope value than the GMWL, suggesting major changes in the origin of precipitation during the seasonal rain cycles. Although we called LMWL, we are fully aware that the isotopic compositions undergoes variations on event-based and therefore, our LMWL solely reflects the conditions during those 8 days of sampling, therefore, the results need to be considered as preliminary and used with caution if comparisons with other regions or data sets are sought.

Table 3. Summary of the stable isotope data. 1: Trung Han cave system; 2: Bao Lac; 3: Thang Hen cave system.

Sample	$\delta^{18}O$ (‰)	δD (‰)	*d*-excess (‰)
[1]Trung Han Spring 1HQ 31	-7.86	-49.12	13.74
[1]Trung Han Spring 2HQ 32	-7.78	-46.19	16.06
[2]Bao Lac Spring	-8.93	-55.23	16.22
[2]Bao Lac Sump in Hang Kanh Xuan Cave	-9.00	-52.54	19.49
[3]Tra Linh sinking stream	-7.76	-45.34	16.73
[3]Tra Linh Water Fall Cave TH 07	-7.63	-42.35	18.66
[3]Tra Linh Sinking Stream Ponor 045	-7.98	-44.29	19.52
[3]Karst Window 105	-7.66	-53.96	7.31
[3]Tra Linh Sinking Stream Ponor 107	-7.62	-54.15	6.85
[3]Thang Hen Lake	-7.71	-48.51	13.16
[3]Tra Linh Spring	-8.08	-45.27	19.37
Bang Ga gour	-8.39	-42.49	24.60
Bang Ga Spring T4	-8.24	-50.79	15.10
Rain Water	1.37	26.80	15.85

More samples of precipitation and fresh groundwater are needed to construct a real LMWL for this region, and to calculate the deuterium excess value, defined as:

$$d = \delta D - 8\delta^{18}O \text{ (‰)}.$$

This parameter is a valuable indicator of the source area of the water vapor. Values around +10‰ are typical for most continental meteoric waters, whereas values well above +10‰ suggest more evaporated moisture being added to the atmosphere (Rozanski et al. 1992).

Acknowledgments

We are grateful to the following organizations that provided us with the hydrogeological analyses: Institute of Geosciences and Mineral Resources and PELA GeoEnvironmental and to members of the Geokarst Adventure for their help during the fieldwork.

References

Brouquisse F, 1998/1999. Données physico-chimiques, Federation Francaise de Speleologie, Societa Speleologica Italiana (Unpublished report).

Cao Bang 2007, Italo-french-vietnamese caving project in Vietnam (Unpublished report).

Clements R, Sodhi NS, Schilthuizen M, Ng KLP, 2006. Limestone karsts of Southeast Asia: imperiled arks of biodiversity. BioScience, 56(9), 733–742.

Craig H, 1961. Isotopic variations in meteoric waters. Science, 133, 1702–1703.

Dansgaard W, 1964. Stable isotopes in precipitation. Tellus, XVI (4), 436–468.

Ford DC, Williams PW, 2007. Karst Hydrogeology and Geomorphology. John Wiley & Sons, London, 562.

Holroyd M. and team, 2003, 2005, 2010. Vietnam Expedition (Unpublished reports).

Limbert H. and team, 1999, 2007, 2009. Vietnam Caving Expedition. http://www.vietnamcaves.com/report-2009

Nguyen Thi Thuy, 2007. Application of stable isotope geochemistry in a study of paleoclimate and environment. Case study in Son La, Vietnam. Master Dissertation, Universiteit Gent, Vrije Universitei Brussels, Belgium.

Rozanski K, Araguás-Araguás L, Gonfiantini R, 1992. Relation between long-term trends of oxygen-18 isotope composition of precipitation and climate. Science, 258, 981–985.

Topographic map of Na Khoang, 1:50,000.

Topographic map of Cao Bang, 1:50,000.

INCIDENCES OF THE TECTONICS IN THE KARSTIFICATION OF CHALK LIMESTONES IN THE WESTERN PARIS BASIN: EXAMPLE FROM THE PETITES DALES CAVE (SAINT MARTIN AUX BUNEAUX, FRANCE)

Joël Rodet[1], Kun Ma[2], Jean-Pierre Viard[3]
[1]UMR 6143 CNRS-M2C-Université de Rouen, Laboratoire de Géologie, CNEK, 76821 Mont Saint Aignan, France, joel.rodet@univ-rouen.fr
[2]Université de Rouen, UMR 2795 CNRS-IDEES, Institut de Géographie, 76821 Mont Saint Aignan, France
[3]Centre Normand d'Etude du Karst et des Cavités du Sous-sol, 97 rue du 8 mai, 27400 Montaure, France

The classical approach to study the karstification attributes a major role to the structure in the establishment of concentrated drainage of groundwater. This structure, essentially tectonics and stratigraphy, serves to guide the water, which gradually opens up these discontinuities to build a network, from the introduction to the resurgence. This too idealistic view does not reflect the complexity of the establishment of a karst system. Indeed, experience shows that some bedrocks contain karst drains in the absence of any cracking. What's more, some conduits can go through the structural elements without undergoing any morphological changes. In the chalk of Western Paris Basin, the Petites Dales Cave proves an excellent observatory. We have conducted a study on the relationship between the main conduit, restitution collector of the underground system, and observable fissures in the roof and walls of the conduit. Along a drain of 421 m, we counted 374 fissures, the total length of which being a little more than 867 m. Examination of the orientation of the drain and fissures reveals four types of relationship: (1) parallel (2) oblique, (3) perpendicular and (4) no joints. No correlation could be established between the development of the collector and the presence of fissures, other than very occasionally or during episodes of overflow. In fact, the relationship between fissure and karstic conduit cannot be established, therefore it is necessary to introduce other factors in the speleogenesis, such as porosity of the chalky bedrocks, and the direct effect of the hydraulic gradient.

1. Introduction

Typically, it is assumed that the development of karst drains depends on the structure, especially the tectonics. "Structural cracking is the main factor of permeability to water in a limestone" (Jakucs 1977). Explorations in the chalky limestone of the Paris Basin showed that this was not always the case (Rodet 1992). So we started the study on the relationship between drain and fissures in one of the largest caves of Normandy, the Petites Dales Cave.

Petites Dales Cave opens in the eponymous valley, 1.2 km from its outlet on the coast of the English Channel (Fig. 1). Small cavity of only 62 m of development at its speleological recognition in 1966, this site became one of the most important underground excavation sites in France since 1991 (Rodet et al. 2007). To date, with more than 710 m of explored galleries, the cavity is the largest in Seine Maritime. It hosts a multidisciplinary karst research program (Laignel et al. 2004; Rodet et al. 2006), being referenced as the chalk karst of Normandy Region (Rodet and Viard 2009).

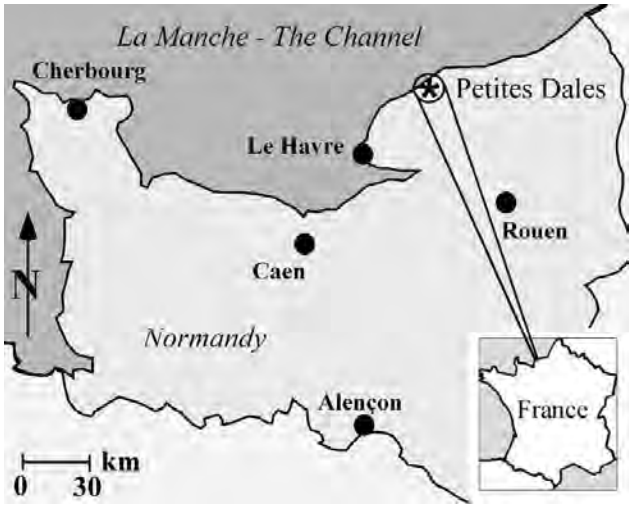

Figure 1. Location of the study area.

As part of this research program, we studied specifically the relationship between visible tectonics and directions of drain to verify the applicability of the concept of the drainage network establishment based on the tectonic frame (Hauchard et al. 2002, 2008) for cavities in chalk. Our approach is limited to observable fissures in the main gallery of the cave between the entrance (topographic point # 1 – pt. 1) and the impact of the first solution pipe (topographic point # 43).

2. Methodology

The topographic map of the Petites Dales Cave was surveyed from a network of fixed and materialized stations, which are therefore easy to locate (Fig. 2).

The topography of the collector was completely established along a length of 460 m, till the foot of the second solution pipe where we have not found upstream gallery. The impact of trepanation of the two solution pipes makes it illusory the study of fissures upstream of the pt. 43, which is 421 m from the entrance (Rodet et al. 2009). As a result, we limited our study area between the pt. 1 (entrance) and the pt. 43.

From this topography, we carried out a campaign of systematic survey, *in situ*, of (i) the orientation of the

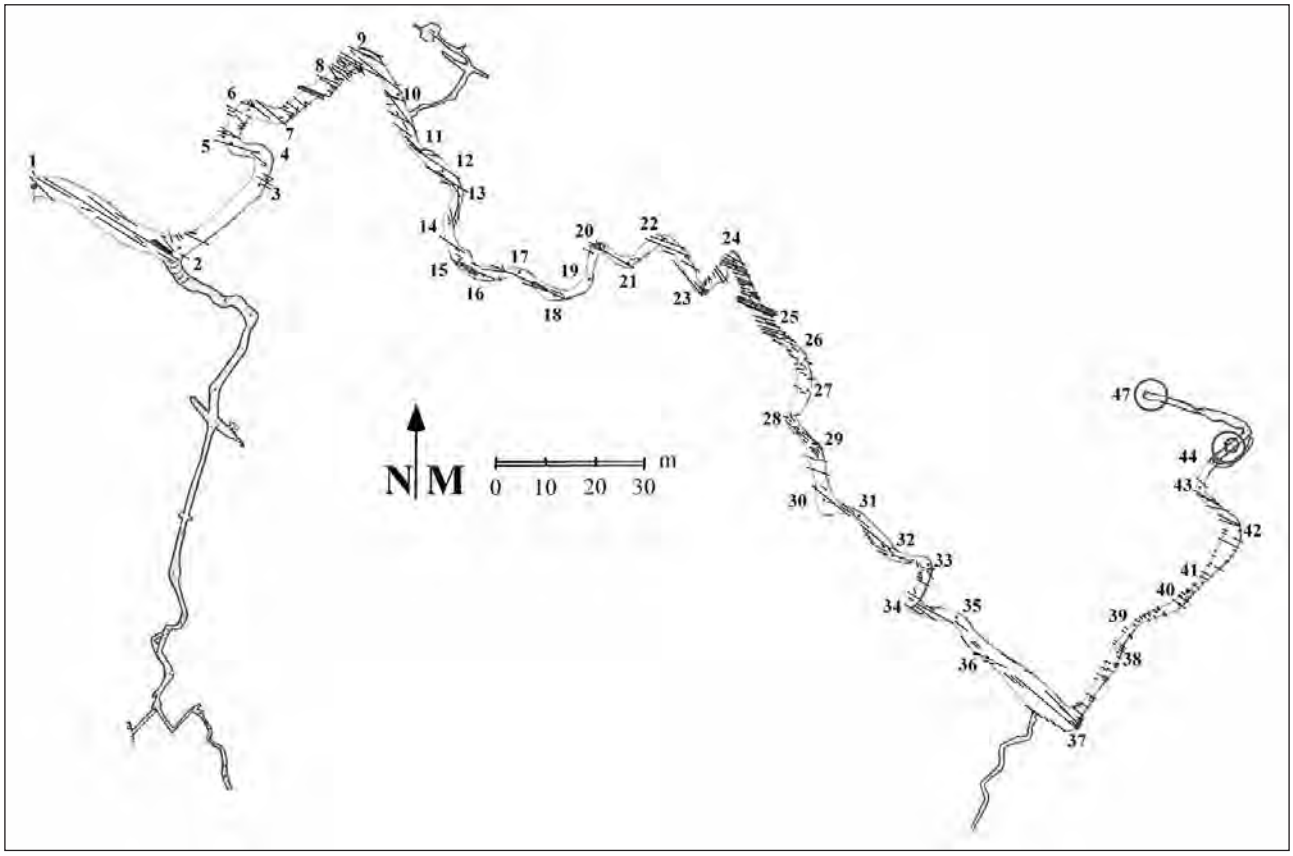

Figure 2. Survey of the Petites Dales Cave, with the tectonic network.

sections of the collector, (ii) the length of these sections, (iii) the orientation of visible fissures in the roof and the walls of the sections, (iv) the length of the fissures. Every joint was oriented (az degree) and measured with a tape measure. For fissures in the form of broken line or curve, we measured the orientation between the two extreme points. Each joint was numbered and plotted on the spot on a 1/100 topographic map. The measures were then introduced into a spreadsheet. By combining these data, we can define drain / joint relation models to assess the impact of visible tectonics on the karst development, and the impact of hydraulic gradient supported by the porosity of the bedrocks.

The first element to consider is the spatial organization of the 42 segments which compose the drain being studied, according to their orientation and accumulated length of development by azimuth class. The second element is the tectonic network survey, according to its frequency, directional distribution and accumulated length of development by class. Finally, the comparison of the two types of data aims to understand the relationship between tectonics and karst drain under discussion.

As indicated by the reference point pt. 43, the 42 oriented segments of gallery were grouped by class of 5° (Fig. 3a). The 374 inventoried joints were grouped according to their magnetic orientation (az value) by class of five degrees.

3. Results

The cavity was examined along the 421 m of the drain. 374 joints, with a total length of 867.70 m of fissures (f), were identified.

3.1. Collector directions

The distribution of the 42 directions is very dispersed: no class contains more than 4 sections and thus reaches 10 %. It is relatively uniform across all classes, with a slight concentration in two large sets (11–70° and 106–155°), in the middle of less relevant values.Concerning the cumulative length of the conduits (Fig. 3b), two sets are slightly reinforced. The first set is bipolar with a first peak around 11°/15°, a second around 31°/50°, and more specifically between 40° and 50°, clearly in SW/NE direction. The second set is more uniform with a maximum in the 136°/140° Class, the maximum being further accentuated as to the cumulative of NW/SE segment lengths.

Both directions, and especially values between 120° and 150°, correspond to lineaments and faults of the Pays de Caux (Hauchard et al. 2002, 2008).

3.2. Joints in the collector

The output gallery is marked regularly with topographic stations used as a benchmark to locate oriented gallery segments and fissures identified in the roof and the walls of the gallery. The total development of drain is 421 m (420.90 m), in which 374 joints are identified with a total fissure length of 867.70 m. Thus, the average length of fissure is 2.32 m, the number of fissures per linear meter of drain is 0.89, and the length of fissure (mf) per meter of drain is 2.06 m.

For morphological reasons (Fig. 2), we divided the main gallery into four sectors, namely:

3.2.1. From pt 01 to pt 11

In this first sector, the length of conduit is 119.30 m, which represent 28.34 % of the total length of gallery. We identified 101 joints or 27.1 % of all fissures identified throughout the gallery. We obtain a density of 0.85 fissure per meter of gallery. The total length of joints rises to 336.80 m, which means a ratio of 2.82 m of fissure per meter of drain.

3.2.2. From pt 11 to pt 24

In this second sector, the length of conduit is 100.80 m, which represent 23.95 % of the total length of conduit. We identified 67 joints, or 17.91 % of all fissures identified throughout the gallery. We obtain a density of 0.66 fissures per meter of gallery. The total length of joints rises to 196.10 m, which means a ratio of 1.95 m of fissure per meter of drain.

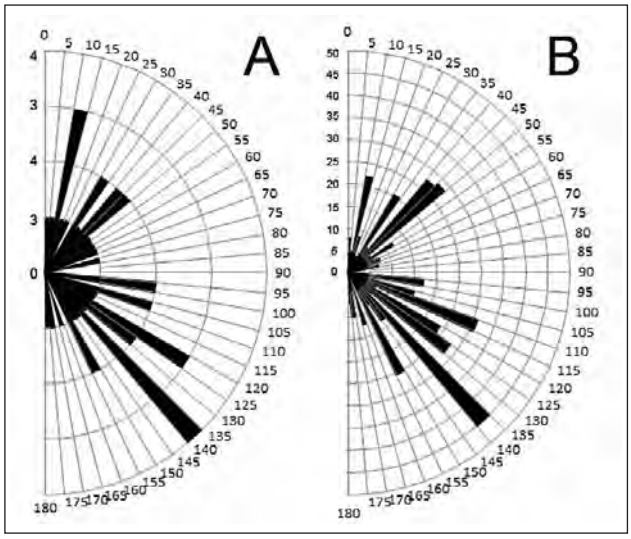

Figure 3. Distribution of the segments in the main gallery. A: number of segments by 5° sets. B: cumulative length of the segments by the same sets.

3.2.3. From pt 24 to pt 37

In this third sector, the length of conduit is 136.40 m, which represent 32.41 % of the total length of conduit. We identified 118 joints, or 31.55 % of all fissures identified throughout the gallery. We obtain a density of 0.87 fissure per meter of gallery. The total length of joints rises to 267.50 m, which means a ratio of 1.96 m of fissure per meter of drain.

3.2.4. From pt 37 to pt 43

In fourth sector, the length of conduit is 64.40 m, which represent 15.30 % of the total length of conduit. We identified 88 joints, or 23.53 % of all fissures identified throughout the gallery. We obtain a density of 1.37 fissures per meter of gallery. The total length of joints rises to 67.30 m, which gives a ratio of 1.05 m of fissure per meter of drain.

3.2.5. Summary of all sectors

There is therefore a medium density of joints in the first sector (0.85 f/ml). It falls in the second sector to 0.66 f/ml, returns to the average of the first sector in the third sector (0.87 f/ml), and increases significantly in the fourth sector (1.37 f/ml).

We also note that the joint density is not in the pair with the joint length, since the ratio decreases from the entrance to the end where the lowest ratio (1.05 mf/ml) accompanies the highest fissure density (1.37 f/ml). Only in the two intermediate parts the overall average is approached. Is this increasing ratio from the end to the entrance reflecting a possible relaxation effect of the massif induced by the opening of the Petites Dales Valley?

3.3. The directions of joints

They are 374 inventoried joints grouped according to their magnetic orientation (Fig. 4). There is an overwhelming concentration of orientations between 100° E and 145° E. The rest is trivial: a small class of 15–20 ° and an even smaller one near 180° (Fig. 4a). This NW/SE orientation dominance is even stronger. It concentrates around 115–125° when we focuse not on the number of joints but their cumulative development (Fig. 4b).

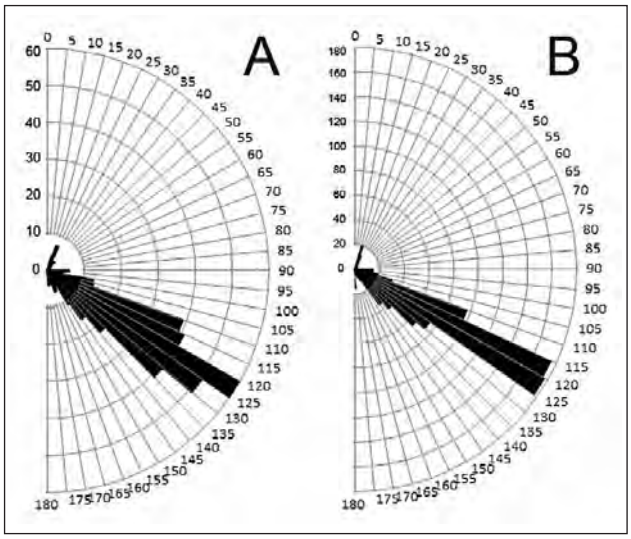

Figure 4. Distribution of the fissures in the main gallery. A: number of joints by 5° sets. B: cumulative length of joints distributed in the same classes.

4. Discussion

What do the results mean?

4.1. Drain/joint directional relations

The relations between the direction of the drain and the joints reveal four cases.

4.1.1. The joints accompany or frame the drain

We can suppose that there is a relationship between joint and drain, as a lot of studies shows in numerous conventional caverns in limestone with low permeability or porosity (White, 1988). Certainly the combination of fissures and hydraulic gradient provides the best conditions for the development of karst. In the main gallery, it represents 148.4 m, therefore 35.26% of the gallery.

4.1.2. The joints intersect obliquely the drain

The joints intersect obliquely the drain without thereby deviating the gallery. We must therefore conclude that the

oblique fissures do not affect directly the conduit. In the collector, it represents 130.2 m and therefore 30.93% of the gallery.

4.1.3. The joints intersect perpendicularly the drain

The joints intersect perpendiculary the drain without impacting the morphology of the walls. Joint does not influence the flow. As in the previous case, only the phases of flooding with a very reduced flow speed affect the morphology of the drain by the establishment of equilibrium chimneys. In the collector, it represents 86.8 m and therefore 20.62 % of the gallery.

4.1.4. The joints are absent from the drain

In the collector, there is no joint along 55.5 m, that is to say, 13.19 % of the gallery has no relationship with tectonics (Fig. 5).

In total, 365.40 m of the gallery exhibit fissures in the ceiling or walls, that represent 86.81 % of the total length of the collector, but in which only 148.4 m, or 35.26 %, show a clear relationship between tectonic and karst drain.

We conclude that tectonics is not the only responsible for the establishment of all sections of the collector. Other factors involve either stratigraphy (favorable interbedding) or porosity (with direct impact of the hydraulic gradient). Some authors, supporters of the "all tectonics", suggest the existence of a network of micro-cracks, unproven to date: curiously this network should be large enough to guide the drain, but at the same time it would not be revealed by the flooding phases…

Figure 5. Segment of the main gallery of the Petites Dales, without joint, between pt. 2 and pt. 3 (photo by D. Guillemette).

4.2. Drain and joint

The last approach was made by comparing the drains and joints. It shows significant disparities, where there are areas with many joints or significant accumulated metrics of joints, and areas almost without joint. We have established a ratio between length of joint (mf) and length of gallery (mlg), which reveals three classes, depending on whether the ratio is close to the average ratio of the cavity, higher, or on the contrary, lower:

4.2.1. Gallery with a low ratio of fissure

The ratio is low (< 1 mf/mlg). 11 of 42 sections provide a ratio of less than 1 m of fissure per lineal meter of drain. This represents 26 % of the sections.

4.2.2. Gallery with a ratio close to the average

The ratio is close to the average of joint (2.06 mf/mlg) of the whole gallery, between 1 and 3 m of fissure per meter of drain. This represents 25 of the 42 sections of the collector, i.e. 60 % of the sections.

4.2.3. Gallery with a strong relationship to tectonics (> 3 mf/mlg)

Only 6 sections provide a ratio greater than 3 between the meter of fissure and the linear meter of the gallery. Those sections represent 14 % of the segments of the collector. Strangely, the sectors with a high ratio of fissure are those which were strongly influenced by episodes of significant flooding associated with sudden and torrential floods from the downstream solution pipe (pt. 44). Therefore, it relates to the morphology after the establishment of the drain collector, thus the tectonic factor cannot be applied as a determinant factor to the morphogenesis of the former drain.

The last graphic (Fig. 6) oppose the cumulative length of drains grouped into orientation classes by 5° to the cumulative length of fissures, which are also grouped by class of 5°. There is a wide difference in the distribution of the orientations between the development of drains and the development of joints. In particular, note that while the cumulative lengths of conduits (classes 116–120° and 121–125°) are from 7 m to 24 m, giving a ratio of 3.5, the cumulative lengths of joints are equal (175.9 m and 177.2 m), giving a difference of 1.3 m or a ratio of only 1.007.

Moreover, it should be noted that values equivalent to the linear meters of drains (24 m for 121–125°, and 28 m for 41–45°) are completely opposite to the those of joint (177.2 m and 2.1 m), i.e. a ratio of 84. The lack of relationship between classes of drains and those of fissures, shows very clearly in this case that the development of drains does not depend on the tectonics of bedrock, but on other speleogenetic factors and constraints which must to be identified.

5. Conclusion

The collector of the Petites Dales Cave offers several sectors without joint (Fig. 5). Sections where there are oblique (Fig. 7) or perpendicular joints which do not affect the morphology of the collector drain are not linked to the structure of the bedrock. It is only in the presence of joints / drain correlation that tectonics can be considered with

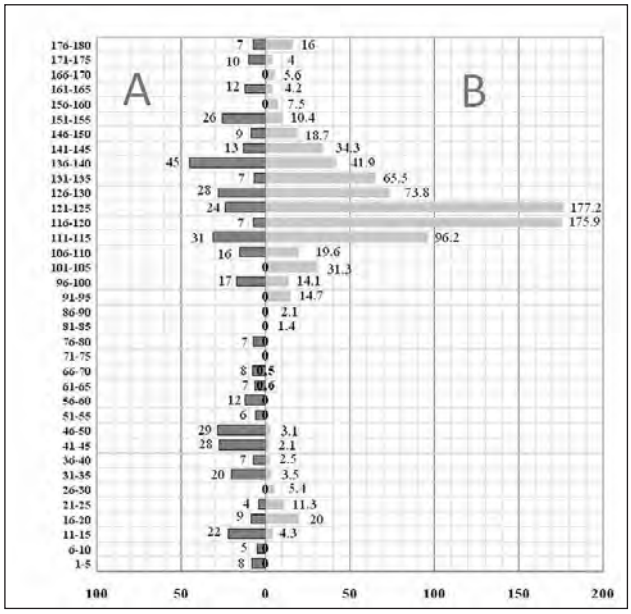

Figure 6. Dual graph of distribution by class of orientation (5°). A: cumulated length of the segments in the main gallery. B: cumulated length of the joints observed in the main gallery. We note the absence of correlation between A and B.

certainty to affect the karstification. In theory, it is one out four cases. Concerning the development of collector of the Petites Dales Cave, it represents less than 150 m of the drain, that is to say, just over 35 % of the main drain.

Clearly, porosity, by allowing the dispersion of the flow, promotes the expression of the hydraulic gradient. This dimension reduces, sometimes even annihilates the impact of the structure. Thus, it is in the phases of saturating flooding, when the flow velocity is minimized by effect of damming, that the weaknesses of the bedrocks manifest, especially through joints.

As a result, the correlation or the non-correlation between the direction of the drains and the structure of the bedrock reflects the impact of bedrock on drains. For a long time, chalk was compared to a sponge and thus the existence of karst within it was denied. Today, no one denies any more the obvious, but the chalk, porous limestone, has its specificities, both morphologically and hydrologically, which are shown by the development of the karst.

References

Hauchard E, Laignel B, Delahaye D, 2002. Proposition d'un nouveau schéma structural du Nord-Ouest du bassin de Paris reposant sur l'analyse fractale de la morphologie des réseaux de thalwegs et les données récentes de la géologie régionale. C. R. Geoscience, 334, 295–302.

Figure 7. Segment of the main gallery, with obliquily intersection of joints, between pt. 24 and pt. 25 (photo by J. Rodet).

Hauchard E, Laignel B, 2008. Evolution morphotectonique de la marge nord-occidentale du Bassin de Paris. Zeitschrift für Geomorphologie, 52 (4), 463–488.

Jakucs L, 1977. Morphogenetics of karst regions – variants of karst evolution. Adam Hilger, Bristol: 284.

Laignel B, Dupuis E, Rodet J, Lacroix M, Massei N, 2004. An example of sedimentary filling in the chalky karst of the Western Paris Basin: Characterization, origins and hydrosedimentary behaviour. Zeitschrift für Geomorphologie N.F., 48 (2), 219–243.

Rodet J, 1992. La craie et ses karsts. Ed. Groupe Seine CNRS Caen & CNEK, Elbeuf, 560.

Rodet J, Laignel B, Dupuis E, Brocard G, Massei N, Viard J-P, 2006. Contribution of a sedimentary study to the karstic evolution concept of a chalk cave of the Western Paris Basin (Normandy, France). Geologica Belgica, 9 (3–4), 287–296.

Rodet J, Viard J-P, Poudras J, 2007. A la découverte de la grotte des Petites Dales (Saint Martin aux Buneaux, Seine Maritime, France). Spéléo-Tract, 6, 38.

Rodet J, Viard J-P, 2009. La grotte des Petites Dales, un patrimoine normal? non! normand! Spelunca, 114, 28–34.

Rodet J, Willems L, Brown J, Ogier-Halim S, Bourdin M, Viard J-P, 2009. Morphodynamic incidences of the trepanning of the endokarst by solution pipes. Examples of chalk caves in Western Europe (France and Belgium). Proceedings of the 15th International Congress of Speleology, Kerrville (Texas, USA), 19–26 July 2009, UIS, vol. 3, contributed papers: 1657–1661.

White WB, 1988. Geomorphology and hydrology of karst terrains. Oxford University Press, 464.

CEILING CHANNEL AND INPUT KARST. EXAMPLE OF THE PETITES DALES CAVE, NORMANDY, FRANCE

Joël Rodet[1], Laurent Magne[2], Jean-Pierre Viard[3]
[1]CNRS UMR 6143-Laboratoire de Géologie, Université de Rouen and CNEK, 76821 Mont Saint Aignan, France, joel.rodet@univ-rouen.fr
[2]Hydrogeologist engineer and CNEK, 94430 Chennevières sur Marne, France, lmim.ber@gmail.com
[3]Centre Normand d'Etude du Karst et des Cavités du Sous-sol – CNEK, 27400 Montaure, France, follainjanine@orange.fr

Within the endokarstic forms, the ceiling channel is often put forward because of its morphodynamic significance. Generally, the ceiling channel demonstrates a breaking into the initial drainage and a reduced stream flow resumes in a very congested drain. This top incision plays a new collection role on a filled drain which is also hydrologically disconnected, and gradually the channel becomes more and more important downstream. Studies made for more than twenty years in the Petites Dales Cave (Saint Martin aux Buneaux, France) revealed that the ceiling channel excavated in the roof of the collector-gallery presents an atypical development, which does not correspond to the classic scheme because it is much more developed upstream than downstream. This progressive morphology shows a huge variation of dimension linked to abrupt changes in the collector's orientation. These elements help to affirm that the ceiling channel of the main drain of the Petites Dales Cave is a form of introduction whose function is the absorption of brutal introductions by the water chasms which hydrate the underground network.

1. Introduction

In karstic geomorphology, the ceiling channel is an important indicator about the evolution of the drain, even the system (Jennings 1985). In a classic approach, it deals in fact with an erratic drainage of restitution which develops at the top of a filled drain, temporarily non-operational (Renault 1968). As a consequence, the channel becomes bigger downstream, in link with the collector function of the conduit (Slabe 1995). But sometimes, the channel can work differently, with another kind of drainage: the absorption of an introduction as a consequence of the trepanation of the restitution drain by a pothole or a solution pipe (Rodet et al. 2009). In the latter case, the channel becomes smaller and smaller as it develops downstream, by reducing the flow absorbed by the restitution drain. This is what we focused on in the main gallery of the Petite Dales Cave.

The Petites Dales Cave is an important chalk cavity in the Western Paris Basin (Fig. 1) because of its dimensions and moreover because of the section of its main gallery, from 2 to 5 m large for 10 m high, almost completely filled (Rodet et al. 2007). The Norman speleologists' work, under the direction of Jean-Pierre Viard, by a partial emptying of the soil runoff landfill since 1991, revealed day after day the importance of this cavity whose size was 62 m when speleologists discovered it in 1966, now there are more than 710 m of developed length (Rodet and Viard 2009). Poorly developed downstream, the channel, which develops at the roof of the collector, increases upstream. Several hypothesis were envisaged, that the discoveries linked to the cleaning, easily rejected, until the base of solution pipes was cross-check by exploration.

We have also studied the conditions of contact between introduction and restitution dynamics, leading to the notion of trepanation (Rodet et al. 2009). In this context, the ceiling channel is at least significant.

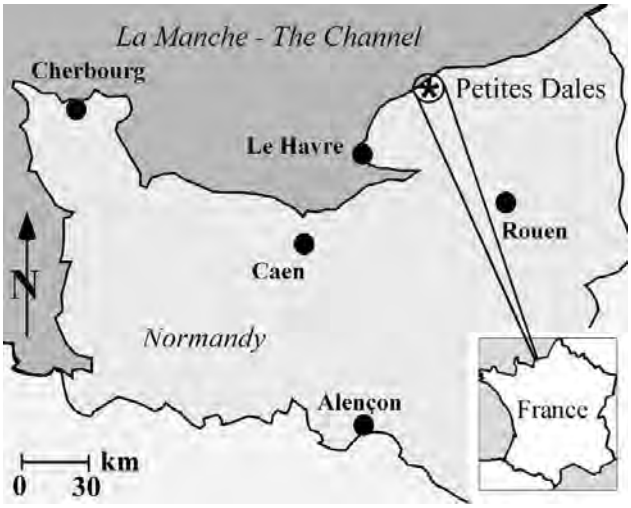

Figure 1. Location of the study area.

2. Methodology

The Petite Dales Cave benefits from a good organization: its topographic stations are easy to find (Fig. 2). Referring to this topographic network we directly checked the height and width of the ceiling channel in the main gallery between the topographic points (pt.) 2 and 43. To this finality we used a flexible panta-decametre, a level and an electronic laser meter. The data were noted on a notebook and registered in our office computer. We excluded (i) the downstream first segment of the gallery, between the entry (pt. 1) and the confluence (pt. 2) because the channel is absolutely absent, erased by the calibration of the collector during the reactivation of the siphon and (ii) the segment between pt. 42 and pt. 43 because the channel exactly corresponds to the topographic drain, because the underlying collector has not been cleared.

The topographic statement is composed of 259 stations which represent a metric measure if sectors without channel

are excluded. Each station has been subject to 3 to 8 measures, totaling more that 1,000 measures. With this morphometric statement we have realized more than 600 photographic cross-sections, set to the topographic network. A longitudinal cross-section was then designed by a computer, enabling a study of the latter. This approach was completed by perpendicular sections from the morphometric statements and the photographic cross-sections.

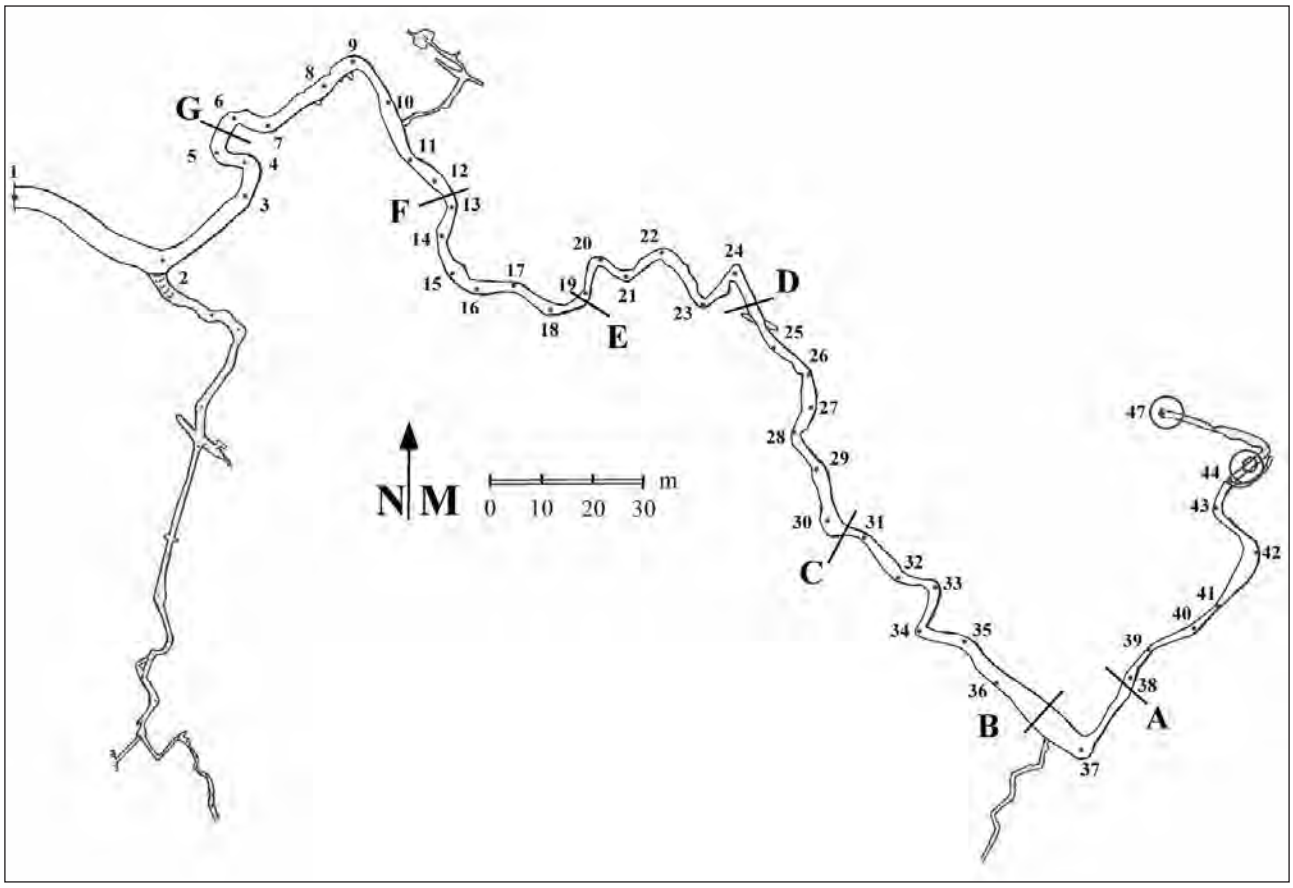

Figure 2. Cave survey with topographic stations (pt) and cross sections (A to G; see Fig. 4).

3. Results

All data have been gathered and studied, and this enabled us to build a longitudinal profile between pt 2 and pt 42 (Fig. 3). It can be noticed that the channel does not evolve in a regular way downstream to upstream and upstream to downstream. Then this is not a regular linear flow. Then what is its function?

If it is a concentration drainage (output or restitution karst), its most evolved parts should contain significant lateral contributions (tributaries). If it is an introduction drainage (input karst), sudden entries leading to flows and sedimentary disruption inside the collector.

The longitudinal profile reveals 4 sectors from upstream to downstream which can be linked to the cave plan (Fig. 2)

3.1. The upstream ceiling channel and the "Espace des Six" chamber

Between upstream (pt. 42) and 315 m from the entry (pt. 35) we can observe a 2 m high ceiling channel, well distinguished and almost rectilinear, easily penetrable by a man. It is rooted to the base of a solution pipe (pt. 44).

This channel, almost separated from the support-gallery (Fig. 4A) leads in a perpendicular way to the most elevated sector of the collector, the "Espace des Six" chamber whose volume is imposing and seems to hang above the collector (Fig. 4B). Its roof rises more than 8 m above the ground of the collector.

3.2. The central part

Between pt. 35/315 m (downstream of the "Espace des Six" chamber and pt. 27/240 m, the sector is low and sinuous, in which the channel is more discreet and above all discontinuous (Fig. 4C). It is rarely higher than 0.5 to 1 m with plenty of small equilibrium chimneys. It is not easily penetrable by a man.

3.3. The great curve

Between pt. 27/240 m and pt. 22, 190 m, the channel rises again between 1 and 2 m above the collector and shows a width which can merge with the width of the collector (Fig. 4D). We can observe a high density of equilibrium chimneys, which can rise higher than 5 m. Between pt. 27 and pt. 24, the drain is almost straight and presents the longest straight line since the "Espace des Six" chamber.

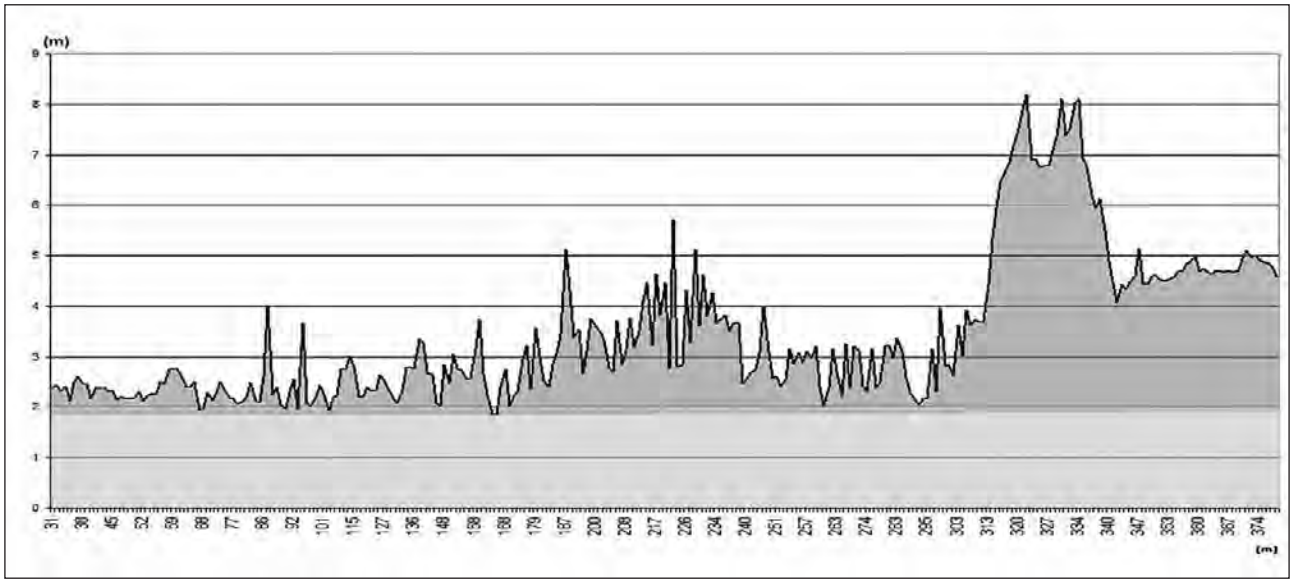

Figure 3. Longitudinal profile of the main gallery. Between 374 m and 319 m, a well developed ceiling channel with downstream a large reservoir; between 319 m and 187 m, a moderately developed ceiling channel with downstream a smaller reservoir; between 187 m and 31 m, a punctually developed ceiling channel without reservoir, only equilibrium chimneys.

This area offers a large volume, which can be compared to the "Espace des Six" chamber, with smaller dimensions. Between pt. 24 and pt. 22, the channel remains high but becomes narrower. Moreover, pt. 22 presents the last dome which rises higher than 5 m above the rolling ground of the collector.

3.4. The downstream ceiling channel

Beyond this dome, from pt. 22/190 m to outside, the channel tends to reduce as well as presenting more frequent and larger interruptions (Fig. 4E). It rarely goes higher than 0.50 m and gets too narrow for a man to fit in (Fig. 4F). The dissolution pockets do not rise higher than 3 m above the rolling ground, except for 3 exceptions which are not higher than 4 m. From pt. 4/60 m, the channel becomes discrete to anecdotal (Fig. 4G). Between pt. 2 and pt. 1, on the last 31 m, the collector has been re-calibrated and the channel has been completely erased.

The ceiling half-tube is therefore much larger in its up-collector part then in its down-collector part. Why is that?

4. Discussion

Two aspects are particularly noticeable: (i) what does the size reduction of the channel from upstream to downstream mean?, and (ii) why do we observe a great irregularity in the longitudinal profile?

The reduction from upstream to downstream of the dimension of a drain often means a reduction of the flow which digs it. If the flow decreases, it means that the drainage scatters instead of concentrating itself, which means that it is not a restitution drainage which collects underground waters, but, on the contrary, an introduction drainage from the surface, which is absorbed along the drain.

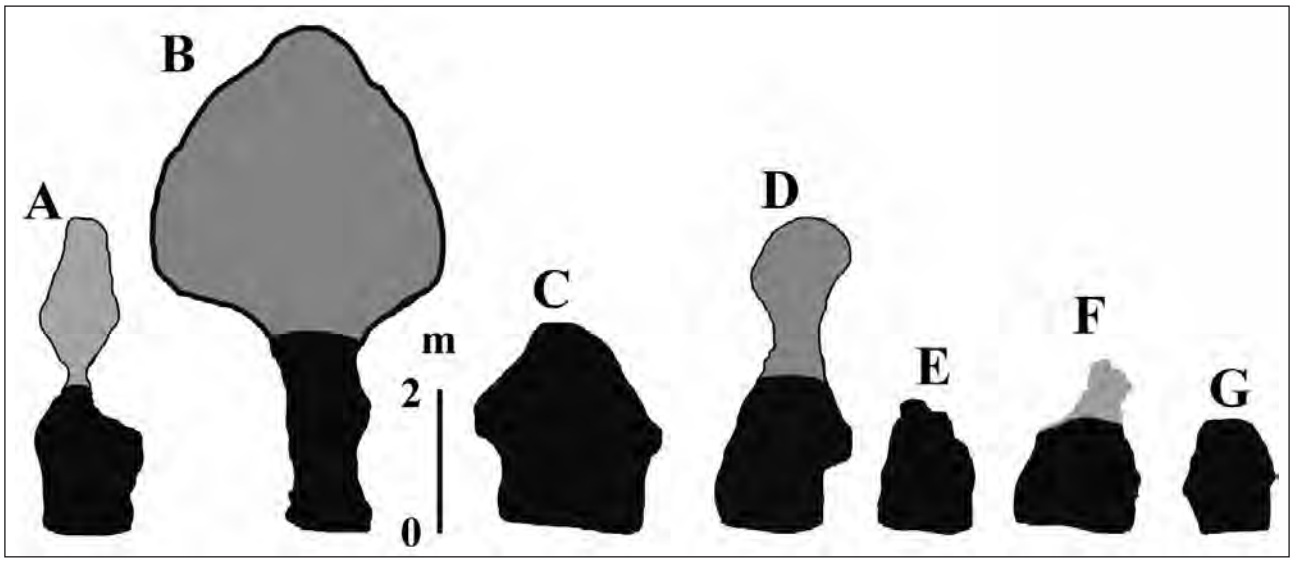

Figure 4. Selected cross sections of the main gallery in the Petites Dales Cave. The black section represents the gallery and the grey section, the development of the ceiling channel. A: pt. 38; B: between pt. 36 and pt. 37 ("Espace des Six" dam chamber); C: between pt. 30 and pt. 31; D: between pt. 24 and pt. 25 (dam-equilibrium chimneys); E: pt. 19; F: between pt. 12 and pt. 13; G: between pt. 5 and pt. 6 (lower point of the main gallery's roof). See the Figure 2.

Consequently it is an introduction and we have to identify the source, meaning, the input point.

Right up pt. 44, the clearance work has shown the base of a solution pipe. In a spectacular way, and without a doubt, this solution pipe has a morphodynamic link with the ceiling channel which starts there, and is, therefore, the source of this introduction channel. This is proved by the morphological continuity (Rodet et al. 2009), confirmed by the sedimentary continuity (Laignel et al. 2004; Rodet et al. 2006). We can particularly notice the complexity, mid-study, of the fluvial sedimentary deposits, strongly upset by many torrential introduction phases which have affected this part of the cavity.

This torrential dynamic is included in the ceiling channel, of which the morphology strongly contrasts with the rest of the cavity. Three particularly noticeable morphological elements illustrate invasive torrential dynamics from the solution pipe. They demonstrate an adaptation of the cavity to these sudden and abrupt external inputs, and their effects on the restitution networks.

4.1. The upstream channel of the Espace des Six

We can notice that the ceiling channel is an introduction pipe coming from the pt. 44/45 solution pipe which joins tangentially the main gallery previously calibrated by the earlier trepanation of the upstream pt. 47 solution pipe. We can observe the junction of a superior drain which quickly loses its erosive and transport dynamic (the drainage loses speed), as well as its drainage mass, which is partially absorbed by the underlying completely filled collector.

Figure 5. Between pt. 37 and pt. 39, the channel seems to be separate over the main drain by a platform in the bedrock (photo by J. Rodet).

This explains why the ceiling channel appears more distinctly above the collector as we get closer to the "Espace des Six" chamber, particularly with an input with tends to isolate both drains (Figs. 4A, 5). Upstream, in the "draw point 404" (pt. 42), channel and collector are fused with the same width, and it is more difficult to show their limit. This evolution can explain the number and the size of big chalk blocks seen in the "draw point 404", which can result in a destruction of the intermediary floor: no water circulation could explain the movement of such volumes, without leaving traces on the walls. On the contrary, we have to consider a stock of introduction water of which the geochemical activity would dissolve the bedrock. The blocks are almost *in situ* and underline the destruction of the floor which isolated the ceiling channel coming from the pt. 44 solution pipe and the calibrated gallery coming from the upstream solution pipe (pt. 47).

4.2. The "Espace des Six" chamber

Located right downstream, the "Espace des Six" chamber (pt. 36/37) is a noticeable point, nonesuch in the whole Petites Dales Cave. Indeed, nowhere else in the cavity can we observe such a large volume. We can also note that the enlargement concerns the top part and not the whole volume (Figs. 4B, 6). Another important element: the inferior third is narrow and was infilled, the intermediary third widens and was infilled too, and the superior third is wide and was empty, except for chalk blocks fallen from the walls and from the roof, underlining submergence phases. It clearly appears that this large volume hanging above the collector is an underground tank, stocking important water inputs during sudden introductions.

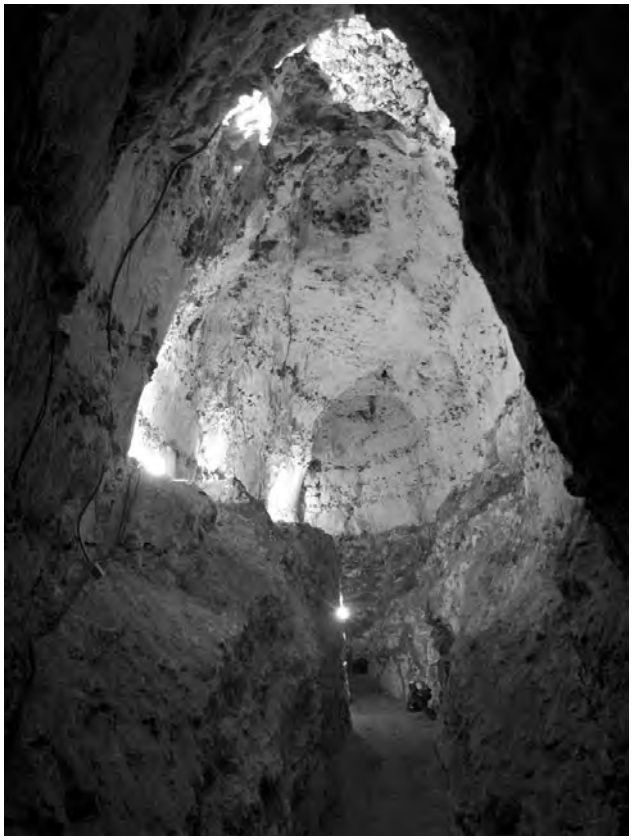

Figure 6. Between pt. 36 and pt. 37, the "Espace des Six", large dam chamber perched on the more narrow main gallery (photo by L. Magne).

4.3. Point 24 turning point

It is the third point morphologically remarkable that can be observed from the upstream part of the main gallery. It clearly shows a high contrast between the upstream side of the drain, almost rectilinear for about 30 m, and downstream which contains not less than four right angle bends on a few dozen meters, except the extremely tight curve of point 24 *sensu stricto*, which almost enables a half turn to the flow thanks to a 45° angle.

If the channel worked like a collection and restitution water drain, the abrupt changes in direction would not have such an incidence. What can be seen?

- Downstream: close and tight turns, in a quite reduced drain, highly congested by sediment filling and with a narrow and high ceiling channel.
- Upstream: a long straight line, one of the most important in the cavity. The roof presents a larger channel which is however largely disemboweled by a succession of equilibrium chimneys, that are high (about 6 m), more and more numerous reaching point 24, giving a beginning coalescence which strangely enough reminds of the draft of a reservoir similar to the "Espace des Six" chamber (Figs. 4D, 7).

The difference is essentially due to the positioning of the joints. If in the "Espace des Six" chamber, the parallel positioning of the drain and of the fissures facilitates the development of a large volume, at point 24, the joints located upstream are oblique compared to the axis of the drain. They generate a succession of equilibrium chimneys, approximately ten along 20 m.

The dynamic responsible for the morphology is the one of a rising which hastily flow out from the upstream through the sinkhole and the solution pipe and hammers the wall of the sudden bend of point 24. It leads to a sudden stopping of the dripping and thus the quasi-instant loss of its sedimentary load which settles and partially or totally blocks the drain downstream. Whereas water accumulates and generates a pressure to the ceiling which is responsible for the digging of equilibrium chimneys on the weak points that the fissures are. Their coalescence draws a chamber typed tank.

Figure 7. Flooding reservoir resulting of coalescence of several equilibrium chimneys developed on the structure, obliquely to the axis of the drain, between pt. 26 and pt. 24 (photo by J. Rodet).

From these different elements, it can be deduced that the ceiling channel of the Petites Dales Cave is a feature which results from concentrated introductions from the surface, in a restitution drain. The episodic and torrential dynamic leads to transport solid elements which deposit and settle out as soon as the stream slows down because of the well-defined turnings of the drain, creating an obstacle to the flow and phases of submergence upstream with diggings of dam chambers. Both the drain morphology and the sedimentation figures in the fillings confirm this model of speleogenesis.

5. Conclusion

The geometry of such a kind of ceiling channel is not compatible with the classic model of restitution drain of the underground waters. The decreasing section of the ceiling channel toward downstream shows indeed that competence is lost and that the latter is opposed to the notion of flow concentration. Then the examination of the longitudinal profile shows a relation between the development of a volume reservoir and brutal orientation changing of the flow. Such an association (upstream: reservoir/downstream: brutal direction changing) shows the process of a very concentrated flow penetrating a pre-existing drain. Unlike the common image of the ceiling channel, which is an erratic circulation collector, the example of the Petites Dales Cave shows a model of concentrated introduction of surface water in a restitution network. This aspect seems it has never been studied through a karstological approach, in spite of the consultation of a wide bibliography, although it gives plenty of information about the dynamics of underground waters, and enables a better understanding of the proccesses of some physical and chemical characters, such as for instance the turbidity in emergences and catchment areas.

Acknowledgments

The authors would like to thank the French Federation of Speleology to have classified the Petites Dales Cave in the Underground Heritage Conservatory Agency, and all those who donated time and energy to allow this big clearing site in the absence of which this study could not have existed.

References

Jennings JN, 1985. Karst geomorphology. Basil Blackwell, Oxford: 293.

Laignel B, Dupuis E, Rodet J, Lacroix M, Massei N, 2004. An example of sedimentary filling in the chalky karst of the Western Paris Basin: Characterization, origins and hydrosedimentary behaviour. Zeitschrift für Geomorphologie N.F., 48 (2): 219–243.

Renault P, 1968. Contribution à l'étude des actions mécaniques et sédimentologiques dans la spéléogenèse. Annales de Spéléologie, tomes 22 (1967): 5–21, 209–267 and 23 (1968): 259–307, 529–596, 317–337.

Rodet J, Laignel B, Dupuis E, Brocard G, Massei N, Viard J-P, 2006. Contribution of a sedimentary study to the karstic evolution concept of a chalk cave of the Western Paris Basin (Normandy, France). Geologica Belgica, 9 (3–4): 287–296.

Rodet J, Machado MMM, Ruchkys de Avezedo Ú, 2012. Thoughts about the karstic heritage management and its enhancement: examples from Normandy and Brazil. Proceedings of the 13th National Congress of Speleology, Muotathal (CH), 29 sept.–01 oct. 2012: 305–306, abstract, PPT.

Rodet J and Viard J-P, 2009. La grotte des Petites Dales, un patrimoine normal? non! normand!. Spelunca, 114: 28–34.

Rodet J, Viard J-P, Poudras J, 2007. A la découverte de la grotte des Petites Dales (Saint Martin aux Buneaux, Seine Maritime, France). Spéléo-Tract, 6: 38.

Rodet J, Willems L, Brown J, Ogier-Halim S, Bourdin M, Viard J-P, 2009. Morphodynamic incidences of the trepanning of the endokarst by solution pipes. Examples of chalk caves in Western Europe (France and Belgium). Proceedings of the 15th International Congress of Speleology, Kerrville (Texas, USA), 19–26 July 2009, UIS, vol. 3, contributed papers: 1657–1661.

Slabe T, 1995. Cave rocky relief and its speleogenetical significance. Znanstvenoraziskovalni Center SAZU, 128.

GULLS, GULL-CAVES AND CAMBERING IN THE SOUTHERN COTSWOLD HILLS, ENGLAND

Charles Self[1], Andrew Farrant[2]
[1]University of Bristol Spelaeological Society, UK., self@globalnet.co.uk
[2]British Geological Survey, Keyworth, Nottingham, NG12 5GG, UK, arf@bgs.ac.uk

The study of fissures and caves formed by mass movement is important not only because they are a significant geohazard, but because such caves can be repositories for palaeogeographic information. In southern Britain, such open joints in solid strata are known as *gulls.* In the southern Cotswold Hills, a sequence of interbedded limestones and mudstones has been deeply dissected by the River Avon and its tributaries. Mass movement and cambering has opened up narrow gulls and larger gull-caves to a far greater extent than had previously been realized. Gull-cave surveys and the mapping of gulls inside the extensive abandoned Box Freestone Mine have allowed the spatial distribution of these features to be studied. We found that the direction of extension is not always in the direction of topographic gradient; locally it can be influenced by the stratal dip direction. In some areas, abrupt changes in the orientation of valley sides have allowed mass movement in two directions, creating rectilinear networks of gull-caves. A quantitative assessment of the valley-ward extension of the strata caused by gulling was made in Box Freestone Mine. Extension may often exceed 5%, and locally may reach 9% in discrete zones. Evidence of preferential dissolution along the NW–SE joint set in both gulls and gull-caves suggests former groundwater flow to the north-west, not to the present River Avon valley. This indicates that the River Avon has subsequently captured the dip slope streams that once fed the headstreams of the River Thames. The greatly enhanced flow of the River Avon after this capture caused rapid over-deepening of the valley, which triggered the original cambering and thus formation of the gull-caves themselves.

1. Introduction

The Cotswold Hills, located in the south-western part of the English Midlands, forms a significant escarpment about 100 km long and generally 20 km wide, reaching a maximum elevation of just over 300 m near Cheltenham. They comprise a sequence of interbedded limestones and mudstones of Middle Jurassic (Bathonian) age, with a steep scarp slope facing to the west and a shallow dip slope to the east (Barron et al. 2011). Rivers rising on the dip slope flow east towards the River Thames and the North Sea, scarp streams flow west to the River Severn and the Atlantic Ocean. The exception to this is the (Bristol) River Avon which rises on the dip slope of the southern part of the Cotswold Hills, then cuts through the escarpment via the Claverton Gorge near Bath; it continues west, picking up scarp stream tributaries, and passes through the cities of Bath and Bristol before reaching the River Severn.

This paper describes part of the southern Cotswold Hills to the east of Bath which has been deeply dissected by the River Avon and the By Brook, a major tributary which joins from the east (Fig. 1). In the valley floor, the rivers have incised through the Middle Jurassic sequence into Lower Jurassic strata of the Lias Group, which are mainly mudstones with subordinate limestones. The lower part of the valley sides are cut in the Inferior Oolite Formation, a rubbly oolitic limestone up to 23 m thick.

Above this is the Fuller's Earth Formation, a series of calcareous mudstones with occasional beds of flaggy limestone, approximately 46 m thick. The Fuller's Earth mudstones are over-consolidated, highly plastic clays prone to mass movement. Capping the interfluves is the Chalfield Oolite; a succession of largely matrix-free oolitic limestones 35–40 m thick. Succeeding these limestones on the dip slope is the Forest Marble Formation, a sequence of coarse bioclastic limestones and mudstones. The regional dip is about 2° to the south-east.

These Jurassic mudstones and limestones are all prone to mass movement. The valley sides of the River Avon and its tributaries have extensively foundered, with significant land slipping in and around the city of Bath. These mass movements include both rotational landslips and extensive cambering. Gulls are common in the more competent oolitic limestones. The term *gull* (derived from gully) is an old quarryman's term, used to describe open joints in solid strata (Fitton 1836). They are particularly well developed in the Chalfield Oolite where the major joints have opened as the stata has extended valley-ward. When large enough to be explored by cavers, they are termed gull-caves; the anthropomorphological element of this definition is important because it means that they are accessible to direct study. Gull-caves are different from normal dissolutionally widened fissures and caves, and can be identified by their distinct morphology. Gulls are typically narrow, parallel-sided, joint orientated rifts, often with symmetrically opposing wall morphologies ("fit features" of Self 1986), but where there has been vertical as well as lateral movement, bedding planes or other discontinuities may also have parted.

In the Bath area, the Jurassic oolitic limestones are excellent building stones, as they can be cut as "freestones" which then harden on exposure to air. Consequently they have been extensively mined. Several large abandoned pillar and stall workings, with several hundred kilometres of surveyed passages occur in the Bath area. The effects of cambering can be seen in many of these mines. Gulls are common and there are also gull-caves large enough to be accessible for direct study. Moreover, these extensive stone mines enable the spatial extent of the gulls to be mapped out over wide areas, and can be used to identify zones of maximum extension.

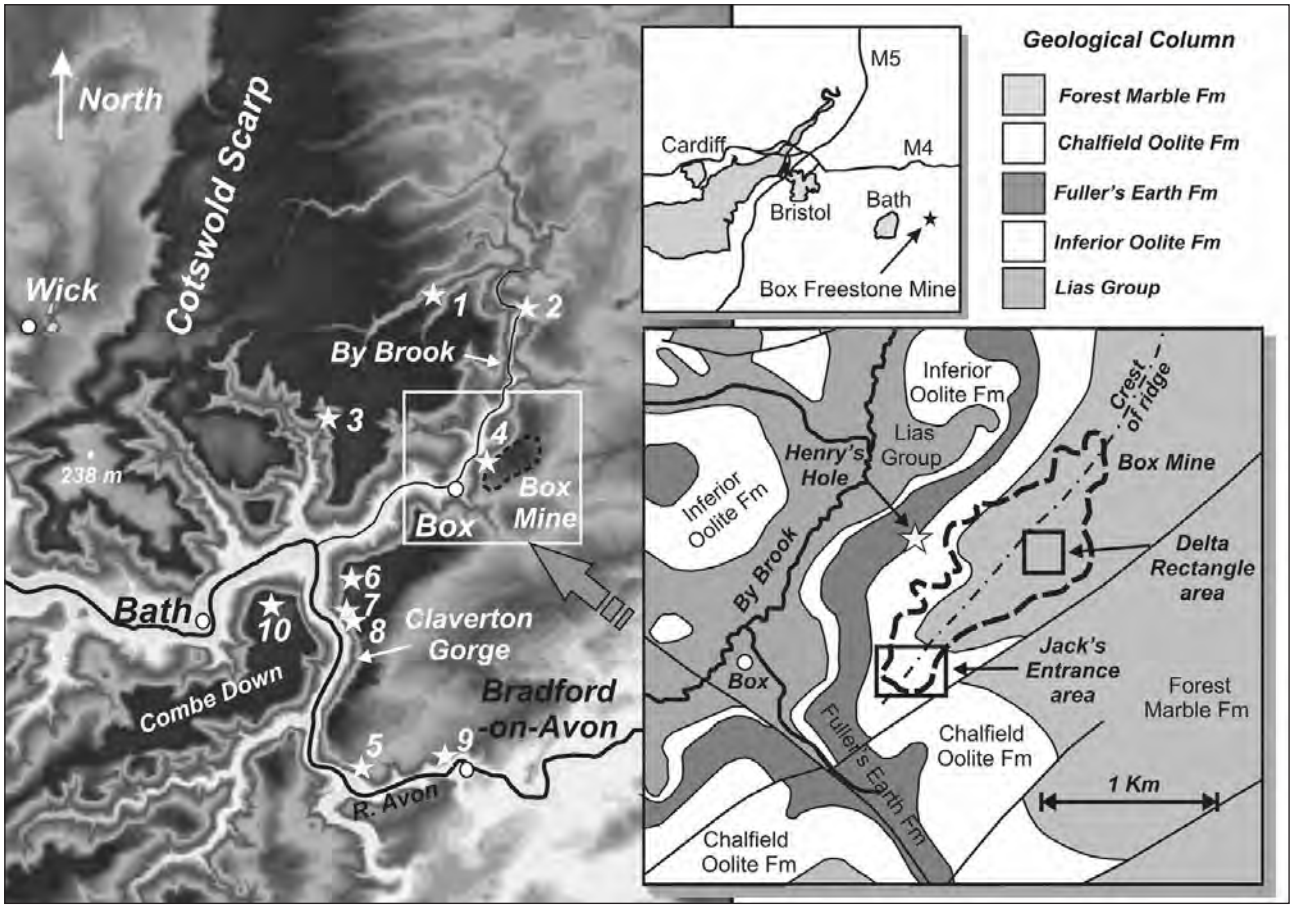

Figure 1. Map of the Avon valley around Bath. The topography is based on a NextMap digital terrain model, with a 5 m spacing greyscale ramp. The inset map is a geological map of the Box area (based on the British Geological Survey digital geological 1:50,000 scale data). Gull caves are marked with a star and numbered: 1. Bury Wood Camp [ST 8162 7397]. 2. Guy's Rift [ST 8450 7372]. 3. The Rock's Rift [ST 7896 7057]. 4. Henry's Hole [ST 8360 6944]. 5. Murhill Rift [ST 7956 6073]. 6. Gully Wood Cave No. 5 [ST 7937 6600]. 7. Sally's Rift [ST 7941 6506]. 8. Gully Wood Cave No. 4 [ST 7946 6500]. 9. Gorton's Rift. 10. Bathampton Down and Bath University. Detailed descriptions of the gull caves are in Self and Boycott (2000).

2. The formation of cambers and gull caves

Gulls form on steep hillsides as a result of mass movement, when well-jointed strata are unsupported on their downhill side. In sedimentary rocks, extension takes place along bedding planes with bed-over-bed sliding and the opening of joints (Hawkins and Privett 1981). Gulls are particularly common in flat-lying or gently inclined strata affected by cambering. *Cambers* are caused by the gravitational lowering of outcropping or near-surface strata towards an adjacent valley. They occur where competent and permeable rocks overlie incompetent and impermeable beds such as clays. The competent beds develop a local dip towards the valleys, swathing the hill-tops and draping the valley sides (Hollingworth et al. 1944). The incompetent material is extruded from beneath the cap-rock, initially as a result of stress relief.

Parks (1991) has suggested that as a camber develops, the competent cap-rock breaks up into joint-bounded blocks above a basal shear plane in the underlying material. A Quaternary cold stage with permafrost conditions is then required, since the underlying strata (if it is mudstone) is much more susceptible to creep when frozen. Thawing at the end of the glacial cycle increases the water content of the mudstone, potentially saturating it and drastically reducing its shear strength. This causes it to behave as a plastic fluid and the competent cap-rock migrates in the direction of slope, opening the joints to form gulls.

The Parks model shows how gulls that are open to the surface can form in a thin cap-rock. In the Cotswold Hills, the limestone cap-rock is much more substantial and the gulls and gull caves generally have intact roofs. They have formed in the lower part of the limestone strata, with little or no mass movement having taken place in the upper part. This requires not only a basal shear plane, but also an upper parting/ sliding plane within the limestone sequence. A possible mechanism, involving the sequential unloading of joint-bounded blocks, was suggested by Self (1986). As extension occurred, individual blocks were able to settle slightly and then move laterally over the mudstone. The blocks move in the same direction but independently of each other, with neighbouring blocks supporting the overlying strata in turn, creating a gull network that propagates away from the valley.

Other features seen in the caves and mines of the southern Cotswolds appear to contradict the Parks model. Significant camber angles are limited in extent, only affecting the strata closest to the hillside margins, whereas gulls continue to occur deep within the stone mines. A possible contributing factor is pyrite oxidation in the upper horizons of the Fuller's Earth mudstone, with chemical leaching of the calcite cement greatly reducing its shear strength (Brown 1991) and allowing mass movement at very shallow camber

angles. Mass movement in the study area seems to have been triggered by the rapid over-deepening of the valley system resulting from the capture by the River Avon of dip slope streams of the palaeo-Thames drainage. High pore pressures in the mudstone need not have been caused by permafrost, but could have been a result of groundwater percolation from above. The stability of the gulls since their creation (with the growth of speleothem deposits) suggests that there was only one major episode of mass movement. A possible explanation is that mass movement ended when the valleys cut down into the more competent Inferior Oolite limestone, which gave stability to the hillsides above.

3. The gull caves

Typically, cave entrances in the southern Cotswolds are found in the cliff faces of abandoned small valley-side quarries (Self and Boycott 2000). Some are single fissures a few metres long, while others form more extensive systems. The main jointing directions are NW–SE and NE–SW, so the more complex gull caves tend to be rectilinear networks. N–S and E–W joints are also present in the study area, but they generally have not been opened by mass movement. The known caves all occur on north- or west-facing (up-dip) slopes, probably because such slopes are less prone to rotational failure. Many more caves certainly exist, but these either do not intersect the surface or are buried under colluvium.

Two main groups of gull-caves occur (Fig. 1). In the By Brook valley, Guy's Rift has 42 m of surveyed passages. Archaeological material in the cave includes the remains of four human adults, three children and pottery of early Iron Age. Downstream, Henry's Hole is a narrow gull which gives access to a small area of independent mine workings, close to the vast Box Freestone Mine complex. The mine intersects other gulls, but one mined passage crosses (with an intact roof) beneath a substantial gull cave, 4 m tall and 40 cm wide. This is evidence for a high-level disturbance within the Chalfield Oolite. In the neighbouring valley, the Rocks Rift is entirely filled with sediment, including calcite flowstone fragments and limestone boulders; it had been previously excavated for 36 m to create a garden folly.

The largest gull caves occur in the Claverton Gorge where the River Avon cuts through the Cotswolds escarpment (locations 5–10 on Fig. 1). Gorton's Rift is a very deep gull accessed from within a small stone mine. The rift is 24 m deep from the mine level and must reach almost to the lithological boundary with the underlying Fuller's Earth mudstones. Several caves can be found on the east side of the gorge. Gully Wood Cave No. 5 is a network of 50 m, developed on several levels whilst Gully Wood Cave No 4 is a 90 m long contour-aligned gull with impressive passage dimensions (Figure 2). Murhill Rift comprises a major passage 80 m long linked to a complex network of rifts and passages on three levels close to the hillside, giving a total length of over 300 m.

The largest cave in the region is Sally's Rift (Fig. 2). It has three entrances and is 365 m long. The passages are typically over 10 m tall and between 20 cm and 50 cm wide; the largest passage lies closest to the hillside and is 15 m tall and 2 m wide. The cave is a series of contour-aligned gulls linked by gulls aligned along a camber spreading axis which runs NE, directly into the hill side.

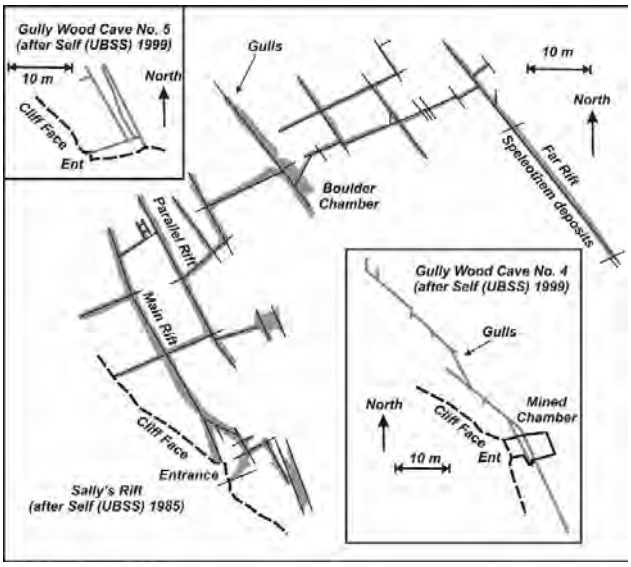

Figure 2. The Gully Wood gull-caves, including Sally's Rift.

This zone of lateral extension is the result of an abrupt change of direction of the River Avon valley just north of the cave, resulting in mass movement in two different directions (Self 2008). The cave has several examples of "fit features", whereby a ledge on one wall matches an overhang at the same level on the opposite wall. In both Sally's Rift and Gully Wood Cave No. 4, there are localized deposits of gravel containing Cretaceous flints with occasional clasts of Carboniferous rocks; these are identical to local superficial deposits preserved in rare patches on the plateau above the cave, identified by Donovan (1995) as an early Quaternary deposit.

4. Gulls in Box Freestone Mine

The Box Freestone Mine complex was worked mostly during the late 19th century using cranes and a network of horse drawn tramways. Over 60 km of passages are still accessible in an area of less than one square kilometre. Gull fissures are pervasive throughout the system and reach into the remotest parts, more than 600 m from the escarpment. The fissures range in width from a few centimetres up to gull-caves over a metre wide and many tens of metres long. Locally they can extend up to 10 m above the level of the mine floor. These larger gulls are sometimes passable, but many have been used for storage of waste stone. A detailed survey of the gull fissures was made in two separate parts of the mine, around Jack's Entrance and in the Delta Rectangle area (see Fig. 1), in an attempt to determine their spatial extent. In the Jack's Entrance area, the majority of gulls are aligned on the 150° joint set and are fairly regularly spaced around 3–8 m apart (Fig. 3). Thirty-five gulls were recorded along a 200 m transect due east from the entrance, showing an average extension of the strata of just over 5% along the length of the passage (Fig. 4). However, in the middle part of the transect, there is a zone with much larger gulls, which give an extension value of 9% for this part of the survey. These *zones of extension* were first reported by Hawkins and Privett (1981) on a

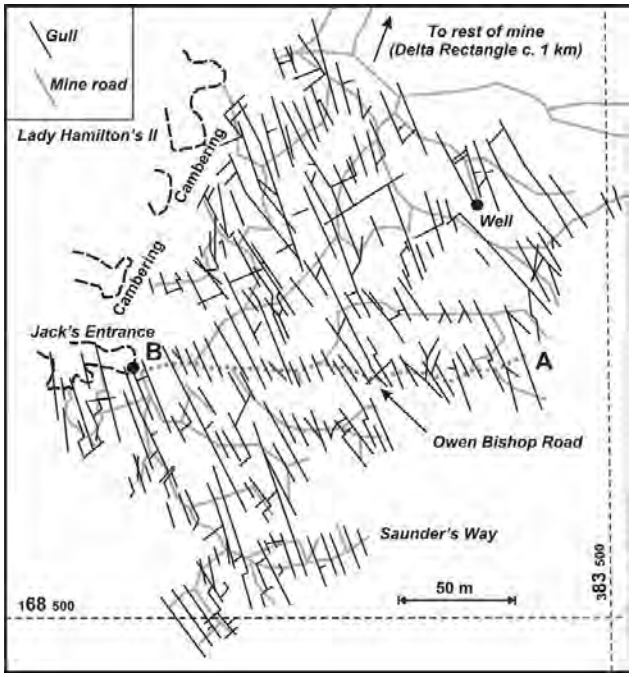

Figure 3. Gulls in the Jack's Entrance area of the Box Freestone Mine.

building site in cambered lower Jurassic strata. Cambering is obvious along the western edge of the mine, reaching a maximum of 11° close to a collapsed former entrance. However, the camber angle decreases sharply a short distance into the mine and within 200 m the bedding becomes essentially horizontal.

In the Jack's Entrance area, the nearby hillside is aligned approximately north-south. Ordinarily, this valley orientation might have caused both the NW and NE joint sets to open. However the regional dip of the strata, around 2° to the southeast, prevents this. Opening of the NE joint set would require cambering up-dip, whereas for the NW joint set cambering is in the much easier direction of strike of the strata. The measured camber directions are not in the direction of slope, which is to the west, but consistently have a dip component which explains the dominance of NW aligned gulls.

The Delta Rectangle area lies almost directly beneath the summit of Box Hill, about 400 m from the nearest escarpment edge. Numerous gull fissures are present but they are more widely spaced than those seen in the southern part of the mine. The gulls are typically 5 to 20 cm wide and both joint sets have opened, with no clear direction of extension (Fig. 5). A 200 m east-west transect recorded seventeen gulls with ca. 1% extension of the strata along the length of the passage. Throughout the mine, the NW joint set is heavily corroded with extensive dissolutional fretting while the walls of the NE joint set are smooth. This suggests that preferred orientation of groundwater flow was in a NW–SE direction.

5. The development of the Claverton Gorge

The Chalfield Oolite is an important aquifer, but it is only weakly karstic and groundwater travels freely along the joints. On the south side of the By Brook and the east side of the Claverton gorge of the River Avon, dissolutional etching is very pronounced in the NW–SE joint set (Self 1995). This etching of the joint walls is the result of slow groundwater movement which pre-dates the onset of cambering (and de-watering of the strata). Drainage could not have been down-dip to the south-east because the Forest Marble forms an impermeable cap-rock. The outlet was therefore up-dip. Up-dip springs contribute to the present drainage of the By Brook valley.

The significance of the up-dip palaeodrainage of the NW joints in Sally's Rift is that the nearby River Avon flows in this direction. The Claverton Gorge (and the entire River Avon valley system upstream) could not have existed at this time, otherwise the groundwater movement would have been towards this valley using the conjugate joint set. This suggests that the proto-River Avon was an aggressive scarp

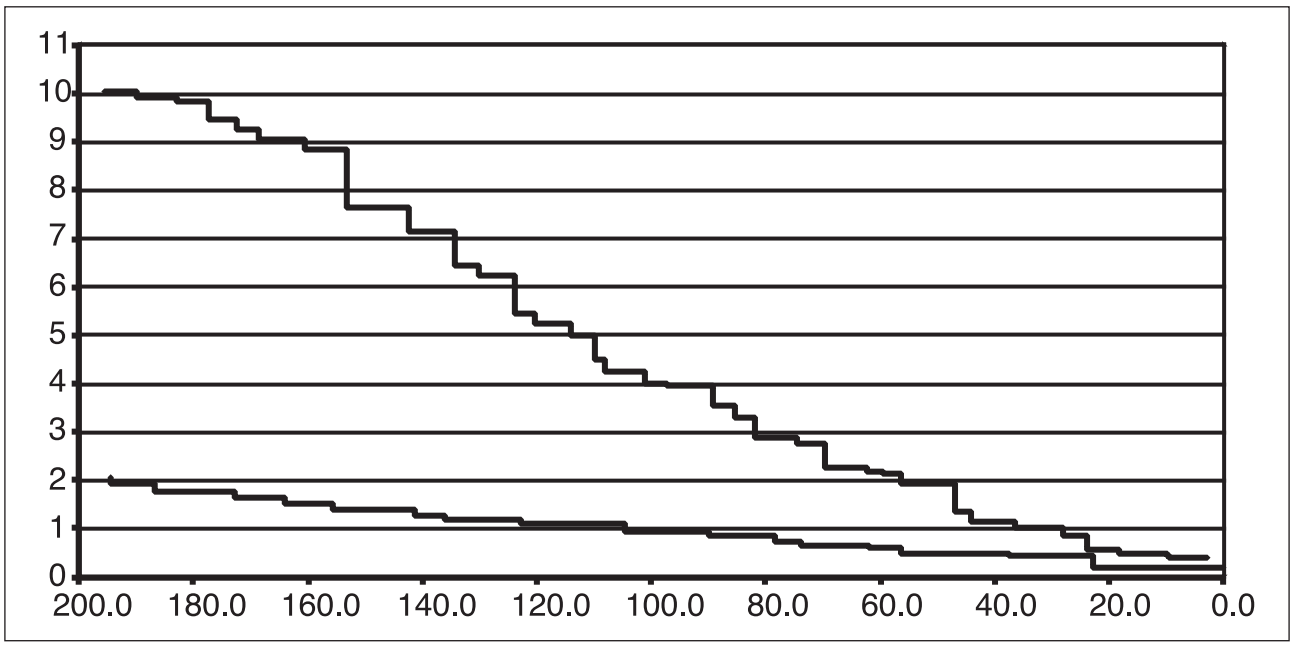

Figure 4. Transects through Box Freestone Mine: 1. Owen Bishop Road close to Jack's Entrance and the hillside (Jack's Entrance to the west); and 2. Delta Rectangle Passage in the interior of the mine beneath the interfluve. Two zones of extension are apparent on Owen Bishop Road in the Jack's Entrance area.

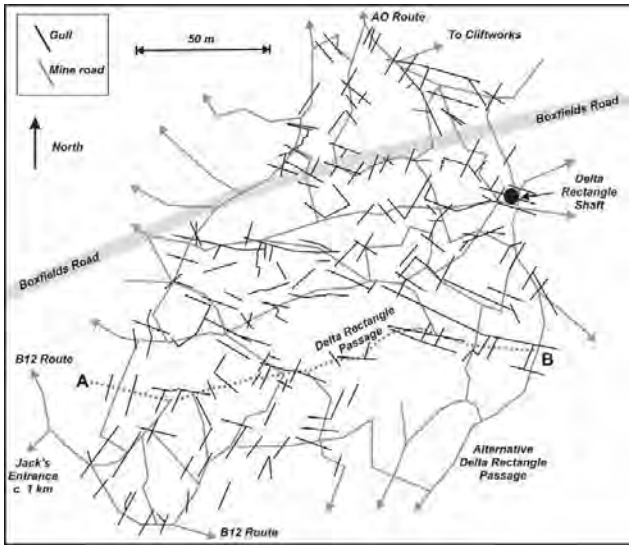

Figure 5. Gulls in the Delta rectangle area of the Box Freestone Mine.

stream tributary to the By Brook, while the Cotswold dip slope drainage was originally east to the River Thames. Eventually, head-ward erosion by the River Avon allowed it to break through into dip-slope territory and capture these former Thames headstreams. With a greatly enhanced flow, the River Avon rapidly over-deepened its valley and formed the steep-sided Claverton Gorge. The tributary valleys also cut down to this new base level and the entire valley system was primed for cambering.

References

Barron AJM, Sheppard TH, Gallois RW, Hobbs PRN, Smith NJP, 2011. Geology of the Bath district: a brief explanation of the geological map sheet 265 Bath. Nottingham, UK, British Geological Survey, 35.

Brown CJ, 1991. A geotechnical study of abandoned mineworkings in the Bath area. Ph.D. thesis, Bristol Univ. UK.

Donovan DT, 1995. High level drift deposits east of Bath. Proceedings of the University of Bristol Spelaeological Society, 20, 109–126.

Fitton WH, 1836. Observations on some of the strata between the Chalk and the Oxford Oolite in the South-East of England. Transactions of the Geological Society, 2(4), 103.

Hawkins AB, Privett KD, 1981. A building site on cambered ground at Radstock, Avon. Quarterly Journal of Engineering Geology, London, 14, 151–167.

Hollingworth SE, Taylor JH, Kellaway GA, 1944. Large scale superficial structures in the Northampton Ironstone Field. Quarterly Journal of the Geological Society, 99, 1–44.

Parks CD, 1991. A review of the mechanisms of cambering and valley bulging. In: A Forster, MG Culshaw, JC Cripps, JA Little, CF Moon (Eds). Quaternary Engineering Geology. Geological Society, London, 7, 373–380.

Self CA, 1986 (for 1985). Two gull caves from the Wiltshire/Avon border. Proceedings of the University of Bristol Spelaeological Society, 17, 153–174

Self CA, 1995. The relationship between the gull cave Sally's Rift and the development of the River Avon east of Bath. Proceedings of the University of Bristol Spelaeological Society, 20, 91–108.

Self CA, 2008 (for 2007). Cave passages formed by a newly recognized type of mass movement: a gull tear. Proceedings of the University of Bristol Spelaeological Society, 24, 101–106.

Self CA, Boycott A, 2000 (for 1999). Landslip caves of the Southern Cotswolds. Proceedings of the University of Bristol Spelaeological Society, 21, 197–214.

THE ROLE OF FOLD-AND-THRUST STRUCTURE IN THE LARGE SHAFTS AND CHAMBERS DEVELOPMENT: CASE STUDY OF THE POLISH TATRA MTS.

Jacek Szczygieł
Faculty of Earth Science University of Silesia, Będzińska 60, 41-200 Sosnowiec, Poland, j_szczygiel@tlen.pl

The Tatra Mts. are characterized by a geological structure typical to fold-and-thrust alpine belt. This paper focuses on four caves belonging to the largest in the Tatra Mts.: the Ptasia Studnia System, the Mała w Mułowej Cave, the Kozia Cave, the Śnieżna Studnia Cave. The caves are developed in the Czerwone Wierchy Unit. A deep shaft or a series of shafts and a large chamber characterize each of these caves. All these large underground features are located within hinge zones of the main synclines of the Ździary or Organy Units (the sub-units of the Czerwone Wierchy Unit). The Organy Syncline has chevron geometry, the Ździary Syncline is characterized by a concentric geometry. Large chambers are formed in hinge zones of chevron folds and in the hinge zones closer to the core of concentric folds. A strong compression in this zone has resulted in a large number of sub-structures (folds, faults, fractures). This zone is relatively narrow which results in the occurence of forms of similar horizontal and vertical dimensions. Chambers are characterized by breakdown features. The extent of chamber is correlated to the strike of strata and faults perpendicular to beds. Deep shafts are developed in the outer part of the concentric folds. The shafts based on long steep stratification surface loosen and dislocated each other by flexular slip, which is an effect of the local extension zone.

1. Introduction

The relationships between the geological structure of the massif and the development of karst features discussed by Grodzicki (1970), Hauselmann et al. (1999), Klimchouk and Ford (2000), Tognini and Bini (2001) and others. The shape and direction of cave passages, as well as volume and extent depend on litology, tectonic and geometry of specific structures. The geometry and extent of specific structures are particularly important in case of a fold-and-thrust orogens. Groundwater flows by the most convenient and the easiest way. Overthrusts and folds can either facilitate waterflow or prevent it (Goldscheider 2005).

Presented examples from the Tatra Mts. Illustrate the controling role of the structures geometry of the major folds on the large shafts and chambers.

2. Study area

The Tatra Mts. are the northernmost part of the Central Western Carpathians, they are composed of a crystalline core and are overcast by autochthonous sedimentary cover, Hight-Tatric Nappe (Czerwone Wierchy Unit, Giewont Unit) and Sub-Tatric Nappes (Križna and Choč nappes; Fig. 1A).

Approximately 1,200 caves have been described in the Tatras so far, of which just over 800 are in Poland (Gradziński et al. 2009). Karst in Polish Tatra Mts. occurs mainly in the Czerwone Wierchy Massif. In this paper the presented data comes from the four caves located in the N part of the Czerwone Wierchy Massif. These are Ptasia Studnia System, Mała w Mułowej Cave, Kozia Cave, Śnieżna Studnia Cave. Large forms of caverns have developed in those caves.

2.1. Geological setting

The caves are located in the Czerwone Wierchy Unit (Fig. 1B) which consists of a sedimentary sequence from Triassic to Lower Cretaceous. Simplified profile of Mesozoic succession is (based on Kotański 1963; Lefeld et al. 1985; Piotrowska et al. 2009):

- Early Triassic "Campilian" limestone and dolomite with shale interbeds (the Myophoria Beds);
- Middle Triassic limestone and dolomite with bioturbate beds;
- Middle Jurassic "Doggerian" crinoida limestone (Smolegowa Formation – Bajocian), red nodular limestone (Krupianka Formation – Batonian);
- Late Jurassic to Lower Cretaceous (Hauterivian) "Malmo-Neokomnian" thick-bedded limestone (Raptawicka Turnia Formation);
- Lower Cretaceous (Barremian, Aptian) "Urgonian" – organodetritic thick-bedded limestone (Wysoka Turnia Formation)
- Lower Cretaceous (Albian-Cenomanian) – green marly shale, (Zabijak Formation)

The Czerwone Wierchy Unit is composed of two sub-units: more northern – Organy and lower southern – Ździary, separated by Organy Fault extending latitudinally along the major unit, from the Kościeliska Valley to Mała Łąka Valley (Kotański 1963).

In spite of numerous studies the character of the Organy and Ździary units is not clearly defined. Kotański (1963, 1965) and Bac et al. (1984) presented these units as a syncline. Grodzicki (1978) based on measurements of the caves ascertained that the Organy Unit is made up of two

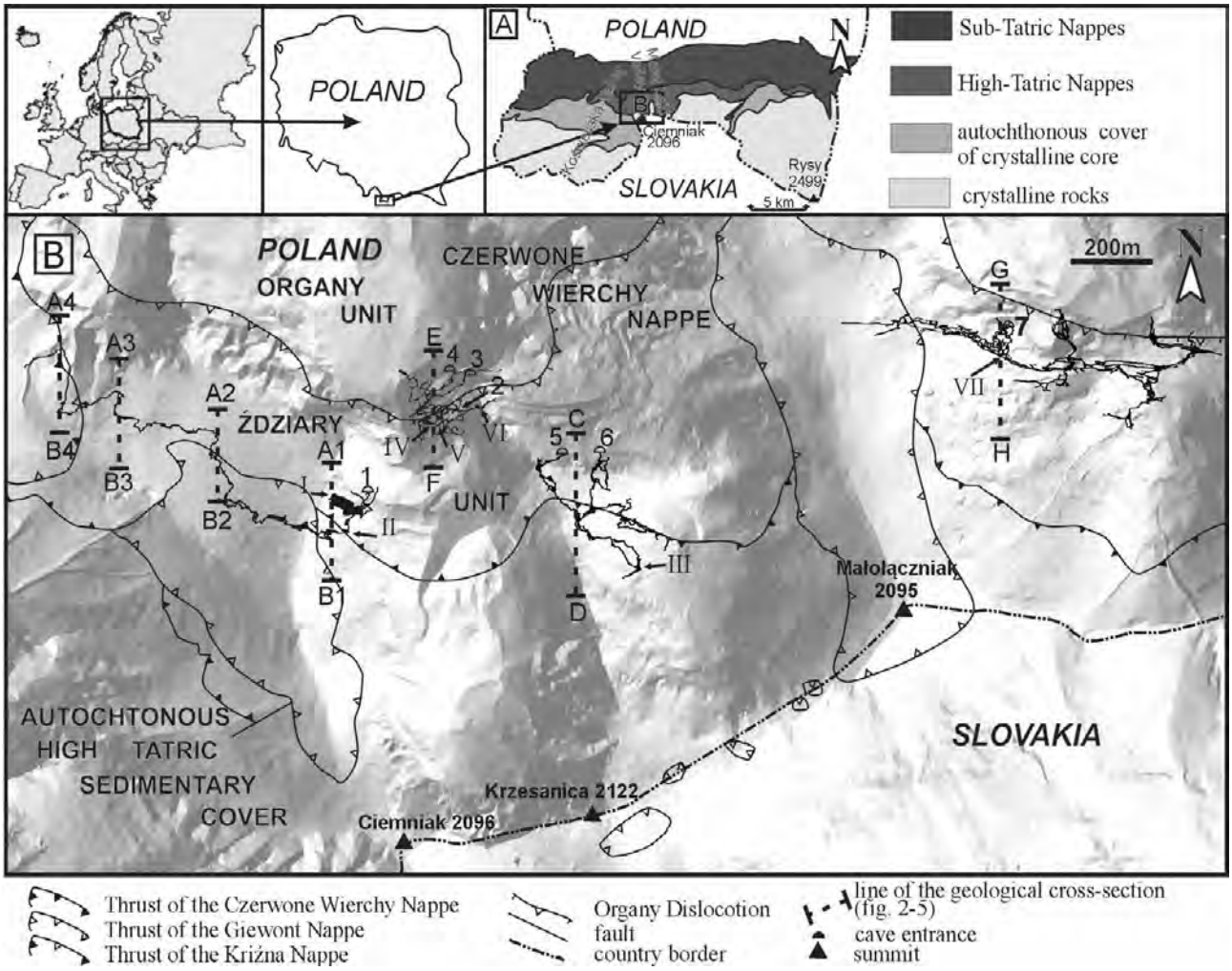

Figure 1. Location of study area; A – Main tectonic units of the Polish Tatra Mts.(after Kotański 1963); B – Schematic tectonic map of the study area with caves location (after Piotrowska et al. 2009); 1 – Mała w Mułowej Cave; 2 – Ptasia Studnia Cave; 3 – Lodowa Litworowa Cave; 4 – Nad Dachem Cave; 5 and 6 – Kozia Cave; 7 – Śnieżna Studnia; I – Fakro Chamber; II – Czesank Shaft; III – Large Shaft; IV – Dante Chamber; V – Chamber Under Colossal Boulder; VI – chamber with Wielki Kłamca lake; VII – Wazeliniarzy Shaft.

elements, the lower – Upłaz Mietusi Anticline and the upper – Organy Syncline. Then Grodzicki and Kardaś (1989) based on geological measurements from the caves interpreted geological structure as a duplex style. Jurewicz (2005) confirmed that the Tatra nappes have been formed in a manner similar to duplexes, but also showed a much more complicated history and dynamics of the Tatra massif proving primary southern inclined of the major overthrust plane.

2.2. Characteristic of caves

The Ptasia Studnia System has 3 entrances: Ptasia Studnia (1,627 m a.s.l.), Lodowa Litworowa Cave (1,576 m a.s.l.) and Nad Dachem Cave (1,522 m a.s.l.). All within the N wall of the Kozi Ridge (Fig. 1B). The cave is a network of passages of different nature and origin: phreatic pipe sometimes remodeled by vadose meanders, tectonic conduit, deep shafts of probably invasive (vadose). On the 1,480 m a.s.l. Dante Chamber is located, one of the largest cave rooms in the Tatras measuring approximately 12 × 35 m and 50 m height. The cave has a length of 6,000 m and 352 m of denivelation (Lorczyk 2010).

The Kozia Cave has two entrances located in Kozi Ridge (Fig. 1B) at 1,850 m a.s.l. The cave consists of two parallel main conduits with many branches. One of the meanders at a depth of approximately 245 m goes into aven type, reaching a depth of -389 m. The second conduit at the upper part continues as a tectonic corridor. Below a depth of 100 m is a typical vadose passage and reaches a depth of -263 m. The connective passages of two conduits are a level at a depth of approximately 100–120 m. Kozia Cave is 3,470 m long (Wiśniewski and Kotarba 2010).

The Mała w Mułowej Cave is located at NE slope of the Ciemniak (Fig. 1B). Entrance is situated at 1,757 m a.s.l. Mała w Mułowej Cave is 555 m deep and 3,863 m long (Antkiewicz and Lorczyk 2010). The cave has two main conduits which separate at a depth 60 m. The first conduit is a vertical type and contain the biggest chamber in Tatra Mts. of dimensions 85 × 35 × 90 m. The second conduit is of Aven type too, but only to 300 m deep. At a depth of -160 m begins the Czesanka Shaft with a depth of 130 m. Further passages run 800 m westwards in a straight line to a depth of 555 m.

The Śnieżna Studnia cave is known only by one entrance. It is located at a height of 1,747 m a.s.l. at the NE slope of the Małołączniak (Fig. 1B). In the cave there are two basic types of corridors. Sub horizontal corridors of phreatic or

tectonic origin, with the general course W-E and the extent of 900 m. Old inactive conduits are developed between 1,350 and 1,200 m a.s.l., the known active conduit (zone of sump) extends from the 1,100 m to 1,030 m asl. The second type is vertical. Within parts from the entrance to the level -500 the deepest shaft is located in Tatra Mts. – Wazeliniarzy Shaft (200 m deep). The cave has 763 m of denivelation and length of 12,050 m (Fuja et al. 2010).

3. Methods

Fieldwork has covered measurements of bedding planes, fractures, faults and tectogliphs. Observations of relationship between measured structures and the course of the cave have been made. Rock samples for stratigraphic position of studied units were collected. All data are presented as structural plans of caves and geological cross-sections.

Structural studies were carried out on the basis of the detailed structural analysis in order to recognize geometric, kinematic and dynamic features of minor tectonic deformation structures represented by: joints, mesofaults (with accompanying minor structures on the fault surfaces and shears) and veins. The studies were based mainly on the geometric analysis of various mesoscale tectonic structures: their morphology, spatial orientations and superposition. Collected data were summarized in the form of structural diagrams (great circles and contours) made in equal-area Lambert-Schmidt projection on the lower hemisphere using SpheriStat software. Rose diagrams – presenting strike directions and dip angles of studied structures – were prepared in TectonicsFP software.

4. Results of geological observations

4.1. Ptasia Studnia System

The Ptasia Studnia System has been investigated by Grodzicki and Kardaś (1989). They have recognized at the Organy Fault plane depth of 15 m below Ptasia Studnia Cave entrance. Below documented hinge of the Organy Syncline around 1,450 m a.s.l. Detailed revision confirms the presence of overthrust separates the two units at a depth of approximately 15 m. In the depth the cave develops mainly in Middle Traissic limestone and dolomites. The Nad Dachem Cave developed in limestone of the Raptawicka Turnia Formation up to 1,450 m a.s.l. where there is the boundary between the limestone of the Raptawicka Turnia Formation, Middle Jurassic limestone and Middle Triassic rocks (Fig. 2). Beds in the inverted limb of the Organy Syncline oscillate from 55° to 35°, locally to 20°. The dip direction of bedding is S and SSE less frequently SSW. In the lower limb of the syncline the dip of bedding are between 55° and 3° to NE direction (Fig. 2). Axial surface orientation is 109/22. The syncline is a chevron type fold with gently inclined axial surface. Dominated joints in the cave are orientated NNE–SSW, very steeply occurs The NE–SW-trending and steep re slightly less frequent. There are also sub-latitudinal and NNW–SSE trending fractures (Fig. 2). Comparison of fracture diagrams of the upper and lower fold limbs shows similarities, which proves the formation of these fractures after the folding. Three faults are documented in the cave. They are in the Canyon (160/70, about 0.5 m dip separation, normal fault; Fig. 2), in the Dante Chamber (210/50), which probably extends to the Chamber Under Colossal Boulder, and in the chamber with Wielki Kłamca lake (120/80).

4.2. Kozia Cave

Geology of the Kozia Cave has been generally described by Grodzicki and Kardaś (1989). They recognized the cave developed in inverted series of the Middle Triassic limestone and dolomites. They described that beds are inclined to S and dip increase with depth, and the cave developed in the vertical joints. The research shows that in the western conduit, dip of beds to a depth of approximately 140 m oscillates between 40 and 25° to the SSE, and then grow to a depth of 245 m where achieves 60°. Here, the cave changes the charater of meander to aven (shafts serie; Fig. 3), and dip further increase to 75° to the SSE and at the bottom reaches 85° to NNW. In the eastern conduit the dip of bedding is between 32 and 45° to the SSE, and at a depth of about 200 m grows to 60°. At the bottom dip is 65° to the SSE. The cave is dominated by very steep NE SW striking joints. This set can be identified with the same set occurring in the Ptasia Studnia System which is younger than folds. Meridional steeply fractures, very steep latitudinal fractures and of WNW–ESE-oriented fractures are of similar participation in the cave. Meridional and WNW–ESE trending fractures often occur together (Fig. 3).

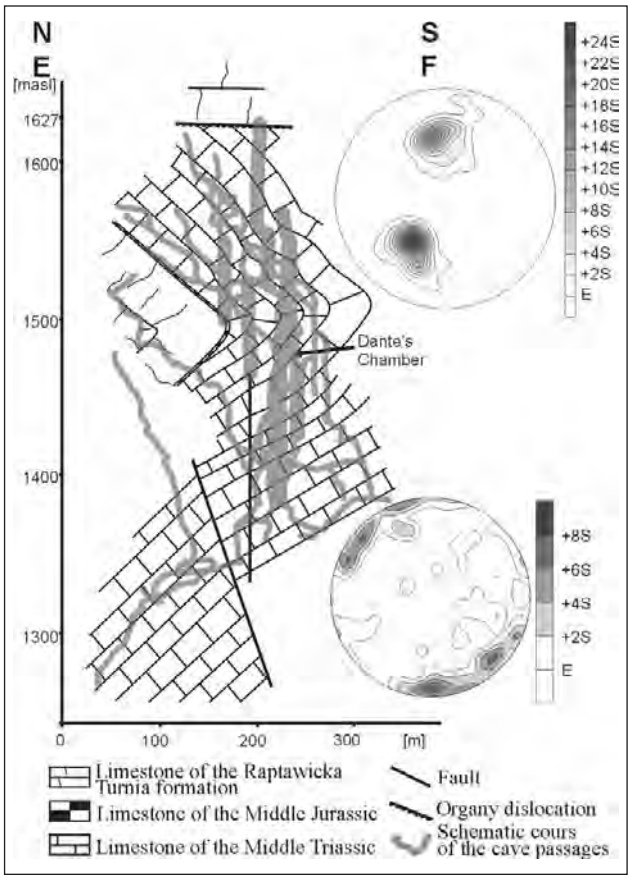

Figure 2. Geological cross-section of the Ptasia Studnia System; upper contour diagram is projection of stratification in the cave, lower is showing fracture; line of the cross-section on the Figure 1B.

An angle of 60° between them and flat fractures plane can point that this fractures are complementary shears system. Φ1 direction (about 335°) which bisects 60° angle is the same as the direction of the main tension of folding. At the depth of -160 to -190 a series of parallel faults of the two cave conduits has been found. Faults planes are gently eastwards inclined (15–25°). In the W conduit observed drag indicates left-rotation. In the E conduit the fault is rejuvenated after the cave development becouse the passages are dislocated by right-rotation. The presence of this fault is correlated with interpretative geological cross-section through Krzesanica by Bac-Moszaszwili and Nowicki (2006).

4.3. Mała w Mułowej Cave

The geological setting of the Mała w Mułowej cave has been described by Bac-Moszaszwili and Nowicki (2006). Their conclusions were based on the surface studies. Preliminary and incomplete studies have been carried out by Recielski and next interpreted by Grodzicki (2008).

The Mała w Mułowej Cave developed in the Middle Triassic limestone and dolomites banding up to 300 m of depth. The beds are arranged in concentric brachysyncline with sub-horizontal axes and axial surface inclined 37º toward N. The upper limb is oriented middling 170/45, the lower 5/65 (Fig. 4). This characteristic is not similar to the interpretations of Bac et al. (1984), Grodzicki and Kardaś (1989), Bac-Moszaszwili and Nowicki (2006). The closest is the interpretation of Kotański (1965).

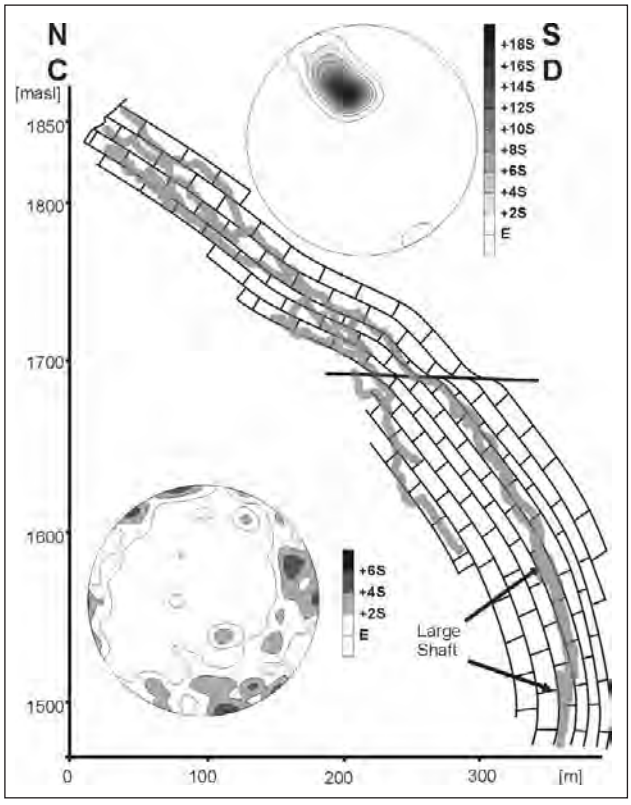

Figure 3. Geological cross-section of the Kozia Cave; upper contour diagram is projection of stratification in the cave, lower is showing fracture; line of the cross-section on the Figure 1B; legend at the Figure 2.

About 300 m under the cave entrance passages are formed mainly at the contact between the autochthonous High Tatric sedimentary cover and the Ździary Unit (Fig. 4). The first Unit consists of calcareous shale of the Zabijak Formation and limestone of the Wysoka Turnia Formation, the second one is formed by the Middle Triassic limestone and dolomites and the Early Triassic limestone with shale interbeds. The contact is tectonic (overthrust), the surface is inclined at an angle of 52 to 83° toward the SW. Shales are oriented at contact consequently or rarely insequently. Triassic rocks contact the overthrust plan insequently, inclined 20–55º toward N. The contact is dislocated by strike-slip faults perpendicular to them.

4.4. Śnieżna Studnia Cave

Geological research in the Śnieżna Studnia Cave was not undertaken before. The geological structure of the cave was outlined in Bac-Moszaszwili and Nowicki (2006). They interpreted the surface data. Fieldwork in the cave still needs to be completed. Measurements were made in the main conduit to the bottom and in horizontal passages. It is expected to work further below the horizon -500. Paper presents preliminary interpretation of the data obtained so far. However, the main feature of this study is the Wazeliniarzy Shaft which is included in the research.

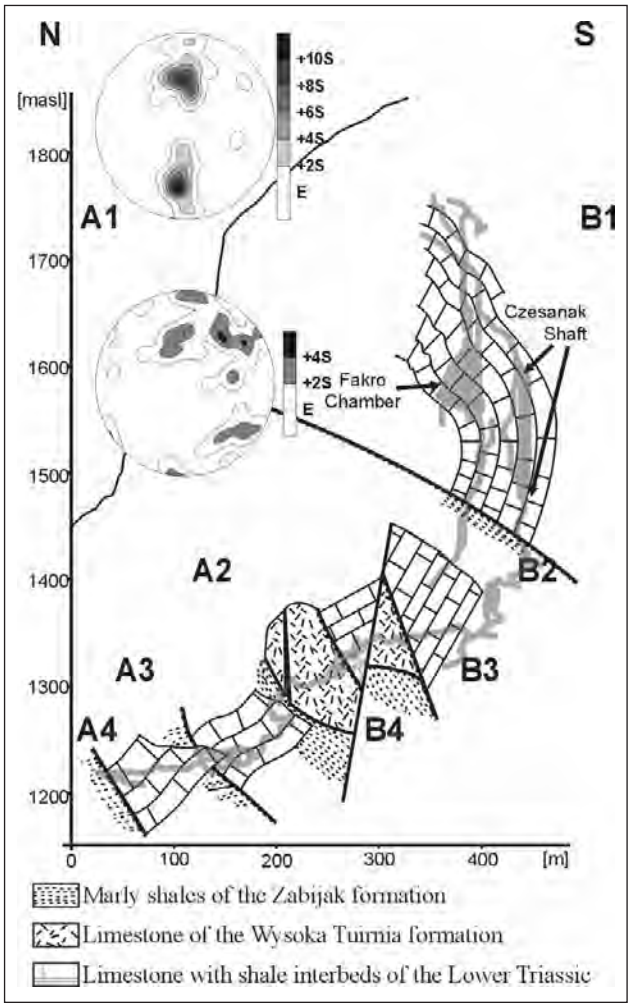

Figure 4. Geological cross-section of the Mała w Mułowej Cave; upper contour diagram is projection of stratification in the cave, lower is showing fracture; line of the cross-section on the Figure 1B; rest of the legend at the Figure 2.

Bac-Moszaszwili and Nowicki (2006) presented that the Śnieżna Studnia cave, to 1,350 m a.s.l., developed into a inverted series of Triassic and Jurassic rocks, doubled by a fault. The vertical part of the cave, included the Wazeliniarzy Shaft, developed in the limestone of the Raptawicka Turnia Formation belonging to Ździary Unit. The horizontal passages at the depth of -500 are developed along the Organy Fault and parts under -500 m are developed in the Triassic rocks of the Organy Unit. However, this cross-section was set too far to the west.

The fieldwork shows that the layers are inverted. In the cave entrance the Middle Triassic limestone are inclined at an angle of 35° toward the SE. At a depth of 60 m there is the boundary with Bajocian limestones, a few meters below the contact with the limestone of Raptawicka Turnia Formation. At a depth of 150 m the fault is observed, most likely the Organy Fault. Fault plane inclined 40° toward S. Limestone interbeded by greenish shales was found, which probably are the Lower Triassic. Just below the cave is developed in banding Middle Triassic limestone inclined 50° southward (Fig.5). From a depth of 200 m the cave is developed in the fault zone. Fault plane is initiated at bedding planes. Dip of fault plane increases from 55° to 75° to the S and SSE up to a depth of 270 m. Dislocation has been identified in the cave from the western to the eastern limits. The fault plane is mineralized and tectogliphs indicate normal dextral movement. This fault was rejuvenated in the recent past because it dislocated the passages, dip separation is equal to 22 cm. Apart the main dislocation, discontinuities in the cave in the upper part especially can be seen, where stratification is not too steep, the cave is formed rather along the cracks. Dominant fractures are NE–SW, NW–SE, WNW–ESE mainly by steep and very steep planes (Fig. 5).

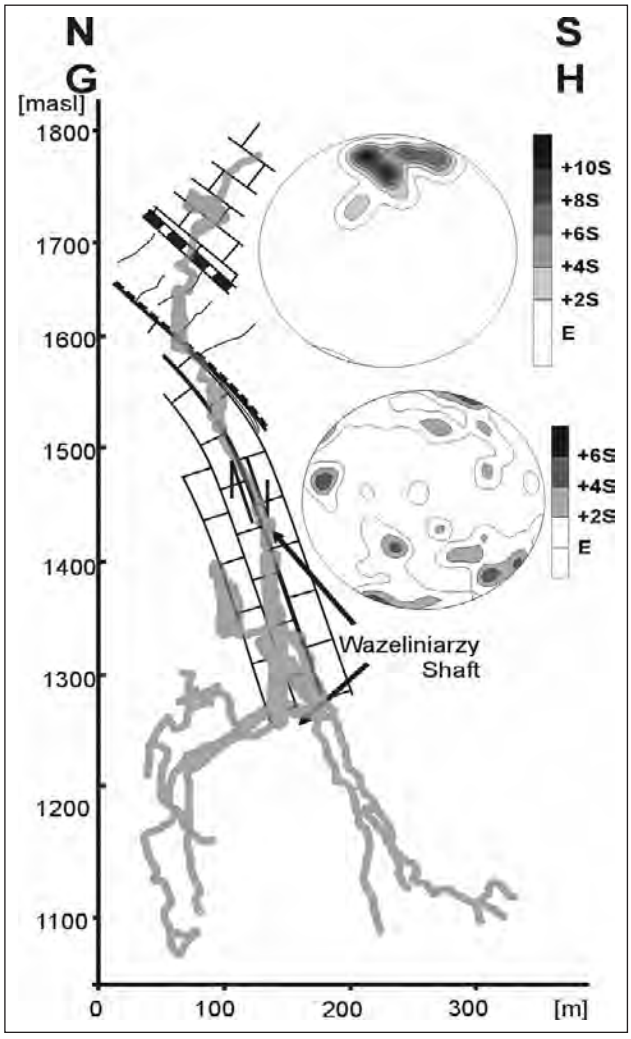

Figure 5. Geological cross-section of the Śnieżna Studnia Cave; upper contour diagram is projection of stratification in the cave, lower is showing fracture; line of the cross-section on the Figure 1B; legend at the Figures 2 and 4.

5. Relations between large shafts and chambers and main folds

Large volume features in the Ptasia Studnia System are presented at the depth of -100 to -160 especially. From Dante Chamber to the West to the chamber with Wielki Kłamca Lake to the East. The whole zone has cracked character. In the above-mentioned interval hinge zone of the Organy Syncline is located. Breakdown parts (bottom of the Dante Chamber, the Chamber Under Colossal Boulder, the Shaft with the Pirates Bridge). The Wielki Kłamca Lake covers the entire surface of the hall so it is hard to assess clearly the nature of the chamber bottom. However, the irregular shape of the plan of the hall and observations from the walls show a significant impact of the tectonics on chamber development. Cave parts between the Dante Chamber to the Chamber Under Colossal Boulder are probably partly conditioned by discontinuity 210/50, which direction correlates with the direction of the cave and a prominent fault visible at the roof of the Chamber Under Colossal Boulder.

Below the depth of 254 m in the Kozia Cave the cave changes the nature from meander to aven, which correlates with increasing dip of layers. Caves along their whole length allude strongly to stratification, regardless of the type of passages (vadose or tectonic). Water penetrating the Kozia Cave used the conjugation of stratification and fractures. The bedding plane is influencing on inclination of passage, joints and shears on their direction. However, conduit from -245 m to the bottom (-389) is developed on the steep and vertical stratification, the fractures receded into the background. In this lower part the stratification determines not only inclination but also direction of passages. Fieldwork confirms the geological interpretation of Bac-Moszaszwili and Nowicki (2006). Thus it can be concluded that the increasingly steep layers are associated with the main syncline of the Ździary, and its open interlimb angle is the result of the cave course in the outer part of the concentric fold.

In the Mała w Mułowej Cave the large volume parts, as the Fakro Chamber and the Czesanka Shaft, are located at the altitude interval of 1,650–1,470 m, where hinge zone of the Ździary Syncline is located. The Fakro Chamber is developed in the N part closer to the core of the fold. This chamber is a breakdown type. Above the hall and on the walls minor folds are very visible, some of which are dislocated. The Czesanka Shaft is located in southern outer part of syncline. The shaft is developed at very steep and vertical bedding plan. Both forms have a latitudinal extent, referring to the strike of layers.

The deepest shaft in the Tatra Mts. – the Wazeliniarzy shaft, which is 200 m deep, is located in the Śnieżna Studnia Cave. Comparably to the Kozia Cave, it is associated with increasingly steep layers, which in this case were also moved relative to each other. Similarly as in the Kozia Cave gentle change of dip is likely due to the location of the cave in the outer zone of the fold. The direction of surface displacement of stratification are consistent with flexural slip (Fig. 6).

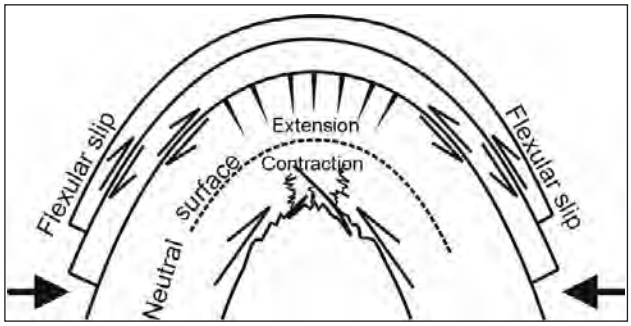

Figure 6. Schematic of a minor deformations in major fold (based on Ramsey and Huber 1987, changed).

All of these forms are located within the hinge zones. During folding sub-structures were formed in the manner that could have a major impact on the relationship discussed. Within the complex of folding rocks the highest compression zone and the local zone of extension can be distinguish. This zone is located closer to the core of the fold. Local zone of extension is located in the outer zone (Fig. 6). Zones are separated by a neautral surface (Ramsey and Huber 1987). In the contraction zone were developed faults and minor folds. In the extension zone were formed fractures perpendicular to strata. Flexural slip is a common phenomenon during folding (Ramsey and Huber 1987; Fig. 6). It seems that in the case discussed above, in thin limestone layer, all types of movement relative to one to another is an easy way to discharge stress rocks through the use of existing surfaces.

6. Conclusions

Presented folds are gently inclined or moderatly of an axial surface and interlimb angles are open or wight. The Organy Syncline in which the Ptasia Studnia System has evolved have chevron geometries and regardless of distance from the core, inclined of individual packages of rocks do not change. While the Ździary Syncline has concentric geometries where closer to the core dip of layers is changing rapidly, it is a significant number of folds associated by minor faults and high density fractures. In the outer zone, layer on a very long stretch are very steeply and continuous of layers is interrupted by extensions fractures. The conducive role of hinge zone to the development of karst forms has been described by Tognini and Bini (2001). However, theirs research discussed the standing folds conditions where the cave galleries formed in extension zones and neutral surface is something of a barrier to karst processes. The geological situation of the Czerwone Wierchy Unit leads to the conclusion that the whole hinge zone will favour development of large chambers and deep shafts.

Large chambers are formed in hinge zones of chevron folds and in the hinge zones closer to the core of concentric folds. Relatively large concentration of deformations in small vertical distance induces development of forms of similar horizontal and vertical dimensions. Chambers are characterized by brakdown feature. The extent of rooms is linked to the strike of layers and faults which are perpendicular to bedding.

Deep shafts are developed at the outer part of the concentric folds. Shafts are based on long, very steep stratification surface which are loosen and dislocated each other by flexular slip.

Acknowledgments

Studies in caves would not be possible without permission of the authority of the Tatra National Park. The research has been funded by “Grant for young scientist” at the Faculty of Earth Sciences, University of Silesia.

References

Antkiewicz A, Lorczyk M. 2010. Jaskinia Mała w Mułowej. Portal CBDG http://geoportal.pgi.gov.pl/jaskinie-pub/jaskinie (in Polish).

Bac-Moszaszwili M, Jaroszewski W, Passendorfer E, 1984. On the tectonics of Czerwone Wierchy and Giewont area in the Tatra Mts. (Poland). Annales Societatis Geologorum Poloniae, 52(1/4), 67–88 (in Polish).

Bac-Moszaszwili M, Nowicki T, 2006. Remarks on caves development in the Czerwone Wierchy Nappe in the Tatra Mts.. Przegląd geologiczny, 54(1), 56–60 (in Polish).

Fuja D, Filar F, Albrzykowski G, 2010. Jaskinia Śnieżna Studnia. Portal CBDG, http://geoportal.pgi.gov.pl/jaskinie-pub/jaskinie (in Polish).

Goldscheider N. 2005. Fold structure and underground drainage pattern in the alpine karst system Hochifen-Gottesacker. Eclogae Geologicae Helvetiae, 98, 1–17.

Gradziński M, Hercman H, Kicińska D, Barczyk G, Bella P, Holúbek P, 2009. Karst in the Tatra Mountains—developments of knowledge in the last thirty years. Przegląd Geologiczny, 57(8), 674–684 (in Polish).

Grodzicki J, 1970. Rola tektoniki w genezie jaskiń masywu Czerwonych Wierchów. Speologia, 5, 33–48 (in Polish).

Grodzicki J,1978. Nowe elementy strukturalne jednostki Organów między Doliną Kościeliską i Doliną Miętusią. Kras i Speleologia, 2, 77–81 (in Polish).

Grodzicki J, 2008. Remarks on caves development in the Czerwone Wierchy Nappe in the Tatra Mts.-how to fabrykowac fakty by potwierdzić własna teorie. Proc. of 42. Speleological Symp. Tarnowskie Góry, Poland, 57–60.

Grodzicki J, Kardaś R 1989. Tectonics of the Czerwone Wierchy (Massif Tatra Mts.) in the light on observations in caves. Annales Societatis Geologorum Poloniae, 59, 275–293.

Häuselmann P, Jeannin PY, Bitterli T, 1999 Reltionships between karst and tectonics: case-study of the cave system North of Lake Tun (Bern, Switzerland). Geodinamica Acta, 12(6), 377–387.

Jurewicz E, 2005. Geodynamic evolution of the Tatra Mts. and the Pieniny Klippen Belt (Western Carpathians): problems and comments. Acta Geologica Polonica, 55, 295–338.

Klimchouk A, Ford D, 2000. Lithologic and structural controls of dissolutional cave development. In: AB Klimchouk, DC Ford, AN Palmer, W Dreybrodt (Eds.). Speleogenesis. Evolution of Karst Aquifers. National Speleological Society, Huntsville, Alabama, 54–64.

Kotański Z, 1963. Nowe elementy budowy masywu Czerwonych Wierchów. Acta Geologica Polonica, 13, 149–181 (in Polish).

Lefeld J, Gaździcki A, Iwanow A, Krajewski K, Wójcik K, 1985. Jurassic and Cretaceous lithostratigraphic units of the Tatra Mountains. Studia Geologica Polonica, 84, 1–93.

Lorczyk M. 2010. Ptasia Studnia-Jaskinia Lodowa Litworowa-Jaskinia Nad Dachem. Portal CBDG; http://geoportal.pgi.gov.pl/jaskinie-pub/jaskinie (in Polish).

Piotrowska K, Cymerman Z, Rączkowski W, 2009. Detailed geological map of the Tatra Mts. in scale 1:10,000 – sheet Czerwone. National Geological Institut-Polish Reserch Institut. Warszawa.

Ramsay JG, Huber MI, 1987. The technigues of modern structural geology. Vol. 2:Folds and Fractures. Academic Press. London.

Tognini P, Bini A, 2001. Efects of structural setting endokarst system geometry in the Valle del Nose (Como Lake, Northern Italy). Geologica Belgica, 4(3/4), 197–211.

Wiśniewski WW, Kotarba S, 2010. Jaskinia Kozia. Portal CBDG, http://geoportal.pgi.gov.pl/jaskinie-pub/jaskinie (in Polish).

HYPOGENIC CAVES OF SICILY (SOUTHERN ITALY)

Marco Vattano[1], Philippe Audra[2], Fabrizio Benvenuto[3], Jean-Yves Bigot[4], Jo De Waele[3], Ermanno Galli[5], Giuliana Madonia[1], Jean-Claude Nobécourt[6]

[1]Department of Earth and Sea Sciences, University of Palermo, Via Archirafi 22, 90123 Palermo, Italy, marco.vattano@unipa.it, giuliana.madonia@unipa.it

[2]Polytech'Nice-Sophia, Engineering School of Nice – Sophia Antipolis University, & I'CiTy (IMREDD), 930 route des Colles, 06903 Sophia-Antipolis, France, audra@unice.fr

[3]Department of Biological, Geological and Environmental Sciences, Bologna University, Via Zamboni 67, 40126 Bologna, Italy, fabrizio.benvenuto2@studio.unibo.it; jo.dewaele@unibo.it

[4]Association Française de Karstologie (AFK), 21 rue des Hospices, 34090 Montpellier, France, catherine.arnoux@club-internet.fr

[5]Department of Earth Sciences, University of Modena and Reggio Emilia, Largo S. Eufemia 19, 41121 Modena, Italy, gallier@unimore.it

[6]CRESPE, Le Hameau de l'Ara, 259 Bd Reine Jeanne, 06140 Vence, France, jcnobecourt@free.fr

First results of a study on hypogenic caves in Sicily are presented. Inactive water-table sulphuric acid caves and 3D maze caves linked to rising of thermal waters rich in H_2S were recognized. Cave patterns are guided by structural planes, medium and small scale morphological features are due mainly to condensation-corrosion processes. Calcite and gypsum represent the most common cave minerals. Different types of phosphates linked to the presence of large bat guano deposits were analyzed.

1. Introduction

Hypogenic caves are recognised as generated by water recharging from below independently of seepage from the overlying or immediately adjacent surface. Waters are often thermal and/or enriched in dissolved gases, the most common are CO_2 and H_2S. Hypogenic caves can be thermal caves, sulphuric acid caves, and basal injection caves. They differ from epigenic caves in many ways, such as: speleogenetic mechanisms, morphological features, chemical deposits, and lack of alluvial sediments (Klimchouk 2007; Klimchouk and Ford 2009; Palmer 2011). Several studies were conducted to evaluate the hypogenic origin of a large number of caves (Klimchouk and Ford 2009; Stafford et al. 2009; Audra et al. 2010; Plan et al. 2012; Tisato et al. 2012). A significant contribution was given by the work of Klimchouk (2007) that systematically provided instruments and models to better understand and well define the hypogenic karst processes and landforms.

Studies on hypogenic caves in Italy were carried out since the 90s in different karst systems, especially in the central and southern Appenines. These studies mainly concerned chemical deposits related to sulphuric ascending water and micro-biological action (Galdenzi and Menichetti 1995; Galdenzi 1997; Piccini 2000; Galdenzi and Maruoka 2003; Forti and Mocchiutti 2004; Galdenzi 2012; Tisato et al. 2012).

This paper aims to describe preliminary the first results of a study conducted in some hypogenic caves in Sicily, highlighting their main features such as pattern, morphology, mineralogy and speleogenesis. These are Monte Inici karst system and Acqua Fitusa Cave. For this purpose topographic and geomorphological surveys were carried out, and about 40 samples of cave minerals were taken in different parts of the caves. In addition, a brief description of Monte Kronio karst system is given. It represents one of the most important hypogenic karst systems of Sicily, characterized by flows of hot air and vapor rising from below.

2. Karst in Sicily

Karst in Sicily is widespread and exhibits a great variety of surface and underground landforms related to the wide distribution of soluble rocks (Di Maggio et al. 2012). About 20% (more than 6,000 km^2) of the land area consists of carbonates and evaporites, primarily gypsum (Fig. 1). Carbonate karst lies mainly in the northwestern and central sectors of the Apennine chain and the foreland area in southeastern Sicily; gypsum karst occurs chiefly in the central and southern areas of the island, though evaporite landscapes are also present in the northern and western parts of Sicily.

Carbonate and gypsum karst systems develop under unconfined conditions and in most cases constitute epigenetic systems fed by meteoric waters. Hypogene caves are located only in carbonate rocks and are linked to the presence of deep thermal waters.

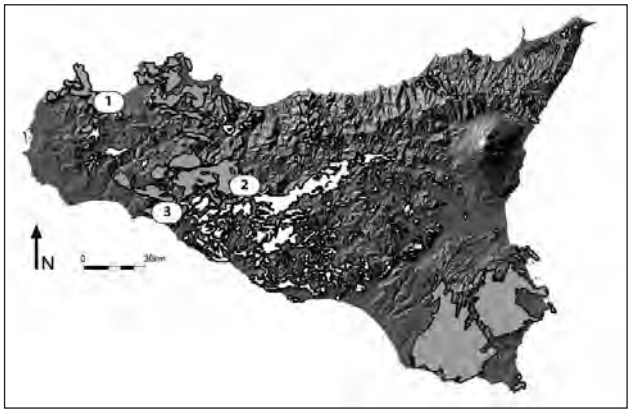

Figure 1. Gypsum (white) and carbonate karst areas (grey) and localization of investigated hypogenic karst systems. 1. Monte Inici; 2. Acqua Fitusa. 3. Monte Kronio.

3. Hypogenic caves

3.1. Acqua Fitusa Cave

Acqua Fitusa Cave opens in the eastern section of the Sicani Mounts (west-central Sicily), along the north-eastern fault scarp of a N-S anticline, westward vergent, forming the Mt. La Montagnola (Fig. 1). The cave formed in the Upper Cretaceous Rudist breccias member of the Crisanti Fm., composed of conglomerates and reworked calcarenites with rudist fragments and benthic foraminifera (Catalano et al. 2011).

At present it is inactive with a thermal spring occurring 300 m north and 30 m below the cave. The waters have a temperature of about 25 °C, and are indicated as chlorine-sulphate alkaline (Grassa et al. 2006 and references therein). During the spring-summer-early autumn the cavity hosts a large colony of bats, including *Myotis myotis* and *Miniopterus schreibersii* species (Mucedda pers. comm.), that produce significant amounts of guano.

The first explorations of Acqua Fitusa were carried out in the early XXth century by some inhabitants of the neighboring villages, but the first human frequentations of the cavity have to go back to the Paleolithic and Chalcolithic periods, as evidenced by the discovery of numerous lithic fragments, remains of food and burials (Bianchini and Gambassini 1973). Lombardo et al. in 2007 gave a description of the cave and some studies concerned the hydrogeochemistry and isotopic composition of the nearby spring waters (Grassa et al. 2006 and references therein).

According to the survey made in 2011, the cave consists in at least three stories of subhorizontal conduits, displaying a total length of 700 m, and a vertical range of 25 m (Fig. 2). The main passages are generally low and narrow and follow sets of joints oriented in ENE-WSW, E-W and N-S directions. Very small passages develop from these galleries making incipient mazes.

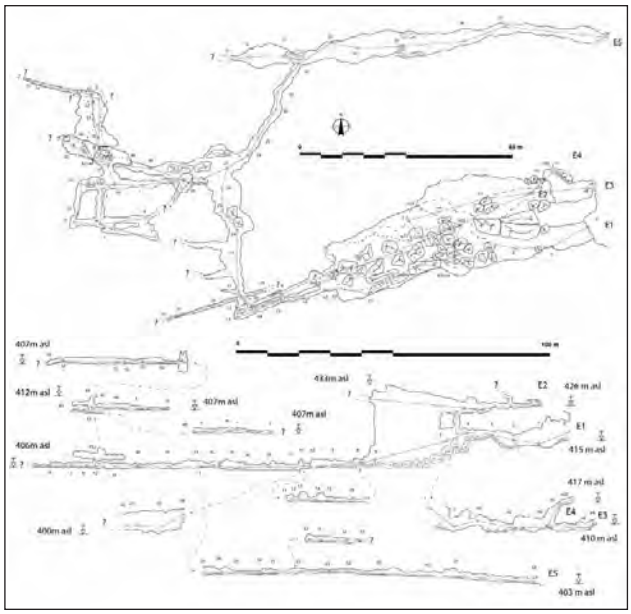

Figure 2. Acqua Fitusa Cave: plan view and extended profile (Survey: Ceresia, Inzerillo, Provenzano, Sausa, Scrima and Vattano, 2011).

The conduits breach the fault scarp in more points at different heights. The main entrance leads to a large chamber enlarged both by corrosion and breakdown processes, connected to an upper subhorizontal passage that likely formed during a past higher karst base level.

Acqua Fitusa Cave represents a clear example of inactive water table sulphuric acid cave (Audra et al. 2009). Despite the small size, the cave is very interesting for the abundance and variety of morphologies and deposits formed at and above the water table where H_2S degassing and thermal convection produced strong condensation-corrosion processes.

The floor of some passages is breached for several meters by an inactive thermo-sulphuric discharge slot that can reach a depth of 7 m (Fig. 3). In some sections of the caves, notches with flat roof, linked to lateral corrosion of a water table with concentrated sulphuric acid, carve the walls at different heights, recording past stages of base-level change.

Several forms of small and large sizes, generated by condensation-corrosion processes above the water table, can be observed along the ceiling and walls. Ceiling cupolas and large wall convection niches occur in the largest rooms of the cave. Here and in the upper gallery, pendants at junctions of more cupolas or between braided channels are widespread. Cave walls of many passages are carved at different heights by deep wall convection niches that in places form notches (Fig. 3). Condensation-corrosion channels similar to ceiling-half tubes carve the roof of some passages; replacements pockets due to corrosion-substitution processes are widespread; boxwork created by differential condensation-corrosion were observed in the upper parts of the conduits.

Figure 3. Acqua Fitusa. Passage with discharge slot at the floor and different levels of wall convection niches.

The most abundant cave mineral is gypsum which displays different shapes and colours. Replacement gypsum crusts are common in many passages; the gypsum is located in large vertical fissures along the walls, it can partially cover wall convection notches, or replacement pockets. A gypsum body of about 50 cm of thickness was found on the floor of the biggest room in correspondence of which small ceiling cupolas and pendants are associated on the roof. Centimeter-sized euhedral gypsum crystals grew inside mud sediments. Finally, the walls of a feeding fissure are covered with a network of gypsum “roots” in which the

biological control is obvious. Further investigation on these apparently subaqueous gypsum speleothems is still ongoing.

Phosphate minerals, such as apatite [$Ca_5(PO_4)_3(OH)$], were found in the form of thin crusts near large deposits of bat guano.

3.2. Monte Inici Complex

Monte Inici karst system is situated in northwestern Sicily (Fig. 1), in the eastern sector of the Trapani Mountains, and opens along the southeastern slope of Mt. Inici, a gently westward – dipping monoclinal relief affected by NW-SE, NE-SW and NNW-SSE high angle faults. The karst system is composed of two caves, Grotta dell'Eremita (or Grotta del Cavallo) and Abisso dei Cocci, formed in Jurassic limestones and dolomitic limestones. Thermal waters emerge from three hot springs east and at lower altitude respect to the caves (Fig. 4). These are of chloride-sulphate alkaline-earth type and have a temperature respectively of 48.3 °C (Gorga 1), 49.6 °C (Gorga 2), and 44.2 °C (Terme Segestane) (Grassa et al. 2006 and references therein).

The caves preserve clear signs of prehistoric and medieval human presence, such as several lithic and bone fragments, food remains, ceramic finds typical of the Middle Neolithic-Middle Chalcolithic (Grotta dell'Eremita), and large amounts of medieval pottery (XIth–XVth century), identified mainly within Abisso dei Cocci (Tusa 2004). These caves were explored and described in the early 90s. On the basis of morphological features a genesis linked to thermal waters was supposed (Biancone 1993; Messana 1994).

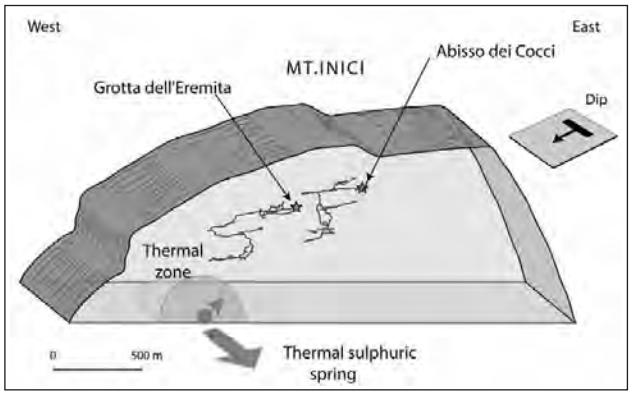

Figure 4. Sketch of Monte Inici karst system and localization of the thermal zone.

3.2.1. Abisso dei Cocci

Abisso dei Cocci is an inactive 3D maze cave formed in Lower Jurassic limestones and dolomitic limestones (Inici Fm.), arranged in decimetric westward dipping beds. The cave is one of the largest of Sicily, reaching a total length of over 2,053 m and a vertical range of -300/+61m. It consists of several stories of large subhorizontal galleries and chambers connected by deep shafts. In plan view the galleries are mainly oriented in NW-SE and NE-SW direction, parallel with the main tectonic discontinuity lines. Some conduits are gently inclined and follow the dip of bedding planes, whereas the shafts develop along vertical fissures or fault planes. Passages display sub-circular cross-sections, sometimes with vadose entrenchments (Fig. 5).

Several features linked to rising thermal water and air flow were recognized in many sections of the cave. Many passages are characterized by large convection wall niches, mega-scallops, ceiling cupolas, and ceiling spheres. In some cases adjacent passages are separated by partitions (Fig. 5).

The cave lacks alluvial sediments; on the other hand chemical deposits are abundant mainly in the middle level of the cave, where dripping is still active. Here, a large variety of calcite speleothems, such as stalactites, stalagmites, flowstones, shelfstones, etc., occur. Calcite is present also in the shape of powder, thin crusts, and frostwork. Gypsum was recognized in the middle and deepest sections of the cave in the form of tabular or acicular colourless small crystals (Fig. 5).

Figure 5. Abisso dei Cocci. Passages displaying sub-circular cross-section with vadose entrenchment characterised by uncovered ceiling and walls with cupolas and gypsum in the lower parts.

Different types of phosphate minerals were found in several parts of the caves. Hydroxylapatite occurs as thin crusts or powder above the bedrock, and even forms true stalactites. Crandallite [$CaAl_3(PO_4)_2(OH)_5 \cdot H_2O$] is present as soft white grains at the contact between weathered rock and bat guano, in association with green small spherical masses of montgomeryite [$Ca_4MgAl_4(PO_4)_6(OH)_4 \cdot 12H_2O$]. Phosphates are linked to the presence of large fossil bat guano deposits occurring in many parts of the cave.

3.2.2. Grotta dell'Eremita

Grotta dell'Eremita formed in Middle-Upper Jurassic reddish-gray limestones with ammonites (Buccheri Fm.), and in Lower Jurassic limestones and dolomitic limestones (Inici Fm.) in its deepest parts. The cave is a relict 3D maze cave, which reaches a total length of 2880 m, and a vertical range of -306 m. The air temperature, measured in

December 2011, was 17.6 °C in the passages near the entrance area, gradually increasing up to 21.0 °C in deepest chamber of the cave.

Grotta dell'Eremita shows many morphological and depositional features similar to Abisso dei Cocci, although some differences were recognized. The cave is made up of large subhorizontal passages and big chambers connected by deep shafts, which are guided by the main tectonic discontinuity planes. Some galleries are gently inclined following the dip of bedding planes and display sub-circular cross-sections. Along the walls of these passages, in correspondence of the bedding planes, several small conduits filled by well-cemented fine reddish sediment of continental nature, are visible. Large convection niches, mega-scallops, ceiling cupolas, ceiling spheres, and drip holes are widespread in the chambers and in the largest passages of the cavity (Fig. 6).

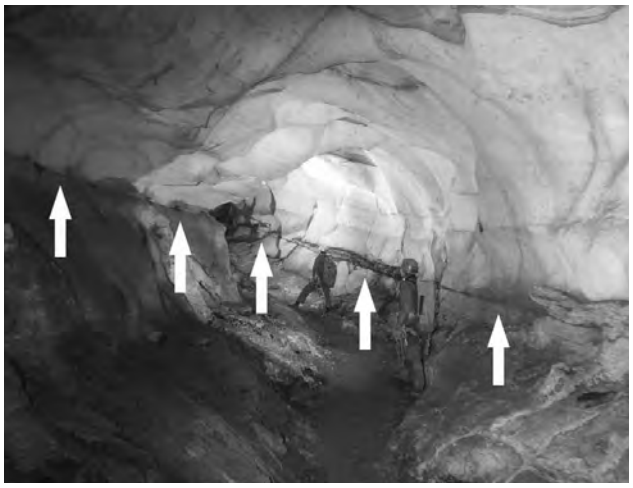

Figure 6. Grotta dell'Eremita. Passage along a bedding plane where filled protoconduits are visible. Walls and ceiling are characterised by large convection niches and cupolas.

A breccia consisting of decimetric carbonatic clasts in a reddish silt matrix characterized by thin laminas and decantation structures is exposed at walls and ceiling of some deep passages.

Different chemical deposits were identified: besides calcite, occurring in the form of white cigar-shaped crystals grown under old bat guano, reddish laminae, or coralloids, gypsum was found as tabular or fibrous crystals. Phosphate minerals, such as hydroxylapatite and taranakite, occur mainly in form of powders or crusts near or above deposits of bat guano. Carbonate-apatite was recognised as crusts or small stalagmites (Messana 1994). As in Abisso dei Cocci clastic sediments are absent.

3.3. Monte Kronio karst system

Monte Kronio karst system opens in the southern scarp of Mt. Kronio or Mt. San Calogero, north-east of Sciacca town (southern Sicily) (Fig. 1). Mt. Kronio consists of an imbricate fan system linked to ENE-striking, closely spaced imbricate thrust sheets, involving Triassic to Miocene platform and pelagic platform carbonate deposits (Monaco et al. 1996). The karst system is made up of a series of cavities characterized by rising of hot air and vapour flow at temperature of about 38 °C, connected to the presence of thermal waters. These waters, emerging along the southern slope of Mt. Kronio at lower altitude respect to the cave entrances, are of chloride-sulphate alkaline type and have a temperature ranging between 32 and 55 °C (Grassa et al. 2006 and references therein; Capaccioni et al. 2011). Actually they are used for aesthetic and therapeutic purposes.

The caves were visited by man since the end of the Mesolithic for residential use, place of worship, necropolis, and from the Ist century BC for thermal purposes. The first attempts to explore the caves date back to the end of the XVIIth century; since the 40s several exploration campaigns conducted by the Commission Grotte "E. Boegan" of Trieste identified and surveyed the cave system nowadays known. The explorations, carried out with great difficulty, due to the critical environmental conditions with temperatures of about 38 °C and humidity of 100 %, have allowed the discovery of an extended maze cave system about 200 m deep (Perotti 1994).

The system is composed of more cavities, located at different altitude, characterized by subhorizontal passages connected by deep shafts or steep passages, but there is not always a passable connection between the several branches of the caves. Some galleries breach the southern scarp of Mt. Kronio through small openings some of which emit hot air, other ones aspire cold air from outside (Perotti 1994).

The upper section of the system, known also as Stufe di San Calogero, consists of a series of chambers separated by man-made walls, connected to a maze of narrow passages. Some chambers are characterized by hot vapour flow rising from a deep shaft which connects these passages with two large hot galleries, oriented in NW-SE direction, where abundant archeological finds were discovered. A small cave (Grotta del Lebbroso), interested by rising of hot vapour flow, develops eastward at the same altitude, but to date no passable connection to the rest of the system was recognized. The deepest part of the cave is represented by a large and deep shaft (Pozzo Trieste), from which more levels of narrow passages, both hot and cold, develop breaching the southern cliff of Mt. Kronio (Fig. 7). A large breakdown deposit occurs at the bottom of the shaft.

Walls and ceiling of the caves are weathered and important gypsum deposits, in form of powders or crusts, were observed (Perotti 1994).

Figure 7. Monte Kronio. Forms linked to condensation-corrosion (on the right); weathered flat roof affected by condensation (on the left).

4. Discussion and Conclusions

The study of the geological setting, cave pattern, medium and small scale morphological features, and the analysis of cave minerals allowed defining a hypogenic genesis for the investigated karst systems. All the caves developed along structural planes, such as bedding, fracture or fault planes, whose enlargement is due to corrosion by H_2S-rich thermal waters, and to condensation-corrosion processes by air flow in the cave atmosphere.

Acqua Fitusa cave is an inactive water-table sulphuric acid cave linked to corrosion processes of carbonate rock with replacement of gypsum by H_2S-rich thermal water (Fig. 8). Occurrence of notches with flat roof indicates lateral corrosion processes by sulphuric thermal water fed through discharge slots still open on the floor of some passages. Ceiling cupolas, large wall convection niches, condensation-corrosion channels, boxwork testify that enlargement of voids occurred mainly above the water table where H_2S degassing in the cave atmosphere, oxidation of sulphides and thermal convection produced strong condensation-corrosion processes. In addition, large amounts of gypsum, replacement pockets, in places containing gypsum, suggest the corrosion of the carbonate rock occurred with replacement of gypsum according to the sulphuric acid speleogenesis (Galdenzi and Maruoka 2003; Audra et al. 2010 and references therein). Like other sulphuric acid systems (Galdenzi and Menichetti 1995) the different levels of passages record past stages of the water table, in relation to changes of the base-level.

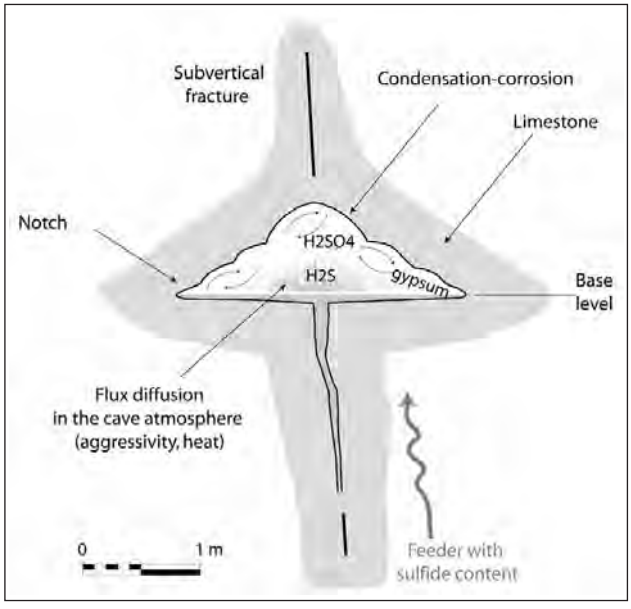

Figure 8. Acqua Fitusa. Genetic mechanism of cave passages due to H_2S degassing in the cave atmosphere.

Grotta dell'Eremita and Abisso dei Cocci caves were identified as inactive 3D maze caves. Pattern and cross sections of the main passages of Abisso dei Cocci suggest the early speleogenetic phases to have occurred in phreatic conditions by rising thermal water which formed a well developed 3D maze system. An important role in the evolution and widening of the subterranean voids was played by air flow when the cave passages switched from phreatic to vadose conditions, as a consequence of the uplift phases of this sector of the Sicilian chain. In this case, the processes of corrosion by condensation from air flow rich in H_2S, favoured on one hand the enlargement of the early voids with the formation of large megascallops and ceiling cupolas, on the other hand the deposition of gypsum in the lower parts of the passages (Fig. 9).

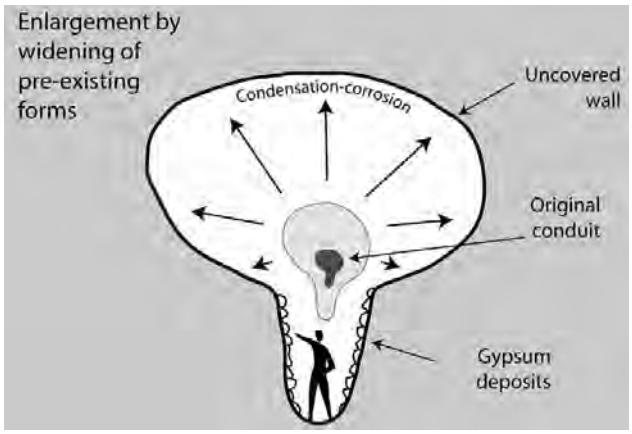

Figure 9. Abisso dei Cocci. Enlargement of passages by widening of pre-existing forms due to condensation-corrosion.

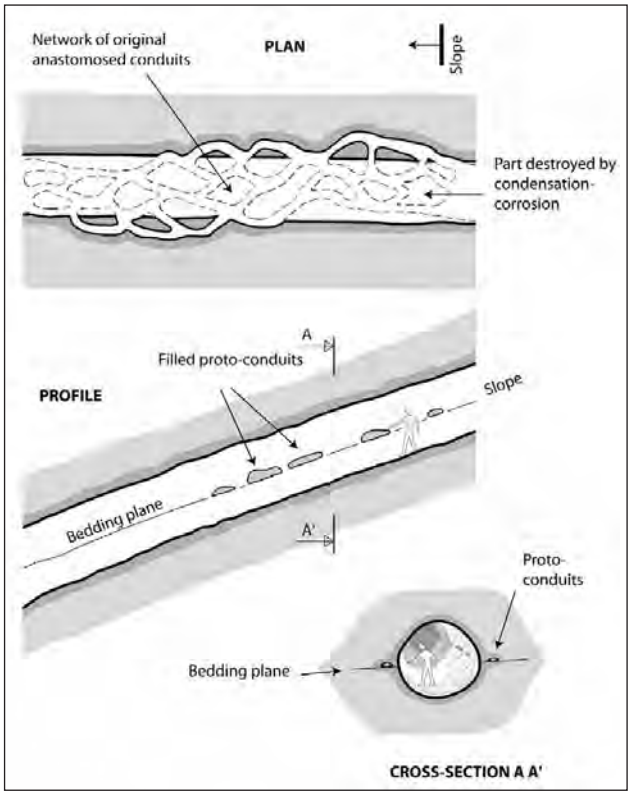

Figure 10. Grotta dell'Eremita. Genesis of passages along a bedding plane with formation of protoconduits enlarged by condensation-corrosion.

The first speleogenetic phases in phreatic conditions of Grotta dell'Eremita are recorded, beside the pattern, by the presence of several filled anastomosed protoconduits visible at the bedding plane, along which the passages develop. The next phase of evolution of the system may have followed two possible ways: a) enlargement of voids by condensation-corrosion processes which destroyed the network of protoconduits and formed the main passages as testified by the presence of megascallops, ceiling cupolas, etc. (Fig. 10); b) corrosion processes by a deep sulphuric thermal water enlarging the early voids, destroying the protoconduits and forming the main passages in phreatic

conditions. Successively, condensation-corrosion processes by acid sulphuric air flow enlarged the early phreatic voids with the formation of megascallops, ceiling cupolas etc., and deposition of gypsum. The question is open, future studies will clarify the issue.

Finally, in all the investigated caves the presence of different types of phosphate minerals is linked to the large deposits of bat guano (Hill and Forti 1997).

Monte Kronio system is an active hypogenic karst system and is unique in Sicily and probably in the world. It owes its peculiarity to the rising of hot air and vapour flow, linked to a deep thermal aquifer, still not identified within the system. Although this system is known since prehistoric times, yet little is known about its real development and speleogenetic mechanisms due to the harsh environmental conditions that make exploration extremely difficult. Multidisplinary studies are currently in progress.

Acknowledgements

G. Ceresia, S. Inzerillo, A. Provenzano, L. Sausa, A. Scrima contributed to resurvey Acqua Fitusa cave. G. Ceresia, A. Provenzano, P. Tordjman and G. Valdese helped sampling. Mr. Mancuso helped visiting to Monte Inici karst system. Commissione E. Boegan and La Venta for facilitating the field activities in the Monte Kronio caves. Michal Philippi and Jiří Bruthans for the review of this paper.

References

Audra P, D'Antoni-Nobecourt J-C, Bigot J-Y, 2010. Hypogenic caves in France. Speleogenesis and morphology of the cave systems. Bulletin de la Société Géologique de France, 181 (4), 327–335.

Audra P, Mocochain L, Bigot J-Y, Nobécourt J-C, 2009. The pattern of hypogenic caves. Proceedings of the 15th International Congress of Speleology, Kerrville (TX), 2, 795–800.

Bianchini G, Gambassini P, 1973. Le Grotte dell'Acqua Fitusa (Agrigento) I – Gli scavi e l'industria litica. Rivista di Scienze Preistoriche, 28 (1), 1–55.

Biancone V, 1993. Monte Inici. Una sorpresa tutta siciliana! Speleologia, 29, 72–77.

Capaccioni B, Vaselli O, Tassi F, Santo AP, Huertas AD, 2011. Hydrogeochemistry of the thermal waters from the Sciacca Geothermal Field (Sicily, southern Italy). Journal of Hydrology, 396, 292–301.

Catalano R, Agate M, Avellone G, Basilone L, Gasparo Morticelli M, Gugliotta C, Sulli A, Valenti V, Gibilaro C, Pierini S, 2011. Walking along a crustal profile across the Sicily Fold and Thrust Belt. AAPG International Conference & Exhibition, Post conference field trip 4, 27–29 October 2011.

Di Maggio C, Madonia G, Parise M, Vattano M, 2012. Karst in Sicily and its conservation. Journal of Cave and Karst Studies, 74(2), 157–172.

Forti P, Mocchiutti A, 2004. Le condizioni ambientali che permettono l'evoluzione di speleotemi di zolfo in cavità ipogeniche: nuovi dati dalle grotte di Capo Palinuro (Salerno, Italia). Le Grotte d'Italia, 4 (5), 39–48.

Galdenzi S, 1997. Initial geological observations in caves bordering the Sibari plain (southern Italy). Journal of Cave and Karst Studies, 59 (2), 81–86.

Galdenzi S, 2012. Corrosion of limestone tablets in sulfidic ground-water: measurements and speleogenetic implications. International Journal of Speleology, 41 (2), 149–159.

Galdenzi S, Maruoka T, 2003. Gypsum deposits in the Frasassi Caves, central Italy. Journal of Cave and Karst Studies, 65, 111–125.

Galdenzi S, Menichetti M, 1995. Occurrence of hypogenic caves in a karst region: examples from central Italy. Environmental Geology, 26, 39–47.

Grassa F, Capasso G, Favara R, Inguaggiato S, 2006. Chemical and isotopic composition of waters and dissolved gases in some thermal springs of Sicily and adjacent volcanic islands, Italy. Pure and applied geophysics, 163, 781–807.

Hill C, Forti P, 1997. Cave mineral of the world. National Speleological Society, Huntsville, 463.

Klimchouk AB, 2007. Hypogene Speleogenesis: hydrogeological and morphogenetic perspective. National Cave and Karst Research Institute, Special Papers, 1, Carlsbad, NM, 106.

Klimchouk AB, Ford DC (Eds) 2009. Hypogene Speleogenesis and Karst Hydrogeology of Artesian Basins. Ukrainian Institute of Speleology and Karstology, Special Paper, 1, Simferopol, 280.

Lombardo G, Sciumè A, Sollano G, Vecchio E, 2007. La Grotta dell'Acqua Fitusa e l'area della Montagnola nel territorio di San Giovanni Gemini (Ag). Speleologia Iblea, 12, 125–132.

Messana E, 1994. Il sistema carsico del gruppo montuoso di M. Inici (Castellammare del Golfo, TP). Bollettino dell'Accademia Gioenia Scienze Naturali, 27 (348), 547–562.

Monaco C, Mazzoli S, Tortorici L, 1996. Active thrust tectonics in western Sicily (southern Italy): the 1968 Belice earthquake sequence. Terra Nova, 8, 372–381.

Palmer AN, 2011. Distinction between epigenic and hypogenic maze caves. Geomorphology, 134, 9–22.

Perotti G., 1994. Kronio. – Le stufe di San Calogero e il loro flusso vaporoso. Bollettino dell'Accademia Gioenia Scienze Naturali, 27 (348), 435–475.

Piccini L, 2000. Il carsismo di origine idrotermale del Colle di Monsummano (Pistoia – Toscana). Le Grotte d'Italia, 1 (5), 33–43.

Plan L, Tschegg C, De Waele J, Spötl C, 2012. Corrosion morphology and cave wall alteration in an Alpine sulfuric acid cave (Kraushöhle, Austria). Geomorphology, 169–170, 45–54.

Stafford KW, Land L, Veni G (Eds.) 2009. Advances in Hypogene Karst Studies. National Cave and Karst Research Institute Symposium, 1, 182.

Tisato N, Sauro F, Bernasconi SM, Bruijn R, De Waele J, 2012. Hypogenic contribution to speleogenesis in a predominant epigenic karst system: A case study from the Venetian Alps, Italy. Geomorphology, 151–152, 156–163.

Tusa S, 2004. Grotta del Cavallo e la preistoria del comprensorio di Inici. In: CAI Palermo (Ed.). I Tesori di Monte Inici, 85–95.

SEDIMENTS AT THE MÜNNICH PASSAGE IN THE BARADLA CAVE (HUNGARY): MINERALOGICAL AND PETROLOGICAL STUDY

Gábor Vid[1], István Berényi Üveges[1], Orsolya Viktorik[1], Tibor Németh[2,3], Zsolt Bendő[4], Sándor Józsa[4], Judit Berényi Üveges[1]

[1]Niphargus Cave Research Association, Kaffka Péter 4., H-3758 Jósvafő, Hungary, info@niphargus.hu
[2]HAS Institute for Geological and Geochemical Research, Budaörsi út 45., H-1112 Budapest, Hungary
[3]Department of Mineralogy, Eötvös Loránd University, Pázmány Péter stny. 1., H-1117 Budapest, Hungary
[4]Department of Petrology and Geochemistry, Eötvös Loránd University, Pázmány Péter stny. 1., H-1117 Budapest, Hungary

Unconsolidated sediments at Münnich Passage in the Baradla Cave were studied by sedimentological and mineralogical methods (grain size distribution, sorting by grain size fractions and studying them by, XRD and SEM). In silty sediments filling the cavern in 755 cm thickness quartz is the dominant mineral. Mica-illite, illite/smectite, kaolinite, limonite (goethite) are present in all layers. The mineral composition of the clay fraction, the presence of iron minerals and idiomorphic quartz and tourmaline crystals, as well as the absence of calcite suggests short transport pathway. This means that the fine sediments found at Münnich Passage may originate from the soils and fine sediments of the surface area nearby.

1. Introduction

Our research group has studied the sediments of Baradla Cave since 2002. The research was started at Münnich Passage because this place seemed most promising to find sediments of several meters thick according to unpublished former studies (mid 1980's) of the Hungarian Geological Institute. Since 2002 seven other sites were sampled by drilling where sediments in various thickness were found. Based on these experiences a more detailed study using more sensitive methods with repeated sampling at this site can contribute to the understanding of the genesis of the cave particularly on the cyclic filling and depleting of the sediments (Berényi et. al. 2006).

Baradla Cave is located on the north-eastern part of Hungary at the border with the Slovak Republic in the mountains called "Gömör-Torna Karst" (Fig. 1). The cave is part of the Aggtelek National Park, belongs to the World Heritage and is protected by the Ramsar Convention.

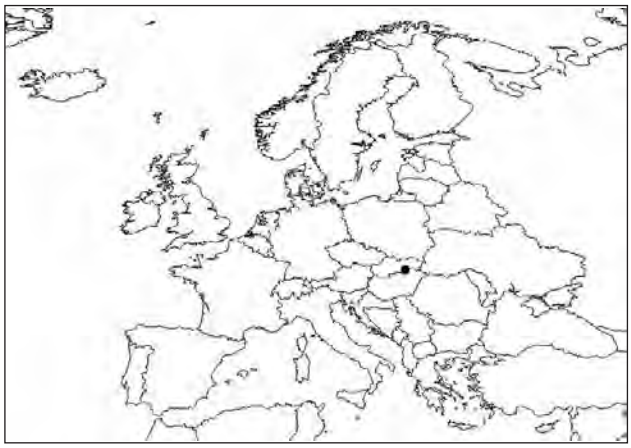

Figure 1. Location of Baradla Cave.

Baradla Cave is the longest known cave in Hungary with the total length of 27 km. It is developed in Triassic limestone that is covered by younger sediments (gravel, sandy gravel, red clay). Ground-water tracing studies proved the presence of the second level under the main branch. There is no passage accessible for man between the two levels. The cave creek is temporary, flowing water occurs only during the time of great floods.

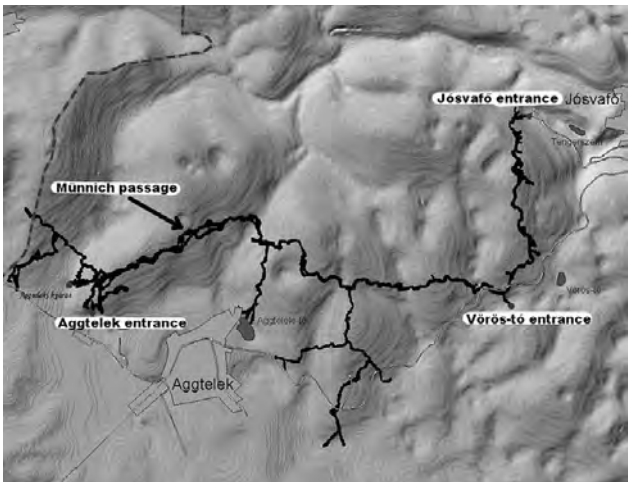

Figure 2. Map of Baradla Cave. (Map from National Cave Register).

The Münnich Passage is located 1,300 m from the entrance at Aggtelek village. It's a man-made path named after Kálmán Münnich who recognised that by digging out a short section filled by sediments a convenient tourist route can be formed that exclose a difficultly accessible section called "Nehéz-út (Hard Road)" (Figs 2, 3, 4). The height of the roof here is about 1.5–2.5 m now. Adding the thickness of the sediment (755 cm according to our sampling), the cavern of about 10 meters high can be assumed. It corresponds to the characteristic size of the cave at Aggtelek section.

According to the findings (Bosak et. al. 2004) the age of the top part of the sediment at Münnich Passage is 114 ka based on U/Th series dating.

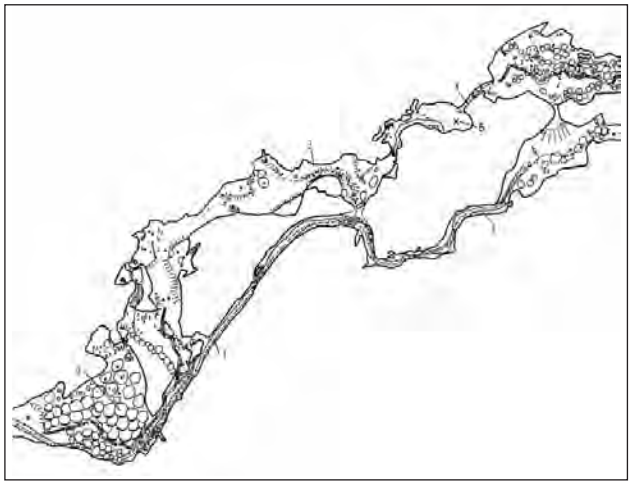

Figure 3. Map of Münnich passage and it's region (Ország et al. 1989), left side: direction to Aggtelek, right side direction to Jósvafő. Legend: 1: Hard Road, 2: Hill of Mórea, 3: Wax street, 4: Münnich passage, 5: Place of borehole.

Figure 4. Baradla-Cave Münnich-Passage (from Aggtelek side). Legend: Place of undisturbed sample.

2. Materials and Methods

The sediments were sampled by hand operated helical (D = 55 mm) soil sampler. Material forming a uniform layer was collected in one sample. If the uniform layer was thicker than 50 cm samples were taken at 50 cm intervals. Undisturbed samples were also taken from the wall of the passage (Fig. 4).

Particle size distribution was determined by sieving combined with sedimentation method. Mineralogical composition was studied after wet sieving and heavy mineral separation (SPT method) by binocular microscopy.

X-ray diffraction studies were carried out by a Phillips PW 1710 equipment with Cu K-alpha radiation 35 mA tube current and 45 kV acceleration voltage. Semi quantitative analysis was carried out on the disoriented powdered sample. Clay minerals were studied after separating the fraction less than 2 micrometers by sedimentation. Ethylene-glycol and heat (350 °C and 550 °C) treatments were also applied.

SEM studies were carried out on the undisturbed dried samples. The samples were impregnated into two component clear epoxy adhesive (Araldite 2020) by vacuum impregnator. The measurements were carried out on the AMRAY 1830 I/T6 SEM/EDX.

3. Results and discussion

At the entrance of the passage the thickness of the sediments is 755 cm. Table 1. presents the sediment characteristics in the borehole. The sediments found in the borehole and in the wall of the passage are uniform. The particle size distribution curves are presented in Figure 5.

Table 1. Sediment characteristics in borehole.

Depth	Material
0–195 cm	reddish brown silt
195–202 cm	silt with charcoal
202–220 cm	light brown silty sand
220–245 cm	reddish brown silt
245–400 cm	yellowish brown silt
400–710 cm	yellowish brown silty sand
710–755 cm	yellowish brown silty sand with black grains

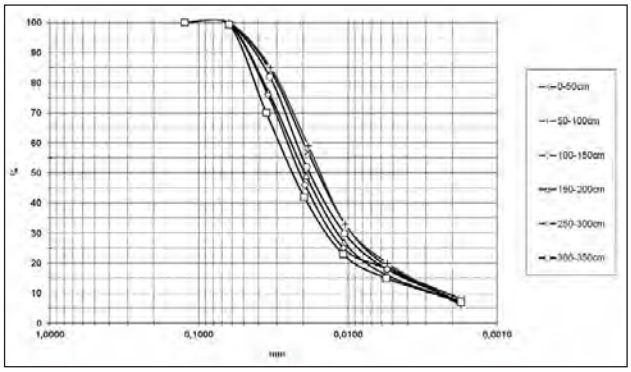

Figure 5. Particle size distribution curves measured in the sequence.

According to the particle size distribution curves (Fig. 5) and the SEM study (Fig. 6) the particle size ranges between 10–60 micrometers and the smallest fraction is between 20 and 30 micrometers. Particle size characteristics are very similar to that of loess. The structure of the sediment is closely packed and only a few laminar voids can be found. Particles are angular and fragmented.

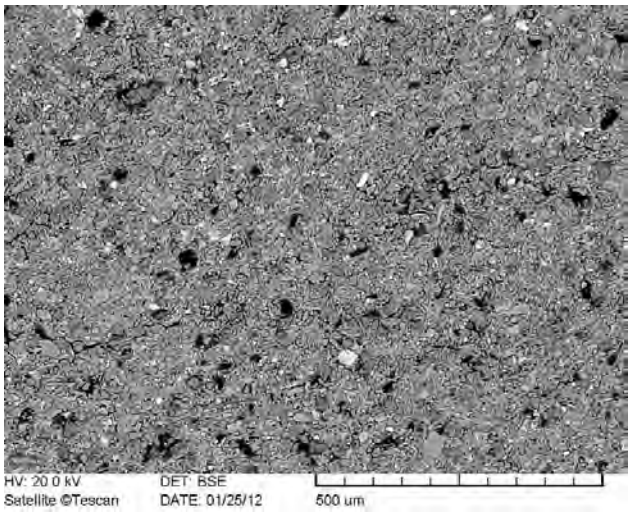

Figure 6. Backscattered electron image of the undisturbed sample taken from the sidewall of the Münnich-passage.

The results of SEM, XRD and microscope studies are in mutual agreement. The mineralogical composition of the sediments are: quartz 50–70%, 5% feldspars (both plagoiclase and K-feldspars), and 20–25% phyllosilicates (mica-illite, kaolinite, illite/smectite mixed layer mineral, smectite). Carbonates are not present in the sediments, except the layer where dropstone fragments were found. Goethite is present in less than 5% in the bottom part of the sequence.

Limonite aggregates were also found. Binocular microscope study showed that the forms of limonite aggregates are laminar on the top of the sequence. Fine grained aggregates or nodules occur at the bottom. Tourmaline (dravite composition), monacite and xenotime were also detected by SEM-EDX.

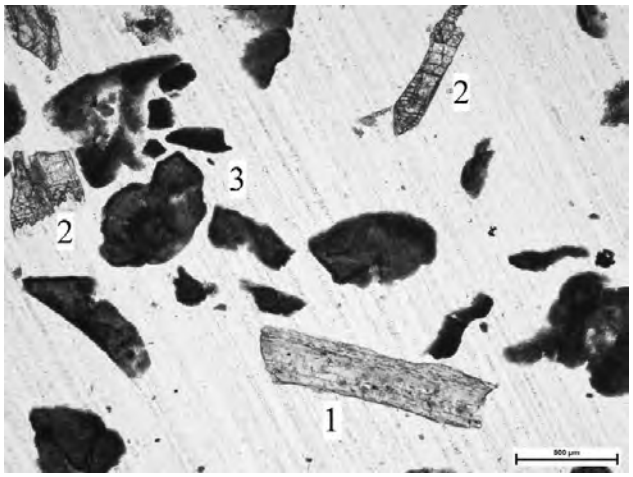

Figure 7. Part of bedded thin section sample from 0–50 cm depths, >250 μm grains. Legend: 1: bone fragment, 2:calcite, 3: limonite aggregates.

Dominant clay minerals are illite and kaolinite, their ratio is the same throughout the sequence. Smectite is present in a smaller amount in the form of illite/smectite. The amount of smectite increases upwards, and reaches its maximum in the top layer of the sequence (Fig. 8). The interlayer cation of the smectite is dominantly Ca – and based on SEM-EDX it is rich in iron substitution in the octahedral sheet. It is noteworthy that the bottom layers do not contain chlorite, it occurs only in the uppermost layer in a small amount. In the bottom part goethite is detectable in the clay fraction which indicates its pedogenic origin.

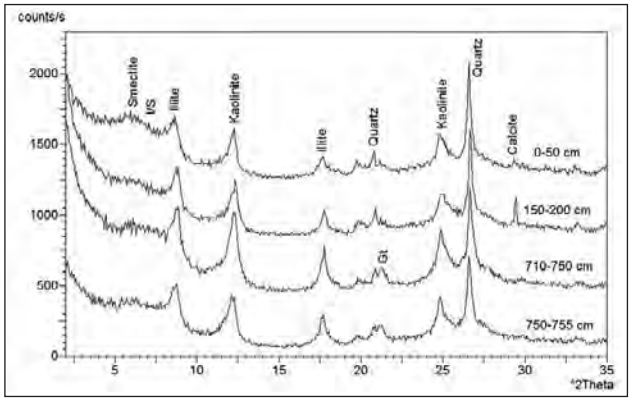

Figure 8. XRD patterns of the clay fractions by depth. Legend: I/S = illite/smectite, Gt = goethite.

The shape and sorting of the particles indicate a short transport distance, they sedimented from a still or slowly percolating water.

SEM investigation showed that the cracked parts of quartz, tourmaline monacite grains are next to each other. This indicates that the cracking took part after the sedimentation. The origin of a high pressure cracking these particles is unknown; perhaps frozen water on the surface of the sediment or in the pores can be responsible for that.

Reddish clayey sediments and soils can be found at the surface of the Aggtelek-karst having goethite as dominant iron mineral, and kaolinite with smectite as characteristic clay minerals (Fekete et al. 2008). Other studies found hematite and kaolinite in red soils of the same region (Czirbus et al. 2010).

The absence of carbonates in the sediment indicates that the sediment transported into the cave did not contain carbonates originally or they were eluviated (washed out and totally dissolved) – similar to present day soils – before the sediment entered the cave.

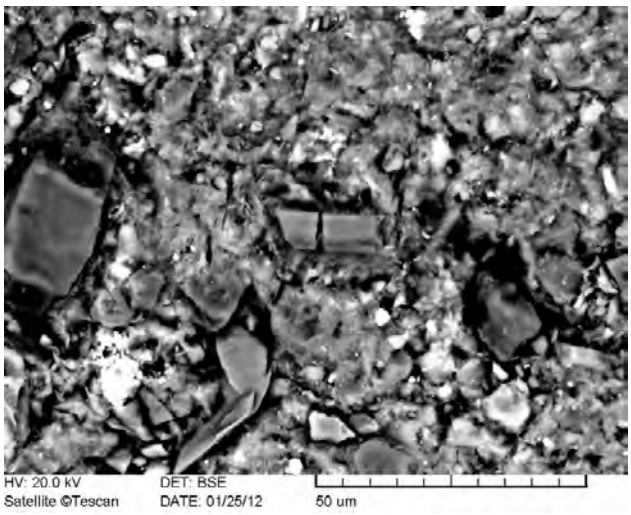

Figure 9. SEM image of a cracked tourmaline. (Undisturbed sample taken from the sidewall of the Münnich-passage).

4. Summary

Based on our mineralogical studies, the fine sediments found at Münnich Passage can be originated from the soils and fine sediments of the surface area nearby. Short transport distance is indicated by the presence of idiomorphic quartz and tourmaline. To support this assumption a detailed study of the sediments on the surface is planned.

Acknowledgement

The authors are grateful to the Aggteleki National Park, the Soliform Plc., András Varga Eötvös Loránd University and friends from the Nyphargus research association.

References

Berényi Ü. I., Berényi Ü. J., Vid Gábor, 2006: Adalékok a Baradla-barlang fejlődésének elméletéhez üledékvizsgálatok alapján. Karszt és Barlang 2006 I–II (in Hungarian).

Bosák P., Hercman H, Kadlec J, Móga J, Pruner P, 2004: Paleomagnetic and U-series dating of cave sediments in Baradla cave, Hungary. Acta Carsologica, 33(2), 219–238.

Czirbus N, Nyilas T, Bozsó G, Hetényi M, 2010: Az aggteleki-karsztról származó vörösagyagos rendzina talaj szerves anyagának geokémiai jellemzése Rock-Eval pirolízissel. Kárpát-medencei Doktoranduszok Nemzetközi Konferenciája, Konferencia Kötet, 46–54 (in Hungarian).

Fekete J, Csibi M, Stefanovits P, 2008: Magyarországi vörösagyagok jelentősége, fontosabb talajtani jellemzőik. Talajvédelem különszám 585–594 (in Hungarian).

National Cave Register, http://www.termeszetvedelem.hu/index.php?pg=cave_5430-1

Ország Gy, Vid Ö, Szilágyi F, Végh Zs, Gyuricza Gy, Frunyó E, Tóth Zs, 1989: Baradla-barlang 1:1,000, Magyarország barlangtérkepei 7. kötet (in Hungarian).

ENDOKARSTS AND CRYPTOKARSTS IN CRETACEOUS COARSE AND HIGHLY POROUS CHALK AT THE BELGIAN-DUTCH BORDER

Luc Willems[1], Joël Rodet[2]
[1]*Department of Geology, Sedimentary Petrology, Bd du Rectorat, B20, Sart Tilman, 4000 Liège, Belgium. L.Willems@ulg.ac.be*
[2] *UMR 6143 CNRS, Morphodynamique continentale et côtière, Laboratory of Geology, University of Rouen, 76821 Mont-Saint-Aignan Cedex, FRANCE*

Abstract. Since 2003, the study of several quarries at the Belgian-Dutch border has made it possible to identify numerous karsts essentially developed in coarse chalk (calcarenites) of the Maastricht Formation (Upper Cretaceous). This lithology is highly porous and is often considered unfavorable to karstification. However, caves, solution pipes, sponge networks, roof channel, pockets (alveoli) several meters in diameter developed inside without connection to fractures. These karsts belong to flooded karsts (caves and pockets) or to younger cryptokarsts (input karst type – thousands of solution pipes). When the endokarsts dewater, the high porosity of calcarenites inhibits closed caves from evolving. Tubular solution pipes are produced by the seepage water under fluvial terrace gravels and can exceed 30 m deep under the surface plateau. Sometimes, they encounter caves which are consequently filled and fossilized. By this process, they preserve caves from further collapsing inside a crumbly lithology.

Abstrait. Depuis 2003, l'étude de différentes carrières, à la frontière belgo-néerlandaise, a permis d'identifier un grand nombre de karsts essentiellement localisées dans des calcarénites de la Formation de Maastricht (Crétacé supérieur). Cette lithologie très poreuse est souvent considérée peu karstifiable car elle devrait inhiber une concentration des altérations. Pourtant, grottes, racines du manteau d'altération, réseaux en éponge, chenaux de voûte, alvéoles plurimétriques y sont développés, hors fracturation. Ces morphologies sont rattachées soit à des endokarsts noyés (grottes, alvéoles) soit à des cryptokarsts plus récent de type « karsts d'introduction » (plusieurs milliers de racines du manteau d'altération). Au moment de l'exondation des endokarsts, la porosité élevée des calcarénites stoppe l'évolution des grottes fermées. Des racines du manteau d'altération, formes tubulaires générées par les eaux d'infiltration sous un cailloutis de terrasse fluviale, peuvent s'enfoncer de plusieurs dizaines de m sous la surface du plateau. Elles peuvent recouper des grottes qu'elles colmatent et qu'elles préservent d'effondrement ultérieur dans une lithologie très friable.

1. Introduction

Cretaceous chalks and calcarenites (coarse chalks) at the Belgo-Dutch border (Fig. 1) develop numerous endokarsts and cryptokarsts without connection with fractures and in spite of a high porosity of the rock (Willems et al. 2004, 2005a, b; 2007a, 2007b, 2010; Lagrou et al. 2008; Rodet et al. 2009b). These cryptokarsts are essentially vertical tubes, solution pipes, which can reach more than 30 m deep under the plateau surface. In the area, they take place only under fluvial terrace gravels. The endokarsts are centimeters to several meters in size closed pockets which can be organized in subhorizontal blind tunnel-like caves which can be more than 60 m long. These caves had functioned as drains in the top of an aquifer.

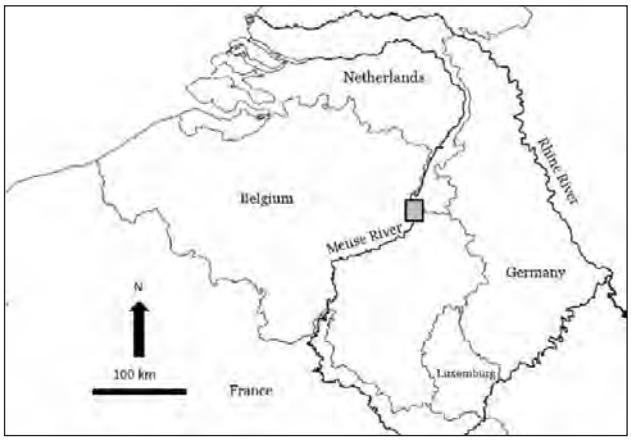

Figure 1. Localization of the studied area.

2. Physical environment

The studied karsts are intersected by underground or surface quarries opened in the Gulpen and Maastricht Formations (Cretaceous), exposed with a thickness of 100 m. The upper-lying Maastricht Formation consists in macroporous calcarenites rich in flint nodules and subdivided by hardgrounds. Porosity between 37 % and 44 % (Willems et al. 2010) is determined near cavities. These values are much reduced at hardgrounds or fossiliferous beds, which have no influence on the studied karst morphologies.

The underlying Gulpen Formation consists of very fine calcarenites grading downwards to chalk rich in flint beds. Pure white chalk and impervious marls of Campanian age separate the exposed Maastrichtian carbonates from the underlying deeply weathered and kaolinized Carboniferous limestones (Felder and Bosch 1998). Above the Cretaceous layers, Oligocene marine sands were deposited. In some places these sands are preserved in dolines developed in the Cretaceous formations. During Pliocene time, the river Meuse drainage system came into existence and progressively incised down to its present level, as testified by peneplain surfaces and gravel terraces. The high terrace of the river is a Middle Pleistocene gravel formation. This coarse and loamy river deposits armour the underlying Cretaceous chalk and lead to a local relief inversion (Juvigné 1976). During the Weichselian glaciation, about

ten meters of loess was deposited, burying the pre-existing landscape (Haesaerts, 1984).

High rates of underground water flow (2.2 to 13 km/day) have been reported (Dassargues and Montjoie 1993). They are similar to highly karstified aquifer (Harold 1937; Atkinson and Smith 1974; Rodet 1992; Maurice et al. 2006). They could be due to horizontal narrow pipes observed in drainage galleries (Van Den Broeck et al. 1910; Ministère de la Région wallonne and Université de Liège 2006), but also to the caves and sponge networks found in the Maastricht Formation. Deep weathered nodes are also generated in chalks of the Gulpen Formation, tens of meters under the Meuse alluvial plain (Willems et al. 2007a, b; 2010). They could also favour high rates of flows.

3. Cryptokarsts

The cryptokarsts are essentially tubular solution pipes (raciness du manteaux d'altération) (Fig. 2) developed under terrace gravels of the river Meuse. They have quite regular sections and their diameters vary between a few centimeters to over two meters. They may exceed 30 m deep under the plateau surface. The solution pipes contain Oligocene sands and/or sandy clays, and also rounded pebbles coming from the upper Meuse river terrace. The descent of superficial deposits into the Cretaceous strata supports evidence of deepening of the solution pipes. Their widening results from the coalescence of smaller ones. Juvigné (1992) connected their genesis to lithological variation in terrace deposits. The coarse parts of the terraces produce local concentrations of seepage water and initiate these solution pipes (Rodet et al. 2009a). A local flint accumulation could trigger the same water concentration process. On the contrary, when sand deposits partially cover the Cretaceous formations, no evidence of solution pipes are found. The reason for this could be the dispersion of seepage water in this kind of lithology. Several observations show that these cryptokarsts stopped enlarging at around 75–80 ka BP, i.e. the Upper Weichselian (Juvigné 1992; Juvigné et al. 2008; Willems et al. 2010). Juvigné (1992) suggests a permafrost, which inhibited the seepage water. Another hypothesis is a fast loess deposit on the terrace gravel playing the same role as a sand cover (Willems et al. 2010). The rapidity of loess deposits is supported by a non-eroded tephra inside the loess. Some solution pipes encountered lower horizontal caves, their filling are withdrawn, and small swallow holes are generated (Willems et al. 2010).

4. Endokarsts

Most endokarsts consist of meters to several meters sized blind cavities with similar altitudes. They are located between 20 and 30 m below the plateau surface and between 10 and 20 m below the contact Oligocene/Cretaceous (Willems et al. 2007, 2010). Two types of cavities can be identified: the first one consists in a corridor with an ellipsoidal section, developed in a parallel to the subhorizontal stratification. The second one is made of a single room with rounded walls, which are in turn generated

Figure 2. Solution pipes opened in the underground quarry (Caster, Belgium).

by the coalescence of many centimetric to decametric pockets. There is an obvious continuum between sponge networks, single-room caves, and corridor caves (Fig 3).

Endokarsts have the following characteristics:

1. The caves are formed outside the fractures. If fractures are present, they are poorly karstified and they dissect the caves.
2. Numerous small horizontal pipes are connected to the main cave without a preferential orientation.
3. The cave floor is made of mixed collapsed blocks and weathered calcarenite powder. There is a transition between this powder and the fresh bedrock without a clear limit. Traces of oxide migrations inside the weathered part of the floor attest to slow water flows. In some cases, the cave floor consists in pockets.
4. Some corridor caves are completely clogged up by superficial deposits (Tertiary sands, loess) (Fig. 3c) and show sedimentary fill typical of low energy flow. These observations show that some caves had functioned as drain in the top of an aquifer.
5. Trace of an ice-wedge is observed in the floor deposit of a cave (Willems et al. 2010). It demonstrates the top of an old permafrost tens meters under the plateau surface. Figures of hydromorphy under this structure (traces of iron hydroxide remobilization) could result from a perched aquifer due to the impermeable permafrost. It could explain the temporary concentrated flows from the seepage water and promotes drains and a slow moving of the brecciated materials of the floor.

6. Some caves are encounter by solution pipes. The superficial materials (loess, terrace pebbles, etc.) which constitue the central part of the solution pipe partially dump in the caves. The deposit shows evidence of a process in an unsaturated zone. It shows that the cave was dewatered before it was encountured by solution pipes.

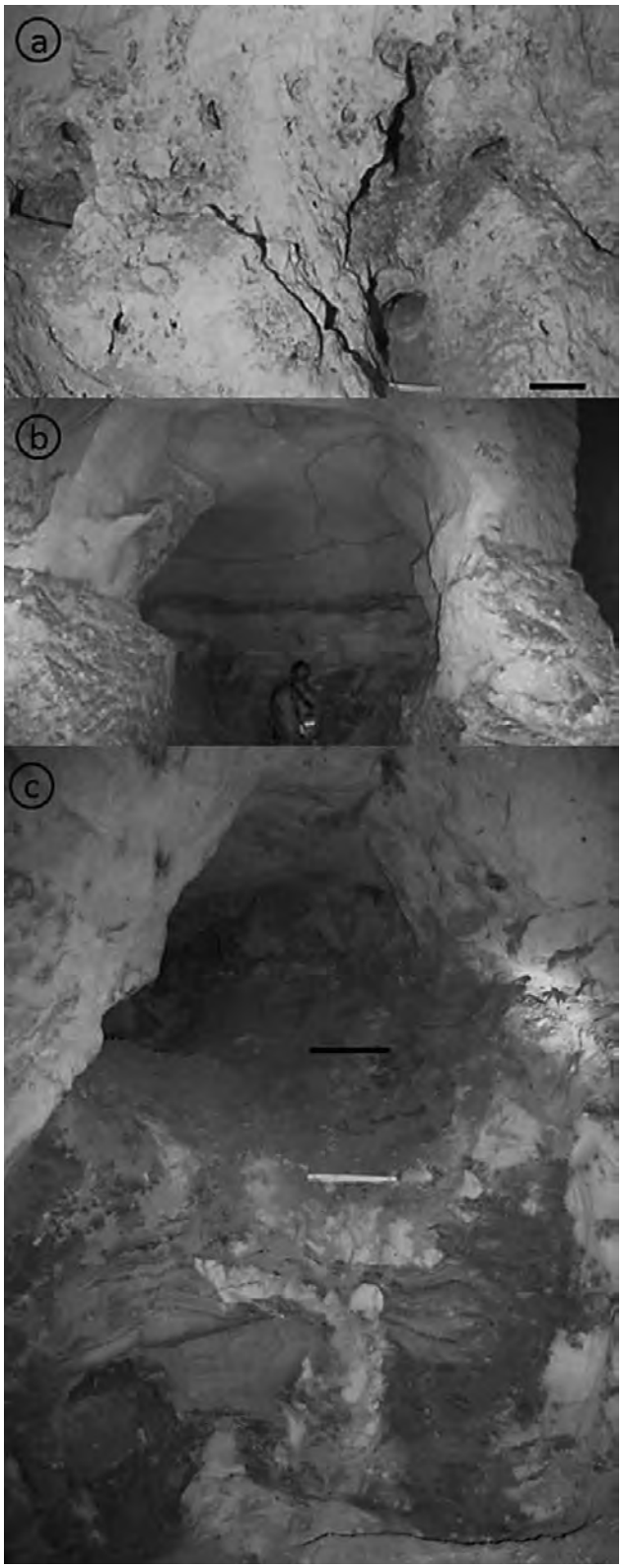

Figure 3. Several types of endokarsts: a.) sponge network inside the calcarenite – Petit Lanaye Supérieur (scale bar: 20 cm); b). single room cave – Petit Lanaye Supérieur; c). corridor cave with Tertiary sands and Quaternary loess filling – CRSOA cave – Petit Lanaye inférieur – Belgium (scale bar: 20 cm).

5. Discussion – Conclusion

At least three stages are identified in evolution of the karsts:

Firstly, the developments of caves, deep under the surface of the plateau, in phreatic zone, as evidenced by sponge networks, micro and macro pockets.

Secondly, a dewatering of the caves and a widespread terminated of dissolution process.

Thirdly, the development of fractures which dissect the caves or solution pipes which encounter them. In this stage, the caves can be completely filled and fossilized (Fig. 4).

Various caves listed are sometimes several kilometers away from each other and have similar altitudes. Their genesis can be related to a paleo aquifer. The caves could also result in the evolution of deep weathering nodes (Fig. 5) such as those found twenty meters below the Meuse alluvial plain (Willems et al. 2007). These nodes are similar to "ghost-rocks" found within the Tournaisian limestone (Quinif et al. 1994; Vergari 1998). The ghost-rock is "in situ" limestone weathering with residual weathered-rock ("ghost-rock") that keeps its initial volume.

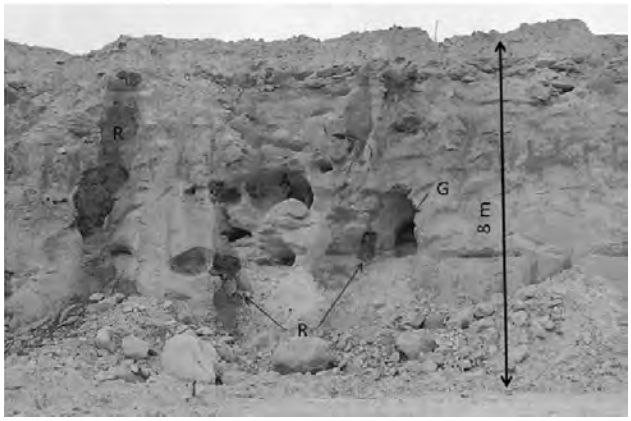

Figure 4. Complex karst network in the quarry of Romont-Belgium. Horizontal corridor cave (G) – single room caves(A) encountered by solution pipes (R) which intersect previous forms.

The caves could be related to slow water circulations within the Cretaceous Formations and under the regional thalwegs (Willems et al. 2007 a, b) The dismantling of this paleo aquifer can be due to the downcutting of the Meuse River and its tributaries.

Studies of karst in high porosity carbonate rocks are still few (Rodet 1992). However, the example of the Cretaceous chalk karstification at the Belgian-Dutch border shows that they can be very numerous. Their genesis results of a much more complex history than a simple fracture karstification. Their impact on water resources needs to be evaluated.

References

Atkinsons C, Smith DI, 1974. Rapid groundwater flow in fissures in the Chalk: An example from South Hampshire. Quarterly Journal of Engineering Geology, 7: 197–205.

Dassargues A, Monjoie A, 1993. Hydrogeology of the chalk of North-West Europe. Chap. 8: Chalk as an aquifer in Belgium, Oxford University Press, 153–169.

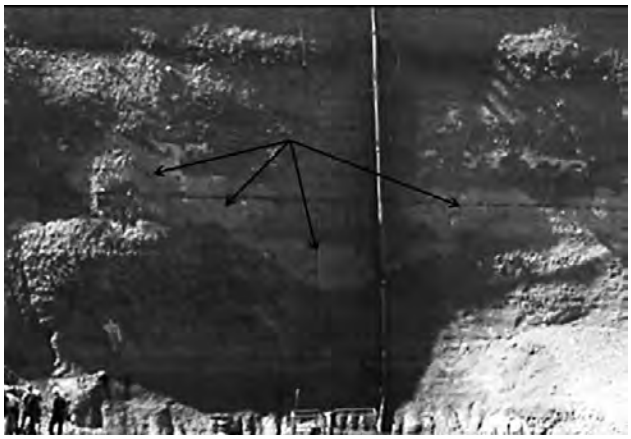

Figure 5: deep weathering nodes – ENCI quarry – Maastricht-Netherlands.

Felder WM, Bosch PW, 1998. Geologie van de St. Pietersbergbij Maastricht. Grondboor & Hamer, 52: 53–63.

Haesaerts P, 1984. Aspects de l'évolution du paysage et de l'environnement en Belgique au Quaternaire, in: Cahen, D., Haesaerts, P. (Eds.), Peuples chasseurs de la Belgique préhistorique dans leur cadre naturel, Bruxelles, 27–39.

Harold C, 1937. The flow and bacteriology of underground water in the Lee Valley. Metropolitan Water Board 32nd Annual Report, London, England. 89–99, in Maurice et al. 2006.

Juvigné E, 1976. La stratigraphie du Quaternaire. Géomorphologie de la Belgique, in Hommage au Prof. P. Macar, Laboratoire de Géologie et Géographie physique, Université de Liège, 169–179.

Juvigné E, 1992. Les formations cénozoïques de la carrière C.B.R. du Romont (Eben/ Bassenge, Belgique). Ann. Soc. Géol. de Belgique, 115: 159–165.

Juvigné E, Tallier E, Haesaerts P, Pirson ST, 2008. Un nouveau stratotype du téphra de Rocourt dans la carrière de Romont (Eben/Bassenge, Belgique). Quaternaire, 19 (2), 2008, 133–139.

Maurice LD, Atkinson TC, Barker JA, Bloomfield JP, Farrant AR, Williams AT, 2006. Karsticbehaviour of groundwater in the English Chalk. J. of Hydrology, 330: 63–70.

Ministère de la Région wallonne (DGRNE) & Université de Liège, GéomacHydrogeologie, 2006. Carte hydrologique de Wallonie, Alleur-Liège 42/1-2,Notice explicative, 52.

Quinif Y, Vergari A, Doremus P, Hennebert M, Charlet JM, 1994. Phénomènes karstiques affectant le calcaire du Hainaut. Bull. Soc. Bel. de Géologie, 102: 379–384.

Rodet J, 1992. La craie et ses karsts, Caen, Centre normand d'Étude du Karst et des Cavités du Sous-sol. Elbeuf, & Groupe Seine-CNRS, 560.

Rodet J, Brown J, Dupont J-P, 2009a. Development and function of a perched aquifer in the covering layers of the chalk limestones in the Paris Basin. Proceedings of the 15th International Congress of Speleology, Kerrville (Texas, USA), 19–26 july 2009, UIS, vol. 3, contributed papers: 1662–1666.

Rodet J, Willems L, Brown J, Ogier-Halm S, Bourdin M, Viard JP, 2009b. Morphodynamic incidences of the trepanning of the endokarst by solution pipes. Examples of chalk caves in Western Europe (France and Belgium). Proceedings of the 15th International Congress of Speleology, Kerrville (Texas, USA), 19–26 july 2009, UIS, vol. 3, contributed papers: 1657–1661.

Speleogenesis, 2012. Info KarstBase Glossary of Karst and Cave Terms. www.speleogenesis.info/directory/glossary/index.php

Van Den Broeck E, Martel EA, Rahir E, 1910. Les Cavernes et les Rivières souterraines de la Belgique. Lamertin, Bruxelles, Vol. I, p. VIII.

Vergari A, 1998. Nouveau regard sur la spéléogenèse: le "pseudo-endokarst"duTournaisis (Hainaut, Belgique). Karstologia, 31/1: 12–18.

Willems L, Rodet J, Massei N, Fournier M, Laignel B, Dussart-Baptista L, Schyns JCH, Ek C, 2004. Chalk karsts – Saint-Pierre Mountain – Basse-Meuse (Belgium). Poster – Meuse-Rhine EuregioGeologists Meeting, Maastricht, 28–29 Mai 2004.

Willems L, Rodet J, Massei N, Fournier M, Laignel B, Dussart-Baptista L, Schyns JCH, EK C, 2005a. Genèse d'un système karstique dans la craie en Basse Meuse (Frontière belgo-néerlandaise). Poster, Coll. Intern. "Karst et aménagement du territoire ", Région wallonne, Jambes, Mai 2005.

Willems L, Rodet J, Fournier M, Massei N, Laignel B, Dussart-Baptista L, Schyns JCH, Dusar M, Lagrou D, Ek C, 2005b. Karst system genesis in the chalk of the lower Meuse (Belgian-Dutchborder)", 14e Congrès de l'UIS, Athènes- Kalamos, 23–28 Août 2005, CDRom Full Paper: 0–36 (6 p).

Willems L, Rodet J, Fournier M, Laignel B, Dusar M, Lagrou D, Pouclet A, Massei N, Dussart-Baptista L, Compère PH, Ek C, 2007a. Polyphase karst system in Cretaceous chalk and calcarenite of the Belgian-Dutch border. Z.Geomorph. N.F., Berlin-Stuttgart, 51 (3): 361–376.

Willems, L., Rodet, J, Ek, C., Dusar, M., Lagrou, D., Fournier, M., Laignel, B. & Pouclet, A., 2007b. Karsts des craies et calcarénites de la Montagne Saint-Pierre (Basse Meuse liégeoise)". Bull. des Chercheurs de la Wallonie, 46: 171–186.

Willems L, Rodet J, Ek C, Pirson ST, Juvigné E, 2010. Karsts des calcarénites de la carrière du Romont (Eben – Belgique). Bull. Chercheurs de la Wallonie, hors-série No. 3, 115–130.

THE TUPPER GLACIER SINK – RASPBERRY RISING CAVE SYSTEM, GLACIER NATIONAL PARK, CANADA: A REMARKABLE EXAMPLE IN STRIPE KARST

Charles Yonge, Nicholaus Vieira, Adam Walker
Alberta Karst Consulting, 1009 Larch Place, Canmore, Alberta, Canada, chas-karst@telus.net

The large spring in Rogers Pass named by cavers as Raspberry Rising, and by Parks Canada as Cascade Cave, has been known of for over a hundred years. In the late 1960's, Derek Ford and others from the Karst Research Group at McMaster University inserted dye at the Tupper Sink, which takes the large outflow from the Tupper Glacier, recording an unprecedented underground flow time to Raspberry Rising (almost 500 m lower and 2 km away) of 53 minutes. Such a rapid flow-through indicates a very direct route through an open cave system, which is contained within a sub-vertical, narrow sheet of marble – a classic Type 1 stripe-karst hydrology. The Tupper-Raspberry cave system is compared to 3 other significant stripe karst caves in the vicinity and to Raggejavri-Raigi Cave in Norway.

A short (10 m) sump encountered 70 m into Raspberry Rising had been repeatedly dived from 1971 onward. Progress had been halted at a large waterfall, with only one attempt being made to climb it by mapole in 1981. Now while the system's proximity to the TransCanada Highway makes it accessible, high water levels in the summer necessitate winter travel into one of the Pass's largest, most highly restricted avalanche zones (the Connaught Slide Path). Despite this however, the winters of 2011 and 2012 saw success in climbing the waterfall and the mapping of around 2.4 km of large, well-decorated passageways, with almost half of the distance to the Tupper Glacier Sink reached. Work is in progress.

1. Introduction

The large spring in Rogers Pass named by cavers as Raspberry Rising, and by Parks Canada as Cascade Cave, has been known of for over a hundred years. In the summer of 1966, Derek Ford and others from the Karst Research Group at McMaster University dye-traced the water at Tupper Sink, the source of which is the large Tupper

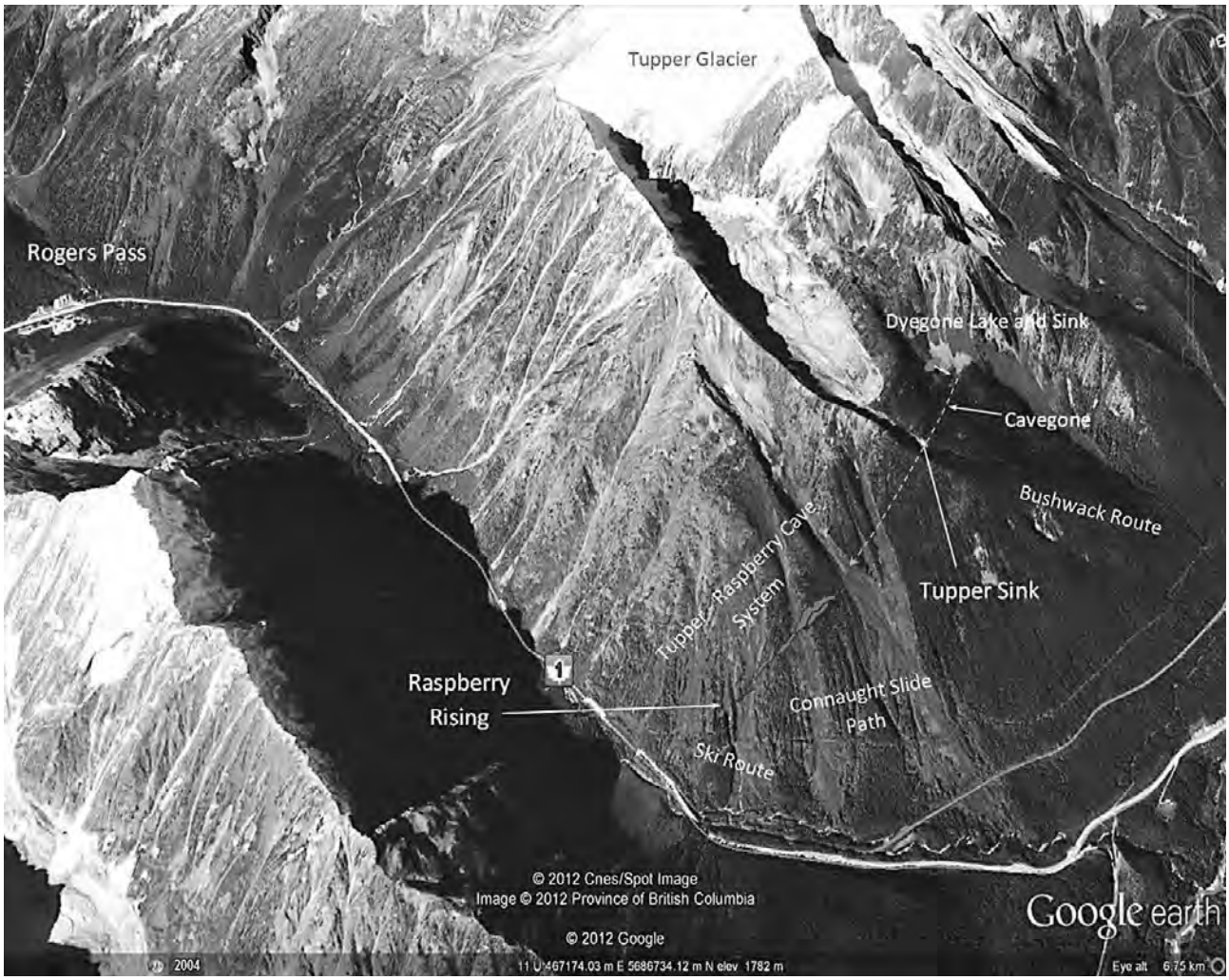

Figure 1. Location of the Tupper–Raspberry Cave System.

Glacier, and getting a positive and rapid response at Raspberry Rising, 483 m lower and 1.94 km away, in 53 minutes (Ford 1967). An open, vadose cave system seemed likely, especially as both sink and spring appeared to be contained within a narrow, sub-vertical band of marble. Its proximity to the highway makes it very accessible (Figure 1) although winter travel into one of the Pass's largest avalanche zones (the Connaught Slide Path) is highly restricted.

Figure 3. Steeply dipping beds at the Nick Point. Note thinner bands of schist within the marble.

Once inside Raspberry Rising, the first serious obstacle preventing exploration comes 70 m from the entrance where there is a 10 m sump. This sump was first passed in 1971 by Mike Boon, but he was soon stopped by a high waterfall. While other dives followed the only progress made was by Mike Boon, Pete Lord and Randy Spahl in 1981 (see Yonge 2012 for the history of these dives). Boon ascended the lower part of the waterfall using a maypole, but was ultimately overwhelmed by the volume of falling water and Pete Lord had been able to climb ledges to the right of the waterfall, apparently finding 65 m of passage to a dig (this likely leads to the passage system above the waterfall found later).

Thus Vieira, with us in support as far as the sump – made it to the top of the waterfall via modern bolting methods on February 2nd, 2012; it is 25 m high and named the Nick Point. What he discovered beyond (The Dream Collector) was astounding; he saw that the passage ran ahead as a field of massive tumbled boulders with the stream running under them, 15 m wide and 20 m high.

Later that winter and spring plus this winter, we conducted several diving and mapping trips into the system, penetrating 800 m into the mountain with some 2.4 km of survey completed. We also undertook basic photography of

Figure 2. Copious speleothems in the T-R System. The curtain at right is ~2 m long.

the very extensive speleothems (Figures 2 and 7) and made preliminary observations of the surprisingly sparse biological/organic material.

2. Geology and Geomorphological Setting

The Tupper-Raspberry cave system (T-R) is confined to a 20 m to 60 m-wide marble band sandwiched between calcareous slates and garnet schists (the Precambrian Horsethief Creek Group of the Shuswap Metamorphic Complex (SMC): Poulton and Simony 1980). It varies in dip from near vertical to 45° (Figure 3), giving a practically straight-line path between sink and rising. Furthermore the band extends eastwards to another sink from a small lake known as Dyegone, 371 m above Raspberry Rising (Figure 1). Dye placed in this sink by the McMaster Group travelled to the rising in approximately 8 hours.

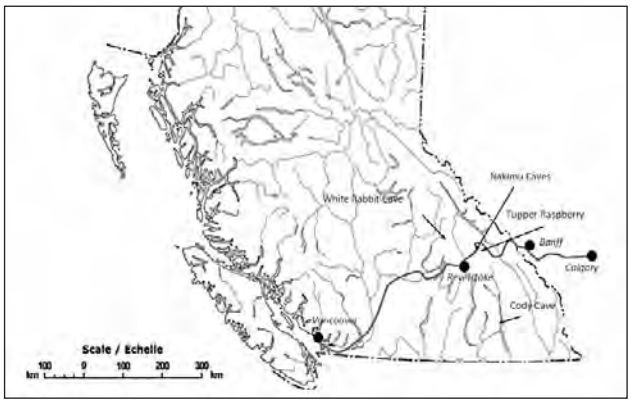

Figure 4. Location of stripe karst caves in the area.

The nearest caves of any significance, also in marble stripe karst, are White Rabbit, Cody and Nakimu Caves (Figure 4 and Table 1). The closest, 11.5 km west of the T-R system, are Nakimu Caves (Rollins 2004) in the highly fractured, veined crystalline Badshot Limestone of Lower Cambrian age (Poulson and Simony 1980). Actually, it comprises a system of three caves with a common meltwater stream separated by collapsed sections, which yielded a total surveyed length of 5.49 km and and depth of 286 m. It is of the Type 3 perched stripe karst type. The next nearest cave of any significance, albeit at an early stage of exploration (< 400 m mapped) is White Rabbit which is 100 km west

of the T-R system. It is in a late Precambrian to early Cambrian marble of the Mount Grace Formation (Hoy and Pell 1985) with a possible length of > 2 km and depth of ~ 400 m. Dips are low at an average of 23°, qualifying it as a Type 3 stripe karst i.e. the marble band is narrow at ~50 m and the cave appears perched on the lower impermeable unit. Cody Cave 180 km to the south is ~1.5 km long and ~60 m deep. It is in the Milford Group of Triassic age (Fyles 1967) and has some relationship to Nakimu lying in the same north-south metamorphic belt. It is an example of the Type 2 stripe karst being confined to development at the upper contact (Lauritzen 2001 and Table 1). The four caves (including the TR system – Figure 4) are indicative of the rareness of speleogenic carbonate rocks in the area and the diversity of relationship (age of rock and setting) between them. All lie within the extensive Shushwap Metamorphic Complex of the Middle to Late Jurassic.

3. Results and Discussion

3.1. The Tupper-Raspberry Stripe Karst

The Tupper-Raspberry System is a fine example of a Type 1, sub-vertical marble stripe karst (the Scandanavian Caledonides or "Norwegian Karst Type" exemplifies the 3 types or classes of stripe karst defined in the Norwegian setting – Lauritzen 2001 and 2004). The Tupper-Raspberry System meets the Type 1 criteria, consisting of a narrow outcrop of steeply dipping karst rock, where the allogenic contact perimeter (P) is very large relative to the area (A) of karst i.e. the outcrop is very narrow compared to its length. Lauritzen (2001) defines a quantity *r* based on the P/A where γ is the ratio of the length of the "stripe" λ to its width w (i.e. $\gamma = \lambda/w$) which replaces λ and w in the expression. We have used a modified expression to give a dimensionless integrity to the relationship by defining a ratio of $r' = P/A^{1/2}$ (Figure 6), yielding:

$$r' = P/A^{1/2} = 2(\gamma^{1/2} + \gamma^{-1/2}) \quad (1)$$

The right-hand side of the expression is the same as that used by Lauritzen (2001) and is a sigmoidal function with its differential having a maximum at $\gamma = 3$.

$$dr'/d\gamma = P/A^{1/2} = \gamma^{-1/2} + \gamma^{-3/2} \quad (2)$$

The modified *r* does not change the essential discussion given by Lauritzen (2001), and it can easily be shown that the minimum for P/A is a square (i.e. $\gamma = 1$). The dimensionless $r' = P/A^{1/2}$ also yields a minimum at $\gamma = 1$. The differential is a measure of the sensitivity of the perimeter to area of stripe karst in which values of $3 > \gamma > 30$ which Lauritzen refers to as the region of development to a full stripe karst geometry.

Thus based on the distance between Raspberry Rising and the known sink-points of 1.94 and 2.63 km, and an in-cave horizontal expression of the marble from 20–30 m (average 25 m), $\gamma = 78$ to 105 is indicative of a fully developed karst geometry $\gamma > 30$. (Note that White Rabbit, Cody and Nakimu Caves have $\gamma = 44$, 19 and 3 respectively, which defines all as stripe karst, although the latter represents an end member.)

Narrow, steeply-dipping stripe karst gives rise to solution on both contact faces with greater karstification at the hanging wall. Furthermore, the confining walls of schists and slates containing sulphides and ferrous oxides, which tend to impregnate the enclosed marbles, allows sulphuric acid dissolution to take place (rust staining on the marble at the contact suggests this). However, because of metamorphism, primary voids tend to be absent, but the brittleness of the marble leads to prevalent fractures and joints for which extensive speleogenesis is required (Lauritzen 2001 and Figure 5).

Figure 5. Person standing on breakdown in the main passage. Note bedding and jointing sets.

The Tupper–Raspberry system does show extensive fracturing with enormous, truck-sized breakdown blocks. The rotation of the marble band from near vertical at the rising to 45° at the midpoint back to around 80° at Tupper Sink suggest tectonic flexing of the unit leading to additional fracturing beyond that due to initial uplift and regional folding (Figures 5 and 7). This system can be compared to the celebrated Type 1 stripe karst cave at Hellemofjord, Norway known as Raggejavri-Raigi (RJR – Lauritzen et al. 1991 and Table 1). RJR descends a sub-vertical vertical marble from a plateau to the base of the fjordal wall rising just below sea level (a dry, relict entrance allows for a through trip). Whereas the marble band in this case is oriented at a right-angle to the fjord wall, the T-R system is angled (Figure 1). However while similar in depth (RJR = 580 m), the distance from sink to rising is much less

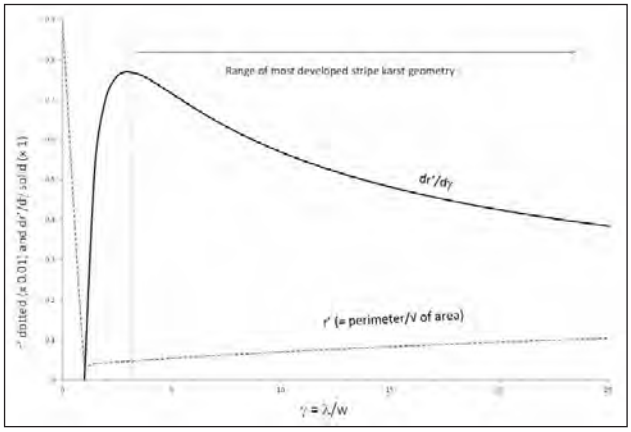

Figure 6 (modified from Lauritzen, 2001). Eqn. (1) and its first derivative plotted, showing a maximum sensitivity of $\gamma = 3$. The sensitivity of $P/\sqrt{A}$ with increasing γ dies out above $\gamma = 30$, i.e. stripe geometry is fully developed. Most stripe karsts display γ in the interval $10 < \gamma < 200$.

Figure 7. Strike view of the Tupper-Raspberry System at 70°. Note that the beds at the north end of the system at 45° splay the passage network.

for RJR at 0.79 km compared to 1.94 km for T-R. This gives RJR a high hydraulic gradient 0.73 compared to 0.25 for T-R, and results in some large pitches and likely rapid flowthrough times, although this has not yet been determined (Lauritzen, percomm.). Unlike RJR, where large chambers have consumed almost all of the surrounding rock (a width of between 20–30 m) the T-R system appears to wander between the confining walls. This occurs because thin discontinuous schist horizons in the marble limestone temporarily confine the passage width. Indeed the initial sump penetrates through a narrow slot in a thin schist unit dividing one massive marble unit from another.

3.2. Hydrology and Speleogenesis

The rapid flow-through time for the Tupper-Raspberry link can be compared to some of the fastest vadose karstic flows anywhere. The summer T-R breakthrough of < 53 minutes yields an average flow speed of 61 cm/s. Worthington *et al* (2000) have compiled linear karst groundwater velocities, based on a global data set of 3,015 trace experiments (compensated for a sinuosity of 1.2) and finds that only 0.5 % of karstic flows have speeds greater than this. The high T-R hydraulic gradient (483 m / 1,940 m = 0.25) combined with open passages in a linear, narrow, sub-vertical carbonate band leads to this rapid flow. Dygone Sink is at a lower altitude and is further away, giving a hydraulic gradient of 0.14 (371 m / 2,630 m). With an 8-hour summer breakthrough, this yields a flowspeed of 9 cm/s; we suspect that additional sedimentary blocking and possible siphons are responsible for the slower flow. Despite this, Dygone falls within the top 10 % of the fastest karst flow-through times.

The combined flow of Tupper, Dygone and the many other inlets (both seen and unseen) yields summer flows of 0.71 cumecs. Based on increasing flows at Raspberry during a typical summer's day; Ford (1967) estimated that 75 % of the water comes from the Tupper Glacier. In winter, we have calculted average flows of around 0.05 cumecs or 7 % of summer flow, but the relative contributions from the various sinks is unknown (we have already encountered many inlets so far).

While the T-R system has obstructions at both ends – a blocked sink at the top and sump at the bottom – it (so far) appears open in between. Although we have reached a second 1m sump (duck) which leads to a series of cascades, including one pitch, and a third longer siphon, these are unlikely to hold up the flow. The average gradient (thalweg) of the cave thus far is ~11.5° (figure 8) which suggests a significant increase ahead (> 300 m) to arrive at the Tupper Sink (an overall gradient of 14°). Dygone has a gradient of 8°, suggesting that it may actually be an earlier sink point. Alternatively, the current stream profile extrapolates to an area of depressions and one abandoned cave (Cavegone) between Tupper Sink and Dygone, which may be the original sink point (Figure 1; see discussion below). Higher gradient relict passages such as the Dream Collector and Freedom 65 suggest major inlets, and these may be provided by the sizeable valley system cutting the middle of the Cannaught Slide (informally named Grizzly Paradise – figure 1). These latter, storeyed passages are expected in Type 1 stripe karst (Lauritzen 2001 and 2004), indicating a deep karstification of the marble unit. Passage below the Nick Point and out to the current entrance appears to be junvenile, so further exploration may yield a relict rising as a downward continuation of the main passage.

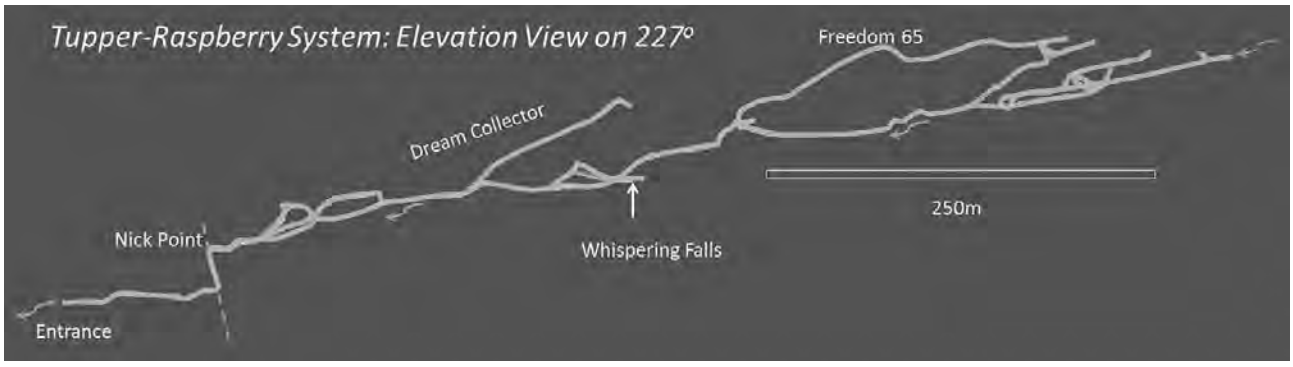

Figure 8. Elevation view on 227° of the Tupper-Raspberry System.

While Tupper is a massive sink compared to Dygone, the latter may actually be older or at least contemporaneous. Using a 1956, 1:50,000 topographic map and current Google Earth imagery, it can be seen that the Tupper Glacier has retreated 1.2 km (21 m/year). The glacier currently lies 1.85 km from Tupper Sink at an altitude of 2,100 m; in 1956 it was 0.65 km distant at 1920 m. This suggests that in post-Wisconsin times an extensive glacier lay above both sinks. We note that in the Western Cordilleras of Canada, karst and caves are more developed in south-facing valleys and cirques, where solar melting is considerably more extensive. In the case of Tupper, the west side of the valley cirque is shaded by the high Mount Tupper ridge, whereas the east side receives long daylight sun. We would then be expect to see an earlier karst develop on that side with Dygone (or at the aforementioned area of depressions)

Table 1. Data on stripe karst caves discussed in text. ** After Lauritzen et al (1991).*

Cave/System	Estimated length (m)	Estimated depth (m)	Marble width (m)	Marble dip (°)	Sink elev. (m)	Resurge elev. (m)	Sink to resurg. (m)	Hydraulic gradient	Stripe Karst
White Rabbit	2,500+	398	50	20–27	1,443	1,045	2,220	0.18	Type 3
Cody Cave	3,000+	60	110	55	1,440	1,380	2,040	0.03	Type 2
Nakimu Caves	5,500	285	300	40–50	1,708	1,423	910	0.31	Type 3
Tupper-Rasp.	6,700	483	20–30	45–80	1,748	1,265	1,940	0.25	Type 1
Dygone-Rasp.	9,000	371	20–30	45–80	1,636	1,265	2,630	0.14	Type 1
RJR Norway*	2,000+	580	20–30	65	580	0	790	0.73	Type 1

receiving meltwater at the contact for a longer time. Eventually the glacier would have retreated back over the cirque sill, depriving Dygone (and other area) of the main supply. Currently all of the glacial meltwater cascades over the low west side of the sill to sink entirely at Tupper (except in very high water when the residual flows down the overflow channel on the surface – Figure 1). In respect of the marble band cutting across the front of the glacier, it is possible that the Tupper Sink had an anchoring effect on the glacier, causing it to pivot on the east side down the steep slope above Dygone thus enhancing the ice flow on that side and under a regime of greater melting. Anchoring of glaciers on karst by depriving them of basal, lubricating regelation water has been observed in Norway (Lauritzen 1996).

Figure 9. Surveying carefully around soda straws in a side passage (note use of laser for distance).

4. Conclusions

While the Tupper-Raspberry System is still at an explorative stage, we can nevertheless conclude that it is a mature karst with a very high degree of development toward a full stripe geometry (γ = 78 to 105, the latter if Dygone is included). In fact it represents an end-member. Furthermore, its storeyed or tiered network is typical of a mature, Type 1 sub-vertical stripe karst. While we are uncertain of the relative age relationships of the two main sinks (Tupper and Dygone), it may be that the smaller Dygone and adjacent area of depressions represent an earlier phase of karstification. Work establishing a primarily baseline survey (Figure 9), but complemented with some spelothem dating, will be continued over the next few years.

References

Ford DC, 1967. Sinking creeks of Mount Tupper: A remarkable groundwater system in Glacier National Park. Can, Geog, XI(1), 49–52.

Hoy T, 1987. Geology of the Cottonbelt lead-zinc-magnetite layer, carbonatites and alkilic rocks in the Mount Grace Area, Frenchmans Cap Dome, southeastern BC. BC Ministry of Energy, Mines and Petroleum Resources. Bulletin 80, 43 pages.

Lauritzen S-E, 2004. Stripe karst. In: J Gunn (Ed). Encyclopedia of Caves and Karst Science. Fitzroy Dearborn, NY & London, 705–706.

Lauritzen S-E, 1981 Marble stripe karst of the Scandanavian Caladonides: An end-member in the contact karst spectrum. Acta Carsologica, 30(2), 47–79.

Lauritzen S-E, 1996. Karst Landforms and Caves of Nordland, North Norway: Excursion Guide 2. In: JE Mylroie and S-E Lauritzen (Eds). Climate Change: the Karst Record, 29–30.

Lauritzen S-E, Kyselk J, Lovlie R, 1991. A new survey of Raggejavri-Raigi and the Hellemofjord karst, Norway. Cave Science 18(3), Trans. British Cave Research Association, 131–137.

Poulton TP, Simony PS, 1980. Stratigraphy, sedimentology and regional correlation of the Horsethief Creek Group (Hadrynian, Late Precambrian) in the northern Purcell and Selkirk Mountains, British Columbia. Canadian Journal of Earth Sciences, 17, 1708–1724.

Rollins J, 2004. Caves of the Canadian Rockies and Columbia Mountains. Rocky Mountain Books ISBN 0-921102-94-1, 336 pages.

Safford K, 2010. Following the White Rabbit. BC Caver, vol. 24(4), 18–20.

Rogers JP, Coates D, 1980. Cody Cave survey. Vancouver Island Cave Exploration Group 10(8).

Thompson P, 1976. Cave exploration in Canada. A special issue of the Canadian Caver, 183 pages.

Worthington SRH, Ford DC, Beddows PA, 2000.Porosity and permeability enhancement in unconfined carbonate aquifers as a result of solution. In: A Klimchouk, DC Ford, AN Palmer, W Dreybrodt (Eds.). Speleogenesis: Evolution of Karst Aquifers. NationalSpeleological Society, Huntsville, AL, USA, 463–472.

Yonge CJ, 2013. Exploration of the Tupper Sink–Raspberry Rising Cave System. Canadian Caver #77. In press.

CAVE AND KARST PROSPECTION IN RAS AL-KHAIMAH MOUNTAINS, NORTHERN UNITED ARAB EMIRATE

Nadja Zupan Hajna[1], Asma Al Farraj Al Ketbi[2], Franci Gabrovšek[1], Metka Petrič[1], Tadej Slabe[1], Martin Knez[1], Janez Mulec[1]

[1]Karst research Institute ZRC SAZU, Titov trg 2, Postojna, Slovenia, zupan@zrc-sazu.si

[2]United Arab Emirates University, Geography Department, P.O. Box: 17771, Al Ain, United Arab Emirates, asma@uaeu.ac.ae

In January 2011, we were visiting Ras Al-Khaimah Mountains in the Northern Emirate of United Arab Emirates with the purpose to find some new caves. There are several big caves known in Oman, but none really big in the UAE. Several areas in Ras Al-Khaimah emirate on the Musandam Peninsula were surveyed, particulary in the northern part of Oman Mountain range near the border with Oman. We found several small caves on the northern slopes of Mount Al Jeer, at the entrance to Wadi Haqil and at different locations in Wadi Al-Bih and Wadi Taweeyan and also in its tributary Wadi Maai. Unfortunately we didn't find any big caves, almost all were short horizontal caves on the wadi slopes and the longest one was not even formed by solution, but was an opening along the relaxation fissure.

1. Introduction

There were many studies done on caves and karst in different areas of the Arabian Peninsula. The most extensive research has been done in Saudi Arabia (Edgell 1990; Forti et al. 2005; Kempe and Dirks 2008) and Oman where the biggest caves of the region are known. In Oman for instance were done several studies on speleothems; especially on dating and climatic changes (Fleitmann and Matter 2009; Burns et al. 1998, 2001; Sadiq and Nasir 2002).

But karst and caves in the United Arab Emirates are not very much explored. There have been only few research expeditions and the existing studies have been mainly undertaken by the Emirates Natural History Group in Jebel Hafit (Jeannin 1992; Waltham and Jeannin 1998; Fogg et al. 2002; Aspinall and Hellyer 2004).

Figure 1. Locations of our studied areas in Ras Al-Khaimah Emirate in UAE (source Google Earth).

Here are presented preliminary research results of field observations in January 2011 when our group explored and mapped few new caves and other karst features on the western slops of Musandam Mountains, which are northern part of Oman Mountains, in Ras Al-Khaimah Emirate. Our study areas were located close to the United Arab Emirates (UAE) – Oman state border, where the Musandam Mountains are over 2,000 m high. The locations of our explorations are shown on map (Fig. 1).

2. Geology

Oman and the UAE are located on the NE margin of the Arabian plate (Ricateau and Riche 1980; Kusky et al. 2005). This plate is bounded to the south and SW by the active spreading axes of the Gulf of Aden and Red Sea. On the east and west its border is marked by transcurrent fault zones. On the north the plate is marked by a complex continent–continent to continent–ocean collision boundary along the Zagros and Makran fold and thrust belts. During the Cretaceous spreading of the Tethyan Sea, Gondwana Land continued its dispersal, and the Arabian-African plate drifted northward about 10°. These events combined with the opposite rotation of Eurasia and Africa initiated the closing of the Tethyan during the Late Cretaceous. At the early stages of closure, downwarping of the Arabian continental margin combined with the compressional forces of closure from the Eurasian plate initiated obduction of the Tethyan oceanic crust along preexisting transform faults, and still hot oceanic crust was detached along oblique northeast dipping thrust faults.

The Musandam Mountains are built up of several major structural units ranging in age from Precambrian to Miocene. These include a pre-Permian Basement, the Hajar Unit, the Hawasina Nappes, the Samail Ophiolite and metamorphic sole, and the postnappe structural units. The main structure of the Musandam Mountains is a complex interaction of Late Cretaceous thrust sheets folded over the Musandam mid-Tertiary culmination, with two foreland basins developed in front of the rising mountains (Searle 1988). The Musandam Carbonates were deposited in shallow water on the Arabian continental margin. The Samail Ophiolite represents a portion of the Tethyan ocean crust formed at a spreading center of Middle Cretaceous age (Cenomanian). During the late Cretaceous the Musandam Carbonates and Semail Ophiolites were

tectonically shifted over the Hawasina Unit (Glennie et al. 1974). The Musandam Mountains are separated from the rest of the Oman Mountains by the very distinct Dibba fault zone.

The emergence and uplift of the Musandam Peninsula in the Miocene caused the initiation of the drainage network in the northern UAE. However, the UAE–Oman mountain range has only been a barrier for the last fifteen to twenty million years, which has also influenced the climatic conditions there.

In the Pleistocene, huge terraces of alluvial sediments accumulated in wadis at the feet of the Musandam Mountains (Al-Farray and Harvey 2000). The limestone mountain ranges are dissected by wadis of various sizes ranging from smaller gorges to large valleys, which present a unique image of fluvial relatively densely dissected karst. Unique caves with characteristic rock relief forms developed in their slopes.

Our studied areas were dominated by carbonate rocks of the Musandam Group (Lower, Middle, Upper Musandam limestone) of Upper Jurassic to Lower Cretaceous age, but carbonates of the Russ al Jibal Group (Bih dolomites, Haqil limestone, Ghail limestones) of Middle Permian to Middle Triassic age and of the Elphinstone Group (Milaha limestone, Ghalilah limestones and mudstones) of Upper Triassic to Lower Jurassic age may also be found (Hudson and Chattan 1995; Hudson 1960).

Thirty-nine samples were taken at 6 locations in the wider surroundings of the city of Ras Al-Khaimah to make fiftynine microscopic thin-sections that were examined from the petrological and lithostratigraphic aspects. All samples were also subjected to calcimetric analyses. The main result was that the samples are made of shallow sea carbonates which were partly recrystallized and dolomitized.

3. Hydrogeological characteristics and water quality

Hydrogeological characteristics of the UAE are significantly influenced by low amount of precipitation and high potential evaporation. The annual precipitation ranges between 15 mm in very dry years to 600 mm in extremely wet conditions. Practically all rain water drains as surface flow in a form of seasonal floods, and according to some estimation only 2 to 3% of it recharges the groundwater (Rizk and Alsharhan 2003).

Groundwater is stored in 4 main types of aquifers: karst in carbonate rocks, fissured in ophiolites, and intergranular in gravel and sand dunes. For the wadis karst aquifers of rocky slopes and intergranular aquifers of alluvial deposits are characteristic. The main source of recharge of the intergranular aquifers in Quaternary alluvial deposits, which are composed of gravel and sand with thin interbeds of silt and clay (Rizk and Alsharhan 2003), is surface water that drains in the wadis. The karst aquifers are composed of limestone and dolomite. They are recharged by infiltration of rain and discharged through karst springs at the contact with less permeable rocks or directly into the sea.

During our field work the karst springs named Khatt and MeBreda, which differ significantly in their hydrogeological characteristics, were studied in more detail. For the comparison only, the basic physical and bacteriological parameters of samples taken at the pumping station in an intergranular aquifer and in a small collector of surface water in a rocky slope of the wadi Haqil were defined additionally.

The Khatt spring with two main outflows Khatt north and Khatt south is located 15 km south of the town Ras Al-Khaimah at the extreme east of the gravel plains at the foot hills of the Northern Oman Mountains. The gravel aquifer in the plain is overlying very poorly permeable rocks of Cretaceous age (marls and shales with varying admixtures of coarse detrital debris of chert, basic igneous rocks, and limestone). The karst recharge area of the spring is composed of dolomitic limestone and limestone of Jurassic and Cretaceous age. In the period from 1979 to 2004 the average annual discharge of the Khatt north spring ranged between 1 and 60 $l.s^{-1}$, and of the Khatt south spring between 4 and 55 $l.s^{-1}$ (Wycisk et al. 2008). The oscillation of discharges clearly reflects the influence of the amount and distribution of precipitation. In dry years with low amount of rain the discharges were significantly lower. The spring with the water temperature of approximately 39 °C is used for balneological purposes.

In the MeBreda area in the rocky slope of the Wadi Shehah (a tributary to the Wadi Al-Bih) a karst spring is situated at the altitude of 710 m a.s.l. The name MeBreda is used also for the spring. At the point of a small, permanent outflow of water through a fissure in dolomite rock a group of local people built in 1925 two pools for collecting water. The location of the spring is most likely conditioned by the existence of a less permeable zone within the carbonate sequence. This enables the water storage in a small perched aquifer, which recharges a perennial spring with the discharge of several $l.s^{-1}$. Water flowing out of the fissure is first collected in the upper pool (our local guide used it as drinking water), and then flows in the lower pool (water used by goats and for irrigation of a small plantation).

Several small holes, which are artificially arranged as collectors of rain water, were seen in the rocky slope of the Wadi Haqil. One of them was partly filled with water in the time of our visit. Stored water is probably used by herds and goats as drinking water. In the nearby pumping station the groundwater is pumped from a gravel aquifer and used for irrigation of agricultural land, mostly for cultivation of date palms.

At all described locations we measured physical and chemical parameters and did basic bacteriological analyses, because drinking water in arid areas is of great concern. Already the comparison of basic physical parameters shows very different types of analyzed waters. The EC value of groundwater from the gravel aquifer is very high due to salinization. In the small collector of rain water in the rocky slope of the Wadi Haqil stagnant water was sampled, which has been altered by some additional influences.

The results show that although both, the MeBreda and Khatt springs, are recharged from karst aquifers, they differ significantly. In the MeBreda spring the anions arranged

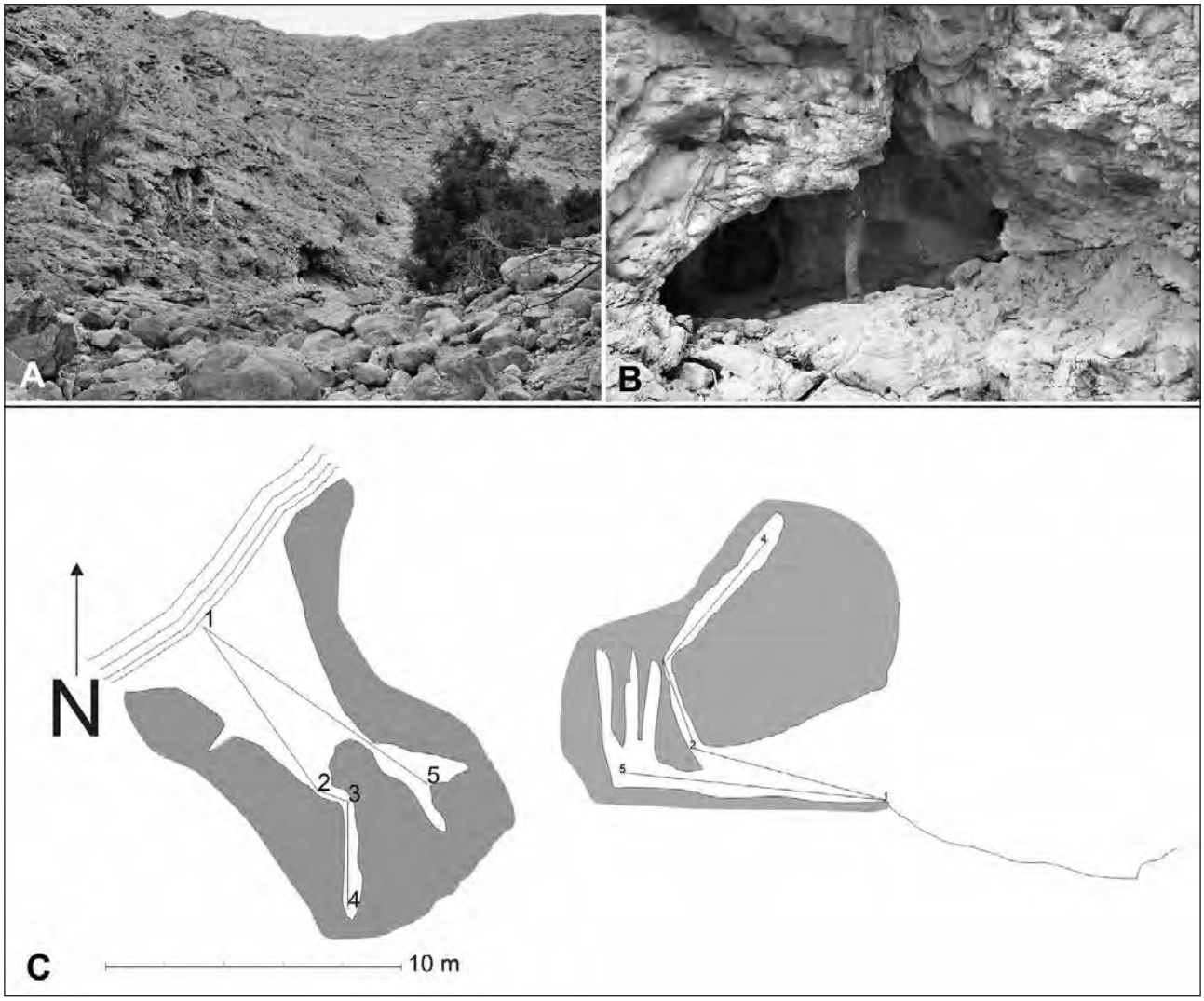

Figure 2. A) The slopes above Wadi Maai with numerous opening to the small caves; B) entrance to the largest cave; C) plan view (left) and extended elevation (right) of the cave (Photos and map - Karst Research Institute ZRC SAZU).

according to their decreasing concentrations are HCO_3^-> SO_4^{2-}> Cl^-> NO_3^-, and in the Khatt spring HCO_3^-> Cl^-> SO_4^{2-} > NO_3^-. The springs have significantly different T, EC, and concentrations of anions. Relatively low EC, the chemical composition of water, and the ratio Ca^{2+}/Mg^{2+}=1.6 in the MeBreda spring indicate an outflow from a carbonate aquifer with a larger share of dolomite. Increased concentrations of nitrates are due to grazing goats around the spring.

According to its high temperature of 38.5 °C the Khatt spring can be characterized as a thermal spring with deep circulation of groundwater. For other springs in the northern part of the UAE the temperatures of springs range from 25 to 32 °C (Wycisk et al. 2008). Viable microbes on Ridacount test plates were retrieved from all sampling sites except from water pumped from the underground which had high conductivity. Surprisingly, the traditionally collected rainwater in natural crack had low number of total bacterial count; however detected E. coli indicated probable fecal contamination of water from pasturing goats. Considering two ISO standards SIST EN ISO 9308-1 (coliforms and E. coli) and SIST EN ISO 6222 (total bacteria) none of the water from any of the tested sites matched the ISO criteria for direct human consumption.

4. Characteristics of explored caves

Even though the geology of the area has been studied thoroughly, few references report on caves and karst phenomena in UAE (Jeannin 1992; Waltham and Jeannin 1998; Fogg et al. 2002). Our primary target was mountainous region in the NE part of the emirate Ras Al-Khaimah, where some potential caves had been reported. Some of these caves came out to be small cavities or even rock shelters. As information on our work was well spread several more caves and areas with caves were reported to us by locals. Nevertheless, extended caves are not common for the area. Arid climate and local geology with relatively impure limestones and marls do not favor formation of big cave systems. Climate in Pleistocene however resulted in higher accumulation of clastic sediments in river terraces and diamicts at the wadis bottoms, probably also in some caves. Such sediments have been found in all visited wadis (Wadi Al-Bih, Wadi Taweeyan and Wadi Maai).

We first explored caves on the very eastern border with Oman on the slopes of Mount Al-Jeer where the local people knew of several cave entrances that no one had previously entered. The surface of the rock was finely and shallowly corroded, and we found several solution pans with outflow channels. We examined many small passages

along bedding planes that had developed in thin-layered limestone that alternated in places with layers of dolomite. All the passages ended after a few meters, and all narrowed characteristically from the entrance inwards. Their floors were covered with material from the walls of the passages, light grey clay, bones, and larger plant seeds.

North East from Ras Al-Khaimah a large number of small cavities and caves have been found in a hill at the entrance of Wadi Haqil. Small ridge, which rises about 45 m high from the wadi bottom is intersected by numerous cavities, small conduits and roofless caves. Looking as whole, the hill looks like a block of limestone characterized by vuggy porosity. However, caves are short, cavities unlinked and isolated. There was only one cave longer than 10 m. It is a relatively simple channel with oval cross-section. Some of the channels are fully and some partially filled with yellow clastic sediments. Also few layers of flowstone between clastic sediments and many calcite crystals were detected. Few samples were after analyzed by x-ray diffraction method in the Laboratory of Physical Methods at Institute of Geology ASCR in Prague. All samples contained quartz, gypsum and kaolinite, almost all of them also calcite, palygorskite, smectite and illite. Calcite and gypsum represent precipitates from the cave (crusts, crystals, cements) and other minerals were brought to the cave most probably by water or wind from eroded rocks and/or soils from wadi catchment area. In caves in Wadi Haqil mouse-tailed bats (Rhinopomatidae) were observed which belong to the species Rhinopoma cystops.

Along Wadi Taweeyan, for instance in the area of Jebel Al Khab and tributary wadi Maai (Fig. 2), many small cavities can be observed in several places. More or less all were short horizontal channels with some rest of fluvial sediments.

In Wadi Al-Bih we checked two tributary wadis. First was wadi Shie Haft, where was 50 m above river located bigger cave entrance. But unfortunately after few meters cave finished. There was big accumulation of debris and clays in the cave bottom.

A cave close to the top of MeBreda, above Wadi Shehah which is also tributary to Wadi Al-Bih, at 825 m above sea level, was very distinct from the others found. The cave follows a set of vertical relaxation fissures with absolutely no solutional features. A block of the massive, with well expressed fold, has separated from the plateau and is sliding into a valley (Fig. 3). The only sediment in the cave is breakdown material. We have measured about 70 m of the cave. Temperature in the cave was 17.5 °C, relative humidity 57.8 % and carbon dioxide concentration 380 ppm (January 27, 2011).

4.1. Rock relief of wadis and caves

Characteristic rock relief dissects the circumference of the special caves forming in the walls of the wadis that were studied comprehensively for the first time. The slopes of the wadis are often dissected by large recesses, relatively rare subsoil forms, and karren with microrills and rain flutes. Karren-like rock surface also occurs between wadis, and rock forms are found on rocks that have broken off from the slopes as well as on and in the sediments covering the bottoms of the wadis. More extensive karren are found on the tops of the mountains. The rocky riverbeds of wadis were shaped by rapid water currents and corrosion at the contact with sediment. Rock forms are an important trace of the formation and development of caves and karst surfaces.

Caves in wadis are located just above the sediment level and are therefore periodically flooded and dry at various levels above it. They also share similar rock relief. Ceiling pockets are found on the ceilings of niches that developed at the contacts of passages and at their sharp bends in areas of emphasized swirling of water. As a rule, their diameters do not exceed one meter but they are usually deeper, with a 1:3 ratio, and wider in the upper part. In places, pockets are also found on walls, but their lower parts are flat and their upper parts are vaulted. The lower parts were frequently covered by sediment that protected the rock from dissolving and erosion and therefore grew upwards and sideways. The walls of passages are smooth and rounded. The mechanical erosive action of water currents carrying material appears to play an important role in their formation. The ceilings of passages are usually covered by above-sediment channels that along with the paragenetically raised cross sections of passages indicate the frequent filling of caves with sediments and the flow of smaller quantities of water above them. The largest reach a depth of one meter, the consequence of the relatively long-term formation of caves of this kind and their filling with sediment. Along-sediment wall notches, up to one meter deep, indicate periodic partial filling of the caves and a long lasting sediment level in the cave. Along-sediment rock forms are the trace of relatively frequent filling of wadis with sediment and its removal.

5. Discussion and Conclusions

In our studied, very arid area, with an average annual precipitation only slightly above one hundred millimeters, of which only a small percentage recharges the groundwater, karst surface forms, caves, spring caves, and springs are rare.

The described caves along with several smaller ones show some common characteristics that could point to their origin. The passages are generally round with well expressed ceiling channels, wall and ceiling pockets, and dead ends. There are no obvious flow paths along which caves developed. In some areas the vuggy porosity resembles that found in caves of hypogene origin. However, we did not observe any other typical indicators of hypogene origin. The dimensions of passages decrease from the entrance toward the interior of caves. Most caves end with solid walls with no leads continuing into the massif. Scallops are rare or non-existent.

Detailed geological studies have shown that the significant factors for the karstification and the growth of the caves in the studied wadis were like everywhere: bedding planes and slips along them, older tectonically broken zones in the carbonate rocks, occurrence of large concentrations of calcite, contacts between dolomitized and non-dolomitized rocks, and last but not least, recent fissures and faults.

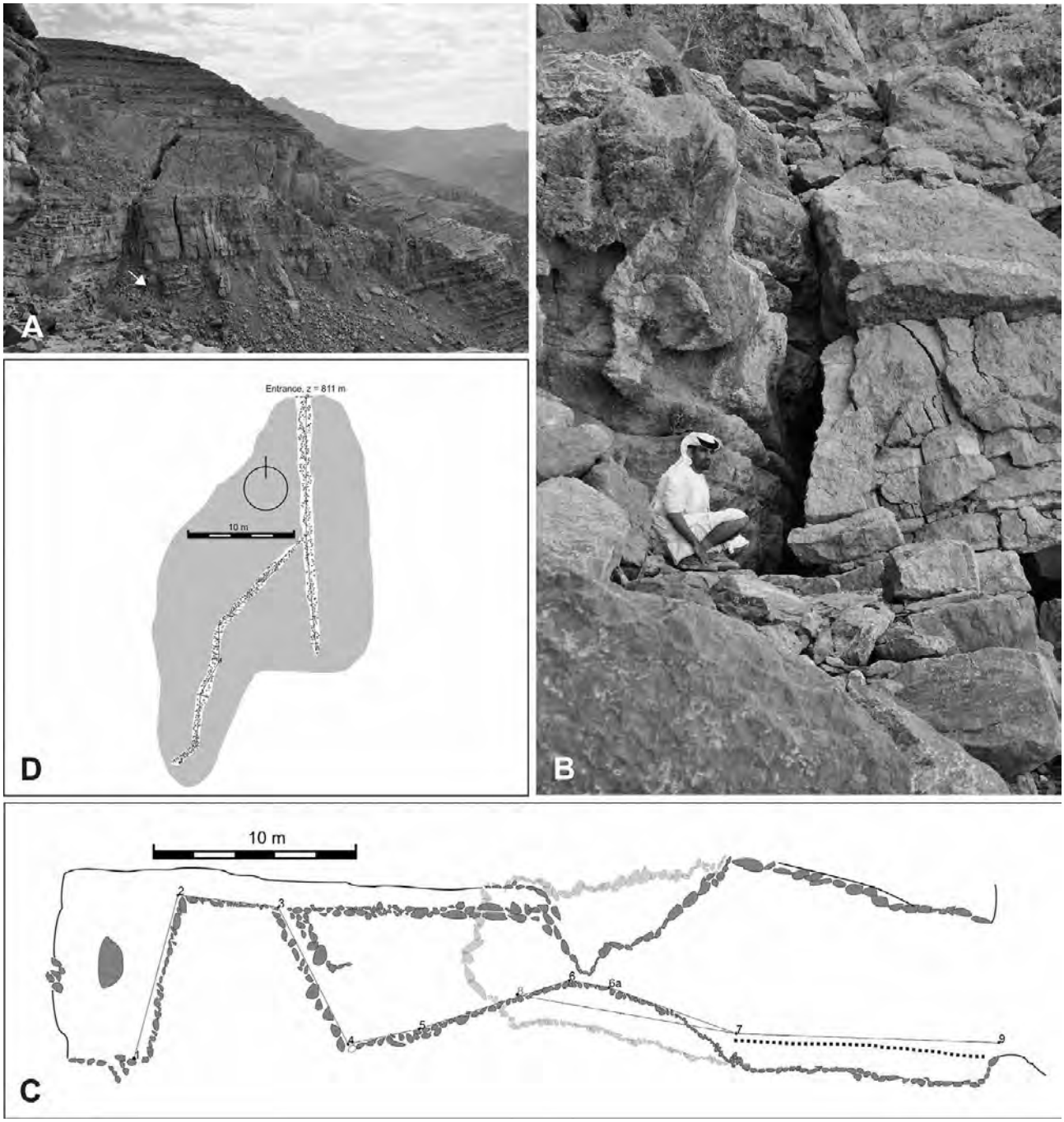

Figure 3. Mountaine at MeBreda above Wadi Shehah A) broken and fissured slope above the cave; B) entrance to the cave marked by an arrow on Fig. 3A.; C) extended elevation of the cave; D) map of the cave. (Photos and maps - Karst Research Institute ZRC SAZU).

At this stage we do not have firm arguments for any mechanism behind the origin of these caves; however, some of the characteristics mentioned above indicate that the caves originated from near-surface processes. We found and studied mainly clastic sediments. Speleothems are rare, probably due to the arid climate and the very low and diffuse infiltration from the surface. Sediment samples differ in content due to their origin in different rock. Along with fluvial cave sediments, eolian sediments and sediments of organic origin (guano, bones, seeds) are also present.

Cave rock relief and surface rock relief indicate the major significance of along-sediment and subsoil formation of the wadis and the karst between them. We can observe the development of wadis through extensive filling with sediment and rocks from the slope, the shaping of rock at the contact with sediment, and the emptying or distinct change of the sediment level. The majority of caves, including those currently located high above any sediment, were filled with sediment over a longer period. The walls on the sides of wadis commonly exhibit individual or linked cavities that resemble tafoni of various sizes. Some of these, although rare, are large enough to enter.

The general morphology of caves can be linked to floodwater patterns (e.g., Palmer 2007). The flow patterns in bed sediments of wadis are known to be very complex. The carbonate bedrock at the side of the wadis is therefore exposed to dissolution by both superficially flowing water and water flowing within the sediments. The dissolution could occur along the sediment-bedrock contact resulting in cave geometry defined by the combined action of dissolution and sediment morphology. This suggests that caves could form as the wadis develop. However, this hypothesis needs further field and theoretical verification.

The lack of fluvial sediments in the caves surely raises doubts about the genesis.

One possible explanation of why there are not many caves in the studied area of Ras Al-Khaimah is that little water penetrates the steep karst slopes of wadis, which does not create ideal conditions for the development of caves, especially in recent climate conditions. The annual precipitation values here are very low and most of the precipitation falls in the form of downpours causing major surface runoff in the mountainous areas due to large inclination of slopes and the thin-layered impure limestone with intermediate marl layers.

Acknowledgments

In January 2011, at the invitation of Prof. Dr. Asma Al-Farraj, a team from the Karst Research Institute at the Research Centre of the Slovenian Academy of Sciences and Arts went to study the karst and caves in the mountainous regions of the northeastern Emirate of Ras Al-Khaimah in the United Arab Emirates. The research was also supported by Saud bin Saqr Al Qasimi, Sheikh of the RAK Emirate. The research was supported also by the research program Karst research financed by Slovenian Research Agency.

References

Al-Farraj A, Harvey AM, 2000. Desert pavement characteristics on wadi terrace and alluvial fan surfacesWadi Al-Bih UAE and Oman. Geomorphology, 35 (2000), 279–297.

Aspinall S, Hellyer P, 2004. Jebel Hafit, A Natural History. Abu Dhabi.

Burns SJ, Fleitmann D, Matter A, Neff U, Mangini A, 2001. Speleothem evidence from Oman for continental pluvial events during interglacial periods, Geology, 29, 623–626.

Burns SJ, Matter A, Frank N, Mangini A, 1998. Speleothem-based paleoclimate record from northern Oman. Geology, 26, 499–502.

Clesceri LS, Greenberg AE, Eaton AD, 1998. Standard methods for the examination of water and wastewater. 20th Edition, American Public Health Association, Washington.

Edgell HS, 1990. Karst in Northeastern Saudi Arabia. J.K.S.A.U, Earth Science, Special issue: 1st Saudi symposium on Earth Science, Jeddah, 3, 81–94.

Fleitmann D, Matter A, 2009. External geophysics, climate and environment, The speleothem record of climate variability in Southern Arabia. C. R. Geoscience 341, 633–642.

Fogg T, Fogg P, Waltham T, 2002. Magharet Jebel Hafit – a significant cave in the United Arab Emirates. Tribulus Journal of the Emirates Natural History Group. 12, 1, 5–14.

Forti P, Galli E, Rossi A, Pint J, Pint S, 2005. Cave Minerals Of Some Limestone Caves Of Saudi Arabia. Hellenic Speleological Society. Research made within the MIUR 2002 Project "Morphological and Mineralogical Study of speleothems to reconstruct peculiar karst environments" Resp. 21–28 August 2005, Kalamos, Hellas.

Glennie KW, Boeuff MGA, Hughes-Clarke MW, Moody-Stuart M, Pilaar WHF, Reinhart BM, 1974. Geology of the Oman Mountains. Kon. Ned. Geol. Minnhoukundia Genoot. Vern., 33, 423.

Hudson RGS, Chattan M, 1959. The Musandam Limestone (Jurassic to lower Cretaceous) of Oman Arabia. Notes Memoirs. Moyen-Orient., 3, 69–93.

Hudson RGS, 1960. The Permian and Trias of the Oman peninsula, Arabia. GeologicaMagazine, 97, 299–308.

Jeannin P-Y, 1992. Expedition suisse aux Emirats Arabes Unis. Stalactite (Switzerland), 42(1), 47–55.

Kempe K, Dirks H, 2008. Layla Lakes, Saudi Arabia: The World-wide largest lacustrine Gypsum Tufa. Acta Carsologica, 37(1), 7–14.

Kusky T, Cordula Robinson C, El-Baz F, 2005. Tertiary–Quaternary faulting and uplift in the northern Oman Hajar Mountains. Journal of the Geological Society, 162, 871–888.

Palmer AN, 2007. Cave Geology. Cave Books, Dayton, OH.

Ricateau A, Riche PH, 1980. Geology of the Musandam peninsula (Sultanate of Oman) and its surroundings. Journal of petroleum geology, 2(3), 139–152.

Rizk ZS, Alsharhan AS, 2003. Water resources in the United Arab Emirates. In: Alsharhan AS, Wood WW (Eds.) Water Resources Perspectives: Evaluation, Management and Policy, Elsevier, 245–264.

Sadiq AM, Nasir SJ, 2002. Middle Pleistocene karst evolution in the State of Qatar, Arabian Gulf. Journal of Cave and Karst Studies, 64(2), 132–139.

Searle MP, James NP, Calon TJ, Smewing JD, 1983. Sedimentological and Structural evolution of the Arabian continental margin in Musandam Mountains and Dibba zone, U.A.E. Geological Society of America, Bulletin, 94, 1381–400.

Waltham AC, Jeannin PY, 1998. Forum: Caves in the United Arab Emirates. Journal Cave and Karst Science, 25(3), 149.

Wycisk P, Al Assam M, Akram S, Al Mulla M, Schlesier D, Sefelnasr A, Al Suwaidi NB, Al Mehrizi MS, Ebraheem A, 2008. Three-dimensional geological and groundwater flow modelling of drought impact and recharge potentiality in Khatt springs area, Ras Al Khaimah Emirate, UAE. In: WASTA 8th Gulf Water Conf., Bahrain, Proceedings, 1–14.

INFLUENCE OF THE PLEISTOCENE GLACIATIONS ON KARST DEVELOPMENT IN THE DINARIDES – EXAMPLES FROM VELEBIT MT. (CROATIA)

Neven Bočić[1], Sanja Faivre[2], Marijan Kovačić[3], Nada Horvatinčić[4]

[1]University of Zagreb, Faculty of Science, Department of Geography, Marulićev trg 19/II, HR-10000 Zagreb, Croatia, nbocic@geog.pmf.hr

[2]University of Zagreb, Faculty of Science, Department of Geography, Marulićev trg 19/II, HR-10000 Zagreb, Croatia, sfaivre@geog.pmf.hr

[3]Marijan Kovačić, University of Zagreb, Faculty of Science, Department of Geology, Horvatovac bb, HR-10000 Zagreb, Croatia, mkovacic@geol.pmf.hr

[4]Nada Horvatinčić, Ruđer Bošković Institute, Division of experimental physics, Laboratory for Measurements of Low-level Radioactivity, Bijenička 54, HR-10000 Zagreb, Croatia, Nada.Horvatincic@irb.hr

Traces of the Pleistocene glaciations in the Dinarides have attracted attention of many researchers. Thus in the Velebit Mt. area in Croatia numerous surface traces of ice influence were explored (destructive and accumulation). As Velebit is dominantly composed of carbonate karstified rocks the interaction between glacial and karst processes is expressed. Such phenomena are visible on the surface and in the karst underground. The aim of this paper is to explore this interaction on three examples in northern and central Velebit Mt.

1. Introduction

Velebit Mt. is a part of the Dinaric karst mountain range. It is located in Croatia and extends to the length of 145 km along the northern part of the eastern coast of the Adriatic Sea. The highest peak is 1,757 m high. Velebit mostly consists of karstified carbonate rocks (limestone, dolomite and breccias consisting of carbonate rock fragments). Former glaciation of this region has long attracted researchers (e.g., Hranilović 1901; Gavazzi 1903). Studies have shown that a large part of the area was affected by the Pleistocene glaciations. The best preserved glaciations traces in landscape are from the last glaciation period – Würm. Studies of these glaciations were more detailed in the southern Velebit area (e.g., Nikler 1973). Glaciation of north Velebit was first studied by Bauer (1935), while the central Velebit glaciations were less known. Research of the glaciations of northern and central Velebit were particularly intensified during the past twenty years (Bognar et al. 1991; Bognar and Faivre 2006; Velić et al. 2011). In those works they found morphological traces of different types of glaciers, and the surface morphology evidence of their propagation (denudation phenomena and material accumulation in moraines). These results have prompted questions about the impact of glaciation on the development of karst, especially the underground karst formations – caves in this area. This question has been studied so far in the areas outside the Dinarides (e.g., Glover 1977; Kunaver 1983; Mylroie 1984; Audra 2000; Woodward and Goldberg 2001).

2. Aims and methods

This paper explores the impact of the Pleistocene glaciations on the karst development in northern and central Velebit. Special emphasis has been given to the research of the impact of the glaciations on the development and morphology of the caves in the area (Fig. 1). The main methods used in this study were geomorphological mapping and speleological research. Also, some sedimentological methods were used and dating of the flowstone crust was provided. It was sampled and dated by the ^{14}C method in the Laboratory for Low-Level Radioactivity at Ruder Boskovic Institute. The measurements were carried out with a Liquid Scintillation Counter, Quantulus 1220, using the benzene synthesis method (Horvatinčić et al. 2004).

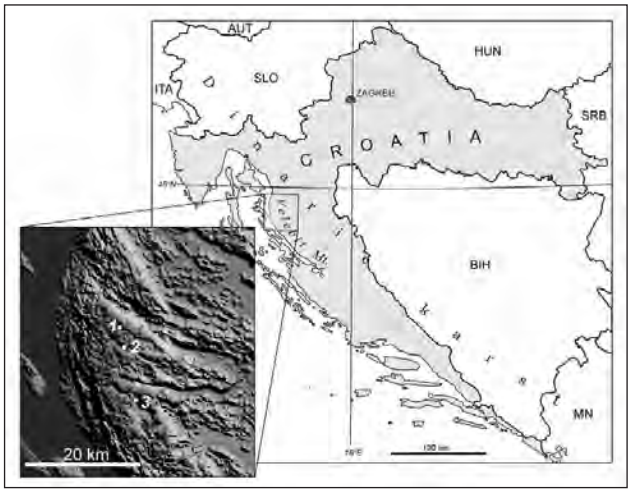

Figure 1. Location of the researching sites: 1 – Jezera area; 2 – Ledena jama u Lomskoj dulibi (Ledena Ice Cave); 3 – Štirovača Ice Cave.

3. Results

The paper presents two examples of northern Velebit, and one which is in the border area of northern and central Velebit. In the area of Jezera (*Lakes* in Croatian, ~1,400–1,500 m a.s.l., Fig. 1) it was noticed that the moraine material (which is relatively impermeable) affected the appearance of small occasional streams. These streams cause cutting in small torrents and increase the surface erosion processes in karst environment. In the areas where

the moraine cover is thinner or missing rekarstification of bedrock is visible, and occasional short streams sinking at the contact zone of the moraine material and bedrock (Jurassic carbonate rocks). In this way several small blind valleys were formed.

In the glacial valley Lomska duliba (Fig. 1) is the Ledena jama (Ledena Ice Cave), 536 meters deep, characterized by ice accumulation thicker than 50 m. During this study we mapped the moraine forms along the valley and found that the same material plugged entrance part of the cave (Bočić et al. 2012a). The entrance to the cave is located on the route of the former glacier at 1,256 m a.s.l.). Morphology and sediment traces indicate that the water flow (from melting ice) was sinking into the cave. So, the entrance part of the cave was filled with glacial and fluvio-glacial materials. In this way, the former canyon of the incoming surface water flow is now completely filled (Fig. 2). Based on the residue of moraine material one can conclude that the entrance part of the cave was filled with more quantity of that material and perhaps even the whole entrance part of the cave was completely filled. In the cave channel that is below these materials (at the depth of 60 m) the sample of speleothem was taken and dated with $^{230}Th/^{234}U$ method. There was assessed the age of 301,000 ± 55,000 years BP (Jelinić et al., 2001). It suggests that glaciations older than Würm also had the influence on the genesis of the cave.

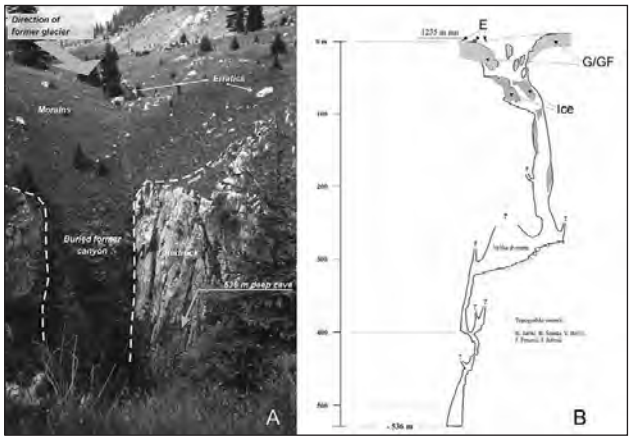

Figure 2. Ledena jama u Lomskoj dulibi (Ledena Ice Cave): A – Entrance with moraine material, erratic and buried canyon, B – Survey of the cave, GF/G – glaciofluvial and glacial material, E – erratics (cave topography according to Jelinić et al. 2001).

Great influence on the development of glaciation surface and underground karst forms was studied in Štirovača (middle Velebit area). Here is the 351 m long Štirovača Ice Cave with abundant erosional remnants of the fluvioglacial deposits that fully filed much of the known part of the cave in the past (Bočić et al. 2012b). Coarse-grain clastic sediments, generally rarely present, have been discovered in this cave (Fig. 3). They occur as erosional residues and pebbles are cemented with calcitic cement. This sediment is defined as a coarse-grained, moderately to weakly sorted, porous, polymictic ortoconglomerate, and formed by sedimentation resulting from polyphased torrential flows. We may presume that we are dealing with sediments of fluvioglacial origin, i.e. with material that was transported from the fluvioglacial fans, and which was finally sedimented in the cave's channels. On the northern edge of the cave another sedimentary body has been found, 20–40 cm thick, which has been defined as limestone debris. The sediment is mainly composed of unrounded limestone fragments, rarely of sandstone fragments and pelitic pebbles. The material is moderately sorted. The upper part of this sediment body is covered with a flowstone layer. The presented results show that all the sediments are of different ages. Based on the age of the flowstone crust of 8,230 ± 150 years BP, as well as on its position, it may be concluded that coarse-grain clastic sediment and limestone debris are older. Based on the sedimentological properties, primarily on their cementation properties, it can be assumed that limestone debris is significantly younger then the fluvioglacial fan material. This indicates that the fluvioglacial fan cannot be related to the Würm/Holocene transition, although we may presume that the limestone debris was deposited at that time. During cold periods, glacial exaration produced a particularly significant quantity of sediments. Consequently, the underground karst conduits situated below the snow line during the Pleistocene were filled with high-energy sedimentary structures, glacial and fluvioglacial sediments. That reduced or even stopped their conduit function, and led to difficulties in the drainage of meteoric water, to lake formation within morphological depressions and to a rise in the local water-table level. With the denudation of these deposits, conduit reactivation and a drop in the underground water level occurred. Stabilisation during milder climatic conditions led to aggradation of the cave and to deposition of the flowstones from 8,230 ± 150 years BP.

Figure 3. The coarse-grain clastic sediments in the Štirovača Ice Cave.

4. Conclusions

It can be concluded that the Pleistocene glaciation had multiple effects on the development of karst in this area. Moraine deposits, relatively impermeable, promote local development of surface runoff and erosion. In this way, they temporarily slow down the process of karstification below, but because of the contact process they accelerate karstification along their edges. Moraine-derived material can also be accumulated in the caves, directly or after resedimentation as fluvioglacial material. In this way it fills the underground channels and then reduces and hinders drainage function of these channels. These studies are being continued.

References

Bauer B, 1935. Uber des Nordlichen Velebit.- Jahresber des Bundesrealgymnasium in Knittenfeld, 35–37.

Bočić N, Faivre S, Kovačić M, Horvatinčić N, 2012a. Uloga pleistocenske oledbe na razvoj krša na području Velebita. Znanstveno-stručni skup "Posebne vrijednosti dubokog krša", Krasno, 21.–22. 4. 2012. Book of Abstact, 27–28.

Bočić N, Faivre S, Kovačić M, Horvatinčić N, 2012b. Cave development under the influence of Pleistocene glaciation in the Dinarides – an example from Štirovača Ice Cave (Velebit Mt., Croatia). Zeitschrift für Geomorphologie, 56(4), 409–433.

Bognar A, Faivre S, Pavelić J, 1991. Tragovi oledbe na Sjevernom Velebitu. Geografski glasnik, 53, 27–39.

Bognar A, Faivre S, 2006. Geomorphological Traces of the Younger Pleistocene Glaciation in the Central Part of the Velebit Mt. Hrvatski geografski glasnik, 68(2), 19–30.

Gavazzi A, 1903. Trag oledbe na Velebitu. Glasnik Hrvatskog naravoslovnog društva, 14, 174–175.

Glover RR, 1977. A conceptual model of cave development in a glaciated region. – 7th International Congress of Speleology, Proceedings, 220–221.

Horvatinčić N, Barešić J, Krajcar Bronić I, Obelić B, 2004. Measurement of low ^{14}C activities in Liquid Scintillation Counter in the Zagreb Radiocarbon Laboratory. Radiocarbon, 46, 105–116.

Hranilović H, 1901. Geomorfološki problemi iz Hrvatskog krasa, Glasnik Hrvatskog naravoslovnog društva, XIII(1–3), 93–133.

Jelinić I, Horvatinčić N, Božić V, 2001. Ledena jama u Lomskoj dulibi. Senjski zbornik, 28, 5–20.

Kunaver J, 1983. Geomorphology of the Kanin Mountains with special regard to the glaciokarst. Geografski zbornik, 22 201–344.

Mylroie JE, 1984. Pleistocene climatic variation and cave development. Norsk Geografisk Tidsskrift, 38(3–4), 151–156.

Nikler L, 1973. Novi prilog poznavanja oledbe Velebita. – Geološki vjesnik, 25, 109–112.

Velić J, Velić I, Kljajo D, 2011. Sedimentary bodies, forms and occurrences in the Tuderevo and Mirevo glacial deposits of northern Velebit (Croatia). Geologia Croatica, 64(1), 1–16.

Woodward JC, Goldberg P, 2001. The sedimentary records in Mediterranean rockshelters and caves: archives of environmental change. Geoarchaeology: An International Journal 16, 327–354.

CONTRIBUTION OF THE KARSTIC ENVIRONMENT ON THE ORIGIN OF THE COLLOPHANITES OF ITATAIA URANIUM-PHOSPHORUS DEPOSIT, BORBOREMA PROVINCE, BRAZIL

José Adilson Dias Cavalcanti[1], Cesar Ulisses Vieira Veríssimo[2], Maria Dulcinea M.R. Bessa[3], Clovis Vaz Parente[4]
[1]Geological Survey of Brazil, Av. Antônio Sales, 1418, Fortaleza-CE, Brazil, jose.adilson@cprm.gov.br
[2]Federal University of Ceará, Pici Campus, Fortaleza-CE, Brazil, verissim@ufc.br
[3]Geological Survey of Brazil, Av. Antônio Sales, 1418, Fortaleza-CE, Brazil, dulcinea.bessa@cprm.gov.br
[4]Federal University of Ceará, Pici Campus, Fortaleza-CE, Brazil, clovis@ufc.br

The U-P Itataia deposit, which occurs in the northern portion of the Borborema Province, northeastern Brazil, has the largest uranium reserves in the country. It is a phosphate deposit which has byproduct uranium. However, there is no uranium mineral. All uranium content is in the apatite structure in the micro- to cryptocrystalline masses called collophanites. The collophanites hosted in dolomitic marbles of Alcantil Formation of the Neoproterozoic age, belonging to the Ceará Complex. These collophanites occur as massive bodies very porous filling brittle faults and fractures, fractures at the edges as part of calcite veins, the walls of open fractures with botrioidal habit, filling voids in epissienites dikes hosted in marble and as fragments filling karst features.

The origin of the deposit remains enigmatic to this day. The genetic models for the source of the mineralizing fluids points to two main strands: hydrothermal with magmatogenic source or metamorphic-hydrothermal with sedimentogenic source, both with late supergene enrichment by karstification. The karstification phase is marked by a profile of supergene alteration that reaches up to 300 meters deep, with precipitation of collophanites in fracture zones in subaqueous environment of low temperature. The collophanites normally exhibit botryoidal habit characteristic of subaqueous environments. It's composed mainly of fluorapatite, but may contain newly formed calcite and fragments of preexisting minerals (feldspar, hornblende, biotite and opaque minerals). The content of P_2O_5 may be above 25 % and the contents of U_3O_8 are averaged 0.23 %.

1. Introduction

The Itataia uranium-phosphorus deposit was discovered in 1976 by NUCLEBRÁS during Canindé Project, from a radiometric anomaly located in Santa Quitéria, Ceara, northeastern Brazil. From the discovery were conducted geophysical surveys, geological mapping, 37,000 m of diamond drilling, 1,270 m of galleries and several wells.

Total reserves of the deposit are estimated at 9 million tons of phosphate and 80,000 tonnes of uranium. In addition to the reserves of phosphate and uranium, the field also has potential for explotation about 32 million tonnes of marble. The richest ore has P_2O_5 content of 21.2 %, intermediate 11.8 % P_2O_5 and the poor ore 2.5 % P_2O_5 is discarded in the tailings pile (Source: FIEC, 2008). From laboratory tests and pilot plant expected to yield a final concentrate of 34.4 % P_2O_5 and 0.228 % of U_3O_8 (Vidal et al. 2005).

The mineralization occur in the setentrional domain of the Borborema Province in metasedimentary sequence of passive margin of Neoproterozoic, metamorphismsed in amphibolite facies and individualized as Itataia Group which is formed by a sequence that is divided into four units, from bottom to top by: i) migmatites and gneisses, ii) quartzites, iii) migmatitic paragneisses, iv) marbles, Bt gneisses and calc silicates rocks (Figs. 1 and 2). Mendonça et al. (1982) assigned the following names for these formations: Serra do Ceú, Laranjeiras, Barrigas and Alcantil. The mains uranium-phosphorus bodies hosted in marbles of the Alcantil Formation. The Alcantil formation is composed for gray to white marble with green horizons of pure calcitic marbles or nearly pure, passing dolomitic marbles and even more impure types rich in pyroxene, hornblende, biotite-phlogopite, calcic plagioclase, garnet, quartz, titanite and scapolite, marking the gradual passage between the carbonate sequence and gneiss on the top. The presence of this lithological association could indicate that the mineralization is related with the deposition of marine or paralic restricted platform (Castro 2005).

The Itataia phosphorus-uranium deposit has complex geometry, but two bodies were individualized. The main ore body of ellipsoidal shape occurs at an elevation, with dimensions 800 m × 400 m and a depth of 180 m, with east plunge. The other ore body is elongated in the NW direction, withextension of approximately 800 m and depth ranging from 100 m to 200 m. The ore bodies are collophanites that occur in different forms and associations, but preferentially hosted in marbles and calc silicates rocks (Castro et al. 2005). Regarding the typology of collophanites main body, defined the following types: solid; botrioidal, filling open fractures; fragmented, filling karst features (paleokarst); thin vein; and disseminated in the host rocks and episyenites.

2. Climate and Physiographic Features

In Ceará state, the tropical hot semi-arid occurs in 68 % of its total area (IPECE 2008). Other climatic types also occur in the state in potions more restricted, as is the case in tropical hot semi-arid mild that occurs in the south, north and northwest of the state. Already, the tropical hot and humid and sub-humid tropical wet subquente, are restricted to the Baturité and Ibiapaba saws.

The relief in the Ceará were defined five geomorphological

units that are related to geological (lithology and structure), paleogeographic, climatic and environmental variables. These units are the coastal plain, the glacis pre-coastal, sertanejos highlands, waste massive and hinterland depressions (IPLANCE 1995). Making a correlation between morpho-structural compartments defined from SRTM image of the IBGE (www.ibge.gov.br) were earmarked by three compartments: hinterland depression with elevations below 400 m, the sertanejo plateau with elevations between 401 m and 600 m and massive waste with altitudes between 601 m and 850 m.

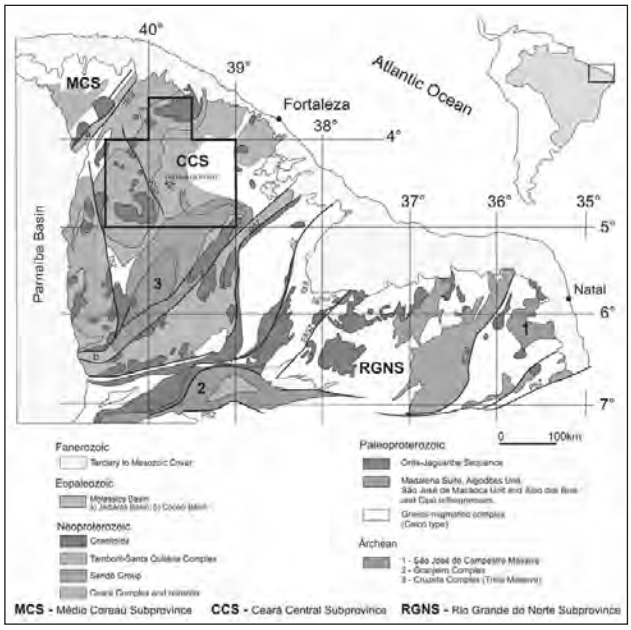

Figure 1. Setentrional portion of Borborema Province with the location of Itataia deposit (compiled and modified of Arthaud et al. 2008).

3. Methods

The field activities were conducted geological profiles, surface sampling and diamond core samples. Subsequently, thin and polished thin sections were prepared and were analyzed by optical microscopy and scanning electron microprobe. Geochemical whole rock analyzes were also performed for major oxides, trace and rare earth elements.

The microprobe used was a Cameca SX50 with 4 WDS spectrometers and a spectrometer Kevex EDS, of the Mineralogy and Petrography Department, Brasília University. The whole rock geochemical analyzes were performed at SGS Geosol, Brazil. We analyzed the major oxides (SiO_2, TiO_2, Al_2O_3, Fe_2O_3, MgO, CaO, MnO, Na_2O, K_2O P_2O_5) by fusion with lithium metaborate determination by ICP-ES and minor, trace and rare earth elements including (Ba, Be, Co, Cs, Ga, Hf, Nb, Rb, Sn, Sr, Ta, Th, U, V, W, Zr, Y, La, Ce, Pr, Nd, Sm, Eu, Gd, tb, Dy, Ho, Er, Tm, Yb, Lu) by fusion with lithium metaborate determination by ICP-MS. The elements Mo, Cu, Pb, Zn, Ni, As, Cd, Sb, Bi, Ag, Au, Hg, Tl and Se were held open by dilution with aqua regia and determination by ICP-MS.

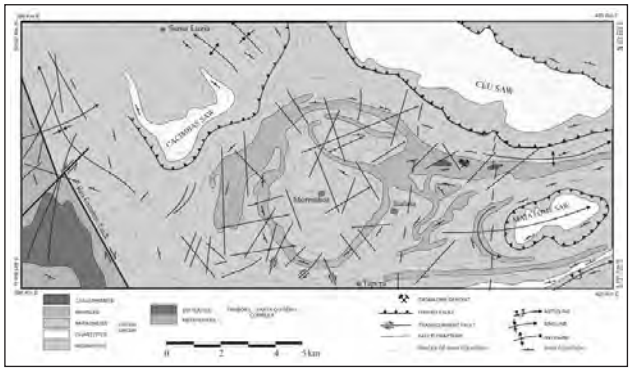

Figure 2. Geologic setting and localization of Itataia ore deposit (Modified of Angeiras, 1988).

4. Results

4.1. Field and Petrography

The collophanites are epigenetics and confined mainly in marbles and secondarily in calc-silicate rocks belonging to metasedimentary sequence of sillimanite-garnet-biotite gneisses, marbles, quartzites and calc-silicate rocks, locally designated Itataia Group and regionally disigned Ceará Complex (Fig. 2). It is a rock composed essentially of collophane (or microcristaline apatite), fine-grained, homogenous texture, reddish brown color, has cavities filled with powdery material and carbonates, exhibit massive, botryoidal and fragmented aspects (Figs. 3, 4, 5 and 6).

These collophanites occur as massive lenticular lodes filling large cavities, and as veins and veinlets arranged in stockwork (Fig. 3), and filling open fractures, border of calcite veins in contact with marbles, and also in the main foliation planes and voids filling episyenites bodies. Marble filled fractures by collophanite of the main ore body are preferentially N5°–15°E and N40°–45°E (Alcântara e Silva, 2003). Another mode of occurrence is lithic fragments in breccias and filling cavities of karstic marbles (Fig. 6).

Under the microscope, the collophanites has reddish brown, fine-grained (Fig. 7), light displays scores (carbonate and feldspar altered) and dark (amphibole, pyroxene and opaque minerals). It comes in a massive way, botryoidal, stockwork and veining. Often, displays or empty cavities filled with secondary material, such as calcite, clay or silica finely granulated. It consists essentially of a mass of micro- to cryptocrystalline brownish coloration of collophane that may contain feldspar, pyroxene, amphibole and accessory phases such as carbonate and titanite, apatite and opaque, subordinate.

The other peculiar form of collophanite occurrence is filling voids in episyenites dikes. The episyenites rock is a coarse-grained to pegmatoide texture, vesicular, with pinkish to reddish mainly composed of albitized feldspar. The vacuoles, which in the literature are described, as a result of desilicification are usually filled by collophane and carbonate. In blade exhibit granular texture and consisting essentially of large crystals of albitized feldspars (80%) and subordinately for collophane. The opaque minerals occur in ancillary quantity and carbonate is secondary. The plagioclase feldspar is represented by albitized like crystals, altered to sericite and clay minerals. Apatite (collophane) has a dark color due to the presence of oxidizing material filling the interstices between larger crystals of feldspar and the edges of the cavities (Fig. 8). Calcite also occurs filling cavities and also as a product of alteration of plagioclase.

4.2. Mineral Chemistry

Apatite is a generic term used to describe calcium phosphates with simplified formula $Ca_5(PO_4)_3$ X (where X = F, Cl, OH). Since a long time (1856–1860), has been called fluorapatite, and hydroxyapatite cloroapatita, depending on the predominance of anion X-(Pasero et al. 2010). Currently, the IMA (International Mineralogy Association) has inserted several mineral species within the apatite supergroup, which was divided into 5 groups (Apatite, Hedyphane, Belovite, Britholite and Ellestadite). The apatite group is composed of apatite-(CaF), apatite-(CaCl) and apatite (CaOH), having the following idealized formula $Ca_5 (PO_4)_3F$, $Ca_5 (PO_4)_3$ Cl and $Ca_5 (PO_4)_3OH$, respectively.

Figure 3. Outcrop of marble of Alcantil Formation with collophanites filling fractures.

The collophanite is a rock composed essentially of microcrystalline apatite. In Itataia deposit occur apatite-(CaF), known as fluorapatite, with content of F between 4.1–2.6% and Cl < 0.1% (Table 1). The content of MnO is less than 0.07% and Fe > 1% and S (expressed as SO3%) < 1%. The presence of Fe and S in the apatite may be related to the redox conditions of the mineralizing fluid, oxidizing the ore. SO occurs as $SO4^{-2}$ which is easily replaced by the $(PO_4)^{-3}$ in the apatite (Pasero et al. 2010). In collophanites of Itataia $SO4^{-2}$ is relates with an increase of FeO.

There is also a strong correlation between sodium (Na_2O), strontium (SrO) and uranium (UO_2). With increasing contents of Na_2O and SrO, is also increased UO_2.

4.3. Geochemistry

The whole rock geochemical analyzes showed the phosphate content of collophanite that occurs almost always

Figure 4. Detail of outcrop of marble of Alcantil Formation with collophanites filling fractures.

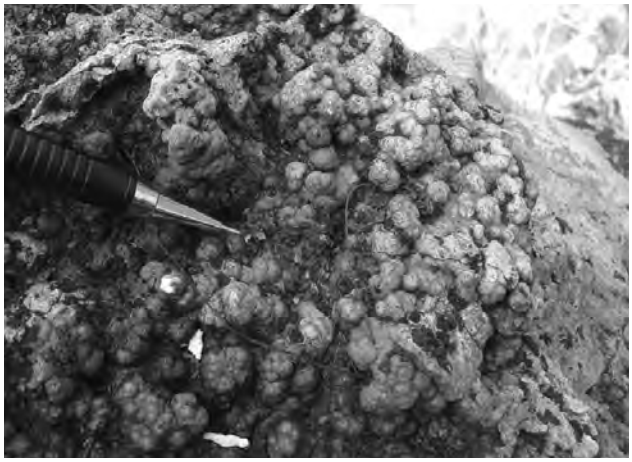

Figure 5. Botryoidal collophanite on the top of main ore body of Itataia deposit.

Figure 6. Paleokarst features in marble, such as conduits, filled with fragments colofanito in clay matrix.

above 25% in the samples richest and around 20% in the samples poorest. The content of P_2O_5 increasing with of increasing CaO and decreasing of SiO_2. Already uranium (3,689–1,582 ppm) has positive correlation with Fe and Mg. The samples richer in MgO and Fe_2O_3, also have a higher content of uranium (Tables 2 and 3).

In relation to REE, the collophanites are enriched by up to 100 times chondrite standard, planar displays, slightly enriched in light rare earth elements relative to heavy and has a mild anomaly of Eu (Fig. 9). In relation to the trace elements, have U and P positive anomalies and K, Zr, Ti negative (Fig. 10).

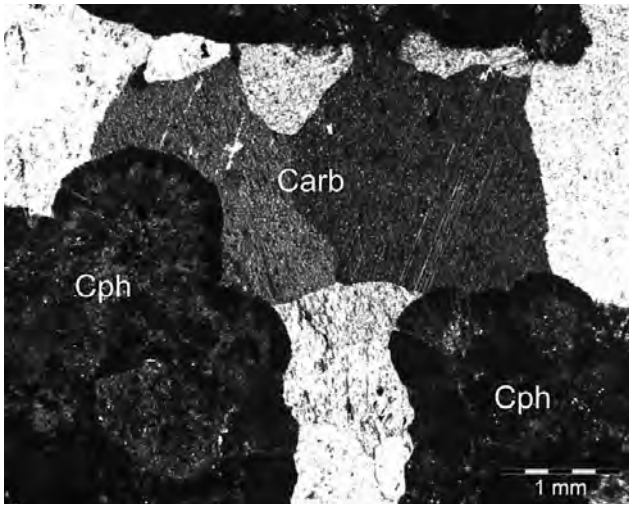

Figure 7. Microphotograph showing botryoidal collophanite associated with calcite veins hosted in marble.

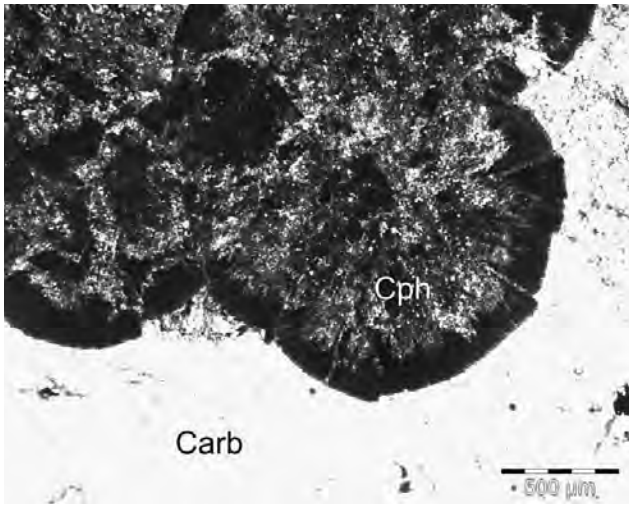

Figure 8. Microphotograph showing detail of botryoidal collophanite associated with calcite veins hosted in marble.

Table 1. Mineral chemistry of apatite.

SAMPLE	P2O5	CaO	FeO	MnO	Na2O	SrO	Nb2O5	UO2	F	Cl	SO3	Total
1	41,76	55,05	0,04	0,00	0,01	0,07	0,16	0,09	3,78	0,01	0,00	99,79
2	40,73	54,84	0,08	0,00	0,00	0,03	0,00	0,01	3,87	0,07	0,01	98,28
3	40,52	54,78	0,04	0,00	0,01	0,00	0,00	0,01	4,10	0,09	0,07	98,12
4	40,31	52,81	0,09	0,02	0,27	0,22	0,12	0,12	2,66	0,00	0,08	95,68
5	40,05	53,46	0,03	0,06	0,25	0,34	0,37	0,06	3,30	0,02	0,13	96,84
6	40,01	53,29	0,01	0,06	0,26	0,26	0,03	0,01	3,11	0,01	0,16	96,06
7	39,97	53,26	0,04	0,04	0,18	0,32	0,00	0,16	2,74	0,02	0,09	95,76
8	39,46	53,59	0,15	0,01	0,38	0,60	0,02	0,19	3,38	0,01	0,35	96,83
9	39,42	53,61	0,07	0,00	0,23	0,14	0,17	0,01	2,91	0,01	0,12	95,54
10	39,39	52,25	0,67	0,02	0,71	0,26	0,22	0,52	2,99	0,02	0,34	96,49
11	38,67	52,33	0,39	0,05	0,76	0,44	0,00	0,30	2,93	0,01	0,36	95,38
12	38,62	53,49	0,35	0,03	0,39	0,74	0,72	0,28	3,52	0,01	0,39	97,80
13	38,60	53,09	1,03	0,02	0,39	0,53	0,25	0,10	3,30	0,02	0,42	96,51
14	38,45	51,86	0,33	0,05	1,09	0,50	0,00	0,67	3,38	0,01	0,66	95,72
15	38,31	52,64	0,43	0,00	0,57	0,40	0,00	0,10	3,45	0,01	0,36	95,00
16	37,38	52,85	0,33	0,01	0,59	0,66	0,18	0,00	3,62	0,04	0,53	95,04
17	36,87	49,22	3,39	0,00	0,79	0,57	0,00	0,30	3,26	0,02	0,39	95,15
18	36,27	52,33	0,63	0,02	1,11	0,75	0,13	0,11	3,73	0,01	0,58	95,37
19	36,24	48,81	1,55	0,04	1,41	0,47	0,00	0,51	2,90	0,00	1,05	95,21

Table 2. Lithogeochemistry of oxides in collophanites.

P2O5	CaO	SiO2	TiO2	Al2O3	Fe2O3	MnO	MgO	Na2O	K2O	LOI	Sum
>25	43,1	13,8	0,3	1,4	3,5	0,1	2,3	0,4	<0.01	7,47	98,66
>25	44,0	12,4	0,1	1,4	4,5	0,0	1,0	0,5	0,3	2,9	98,75
21,1	31,9	22,3	0,5	6,6	3,9	0,1	3,9	2,1	1,3	4,09	97,66
20,1	44,6	12,0	0,1	1,8	2,5	0,1	1,1	1,3	0,1	11,95	95,68
>25	42,5	13,6	0,1	1,6	2,5	0,1	1,7	1,0	0,1	6,62	97,41
>25	52,0	6,3	0,0	0,2	1,2	0,0	0,0	0,4	0,0	1,15	97,34
>25	44,1	12,8	0,2	1,8	2,4	0,0	2,0	1,5	0,0	1,59	99,77

Table 3. Lithogeochemistry of REE in collophanites.

	1	2	3	4	5	6	7
	3689	1913	1822	1685	1602	1542	973,9
La	37,8	43,2	63,1	61,7	27,9	102,8	9,4
Ce	101,9	83,6	146,8	180,6	59,7	238	19,9
Pr	13,52	8,75	18,57	25,8	7,36	33,57	2,5
Nd	66,2	34,1	92,8	129,6	33,7	163	11,8
Sm	20,9	8,2	28,2	40,1	10,2	49,9	3,2
Eu	4,43	2,23	6,2	8,14	3,33	10,23	1,02
Gd	22,35	9,36	28,42	39,87	11,81	49,86	4,43
Tb	4,2	1,73	4,54	6,37	2,25	8,07	1,02
Dy	31,96	12,16	29,73	46,74	20,06	58,54	9,49
Ho	8,18	2,71	6,54	13,19	5,91	14,17	3,03
Er	32,8	10,28	20,54	60,31	24,98	48,83	14,98
Tm	6,51	2,29	3,52	12,32	5,27	8,66	3,31
Yb	53	25,1	28,1	103,1	46,3	62,1	29,6
Lu	6,39	3,68	3,51	12,59	5,92	7,21	4,94

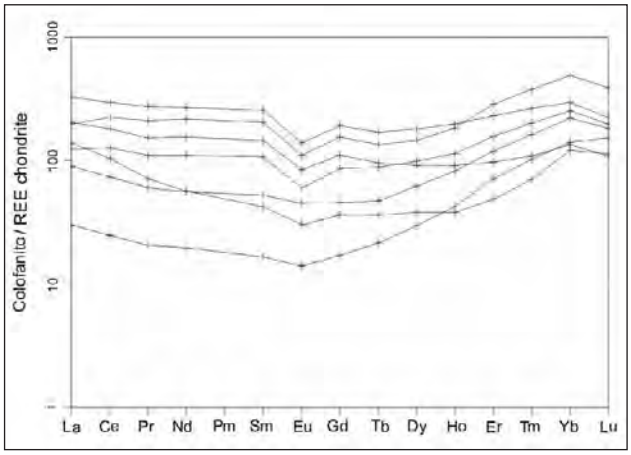

Figure 9. Diagram of rare earth elements for collophanites, according Boynton 1984.

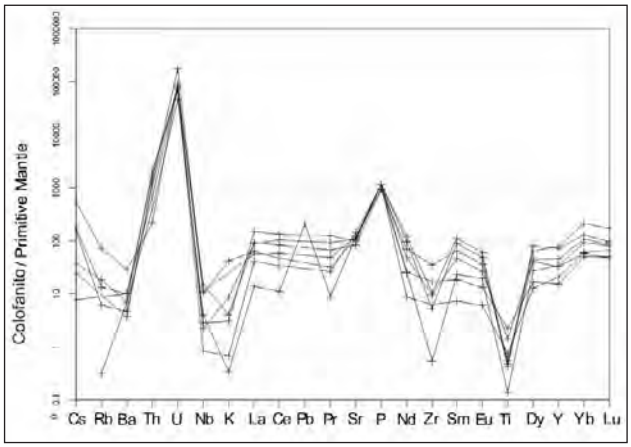

Figure 10. Diagram of trace elements for collophanites, according to Sun and McDonough (1989).

5. Discussion and Conclusions

In the study area, the intense magmatism that occurred in the period between the Neoproterozoic and Cambrian marked the evolutionary history of the Province Borborema. This story begins with the collision of cratons West Africa and São Luis, around 660 Ma, followed by magmatism of the Tamboril – Santa Quitéria Complex between 657–591 Ma, through high-grade metamorphism at 620 Ma, the anorogenic magmatism in around 470 Ma and the Rio Ceará-Mirim magmatism related to the opening of the South Atlantic at 130 Ma (Brito Neves and Cordani 1991; Fetter 1999, Brito Neves et al. 2001, Hollanda et al. 2006).

In this geological context of Brasiliano mobile belt that fits the Itataia deposit and other phosphorus-uranium occurrences of this region. The geological setting and structural control of the collophanites ore bodies are in brittle structures and infers different sources for mineralizing fluids. The genetic models existing on the deposit Itataia point to two main strands, a hydrothermal with magmatogenic source and metamorphic-hydrothermal with sedimentogenic source, both with supergene enrichment through the phenomenon of karstification.

From the new studies, a new frame can be painted. In the proposed model, alkaline rocks associated with the final stages of consolidation Tamboril-Santa Quitéria Complex (Neoproterozoic) are considered the primary source of phosphate and uranium. In the study area were described feldspathic affinity alkaline rocks rich apatite with contents of up to 10% P_2O_5 and 0.08% U. These rocks have undergone processes of albitization, desquatzification (episyenitization) at temperatures between 550–350 °C (Cuney 2010), becoming the protore phosphate uranium-rich. The processes of albitization and episyenitization correspond to the early stages of mineralizing process. In the study area were described sterile and mineralizaded albitites, and breccias locally enriched in phosphate (up to 15% P_2O_5) and uranium (2,300 ppm).

The collophanites of Itataia deposit were to be formed later with the introduction of a hot spring, Rio Ceara-Mirim dykes, related to rifting on a global scale and activity hotspot during the opening of the South Atlantic and Equatorial. Based on thermo-geochronological studies of fission track in apatite, Netto et al. (1991) obtained the age of 91±6 Ma for the formation of collophanites associated with a Cretaceous thermal event. During this event, great faults of gravity and combined fractures that became the main sites of ore deposition. This hot spring associated with the exhumation of the land would have generated a convective system hydrothermal involving a mixture of meteoric and magmatic fluids, which removed the phosphate and uranium from alkaline rocks and depositing apatite rich in uranium as collophane at low temperatures (140–50 °C), giving rise to collophanites in an environment subaqueous karst. Subsequently, a new phase of karstification reworked this material, fragments of reconcentrating collophanites in karst depressions.

Acknowledgments

Thanks INB (Brazilian Nuclear Industries) for having given piece of data CPRM and UFC. Collaboration of Brasília University, by Procad.

References

Alcântara e Silva JR, 2003. Caracterização hidrogeológica da Jazida de Itataia-CE. Master Science Thesis, Geology Department, Federal University of Ceará, 150.

Angeiras AG, 1988. Geology and metallogeny of the northeastern Brazil uranium-phosphorus province emphasizing the Itataia deposit. Ore Geology Reviews, Amsterdam, 3, 211–225.

Boynton WV, 1984. Cosmoghemistry of the rare earth elements: meteorite studies. In: HENDERSON, P. (Ed.). Rare earth element geochemistry. Amsterdam: Elsevier, 1984. 63–114. (Development in Geochemistry, 2).

Brito Neves BB, Campos Neto MC, Van Schmus WR, Santos EJ, 2001. O sistema Pajeú-Paraiba e o maciço São José do Campestre no leste da Borborema. Revista Brasileira de Geociências, 31(2), 01–15.

Brito Neves BB, Cordani UG, 1991. Tectonic Evolution of South America during the Late Proterozoic. Precambrian Research, 53, 23–40.

Castro GL, Parente CV, Veríssimo CUV, Sial NA, Garcia MGM, Santos, RV, Melo, RC, Santos, AA, 2005. Isótopos de carbono e oxigênio dos mármores associados com o depósito fósforo-uranífero de Itataia, Ceará. Revista Brasileira de Geociências, 35(2), 199–208.

Cuney M, 2010. Evolution of uranium fractionation process through time: driving the secular variation of uranium deposit types. Economic Geology, 105, 553–569.

Fetter, AH, 1999. U/Pb and Sm/Nd Geocronological Constraints on the Crustal Framework and Geologic History of Ceará State, NW Borborema Province, NE Brazil: Implications for the Assembly of Gondwana. Departament of Geology, Kansas University, Lawrence, PhD Thesis, 164.

Hollanda, MHBM, Pimentel, MM, Oliveira, DC, Jardim de Sá, E.F, 2006. Lithosfere-asthenosphere interaction and the origin of Cretaceous tholeiitic magmatism in Northeastern Brazil: Sr-Nd-Pb isotopic evidence. Lithos 86, 34–49.

IBGE, 2009. Cidades @. In: www.ibge.gov.br/cidadesat/topwindow.htm?1. Access in november, 2010.

IPECE, 2008. Caracterização territorial. Governo do Estado do Ceará. In: http://www.ipece.ce.gov.br/atlas/capitulo1. Access in 2010. Brasília, 73.

IPLANCE – Instituto do Planejamento do Ceará, 1995. Atlas do Ceará, Governo do Estado, Fortaleza, 64.

Mendonça JCGS, Campos M, Braga APG, Souza EM, Favali JC, Leal JRLV, 1985. Jazida de Urânio de Itataia-CE. In: Principais Depósitos Minerais do Brasil, DNPM, v.1, 121–131.

Netto AM, Meyer A, Cuney M, Poupeau G, 1991. A thermo-geochronological study of the Itataia phospho-uraniferous deposit (Ceará, Brazil) by analyses: genetic implications. In: Source Transport and Deposition of apatite fission track Metals, Pagel, M. and Leroy, J.L., eds., Proceedings of the 25 Years SGA Anniversary Meeting, 1991.

Pasero M, Kampf AR, Ferraris C, Pekov IV, Rakovan J, White TJ, 2010. Nomenclature of the apatite supergroup minerals. European Journal of Mineralogy, 22, 163–179.

Sun SS, McDonough WF, 1989. Chemical and isotopic systematics of oceanic basalts: implications for mantle composition and processes. In: SUNDERS, AD; NORRY, MJ (Eds.). Magmatism in ocean basins. Oxfor: Geological Society of Lonfon; Blackwell, 1989. (Geological Society of London Special, 42).

Vidal FWH, Sales FACB, Costa Roberto FA, Sousa JF, Mattos IC, 2005. Rochas e minerais industriais do Ceará. FUNCAP, Fortaleza, 180.

NA JAVORCE CAVE – A NEW DISCOVERY IN THE BOHEMIAN KARST (CZECH REPUBLIC): UNIQUE EXAMPLE OF RELATIONSHIPS BETWEEN HYDROTHERMAL AND COMMON KARSTIFICATION

Jiří Dragoun[1], Karel Žák[2], Jiří Vejlupek[1], Michal Filippi[2], Jiří Novotný[1], Petr Dobeš[3]
[1]Czech Speleological Society, ZO 1-11 Barrandien, Working Group Babyka, Trachtova 1/1129, 158 00 Prague 5, Czech Republic, drzahr@seznam.cz; vejlupj@seznam.cz; jinoli.centrum.cz
[2]Institute of Geology AS CR, v. v. i., Rozvojová 269, CZ-165 00 Prague 6, Czech Republic, zak@gli.cas.cz; filippi@gli.cas.cz
[3]Czech Geological Survey, Klárov 3, 118 21 Prague 1, Czech Republic, petr.dobes@geology.cz

The Na Javorce Cave is located in the Bohemian Karst, Czech Republic, near the Karlštejn castle, about 25 km SW of Prague. The cave was discovered as a result of extensive exploration including cave digging and widely employed capping of narrow sections. Exploration in the cave has already lasted 20 years. The cave is fitted with several hundred meters of fixed and rope ladders and several small fixed bridges across intra-cave chasms. Access to the remote parts of the cave is difficult because of long narrow crawl passages and deep and narrow vertical sections. The Na Javorce Cave became the deepest cave discovered to date in Bohemia with the discovery of its deepest part containing a lake in 2010. The cave was formed in vertically dipping layers of Lower Devonian limestone; it is 1,723 m long and 129 m deep, of which 9 m is permanently flooded (data as of December 2012). The cave is polygenetic, with several clearly separable evolutionary stages. Cavities discovered to date were mostly formed along the tectonic structures of two main systems. One of these systems is represented by vertical faults of generally N-S strike, which are frequently accompanied by vein hydrothermal calcite with crystal cavities. The second fault system is represented by moderately inclined faults (dip 27 to 45°, dip direction to the W). Smaller tube-like passages of phreatic morphology connect the larger cavities developed along the two above-mentioned systems. The fluid inclusion data obtained for calcite developed along both fault systems in combination with C and O stable isotope studies indicate that the hydrothermal calcite was deposited from moderately saline fluids (0.5 to 8.7 wt. % NaCl equiv.) in the temperature range from 58 to 98 °C. The fluids were NaCl-type basinal fluids, probably derived from the deeper clastic horizons of the Barrandian sedimentary sequence. The age of the hydrothermal processes is unknown; geologically it is delimited by the Permian and Paleogene. The hydrothermal cavities are small compared to cavities formed during the later stages of karstification. The majority of the known cavities were probably formed by corrosion by floodwater derived from an adjacent river. This process was initiated during the Late Oligocene to Early Miocene, as was confirmed by typical assemblage of heavy minerals identical in the surface river sediments and in clastic cave sediments. The morphology of most cavities is phreatic or epiphreatic, with only local development of leveled roof sections ("Laugdecken"). The phreatic evolution of the cave is probably continuing into the present in its deepest permanently flooded part, which exhibits a water level close to that of the adjacent Berounka River. Nevertheless, the chemistry of the cave lake differs from that of the river water. The cave hosts all the usual types of cave decoration (including locally abundant erratics). The most interesting speleothem type is cryogenic cave carbonate, which was formed during freezing of water in relation to the presence of permafrost during the Glacial period. The occurrence of cryogenic cave carbonate here indicates that the permafrost of the Last Glacial period penetrated to a depth of at least 65 m below the surface.

1. Introduction and history of the cave exploration

Two small cave entrances, located high in the eastern slope of the Javorka Hill, close to the famous Karlštejn castle, already attracted attention at the end of the nineteen forties and beginning of the nineteen fifties. Jaroslav Petrbok, a well-known karst researcher, archaeologist and zoologist focusing on terrestrial mollusks, performed excavations in both entrances. Radvan Horný and Jiří Kovanda helped him during this work (both later became well-known geologists). Only a few meters of the entrance sections were explored, with finds of several ceramic fragments of the Hallstatt culture and an iron spear point dated to the Middle Ages (Petrbok and Horný 1950; Petrbok 1955). Allegedly Mesolithic finds, fragments of antlers, were later suggested not to be artifacts by Fridrich and Sklenář (1976) and Sklenář and Matoušek (1992). This stage can be considered not to be important from the viewpoint of cave exploration.

A new exploration phase was initiated by the members of the Czech Speleological Society, Unit 1-11 Barrandien (who are also the authors of this paper), in the upper entrance in March 1993. Clay sediments, with only small open spaces near the roof, filled the passages of the upper entrance behind the section explored archaeologically. The excavated material was transported using a special suspended mini-railway. The excavation performed in the complicated space of karstified tectonic structures with large unstable blocks of rock reached a length of 49 m in 1997. The work was interrupted here because of the instability of the walls of the excavated space. The next effort was focused on the lower entrance after an interruption of 3 years, again using a similar mini-railway suspended near the roof of the passage. Narrow sections had to be widened using capping. After 15 m of difficult work, the first open cavities with attractive decorations were reached in 2001 (Fig. 1).

Figure 1. Speleothem decoration in the cavities of the lower entrance (a cavity called Digital Chimney) discovered in 2001. Photo by J. Novotný.

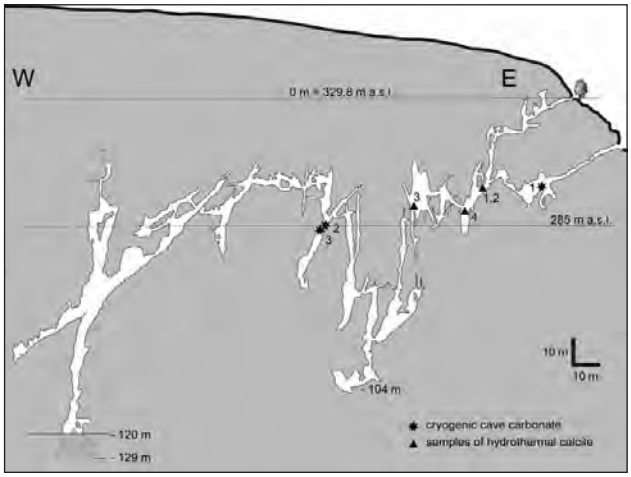

Figure 2. Simplified longitudinal E-W section (side view) of the Na Javorce Cave. The horizontal line at 285 m a.s.l. corresponds approximately to the base of the Neogene river terraces, and simultaneously to the base of the oldest Early Pleistocene river terraces in the adjacent valley. The sites of sampling of cryogenic cave carbonates (stars) and of hydrothermal vein fill (triangles) are also depicted. Based on mapping of J. Dragoun, J. Vejlupek and J. Novotný in 2010.

The discovery initiated more intensive work, which enabled further uncovering of this morphologically complicated cave, which is very difficult to explore. It became clear that the cave developed in a structurally complex space, affected by low-temperature hydrothermal activity with deposition of calcite crystals in cavities.

The cave generally consists of several types of cavities. The first type is represented by narrow, flat cavities developed along the N–S faults with calcite veins. The cavities are up to 1–2 m wide (frequently only 0.3–0.4 m), but up to several tens meters long and commonly several tens of meters high in the direction along the faults. The second important type of cavities is represented by both narrow and larger corridors that developed along faults moderately dipping to the W. The two systems of cavities are interconnected by narrow, tube-like phreatic channels.

Further exploration resulted in the interconnection of the upper and lower cave entrances in 2005. Together with further minor discoveries, the cave was explored to a length of 500 m that year. Difficult access to the above-mentioned connecting tubes between the vertical cavities required the construction of small hanging platforms, from which further exploration was possible. Difficult digging at the bottom of a narrow shaft called Zubatá finally resulted in penetration into larger open spaces in 2006. The cave was explored to a depth of 104 m in that year (Figs. 2, 3).

Further exploration was more rapid in the following several years. After cleaning of another connecting tube, a high parallel cavity was reached and, following difficult climbing up this chimney (in 2007), the upper levels of the cave have been gradually explored. This upper part of the cave also has rich decoration, including long soda straws and abundant erratics (Fig. 4). Any work in this distant cave section requires long access, which was facilitated by the construction of small bridges across the chasms. Cave digging in the narrow passages of the upper part of the cave enabled further discoveries in 2008 and 2009. The largest cavity, an inclined irregular passage called Sešup, was discovered in this period. Exploration of vertical cavities in this part resulted in the discovery of the deepest cave section with a lake in 2010.

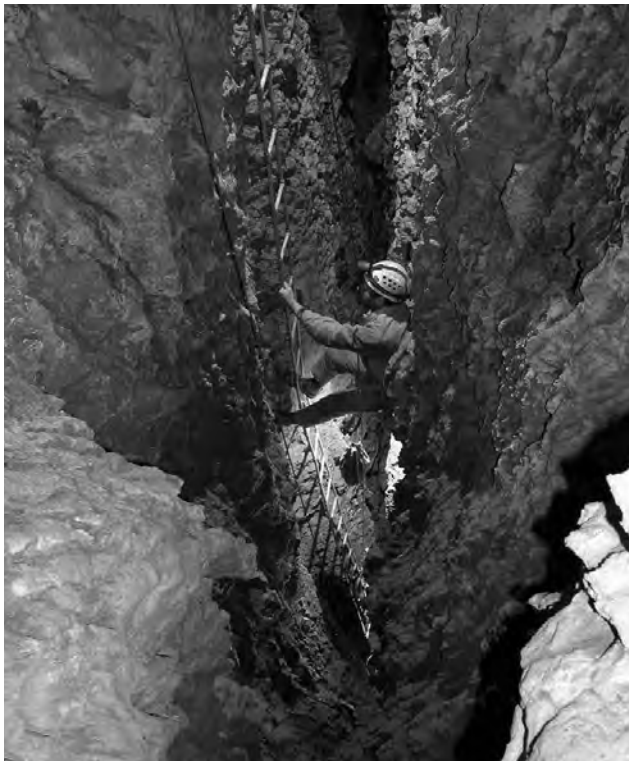

Figure 3. Typical appearance of vertical cavities of the Na Javorce Cave. The photo is taken in a vertical cavity above the point of -104 m (cf. Fig. 2). Photo by J. Novotný.

The water level of the lake has lies at 120 m below the upper entrance (Fig. 5). Measurement of the water depth and first diving explorations demonstrated a water depth of 9 m, which corresponds to a total cave depth of 129 m. The cave became the deepest one discovered in Bohemia. Further cave exploration performed at several locations within the cave since 2010 did not result in new discoveries. Altogether, 498 one-day or two-day work shifts have been spent in the cave during the last 20 years. The cave became not only the deepest discovered in Bohemia, it is also the third longest cave discovered in the Bohemian Karst.

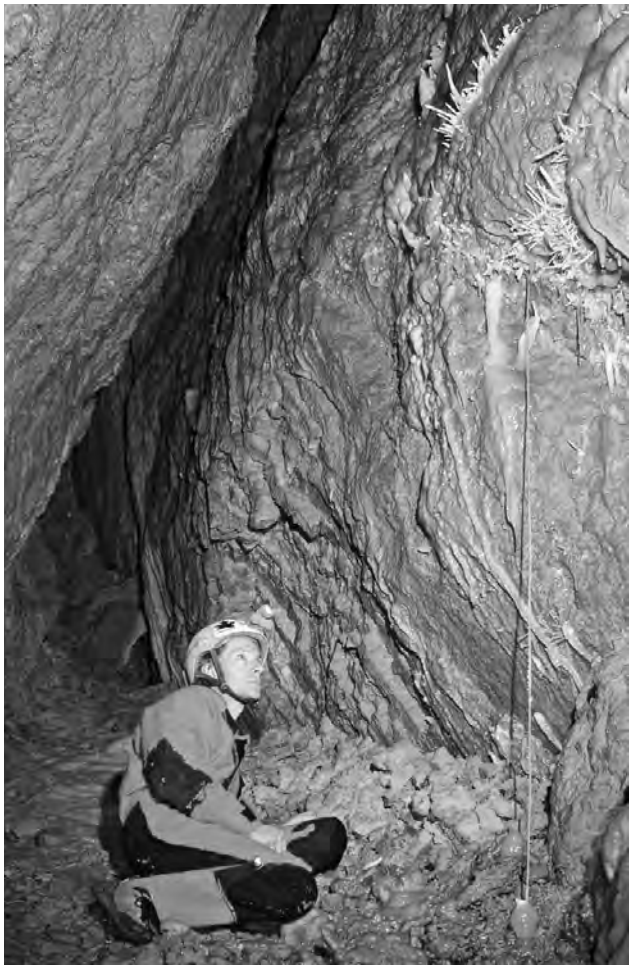

Figure 4. Speleothem decoration in the Radvanská Passage (distant upper part of the cave) with erratics and long soda straw. Photo by J. Novotný.

Figure 5. Lake in the deepest part of the Na Javorce cave. Photo by J. Novotný.

2. Cave location, geology, hydrothermal calcite and cave decoration

The two cave entrances are located in the steep eastern slope of the Javorka Hill at elevations of 329.8 and 313.3 m a.s.l. The upper entrance opens 120 m above the water level of the Berounka River flowing at a distance of several hundred meters (the usual water level in the river is at 209.5 m a.s.l.). The cave is located below the S and SE slopes of the hill close to its summit. This results in only a small geographical catchment of the cave under the present-day topography. The major lithology hosting the cave is Lower Devonian Kotýs Limestone, especially pure limestone layers in the upper part of the Lochkovian Stage. Nevertheless, cavities frequently also penetrate to the lower lithology, Kotýs Limestone with siliceous chert lenses and layers, and rarely also to the upper Loděnice Limestone and Dvorce-Prokop Limestone, both of which already belong to the Pragian Stage. Layers of all types of limestone dip almost vertically in this part of the Javorka Hill (the strike of the layers is almost E–W, 80 to 85°; the layer dip is around 90°). The main Hercynian folding, producing a complicated structure including abundant large overthrusts, occurred in the Late Devonian and Early Carboniferous in the area.

The vertically dipping sedimentary sequence is affected in the cave area by the faults of two main systems. Vertical faults of N–S strike (the whole range of strikes is 155 to 180°), represent the most important fault system. The limestone layering had a small effect on the cave morphology. The layering is roughly parallel to the E–W simplified section (Fig. 2), while the N–S faults and cavities developed along them are perpendicular to this section. The second fault system is represented by moderately inclined faults (dip 27 to 45°, dip direction 240 to 270°). Both entrance passages and the large Sešup Passage developed along the faults and joints of this second system (Fig. 2).

Calcite veining and crystal cavities were formed especially along the structures with N–S strike. Locally they also penetrated into inclined faults. Calcite is coarsely crystalline, with scalenohedrons and rhombohedra with sizes up to 10 cm, of white, yellowish or brownish color. The evolution of calcite veins was irregular. Locally, they reach a thickness of several tens of cm, while at other places they are completely absent on the faults. Hydrothermal calcite was more resistant to corrosion during the later cave evolution, so that the calcite veins locally protrude out of the cavity walls, producing typical boxwork. Limestone alteration (inter-granular corrosion) locally produced rock with sandy disintegration and small accumulations of carbonate sand at several places. Cavities of tectonic and hydrothermal origin represent only a small portion of the known cavities. Most cavities developed during the later stages by common corrosion in the phreatic karst zone. Corrosion occurred along all the types of faults and calcite veins, so that the extent of earlier hydrothermal corrosion (if present) cannot be evaluated. Phreatic corrosion, a dominant process shaping the cave, is well-recorded in the morphology of the cavities. A small section of leveled roofs ("Laugdecken"), indicating long-term stagnation of the water level, developed only locally.

There are several types of clastic cave sediments. The most interesting are quartz-dominated gravels with well-rounded pebbles and quartz-dominated sands of white to grey color. They occur in the upper part of the cave in a small quantities (up to several m^3), especially in sections located close to the lower entrance. They represent the lowermost part of the cave sedimentary filling here. Since they show lithological similarity to the surface sediments of a river flowing not far from the cave during the Late Oligocene to Early Miocene, they have been subjected to study of the

heavy mineral assemblage (see below). Quaternary speleothems can be found in the cave in a variety of morphological types, including long soda straws and locally abundant erratics (Fig. 4). Several chambers and corridors are well decorated, while the majority of the cave does not have any speleothems. Cryogenic cave carbonates formed by crystallization accompanied by water freezing occur at several sites (see the star symbols in Fig. 2; cf. Žák et al. 2012). They occur as accumulations of free crystals and crystal aggregates loosely deposited on the bottom of the cavities (Fig. 6 and the discussion below).

3. Analytical methods

New analytical research in the cave included study of the hydrothermal processes using fluid inclusion and stable isotope data on hydrothermal calcite, study of pre-Quaternary clastic sediments in the cave using the assemblage of heavy minerals, research on specific types of speleothems – cryogenic cave carbonates (cf. Žák et al. 2012), and a pilot study on the chemistry of the lake water.

Microthermometric analyses of fluid inclusion entrapped in hydrothermal vein calcite and calcite crystals in cavities were performed on cleavage chips (of about 300 μm thick) using Chaixmeca apparatus (Poty et al. 1976). The apparatus was calibrated in the temperature range -100 to +400 °C using Merck chemical standards, the melting point of distilled water, and phase transitions in natural pure CO_2 inclusions. The reproducibility of temperatures of homogenization up to +200 °C was ±3.0 °C; the reproducibility of the temperatures of ice melting in fluid inclusions below 0 °C was ±0.2 °C. The salinity of fluids was calculated according to Bodnar and Vityk (1994) and the composition of the salt system was evaluated after Borisenko (1977).

C and O stable isotope composition of hydrothermal calcite was determined using the standard method of McCrea (1950). The isotopic composition of the CO_2 gas produced by decomposition of samples was measured using a Finnigan MAT 251 mass spectrometer. The heavy minerals were separated from a sieved 0.2 to 0.6 mm fraction of the cave sands using tetrabromethane with a density of 2.95 g.cm^{-3}. Methods used for the study of cryogenic cave carbonates are contained in Žák et al. (2012). Minerals were determined by X-ray powder diffraction using a Bruker D8 apparatus. The chemistry of water in the cave lake was determined using standard analytical methods (AAS, HPLC).

4. Results and discussion

4.1. Fluid inclusions in hydrothermal calcite

The Jav1, Jav2 and Jav3 samples (see Fig. 2 for the sample location) contained relatively small amounts of primary fluid inclusions in 3D distribution. The inclusions were of irregular shape, from 5 to 60 μm in diameter, and with variable liquid to vapor ratios (LVR = L/L+V). The most common (about 80 %) were liquid-only inclusions, followed by liquid-rich two-phase inclusions with LVR of about 0.9 (about 15 %), and inclusions with prevailing vapor phase were relatively rare. In a contrast, the Jav4 sample contained a very large number of tiny primary inclusions with variable LVR ratio in 3D distribution ("sponge texture"). The inclusions were of oval to irregular shape and from 5 to 20 μm in diameter.

Only fluids of the H_2O-type were found in primary inclusions of all the studied samples. No fluid inclusions with a gaseous phase, such as CO_2 or CH_4, were recorded. Due to the variable LVR, the homogenization temperatures (Th) were measured in clusters of inclusions with LVR of 0.90 to 0.95. The values of Th of the primary inclusions fluctuated from 58 to 91 °C; the salinity of an aqueous solution, calculated from the melting temperature of the last ice crystal (Tm), varied from 0.5 to 7.0 wt.% NaCl equiv. The eutectic temperature (Te = -22.0 to -23.2) indicated that NaCl was the major component of the aqueous solution (Tab. 1).

Table 1. Fluid inclusion data. FIA – fluid inclusion assemblage; Th – temperature of homogenization; Tm – temperature of melting of the last ice crystal; Te – eutectic temperature.

No.	FIA generation	FIA type	Th (°C)	Tm (°C)	salinity (wt.% NaCl eq.)	Te (°C)
Jav1	primary	H_2O	58–68	-2.1 to -4.4	3.6–7.0	-23.2
	pseudosec.	H_2O	79–98	-1.2 to -2.1	2.1–3.6	
	secondary	H_2O	65–94	-0.1 to -0.4	0.2–0.7	
Jav2	primary	H_2O	84–91	-1.1 to -3.3	1.9–5.4	
	pseudosec.	H_2O	72–86	-0.7 to -0.8	1.2–1.4	-21.5
	secondary	H_2O	75–112	-1.2 to -2.1	2.1–3.6	
Jav3	primary	H_2O	–	-0.3 to -1.2	0.5–2.1	-22.0
	pseudosec.	H_2O	–	–	–	
	secondary	H_2O	85–112	-0.8 to -3.4	1.4–5.6	
				-12.6 to -13.9	16.5–17.7	-21.5
Jav4	primary	H_2O	58–74	-1.4 to -3.5	2.4–5.7	-22.5
	pseudosec.	H_2O	74–94	-2.6 to -5.6	4.3–8.7	
	secondary	H_2O	–	–	–	

Pseudosecondary fluid inclusions were observed in the studied samples along short healed microfractures. The inclusions were mostly of oval shape, up to 20 μm in diameter, and exhibited consistent LVR ratios from 0.90 to 0.95. The Th values yielded valuable data in the range from 72 to 98 °C, the salinity of the aqueous solution was calculated between 1.2 and 8.7 wt.% NaCl equiv., and NaCl was assumed to be the major compound of the aqueous solutions (Te = -21.5 °C).

Two generations of secondary inclusions were found in the studied calcite samples. They were observed either along longer healed microfractures, where they are of oval shape, up to 20 μm in diameter, and with consistent LVR from 0.90 to 0.95, or along cleavage planes, where they are of irregular shape, from 10 to 200 μm in diameter, and with variable LVR. The obtained Th values in the inclusions of the first generation ranged between 65 and 112 °C, and the salinity of the solution was found to be from 0.2 to 5.6 wt.% NaCl equiv. The Th value of the second generation of secondary fluid inclusions was not determined because of variable LVR. The obtained Tm values yielded two intervals of salinity, from 1.9 to 1.9 wt.% NaCl equiv., and from 16.5 to 17.7 wt.% NaCl equiv.

4.2. Carbon and oxygen stable isotopes in hydrothermal calcite and origin of fluids

The carbon isotope data of the hydrothermal calcite ($\delta^{13}C$ from -6.37 to -3.33‰ vs. VPDB) and the oxygen isotope data ($\delta^{18}O$ from -10.74 to -9.20‰ VPDB) were obtained on identical hydrothermal calcite cleavage chips, which were also used for the fluid inclusion study. This enabled recalculation of the mineral C and O isotope data to the stable isotope parameters of the fluids. HCO_3^- was assumed to be the dominant carbonaceous component of the fluids. The fluids depositing the calcite had $\delta^{13}C$ values in the range from -8.1 to -4.8‰ VPDB and $\delta^{18}O$ values in the range from 0 to +5‰ VSMOW. These characteristics are typical for basinal fluids. Meteoric waters of shallow circulation cannot be considered for the deposition of hydrothermal calcite because of the fluid $\delta\ ^{18}O$ values and also their temperature and salinity.

4.3. Pre-Quaternary clastic cave sediments and the evolution of cavities in the phreatic zone

Well size-sorted, white to gray, quartz-dominated sands from the passages of the lower cave entrance are locally accompanied by white to light-gray clays. The heavy mineral assemblage of the sands (2–5% andalusite, 5–15% secondary Fe-minerals, 30–40% ilmenite, 5% kyanite, 2–10% leukoxene, 1–5% magnetite, 10–15% rutile, 3–5% turmaline and 10–15% zircon) contained only stable minerals typical in the studied area for Late Oligocene and Early Miocene river sands. In contrast, minerals typical for Quaternary river terraces (amphiboles, pyroxenes, garnets, etc.) were completely missing in the studied cave sands. The relationship of the studied cave sands to an Oligocene/Miocene river can be considered as proved. The mineralogy of the spatially related light-colored clays (kaolinite, illite/muscovite) supports the pre-Quaternary origin of the cavities hosting these clastic sediments.

We assume that these clastic sediments penetrated into the cave together with floodwater injection from the Oligocene/Miocene river. The cavities were rapidly enlarged by corrosion by the river water, possibly with a contribution from mixing corrosion during mixing of the river and karst waters. As the Quaternary valley network started to develop, the upper parts of the cavities became drained, and the phreatic zone moved deeper and deeper.

4.4. Cryogenic cave carbonates and permafrost during the Glacial

Freezing of mineralized karst water is inevitably accompanied by cryogenic mineral precipitation. The cryogenic cave carbonates exhibit typical modes of occurrence, morphology and geochemistry. The low-ventilation caves can be cooled to freezing temperature only as a result of formation of permafrost. The occurrence and dating of cryogenic cave carbonates in these caves can be used for estimation of the permafrost depth of former glacials (Žák et al. 2012). The low ventilation of the Na Javorce Cave is reflected in the elevated content of CO_2 in the cave atmosphere (around 2%) and by its almost constant temperature. The occurrences of cryogenic cave carbonates in the Na Javorce Cave (stars in Fig. 2) have been studied and dated in detail by Žák et al. (2012). Site 1 yielded U-series ages of 50.04±0.39 and 28.56±0.17 ka BP, Site 2 an age of 14.98±0.17 ka BP and Site 3 an age of 9.19±0.07 ka BP. The data show that the rock massif and the cave were in a permafrost zone down to at least 65 m below the surface during the Last Glacial.

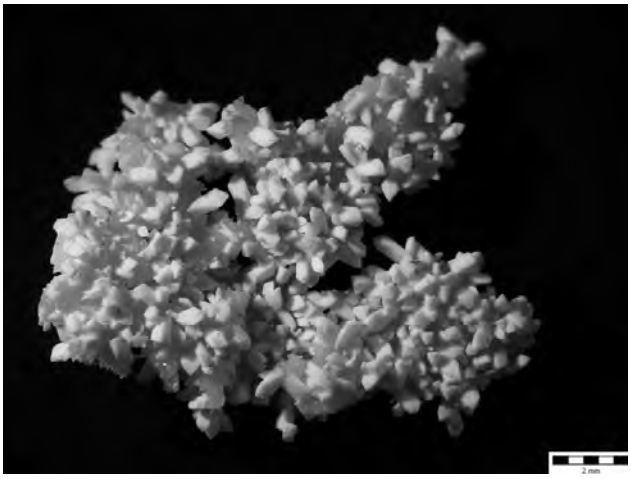

Figure 6. Cryogenic cave carbonate of raft type with two generations of crystals, Na Javorce Cave, location 1 in Fig. 2. Photo by M. Filippi.

4.5. Present-day cave hydrogeology

The cave lake (Fig. 4) contains low-mineralized karst water (sampling on 27 December 2010; composition in $mg.L^{-1}$: Li^+ 0.0042; NH_4^+ <0.02; Na^+ 7.00; Mg^{2+} 29.94; Al <0.20; K^+ 2.34; Ca^{2+} 71.9; Mn^{2+} 0.015; Fe 0.11; Zn^{2+} <0.005; HCO_3^- 311.2; NO_3^- 13.6; F^- 0.09; SO_4^{2-} 20.2; Cl 15.84; pH 7.42; conductivity 503 $\mu S.cm^{-1}$). This water chemistry differs from that of the adjacent Berounka River (which exhibits a higher content of sulfate and chloride). It also differs from the water of karst springs with deep circulation, and from the water of a polluted creek flowing through the village of Karlštejn. The water in the cave lake is therefore local infiltration water derived from the forested Javorka Hill itself. The present-day hydrogeological behavior of the lake is unknown. Detailed studies in the past few years clarified the hydraulic relationships between the river and adjacent caves (Vysoká et al. 2012). Nevertheless, the cave lake in the Na Javorce Cave is farther away from the river than any of the lakes studied by Vysoká et al. (2012).

5. Conclusions – overview of the cave evolution

The cave evolution was initiated by tectonic processes. The inclined structures of western dip are probably older than the vertical tectonic structures of approximately S-N strike. Movements on these vertical structures locally opened small tectonic cavities. These cavities were later filled by hydrothermal calcite, containing abundant crystal cavities. Neither the tectonic phases nor the hydrothermal phase have been precisely dated. Dating is lacking for any of the abundant calcite veins of the Bohemian Karst. Geological observation indicates that the movement along vertical faults could have occurred from the Carboniferous to the

Cretaceous, and the hydrothermal phase could have occurred at any time between the Permian and the Paleogene. Movements along faults after the formation of hydrothermal calcite were either absent or only of small amplitude. The hydrothermal phase occurred at temperatures between 58 and 98 °C. Moderately saline fluid (0.5 to 8.7 wt.% NaCl equiv.) with $\delta^{18}O$ in the range between 0 and +5‰ VSMOW and $\delta^{13}C$ in the range between -8.1 to -4.8‰ VPDB was most probably some kind of basinal water derived from a deeper part of the sedimentary sequence. The extent of hydrothermal corrosion is difficult to evaluate, since later karst corrosion in the phreatic zone overlaps the earlier hydrothermal corrosion.

The upper parts of the Na Javorce Cave (above approximately 285 m a.s.l., which is the upper limit of the Quaternary river terraces) were formed by phreatic corrosion in the pre-Quaternary period, most probably during the Late Oligocene and Early Miocene. The relationship between the river of this age and the cave is reflected in the presence of quartz-dominated sands in the cave, which contain identical heavy mineral assemblage like the surface sediments. The surface fluvial sediments at a site located 2 km away from the cave are dated by paleontology (Žák et al. 2003). The principal processes of cave formation were probably floodwater injection and mixing corrosion. These processes resulted in irregular morphology of the cavities. The cavities below a level of 285 m a.s.l. could also have been formed (or their formation initiated) during the Oligocene or Miocene. In relation to the deep incision of the river during the Quaternary, the upper parts of the cave became drained and the phreatic evolution could continue only in deeper part of the cave. The present-day hydraulic relationship between the cave phreatic zone and the 400 m distant river is unknown (the cave lake was discovered in 2010 and has very difficult access). The water level in the cave lake and in the river are approximately equal (within the measuring error). It is clear that the cave was “trapped” in the Javorka Hill during the Quaternary. It has very limited geographic catchment area. The cave-lake water chemistry is different from those of the river and of a creek flowing through the town of Karlštejn. The water chemistry probably reflects infiltration in the forested area of Javorka Hill itself. Water flow along the N-S faults from a more northern area is another possibility.

The Quaternary evolution of the cave is poorly understood. Sections with vadose morphology are generally rare in the cave (corrosion by drip-water is locally present) and the speleothems have not been dated yet, except the cryogenic cave carbonates of the Last Glacial. These cryogenic cave carbonates indicate that, during the Glacial, especially during the Last Glacial Maximum (between ca. 26.5 and 19.0 ka BP), the permafrost extended to a depth of at least 65 m below the surface. Cryogenic cave carbonates were found at several sites within the cave (Fig. 2) and were dated and studied in detail by Žák et al. (2012). The youngest age of the cryogenic cave carbonate of 9.19±0.07 ka BP was obtained for the sample with the deepest location within the cave. This possibly indicates that the relic permafrost lenses could have survived until the Early Holocene. Late Glacial and Early Holocene age have also been attributed to the bone finds in the entrance cave sections, transported into the cave by predators. The presence of animals and prehistoric humans was restricted to only a few meters behind both entrances, because of the sediment fill of the passages.

Exploration work done in the cave since 1993 (intensive since 2001) resulted in the discovery of this interesting cave, which became the deepest cave of Bohemia in 2010. It is clear that the Na Javorce Cave has not yet revealed all its secrets.

Acknowledgments

The research in the cave was performed within project P210/10/1760 of the Czech Science Foundation. The authors would like to thank Z. Táborský for heavy mineral separation and determination, R. Skála for XRD mineral identification and I. Jačková and B. Čejková for the C and O stable isotope determinations.

References

Bodnar RJ, Vityk MO, 1995. Interpretation of microthermometric data for H_2O-NaCl fluid inclusions. In: Fluid Inclusions in Minerals, Methods and Applications, B De Vivo and ML Frezzotti (Eds.). Virginia Tech, Blacksburg, VA, 117–130.

Borisenko AS, 1977. Izutchenye solevogo sostava rastvorov gazovozhidkych vklyutcheniy v mineralach metodom kriometrii. Geologia i Geofyzika, 8, 16–28. Moscow (in Russian).

Fridrich J, Sklenář K, 1976. Die paläolitische und mesolitische Höhlenbesiedlung des Böhmischen Karstes. Fontes Archaeologici Pragenses, 16, 1–122. Prague.

McCrea JM, 1950. On the isotopic chemistry of carbonates and a paleotemperature scale. Journal of Chemical Physics, 18, 849–857.

Poty B, Leroy J, Jachimowicz L, 1976. Measuring temperature under microscope – Chaixmeca micro-thermometry apparatus. Bulletin de la Societe Francaise Mineralogie et de Cristallographie, 99(2–3), 182–186.

Sklenář K, Matoušek V, 1994. Die Höhlenbesiedlung des Böhmischen Karstes vom Neolithikum bis zum Mittelalter. Fontes Archaeologici Pragenses, 20, 1–212. Prague.

Vysoká H, Bruthans J, Žák K, Mls J, 2012. Response of the karst phreatic zone to flood events in a major river (Bohemian Karst, Czech Republic) and its implication for the cave genesis. Journal of Cave and Karst Studies, 74(1), 65–81.

Žák K, Táborský Z, Lachmanová M, Pudilová M, 2001. Heavy mineral assemblages in allochthonous clastic cave sediments of the Bohemian Karst: A pilot study. Český kras, XXVI, 5–14. Beroun (in Czech with abstract in English).

Žák K, Teodoridis V, Sakala J, 2003. Find of flora in Tertiary sediments near Karlštejn. Geoscience Research Reports for 2002, 47–49. Prague (in Czech with abstract in English).

Žák K, Richter DK, Filippi M, Živor R, Deininger M, Mangini A, Scholz D, 2012. Coarsely crystalline cryogenic cave carbonate – a new archive to estimate the Last Glacial minimum permafrost depth in Central Europe. Climate of the Past, 8, 1821–1837.

FIELD MEASUREMENTS OF GYPSUM DENUDATION RATE IN KULOGORSKAYA CAVE SYSTEM

Nikolay Franz[1], Sergey Sorokin[2,3], Alexandra Alexeeva[4], Irina Inshina[4], Olga Novysh[3], Anton Kazak[3]
[1]Arkhangels Speleological Association "Labirinth", Arkhangels, Russia, franikol@mail.ru
[2]Tver State University, Zhelyabova 33, Tver, Russia, sergey@tversu.ru
[3]Arkhangels Speleological Association "Labirinth", Arkhangels, Russia
[4]Tver State University, Tver, Russia

Results of measurements of karst denudation rate in natural conditions in Kulogorskaya cave system are reported. Taking into consideration relatively high rate of denudation in gypsum caves we have used simplified MEM measurement method. Observation of hydrological situation suggests that most of the dissolution in caves of the area occurs during a few days of spring flood. Here we report results of measurement at 62 points located at 6 sites for the period from 2003 to 2012. Data analysis gives us average retreat rate of 0.0448 mm/day, while point is underwater. Confidence interval for this value is 0.0379 to 0.0516 mm/day.

1. Introduction

Kulogorskaya cave system includes 7 caves, three of which constitute the largest cave system in Russia in a gypsum, with a total length of surveyed passages more than 17.5 km.

Cave system is studied by speleologists from Arkhangels, St. Petersburg, Moscow, Tver and other cities under the guidance of Arkhangels Speleological Association "Labirinth".

This report presents the preliminary results of the measurements of dissolution of gypsum in the natural conditions, which are held from 2003.

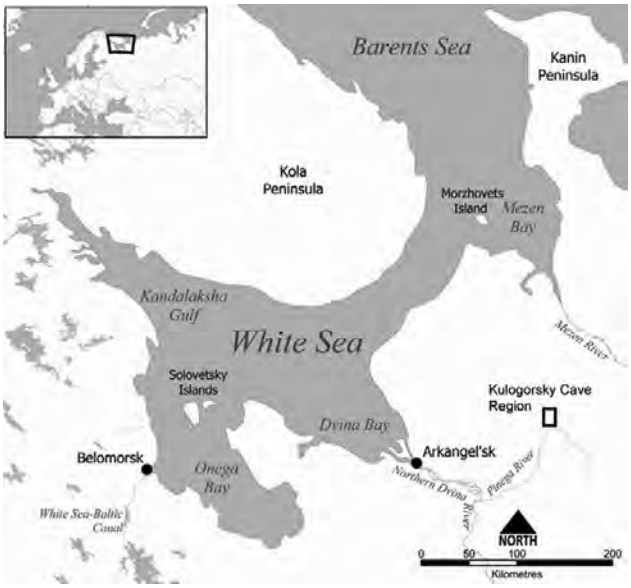

Figure 1. Geographical position of Kulogorsky Cave Region.

2. Geography and geology

Geographically Kulogorskaya cave system is located in the north of the East European Plain, in the watershed of Pinega (tributary of Northern Dvina) and Kuloi (Fig. 1).

The climate here is quite severe, with low air temperatures and high humidity, rainfall exceeds evaporation. The multi-year average annual temperature is +0.2 °C. The average annual rainfall 560 mm. The coldest month – January (average long-term temperature -13.0 °C). The warmest month – July (average long-term temperature +15.4 °C).

Karstifiable rocks of massif are represented by gypsum and dolomite of Permian age. Primary karst rock is gypsum, forming homogeneous strata ranging from 0.2 to 7 m, interleaved with dolomites. Average total width of sedimentary cover above caves is 20 m.

Caverns in the massif are well represented in all hydrodynamic zones: vertical transfer zone, zone of seasonal fluctuations of water table levels and phreatic zone. Human-passable channels are located only at the zone of water table. In karst dissolution infiltrational, condensational and floodwaters are involved. Local erosion bases for caves in Kulogorskaya cave system is Pinega River and Pinega-Kuloy channel.

3. Conditions of karst denudation

The most important role in the process of dissolution of gypsum walls in the water-table zone play floodwater penetrating the karst massif through numerous small ponors laid along the Kulogorsky ledge in the area of contact between the karst rocks and the floodplain alluvium.

The penetration of floodwater into massif mainly occurs in spring (April–May) when Pinega waters rise by 4–5 meters above the winter low water (in the caves in this period water rises up to 2–3 meters, completely flooding almost all horizontal passages). During this period water flows in horizontal passages in water-table zone, which are typically dry in other seasons. Absorbed water temperature typically ranges around 1 °C.

Autumn floods in the river and caves are less affluent: the rise of water in the river – up to 2–3 m, in caves – up to 1 m. The inflow of water into the massif in this period is only through channels of phreatic zone (flooding of caves is caused by raising of the water-table level). Reverse runoff after autumn flood occurs on the same path in the opposite direction (the horizontal filtering through the thickness of the alluvium in the direction of erosion basis).

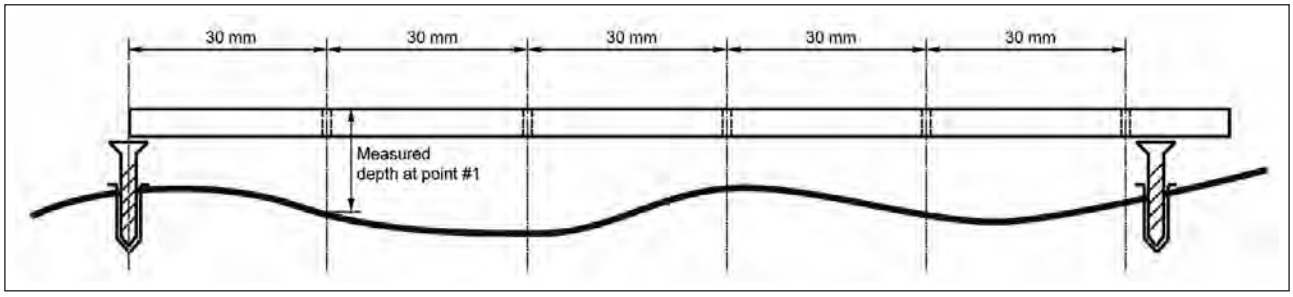

Figure 2. Measurement method.

The main feature of the hydrogeology of Kulogorsky massif is absence of significant inverse flow of flood waters after passing through the peak of the spring flooding. In other words, floodwaters which penetrate the caves from the floodplain, never pour back by the same horizontal channels. Our current understanding is that at mean water period the water from caves is unloaded by slow horizontal filtering through the thickness of alluvium in the direction of the local base level of erosion.

To determine the saturation of cave waters with gypsum, we measure its electrical conductivity, which is directly proportional to the salinity of water – both according to the data of other researchers (Krawczyk and Ford 2006), and confirmed by our observations.

In 2004 we conducted experiment in K-2 cave on the dissolution of gypsum powder in the water from underground lake (initial conductivity 2.1 mS) at natural cave temperature +2.2 °C, which gives us maximal conductivity of 2.5 mS.

But these values are not reachable in the natural underground water exchange, which is convincingly shown by the results of long-term observations of hydrochemical karst springs in the river Pinega: conductivity of discharged water is never more than 2.2 mS (88 % of maximum mineralization).

Since caves are inaccessible to humans during flood, we have used the tanks with automatic closure to determine the salinity of flood waters. These tanks have been installed by us in 2005 at a different distance from ponors.

Analysis of the data showed, that conductivity of aggressive flood water, which penetrates the massif is 0.5–0.6 mS (20–24 % of maximum). After passing for many hundreds of meters underground transit, these waters are saturated to 1.8–1.9 mS (72–76 %). Then, in a few months of slow water level drop, conductivity of underground water reaches 2.2–2.3 mS (88–92 %).

Thus, during the transit time (in a few days at the peak of the spring flood) in conditions of heavy water exchange, floodwaters are saturated with the products of dissolution of sulphate rocks up to 50 % approximately. Over the following months, during slow level decline, water gather additionally about 15 % to reach the maximum observed mineralization of 2.2–2.3 mS, or 88–92 % of the maximum possible in these climatic conditions.

Since, as mentioned above, main floodwater flow occurs in the zone of water-table, we can assume that maximal denudation of cave walls happens in this zone. That is why all karst denudation rate measurement sites ("SKD" for Rate of Karst Denudation in Russian) were fitted by us only in the passages of this zone.

4. Methods

To study the rate of dissolution of gypsum in the natural conditions since 2003, we have equipped 15 measurement sites in five caves. Almost all sites were equipped on the surfaces of the ceilings and walls of passages laid in the massif of white-and fine-grained gypsum with rare clusters of large gypsum crystals.

Since the expected rate of dissolution of gypsum is higher than that of limestone, we used a simplified, compared to the classic version of the MEM method (Smith, 1977).

Each SKD site includes from 1 to 4 rows of control points. Rows of control points may be oriented horizontally or vertically. Each row, in turn, includes from 4 to 7 observation points located with an interval of 3 cm along a straight line between the two fixed reference points.

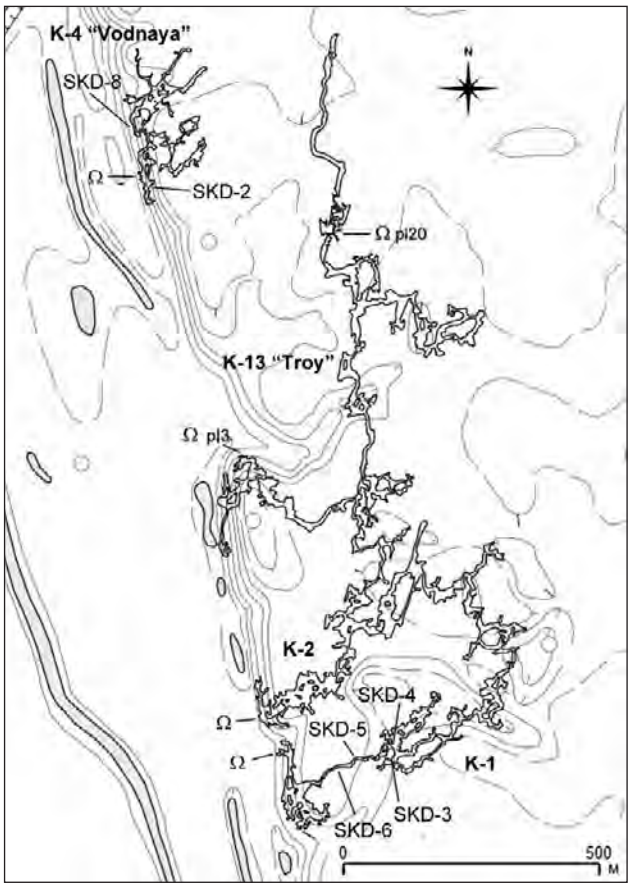

Figure 3. Location of measurement sites.

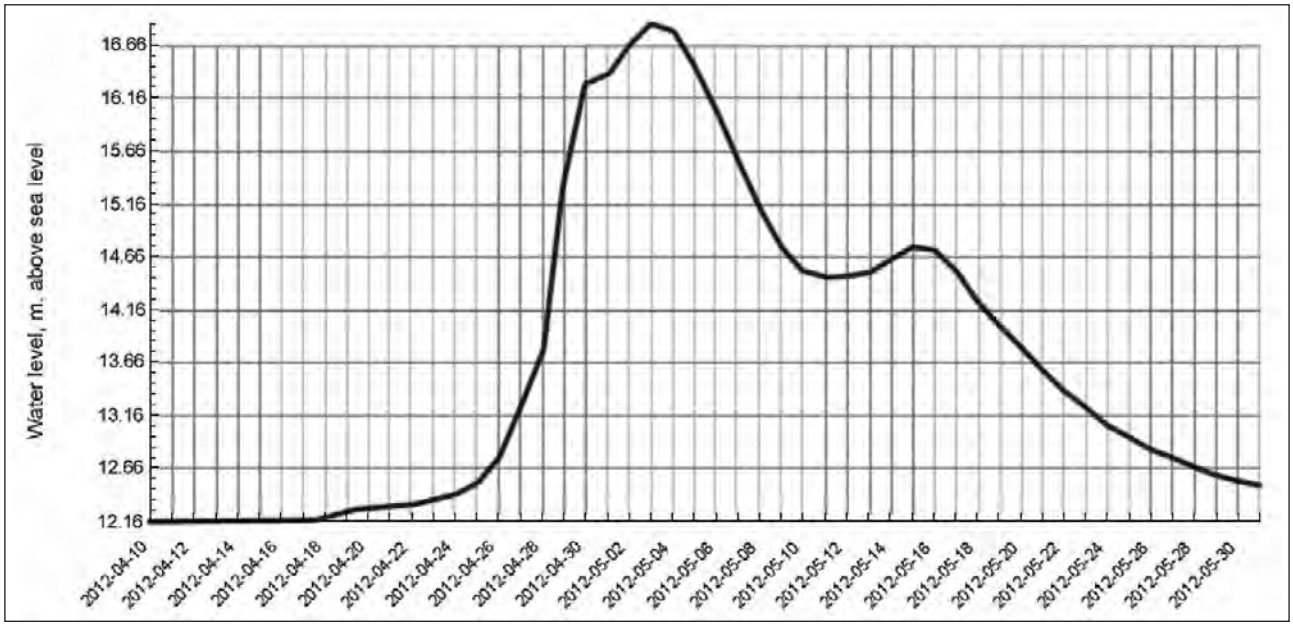

Figure 4. Hydrograph of spring flood at Pinega river. Data from the state gauging station in Kulogory village in the immediate vicinity of the cave system (Federal State Unitary Enterprise "Centre of Russian water works inventory and state water cadaster", 2012).

Reference points are stainless steel screws fixed to the wall with plastic plugs to a depth of 50–60 mm. During the measurement special aluminum rod of square section with test holes every 3 cm is imposed on the heads of the screws (Fig. 2).

Vernier caliper probe is inserted to each hole and distance between wall surface and outer surface of the rod is measured.

On every SKD site we made a special "passport" with the tables of the measured values on each set of control points. We also made an exact measurement of height above sea level of each control point row.

5. Results and discussion

This report presents the results of observations on six oldest SKD sites equipped in 2003–2004 and affected by nine spring floods (2004–2012). Locations of sites are shown in Fig. 3. Totally 62 points were analyzed.

Obviously, in the existing hydrogeological environment hypsometric position of the observation point plays a significant role. Thus, the higher (in absolute elevation) is the reference point, the less time it is exposed to dissolving effects of flood waters, and vice versa. This is illustrated by a spring flood hydrograph of Pinega River in 2012 (Fig. 4), which is fairly typical.

Therefore, in the analysis of the data, we took into account the absolute height of each of the control points. Taking into consideration available data on the dynamics of the spring floods of the river Pinega for 2004–2012 years, it was possible to determine the estimated time (in days) of the interaction between gypsum surface and aggressive floodwater for each control point for the entire observation period.

The resulting values of the total retreat (in mm) at each test point and the data on the duration of flooding of each of them allowed us to determine the retreat rate (Tables 1 and 2).

We have used Smirnov-Grabbs criterion on the values of the retreat rate to identify outliers. Four points with exceptionally high rate where identified. They are shown with "high rate" comment in tables 1 and 4, and they are not used for any calculations.

Using data from the remaining points we calculate mean retreat rate for every measurement row and site.

Average retreat rate for all observation points is 0.0448 mm/day. The confidence interval for this value from 0.0379 to 0.0516 mm/day.

The column "conditions" of Tables 1 and 2 provides an assessment of denudation conditions for each of the sites. In the sites marked "Corrosion" there is no signs of water flow. "Erosion" – conditions are suitable for water flow and there are signs of such flow.

It is interesting to note that the maximum retreat rate on surfaces of walls and the roof was measured at the SKD-8 site, equipped in one of the passages of Vodnaya (Water) Cave, where the nature of water deposits suggests flood-flow velocities above 1 m/sec. and here, respectively, there is a very intense water exchange.

From these data it is clear that the denudation rate of cave channels depends strongly on the local conditions, which is characteristic for gypsum karst (Klimchouk et al. 1996). On the example of SKD-2 site one can see that the dissolution rate can vary significantly even at points located in close proximity to each other. However, the obtained confidence limits give hope that average rate really characterizes the process of denudation within all massif.

Another trend that can be observed in collected data, is higher rate of dissolution of horizontal surfaces (ceilings) than of vertical (walls). However, the existing data does not reliably establish that fact. We hope to clarify this point, after completing the measurements on the other sites.

The resulting average speeds of karst denudation in real hydrogeological conditions of Kulogorskaya cave system can later be used to build a variety of mathematical models and reconstructions of paleogeography environments and stages of development of the caves of massif.

We continue to equip new measurement sites and are working on improvement of our techniques. Long-term monitoring of natural karst denudation processes will undoubtedly allow us to deepen our knowledge of the laws of development of not only Kulogorskaya cave system, but also of the entire northern sulfate karst.

References

Federal State Unitary Enterprise "Centre of Russian water works inventory and state water cadaster". http://www.waterinfo.ru/ (in Russian).

Klimchuk A, Cicchi F, Calaforra JM, Aksem S, Finocchiaro F, Forti P, 1996. Dissolution of Gypsum from Field Observations. Gypsum Karst of the World. International Journal of Speleology, Theme issue, 1996, Vol 25, Issue 0, 37–48.

Krawczyk WE, Ford DC, 2007. Correlating specific conductivity with total hardness in gypsum karst waters. Earth Surf. Process. Landforms, 32: 612–620. doi: 10.1002/esp.1409.

Smith DI, 1977. The Micro Erosion Meter: Its application to the Weathering of Rock Surfaces. Conservation of Rock Art. Proceedings of the International Workshop on the Conservation of Rock Art, Perth, September 1977 (1978), 44–53.

Table 1. Measurement data and statistics, part 1.

Site	Conditions	Row	Sufrace	Point	Pecularities	Height, m a.s.l.	Days underwater	Depth in 2004 mm	Depth in 2012 mm	Total retreat, mm	Retreat rate, mm/day	Avg. rate for row, mm/day	Avg. rate for location, mm/day
SKD-2	Erosion	A	Wall	1		16.69	25	22.0	23.7	1.7	0.0680	0.0690	0.0475
				2		16.66	25	27.7	29.4	1.7	0.0680		
				4		16.60	25	35.0	36.4	1.4	0.0560		
				5	high rate	16.57	25	33.6	36.8	3.2	0.1280		
				6		16.54	25	29.2	31.3	2.1	0.0840		
		B	Wall	1		16.36	36	26.5	28.2	1.7	0.0472	0.0299	
				2		16.33	36	31.2	32.1	0.9	0.0250		
				3		16.30	36	32.6	33.1	0.5	0.0139		
				6	crystall	16.21	36	29.1	30.3	1.2	0.0333		
		C	Wall	1		16.02	46	35.0	38.4	3.4	0.0739	0.0591	
				2		15.99	46	34.2	36.0	1.8	0.0391		
				3		15.96	46	28.4	31.2	2.8	0.0609		
				4		15.93	46	27.8	30.5	2.7	0.0587		
				5	crystall	15.90	46	25.0	27.9	2.9	0.0630		
		D	Wall	1		15.35	79	25.0	27.3	2.3	0.0291	0.0352	
				2		15.32	79	23.0	25.1	2.1	0.0266		
				3		15.29	79	25.6	28.5	2.9	0.0367		
				4		15.26	79	23.3	26.6	3.3	0.0418		
				5		15.23	79	26.2	29.3	3.1	0.0392		
				6		15.20	79	28.0	31.0	3.0	0.0380		
SKD-3	Corrosion	A	Wall	1		15.57	51	18.1	19.9	1.8	0.0353	0.0196	0.0330
				2		15.57	51	16.2	16.8	0.6	0.0118		
				3		15.57	51	16.0	16.9	0.9	0.0176		
				4		15.57	51	13.8	14.5	0.7	0.0137		
		B	Wall	1		16.27	33	18.0	19.2	1.2	0.0364	0.0436	
				2		16.27	33	17.3	18.3	1.0	0.0303		
				3		16.27	33	17.2	18.3	1.1	0.0333		
				4		16.27	33	18.0	18.8	0.8	0.0242		
				5		16.27	33	17.7	20.8	3.1	0.0939		
SKD-4	Erosion	A	Wall	1		15.18	80	16.4	17.3	0.9	0.0113	0.0148	0.0148
				2		15.18	80	12.0	13.1	1.1	0.0138		
				3		15.18	80	17.8	19.5	1.7	0.0213		
				4		15.18	80	18.5	19.7	1.2	0.0150		
				5		15.18	80	20.0	21.0	1.0	0.0125		
SKD-5	Erosion	A	Wall	1		15.34	72	11.2	13.0	1.8	0.0250	0.0378	0.0372
				2		15.34	72	14.8	16.8	2.0	0.0278		
				3		15.34	72	16.0	19.2	3.2	0.0444		
				5		15.34	72	25.4	29.3	3.9	0.0542		
		B	Wall	1		15.70	50	14.4	16.5	2.1	0.0420	0.0365	
				2		15.70	50	18.5	20.1	1.6	0.0320		
				3		15.70	50	16.3	18.6	2.3	0.0460		
				4		15.70	50	20.1	21.4	1.3	0.0260		
SKD-6	Erosion	A	Wall	1		15.94	44	21.5	22.5	1.0	0.0227	0.0352	0.0352
				2		15.94	44	21.0	23.0	2.0	0.0455		
				3		15.94	44	20.0	21.4	1.4	0.0318		
				4		15.94	44	20.8	22.3	1.5	0.0341		
				5		15.94	44	21.5	23.0	1.5	0.0341		
				6		15.94	44	20.8	22.7	1.9	0.0432		

Table 2. Measurement data and statistics, part 2.

Site	Conditions	Row	Sufrace	Point	Pecularities	Height, m a.s.l.	Days underwater	Depth in 2004 mm	Depth in 2012 mm	Total retreat, mm	Retreat rate, mm/day	Avg. rate for row, mm/day	Avg. rate for location, mm/day
SKD-8	Erosion, high-speed currents	A	Celling	1	high rate	15.90	45	14.2	21.9	7.7	0.1711	0.0844	0.074
				2		15.90	45	15.2	20.3	5.1	0.1133		
				3	high rate	15.90	45	15.2	23.5	8.3	0.1844		
				4		15.90	45	14.2	18.6	4.4	0.0978		
				5		15.90	45	15.0	16.9	1.9	0.0422		
		B	Wall	1		15.60	52	14.3	18.2	3.9	0.0750	0.0723	
				2		15.60	52	15.5	19.8	4.3	0.0827		
				3		15.60	52	21.0	24.1	3.1	0.0596		
				4		15.60	52	22.6	26.3	3.7	0.0712		
				5		15.60	52	19.6	23.4	3.8	0.0731		
		C	Wall	1		15.30	73	20.1	25.5	5.4	0.0740	0.0667	
				2		15.30	73	16.1	21.4	5.3	0.0726		
				3	high rate	15.30	73	13.2	23.2	10.0	0.1370		
				4		15.30	73	16.0	19.9	3.9	0.0534		

GEOLOGY AND STRUCTURE OF PARIAN CAVE, ISFAHAN, IRAN

Ghassem Ghaderi , Leila Karimi
Iran Speleology Society, 71438-54941, Gas S., Shiraz, Iran, ghaderi1348@yahoo.com, L_karimi2007@yahoo.com

Parian Cave is located in Meimeh, Isfahan Province and formed in to the Triassic dolomites (Shotori Formation). The cave was discovered in 1999 and about 1,400 m of it has been surved. The cave developed above the water level (vadose zone) and has a very beautiful carbonate speleothems such as stalactites, stalagmites, columns, coralloids, flowstones, draperies, helectites, anthodites, frostworks, crusts, flowers, sodastraws, rimestones and shields.

This survey is geological, morphological and structural viewpoints and the study results shows that the cracks and fissures have created enough porosity in the host stone and rainfalls have provided internally karst conditions. The cave passages follow discontinuity surfaces. They look are like a network of related underground spaces. Depending on the morphology of the passage and cave climate, every passage creating special speleothems and should be examined separately because each underground space has its special morphologic, hydrogeologic and hydrochemic conditions. The Parian Cave is a maze cave and has a pool with carbonate type elements.

1. Introduction

Vast regions in Iran including Zagros, Elburz and central Iran mountains consist of karst rocks which are important source of drinkable water for the population arid and semiarid climate of Iran. On the other hand, the hydrocarbon sources (oil and gas) are mostly located in karst regions in Iran and many silver, lead, zinc and bauxite sources are situated in similar locations.

In this article the geology, geomorphology and tectonics of the Parian Cave were studied. The research is divided into two parts: (1) superficial and (2) subsurface examinations. The geologic map (1:2,000) and structural map including joints, faults, strata dip and strike and fold axes by the satellite photos are obtained. All discontinuous surfaces including fissures, faults, joints and beddinging in 14 places on the surface around the cave entrance were sampled and analyzed.

The cave was mapped by compass and all the discontinuities were measured and analyzed by “rockwork” and finally the gained superficial and internal data were compared and the formation and development ways were analyzed.

Figure 1. Satellite photo of the Parian Cave.

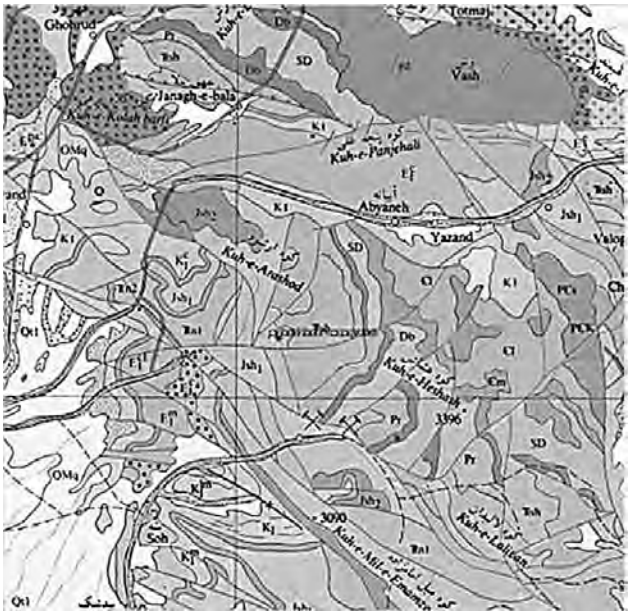

Figure 2. The Parian Cave in geologic map.

2. Discussion

The Parian Cave is formed in Middle Teriassic dolomite. Lithology around the cave was mapped by meter and compass in the field (Tab. 1). Five main layers and eleven secondary layers were found in the travers from the valley bottom, hill summit up to the next valley.

Limestones are light and dark colored with sandstone interbed deposited in shallow coastal environment. The Parian Cave is located in massive limestone layer. Dolomitic layers form cave walls. The change in the carbonate rock lithology and its impurities represents an important factor increasing potential for the karst formation in this region.

Table 1. Lithology of the layers measured during field.

Symbol	Thickness	Lithology
Rash5		Alternation of green shale with layers of sandstone and thin layers of limestone and dolomite, sometimes ferrous
Rash4	5	Light cream crushed limestone
	7.4	Light cream limestone
	2.9	Dark grey limestone
	2.9	Alternation light and dark limestone
	11.2	Cream crushed limestone
	14	Alternative dark and sandy limestone
	23.2	Brown ferruginous sandy limestone
	7.4	Dark grey limestone
	35.1	Alternation of grey limestone and red ferrous sandstone
	20.7	Alternation of grey limestone and sandstone
	10.8	Dark and cream limestone
Rash3	184	Fissured cream limestone with fault and superficial karen
Rash2	62	Green shale with sandstone and limestone interbeds
Rash1		Light cream thickly-layered limestone with small caves

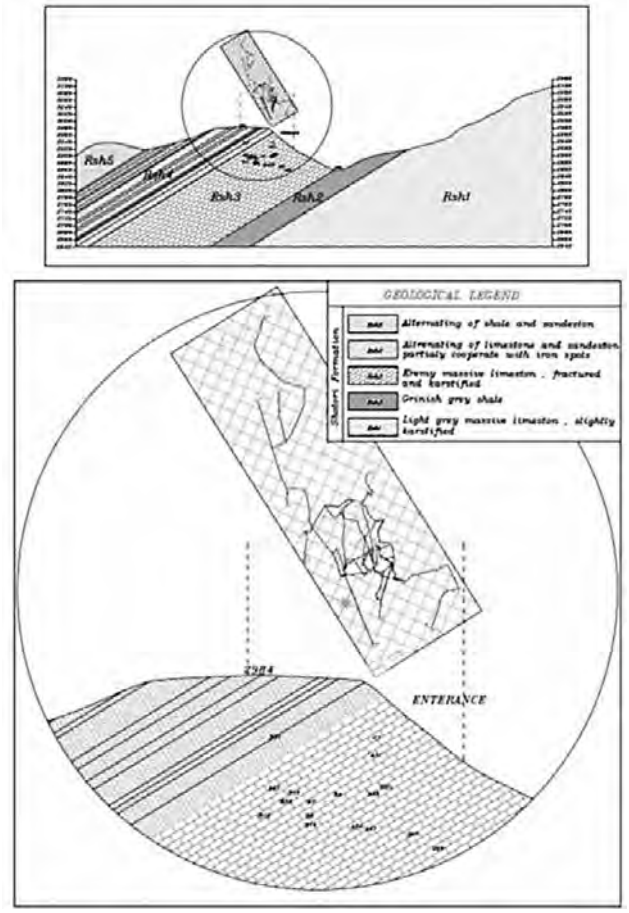

Figure 3. Geological section of The Parian Cave.

By virtue of the joint studies on 14 parts around the cave entrance, 3 sets of discontinuous surfaces are found. The joint surface properties included planar, semi-open, unfilled or filled partly with loam, and rough surface and moderately weathered. Countour and rose diagrams are shown three joint sets with northeast to southwest trend (Fig. 4).

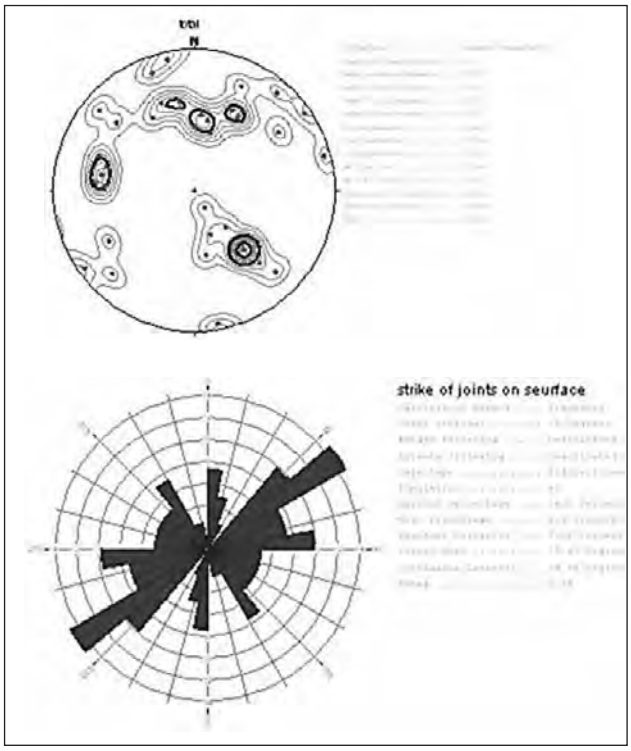

Figure 4. The countour and rose diagram of discontinuous surfaces on the ground.

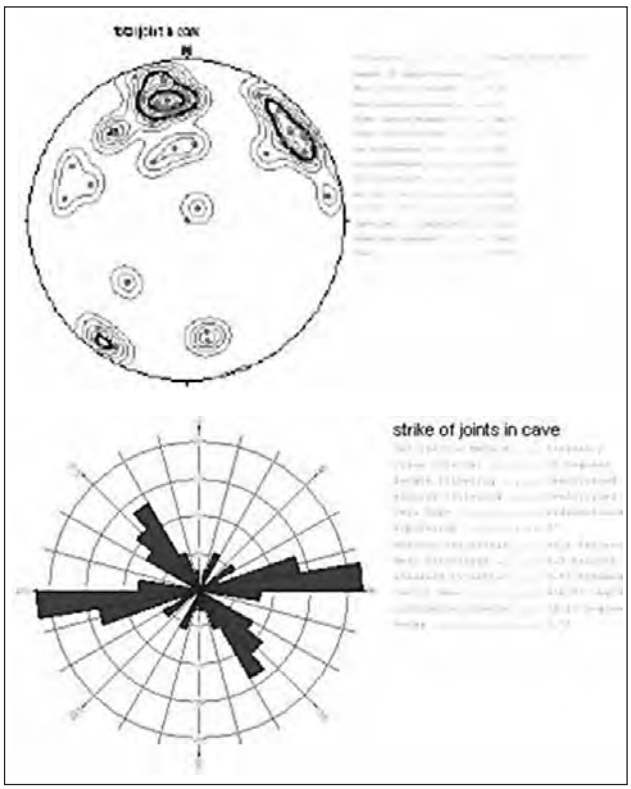

Figure 5. The countour and rose diagram of discontinuous surfaces in the cave.

The internal fissures were measured in the passages and chambers of cave (Fig. 5). The stereographic diagram shows that the cave fissures pattern is approximately similar to the earth surface; only the dip of discontinuities in the cave are less than the surface ones and have a 20–30° turning. The cave discontinuous surface properties are open and not filled.

The Parian Cave was surveyed completely in four weeks by meter and compass and data drawn by the software compass. Figures 6 and 7 show the plan and profile drawn by software and Table 2 shows statistic analysis of the cave.

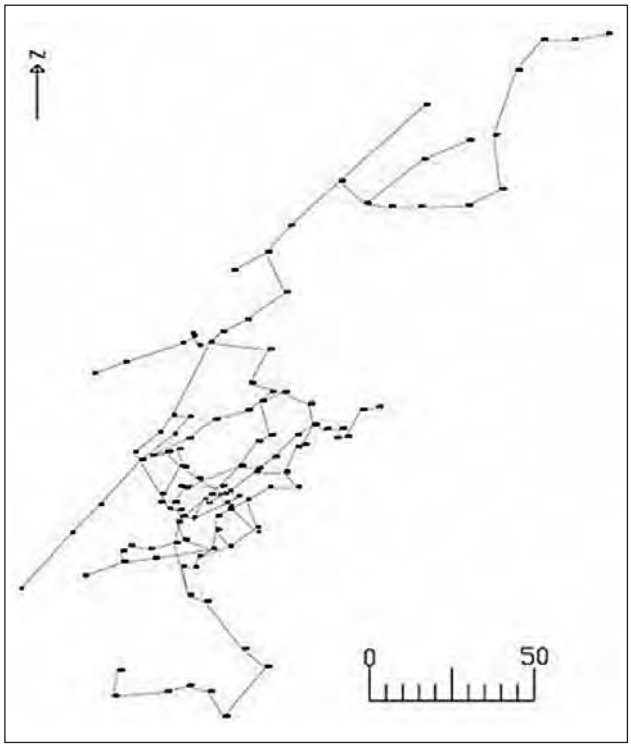

Figure 6. The Parian Cave plan.

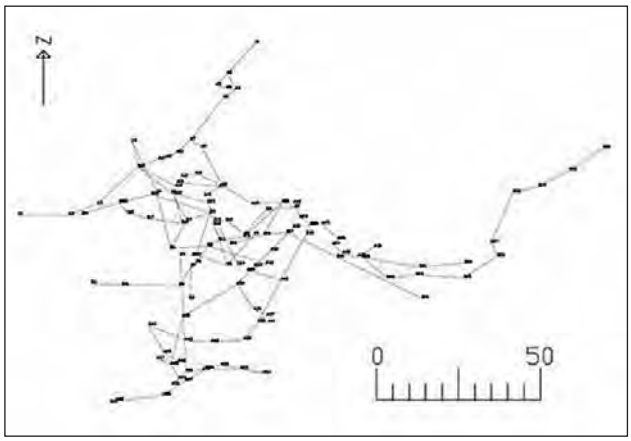

Figure 7. The Parian Cave profile.

The azimuth of the cave has the NE–SW trend and is completely similar to the discontinuities on the surface and inside the cave (Fig. 8). The cave has the negative or positive 20° dip (Fig. 9) and also 70 % of cave length is in the depths of 30 to 70 m (Fig. 10).

Table 2. The specifications of the statistic analysis of The Parian Cave.

Included Length	1,401.5 m
Total Surveyed	1,401.5 m
Horizontal Length	1,185.7 m
Cave Depth	110.1 m
Surface Length	178.5 m
Surface Width	209.0 m
Surface Area	37,308.3 m^2
Cave Volume	99,409.4 m^3
Average Diameter	8.4 Meters
Wall Area	39,593.5 m^2
Floor Area	10,349.5 m^2
Average Inclination	25.8°

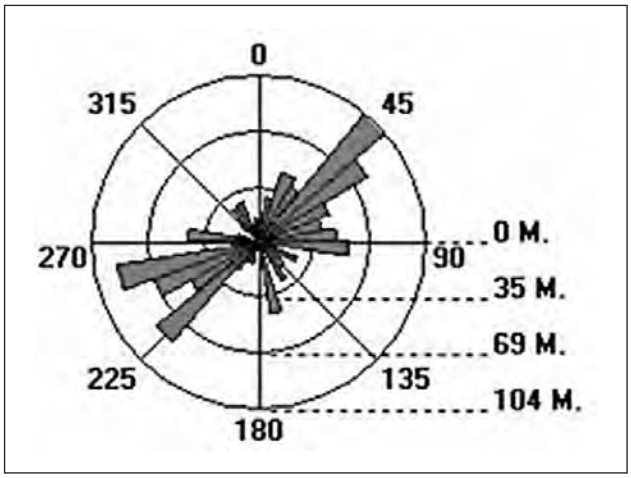

Figure 8. Rose diagram of the cave passages.

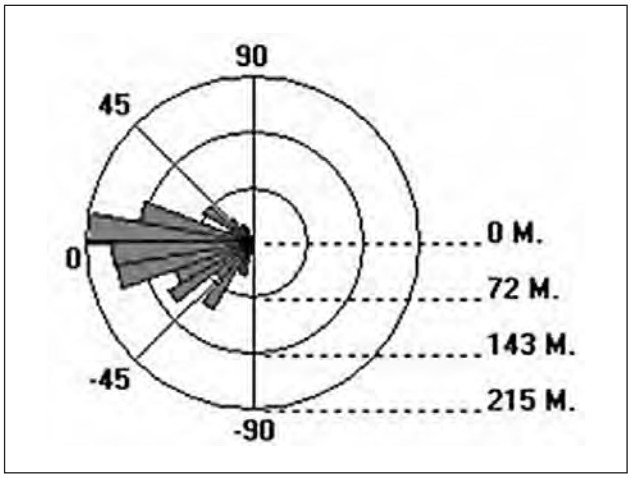

Figure 9. The dip diagram of The Parian Cave.

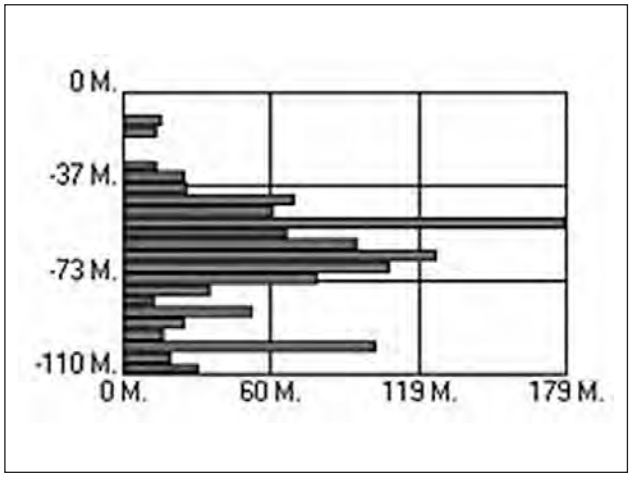

Figure 10. The passage length versus passage dip of The Parian Cave.

This survey shows that two systems effect to form of speleothems. Internal cave system and external cave system. External cave system relates to near-surface hydrological cycle and internal cave system refers to every process that has happened in the cave. In this point of view, all of the speleothems in the Parian Cave have classified to two major groups.

1. Speleothems controlled by physico-chemical conditions of the External cave system that has recorded in infiltered water and goes down to cave and can be recognized in speleothems which were formed by dripping water(such as stalactite, stalagmite, column, sodastra) and flowing water (flowstone, drapery, shield).
2. Speleothems controlled by physico-chemical conditions of the internal cave system that related to microclimate conditions in cave and can be recognized in speleothems which were formed by seeping water(coralloid, helectite, frostwork, anthodite) and speleothems that formed under pools (crystal lining, gours).

3. Conclusions

The findings concerning the Isfahan Parian Cave studies are as follows:

1. The Parian Cave is developed mostly in the massive limestone layers. Dolomite layers are mostly in cave walls so the change in the lithology and rock impurities has been an important factor increasing karst evolution potentiality in one region and undeveloped potentiality in other ones.
2. The discontinuous surfaces which developed on the earth and deep fissures transfer the rains into the cave and create the porosity necessary for karst development. The rose diagram in the cave is completely similar to the surface. Also, the properties of discontinuity are similar to the surface; only the cave fissures are open and unfilled completely.
3. The Parian Cave represents a set of related passages and corridors following the discontinuity pattern on the surface and in fact, it is a maze cave.
4. Total length of the cave is 1,401 m with an area of 37,000 m^2. The mean diameter of the disintegration passages is 8.4 namely the disintegration is effective. The lowest part of the cave is in 110 m depth from the entrance.
5. The mean slope is positive and negative 20° and the most development is the depth of 30–70 m.
6. Internal and External cave systems are effect to form Parian speleothems. Speleothems which were formed by dripping water and flowing water controlled by physico-chemical conditions of outer cave system. Also Speleothems which were formed by percolating precipitation and speleothems which formed within pools controlled by physico-chemical conditions of external cave system.

Acknowledgments

The study was done with the kind help and generous grace of Chakad Mountain Climbing Group and many spelunkers from Tehran, Isfahan and Shiraz to map and survey the cave. Also I continue to be indebted to Mr. Behrooz Mohammadi, Mr. Mansoor Khojasteh, Mr. Mahdi Hajhashemi, Ms Mehrnoosh Noorelahi, Mr. Mahdi Shahkarami, and Mr. Ahmad Emadzadeh for their kind cooperation.

References

Darvishzadeh A, 1991. Iran Geology, Emrooz Publications.

Memarian H, 1995. Engineering Geology and Geotechnique, Tehran University Press.

Ghobadi MH, 2007. Karst Engineering geology, Booali Sina University Press, Hamedan.

Topographic maps with the scale 1:25,000, State Topography Organization.

Kashan Geological Map with the scale: 1:250,000, Iran Oil National Company.

PRELIMINARY STUDIES ON CORROSIVE FORMS AND CLASTIC DEPOSITS IN THE ŚNIEŻNA CAVE (THE TATRA MTS., POLAND)

Ditta Kicińska
Institute of Geology, Adam Mickiewicz University, ul. Maków Polnych 16, 61-606 Poznań, Poland, kicinska@amu.edu.pl

The Wielka Śnieżna Cave is the deepest and the longest system in Poland, which consists from group of vertical shaft with horizontal parts among of which the highest situated on depth of 300 m (the part of Wodociąg and Ciągi Zakopiańskie passages). New data on basis observation of corrosive forms and heavy minerals analyses indicate that some passages of the Śnieżna Cave could be formed on several stage and under phreatic or epiphreatic conditions.

1. Introduction and geological settings

The Wielka Śnieżna Cave System (denivelation of 824 m, length of 23 km) is situated in the Czerwone Wierchy Massif, which is surrounded on the northern part by the Mała Łąka, Miętusia and Kościeliska valleys. The system includes 5 caves: Śnieżna, Wielka Litworowa, Nad Kotliny, Jasny Aven and Wilcza (Fig. 1). Preliminary studies were conducted in the Śnieżna Cave up to depth of 300 m where the horizontal part named Wodociąg and Ciągi Zakopiańskie passages occur (Grodzicki 2002).

The system is developed in Mesozoic limestones, which belong to the High Tatric sequence (Kotański 1959). Three E–W-trending carbonate belts (southern, middle and northern) separated by zones of non-karstic rocks occur in this sequence. The belts run across river valleys. The Wielka Śnieżna Cave System belongs to the middle belt, in which the longest and the deepest caves of Poland are located. This part of the Czerwone Wierchy Massif is discharged by an ascending Lodowe Źródło Spring (in the Kościeliska Valley).

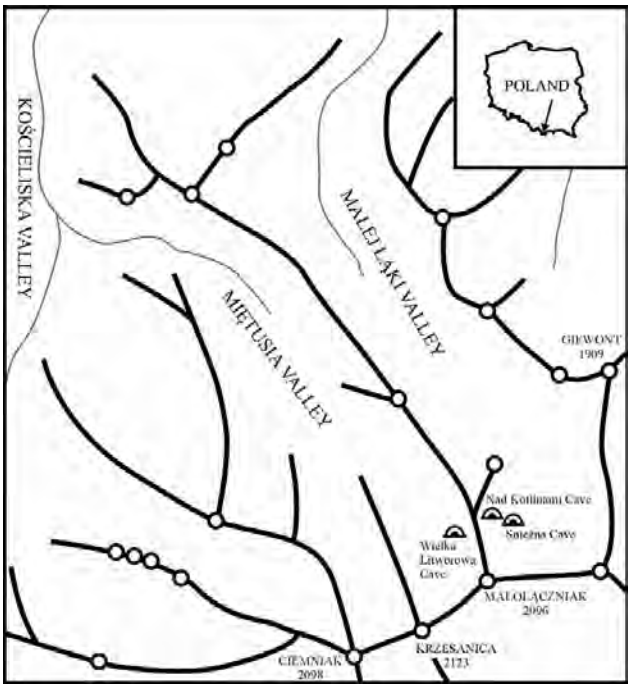

Figure 1. Location of Śnieżna Cave.

2. Investigations in the cave

The first observation on karst was published by Kowalski (1953), who claimed that the Lodowe Spring in the Kościeliska Valley drains the western part of the Czerwone Wierchy Massif between the Kościeliska and Miętusia valleys and possible the eastern part of Czerwone Wierchy Massif too. Zwoliński (1955) suggested that the Lodowe Spring drains the massif between peaks of Ciemniak and Małołączniak. The tracing of underground water in the Śnieżna Cave revealed flow to the Lodowe Spring during 6 days (Dąbrowski and Rudnicki 1967).

Investigations of origin and age of Śnieżna Cave were made by Wójcik (1978), Głazek et al. (1979), Grodzicki (1991, 2002) and Głazek and Grodzicki (1996) who concluded that the main reason of development of cave is tectonic widening of fissures, which formed during deglaciations. Following researches were conducted by Kicińska (2002) and Pawłowska – Bielawska (2007) who origin horizontal passages related to be formed under phreatic or epiphreatic conditions.

Observation and measurements of scallops were performed in the main passages of the Wodociąg and Ciągi Zakopiańskie passages (toward Salka Rysi). Asymmetry of scallops indicate a west paleocurrents direction (towards the Kościeliska Valley) (Fig. 2). Composition of heavy minerals in particular parts is varied. Predominance instable minerals in the Wodociąg passages and chemostable and mechanostable minerals – in the Ciągi Zakopiańskie passages provides that analyzed horizontal passages

of Śnieżna Cave has been not formed on one stage (Fig. 3). The cross section of passages confirmed suggestion made by Głazek et al. (1977) that the vertical elements developed on tectonic discontinuities during deglaciation of Pleistocene and Holocene age as the invasion caves (proglacial). Ellipsoidal cross section of the Wodociąg and Ciągi Zakopiańskie passages, paleocurrents direction based on scallops and composition of heavy minerals show that the horizontal parts were formed under epiphreatic or phreatic conditions, what sheds a new light on the origin, evolution and probably age of the Śnieżna Cave. To better understand the Wielka Śnieżna Cave System more researches is needed such as analysis of spatial patterns of cave and cross-section of passages, analysis of corrosive forms and dating of speleothems.

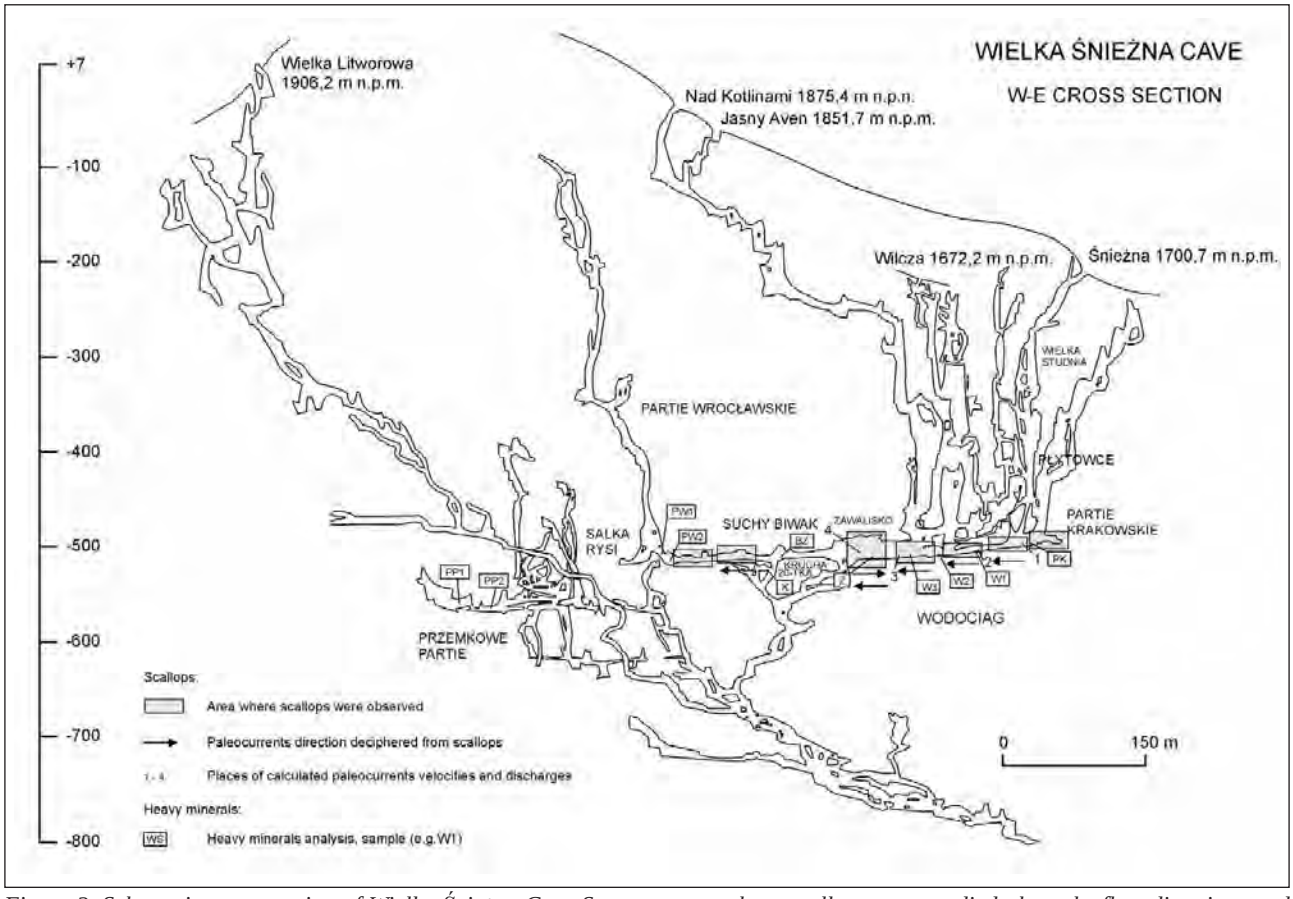

Figure 2. Schematic cross-section of Wielka Śnieżna Cave System, areas where scallops were studied, the paleoflow directions and sampling places of clastic deposits.

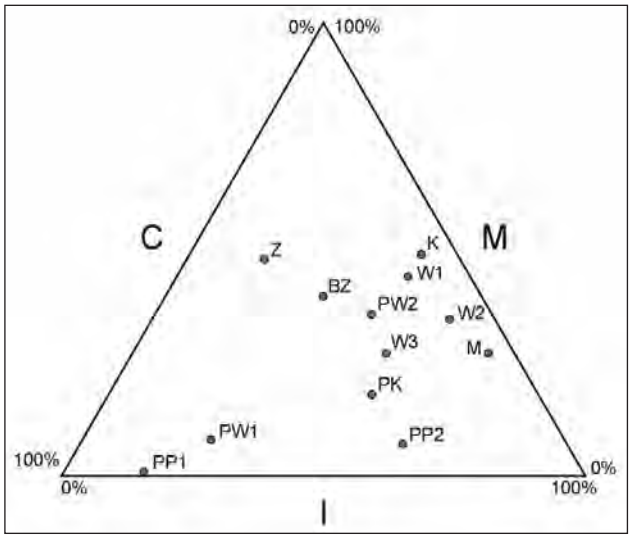

Figure 3. Relationship between instable (apatite, amphinole, epidot), chemostable (rutile, staurolite, disthene, tourmalines) and mechanostable (garnets, zircon) heavy minerals in the studied samples, classification diagram after Burkhardt (1978).

References

Bielawska-Pawłowska P, 2007. Evolution of Wielka Śnieżna Cave in the light of geomorphologic observations. Karst and Cryokarst, Uniwersytet Śląski, 155–164.

Dąbrowski T, Rudnicki J., 1967. Wyniki badań przepływów krasowych w masywie Czerwonych Wierchów. Speleologia, 3, 1, 31–33.

Głazek J, Grodzicki J, 1996. Kras i jaskinie. In: W: Mirek Z. (Ed.). Przyroda Tatrzańskiego Parku Narodowego. Wyd. Inst. Ochr. Przyrody PAN, 139–169.

Głazek J, Rudnicki J, Szynkiewicz A, 1977. Proglacjal caves – a special genetic type of caves in glaciated areas. Proceedings 7th International Speleological Congress, Sheffield, England, Semptember, 1977. British Cave Research Association, Bridgewater. 215–217.

Grodzicki J, 1991. Geneza i ewolucja jaskiń Tatr Zachodnich. In: Grodzicki J. (Ed.) Jaskinie Tatrzańskiego Parku Narodowego. T. 1. Jaskinie Doliny Chochołowskiej i dolinek reglowych. Polskie Towarzystwo Przyjaciół Nauk o Ziemi. 11–41.

Grodzicki J, 2002. Jaskinie Tatrzańskiego Parku Narodowego. Wielkie jaskinie Doliny Małej Łąki. T.9. Polskie Towarzystwo Przyjaciół Nauk o Ziemi, Warszawa, 1–278.

Kotański Z, 1959. Profile stratygraficzne serii wierchowej Tatr Polskich. Biuletyn IG, 139, 1–160.

Kowalski K, 1953. Jaskinie Tatr Polskich. Wyd. Państw. Muz. Archeol., 1–186.

Wójcik Z, 1978. O wieku jaskiń tatrzańskich. Prace Muzeum Ziemi, 28, 123–131.

Zwoliński S, 1961. W podziemiach tatrzańskich. Wyd. Geol., 1–277.

GEOCHEMICAL AND STABLE ISOTOPE CHARACTERIZATION OF DRIP WATER FROM THE POSTOJNA CAVE, SLOVENIA

Magda Mandić[1], Andrej Mihevc[2], Albrecht Leis[3], Ines Krajcar Bronić[4]
[1]Department of Physics, University of Rijeka, Rijeka, Croatia, mmandic@phy.uniri.hr
[2]Karst Research Institute, Postojna, Slovenia
[3]Joanneum Research Institute, Graz, Austria
[4]Ruđer Bošković Institute, Zagreb, Croatia

Comprehensive investigation of geochemical and isotopic characteristics of drip water in Postojna Cave (Classical Karst, SW Slovenia) is presented here. Sampling of drip water was performed at 9 locations within the cave from March 2010 to April 2011. Air and water temperature, pH value, drip rate, conductivity, ion concentrations, $\delta^{18}O$ of water and $\delta^{13}C$ of DIC were determined. All drip waters belong to the Ca – HCO_3 type according to chemical composition and to the seepage-flow type according to drip rate and its variability. Cave temperature is relatively constant during the year and reflects the average temperature in the region. Relatively constant $\delta^{18}O$ values of drip water reflect mean $\delta^{18}O$ of precipitation. A process of prior calcite precipitation (PCP) is proposed for explaining observed differences in some parameters at location 05 – Podrti kapnik in comparison with all other locations.

1. Introduction

The Postojna Cave (Slovenia) is one of the most famous karst caves in the South-eastern Europe. The comprehensive investigation of speleothems and cave environment has been undertaken with the aim to map recent geochemical and stable isotope characteristics of the Postojna Cave which could help in providing insights into climate and environmental changes. In this work we present results that relate to various geochemical and isotopic parameters in drip water.

2. Site description

The Postojna Karst is situated in Slovenia on NW part of the Dinaric Karst (Figure 1). More than 60 caves are known in the Postojna Karst. The largest cave system (20.5 km long) is the Postojna Cave system. One of the caves in the system is the Postojna Cave, 10,399 m long (Šebela 1997). The Postojna Cave was formed by the sinking Pivka River. There are two main levels of the cave passages: the upper, which is mostly dry, and the lower where the Pivka River flows. Modern entrance of the Postojna Cave is at 529 m a.s.l. It is 18 m above the Pivka River sinkhole. The entrance leads to the upper level of cave passages and larger halls which are also connected with lower river passage. In the whole length cross section is rounded and shows leveled ceilings. On the walls and ceiling of the cave interior there are marks and remains of sediments, indicating that in the cave evolution there were cycles of filling and flushing out the cave passages during the past (Brodar 1966).

3. Sampling

Monitoring in the Postojna Cave was performed in the period from March 2010 to April 2011. Sampling of drip water was done at 9 locations within the cave (Figure 2). Additionally, the Pivka River was sampled at two locations: at the entrance to the Postojna Cave and 2.5 km inside the cave. On the field were measured pH, conductivity, air and drip water temperature and drip rate. Laboratory chemical analysis of water samples included measurements of Ca^{2+}, Mg^{2+}, HCO_3^- concentrations and twice a year measurement of Na^+, K^+,Cl^-, SO_4^{2-} and NO_3^- concentrations. Stable isotope compositions of water ($\delta^{18}O$) and dissolved inorganic carbon DIC ($\delta^{13}C_{DIC}$) were determined.

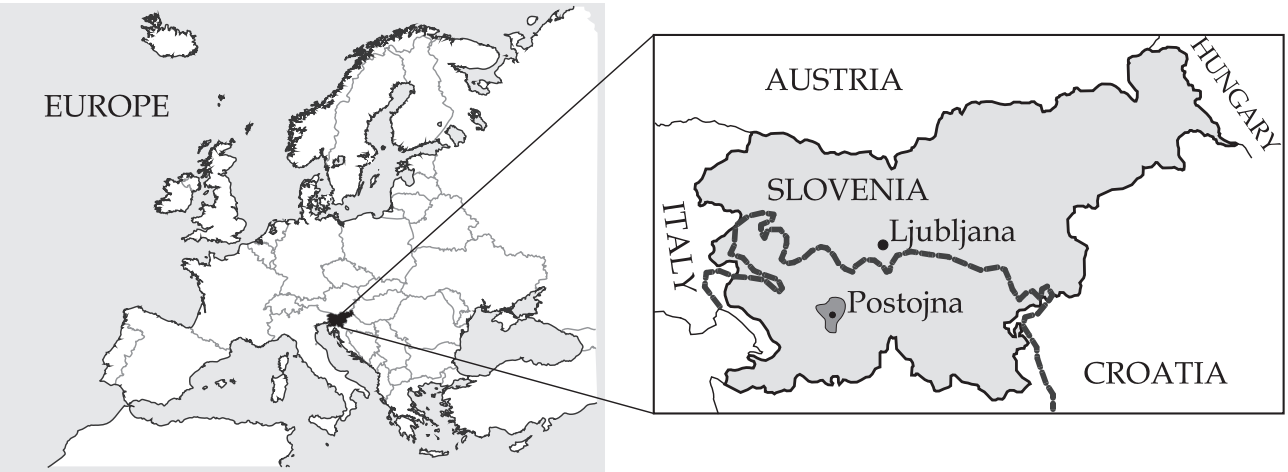

Figure 1. Map of Europe with position of Slovenia (left); (right) map of Slovenia with Postojna Karst area (darker shadowed area). The boundary of the Dinaric karst (dashed line) is shown (Gams 1974).

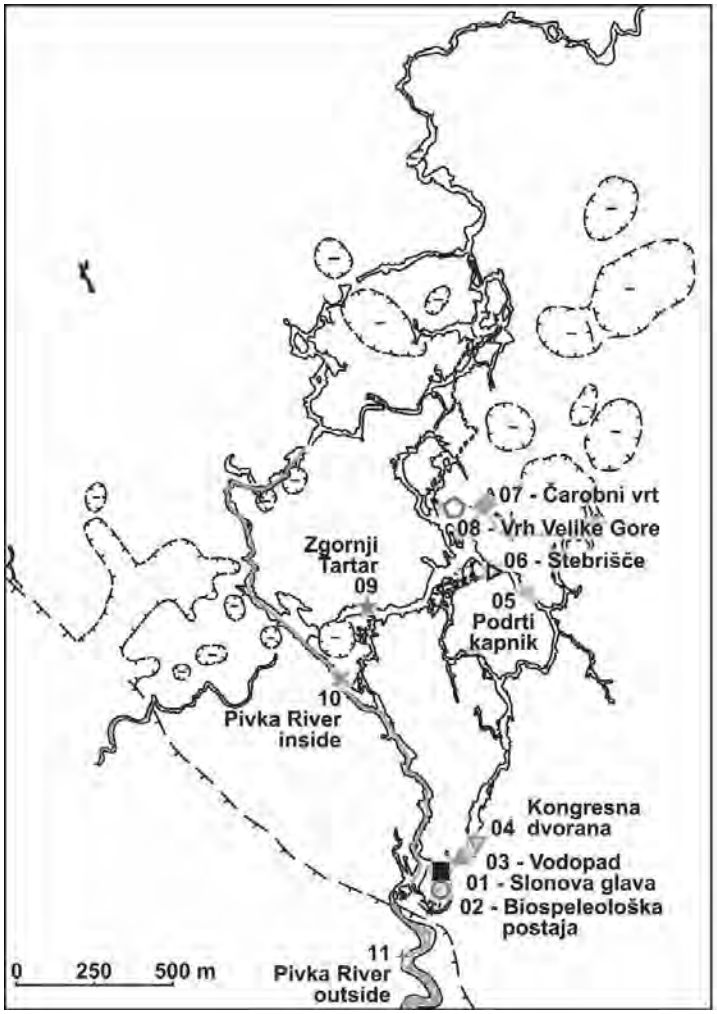

Location number and name	Symbol
01 - Slonova glava	■
02 - Biospeleološka postaja	○
03 - Vodopad	▲
04 - Kongresna dvorana	▽
05 - Podrti kapnik	◁
06 - Stebrišče	▷
07 - Čarobni vrt	◆
08 - Vrh Velike Gore	⬠
09 - Zgornji Tartar	★
10 - Pivka River inside	×
11 - Pivka River outside	+

Figure 2. Sampling locations in the Postojna Cave (left). List of names of the sampling locations and their numbers, and the symbol applied in this paper (right).

4. Measurement

Physical (temperature) and chemical parameters (pH and conductivity, both corrected to 25 ºC) in drip waters were measured *in situ* by the WTW multiline pH/Conductivity 340i Ph Meter. Chemical analyses of water samples were performed by certificated methods using ion chromatography. Stable isotope analyses were carried out in Laboratory Centre for Isotope Hydrology and Environmental Analytics, Joanneum Research Institute (Graz) by an on-line continuous-flow system (Gasbench II) linked to a Thermo Fisher Scientific DELTA^{plus}XL isotope ratio mass spectrometer. The $\delta^{18}O$ values are reported relative to the VSMOW scale and $\delta^{13}C_{DIC}$ relative to the VPDB scale. Calibration of the mass spectrometer was accomplished using in-house water and calcite reference materials whose stable isotopic composition had previously been calibrated (Spötl 2005).

5. Results and discussion

Air temperature (Fig. 3) within the Cave varies slightly around 10 °C, which is close to the mean air temperature measured at the meteorological station during last decade (9.7 ±0.5 °C). Variations around the mean are larger at locations closer to the entrance to the Cave. Drip water temperature also slightly varies around 10 °C, while the river water follows more closely the outside air temperature. Monthly amount of precipitation and drip rate are shown in Figure 4. According to drip rate and its variability, all drip waters belong to the seepage type (Smart and Friedrich 1987). The lowest drip rate is measured in summer (August 2010), and the highest in November 2010, about two months after abundant precipitation in September 2010. During winter period (February 2011), preceded by two months of low precipitation, the drip rate is again low. Low discharge in winter may be observed also because of snow cover during winter months.

At location 08 – Vrh Velike gore the highest drip rate is measured in November 2010 due to the high amount of precipitation during September 2010. In the time with low

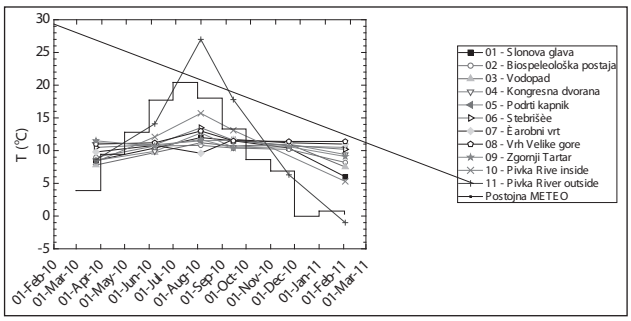

Figure 3. Air temperatures on sampling locations in Postojna cave, together with data from Slovenian meteorological survey for Postojna during sampling period (step line).

precipitation amount the drip rate at location 08 – Vrh Velike gore is low. That would appoint to short mean residence time (MRT) at location 08 – Vrh Velike gore. The response of the drip rate to abundant precipitation is delayed for about 2 months at locations 07 – Čarobni vrt, 08 – Vrh Velike gore and 09 – Zgornji Tartar, as opposed to location 02 – Biospeleološka postaja where high precipitation amount has negligible influence on drip rate, i.e. drip rate is relatively constant and not dependent on the amount of precipitation (Fig. 4).

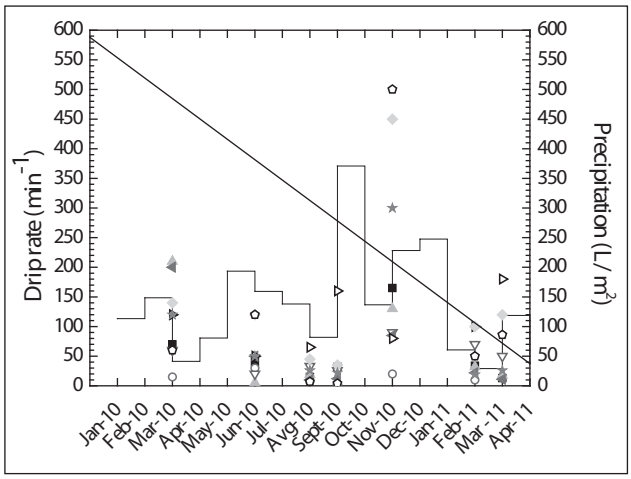

Figure 4. Monthly precipitation amount (—) and drip rate.

The pH values of the drip water show seasonal fluctuation – lowest pH values are measured in August and September and highest during winter months (November–March).

Calcium concentrations range between 74 and 89 mg.l^{-1} (Fig. 5). Largest variation from mean value for calcium concentration is found at location 01 – Slonova glava (89 ±16 mg.l^{-1}), and at location 08 – Vrh Velike gore deviation from mean value is the lowest (82 ±3 mg.l^{-1}). Location 05 – Podrti kapnik has the lowest mean value (65 ±12 mg.l^{-1}). Mean HCO_3^- concentrations range between 200 and 273 mg/L at all locations except for Podrti kapnik (152 mg.l^{-1}).

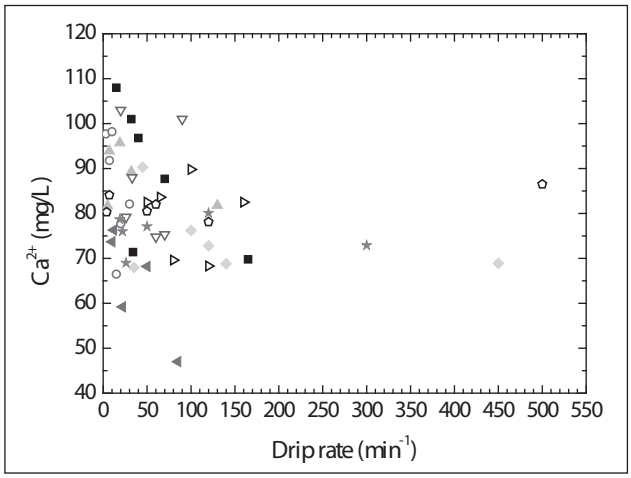

Figure 5. Dependence of calcium ion concentration on drip rate.

Relation of calcium ion concentration and drip rate is different for different locations (Figure 5). At locations 07 – Čarobni vrt, 08 – Vrh Velike gore and 09 – Zgornji Tartar where drip rate has large variations calcium concentration is stable. The larger variation of calcium ion concentration has been observed at location 02 – Biospeleološka postaja, where the drip rate is constant and low.

The average concentration of calcium ion is plotted as a function of the caprock thickness in Figure 6. Higher calcium concentration (from 86 mg.l^{-1} to 89 mg.l^{-1}) is determined at outer locations (01, 02, 03 and 04) with caprock thickness between 40 m and 90 m. At other (inner) locations (06, 07, 08, 09) with caprock thicknesses from 65 m to 85 m, Ca^{2+} concentration is lower (73 to 82 mg.l^{-1}).

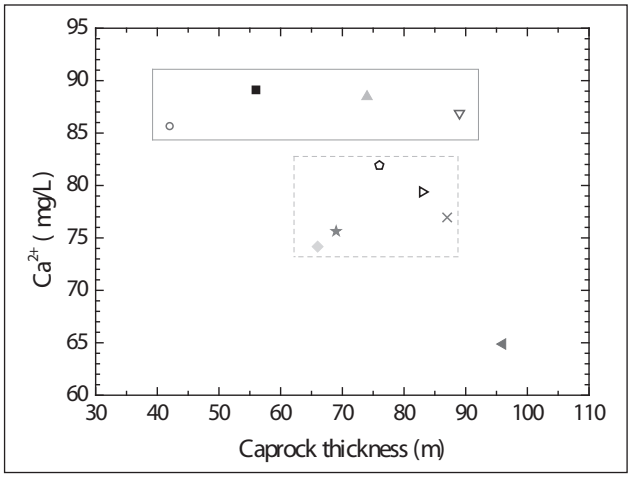

Figure 6. Mean values of calcium ion concentration vs. caprock thickness. There are two groups of locations. Full line square points out outer locations (0 04) and dashed line square inner locations (06–09). Location 05 does not belong to any of the two groups.

Therefore, concentration of calcium ion in the drip water is not determined only by caprock thickness, but also by geomorphology of the karst terrain itself, i.e. by the routes that drip water undergoes before reaching the drip site (Baker et al. 2000; Fairchild et al. 2000; Tooth and Fairchild 2003). Most dissolution of limestone occurs in the epikarst zone (up to 60 m terrain depth) (Ford and Williams 2007). In Figure 6, location 11 – Pivka River inside is plotted only for comparison and demonstration that calcium ion content of water is not influenced by caprock thickness. Location 05 – Podrti kapnik is an exception and will be discussed separately. Other chemical parameters are neither influenced by caprock thickness.

At all locations, magnesium concentrations are lower than 1.5 mg.l^{-1}, with the mean value of 0.85 ±0.18 mg.l^{-1}. Both sampling locations of the Pivka River show higher concentrations of magnesium ions (>3 mg.l^{-1}) due to the Pivka River origin and flow path. Concentrations of other minor ions are negligible at all locations.

The $\delta^{18}O$ values of drip water vary between -10 and -8‰ with practically now seasonal variations. The variations in

$\delta^{18}O$ of drip water at all 9 locations are than that in local precipitation, indicating good mixing of waters in the epikarst zone and relatively long MRT of water, from several months (at locations 01, 02 and 08) to about 1 year at locations 03, 05 and 09 and reaching several years (locations 04, 06, 07).

The $\delta^{13}C_{DIC}$ values measured in the Pivka River water at location 10 – Pivka River inside and at location 11 – Pivka River outside are approximately the same, i.e. -12.4 ±2.0‰ and -12.4 ±2.2‰, respectively. The drip water at location 05 – Podrti kapnik (mean value -9.90 ±2.26‰, ranging from -11.78‰ to -5.64‰) has more positive $\delta^{13}C_{DIC}$ values than other drip waters, where $\delta^{13}C_{DIC}$ mean values range from -12.32 ±0.28‰ at location 07 – Čarobni vrt to -13.30 ±0.33‰ at location 01 – Slonova glava. Smallest variations have been measured at location 06 – Stebrišče (-13.06 ±0.11‰).

The highest average conductivity value has been measured at location 01 – Slonova glava (454 ±76 $\mu S.cm^{-1}$), where maximum value of 556 $\mu S.cm^{-1}$ is measured in November 2010. The lowest average value is found at location 05 – Podrti kapnik (277 ±42 $\mu S.cm^{-1}$), where the minimum conductivity of 197 $\mu S.cm^{-1}$ is measured in February 2011. At location 06 – Stebrišče minimum deviation from mean value is found 366 ±17 $\mu S.cm^{-1}$, i.e. this location shows most stable conductivity condition of all sampling locations.

Correlation between mean values of HCO_3^- and Ca^{2+} ions for all locations is shown in Figure 7. Good correlation ($R^2 = 0.94$) is in agreement with classical processes in karst where higher concentrations of bicarbonate HCO_3^- in drip water causes higher concentrations of dissolved minerals, in the case of limestone, the calcium minerals.

Mean conductivity and drip rate show linear relationship ($R^2 = 0.51$; Fig. 8). Conductivity is in direct correlation with concentration of dissolved minerals in the solution. Locations with higher drip rate show stronger response to the rain events. For drip water at location 08 – Vrh Velike gore and 07 – Čarobni vrt with short residence time conductivity is low because of shorter time for water – rock interaction, i.e. for dissolution of the overlying limestone bedrock, which is opposite to the situation at location 02 – Biospeleološka postaja.

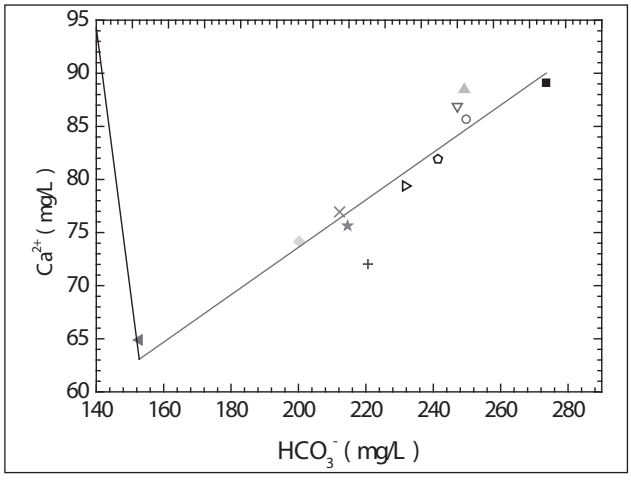

Figure 7. Correlation between mean values of HCO_3^- and Ca^{2+} ion concentration for all sampling locations.

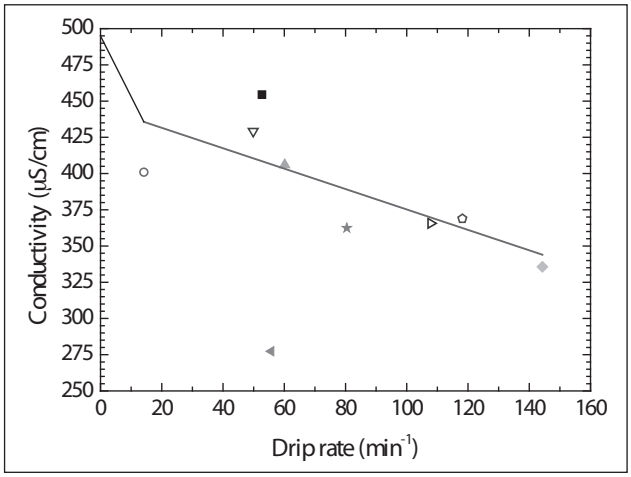

Figure 8. Correlations of mean annual conductivity and drip rate with linear fit.

The mean values of saturation index I_{sat} vary from 1.94 ±0.81 at location 01 – Slonova glava to 6.19 ±4.12 at location 04 – Kongresna dvorana. The highest value (12.82) is observed at location 04 in February 2011 (Figure 9), and the lowest value of 0.58 at location 02. Line on the Figure 9 presents equilibrium solution, i.e. $I_{sat} = 1$. If $I_{sat} < 1$ there is no possibility for carbonate precipitation, and if $I_{sat} > 1$ then carbonate precipitates. Most of drip water I_{sat} values lye in the region above the line, and only several I_{sat} values are close to or slightly lower than 1.

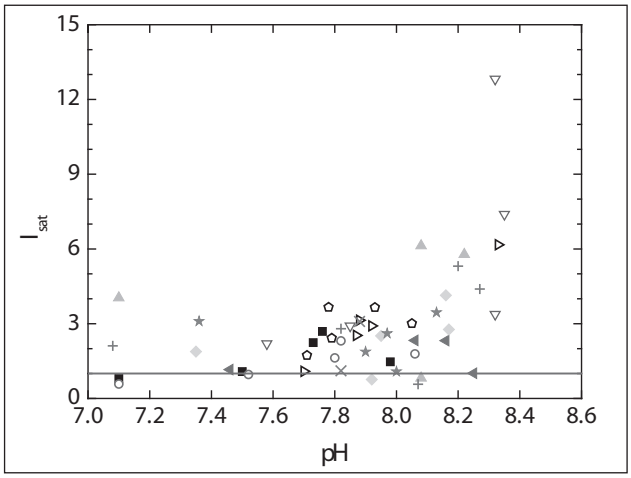

Figure 9. Relation between I_{sat} and pH. Red line presents equilibrium solution, $I_{sat} = 1$.

Location 05 – Podrti kapnik has been mentioned several times as an exception in comparison with other locations, e.g., concentrations of calcium and bicarbonate ions (Figures 6, 7) and conductivity (Figure 8) are lower, while the $\delta^{13}C$ values of DIC are on average 2–3‰ higher than at other studied locations. The differences are more pronounced during dry periods when the Mg/Ca ratio also increases. All these observations indicate the possibility of the loss of calcium and bicarbonate ions due to carbonate precipitation in some voids within the caprock above this locations caused by degassing of CO_2 from the percolating water. This process in known as prior calcite precipitation (PCP; Horvatinčić et al. 2003; Spötl et al. 2005; Fairchild et al. 2007). In the period after abundant precipitation when the water level is high, the voids are filled with water and do not allow CO_2 degassing, the mentioned parameters at

location 05 do not show different values compared to other locations, justifying our assumption of PCP.

6. Conclusion

The one-year monitoring of various chemical and isotopic parameters in drip waters of the Postojna Cave leads to the following conclusions. Air temperature and drip water temperature reflect the mean annual temperature of the area, but the seasonal variations in the cave are much smaller. Similarly, the mean $\delta^{18}O$ values of drip waters reflect the $\delta^{18}O$ of the local precipitation, but without pronounced seasonal variations. According to its chemical composition, all drip waters belong to the same type (Ca – HCO_3^-). According to drip rate and its variability, all drip waters belong to the seepage type, although some differences in the drip rate response to the precipitation amount are observed among the studied locations. Location 05 – Podrti kapnik is often an exception when compared to all other monitored locations by its lower Ca^{2+} and HCO_3^- concentrations, lower conductivity, higher Mg/Ca ratio, and higher $\delta^{13}C_{DIC}$ values. All these characteristics indicate the possibility of prior calcite precipitation on the way of the drip water from the epikarst zone to the cave.

References

Baker A, Genty D, and Fairchild I, 2000. Hydrological characterization of stalagmite drip waters at Grotte de Villars, Dordogne, by the analysis of inorganic species and luminescent organic matter. *Hydrology and Earth System Sciences* Discussions, 4(3), 439–449.

Brodar S, 1966. Pleistocenski sedimenti in paleolitska najdišča v Postojnski jami. *Acta carsologica*, 4, 57–138.

Fairchild I, Borsato A, Tooth A, Frisia S, Hawkesworth C and Huang Y, 2000. Controls on trace element (Sr-Mg) compositions of carbonate cave waters: Implications for speleothem climatic records. Chemical Geology 166, 255–269.

Fairchild I, Frisia S, Borsato A and Tooth A, 2007. Speleothems. In Nash, D. and McLaren, S., eds., *Geochemical Sediments and Landscapes*. Wiley-Blackwell, Oxford.

Ford D, and Williams F, 2007. *Karst hydrogeology and geomorphology*. John Wiley and Sons, West Sussex.

Gams I, 1974. Kras – zgodovinski, naravoslovni in geografski oris. – Slovenska matica, Ljubljana, 359.

Horvatinčić N, Krajcar Bronić I, and Obelić B, 2003. Differences in the ^{14}C age, $\delta^{13}C$ and $\delta^{18}O$ of Holocene tufa and speleothem in the Dinaric Karst. *Palaeogeography, Palaeoclimatology, Palaeoecology* 193(1), 139–157.

Smart P, and Friedrich H, 1987. Water movement and storage in the unsaturated zone of a naturally karstified aquifer unsaturated zone of a maturaly karstified aquifer, Mendip Hills,England. In Zeitschrift fur Geomorphologie / Proceedings of Conference on Environmental Problems in Karst Terrains and their Solutions, volume 59–87. National Water Well Association, Bowling Green, Kentucky.

Spötl C, 2005. A robust and fast method of sampling and analysis of $\delta^{13}C$ of dissolved inorganic carbon in ground waters. Isotopes in Environmental and Health Studies 41(3), 217–221.

Spötl C, Fairchild I, and Tooth AF, 2005. Cave air control on dripwater geochemistry, Obir Caves (Austria): Implications for speleothem deposition in dynamically ventilated caves. *Geochimica et Cosmochimica Acta* 69, 2451–2468.

Šebela S, 1998. *Tectonic structure of Postojnska jama Cave System*. ZRC SAZU, Postojna.

Tooth AF, and Fairchild IJ, 2003. Soil and karst aquifer hydrological controls on the geochemical evolution of speleothem-forming drip waters, Crag Cave, southwest Ireland. Journal of Hydrology 273, 51–68.

THE SKALISTÝ POTOK CAVE IN THE RELATIONSHIP TO THE RELIEF OF THE SOUTH PART OF JASOVSKÁ PLATEAU (SLOVAK KARST) AFTER 25 YEARS OF RESEARCH

Alena Petrvalská, Zdenko Hochmuth
Institute of geography, Faculty of Natural Sciences, P. J. Šafárik University, Jesenná 5, Košice 040 01, Slovakia, alena.petrvalska@upjs.sk, zdenko.hochmuth@upjs.sk

The Skalistý potok Cave is situated on the south slope of the Jasovská Plateau. In present, it is the longest and deepest cave in the Slovak Karst. It consists of three different parts, having different genesis and relationship to relief of slopes and plateau. We analyze location of cave corridors and relief above them. We can confirm that cave corridors do not have relation to the relief itself, they do not pass under dolines and they do not correspond to doline lines or lines of slope valleys. We deal with further perspectives of the research, possibilities and applications of new progressive methods that can help us solve some research problems (relationship of microclimate and discharge, neotectonic movements etc).

1. Introduction

The Slovak Karst is situated in the eastern part of south Slovakia. It forms the largest continuous karst area in the Slovakia overreaching to Hungary where it is called the Aggtelek Karst. In Slovakia, it occupies an area of about 800 km^2 and is built up of karst rocks.

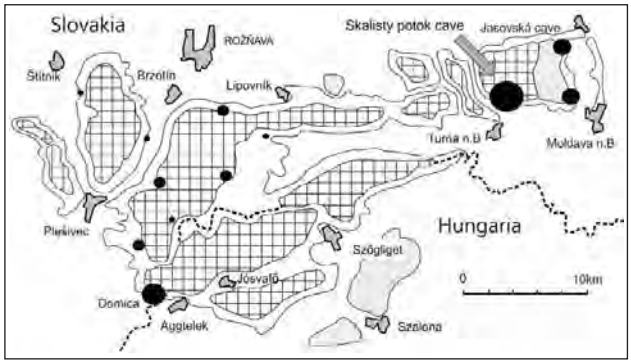

Figure 1. Slovak karst plateaus and the most important caves.

2. Geological and geomorphological character of Slovak Karst

The Slovak Karst has a complicated geological structure with five tectonic units (nappes): Silicicum, Gemericum, Bôrka Nappe, Meliaticum and Turnaicum. A bottom part of nappes are built up of Lower Triassic non-karstifying rocks overlain by dominantlight grey and white Wetterstein Limestone, and Wetterstein Dolomite, Guttenstein Limestone and Dachstein Limestone (with megalodont fossils).

The Slovak karst is characterized by uniform pediplanation surface. We expect that whole area of the Slovak Karst was in the time of tectonic calm in Miocene (Pannonian age) cut into the planation surface peneplain. New ideas on the evolustion of the Slovak Karst were presented by Jakál (2001), Gaál and Bella (2005), Gaál (2008), Hochmuth and Labunová (2008), Hochmuth and Petrvalská (2010).

After the uplift in the Rhodanian phase of Carpatian orogenesis, canyon- and gorge-like valleys were created. They separate the area into several plateaus: Koniar, Plešivecká, Silická, Horný vrch, Dolný vrch, Zádielska, Borčianska and Jasovská. The altitude difference between valley and plateau surface is 400 m on average. On the plateau surfaces, karst forms (exokarst) are well-developed. Lot of Aven- and Lighthole-type abysses were found there. It is interesting that active karst hydrological systems with active flow are known only from the edge of the Slovak Karst.

3. Skalistý potok Cave

Both known and used entrances into the Skalistý potok Cave (Rocky brook Cave) are man-made. The first was punctured by workers from the IGHP (Engineer-geological survey) in 1968 in the place of the periodic spring on the feet of the Jasovská plateau in the altitude of 205 m a.s.l.

The second one was punctured by cavers on the southern plateau slope in 2007 at 460 m a.s.l. Most of passages are overflowed by active underground river, 42 sumps are already mapped (with a length of about some meters up to 130 m). Finally, the cave is interesting speleodiving locality, but there are many vertical parts. These passages rank the cave to the deepest caves in the Slovak Karst and among Slovak caves it ranks the fourth. The topical length is 7,983 m and denivelation 373 m.

4. History of a speleological and speleodiving survey in the Skalistý potok Cave

1968: In the place of the periodic spring on the feet of the Jasovská plateau, workers from the IGHP Co. from Žilina gapped a 13 m long exploration tunnel and they find underwater parts of the natural cave. Cave passages were surveyed by Mikuláš Erdős.

1982: Speleodiver J. Kucharovič from Trenčín city overcame two sumps and reached a distance 258 m from the cave entrance, he tentatively surveyed the passages.

1985: renewal of research by regional caving club in Ružomberok city, later renamed a group Východ – East as a part of the Commission for speleodiving.

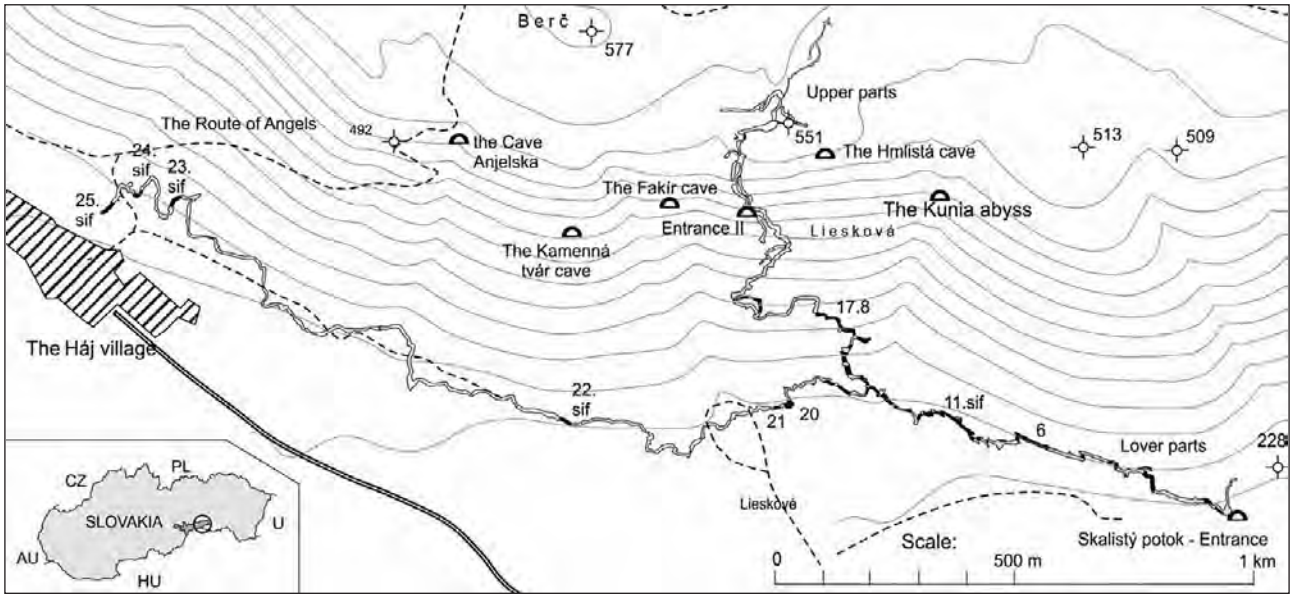

Figure 2. Map of the Jasovská Plateau and the Skalistý potok Cave position.

1986: In the Skalistý potok Cave, speleodivers Hochmuth, Koľbik, Šimkovič and Ďurček managed 11. sump in the distance of 600 m from the cave entrance.

1987: 21. sump was reached, the length of the cave is 1,500 m. Detailed mapping with mining set (Meopta) was running.

1988: Discovery of the tributary flow in the section of 17. sump.

1989, February 11: Cavers overcame sump No. 17.11, longest in the cave with a length of about 130 m. In the same year they discovered new areas of the cave, ascendent dry cave with waterfalls and sinuous horizontal parts.

1991: In the ascending passage new research and mapping by classical methods started. The new highest point was attained (Vrchol 91 – Peak 91) in the height of 441 m.

1992: Resumption in the passages against the underground river. The new highest point was discovered – Vrchol "peak" 92 on the slope of a huge hall with waterfall.

1993: D. Hutňan is going to help with new research in the cave. Climbing up the 31 m high waterfall and discovery of new subhorizontal parts with halls and sump No. 17.14. At this point the research was stopped. Denivelation of the cave is 287 m.

1994: A progress in the lower parts of the cave (Hochmuth, Ďurček), overcome of the 31. sump and discovery of a long horizontal passage with sump No. 22. Damping of the speleodiving activity.

1999–2000: Research of the Speleoaquanaut Club from Prague (the Czech Republic) and group from Kladno heading by D. Hutňan. Overcome of sump 17.13 and discovery of next passages with sump and shallow inflow. In this time Peak 91 was overcome and the passage was near to the Jasovská Plateau slope.

2000: Overcome of 22. sump and discovery of more than 1 km long new passages that are occurring nearby built areas of the Háj village. Caver began to perforate a tunnel from the surface to the "Contact hall".

2002–2007: A progress in the horizontal part, sumps No. 23 and 24 were overcome.

2007: Opening of the 2nd cave entrance on the plateau slope, revival of the speleodiving research in the upper parts.

2008: Sump No. 17.13 was overcome by M. Mahart and D. Hutňan from Speleoaquanaut Prague.

2010: Gap of the crosscut above sump No. 17.13.

2011: The ascending part above Kladenská Passage and record denivelation 373 m was reached.

2012: The waterfall was overcome, new waterpassage with sumps Nos. 17.14, 17.15 and 17.16 was discovered, in the siphon 17.17 wasn`t attained. The cave length is under 8 km already.

Many papers were published about this cave, for example Hochmuth (1989, 1992, 1994), Hochmuth, Danko and Hutňan (2011), Hochmuth and Hutňan (2012) etc.

5. Genetic parts of the cave

The Skalistý potok Cave has 3 genetically different parts.

Lower subhorizontal part of the cave is situated between 164–200 m a.s.l. (the lowest localities are in sumps). It spreads into WSW and in some parts it generates meanders. In the straight direction the passages are more than 2,8 km long. Most of these passages are tectonically conditioned by fault area between the foothill of the plateau and the hollow basin. But typical are freatic, meander segment and flooded vertical "well". A schematic profile of the cave is included in the paper Hochmuth (1994). Only a third of this part is overflowed by underground flow from a vertical passage. West heading passage is mainly dry, overflowed only in flood period of the year. It is interesting that this part of the cave is not increasing, but horizontal and every each siphon is in greater depth.

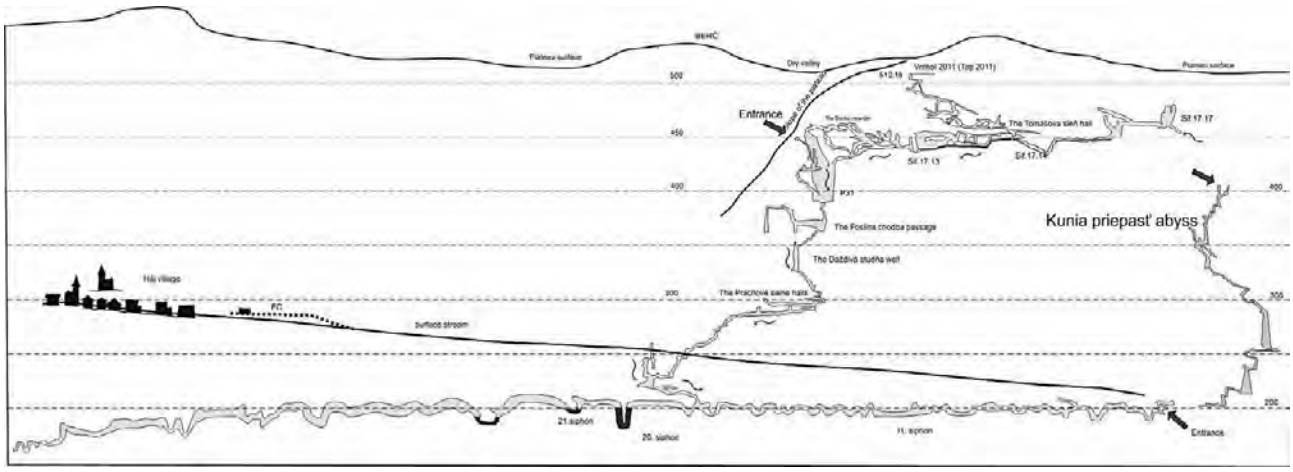

Figure 3. Schematic profile of the Jasovská Plateau (under the angle of 45–225°).

We proposed a solution to this question by "divergention against the water flow" longer time ago. A extension of this branch is problematic since there are permanent siphons (Nos. 23–25) situated, passages on the fault zones are tight and collapse-like. In sediments of this part, boulders of metamorphic rocks are occurring indicating transport by flood waters from the west-situated Hájska Valley. The surface flow of the Hájsky Brook contains these bulders as well. In the fine fraction of sediment we observed heavy minerals that outline the catchment area of the stream. There is an evidence of hydrological connection with underground stream in the Kunia Abyss (250 m) by tracers. The water passed from the siphon to the spring in 5 weeks in minimal discharge. It is possible to consider this part of the cave as relatively young developing in parallel with river plain of the Hájsky Brook and its alluvial cone.

Vertical parts with meander passages. The passages that P. Bella called "vadose canyons" and other authors (P. Hipman, Z. Hochmuth) called "caves of the mountain type", are known from the Alps and in Slovakia and Poland from higher mountains in the Carpathian range (the High and Low Tatras). Their existence in the Slovak karst region was surprising. The waterfalls of 2–31 m height alternate with meander passages of oval shape (profile) and with "vertical canyons". This part heads generally to the north however not following tectonic line or lines. Some parts even avoid tectonic structures identified on the slope surface. Into these parts a new entrance was made to better access to the highest passages of the cave. Water channel is currently developing, in some parts completely without sediments and in other parts with corroded sinter crusts. These parts witness of accumulation phase in long-term period (paleomagnetic research of speleothem has been in progress). "Vadose canyon" is on some places 20–30 m high and higher parts have interesting crystal trappings and speloethem forms similar to helictits.

Upper subhorizontal part is situated between 480–520 m a.s.l. There was an active underground flow with the existence of sumps in this part. Their position is not typical for such a high altitude. Passages are oriented northwards generally and east-west parts are tectonically conditioned by fault area. These passages are 200 m from the rim of the plateau and situated only 25–60 m under the plateau surface. This subhorizontal part consists of fossil freatic level 10–20 m above active flow, in the highest fossil passages an acoustic connection was established.

6. Topical problems of research

The research of the cave with classical methods, after the opening the upper parts of the cave, reached the top. At present time, there is research in three ways running:

Observation of neotectonic movements with exploitation of TM 71 dilatomer, which was installed on the active zone. This fault formed north-south direction of the "Upper level" in the cave.

Measurement of water discharge with automatic depth sensor which was installed on Thompson weir situated on the upper stream in the cave. It helps us understand relationship between rainfall, temperature and snow melting on the plateau surface.

Figure 4. Character of water channel in the upper parts. Photo by J. Stankovič.

Figure 5. Fossil freatic passages in the upper parts. Photo by J. Stankovič.

Research of sediments with classical mineralogical and petrographical methods to recognize a catchment area of non-karstic components.

Prolongation research was centered on the area behind sumps Nos. 17.14–17.17 with major inflow. Direction of this passage to the NE only a few meters under the plateau surface is seemingly interesting and it will be necessary to work in here in the future. For practical survey in the cave it would be helpful to gap a next entrance from the plateau surface (near the Vrchol – Top 2011). The survey in the down parts of the cave is possible only with change in research philosophy, methods and new generation of speleodivers. Another problem is a speleological connection with Kunia Abyss. It belongs to the catchments area of the Skalistý potok spring and the research in past was in progress in both ways (from the Kunia Abyss bottom and in Skalistý potok Cave from the sump No. 17.9). The revival of the research by group of new cave divers would be desirable.

7. Summary

Relation of corridors in the Skalistý potok Cave and its relief above them is shown on the map. This cave, similarly to other caves "avoids" to depressions on the relief. The best evolved parts of the cave are under the crest (covered by karren) of the Jasovská plateau, however not under the slope valleys as we expected. The passing of spaces under the relief does not imply it. One part lying under the plateau relief nearby the slope and dry valley does not copy the line of the valleys (tectonic line of N–S direction), but runs

Figure 6. Specific forms of stalactites and stalagmites formed under the conditions of flowing aerosol from the waterfalls. Photo by P. Šuster.

Figure 7. Specific forms of stalactites and stalagmites formed under the conditions of flowing aerosol from the waterfalls. Photo by P. Šuster.

through the valley bottom to the second site, and it continues there. In the cave one can find recrystalised sinter, which can, according to Hochmuth (in verb.) show the older age (pre-Quaternary), similar sinters were found in the older upper fossil level in the Drienovecká Cave. On the cave

wall, large manganese surface films (layers) under the sinters can be observed. It will be very interesting to run further research in this cave.

The exploration of the Skalistý potok Cave gradually sheds more light on understanding of this part of the Jasovská Plateau. After more than 25 years of surveying the cave, many speleological problems remain unresolved. Moreover, prolongation of surveyed corridors in every direction is likely to be made. After opening the entrance in the upper parts of the cave, detailed mapping and research of the reachable parts we compiled enough useful facts to understand the main questions of the genesis. On the basis of these findings, we can identify several paleolevels 250 m above the bottom of the valley in the length of 2 km. They are drained by a water stream of unknown origin and source location. The pre-Quaternary age is indicated by old, corroded speleothems, large calcite crystals and manganese crusts. There is no apparent affinity towards superficial landforms, dolines, even though these were ground surveyed and mapped in detail. Only some corridors of the W–E directions can be related with the fault directions in the marginal parts of the karst plateau.

We suggest the horizontal level of the cave (i.e. its fossil part) was formed in the Upper Pliocene. At that time, the relative relief between the plateau and the valleys was about 50–100 m. This is indicated by the high age of the speleothems and Fe and Mn sediments which were not formed during the Quaternary. Tectonic uplift caused individualisation of particular plateaus in the subsequent evolution. For that reason, the cave area lost its original function and they became the current water collector only later on. This water changes the lower parts of the cave, destroys the speleothems and it creates waterfalls and abyssal sections by attempting to reach the current water level in the karst massive.

Acknowledgments

This work has been funded by project Nr. 1/1251/12 with financial support of the VEGA grant agency.

References

Gaál Ľ, 2008. Geodynamika a vznik jaskýň Slovenského krasu. Speleologia Slovaca, 1, ŠOP SR, Správa slovenských jaskýň, Liptovský Mikuláš, 166 (in Slovak).

Gaál Ľ, Bella P, 2005. Vplyv tektonických pohybov na geomorfologický vývoj západnej časti Slovenského krasu. In Slovenský kras, XLIII, Liptovský Mikuláš, 17–36 (in Slovak).

Hochmuth Z, 1989. Výsledky speleologického prieskumu jaskyne Skalistý potok. Slovenský kras 1989, Martin, 3–16 (in Slovak).

Hochmuth Z, 1992. Novšie poznatky z prieskumu jaskyne Skalistý potok a morfológia častí objavených v rokoch 1989–1990. Slovenský kras, XXX, Martin, 3–15 (in Slovak).

Hochmuth Z, 1994. Skalistý potok – ďalší príklad divergencie podzemného toku. Spravodaj SSS, 4, XXV, Liptovský Mikuláš, 15–17 (in Slovak).

Hochmuth Z, Danko S, Hutňan D, 2011. Prieskum, topografia a náčrt genézy horných častí jaskyne Skalistý potok (Slovenský kras). Slovenský kras, Acta carsologica slovaca 49, 2, 111–122 (in Slovak).

Hochmuth Z, Hutňan D, 2012. Sifóny v horných častiach jaskyne Skalistý potok (Slovenský kras). Speleofórum, ČSS, Brno, 31, 94–98 (in Slovak).

Hochmuth Z, Labunová A, 2008. K priebehu podzemných priestorov významných jaskynných systémov Slovenského krasu vzhľadom na súčasný relief. In: Stav geomorfologických výzkumů v roce 2008, Brno, 15–16 (in Slovak).

Hochmuth Z, Petrvalská A, 2010. Povrchové a podzemné krasové formy Jasovskej planiny. In: Geografie pro život ve 21. století: Sborník příspěvků z XXII. sjezdu České geografické společnosti pořádaného Ostravskou univerzitou v Ostravě 31. srpna – 3. září 2010. Ostrava: Ostravská univerzita v Ostravě, 15–19 (in Slovak).

Jakál J, 2001. Vývoj reliéfu Slovenského krasu v etape neotektonického vyzdvihnutia územia. Slovenský kras, XXXIX, Liptovský Mikuláš, 7–14 (in Slovak).

CAN CONDUIT VOLUMES OBTAINED FROM ARTIFICIAL TRACER TESTS BE TRUSTED?

Anna Vojtěchová[1], Jiří Bruthans[1], Ondrej Jäger[2], Frantisek Krejča[3]
[1]Faculty of Science, Charles University in Prague, Albertov 6, Praha 2, Czech Republic, bruthans@natur.cuni.cz
[2]AQH s.r.o., Frýdlantská 1310/23, 182 00 Praha 8, jager@aqh.cz
[3]Management of Chýnov Cave, Dolní Hořice 54, 391 55 Chýnov, Czech Republic, krejca@caves.cz

Phreatic loop in a natural carbonate cave was used to test the reliability of artificial-tracer tests for estimating the volume of a flooded karst conduit (Fig. 1). The volume of a phreatic tube was measured by filling a drained phreatic loop with a constant inflow over a known time period. The volume of the phreatic loop is 190 ±20 m^3, and it was compared to independent calculations of conduit volumes based on values based on tracer breakthrough curves (Vojtechovska et al. 2010). The best results were for mean transit time, where tracer-test calculations yielded volumes very similar to the volume obtained by direct filling of the loop (Table 1). On the other hand, using the first-arrival time or peak time in the volume calculation resulted in considerable underestimation of the phreatic tube's volume, and these methods should be avoided except when breakthrough curves are affected by molecular diffusion. This demonstrates that volume estimation by tracer tests may be quite precise for common natural conduits, but results are strongly affected by the chosen breakthrough-curve parameter.

Acknowledgments

Research was supported by institutional project No. MSM0021620855.

References

Vojtěchovská A, Bruthans J, Krejča F, 2010. Comparison of conduit volumes obtained from direct measurements and artificial tracer tests. Journal of Cave and Karst Studies 72, 3: 156–160.

Table 1. Times and corresponding calculated volumes (modified from Vojtěchovská et al. 2010).

Time	Minutes after injection	Corresponding volume (m^3)	Compared to real volume (%)
Real volume (pumping)	–	190	100
t_A first arrival time	116	85	45
t_P peak time	176	129	68
t_R mean residence time	231	169	89
t_C mean transit time	290	212	112

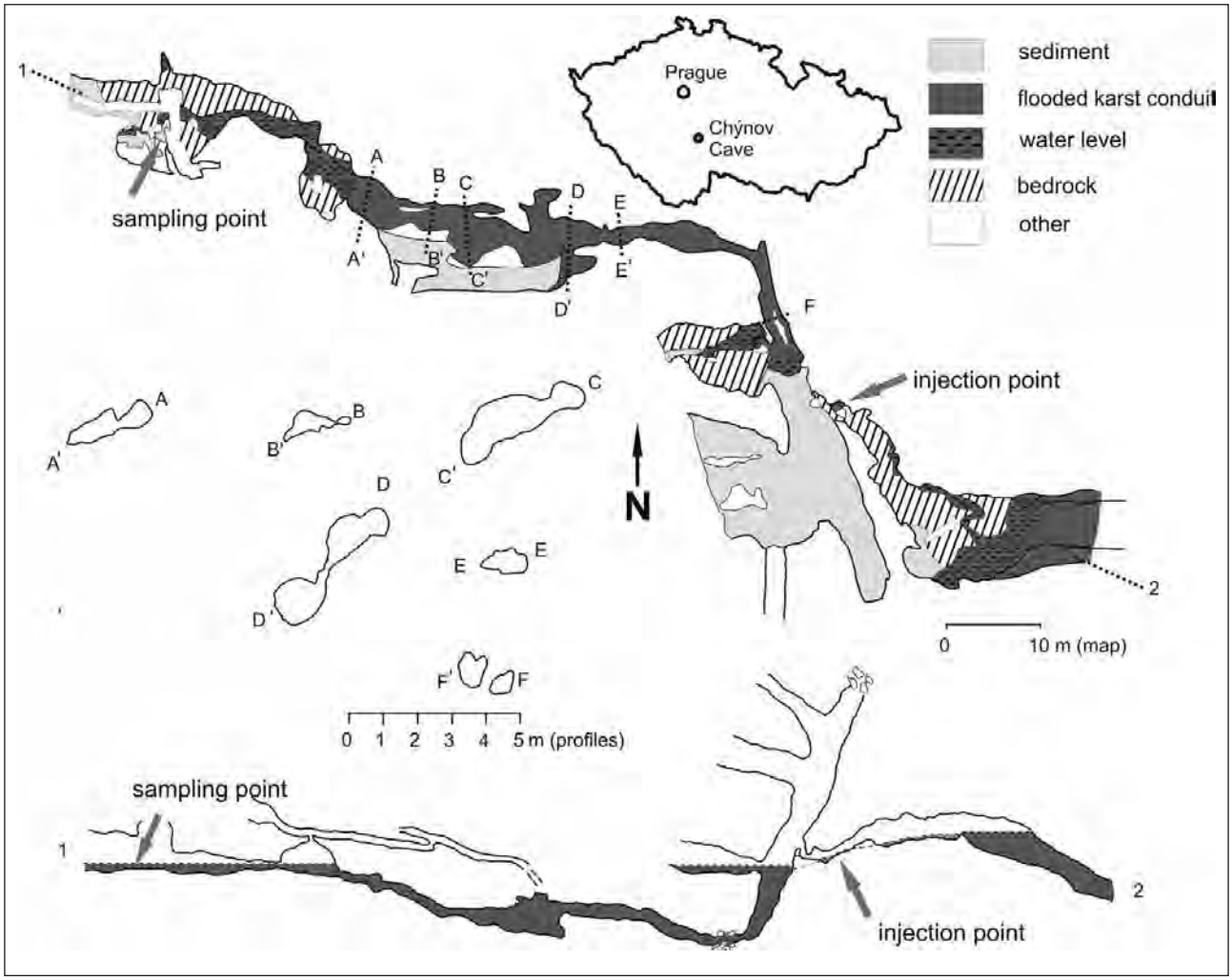

Figure 1. Map and longitudinal vertical section of sump in Chýnov Cave (modified from Vojtěchovská et al. 2010).

THE TECTONIC CONTROL OF AN UNDERGROUND RIVER NETWORK, AGIA TRIADA CAVE (KARYSTOS, GREECE)

Emmanuel Vassilakis[1], Kyriaki Papadopoulou-Vrynioti[2]
[1]National and Kapodistrian University of Athens, Department of Dynamics, Tectonics and Applied Geology, Panepistimioupolis Zographou, 15784 Athens, Greece, evasilak@geol.uoa.gr
[2]National and Kapodistrian University of Athens, Department of Geography & Climatology, Panepistimioupolis Zographou, 15784 Athens, Greece, papadopoulou@geol.uoa.gr

The water pathways of the underground river of Agia Triada (Karystos, Greece) and their generation are examined in this study. One of the longest caves explored in Greece is formed at heavily deformed metamorphic rocks and the suggested combined methodology, which includes traditional geological mapping, speleological exploration and remote sensing image interpretation, led us to the conclusion that the water flows along the hinge of a NE–SW-trending mega-fold. A number of faults that have been activated after the generation of the underground river, have altered its pathway by creating "knick-points" which host impressive subsurface waterfalls, the largest of which is about 20 m high. The extraction of morpho-lineaments from ortho-rectified satellite images revealed the importance of structures that were identified on the open surface mainly by high-resolution remote sensing data interpretation and are related to the cave development. This was made feasible with the use of the Geographic Information Systems as all the collected data were converted into layers for further interpretation. It proved to be very useful as the projection of the cave trace on the ortho-rectified data revealed the underground linkage between two adjacent hydrological basins. This explained the unusual large quantities of water discharged by the Agia Triada spring.

1. Introduction

It is quite often to study an underground karstic landform only regionally, since the major subject is the generation and operation of a cave. Especially in caves that act as underground river flows, the main question that arises is whether this subsurface network should be part of the surface drainage or not (Papadopoulou-Vrynioti 2002; Papadopoulou-Vrynioti and Kampolis 2011). In this paper we investigate the role of the tectonic structures at the local karstification and the influence of several tectonic structures at the underground connection between two separate sub-basins at the area of Karystos (southern Evia, Greece), where the Agia Triada Cave has been found. It is classified as one of the longest caves in Greece (Petrochilou 1981). The existence of an impressive underground waterfall, among lakes and other unique speleological features attracted a great number of expeditions for investigating the cave since 1932 (Zervoudakis 1959; Avagianos 1981).

The first fieldwork was carried out during 1994 by doing a speleological expedition as well as geological mapping at the open surface around the cave trace (Vassilakis and Vlachou 1995). Remote sensing techniques were also applied on an ortho-rectified multi spectral IKONOS satellite image and panchromatic aerial photographs by using a 25 m Digital Elevation Model, for increasing the mapping accuracy of the area around the Agia Triada spring which discharges the underground river. Moreover digital and fieldwork data were imported, combined and interpreted extensively in a Geographic Information System. The orientation of the cave mapping (by SPELEO Club speleologists) as well as the projection of the cave trace on the surface and combined with all kinds of the available data, proved to be very helpful as it was really important to relate the fieldwork results (geological and speleological) with the remote sensing data interpretation.

The applied methodology seems to be ideal for cases like this one as underground rivers are more often related to tectonic structures that might have surface expression. In such cases remotely sensed datasets with proper interpretation can lead to the structures that were responsible for the cave generation.

2. Geomorphological and geological setting

The discharge of the studied underground river is done by a karstic spring, which is located at an elevation of 250 m, next to the Agia Triada chapel just north of the coastal town of Karystos, at southern Evia, in Greece. The cave extends NE beneath the mountain of Ochi and great amount of precipitation water that is infiltrated through its permeable rocks cropping out on the surface, flows along a naturally constructed tunnel. The quantity of the water discharge is large enough for providing Karystos and the surrounding villages, domestic, potable water throughout the duration of the year.

The cave is located in a hydrological basin which covers an area of about 20 km^2 discharging most of the WSW slopes of Ochi Mt. since its watershed reaches the highest peak of the mountain at nearly 1,400 m of elevation (Fig. 1). The hydrographic network reaches the 5th order of Strahler classification (Strahler 1957). It comprises of two 4th order branches, which divide the triangular shaped basin into two asymmetrically developed sub-basins. The westernmost main branch flows almost parallel and in a relatively small distance from the watershed margin, as well as the easternmost branch flows next to the eastern margin of the basin.

The cave entrance is located almost at the central area of the basin and in the westernmost sub-basin. The projection of the underground river, which was mapped by SPELEO

Club speleologists during several explorations, onto the surface shows a subsurface connection between the two sub-basins. The main cave trace – at least from the known mapping information – has a SW–NE orientation and it is clear that large amount of infiltrated water coming from precipitation on the eastern sub-basin flows through the underground river to the western sub-basin.

The area comprises mainly of metamorphic rocks, parts of the Ochi unit (Papanikolaou 1986). Intercalations of marbles with sipolines and mica schists have been observed throughout the entire area and are geotectonically placed between a series of ophiolitic rocks and amphibolites on top and the basement rocks comprised of gneiss (Latsoudas and Triantafyllis 1993; Moustaka 2011) (Fig. 2).

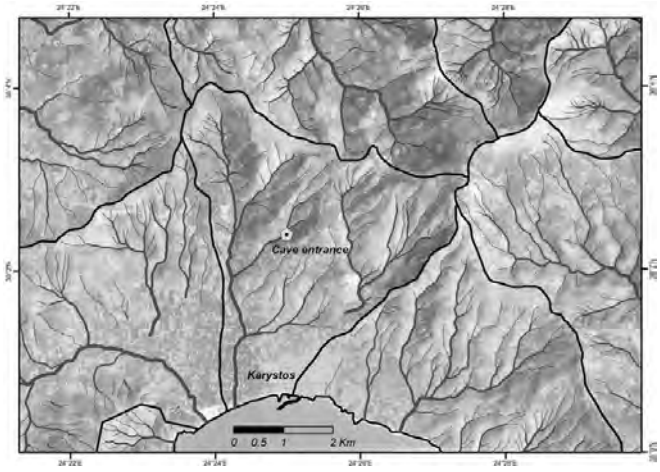

Figure 1. Shaded relief map showing the geomorphology of the hydrological basin where the entrance of the cave is located.

The formations that host the cave and can be identified on the surface along its projected trace (Fig. 2) are the sipolines and the schists. Quite often caves are guided by changes in lithology with passages developing along or close to the contact of carbonate rocks and underlying shales (Gillieson 1996). It is rather clear that in this case the underground river is developed on the contact between the permeable carbonate marbles and the impermeable schists. It is not quite clear if this contact is of tectonic or stratigraphic origin, since the host rocks are heavily deformed by various generations of folding.

The deformation led to the generation of a dense network of discontinuities, which was identified either by fieldwork but also during the interpretation of the remote sensing data (see section 3.2). Our interpretation led us to the simplest model concerning the cave generation, arguing that the cave has been developed along a NE–SW-trending mega fold axis. Several open, erodible and karstified discontinuities were used by the water flow to offset its way to the discharge point at Agia Triada, but the general trend remains NE–SW and no major or minor fault of similar orientation has a surface expression near the projected cave trace. On the contrary quite a few NW–SE-trending structures seem to crosscut the cave normally to its development, possibly affecting and altering the water pathways.

3. Methodology

The general idea of the applied methodology was to enhance the classic fieldwork of speleological exploration and geological mapping with the aid of the GIS and high-resolution remote sensing datasets.

3.1. Fieldwork data

The geological and structural mapping revealed that the entire area has been folded during the alpine period (late Jurassic – early Cretaceous). Most of the folds that are observed in all kinds of scales have axis trending generally along the NE–SW orientation. This orientation is compatible with deep ductile deformation (Katsikatsos et al. 1976). It is expressed with isoclinal, overturned and recumbent folds with many orders of folding.

A second deformation incident seems to have happened after the previous one as folding of the already folded rocks is observed. It is expressed by open folds with almost vertical axial plane and NNW–SSE-trending axis. The most likely age of this deformation is during Oligocene (Papanikolaou 1978).

Additionally, three main systems of faulting were identified throughout the wider area of southern Evia. Most of the faults trend in the NW–SE direction but there is also a large number of faults trending either NE–SW or ENE–WSW (Latsoudas and Triantafyllis 1993).

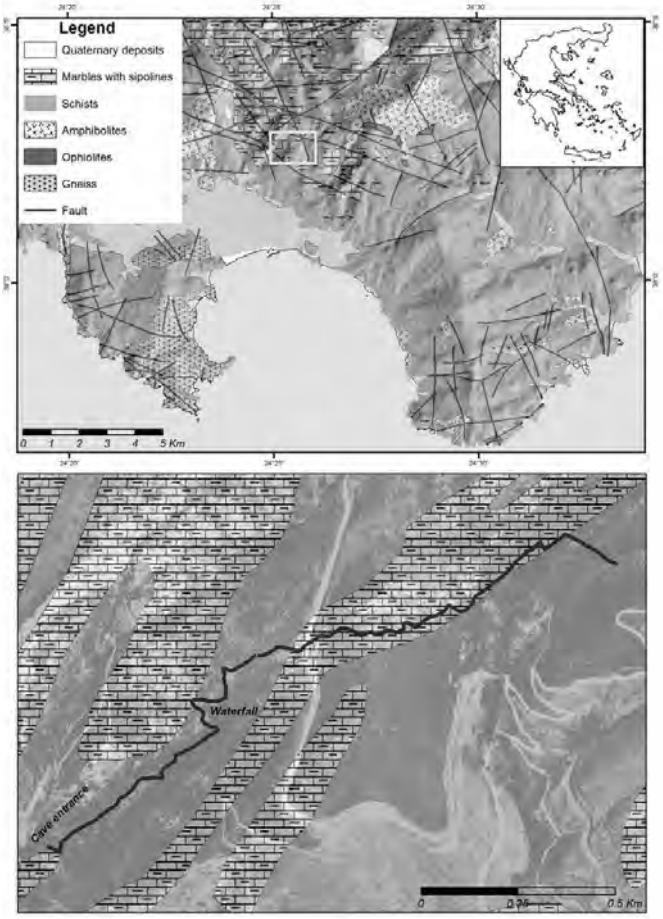

Figure 2. Simplified geological map of southern Evia (upper plate). The white box shows the magnified area (lower plate) around the surface projection of the cave trace (blue line) where metamorphic rocks are cropping out. The cave entrance and the waterfall locations are also noted.

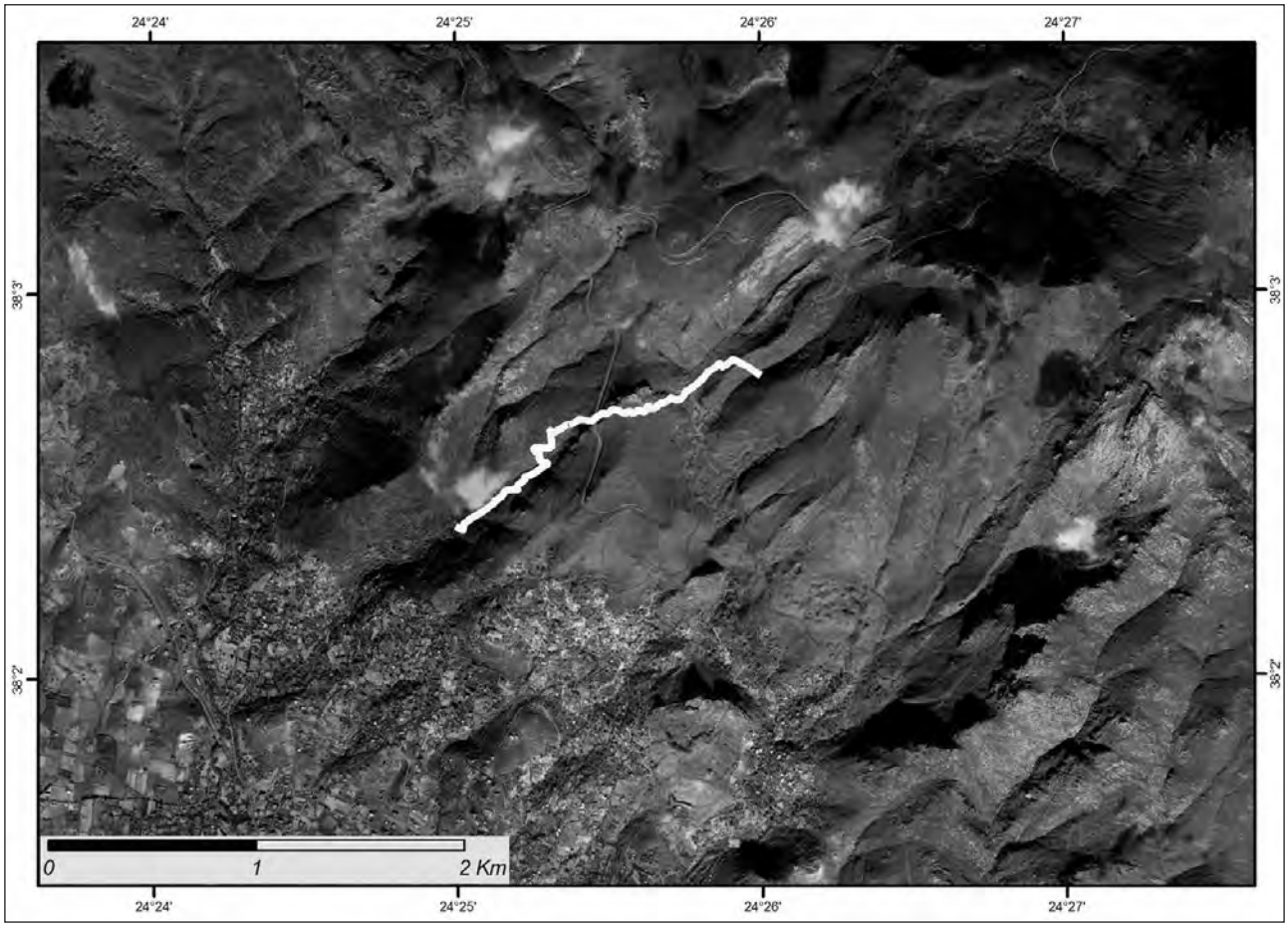

Figure 3. Pseudo-colour ortho-rectified image produced by digital interpretation of high spatial resolution (1 m) IKONOS satellite image (2,4,1/R,G,B). The yellow line represents the projected cave trace on the surface.The green colours represent the vegetation cover whilst the bluish colours represent the uncovered rocks. The purple colours at the top represent an open excavation field for decorative stones (Plaka Karystou).

3.2. Remote sensing data

We combined a few remote sensing datasets for completing the required tasks and finally relate the fieldwork findings to the cave trace. Initially a medium resolution (25 m) DEM was constructed after digitizing the 20 m contours from scanned topographic maps of scale 1:50,000, for the entire area of southern Evia. The product was combined with a high-resolution ortho-photo mosaic constructed by panchromatic aerial photographs and both of the datasets were used for the ortho-rectification of a high-resolution satellite image captured by the IKONOS satellite. These tasks are necessary for merging the produced datasets with the cave trace projection, since the final interpretation needs to be performed in a large scale of the order of 1:5,000.

The initial geological mapping was edited and finalized in a GIS where the basemap consisted of the four-spectral-band IKONOS image (three bands in the visible and a fourth in the infrared spectra). Different band combinations lead to the production of several true- and pseudo-colour digital map compositions, aiming to reveal formations of similar mineral composition and especially the contacts between the various rock outcrops (Fig. 3).

The orientation of all the mapped structures during fieldwork is in full agreement with the morpho-lineaments, which were extracted after the digital interpretation and combination of the DEM and the 1 m resolution ortho-rectified remote sensing data. These datasets were required for the construction of a morpho-lineament map for the upstream area of the underground river within a buffer zone of 1 km around the cave trace (Fig. 4). The morpho-lineaments are surface expressed lineament features, which might be either geological or geomorphological structures or neither of both. In any case these can be related to more or less significant structures that have affected the study area and left their imprints on the surface (Vassilakis 2006).

The statistical analysis of 282 lineament features in total, which were identified on the produced pseudo-colour and true-colour images, show the exact main orientations with the field observations and measurements. It is more than clear by reading the rose diagram that the main orientation of the lineaments is along NE–SW (Fig. 4). Nevertheless, a secondary trend of NW–SE is also identified. Even though both of the main calculated orientations are identical to those revealed by the field observations, it is clear that the remote sensing data interpretation altered the significance of the recorded orientation, by promoting the NE–SW-trending as the most significant.

Moreover, the cave trace is developed along the very same orientation as the one that is suggested by the satellite image interpretation but on the other hand some sharp bendings seems to be related to the NW–SE trends.

3.3. Speleological data

The cave has been developed along the initial stratigraphic contact of the sipoline marbles and the schists that are found

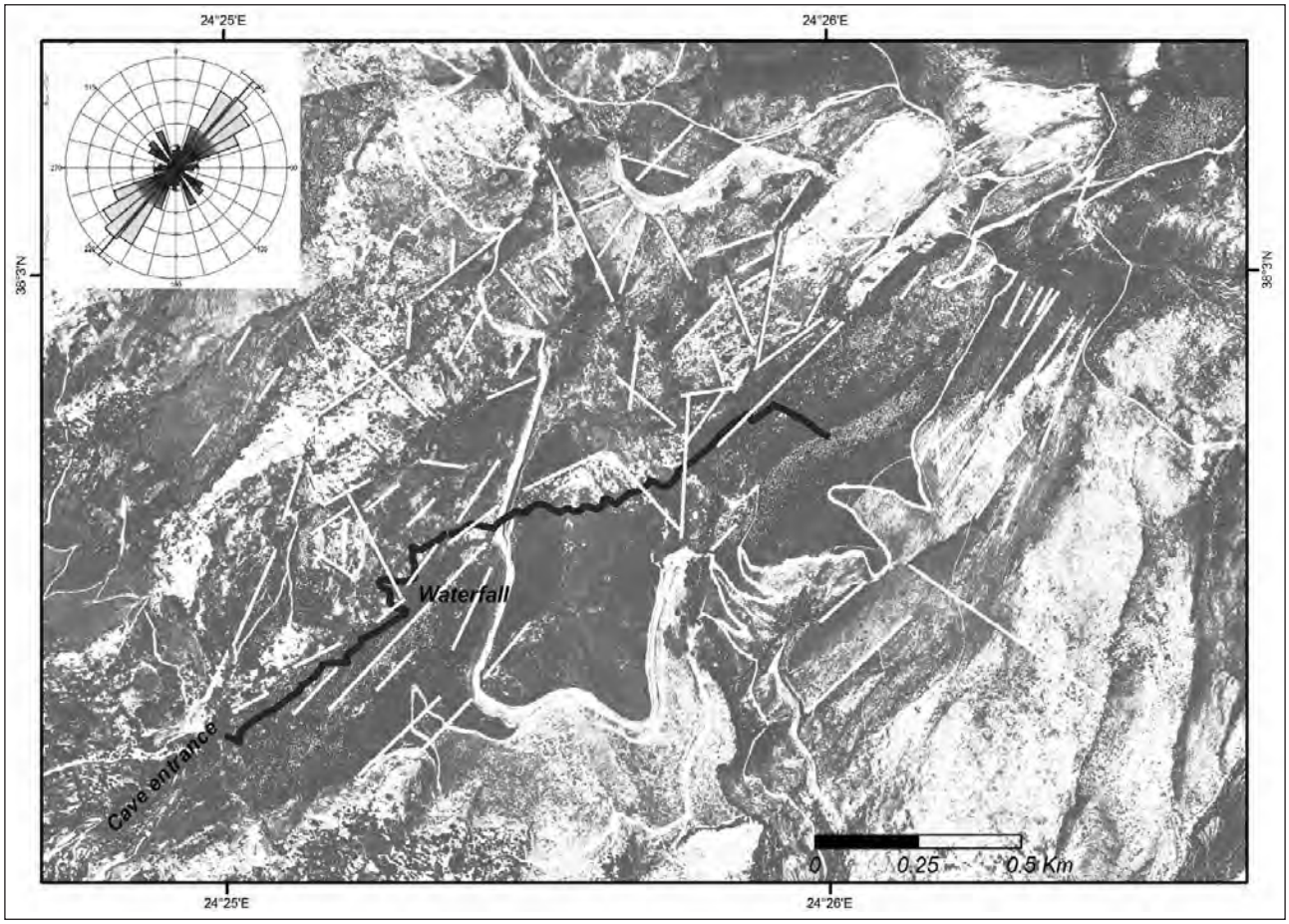

Figure 4. Morpho-lineament map at a buffer zone of 1 km upstream the cave trace (blue line). The statistical interpretation of the lineament features is shown at the inset rose-diagram.

all over the surrounding area. It is almost 1,800 m long and in spite of all the individual chambers, waterfalls, lakes and branches, it has all the characteristics of an underground river flowing along a naturally constructed tunnel. According to Boegli (1980), the classification the Agia Triada Cave is a contact large cave.

The corrosion of the permeable carbonate rocks allowed the water to create a relatively high tunnel with a naturally created passage above the subsurface flow (Fig. 5). During the first few hundreds of meters no impressive stalagmitic decoration is being observed although the walls of the tunnel are usually covered by stalagmitic material, which in many cases make the passing through quite difficult.

During the next part of the cave several lakes and high-energy water flow are observed until the arrival to a wide chamber with a large asbestite cover of 3 m wide and 6 m high, under which the river flows (Fig. 6). It seems that at this location there is a petrified waterfall since the water has managed to find a lower passage more recently.

This section of the cave (420 m from the entrance) ends at a lake that covers an underwater passage, where diving equipment is necessary. There is also a very small passage next to this lake, which can be used for diverting it, after climbing on a 6 m high wall. It is an older branch of the river, which used to be active during the early stages of the cave generation and it was filled up with sandy material later. The widening of this passage was made recently by several exploring teams coordinated by the SPELEO Club.

The next part of the cave is quite similar to the aforementioned one as the power of the water corrosion created another tunnel with many stalagmitic decorations hanging from its roof. After 150 m huge unstable boulders block the tunnel. Right after these there is a large opening where a deafening noise dominates. It is the noise of high water flow energy and it is caused by a 20 m high underground waterfall. The height of the chamber that hosts the impressive waterfall and the lake, which is formed at its bottom, is almost 40 m and its width about 20 m. The intercalations of the sipolines and the schists can be observed all over the walls of the chamber and it seems that this is a hinge of a mega-fold with several orders of minor asymmetric folding and the water path is created along the folding axis. The waterfall is formed normal to a "knick-point" which seems to have been created by NW–SE-trending fault.

The cave is extending towards NE for at least 1,000 m beyond this chamber but reaching the mouth of the waterfall needs good climbing skills and equipment. Passing through this location a series of quite deep-formed lakes (> 4 m) are observed and the way leads to another "knick-point", which should be also overtaken by climbing. The final part of the cave extends into an impressively decorated NE–SW-trending tunnel with stalagmites and asbestitic covers until reaching the end of it about 1,800 m away from the entrance.

It is worth to mention that at a close distance from the entrance, findings of Early Bronze Age were identified, as well as Final Neolithic material in large quantities (Nikolaidis and Tazartes 1998; Mavridis and Tankosić 2009).

Figure 5. The underground river flows beneath the naturally created passage along the first few hundred meters after the cave entrance (Photo by Emm. Vassilakis).

Figure 6. Petrified waterfalls above the contemporary water flow show a more recent migration of the underground river water path at a lower level (Photo by Emm. Vassilakis).

4. Conclusions

The combination of traditional field mapping, speleological exploration and innovative techniques of the GIS data manipulation and remote sensing image interpretation provided useful tools for generating an effective methodology.

The underground river of Agia Triada is clearly controlled by tectonic structures. It is formed and developed along pre-existing tectonic structures, which are dominant at the area of southern Evia. The main structure is a NE–SW-trending hinge of a mega-fold affecting marble sipolines and mica schists cropping out all over the wider area.

The water pathway is placed on the contact between the permeable carbonate layers and the impermeable schists. An underground – almost linear – linkage between two sub-basins is created and this explains the unusually large quantities of water that are discharged at the Agia Triada spring.

Several faults trending normally (NW–SE) to the cave orientation have vertically offset the hinge resulting "knick-points" of various scales and consequently impressive subsurface waterfalls. These morphological discontinuities are not visible at the open surface where erosional proceedures smoothened the relief.

Acknowledgments

The authors would like to thank P. Stylianos, J. Speis and J. Froudarakis for their valuable assistance and participation during the speleological fieldwork. The IKONOS scene was kindly offered by TotalView Inc. The comments on the original manuscript by P. Bosak and M. Filippi were highly appreciated.

References

Avagianos G, 1981. Recent achievements in underwater speleology and in exploration of deep potholes. Bulletin H.S.S., 18, 553–563.

Boegli A, 1980. Karst hydrology and physical speleology. Springer, Berlin, 284.

Gillieson D, 1996. Caves: Processes, Development, and Management. Blackwell, Oxford, 324.

Katsikatsos G, Mercier J, Vergely P, 1976. L'Eubée méridionale: une double fenêtre polyphasée dans les Hellénides internes (Grèce). C. R. Acad. Sci. Paris, 283, 459–462.

Latsoudas C, Triantafyllis E, 1993. Geological map of Greece, 1:50,000, Sheet Karystos-Platanistos. IGME, Athens.

Mavridis F, Tankosić Z, 2009. The Ayia Triadha cave, southern Euboea: finds and implications of the earliest human habitation in the area (a preliminary report). Mediterranean, Archaeology and Archaeometry, 9, 47–59.

Moustaka E, 2011. Structural analysis and geochemical stydy of minerals of the metamorphic rocks of Mt. Ochi, Southern Evia. MSc Thesis, Faculty of Geology & Geoenvironment. NKUA, Athens, 169.

Nikolaidis S, Tazartes N, 1998. Ayia Triada cave (Karystos), Conf. on Human and Speleoenvironment, Athens, 179–180.

Papadopoulou-Vrynioti K, 2002. Lost rivers associated with hazard pollution in Greece, 6th Int. Symposium on History of Speleology and Karstology. ALCADI, Gorizia, Italy, 55–61.

Papadopoulou-Vrynioti K,.Kampolis I, 2011. The "Selinitsa-Drakos" coastal karstic system in the Messinian Mani Peninsula (southwestern Greece) in relation to the terrestrial geoenvironment. Geologica Balcanica, 40(1–3), 75–83.

Papanikolaou D, 1978. Contribution to the geology of Aegean Sea: The Island of Andros. Ann. Geol. Pays Hell., 29, 477–553.

Papanikolaou D, 1986. Geology of Greece. (in Greek). Eptalofos Publ., Athens, 240.

Petrochilou A, 1981. The deepest and longest caves of the world and Greece. Bulletin H.S.S., 18, 375–389.

Strahler AN, 1957. Quantitative analysis of watershed geomorphology. Trans. Amer. Geophys. Union, 38(6), 913–920.

Vassilakis E, 2006. Study of the tectonic structure of Messara basin, central Crete, with the aid of remote sensing techniques and G.I.S. Ph.D. Thesis, NKUA, Athens, 546.

Vassilakis E, Vlachou S, 1995. Operation mechanisms of southern Evia springs. BSc Thesis, Faculty of Geology. NKUA, Athens, 125.

Zervoudakis I, 1959. Agia Triada cave, no 115. Bulletin H.S.S., 5, 76–89.

Session:

Karst and Caves in Other Rocks, Pseudokarst

CAVE FORMATION INITIATED BY DISSOLUTION OF CARBONATE CEMENT IN QUARTZOSE SANDSTONES

Jiří Adamovič[1], Radek Mikuláš[1], Tomáš Navrátil[1], Jan Mertlík[2]
[1]*Institute of Geology AS CR, v. v. i., Rozvojová 269, CZ-165 00 Praha 6, Czech Republic, adamovic@gli.cas.cz*
[2]*Bohemian Paradise PLA Administration, A. Dvořáka 294, 511 01 Turnov, Czech Rep., mertlik@cesky-raj.info*

Besides cavities of irregular shape, European sandstones also feature symmetrical cavities of spherical, ellipsoidal or tear-drop shapes. Most of them are tens of centimetres across but some reach as much as 2–3 m in diameter and may coalesce into large caves tens of metres in length. Their origin has not been clearly explained yet. Based on the field comparison between such cavities in quartzose sandstones and incompletely developed cavities in carbonate-cemented sandstones, it can be demonstrated that the symmetrical cavities form by carbonate dissolution within the limits of former carbonate concretions. The diagnostic features of post-concretionary cavities include their circular or elliptical cross-section, a uniform orientation of their long axes across the region, and the presence of a set of parallel vertical joints or grooves/ribs on their inner walls. In some sandstone areas (e.g., Petite Suisse area in Luxembourg, Kokořín area in the Czech Republic), a wide variety of transitional forms can be found between the cavities and concretions forming positive relief on a vertical cliff face, depending on the position of the carbonate dissolution front in the present landscape.

1. Introduction

Symmetrical cavities and caves in sandstone tens of centimetres to several metres in diameter were studied in the temperate zone of Europe: in the Petit Suisse area in Luxembourg and Germany, in the Kokořín area and Klokočské skály Cliffs in the Czech Republic, and in the Outer Flysch Belt of the Carpathians in Poland and Slovakia. The origin of many symmetrical (spherical or tunnel-like) caves in quartzose sandstone can be hardly explained by processes like salt weathering or stream erosion and must be attributed to processes of epigenetic carbonate dissolution.

2. Preconditions of symmetrical cave origin

Depositional systems giving rise to thick packages of quartzose sandstones are characterized by high supply of detrital material from the source area and relatively dynamic sedimentary environments separating the deposited sand from finer particles which remain in suspended load. At tropical/subtropical climates with enhanced carbonate production, sand deposited in marine and lacustrine environments may become mixed with lime mud. At protected places, bottoms of seas/lakes are colonized by molluscs with calcareous shells. These may get preserved *in situ* or redeposited into shell lags during storm events. Under diagenetic conditions, lime mud and calcareous shells become recrystallized into sparitic cement (Adamovič 2005).

Where nucleation centres are regularly dispersed in sandstone, newly formed cement grows into spherical concretions or elongate, cigar-shaped forms. Later during diagenesis, these forms get vertically compressed to a variable degree and their cross-sections become somewhat elliptical. Where carbonate crystallization is bound to a specific bedding plane (e.g., a shell lag), irregular but more-or-less continuous sheet-like bodies of cemented sandstone are formed. Under regional tectonic stress, cemented sandstone is prone to brittle deformation. This is caused by its higher elastic modulus compared to uncemented sandstone. A network of fractures forms within the concretions, parallel to the maximum principal stress (Bessinger et al. 2003; Quesada et al. 2009).

With the emergence of the rock massif to near-surface conditions, pore spaces in the sandstones become flushed with meteoric waters. Dissolution of the sandstone compounds by infiltrating meteoric waters represents a natural process of acidification. The most reactive minerals such as calcium carbonate can buffer the acidity from deposition. At some sites the pH of atmospheric precipitation became extremely low due to the anthropogenic pollution. The low pH of precipitation in central Europe caused by high concentrations of acidifying compounds (especially SO_4 and NO_3), can be further decreased upon infiltration into the sandstone by many processes, e.g., dissolution of organic material derived from the biomass (recent vegetation). Edmunds et al. (1992) reported pH values of interstitial waters ranging between 4.0–4.5 in the United Kingdom and pH values of 3.5–4.5 were reported in the Bohemian Switzerland National Park in N Bohemia (Vařilová et al. 2011; Navrátil et al. 2013 in press). The relatively slow buffering of infiltrating interstitial waters in low-Ca sandstones is usually due to their overall low buffering capacity. While resistant minerals such as quartz remain relatively stable under acidic conditions, carbonate cement (if present) will be readily dissolved.

3. Areas of study

In the Petit Suisse area in Luxembourg and Germany, the shallow marine Lower Jurassic Luxembourg Sandstone provides vast outcrops in the basin of the Sûre (Sauer) River and its tributaries. Quartzose sandstones contain 0.1 to 2 m thick beds and concretions of calcite-cemented sandstone (Van den Bril and Swennen 2009). While most of them form positive relief on vertical cliff faces, others are partly or completely altered – disintegrated into loose sand. The caves formed by calcite dissolution are strata-bound, max. 8 m long and 1.5 m high.

Late Cretaceous quartzose sandstones of shallow marine origin are well exposed in the Kokořín area N of Prague, Czech Republic. Intercalations of calcareous sandstone are preserved in marginal areas of siliciclastic deposition, at levels corresponding to highstand systems tracts (e.g., several metres above the Upper Turonian base). In the centre, symmetrical cavities as much as 2 m in diameter are displayed at the same levels, with occasional loosened cores of calcareous sandstone (Kokořín, Vrtořez Gorge). At Ješovice, tube-shaped caves max. 10 m long and 2 m in diameter are a common phenomenon (Zimerman 1995; Adamovič and Mikuláš 2011).

Quartzose sandstones of the same age (Upper Turonian) form a 140 m thick body in Klokočské skály Cliffs near Turnov, Czech Republic. Spherical cavities 1 m to several metres in diameter concentrate at a level ca. 15 m below the top of the body. These cavities merge to form caves tens of metres long (Vítek 1987, Mertlík and Adamovič 2005). Spherical concretions max. 1 m across can be also occasionally found on vertical cliff faces, forming positive relief.

The Ciężkowice Sandstone in Slovakia and Poland (Paleocene to Lower Eocene) is a unit of quartzose sandstones and subarkoses belonging to the Outer Flysch Belt of the Carpathians. In Slovakia, spherical calcite-cemented concretions max. 2.6 m in diameter are found in fresh exposures (Megonky) and on cuesta edges (Klokočov), forming positive relief (Adamovič et al. 2010). Further east in the Beskidy Mts. (Ciężkowice rock city, Prządki rock city near Krosno), the calcareous cement is dissolved, leaving behind cavities and rock basins.

4. Weathering forms observed

The presence of carbonate cement in packages of quartzose sandstone is associated with a range of weathering forms. The following typical forms were encountered.

1. Carbonate-cemented beds and concretions forming positive relief on vertical cliff faces are a typical feature of the Luxembourg Sandstone, although they can be found at favourable sites in almost all areas. Cemented sandstone is characterized by a higher resistance to physical weathering and a lower total effective porosity than the ambient uncemented rock. Dense vertical fracturing is limited to the cemented part and maintains uniform strikes throughout the particular area. A thin (several cm) zone of onion-like scaling lines the outer edge of the concretions, particularly the spherical ones.

2. Concretions lined by a groove on their outer edge. The groove marks a zone more susceptible to granular disintegration and is sometimes composed of a series of honeycomb pits. Within the concretion, carbonate cement is either preserved or dissolved. The transition from #1 to #3 is associated with solutional widening of the vertical fractures, especially around their top ends.

3. Spherical or ellipsoidal cavities are typical for sandstone areas in the Czech Republic and for the Beskidy Mts. in Poland. Relics of carbonate-cemented sandstone are occasionally found inside the cavities. If not, their affinity to carbonate-cemented concretions can be deduced by the presence of dense vertical fractures on the inside walls, usually widened into morphologically prominent ribs, or the preserved onion-like weathering pattern on their outer edge.

Figure 1. Calcite-cemented concretions in quartzose sandstone forming positive relief. Perekop near Berdorf, Luxembourg. 49.81794°N, 6.37528°E.

Figure 2. Partly dissolved calcite-cemented concretion inside an elliptical cavity in quartzose sandstone at Perekop near Bedorf, Luxembourg. Note the dense vertical jointing within the concretion limits. 49.81816°N, 6.37470°E.

Figure 3. A relict of a vertically jointed calcite-cemented concretion inside an elliptical cavity partly re-modelled by salt weathering. Quartzose sandstone at Kokořín, Czech Republic. 50.42958°N, 14.57294°E.

4. Symmetrical cavities with flattened bottoms and arched tops (teardrop-shaped cavities), partly filled with loose sand, can be attributed to this group based on their symmetrical shapes and topographic and/or stratigraphic co-occurrence with #1–3. Vertical ribs are sometimes present on the inside walls.

5. Mineral composition of cement

Mineral cement was studied using optical microscopy (Olympus DP70 polarizing microscope) and X-ray diffraction method (Bruker D8 Discover powder diffractometer) at Institute of Geology AS CR, v.v.i. in Prague. Calcite was detected in samples of carbonate concretions from Perekop near Berdorf, Luxembourg, in a sample of a relict of a carbonate concretion from Kokořín, Czech Republic, and in a sample from the core of a large spherical concretion at Megonky, Slovakia. Samples taken from concretions in the Klokočské skály Cliffs, Czech Republic, show mostly no mineral cement; previous existence of carbonate or silica cement can be supposed.

Figure 4. A cave with dense vertical jointing on its interior walls formed by dissolution of carbonate cement within the limits of a former concretion. Luxembourg Sandstone, Teufelsschlucht area, Germany. 49.84750°N, 6.43826°N.

Figure 5. A cave in quartzose sandstone with vertical joints on its walls. The joints do not continue to the ambient rock, suggesting a carbonate-concretion precursor of the cave. Žabí jeskyně Cave near Ješovice, Kokořín area, Czech Republic. 50.44203°N, 14.44529°E.

6. Initiation and enlargement of cavities

The pore space of aquifers in sedimentary basins is affected by fluids of various pH and various red-ox conditions throughout the basin history. With the emergence of the aquifer to near-surface conditions, exposure to waters of meteoritic origin becomes a rule. The slightly acidic reaction of rainwater due to pCO_2 in the atmosphere becomes strongly acidic in areas where organic-rich soils develop on a quartzose sandstone bedrock. With ongoing erosion and lowering of the base level, the acidification front is progressively sinking. Carbonate cement within the concretions in sandstone becomes dissolved and their quartz grains are set loose, creating "sand nests" inside a compact sandstone. When a former carbonate-cemented bed or a level of former concretions become reached by valley incision, the loose sand becomes evacuated, leaving behind open cavities. The "sand nests" in Late Cretaceous sandstones as a stage transitional to cavity formation were previously reported from Saxony (Seifert 1936) and Poland (Dumanowski 1961).

Field evidence from the European sites suggests that the preservation potential for carbonate cement in quartzose sandstones is enhanced basically by three factors: 1, low precipitation. This is evidenced by the contrast between complete carbonate dissolution in the Góry Stołowe National Park in Poland with a total annual precipitation of max. 1,100 mm vs. weak carbonate dissolution in the Petite Suisse area in Luxembourg with a total annual precipitation of 700–800 mm; 2, local topography. The least carbonate dissolution is observed near the base level at sites with high relief dynamics, such as cliff bases in narrow valleys (Kokořín); 3, the presence of carbonate-rich beds at topographically higher positions. This is best visible in the area around Turnov, Czech Republic where carbonate is presently precipitated in sandstones overlain by loess deposits (Trosky, Příhrazy).

Symmetrical cavities in most areas are larger in size than the observed carbonate concretions. Those with arched tops (form #4) seem to be enlarged by the process of salt weathering, as evidenced by the presence of honeycomb pits inside the cavities and by salt efflorescences. Their flat bottoms can be equally shaped by frost weathering. Some of the spherical cavities still possess a lining of concentric onion-like scales, which suggests only a slight or no enlargement after the concretion has been removed (gravitational detachment of big parts of concretions from the Ciężkowice Sandstone was observed with no solution involved). Other spherical cavities have been enlarged considerably and coalesced into caves tens of metres long. Their walls bear no honeycomb pits, which suggests a slow grain-by-grain disintegration (Klokočí area). By dating calcitic speleothems on their walls, Bruthans et al. (2012) found that no enlargement occurred after the Late Glacial and attributed the "growth" of such cavities to their ventilation in the Glacial period.

7. Conclusion

The variety of carbonate-solutional forms observed across Europe allows to conclude that the origin of symmetrical cavities in sandstone through dissolution of carbonate cement is a widespread phenomenon in humid temperate regions. After cement dissolution, sandstone within the limits of the original carbonate concretion or bed turns into loose sand which becomes evacuated upon subaerial exposure. The enlargement and coalescence of the cavities thus formed involves salt weathering, frost weathering and other processes leading to granular disintegration of their walls. In larger cavities/caves, a specific ventilation system may play a role.

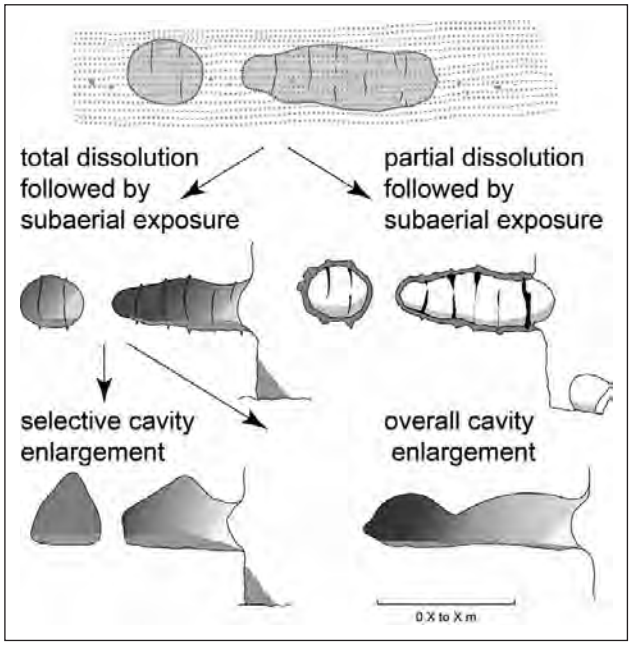

Figure 6. A succession of forms during the formation of symmetrical cavities by the dissolution of carbonate cement in quartzose sandstones.

Acknowledgments

This research was supported by Project IAA300130806 of the Grant Agency of the Academy of Sciences of the Czech Republic and falls within the Research Plan RVO 67985831Z of the Institute of Geology AS CR.

References

Adamovič J, 2005. Sandstone cementation and its geomorphic and hydraulic implications. Ferrantia, 44, 21–24.

Adamovič J, Mikuláš R, 2011. Vznik některých elipsoidálních dutin rozpouštěním karbonátového tmelu v pískovcích jizerského souvrství na Kokořínsku. Zprávy o geologických výzkumech v roce 2010, 9–13 (in Czech).

Adamovič J, Mikuláš R, Cílek V, 2010. Atlas pískovcových skalních měst České a Slovenské republiky. Academia, Praha.

Bessinger B, Cook NGW, Myer L, Nakagawa S, Nihei K, Benito P, Suarez-Rivera R, 2003. The role of compressive stresses in jointing on Vancouver Island, British Columbia. J. Struct. Geol., 25, 983–1000.

Bruthans J, Schweigstillová J, Jenč P, Churáčková Z, Bezdička P, 2012. ^{14}C and U-series dating of speleothems in the Bohemian Paradise (Czech Republic): retreat rates of sandstone cave walls and implications for cave origin. Acta Geodyn. Geomater., 9(1), 93–108.

Dumanowski B, 1961. Forms of spherical cavities in the Stołowe Mountains. Zeszyty nauk. Univ. Wrocław., Ser. B, 8, 123–137.

Edmunds WM, Kinniburgh DG, Moss PD, 1992. Trace metals in interstitial waters from sandstones – acidic inputs to shallow groundwaters. Environmental Pollution, 77(2–3), 129–141.

Mertlík J, Adamovič J, 2005. Some significant geomorphic features of the Klokočí Cuesta, Czech Republic. Ferrantia, 44, 171–175.

Navrátil T, Vařilová Z, Rohovec J, 2013. Mobilization of aluminum by the acid percolates within unsaturated zones of sandstones. Environmental Monitoring and Assessment**.** Online First. DOI 10.1007/s10661-013-3088-4.

Quesada D, Leguillon D, Putot C, 2009. Multiple failures in or around a stiff inclusion embedded in a soft matrix under a compressive loading. Eur. J. Mechanics, A–Solids, 28, 668–679.

Seifert A, 1936. Sandnester im Turon-Sandstein der Sächsischen Schweiz und ihre Bedeutung für Verwitterungsformen (Wannen, "Opferkessel" und Höhlchenbildungen). Sitzungsberichte und Abhandlungen der Naturwissenschaftlichen Gesellschaft Isis in Dresden 1935, 136–152 (in German).

Van den Bril K, Swennen R, 2009. Sedimentological control on carbonate cementation in the Luxembourg Sandstone Formation. Geol. Belgica, 12, 3–23.

Vařilová Z, Navrátil T, Dobešová I, 2011. Recent atmospheric deposition and its effects on sandstone cliffs in Bohemian Switzerland National Park, Czech Republic. Water, Air and Soil Pollution 220 (1–4), 117–130.

Vítek J, 1987. Pseudokrasové tvary v pískovcích Klokočských skal. Českosl. Kras, 38, 71–85 (in Czech).

Zimerman V, 1995. Jeskyně Kokořínska – místo průvodce. Místní noviny Podbezdězí, Kruh (in Czech).

ARENITIC CAVES IN VENEZUELAN TEPUIS: WHAT DO THEY SAY ABOUT TEPUIS THEMSELVES?

Roman Aubrecht[1,2], Tomáš Lánczos[3], Ján Schlögl[1], Lukáš Vlček[4], Branislav Šmída[5]
[1]Department of Geology and Paleontology, Faculty of Natural Sciences, Comenius University, Mlynská dolina – G, SK-842 15 Bratislava, Slovakia, aubrecht@fns.uniba.sk
[2]Geophysical Institute, Slovak Academy of Sciences, Dúbravská cesta 9, SK-845 28Bratislava, Slovakia
[3]Department of Geochemistry, Faculty of Natural Sciences, Comenius University, Mlynská dolina – G, SK-842 15 Bratislava, Slovakia, lanczos@t-zones.sk
[4]Slovak Speleological Society, Hodžova 11, SK-031 01 Liptovský Mikuláš, Slovakia, lukasvlcek@gmail.com
[5]Speleoclub of Comenius University, Department of Geology and Paleontology, Faculty of Natural Sciences, Comenius University, Mlynská dolina – G, SK-842 15 Bratislava, Slovakia, brano.smida@gmail.com

Geoscientific research was performed in the two largest sandstone cave systems in the world – Charles Brewer Cave System on the Chimantá Massif and Ojos de Cristal Cave System in the Mt. Roraima, both in South American table mountains (tepuis). These cave systems consist of subhorizontal caves. The research revealed that erosion of non-cemented layers and lateritization of arkosic arenites (hydrolysis of feldspars and micas) played a substantial role in their genesis. Softer beds in which the caves were initially formed show a lack of cementation or cementation by kaolinite. The hard overlying and underlying beds, as well as the "finger-flow" pillars which penetrate the uncemented arenite beds, are cemented by opal and quartz cements. The "finger-flow" pillars indicate that the main diagenetic phase was represented by descending silica-bearing fluids. The pillars originated when the fluid flow reached a coarse-grained arenitic bed, where the continuous fluid front splited to narrow channels. This caused lithification of the arenitic material in the channels and the rest of arenites in these beds escaped from lithification (softer beds) and was easily erodable.

This unusual way of arenite lithification in tepuis infers new views on their genesis and on the geomorphological evolution of the north of South America. Tepuis were formed from hard quartzites and sandstones of the Matauí Formation, which are underlain by arkoses of the Uaimapué Formation. These are the uppermost formations of the Roraima Supergroup which is the Paleoproterozoic detritic cover of the Archean Guyana Shield. From the speleogenetic and geomorphological observations it is evident that the main lithification phase of the Matauí Formation which caused their hardening to quartzites was represented by descending silica-bearing fluids which did not penetrate to the underlying arkoses which remained almost unlithified. The question is: what was the source of these fluids? A new theory concerning the origin of tepuis is presented in this paper. According to this theory, tepuis originated in places where there was an intensive descending fluid flow, most likely emanating from surface water reservoirs, such as rivers or lakes. This continuous flow carried SiO_2 from the lateritized surface beds. Thus, the underlying part of the Roraima Supergroup was impregnated with SiO_2 and strongly lithified. These indurated parts of the formation remained as tepuis, while the remainder of the formation was removed by erosion. The softness of the underlying, non-lithified sediment below the tepuis caused undercutting of their margins thus maintaining the walls vertical.

1. Introduction

Discoveries of large arenitic caves in famous Venezuelan table mountains (tepuis) were unexpected. Caves in silicate rocks are not so ubiquitous as caves in much more soluble material, such as limestones or gypsum. The previously most accepted model for the genesis of the sandstone caves was based on the arenization concept presented first by Martini (1979). The term "arenization" involves the dissolution of the quartz cement in arenitic rocks, with subsequent erosion and winnowing of the loose sand material. However, recent data from the research in the largest sandstone cave systems in the world – Charles Brewer Cave System on the Chimantá Massif and Ojos de Cristal Cave System in the Mt. Roraima (Aubrecht et al. 2008, 2011, 2012) showed that the dominant role of quartz and/or quartz cements dissolution is questionable. Geological and geomorphological research showed that the most feasible way of speleogenesis is winnowing of unlithified or poorly lithified arenites which remained as isolated "pockets" among hard-lithified quartzites and sandstones. Another frequently observed phemomenon, which contributes to the formation of the cave systems is weathering of aluminosilicate minerals, i.e. lateritization. While the latter is related to the recently ongoing processes, the first mentioned speleogenetic factor was related to the processes which created the tepuis themselves. Analysis of this process and the consequences resulting from it are the main aim of this paper.

2. Geology of the studied area

The main morphological feature of Guyana Highlands, encompassing southern Venezuela, Northern Brazil and Guyana are its tepuis. These are table mountains characterized by steep cliff walls and relatively flat mesetas, composed of Precambrian quartzites and sandstones covering the Guyana Shield. More than 100 table mountains can be found in the area. They provide important habitats for a great variety of endemic flora and fauna.

From a geological viewpoint, the caves and surface areas

analyzed herein are situated in the Venezuelan Guyana, in the northern part of South America (southeastern Venezuela, Gran Sabana). This area comprises Archaean rocks of the Guyana Shield which is the northern part of the Amazonian Craton. The Guyana Shield has a Proterozoic sedimentary cover named Roraima Supergroup which is formed mainly by clastics derived from the northern Trans-Amazonian Mountains. Sedimentological studies showed that the depositional environments ranged from alluvial fans to fluvial braided-river deposits together with lacustrine, aeolian, tidal, shallow-marine deposits and some shallow water turbidites (Reis and Yánez 2001; Santos et al. 2003). Sandy continental deposits are dominant here. The thickness of the group ranges from 200 m to approximately 3,000 m, and it consists of the following lithostratigraphic units arranged in stratigraphic order: Arai Formation, SuapiGroup, Uaimapué Formation and the Matauí Formation (Reis and Yánez 2001). Tepuis developed mainly in the uppermost, Matauí Formation formed by quartzites and sandstones, whereas the underlying Uaimapué Formation is mainly formed by arkoses. Their age was determined as 1,873 ±3 Ma (late Paleo-Proterozoic). This was achieved by U-Pb analyses of zircons from a green ash-fall tuff of the Uaimapué Formation (Santos et al., 2003). Since most of the previous authors accepted the theory that quartz dissolution requires a long time, the recent landscape, including commencement of the cave-forming process, is considered to be inherited from the Mesozoic period (e.g., Cretaceous – Galán and Lagarde 1988; Briceño et al. 1991; Piccini and Mechia 2009).

3. Methods

Our geological, geomorphological and speleological observations were focused on phenomena relevant to the solution of the speleogenetic problems. This mainly centered on the differential physical and mineralogical properties of the various kinds of arenites on the tepuis surfaces and caves in the Matauí Formation, and also on morphological aspects of the various stages of speleogenesis and its final manifestations on the surface.

Along with geomorphological observations, petrological and mineralogical analyses were performed on the rocks of the Matauí Formation. This mainly encompassed petrography of thin-sections of the arenites under polarized light, as well as SEM observations. Mineralogical composition of the samples was determined optically and also by X-ray diffraction analysis (XRD).

4. Results of geomorphological, petrographical and speleogenetic research.

Erosion and rockfalls, which recently prevail in the Charles Brewer and Ojos de Cristal cave systems (for position of the tepuis see Fig. 1) have concealed their true speleogenetic processes. The trigger and structural factors acting during initial stages of the cave evolution are now mostly obliterated in the mature parts of the cavern systems. Therefore, many of the most important clues resulted from caves which are still in their initial stages of evolution.

Figure 1. Location of the examined tepuis.

The sandstone surfaces of tepuis are very uneven and bizarre, which we interpreted as originated due to an inhomogeneous lithification of the Proterozoic arenites. This is especially apparent in areas where arenite beds form overhangs. The overlying and underlying beds are hard, well-lithified sandstones to quartzites, so that sampling was possible only with strong hammering. However, the beds inbetween are considerably soft, consiting of sands or soft sandstones, so that it was almost impossible to take solid samples for petrographic microscopic study, even after digging 30 cm deep by hand. This contrast in hardness was also verified by Schmidt hammer measurements (Aubrecht et al. 2011, 2012). These soft beds are penetrated by perpendicular pillar-shaped bodies (Fig. 2). These are narrower in the middle, but they have funnel-like widening at either end, with the lower funnel often less developed than the upper one. They are relatively hard rocks, ranging from sandstones to quartzites. In our interpretation, the origin of these pillars is purely diagenetic and their presence proves that the softness of the beds is due to a poor lithification and, therefore, it is primary rather than being secondary, related to weathering (see the discussion between Sauro et al. 2013 and Aubrecht et al. 2013). The pillars are considered to originate by a “finger flow” mechanism (cf. Aubrecht et al. 2008, 2011, 2012, 2013). The main factors influencing diagenetic variability were the differing hydraulic properties of the sediment in different layers which influenced its hydraulic conductivity.

Figure 2. Well preserved “finger-flow” pillars in the uncollapsed main corridors of Cueva Cañon Verde revealing their origin from descending silica-bearing fluid flow (note the similarity to leaking thick syrup).

The diagenetic fluids most likely penetrated vertically from the overlying strata as a descending diagenetic fluid flow. In finer-grained sediments, these diagenetic fluids filled the intergranular spaces evenly and resulted in the formation of diagenetically well-lithified beds, resistant to weathering. In coarse-grained arenites with higher hydraulic conductivity below the fine-grained beds, the evenly distributed descending diagenetic front divided into "fingers", where the fluid flow accelerated and formed separate, finger-like flows. This process has been described in detail by various authors working with transport processes in unsaturated zones of sandy aquifers and also in soils (Liu et al. 1994 and Bauters et al., 2000). A similar process is seen in snow penetrated by descending water as it leaks from melted snow above (Marsh 1988 – Fig. 2). Liu et al. (1994) considered that when these finger flows are generated in originally dry sandstones they are conserved as the most preferred method of infiltrating solutions. This is the way pillars originated in the unlithified sands. The downward diminishing funnel shape of the upper part of the pillar originated from flow acceleration, which continued until it decelerated when approaching the less permeable bottom. This retardation process is manifested in the reversely oriented funnel shape in the lower part of the pillar.

Observations in the Charles Brewer and Ojos de Cristal cave systems show that pillars are present in most of the caves and in their galleries, which are still in younger stages of their evolution. These usually possess low ceilings and strictly maintain one distinct layer. However, relic finger-flow pillars were also observed in the marginal, uncollapsed parts of the larger galleries.

When several superimposed winnowed horizons evolve together, a second collapse stage follows, leading to formation of much larger subterranean spaces. Galleries in the Charles Brewer Cave System are typically 40 metres wide, but they can also be much larger. The largest chamber found in the cave is Gran Galería Karen y Fanny. This is 40 metres high, more than 355 metres long and 70 metres wide, giving a volume of approximately 400,000 cubic metres.

The final stages of cave evolution often lead to huge collapses, and these are evident also on the tepui surfaces. This process most likely led to the creation of the large abysses in the Sarisariñama Plateau (Sima Mayor and Sima Menor).

Mineralogical and petrological analyses showed that softer beds in which the caves were initially formed lack cementation, or only kaolinite cementation is present, while the hard overlying and underlying beds and the "finger-flow" pillars are cemented by opal and quartz.

Some workers, e.g., Sauro et al. (2013) argumented against differential diagenesis by the metamorphic overprint of the entire Matauí Formation. They suggested that the metamorphism is evidenced by presence of pyrophyllite and pressure dissolution of quartz. Pressure dissolution also takes place in higher degrees of diagenesis and it can be neglected as a metamorphic indicator. Concerning pyrophyllite, although it is mentioned as a metamorphic indicator in the literature (anchizone to epizone) it does not explain presence of vast quantity of kaolinite in the soft arenitic beds that did not react with quartz to form pyrophylllite. Instead, pyrophyllite without kaolinite is present in hard lithified arenites (Aubrecht et al., 2013 – Fig. 3). Literature studies revealed that there is some evidence that pyrophyllite may also originate by hydrothermal alteration at lower temperatures (e.g., Ehlman and Sand 1959; Bozkaya et al. 2007; Bauluz and Subías 2010). The most important information is that some part of the aluminosilicate mineral phases existing at atmospheric pressure and 25 °C shows that H_4SiO_4 concentration is the critical factor in kaolinite/pyrophyllite transition (Aubrecht et al. 2013 – Fig. 4). Here, increased H_4SiO_4 concentration can theoretically cause the transformation of kaolinite to pyrophyllite without increased temperature or pressure (Aubrecht et al. 2013).

Lateritization, which also contributes to cave-forming processes, is important, but as we are now focused to the very early diagenetic processes that affected the Matauí Formation, it is beyond the scope of this paper.

5. Interpretation of the descending silica-bearing fluid flow: a new view on the origin of tepuis

Summarizing the results of the speleogenetic research, several important points were discovered concerning the origin of the tepuis. Although the research elucidated many aspects of the speleogenetic process, it also created new questions and problems. The most conspicuous finding was that the Matauí Formation is formed not only of quartzites but that its arenites show various degrees of lithification. Our research provided evidence of variability in vertical profiles. But what about the lateral variability? Are tepuis with a dominant presence of hard-lithified quartzites typical examples of the Matauí Formation? What about the larger, missing portion of the formation which was removed by erosion? Why are tepuis usually isolated islands rising up from the flat Gran Sabana? And also, why there are no "ruins" of tepuis formed by accumulations of quartzite boulders dispersed throughout the Gran Sabana?

Answers to these questions are currently purely theoretical as the missing, eroded portion of the Matauí Formation can no longer be examined. However, knowledge gathered from our research of this formation's remnants can be grouped under one common image which entails a new theory of the origin of tepuis.

"Finger-flow" pillars in the arenites forming these tepuis indicate that the descending flow of silica-bearing diagenetic fluids provided induration to arenites even to very hard quartzites. This flow penetrated deeply enough to lithify hundreds of metres of arenites in a vertical profile, and the indurated rocks then protected less lithified portions of the formation below. Most of the tepuis are limited by vertical cliffs, and undercutting of these cliffs often occurs because the lower parts of the massifs are less lithified (see also Young et al. 2009 – p. 58–60). Undercutting and the subsequent rockfall would be responsible for creation of the rock talus around tepuis (Montañas al pie del escarpado – see Briceño and Schubert, 1992 – Fig. 4.3). The talus then passes to flat country surrounding the tepuis, without retaining any remnants of quartzite boulder accumulations. However, closer inspection of the talus around Roraima indicates that

it is formed by less lithified, soft arenites of the Roraima Supergroup, which most likely underlie the sandstones and quartzites, rather than by fallen quartzite blocks (Fig. 3). Erosion of these soft arenites causes undercutting of the Roraima cliffs and keeps them steep.

Figure 3. A view on Mt. Roraima (and Mt. Kukenan – left). The mountain consists of quartzites, which form steep cliffs (C) and surrounding talus (T).

All these observations suggest that the patchy distribution of tepuis in Gran Sabana was formed long ago by vertical lithification of the Matauí Formation. This lithification required a voluminous source of soluble SiO_2 and sufficient fluids. Exactly as evident today from the recent lateritization, the best source of SiO_2 were the clay and rocks with micas and feldspars above the actually preserved Matauí Formation. These rocks were easily affected by lateritization, which most likely occurred after the Late Carboniferous, when the northern-most part of South America reached the tropical zone (see Scotese 2001). The best source of fluids would undoubtedly have been water reservoirs on the surface, and thus the recent distribution of tepuis may have copied the distribution of ancient lakes and rivers. Alternative explanations for the erosion of the missing portions of the Roraima Supergroup include the inference of Galán et al. (2004 – Fig. 1) that this erosion mainly affected tectonically disrupted parts of the Roraima Supergroup. However, this contradicts the lack of boulder accumulations on Gran Sabana. Moreover, the disrupted parts of the Roraima Supergroup had to be more widespread than the undissected ones, and this is considered most unlikely in this firm, rigid block of the Guyana Shield.

This theory is currently based on a limited set of data and further research is necessary. Although new data may support or refute our theory, it is very satisfying to provoke future research in this area.

6. Conclusions

1. The following speleogenetic model can be inferred from the obtained geomorphological and geological results (Fig. 4): Stage 1 – The descending, SiO_2-bearing diagenetic solutions caused complete lithification of some beds, whereas other beds with more coarse-grained arenites were only penetrated by narrow channels through which fluids flowed to completely fill some of the lower beds. This resulted in the contrasting diagenesis, where most beds turned to sandstone and quartzite while parts of other beds remained intact. Stage 2 – Hard, isolated beds were broken, and the flowing water which penetrated the poorly lithified beds started initial erosion. Lateritization then began in aluminosilicate-rich beds with the subsequent emptying of spaces by winnowing of sand and other products of lateritization. The empty spaces were then supported solely by "finger-flow" pillars. Stage 3 – Empty spaces collapsed further, thus creating larger caves, and superior propagation of these collapses created large collapse depressions on the surface.

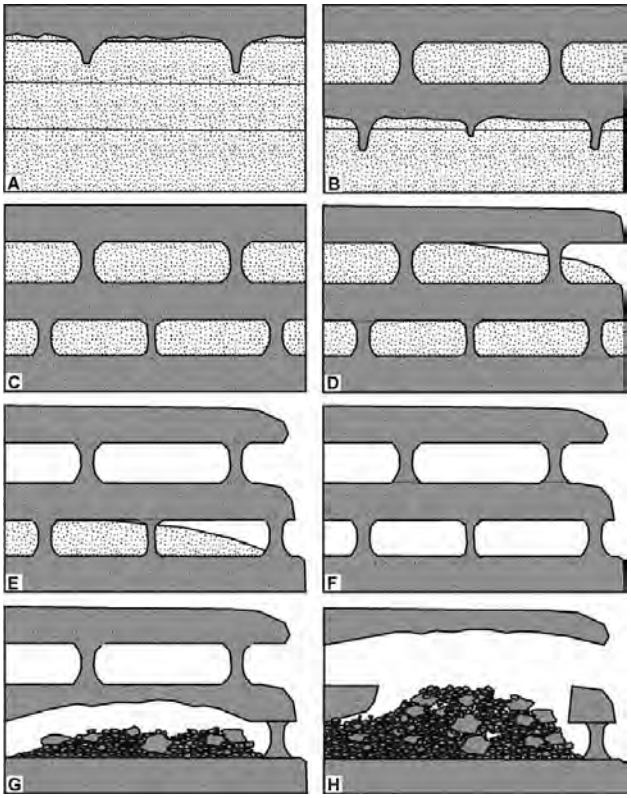

Figure 4. Schematic overview of the speleogenesis in the arenites of the Roraima Supergroup. Grey – well-lithified arenites, pale – poorly lithified arenites (caves formed by lateritization are omitted). A–B – The gradual diagenesis to arenites caused by descending silica-bearing fluids (Stage 1). C – Two poorly-lithified horizons superimposed on each other. D–E – Flowing water penetrated the vertical cleft (on the right side) causing gradual winnowing of the poorly lithified sediment (Stage 2). F – Two horizons remained empty (two superimposed initial caves), with lithified pillars offering the only support against collapse. G–H – Collapse of both floors, forming a large cave (Stage 3).

2. A new theory concerning the origin of tepuis can be proposed, based on the fact, that diagenesis by descending silica-bearing fluids appears to be the main phase that indurated the Matauí Formation quartzites (Fig. 5). According to this theory, tepuis originated in places where there was an intensive descending fluid flow, most likely emanating from surface water reservoirs, such as rivers or lakes. This continuous flow carried SiO_2 from the lateritized surface beds. Thus, the underlying part of the Roraima Supergroup was impregnated with SiO_2 and strongly lithified. These indurated parts of the formation remained as tepuis, while the remainder of the formation was removed by erosion. The softness of the underlying, non-lithified sediment below the tepuis caused undercutting of their margins thus maintaing steep walls. Speleogenesis in the tepuis was a process which most likely began at a later stage, with initial incision of the valleys followed by erosion.

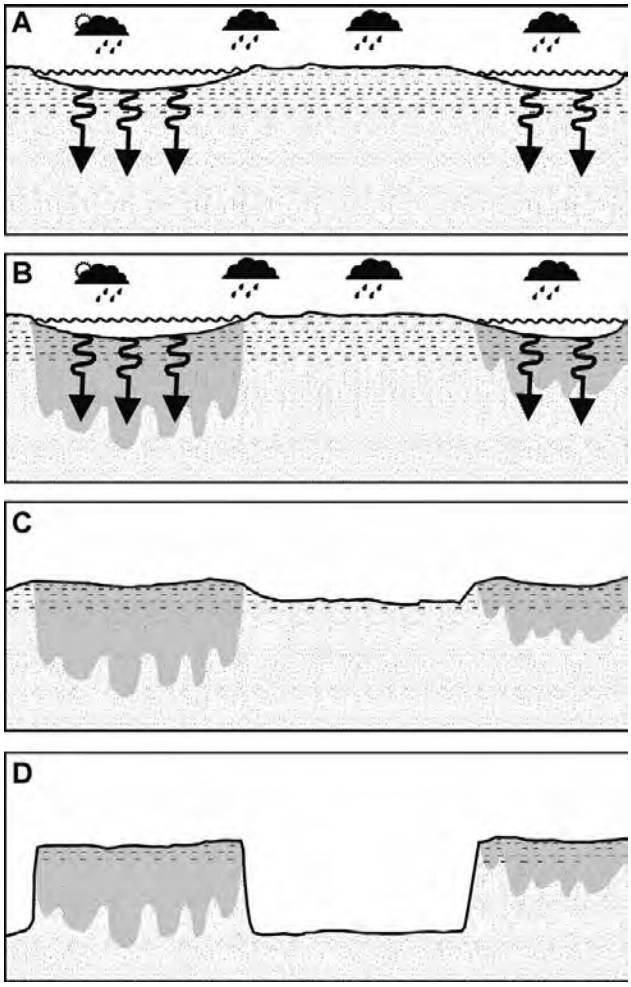

Figure 5. The newly proposed model of the origin of the tepuis. A – The Roraima Supergroup was originally capped by sediments rich in micas, feldspars or clay minerals which were prone to lateritization. This lateritization may have begun in the Late Carboniferous when the northern part of present South America reached tropical areas (Scotese, 2001). B – The lateritization occurred mostly in the areas with excess fluids, such as rivers and lakes. The descending fluids brought silica from the lateritization zones downwards, causing additional cementation of the Matauí Formation. This cementation was patchy, and concentrated only in the zones with sufficient water. C–D – In the later geomorphological evolution stages, the uncemented portions of the Roraima Supergroup were subjected to erosion and the cemented, quartzitic parts were preserved, together with the softer, uncemented parts protected below them. The steep cliffs of the tepuis are maintained by erosion of the softer, uncemented arenites below with subsequent undercutting of the quartzite layers.

Acknowledgements

The authors are deeply indebted to Francesco Sauro and Jo De Waele (Bologna University, Italy) for their review and useful corrections and comments that helped to improve the text of this paper. The research was financed by grants APVV 1-0251-07 and VEGA 1/0246/08.

References

Aubrecht R, Lánczos T, Šmída B, Brewer-Carías Ch, Mayoral F, Schlögl J, Audy M, Vlček L, Kováčik Ľ, Gregor M, 2008. Venezuelan sandstone caves: a new view on their genesis, hydrogeology and speleothems. Geologia Croatica, 61, 345–362.

Aubrecht R, Lánczos T, Gregor M, Schlögl J, Šmída B, Liščák P, Brewer-Carías Ch, Vlček L, 2011. Sandstone caves on Venezuelan tepuis: return to pseudokarst? Geomorphology, 132, 351–365.

Aubrecht R, Barrio-Amoros C, Breure A, Brewer-Carías Ch, Derka T, Fuentes-Ramos OA, Gregor M, Kodada J, Kováčik Ľ, Lánczos T, Lee NM, Liščák P, Schlögl J, Šmída B, Vlček L, 2012. Venezuelan tepuis – their caves and biota. Acta Geologica Slovaca – Monograph, ISBN 978-80-223-3349-8, 1–168.

Aubrecht R, Lánczos T, Gregor M, Schlögl J, Šmída B, Liščák P, Brewer-Carías Ch, Vlček L, 2013. Reply to the Comment on "Sandstone caves on Venezuelan tepuis: Return to pseudokarst?" Geomorphology (DOI: 10.1016/j.geomorph.2012.11.017).

Bauluz B, Subías I, 2010. Coexistence of pyrophyllite, I-S, R1 and NH_4^+-rich illite in Silurian black shales (Sierra de Albarracín, NE Spain): metamorphic *vs*. hydrothermal origin. Clay Minerals, 45, 3, 383–392.

Bauters TWJ, Dicarlo DA, Steenhuis TS, Parlange J-Y, 2000. Soil water content dependent wetting front characteristics in sand. Journal of Hydrology, 231–232, 244–254.

Bozkaya O, Yalcin H, Basibuyuk Z, Bozkaya G, 2007. Metamorphic-hosted pyrophyllite and dickite occurrences from the hydrous Al-silicate deposits of the Malatya-Puturge region, central eastern Anatolia, Turkey. Clays and Clay Minerals, 55, 4, 423–442.

Briceño HO, Schubert C, 1992. Geomorfología. In: Huber O. (Ed.): Chimantá. Escudo de Guayana, Venezuela. Un Ensayo Ecológico Tepuyano. Oscar Todtmann Editores, Caracas, 61–74.

Briceño HO, Schubert C, Paolini J, 1991. Table-mountain geology and surficial geochemistry: Chimantá massif, Venezuelan Guayana Shield. Journal of South American Earth Sciences, 3, 179–194.

Ehlmann AJ, Sand LB, 1959. Occurrence of shales partially altered to pyrophyllite. Clays and Clay Minerals, 6, 368–391.

Faure G, 1991. Principles and applications of inorganic geochemistry: a comprehensive textbook for geology students. Macmillan, New York, 626.

Galán C, Lagarde J, 1988. Morphologie et evolution des cavernes et formes superficielles dans les quartzites du Roraima. Karstologia, 11–12, 49–60.

Galán C, Herrera FF, Carreño R, 2004. Geomorfología e hidrología del Sistema Roraima Sur, Venezuela, la mayor cavidad del mundo en cuarcitas: 10,8 km. Bol. SVE, 38, 2–16.

Liu Y, Steenhuis TS, Parlange J-Y, 1994. Formation and persistence of fingered flow fields in coarse grained soils under different characteristics in sands. Journal of Hydrology, 159, 187–195.

Martini JEJ, 1979. Karst in Black Reef Quartzite near Kaapsehoop, Eastern Transvaal. Annals of the Geological Survey of South Africa, 13, 115–128.

Piccini L, Mecchia M, 2009. Solution weathering rate and origin of karst landforms and caves in the quartzite of Auyan-tepui (Gran Sabana, Venezuela). Geomorphology, 106, 15–25.

Reis NJ, Yánez G, 2001. O Supergrupo Roraima ao longo da faixa fronteirica entre Brazil-Venezuela (Santa Elena del Uairen-Roraima Mountain). In Reis N.J. & Monteiro M.A.S. (Eds.): Contribuicao a geologia da Amazonia, Vol. 2: Manaus, Brazil, Soc. Brasil. Geol. 113–145.

Santos JOS, Potter PE, Reis NJ, Hartmann LA, Fletcher IR, McNaughton NJ, 2003. Age, source, and regional stratigraphy of the Roraima Supergroup and Roraima-like outliers in northern South America based on U-Pb geochronology. Geological Society of America Bulletin, 115, 331–348.

Sauro F, Piccini L, Mecchia M, De Waele J, 2012. Comment on "Sandstone caves on Venezuelan tepuis: Return to pseudokarst?" by R. Aubrecht, T. Lánczos, M. Gregor, J. Schlögl, B. Smída, P. Liscák, Ch. Brewer-Carías, L. Vlcek. Geomorphology 132, 351–365. Geomorphology.

Scotese CR, 2001. Atlas of Earth History. PALEOMAP Project, Arlington, Texas, 1–52.

Young RW, Wray RAL, Young ARM, 2009. Sandstone landforms. Cambridge University Press, 1–304.

INFRARED THERMOGRAPHIC SURVEY OF PSEUDOKARST SITES IN THE FYSCH BELT OF OUTER WEST CARPATHIANS (CZECH REPUBLIC)

Ivo Baroň[1, 2], David Bečkovský[3], Lumír Míča[3]
[1]*Speleological Society of Vienna and Lower Austria, Obere Donaustraße 97/1/61, A-1020 Wien, Austria*
[2]*Geological Survey of Austria, Neulinggasse 38, 1030 Vienna, Austria, ivo.baron@geologie.ac.at*
[3]*Faculty of Civil Engineering, Brno University of Technology, Kounicova 966/67a, 60200 Brno, Czech Republic*

The paper presents a test study of application of infrared thermography (IRT) for mapping thermal characteristics of pseudokarst crack caves related to deep-seated gravitational slope failures in the Flysch Belt of the Outer West Carpathians, and for locating new systems. The method was tested at four pseudokarst sites: Křížový, Smrdutá, Pustevny and Záryje in E Czech Republic. The IRT images excelently showed spatial pattern and thermal characteristics and gradients of the crack systems opened to the ground surface promising new cave discoveries. The method is, however, constrained by very specific meteorological conditions, such as cold weather with ambient air temperatures lower than the local annual mean rock temperature at depth, good visibility, lack of direct insolation, absence of thick snow cover, adequate sensor resolution and accuracy, and reasonable distance and sensing angle from the rock surface.

1. Introduction

Thermal gradients between deep rock and colder ground surface often help cavers identify unexplored caves by searching for melted snow cover in the winter season (Rinker 1975; Lešinský 1999; Baroň 2002). The Infrared Thermography method (IRT) has been proposed as a useful tool for detecting karst cave openings (Rinker 1975; Wynne et al. 2008; Baroň et al. 2012) and hydrological features in karst watersheds (Campbell et al. 1996).

Here we present a test study of application of IRT to pseudokarst sites in E Czech Republic, which follows our previous work focused on detection of open cracks within deep-seated rockslides in Outer West Carpathians and Northern Calcareous Eastern Alps (Baroň et al. 2012). The main aim of this study is testing the reliability of the method for pseudokarst crack caves within gravitational rock-slope failures.

Figure 1. A) Location within the Czech Republic, and B) detailed location of the study sites within the topography of the central-eastern part of the Czech portion of the Outer West Carpathians. The black rectangle indicates the extent of B) (Source of SRTM data: USGS/NASA).

2. Methods

The IRT detection method of pseudokarst caves relies on air circulation and ventilation though open joints and cracks when, in winter, the warmer subsurface communicates with the (colder) ground surface; crack caves could be identified as relatively warm areas using IRT then (Baroň et al. 2012). For this study, we used a Flir B360 infrared thermal camera, which is a high-sensitivity camera with 320 × 240 IR resolution and thermal sensitivity (N.E.T.D) of 0.05 °C at 30 °C. The sensing temperature range is -20 to 120 °C, and the spectral range varies from 7.5 to 13 μm (far-IR).

IRT mapping in this study was conducted in beginning of cold season on 1st December, 2012, when it was overcast to cloudy weather with external temperatures ranging between 0 and -5 °C. There was no or minimum snow cover at the time of the survey.

3. Description of the Křížový, Smrdutá, Pustevny and Záryje Sites

The case-study sites comprise four pseudokarst localities related to deep-seated rock slope failures in the Flysch Belt of Outer West Carpathians in E Czech Republic.

The Křížový pseudokarst site has developed in a headscarp area of a Holocene rotational deep-seated rockslide at SE slopes of the Křížový Hill (670 m a.s.l.) about 3.5 km west from Vsetín. The slope failure is about 700 m long, 300 m wide with estimated 8–10 million m^3 of affected bedrock and colluvium. The main scarp exhumed faces of several m thick sandstone beds of the Lukov Member of the Soláň Formation. The sandstone cliff reaches height of up to 10 m, with a scree accumulation below; the whole scarp is about 30 m high. About 20 long and 12 m deep crack cave "Zbojnická" occurs at SW flank of the scarp.

The Smrdutá pseudokarst site comprises a deep-seated complex flow-like landslide combined with a deep-seated rockslide and rock sagging in the upper part. It is situated at SW slopes of the Smrdutá Hill within competent sandstones and conglomerates of the Rusava Member and incompetent

claystones and shales of the Raztoka Member of the Rača Unit. Our results of the radiocarbon dating of lacustrine deposits at the base of a palaeo-dam due to the landslide revealed a minimum age of the slope failure about 2055 ±30 14C years BP. Two smaller pseudokarst talus caves developed between conglomerate blocks in the flow part, and six other crack-caves developed within the rockslide and sagging part. The longest caves here are the "Na Smrduté" and "Poschoďová" Caves reaching maximum length of 56 m (Wagner et al. 2009).

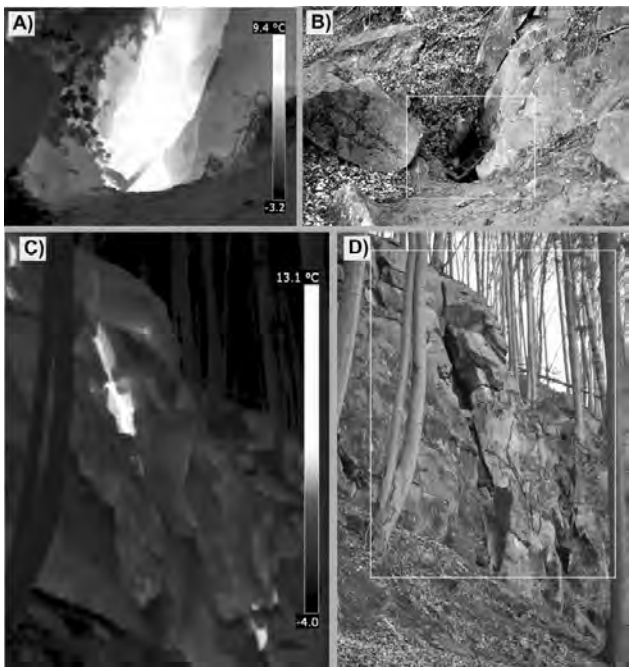

Figure 2. Results of the IRT survey at the Křížový Site: A) IRT image of the entrance of the Zbojnická Cave, B) BW photography of the same area, C) IRT image of a toppled rock column indicating open cracks behind it, D) BW photography of the same area.

The Pustevny Site is well known for the longest pseudokarst cave of the Czech Part of the Outer West Carpathians. The Cyrilka Cave has been recently prolonged to 535 m (J. Lenárt, pers. comm.) and it has developed in the crown of a large deep-seated translational consequent rockslide at the SE slopes of the Radhošť massif near Pustevny. The rockslide is about 2,400 m long, 1,500 m wide and about 20–30 m thick (Baroň and Kašperáková 2007). The sliding surfaces are located within claystone intecalations between several m thick sandstone beds dipping about 9–12° to SSE.

The last studied pseudokarst site at Záryje has, similarly to the previous site, developed in upper part of a large deep-seated translational consequent rockslide at the S slopes of the Radhošť. Several caves are known from this area (Wagner et al. 1990). The longest one is the Szalajka Cave discovered in 2004 (J. Szalai, pers. comm.).

4. Resuls

4.1. The Křížový Site

Several warmer areas were observed at this site; all of them were located along the cliff of the main-scarp. A blowhole with strong air current was related to the entrance the Zbojnická Cave (Figure 2A and B) as well as several warmer spots.

Other melting spots developed on the scree accumulation (warm air originated within small caverns between stones and debris) or behind toppled boulders (Figure 1C and D). The spots related to toppled boulders indicate the future rock-fall hazard. The "pseudokarst doline" below the scarp was thermally neutral. The warm areas are, however, relatively very small, both in dimensions and thermal gradient. Therefore we do not suspect an existence of larger cave systems except of the Zbojnická Cave.

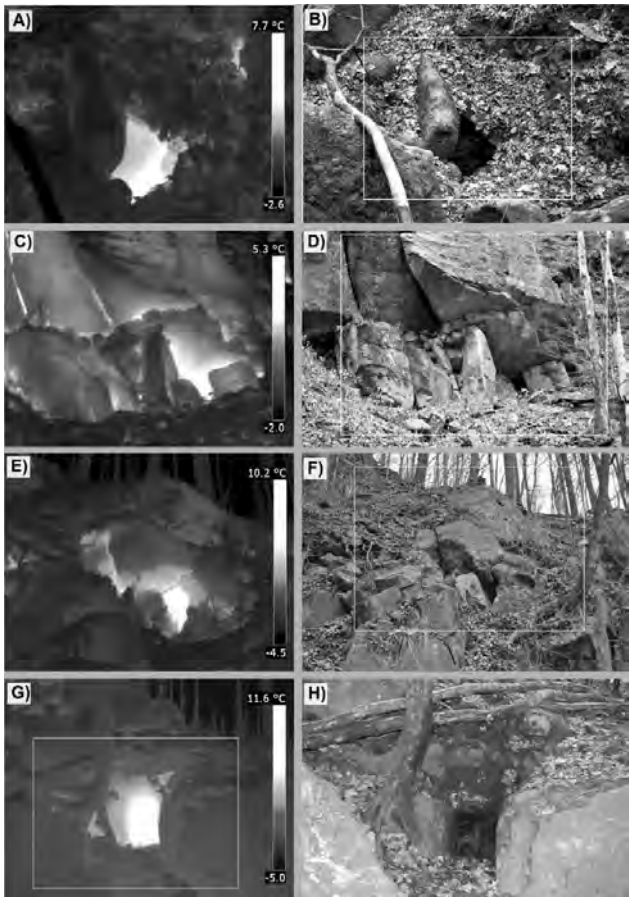

Figure 3. Results of the IRT survey at the Smrdutá Site: A) IRT image of the entrance of the Vodní Cave, B) BW photography of the same area, C) IRT image of the entrance of the Poschoďová Cave, D) BW photography of the same area, E) IRT image of the entrance of an unknown undergroung space, F) BW photography of the same area, G) IRT image of the entrance of the Na Smrduté Cave, H) BW photography of the same area.

4.2. The Smrdutá Site

The IRT survey found several warmer areas related to (i) the highly-porous flow part containing blocks up to 10–15 m in diameter, e.g., at the Vodní Cave (Fig. 3A and B), loosened rock of an incipient deep-seated rockslide part with the Poschoďová Cave (Fig. 3C and D), several other unknown undergound crack caves (Fig. 3 E and F), and to the sagged part with the longest cave here, the "Na Smrduté" Cave (Fig. 3G and H). The IRT images excellently showed the spatial pattern and thermal characteristics and gradients of crack systems opened to the ground surface. The results promise new cave discoveries; however due to dimensions of the slope failure, they would not exceed several tens of meters.

4.3. The Pustevny Site

At the Pustevny Site, we surveyed only the area of the Cyrilka Cave. The site was in several places exposed to the sunshine, therefore the results were acceptable only from few a places. Despite that, thermal characteristics of the entrance of the Cyrilka cave (Fig. 4A and B) and the spatial pattern of its traces at the ground surface (Fig. 4C and D) were achieved by IRT.

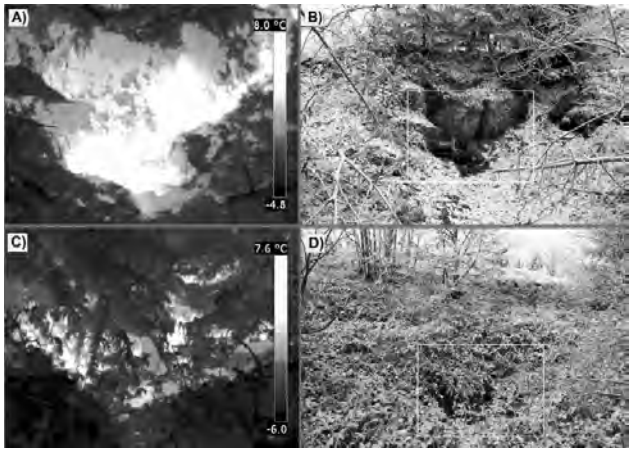

Figure 4. Results of the IRT survey at the Pustevny Site: A) IRT image of the entrance of the Cyrilka Cave, B) BW photography of the same area, C) IRT image of a trace of the Cyrilka Cave at the ground surface, B) BW photography of the same area.

4.4. The Záryje Site

We achieved the best results of the structural pattern of open cracks and the existing and potential cave systems at the Záryje Site. We identified all the known caves and their traces at the ground surface, (e.g., the Szalajka Cave, Fig. 5A and B), and also several up-to date unknown crack systems (Fig. 5C and D and Fig. 6). The site promises new speleological discoveries in near future.

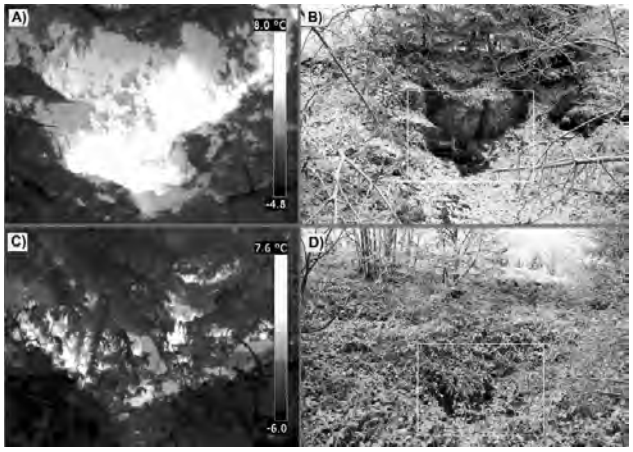

Figure 5. Results of the IRT survey at the Záryje Site: A) IRT image of the entrance of the Szalajka Cave, B) BW photography of the same area,C) IRT image of a superficial trace of an unknown crack-cave system, D) BW photography of the same area.

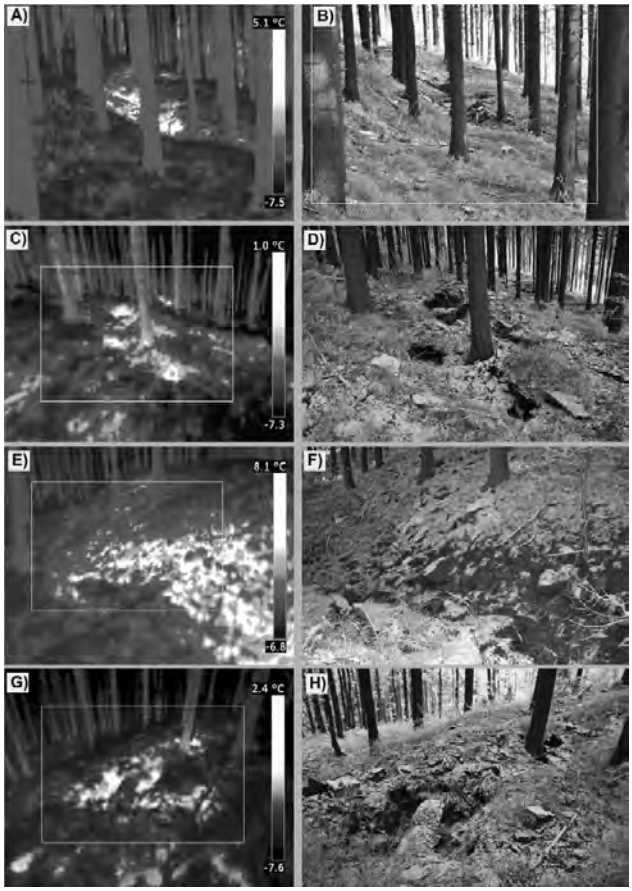

Figure 6. Results of the IRT survey at the Záryje Site: A), C), E) and G) IRT images of superficial traces of unknown crack-cave systems, B), D), F) and H) BW photographies of the respective areas.

5. Discussion and Conclusions

Through our research, we proved great advantages of the IRT ground-based survey for mapping thermal characteristics of pseudokarst crack caves related to deep-seated gravitational slope failures in the Flysch Belt of the Outer West Carpathians, and for locating new cave systems.

The method is, however, restricted to very specific meteorological conditions, similar to the IRT survey for mapping open cracks within unstable rock slopes and rock cliffs for engineering-geological purposes (Baroň et al. 2012); the applicability of the IRT method is restricted to cold weather, when ambient air temperatures are lower than the local mean rock temperature at depth. Good visibility, lack of direct insolation, absence of thick snow cover, adequate sensor resolution and accuracy, reasonable distance from the rock surface, and sparse vegetation between the sensor and rock surface are main considerations of the method (Baroň et al. 2012).

Acknowledgments

The survey was supported by the project “OP VAVpI CZ.1.05/2.1.00/03.0097” AdMaS at the Brno University of Technology. The authors thank to M. Filippi and other anonymous reviewer for careful reading of the manuscript and their comments, which helped improving its quality.

References

Baroň I, 2002. Location of underground spaces in selected slope deformations by observations of melted snow and ventaroles (in Czech). Speleofórum 21, 64–66.

Baroň I, Bečkovský D, Míča L, 2012. Application of infrared thermography for mapping open fractures in deep-seated rockslides and unstable cliffs. Landslides, Springer Verlag. DOI 10.1007/s10346-012-0367-z.

Baroň I, Kašperáková D, 2007. Numerical analysis of Silesian Nappe gravitational disintegration by means of FDM (Case study: Radhošť-Pustevny). Zprávy o geologických výzkumech v roce 2006, 49–52, Czech Geological Survey, Prague (in Czech).

Campbell CW, Abd El Latif M, Foster JW, 1996. Application of Thermography to Karst Hydrology. Journal of Cave and Karst Studies 58(3), 163–167.

Lešinský G, 1999. Comments to caving in winter season with focus on observing melted spots and ventaroles. Spravodaj SSS 1999 (4), 32–33. Liptovský Mikuláš (in Slovak).

Rinker JN, 1975. Airborne infrared thermal detection of caves and crevasses. Photogrammetric engineering and remote sensing 41, 1391–1400.

Wagner J, Demek J, Stráník Z, 1990. Caves of the Moravian-Silesian Beskids and Surrounding. Knihovna ČSS 17: 1–130. Praha.

Wagner J, Baroň I, Bezděčka P, 2009. Pseudokarst caves of the flysch belt of the Outer West Carpathians. In Hromas J. et al. (Eds.), Protected Areas of the Czech Republic, Volume XIV: Caves, Praha – Brno, 536–546 (in Czech).

Wynne JJ, Titus TN, Diaz GCh, 2008. On developing thermal cave detection techniques for earth, the moon and mars. Earth and Planetary Science Letters 272, 240–250.

KAHUENAHA NUI (HAWAII): A CAVE DEVELOPED IN FOUR DIFFERENT LAVA FLOWS

Ingo Bauer[1], Stephan Kempe[1], Peter Bosted[2]
[1]Institute of Applied Geosciences, University of Technology Darmstadt, Schnittspahnstr. 9, D-64287 Darmstadt, Germany, Kempe@geo.tu-darmstadt.de
[2]Cave Conservancy of Hawaii: P.O. Box 7032 Ocean View, Hawaii 96737-7032

Exploration and survey of the Kahuenaha Nui Cave in March 2011 yielded astonishing insights into the processes that act to enlarge the tunnels of underground lava conduits (pyroducts). The cave is situated in lavas of the SW Rift of the Mauna Loa, Hawaii, within the area of the former Kahuku Ranch, south of the Belt Road at an altitude of 564 m a.s.l. On the geological map of Hawaii, these lavas belong to the stratigraphic group Qk2, dated to between 1500 and 3000 a BP. These flows are bordered by the 1868 pahoehoe flow in the E and the 1887 a‘a flow in the W and occupy ca. 70 km^2. The cave survey yielded a total length of 1,850 m, a total vertical extent of 55 m, and an average slope of 5.7° (Bauer 2011). The cave features a main trunk that is up to 18 m wide and 11 m high. Its floor is in parts formed by terminal a‘a. Above this trunk passage, we explored numerous small to very small interconnected pahoehoe ducts. At the entrance puka (breakdown hole) and at a large open puka we were able to study the cave formation process. The trunk passage formed by eroding an underlying a‘a rubble layer. In places even the underlying a‘a core layer has been cut into. Above, a stack of seven superimposed pahoehoe (phh) flows with small ducts occurs, forming the primary roof of the cave. The lava flowing in this stack of sheets managed to combine into one flow, eroding the main trunk underneath. After cave formation first an a‘a flow and then a thin pahoehoe flow transgressed the area. The cave’s roof partly collapsed, not only exposing the transgressed a‘a but also forming the two entrances. This cave forming mechanism is fundamentally different from the “inflation” and the “crusting-over of channels” mechanisms identified as pyroduct formation modes so far.

1. Introduction

Even though many lava tubes are mapped on the island of Hawaii, especially on Mauna Loa, only little is known about the detailed processes taking place during the formation of lava caves. Volcanological literature does not deal in detail with near-surface transport processes of lava and their importance for building shield volcanoes. Description of lava tube forming processes are often limited to “crusting-over of channels”. Despite this many lava cave forming processes are known today due to intense research in this field of study although we are far away from understanding all the features we can observe. In Kahuenaha Nui, a cave situated on the south-west flank of Mauna Loa, we were able to discover a new way to form large pyroducts. A number of small pyroducts in the stack of pahoehoe sheets of the primary roof drained into the main passage eroding an underlying a’a-flow. Astonishingly intense erosion cut down not only through the underlying a’a rubble but also the a’a core beneath was deeply degraded. This results in a cave with its main volume build in older lavas.

2. Geologic setting

The study area is located near Hawaii’s South Point, on the southern flank of Mauna Loa, south of the Mamalahoa highway between Ocean View and Na’alehu. The investigation area between the highway and the coast is 10 km long and covers roughly 70 km^2. Our study concentrated on the Pu’u o Keokeo-Flow. The average surface slope is 3.2°, decreasing towards the coast.

Mauna Loa is the largest active volcano on the island of Hawaii. Eruptions can be discriminated in summit, rift-zone, and flank eruptions. Two rift zones, the Northeast and Southwest rift zone cut through the volcanic edifice. Eruptions from the SW-Riftzone produced the 1868 and 1887 flows, bordering the Pu’u o Keokeo-Flow to the east and west.

Kahuenaha Nui is situated in a series of old lavaflows also erupted from the SW-Riftzone of Mauna Loa. The lavas

are not dated but supposed to be of late Holocene age, between 1500 and 3000 a BP. According to the geological map, these lavas belong to the stratigraphic group Qk2. The surface of the northern area is covered by a hummocky pahoehoe flow, the Pu’u o Keokeo-Flow. It transgressed an older a’a-flow, appearing in patches on the surface. This flow is radiocarbon-dated to 1730±60 a BP.

Mauka (Hawaiian for uphill) Mamalahoa highway aerial photographs allow tracking the Pu’u o Keokeo-Flow for another 3 km. Further uphill vegetation prevents identification. Lavas of the 1926 and 1950 flows cover the surface mauka. Considering the section shape of the SW-Riftzone it is unlikely that the Pu’u o Keokeo lavas originate from a summit eruption. Thus it is probable that the source of the lava is a magma chamber below the SW-rift zone.

The surface above Kahuenaha Nui is covered with phh-lava. In defined narrow areas transition from pahoehoe to a’a can be observed, partially covered by pahoehoe from later events. The area is characterized by the appearance of numerous tumuli. They arise while already cooled surface lava bulges due to varying eruption rates. In the upper Pu’u o Keokeo-Flow no evidence for overflowing lava was found. Therefore one could assume that eruption rates fluctuated with low amplitude and high frequency.

3. Petrology

Thin sections from different Kahuenaha Nui samples were investigated and XRD-analysis was conducted on selected samples in order to characterize different lava flows (Table 1). As expected the composition is tholeiite-basaltic. The pyroxene family is represented by diopside. Sample CS 5 stems from the lower a'a-rubble of the basal a'a-layer. The related a'a-core is partially covered with lining and cannot be traced continuously. Albeit sample CS 5 can be correlated to CS 14 which belongs to the lower a'a core at st. 13. Hematite can be verified in samples CS 5, CS 14, CS 17, and CS 18. It originates from oxidation of magnetite and indicates as reddish boundary layer temporally separated lava flows. During transgression of a'a-lava oxygen reaches the boundary layer through the a'a-rubble. Sample CS 18 belongs to a channel overflow during a late stage of flow activity. In the process lava flowed through a channel in the pyroduct floor, no longer occupying the whole width of the passage. The above placed gas space was connected with the surface through contraction cracks in the cave roof and probably by hot pukas, allowing rapid oxidation of the lava surface resulting in a reddish coloured surface.

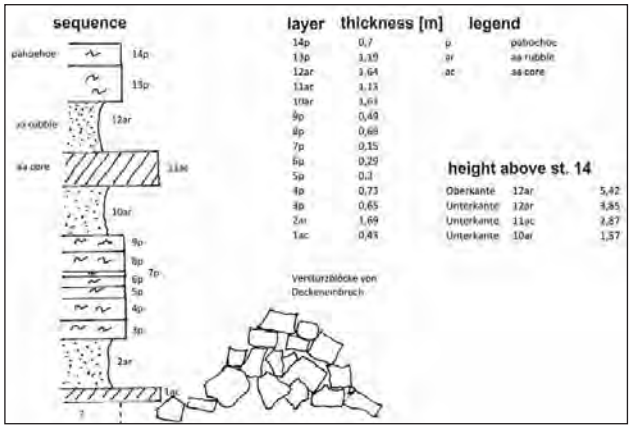

Figure 1. Stratigraphic column of Kahuenaha Nui at Puka 2.

Gibbsite, thenardite, and gypsum are secondary minerals, resulting from alteration of lava due to chemical weathering. They occur in large amounts, covering the cave walls and breakdown.

4. Cave description

The area has numerous pukas and caves of which only a few have been investigated during our field trip.

Two entrance pukas, both formed by cold breakdown give access to the cave. Entrance puka 2, with a width of 9 m and steep overhanging walls, is the bigger one and was found later, after the discovery of Entrance puka 1. Puka 2 exposes the layers responsible for cave formation. Entrance puka 1 led to the discovery of the cave while one of the authors, sitting near the wall suddenly felt a cold breath from behind, arising from an airflow sweeping through a small hole in the wall of the puka. A short dig led to Discovery Hall (DH; Fig. 6a, P1), representing the actually known far N-end of Kahuenana Nui. Makai opened the main passage. Here the original cave roof, represented by a stack of phh-sheets, can be seen. The mauka end of DH is blocked by boulders arising from cold breakdown of the cave roof. The SE-cave wall exposes an a'a-core pinching out to the S, overlain by a reddish hematized a'a-rubble. The cave roof is situated in phh-sheets resulting from a younger eruption event. Even the NNW-wall exposes an a'a-core, petering out northwards, leading to a thick layer of a'a rubble overlain by phh. These observations give evidence that DH developed at the border of two a'a-flows. The absence of a continuous a'a-core allowed upward enlargement while the underlying original cave passage became blocked. The original cave floor is completely covered with boulders and is not exposed. Puka 2 is a wide open cold puka and gives comprehensive insight in the development of the cave.

Table 1. Results from XRD-analysis. Minerals without distinct evidence in italic letters.

Sample Nr.	Location	Mineral composition
CS 5	Kahuenaha Nui, southern wall, St. K6, lower a'a-rubble (layer 0 ar)	anorthite diopside albite cristobalite hematite *thenardite* *hornblende* *marcasite*
CS 14	Kahuenaha Nui, st. 13, lower a'a-core (layer 1 ac)	anorthite diopside high-albite hematite *hornblende* *marcasite*
CS 16	Kahuenaha Nui, entrance flow	augite anorthite high-albite *gypsum*
CS 17	Kahuenaha Nui, southern wall, upper a'a-rubble of lower a'a-layer (layer 2 ar)	anorthite albite diopsid cristobalite hematite magnesite *thenardite* *gibbsite*
CS 18	Kahuenaha Nui, st. 28b, porous overflow	anorthite diopside albite hematite

An alternating sequence of phh- and a'a-layers can be seen in the entrance puka 2 (Figs. 1, 6a, P2). The a'a-rubble layers 12ar and 10ar are undercut while the more resistant a'a-core layers 11ac and the phh-surface layers 13p and 14p form minor overhangs. The primary cave roof is located within the stack of phh-layers 3p to 9p but cannot be determined exactly. The development of Kahuenaha Nui is essentially determined by erosional downcutting of the cave forming phh-lava in underlying a'a-layers 1ac and 2ar. Due to minor resistance of layer 1ar against downward erosion, one can expect fast downcutting through the slightly welded a'a-rubble. Below layer 2ar the flowing phh even cut through the a'a-core (layer 1ac). A cross section at st. 12 gives evidence that the phh-lava cut down through at least 3.5 m of a'a. Further mauka lining covers layer 1ac while it

downwells in breakdown from the ceiling. Even though the a'a-layer below the cave-forming pahoehoe is not continuously exposed, samples from Discovery Hall and puka 2 show similar mineralogical composition (samples CS5 and CS 14), suggesting that both layers belong to the same flow. At least two transgressive events can be determined subsequent to the cave forming process. The primary cave roof is overlain by an a'a-flow (layers 10ar, 11ac,12ar). Not less than two more phh-flows (13p, 14p) form the present surface.

Figure 2. Outcrop of a'a-core with overlying a'a-rubble at st. 12. The phh-flow cut through both layers. View southwest. Photo by Stephan Kempe.

Not far behind st. 20 the main passage splits. While the right passage has numerous 0.2 m deep cataracts, a 1 m deep lavafall cut down into the left passage. Where the passages unite again several initial phh-conduits in the phh stack meet and their lava cut into the underlying a'a (Figs. 3, 6a, P3).

Figure 3. Mauka view from Confluence Hall. Arrow points to one initial conduit in the phh stack that drained into the main passage. Photo by Peter and Ann Bosted.

Makai (Hawaiian for downhill) of st. 34b7 a lavafall drops 2.5 m down into an underlying passage (Fig. 6b, P4). The separation between different conduits in the initial stack of phh collapsed and the cave-in was carried out by the lava in the remaining lower conduits. Occasionally the underlying passage was blocked by lavaballs which gave rise to the spill-over of lava in the overlying passage. Reddish oxidized lava can be observed around the collapse and can be followed makai. However the reddish lava cannot be traced mauka giving evidence for a post collapse event.

In the center of the cave, the main passage got so wide and deeply entrenched, that a secondary ceiling formed (Fig. 6b, P5). No evidence of hot pukas can be found. At the "Ball Room", several small conduits unite to form a larger cavity (Fig. 6b, P6). The r-passage incorporates a number of small initially formed conduits. (Fig. 6c, P7). Several small tubes in different phh-sheets can be observed. No lavafall established at st. ra1 or st. rb2, giving evidence that the overlying conduits have already been drained earlier. However at st. r2a1 a lavaflow can be determined, draining a high-lying small pyroduct. Makai of the "Misery Crawl" the b-passage cuts an overlying passage. Partial lining can be found, indicating that the phh-stack collapsed, connecting both passages while at least the lower passage was still active. However no lavafall from the upper passage developed. The upper passage points towards the mauka end of "Peters Challenge" (Fig. 6c). This passage was cut from the active flow at st. r2a6 (Fig. 6c, P7).

Figure 4. Collapse connects two simultaneously active and overlying passages, draining the upper passage. Photo by Peter and Ann Bosted.

5. Survey data

The main trunk´s length is 458 m with a total extent of 1,850 m. The main passage is mostly covered with breakdown blocks. It reaches a maximum width of 18 m and a maximum height of 11 m (Table 2). Although the average slope is 5.4° just a few lavafalls contribute to this gradient. In comparison, lavafalls represent 25 % of the vertical extent of the Huehue-Flow (Oberwinder 1996).

Table 2. Kahuenaha Nui survey data.

Total length	1,846 m
Total depth	-55 m
Horizontal length	1,812 m
Horizontal extension	560 m
Highest survey point	564 m a.s.l.
Lowest survey point	509 m a.s.l.
Longest way to origin	660 m
Area coverage	1.54 km^2
Average slope	5.7°
Average surface slope	4.0°
Sinousity	1.18 m
Maximum width	18.9 m
Maximum height	11 m
Striking direction	224° (NE–SW)
Main trunk length	458 m

6. Discussion

Erosion of underlying rock beds plays an important role during the formation of pyroducts (Greeley et al. 1998; Kempe, 1997, 2002, 2009, 2012). Two a'a flows are of significance for the genesis of Kahuenaha Nui. The first one (layers 1 ac and 2 ar, Fig. 1) is seated at the base of the pyroduct, the second transgressed during a later eruption (layers 10 ar, 11 ac, 12 ar). Initially a network of numerous small pyroducts established, basically following the surface morphology. These pyroducts interact while the phh flow branches at pre-existing tumuli. The parallel flows erode the underlying lava. Due to variations in flow velocity and resistance of the base layer one branch degrades the lower bed faster, draining other small pyroducts. These initial pyroducts can be seen at several places in Kahuenaha Nui. At the "Deutsches Eck" (Fig. 3, Fig. 6a, P3) numerous initial conduits can be observed, depicting a dense network of contemporaneous active pyroducts. The erosion rate increases as the main flow hits the underlying a'a-rubble, resulting in fast lateral and downward extension. The small number of lavafalls gives evidence for fast downward erosion. Rather than local erosion by lavafalls the base layer denudates. Fast lateral erosion produces quite a number of lavaballs, causing temporary blockage of cave passages. The created afflux boosts the establishment of parallel, simultaneously active pyroducts. If there is enough time for the cave roof to consolidate, the newly generated flow can superimpose the older flow, while both trunks are still active. We name this "superimposed trunk system". Fast downward erosion of basal a'a-layers facilitates this process. The emerging gasfilled space above the flowing lava effects thermal insulation, resulting in fast cooling of the cave roof. Skylights between the different levels allow interaction between the two flows. Up to now three modes of lava tunnel formation have been described (Kempe 2010). Figure 5 shows the already known inflation mode (1a) and two modes of crusting over of channels (1c and 1d). Our investigations led to the conclusion that Kahuenaha Nui seems to represent a fourth type of genesis: Confluence of lavas from smaller conduits of superimposed sheets of pahoehoe (1d). While a first sheet of phh establishes a pyroduct it is overridden and buried by a second sheet, likewise establishing a pyroduct. This process happens several times. At the same time the lowest phh-flow erodes down. The tubes merge and drain into the main passage until the lowest tube contains all the flow. Lateral and downward erosion creates a large tunnel. In addition upward erosion enlarges the passage.

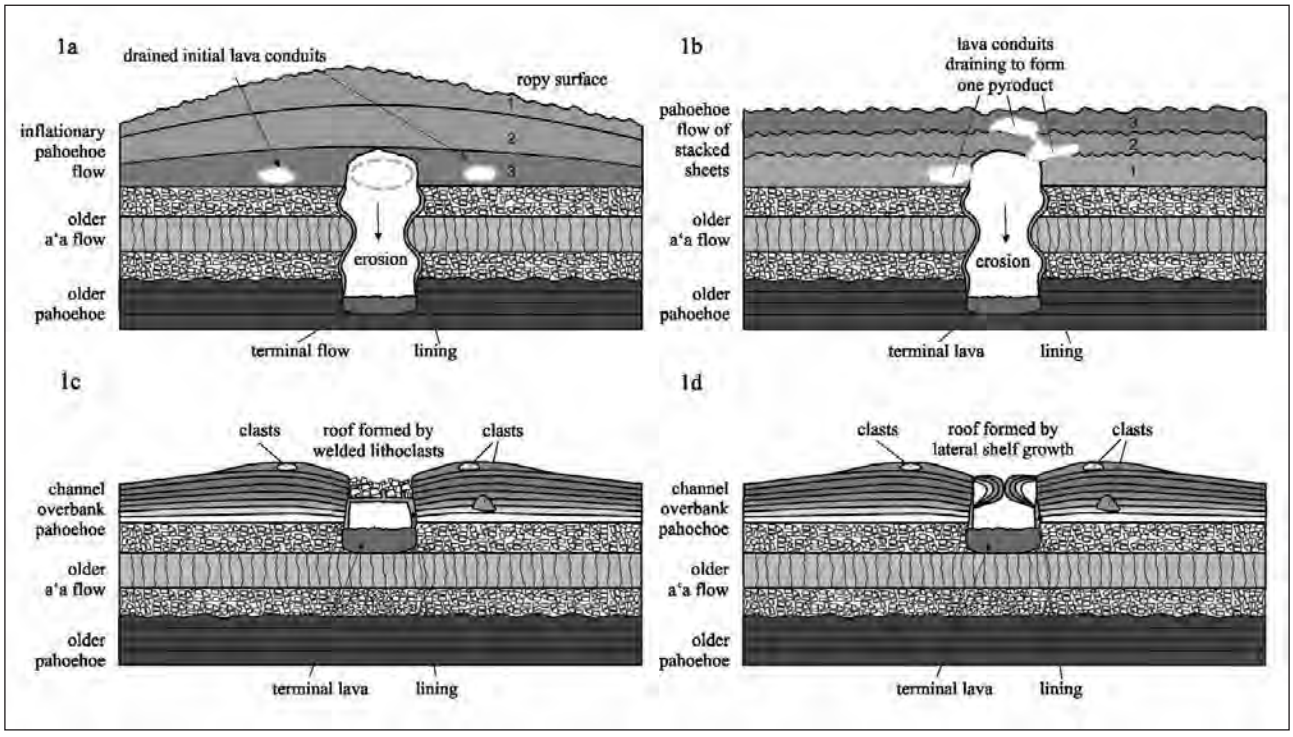

Figure 5. Three modes of lava tunnel formation are already known (1a, 1c, 1d). 1a shows the inflationary type. 1c and 1d represent two modes of crusting over of channels, Kahuenaha Nui seems to represent a fourth type of genesis (1b).

7. Conclusions

Kahuenaha Nui is a new cave type that so far was not documented in detail. The cave involved four lava units from different eruptions. It eroded into an underlying a'a, visible nowhere else in the vicinity. The lava that formed the cave was carried initially in several superimposed small conduits in a 3 to 4 m thick stack of surface pahoehoe sheets. After the cave formation, the phh stack was transgressed by a 3.5 m thick a'a flow and a 2 m thick pahoehoe flow forming the flows visible at the surface. The confluence of lava from different conduits involves consequent downcutting into the lower bed below the phh stack. This type of conduit formation is most likely favoured where there are easily erodible layers below the active flow. However, once the flow is concentrated in this new conduit, it may also erode even through a'a core layers.

Acknowledgments

The authors wish to thank the members of the Hawaiian Volcano Observatory for their support. Ann Bosted, Ron Carlson, Don Coons, Harry Shick, Emily Davis, Bob South,

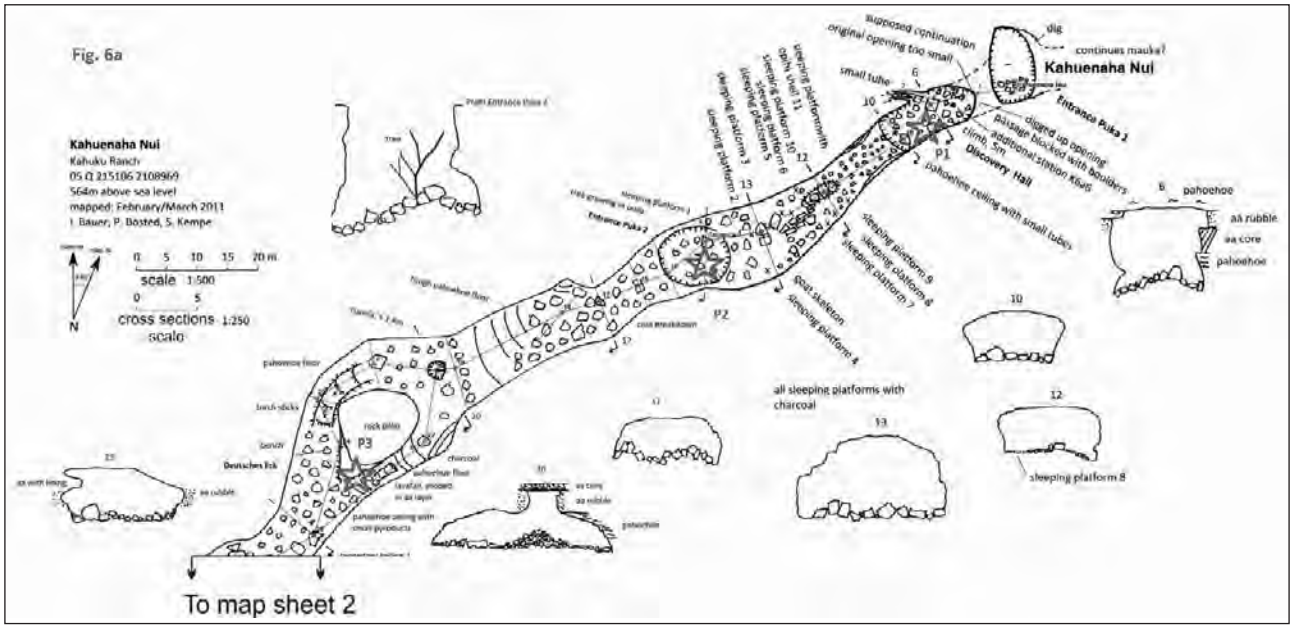

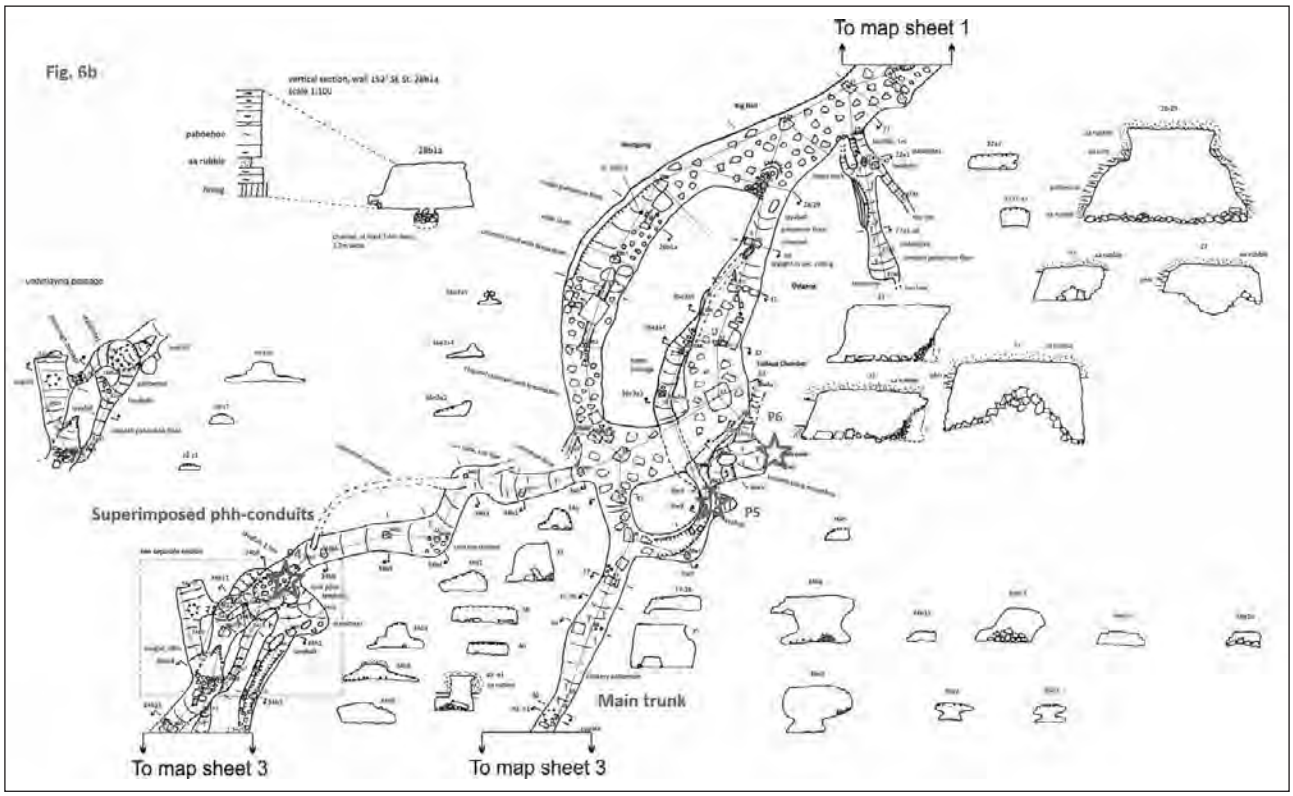

Mike Warner, Susan and Nick White, and John Wilson assisted during field work. XRD-analysis and polarizing microscopy was conducted at the Institute of Applied Geosciences, Technical University Darmstadt.

References

Bauer I, 2011. Geologie, Petrographie und Pyroductgenese des Kahuku-Ranch-Gebiets, Big Island, Hawaii. Dipl. Thesis, Institute of Applied Geosciences, Technical University Darmstadt, Germany (unpubl.).

Greeley R, Fagents SA, Harris RS, Kadel SD, Williams DA, 1998. Erosion by flowing lava, field evidence. J. Geophys. Res., 103 (B11), 27, 325–327, 345.

Kempe S, 1997. Lavafalls: a major factor for the enlargement of lava tubes of the Ai-la'au Shield phase, Kilauea, Hawaii. Proc. 12th Int. Congr. of Speleology, La Chaux-de-Fonds, Switzerland, 1, 445–448.

Kempe S, 2002. Lavaröhren (Pyroducts) auf Hawaii und ihre Genese. In: Angewandte Geowissenschaften in Darmstadt, Rosendahl W, Hoppe A (Eds.), Schriftenreihe der Deutschen Geologischen Gesellschaft, 15, 109–127.

Kempe S, 2009. Principles of pyroduct (lava tunnel) formation. Proc. 15th Int. Congr. of Speleology, Kerrville, Texas, July 19–26, 2009, 669–674.

Kempe S, Bauer I, Bosted P, Coons D, Elhardt R, 2010. Inflationary versus crusted-over roofs of pyroducts (lava tunnels). Proc. 14th. Int. Symp. Volcanospeleol., Undara, Australia, 2010, 93–101.

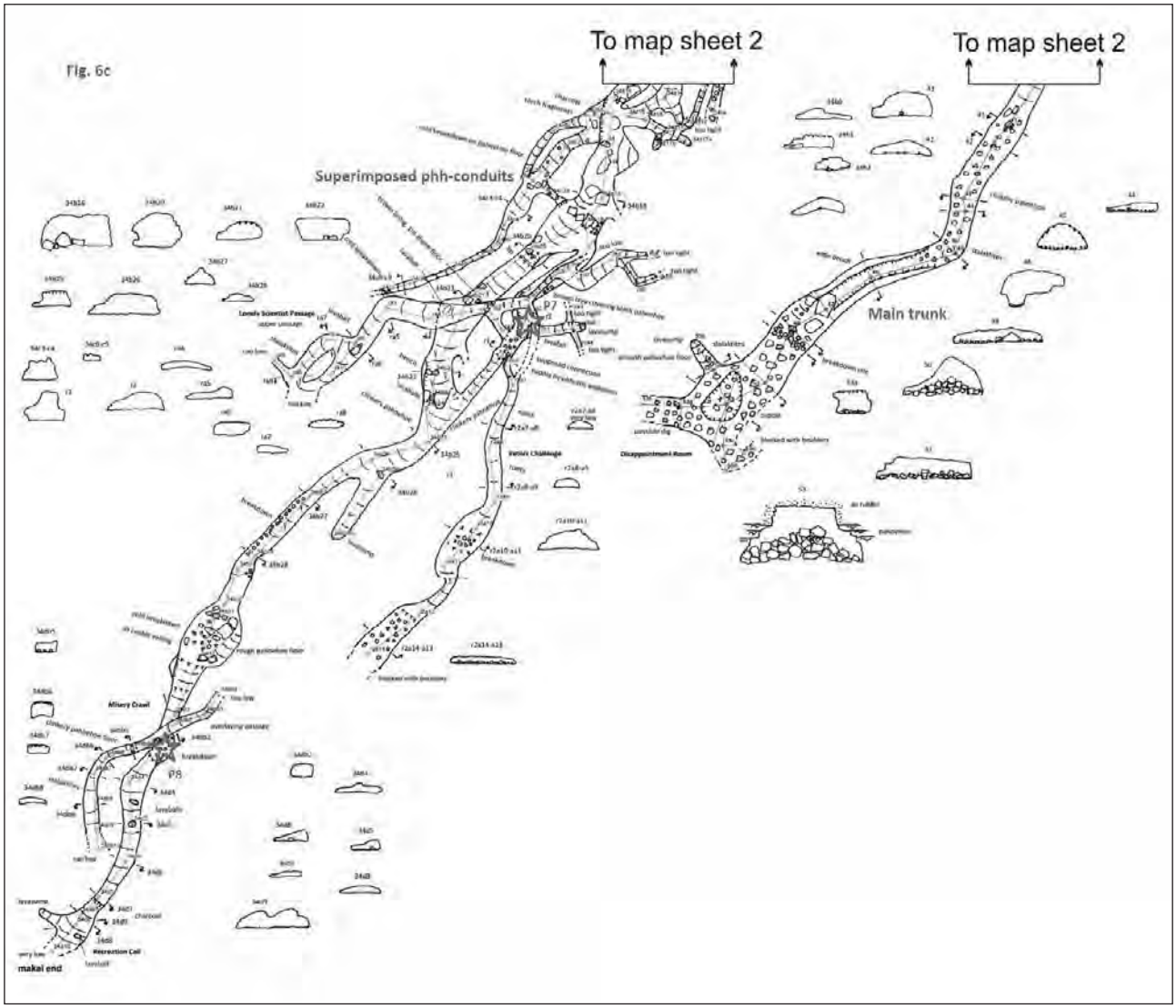

Figure 6 a, b, c. Kahuenaha Nui cave map, split in three parts.

Kempe S, 2012. Volcanic rock caves. In: White WB, Culver DC (Eds.), Enzyclopedia of Caves, 2nd ed., Academic Press/ Elsevier, Amsterdam, 865–873.

Oberwinder M, 1996. Genese und interne Struktur des oberen Teils des Lavastroms von 1801 (Huehue Flow, Hualalai, Hawaii). Dipl.-Thesis Institute of Applied Geosciences, Technical University Darmstadt, Germany (unpubl.).

GENETIC TYPES OF NON-SOLUTION CAVES

Pavel Bella[1,2], Ludovít Gaál[1]
[1]State Nature Conservancy of the Slovak Republic, Slovak Caves Administration, Hodžova 11, 031 01 Liptovský Mikuláš, Slovakia, bella@ssj.sk, gaal@ssj.sk
[2]Department of Geography, Pedagogical Faculty, Catholic University, Hrabovská cesta 1, 034 01 Ružomberok, Slovakia, Pavel.Bella@ku.sk

Many caves were originated by various mechanical processes in both non-soluble and soluble rocks. The genetic classification of the specific group of caves presents one of important and actual speleogenetic problematics. The paper gives a basic categorisation of non-solution caves according to their origin. The group of non-solution caves originated by endogenous processes consists of magmatic, volcanic and tectogene caves. Fluvial erosion caves, caves formed by moving glacier and deposition of moraine sediments, suffusion caves, constructional travertine caves, mudlow caves, wave cut caves, caves originated by deformation of rocks caused by their volumetric changes, caves originated by gravity disintegration of rocks, mechanically weathered caves, eolian caves, caves of biogenic origin, pyrogenic caves, and caves formed as a result of the technogenic activatisation of natural processes are distinguished within the group of non-solution caves originated by exogenous processes.

1. Introduction

During last years much knowledge was obtained about the caves originated by non-solution processes. But their genetic classification is not completed until now. Only partial classifications of some genetic groups of non karstic caves were worked up, mostly without the unified terminology (Halliday 1960, 2004; Wood 1974; Grimes 1975; Vítek 1983; Andrejčuk 1985; Sjöberg 1986; Striebel 1999; Honda 1999; Bella and Gaál 2007, and others). Based on clearly defined geological and geomorphologic criteria (action of endogenous or exogenous processes, type of geomorphic process and mechanism of cave origin) the basic categorisation of non-solution caves is presented in the paper (more detailly elaborated by Bella 2012). We do not deal with caves originated by solution in hardly soluble rocks, conglomerates or other lithified sedimentary rocks and by melting of ice.

2. Caves originated by endogenous processes

This group of caves originated by natural processes induced by the inner dynamics of the Earth, i.e. magmatism, volcanism, earthquake or tectonic processes.

2.1. Magmatic caves

They are smaller **geode-like magmatic cavities** created by intrusive magmatism under the Earth´s surface, often without natural entrance (cavities uncovered in the mines or quarries). They often contain many crystals of various minerals formed by slowly cooled solution in magma bubbles (Dubljanskij and Andrejčuk 1989).

2.2. Volcanic caves

This wide group includes the caves created by volcanic explosion, lava effusion and various volcanic – rheogenetic, pneumatogenetic and pyrogenic processes.

Roofed lava channels – subcrustal lava caves originated by gradual growing of hardening lava from both sides of roof. The roofing happened also by connecting of flowed blocks of hardened lava and by lateral levees of inunded lava (Greeley and Hyde 1972; Atkinson et al. 1975; Calvari and Pinkerton 1999; Grimes 2008; Harris et al. 2009).

Lava tube caves – tubes or tunnels formed by outflowing of hot lava from the bellow solidified roof crust. If the liquid lava has been locked inside the tunnel, in these places large rooms originated. Straight tunnel has symmetric profile while asymmetric profile is resulted by the change of a direction of flowing lava (Greeley 1971; Wood 1974; Calvari and Pinkerton 1999; Halliday 2004b). Also lateral narrow subcrustal simple or branched tubes (lava overflow caves) can be formed on the side of main lava flow (Grimes 2008). Kempe (2009) distinguishes single-trunked, double- or multi-trunked, and superimposed-trunked systems of lava flows.

Drainage tubes of active rift zones – underground spaces looking like lava tube caves can occur within large dykes intruded along fractures, eruptive fissures or rift zones lava. The fissures are remodelled by intruded lava and the spaces have an oval shape (Harter 1976; Favre 1993; Okubo and Martel 1998; Halliday 2008).

Lava rise caves – some places of horizontal lava surface raised by pressure of accumulated hot lava about 0.5–1 m thereupon the low-lying underground spaces are created (Halliday 1998; Gadányi 2008).

Lava ridge caves – smaller triangle-shaped caves occur in the lateral part of lava flows in consequence of decreasing in central zone of lava surface, also in the toe part of lava flow by pressure of flowing lava (Chitwood 1989; Gadányi 2008).

Lava tumulus caves – occur under elliptic elevation of lava surface (tumulus) in consequence of decreasing of solidified lava. They can reach about 5 m of height (Ollier 1962; Chitwood 1989; Halliday 1998; Gadányi 2008).

Boulder caves in lava flows – generally occur in the frontal part of aa lava between larger blocks of solidified lava surface.

Volcanic crater shafts – vertical shafts originated by decreasing lava into the diatremas and necks of crater structure. They have floater or bell-like shape (Stefánson 1992; Favre 1993).

Volcanic exhalation caves – smaller caves created by exhalation or explosion of ascending volcanic gases in scoria cone. In an ideal case the chimney, which flowed into small horizontal cave, is preserved (Eszterhás 2004; Gaál and Balciar 2008).

Chimneys of spatter cones and hornitos – open vertical volcanic conduits formed by blowing of very liquid lava from primary fractures which creates spatter cones or hornitos (Ollier 1964; Licitra 1993).

Lava blister caves – lava bubbles of diameter about 1 m, rarely to 5 m originated by accumulation and pneumatic expansion of gas in lava (Ollier 1962).

Polygenetic spatter cone caves in carbonatite volcanoes – a rare case of cave origin in spatter cones in the summit crater of Ol Doinyo Lengai in Tanzania, cavities under spatter cones originated by thermal erosion, and meteoric water and condensation corrosion of natrocarbonatite lava (McFarlane et al. 2004).

Volcanic pyrogenetic tree moulds – formed by burning-out of trees in glowing lava (Finch 1931; Balázs 1974; Honda 1999; Gaál 2003a; Bella and Gaál 2007). According to the position of tree trunks they can be vertical, inclined or horizontal. Tree moulds are known as simple type, compound type with several trees and tree-break type. From a morphological point of view the mushroom type, plate type, bottle type, "narusawa" type (cedar-like cave after burning of gase) and "hudoiwa" type (with accumulated lava in a frontal part of tree) are distinguished (Tachihara et al. 2002).

Volcanic eruptive fissure caves – along the fissures originated by movement or quake eventually by pneumatic pressure during volcanic eruptions. Generally they have fissure character sporadically with marks of flowing lava (Ogawa 1986; Leotta and Liuzzo 1998; Halliday 2004b).

2.3. Tectogene caves

The group includes the caves originated in consequence of endogenous tectonic movement and earthquake. They occur mostly along the fissure, rarely on the fold structure.

Fault caves – along the disjunctive fault and fissures formed by extension tectonic movement. They have linear character with narrow and long passages (Kiernan 1982; Dubljanskij and Andrejčuk 1989).

Rift caves – fault caves in the margin part of the rift zone and trench fault along the mobile zones of the Earth (Davis 1998).

Fold caves – rare occurring caves on the flexion of folds (Kiernan 1982).

Collapsed pit crater caves – vertical circular or elliptic shafts along the active rift zone in the crossing place with structural or stratigraphic discontinuity. They occur mostly in areas of large shield volcanoes (Halliday 1998; Okubo and Martel 1998).

Seizmotectonic fracture caves – caves along the narrow fissures created in consequence of decompression seismic quake after melting of glacier and isostatic uplift in Scandinavia (Sjöberg 1986).

Seismotectonic boulder caves – underground spaces between rock blocks originated by disintegration of granite massive disturbed by seismic quake. The seismotectonic boulder caves can also be originated by earthquake-induced rockfall (Sjöberg 1986, 1987).

3. Caves originated by exogenous processes

This group involves the caves, which originated by fluvial erosion, glacier moving, suffosion, marine abrasion, gravity disintegration (sliding and falling of rock blocks), mechanical weathering (fissure and boulder exfoliation), frost weathering, eolian processes (corrosion and deflation), biogenic way, pyrogenic processes and the caves of technogenic activatisation of natural processes.

3.1. Fluvial erosion caves

The genetic group of caves originated by mechanical erosion of water flow that means abrading of rock walls and scouring of river channels.

River bank erosion caves – formed in the rock banks of river channel by lateral erosion mainly in meanders along horizontal bedding plane (Trimmel 1968; Striebel 1999; Day 2001).

Waterfall erosion caves – formed by backward erosion of falling water under occasional or constant waterfall (Striebel 1999; Day 2001).

Fluvial channel erosion caves – occur at the contact of rocks of different permeability and hardness or along fractures, the water course become engrosses in the floor (Kempe and Werner 2003).

3.2. Caves formed by moving glacier and deposition of moraine sediments

This group includes the caves formed by mechanical deformation of glacier and underlying rocks, also subglacial caves formed as glacier slides over abrupt changes in the bedrock surface, and glacial boulder caves.

Glacier crevasse caves – formed by extension strain on the elevation of bedrock (V shape crevasse) or by compression in depression (A shape crevasse). The other diagonal crevasses can be formed in consequence of unequal moving of glacier in its central and side parts (White 1988). Crevasses formed by rotation of ice masses in the steep upper part of glacial cirques are named "bergschrunds" (Battle and Lewis 1951).

Crevasse caves under glacier in bedrock deformated and fractured by pressure of moving glacier, so-called "glaciotectonic" caves (Schroeder et al. 1986; Sjöberg 1986, 1989; Schroeder 2004).

Subglacial cavities formed as glacier slides over abrupt changes in the bedrock surface, the ice separated from bedrock in the lee of a downward step (Pulina et al. 2003; Fountain 2005).

Glacial boulder caves – irregular, chaotic cavities between large blocks of moraine or erratic boulders (Kiernan 1982; Sjöberg 1986).

3.3. Suffosion caves

Suffosion or piping caves formed by washing out of soft clastic material by infiltration or flowing underground water. They originated mainly in less consistent clastic rocks as clay, loess, silt, laterite, weathered sandstone and volcaniclastic rocks.

Suffosion tunnel caves – originated by suffosion and erosion generally on the contact of loose rocks and impermeable background (Clausen 1970; Cílek 1997; Bella et al. 2005; Grimes and Spate 2008).

Suffosion collapse shafts – formed by decrease and subsequent collapse of hanging rock upper suffosion tunnels (Clausen 1970; Urban 2004).

3.4. Synsedimentary travertine caves

Constructional caves originated by precipitation of travertine from solutions.

Travertine crater caves – spring travertine throats inside travertine craters (Bella 2005; Halliday 2011).

Travertine fissure ridge caves – rare occurring longitudinal narrow cavities along an effluence fissure (Pisarowicz 2003; Halliday 2011).

Caves of constructive travertine waterfalls – mostly longitudinal cavities along the foot of constructive travertine waterfalls (Trimmel 1968; Bella 2005).

3.5. Mudflow caves

They present sporadic caves formed by outflowing of liquid mud from under and upper dried indurate crust on slopes of mud volcanoes (Kalenda 2010).

3.6. Wave-cut caves

They are formed by mechanical wave abrasion at the foot of costal cliffs of sea or large lake formed by insoluble rocks (Moore 1954; Bunnell 1988).

3.7. Caves originated by deformation of rocks caused by their volumetric changes

These are rarely occurring caves formed by enlarging of volume of evaporite caused by water absorbing. In consequence of hydratation of anhydrite to gypsum the rock can expand till 50–60 % whereby some hydratation raised subcrustal cavities is formed.

Hydratation raised caves – upward raised subcrustal cavities between hydrated gypsum upper anhydrite or subjacent beds. Some narrow cavities – gypsum tumuli – are also created by rising caused by precipitation or recrystallization of gypsum (Gorbunova 1978; Reinboth 1997; Callafora and Pulido-Bosch 1999).

Subcrustal cavities of "tepee" structure – upward cambered margin of expanded megapolygons of agglutinated crust of carbonate-evaporite coastal sediments in periodic inundated and shrinkages basins (Kendall and Warren 1987).

Salt diapire fissure caves – occur in the raising salt stump or diapire of hydrated anhydrite (Vendeville and Jackson 1992).

3.8. Caves originated by gravity disintegration of rocks

Such caves occur in areas with vertically dissected relief and suitable geological conditions (rigid rocks with underlying soft or plastic beds).

Crevice caves – formed by gravity movement of marginal rigid blocks upper underlying plastic beds on the slopes (Campbell 1968; Vítek 1983; Self 1990; Turchinov 1990; Filippov 1997; Margielewski and Urban 2003; Halliday 2004 and others). Gaál (2003b) distinguishes deflection crevice caves (formed in initial or opening phase by deflection of marginal blocks), inclination crevice caves (formed by backward inclination of blocks in relation to their rotation), decrease crevice caves (horizontal or subhorizontal caves formed by decreasing of blocks in the initial phase), displacement crevice caves (caves in "wide crevice" formed by gravity transfer of block in the sliding phase, mostly combined crevice-boulder caves are formed). The crevice caves are also formed on the coastal cliffs of a sea or lake and on the gravity disintegrated steep coast of carbonate platforms. The bank-margin fracture type of "blue holes" in Bahamas probably was formed during glacioeustatic decrease of sea level (Smart et al. 1988; Mylroie 2004).

Falling-out caves – small caves formed after gravity falling-out of released blocks. Disintegration and releasing can be supported by termomechanical weathering (Striebel 1999).

Rockfall / rockslide boulder caves – chaotic cavities formed by deposition of disintegrated large angular boulders from falling or sliding rock blocks at the base of cliffs on slopes, in the bottom of valleys or at the foot of coastal cliffs. Rockfall boulder caves are originated by sudden falling of rocks, rockslide boulder caves by sliding and subsequent disintregration of rock blocks (Kiernan 1982; Vítek 1983; Striebel 1999; Bella and Gaál 2010 and others). Outside arid regions, in-valley boulder caves (so-called "purgatory caves" in California and the northeastern United States) are commonly featured by mechanical erosion of underground streams (Finlayson 1981; Halliday 2004a).

3.9. Caves originated by mechanical weathering

This group involves caves originated by mechanical weathering and associated slope processes: caves in rock structures disintegrated by macroexfoliation, frost weathering caves, and caves formed by insolation and salt weathering.

Exfoliation caves – formed in consequence of segregation of rock squama mostly parallel with rock surface. Therefore the exfoliation cracks are often curved like an onion. Exfoliation caves are formed along the fissures (fissure exfoliation cave), by falling-out of block along the fissure (fissure-falling-out exfoliation cave), among boulders formed by exfoliation disintegration along the bedding or cubical jointing "in situ" (boulder exfoliation cave), wide and narrow simple exfoliation

underground spaces (woolsack cave), weathered exfoliation caves and small deltoid caves of A-tents type (Ollier 1965; Jennings 1978; Striebel 1999; Twidale 2009).

Frost weathering caves – generally shelter type caves originated by break-up of host rock in consequence of frost (Schroeder 1979; Mitter 1983; Cílek 1996; Striebel 1999). Belong them also weathered boulder caves in glacial and periglacial regions (Striebel 1999).

Tree moulds formed by mechanical disintegration of silicified or carbonified trees covered by volcaniclastic beds or lahars (Gaál 2003a; Bella and Gaál 2007).

Tafoni caves – originated by insolation weathering along the contact plane of primary cubical jointing of granite and similar rocks. The favorable conditions of its origin are in repeated moistly and dry climatic areas (Martini 1978; Twidale 1982; Vidal Romani 2007).

Salt weathering caves – small caves originated by change of volume in consequence of crystallization of salt in poruses and cracks. They are as foot-cliffs shelter caves or caves formed along lithologically or tectonically weakened parts of rocks (Gavrilović 1981; Cílek 1998).

3.10. Eolian caves

This group involves smaller caves originated by wind corrasion and deflation mainly in soft and loose rocks located mainly in arid and semiarid regions.

Corrasion caves – simple elliptic cavities originated by mechanical abrasion by wind (White 1988; Dubljanskij and Andrejčuk 1989).

Deflation caves – short cavities generally with two entrances along which wind insufflate the soft particles of weathered rock. They occur most frequently in mountain ridges and elevation in open terrains (Dubljanskij and Andrejčuk 1989).

3.11. Caves of biogenic origin

Reef caves – small irregular constructional cavities in barrier reefs and atolls formed by growing of corals under sea level (Trimmel 1968).

Caves excavated by animals – small cavities excavated mainly as hiding-place (salt ingestion caves). These caves occur in rock with salt because salt is searched by elephants, buffalos, antelopes and other animals (Carey and Middleton 1973; Lundquist and Varnedoe 2006).

Biogenic tree moulds – formed by biogenic disintegration of necrotic tree trunks by funguses and microorganisms. They are known mainly in travertine (Bella and Gaál 2007; Gradziński 2008).

3.12. Pyrogenic caves of self-kindled fires

These caves represent cavities after burned out of coal layers or other burnable raw material (Maximovich 1969; Dubljanskij and Andrejčuk 1989). In volcanic rocks tree moulds formed by burning was described as volcanic pyrogenic tree moulds.

3.13. Caves of technogenic activatisation of natural processes

This group involves caves originated by natural processes but in consequence of human activity, mostly mining, exploitation of raw material or violation of slope stability.

Consequent crevice and breakdown caves – formed by gravity block movement anthropogenically induced by rock instability (Eszterhás 1993).

Technogenic pyrogenic caves – created by underground burning of coal in order to obtain of gas for electric energy (Andrejčuk 1985; Dubljanskij and Andrejčuk 1989).

4. Conclusion

Totally 56 types of non-solution caves are distinguished and briefly characterised in this paper (21 types are related to endogenous processes, 35 types to exogenous processes). Various genetic types of non-solution caves point to a high diversity of their formation in varied environments with different lithological, structural-tectonic, geomorphologic and climatic conditions. Non-solution caves originated mostly in magmatic, volcanic and volcaniclastic rocks, crystalline shales and clastic sedimentary rocks, constructional caves also in travertine and coral limestone. Some specific types of non-solution caves are known in gypsum and salt. A higher variety of cave formation by exogenous processes is linked with a higher heterogenity of the Earth-surface dynamics. Comparing with solution caves, an occurrence of non-solution caves is lower but their genetic diversity is higher. Several non-solution caves are important sites of nature and human history. Therefore they are protected as natural monuments or are included within protected areas.

References

Andrejčuk VN, 1985. Klassifikacija podzemnych polostej. Izvestija VGO, 117, 4, 341–348 (in Russian).

Atkinson A, Griffin TJ, Stephenson PJ, 1975. A major lava tube system from Undara Volcano, North Queensland. Bulletin of Volcanology, 39(2), 266–293.

Balázs D, 1974. Lávaüregek keletkezése, típusai és formakincse. Földrajzi Közlöny, 2, 135–148.

Battle WRB, Lewis WV, 1951. Temperature observation in bergschrunds and their relationship to cirque erosion. Journal of Geology, 59(6), 537–545.

Bella P, 2005. Syngenetické travertínové jaskyne na Slovensku. Geomorphologia Slovaca, 5(2), 23–29 (in Slovak).

Bella P, 2012. Genetické typy jaskýň. Verbum, Ružomberok (in Slovak).

Bella P, Gaál Ľ, 2007. Tree mould caves within the framework of cave genetic classification. Nature Conservation, 63, 7–11.

Bella P, Gaál Ľ, 2010. Medzibalvanové jaskyne – terminológia a genetické typy. Aragonit, 15(1), 3–10 (in Slovak).

Bella P, Gaál Ľ, Inokura Y, 2005. Sufózne jaskyne vo vulkanoklastických horninách v doline Nagatani pri Kagošime. Slovenský kras, 43, 67–80 (in Slovak).

Bunnell D, 1988. Sea caves of Santa Cruz Island, Santa Barbara, California. McNally and Loftin Publishers.

Calaforra JM, Pulido-Bosch A, 1999. Genesis and evolution of gypsum tumuli. Earth Surface Processes and Landforns, 24(10), 919–930.

Calvari S, Pinkerton H, 1999. Lava tube morphology on Etna and evidence for lava emplacement mechanism. Journal of Volcanology and Geothermal Research, 90(3–4), 263–280.

Campbell NP, 1968. The Role of Gravity Sliding in the Development of Some Montana Caves. Bulletin of the National Speleological Society, 30(2), 25–29.

Carey SD, Middleton AL, 1973. The Rock House – An Unusual Mississippi Shelter Cave. NSS News, 31(11), 198.

Cílek V, 1996. Vznik previsů a jeskynních výklenků v bralné časti Velké Fatry. Speleofórum, 15, 34–36 (in Slovak).

Cílek V, 1997. Sufozní podzemní systém ve sprašové rokli v Zeměchách u Kralup. Speleo, 25, 19–23 (in Czech).

Cílek V, 1998. Fyzikálne-chemické procesy vzniku pískovcového pseudokrasu. In: V Cílek, J Kopecký (Eds.) Pískovcový fenomén: klíma, život a reliéf. Knihovna ČSS, 32, Praha, 134–153 (in Czech).

Clausen EN, 1970. Badland caves of Wyoming. Bulletin of the National Speleological Society, 32 (3), 59–69.

Davis RA, 1998. Tectonic caves of Solai in the Kenyan Rift Valley. International Journal of Speleology 27B(1–4), 69–74.

Day MJ, 2001. Sandstone caves in Wisconsin. Proceedings of the 13th International Congress of Speleology, 1, Brasilia, 88–92.

Dubljanskij VN, Andrejčuk V N, 1989. Speleologija (terminologia, svjazi s drugimi naukami, klassifikacija polostej). Uraľskoe otdelenie AN SSSR, Kungur (in Russian).

Eszterhás I, 1993. Konsequenzhöhlen. Jahresbericht der Höhlenforschergruppe Rhein-Main, Frankfurt a. M., 43–44 (in German).

Eszterhás I, 2004. Durch exhalation entstandene höhlen im Karpatenbecken. In: L Gaál (Ed.) Proceedings of the 8th International Symposium on Pseudokarst, Teplý Vrch, 7–13.

Favre G, 1993. Some observations on pits craters and relations with lava tubes. In: WR Halliday (Ed.) Proceeding of the 3rd International Symposium on Vulcanospeleology (Bend, Oregon), Washington, 37–41.

Filippov AG, 1997. Gravity caves of the Siberian Platform. In: PY Jeannin (Ed.) Proceedings of the 12th International Congress of Speleology, 1, La Chaux-de-Fonds, 465–468.

Finch RH, 1931. Lava tree casts and tree molds. The Volcano Letter (Hawaiian Volcano Observatory), 316, 1–3.

Finlayson B, 1981. Underground streams on acid igneous rocks in Victoria. Helictite, 19(1), 5–14.

Fountain AG, 2005. Glacier Caves. In: DC Culvier, WB White (Eds.) Encyclopedia of caves. Elsevier Academic Press, 271–275.

Gaál Ľ, 2003a. Tree mould caves in Slovakia. International Journal of Speleology, 32, 1–4, 107–111.

Gaál Ľ, 2003b. Genetické typy rozsadlinových jaskýň na Slovensku. Slovenský kras, 41, 29–45 (in Slovak).

Gaál Ľ, Balciar I, 2008. Caves in the youngest volcanic structure in Slovakia. Proceedings of the 10th International Symposium on Pseudokarst, Gorizia, 165–167.

Gadányi P, 2008. Caves under uplifted surface crusts of basalt lava flows. Proceedings of the 10th International Symposium on Pseudokarst, Gorizia, 119–126.

Gavrilović D, 1981. Genetic types of caves in Sahara. Evropejska regionalna konferencia po speleologija, Sbornik ot materiali, 2, Sofia, 137–139.

Gorbunova KA, 1978. Peščery gidratacii. Peščery, 61–63 (in Russian).

Gradziński M, 2008. Origin of a unique tree-mould type cave in travertine based on examples from the village Lúčky (Liptov, Slovakia). Slovenský kras, 46(2), 325–331.

Greeley R, 1971. Observations of actively forming lava tubes and associated structures, Hawaii. Modern Geology, 2, 207–223.

Greeley R, Hyde JH, 1972. Lava Tubes of the Cave Basalt, Mount St. Helens, Washington. Geological Society of America Bulletin, 83(8), 2397–2418.

Grimes KG, 1975. Pseudokarst: Definition and types. Proceedings of the 10th Biennial Conference of the Australian Speleological Federation (Brisbane, 27–29 December 1974), Sydney, 6–10.

Grimes KG, 2008. Subcrustal Drainage Lava Caves; examples from Victoria, Australia. In: R Espinasa-Pereña, J Pint (Eds.) Proceedings of the X, XI, and XII International Symposia on Vulcanospeleology. AMCS Bulletin, 19, 35–44.

Grimes K, Spate A, 2008. Laterite Karst. Australasian Cave and Karst Management Association Journal, 73, 49–52.

Halliday WR, 1960. Pseudokarst in The United States. Bulletin of the National Speleological Society, 22(2), 109–113.

Halliday WR, 1998. Hollow volcanic tumulus caves of Kilauea Caldera, Hawai County, Hawaii. International Journal of Speleology, 27B(1–4), 95–105.

Halliday WR, 2004a. Talus caves. In: J Gunn (Ed.) Encyclopedia of Caves and Karst Sciences. Fitzroy Dearbon, New York – London, 723–724.

Halliday WR, 2004b. Volcanic caves. In: J Gunn (Ed.) Encyclopedia of Caves and Karst Sciences. Fitzroy Dearbon, New York – London, 760–764.

Halliday WR, 2008. What Is a Lava Tubes? In: R Espinasa-Pereña, J Pint (Eds.) Proceedings of the X, XI, and XII International Symposia on Vulcanospeleology. AMCS Bulletin, 19, 48–56.

Halliday WR, 2011. Karst and pseudokarst at Mammoth Hot Springs, Yellowstone National Park, USA. International Union of Speleology, Pseudokarst Commission Newsletter, 22, 10–19.

Harris AL, Massimiliano F, Francesco M, Hamilton CW, 2009. Construction dynamics of a lava channel. Bulletin of Volcanology, 71, 4, 459–474.

Harter JW, 1976. Morphologic Classification of Lava Tubes. In: WR Halliday (Ed.) Proceedings of the International Symposium on Vulcanospeleology (White Salmon, Washigton). NSS, Seattle, 74–85.

Honda T, 1999. Classification of lava tree molds with/without remelted inner surface according to its formation process. In: N Barone, G Licitra (Eds.) Proceedings of the IXth International Symposium on Vulcanospeleology, Catania, Italy, 123–124.

Chitwood LA, 1989. Inflated lava. Desert Ramblings, The Newsletter of the Oregon Natural Desert Association, 2(1), 1–4.

Jennings JN, 1978. Genetic variety in a-tents and related features. Australian Geographer, 14(1), 34–38.

Kalenda P, 2010. Ázerbajdžán – země bahenních sopek a také bahenních jeskyní. Speleo, 54, 16–19 (in Slovak).

Kempe S, 2009. Principles of pyroduct (lava tunnel) formation. In: WB White (Ed.) Proceedings of the 15th International Congress of Speleology, 2, Kerrville, Texas, USA, 668–674.

Kempe S, Werner MS, 2003. The Kuka´iau Cave, Mauna Kea, Hawaii, created by water erosion, a new Hawaiian cave type. Journal of Cave and Karst Studies, 65(1), 53–67.

Kendall CGSt, Warren J, 1987. A review of the origin and setting of tepees and their associated fabrics. Sedimentology, 34(6), 1007–1027.

Kiernan K, 1982. Mechanically shaped pseudokarst: talus, joint and fault caves and their potential in Tasmania. Journal of Sydney Speleological Society, 26(3), 41–51.

Leotta A, Liuzzoi M, 1998. The 1981 eruptive fissure on Mt. Etna: considerations on its exploration and genesis. International Journal of Speleology 27B(1–4), 147–153.

Licitra GM, 1993. Essay on genetic classification of volcanic caves. In: WR Halliday (Ed.) Proceedings of the 3th International Symposium on Vulcanospeleology (Bend, Oregon), Vancouver, Washington, 118–120.

Lundquist ChA, Varnedoe WW, 2006. Salt ingestion caves. International Journal of Speleology, 35(1), 13–18.

Margielewski W, Urban J, 2003. Crevice-type caves as initial forms of rock landslide development in the Flysch Carpathians. Geomorphology, 54(3–4), 325–338.

Martini IP, 1978. Tafoni weathering, with examples from Tuscany, Italy. Zeitschrift fűr Geomorphologie, 22(1), 44–67.

Maximovich GA, 1969. Peščery podzemnych požarov. Peščery 7(8), 87–88 (in Russian).

McFarlane DA, Lundberg J, Belton F, 2004. An Unusual Lava Cave From Ol Doinyo Lengai, Tanzania. Journal of Cave and Karst Studies, 66(3), 98–101.

Mitter P, 1983. Frost Features in the Karst Region of the West Carpathian Mountains. In: TL Pewe, J Brown (Eds.) Permafrost: Proceedings of the Fourth International Conference, Fairbanks July 17–22, 1983. Washington DC, 861–865.

Moore DG, 1954. Origin and development of sea caves. Bulletin of the National Speleological Society, 16, 71–76.

Mylroie JE, 2004. Blue holes of the Bahamas. In: J Gunn (Ed.) Encyclopedia of Caves and Karst Sciences. Fitzroy Dearbon, New York – London, 155–156.

Ogawa T, 1986. The formation of lava caves. Communications, 9th International Congress of Speleology, 2, Barcelona, 47–51.

Okubo C, Martel S, 1998. Pit crater formation on Kilauea volcano, Hawaii. Journal of Volcanology and Geothermal Research, 86 (1–4), 1–18.

Ollier CD, 1962. Tumuli and Lava Blisters of Victoria, Australia. Nature, 202, 1284–1286.

Ollier CD, 1964. Caves and related features at Mount Eccles. Victorian Naturalist, 81, 64–71.

Ollier CD, 1965. Some features of granite weathering in Australia. Zeitschrift für Geomorphologie, NF, 9, 285–304.

Pisarowicz J, 2003. Beneath Yellowstone. Rocky Mountain Caving, 20(4), 12–18.

Pulina M, Řehák J, Schroeder J. 2003. Les cavités glaciaires sous le regard spéléologique. Karstologia, 42(2), 23–36.

Reinboth F, 1997. Die Zwerglöcher bei Walkenried am Südharz-Bemerkumgen zur Frage der Quellungshöhlen. Die Höhle, 48(1), 1–13 (in German).

Self C, 1990. A gravity sliding cave in Western England. In: J Wagner (Ed.) IV. symposium o pseudokrasu, sborník referátů. Knihovna ČSS, 23, Praha, 139–145.

Schroeder J, 1979. Dévelopement de cavités d'origine mécanique dans un karst froid (Nahanni, T. N. O., Canada). Annales de la Société géologique de Belgique, 108, 59–67.

Schroeder J, Beaupré M, Cloutier M, 1986. Ice-push caves in platform limestone of the Montreal area. Canadian Journal of Earth Sciences, 23(11), 1842–1851.

Schroeder J, 2004. Glaciotectonic cavities. In: AS Goudie (Ed.) Encyclopedia of Geomorphology. Routledge, London, 470–471.

Sjöberg R, 1986. A proposal for a classification system for Granitic Caves. Communications, 9th International Congress of Speleology, 2, Barcelona, 25–27.

Sjöberg R, 1987. Caves as indicators of neotectonics in Sweden. Zeitschrift für Geomorphologie, NF, Suppl. 63, 141–148.

Smart PL, Palmer RJ, Whitaker F, Wright VP 1988. Neptunian Dikes and Fissure Fills: An Overview and Account of Some Modern Examples. In: NP James, PW Choquette (Eds.) Paleokarst. Springer-Verlag, New York – Berlin – Heidelberg – London – Paris – Tokyo, 149–163.

Stefánson ÁB, 1992. Príhnúkargígur. In: GT Rea (Ed.) Proceeding of the 6th International Symposium on Vulcanospelogy, 197–203.

Striebel T, 1999. Typen von Sandsteinhöhlen und Granithöhlen in der Umgebung von Bayreuth. Pseudokrasový zborník, 1, Knihovna ČSS, 35, Praha, 51–57.

Tachihara H, Sawa I, Kuroishikawa Y, Ogawa T, Honda T, Kim B, Makita T, Watanabe N, Ninata H, Nakau K, 2002. The shape classification and formation model by observation of lava tree-mold. Review of Osaka University of Economics and Law, 84, 46.

Trimmel H, 1968. Höhlenkunde. Friedr. Vieweg und Sohn, Braunschweig.

Turchinov I. 1990. Pseudokrasové jeskyně ve Skolevských Beskydech (Ukrajinské Karpaty). In: J Wagner (Ed.) IV. symposium o pseudokrasu, Knihovna ČSS, 23, Praha, 119–124 (in Czech).

Twidale CR, 1982. Granite landforms. Elsevier, Amsterdam.

Twidale CR, 2009. On the origin of A-tents (pop-ups), sheet structures, and associated forms. Progress in Physical Geography, 33(2), 147–162.

Urban J, 2004. Morphological evolution of the pseudokarst forms in Quaternary loesses of Southern Poland – a case study of Bugaj near Pinczów, Nida Basin. In: L Gaál (Ed.) Proceedings of the 8th International Symposium on Pseudokarst, Teplý Vrch, 75–83.

Vendeville BC, Jackson MPA, 1992. The rise of diapirs during thin-skinned extension: Marine and Petroleum Geology, 9(4), 331–353.

Vidal Romaní JR, 2007. Origin of tafoni elastic deformation. International Conference on Granite Caves. Abstracts, La Coruña, 20–21.

Vítek J, 1983. Classification of Pseudokarst Forms in Czechoslovakia. International Journal of Speleology, 13(1–4), 1–18.

White W B, 1988. Geomorphology and Hydrology of Karst Terrains. Oxford Univ. Press, Oxford – New York.

Wood C, 1974. The genesis and classification of lava tube caves. Transactions of the British Cave Research Association, 1(1), 15–28.

THE KEOKEO LAVA TUBE SYSTEM IN HAWAII

Peter Bosted[1], Tomislav Gracanin[2], Veda Hackell[2], Ann Bosted[1], Ingo Bauer[3], Stephan Kempe[3]
[1]PO Box 6254, Ocean View, HI 96737 USA, peter@cavepics.com
[2]Houston, Texas, tnv@att.net
[3]University of Technology Darmstadt, Schnittspahnstr. 9, D-64287 Darmstadt, Germany, kempe@geo.tu-darmstadt.de

The Keokeo lava tube system lies within a lava flow that apparently originated in the Pu‘u o Keokeo vent on the Southwest Rift zone of Mauna Loa, on the Big Island of Hawaii. The lava flowed 1,500–3,000 years ago from the source near 2,200 m elevation all the way to the ocean, a distance of some 28 km. A large lava tube system has been discovered in most of the flow. The cave system is often braided into parallel branches, as well as being formed on up to four vertical layers. The system is sometimes segmented by ceiling collapse or lava sumps. As of this writing, about 22 km of passage has been surveyed in segments ranging from 10 m to 4 km long. The deepest passages are readily distinguished because the lava downcut through a thick layer of a‘a, which is seen when the wall linings peel away. In places, there is evidence of downcutting through two a‘a layers. There are many white and orange crusts, frostwork, and coatings throughout the system, which could be the subject of a mineralogical investigation. Microbial mats are fairly common as well. Ohi‘a tree roots support a variety of cave-adapted species, including crickets, spiders, isopods, planthoppers, and moths. Other interesting resources in the system include fossil bird bones and occasional native Hawaiian water collection and shelter sites.

1. Introduction

The Big Island in the U.S. state of Hawai‘i is home to the majority of major lava tube (pyroduct) systems (e.g., Kempe 2012) in the world. The second longest system in the world, the Kipuka Kanohina system, originates in the SW rift zone of Mauna Loa, within the Kahuku Unit of Hawaii Volcanoes National Park (HAVO), and passes under the Hawaiian Ocean View Estates (HOVE) and Kula Kai subdivisions, reaching almost to the ocean. Recently, another major system has been identified, also originating in the SW rift zone. The approximate location of the system is shown as the thin and thick black lines in Figure 1. The system is formed in the Qk2 Mauna Loa flow which extends from the presumed source at Pu‘u o Keokeo (altitude of 2,200 m), all the way down to the ocean, some 28 km distant. The estimated age of the flow is 1,500 to 3,000 aBP (Sherrod 2007).

2. Exploration History

Some of the lava tubes in the system were used by the original Polynesian settlers, possibly as long as 1,000 years ago. They likely explored the caves looking for good places to collect water in thisdry environment. They also used some entrance areas for temporary shelters and defense in times of war.

In most of the 1800’s and 1900’s, the entire flow was on the property of the very large Kahuku Ranch. Ranch-hands and farm children sometimes visited the caves, although there is no written record of their activities. The upper portion of the Keokeo flow became part of Hawaii Volcanoes National Park (HAVO) in 2004. The lower portion was sold to private developers (Nani Kahuku Aina) in 2006.

Systematic exploration of the Keokeo system began in 2011. Some entrances were found from satellite and aerial photos. The great majority of them were found on surface hikes, or by entering one entrance and coming out another one. To date, about 300 entrances have been identified. Of these, less than 100 have been explored and surveyed. For the entrances within HAVO, an initial reconnaissance of all of the passages accessible from a given entrance was made with archaeologist Dr. Tim Scheffler, in order to determine if sensitive cultural resources were present.

To date, there have been about 110 field trips to the flow, of which roughly one quarter were to locate entrances, one quarter for archaeological reconnaissance, and half for detailed mapping and photography. About 22 km of passage has been mapped in segments ranging from less than 10 m to over 4 km in length. The segments are usually separated by trenches formed by the collapse of the original tube. In other cases, especially where the gradient is low, the lava completely filled the passages when it cooled, making for lava sumps.

3. Geology

The geology of one of the longest segments of the system, Kahuenaha Nui, was studied by Ingo Bauer as part of his Master’s thesis (Bauer 2011). The cave survey of this segment yielded a total length of 1,850 m, a total vertical extent of 55 m and an average slope of 5.7°. The cave features a main trunk that is up to 18 m wide and 11 m high. Its floor is in part formed by terminal a‘a. Above this trunk passage, there are numerous small to very small interconnected pahoehoe-floored passages. It was possible to study the cave formation process at the two entrance collapses (pukas in Hawaiian). The trunk passage appears to be formed by eroding an underlying a‘a rubble layer. In places even the underlying a‘a core layer has been cut into. Above, a stack of seven superimposed pahoehoe flows with small meandering passages occurs, forming the primary roof of the cave. The lava flowing in this stack of sheets managed to combine into one flow, eroding the main trunk underneath. After cave formation first an a‘a flow and then a thin pahoehoe flow transgressed the area. The cave’s roof partly collapsed, not only exposing the transgressed a‘a, but also forming the two entrance pukas. This cave-forming mechanism is fundamentally different from the standard

lava tube formation modes “inflation” and the “crusting-over of channels” (e.g., Kempe 2012).

Figure 1. Geologic overview of the Keokeo flow on the south slope of Mauna Loa. The thick black lines show the approximate location of explored passages, while the thin black lines are likely extensions to the north and south. The distance from the top to bottom of the figure is about 30 km, and north is up. The Keokeo flow is colored light green. Older flows are yellow and green, while modern flows are colored blue. Highway 11 crosses the figure from left to right just below the middle.

While detailed geologic studies have not been done in other segments of the system, the mode of down-cutting into an a‘a layer appears to persist throughout the main, lower level trunk passages. This is most often revealed by wall coatings, typically 0.2 to 1 m thick, that have peeled away, generally falling towards the center of the passage, and leaving a pile of exposed a‘a rubble behind. Often the a‘a rubble is stained orange or red, by oxidation of the iron in the basalt. One of the more dramatic examples is shown in Figure 2.

Throughout the system, the larger entrances are often the best place to study the stratigraphy. Where there are clean ceiling collapses, it is sometimes possible to count the number of pahoehoe sheets and a‘a layers.

The lava tube passages often contain white, orange, and sometimes pink or green minerals. These most commonly occur as crusts or coatings on the ceiling, walls, and sometimes on the floor. There is a noticeable correlation of mineral coatings with high wind velocities near major

Figure 2. Illustration of wall-lining peeling away to reveal a thick layer of red a‘a rubble behind. Bob South is the model. Photo by Peter and Ann Bosted.

Figure 3. Stephan Kempe (in red) and Tim Scheffler above the largest entrance of the system found so far. Photo by Peter and Ann Bosted.

entrances and constrictions where the Venturi effect makes for strong air flow. The very dry climate of the region likely stops the minerals from being dissolved, because they are much more common here than in the wet areas of Hawai‘i. Based on sampling in the nearby Kanohina system, most of the white minerals are probably calcite, gypsum or opal, although epsomite and mirabilite can be found. A typical medium-size passage with white, orange, and red coatings, and an a‘a floor over smooth linings, is shown in Figure 4. In some areas, the minerals are in a frostwork morphology, as illustrated in Figure 5.

4. Biology

The Keokeo flow covers a large elevation range (from sea level to about 2,200 m), but the endemic Hawaiian Ohi‘a tree can be found throughout almost the entire range. This tree is very important to the cave biology, because it is adapted to putting its roots down into lava tubes, often going right through to the floor below. Some of the roots are well over 10 m long and bundles up to 30 cm in diameter occur. An example of thick forest of Ohi‘a tree roots is shown in Figure 6.

Figure 4. Ann Bosted in typical medium-sized passage with many mineral coatings. Photo by Peter and Ann Bosted.

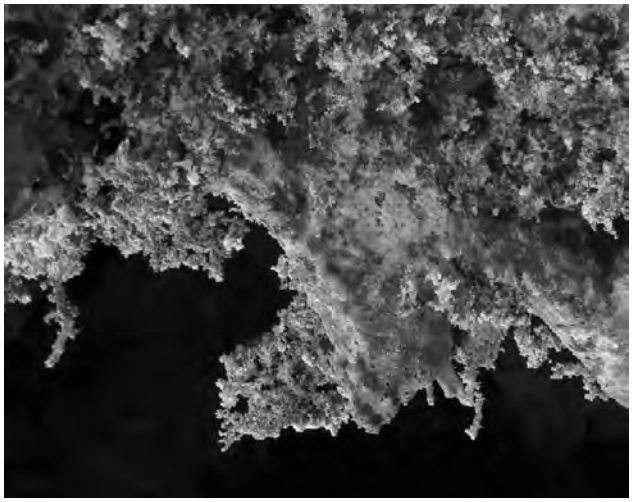

Figure 5. Delicate frostwork minerals on ceiling lava drips. Photo by Peter and Ann Bosted.

The tree roots are an important source of nutrition and water for a host of cave-adapted species. While no professional biologist has studied this system as of this writing, we have sent photographs to biologist Fred Stone, who has identified various crickets, spiders, isopods, moths, and planthoppers.

Another important source of the cave biology is the large number of goats that use the caves as night-time shelters.

They supply nutrition by their excrements and the degradation of their dead bodies. The goats are generally found at lower elevations. At higher elevations, the most common mammal bones are Mouflon (a form of wild sheep), cattle, occasional horses, rats, and mongeese. A typical passage with an ungulate skull is shown in Figure 7.

Well-preserved fossil bird bones are also sometimes found, especially in deep passages far from entrances, where they are protected from wheathering. Some of these may be from now-extinct species. A systematic study has not been done yet, however. One of the best-preserved examples is shown in Figure 8. This is most likely the head of one of the petrel varieties.

Microbial mats are found throughout the system. None have been studied as of this writing.

Finally, the deep entrances provide a haven for certain rare and endangered plants. The moister climate is a boon to the

Figure 6. A thick forest of ohi'a tree roots. Photo by Peter and Ann Bosted.

Figure 7. Typical passage with mouflon skull in the foreground. Photo by Peter and Ann Bosted.

Hapu'u (tree fern). Large Koa trees can also be found in deep pukas where the steep sides have excluded cattle, which would otherwise eat and trample the young trees. An example of abundant native vegetation in a skylight puka is shown in Figure 9.

5. Prospects

With about 200 or more entrances to investigate, there is clearly a lot more work just to finish the exploration, mapping, and photo-documentation of the Keokeo system. Meanwhile, there are many opportunities for detailed studies of the geology, biology (both macro and micro), extinct birds, and archeology. Potential investigators would need to obtain a permit from the National Park Service or other land owners.

Acknowledgments

We are extremely grateful to Tim Scheffler for archeological monitoring assistance during many more long field trips than originally anticipated. Thanks to the numerous cavers who helped with mapping and photography, especially Bob South. We thank the National Park Service for their support.

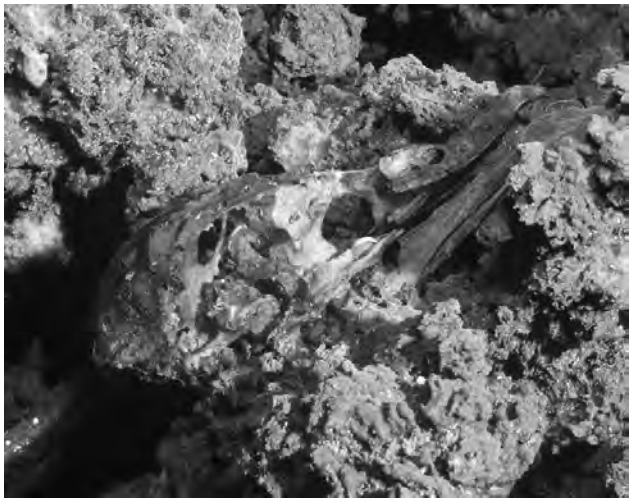

Figure 8. Fossil bird head. Photo by Peter and Ann Bosted.

Figure 9. An entrance skylight with native vegetation. Photo by Peter and Ann Bosted.

References

Bauer I, 2011. Geologie, Petrographie und Pyroductgenese des Kahuku-Ranch-Gebiets, Big Island, Hawaii. MSc thesis, Inst. of Appl. Geosciences, Techn. Univ. Darmstadt, 139, unpublished.

Sherrod E, David R, Sinton, JM, Watkins S, Brunt, KM, 2007. Geologic map of the State of Hawai'i: U.S. Geological Survey Open-File Report 2007-1089, http://pubs.usgs.gov/of/2007/1089/

Kempe S, 2012. Volcanic rock caves. In: White W, Culver DC (Eds.), Encyclopedia of Caves, 2nd ed. Academic Press /Elsevier, Amsterdam, 865–873.

Nani Kahuku Aina, LLC in Draft Environmental Impact Statement, PBR and Associates, Honolulu, 2011. http://oeqc.doh.hawaii.gov/Shared%20Documents/EA_and_EIS_Online_Library/Hawaii/2010s/2011-09-23-DEIS-Kahuku-Village-Vol1.pdf

ORIGIN OF "ROCK CITIES", PILLARS AND CLEFT-CONDUITS IN KAOLINITE-BONDED SANDSTONE: NEW INSIGHT FROM STUDY IN SANDSTONE QUARRY WHERE LANDFORMS RECENTLY EVOLVE

Jiri Bruthans[1], Jan Soukup[1], Jana Schweigstillova[2], Jana Vaculikova[1], Daniel Smutek[3], Alan L. Mayo[4], Lukas Falteisek[1]

[1]Faculty of Science, Charles University in Prague, Albertov 6, Praha 2, Czech Republic, bruthans@natur.cuni.cz
[2]Institute of Rock Structure and Mechanics AS CR, v.v.i., V Holešovičkách 41, 182 09, Praha 8, Czech Republic,
[3]Vodní zdroje Chrudim sro., U vodárny 137, Chrudim II, Czech Republic
[4]Brigham Young University, Department of Geosciences, Provo, UT 84602, USA

Various ideas exist on the origin of landforms like rock cities, pillars, clefts, rock shelters and lenticular hollows in kaolinite-bonded sandstone. Sandstone surfaces and processes were studied in Střeleč Quarry, the Czech Republic in Cretaceous marine quartz sandstone, where forms similar to landforms at natural exposures (clefts-conduits, lenticular hollows) are evolving at present time. The quarry offers a unique opportunity to characterize the erosion processes, which may form natural landforms prior to stabilization by case hardening. Based on measurements of relative erodibility, ambient and water-saturated tensile strength at natural and quarry exposures three distinct kinds of surfaces were distinguished: 1) Sandstone directly erodible by flowing water. 2) Sub-vertical fracture surfaces that are non-erodible and formed tectonically (slip faces of microfaults). 3) Case hardened surfaces that start to form after exposure. In favorable conditions case hardened surfaces become non-erodible and reach the full tensile strength in just 6 years. Flow in openings with a discharge 1 ml/s and hydraulic gradient > 0.05 exceeds the erosion threshold and initiates piping. In the first phase of conduit evolution, fast concentrated flow mobilizes erodible sandstone between sets of parallel fractures in the shallow phreatic zone. In second phase the conduit opening mainly expands vertically upward into the vadose zone by mass wasting of undercut sandstone slabs. Mass wasting is responsible for > 90 % of mobilized sandstone. Sides of the mature conduits are protected by non-erodible fracture surfaces. Natural landforms were probably formed rapidly by piping and possibly overland flow and fluidization during, or at, the end of the glacial periods when sandstone was not protected by case hardening yet. Erosion proceeded along highly fractured zones. The study does not support the existence of deep weathering along fractures proposed by some authors (etching).

1. Introduction

The weathering and erosion of sandstone result in the formation of interesting morphology features in many areas including the Colorado Plateau (United States) and the Bohemian Cretaceous Basin (Czech Republic, Germany) (Härtel et al. 2007). The landscape of many areas in the northern Czech Republic, in Saxony, Germany, in Weald, SE England and elsewhere are developed in quartz sandstones bonded by kaolinite, whose tensile strength decreases strongly if sandstone is wetted (Bruthans et al. 2012b). The effect of wetting weakening is well known to local climbers who by regulation are prohibited from climbing in sandstone terrains for one or two days after rain events not to damage sandstone surfaces (HOROSVAZ 2011).

Various landforms are known from these sandstones including caves, clefts separating individual sandstone pillars (castellated sandstones), rock overhangs (shelters) and also small-scale features like lenticular hollows and honeycombs (Härtel et al. 2007; Fig. 5). Honeycombs are clearly evolving at present time, as they cover also few hundred years old quarry faces as well as sandstone blocks at cemeteries and walls of medieval castles (Härtel et al. 2007).

Based on radiocarbon and U-series dating of secondary carbonates in sandstone cave ceilings and archeological evidence, sandstone erosion in caves and sandstone overhangs ceased at least 8 kyr ago in Bohemian Paradise and wider surroundings of Česká Lípa (Cílek 2007; Bruthans et al. 2012a). Continuous peat bog sedimentation for the last 7.5 kyr in valleys directly below sandstone exposures in Adršpach region (60 km east of the studied locality) demonstrates that at least some sandstone exposures have not been eroded in this period (Kuneš and Jankovská 2000; our study, unpublished).

At present time the sandstone exposures and even sides of many overhangs are reinforced by case hardening, which makes sandstone exposures unerodible (Härtel et al. 2007). Important question is how quickly case hardening is formed and what the properties of the sandstone were before the case hardening was formed. So far the evolution of sandstone landforms has been studied at natural exposures. Due to protection measures the studies were mostly limited to observation and documentation of landform shapes and taking small samples of rock crust for mineralogical analysis of salts and cements (e.g., Adamovič et. al. 2011). So far such studies failed to bring clear evidence for origin of landforms in clay-bonded sandstone except perhaps honeycombs. As a consequence, a wide variety of different ideas exist on processes responsible for evolution of landforms including deep weathering along fractures followed by the frost, salt and biogenic weathering (Cílek 2010), dissolution of carbonate cement (Adamovič and Mikuláš 2011) and many others.

Interestingly, some landforms (cleft-conduits, lenticular hollows) whose origin is discussed above are actively evolving at present time in Střeleč quarry (Fig. 5). In the quarry, Cretaceous Hrubá Skála quartz sandstone is mined (for geotechnical and hydraulic parameters see Bruthans et al. 2012b). In this sandstone, a wide variety of natural forms

occur in the so-called Bohemian Paradise (Härtel et al. 2007). There are two strong advantages to study the landforms in the quarry: 1) All landforms are doomed to be destroyed by quarrying and therefore destructive methods can be fully applied; 2) Newly quarried surfaces are unprotected by case hardening, unlike natural surfaces. Possibility to observe presently evolving forms and potential to apply destructive techniques creates a unique opportunity to resolve the origin of landforms and study directly the erosion processes.

Many fresh sandstone faces in the quarry are weak enough to be eroded by running water and rain, and the sandstone was even mined for decades by spraying a jet of pressurized water. The same sandstone, however, has to be mined by explosives when dry, and it has formed stable (up to 40 m high) vertical mining faces before the present safety regulations. The significant decrease in the strength of the wet sandstone compared to its dry state is known as wetting weakening (Lin et al. 2005).

The aim of this study is to describe: 1) Sandstone surfaces in a quarry in terms of the erodibility, tensile strength and geomorphological functioning; 2) Erosion processes operating in the quarry; 3) Apply the findings from the quarry to understand the evolution of natural sandstone landforms.

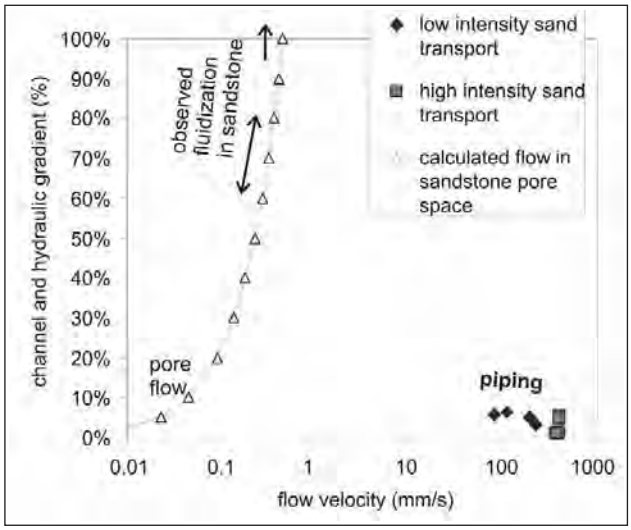

Figure 1. Measured flow velocity in conduits compared to calculated flow velocity in sandstone pores as a function of channel gradient or hydraulic gradient. While piping is characterized by high flow velocity and low hydraulic gradient (conduit flow) the fluidization is characterized by steep hydraulic gradient and very low flow velocity (due to extreme friction in small pores). Modified from Bruthans et al. (2012b).

2. Methods

The geometry, locations and gradients of underground conduits were mapped by compass, precision clinometer, and a tape or a laser distance meter. Tracer tests in underground streams were performed with dissolved NaCl and fluorescent dye. Maximum flow velocity was measured by a tracer test (first arrival of dissolved tracer) and the leading edge of the breakthrough was photo-documented based on fluorescein dye.

The tensile strength of surfaces was measured in the field. Metal plates were glued by epoxy to sandstone surfaces. After hardening a tensile force was gradually increased perpendicular to sandstone surface until the sandstone beneath the epoxy failed. The maximum (pull off) force and effective area was measured and calculated as kPa. The ambient tensile strength (TSa) and saturated tensile strength (TSs) were measured (Bruthans et al. 2012b).

The relative susceptibility to erosion by flowing water was measured by means of a water jet. A sprayer device equipped by a pressure gauge was used to create a jet of water 1 mm in diameter. The reservoir was pressurized to 180 kPa during all tests. The water jet was applied to tested points at the sandstone surface with a 10 cm-long stream of water for 5 seconds (Bruthans et al. 2012b). The depth of the water jet drill holes was measured by a caliper. The drilled depth is herein designated as the "relative erodibility indicator" (REI). The REI technique is based on a similar principle as the "jet test" developed by Hanson and Cook (2004).

3. Results and discussion

3.1. Characterization of conduits

Up to several hundred meters long conduits developed in the quarry due to artificial water level decrease by 20 m (Fig. 5a). At several locations the underground conduits were mainly enlarging upward by mass wasting. At several locations the mass wasting broke through to the ground surface resulting in vertical shafts similar to natural clefts.

A striking feature of the underground conduits is the fact that most of the sides of the passages do not display erosion features made by flowing water (Fig. 5a). Instead, conduit sides are smooth fracture surfaces. The measured stream gradient in major and minor conduits is ~0.01 and ~0.05, respectively with flow velocity ~40 cm/s (Fig. 1).

Flow in the smallest channels transporting sand grains was investigated by studying the propagation of the leading edge of fluorescein dye. Small inflow trickles with flow rates as low as 1–4 ml/s had a maximum a velocity 8–19 cm/s in several cm-wide channels with gradients of 0.05–0.06.

3.2. Strength and erodibility of sandstone surfaces

Surfaces measured by REI and TS included: 1) Fracture surfaces that are smooth and planar, 2) Case hardened surfaces that have a thin surface crust, 3) Water eroded surfaces that show traces of fluvial erosion, 4) Non-eroded surfaces that are a subset of fracture surfaces, which were in contact with flowing water but do not show traces of any erosion, and 5) other surfaces which include all other surfaces (mainly measurement at the quarry faces).

More than 750 REI measurements were made, with drill hole depths ranging from < 1 mm to 152 mm (Fig. 2). Ninety percent of the water eroded surfaces have REI > 20 mm and 93% of non-eroded surfaces have REI < 20 mm (Fig. 2). Therefore, the REI threshold for erodible sandstone and non-erodible sandstone is defined for the quarry sandstone as 20 mm.

To estimate the percentage of erodible sandstone in the quarry, REI measurements were performed along a 240 m-long horizontal profile of the quarry face. On average 64% of

sandstone in this profile is erodible (Bruthans et al., 2012b).

REI measurements demonstrated that fracture surfaces are in many cases less erodible than the sandstone located several millimeters below the fracture surface. REI < 20 mm shows 83 % of fracture surfaces. The REI of 86 % of case hardened surfaces < 5 mm, which makes case hardened surfaces the least erodible surfaces in the quarry (Fig. 2).

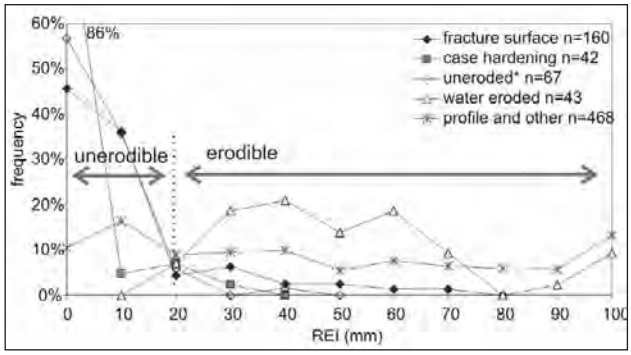

Figure 2. Histogram of REI. Values were rounded to tens. Category REI 100 contains also readings exceeding REI 100 mm. Modified from Bruthans et al. (2012b).

Surfaces of erodible sandstone have an ambient tensile strength (TSa) of 2.2–14 kPa (Fig. 3). The tensile strength of the sandstone decreases substantially when the sandstone is water saturated. The saturated tensile strength (TSs) of erodible sandstone is only < 0.6 kPa. Measurements suggest that the ambient tensile strength is at least about 2 orders of magnitude greater that the saturated tensile strength.

Fracture surfaces and case hardened surfaces, which are not erodible, have a TSa of 27–216 and 64–183 kPa, respectively. The TSs of vertical fracture planes is between 0.9 and 38 kPa, which is less than fracture surface TSa. The TSs of fracture planes are nevertheless much greater than the those of erodible sandstone (Fig. 3).

3.3. Binding and microfabric of surfaces

To explain the distinct difference in tensile strength and erodibility of sandstone surfaces in the quarry, the binding and sandstone microfabric were studied. Erodible sandstone shows a looser packing between grains compared to fracture surfaces. Neither silica nor calcite and iron-oxide cement were identified in any sample of erodible sandstone based on SEM and cathodo-luminescence inspection. Opal was not detected by FTIR in silt and clay separates from erodible sandstone. Only kaolinite was identified as binding agent in erodible sandstone (for details see Bruthans et al., 2012b). The decrease in tensile strength from relatively dry to the saturated state confirms that erodible sandstone is not bonded by permanent cement, but only by clay.

Fracture surfaces are formed by zones of densely packed grains, which are several millimeters thick (Fig. 5h). Unerodible fracture surfaces were found at exposures as well as inside the conduits, tens of meters below the quarry surface. Fracture surfaces were thus non-erodible already prior to exposure at ground surface. Fracture surfaces correspond to slip faces or possibly deformation bands in sense of Antonellini et al. (1994).

Case hardened surfaces are formed by a 0.5–1 mm thick layer sandstone where most of the pores become filled by clay. Lichen hyphae were found in large numbers at case hardened surfaces (Fig. 5j). Sample of case hardened surface left for 5 days in hydrogen peroxide (30 %) was disintegrated to loose sand, while control sample left in water was stable. As hydrogen peroxide decomposes organic matter, the hyphae organic fibers are probably responsible for stabilization of surfaces. Unlike fracture surfaces, case hardened surfaces start to develop after sandstone is exposed at ground surface. At the bottom of the quarry, parent surfaces had unlimited moisture supply and were directly exposed to sun radiation. The case hardened surfaces with firm surface crust (TSa 64–180 kPa) developed at places which were excavated just 6 years ago (Bruthans et al. 2012b).

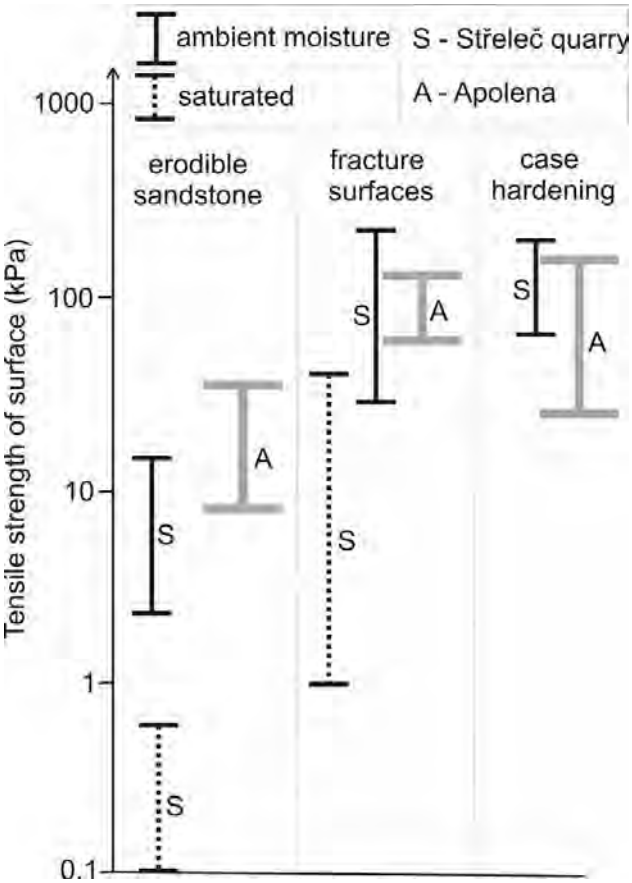

Figure 3. Tensile strength of surfaces in the quarry and natural outcrop Apolena, both formed by the Hrubá Skála sandstone.

3.4. Erosion processes

Field evidence proves the critical role of piping and mass wasting in conduit enlargement. Conduit flows were observed to erode by piping the most erodible sandstone surfaces at rates as high as several centimeters per minute. In one case a 3 m deep, 1 m wide, and 15 m long gully was cut into sandstone in less than 12 hours by water discharging from one spring (Bruthans et al. 2012b). Mass wasting of undercut sandstone blocks, along sub-vertical fractures, is the dominant mechanism in conduit enlargement because more than 90 % of conduit volumes are excavated above the conduit stream surfaces.

The potential role of fluidization in the enlargement of fracture openings is unclear. Fluidization may potentially contribute to erosion due to initial steep hydraulic gradients

in the surroundings of new conduits. To test this possibility the critical hydraulic gradient for the onset of fluidization was measured in eight rectangular blocks of erodible sandstone. In two of the blocks, erosion due to fluidization occurred when the hydraulic gradient ≥0.7. In other blocks, no erosion was observed even under very steep hydraulic gradients (1.2–1.5).

Lenticular hollows are relatively common in conduits and lake sides in the quarry (Fig. 5e). Active erosion was not observed under ambient conditions. In an attempt to better understand the process responsible for origin of lenticular hollows the overland flow and fluidization experiments were performed in the quarry. The experiments consisting of flowing water across erodible sandstone surfaces and via sandstone matrix in the quarry demonstrated that two different processes can create lenticular hollows: 1) Fluidization, and 2) Overland and/or pipe flow.

3.5. Evolution and propagation of conduits

Incipient conduits probably propagate along bedding planes or subhorizontal cracks in several cm to few tens of cm thick sub-vertical slabs of sandstone. Conduits are formed by erosion of narrow sandstone slabs between sets of parallel subvertical fractures. Conduit width increases by mass wasting along parallel fractures (Fig. 4).

3.6. Origin of natural sandstone landforms

To evaluate if the processes observed in Střeleč quarry are partially responsible for the sandstone landscape evolution observed elsewhere, exposures of the same sandstone were studied in the Apolena area 1.7 km from the quarry. In Apolena the sandstone forms pillars up to 30 m high, rock shelters, arches and lenticular hollows (Figs. 5 d, e). The pillars and parts of sandstone massif are separated by deep clefts. Outer faces of the sandstone outcrops are often defined by vertical fracture planes. Such landforms are a very common feature in sandstones in the Czech Republic and Saxony, Germany (Härtel et al. 2007). At Apolena and other natural sandstone exposures (e.g., Adršpach), the features have similar appearance to those found in the quarry (Fig. 5). Some natural springs in the surroundings of the Střeleč quarry have feeding conduits of the same shape as that found in the quarry (Bruthans et al., 2012b).

At Apolena fresh surfaces of sandstone boulders, which are the residual of pillar collapse, have similar values of TS and REI as fresh sandstone faces in Střeleč Quarry and are erodible. Case hardening in Apolena area is similar to the recent case hardening in Střeleč quarry. Hydraulic gradients of ~0.03 responsible for the onset of conduit development in the quarry surroundings (Bruthans et al. 2012b) could occur in the past under natural conditions. Observations made in the quarry are thus fully applicable to this natural sandstone outcrop.

It may be possible to extrapolate the erosion processes observed in the Střeleč quarry to the landforms found in the Apolena area and elsewhere in the clay-bonded sandstone. Clefts were excavated probably by piping and consequent mass wasting of undercut sandstone slabs in erodible sandstone. Overland flow and fluidization may be considered too. Lateral enlargement of clefts by mass wasting of sandstone slabs was responsible for the formation of pillars and rock cities. Fracture planes were the only surfaces limiting erosion in erodible sandstone since case hardening was not yet formed. Unerodible parts of sandstone may have disintegrated by ice wedging. Rain water collected at ground surface was probably the major source of water feeding cleft conduits. The erosion was active during glacial periods, when sandstone was impermeable (except shallow subsurface in warm period of year) due to >30 m thick permafrost (Žák et al. 2012) and possibly also at glacial/interglacial transition.

With the establishment of warmer climate and forest cover during the Holocene (Kuneš and Jankovská 2000), the amount of water available for surface erosion and piping decreased considerably due to transpiration consumption of forest cover. Eroded surfaces were probably case hardened at this time, thus fossilizing the sandstone landforms into their present shapes. The postulated timing of erosion, formation of case hardening and consequent fossilization of landforms are in good accord with the results of dating studies (Cílek 2007; Bruthans et al. 2012a, undisturbed peat bog sedimentation below sandstone exposures mentioned above).

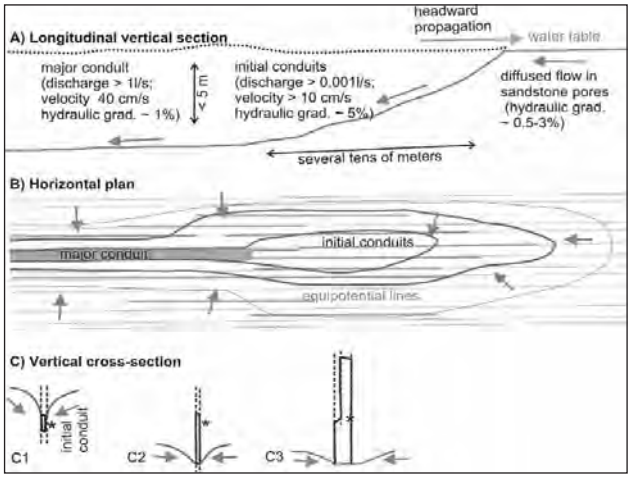

Figure 4. Conceptual model of conduit propagation. A) Evolution in longitudinal vertical section; B) Horizontal plan of headward part of propagating conduit. Bedding planes provide a permeable path in a direction oblique to fractures; C) Evolution of conduit cross-section. Asterisk shows the original position of proto-conduit. Modified from Bruthans et al. (2012b).

4. Conclusions

Three distinct kinds of sandstone surfaces can be defined based on field appearance, erodibility and tensile strength: A) Erodible sandstone is defined as sandstone with REI readings >20 mm based on field calibration. Erodible sandstone does not contain permanent cement. Sandstone is bonded by kaolinite, capillary forces and interlocking of sand grains. Erodible sandstone loses as much as 99% of its surface tensile strength when submerged below water. B) Sub-vertical fracture surfaces (slip faces of microfaults) are generally not erodible by piping or overland flow based on REI and field observations. Tensile strength is several times higher (TSa 27–220 kPa) compared to sandstone in the subsurface of a fracture plane. Unlike the erodible sandstone, fracture surfaces often keep considerable tensile

strength if fully saturated. The non-erodible zone is several millimeters thick. Non-erodible fracture surfaces have clearly developed before the sandstone was exposed at ground surface and were recognized as a factor affecting shape of many sandstone landforms at natural outcrops. C) Case hardened surfaces cover most of the natural sandstone exposures, but also many exposures in the quarry, which are more than few years old. They evolve after the sandstone was exposed at ground surface, with a contribution of lichens. Case hardened surfaces consist of a 0.5–1 mm thick zone of sandstone where most of the pores become filled by kaolinite clay reinforced by lichen hyphae. Case hardened surface are not erodible by overland flow. Under optimum conditions (sun irradiation, moisture abundance), case hardening developed in the quarry within just 6 years reaching the same tensile strength as the case hardened surfaces at natural exposures (TS 23–180 kPa).

The critical requisite for erosion of sandstone is the development of a zone of locally steep hydraulic gradient (~0.05), which resulted in an increase in flow velocity in small openings. The zone of steep gradient migrates headward in front of the propagating conduit. Openings with flow > 1 ml/s and hydraulic gradient > 0.05 exceed the threshold for initiation of piping in erodible sandstone.

The conduit evolution is initiated by piping of narrow slabs of erodible sandstone between sets of parallel fractures in shallow phreatic zone. In the second phase, the conduits mainly propagate vertically upward via the vadose zone by mass wasting of undercut sandstone slabs. Mass wasting is responsible for > 90 % of mobilized sandstone. No traces of erosion are left on fracture planes that form the conduit sides. Clefts in natural sandstone landscape may thus be developed by water erosion even if there are no traces of such erosion left. Based on physical modeling, the fluidization may occur in vadose zone at seepage face under a steep hydraulic gradient (> 0.7).

Based on the observations in the quarry, the following origin of various phenomena in clay-bonded sandstones is proposed. A) Clefts and eroded zones separating pillars and other rock masses in rock cities were initiated by piping and enlarged by mass wasting along subvertical fractures. Overland flow and fluidization erosion formed the undulating sandstone surface and lenticular hollows at pillars and other sandstone exposures. Erosion was active during glacial periods or at glacial/interglacial transitions. Frost weathering disintegrated firmer parts of sandstone. Landform evolution might be very fast (centuries). B) The case hardening started to form at sandstone exposures during the Holocene climate conditions, which decreased the erodibility below the threshold for natural flow and fossilized the forms into present shape except honeycombs, which are recently evolving. The postulated timing of erosion and formation of case hardening is in good accordance with published dating studies.

The study does not support the existence of deep weathering along fractures (cf. Cílek 2010). Sandstone is weak in massive blocks (forming pillars) as well as in fractured zones (forming clefts). In our opinion it is the mechanical weakness of narrow slabs of sandstones what enables the piping, triggers mass wasting and finally forms clefts.

Acknowledgments

Many thanks to Petr Mikuš, Lukáš Hronec, Iva Kůrková, Vojtěch Stejskal, Michal Filippi, Ondřej Jäger and Stanislav Šlechta for assistance with field measurements in 2009–2012 and to the management of Střeleč Quarry for facilitating the research, and Jiří Adamovič and Tomáš Lánczos for very valuable comments. The research was supported by grant projects GAUK 380511, GAČR 13-28040S research plan MSM0021620855 and research plan AV0Z30460519.

References

Adamovič J, Mikuláš R, 2011. Origin of some ellipsoidal cavities by carbonate cement dissolution in the Jizera Formation sandstones, Kokořín area. Geoscience Research Reports for 2010, 9–13. Czech Geological Survey.

Adamovič J, Mikuláš R, Schweigstillová J, Böhmová V, 2011. Porosity changes induced by salt weathering of sandstones, Bohemian Cretaceous Basin, Czech Republic. Acta Geodynamica et Geomaterialia 8, 1, 29–45.

Antonellini MA, Aydin A, Pollard DD, 1994. Microstructure of deformation bands in porous sandstones at Arches National Park, Utah. Journal of Structural Geology 16, 7, 941–959. Amsterdam.

Bruthans J, Schweigstillová J, Jenč P, Churáčková Z, Bezdička P, 2012a. 14C and U – series dating of speleothems in the Bohemian Paradise (Czech Republic): Retreat rates of sandstone cave walls and implications for cave origin. Acta Geodynamica et Geomaterialia 9 (1), 93–108.

Bruthans J, Svetlik D, Soukup J, Schweigstillova J, Valek J, Mayo AL, 2012b. Fast evolving conduits in clay-bonded sandstone: Characterization, erosion processes and significance for origin of sandstone landforms. Geomorphology 177–178, 178–193.

Cílek V, 2007. Climate, microclimate and paleoclimate of sandstone areas of Central and Northern Bohemia (Czech Republic). In: Härtel H, Cílek V, Jackson A, Williams R. (Eds.), 2007. Sandstone Landscapes. Academia, Praha, 97–103.

Cílek V, 2010. Saxon-Bohemian Switzerland: sandstone rock cities and fascination in a romantic landscape. P. Migon (ed.) Geomorphological Landscapes of the World, 201–209. Springer.

Hanson GJ, Cook KR, 2004. Apparatus, test procedures and analytical methods to measure soil erodibility in situ. Applied Engineering in Agriculture 20 (4), 455–462.

Härtel H, Cílek V, Jackson A, Williams R. (Eds.), 2007. Sandstone Landscapes. Academia, Praha.

HOROSVAZ, 2011. Pravidla sportovního lezení na pískovcových skalách v Čechách. Czech Mountaineering association. http://www.horosvaz.cz/index.php?cmd=page&type=2&article=35

Kuneš P., Jankovská V., 2000. Outline of Late Glacial and Holocene vegetation in a landscape with strong geomorphologic gradients. Geolines 11, 112–114.

Lin ML, Jeng FS, Tsai LS, Huang TH, 2005. Wetting weakening of Tertiary sandstones – microscopic mechanism. Environmental Geology 48, 265–275.

Žák K, Richter DK, Filippi M, Živor R, Deininger M, Mangini A, Scholz D, 2012. Cryogenic cave carbonate – A new tool for estimation of the Last Glacial permafrost depth. Climate of the Past Discussions 8, 2145–2185.

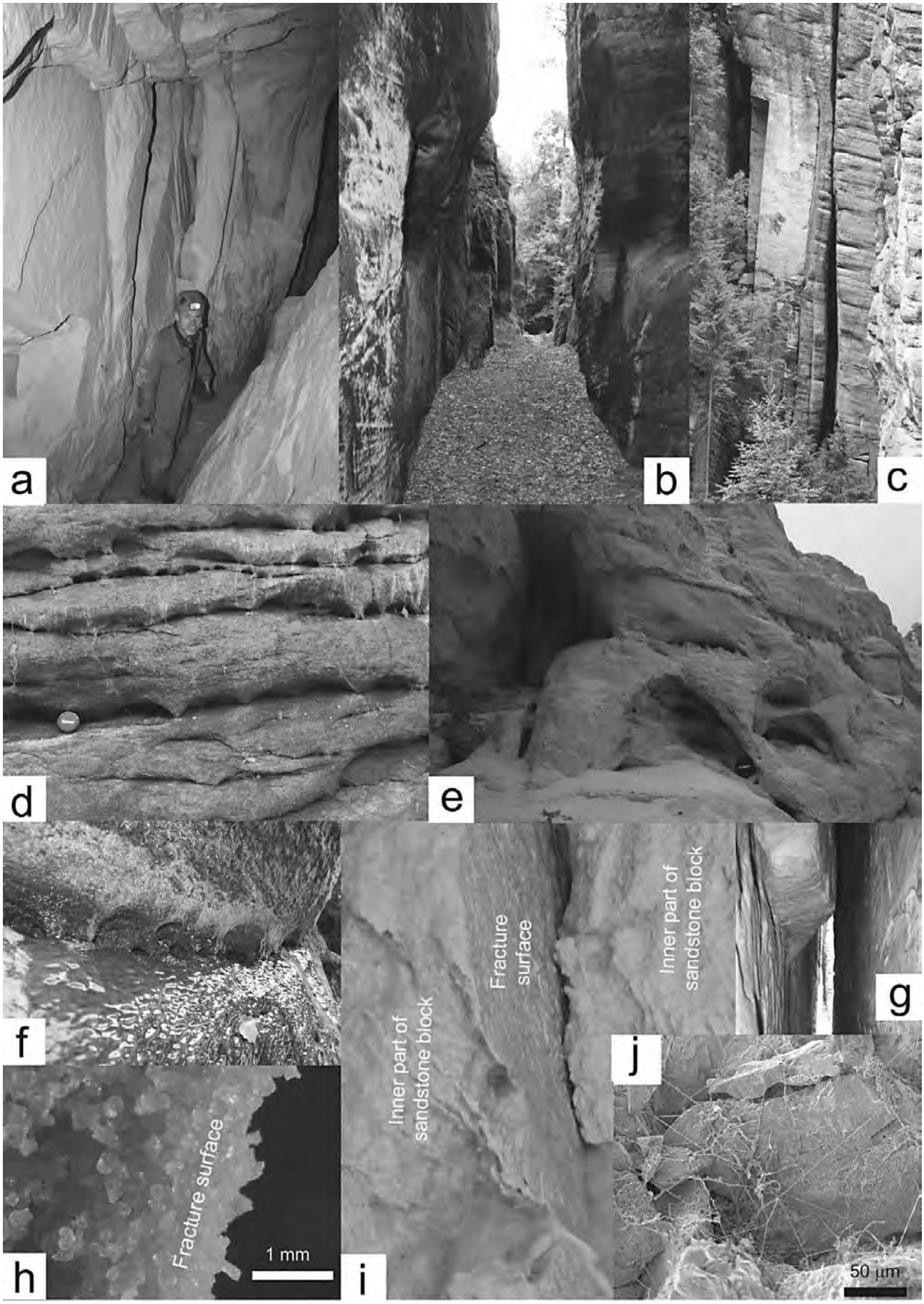

Figure 5 a) Conduit developed by flowing groundwater in Střeleč quarry propagating mainly upwards along parallel sub-vertical fractures. Photo M. Filippi; b) Cleft limited by subvertical fractures in Apolena area; c) Fracture-guided opening in Adršpach nature reserve. Note the highest width at base and multiple fractures dying out upward; d) ¨Lenticular hollows in Adršpach-Teplice nature reserve; e) Lenticular hollows developed at the side of a quarry lake (< 6 years old); f) Freezing groundwater seeping out of the lenticular hollows (Adršpach); g) Fracture-guided opening in Adršpach area. Note remaining block in the ceiling; h) Cross-section via fracture surface (quarry); i) Inner part of the sandstone block is much easily erodible by flowing water than fracture surface (quarry); j) Lichen hyphae in a case hardened surface (quarry).

ORIGINS OF THE KARSTIC SEDIMENT FILLING OF THE NORTHWESTERN PARIS BASIN CAVES

S. Chédeville[1], J. Rodet[2], B. Laignel[1], D. Todisco[3], E. Dupuis[1], G. Girot[1], G. Hanin[1]
[1]Université de Rouen, UMR 6143 M2C CNRS, SFR SCALE, 76821 Mont-Saint-Aignan, France, chedeville.stephane@gmail.com
[2]CRNS UMR 6143 M2C, Université de Rouen, SFR SCALE, 76821 Mont-Saint-Aignan, France
[3]Université de Rouen, UMR 6266 IDEES CNRS, SFR SCALE, 76821 Mont-Saint-Aignan, France

Petites Dales, Villequier II and Orival are three privileged caves to study the sedimentary fillings in the chalk karst of the Northwestern Paris Basin (France). The present study is based on sedimentological characterization of the sediments from these caves using stratigraphy, grain-size and geochemical analysis. Observations and analysis point out a sedimentary variability both within and between sites. This may be explained by the variation of two main parameters: (i) the origin of karst sediments and (ii), their hydrodynamic behaviour in the karst system. The methodology used to analyse karst fillings allows identifying the origin of the components: (i) fillings made of surface formations (loess, sand deposits, or a mixture of them) and (ii), insoluble residue of chalk (clay with flints).

1. Introduction

Karstification processes occur in different parts of the world on different carbonated or not bedrocks (Rodet 1991; Willems 2000). These processes create voids on the surface (e.g., sinkhole) and within the bedrock (i.e. karstic conduit) by chemical weathering and/or mechanical erosion (Mangin 1975). Depending on the hydrodynamics and sediment sources, these voids may present three kinds of karstic filling: (i) allochthonous (supply of sediments by mechanical erosion), (ii) autochthonous (insoluble residues from chemical alteration of the bedrock) or (iii), a mixture of both (Laignel et al. 2004; Rodet et al. 2006). The sedimentary fillings of karst are excellent recordings of hydrodynamic changes in the karst (Losson and Corbonnois 2006). Their studies allow understanding of the hydrosedimentary processes at the origin of sedimentation, and subsequently to determine past climatic conditions (Falguères et al. 2001; Quinif 2006; Rodet et al. 2006; Hanin et al. 2011).

Karstification phenomena are well developed in the chalk of the Northwestern Europe (NWE), particularly in the Northwestern Paris Basin (NWPB) in France, North-East Wallonia in Belgium and South-East England. In these areas, karstic introductions, networks and sedimentary fillings are most often similar (Rodet 1991; Laignel et al. 2004; Quinif 2006; Van Den Eeckhaut et al. 2007; Willems et al. 2007a; Cooper et al. 2011; Farrant and Smart 2011; Hanin et al. 2011). In limestone bedrocks, the weathered surface and karstification are linked (Rodet 1991; Laignel 2003; Laignel et al. 2004). The karstic network could be considered as zones of alteration, storage volumes of eroded material and also of transit.

Whereas a lot of studies on karstic fillings are focused on archeology (Madeyska 2002; Cyrek et al. 2010) or climate change (Quinif 2006), for example, very few deal with the characterization and comparison of several karstic fillings (Rodet et al. 2009). The objective of the present study is then to propose a comparison between several karst sedimentary fillings in the NWPB. Three sites with karstic filling have been studied in the NWPB (Seine-Maritime, France): Villequier II, Orival and Petites Dales Caves (Fig. 1).

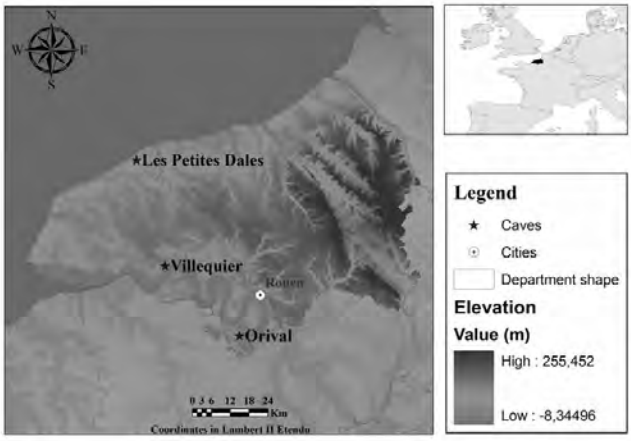

Figure 1. Location map of caves.

The karstic sediment fillings of these sites have been characterized with stratigraphical and sedimentological analysis in order to determine the origin of the sediments. After defining the origin of sediment sources, a comparison is drawn between the obtained results with those from Belgium (Quinif 2006; Willems et al. 2007a) and England (Farrant and Smart 2011).

2. Context and methodology

In the NWPB, caves and karst conduits are found in Cenomanian to Campanian chalk formations. The Upper Cretaceous chalks are covered by surface formations including from bottom to top: (i) Pliocene–Quaternary clay with flints (CWF), produced by atmospheric weathering of chalk (Quesnel et al. 2000; Laignel et al. 2002), (ii) Tertiary detrital deposits occurring as pockets at the top of CWF (Auffret et al. 1975), and (iii) Quaternary loess (Lautridou 1985).

The three studied sites are located in the NWPB, in the North of the Haute-Normandie region (Fig. 1). The Upper Cretaceous chalk formations of this region are subject to current or fossil karstification and voids may be filled by sediments. The three selected sites can be defined as undercovered karsts, covered with unkarstifiable/insoluble layers, which not prevent the limestone to be weathered

(Salomon et al. 1995; Salomon 2006). According to classification of Nicod (1992), under-covered karsts may have alterite coverage.

2.1. Presentation of study sites

The studied sites are karst systems without current flooded network.

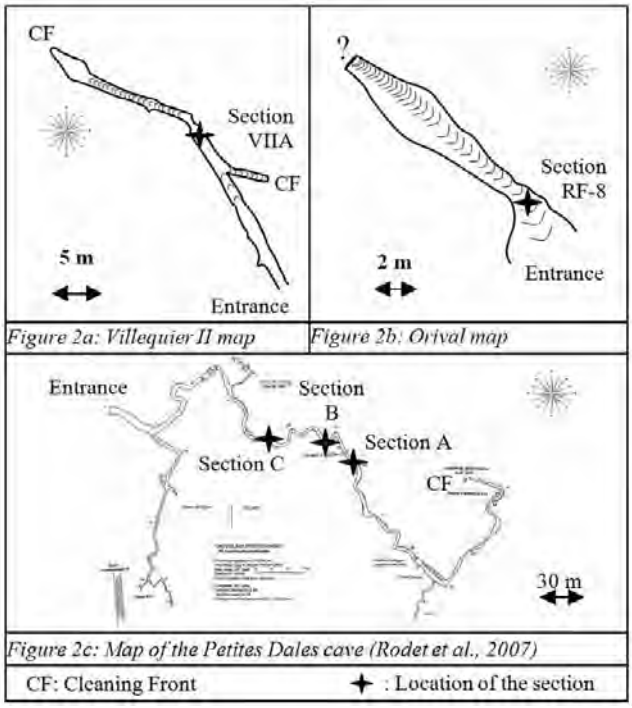

Figure 2a: Villequier II map

Figure 2b: Orival map

Figure 2c: Map of the Petites Dales cave (Rodet et al., 2007)

Figure 2. Map of the studied caves: Villequier II, Orival and Petites Dales.

Villequier II site (Fig. 2a)

The Villequier II gallery is located in Villequier (N49°29'45.2" E 000°39'48.9"; Z +8 m a.s.l). This gallery of 34.5 m length, develops in the white chalk of Upper Coniacian at the base of a 30 m high cliff. According to the spatial distribution of superficial deposits in the Western Paris Basin (Laignel 1997, 2003), the area include Saint-Eustache and Lozere sands, but also CWF (2–4 m) and lœss (<0.5 m).

Orival RF8 site (Fig. 2b)

The Roche Foulon karst system develops in senonian chalk cliffs on the left bank of the Seine River, in the town of Orival (N49°19'08.7" E001°00'14.0"; Z +75 m a.s.l). These delimit the concave side of the Elbeuf-Oissel meander, downstream of the confluence of the Essarts/La Londe Valley (Rodet 1991). Walking by the GR2, regional hiking trail, an abandoned quarry and rock-shelter houses are observed and also many karst conduits, some of which revealing a sedimentary filling. The site called RF8 has been the subject of a sedimentary study (Rodet 1991). The RF8 section was taken over 1.36 m. According to the spatial distribution of superficial deposits in the Western Paris Basin (Laignel, 1997, 2003), the area include the Saint-Eustache, Lozere and Ypresian sands but also CWF (2–4 m) and lœss (<0.5 m).

Petites Dales site (Fig. 2c)

The Petites Dales Cave entrance is open in the Petites Dalles non drained valley, in the town of Saint-Martin-aux-Buneaux. This karst is very close to the sea-coast, at 1,200 m from the Channel border. The current access to the cavity is through the working face of an open chalk quarry into the NE valley slope (N49°48'94.8" E000°31'91.0"; Z +30 m a.s.l). The cavity does not have perennial flow; only re-flooding in the lower parts was recorded in 1995 and 2000. The gallery develops in the coniacian chalk with flint (Rodet and Viard 1996; Laignel et al. 2004).

The Petites Dales Cave, described by Rodet et al. (2007), consists in a main gallery, recognized over 710 m of development (Viard and Rodet 2011), with 10 m height (according to a core) and a width of 2 to 5 m (maximum width in the karst entrance). It is the most important cave of the Seine Maritime department. The main axis shows a succession of rectilinear and sinuous sections. In this axis, three secondary drains join the main one. The drains morphology gives evidence of an evolution from an anastomosed network which was reduced to a main collector by concentration of drainage. According to the spatial distribution of surperficial deposits in the Western Paris Basin (Laignel 1997, 2003), the area include Saint-Eustache and Lozere sands, but also CWF (6–8 m) and lœss (>5 m).

2.2. Methodology

The initial contact with the sedimentary fillings was made with section surveys representative of the sites. Both the color and texture of the sediments were described. The color was determined from the Munsell soil color chart. Units were defined integrating relatively homogeneous sedimentary facies in terms of color, components and grain size. Sampling was then performed for grain-size and geochemical analysis.

Grain sizes were performed by using the laser particle size analyzer LS230 BECKMAN-COULTER in the Laboratory of Continental and Coastal Morphodynamics (M2C) of the University of Caen. The results are expressed as percentages of sand (>63 µm), silt (63–4 µm) and clay (<4 µm). Geochemical analyses were performed by the SRAM laboratory at CRPG-CNRS (Center of Petrographic and Geochemical Research), at Nancy. Major elements were measured by emission spectrometry (ICP-AES) Jobin Yvon JY-70® and absorption spectrometry (ICP-MS) Perkin-Elmer ELAN 5000 and 6000®. Three major elements were used for the present study (SiO_2, Al_2O_3, Fe_2O_3. They are given in mass percent.

Flow velocities were determined with Hjulström diagram using the 95 percentil of grain size samples.

3. Lithological characterization of the karst sedimentary fillings

3.1. Observations of the karstic sediment fillings

In Villequier II Cave, a section of 67 cm was survey in the middle of the gallery. The filling of the section VIIA has a

vertical organization with alternating beds of variable thickness, in the order of 1 mm to 14 cm. The fill is dominated by pale beige sands 10YR/8/3 (VIIA2 and VIIA5) to beige 10YR/7/3, which can be a little more silty (VIIA3). Stratifications are observed that can be crossed (VIIA3) or slightly oblique to sigmoidal (VIIA6). Seven units were identified on the section VIIA. In these units, three main kinds of sediments are distinguished (Table 1).

In the Petites Dales cave, three sections were surveyed in the middle of the gallery. The height of the A, B and C sections was measured respectively at 160 cm and 126.5 cm and 217 cm. The sediments of the three sections are vertically organized in beds of different thicknesses (0.1 to 20 cm) with a rhythmicity in millimetre to centimetre scale. The A and B sections consist of 14 units each and 13 have been identified in the C section. A similar filling was observed between A and B sections and a stratigraphic continuity can be underlined with the C section thanks to a benchmark of calcite. On A, B and C sections, three main kinds of sediments are described (Table 1). In addition, a coarse sand unit is also only observed at the base of C section.

In the Orival site, the RF8 section, of 138 cm high, was surveyed. The filling has a vertical organization of alternating beds with variable thickness: in the order of 1 mm to 22 cm. Fifteen units were found in the very heterogeneous filling. The section includes silty beds (e.g., RF8-8, RF8-6) and heterogeneous medium to coarse sand, more or less clayey, sometimes with beds of rounded quartz (RF8-15). According to Laignel (2003), such a sediment is characteristic of Lozere sand facies. In some units, pieces of flint can be found in a silty matrix (RF8-10, RF8-8 in particular). Three kinds of sediment were identified in this section (Table 1) with the presence of reddish Lozere sands facies in the filling (RF8-13).

Table 1. Lithological characterization of karstic fillings and origin of sediment sources. Main source of sediment in the filling in bold.

Site	**Villequier II**			**Petites Dales**			**Orival**		
Kind of sediment	Pale beige sands	Pale beige silty sands	Brown sandy silts	Pale beige silts	Beige silts	Brown clayey silts	Lozere sands facies	Sands to silty sands	Silts
Samples	VIIA2, VIIA6, VIIA7	VIIA1, VIIA5	VIIA3, VIIA4	A12, B10, B12	A1, A2, A5, A6, A8, A9, A11, B1, B4, B6, B7, B9, B11, B14	A4, A7, A10, B3, B5, B8, B13	RF8-15 RF8-13	RF8-12, RF8-7, RF8-5, RF8-3, RF8-2	RF8-14, RF8-11, RF8-10, RF8-9, RF8-8, RF8-6, RF8-4, RF8-1
Clay (%) (0–4 µm)	0.6 to 0.9	1.9–2.2	3.1–3.4	0	0–0.4	0.0–1.7	1.0–1.3	1.0–2.5	4.6–23.9
Silt (%) (4–63 µm)	6.9–12.4	26.2–32.2	50.7–63.4	76.5–93.1	81.1–99.8	86.5–99.7	12.5–12.9	11.8–47.8	49.5–93.2
Sand (%) (63–2000 µm)	86.8–92.5	65.8–71.6	33.5–45.9	6.9–23.5	0.1–18.9	0.3–11.7	86.0–86.2	49.7–87.3	1.7–44.5
SiO_2 (%)	97.0–97.8	95.7–96.0	94.0–94.9	90.6–91.2	85.0–89.9	79.0–81.7	83.4–83.8	88.7–91.5	76.3–88.9
Fe_2O_3 (%)	1.4–1.9	2.8–3.0	3.6–4.2	6.5–7.0	7.3–10.5	13.0–14.9	9.2	4.3–7.9	7.4–15.7
Al_2O_3 (%)	0.8–1.1	1.2–1.3	1.6–1.8	2.3–2.4	2.7–4.4	5.3–6.1	7.0–7.4	2.9–4.2	3.3–8.2
Flow velocity sedimentation (cm/sec)	1.7–2.5	0.9–1.5	0.7	1.0–1.6	0.9–1.1	0.4–0.5	9.1	5.2–6.3	0.3–1.2
Sediment origin	**Saint-Eustache sands**	**Indeterminate sands**, Saint-Eustache sand	**Indeterminate sand / læss mixture**	**Læss,** Saint-Eustache sands	**Læss**	**Læss**, weathered chalk	**Lozere Sands**	**Undetermined sands**, læss	**Læss** undetermined sand, clay-with-flints
Surrounding surface formations	Saint-Eustache sand, lozere sand, læss, clay-with-flint, chalk			Læss, lozere sand, Saint-Eustache sand, clay-with-flints, chalk			Lozere sand, Saint-Eustache sand,Ypresian sand, clay-with-flints, læss, chalk		

3.2. Grain size distribution and geochemical characterization of the karstic sediment fillings

In the Villequier II site, the main grain size of the filling is sandy to sandy silt (Table 1). We have a fairly significant heterogeneity in the filling: values are rather different in Table 1. The clay content could be described as "background noise" with a ratio between 0.64 % to 6.42 %. The particle size confirms the observations with the exception of two samples, VIIA3 is really sandy silt rather than silty sand and VIIA5 is silty sand instead of sandy. Geochemistry of the filling is very siliceous: the values of SiO_2 are above 94 % for all samples. The contents of Fe_2O_3 and Al_2O_3 are very low and do not exceed 4 % and 1.8 % respectively. The values are very narrow, indicating a homogeneous geochemical composition (Table 1). The coarser the sediment, the higher percentage in SiO_2.

Samples from the A section of Petites Dales are silty with values greater than 75 % silt, and more than 80 % of silt to B section (Table 1). The grain-size distribution variations are weak between samples. Observations and grain-size analyze point out a homogeneity between the A and B sections. Geochemical characteristics of sediments from the B section reveal that these are highly siliceous with values above 79 % for all samples. The Fe_2O_3 contents begin to be

significant for samples B13, B3 and B8 with percentages of 13–15 %. For Al_2O_3, levels are low and do not exceed 6 %. Such values also likely indicate a relative homogeneity in the filling. For each kind of sediment, a slight geochemistry difference appears. Once again, the coarser the sediment, the higher the percentage in SiO_2.

The Orival sedimentary filling is heterogeneous with grain size ranging from sandy to silty (Table 1). The clay percentage is higher than in the two other sites, even if clay is less than 10 % for most samples. In addition, four samples have percentage between 10 and 25 %. The grain size confirms the observations with the exception of two samples which are really silty clay instead of silt (RF8-4, RF8-8). The filling is very siliceous, with SiO_2 values above 76 % for all samples. The analysed section reveals a relative homogeneity but values are a little more scattered than Petites Dales and Villequier II (Table 1). The contents of Fe_2O_3 and Al_2O_3 are most often below 10 % (except for RF8-08, RF8-10, RF8-06 respectively 15.7 %, 14.2 % and 11.7 % in Al_2O_3). For each kind of described sediment, a slight geochemistry difference is again observed. The coarser the sediment, the higher the percentage in SiO_2, with the exception of the sediment with Lozere sand facies. The latter have high levels of Fe_2O_3 and Al_2O_3 (respectively 6.96 % to 7.42 % and 9.17 % to 9.24 %).

3.3. Lithological synthesis of the karstic sediment fillings

All the sediments from the studied karst fillings are dominantly siliceous, fine, mostly silty sediments, but can also be sandy and poor in clay (Table 1). Each filling has a relatively characteristic grain size: sediments of Petites Dales are mainly silty whereas those of Villequier II are primarily sandy. The Orival site presents the most heterogeneous filling, with the most variable size including sandy to silty clay samples. For each site, three kind of sediments are found, each of them having its own grain size and geochemistry properties. A similarity in the sedimentary organization is noticed between the three studied karst fillings, with variable thickness of horizontal beds as well as rhythmicity. Nevertheless, there is an inter-site variability based on the nature and origin of sedimentary material.

4. Sources of the karst sediments

According to the geological context of the three sites described above, several sediment sources are possible: (i) læss, CWF and residual Tertiary sandy deposits (i.e. Lozere, Saint Eustache and indeterminate sands) through mechanical erosion, and (ii) insoluble residue of chalk through chemical weathering of the bedrock. Once deposited in karst, the insoluble residue of chalk is considered autochtonous (endogenous) deposits, whereas læss deposits, CWF and Tertiary sandy deposits are allochtonous (exogenous). The terms “endogenous” and “exogenous” correspond to the Ford and Cullingford English classification (1976) in Ek and Quinif (1988).

In order to determine the likely sources, of each kind of karstic sediments, geochemical data have been used and compared (karstic fillings, surface formations, chalk; Fig. 5), in addition to field observations and grain size data.

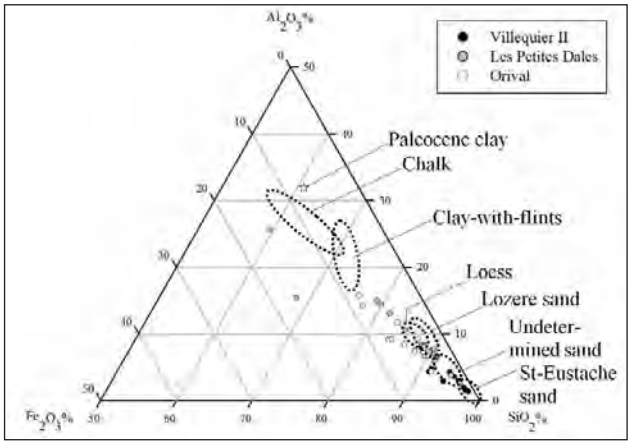

Figure 3. Ternary plot of the geochemistry of the potential sedimentary sources and of Villequier II, Petites Dales and Orival karstic sedimentary fillings.

For each site, a summary of what surface deposits could be at the origin of the filling was made (Table 1). The results given by the geochemistry (Fig. 3) are in the penultimate line, the main source is in **bold**. It appears that loess is the main source of fillings, but in varying proportions, explaining a relative homogeneity of fillings. Nevertheless, the characterization shows both an intra and inter-site variability. The latter is partly explained by the presence of several sediment sources in addition to loess, such as the Saint-Eustache, Lozere, and indeterminate sands, but also possible *in situ* alteration of chalk, even if in very small quantities (on a single site).

The surface deposits are constitutive of the karst fillings, but in different proportion. For the Petites Dales, the filling mainly consists of three kinds of surface deposits whereas five are present in the watershed. Loess is found in each site, but in varying proportions, in relation to its large coverage of the NWPB (Laignel 2003). By contrast, the Tertiary sands are only present as pockets, which are covered by loess. Saint-Eustache sands are present in the watersheds of the three sites, however they are present in only two fillings (Villequier II and Petites Dales). The same observation is made for the Lozere sands, present in all three watersheds, but only found in the Orival filling. Two conditions may explain the presence of one type of Tertiarty sands, i.e. a pocket that is intersected by the karstic network, in addition to specific hydrodynamic conditions allowing erosion, transport and deposition of Tertiary sands in karst conduit.

CWF are made of flint packed in a clayey silty sand matrix, whose proportions of the different constituents vary from one site to another, covering a very large part of the NWPB (Laignel 1997; Laignel et al. 1998, 2002; Laignel 2003). Such components are however absent in the fillings, even if solution pipes are observed, forming the input karst which cut the output karst network. Because of its nature, CWF is very cohesive then difficult to be eroded (Laignel 1997; Quesnel et al. 2000). If CWF drown downward solution pipe into the karstic network, they tend to stay *in situ*. Only the most erodible particles, such as læss (Le Bissonnais 1988) and sands (if a pocket is connected with a solution pipe) will undergo transport and deposition in the endokarst.

We agree with the hypothesis of Laignel et al. (2004) to explain the absence of CWF in significant proportions in

the fillings. Therefore, our results do not reach those of Sweeting (1973), suggesting that clay particles come from erosion of CWF. Our studies are consistent with those of Reams (1968) showing that clay have two possible origins: the *in situ* alteration of the chalk in the endokarst and/or arrivals of surface sediments by mechanical erosion.

To summarize, the most erodible sediments are primarily deployed in the karst network. Different sediment origins partly explain the variability between each site. Within a single site, sediment origin is probably not the only cause of the variability of the filling. Another parameter influences intrakarstic sedimentation, especially hydrodynamic conditions.

5. Discussions and conclusions

Karsts of NWPB present introduction forms as sinkholes (Laignel et al. 1997; Quesnel et al. 2000) and current or ancient restitution forms, as springs or caves (Rodet 1991; Laignel et al. 2004; Hanin et al. 2011). Ancient karst systems could be filled depending on the hydrodynamic conditions and sediment sources. Sedimentary fillings characterization is essential to understand sediment dynamics in endokarst (Coquerel et al. 1993; Laignel et al. 2004; Hanin et al. 2011) and also to determine the paleoenvironmental conditions in a given area.

Karst fillings from NWPB are made of surrounding superficial formations, from clayey silt to coarse sandy material, according to the sediment sources and the hydrodynamics in karst (Laignel et al. 2004). Studies in the North-East Wallonia (Belgium) have shown the same kind of karst introduction (solution pipes) associated with filled caves (Van Den Eeckhaut et al. 2007; Willems et al. 2007a, 2007b; Rodet et al. 2009). Fillings mainly consist in silty to sandy particles as examplified by the Montagne Saint Pierre (Willems et al. 2007a). The latter study has been shown that the filling is primarily made of sands and loess (surrounding surface formations) with also slight proportion of residual material from chalk alteration.

South-East of England has similar forms of introduction as NWPB and North-East Wallonia like solution pipes and cave fillings with similar size particles (Cooper et al. 2011). Farrant and Smart (2011) have also shown that filling is partly composed from surrounding surface formations with also residuals from chalk alteration.

To conclude, a sedimentological characterization of karst fillings allows determinating sediment sources. By comparing the sediment fills and the surface formations several sources were identified in studied caves: surface formations (Tertiary sand, clay-with-flints, and lœss) and insoluble of residual alteration of chalk bedrock. A similarity is apparent between karst of the NWPB and that of NWE when considering (i) karst morphology, (ii) sediment fillings, and also (iii) particle sizes of the allochtonous material. One of the future perspectives is notably to apply GIS to the study of karst, e.g., in integrating data concerning surrounding surface formations and to draw comparisons between caves from different regions of the NWE. Such study should also be associated with large sedimentological analyses and when possible, accurate dating of the endokarstic deposits.

Acknowledgement

We wish thank the members of CNEK (Centre Normand d'Étude du Karst – http://www.cnek.org/) for their outstanding work at the Petites Dales cave. More than twenty years of cave excavation until today for the access to the site. Thank for keeping the history of works in referenced pictures archives. Thanks to the SCALE and the Upper Normandy Council for the study grant allocation.

References

Auffret JP, Bignot G, Blondeau A, Cavelier C, Pomerol C, 1975. Geologie du Bassin Tertiaire de la Manche Orientale au Large du Pays de Caux [and Discussion], Philosophical Transactions of the Royal Society of London. Series A, Mathematical and Physical Sciences, 279(1288), 169–176.

Cooper AH, Farrant AR, Price SJ, 2011. The use of karst geomorphology for planning, hazard avoidance and development in Great Britain. Geomorphology, 144, 118–131.

Coquerel G, Lefebvre D, Rodet J, Staigre J-C, 1993. La grotte du Funiculaire. Spéléogenèse et étude d'un remplissage ferro-manganique. Karstologia, 22(2), 35–42.

Cyrek K, Socha P, Stefaniak K, Madeyska T, Miroslaw-Grabowska J, Sudol M, Czyzewski L, 2010. Palaeolithic of Bisnik Cave (Southern Poland) within the environmental background, Quaternary International, 220(1–2), 5–30.

Ek C, Quinif Y, 1988. Les sédiments détritiques des grottes: aperçu et synthétique. Annales de la Société Géologique de Belgique, 111, 1–7.

Falguères C, Bahain J-J, Yokoyama Y, Bischoff JL, Arsuaga JL, De Castro JMB, Carbonell E, Dolo J-M, 2001. Datation par RPE et U-Th des sites pléistocènes d'Atapuerca: Sima de los Huesos, Trinchera Dolina et Trinchera Galeria. Bilan géochronologique. L'Anthopologie, 105, 71–81.

Farrant AR, Smart PL, 2011. Role of sediment in speleogenesis; sedimentation and paragenesis. Geomorphology, 134, 79–93.

Ford TD, Cullingford CHD. 1976. The science of speleology. London Academic Press.

Hanin G, Laignel B, Massei N, Hauchard E, Ladhui V, Chédeville S, 2011. Hydrological variations and sediment transfer in a karst system (Radicatel springs, Upper Normandy, France) controlled by climate fluctuations. Proceedings of Hydrology & Hydrogeology of the Karst, 9th Conference on Limestone Hydrogeology, Besançon (France), 221–224.

Laignel B, 1997. Les altérites à silex de l'ouest du bassin de Paris: caractérisation lithologique, genèse et utilisation potentielle comme granulat., Thèse de Doctorat, Université de Rouen, édition BRGM, Orléans, France.

Laignel B, 2003. Caractérisation et dynamique érosive de systèmes géomorphologiques continentaux sur substrat crayeux. Mémoire de HDR., Université de Rouen.

Laignel B, Dupuis E, Rodet J, Lacroix M, Massei N, 2004. An example of sedimentary filing in the chalk karst of the Western Paris Basin: characterization, origins and hydrosedimentary behaviour. Zeitschrift für Geomorphologie, 48(2), 219–243.

Laignel B, Quesnel F, Meyer R, 2002. Classification and origin of the clay with flints of the Western Paris Basin (France). Zeitschrift für Geomorphologie, 46(1), 69–91.

Laignel B, Quesnel F, Meyer R, Macaire J-J, 1998. Relations quantitatives entre les craies à silex et les formations résiduelles à silex de l'ouest du Bassin de Paris, Geodinamica Acta, 11(4), 171–181.

Laignel B, Quesnel F, Spencer C, 1997. Une nouvelle ressource en granulats: les formations résiduelles à silex, Géochronique, 63, 9–10.

Lautridou J-P, 1985. Le cycle périglaciaire pléistocène en Europe du Nord-Ouest et plus particulièrement en Normandie. Thèse de Doctorat d'Etat, Université de Caen.

Le Bissonnais Y, 1988. Analyse des mécanismes de désagrégation et de la mobilisation des particules de terre sous l'action des pluies. Thèse de Doctorat es Sciences, Ecole Doctorale I.N.R.A., Université d'Orléans.

Losson B, Corbonnois J, 2006. Les modes de sédimentation détritique: nouvelle méthode de détermination appliquée à des remplissages endokarstiques. Geologica Belgica, 9(3–4), 257–265.

Madeyska T, 2002. Evidence of climatic variations in loess and cave palaeolithic sites of Southern Poland and Western Ukraine. Quaternary International, 91(1), 65–73.

Mangin A, 1975. Contribution à l'étude hydrodynamique des aquifères karstiques. Thèse de Docteur en Sciences, Université de Dijon 1975; Annales de Speléologie, 1974, 29, 3, 283–332; 1974, 29, 4, 495–601; 1975, 30, 1, 21–124.

Nicod J, 1992. Les karsts sous couverture (sableuse, argileuse et/ou détritique) en France, d'après des travaux récents. Cuadernos de Seccion, Historia, Donastia: Eusko Ikaskuntza, 20, 165–185.

Quesnel F, Laignel B, Bourdillon C, Meyer R, 2000. Les altérites à silex de Seine-Maritime (France): typologie, chronologie et géodynamique. Bulletin d'Information des Géologues du Bassin de Paris, 37(1), 17–31.

Quinif Y, 2006. Complex stratigraphic sequences in Belgian caves correlation with climatic changes during the middle, the upper Pleistocene and the Holocene. Geologica Belgica, 9(3–4), 231–244.

Reams MW, 1968. Cave sediments and the geomorphic history of the Ozarks. Ph.D. thesis, Washington University, St Louis, Missouri.

Rodet J, 1991. Les karsts de la craie: étude comparative. Thèse de Doctorat d'Etat, Université de Paris IV-Sorbonne.

Rodet J, Viard J-P (eds.), 1996. La grotte des Petites Dales, Spéléo-Drack.

Rodet J, Laignel B, Brocard G, Dupuis E, Massei N, Viard J-P, 2006. Contribution of a sedimentary study to the concept of karstic evolution of a chalk cave in the werstern Paris Basin (Normandy, France), Geologica Belgica, 9(3–4), 287–296.

Rodet J, Viard JP, Poudras J, 2007. À la découverte de la grotte des Petites Dales (Saint Martin aux Buneaux, Seine Maritime, France), Spéléo-Tract.

Rodet J, Willems L, Brown J, Ogier-Halim S, Bourdin M, Viard J-P, 2009. Morphodynamic incidences of the trepanning of the endokarst by solution pipes. Examples of chalk caves in Western Europe (France and Belgium). Proceedings of the 15th International Congress of Speleology, Kerrville (Texas, USA), 19-26 july 2009, UIS, vol. 3, contributed papers: 1657–1661.

Salomon JN, 2006. Précis de karstologie, 2ème ed., Presses universitaires de Bordeaux, Collection Scienteren.

Salomon J-N, Pomel S, Nicod J, 1995. L'évolution des cryptokarsts: comparaison entre le Périgord-Quercy (France) et le Franken Alb (Allemagne). Zeitschrift für Geomorphologie, 39(4), 381–409.

Sweeting MM, 1973. Karst landforms. Mc Millan, London.

Van Den Eeckhaut M, Poesen J, Dusar M, Martens V, Duchateau P, 2007. Sinkhole formation above underground limestone quarries: A case study in South Limburg (Belgium). Geomorphology, 91(1–2), 19–37.

Viard JP, Rodet J, 2011. Seine-Maritime: Grotte des Petites Dales, Saint-Martin-aux-Buneaux. Spelunca, 122(5), 0242–1771.

Willems L, 2000. Phénomènes karstiques en roches silicatées non carbonatées. Cas des grès, des micaschistes, des gneiss et des granites en Afrique sahélienne et équatoriale. Thèse de Doctorat, Université de Liège (Belgique).

Willems L, Rodet J, Ek C, Dusar M, Lagrou D, Fournier M, Laignel B, Pouclet A, 2007a. Karsts des craies et calcarénites de la Montagne Saint-Pierre (Basse Meuse liégeoise). Bulletin des Chercheurs de la Wallonie, 46.

Willems L, Rodet J, Fournier M, Laignel B, Dusar M, Lagrou D, Pouclet A, Massei N, Dussart-Baptista L, Compère P, 2007b. Polyphase karst system in Cretaceous chalk and calcarenite of the Belgian-Dutch border. Zeitschrift für Geomorphologie, 51(3), 361–376.

SANDSTONE CAVES IN THE SYDNEY BASIN: A REVIEW OF THEIR CULTURAL AND NATURAL HERITAGE

John R. Dunkley
5 Coleman Street, Pearce ACT 2607, Australia, jrdunkley@gmail.com

Small caves are found throughout the onshore Sydney Basin, but an inventory of over 1,100 has only recently been compiled for the database of the Australian Speleological Federation Inc. Aboriginal sites have been studied for a century, but only a few academic studies of the development of the caves and karst features have been highlighted in recent research findings. Most caves are clustered low in the landscape, close to watercourses and to urban areas, and exhibit a variety of distinct processes: marine action, piping, block-gliding and other forms of mass movement, waterfall retreat, lateral meandering and deep canyon incision. In total they attract large numbers of visitors. They are, nevertheless, largely underappreciated and underestimated in cave and karst literature and by heritage managers, as well as by recreational cavers. On balance, the caves are of importance mostly for their association with human activity. However some contain unusual features such as silicate and other deposits worthy of research and proper management.

1. People and Landscape

Caves are scattered widely throughout the onshore 36,000 km² of the Sydney Basin in some of the planet's most spectacular landscapes, including World Heritage Areas which, however, gained that status primarily for their natural biological values. Most are small but over 1,100 are recorded as greater than 3m in length in the database of the Australian Speleological Federation Inc., the longest being 263 m (Dunkley, in press). Their density varies considerably, from less than one per 100 km², up to 3–4 per km². Most are clustered low in the landscape, beside or on mid-slopes above watercourses, some in the middle of the Sydney metropolitan area. The higher, usually drier sandstone ridges have few caves. Sandstone covers over 30 % of the Basin and most of that is in the quarter of the Basin that is almost uninhabited national park and declared wilderness. Yet about 800 caves lie within at most a 30-minute drive and 20 minutes walking distance, of the population (nearly 6 million people) in the Greater Sydney urban region. Indeed many are in valleys within the metropolitan area. Although mostly small, in total the caves may attract more visitors, albeit fleetingly and only occasionally as a specific destination, than all the well-known limestone caves in the state combined.

Figure 1. Characteristic landscape of upper Blue Mountains. Caves typically occur near breaks of slope, mainly near the edge of the plateau, often in canyons.

Aboriginal sites have been studied for a century, and although a few academic studies of karst and caves have occurred (e.g., Johnson 1974; Wray 1993, 1995; Young et al. 2009), these features are consistently underappreciated and underestimated in cave and karst literature and by natural heritage managers, as well as by recreational cavers, the last perhaps because their speleological pedigree is not recognised. The inventory includes about 114 sea caves, 20+ block-gliding caves, 40+ in narrow, deep and often dark canyons, 30–40 with unusual iron and silica concretions, and 2 stream caves. In addition, at least 200 contain evidence of Aboriginal occupation; 45 have white historical associations; 25 were used for a period as homes, mainly by destitute people in the last century; 23 are camping caves used by bushwalkers; 20 are connected with bushranger legends; 20 are used for rock climbing and bouldering; 14 inspired poetry, music or art, and 10 or 20 contain glow worm populations.

1.1. Aboriginal significance of caves

The oldest of about 200 Aboriginal occupation cave sites dates back 22,000 years, and a further 100+ have been identified which, by location, size and aspect are potential aboriginal sites. For a century after white settlement, passing scientists just observed and described Aboriginal people and their customs, taking little interest in their cave sites and less in prehistory. Nearly a century passed before serious studies were undertaken of cave art sites and properly documented and scientifically executed excavations were undertaken. Even then, much of the work was undertaken by professional polymaths from other fields such as geology (Edgeworth David), palaeontology (Robert Etheridge) and surveying (R.H. Matthews), the last of whom apparently studied 50 caves and 70 rock art sites. In recent years Australian archaeology has been revolutionised by many more qualified archaeologists, and intensive studies have been undertaken in restricted areas in military reserves and water catchment areas, aiding site conservation. Attenbrow (2002) provided a comprehensive review. Important caves continue to be identified in remote areas of Wollemi and other national parks and there are undoubtedly many more awaiting rediscovery.

Figure 2. A former Aboriginal habitation site below houses in the Sydney metropolitan area, now used by walkers and bouldering enthusiasts.

1.2. European perspectives and perceptions

First Fleet settlers recorded Aboriginal life in caves around Sydney Harbour from the day they arrived in January 1788. A few caves gained historical significance when recorded during the first attempts to cross the Blue Mountains, in one case settling a long debate about an explorer's route. About 20 caves are named after known or alleged early outlaws (called bushrangers in Australian legend), or in connection with other illegal activity such as stills and stolen goods. Then for many years the sandstone around Sydney became country to be hurried across rather than settled, and for nearly a century caves were used to house military guards, road gangs, railway and other itinerant builders and workers. Partly as the result of gold rushes, by the 1880s Australia was a wealthy country and railways began to deliver tourists to these wild landscapes. Over the next 50 years wealthy landowners, hotel entrepreneurs and local councils constructed walking tracks totalling 300 km in length to pleasant sights (Smith 1999), including numerous small caves which in turn acquired romantic or fanciful names, and which appeared on postcards and souvenir books. The early reservation of sites such as Mermaids Cave at Blackheath in 1882 began a period during which, eventually, nearly all sandstone caves in the region would remain in public ownership. However, after 1935 many such caves were forgotten or neglected, but most trails have survived because the more rugged land became incorporated into public reserves and later national parks.

Over 30 caves are known to have been used for bush camping by walkers and climbers, and most still are, especially in rugged country more than a day's walk from roads. Some caves were appropriated as weekend and holiday retreats by walkers, fishermen and others, and partly as a result have inspired works by writers, poets, artists and musicians. A number were used as permanent homes by recluses and the indigent, especially in the early 20th century and during depression years. As recently as 2011 inhabitants of several caves in Royal National Park on the southern outskirts of Sydney were removed by authorities.

In recent decades the sports of rock-climbing, bouldering and canyoning have flourished throughout the region, especially in the upper Blue Mountains. At least 20 caves are used by climbers, some with fixed climbing routes. Caves in the splendid deep and narrow canyons are less frequented and more robust because of regular flooding.

2. Geology and Landscape

Most caves are developed in either the Middle Triassic Hawkesbury Sandstone, or the Early Triassic Narrabeen Group of massive sandstones interbedded with claystones and shale. Beyond the Cumberland Plain of Sydney's metropolitan area, outcrops of the former are dominant over most of the coastal zone and from the Southern Highlands district to ridges north of the Hawkesbury River, while the latter predominate in the upper Blue Mountains west of Woodford. Block-gliding caves occur in a smaller area of Permian Shoalhaven Group sandstones near Nowra. Current research suggests that uplift of all these rocks occurred no more recently than the early Palaeogene period,

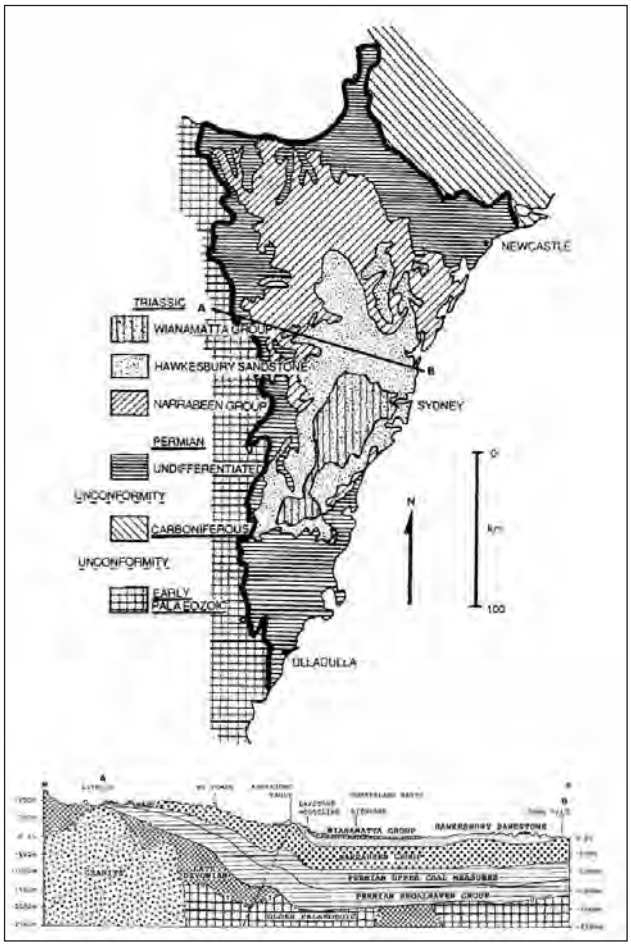

Figure 3. Sydney Basin showing location of Hawkesbury, Narrabeen and Shoalhaven groups of sandstone. Cross-section AB is from Lithgow to Mona Vale, near Sydney.

at least 65 Ma, after which the area has been relatively stable. Rivers maintained their courses, eroding deep gorges in relatively level plateaux surrounding Sydney.

Over 100 sea caves up to 100 m+ long are developed extensively in cliffs lining most of the coastal exposure of Sydney Basin rocks north and south of the city, some being essentially eroded dykes of mostly Neogene age. There are no known volcanic caves.

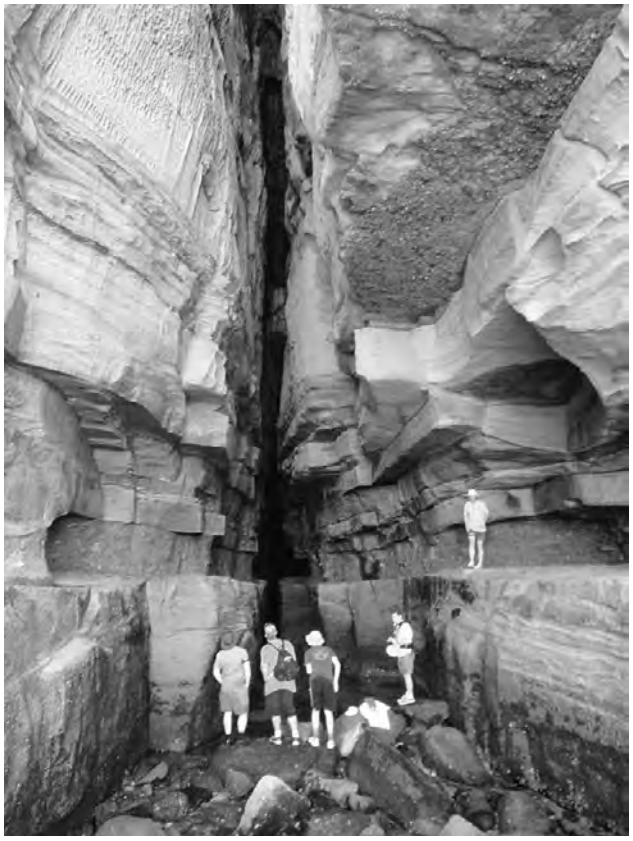

Figure 4. Typical sea cave at Avalon, near Mona Vale.

In the Nowra Sandstone of the Shoalhaven Group there are at least 25 block-gliding caves up to 240 m long in riverside cliffs, probably primarily the result of rock deformation and sliding on a clay base, and a few other mass-movement caves have been identified from this study elsewhere in the region.

In the Hawkesbury and Narrabeen sandstones most caves are similar in form and at least partly solutional in origin. In the Narrabeen Group caves are commonly associated with knickpoints, waterfalls and intercalated beds of claystone, and at least 40 or 50 are found in deep, narrow and often quite dark canyons, which in some cases are no more than a metre wide at base. The paucity and lenticular nature of such beds in the Hawkesbury Sandstone produces few canyons but simpler and still numerous caves.

The growing evidence of solutional activity in non-carbonate rocks such as quartz sandstone is discussed in Young et al (2009), the authors of which carried out extensive work in the Sydney Basin.

A variety of karst-like surface features exists. Minor solution forms such as grikes and runnels occur, and solution basins (gnammas) were important sources of water for Aboriginal groups, especially on the dry, higher ridges. Ruiniform landscapes resembling ruined cities and towns are developed extensively in the Narrabeen Group, particularly above Wolgan Valley and in Gardens of Stone National Park, both with small caves usually at the base of sandstone towers locally called pagodas, analogous to remnant towers in limestone country (Washington and Wray 2011). Also in the Narrabeen Group are most of the 40+ deep canyons, some over 100 m deep, often with waterfalls associated with knickpoints. Nearly all incorporate lateral incision caves, especially where the canyon intersects a claystone bed. About a dozen natural bridges, some across streams, are recorded.

2.1. Formation, enlargement and age of the caves

There is a long-entrenched popular belief that these caves (other than the sea caves) are formed by wind, sandblasting or at least by enlargement upwards due to convectional air currents. There is no evidence of this. Their real origin, well established for many years, is through the essential "trigger" role that solution plays in initiating caves and enabling them to enlarge. The host rocks are commonly characterised by matrices of silt, clay and soluble cements such as iron carbonate (siderite). The process commences with naturally acidic water (percolating from swamps carrying organic acids in the upper Blue Mountain) interacting with and removing the matrix. Hydration then releases iron, silica and other elements. The rock becomes less coherent and more susceptible to physical disintegration, and the grains disaggregate, fall or are washed away. Enlargement then takes place due to the interrelationship between the high permeability and higher rates of weathering in the less coherent interior, which weathers chemically faster than the entrance and surrounding case-hardened surface rock (Johnson 1974). Salt is not as active a factor in the Sydney region as commonly believed, and its presence assists chemical rather than mechanical processes (Young 1987).

Field studies show that this process is very slow. However sufficient time has been available in the Sydney Basin since the end of the Triassic. Indeed, it may be that these caves can form only BECAUSE the process is so slow. If water movement through the rock matrix were too rapid, widespread surface lowering would occur. Hughes and Sullivan (1983) suggested that natural rate of cavern growth is generally less than 2 to 5 mm / 1,000 years. On this basis, it seems likely that some caves are of the order of at least a few million years old.

2.2. Types of caves

In addition to sea caves and mass-movement caves, several overlapping types of solutional and non-solutional caves are apparent: undercuts, lateral meanders and incisions, piping caves, those associated with waterfalls, a small number of through stream caves, caves in deep narrow canyons, and other small caves.

Undercuts, some quite long, are usually associated with relatively thin (2–3 m) beds or lenses of claystone or shale, sufficiently high above valleys that it is difficult to attribute them to old lateral stream incision. Lateral meanders and incisions are particularly common where streams have incised through one or more claystone beds, sometimes on the outside of tight, entrenched meanders. Only a few caves are located predominantly behind waterfalls, negating an origin due primarily to plunge pools. Much more often they form laterally downstream, possibly from spray and/or interstratal seepage, lengthening as the waterfall retreats. The longest cave, 263 m, is a horseshoe-shaped example of this. Small-scale piping is evident in many caves such as in the Budawang Mountains south of Nowra, but two in particular, at Kincumber and Leura, are clearly formed primarily by this process.

There are two excellent examples of through stream caves similar in all regards to those in limestone. The

Underground River at Blackheath resulted from a landslip filling a tight incised meander, forcing water through joints in the meander neck. Although a fossil dry valley exists nearby, Hill Top Cave at Mittagong appears to have formed by a combination of a relatively weak joint and upstream migration of a knickpoint.

2.3. Speleothems and Speleogens

The most widespread and characteristic forms are speleogens, notably cavernous weathering forms such honeycombing. Protruding plates of eroded bedrock are prominent in several caves, usually at a shallow sub-parallel angle to the back wall, for distances as great as a metre and invariably associated with cross-bedding. Their aesthetic attraction is enhanced by characteristic bands and swirls of iron staining of the sandstone, so that colour can vary from dark red and brown through orange and yellow to white.

Figure 5. Protruding bedrock plates (speleogens) in a Hawkesbury Sandstone cave north of Sydney.

Many are very vulnerable to damage and deserve closer management, informed by further research, documentation and discussions with local Councils and other management authorities.

Both carbonate and silicate speleothems are found, noticeably smaller than in limestone caves but still fairly common, including flowstone, cave coral, stalactites, stalagmites and small columns. A few caves in deep valleys with sheltered aspects facing east to south exude sticky gelatinous nodules presumed to be of partly dissolved limonite or other minerals, along with unidentified forms of what appear to be thin, parallel bands of mud stalactites possibly indurated with calcite, limonite and/or vegetation matter. Depositional minerals include carbonates of both calcium and iron, silicates, iron oxides, generic alum, alunite (potassium aluminium sulphate), and manganese. Secondary growths of both silica and carbonates long ago raised questions about origins (Osborne 1948; Lovering 1951).

3. Significance, Conservation and Management

Most caves are quite robust and have survived well, some having been used by humans for thousands of years, although evidence is that Aboriginal occupation did hasten

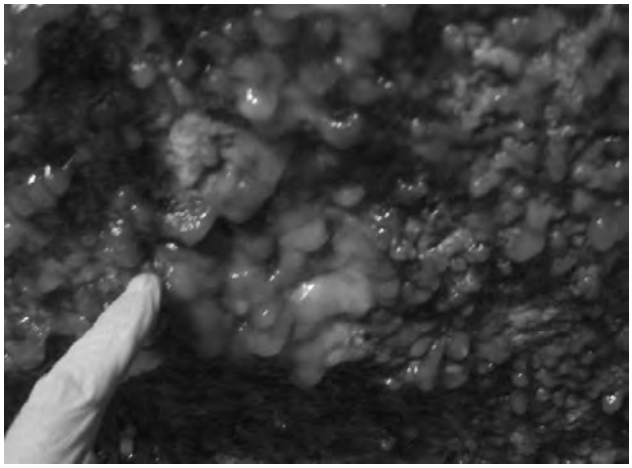

Figure 6. Gelatinous nodules containing suspected iron minerals in a cave near Blackheath.

deterioration of caves and art sites. Their location in the more rugged terrain along and on the steep slopes above water courses rather than on ridge tops also aided survival. Intensive research has concentrated on Aboriginal sites, such as that relating to survival of cave art sites (Hughes 1978). Many sensitive sites are protected only by lack of publicity and/or by their location in military and water catchment or remote and rugged areas. A few close to urban settlement have suffered inexcusable vandalism, but some protective measures are now in place. Caves with aesthetically pleasing, thin protruding bedrock plates are vulnerable, with no additional protective measures provided; the same applies to those with unusual mineral deposits. The greatest environmental pressure comes from urban development which has concentrated run-off and thus flooding, sedimentation, pollution, infiltration of garden and other chemicals, and has increased graffiti. Although improvements have occurred in recent years, geoheritage has not enjoyed high priority among management authorities, and important landscapes such as that of Gardens of Stone National Park have not been adequately studied. Further persuasion of responsible public authorities, both state and local, is called for.

The caves are worth celebrating primarily for their association with human life and endeavour, in other words, for their intangible cultural and heritage value. Some contain unusual features and deposits worthy of further research and proper conservation measures.

4. Acknowledgments

Field work was greatly assisted by members of Highland Caving Group, and advice on documentation procedures was provided by Peter Dykes. The paper benefitted from critical comments from Dr Susan White, Latrobe University, Melbourne, and by Cathy Brown, Geoscience Australia, Canberra. Photographs by author except for Fig. 4 (J. Sydney).

References

Attenbrow V, 2002. Sydney's Aboriginal Past. Univ. NSW Press, Sydney, 225.

Dunkley J, 2013 (in press). Caves, people and land: Sandstone caves of the Blue Mountains and Sydney Region. Australian Speleological Federation Inc., Sydney.

Hughes PJ, 1978. Weathering in sandstone shelters in the Sydney Basin and the survival of rock art. Proc. International Workshop on the Conservation of Rock Art, Perth, Sept. 1977, 36–41.

Hughes PJ, Sullivan ME, 1983. The geoarchaeology of the Sydney Basin sandstones. In Young, R.W. & Nanoson, G.C. eds. Aspects of Australian sandstone landscapes. Australian and New Zealand Geomorphological Group, Wollongong, 120–126.

Johnson ARM, 1974. Cavernous Weathering at Berowra, N.S.W. Aust. Geographer XII, 6. 531–535.

Lovering JF, 1951. The Mystery of the "Limestone" Caves in National Park. Aust. Museum Magazine, March 12, 1951. 155–157.

Osborne GD 1948. A Review of Some Aspects of the Stratigraphy, Structure and Physiography of the Sydney Basin. J.Proc.Linn.Soc.NSW 83 pts 1–2, 4–37.

Smith J, 1999. Blue Mountains District walking track heritage study: Historical report prepared for NSW National Parks and Wildlife Service. Heritage assessment & conservation guidelines prepared for NSW National Parks and Wildlife Service by MUSEcape Pty Ltd & David Beaver.

Washington H, Wray RAL, 2011. The Geoheritage and Geomorphology of the Sandstone Pagodas of the North-western Blue Mountains Region NSW. Proc.Linn.Soc. NSW 132, 131–143.

Wray, RAL 1993. Solutional Landforms on Silicates: largely ignored or simply unrecognised? In Proc. 19th Biennial Conf. Aust.Speleol.Federation, Launceston, 110.

Wray, RAL, 1995. Solutional Landforms in Quartz Sandstones of the Sydney Basin. PhD thesis, Univ. Wollongong, 381.

Young, ARM, 1987. Salt as an agent in the development of cavernous weathering. Geology 15, 962–966.

Young R, Wray RAL, Young A, 2009. Sandstone Landforms. Cambridge UP, Cambridge, 304.

KARST EVOLUTION IN SANDSTONE: THE CHAPADA DOS GUIMARÃES SITE, BRAZIL

Rubens Hardt[1], Joël Rodet[2], Sergio dos Anjos Ferreira Pinto[3]
[1]Instituto do Carste, Rua Seis, 1043 apto 112, 13500-050, Rio Claro, SP, Brazil, rubens.hardt@gmail.com
[2]UMR6143CNRS/Université de Rouen, 76821, Mont Saint Aignan, France, joel.rodet@univ-rouen.fr
[3]UNESP, Rua 24A, 1515, 13506-900, Rio Claro, SP, Brazil, sanjos@rc.unesp.br

Karstification of sandstone was considered a controversial topic in the past, but it has become increasingly accepted by karst researchers in recent decades. A large area of Brazil's territory has sandstone and metasandstone outcrops. The country's tropical climate, abundant rainfall and vegetation, allied to the presence of organic matter, iron oxides, salts and long weathering processes, among other factors, accelerated the chemical weathering of quartz. This combination of factors has produced a wide variety of karst landforms as well as a spatial organization that allows them to be referred to as Sandstone Karst Systems. The area under study was the Chapada dos Guimarães. This study allowed the determination of the karst topography by understanding the organization of these landscape's processes and their systemic integration. The knowledge thus gained, served to underpin the formulation of hypotheses about the processes involved in the structuring of these landforms and systems. Above all, it shows the importance of vegetation as an aid for quartz dissolution, on the process of rock weathering ("*in situ*" alteration), and subsequent removal of modified material by complete dissolution or by mechanical means. That resulted in karst landforms and systems. The aforementioned hypotheses served as the basis for the proposal to amend the definition of karst with respect to the term "chemical dissolution", by using a broader term "chemical weathering". This will allow the inclusion of changes in rock resulting from chemical processes and mechanical removal as karst, since they produce the same type of system and function in the same way as systems typically developed by dissolution of carbonaceous rocks.

1. Introduction

Sandstone karst is still a controversial subject, even after several studies showing its reality (Mainguet 1972; Jennings 1983; Young 1988). Although the term is accepted by some karst researchers, several questions remain open. Therefore, others still disagree with the possibility that sandstone is a substrate for karstification, without studying or even visiting a sandstone site themselves.

In tropical areas, like in Brazil, it is possible to find large areas of sandstone, most of them presenting several aspects of karst (Hardt 2011). These include caves, kamenitzas, closed depressions, several types of karren, underground rivers and even some speleothems, showing not only the dissolution, but also precipitation of minerals.

Since hydraulic gradient is needed to provide some movement to groundwater, usually these karstification areas are associated with gentle slope reliefs (e.g., cuesta backslopes) where the altitude provides such gradient and large area of exposition to weathering processes, giving rise to a karst system.

One of these areas, the Chapada dos Guimarães site, in Mato Grosso State, Brazil (Fig. 1) has developed a complex, polyphase karst system.

In this area, a cuesta relief can be found, where water is abundant, and the gradient on the cuesta backslope side is low, providing conditions to the development of karstic features. The proximity of the cuesta front also has interfered with the system, generating some captures that altered the gradient and influenced the evolution of the karst system in the late stage.

The occurrence of caves is in the contact from the sandstones of Ordovician Alto Garças formation to the sandstones of Silurian Vila Maria formation. The contact between the formations shows discontinuity. According to Köppen's system the contemporary climate is classified as Aw, with dry season in autumn and winter, and wet season in spring and summer.

Figure 1. Location in Mato Grosso State, Brazil.

2. Methods

In the field, most of the work consisted of exploration guided by the knowledge of the main caves' locations, in addition to the previous analysis of maps and satellite images from China-Brazil Earth Resource Satellite (CBERS), morphometric analysis of landforms, topography of caves and depressions.

Exploration of sites that may present elements not described or known by previous researchers, but with the potential to have something important complementing the knowledge of the site, allowed to build a database of forms, measurements, spatial location and distribution.

The endokarst measurements provide the morphometric characteristics of the conduits allowing one to understand the evolution of the caves.

A map of the area was created with the spatial distribution of the forms, their organizations and the connections between them. This helps to understand how water dynamics behaves in the system by generating forms, describing, this way, the system's morphodynamics.

At the end, a conceptual model was proposed, describing the evolution of the system through time and its consequences on landforms.

3. Data and observations

Several exokarstic features were found in the area, including varieties of karren, kamenitzas, arches, unroofed caves and closed depressions.

Two of these closed depressions, referred from now on as poljes, are very important for the comprehension of the system. The first one, denominated "the upper polje", has about 45,300 m^2 of area, ellipsoidal form, and feeds with water the Kiogo-Brado cave. The other depression, denominated "the central polje", has an area of 150,000 m^2, and resembles the shape of a banana, an elongated ellipse with a turn in its center. Its water feeds the Aroê-Jari system, and Lagoa Azul cave.

The endokarst is complex but organized, showing a mature system evolving to a senile system with abandoned galleries, residual pillars, dendritic drainage, dissolution cupolas and speleothems.

The main cave system, Aroê-Jari, is 1,500 m long, with galleries going from sub-metric to more than 15 m high, and forming saloons more than 50 m wide by 100 m long. The main drain is about 1 km across the massif, with an average height of 12 m and width of 10 m.

The Kiogo-Brado cave is about 210 m long with an average height of 13 m and width of 7 m. Its height can reach 16 m and the main entrance is about 33 m wide by 15 m high, but over an accumulation of blocks the "void" of the cave itself probably goes down under 10 m more.

Another important cave is the Lagoa Azul Cave, a large flooded saloon 50 m × 30 m, of a trapezoidal shape, with several underwater conducts at the end of the saloon going into the massif, following the main joints.

Elements of an ancient karst system can be found above the current system. There are arches, unroofed caves, and fragmented conduits in residual rock and ancient deposits above the present day level.

4. Results and discussion

The existence of a residual karst above the present day one demonstrates that the evolution of the landscape has involved several phases, while the water had to find its way down.

But the complexity of the endokarst is the most important information about this system, since it is quite identical to several others in limestone.

In the backslopes of the cuesta relief, the water following the gradient generates depressions by dissolution, where it accumulates. The weathering of the rock generates clay, which is deposited at the bottom of the depression, making it waterproof. For being filled with water and finding a barrier of rock at the side, the water penetrates amidst the rocks following the joints of the bedding plane or the structure, trying to find a way to cross the massif.

Several pipes started to develop in those joints, especially in the gradient direction by dissolution, creating essays to cross the massif. These pipes were abandoned when one of them succeeded and concentrated the flux. The walls of these tubes are covered by a crust, which demonstrates the mobility of silica (Fig. 2). This is common to depressions, the upper polje and the central polje.

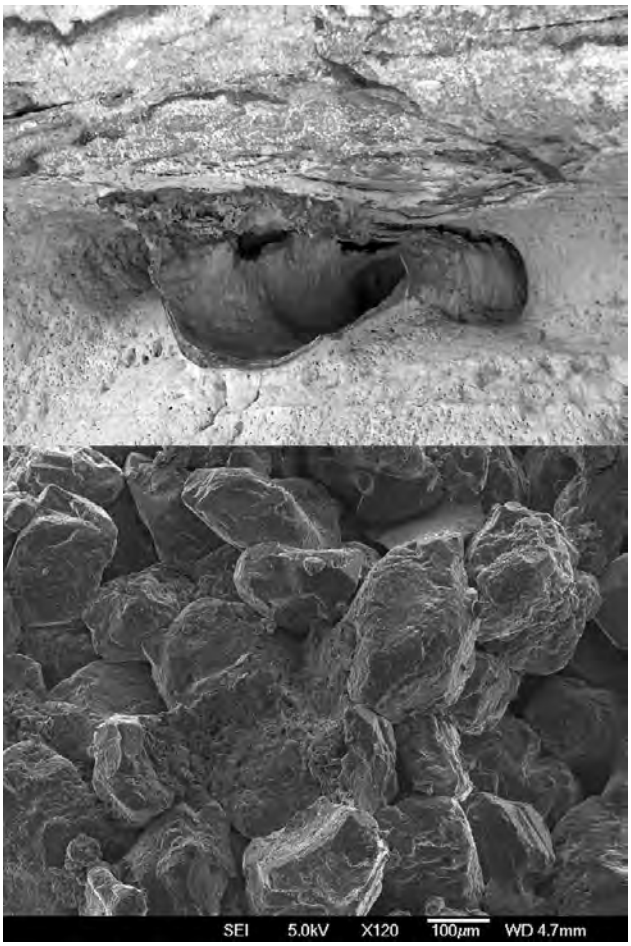

Figure 2. One of the tubes and SEM image, demonstrating the chemical mobility of the silica. Photos by Rubens Hardt.

After some time these pipes were abandoned in favor of one of them where flow has been concentrated, since it reaches the other side of the massif.

Now it is important to separate what happened in the connection between the upper polje and the central polje, in Kiogo-Brado cave, and the central polje and whatever could have been after Aroê-Jari cave: a polje or a valley.

One of the essays to cross the first massif had reached the other side but it found another great depression, filled with water, and the flow had been blocked. That has allowed the deposition of sediments, partially provided by the incomplete solution of the rock, and partially transported by allogenic fluxes. This allowed a paragenetic evolution inside the caves.

It is important to understand that the incomplete dissolution of rock is here regarded as in carbonate rocks, where the process denominated "ghost rock" formation (Quinif 2010), previously described as "*in situ*" alteration (Rodet 1996), is the main process in the formation of caves and its galleries, since residual alterite (ghost rock) was found in several places inside the caves.

This circumstance allows a paragenetic evolution, with the water flowing above sediments, enlarging the galleries. Sediments trapped above the contemporary level (Fig. 3) and roof channels are the evidence of this phase.

Figure 3. Sediment trapped on the roof. Photo by Rubens Hardt.

At Aroê-Jari much of the protogalleries was filled with residual rock, and the water was running above it, so this cave also had a paragenetic evolution in a certain period.

After a continuity solution (a connection between two points by a conduit) has been established from the upper polje via Kiogo-Brado to the central polje, and from the central polje via Aroê-Jari to a polje or valley beyond Aroê-Jari, the paragenetic evolution ceased and, in the Aroê-Jari Cave many parallel conduits have coalesced, giving a large central collector as attested by residual pillar in the central collector and the double-roof channel on affluent conduit (Fig. 4).

Figure 4. Double-roof channel. Photo by: J. A. Labegalini.

This characterizes a karst with captures of surface flow to the underground system.

Then, the evolution of the landscape brings the front of the cuesta nearby the area where the karst has evolved, inducing the capture of the central polje by a drainage running into the depression, resulting in two different reactions in both caves.

In the Aroê-Jary, the lack of water converted the cave in an almost fossil cave, with too little water coming in and without enough energy to transport the sediments and organic matter from one side to another. The large saloons inside have become sediment traps and only the water that rises from a diffuse spring in the center of the central polje is captured to the cave.

In the Kiogo-Brado Cave the fast drain created by the opening of the polje, lowered the cave in a syngenetic evolution, attested by the residual deposits on the side walls.

After that, the upper polje has been captured and reduced the amount of water which feeded the Kiogo-Brado Cave, what originates a much smaller incision at the basement of it, giving the key role shape in the cross-section of the conduit.

This is the actual situation at Chapada dos Guimarães site (Table 1).

Table 1. Comparative schema between Kiogo-Brado subsystem and Aroê-Jari subsystem.

From Upper polje to center polje (Kiogo-Brado connection):	From center polje to the valley or lower polje (Aroê-Jari connection):
I – Progradation fronts, primokarst.	I – Progradation fronts, primokarst.
II – Hydrokarstic connections, paragenesis.	II – Hydrokarstic connections, paragenesis. Water concentration, fully developed main conduit.
III – Lowering of water table due to central polje opening. Syngenetic evolution.	III – Lowering of water table due to central polje opening. System's fossilization, reduced drainage, sediment trap.
IV – Upper polje opening, system's fossilization.	

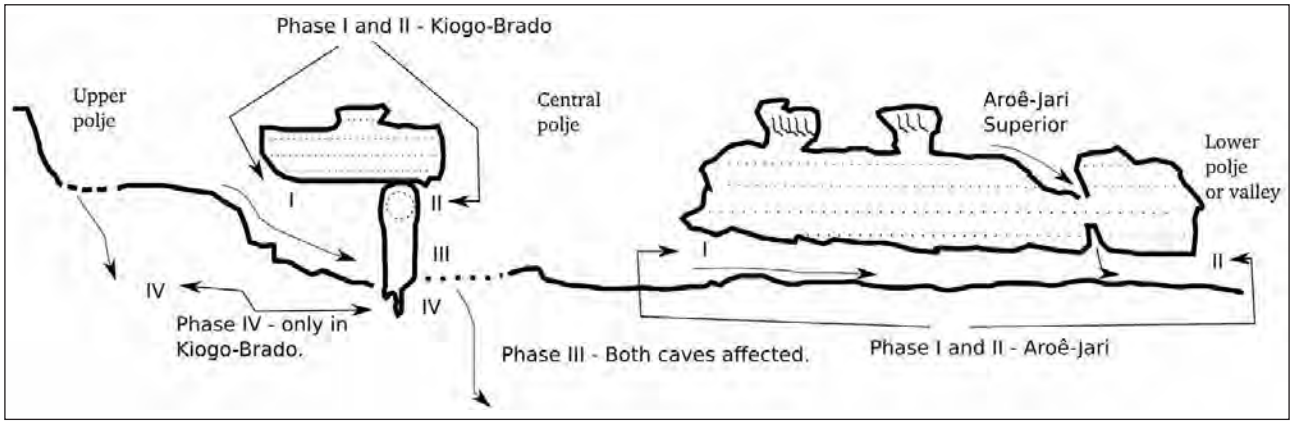

Figure 5. Schematic view (see table 1 for phase's description).

5. Conclusions

Such a karstic system in sandstone as described here is quite rare, since sandstone is much more susceptible to other forms of erosion that competes with chemical erosion or alteration. Karst in sandstone is not usually a pure karst with elements of a fluvial system competing in the structure of the system.

But even when the system is not a pure karst, it is possible to state that karst in sandstone is a reality, since the processes (dissolution/alteration), the landforms (closed depressions, underground drainage, several small scale surfaces and underground forms) and finally the system may develop in this rock.

The complex evolution and the response of the system to external factors put the sandstone karst in a similar level to carbonate karst.

References

Hardt R, 2011. Da carstificação em arenitos. Aproximação com o suporte de geotecnologias. À propos de la karsification dans les grès. Traitement par les technologies SIG. (Ph. D. Thesis) Instituto de Geociências e Ciências Exatas. Universidade Estadual Paulista Júlio de Mesquita Filho. Em co-tutela com Morphodynamique Continentale et Côtière. Laboratoire de Géologie. Université de Rouen. 224.

Jennings JN, 1983. Sandstone pseudokarst or karst? In: Young RW; Nanson GC, Aspects of Australian Sandstone Landscapes. Wollongong: Australian and New Zealand Geomorphology Group Special Publication no. 1, 21–30.

Mainguet M, 1972. Le modelé des grès: Problèmes Généraux. Paris: Institut Géographique National, 228.

Quinif Y, 2010. Fantômes de roche et fantômisation. Karstologia Mémoires 18, 184.

Rodet J, 1996. Une nouvelle organisation géométrique du drainage karstique des craies: le labyrinthe d'altération, l'exemple de la grotte de la Mansonnière (Bellou sur Huisne, Orne, France). Comptes Rendus de l'Académie des Sciences de Paris, t. 322 (12), série II a: 1039–1045.

Young RW, 1988. Quartz etching and sandstone karst: Examples from the East Kimberleys, northwestern Australia. Zeitschrift fur Geomorphologie 32, 409–423.

THREE TYPES OF CREVICE-TYPE CAVES IN THE AREA OF CZECH FLYSCH CARPATHIANS

Jan Lenart[1,2], Tomáš Pánek[1]

[1]Department of Physical Geography and Geoecology, Faculty of Science, University of Ostrava, Chittussiho 10, 71000, Ostrava-Slezská Ostrava, Czech republic, honza.lenart@seznam.cz

[2]ZO ČSS 7.01 Orcus, Čáslavská 407, 73581, Bohumín, Czech republic, honza.lenart@seznam.cz

The crevice-type caves of the Czech part of the Outern Western Carpathians are formed by the processes of the gravitationall slope movements: spreading (or incipient translational sliding), toppling and rotational sliding. The Outern Western Carpathians are built by the flych Mesozoic rocks: sandstones, conglomerates and shales. The aim of the research was to detect types of the process and to divide the caves into the cathegories.

1. Introduction

Caves are among the most distinctive forms of pseudokarst phenomena (Halliday 2007). Most extensive and widespread pseudokarst caves are crevice-type caves formed during evolution of slope failures (Vítek 1978). Margielewski and Urban (2003) considered the crevices to be free spaces between two rock blocks, when at least one of them is affected by slope movement. Most commonly, they accompany evolution of deep-seated gravitational slope deformations (DSGSDs); i.e. types of large-scale and relatively short-displacement mass movements affecting large volumes of mountain ridges (Němčok 1972; Dramis and Sorriso-Valvo 1994) and reaching the depth at least 30 m (Hutchinson 1988). They are mostly slow or extremely slow mass movements with the average velocity less than 18 mm per year (Varnes 1978). However, besides DSGSDs, the crevice-type caves can be produced also within the shallow and medium-deep (< 30 m according to Hutchinson, 1988) structurally-predisposed landslides (Margielewski 2009).

The crevice-type caves of the same genesis may occur in distinct types of rocks. The crevices very often cut incoherent sedimentary flysch rocks: sandstones and conglomerates with intercalations of shales, but can occur in granites, quartzites, gneisses and other lithologies (Vítek 1978). Crevices originate also in the carbonate karst rocks (limestones and dolomites), but these are usually classified as a karst caves (Vítek 1978). Typically, crevices and crevice-type caves occur within the areas built by anisotropic rigid rocks underlain by the plastic shales (Pánek et al. 2009 and 2010).

Crevice-type caves originate by the process of gravitational widening and movement of tectonically or lithologically predisposed rock massif. This type of caves is mostly regularly narrow-shaped ("A" and "V" or "H" letter in cross-section) with high walls and flat roofs or floors. The corridors may reach appreciable length (Vítek 1978 and 1981). Within the crevice-type cave development, other processes might play a role, such as water erosion, frost weathering, rockfalls, seasonal temperature change etc. (Vítek 1981; Margielewski et al. 2007; Klimeš et al. 2012). In such circumstances, the crevice-type cave is each cave originated in the soluble or insoluble rocks by the influence of gravitationally or tectonically induced widening of fissures (Panoš 2001). Some authors divide the crevice-type caves into the primary endogenic diapiric crack caves, rock-slide caves and primary exogenic frost caves (Panoš 2001). Pokorný and Holec (2009) classify the pseudokarst caves in respect to genesis into a crack type, cleft type, talus type, erosional type and combined type. Crack type is a high, narrow and widening to the bottom cave. The ceiling is flat, fixed and connected with the overlapping rock. If the whole massif is not stable, the cave is indicated as a cleft type (crevice-type) (Pokorný and Holec 2009). This typology seems to be very problematic because different types of ceilings usually occur within a particular crevice. In the flysch rocks of Outern Western Carpathians (OWC), there are specific cases of crevice-type corridors with flat and homogenous ceilings.

These caves were mapped in the OWC systematically since the middle of 20th century. In the Czech Republic, the largest crevice-type caves were mapped by Foldyna and Pavlica (Foldyna 1968; Foldyna and Pavlica 1968) and by Wagner et al. (1990).

The research of gravitational slope deformations and crevice-type caves has converged together in the last ten years (e. g. case studies: Baroň et al. 2003a; Margielewski and Urban 2003; Pánek et al. 2007 and 2010; Klimeš et al. 2012). Thanks to the opened crevices, we can study the internal structure of landslide bodies from inside and make the analysis of slope deformations more properly (Margielewski 2006). Some comprehensive studies of gravitational slope deformations and crevice-type caves use the investigation performed within the caves for the survey of internal structure of landslides and regime of slope movements (Margielewski and Urban 2003; Baroň et al. 2004). The evolution of slope deformations and the origin of crevices in anisotropic rock massifs are predisposed by tectonic and lithological discontinuities (e.g., faults, joints, schistosity and bedding planes; Kirchner and Krejčí 2002; Di Luzio et al. 2004; Margielewski 2006; Brideau et al. 2009; Jaboyedoff et al. 2009) and driven by various gravitational mechanisms like lateral spreading, toppling, sagging (*sackung*), rotational and translational sliding, and/or compound (as an intermediate cause between rotational and translational sliding) movement (e. g. Kleczkowski 1955, Němčok et. al. 1972; Varnes 1978; Hutchinson 1988; EPOCH 1993). Crevice-type caves usually indicate the initial forms of gravitational slope deformation development (Margielewski and Urban 2003; Margielewski et al. 2007; Margielewski 2009), but whilst in karst areas the evolution of a cave is running cyclically (Bosák 2003), in the area affected by mass movement the evolution is running only in one direction – gravitationally downwards.

2. Regional settings

The OWC are formed predominantly by flysch Mesozoic and Paleogene sediments which were folded and thrusted more than 50 km onto the Carpathian foredeep during the lower and middle Miocene alpine orogeny phases (Menčík et al. 1983; Krejčí et al. 2004). The following units (nappes) are distinguished in the region (from the south): Magura Unit, Silesian Unit and Sub-Silesian Unit. The strata consist of thick-bedded sandstones or conglomerates with mica, glauconitic and calcific admixture and thin-bedded intercalations of shales with predominant content of illite and kaolinite clay minerals (Menčík et al. 1983; Eliáš 2000; Pánek et al. 2011). Regarding the dip of strata, ridges are often asymmetrical, with the character of monoclinal ridges and cuestas. This is typically demonstrated within the Silesian Unit (e.g., Moravskoslezské Beskydy Mts.) characterized by steep northern slopes and gentle, long southern slopes predisposed by bedding planes (e.g., Rybář et al. 2008). The flysch massif is strongly disrupted by joints and faults trending in the E-W, N-S and NE-SW (Menčík et al. 1983; Krejčí et al. 2002; Bubík et al. 2004) and WNW-ESE direction (Menčík et al. 1983; Pánek and Duras 2002).

Slope deformations are common features in the OWC (Margielewski 2006). Susceptibility of this region to mass movements is given by (i) overall disequilibrium of flysch nappes which are not in balance with underlying basement consisting of soft Neogene deposits (Krejčí et al. 2004), (ii) strong anisotropy of flysch rocks creating conditions for the development of slip surfaces (Margielewski 2006) and (iii) high precipitation totals which together with summer heavy downpours and rapid snow melt at the end of winter generate high pore pressures within the rock mass. Typical slope movements are represented by DSGSDs and structurally-induced landslides, very often accompanied by the origin of crevice-type caves (Margielewski 2009).

3. Recent movement and forms

The downward movement of a landslide determines the main trend of movements – their direction and velocity. The movement proper for crevice-type cave creation is very slow (creep) and the crevices are typically formed upright to the movement direction (Baroň et al. 2003; Margielewski and Urban 2003). Seasonal movements measured between two opposite walls of crevice are caused by the volumetric change of rocks which are partly elastic. These cyclic movements become evident as a narrowing and widening of crevices. The rate of movements depends on season and water content in rock (Klimeš et al. 2012). The main gravitationally induced movement and seasonal elastic movement is accompanied by secondary movements of relaxed blocks, boulders and sediments.

There are three main types of corridor shapes formed by the distinct gravitational movement of flysch massif: (i) "V-letter-shaped" where the upper part of crevice is significantly wider than lower part, (ii) "A-letter-shaped" crevices when the ceiling is significantly narrower than the bottom and (iii) "H-letter-shaped" forms with no difference in width between lower and upper part of crevice. The first type indicates toppling, the second one is associated with rotational slides and the third one signifies lateral spreading or translational slides. There is a problem with vast subsided and fissured rock blocks which can falsely indicate the type of movements using this approach. This mistake can be eliminated partially by observing and correlating bedding planes which in the conditions of flysch rocks are usually very well detectable. The subtle morphology of cave corridors is shaped by water erosion caused by episodic inflows (Urban 2005).

As for the vertical caves, each level) is usually shifted staircase. The elevation of bedding planes, sedimentary reglets or boundaries in sedimentary sequences between two opposite walls sometimes significantly change along the crevice. These are the signs of vertical displacement or rotational movements. In the horizontally established caves, a typical feature is an intra-bed creep. During this process, the regularly shaped rooms with flat roofs are created by movement of blocks along bedding planes. In the case of an advanced stadium of cave evolution, there could be,,corridor-like" areas created between the fallen, tilted and cracked rock blocks and boulders. Typically, extensive rooms, levels and corridors are connected with each other only by narrow and small scuttles.

4. Methods

There were 8 crevice-type caves investigated in the area of Czech part of Outern Western Carpathians: The Cyrilka Cave (length 535 m, depth 16 m), The Kněhyňská Jeskyně Cave (length 280 m, depth 57 m), The Velká Ondrášova Jeskyně Cave (length 217 m, depth 35 m), The Salajka Cave (length 156 m), The Velryba Cave (length 50 m), The Kyklop Cave (length 40 m), The Na Gírové I Cave (length 46 m) and The Čertova Díra Cave (length 74 m, depth 35 m) (Wagner et al. 1990). The used methods were: (i) Analysis of corridors ("A", "V" or "H") by observing and measuring their dimensions using tape and laser range-finder Leica Disto A3; (ii) measuring of microstructures (cracks, faults) using geological compass; (iii) comparing subsurface cavities with surface trenches and sinkholes using a DEM combined with maps of the caves; (iv) construction of typical cross-sections of cave corridors, using data from microstructural measuring and proportions of corridors measuring.

5. Exemplary results

There are three types of crevice-type caves in the investigated area, exemplified by particular caves:

5.1. The Kyklop Cave

The entrance of the Kyklop cave is situated on the SE slope of the Kněhyně Mt., just 100 m under the summit (Fig. 1). The slope is highly disturbed by the activity of a landslide. Corridors follow the direction of the trench: SW-NE and SSW-NNE. Everywhere within the cave these two directions occur as opened cracks and narrow corridors. In the same directions, also a small secondary cave Žánova Díra originated. This cave (20 m long) is geneticaly connected with the Kyklop Cave and the direction of the main corridor follows the south-western ending of the trench.

The walls are formed by the massive sandstones of the

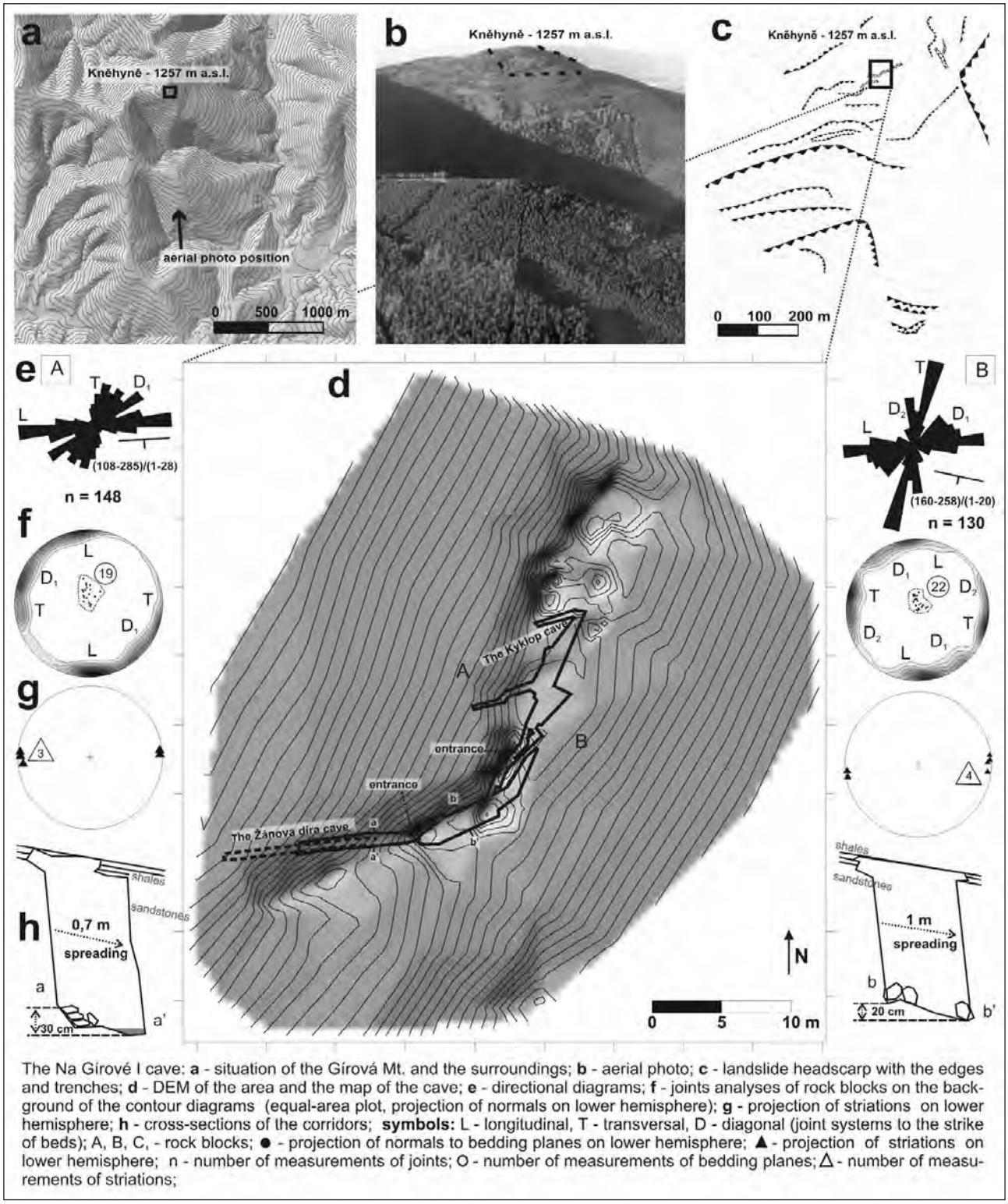

The Na Gírové I cave: **a** - situation of the Gírová Mt. and the surroundings; **b** - aerial photo; **c** - landslide headscarp with the edges and trenches; **d** - DEM of the area and the map of the cave; **e** - directional diagrams; **f** - joints analyses of rock blocks on the background of the contour diagrams (equal-area plot, projection of normals on lower hemisphere); **g** - projection of striations on lower hemisphere; **h** - cross-sections of the corridors; **symbols:** L - longitudinal, T - transversal, D - diagonal (joint systems to the strike of beds); A, B, C, - rock blocks; ● - projection of normals to bedding planes on lower hemisphere; ▲ - projection of striations on lower hemisphere; n - number of measurements of joints; O - number of measurements of bedding planes; △ - number of measurements of striations;

Figure 1. The Kyklop Cave.

Silesian unit with the intercalations of shales. There are also bedding planes exposed within the corridors. On the walls there are striations visible. The ceilings are formed by sandstone blocks as flat lower bedding planes or as accumulation of rock debris. The bottom of the corridors is infilled by rock debris and loam.

5.2. The Čertova Díra Cave

The entrance of the Čertova Díra Cave is situated on the SW slope of the Čertův Mlýn Mt., cca 150 m under the mountain ridge, at the bottom of 30 m long rocky trench (Fig. 2). The cave has distinct vertical character. Corridors are found in three levels. The entrance leads into a first level, which is formed by an extensive room (cca 3 × 10 m). The small scuttles connect the room with the main abyss through the zone of fallen blocks. In the north ending of the abyss the narrow scuttle leads to the third level. Here is the deepest part of the cave: 35 m under the surface. All the corridors follow the direction of the trench: NNW-SSE.

The walls of the cave in the first and second level are formed by very thin sandstone beds with shale intercalations (thin-bedded flysh). Conversely, the third level is formed in massive sandstone beds. In the first and second level there are many bedding planes exposed, in the third level there are the fault zones with subhorizontal striations and slickenside

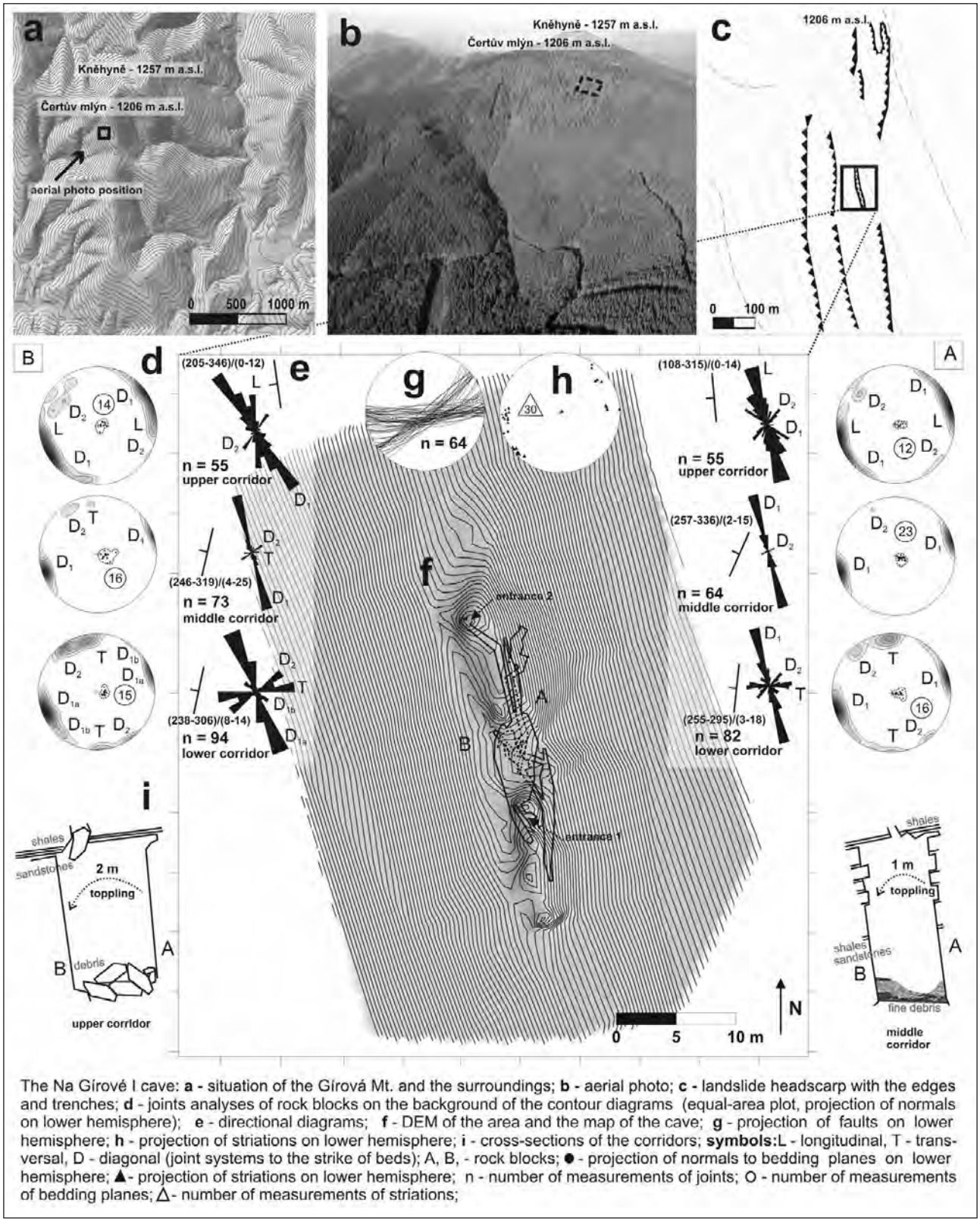

The Na Gírové I cave: **a** - situation of the Gírová Mt. and the surroundings; **b** - aerial photo; **c** - landslide headscarp with the edges and trenches; **d** - joints analyses of rock blocks on the background of the contour diagrams (equal-area plot, projection of normals on lower hemisphere); **e** - directional diagrams; **f** - DEM of the area and the map of the cave; **g** - projection of faults on lower hemisphere; **h** - projection of striations on lower hemisphere; **i** - cross-sections of the corridors; **symbols:** L - longitudinal, T - transversal, D - diagonal (joint systems to the strike of beds); A, B, - rock blocks; ● - projection of normals to bedding planes on lower hemisphere; ▲- projection of striations on lower hemisphere; n - number of measurements of joints; O - number of measurements of bedding planes; △- number of measurements of striations;

Figure 2. The Čertova Díra Cave.

surfaces exposed. The ceilings are formed by sandstone debris or huge blocks, while in the third level the ceiling is formed by sandstone beds. The bottom of the corridors is infilled by sandstone debris and by clayey mud. The whole cave is very unstable and collapses within debris accumulations are very frequent.

5.3. The Na Gírové I Cave

The entrance of the Na Gírové I Cave is situated on the SW slope of the Gírová Mt., within the upper part of the rocky landslide headscarp, cca 150 m under the mountain ridge (Fig. 3).

The cave has two levels. The first of them is represented by the entrance corridor. The connecting abyss (-4 m) leads to the lower level which represents the rest of the cave. The crevices follow the E-W, NW-SE and SW-NE directions. The walls are formed by massive sandstones and conglomerates of the Magura flysch unit, with the intercalations of shales. The ceiling of the entrance corridor is formed by the lower bedding plane of the sandstone bed. In the lower level the ceilings are sometimes not visible because of the shape of the

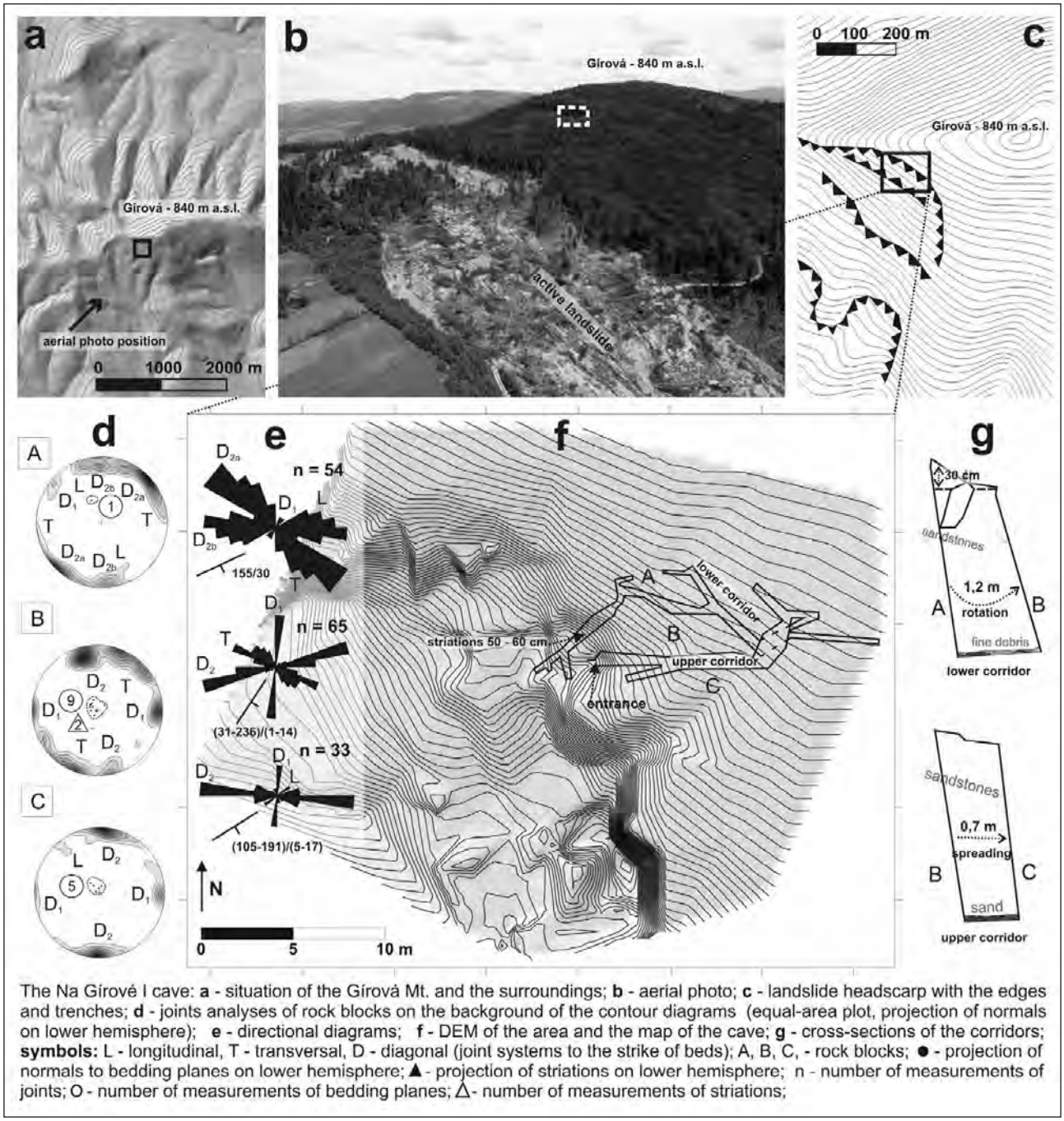

The Na Gírové I cave: **a** - situation of the Gírová Mt. and the surroundings; **b** - aerial photo; **c** - landslide headscarp with the edges and trenches; **d** - joints analyses of rock blocks on the background of the contour diagrams (equal-area plot, projection of normals on lower hemisphere); **e** - directional diagrams; **f** - DEM of the area and the map of the cave; **g** - cross-sections of the corridors; **symbols:** L - longitudinal, T - transversal, D - diagonal (joint systems to the strike of beds); A, B, C, - rock blocks; ● - projection of normals to bedding planes on lower hemisphere; ▲ - projection of striations on lower hemisphere; n - number of measurements of joints; O - number of measurements of bedding planes; △- number of measurements of striations;

Figure 3. The Na Gírové I Cave; captions for all pictures.

corridors when the free space is narrowing to the top. The bottom of the cave is infilled by sand or loam with organic matterial.

6. Discussion

According to microstructural measuring on different rock blocks and opposite walls and according to the change of dip of bedding planes we can estimate the character of process which has led to cave formation. The Kyklop Cave is an example of crevice-type cave which is formed by the process of spreading and incipient translational sliding. Identical or very similar values measured on two opposite walls point to the spreading type of movement. The rock block B was shifted along bedding planes. Also, the measured proportions of corridors indicate the spreading type of movement. The Čertova Díra Cave is an example of crevice-type cave which is formed by the process of toppling. Within the Čertova Díra Cave the inclinations of the blocks B are constantly less than of the A block which reveals toppling process. The dip of strata of the B blocks is evidently larger than that of the A block which is another evidence of toppling. The differences between the A block and B blocks fade away downwards. The greatest differences are in the first level, the smallest are at the bottom of the cave where they totally disappear. The formation of the Kyklop Cave and the Čertova Díra Cave has surface displays – rocky trenches. The lower level of the Na Gírové I Cave is an example of the crevice-type cave formed by rotational sliding. The shape of the corridor – narrowing to the top – and the values of microstructural measuring carried out on two opposite walls point to rotational character of movement. The short entrance corridor is due to spreading process. Thanks to rotational character of the movement, there are no surface displays above the cave – according to the digital terrain model.

In accordance with the currently used nomenclature of the gravitational movements we can term these three exemplary crevice-type caves. The Kyklop cave, which is formed by the spreading movement, pertains to the category of the spreading-type caves. The Čertova Díra Cave, which is formed by toppling movement, pertains to the category of the toppling-type caves. The Na Gírové I Cave, which is formed by the rotation movement, pertains to the category of the rotational-type caves. This nomenclature is based on the criterion of genesis.

7. Conclusion

There were 8 crevice-type caves investigated in the area of the Czech part of the flysch Outern Western Carpathians. These caves have been formed by various processes of gravitational slope movements: spreading, toppling, rotational sliding. The survey involved description of shapes of corridors, microstructural measuring, comparison of subsurface cavities with surface trenches and sinkholes using a DEM combined with cave maps and construction of typical cross-sections of cave corridors, usinga data from the microstructural measuring. In accordance with the currently used nomenclature of the gravitational movements these crevice-type caves was divided into a three cathegories: spreading-type caves, toppling-type caves, rotational-type caves.

Acknowledgments

Survey was co-funded by the financial subsidy within the program “Support for science and research in Moravian-Silesian Region 2012” provided by the Moravian-Silesian Region and by the University of Ostrava Foundation project SGS04/PřF/2012.

References

Baroň I, Cílek V, Melichar R, 2003. Pseudokrasové jeskyně jako indikátory svahových pohybů. Geol. výzk. Mor. Slez. v r. 2002. Brno, 84–87 (in Czech).

Baroň I, Cílek V, Krejčí O, Melichar R, Hubatka F, 2004. Structure and dynamics of deep-seated slope failures in the Magura Flysh Nappe, outer Western Carpathians (Czech republic). Nat. Haz. and Earth Sys. Sc. 4, 549–562.

Bosák P, 2003. Karst processes from the beginning to the end: How can they be dated? Speleogenesis and Evolution of Karst Aquifers 1(3), 1–24.

Brideau MA, Yan M, Stead D, 2009. The role of tectonic damage and brittle rock fracture in the development of large rock slope failures. Geomorphology 103, 30–49.

Bubík M, Krejčí O, Kirchner K, 2004. Geologická minulost a přítomnost Frýdeckomístecka. Muzeum Frýdek-Místek. 54 (in Czech).

Di Luzio E, Saroli M, Esposito C, Bianchi-Fasani G, Cavinato GP, Scarascia-Mugnozza G, 2004. Influence of structural framework on mountain slope deformation in the Maiella anticline (Central Apennines, Italy). Geomorphology 60, 417–432.

Dramis F, Sorriso-Valvo M, 1994. Deep-seated gravitational slope deformations, related landslides and tectonics. Engineering Geology 38, 231–243.

Eliáš M, 2000. Vztahy mezi pústevenskými pískovci a pískovci Malinovské skály (Godulské souvrství s.s.) v Beskydech. Geol. výzk. Mor. Slez. v roce 1999, 64–66, in Czech).

EPOCH (European Community Programme) (1993. Temporal occurence and forecasting of landslides in the European community, (Ed. J-C. Flageollet). 3 volumes, Contract No. 90 0025.

Foldyna J, 1968. Pseudokras v godulských vrstvách dílčího příkrovu godulského (Moravskoslezské Beskydy). Sborník věd. prací VŠB, ř. hor.-geol. 14. Ostrava. 83–103 (in Czech).

Foldyna J, Pavlica J, 1968. Pseudokras masívu Lysé hory a Kněhyně. Sborník věd. prací VŠB, ř. hor.-geol. 14. Ostrava. 69–82 (in Czech).

Halliday WR, 2007. Pseudokarst in the 21st century. Journal of cave and karst studies 69, 103–113.

Hutchinson JN, 1988. Morphological and geotechnical parameters of landslides in relation to geology and hydrogeology. Proceedings, Fifth International Symposium on Landslides, Rotterdam, 3–35.

Jaboyedoff M, Couture R, Locat P, 2009. Structural analysis of Turtle Mountain (Alberta) using digital elevation model: toward a progressive failure. Geomorphology 103, 5–16.

Kirchner K, Krejčí O, 2002. Slope deformations and their significance for relief development in the middle part of the Outer Western Carpathians in Moravia. Moravian geographical reports 10, 10–19.

Kleczkowski A, 1955. Osuwiska i zjawiska pokrewne. Warszawa, Wyd. Geol., 93 (in Polish).

Klimeš J, Rowberry MD, Blahůt J, Briestenský M, Hartvich F, Košťák B, Rybář J, Stemberk J, Štěpančíková P, 2012. The monitoring of slow-moving landslides and assessment of stabilisation measures using an optical–mechanical crack gauge. Landslides 9, 3, 407–415.

Krejčí O, Baroň I, Bíl M, Hubatka F, Jurová Z, Kirchner K, 2002. Slope movements in the Flysch Carpathians of Eastern Czech Republic triggered by extreme rainfalls in 1997: a case study. Physics and Chemistry of the Earth 27, 1567–1576.

Krejčí O, Hubatka F, Švancara J, 2004. Gravitational spreading of the elevated mountain ridges in the Moravian-Silesian Beskids. Acta Geodyn. Geomater. 135, 97–109.

Margielewski W, 2006. Structural control and types of movements of rock mass in anisotropic rocks: case studies in the Polish Flysch Carpathians. Geomorphology 77, 47–68.

Margielewski W, 2009. Problematyka osuwisk strukturalnych w Karpatach fliszowych w świetle zunifikowanych kryteriów klasyfikacji ruchów masowych – przegląd krytyczny. Prz. Geol. 57, 905–917 (in Polish).

Margielewski W, Urban J, 2003. Crevice-type caves as initial forms of rock landslide development in the Flysch Carpathians. Geomorphology 54, 325–338.

Margielewski W, Urban J, Szura C, 2007. Jaskinia Miecharska cave (Beskid Śląski Mts., Polish Outer Carpathians. case study of a crevice-type cave developed on a sliding surface. Nature Conservation 63, 57–68.

Mastella L, Zuchiewicz W, Tokarski AK, Rubinkiewicz J, Leonowicz P, Szczęsny R, 1997. Aplication of joint analysis for paleostress reconstructions in structuraly complicated settings: case study from Silesian nappe, Outer Carpathians, Poland. Prz. Geol. 45, 1064–1066.

Menčík E, Adamová M, Dvořák J, Dudek A, Jetel J, Jurková A, Hanzlíková E, Houša V, Peslová H, Rybářová L, Šmíd B, Šebesta J, Tyráček J, Vašíček Z, 1983. Geologie Moravskoslezských Beskyd a Podbeskydské pahorkatiny. Ústřední Ústav Geologický, Praha, 304 (in Czech).

Němčok A, 1972. Gravitational slope deformation in high mountains. Proceedings of the 24th International Geological Congress. Montreal, vol. 13, 132–141.

Pánek T, Duras R, 2002. The morphotectonics of the eastern marginal slope of The Ropice-range (The Moravskoslezské Beskydy Mts.). Moravian geographical reports 10, 20–27.

Pánek T, Tábořík P, Hradecký J, 2007. Gravitační rozpad hřbetu Čertova mlýna (Moravskoslezské Beskydy). Geol. výzk. Mor. Slez. v r. 2006. Brno, 124–129 (in Czech).

Pánek T, Hradecký J, Šilhán K, Smolková V, Altová V, 2009. Time constraints for the evolution of a large slope collapse in karstified mountainous terrain of the southwestern Crimean Mountains, Ukraine. Geomorphology 108: 171–181.

Pánek T, Margielewski W, Tábořík P, Urban J, Hradecký J, Szura C, 2010. Gravitationally induced caves and other discontinuities detected by 2D electrical resistivity tomography: Case studies from the Polish Flysch Carpathians. Geomorphology 123, 165–180.

Pánek T, Tábořík P, Klimeš J, Komárková V, Hradecký J, Šťastný M, 2011. Deep-seated gravitational slope deformations in the highest parts of the Czech Flysch Carpathians: Evolutionary model based on kinematic analysis, electrical imaging and trenching. Geomorphology 129, 92–112.

Panoš V, 2001. Karsologická a speleologická terminologie. Knižné centrum, Žilina. 352 (in Czech).

Pokorný R, Holec M, 2009. Jeskyně Ústeckého kraje. Nakladatelství XYZ. Praha, 278 (in Czech).

Rybář J, Jánoš V, Klimeš J, Nýdl T, 2008. Strukturně podmíněné svahové pohyby ve východní části Moravskoslezských Beskyd. Zpr. geol. výzk. v roce 2007. Česká geologická služba, Praha, 113–118 (in Czech).

Urban, J, 2005. Pseudokarst caves as an evidence of sandstone forms evolution – a case study of Niekłań, the Świętokrzyskie Mts., central Poland. Ferrantia 44, 181–185.

Varnes, D.J, 1978. Slope movements: type and processes. Landslides: analysis and control. National Academy of Sciences, Washington DC. Special report 176, 12–33.

Vítek J, 1978. Typy pseudokrasových jeskyní v ČSR. Československý kras 30, 17–28 (in Czech).

Vítek J, 1981. Morfogenetická typizace pseudokrasu v Československu. Sborník ČGS 3, 153–165 (in Czech).

Wagner J, Demek J, Stráník J, 1990. Jeskyně Moravskoslezských Beskyd a okolí. ČSS, Praha. 132 (in Czech).

EXHUMATION OF PALAEOKARST BY VADOSE WEATHERING: A TELLING EXAMPLE FROM EASTERN AUSTRALIA

R. Armstrong L. Osborne
Education and Social Work, A35, The University of Sydney, NSW, 2006, Australia, armstrong.osborne@sydney.edu.au

When we encounter an underground space with clean bedrock walls we are inclined to think that it is a product of the most recent phase of speleogenesis, but what if this assumption is wrong? What if an exhumation process can so thoroughly remove the traces of a previous fill that we can mistakenly interpret a cave void that formed hundreds of millions of years ago and was completely filled and stayed completely filled until relatively recently, as a product of recent speleogenesis? This is the interesting possibility raised by recent re-visits to a classic palaeokarst site at Bungonia in eastern Australia, where vadose weathering is almost completely removing traces of an old palaeokarst fill to reveal new-looking cave passages with complex ceiling morphologies.

1. Introduction

Bungonia Caves, located 150 km south southwest of Sydney, NSW, Australia, is one of the most studied limestone karst localities in eastern Australia (Figure 1). Some of the deepest limestone caves on the Australian mainland are developed there in a plateau surface incised by a 360-metre deep limestone gorge.

Figure 1. Map of eastern Australia, showing cavernous karsts and the location of Bungonia.

The caves are developed in two beds of Silurian limestone folded into a southerly plunging syncline. Bedding is steep and the limestone sequence is overlain to the west by late Devonian volcanics and has a faulted/unconformable boundary to the east with Ordovician flysch.

At the plateau surface the limestone is unconformably overlain by remnants of Permian conglomerate and by Tertiary sands, gravel and ferricrete.

Caves at Bungonia intersect caymanite (marine carbonate palaeokarst), crackle breccia and siliciclastic palaeokarst as well as clastic dykes and basic igneous dykes.

The age and origin of the caves has been the subject of much discussion and controversy (see James et al. 1978, Osborne, 1993, 2001a, b, 2005, 2010 and Wray, 1998). Osborne (2001a) noted that many cave passages at Bungonia that had been interpreted as phreatic conduits blindly terminated in bedrock along strike and so could have not been formed by laterally flowing water, while Osborne (2001b) noted that the deep caves at Bungonia have a downward-narrowing profile. This was taken to indicate that the caves had a phreatic, per-ascensum origin followed by minor paragenetic and fluvial vadose invasion modification.

This paper reports new observations in the upper section of Fossil-Hogans Cave close to the Hogans Cave entrance and discusses the significance of these observations for speleogenesis at Bungonia and to interpretation of speleogenetic history generally.

2. Fossil-Hogans Cave (B4-5)

Fossil-Hogans Cave is part of an extensive cave system with multiple entrances, one called Fossil Cave with the cadastre number B4 and another called Hogans Cave with the cadastre number B5. Fossil Cave and Hogans Cave together with their poorly named larger section, the B4-5 Extension form the B4-5 Cave System with a total length of some 2,300 metres (Figure 2). The B4-5 Cave System is the longest and one of the deepest caves at Bungonia. Flying Fortress Cave, described by Osborne (2001a) is an upper level of the B4-5 Cave System.

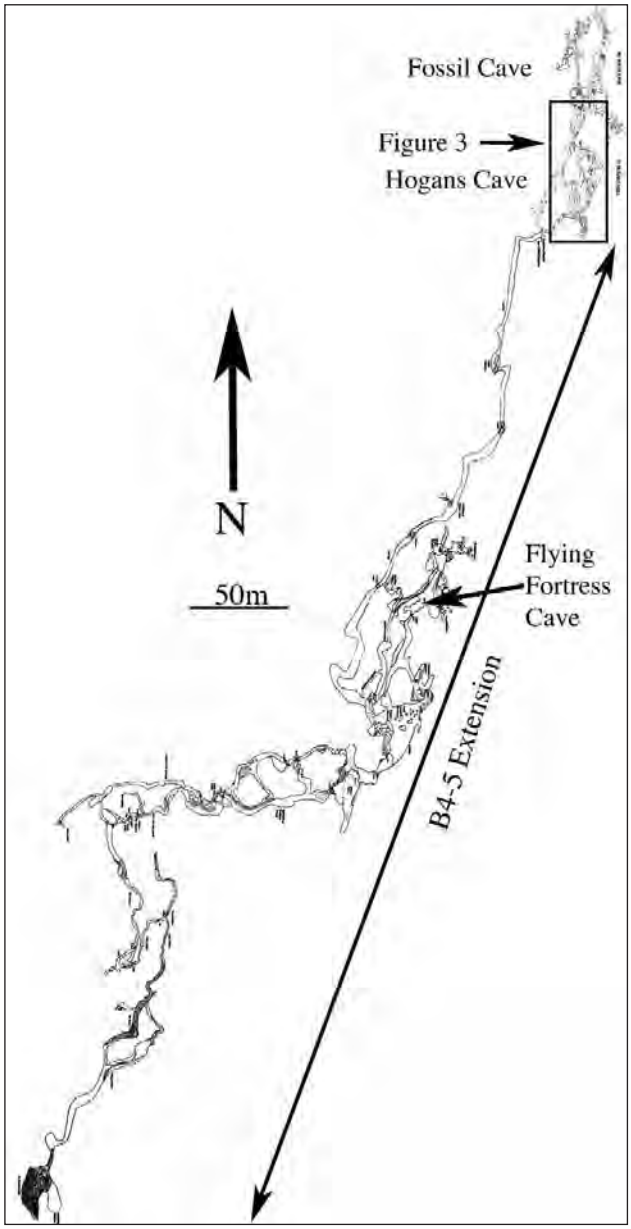

Figure 2. Map of the Fossil-Hogans, B4-5 Cave System modified after Bauer and Bauer (1998).

The B4-5 Cave System is developed in the westerly-dipping Silurian Lookdown Limestone Member in the eastern limb of a southerly plunging syncline.

A simplified plan of the upper section of Hogans Cave, close to its entrance shown in Figure 3 shows the cave consists of north–south trending passages with an elliptical cross-section at different levels guided by strike (A, E and G) and roughly east-west trending rifts guided by cross-joints (C-D and H).

The Hairy Traverse, an easterly sloping notch, "B" in Figure 3 is developed in the southern wall of the east-west trending rift "C-D" in Figure 3.

3. Palaeokarst in Fossil-Hogans Cave

Before the new observations I described the palaeokarst in this part of Hogans Cave in an unpublished manuscript as follows. "In the upper part of the high level passage leading to the Hairy Traverse dolomitic carbonate infilling has irregular boundaries with the limestone ("A" in Figure 3).

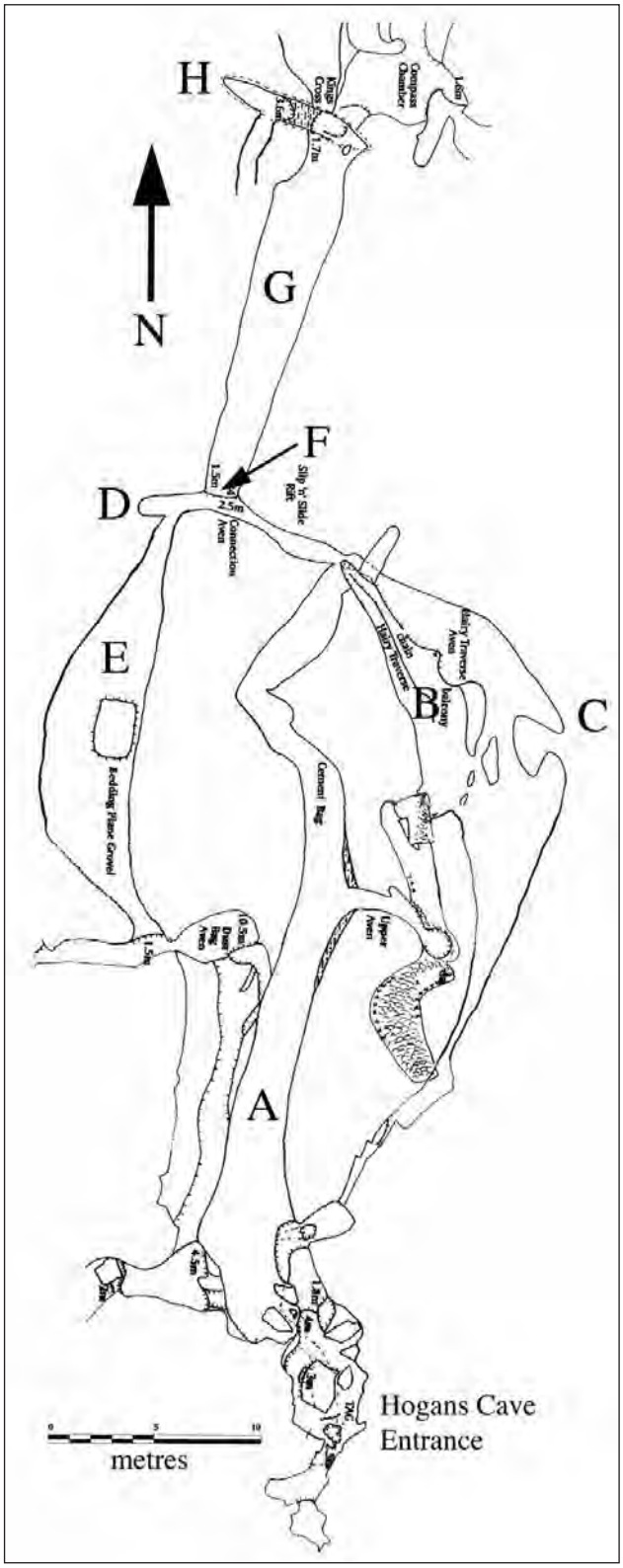

Figure 3. Simplified map of upper section of Hogan's Cave after Bauer and Bauer (1998).

The infilling, is rust-coloured and composed of calcirudite with a muddy dolomitic matrix containing a few spicules. The carbonate clasts range up to 5 mm in size and appear to be biogenic in origin, resembling echinoderm fragments. A similar deposit is exposed at the top of the Hairy Traverse ("B" in Figure 3).

Further east of this deposit, and at a lower level, a laminated palaeokarst deposit is exposed ("C" in Figure 3). This has an unconformable boundary with the bedrock and has almost vertical bedding, striking east-west, cut by a north-

south trending cleavage. The deposit has graded beds which young to the north. In thin section the deposit is seen to consist of coarse laminae composed of calcite clasts, including what appear to be fragments of flowstone and skeletal fragments, interbedded with fine graded laminae containing dolomite. The cleavage seen in the outcrop is not apparent in thin section."

4. New Observations

Two inspections of the cave, one in January 2008 and the other in December 2011 have resulted in new ideas about this section of cave. The first important observation made in 2008 was that palaeokarst deposits in bellholes in the ceiling of passage "A", which were previously interpreted as palaeokarst filing veins intersected by the bellholes were more likely remnants of material that formerly filled what is now open cave space ("A" in Figure 3, Figure 4A). Detailed observations of the western end of the east-west rift showed that it was formerly filled with dark laminated caymanite (Figure 4D).

The second important observation made in 2008 was that the elliptical passages guided by dipping structural planes labelled "A", "E" and "G" in Figure 3 were not guided by bedding planes, which here dip to the west, as suggested by the name " bedding plane grovel" given to passage "E", but by joints dipping to the east. This is similar to what Osborne (2001a) observed in Flying Fortress Cave, an upper level of the B4-5 System some 200 metres to the south, where cave development is guided by joints dipping gently to the east.

The inspection of the cave in December 2011 involved detailed re-examination between "F" and "D" in Figure 3, and for the first time since the 1980s a close inspection of the area between "F" and "H" in Figure 3.

By lying back and looking up at "F" it was possible to see remnants of caymanite fill in the ceiling of the rift and adhering to the northern wall (Figure 4E).

Looking north from "F" along "G" the passage can be seen to be a joint-guided, easterly-sloping rift with a relatively smooth floor and a complex ceiling from which fragments of caymanite are spalling due to crystal wedging (Figure 5A).

The guiding joint forming the space between the floor and ceiling on the western, upper side of the rift, near the "A" in Figure 5A is filled with caymanite. This is weathering and dislodging due to crystal wedging (Figure 5B) and then sliding down the cave floor as disconnected blocks (Figure 5C). The separated blocks continue to disintegrate by crystal wedging as described by Osborne (2004a). The disintegrated blocks finally end up as a dusty residue seen in the lower right of Figure 5A, below Joe Sydney's shoe.

Patches of caymanite fill remain adhered to sections of the ceiling and remnants of caymanite in ceiling pockets indicate that these pockets were once also filled with caymanite (Figure 5D).

At the northern end of passage "G" in Figure 3 there is a "T" intersection with rift "H". "H" is an east-west tending joint-guided rift, essentially a smaller version of "C–D" in Figure 3. At is western end "H" narrows and terminates in a filled joint from which caymanite is being removed by crystal wedging (Figure 5E).

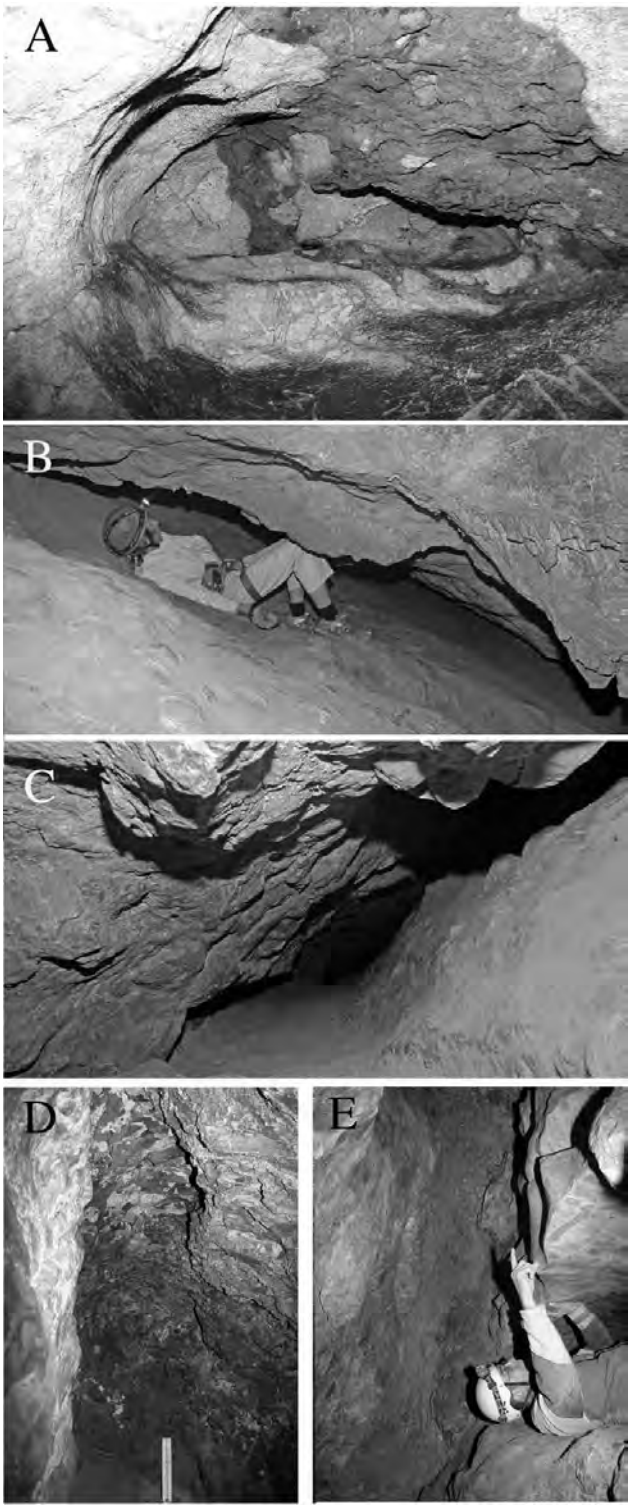

Figure 4. A: Bellhole in ceiling above "A" in Figure 3. B: Looking north along "A" in Figure 3, note floor sloping to the east. C: Looking south into passage "E" in Figure 3. D: Looking west at end of rift, "D" in Figure 3, showing dark caymanite fill in the centre and enclosing limestone walls, light shade. E: Looking west past "F" in Figure 3, author is lying in passage "F–G" pointing to a caymanite fill remnant above.

5. Implications of the New Observations

5.1. Guidance by joints

The traditional view of cave development at Bungonia has been that cave development perpendicular to strike is essentially down dip and in Fossil-Hogans Cave down dip of bedding to the west. The new observations, like those of

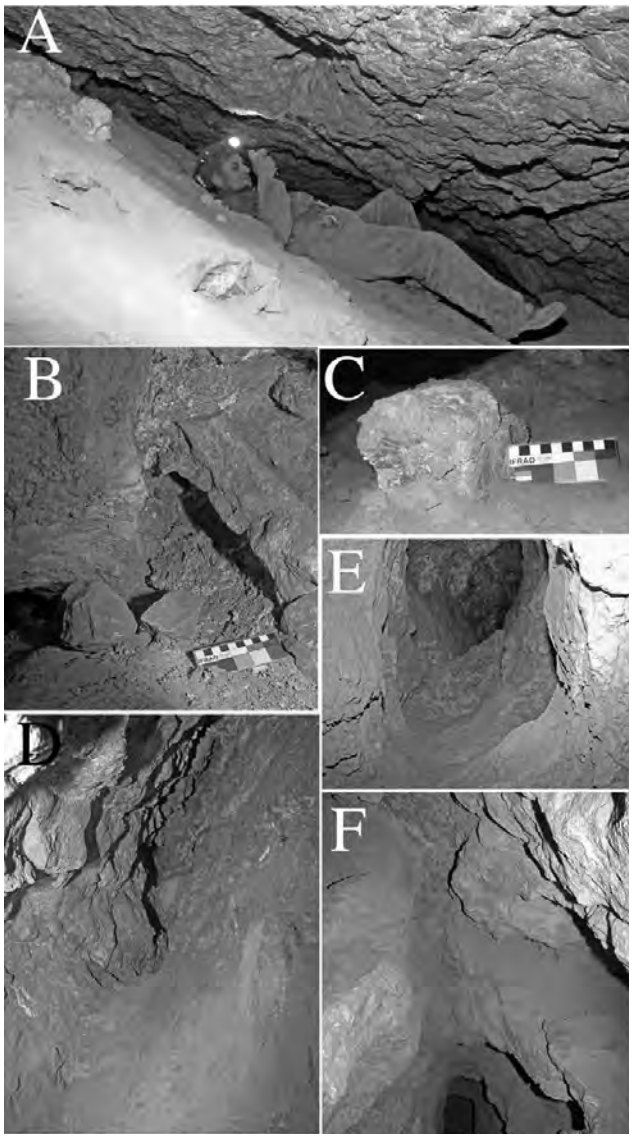

Figure 5. A: Looking north along "G" in Figure 3 note easterly-sloping floor guided by joint and complex ceiling morphology.B: Caymanite at western, upper side of passage "G" in Figure 3 undergoing block failure due to crystal wedging. C: Slipped block on floor of passage "G" in Figure 3 continuing to disintegrate due to crystal wedging after it has separated from caymanite mass. D: Looking up into a ceiling pocket from which caymanite fill is continuing to be removed by crystal wedging. E: East-west trending rift at "H" in Figure 3. Guiding joint adjacent to "E" is filled with caymanite.

Osborne (2001a), suggest that easterly dipping joints, rather than bedding planes, guide so-called "bedding plane flatteners/grovels" like "A", "E" and "G" in Figure 3 and most likely other descending features in the cave.

The idea that the cave developed down dip to the west seems to have its origin in the view that the caves formed under the present hydrological conditions from solution by surface water moving down the dipping bedding planes and then along strike.

The easterly dipping joints dip away from the limestone body and towards the faulted/unconformable boundary with the adjacent Ordovician flysch. Water moving down these joints would eventually be blocked at the contact with the flysch. The easterly dipping joints, however, would provide an upward pathway for water moving into the limestone from the fault along the boundary with the flysch.

The joint-guided cavities and the caymanite filling them must be younger than both the easterly dipping joints and the vertical east-west trending cross-joints. The easterly dipping joints were most likely formed during the last folding event in eastern Australia, the Kanimblan Orogeny, which occurred in the Early Carboniferous. Unfortunately, the age of the vertical joints is unclear.

5.2. Relative age of the cavities

My original thinking about the relative age of the different cavities was that the east-west rifts formed first and were filled with caymanite. They then acted as internal aquicludes (partitions of Osborne, 2003) while the north-south trending passages with an easterly dipping cross-section formed between them. The present pathway through the caves then formed in vadose conditions with the caymanite fill weathering out from the east-west rifts.

A new interpretation of the evolution of the cave chronology is required if both the east-west rifts and the north-south trending passages with an easterly dipping cross-section were both filled with caymanite. This suggests that some time after the Early Carboniferous folding a network cave formed and was filled with caymanite under anoxic conditions. This resulted in the growth of pyrite rhombs in the caymanite matrix. Later, water rising up an easterly dipping joint formed the precursor of the Hairy Traverse, as a phreatic tube along the boundary between the caymanite and the limestone. Very much later the water table was lowered, bringing the caymanite filled cavities into the vadose zone and surface streams invaded through the present entrances.

In vadose conditions, such as those pertaining today, percolating vadose water reacted with the pyrite in the caymanite and the process of exhumation began.

Partial exhumation of the rift "C–D" removed the caymanite that formed the northern wall of the phreatic tube, which was the precursor of the Hairy Traverse, converting the Hairy Traverse from a sloping tube into a sloping notch (a pseudonotch of Osborne, 2004b).

5.3. Almost complete exhumation

Before I observed the active process of crystal wedging and removal of caymanite in passage "G" it did not occur to me that passage "A" or "E" might have also once been filled with caymanite. This observation resulted in the idea that the east-west rifts were older than the passages with an easterly dipping cross-section.

The recognition that caymanite palaeokarst is currently being actively and comprehensively removed by vadose weathering processes and that the rifts and passages "A", "E" and "G" were once completely filled with palaeokarst has significant implications for interpreting the developmental history of caves.

The new observations in Hogans Cave suggest that over time vadose weathering can remove pyrite-bearing carbonate palaeokarst from a filled cavity with almost no trace remaining.

The exhumed ancient cavities are virtually indistinguishable from adjacent much younger features. The exhumed ancient cavities may even be partly re-filled with recent sediment, as has occurred in Hogans Cave, completely obscuring their more ancient origins.

Workers in regions with a complex and long history of speleogenesis need to be alert to the possibility that the bright shiny-walled cavity containing the young sediments may be a very old feature that has benefited from the speleogenetic equivalent of liposuction and a facelift.

Acknowledgments

I would like to thank Neville, Tom and Chris Osborne for their assistance in the field in 2008. Joe Sydney and members of the NSW Cave Rescue Squad and Canberra Speleological Society assisted with fieldwork in 2011. Research at Bungonia Caves was undertaken under the conditions of a NSW National Parks and Wildlife Service Scientific Licence. P. J. Osborne assisted with proofreading.

References

Bauer J, Bauer P, 1998. Eds. Under Bungonia. J.B. Books, Oak Flats.

James JM, Francis G, Jennings JN, 1978. Bungonia Caves and Gorge; a new view of their geology and geomorphology, Helictite, 16(2), 53–63.

Osborne RAL, 1993. A new history of cave development at Bungonia, N.S.W. Australian Geographer, 24(1), 62–74.

Osborne RAL, 2001a. Halls and narrows: Network caves in dipping limestone, examples from eastern Australia. Cave and Karst Science, 28(1), 3–14.

Osborne RAL, 2001b. Non-meteoric speleogenesis: evidence from eastern Australia. Proceedings of the 13th International Congress of Speleology, Brasilia D.F., Brazil, July 15–22, 2001, 1, 97–101.

Osborne RAL, 2003. Partitions, compartments and portals: Cave development internally impounded karst masses. Speleogenesis and Evolution of Karst Aquifers: The virtual Scientific Journal, 1(4), 1–12. www.speleogenesis.info

Osborne RAL, 2004a. Cave breakdown by vadose weathering. International Journal of Speleology, 31(1/4), 37–53.

Osborne RAL, 2004b. The trouble with cupolas. Acta carsologica, 33(2), 9–36.

Osborne RAL, 2005. Dating ancient caves and related palaeokarst. Acta Carsologica, 34(1), 51–72.

Osborne RAL, 2010. Rethinking eastern Australian caves. *In* P Bishop and B Pillans (Eds.) Australian Landscapes. Geological Society of London Special Publication 346, 289–308.

Wray RAL, 1998. Changing ideas on the landscape and speleologic evolution of Bungonia Caves. In J Bauer and P Bauer (Eds.) Under Bungonia. J.B. Books, Oak Flats, 29–39.

AN INTRODUCTION TO SRI LANKAN GNEISS AND GRANITE CAVES

R. Armstrong L. Osborne[1], Pathmakumara Jayasingha[2], Wasantha S. Weliange[3]
[1]*Education & Social Work, A35, The University of Sydney, NSW, 2006, Australia, armstrong.osborne@sydney.edu.au*
[2]*Research Laboratory, Central Cultural Fund, 11 Independence Avenue, Colombo 07, Sri Lanka, jpathma@yahoo.com*
[3] *Postgraduate Institute of Archaeology, Bauddhaloka Mawatha, Colombo 7, Sri Lanka, wasanthaweliange@yahoo.co.uk*

Commencing in 2008 with a focus on caves in metamorphic terrains, the project Cave Science Sri Lanka has investigated forty-eight caves. Thirty-seven caves have been mapped by the Sri Lankan members of the project, twenty-five have been investigated in more detail and samples have been collected from twelve caves for analysis. In addition to rockshelters, boulder caves, tectonic caves and carbonate karst caves developed in marble and dolomite four distinct types of caves, Tunnel Caves, Block Breakdown Caves, Arch Caves and Network Caves have been recognised in Proterozoic gneiss and Cambrian granite in Sri Lanka. While previous workers have suggested that these caves have either formed in what was called gneiss but was really carbonate rock, or are the spaces left behind in the granitic rock after bodies of carbonate rock were removed, field evidence suggests that phreatic solution of granitic rock and/or formation and removal of phantomized granitic rock play a significant role in speleogenesis.

1. Introduction

Sri Lanka is a continental island located off the southern tip of the Indian subcontinent. Geologically it is a Gondwana fragment with most of the bedrock composed of deformed Proterozoic metamorphic rocks (Fig. 1).

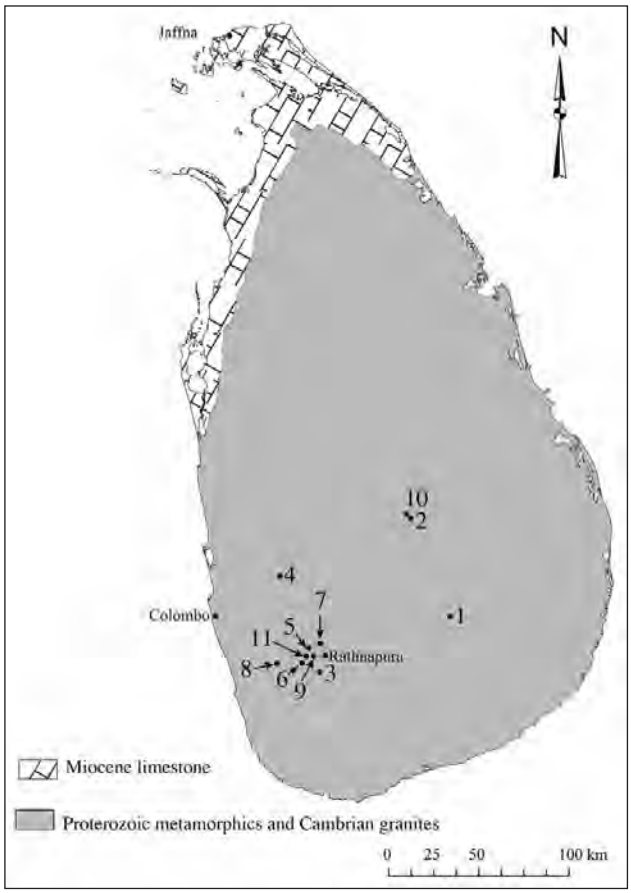

Figure 1. Sri Lanka: 1 = Ravana Ella Cave; 2 = Lunugala Lena Nitre Cave; 3 = Kukuluwa Kanda Rajamaha Viharaya; 4 = Alavala Tunnel Cave; 5 = Batathota Cave & Sthreepura Cave; 6 = Kosgala Vavul Cave; 7 = Batadomba Cave; 8 = Fa-Hien Cave; 9 = Pelpola Cave; 10 = Oil Lamp Cave, Ravana Cave & Twin Cave; 11 = Karannagoda Rajamaha Viharaya.

Sri Lankan caves occur in Proterozoic gneiss, marble and dolomite, Miocene limestone, tufa mounds, and Cambrian granite. There has been little study of Sri Lankan caves except as archaeological sites. A few caves were described by colonial naturalists, Davey (1821) and visiting Europeans: Peet (1945, 1946), Kukla (1958), Siffre (1975) and Brooks (1995a, 1995b), while Gebauer et al. (1996) and Gebauer (2010) provided a cave inventory based on literature research including 310 entries for caves and "cave-like objects" in Sri Lanka. Major Sri Lankan contributions have been by Leiter (1948) who described Nitre Cave and Deraniyagala (1965) who pleaded for international assistance in documenting the caves of Sri Lanka but received no response.

The project Cave Science Sri Lanka, which began in 2008 through the efforts of Dr Wasantha Weliange, is a Sri Lanka–Australia collaboration with the aim of establishing cave science in Sri Lanka by developing local skills in cave exploration and documentation and in scientific research and training. The project is based at the Postgraduate Institute for Archaeological Research, Colombo. The initial focus of the project has been on caves in gneiss and granite as these are significant as archaeological, cultural and religious sites. This research has identified four types of large caves in gneiss; Tunnel Caves, Block Breakdown Caves, Arch Caves and Network Caves.

2. Tunnel Caves

Tunnel caves are a common form of gneiss cave. They are tubes with an elliptical cross-section, which may be horizontal, vertical or sloping depending on the structural setting. Principal axes range in size from 1 to 12 m. Tunnel caves resemble phreatic tubes in karst caves. Large tunnel caves include Ravana Ella Cave (1 in Fig. 1) and Lunugala Lena Nitre Cave (2 in Fig. 1). Some large tunnel caves such as those at Kukuluwa Kanda Rajamaha Viharaya (3 in Fig. 1) are used as temples, one with a large Buddha reclining lengthwise in the cave.

Small tunnel caves form completely in bedrock, but guiding joints that are apparent in the cliff face near their entrance are

often not visible inside the cave. It is unclear if tunnel caves begin as true solution tubes or by some other process such as the removal of phantom rock. Spalling from the cave wall is active and appears to be the main mechanism for lateral expansion of these caves.

Alavala Tunnel Cave (4 in Fig. 1) is good example of this type of cave. It is a tunnel 12.6 m long with an elliptical profile (long axis 1 m; Figs. 2A, B) guided by a westerly dipping joint. After about 5 m the cave steps up to the east. The cave floor is composed of bedrock with a hard, black manganiferous coating. Small elliptical pockets are developed in the western wall of the cave. The only sediments in the cave are two small piles of sub-rounded bedrock fragments, one close to the termination of the lower passage ("i" in Fig. 2A) and the other at the far (northern) end of the cave ("iii" in Fig. 2A). There are signs of active spalling in the cave ceiling, but no spall fragments occur on the cave floor. Small remnant deposits of yellow material that may be phantom rock occur on the eastern wall ("ii" in Fig. 2A) and at the northern end of the cave ("iii" in Figs. 2A, 2C).

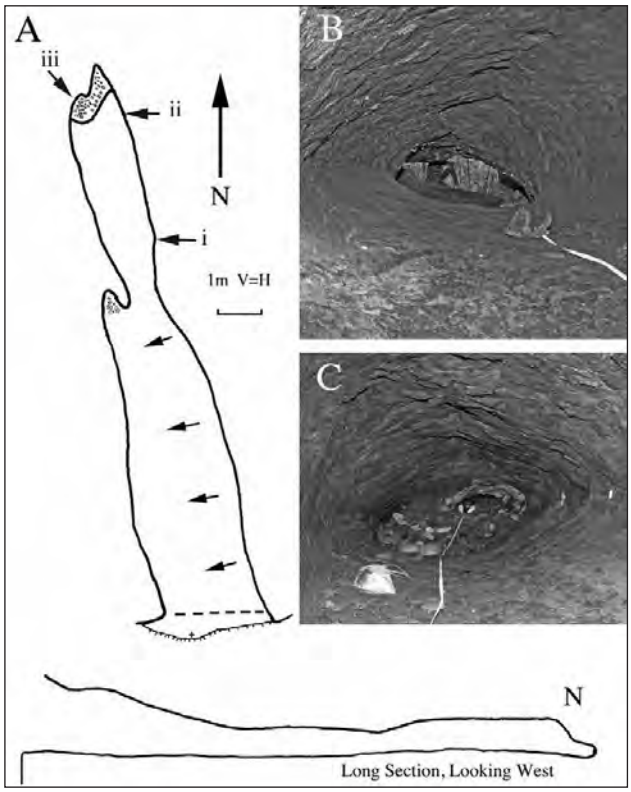

Figure 2. A: Plan and section of Alavala Tunnel Cave. B: Looking south out of Alavala Tunnel Cave note elliptical profile. C: Looking north to end of Alavala Tunnel Cave, note bedrock cobbles and remnant phantom rock (white in B & W image).

3. Block Breakdown Caves

Block breakdown caves are among the larger caves so far investigated in Sri Lanka. They consist of chambers produced by the structurally guided breakdown of gneiss. They are strikingly similar to breakdown chambers in limestone caves. Two block breakdown caves have been investigated in the Rathnapura district**,** Sthreepura Cave (5 in Fig. 1) a system of breakdown chambers and Kosgala Vavul Cave (6 in Fig. 1) a large single-chamber breakdown cave.

Sthreepura Cave is approximately 80 m long and consists of a series of breakdown chambers formed by failure along pairs of conjugate joints most striking NNW–SSE, but in the Guano Chamber breakdown is guided by NE–SW striking joints (Fig. 3A.) This has resulted in the development of "A-type" ceilings (Fig. 3B).

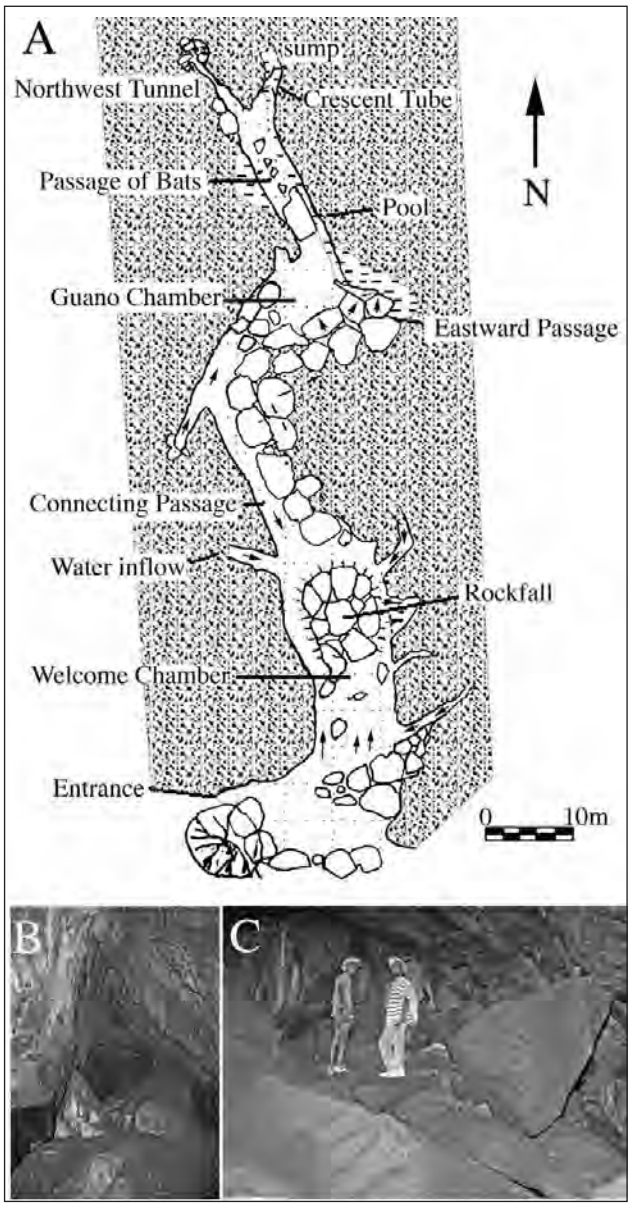

Figure 3. A: Plan of Sthreepura Cave, B: An "A" type ceiling on NNW-SSE joint, connecting passage, Sthreepura Cave. C: Large breakdown blocks Kosgala Vavul Cave.

A remnant half tube is preserved in the ceiling along the axis of the Passage of Bats suggesting that some phreatic-like process proceeded breakdown. A small phreatic tube, the Crescent Tube, extends from the NE corner of the Passage of Bats. Most of the walls, the ceiling and all of the fallen blocks in Sthreepura Cave are composed of gneiss. A small section of the wall and floor in the NW side of Guano Chamber is composed of dolomite. Much of the floor of the cave is covered by dry loose sediment composed of organic silt derived from bat guano and mica flakes derived from the bedrock.

Kosgala Vavul Cave contains breakdown on a much larger scale (Fig. 3C) and like Sthreepura Cave shows remnants of an old small-scale phreatic network with small phreatic tubes exposed as half tubes in joint faces.

4. Arch Caves

Arch caves are large chambers with a triangular-shaped plan and cross-section, their shape and volume makes them ideal for use as temples and as habitation sites. Many such as Batathota Cave (5 in Fig. 1) have been converted into temples and some such as Batadomba Cave (7 in Fig. 1) and Fa-Hien Cave (8 in Fig. 1) are both temples and archaeological sites.

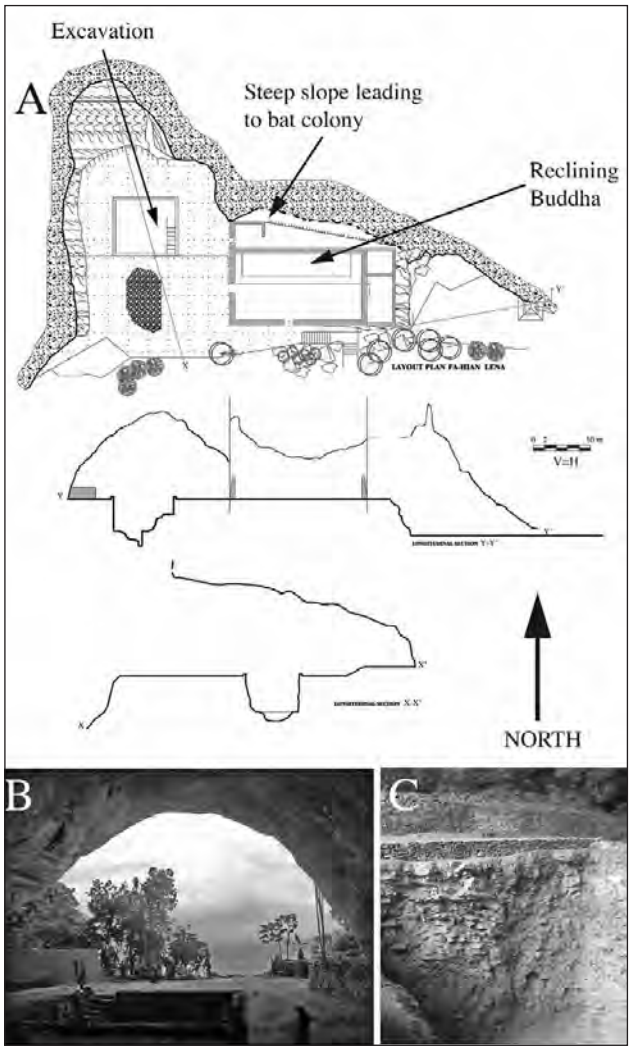

Figure 4. A: Plan and sections of Fa-Hien Cave. B: Looking out through main arch of Fa-Hien Cave, note shape of arch, excavation in foreground. C: Western side of excavation showing relict foliation dipping north.

Fa-Hien Cave is the largest arch cave so far investigated. Its arch chamber is approximately 30 m wide and 14 m high at the entrance and extends 50 m into the rock mass (Fig. 4A). Like other arch caves, Fa-Hien Cave has an arch-like cross section (Fig. 4B).

While the floor of the arch chamber appears to be made of sediment, the exposure in the 6.3 m-deep archaeological excavation shows relict foliation dipping to the north (Fig. 4C). This indicates that the cave floor is not made of fallen matter from the ceiling, as apparently assumed by the archaeologists, but of intensively weathered (? phantomized) bedrock. The base of the excavation reveals a network of small tubes developed in the weathered rock. This has yet to be explored.

Sheet spalling/exfoliation is continuing from the cave walls and masses of spall rubble have been removed from the cave floor and packed around the side of the cave.

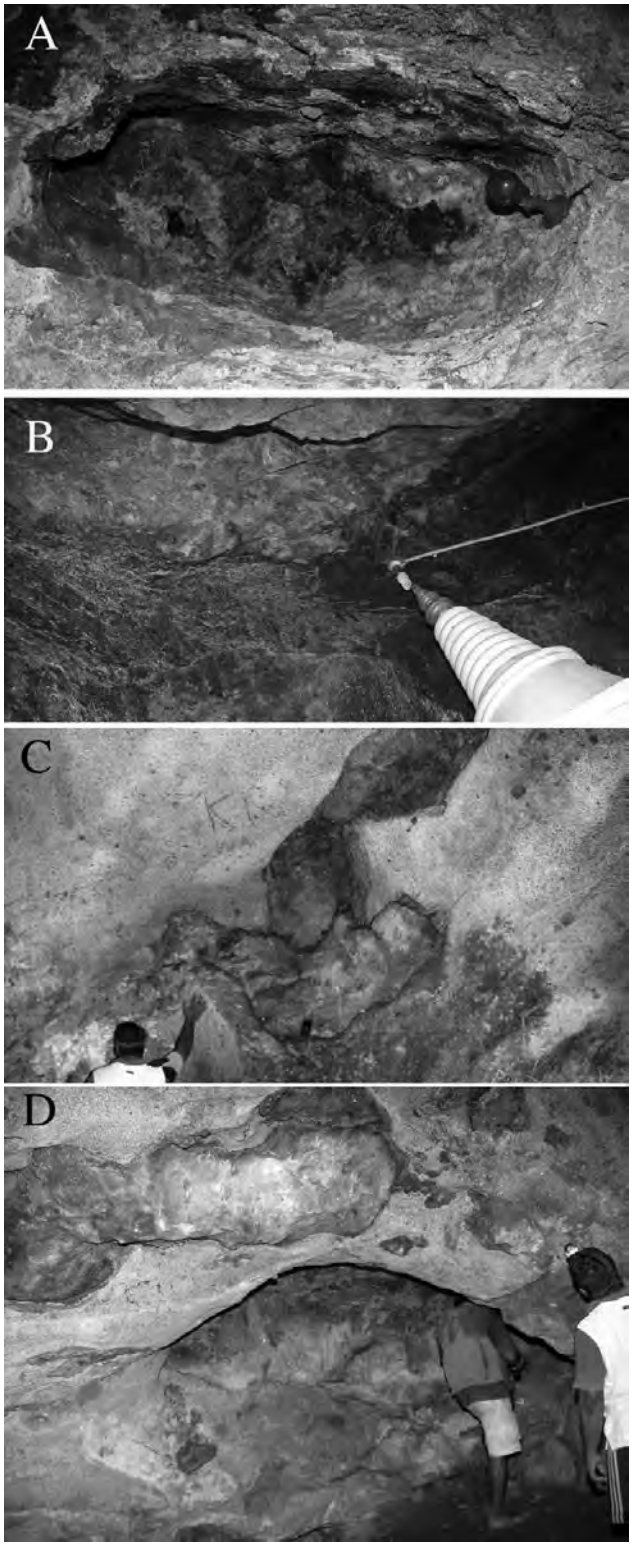

Figure 5. A: Wall pocket, Batathota Cave. B: Ceiling half-tube, Batathota Cave. C: End pocket, Batadomba Cave; lighter rock is gneiss and darker rock is dolomite. D: Ceiling pocket, Batadomba Cave; lighter rock is gneiss, darker rock is dolomite.

The walls and ceilings of arch caves can be quite complex with cupola-like features, wall pockets and ceiling half-tubes developed in Batathota (Figs. 5A, 5B) and Batadomba Cave. The pockets in Batadomba Cave are quite instructive concerning the relationship between speleogens and bedrock. The pocket at the end of Batadomba Cave (Fig. 5C) cuts across both gneiss and dolomite bedrock with minimal effect on its morphology. A similar situation can be seen in Figure 5D where the morphological features below "D" in the image continue with minimal disruption across irregular lithological boundaries.

The origin of these caves remains unclear, while spalling is the main process currently acting to expand the caves, the lack of spall material in the archaeological dig in Fa-Hien Cave suggests that this is probably not the main process involved in cave development over time.

5. Network Caves

Our research so far has focussed on large cavities near the surface and serious attempts at digging in caves have yet to be undertaken, partly because such activities may be interpreted by archaeologists as illegal digs and also because it may lead us to be identified as treasure hunters.

The presence of relict half tubes in block breakdown caves and arch caves and of tubes in the base of the excavation in Fa-Hien Cave, suggests that complex network caves may exist further into the rock mass.

One complex cave with potential for extension by digging is Pelpola Cave (9 in Fig. 1). The entrance to Pelpola Cave is a small collapse doline, much like that seen in limestone karst. At the base of the entrance rubble pile there is a triangular-shaped entrance chamber (Fig. 6A). A passage in bedrock from which mud has been artificially excavated extends downwards from the SE corner of the entrance chamber (1 in Fig. 6A). Figure 6B shows the view looking SE down the passage from "1" in Figure 6A. A profile of the passage is visible in the background showing a triangular upper part and inward-sloping walls in the lower part. After about 10 m an artificial side passage extends to the NE and leads into Treasure Hunters Chamber (2 in Fig. 6A). This chamber has a relatively horizontal bedrock ceiling and a sediment floor, level at the NE end of the chamber that then slopes steeply to the SW. Figure 6C is taken looking east from "2" in Figure 6A. The ceiling above the cavers' heads is composed of siliceous gneiss. The edge of a zone of very large crystals is seen in the upper right corner of the image. The cavers are sitting on a rock shelf composed of dolomite covered by a white mineral paste. There is a large amount of a loose mixture of clay and gravel on the floor of Treasure Hunters Chamber that appears to have been moved from further inside the cave and piled up artificially along the southern edge of the chamber near "3" in Figure 6A. While it was not possible to enter without digging there appears to be a void to the south of "3" and there are indications that the clay/gravel mixture may be retained by timber supports (Fig. 6D). The passage from the Entrance Chamber continues as a trench along the SW wall of Treasure Hunters Chamber and ends in a sediment plug (Fig. 6E). It seems likely that gem miners excavated Pelpola Cave, targeting the clay/gravel mixture as a possible source of gemstones. The clay/gravel mixture appears to be a weathering or alteration product derived from the gneiss bedrock, excavated from further inside the cave.

6. Speleogenesis

While little has been written about Sri Lankan gneiss caves, two explanations for the origin of the caves have emerged in the literature.

The first explanation arises from the idea that if there are caves then they must be in limestone. This idea has been reinforced by Gebauer (2010) locating all caves not in Miocene limestone in "calcareous granulite" or "metamorphosed, crystalline and dolomitic limestone /marble" and by other workers placing caves on dolomite outcrops on low-resolution geological maps.

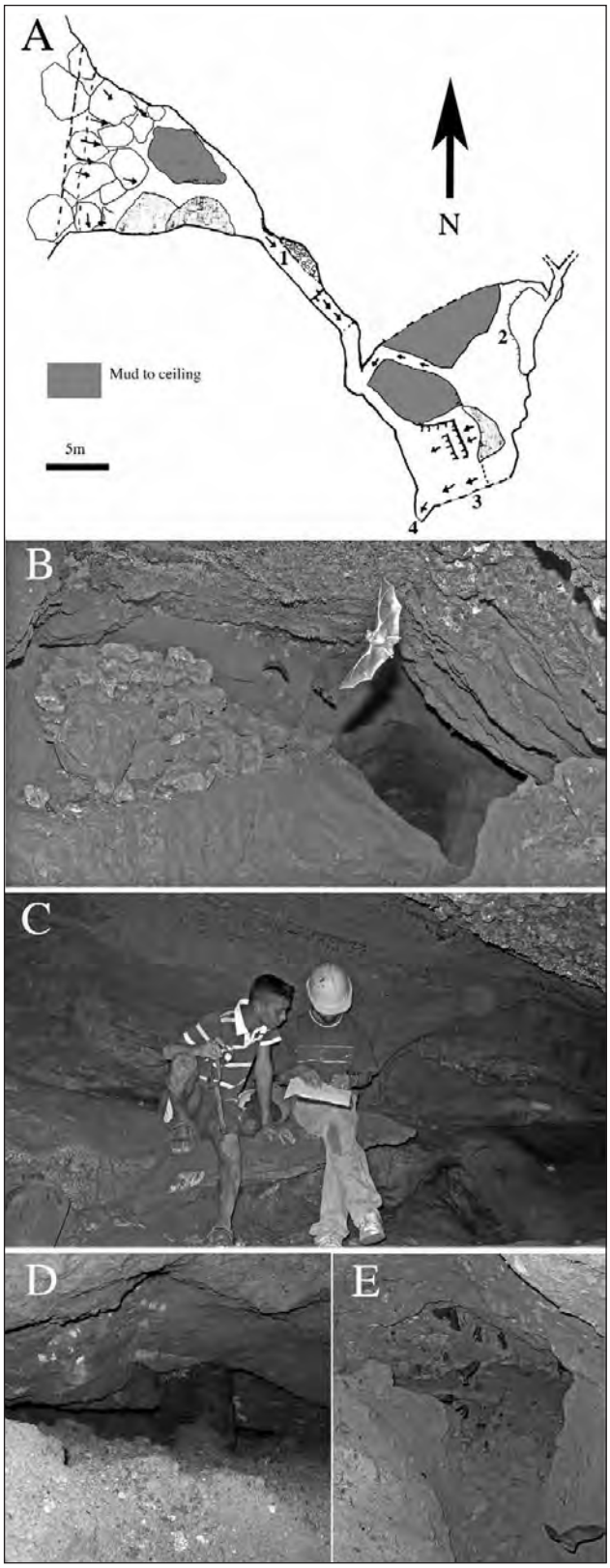

Figure 6. A: Plan of Pelpola Cave. B: View looking SE down passage from "1". C: Looking east from "2". D: Looking south at "3". E: Termination of passage at "4".

Another reason for this idea is that gneiss caves frequently intersect small bodies of marble. This has led to confusion as to what the principal bedrock is. The occurrence of carbonate rock in some gneiss caves lead Davey (1821) to consider that if the gneiss contained caves, then it was so carbonate rich that it should be considered marble. Our observations so far have shown that while many gneiss caves morphologically resemble caves in carbonate rock, most gneiss caves are principally developed in siliceous metamorphic rocks.

The second idea was proposed by Leiter (1948), who considered gneiss caves to be the spaces left behind in the gneiss following the removal of masses of carbonate rock by solution. Since both irregular masses and whole folia of carbonate rock are exposed in many, but not all gneiss caves, this is not an unreasonable suggestion.

We have found a small cave that probably did form this way, Oil Lamp Cave (10 in Fig. 1). Oil Lamp Cave is a small joint-guided passage with a triangular profile and walls composed of gneiss (Fig. 7A). After a few metres the cave comes to a sudden end in a flat surface of solid rock (Fig. 7B). This rock is not siliceous gneiss, but dolomite, with rusting ferromagnesian minerals. The shape of the boundary between the gneiss and the dolomite, indicated by the torch in Figure 7B, matches the profile of the adjacent wall, suggesting that the cave has formed by removal of the carbonate rock from the enclosing gneiss.

While removal of underling folia of carbonate rock is a plausible explanation for the development of block breakdown caves and might explain the initial formation of arch caves, there is too much evidence in Sri Lankan gneiss caves of solution-like speleogens on siliceous gneiss for this mechanism to be universally viable.

Evidence for another mechanism arose on our very first field visit to Kukuluwa Kanda Rajamaha Viharaya (3 in Fig. 1) in 2009. The feature seen in Figure 8A was encountered up hill from the tunnel caves used as temples. This is a structurally-guided, cave shaped depression in the face of a small cliff-like outcrop of gneiss marked by a sign in Singhalese. The cave shape is filled with yellow material. On close inspection the filling appeared not to be sediment but altered/weathered gneiss, the yellow colour resulting from secondary ferruginous cement. The outcrop suggests that natural weathering/erosion has preferentially removed about 1 m of the yellow material. If this were to continue, the result would be a cave with an elliptical profile much like Alavala Tunnel Cave, making this a nascent phantom rock cave. When asked about the sign (right foreground Fig. 8A) the resident monk explained that this was the site of a future meditation hall, he intended to construct by digging out the yellow material to make a new cave. On a return visit in 2012 no progress had been made with the excavation, probably due to the strength of the ferruginous cement.

Further evidence for phantom rock processes in gneiss cave formation is found at Karannagoda Rajamaha Viharaya (11 in Fig. 1) where, in addition to tunnel caves and sections through phantom rock filled tubes, an extensive overhang cave is developed by the partial removal of a horizontal body (folium) of phantomized rock. This cave is approximately 21 m wide by 17 m deep with a ceiling height ranging from 2.1–0.8 m (Fig. 8B).

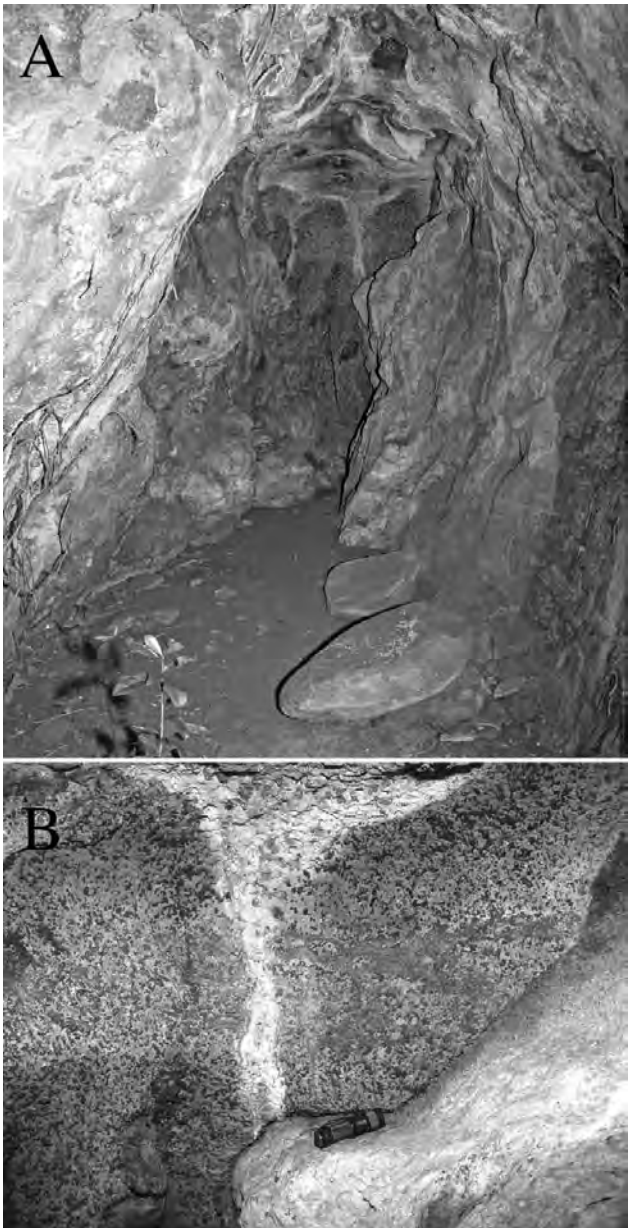

Figure 7. A: Looking into Oil Lamp Cave. B: Bedrock termination of Oil Lamp Cave. Speckled rock is dolomite; white rock below and to the right of black torch is siliceous gneiss. Torch is 95 mm long.

The ceiling slopes to the northeast with the foliation in the bedrock, suggesting that a segment of a whole phantomized folium has ben removed to form the cave. Pillars of phantom rock remain in the cave, separated by curved gaps that resemble the profiles of phreatic tubes suggesting that before mass removal of the phantomized rock there may have been a network of tubes, similar to that in the excavation at Fa-Hien Cave.

The remnant phantom rock in Alavala Tunnel Cave, the deep zone of "weathered" rock in Fa-Hien Cave, the clay/gravel mixture in Pelpola Cave and the observations at Kukuluwa Kanda Rajamaha Viharaya and Karannagoda Rajamaha Viharaya all suggest that formation of phantom rock, followed by its natural, and in places artificial removal is likely to be a major agent for speleogenesis of gneiss caves in Sri Lanka.

Since Vergari and Quinif (1997) have shown that many phreatic-like solutional forms can result from phantom rock processes, it is possible that the range of phreatic-like cavities

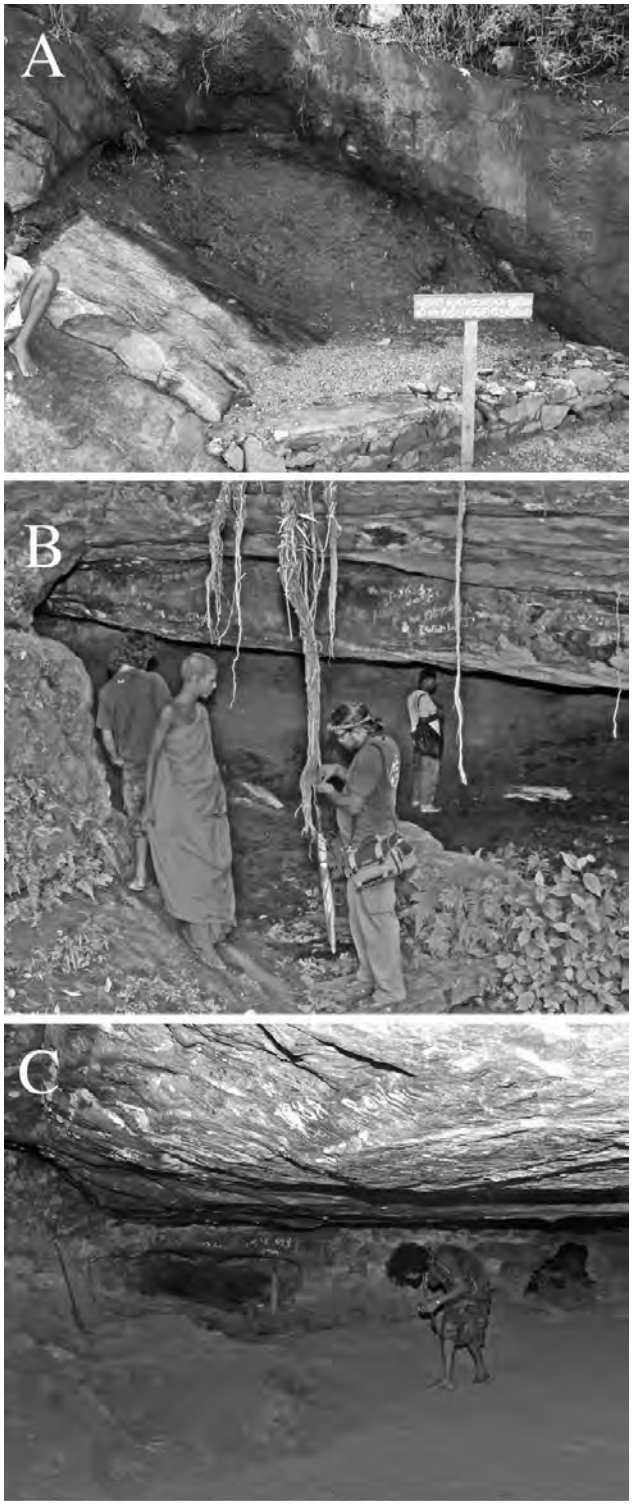

Figure 8. A: Nascent phantom rock cave and meditation hall, Kukuluwa Kanda Rajamaha Viharaya. B: Looking into cave in folium at Karannagoda Rajamaha Viharaya. C: Remnant pillars of phantom rock in cave in folium at Karannagoda Rajamaha Viharaya.

and speleogens found in Sri Lankan gneiss caves are not the product of direct solution of the silicate rock but of its phantomization.

7. On-going Research

In addition to cave morphology and speleogenesis we have also investigated cave sediments and surface karst-like features on gneiss and granite. Minerals and speleothems are being investigated in collaboration with Ross Pogson and David Colchester of the Australian Museum, Sydney. An initial paper (Osborne et al., in prep.) has been submitted to *Acta Carsologica*. Current research is focussed on a 200 m-long network cave, largely developed in phantom rock.

Acknowledgments

We would like to acknowledge the support of professors Nimal de Silva, Jagath Weerasinghe, Prishantha Gunuawardana, Gamini Adikari and Raj Somadewa. Sri Lankan colleagues; A.S. Dandeniya, Prageeth Algiriya, Dinesh Devinuwara, Duminda Alahakoon and Ms Nayomi Sayanara Prasannajith assisted with cave exploration and mapping. We are grateful for the assistance of the clergy and administration of several Buddhist temples and monasteries. Armstrong Osborne would like to thank Dr Weliange, Mrs Aruni Premathilake, Ayoma and Paya for accommodation and assistance in Sri Lanka. Penney Osborne assisted with proofreading.

References

Brooks SJ, 1995a. Caving in Sri Lanka. Orpheus Caving Club Newsletter, 31(5–6), 22.

Brooks SJ, 1995b. Ms 20, Quoted in Gebauer, HD, 2010. Resources on the Speleology of Sri Lanka, http://www.speleologie.de/forschung/lk/general/resources/bhb_2010_lk.pdf, 36.

Davey J, 1821. An account of the interior of Ceylon and of its inhabitants with travels in that island. Longman, Hurst, Rees, Orme & Brown, London.

Deraniyagala PEP, 1965. Some present-day problems of cave research in Ceylon. Studies in Speleology, 1(2–3), 143–147.

Gebauer HD, 2010. Resources on the Speleology of Sri Lanka. http://www.speleologie.de/forschung/lk/general/resources/bhb_2010_lk.pdf

Gebauer HD, Mansfield RE, Chabert C & Kusch K, 1996. Speleological Bibliography of South Asia including the Himalayan regions. Armchair Adventure Press, Kathmandu.

Kukla J, 1958. Jeskyne na Ceylone. Ceskoslovensky Kras, 11, 165–169.

Leiter N, 1948. Geographical study of the Nitre Cave district. Bulletin of the Ceylon Geographical Society, 3(3–4), 61–72.

Osborne RAL, Weliange WS, Jayasingha P, Dandeniya AS, Algiriya AKPP & Pogson RE, In Prep. Caves and karst-like features in Proterozoic gneiss and Cambrian granite, southern and central Sri Lanka: an introduction. Submitted to Acta Carsologica.

Peet GA, 1945. Nitre Cave, Ceylon: An innovatory national park. British Caver, 13, 69–71.

Peet GA, 1946. The Nitre Cave expedition. British Caver, 14, 90–95.

Siffre M, 1975. Dans les abîmes de la terre. Flammarion, Paris.

Vergari A & Quinif Y, 1997. Les paléokarst du Hainaut (Belgique). Geodinamica Acta, 10, 175–187.

ENDO- AND EXO-KARSTIC FEATURES IN BANDED IRON FORMATION AND CANGA, SERRA DA PIEDADE, QUADRILÁTERO FERRÍFERO (BRAZIL)

Manuela Corrêa Pereira[1], Joel Georges Marie Andre Rodet[2], André Augustos Rodrigues Salgado[3]
[1]Instituto Estadual de Florestas/IEF, Cidade Administrativa, Rodovia Prefeito Américo Gianetti, s/n°, 31.630-900, Bairro Serra Verde, Brasil, manuelacp1@gmail.com
[2]UMR/CNRS, 6143, Laboratoire de Géologie de l'Université de Rouen, France, joel.rodet@univ-rouen.fr
[3]Instituto de Geociências/UFMG, Avenida Antônio Carlos, 6.627 Pampulha, Brasil

This research integrates into the theme about karst in non-carbonated rocks, and has as main objective to inventory, describe and analyze the physical aspects of the cavities and superficial karstic features developed in the ferruginous rocks, itabirite and canga in the Serra da Piedade, Brazil. The methodological approach basically consisted in: (1) the prospecting of cavities and superficial features; (2) the selection of the cavities and the superficial features; (3) the description of the physical aspects of the cavities with karstic features; and (4) analysing and debating about the results. Amongst the 52 listed cavities in the Serra da Piedade, five of them contain features that show dissolution processes: Gruta da Piedade, Gruta do Cascalhinho, Gruta da Macumba, Gruta do Chuveirinho and Gruta do Triângulo. These cavities contain shapes that can be seen as karstic features like alveoli, ceiling domes, karstic paleofloors, fillings and rock pendants. Thus, the most common superficial karstic feature in the Serra da Piedade is the kametitza or solution pan. We can come to the conclusion that there is an existence of karstic features developed in the canga and the itabirite of the Serra da Piedade, even though they are not very expressive in comparison with the features in carbonated rocks.

1. Introduction

Since a few times, the number of records and studies about karstic features developed in non-carbonated rocks have tremendously increased. Amongst these studies stand out those made on the sandstone and quartzite rocks, including for instance the works of Sallun Filho and Karmann (2007), Uagoda and Netto (2009), Auler (2004), Hardt (2009), Chalcraft and Pye (1984).

For several researchers, for instance Simmons (1963), McFarlane and Twidale (1987) and Pilo and Auler (2005), the karstic features can also develop in ferriferous formations. According to the researchers, the cavities and others geoforms exist in ferriferous formations and dissolution is an important factor of their genesis. However, despite this fact, the studies on the karstic features in the ferriferous formations are very few. In Brazil, the first studies on the genesis of these features started with Simmons (1963).

By the 21st century, the resurgence of the kartstic features studies in the iron deposite takes place in an environmental protection process opposite to the mineral exploitation which is each time more effective. Nevertheless, despite the augmentation of the number of studies and speleological records in the ferriferous formations around Brazil, we still notice a big lack of academic publications and researches on this subject. This also concerns regions where the iron extraction is very active like for instance in the "Quadrilatero Ferrifero" in Minas Gerais.

In this context, the Serra da Piedade – which belongs to the geological and geomorphological "Quadrilatero Ferrifero" complex – is the subject of this study. Therefore, the main goal of this work is to pick up, describe and analyze the physical aspects of the cavities and superficial karstic features developed in the ferriferous rocks – itabirite and canga – of the Serra da Piedade.

2. Study Area

The Serra da Piedade is located between 19° 48' and 19° 50' in South latitude and between 43° 39' and 43° 42' in West longitude, in the north part of the Quadrilatero Ferrifero – Minas Gerais in Brazil (Fig. 1). It develops in the districts of Sabara/MG and Caeté/MG and has a great signification in the social, cultural and religious history of the Minas Gerais state.

In the region of Serra da Piedade, are shown (Alkmin and Marshak 1998): (i) granito-gneiss of the Archean crystalline substratum; (ii) schists and phyllites also of the Archean era of the Nova Lima Group – Rio das Velhas Supergroup, and (iii) proterozoic rocks of the Minas Supergroup (Figs. 1, 2). In the Serra da Piedade, the Minas Supergroup is represented by the following groups: (i) Caraça, with the ferriferous quartzites of the Moeda Formation; (ii) Itabira, with the itabirites of the Cauê formation, and (iii) Piracicaba, with the schists and phyllites of the Sabara Formation, and with the phyllites and ferriferous quartzites of the Cercadinho Formation. In general, Tertiary-aged formations of canga (Fig. 2) develop and cover the itabirites of the Cauê Formation (Itabira Group).

The topography of the study area, like the whole Quadrilatero Ferrifero/MG shows a strict relation with the substrate and evolved through differential erosion. In this context, the sectors which have canga, quartzites and itabirites for substrate bear the most elevated parts of the relief, and those situated in the schists, the phyllites and the granito-gneiss give the lower topographic parts (Harder and Chamberlin 1915; Tricart 1961; Barbosa 1980; Salgado et al. 2004). Moreover, this range is being distinguished by its steeply slopes with a great drop-off by exposing the clean rock (Fig. 2).

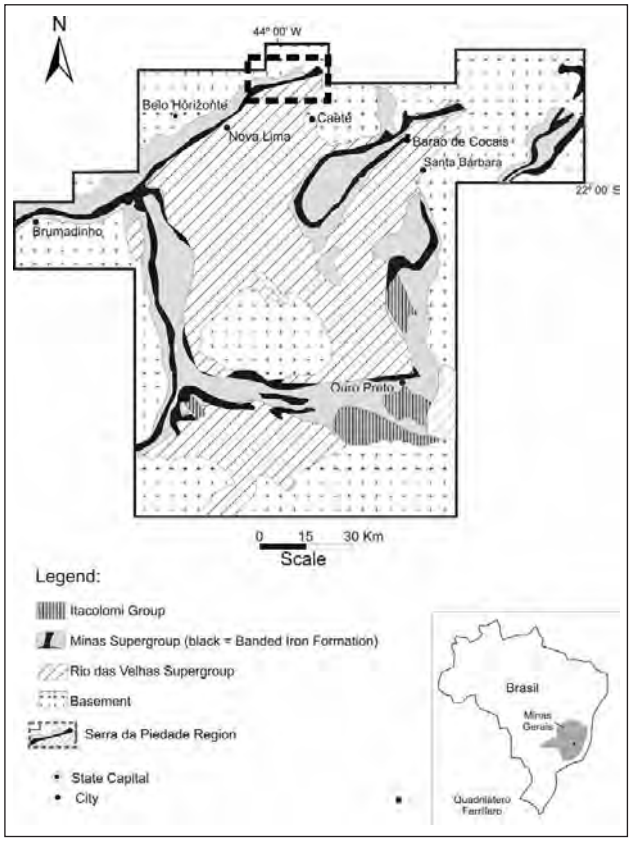

Figure 1. Location and geology of the Serra da Piedade and Quadrilatero Ferrifero. Source: Alkimim and Marshak, S. (1998).

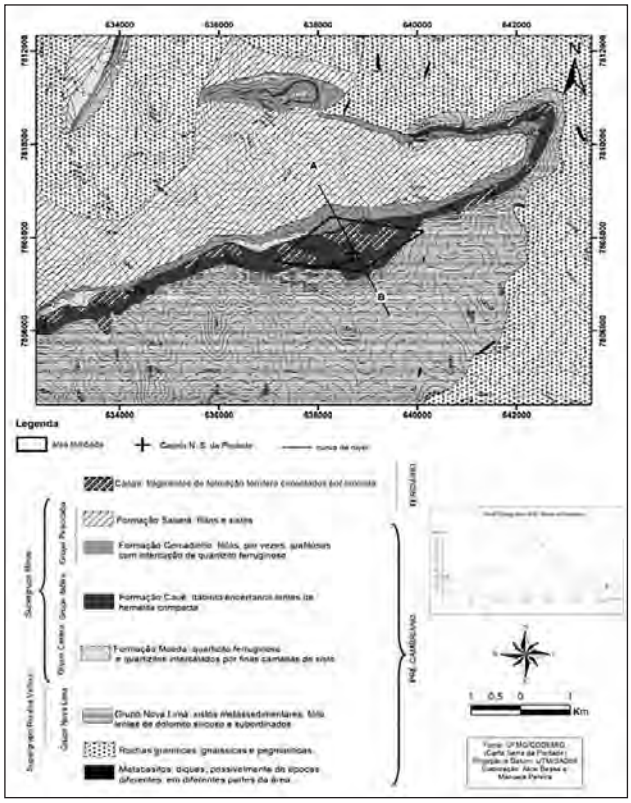

Figure 2. Lithological map of the Serra da Piedade. Regarding the curves of level and cross section A–B, we notice that the southern slope is more abrupt than the northern slope.

3. Methods

The realization of this research can be divided into three steps: (i) bibliographic revision; (ii) collection of data in the field, and (iii) topographical survey of the caves, elaboration of the cartographical material and analyze of the results.

Firstly a bibliographical survey was made about karst in the ferriferous rocks and also an approach of the environmental characteristics of the study area. Moreover, SPOT satellite imagery (2002) was used for a pre-identification of the areas with the most important speleological potential. On the field, cavities were studied, as well as the superficial features that were identified in the study area. The cavities were classified according to three types: (i) cavities formed by the fall of rocks called slope/talus cavities; (ii) cavities which show dissolution features called caves with karstic features, and (iii) cavities which neither have been formed by fall of rocks nor show dissolution geoforms called caves without morphokarstic evidences. In this work, only caves with karstic features are being focused on.

During the field study, was made the topography of the caves with karstic features according to a degree of details and accuracy between 2C and 5D, according to the gradual topology established by the British Cave Research Association. Moreover, we have tried to characterize the physical aspects observed in these cavities: insertion into the landscape, geology, morphology of the conduits, hydrology, clastic deposits, chemical deposits and dissolution features.

4. Results

Fifty-two natural cavities were studied in the study area (1,92 km^2). They split up into 29 talus cavities, 5 caves with karstic features and 18 have been classified as cavities lacking of morphokarstic evidences.

In this work, only the cavities with karstic features will be analyzed: Gruta da Piedade, Gruta do Cascalhinho, Gruta da Macumba, Gruta do Chuveirinho and Gruta do Triângulo (Fig. 3).

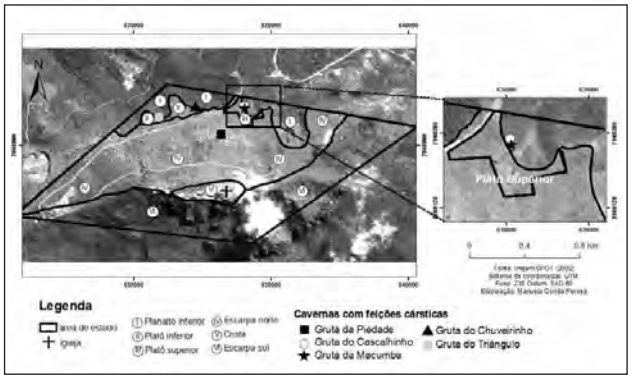

Figure 3. Location of the caves with karstic features in the Serra da Piedade.

4.1. Gruta da Piedade

The cavity was called “Gruta da Piedade” because it is the most developed cave in the study area, thus it received the

same name as the Serra which contains the Nossa Senhora da Piedade sanctuary.

The Piedade Cave develops in the superior part of the Northern Escarpment unity (Fig. 3). This cavity is being distinct because it has a huge development (365 m) and also a height difference of 39 m. This big deep is the cause of the division of the Gruta da Piedade into five altimetric levels: level -1, level 0, level +1, level +2, and level +3. The most significant criterion of the complexity of the Gruta da Piedade is the 15 entries identified during the topography of the cavity.

At -1 level, we can notice the Salão Arredondado and the Conduto Calibrado (Fig. 4). The Salão Arredondado is characterized by the presence of thin sediment on the ground, and we can also notice the contact between the itabirite and the detrital iron crust (Fig. 4A). In this room, it was also possible to look at alveoli-shaped features whose genesis seems associated with dissolution processes. (Fig. 4B).

The Conduto Calibrado presents a tubular form which seems to have been shaped by piping (Fig. 4D) processes. This conduit can be the result of karstification processes. Within the conduit, we can observe the presence of coarse canga deposits, particularly of a block size. Moreover, the main observed karstic feature in this conduit are ceiling pendants (Fig. 4C).

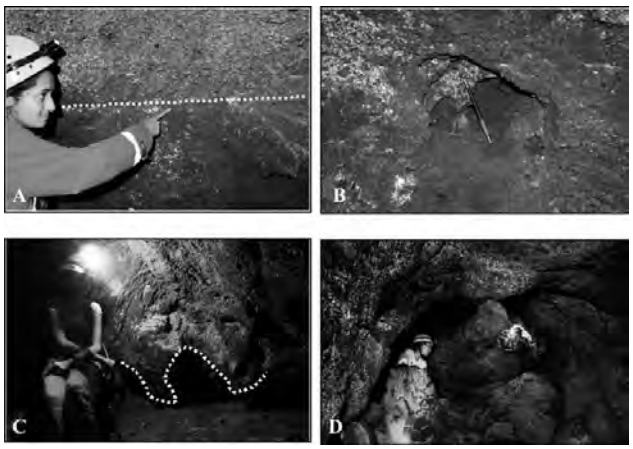

Figure 4. (A) contact between the detrital iron crust and the itabirite in the Salão Arredondado; (B) Alveoli feature located in the Salão Arredondado; (C) Pendants located at the end of the Conduto Calibrado; and (D) Conduto Calibrado, where is possible observe a tubular calibration and the presence of canga blocks.

The 0 level of the Gruta da Piedade consists in a ledge on which the main entrance of the cave stands. In comparison with other studied cavities in the Serra da Piedade, this entrance is wide size, like the dimensions of numerous cavity's entrances in limestone (Fig. 5A). In the entrance room, we can observe several alveoli-shaped features on the walls.

The rooms of the -1 level show a genesis associated with a chaos of itabirite blocks, which signifies that these rooms have not been shaped *in situ*. The interesting features in this part of the cavity are speleothems and small dissolution basins. The speleothems that can be found are coralloid type. The Matacões conduit links the -1 level with the -2 level. In this latter level, the Minhoca conduit is the most interesting. At the end of this conduit we can notice the presence of mischaractized itabirite, regarding the fact that it only gives hematite stratum (Fig. 5B). Thus we can assume that the siliceous stratum was lixiviated, which is a factor that implies dissolution processes. We can also notice the predominance of thin sediments and speleothems shaped in the itabirite.

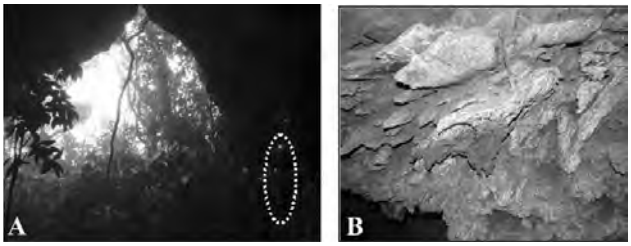

Figure 5. (A) Entrance of the Gruta da Piedade; (B) Altered and crumbly itabirite which does not present anymore the siliceous stratum which takes part in its original composition.

In the main room (0 level), in the south west part, a platform gives access onto the conduits and the other parts of the chambers of the cave. At level +1 is open the Salão dos Morcegos which consists in a big chamber, crossed by temporary drainages. Moreover we can notice that the two first conduits of the west part of this room had a genesis associated with the stratification plans of the itabirite (Fig. 6B).

In the upper parts (levels +2 and +3) develop chambers which appear to be formed by overlap of boulder. In these chambers, the presence of classical coarse deposits is recurrent. In one of the +2 level entrance we can notice alveoli features (Fig. 6A).

Figure 6. (A) Presence of alveoli in the entrance number 13 of the Salão do Alivio; (B) Conduit genesis linked with the bedding planes of the itabirite.

4.2. Gruta do Cascalhinho

The cavity has been called "Cascalhinho" according to the local name given to the plateau on which it is located. The Gruta do Cascalhinho is the first cavity in the W–E direction which develops at the edge of this plateau (Fig. 3). The cave presents two entrances and a development of 30 m.

In the field, we noted that the lithology of the Gruta do Cascalhinho is characterized by the presence of detrital iron crust, showing debris whose dimension is included between the pebble and the rock bolder. Within the debris, we notice that some of them have the banding of the itabirite.

The conduits of this cavity show an irregular morphology, partially oval and partially circular. Moreover, we noted that

a major part of the conduits shows cracks between detrital iron crust and itabirite (Fig. 7A).

As for the hydrologic aspects, we notice that the Gruta do Cascalhinho shows a dripping during the rainy period. However, during this period or during the dry period, the cave shows condensation.

We notice that the clastic deposits show a granulometry which oscillates between the thin sediments and the coarser pebbles, blocks or rock bolder. Within the cavity, we notice speleothems of coralloid type of a dimension from millimeter to centimeter.

In this cavity, a high density of features which highlight karstic processes has been found. Towards these features, pendants detach with millimetric dimension coralloids directly formed on itabirite and ceiling domes which have developed in this lithology (Figs. 7B, C)

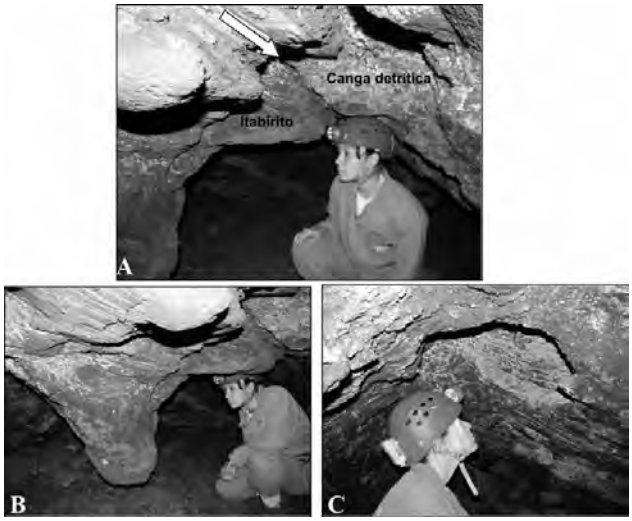

Figure 7. (A) Calibrated conduit with the presence of a crack between the itabirite and the detrital iron crust; (B) Pendant, relic form which indicates the coalescence of conduits related to a dissolution process; and (C) Ceiling dome formed at the top of the Gruta do Cascalhinho.

4.3. Gruta da Macumba

The Gruta da Macumba has that name because of items found inside, these objects are used for this kind of religious ritual. This is the second cavity in the W–E direction which includes in the edge of the Plateau Superior unity (Fig. 3). The cave shows three entrances and a development of 27 m (Fig. 8).

In general, the lithology observed in the field consists in detrital iron crust and itabirite. The more we penetrate the cave, is noticed that the mould of the detrital iron crust become more whitish. The cavity shows numerous cracks all over its development.

As for the hydrologic aspects, we notice that the Gruta da Macumba shows a drip during the rainy period and condensation during the rainy and the dry period.

As for the clastic deposits, we notice that they give a grain size which oscillates from fine-grained sediments to the coarser ones with peebles, blocks, and boulders. The lithology of the most coarse-grained sediments is illustrated by itabirite and canga.

The cavity was classified as karstic according to the presence of features that prove the dissolution processes. Towards the features, a paleofloor detaches in this cavity. The walls of the cavity also show concavities that can be linked with alveoli shapes (Fig. 8).

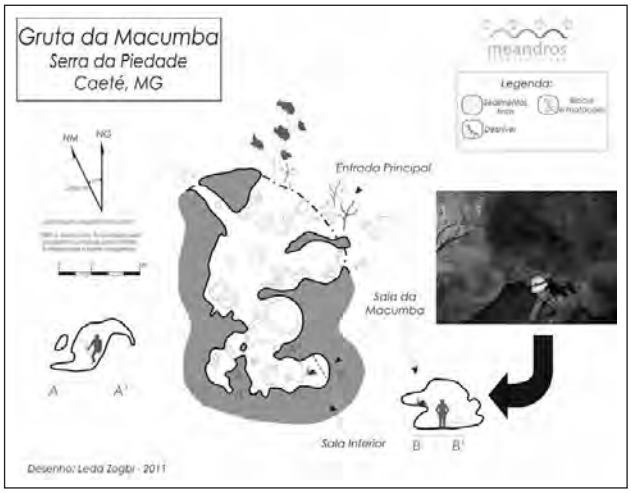

Figure 8. Map of the Gruta da Macumba where we can notice the existence of a paleofloor in the south part of the cavity, and irregular conduits.

4.4. Gruta do Chuveirinho

The cavity was called “Chuveirinho” because of the intense drip during the rainy period. The Gruta do Chuveirinho is the third cavity in the W–E direction and is included in the edge of the Low Plateau (Fig. 3). The cave has only one irregularly shaped entrance and a development of 70 m.

The cavity is composed by four chambers. In general the first two chambers were formed in the detrital iron crust composed of debris, which dimension oscillate between pebble and boulder rock, immerged in a ferriferous mould and densely distributed (plenty of debris by sector). It can be saw the banding of the blocks which compose the iron crust. In the two back chambers is noticed the contact between the detrital iron crust and itabirite. In every chamber, drips have been noticed during the rainy period, whereas, in the dry period, the cave has no perceptible hydrological activity.

The conduits that compose the cavity show an irregular format. We can notice thin to coarse sediments all along the cavity. Moreover, we can notice at the roof and on the walls features that can be assimilated to pockets developed in detrital iron crust (Fig. 9A). However, these features does not have a sufficient rounding degree to be classified as karstic without any doubt.

The presence of a temporal channel and small basin holding back water during the rainy period is the main physical characteristic that can be noticed in the main room. Moreover, we can see the presence of residual columns and ceiling pockets.

In the Salão da Capa, it was noticed the contact between the detrital iron crust and the itabirite. We could also evidenced that the main feature that characterize this karstic cavity is a paleofloor (Fig. 9B). In this room, it was also noticed a basin that conserve the water that penetrates in the cave during the

rainy period. This water brings thin sediments to the basin. These sediments can be allochtonous (dispatched by small channels that connect the surface of the massif to the cave) or autochthonous (extracted from the siliceous stratas of the itabirite).

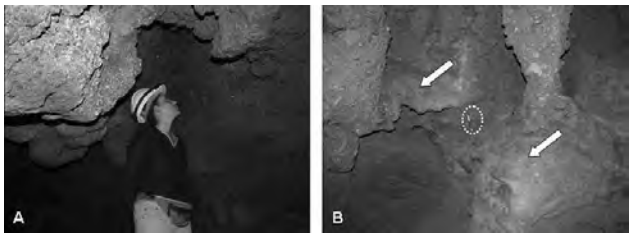

Figure 9. (A) Concavities at the top of the Salão do Sapo; and (B) The arrows indicate the remnant of an eventual paleofloor in the Salão da Capa, where we can also notice some pillars.

4.5. Gruta do Triângulo

The Gruta do Triangulo is located on the Inferior Plateau (Fig. 3). The cavity has this name because of a triangle drawn on the rock near the entrance of the cave. The cavity only has one entrance and irregular conduits. In general, the lithology which predominates in this cavity is the detrital type of iron crust, composed of densely distributed fragments (plenty of debris per area) which dimension oscillate between pebble and block. Moreover, in several chambers, can be noticed the presence of itabirite. As for the hydrological aspects, it was observed the presence of drips associated to the rainy period, temporary channels and condensation were evidenced on rainy and dry period.

The cavity has seven chambers. The first one is characterized by the presence of rocks and blocks. The lithology of these deposits is detrital iron crust. However, in the inferior part of some canga blocks, the itabirite banding can be noticed, which can indicate an eventual contact between these two lithologies. Rounded features were noticed in some of chambers. Between these features, there are several basins that accumulate water during the rainy period (Fig. 10A). In basins, we observed sediments that have been transported by the temporary drainage channel that originates from the canalicules (Fig. 10B).

Sedimentary deposit fixed on the roof of the gallery was noticed in this cavity (Fig. 10C). This element can be interpreted as a witness of a filling in the cavity, in other words this cave had karstification process. The penultimate chamber contains a paleofloor, the main feature which characterize the karstic dimension of the Gruta do Triangulo (Fig. 10D).

Finally, in the last chamber, it was noticed for the first time that the itabirite is dominant upon the iron crust. The chamber is characterized by the presence of blocks and boulders covered with a film. It was also noted that the sand exudation by the canalicules highlights the activity of the alteration processes within.

4.6. Exocarstic Features

During the field period, besides the endokarstic features, the existence of exokarstic features in the Serra da Piedade was noticed. These features can be linked to the dissolution forms

Figure 10. (A) Small basin in the Salão da Bacia which contains thin sediments headed by the temporary dripping of the drainage channels; (B) Thin sediments that can be allochtonous, coming from the canalicules and carried by channels of temporary drainage; (C) Sediment on the roof of the Gruta do Triangulo, deposit that proves that this cave was filled, and thus have known a paragenetic phase; (D) Paleofloor, main feature which characterizes the Gruta do Triangulo as a karstic cavity.

classified as kamenitza. Kamenitza is a Slovenian term that signifies solution pan. According to Ford and Williams (2007), this form is characterized by a flat or sub-horizontal base and by an outfall.

In the case of the kamenitza of the Serra da Piedade, we can notice that the hematite stratum tend to stay in relief in comparison with the siliceous stratum. We can deduce that the solubilization of the siliceous stratum is above the one of the iron stratum. Nevertheless this iron stratum is also subject to dissolution. These features have small dimensions when compared to those observed in limestone (Fig. 11).

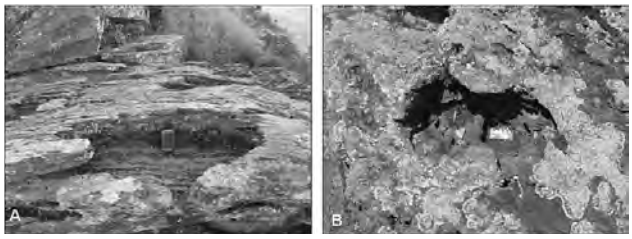

Figure 11. Kamenitzas observed in the Serra da Piedade.

5. Conclusions

From a karst geomorphologic point of view, the shapes observed in the cavities with karstic features and the superficial features of dissolution are very important. They witness the karstification process in the ferriferous rocks, despite the fact that they are not as developed as those of the carbonated and siliceous rocks.

Among the cavities observed and studied, the Gruta da Piedade is the most important. It has 365 m of development, a superior value when compared to the other itabirite and canga cavities already listed in the Quadrilatero Ferrifero (CECAV, 2010). Besides that, the Gruta da Piedade presents particular aspects when compared to other karstic cavities of Serra da Piedade. Among these aspects can be detached: insertion in the relief, vertical drop, number of entrances, conduits and chambers.

It can be concluded that more researches, focused on this specific theme are necessary. More specifically, geological and geochemical analysis shall allow affirmate, with a more systematized approach, the morphogenesis and the morphodynamics of these cavities.

Acknowledgments

To the speleologists Luciano Faria and Roberto Cassimiro for their full support on the field. To the members of Meandros Espeleo Clube and to the students of the Karst Geomorphology class (from the program of the Post-Graduation in Geography – UFMG) for their unrestraint support during the topography phase of the cavities and discussions on the field. Finally to the CNPq for the financing of this research.

References

Alkimim FF, Marshak S, 1998. Transamazonian orogeny in the Sâo Francisco cráton, Minas Gerais, Brazil: evidence for Paleoproterozoic collision and collapse in the Quadrilátero Ferrífero. Precambrian Res. 90, 29–58.

Auler AS, 2004. Quartzite caves of South America. Encyclopedia of Caves and Karst Science (Gunn, J. ed.). Fitzroy Dearborn, New York, 611–613.

Barbosa GV,1980. Superfícies de erosão no Quadrilátero Ferrífero, Minas Gerais**.** Rev. Bros. Gcoc., 10(l): 89–10l.

CECAV – Centro Nacional de Pesquisa e Conservação de Cavernas, 2010. Base de dados das cavernas localizadas em Minas Gerais. Disponível em: www.icmbio.gov.br/cecav. Acesso em: 8 out. 2010.

Chalcraft D, Pye K, 1984. Humid tropical weathering of quartzite in Southeastern Venezuela. Zeitschrift fur Geomorphologie. Berlin: 28(3): 321–332.

Ford D, Williams P, 2007. Karst Geomorphology and Hydrology. London: Chapman and Hall.

Harder EC, Chamberlin RT, 1915. The geology of central Minas Gerais, Brazil. Journal of Geology, 13: 341–378, 385–424.

Hardt R, Pinto SAF, 2009. Carste em Litologias não Carbonáticas. Revista Brasileira de Geomorfologia, v. 10, 99–105.

MCfarlane MJ, Twidale CR, 1987. Karstic features associated with tropical weathering profiles. In: Zeitschrift fur Geomorphologie Suppl. Bd, 64, 73–95.

Piló LB, Auler A, 2005. Cavernas em minério de ferro e canga de Capão Xavier, Quadrilátero Ferrífero, MG. O Carste, 17(3), 92–105.

Salgado AAR, Varajão CAC, Colin F, Braucher R, Nalini Junior HA, Varajão AFD, 2004. O papel da denudação geoquímica no processo de erosão diferencial no Quadrilatero Ferrifero/MG. Revista Brasileira de Geomorfologia. 5(1): 55–69.

Sallun Filho WS, Karmann I, 2009. Dolinas em arenito da bacia do Paraná: evidências de carste subjacente em Jardim (MS) e Ponta Grossa (PR). In: Revista Brasileira de Geociências, setembro de 2007, p. 551–564. Arquivo digital disponível em: www.sbgeo.org.br. Acesso em: 25 de setembro de 2009.

Simmons GC, 1963. Canga Caves in the Quadrilátero Ferrífero, Minas Gerais, Brazil. The National Speleological Society Bulletin 25: 66–72.

Tricart J, 1961. O Modelado do Quadrilátero Ferrífero Sul de Belo Horizonte. Annales de Geographie, 70 (379): 255–272.

Uagoda RSA, Netto ALC, 2006. Depressões Fechadas em Relevo Cárstico-Quartzítico, Bacia do Ribeirão Ribeirão Santana, Médio Vale do Rio Paraíba do Sul. Anuário do Instituto de Geociências da UFRJ, 29 – 87–100.

ENGLACIAL CAVES OF GLACIAR PERITO MORENO AND GLACIAR AMEGHINO, PATAGONIA (ARGENTINA)

Leonardo Piccini[1,2], Marco Mecchia[1]
[1]*La Venta Esplorazioni Geografiche, l.piccini@laventa.it*
[2]*Department of Earth Science, Università di Firenze*

The Glaciar Perito Moreno is one of the few glaciers in the world that is currently affected by recurrent advancements. Conversely, the adjacent Glaciar Ameghino has been affected by a retreat of ca. 4.5 km in the last 40 years, due to surface melting and calving.

Both glaciers host several englacial caves formed by surface and internal melting. Swallow-holes (moulins) are mainly located in the uncrevassed central ablation areas, where the morphological conditions allow the formation of a well-developed runoff network that feeds supraglacial channels up to over a kilometre long. In Glaciar Perito Moreno, the distribution and morphology of glacier swallow-holes in 2010 shows a segmentation of the englacial and supraglacial drainage system, which could be due to an increase in crevassing and the widening of the extensional zone. Glaciar Ameghino shows several minor moulins in a restricted area just above the front and some large but unexplored swallow-holes in the medial sector of ablation area.

1. Introduction

In the ablation area of temperate glaciers, the melting of ice produces a large amount of water which flows over, within or below the ice mass (Shreve 1972; Seaberg 1988; Rothlisberger 1998). Supraglacial streams usually sink in shafts, whose depth is about directly proportional to the amount of water falling in it. This particular kind of caves entirely formed in ice are usually named moulins, a French word meaning “mill”, and develop along vertical fractures where the supraglacial melting water sinks (Holmund 1988; Eraso and Pulina 1992; Piccini 2001; Smart 2003).

In its inception stage a moulin consists of a little conduit, completely water-filled (proto-moulins, after Schroeder 1991). In a few weeks the entrance is enlarged and deepened by the melting action of the inflowing water, until it reaches an equilibrium size. Due to the downward movement of a glacier, a moulin remains active until a new sink-point opens upstream and captures the supraglacial channel that feeds it (Monterin and Somigliana 1930). When a moulin is deactivated, the void begins to close due to the ice collapse, water refreezing or filling with snow. The time lag of this cycle depends on the flow rate of the glacier: the faster the ice velocity the shorter the evolutionary cycle of a moulin.

The functioning of the internal drainage of a glacier and its relationships with the subglacial one are still based on mainly speculative hypotheses or conceptual models, even if the seasonal and diurnal fluctuations of the water level inside moulins suggest in some cases that the drainage of meltwater absorbed by supraglacial sink-points is not directly linked to the subglacial water flow (Piccini 2001; Badino and Piccini 2002; Mavlyudov 2006).

Finally, the shape of moulins reflects the local stress pattern of the ice and can be considered as an indicator of the flow mechanics (e.g., Holmund 1988; Eraso et al. 1998; Gulley et al. 2009a).

Despite their importance in understanding the hydrology of glaciers, the knowledge on englacial caves is still restricted to voids large enough to be accessible by humans and so it suffers of a typical exploration bias. Nonetheless, the exploration of moulins, in glaciers with different dynamics, is a field of research that can give an important contribution to glaciology.

In the last decades the Southern Patagonian Andes have been investigated by many speleologists and karstologists having the main purpose of surveying and studying large glacier caves. Several moulins have been observed in all the major glaciers of the Southern Patagonian Andes: Viedma, Upsala, Marconi, Ameghino, Moreno, Grey, Tyndall and Pio XI (e.g., Eraso et al. 1998; Badino and Piccini 2004; Mecchia and Piccini 2011). In fact, one of the peculiarities of this area is the occurrence of glaciers that descend to very low altitudes (down to sea level), thanks to the large amount of snow that falls onto the Andean ridge. This condition produces a very intensive surface ablation during the summer season (usually from November to March), which feeds a well-developed system of supraglacial channels (named bédières in Europe).

This preliminary note deals with some caves located in the Glaciar Perito Moreno (GPM), investigated in 1995 and 2010, and Glaciar Ameghino (GA), investigated in 2010.

2. Geographical overview

The GPM is situated in the Parque Nacional Los Glaciares and was designated a UNESCO World Natural Heritage site in 1981. The glacier descends about 30 km to the east from the Hielo Patagonico Sur ice sheet. The main watershed lies at an average altitude of about 2,200 m, reaching the highest elevation at the Cerro Pietrobelli (2,950 m a.s.l; Fig. 1). The GPM covers about 250 km^2, 70 % of which belongs to the accumulation area and the remaining 30 % to the ablation area. The equilibrium line lies around 1,150–1,200 m a.s.l. and has been stable in the last years (Aniya and Skvarca 1992; Roth et al. 1998).

The glacier surface is quite clean, with the exception of a medial moraine line recognizable in the central part. The

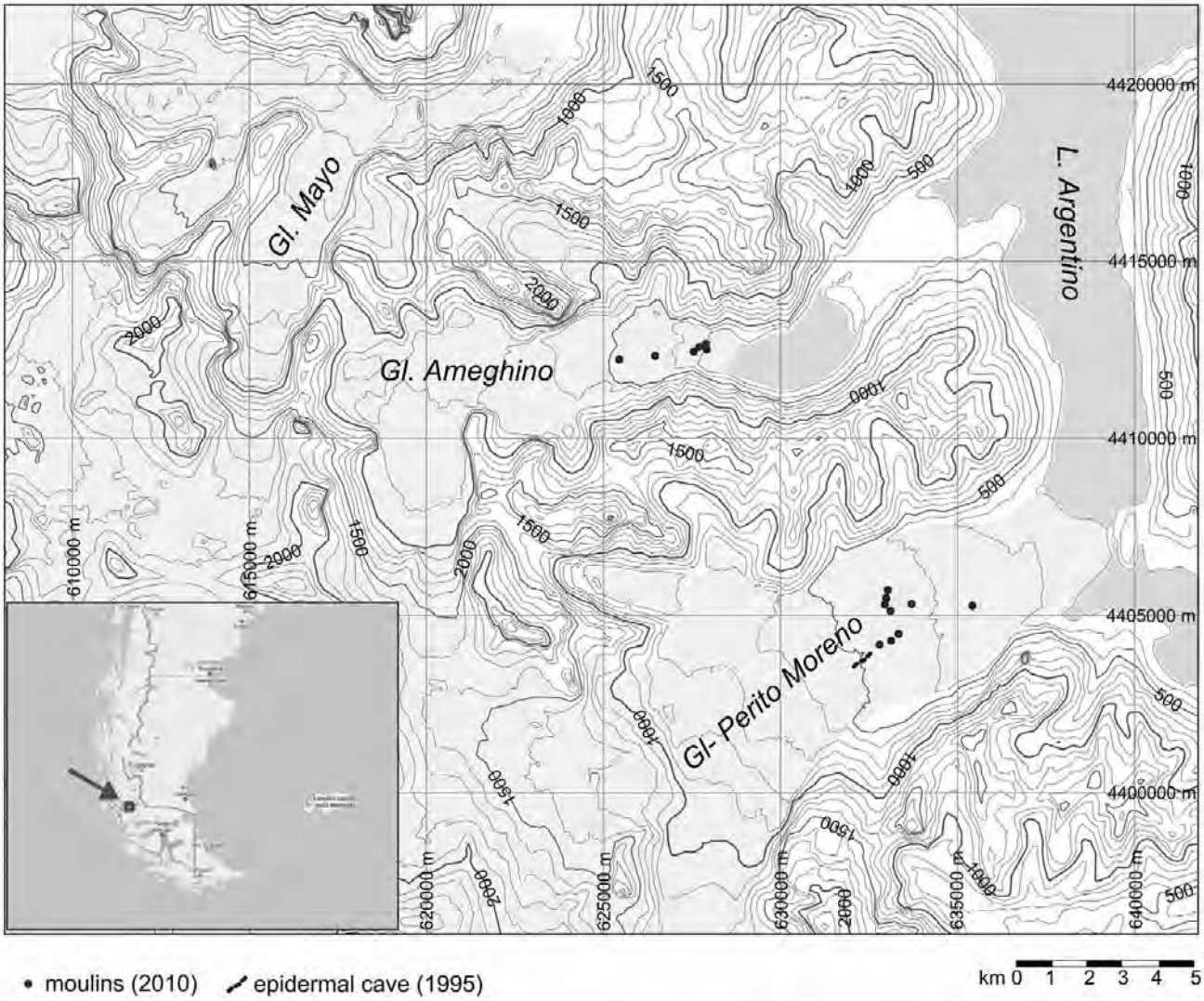

Figure 1. Sketch map of Perito Moreno and Ameghino glaciers with the location of main moulins surveyed in 1995 and 2010 expeditions (contour-lines from GDEM ASTER, modified on the basis of topographic maps).

front overlooks a branch of Lago Argentino (185 m a.s.l.) with a 50–80 m high ice cliff. The thickness of the glacier is about 750 m, at 8 km from the front (Roth et al. 1998), and reduces to 160 m at the terminus (Stuefer et al. 2007).

The GPM can be considered one of the few glaciers that is in an apparent steady state, respect with most of the other glaciers worldwide (Roth et al. 1998; Masiokas et al. 2009). Otherwise, the most famous characteristic of the GPM is the recurrent advancement of the front, which closes the water passage between the two branches of Lago Argentino. This obstruction causes the lake level in the branch upstream to rise 20–25 m. Successively, the increased water head opens a subglacial tunnel which enlarges upward forming a spectacular bridge, until the lake returns to an equilibrium level. The glacier is affected by frequent fall of ice blocks from the front, in the order of several hundred cubic metres per day, at least in the summer season.

The GA lies between latitudes 50°24' and 50°27' South and longitudes 73°10' and 73°21' West. The total extent is about 80 km^2, 45 km^2 of which are in the ablation zone. The highest parts of accumulation area reach 2,260 m a.s.l. (Aniya and Sato 1995), while the front descends to 230 m a.s.l. (Fig. 1).

The ablation zone consists of an about 10 km long tongue, which descends to the east lightly curving to the right. The glacier's front overlooks a lake, which is about 4.5 km long and fills the entire valley from side to side (Fig. 2). The lake is formed by the damming of a terminal moraine, related to a major advance phase occurred during the 18–19th century (Little Ice Age; Aniya and Sato 1995; Aniya, 1996). The GA was affected by a strong retreat of about 4.5 km in the last 40 years.

These two glaciers are emblematic of a very different dynamic state, which cannot be due to different climatic conditions; in fact they have the same feeding area, same orientation (aspect) and almost the same elevation range.

Figure 2. The calving front of Glaciar Ameghino (photo L. Piccini, La Venta).

3. Methods

During the expedition in 2010, the GPM and GA were investigated through field prospection aimed to position all the moulins and the epidermal caves. Positioning of cave entrances was performed by Global Positioning System (GPS) in 2010, and by compass triangulations to the most relevant mountain tops around the glacier in 1995.

During 2010 field surveying, the main supraglacial channels were mapped using the "tracking" tool of the GPS. The tracks and the location of the moulins allowed us to delimitate the areas where supraglacial drainage is well developed and the zones of sinking of supraglacial streams.

This survey cannot be considered very precise, due to the scarce accuracy of the GPS in the area (usual degree of error 30–40 m), anyway, many repeated measures and a cross-check between the GPS and compass positioning has allowed reducing the error to a few tens of metres.

Moulins were descended using standard caving and ice-climbing tools and surveyed using speleological mapping techniques (Palmer 2008). Distances were measured with a 20 m survey tape or with a laser distance-meter (using a rigid plastic tablet as target). Where possible, cross sections were measured through the survey tape, whereas the heights of larger conduits were estimated on pictures. Directions of cave segments were measured with a 1° precision compass, slopes with a 1° precision rolling-disk inclinometer. No tripods were used due to the characteristics of englacial conduits and the difficult operational settings.

Table 1. Main englacial caves explored during 1995 and 2010 expeditions at Glaciar Perito Moreno.

Name	Date	UTMW (18) (WGS84)	UTM S (18) (WGS84)	Elev. (m s.l.m.)	Depth (m)	Length (m)
Perito Meccanico	03/1995	631.965	4403.427	520	-40	1,150
Minas	19/03/1995	631.974	4405.319	435	-25	35
Coltrane	23/03/1995	633.678	4405.238	440	-50	230
Monterin	20/03/1995	632.943	4405.637	445	-55	75
PM10 - a10	17/02/2010	632.683	4405.303	445*	-38	60
PM10 - a13	17/02/2010	632.945	4405.259	445*	-17	20
Coltrane (2010)	19/02/2010	633.455	4405.205	435	>25	>30
PM10 - Coltrane 2	19/02/2010	633.715	4405.392	430	-52	90
PM10 - Guide 1	21/02/2010	635.188	4403.906	370	-43	85
PM10 - Guide 2	21/02/2010	635.276	4403.934	370	-54	65

Table 2. Main englacial caves explored during 2010 expeditions at Glaciar Ameghino.

Name	Date	UTMW (18) (WGS84)	UTM S (18) (WGS84)	Elev. (m s.l.m.)	Depth (m)	Length (m)
AM10-09	26/02/2010	627.726	4412.529	260	-23	25
AM10-12	25/02/2010	627.861	4412.437	255	–	–
AM10-17	26/02/2010	627.978	4412.460	250*	-36	40
AM10-21	26/02/2010	626.631	4412.489	282*	-30	32
AM10-25 - Bingo1	26/02/2010	628.115	4412.615	245*	-43	50
AM10-27 - Murena 1	27/02/2010	628.114	4412.558	240*	-23	30
AM10-28 - Murena 2	27/02/2010	628.119	4412.532	240*	-21	28

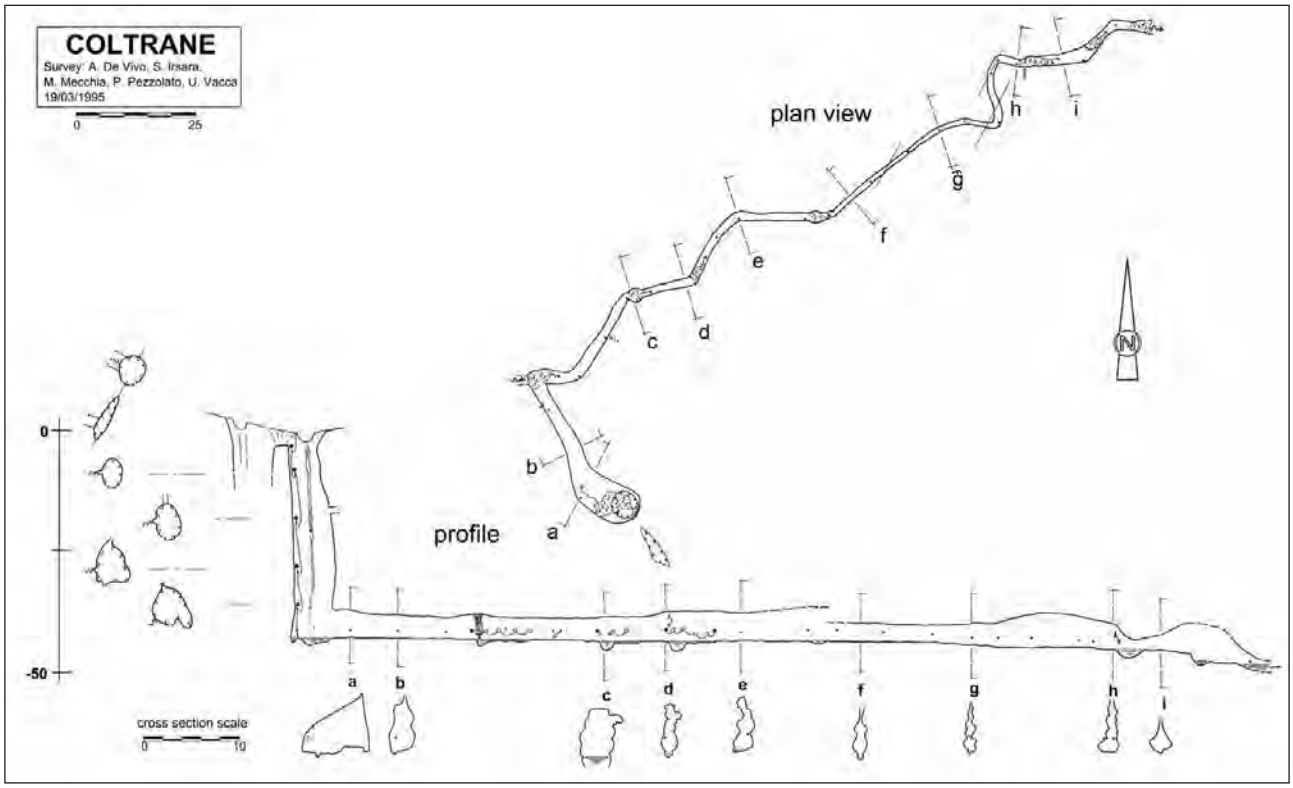

Figure 3. The morphology of the major moulin surveyed in 1995: named "Coltrane". The large bottom gallery is located about 40–45 m below the surface.

4. Results

4.1. Glaciar Perito Moreno

In its current state, the glacier has two main areas having morphological and hydrological conditions suitable for the formation of moulins. A third and upper zone, located between 550 and 650 m a.s.l., was seen from a far panoramic point and aerial photos but was not reached by us.

The two areas occupy a central position in the ablation zone, at elevations situated between 420 and 550 m a.s.l. and 6 to 8 km far from the terminus. In these zones the surface drainage is well developed, with longitudinally oriented bédières running parallel to each other. The larger channels reach discharges up to some cubic metres per second.

In 1995, the main medial torrent fed a large shaft situated slightly above the belt of crevasses that cuts the glacier at about 5.5 km from its front and which separates the two uncrevassed areas. The swallow hole had fortuitously become inactive during the expedition, due to the opening of a new sinking point some dozens of metres upstream. This circumstance allowed descending a 40 m pit (Fig. 3) and reaching a ca. 200 m long horizontal tunnel (Fig. 4). This cave, named "Coltrane" by the first explorers, is one of the largest ever surveyed in the world.

Figure 4. The large englacial gallery at the bottom of the entrance shaft of moulin "Coltrane". Note the vertical fracture on the ceiling of the conduit (photo T. Bernabei, La Venta).

Figure 5. The morphology of the major moulin surveyed in 1995: named "Coltrane". The large bottom gallery is located about 40–45 m below the surface.

In 2010 a moulin fed by the same supraglacial stream was found about 200 m upstream than its 1995 position, but still having similar characteristics. The large amount of water didn't allow us to descend the moulin for more than 20 m. About 300 m downstream, an inactive pit was found, about 60 m deep but not very wide, probably deactivated several months before and in a state of advanced collapse. In the same area, other active pits with depths up to 30 m were descended.

In 1995, a supraglacial stream, located about 700 m further south-west, was captured by a small shaft (that was called "Perito Meccanico") from which a long epidermal conduit develops. The conduit was surveyed for more than 1 km (Fig. 5), walking in a flooded tunnel 5–10 m below the surface (Fig. 6). The tunnel had usually a circular or elliptical section, 2–3 m wide, and was not clearly guided by fractures. This cave wasn't found again in 2010.

Figure 6. A segment of the epidermal tunnel in the "Perito Meccanico" Cave; note the low-angle crack that guides the development of the conduit (photo La Venta).

The lower uncrevassed sector of the GPM is located on the right side of the glacier, about 5 km upstream the terminus and at elevations between 350 and 400 m a.s.l. It is rich in water streams having both longitudinal courses at the centre of the glacier and oblique courses in the southern part. In this zone a large moulin, consisting of a first 20 m pit followed by a gorge with other small vertical drops, was surveyed (Fig. 7); a 43 m depth was reached, while the extension was 80 m. Closely, another 54 m deep moulin was descended, which continued with a narrow meander.

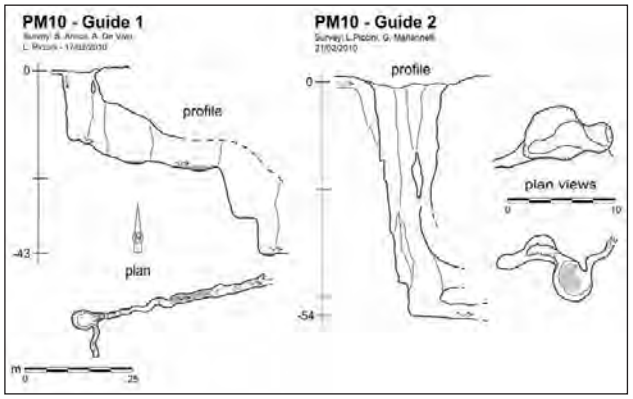

Figure 7. Survey of two moulins explored inn 2010 in the lower sector of Glaciar Perito Moreno.

4.2. Glaciar Ameghino

The ablation area of Ameghino has a wide central plateau, situated between 550 and 750 m of elevation, where the superficial drainage is well developed. Here a series of not yet explored moulins were discovered in 2010. Entrances are aligned in the direction of the ice flow along a central depressed bend close to the medial moraine. Further downstream, there is a transversal belt of crevasses which cut the entire tongue at around 400 m elevation, corresponding to an abrupt increase in its slope. Downstream this crevassed area, there is a relatively regular and flat sector just upstream the frontal zone. In this zone the surface ablation is very intense, due to the low elevation and the exposure to sun. Superficial drainage is very well developed but not very structured. Several bédières occur, having a longitudinal orientation (E–W) in the central zone and an oblique one (NW–SE) in the southern zone. The northernmost sector is intensively crevassed and has no superficial drainage.

In the frontal zone, 15 accessible moulins were found, some of which were quite large and fed by flows having up to several hundred $l.s^{-1}$ of discharge. The deepest moulin was descended for about 30 m and seen for another 20 (Fig. 8). All the explored moulins have similar sizes and morphologies and consist of a first 20–30 m deep pit with a narrow gorge at the base, which is only traversable for a few metres.

Generally, the glacier has very pronounced fusion forms and in the upper zone, the greater rate of superficial runoff allows the occurrence of cavities having larger sizes than the ones explored in the lower zone.

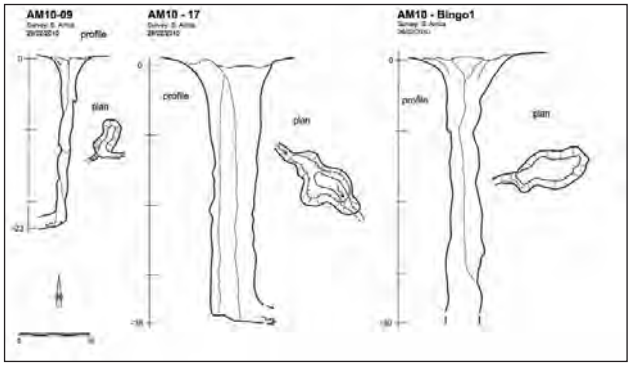

Figure 8. Survey of three moulins explored in 2010 in the lower sector of Glaciar Ameghino.

5. Discussion and conclusions

The epidermal conduit (Perito Meccanico, surveyed in 1995) had a circular or elliptical section, usually 2–3 m in diameter, and was formed along almost horizontal fractures for most of the length. No vertical fractures guiding the direction of the conduit were observed.

Horizontal tunnels can be formed through a "cut-and-closure" type process (Gulley et al. 2009b), but in this case the characteristics of the ice and the shape of the tunnel suggest an origin by melting starting from an englacial conduit. In our opinion this conduit was formed along a series of low-angle fractures, gently dipping upstream. This epidermal cave was located in the central sector of the

ablation zone, where the glacier is affected by a compressive flow, which can form low-angle thrusts almost parallel to the ice surface. This explains the shallow depth of this cave that runs just a few metres below the glacier surface.

The major explored moulins in the GPM are made up of a first vertical shaft, from 20 to 50 m deep, followed by gently inclined canyon. The first shaft is always located along a vertical fracture. In the "Coltrane" Cave (1995), the entrance shaft and the first part of the conduit were clearly guided by a vertical fracture (Fig. 7), whereas the second part of the tunnel did not show any structural control. Conversely, vertical moulins are formed at the downstream borders of the uncrevassed areas, usually just upstream of the transversal crevassed areas, where the mechanical conditions change from compression to extension.

Englacial canyons always go to NE that is the flow direction of the glacier. This is well emphasized by the two graphs in Figure 9, which show the distribution of directions measured in the epidermal tunnel (Perito Meccanico) and in the major moulin (Coltrane) surveyed in 1995. The general trend of the two caves is almost the same, although they were formed in a very different stress pattern, and is consistent with the ice flow direction. This could be due to a limited depth of the fractures in the area where "Coltrane" Cave opened.

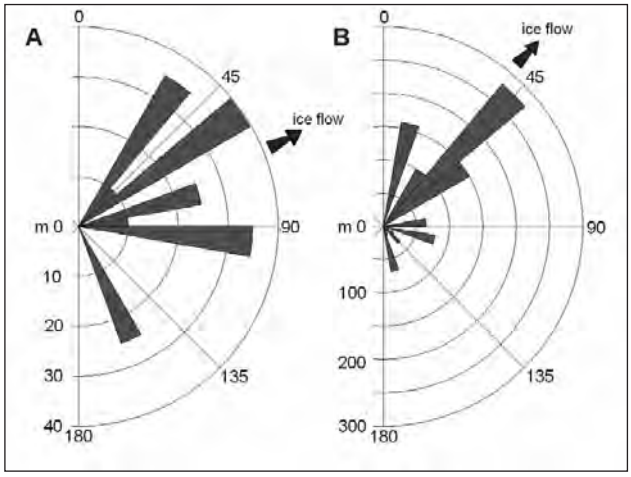

Figure 9. Rose diagrams showing the direction of development of "Coltrane" moulin (A) and "Perito Meccanico" Cave (B).

Acknowledgments

The authors are grateful to Park los Glaciares direction for the permission to access to Perito Moreno and Glaciar Ameghino. The expeditions had a financial support from La Venta Esplorazioni Geografiche association.

References

Aniya M, 1996. Holocene variations of Ameghino Glacier, southern Patagonia. Holocene, 6, 247–252.

Aniya M, Sato H, 1995. Morphology of Ameghino Glacier and landforms of Ameghino Valley, southern Paragonia. Bulletin of Glacier Research, 13, 69–82.

Aniya M, Skvarca P, 1992. Characteristics and variations of Upsala and Moreno glaciers, southern Patagonia. Bulletin of Glaciological Research, 10, 39–53.

Badino G, Piccini L, 2002. Englacial water fluctuation in moulins: an example from Tyndall Glacier (Patagonia, Chile). Nimbus, 23–24, 125–129.

Badino G, Piccini L, 2004. Glacial karst in the world. In: G Badino, A De Vivo, L Piccini (Eds.). "Caves of Sky: a journey in the heart of glaciers. Edizioni Tintoretto, Treviso, 71–100.

Eraso A, Pulina M, 1992. Cuevas en hyelo y rios bajo los glaciares. McGraw Hill, Espana, 242.

Eraso A, Badino G, Mecchia M, Gavilan C, Bernabei T, 1998. Results of the main directions of subglacial drainage prediction method applied to Perito Moreno Glacier. Salzburger Geographische Materialen, 28, 35–46.

Gulley JD, Benn DI, Screaton E, Martin J, 2009a. Mechanisms of englacial conduit formation and their implications for subglacial recharge. Quaternary Science Reviews, 28, 1984–1999.

Gulley GD, Benn DI, Muller D, Luckman A, 2009b. A cut-and-closure origin for englacial conduits in uncrevassed regions of polythermal glaciers. Journal of Glaciology, 55 (189), 66–80.

Holmund P, 1988. Internal geometry and evolution of moulins, Storglaciaren, Sweden. Journal of Glaciology, 34 (117), 242–248.

Masiokas MH, Rivera A, Espizua L E, Villalba R, Delgado S, Aravena JC, 2009. Glacier fluctuations in extratropical South America during the past 1000 years. Palaeogeography, Palaeoclimatology, Palaeoecology, 281, 242–268.

Mavlyudov BR, 2006. Glacial karst, why is it important to research. Acta Carsologica, 35/1, 55–67.

Monterin U, Somigliana C, 1930. Sulla costanza di posizione dei pozzi glaciali. Bollettino Comitato Glaciologico Italiano, 10, 211–225.

Naruse R, Skvarca P, Kadota T, Koizumi K, 1992. Flow of Upsala and Moreno glaciers, southern Patagonia. Bulletin of Glaciological Research, 10, 55–62.

Piccini L, 2001. The glacier caves of Gornergletscher (Switzerland: preliminary notes on their morphology and hydrology. Geografia Fisica e Dinamica Quaternaria, Suppl. V, 151–156.

Rothlisberger H, 1998. The physics of englacial and subglacial meltwater drainage – theory and observation. 4th Symp. On Glacier Caves and Cryokarst in Polar and High Mountain Regions, Salzburg, Austria, 13–23.

Roth H, Stuefer M, Siegel A, 1998. Mass fluxes and dynamics of Moreno Glacier, Southern Patagonia Ice field. Geophysical Research letters, 25(9), 1407–1410.

Seaberg R, 1988. Character of the englacial and subglacial drainage System. Journal of Glaciology, 34 (117), 117–123.

Shreve RL, 1972. Movement of water in glaciers. Journal of Glaciology, 11(62), 205–214.

Schroeder J, 1991. Les cavités du Hansbreen creusées par les eaux de fonte. Svalbard, 77° Lat. N. Proc. of 1st Int. Symp. of Glacier Caves and Karst in Polar Regions, Madrid, 1990, 21–33.

Smart C, 2003. Glacier caves and glacier pseudokarst. In J Gunn (Ed.). Encyclopedia of caves and Karst Science. Routledge, London, 385–387.

Stuefer M, Roth H, Skvarca P, 2007. Glaciar Perito Moreno, Patagonia: climate sensitivities and glacier characteristics preceding the 2003/04 and 2005/06 damming events. Journal of Glaciology, 53(180), 3–16.

SPELEOGENESIS AND SPELEOTHEMS OF THE GUACAMAYA CAVE, AUYAN TEPUI, VENEZUELA

Francesco Sauro[1,2], Joyce Lundberg[3], Jo De Waele[1,2], Nicola Tisato[4], Ermanno Galli[5]
[1]Department of Biological, Geological and Environmental Sciences, Bologna University, Via Zamboni 67, 40126 Bologna, Italy, cescosauro@gmail.com, jo.dewaele@unibo.it
[2]Associazione di Esplorazioni Geografiche la Venta, Via Priamo Tron 35/F, 31030, Treviso
[3]Department of Geography and Environmental Studies, Carleton University, Ottawa, Ontario, Canada, K1S 5B6
[4]ETH Zurich, Geological Institute, Soneggstrasse 5, 8092 Zurich, Switzerland
[5]Department of Chemical and Geological, University of Modena and Reggio Emilia. Largo S. Eufemia 19, I-41121, Modena, Italy

In March 2009 the Guacamaya Cave was discovered on the Auyan Tepui. It represents one of the longest caves explored on this table mountain, the only one known today with a complete horizontal development, comparable with those of the Brewer Cave System, in the Chimanta Tepui (the world largest sandstone cave). Guacamaya Cave presents peculiar morphologies, developed along an obvious bed of iron hydroxides and amorphous silica (Banded Iron Formation, BIF) interposed between hard and massive quartzite banks. In the walls around this layer, a variety of opal speleothems, of unusual dimensions and shapes, together with gypsum flowers and crusts have been documented.

Here we present a compositional and morphological characterization for the BIF layer and one tufa-like bio-speleothem. The speleogenetic control exerted by the BIF stratum is discussed, and in relation to collapse morphologies observed on the surface. An attempt to date the bio-speleothem with the U-Th system shows the difficulties of applying this method to these silica formations, because of post-depositional alteration in this porous material.

1. Introduction

In the last twenty years many new cave systems have been discovered in different "tepuis" (table mountains) of the Guyana Shield (Venezuela and Brazil), formed in the Precambrian quartzite sandstones of the Roraima Supergroup (Piccini and Mecchia 2007; Sauro 2009; Aubrecht et al. 2011). The formation of caves and karst features in quartzite rocks is considered exceptional given the low solubility and solution rates of quartz (Wray 1997a, 1997b). These recent explorations have shown that the largest karst systems in these poorly-soluble siliceous rocks are controlled predominantly by stratigraphic rather than by tectonic factors.

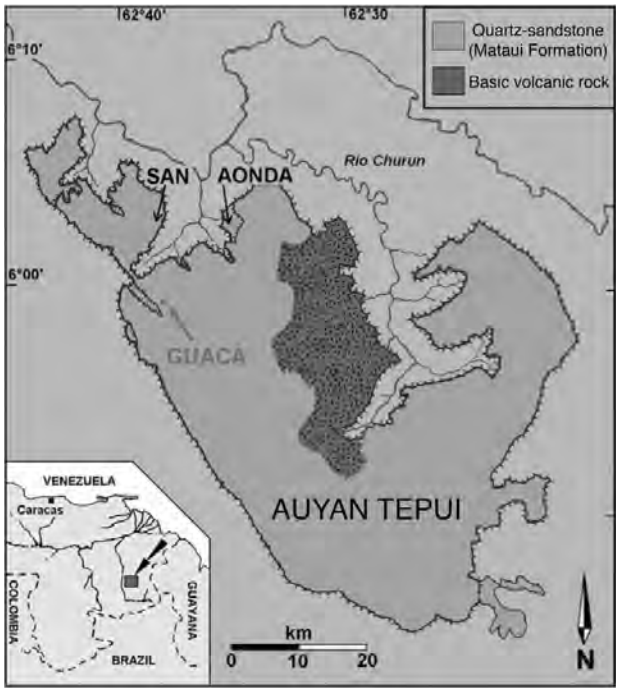

Figure 1. The Auyan Tepuy with caves locations: Guacamaya Cave (Guaca), Sima Aonda (Aonda), Sistema Auyantepui Noroeste (SAN).

Many hypotheses were discussed by previous authors regarding the genesis of these caves, from the weathering process called "arenisation" (Martini 2000; Piccini and Mecchia 2009) to hypogenic processes related to hydrothermal activity (Zawidzki et al. 1976), or even diagenetic predisposition (Aubrecht et al. 2011), but these ideas are still in discussion and there is not yet a clear understanding of the main speleogenetic factors (Sauro et al. 2012b).

In this work we present a morphological description of the Guacamaya Cave, the longest horizontal cave explored in the Auyan Tepui (1.1 km). In addition to the impressive variety of silica bio-speleothems (Aubrecht et al. 2008a) and secondary minerals such as gypsum that were documented in a lateral fossil branch, this cave shows a peculiar characteristic not documented in other quartzite caves of the area: a bed of iron hydroxides (Banded Iron Formation) strictly controls its development.

We performed petrographic studies with thin section and SEM imaging, EDX and XRD chemical analysis on iron hydroxide layers, silica bio-speleothems and gypsum. In addition, following Lundberg et al. (2010), we attempted to date one of the bio-speleothem by the U-Th system.

2. Geographical and geological setting

The Gran Sabana is a wide geographical region located in northern South America, between Venezuela and Brazil, crossed by several tributaries of Rio Caroní, which in turn flows into the Orinoco River. The main massifs of the Gran Sabana, named "tepuis", have the shape of large table mountains. They are delimited by vertical to overhanging walls, often more than 1,000 m high. The massifs are separated from each other by the surrounding lowlands of the

Wonkén planation surface (Briceño and Schubert 1990). More than 60 tepuis are present in the region and Guacamaya Cave opens in the northernmost one, the Auyan Tepui (700 km^2, Fig. 1), not far from the Angel Falls, considered the highest waterfall in the world (975 m).

From a geological point of view the Gran Sabana is part of the Guyana Shield. The igneous and ultra-metamorphic rocks in the northern portion of the shield (Imataca-Bolivar Province, after González de Juana et al. 1980) have an age of 3.5 Ga. The silico-clastic rocks (Roraima Group) belong to the continental-to-pericontinental environment of the Roraima-Canaima Province (Reid 1974). The age of this arenaceous group can be inferred only on the basis of the absolute dating of the granitic basement (2.3–1.8 Ga) and of the basaltic dykes and sills that cross the upper formation of the Roraima Group (1.4–1.8 Ga) (Briceño and Schubert 1990; Santos et al. 2003). The Roraima Group was also intruded by Mesozoic diabases (Hawkes 1966; Teggin et al. 1985). These form thin NE-trending dykes with ages around 200 Ma.

A slight metamorphism, with quartz-pyrophyllite paragenesis in the more pelitic beds, is the result of the lithostatic load of almost 3-km-thick sediments now eroded (Urbani et al. 1977).

Guacamaya Cave is developed in the Mataui Formation, the younger deposits of the Roraima Group, about one and a half billion years old (Santos et al. 2003). These are quartzitic sandstones of 600 to 900 metres thick, which form the highest part of the tepui. These sandstones are made up of quartz grains, representing well over 90% of the composition, held together by a cement, also mostly quartz, which gives them the term “quartz-arenite” (Martini 2000, 2004).

From a structural point of view folds are absent, except for some wide-curvature folds at a very large scale. The bedding in the proximity of the cave is slightly inclined toward the east. Some sets of mainly vertical fractures cut the plateaus, creating a regular network of quadrangular prisms. Important faults have not been observed, at any scale.

Figure 3. Lower valley entrance and the uroofed continuation of the cave.

2.1. Morphological description

The main branch of Cueva Guacamaya is a hydrologic tunnel about 350 metres long. A permanent stream with a discharge of some litres per seconds crosses the cave from the highest entrance (Higher Entrance in Fig. 2) to the resurgence (Lower Entrance in Fig. 2). About one hundred meters from the lower entrance, a lateral fossil branch develops to the south for 700 metres ending in a boulder choke close to the surface (Tramo de los Opales). The passage is of significant size, more than 30 metres wide and about 15 high in some sectors, with a great collapse room (Salon Roberto Campano) at the intersection of the two branches.

It is evident that the cave is part of a more extended system, now dissected and open to the surface: the valleys upstream and downstream of the cave represent the unroofed continuation of the main gallery, showing the same lithological control (Fig. 3). To the east a wide and complex area of tilted and fallen boulders is probably related to the collapse of the gallery in a more fractured sector of the

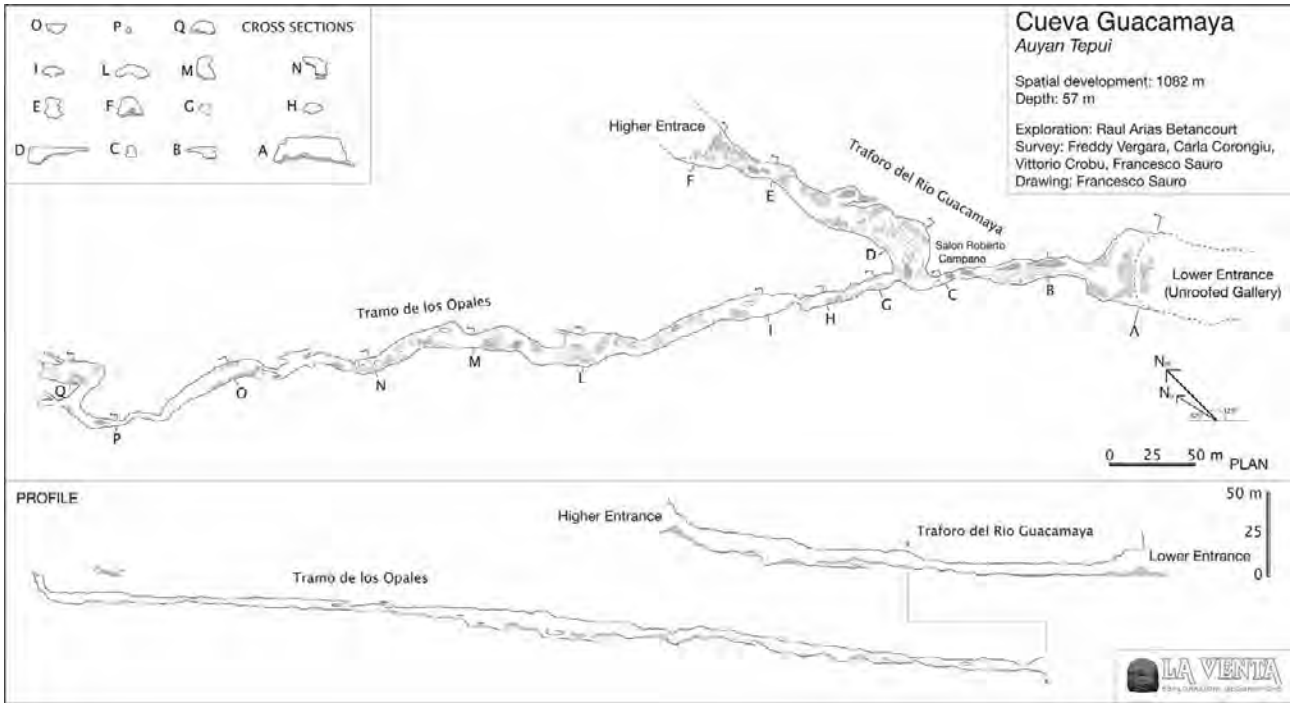

Figure 2. Plan, profile and cross sections of Guacamaya Cave.

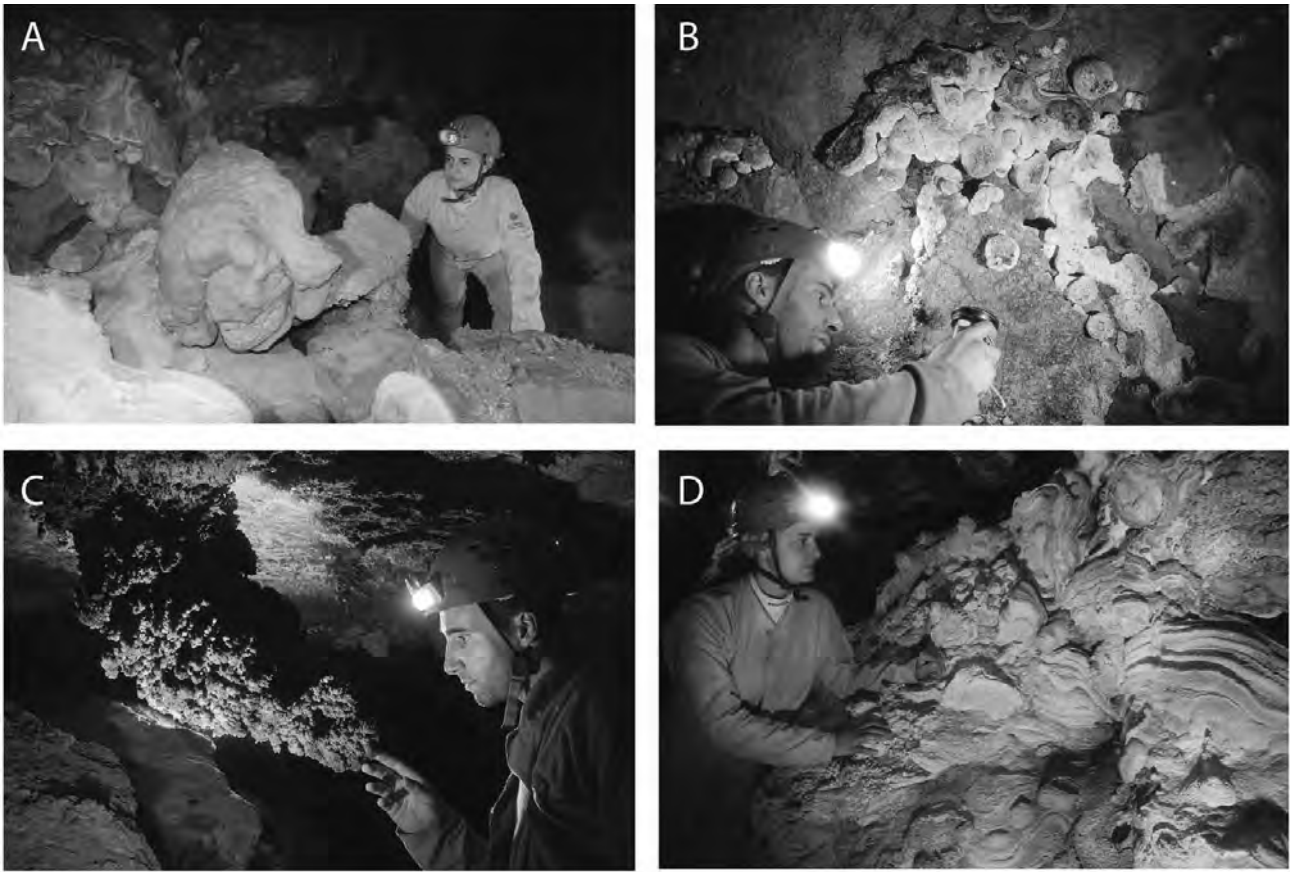

Figure 4. Different morphotypes of biologically mediated silica speleothems. A) tufa-like speleothem; B) champinons agglomerate; C) Giant corralloid wind-guided stalactite; D) "clouds" formations on the wall; (Photos by F. Sauro).

plateau. In general the relict cave is situated at shallow depth from the surface, only 10–5 metres in some places.

Both the active and the fossil branches are developed along a layer of iron hydroxides with minor amorphous silica, similar to typical Banded Iron Formations, from some decimetre to a metre thick. This control is evident in the cross sections of the galleries showing an elliptical or keyhole profile. Original small phreatic conduits entrenched by vadose canyons are recognisable.

2.2. Silica speleothems and gypsum

The cave shows a wide variety of silica and opal speleothems, in particular in the "Tramo de los Opales" (Fig. 4). These formations are concentrated nearby the iron hydroxide layers, preferentially where the gallery cross sections are reduced, with increasing air flow. This branch of the cave is in fact characterised by a strong wind between the two main entrances and the highest final boulder choke open to the surface. Speleothems of different forms and dimensions were observed: coralloid speleothems like "dolls", tufa-like "champignons" (Fig. 4B), "kidneys" and all the morphotypes described by Aubrecht et al. (2008a). More complex composite formations completely cover the cave walls for several square metres (which we have called "clouds", Fig. 4D). A spectacular wind-guided coralloid stalactite 1 metre long was also documented (Fig. 4C).

In general, biologically mediated speleothems such as champignons grow mainly on sharp edges of quarzite blocks or emergent quartz veins (in relief due to differential weathering, resembling boxwork) and they show the tendency to growth toward the centre of the conduit.

Only few speleothems were sampled for this study, in particular a "champignon"-type bio-stromatolite, which we attempted to date.

Gypsum was commonly found in the dry gallery of "Tramo de los Opales". Two different preferential mineralization sites were observed: on the floor, in the form of acicular crystals around weathered blocks of quartzite fallen from the cave ceiling; or as overgrowth on the surface of the amorphous silica bio-speleothems.

3. Methods

For X-Ray Diffraction analyses (XRD) iron-hydroxide bed, silica biospeleothems and gypsum samples were ground to an ultrafine powder in an agate mortar and lightly pressed in a plastic sample holder. XRD patterns were recorded with a Philips PW 1050/25 and a PANalytical X'Pert PRO Diffractometer (experimental conditions 40 Kv and 20 mA tube, CuKα Ni filtered radiation λ = 1.5418 Å) at the Department of Geology of Modena-Reggio Emilia University. In order to better identify iron hydroxides we employed Raman spectroscopy on a fresh cut surface of sample GC3. The Raman spectrometer is an Horiba Jobin YVON – LABRAM HR, with spot size ~2 µm, hole 300 µm, slit 300 µm, 10× optical objective and 632.81 nm wavelength (i.e. red light).

For X ray fluorescence chemical analysis of the banded iron formation the sample was finely ground and analyzed in an Axios PANalitical spectrometer equipped with 5 diffraction crystals in the ETHZ Geologic Institute facilities (Zurich). Because of the uncommonly high iron content, samples had to be diluted with pure silica in order to compare them with

standards. Thus, a variety of powder-pills with different percentages of sample and pure silica were analysed.

For Sem images we used a FEI Quanta 200F SEM equipped with an EDAX Pegasus detector for Energy Dispersive X-ray Spectroscopy mapping (ETH, Zurich).

For the dating attempt of the silica bio-speleothem the methods described by Lundberg et al. (2010) were applied. Small samples (~0.1 g) were taken from two different layers under binocular microscope avoiding the opalized laminations and the vuggy dark-colored material. Samples were ultrasonically-cleaned, spiked with ^{233}U–^{236}U–^{229}Th tracer, dissolved in a mixture of concentrated HNO_3 and HF over 48 h on a hot plate, dried, and then taken up in 7 N HNO_3. U and Th were isolated on anion exchange columns (Dowex AG1-X 200–400 mesh). Measurement of U and Th isotopic ratios was made by thermal ionization mass spectrometry (TIMS) using the Triton thermal ionization mass spectrometer at the Isotope Geochemistry and Geochronology Research Facility, Carleton University, Ottawa. Ontario. The analyses were accompanied by the processing of uraninite in secular equilibrium to ensure accurate spike calibration and fractionation correction. Activity ratios were calculated using half lives from Cheng et al. (2000).

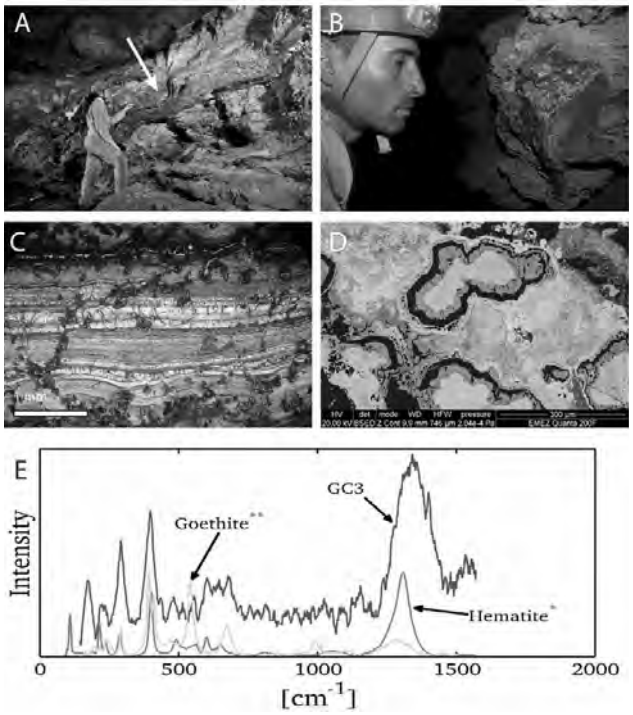

Figure 5. The GC3 sample of the Banded Iron Formation bed: A–B) location of sampling in the Tramo de los Opales; C) thin layers of iron hydroxides in thin section; D) SEM image of iron hydroxides aggomerates in the not laminated part; E) Raman spectrum of GC3 compared with the spectrum of goethite and hematite.

4. Results and discussion

4.1. Banded Iron Formations, their geochemistry and their control on speleogenesis

X-Ray diffraction and Raman analyses show that the Banded Iron Formation is composed mainly of goethite and hematite, together with minor amorphous silica (Fig. 5C). In thin section and SEM images it presents a thin laminations, with nodules and goethite agglomerates. Also rare remnants of siderite and dolomite were identified by EDX punctual chemical analysis, both typical minerals of BIFs (Klein 2005).

WD-XRF Fluorescence analyses show that the BIF layer is composed of 76% of iron with only 18% silica, with minor phosphorus (2%). Phosphorus is also typical of Banded Iron Formation because it tends to be absorbed into iron oxides (Bjerrum and Canfield 2002). Aluminium is below the 2%, with potassium and calcium below the 0.01%.

Of the minor elements, Zn and Cu are present, together with relatively high U and Th concentrations (respectively 96 and 24.5 ppm).

Aubrecht et al. (2011) described similar iron hydroxide deposits in the Churì Tepui as by-product of laterization (clay minerals turned to Fe-hydroxides by weathering).

In the case of Guacamaya Cave the strata consists in a continuous meter thick layer in between the quartz-sandstone beds. Its structure finely laminated (fig. 5C), its high content of iron (more than 70%) and minor amorphous silica are in full agreement with the definition of James (1954) and Trendall and Morris (1983) for Precambrian banded iron formations. The depletion of Al and the lack of a typical latheritic profile suggest that this strata represents a true BIF formation deposited in a shallow marine environment and not a by-product of laterization. Alternatively, this layer could represent a only partially preserved paleo-soil (iron enriched part of the profile), related to weathering and temporary emersion just during the Precambrian (Gutzmer and Beukes 1998; Beukes et al. 2002).

In some place the iron hydroxide bed is folded and stretched, clearly because of shear related to the lithostatic load and the stronger rigidity of the overlying beds of quartz-sandstones. In places, where the layer is stretched it is possible to observe the weathered iron hydroxides flowing out from the strata forming massive brownish flowstone, similar to other goethite speleothems described in other quartzite caves of the Sarisariñama and Chimanta tepuis (Zawidzki et al. 1976; Aubrecht et al. 2011).

Banded Iron Formations are well documented in other areas of South America (Dorr 1973) but were never described before in the Mataui Formation, probably because they are present only locally and because they are much easier weathered than the quartz-arenites.

The role of this bed in guiding the speleogenesis is particularly evident in the Guacamaya Cave, and also in the nearby higher platforms of the Auyan Tepui, where intensive collapses show a predominantly stratigraphical distribution (headwall retreat by basal erosion). It probably represents what is commonly defined as an “inception horizon” in classical karst (Lowe 1992), due to peculiar chemical or rheological characteristics. Many of the hypotheses about speleogenesis in this region are consistent with the petrographic properties and behaviour of this bed. This could include regions of enhanced primary porosity, or even a seepage water alkalinisation effect on the contact with the quartz-sandstone beds, with increasing solubility of quartz and therefore arenization (Martini 2000). Micro-crystalline iron hydroxides in peculiar conditions are also more soluble than silica (Schwertmann 1991) and this factor could enhance

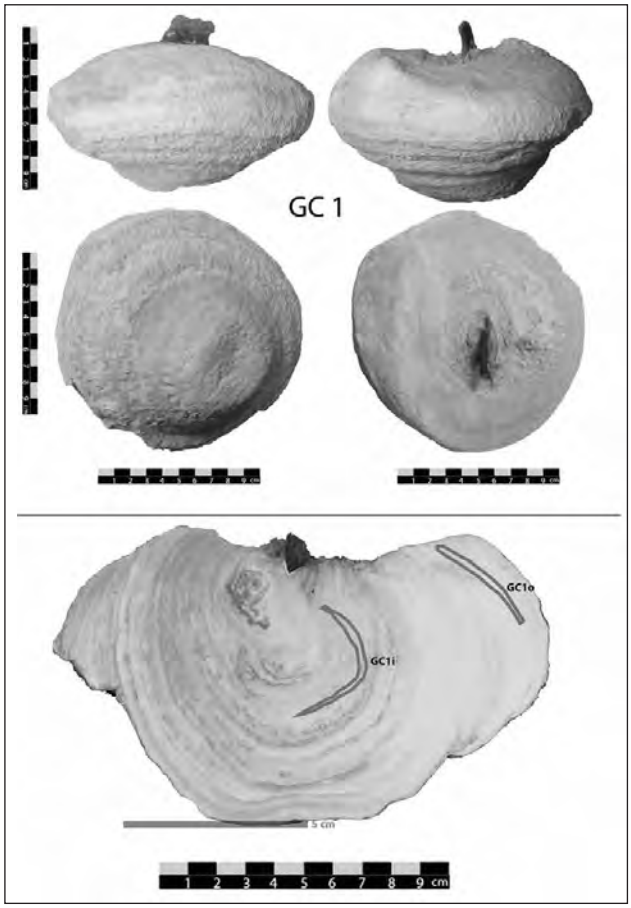

Figure 6. The "champignons" bio-speleothem GC1.

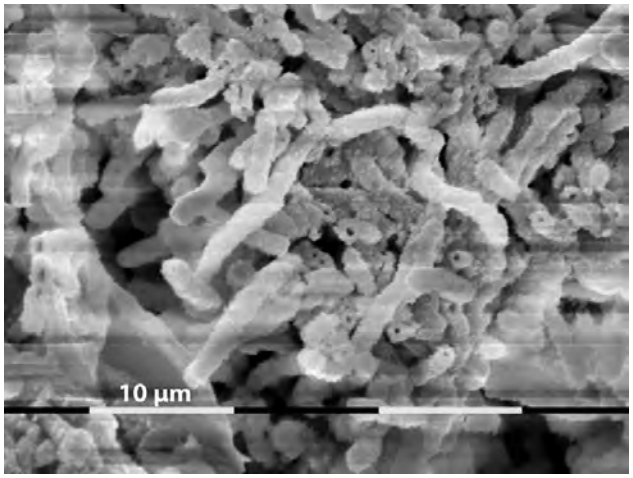

Figure 7. Tubular cast structure of the outer layers in GC1.

weathering. Further research is needed to better understand the main speleogenetic factors enhancing the opening of voids along this peculiar layer.

4.2. Silica biospeleothems

The tufa-like silica bio-speleothem (Fig. 6) is shown to consist of two main textures: tubular casts and peloids (Fig.7). Quartz grains, derived from weathering and arenization of the cave walls, are also common. The inner layers are opalized, while the outer whitish layers are softer and preserve the original structure. The opalization is related to hydration processes, and therefore could be related to longer time of fluids seeping (and therefore with age) or with peculiar events The same opalization of the inner layers was

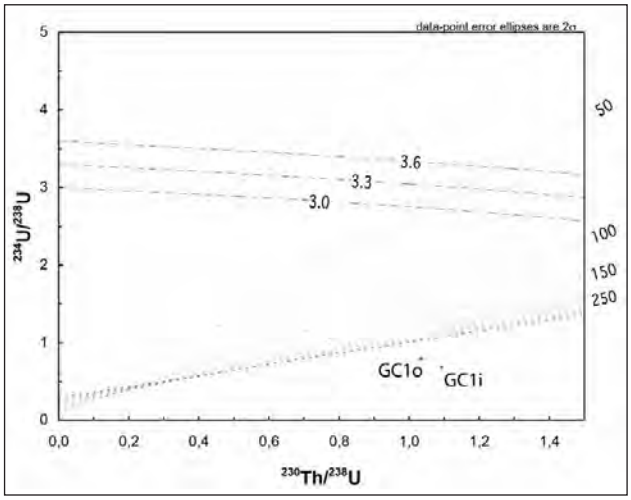

Figure 8. Isotopic ratios from sample GC1 inner(i) and outer (o) layers. The lines labelled "3.6","3.3", and "3.0" are ingrowth curves for initial UU ratios, using ratios from Lundberg et al 2010. Both samples lie outide of the dating envelope (graph was drawn using Ludwig 2000, Isoplot).

observed also in the samples from Chimanta tepui described by Aubrecht et al (2008a) and Lundberg et al. (2010), suggesting that this process could be driven by regional climatic factors.

The two layers sampled for U-Th dating (GCo and GCi in Fig. 6) show high but different contents of uranium: 4.33 ppm in the inner layer, 0.86 in the outer one. This disparity suggests a potential contamination of U rich particles of dust, probably related to the BIF layer that shows really high concentrations of this element. Particles of dust are impossible to observe in thin section or with an optical microscope, but are evident in SEM images. Therefore is not possible to exclude them during the sample preparation.

The isotopic ratios resulted from TIMS analysis are shown in table 1. The $^{230}Th/^{238}U$ versus $^{234}U/^{238}U$, plotted in Fig. 8. The ingrowth curves for initial $^{234}U/^{238}U$ ratios are those from dated speleothem of the Chimanta tepui published in Lundberg et al (2010). Figure 8 shows that both samples from GC1 lie outside of the dating envelope, and therefore cannot be dated by this method. This is due probably to depletion in ^{238}U in comparison with the original ratio, related to leaching, or contamination from other sources of uranium (dust particles). The porous nature of this material suggests that, in spite of the low solubility of silica, the system probably has been open for uranium migration.

With respect to the genesis of this silica bio-speleothem, some observation can be given (Fig. 9). All these speleothems grow on sharp edges, prominent veins of quartz and in proximity of the iron hydroxides layers. A control in their formation by air flow and condensation-evaporation processes is evident also in the anisotropy of the inner layers. These observations not only support the idea of Aubrecht et al. (2008b) that the major source of silica is related to a small-particle aerosol driven by air flows, but also suggest that silica dissolved by condensation waters could be an important source collected on quartz veins and prominent edges of the cave walls. The changing equilibriums between these two sources (growth driven more by aerosol or more by condensation water) in wetter and dryer periods could be the cause of the opalized layers and more porous external ones.

Table 1. Concentrations of 238U in the sample GC1 and isotopic ratios for different isotopes of U and Th.

Sample	Age (ka)	U 238 conc microg/g	230 Th / 234U	2s Error	230 Th / 238U	2s Error	234U / 238U	2s Error
GC1 Inner layer	Not datable	4.33	1.6009	0.00354	1.0927	0.0022	0.6825	0.0007
GC1 Outer layer	Not datable	0.86	1.3124	0.0086	1.0339	0.0033	0.7878	0.0049

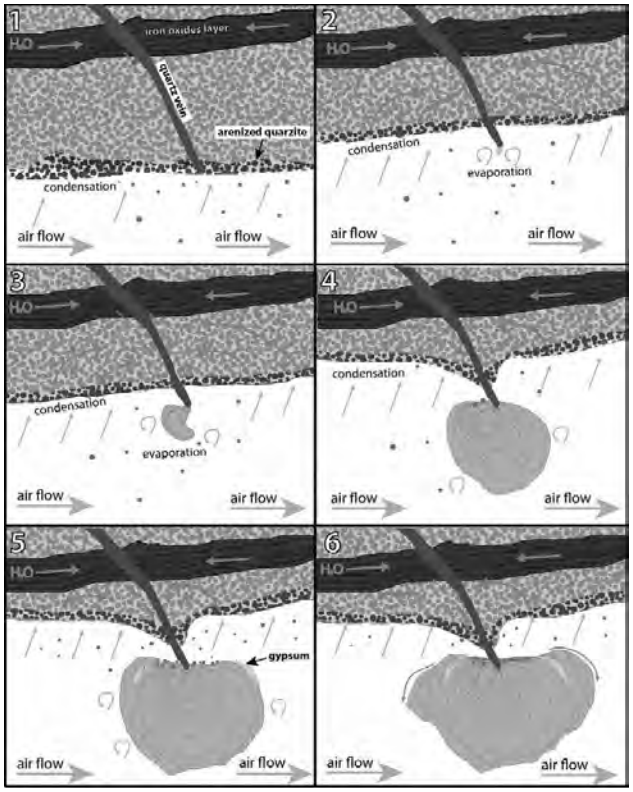

Figure 9. Formation of a "champignons" speleothem on a quartz vein. 1) Initial condition. 2) The surrounding quartzite is weathered, the quartz vein remain in relief and became a preferential collector of seepage water enriched in silica. 3) Air flow controls the evaporation process and the shape of the biological mediated growing speleothems. 4) Grains of quartzite falling by the ceiling in consequence of weathering processes are incorporated in the growing layers. 5) Evaporation causes precipitation of gypsum on the speleothem surface. 6) The formation of a horizontal layer of water on the top of the "apple" leads to the formation of the protruding side of the speleothem.

The presence of gypsum crystals on the speleothem surface and in trace in the inner layers suggests that evaporation processes were active during the formation of the speleothem and in its final growing stage.

5. Conclusions

Guacamaya Cave shows peculiar characters not described before in other quartz-sandstone caves of the Gran Sabana region. The presence of a BIF bed controlling the speleogenesis is evident, and the same layer is probably related to headwall retreat by basal erosion of the higher platform of Auyan Tepui. This layer show a composition typical of primary banded iron formation related to marine sedimentation or, alternatively, of a Precambrian paleo-soil. The cave shows an exceptional variety of biologically mediated silica speleothems of different morphologies and sizes. Their formation is most likely related to aerosol sources of silica and condensation-evaporation processes. Post-depositional alteration, and the possible presence of contaminant dust, limits the ability to date these samples with the U/Th system.

References

Aubrecht R, Brewer-Carías Ch, Šmída B, Audy M, Kováčik L, 2008a. Anatomy of biologically mediated opal speleothems in the world's largest sandstone cave Cueva Charles Brewer, Chimanta Plateau, Venezuela. Sedimentary Geology 203, 181–195.

Aubrecht R, Lánczos T, Šmída B, Brewer-Carías Ch, Mayoral F, Schlögl J, Audy M, Vlček L, Kováčik L, Gregor M, 2008b. Venezuelan sandstone caves: a new view on their genesis, hydrogeology and speleothems. Geologica Croatica, 61, 345–362.

Aubrecht R, Lánczos T, Gregor M, Schlögl J, Šmída B, Brewer-Carías Ch, Vlcek L, 2011. Sandstone caves on Venezuelan tepuis: Return to pseudokarst? Geomorphology, 132, 351–365.

Gutzmer J, Beukes NJ, 1998. Earliest laterites and possible evidence for terrestrial vegetation in the Early Proterozoic. Geology, 26(3), 263–266.

Beukes NJ, Dorland H, Gutzmer J, Nedachi M, Ohmoto H, 2002. Tropical laterites, life on land, and the history of atmospheric oxygen in the Paleoproterozoic. Geology, 30(6), 491–494.

Bjerrum CJ, Canfield DE, 2002. Ocean productivity before about 1.9 Gyr ago limited by phosphorus adsorption onto iron oxides. Nature 417(6885), 159–162.

Briceño HO, Schubert C, 1990. Geomorphology of the Gran Sabana, Guyana Shield, Southeastern Venezuela. Geomorphology, 3, 125–141.

Cheng, H, Edwards RL, Hoff J, Gallup CD, Richards DA, Asmerom Y. 2000, The half-lives of uranium-234 and thorium-230. Chemical Geology, 169, 17–33.

Dorr JVN, 1973. Iron-formation in South America. Economic Geology, 68(7), 1005–1022.

González de Juana C, Picard X, Iturralde JM,1980. Geología de Venezuela y de sus cuencas petrolífera. Edic. Foninvés, Caracas.

Isley AE, 1995. Hydrothermal plumes and the delivery of iron to banded iron formation. The Journal of Geology, 169–185.

Hawkes DD, 1966. Differentiation of the Tumatumari-Kopinang Dolerite Intrusion, British Guiana. Geological Society of America Bulletin, 77(10), 1131–1158.

Klein C, 2005. Some Precambrian banded iron-formations (BIFs) from around the world: Their age, geologic setting, mineralogy, metamorphism, geochemistry, and origin. American Mineralogist, 90, 1473–1499.

Lowe DJ, 1992. The origin of limestone caverns: An inception horizon hypothesis. Manchester Metropolitan University, Ph.D. thesis.

Ludwig KR, 2000. Isoplot: A geochronolgoical Toolkit for Microsoft Excel.Berkeley Geochronology Center, Special Publication No. 1a.

Lundberg J, Brewer-Carias C, McFarlane D.A, 2010 Preliminary results from U-Th dating of glacial-interglacial deposition cycles in a silica speleothem from Venezuela. Quaternary Research, 74, 113–120.

James HL, 1954. Sedimentary facies of iron-formation. Economic Geology, 49(3), 235–293.

Piccini L, Mecchia M, 2009. Solution weathering rate and origin of karst landforms and caves in the quartzite of Auyan-tepui (Gran Sabana, Venezuela). Geomorphology, 106, 15–25.

Martini JEJ, 2000. Dissolution of quartz and silicate minerals. In Speleogenesis-Evolution of karst aquifers. (Klimchouk et al. eds). National Speleological Society, Huntsville, 452–457.

Martini JEJ, 2004. Silicate Karst. In Encyclopedia of Caves and Karst Science (Gunn ed.). Fitzroy Dearborn, London, 1385–1393.

Reid AR, 1974. Stratigraphy of the type area of the Roraima Group, Venezuela. Bolletin de Geologia, Venezuela, Pub. Especial, 6, 343–353.

Santos JOS, Potter PE, Reis NJ, Hartmann LA, Fletcher IR, McNaughton NJ, 2003. Age, source, and regional stratigraphy of the Roraima Supergroup and Roraima-like outliers in northern South America based on U-Pb geochronology. Geological Society of America Bulletin, 115, 331–348.

Sauro F, 2009. Mondi Perduti, sugli altopiani quarzitici del Venezuela. Speleologia, 61, 38–47.

Sauro F, De Waele J, Forti P, Galli E, Vergara F, 2012a. Speleogenesi e speleotemi di opale della Cueva Guacamaya, Auyan Tepui, Gran Sabana, Venezuela. Atti del XXI Congresso Nazionale di Speleologia, Trieste, 291–298.

Sauro F, Piccini L, Mecchia M, De Waele J, (2012b, in press). Comment on “Sandstone caves on Venezuelan tepuis: Return to pseudokarst?” by R. Aubrecht, T. Lánczos,M., Gregor, J. Schlögl, B. Smída, P. Smída, B., Brewer-Carías, Ch., Vlcek, L. Geomorphology.

Schwertmann U, 1991. Solubility and dissolution of iron oxides. Plant and Soil, 130 (1), 1–25.

Teggin D, Martinez M, Palacios G, 1985. Un estudio preliminar de las diabasas del estado Bolivar, Venezuela. Memorias VI Congreso Geologico Venezolano. Caracas, 2159–2206.

Trendall AF, Morris RC (Eds.), 1983. Iron-Formation: Facts and Problems (Vol. 6). Elsevier Science.

Urbani F, Talukdar S, Szczerban E, Colveé P, 1977. Metamorfismo de las rocas del Grupo Roraima. Edo. Bolívar y Territorio Federal Amazonas. Memorias V Congreso Geologico Venezolano, Caracas, 623–638.

Wray RAL, 1997a. A global review of solutional weathering forms on quartz sandstones. Earth Science Reviews, 42, 137–160.

Wray RAL, 1997b. Quartzite dissolution: karst or pseudokarst? Cave and Karst Science, 24, 81–86.

Zawidzki P, Urbani F, Koisar B, 1976. Preliminary notes on the geology of the Sarisariñama plateau, Venezuela, and the origin of its caves. Boletin Sociedad Venezolana de Espeleologia, 7, 29–37.

GOBHOLO CAVE: A LONG GRANITE CAVE IN SWAZILAND (SOUTHERN AFRICA)

Manuela Scheuerer[1], Johannes E. K. Lundberg[2], Rabbe Sjöberg[3]
[1]Carl-Rieder-Weg 6, AT-6130 Schwaz, Austria, manuela.scheuerer@gmail.com
[2]Swedish Museum of Natural History, P.O. Box 50007, SE-104 05 Stockholm, Sweden, johannes.lundberg@nrm.se
[3]Bodviksvägen 14, SE-913 42 Obbola, Sweden, rabbe.sjoberg@telia.com

The results from the 2012 year's reconnaissance expedition to the first major cave reported from Swaziland, southern Africa, will be presented and discussed. The cave is formed by deep weathering and fluvial transport of weathering products in the 2.7 Ga old granites of the Mbabane Pluton, Kaapvaal Craton. So far only a small fraction of the cave has been explored, but with Gobholo River running underground for 1.8 km there is potential for a cave measuring thousands of meters in length. In the higher levels pottery has been found. The biology of the cave is surprisingly rich, with three species of bats, at least five species of spiders and harvestmen, one species of weta, crab, and mollusc, respectively, in addition to observations of springtails and millipeds. There are numerous and diverse non-calcium carbonate speleothems throughout the cave. The exploration of this surprisingly complex cave will continue.

1. Background

Early 2011, during the preparation of the Conference on Granite Caves, one of us (RS) was contacted by Darron Raw who runs Swazi Trails, an adventure agency in Swaziland. He wanted to know more about granite caves, and the reason was that one of the activities Swazi Trail offered is an Adventure Caving trip to Gobholo Cave, a large granite cave near Mbabane, the capital of Swaziland. The trip runs for more than two hours, so the cave had to be of considerable dimensions, and Swazi Trails had run trips there for more than a decade. Still, nothing was known about the cave, its origin or significance. Available sources (Middleton and Waltham 1986; Laumanns 2008) indicated that there are no known caves in Swaziland, at all. Meanwhile, RS wrote a presentation of the cave and its plausible origin (Sjöberg 2011); this paper was the working hypothesis for the geomorphological part of the expedition here presented. All this prompted the idea of a small reconnaissance expedition to Swaziland and Gobholo Cave, and for three weeks in late July-early August 2012 two of us (MS and JL) visited Swazi Trails and Gobholo Cave to initiate the exploration of this remarkable cave.

Figure 1. Gobholo valley, Swaziland. Gobholo River sinks underground near the middle of the image. The distance between the sink and the resurgence is 1.8 km. Source – Google Earth (image date 2009-07-28).

2. Geological and geographic setting

Swaziland is a small landlocked country in subtropical Africa, entirely on the Kaapvaal Craton. Gobholo Cave is in the western part of the country, in the Highveld on the border to the Middleveld (Figure 1). Topographically the Highveld is characterized by higher altitudes, with summits reaching 1,800 m a.s.l., and a large amount of rain (up to 2,000 mm per year). The Highveld is also influenced by jointing and faulting, with many deeply dissecting valleys. The Lowveld has more moderate altitudes (800 m a.s.l. down to 400 m a.s.l.) with less rain.

There are no carbonate rocks known from Swaziland (Laumanns 2008). Most of western Swaziland is instead dominated by Archean intrusive and metamorphic rocks. Gobholo Cave is formed in the c. 2.7 Ga old coarse grained granites of the Mbabane Pluton (Layer et al. 1989), that intruded the up to 3.66 Ga old gneisses of the Ancient Gneiss Complex.

3. Methods

We surveyed most of the tourist cave using ordinary analogue survey techniques (Suunto Compass and Clinometer, together with a Disto DXT for length measurements). The survey data was daily processed in an Excel spreadsheet.

The morphology of the cave was inspected on site, both in the cave and outside at several surface trips.

Speleothems were carefully sampled outside the main tourist part of the cave. The samples have been equally distributed between Prof. Juan Ramón Vidal Romaní, A Coruña, Spain, and the Swedish Museum of Natural History, for later investigation.

Cave life was collected by hand and stored in 70% Et-OH and has been distributed to experts (spiders to Prof. Anise Dippenaar, Pretoria, South Africa, and crickets to Prof. Gianmaria Carchini and Dr. Mauro Rampini, Rome, Italy).

4. Results and Discussion

4.1. Gobholo Cave

Gobholo River sinks underground in the upper part of Gobholo Valley. From there it flows nearly 1.8 km underground until it exits in resurgence in the lower part of the valley. Most of the valley floor is covered by saprolite of unknown thickness. The main entrance to the cave is a few hundred meters upstream the resurgence, between residual boulders forming a small boulder heap. From the large entrance chamber several passages lead steeply down to the middle levels where corestones are still intact. The lowermost part of the cave, with the stream, can be reached in the innermost tourist chamber, at a depth of more than 40 meters under the entrance. The stream passage has not been explored, but there are multiple parallel passages in the middle and higher levels of the cave, forming a 3D-labyrinth. A second source of water in Gobholo Cave has been found in a small middle level passage, where a trickle of moderately warm water can be found, indicating the possibility for at least local scale influences from thermal water.

We surveyed only about 400 meters of the cave, but the surface distance from the extreme points in the survey is slightly more than 100 meters. This gives a factor of at least 3.5 for the length; this number is probably much higher since many parallel side passages were left unsurveyed. Even if the stream only can be followed underground for say 1 km, this indicates that Gobholo Cave eventually will attain a considerable length, possibly measured in kilometers.

Prior to our visit, there have been two competing hypotheses (or rather guesses) for the origin of the cave (D. Raw, pers. info.): that the cave is simply a huge talus cave, formed by boulders that have gravitationally been transported from the sides of the valley; or that it is formed by deep weathering of the granite, and that the boulders are in situ. The presence of free boulders in the upper level of the cave, and well preserved more or less intact corestones in the middle and lower parts (Figure 2), indicates that at least part of the cave is formed by granite deep weathering (Sjöberg 2011). It is likely that the stream primarily has acted as a transport agent for the weathering products, but especially during flooding events it seem to reach high energies and can act as an erosion agent.

4.2. Speleothems

There are numerous speleothems in the cave, forming different morphologies. Most common are coralloids and flowstones (Figure 3), but also draperies are common. Most of the speleothems in the lower parts show signs of erosion from streaming water. No stalactites or stalagmites have been found. It is likely that the speleothems consist of the common granite cave speleothem forming minerals opal-A and pigotite (Vidal Romaní et al. 2010).

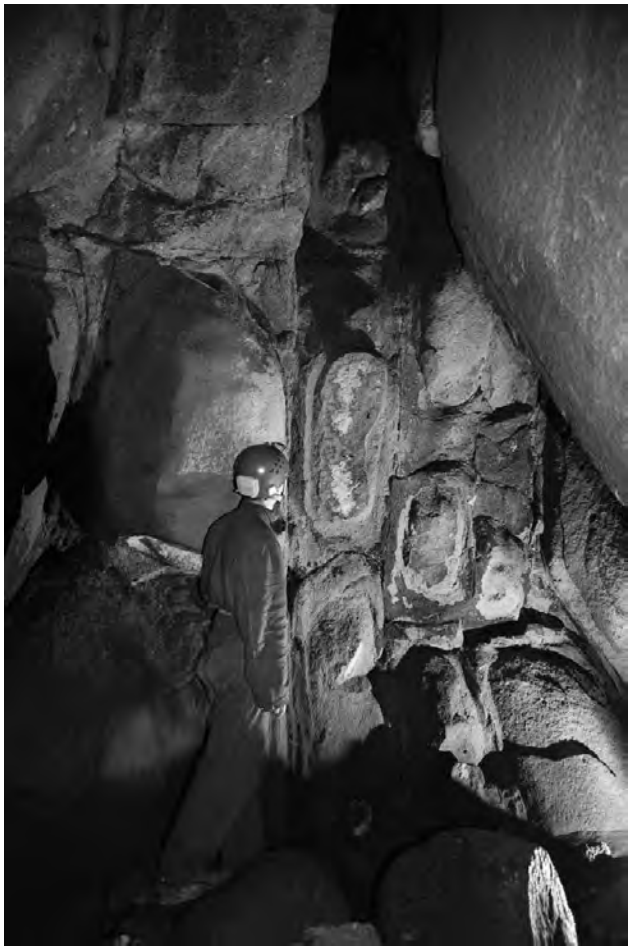

Figure 2. Corestones in the middle level of Gobholo Cave, about 150 m from the entrance. Photo by Johannes Lundberg.

4.3. Biology

The cave ecosystem is surprisingly rich with three species of bats (schreibers' long-fingered bat *Miniopterus schreibersii*, cape hairy bat *Myotis tricolor* (Figure 4), and geoffroy's horseshoe bat *Rhinolophus clivosus*), several species of spiders and harvestman (some with a tendency towards less pigmentation), and numerous individuals of a cave living king cricket (Insecta: Orthoptera: Anostostomatidae). There are also observations of a stationary mollusc, a pigmented crab, and unpigmented springtails as well as millipeds, resting lepidopterans, and small dipterans. Differently coloured colonies of Actinobacteria can be found on the walls, and the guides from Swazi Trail reported the histoplasmosis inducing fungi *Histoplasma* from bat guano (but there are no reported cases of histoplasmosis infection after visits in the cave).

4.4. Archeological potentials

In the upper levels of the cave, near the entrance and in some of the passages leading to the middle levels, scattered pottery has been found. Until fairly recently, western Swaziland was mainly inhabited by Khoisan, hunter-gatherer people now extinct from Swaziland. They were replaced by bantu-speaking people during the Bantu migration reaching the area less than 1,000 years ago. The age and attribution of the pottery is not known. Secret caves in nearby valleys are used as royal burial sites, but no

Figure 3. The large flowstone in the lower part of Gobholo Cave, about 200 m from the entrance. The height of the flowstone is about 2.5 m. Note the graffiti in the left hand of the flowstone. Photo by Manuela Scheuerer.

human remains have been found in any cave in Gobholo Valley.

5. Future research

We are planning to return to Gobholo Cave late this year (2013) or early next year with a larger expedition, together with cavers and researchers from Spain, South Africa and possibly other countries. The goal will be to survey the main passages of the cave, using digital surveying equipment and a digital pipeline for processing the survey data. We will also more thoroughly survey the occurrence of speleothems, their distribution and diversity. A more detailed inventory of the cave life will be undertaken, with special emphasis on the smaller fauna, and we hope to be able to start exploring nearby areas of Swaziland for caves.

*Figure 4. Hibernating cape hairy bat (*Myotis tricolor*) in Gobholo Cave. This is one of three species of bats found in the cave. Photo by Manuela Scheuerer.*

Acknowledgment

We want to thank Darron Raw and Swazi Trails for making us aware of this cave, and inviting us to visit Swaziland and Gobholo Cave. Swazi Trail supported part of the reconnaissanse trip. Many thanks to the guides at Swazi Trails for much assistance while we stayed in Swaziland; in particular we want to thank Sipho Thwale for assistance and company in the cave, and to Anita Raw for help with many practical arrangements. Many thanks to Prof. Gianmaria Carchini and Dr. Mauro Rampini, Rome, Italy, for help with determining the king cricket, and to Prof. Anise Dippenaar, Pretoria, South Africa, for the determination of the spiders we collected, and to Dr. Michal Filippi, Academy of Sciences of the Czech Republic, and one anonymous reviewer for valuable comments on an earlier draft of this manuscript. Thanks also to Prof. Juan Ramón Vidal Romaní, A Coruña, Spain, for a fruitful and valuable cooperation in investigating the cave and its speleothems, and giving us a great learning opportunity.

References

Laumanns M, 2008. Atlas of the Great Caves and Karst of Africa. Part 3. 2nd Edition. Berliner Höhlenkundliche Berichte 30.

Layer PW, Körner A, McMillans M, York D, 1989. Elements of the Archean thermal history and apparent polar wander of the eastern Kaapvaal Craton, Swaziland, from single grain dating and paleomagnetism. Earth and Planetary Science Letters 93, 23–34.

Middleton J, Waltham T, 1986. The Underground Atlas: A Gazetteer of the World's Cave Regions. Hale: London.

Sjöberg R, 2011. Gobholo Caves, Swaziland: världens längsta granitgrotta? Grottan 46(4), 30–32.

Vidal Romaní JR, Sanjurjo Sánchez J, Vaqueiro M, Fernández Mosquera D, 2010. Speleothems of granite caves. Communicações Geológicas 97, 71–80.

SOME SIGNIFICANT CAVES FOUND IN THE NON-KARSTIC ROCKS OF HUNGARY

István Eszterhás[1], George Szentes[2]
[1]Köztársaság-út 157, 8045 Isztimér, Hungary, eszterhas.istvan@gmail.com
[2]Alte Frankfurter Str. 22 b, 61118 Bad Vilbel, Germany, szentesg@yahoo.de

Abstract. Fifteen non-karstic caves have been selected in Hungary in order to study cave development in the different surrounding rocks. Morphological investigations in the granite region has revealed the long weathering process of the granite, which has resulted balancing rocks and among them woolsack caves. In a basalt area the geological observations has resolved the formation of the leaning pseudocave, as the basalt blocks were sliding on the underlying sediments. Further study has shown the cave development in the tuffaceous formations as a consequence of the continuous sliding and the consequent aggradation. The morphological observations in sandstone caves have shown complex cave development such as the tectonic movement and erosion. The morphology of the caves in geyserit and hydroquartzite marks the traces of the alkaline solution and the alteration of the solution and deposition according to the changing pH value. In clay schist a peculiar cave development was studied, where the karstic cavities have broken down in the underlying limestone and the realignment of the hollows has formed the cave.

1. Introduction

In Hungary 4,018 caves have been listed and one quarter of these, 911 caves, have developed in non-karstic rocks. Karst cave development depends on several factors, including acidic solution, erosion, tectonics and fragmentation. On the other hand non-karstic cavities are influenced by more than 50 factors governing cave development due to variations in the composition and structure of magmatic, sedimentary and metamorphic non-karstic rocks.

2. Non-karst caves formed in igneous rocks

Igneous rocks are not subjected to karst processes. Therefore only non-karst caves are formed in these rock types. In Hungary magmatic rocks are found most often and have resulted in the development of many types of non-karst caves. The following describes the most important caves according to their surrounding rock structure (Fig 1).

2.1. Intrusive rocks

In the Velencei Mountains 19 caves are to be found in granite and in granite porphyry. The most extensive cave is the *Zsivány Cave* near the village of Pákozd (Figs. 1, 2). The cave opens in a granite tor, which is composed of rocks balanced one on the other. The cave development is connected to the formation of these rocks. The development process began with the rounding of the granite blocks through chemical weathering below the gravel blanket. After the denudation of the gravel coating the rounded granite blocks reached the surface. Further denudation cleared out the gravel between the granite blocks and as a result of this, accessible woolsack caves have formed. The accessible length of the cave is 15 m and its vertical extension is 4 m. The average height of the passages is 1.2 m (Eszterhás 2006, 2009; Tarsoly 2011).

2.2. Extrusive rocks

Extrusive rocks in Hungary predominantly include rhyolite, dacite, andesite and basalt. Non-karstic caves have formed in each of these rock types. Two-hundred and fifty-two caves are to be found in andesite, 44 in rhyolite, 18 in dacite and 97 caves have been listed in basalt. One significant cave from each rock formation is described below. In the Tokaji Mountains *Rózsa Sándor Cave* near the village of Regéc opens in the pyroxene andesite of Mount Kis-Péter-mennykő (Figs. 1, 3). Due to denudation the lower, north western boulder area of the double peaked mountain was weakened laterally and collapsed to such an extent, that accessible cavities were formed. The cave consists of a lower, 26 m long wide passage and an upper 13 m long crawl way. A 6 m long narrow crevice connects the two levels. The 80 cm wide entrance to the lower passage opens beneath a flat rock slab. Behind the entrance a shaft leads to a small chamber, to the "Anteroom", after which a narrow hole leads to a chamber 4 x 6 m and 4 m high, the "Big Room". An outlaw legend is related to the cave (Eszterhás 2011). In the Tokaji Mountains near the village of Erdőbénye the *Ivan Cave* is to be found in the rhyolite cliffs between Mount Mókus and Veres Peak (Figs. 1, 5). In the cliffs three caves are to be found, among them the most extensive is Ivan Cave. The cave has three entrances in the southern side of the cliff. The western and the middle entrances connect whilst the eastern one is a flat, horizontal crack. Behind the western and the middle entrances runs a high crevice partially filled with huge collapse blocks. The total length of the cave is 29 m. The cave has been formed by the widening of the fissures (Eszterhás 2011). In the Szalánci Mountains near the village of Pusztafalu 10 caves are to be found in the pyroxene-amphiboldacite of Mount Bükkös. The most extensive of the 10 caves is the 11.5 m long *Desem Cave* (Fig 1). The cave is a through cave, which has been formed by the expansion of the surrounding rock. The main passage is 7.5 m long and 1.6 m high. From the main passage three 1.5 m long accessible fissures diverge northward (Eszterhás 2011). The 51 m long *Pokol Hole* is located in the basalt of the Bakony Mountains near the village of Kapolcs (Figs. 1, 4). The basalt is underlain by a

loose sandstone layer and its edge has gradually broken away. The basalt blocks have not slid down on the slope, but rest against the bedrock, leading to the development of a leaning pseudocave, which has formed parallel to the edge of the outcropping rock formation. The main passage along the fault line is 24 m long and it is connected with parallel running side passages. In the sandstone, thick basalt blocks dam up the seeping water, which emerges in the cave as a spring with a changing flow rate. This spring feeds a small lake (Eszterhás 1994).

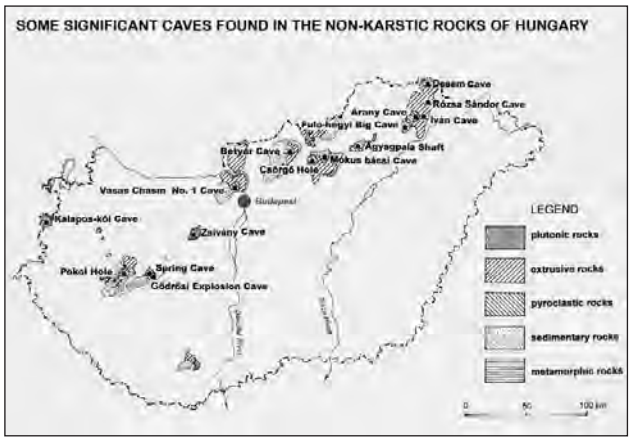

Figure. 1. Location of the caves.

2.3. Pyroclastic rocks

In Hungary 198 caves have been registered in andesite agglomerate, 9 caves in andesite tuff, 23 caves in rhyolite tuff, 6 caves in rhyodacite tuff and 7 caves in basalt tuff. Four caves are described below from different pyroclastic rocks. The *Vasas Chasm No. 1 Cave* in the Visegrádi Mountains has developed in the andesite agglomerate on the northern side of the Mount Cseresznyés (Figs. 1, 10). There, the andesite agglomerate has slid down the clayey andesite tuff, due to erosion deepening the nearby Cseresznyés Creek. As a result of this a 250 m long dilatation fault has evolved, the Vasas Chasm, in which five caves open. The most extensive cave is No. 1 Cave. The cave can be accessed through a 38 m long, 10 m deep and 3–4 m wide crevice. The cave passage is 2–3 m high and 70 cm wide and contains some huge boulders. The southern wall of the passage is bedrock, whilst the northern wall consists of huge boulders. The ceiling is also composed of large boulders and narrow upper passages run through them. The total length of the cave is 50.2 m, its horizontal extension is 40.2 m and its deepest point is 20.4 m. (Szentes 1971; Szilvay 1996). The *Arany Cave* is located in the Tokaji Mountains in rhyolite tuff near the village of Tállya (Figs. 1, 6). The way in which this partly collapsed horizontal cave has developed is complex. Originally it was formed along a fissure by an underground stream. The natural passage was widened in the 17th century as a mining tunnel for gold prospecting, however only pyrite occurs in the surrounding rock. Later, the first part of the tunnel collapsed and was subsequently dug out in 1993. The length of the horizontal cave is 50 m. In the cave there is a slow running acidic knee deep stream. The sulphuric acid content of the water originates from the pyrite weathering. In the middle section the roof is nicely decorated with a large number of 20–40 cm long silicate stalactites. The silicate

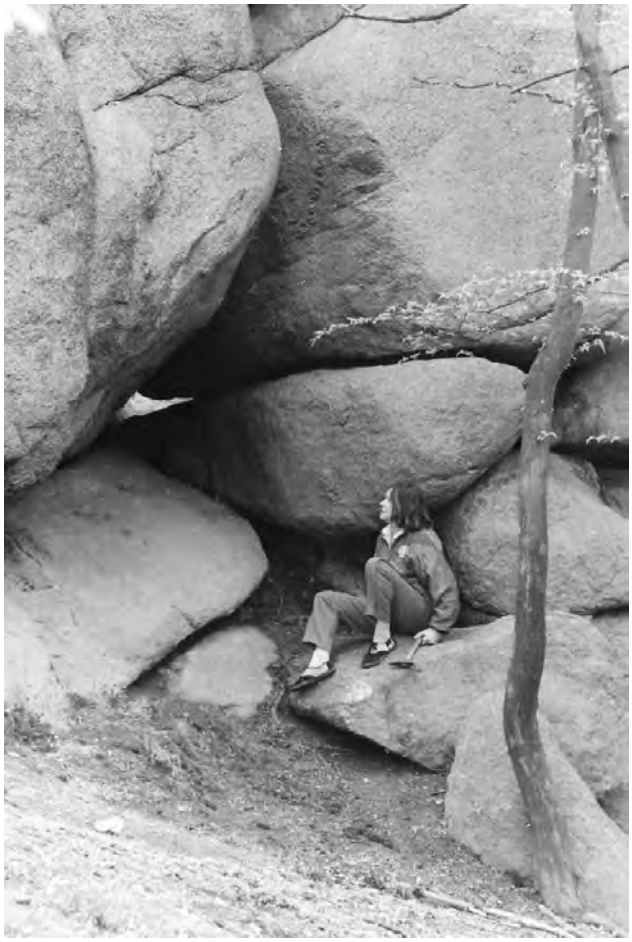

Figure 2. Zsivány Cave in the Pandur-kő Tor.

speleothems are mainly composed of α-tridimite. These rhomboid silicate crystals aggregate into a loose mass and therefore the speleothems are extremely delicate (Dénes 1996; Eszterhás 2011). The *Csörgő Hole* opens in the Western Mátra Mountains in rhyodacite tuff at the southern foot of Mount Ágasvár (Figs. 1, 7). The 428 m long and 29.6 m deep cave is the longest non-karstic cave in Hungary. The Csörgő Hole is an atectonic labyrinth. The development of the cave can be traced back to the continuous sliding of the rhyodacite tuff and the consequent aggradation. The first explorer of the cave, the geologist József Szabó had defined exactly how the landslide had resulted in the development of the cave: *"The position of the surroundings and the direction of the passages indicates that the layers, obeying the pull of gravity, are sliding slowly and continuously toward the bottom of the valley. As a result of this mass movement the layers have broken apart and boulders moving at different rates are piling up on one another…."* (Szabó 1871). The boulders are sliding south-eastwards on a 20^{o} slope, therefore between the accumulated boulders passages have formed following a NE-SW strike. The complicated labyrinth of the cave consists of several chambers passages of various lengths, and shafts. Speleothems are not to be found in the cave. The walls and the ceiling are formed of light grey, granular and partly weathered tuff boulders. The boulders in the Big Room are especially spectacular as are those in the "Prow" and in the M System which contains the 8 m big "Super Cube". In the deepest level of the cave the perennial Vidróczki Spring emerges and in the Bat Chamber an intermittent lake can sometimes be found. The members of the Vulcanospeleological Collective have proved by dye

tracing the connection between the Vidroczki Spring and the Vándor Spring which emerges on the surface. The distance between the two springs is 130 m and the vertical difference is 8 m. The dye tested water emerged after 7 hours. The cave temperature is cooler than the surface temperature. The air temperature in summer is about +4 °C in the deep level. This phenomenon can be explained by the extensive evaporation area of the porous tuff, which results in greater heat extraction (Eszterhás 2010, Ozoray 1962). The survey of the cave has been published in the Proceedings of the 15th International Congress of Speleology (Eszterhás, Szentes 2009). The *Gödrösi Explosion Cave* is is located on the Tihanyi Peninsula (Fig. 1) The cave is the result of a steam explosion, which took place concurrently with the deposition of the basalt tuff. Due to the sudden pressure decrease the upward streaming hot solutions volatilized, which caused explosions. The steam explosion has created a cavity in the basalt tuff, which was filled with lime bearing hot solution. The hole has not collapsed, because the surrounding material has been cemented by the precipitating lime. The cave wall is covered with precipitated calcite pisoliths. The cave was opened by quarry operations in the 1920s. The 15.8 meter long and 6.5 meter deep cave is located on private property (Eszterhás 1987).

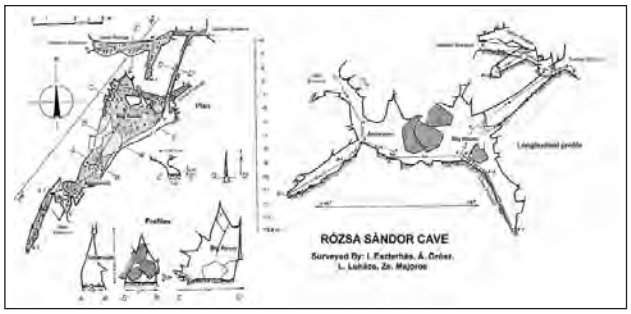

Figure 3. Survey of the Rózsa Sándor Cave.

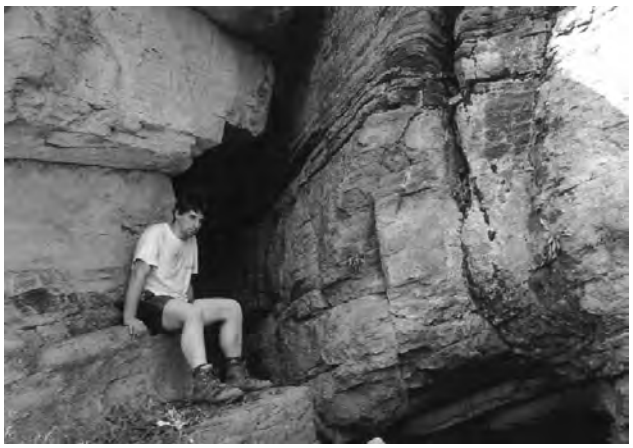

Figure 5. Ivan Cave in the rhyolite cliffs.

3. Non-karst caves formed in sedimentary rocks

3.1. Clastic rocks

In Hungary more than one hundred caves are to be found in conglomerate and in sandstone. These caves have developed mainly in siliceous sedimentary rocks such as conglomerate, sandstone and geyserite. In other sedimentary rock formations very few non-karstic caves are to be found. We describe a significant cave from both sediments. In the Köszörű Valley in the Mátra Mountains the *Mókus Bácsi Cave* (Fig. 1) has formed as a result of the alkaline solution of former geysers. Only a solution with a pH of over 9 would have been able to dissolve the passages in this cave. The alkaline solutions originated from the former geysers of the Gyökeres Peak above the valley. Recently only the remains of the geyser can be observed. The downward-flowing alkaline solutions have dissolved many smaller cavities and also cave sized holes in the conglomerate. The most extensive cave is the 14.6 m long and 0.5–1.0 m wide Mókus Bácsi Cave above the Vasalótalp Cliff (Ezterhás 2010). The *Betyár Cave* in the Cserhát Mountains is 87 m long, and is the longest sandstone cave in Hungary (Figs. 1, 8). The cave was formed in thick calcareous sandstone beds as a result of different types of cave development. It has formed along a fault line. Along the fault, the seeping water has dissolved the limy cementing material and the sand has peeled off from the loose rock surface and accumulated in the lower

Figure 4. The Pokol Hole in basalt.

Figure 6. Silicate stalactites in the Arany Cave.

Figure 7. Accumulated rhyodacite tuff boulders in the Csörgő Hole.

Figure 8. The Betyár Cave in sandstone.

Figure 9. The Kalapos-kői Cave in green schist.

level of the distended fissure. This constant process has resulted in a gradually widening fissure cave filled with loose sand. Excavations in this sand revealed a large number of Pleistocene mammal bones and potsherds dating from the Middle Ages to modern times (Eszterhás 2007).

3.2. Chemically formed rocks

Most limestone, gypsum, salt or dolomite can undergo karstic solution. However some non-karstic caves are to be found in chemically formed rock for instance in calc-tufa deposits. Only non-karstic caves can be formed in sedimentary rocks which are not soluble in an acidic environment such as the geyserites, in which 41 caves occur in Hungary. The well known *Spring Cave* on the Tihanyi Peninsula has developed in geyserite (Fig. 1). The cave opens in the middle of Tihany village in front of the Abbey in Csokonai Grove. The cave is to be found in a geyser cone. It is difficult to recognize the original shape of the cone due to the constructions of Tihany Castle and the Abbey above it. The cave disappeared after the devastation of Tihany Castle in 1702, but was re-opened again in the course of landscaping in 1951. The cave is a gated show cave, illuminated by electric light. The 14 m long, 2.5 m wide and 2–3 m high cave is composed of two chambers and two bigger niches. The cave was developed by alkaline solution. During the slow discharge of the hot solutions the pH value is below 8 and polymeric silicic acid is precipitating, enlarging the geyser cone. The fast discharge of the solutions raises the pH value above 9 and as a consequence of that the precipitated silicate dissolves, forming cavities or cave sized holes. The walls are decorated with spectacular solution forms, which also form the vault of the ceiling (Eszterhás 1987).

4. Non-karst caves formed in metamorphic rocks

The majority of the metamorphic rocks, with the exception of the marble, are not suitable for the karstification. In the metamorphic rocks of Hungary caves occur in clay schist, in calc- and quartz phyllite, in silicified tuff and in green schist.

4.1. Low grade metamorfic rocks

Four caves are to be found in clay schist in the southern part of the Bükk Mountains. The *Agyagpala Shaft* opens 6 km north of Bükzsérc village (Fig. 1). Behind a 1 m diameter opening a 9.6 m gradually widening shaft leads to a 13.8 m long and 3–4 m wide sloping chamber. The volume of the chamber is about 300 m^3. The age of the schist series has been dated to the Carnian (Liassic). The schist overlays the limestone. As the karstic cavities have broken down in the underlying limestone, the realignment of the hollows has formed the cave in the clay schist which lies above. The cave is 23.5 m long and 16.6 m deep. In 1998 an owl family nested in the cave (Eszterhás et al. 1998).

4.2. Metasomatic rocks

The postvolcanic hot siliceous water transformed the rhyolite tuff into hydroquartzite. This, siliceous rhyolite tuff

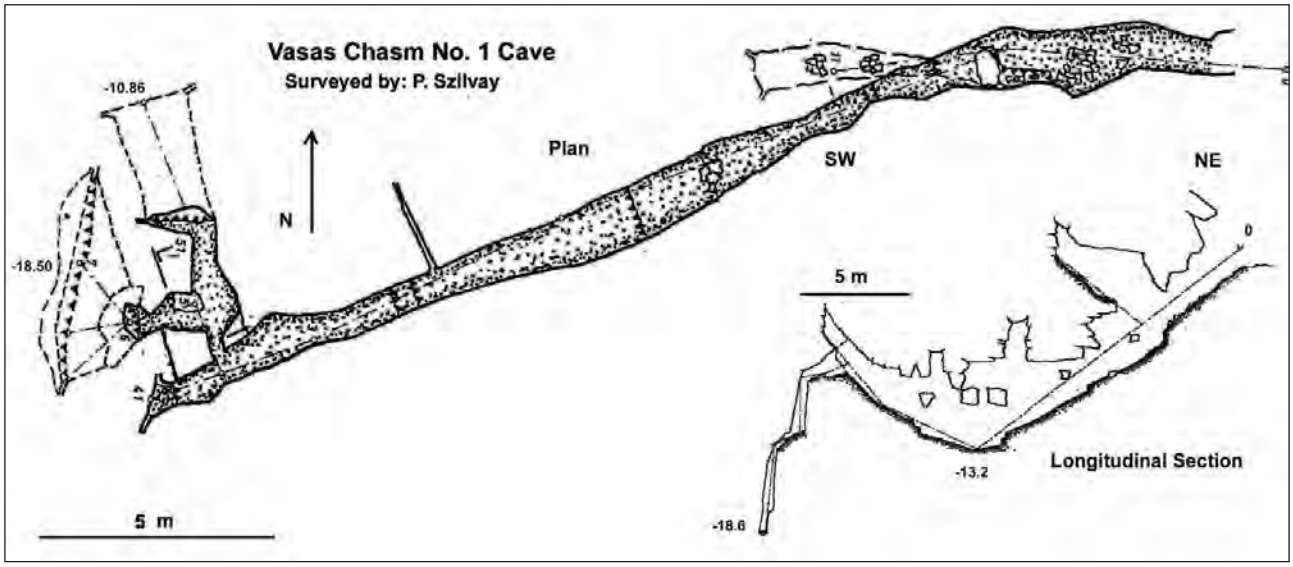

Figure 10. Survey of the Vasas Chasm No. 1. Cave.

occurs in many places in Hungary. In the southern part of the Tokaji Mountains ten caves are to be found in this rock formation. Near the village of Legyesbénye is the *Fuló-hegyi Big Cave* (Fig. 1) formed in the siliceous rhyolite tuff. During the Sarmatian alkaline siliceous hot springs emerged along the fault lines in the rhyolite tuff, which have silicified a part of the tuff. Silicate has been deposited from hot springs below pH8, namely the tuff has undergone silicification. Occasionally the pH value rises above 9 therefore the precipitated silicate dissolves and forms cavities. In the southern slope of Mount Fuló ten caves formed by alkaline solution are to be found. The most extensive cave is the above mentioned 20.4 m long Big Cave. Behind the 3 m high and 4 m wide entrance the cave extends to three larger chambers. In the wall of these chambers spherical solution caldrons and channels can be seen. In 1932 archaeological excavations were carried out in the cave and many artefacts dating from the Bronze Age to the Middle Ages were found (Eszterhás 2011).

4.3. Thermometamorphic rocks

Thermometamorphic rock is the green schist in the Kőszegi Mountains. Fifteen caves have been listed in this formation. The *Kalpos-kői Cave* (Figs. 1, 9) opens in a green schist ledge on the northern slope of Mount Kalapos-kő 2 km northwest of the village of Bozsok. The cave has developed through the extension of a fault which is parallel with the ledge. The northern section of the cave is higher and composed of two levels, southwards the hole gradually descends. The total length of the cave is 30.2 m and the level difference is 4.5 m (Eszterhás 2001).

5. Summary

The study summarises the development and the way in which the 15 most significant non-karst caves in Hungary have formed and reviews the surrounding rock formations. The longest non-karst cave of Hungary is the 428 m long Csörgő Hole in the Mátra Mountains. Most of the non-karst caves, numbering 250 caves occur in andesite. As well as caves which have formed as a result of mass movement and fragmentation, numerous caves have formed as a result of alkaline solution.

References

Dénes Gy, 1996. A pest-hegyi Arany-barlang – Proceedings of the 6th International Symposium on Pseudokarst, Galyatető, 117–135 (in Hungarian).

Eszterhás I, 1987. A Tihanyi-félsziget barlangkatasztere – A Bakony természettudományi kutatásainak eredményei (18. kötet), Zirc, 45–46 (in Hungarian).

Eszterhás I, 1994. A Pokol-lik – Lychnis a Vulkánszpeleológiai Kollektíva kiadványa, Kapolcs, 28–35 (in Hungarian).

Eszterhás I et al., 1998. A Déli-bükk nemkarsztos barlangjai – kézirat a Vulkánszpeleológiai Kollektíva Évkönyvében az MKBT és a BI adattárában, Budapest, 167–178 (in Hungarian).

Eszterhás I, 2001. Barlangok az egykori "Confinia Batthyánia Esterháziána" vidékén – Karszt és Barlang, Budapest, 63–78 (in Hungarian).

Eszterhás I 2006. Felszíni denudációs formák és gyapjúzsákbarlangok a Velencei-hegységben – Karsztfejlődés (XI. kötet), Szombathely, 195–208 (in Hungarian).

Eszterhás I, 2007. A szentkúti Betyár-barlang – Karsztfejlődés (XII. kötet), Szombathely, 331–347 (in Hungarian).

Eszterhás I, Szentes Gy, 2009. Overview of the Non-karstic Caves in Hungary – Proceedings of the 15th International Congress of Speleology, Kerwille, 1474–1480.

Eszterhás I, 2009. Oberflächliche Denudationsformen und Wollsackhöhlen im Granit des Velencei-Gebirges Ungarn – Cadernos Laboratorio Xeolóxico de Laxe (Nº 34), A Coruña, 27–47 (in German).

Eszterhás I, 2010. Barlangok a Mátrában – in Baráz Cs. editor: A Mátrai Tájvédelmi Körzet – a Bükki Nemzeti Park Igazgatóságának kiadványa, Eger, 107–114 (in Hungarian).

Eszterhás I, 2011. A Tokaji-hegység barlangtani vázlatai – Karsztfejlődés (XVI. kötet), Szombathely, 293–314 (in Hungarian).

Eszterhás I, Szentes Gy, 2012. A List of non-karstic Caves in Hungary – http://geogr.elte.hu/nonkarstic, Ozoray Gy, 1962. The genesis of non-karstic natural cavities as elucidatedby Hungarian examples – Karszt- és Barlangkutatás II. évfolyam), Budapest, 127–136.

Szabó J, 1871. Az Ágasvári barlang a Mátrában – Földtani Közlöny (I. évfolyam), Pest 11–12 Szentes Gy, 1971. Caves formed in the volcanic rocks of Hungary – Karszt- és Barlangkutatás (VI. évfolyam), Budapest, 117–129 (in Hungarian).

Szilvay P, 1996. Vasas-szakadék I. sz. barlangja – in Eszterhás-Szabó-Szilvay-Tinn: A Visegrádi – hegység barlangjai (I. rész) – kézirat a Vulkánszpeleológiai Kollektíva Évkönyvében az MKBT és a BI adattárában, Budapest, 118–128 (in Hungarian).

Tarsoly P, 2011. A Velencei-hegység gyapjúzsákbarlangjai – Nyugat- magyarországi Egyetem GEO honlap, Székesfehérvár (in Hungarian).

TYPES OF NON-KARST CAVES IN POLISH OUTER CARPATHIANS – HISTORICAL REVIEW AND PERSPECTIVES

Jan Urban, Włodzimierz Margielewski
Institute of Nature Conservation, Polish Academy of Sciences, Cracow, Poland, urban@iop.krakow.pl

On the basis of historical review of progress in exploration and scientific studies and categorisation of non-karst, mainly gravitational caves in Polish Outer Carpathians (Beskidy Mountains), new concept of these caves' classifications is proposed. Two classifications are suggested. According to the genetic classification, in which the criterion is the relation to the stages of slope evolution, two main types of caves: *initial caves* and *subsequent caves* can be distinguished, however intermediate forms are also observed. According to the geomechanic classification, which accounts the type of phenomenon-process producing caves, three types of caves can be discriminated: *dilation caves*, *dilatancy caves* and strict *boulder caves*.

Introduction

Polish Outer (Flysch) Carpathians, called also the Beskidy Mountains (BMs), with their Foothills, and constituting the predominant part of the Polish Carpathians are principally built of siliciclastic-clayey rocks. In morphological terms the BMs are medium-high mountains composed of several mountain ranges. Such geological structure and relief determine the nature of caves which are relatively frequent in this region. Among more than 1,200 caves recorded in the BMs., karst caves are practically absent, whereas most of caves are genetically connected with gravitational mass movements. Close relation between caves and processes shaping the mountain relief causes that the accurate and comprehensive genetical description and classification of these caves is crucial problem for interpretation and reconstruction of morphogenesis of the region. Therefore, the question of proper classification of these caves is a matter of this paper.

Settings: geological structures controlling the morphogenesis

The BMs are built of flysch, siliciclastic-clayey rocks of the Cretaceous-Palaeogene, occasionally Early Miocene age (with an except of Upper Jurassic, limestone-marly flysch occurring only in the most western part of this belt). The Outer Carpathians represent Alpine orogenic belt tectonically shaped in the Neogene and consisting of several tectonic-facies units overthrust each other toward the north. The following units are distinguished in the region (from the south): Magura Unit, Dukla Unit (and their equivalents), Silesian Unit, Sub-Silesian Unit and Skole Unit. Folded Lower Miocene deposits form Stebnik Unit and Zgłobice Unit situated in the northeastern and northern part of the Polish Carpathians. Lithological sequences of the mentioned above units comprise alternation of sandstone and sandstone-conglomerate usually thick-bedded series, thin-bedded sandstone-shale (heterolithic) series as well as shale (claystone) series (Żytko et al. 1989; Lexa et al. 2000).

The BMs and their Foothills are divided into many ranges, which stand from several tens metres to 800 m above the river valleys separating them (Starkel 1972). Steep slopes of these mountain ranges have been predominantly shaped by gravitational mass movements mainly during the Holocene. The development of gravitational mass movements, among which landslides are very frequent, has been facilitated by geological structures (described above) favourable for the disturbance of slope equilibrium. The gravitational evolution of slopes is prolonged process started from gradual, slow spreading or toppling of massif and finalised with its rapid failure and formation of landslide. The propagation and then widening of rock discontinuities is basic element of the initial, preparation stage of landslide development. The subsequent relatively rapid mass movement can be generated by external factors: fluvial erosion, water overloading of rocks and earthquakes (e.g., Zabuski et al. 1999; Poprawa and Rączkowski 2003; Margielewski 2006).

Apart from rockfall, which is relatively restricted process in the BMs, the following mass movements are typical in these mountains (Dikau et al. 1996; Margielewski 2006):

1. Lateral spreading and rock flow (Sackung/sagging *sensu* Zischinsky 1966), which are usually regarded as initial forms evolving into more advanced ones. They are connected with propagation and widening of cracks, which are often accessible for people, and if roofed, can be recognised as caves.
2. Topple, which does not form a sliding surface and also represents initial phenomenon for development of landslides. This kind of mass movement is linked to the loss of stability of the upper parts of rock massif, detachment and displacement of their fragments.
3. Translational slide – strict landslide, characterised by gravitational movement along flat sliding surface (usually bedding plane, joint surface or fault).
4. Rotational landslide with circular slip surface, developed in homogeneous material, but also typical of deep-seated mass movements developed in anisotropic rocks. In the case of this type of movements influence of natural discontinuities (joints) is reduced due to deep-seated slip surface along which large volume of material is displaced.
5. Compound landslide, understood as form intermediate between translational and rotational types of movements (Dikau et al. 1996).

The caves can be associated with each mentioned above types of mass movements.

State of art as a motivation for the discussion

The caves in the Beskidy Mts. have been mentioned in historical sources for several last centuries, however the first explorations of these caves were reported in 19th and first half of the 20th century (Klassek and Mleczek 2008). In the first modern inventory of caves in Poland 23 caves in the Outer Carpathians were described and mapped. Their non-karst, gravitational origin was stated, but not considered in details (Kowalski 1954). The vigorous exploration of the caves in the Carpathians started in 70-ties of 20th century and has been performed by members of the Speleoclub Bielsko-Biała (SBB) founded in that time as well as members of the Beskidy Caving Club active since the 80-ies of 20th century and Association for the Caves Conservation "Malinka Group" founded at the beginning of the 21st century. It has resulted in discovering and mapping of several tens of caves each year. The work of the cavers was recapitulated in three volumes of the inventory published at the end of the 20th century (Pulina 1997 a, b, 1998), and has been reported during yearly national speleological meetings. According to the last report (Klassek and Mleczek 2012), up to August 2012, 1,246 caves of total length yielding 22,580 m have been recorded in the Beskidy Mts. The longest cave, Jaskinia Wiślańska Cave, is 2,275 m long and 41 m deep; 33 other caves are longer than 100 m. The largest vertical distance between uppermost and lowermost cave parts was measured in the Jaskinia Ostra Cave and yields 60 m, but the deepest cave (measured as the vertical distance between the lowermost part and ground surface directly above) is Diabla Dziura w Bukowcu Cave, 42.5 m deep. 26 caves are deeper than 15 m.

Along with the exploration, morphological-genetic features of the caves have been recognised. The scientific studies of the caves started by J. Janiga and J. Mikuszewski in 1970s, were continued by L. Zawierucha (1986), W Puchejda (1989) and J. Waga (1993) in the 1980s and 1990s (Klassek 2004; Klassek and Mleczek 2008). The work of these authors was recapitulated by Klassek (1989, 1994) as well as Klassek and Mikuszewski (1997), who proposed genetic-morphological categorisation of non-karst caves in Polish Outer Carpathians (BMs). Two general genetic groups of caves occur in the BMs: A. *gravitational caves* and B. *erosional-weathering caves*. Three types of gravitational caves were distinguished by Klassek (1989, English terms after Klassek 1994): A.1. *Landslide caves* – the most common, connected with various elements of landslides and disintegrated (prepared to landslide) slopes; A.2. *Slacking caves* – similar in genesis to the first type, but occurring at the rock outcrops. A.3. *Stone-falling caves* – directly related to rock falls. *Erosional-weathering caves* (type B) have developed on the rock outcrops and usually represent very small cavities.

According to morphological classification proposed by Klassek (1989, 1994; Klassek and Mikuszewski 1997) three general groups of caves occur in the BMs (English terms after Klassek 1994). The first group, *fissured caves*, represents single crevice or systems of crevices, somewhere of maze character. In this group the authors of classification distinguish four types: (a) *grooved-ridged type*, situated in parallel trenches and ramparts within landslide type failures of slopes; (b) *rubbled type*, situated within packet-type landslide colluvia; (c) *cracked caves*, situated upslope of landslide main scarps and (d) *divided caves* occurring in the rock outcrops and connected with initial stages of slope disintegration. The second morphological group is represented by *rock niches* – small forms spatially related to the natural rock forms (crags, cliffs). To the third group belong rare *bedding-type caves*, characterised by horizontal sizes much larger than vertical size (height).

The classification of caves proposed by Klassek (1989, 1994; Klassek and Mikuszewski 1997) is not sufficiently precise. Especially the morphological categorisation is somewhere not clear, combining shape of caves, their spatial situation within the slope (its inner and surface structures) and even genetic features, e.g., in a case of type (d): *divided caves*. But also the genetic categorisation does not determine clear margins between the types of gravitational caves, e.g., *landslide caves* (A.1) and *slacking caves* (A.2). Such impreciseness is at least partly caused by the real complexity of the nature, occurrence of many intermediate forms and phenomena. This supports the tendency to simplify such categorisation. Therefore the Carpathian caves have been also classified applying simpler categorisation, which was introduced by Vítek (1983) in this region. According to this author the gravitationally induced caves can be divided into two types: *crevice type* and *talus type*. Following this author – the *crevice type caves* are the caves "produced by the movements of large blocks … as cracks … widened along tectonic contacts … and clefts (not of tectonic nature), by the breakdown of blocks and rock. In their initial stage the openings are narrow and high …". In turn, the *talus type caves* are "free spaces formed between boulders and rock block debris distributed … in stone fields and piles of boulders" (Vítek 1983). The quoted above description of *crevice type caves* is generally in accordance with common understanding of this term (e.g., Halliday 2004a, 2007) or with the term of *fracture caves* (Kastning 2005), whereas *talus type caves*, named also *boulder caves*, represent widely described type of these objects (Halliday 2004b, 2007, Kastning 2005; Bella and Gaál 2010, 2011). According to these materials, both the terms and types represent rather morphologic than genetic categories, however, especially in the case of *crevice type caves* gravitational context and relation to stage of slope evolution has been emphasized by mentioned authors. In turn, the *talus type caves* are strictly related to their morphological/spatial situation (on the slope), whereas the same objects named *boulder type caves* have been distinguished owing to their shape and relation to boulder agglomerations (the problem was discussed by Bella and Gaál 2010, who prefer the term *boulder caves*).

Materials and methods

The materials used for our analysis are maps and descriptions of caves published in the volumes of cave inventory (Pulina 1997a, b, 1998) and –in a case of recently found caves – papers published in speleological journals for several last years. We analysed in details about 15 caves distributed in various parts of the BMs, particularly in the Beskid Śląski Mts., Beskid Wyspowy Mts., Beskid Sądecki Mts., Beskid Niski Mts and Pogórze Ciężkowickie (Ciężkowice Foothill). The basic method of analysis is, apart from deduction from maps and field observations, mapping

of surface landforms (landslides) spatially related to caves as well as measurements of spatial orientation of the surface and underground elements in order to assessment of nature and stage of slope disintegration (some of such studies have been already published: Margielewski, Urban 2002, 2003a, b, Margielewski et al. 2007, 2008). Recently, also the geophysical method, electrical resistivity tomography (ERT), was used to reconstruct inner slope structures (Pánek et al. 2010; Urban et al. 2011).

Discussion and proposals

Despite the problems described above, the classification applied by Vítek (1983), as simpler than proposed by Klassek (1989, 1994), was used by us in papers discussing the slope structures (failures) and, generally, morphogenesis of the BMs (Margielewski and Urban 2002, 2003a,b, Margielewski 2006). In these papers the *crevice type caves* were interpreted as cracks preceding the landslide formation and preparing a slope to such mass movements, while the *talus type caves* were understood as caves produced within colluvial body of landslide after its formation. However, such interpretation was in some cases misunderstanding due to unclear and combined (morphological and genetic) criteria of discrimination of both these types of caves (see the chapter "State of art …"). For example within the typical landslide body we observed the caves comprising single cracks and fitting the description of *crevice type caves*. Such situations motivated us to discuss the problem of classification and definition of caves and to display our proposals hereafter.

Some approaches to categorisation of non-karst, gravitational caves – or, widely, cracks or irregular voids (if not accessible for man) in the BMs – can be considered. Two the most important for scientific studies are:

- genetic approach, in which the criterion is the relation to the stages of slope evolution,
- geomechanic approach, taking into account phenomena (processes).

Regarding the genetic criterion, two general types of caves can be distinguished: 1. caves preceding formation of typical landslide, which we name *initial caves (cracks)* and 2. caves developed within these structures/landforms named by us *subsequent caves (cracks)* (Figs. 1, 2, 3). Since the predominant stress producing the *initial caves* is tension, these caves are connected with spreading-translation or topple type of movements, however vertical movements and slight rotation are also observed (Fig. 2 C – diagrams show slight toppling). The same types of displacements occur in the case of the *subsequent caves*, but range of topple (tilting) as well as back rotation and rotation around vertical axis (very frequent in the case of translational slide) is usually much higher (Fig. 3 D – diagrams show rotation around vertical axis). Referring to the "classic" Vítek's (1983) classification, *initial cracks* represent exclusively *crevice type caves* (e.g., Fig. 2 B), whereas *subsequent caves* can be both *crevice* and *talus type caves*. Intermediate forms (combining features of both types) are rare caves situated in the zone of landslide main scarp (comprising yielded by tension surfaces). Such cracks are formed before landslide development and they are modified by the main gravitational displacement (slope failure). In this moment their upper parts are transformed to landslide head scarps, while deeper parts are propagated as cracks down the rock massif.

The geomechanic classification (criterion) considers the type of phenomena (processes) causing modification or destruction of slope. In this case two principal phenomena should be accounted: dilation (dilatation) and dilatancy. The dilation is defined as change (of rock massifs) in volume but not in shape. In turn, the dilatancy consists in alteration from

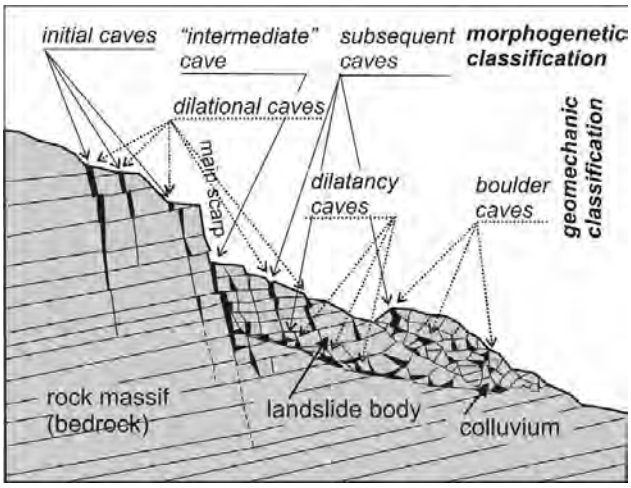

Figure 1. Model illustrating the types of caves (in broader sense: cracks or systems of cracks) in classifications proposed by authors and their situation in the slope.

"close-packed structure" to "open-packed structure", in other words: it generates growth of rocks volume and change in its shape (Dadlez and Jaroszewski 1994). In slope scale the dilation causes propagation and widening of cracks along natural discontinuities (joints, faults) in the initial stage of slope disintegration, as well as during and after the main stage of slope failure (e.g., within landslide body), whereas the dilatancy produces voids within the shear zone (next to slip surface) of landslides during the main stage of slope failure. If such voids are formed along natural discontinuities existing in the massif, the phenomenon is called fissure macrodilatancy (Kwaśniewski 1986). As effects of both types of phenomena two types of caves are distinguished: *dilational caves* and *dilatancy caves* (Figs. 1, 2, 3). The principal feature differing these cave types is their position in relation to shearing zone (slip surface) of landslide: *dilatancy caves* are situated always close to this zone, between stable bedrock and displaced material (Fig. 3 B), whereas *dilation caves* are usually situated in extensional zones close to the surface' It is apparently visible on ERT profiles (e.g., Fig 3 C), where *dilatancy voids* are marked by high and low resistivity bodies distributed close to the sliding surface (A), while the *dilation cracks* are marked by wedge shaped high resistivity anomalies close to the ground surface (B). Although the *initial caves* in morphogenetic classification represent *dilation caves*, the *dilation caves* cannot be automatically identified with *initial caves*, because some of them form in the landside body during the stage of main slope failure. The *dilation caves* are produced principally due to extensional stresses, while shearing strains are initial stresses controlling the development of *dilatancy caves*. However, the size and shape of caves is not decisive feature, the *dilation caves* comprise usually simple widened

cracks, *crevice caves* according to Vítek's (1983) classification, whereas *dilatancy caves*, represent more complex, maze systems of passages – *crevice* or *talus type caves* according to Vítek (1983).

The geomechanic classification includes also the third type of caves, developed within chaotic agglomeration of rock blocks (boulders) within totally disintegrated rock masses of landslide colluvia. Such caves are characterized by irregular structure (framework), not related to original directions of discontinuities in rock massif, (joints, faults etc.) and irregular or rather pyramidal than prismatic shape of chambers. These caves accurately fulfil conditions of *boulder caves*, as they were characterised by Bella and Gaál (2010, 2011), so they can be named *boulder caves*.

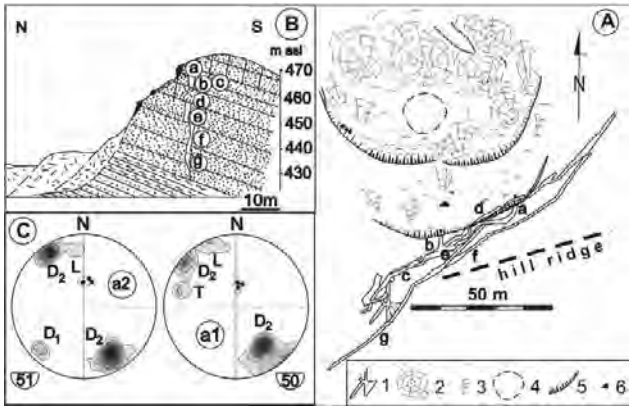

Figure 2. Diabla Dziura w Bukowcu Cave, as an example of initial cave and dilational cave (after Margielewski and Urban 2003b). A – map; B – cross-section (the letters on map and cross-section mark the same parts of cave); C – orientation of joints on contour diagrams and bedding planes on pole point diagrams (equal area plot, projection of normals on the lower hemisphere) in the upslope (a1) and downslope (a2) walls of the upper (a) part of the cave (joint sets: L – longitudinal, T – transversal, D_1 and D_2 – diagonal). Explanations: 1 – cave's outline, 2 – colluvial swells, 3 – colluvial material, 4 – morphological depression, 5 – rocky or soil scarp, 6 – rock form.

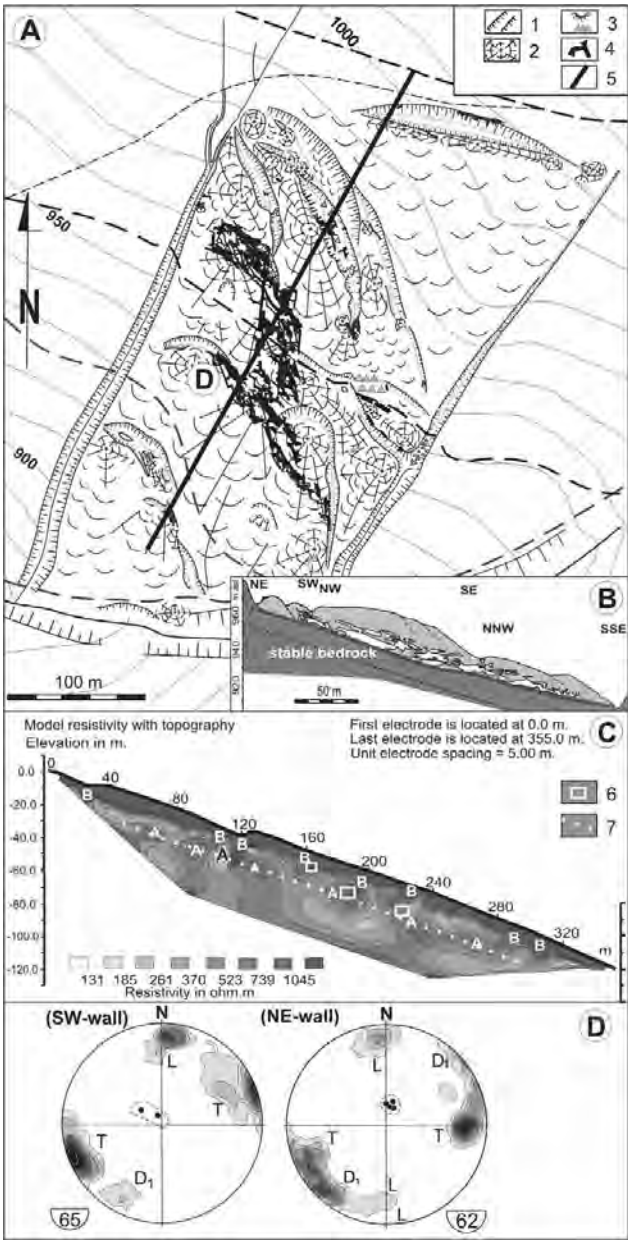

Figure 3. Jaskinia Miecharska Cave (as subsequent and dilatancy cave) and other small caves within the landslide surrounding this cave. A – map (after Margielewski et al. 2007); B – cross-section (after Margielewski et al. 2007); C – ERT profile (after Pánek at al. 2010); D – orientation of joints on contour diagrams and bedding planes on pole point diagrams (equal area plot, projection of normals on the lower hemisphere) in the Sala Grzelaka chamber (letter D in map) in the cave (joint sets: L – longitudinal, T – transversal, D1 and D2 – diagonal) (after Margielewski et al. 2007. Explanations: 1 – rocky or soil scarp, 2 – colluvial swell, 3 – rock forms, 4 – cave's outline, 5 – ERT profile showed in part C, 6 – element of the cave (passage, chamber) crossed by ERT profile, 7 – landslide sliding zone.

Conclusions

Although Polish Outer Carpathians (BMs) are formed of non-karstified rocks, the caves (among which are large ones) are very frequent in this region. Their intensive and efficient exploration has been performed along with the scientific study of these objects. However, classifications of the caves proposed up till now have not been based on clear criteria. The criteria of Klassek's (1989, 1994; Klassek and Mikuszewski 1997) classification combine shape of caves, their spatial situation within the slope and even genetic features. Also classification proposed by Vítek (1983) does not allow unequivocal categorisation of caves and determination of their genetical features. Clearly defined criteria are the crucial problem of proper classification.

Therefore two classifications: genetic and geomechanic, are proposed. The criterion of genetic classification is relation of caves to slope development. It allows to distinguish two main types of caves: *initial caves* and *subsequent caves*, however intermediate forms are also observed. Formation of the *initial caves* precedes main slope failure, whereas the *subsequent caves* develop within the landslide body, during the main mass movements (landslide formation). According to the second, geomechanic classification, considering the type of phenomenon-process producing the caves, three types of caves can be discriminated: *dilation caves*, *dilatancy caves* and strict *boulder caves*. The *dilation caves* are connected with the change in volume (but not in shape) of rock massif, usually with extensional dissection of rocks, whereas *dilatancy caves* are produced by change in shape and growth of volume of rock massif and they are related to the formation of shearing zone during the main mass movements. *Boulder caves* comprise irregular voids within

the chaotic agglomeration of boulders in landslide colluvia.

These two classifications could help in scientific description of caves connected with gravitational mass movements, because application of them (i.e. identification of cave according to their criteria) makes possible clear determination of geomorphologic situation of cave and its genesis.

This study was conducted within a scientific project No. NN306 522 738 granted by Polish Ministry of Sciences in 2010–2013, and statutory works of the Institute of Nature Conservation PAS.

References

Bella P, Gaál L, 2010. Boulder caves – terminology and genetic types (English abstract). Aragonit 15(1), 3–10.

Bella P, Gaál L, 2011. Terminology and genetic types of boulder caves. Pseudokarst Commission Newsletter 22, 1–5 (English and German versions). http://wwwpub.zih.tu-dresden.de/~simmert/pkarst/08 _newsletter/newsletter_022.pdf

Dadlez R, Jaroszewski W, 1994. Tektonika. Wyd. PWN, Warszawa (in Polish).

Dikau R, Brunsden D, Schrott L, Ibsen ML, (Eds.) 1996. Landslide recognition. Identification, Movement and Causes. Willey, Chichester.

Halliday WR, 2004a. Crevice caves. In: J Gunn (Ed.), Encyclopedia of caves and karst science. Fitzroy Dearborn, New York, London, 510–518.

Halliday WR, 2004b. Talus caves. In: J Gunn (Ed.), Encyclopedia of caves and karst science. Fitzroy Dearborn, New York, London, 1544–1550.

Halliday WR, 2007. Pseudokarst in 21st century. Journal of Cave and Karst Studies, 69(1), 103–113.

Kastning EH, 2005. Very small and eclectic caves: conservation and management issues. National Cave and Karst Management Symposium. Albany, New York, 92–101.

Klassek G, 1989. Study of caves in Beskidy Mts. and Carpathian Foothills in Poland. In: 2. Sympozium o Pseudokrasu. Sborník referatů ze sympozia. Janovičky u Broumova, 1985. Czech Speleological Society, vol. 10. Praha, 44–48 (in Czech, German summary).

Klassek G, 1994. Pseudokarst caves in Polish Karpaty Mts. In: 5th Pseudokatrst Sympozium with International Participation, Szczyrk 1994. Proceedings. Bielsko-Biała, 5–9 (in Polish, English summary).

Klassek G, 2004. Caves of the Polish Flysch Carpathians. In: L Gaál (Ed.), Proceedings of the 8th Intern. Symp. on Pseudokarst. Teply Vrch, Slovakia, 2004. Slovak Cave Administration, Liptovský Mikuláš, 69–74.

Klassek G, Mikuszewski J, 1997. Przyrodnicza charakterystyka jaskiń, warunków ich występowania i rozwoju w obszarze polskich Karpat fliszowych. In: M Pulina (Ed.), Jaskinie polskich Karpat fliszowych, v. 1. Pol. Tow. Przyjaciół Nauk o Ziemi, Warszawa, 7–18 (in Polish).

Klassek G, Mleczek T, 2008. Exploration of caves in the Polish Outer Carpathians in the past and nowadays. Zacisk – special issue (9th Intern. Symp. on Pseudokarst). Bull. of the Speleoclub Bielsko-Biała, Bielsko-Biała, 4–6.

Klassek G, Mleczek T, 2012. Eksploracja i inwentaryzacja jaskiń polskich Karpat Fliszowych (sierpień 2011 r. – sierpień 2012 r.). In: J Szulc, W Wróblewski W (Eds.), Materiały 46. Sympozjum Speleologicznego, Góra Św. Anny, 19–21.10.2012. Sekcja Speleologiczna PTP im. Kopernika. Kraków, 42–45 (in Polish).

Kowalski K, 1954. Jaskinie Beskidów i Pogórza Karpackiego. In: Kowalski K. Jaskinie Polski, vol. 3. Narodowe Muz. Archeologiczne, Warszawa, 25–67 (in Polish).

Kwaśniewski M, 1986. Dylatancja jako zwiastun zniszczenia skały. Przegląd Górniczy 42(2), 42–49 and 42(6), 184–190 (in Polish).

Lexa J, Bezák V, Elečko M, Mello J, Polák M, Potfaj M, Vozár J, (Eds.) 2000. Geological map of Western Carpathians and adjacent areas 1:500,000. Geol. Survey of Slovak Republic, Bratislava.

Margielewski W, 2006. Structural control and types of movements of rock mass in anisotropic rocks: case studies in the Polish Flysch Carpathians. Geomorphology 77, 47–68.

Margielewski W, Urban J, 2002. Initiation of mass movement in the Polish Flysch Carpathians studied in the selected crevice type caves. In: J Rybář, J Stemberk, P Wagner (Eds.), Landslides. AA Balkema Publ, Lisse-Abingdon-Exton-Tokyo, 405–409.

Margielewski W, Urban J, 2003a. Crevice-type caves as initial forms of rock landslide development in the Flysch Carpathians. Geomorphology 54, 325–338.

Margielewski W, Urban J, 2003b. Direction and nature of joints controlling development of deep seated mass movements: a case study of Diabla Dziura cave (Polish flysch Carpathians). Geomorphologia Slovaca 3, 58–59.

Margielewski W, Urban J, Szura C, 2007. Jaskinia Miecharska cave (Beskid Śląski Mts., Polish Outer Carpathians): case study of a crevice-type cave developed on a sliding surface. Nature Conservation 63, 57–68.

Margielewski W, Szura C, Urban J, 2008. Jaskinia Miecharska cave (Beskid Śląski Mts., Polish Outer Carpathians), the largest non-karst cave in the flysch Carpathians. Zacisk – special issue (9th Intern. Symp. on Pseudokarst). Bull. of the Speleoclub Bielsko-Biała, Bielsko-Biała, 7–13.

Pánek T, Margielewski W, Tábořík P, Urban J, Hradecký J, Szura C, 2010. Gravitationally induced caves and other discontinuities detected by 2D electrical resistivity tomography: Case studies from the Polish Flysch Carpathians. Geomorphology 123, 165–180.

Poprawa D, Rączkowski W, 2003. Carpathian landslide (southern Poland). Przegląd Geologiczny, 51(8), 685–692 (in Polish, English abstract).

Puchejda W, 1989. Genesis of the cave in Trzy Kopce in the Silesian Beskidy Mts. Kras i Speleologia 6(XV): 66–78 (in Polish, English abstract).

Pulina M, 1997a. Jaskinie polskich Karpat fliszowych, v. 1. Pol. Tow. Przyjaciół Nauk o Ziemi, Warszawa (in Polish).

Pulina M, 1997b. Jaskinie polskich Karpat fliszowych, v. 2. Pol. Tow. Przyjaciół Nauk o Ziemi, Warszawa (in Polish).

Pulina M, 1998. Jaskinie polskich Karpat fliszowych, v. 3. Pol. Tow. Przyjaciół Nauk o Ziemi, Warszawa (in Polish).

Starkel L. 1972. An outline of the relief of the Polish Carpathians and its importance for human management. Problemy Zagospodarowania Ziem Górskich 10, 75–150 (in Polish, English abstract).

Urban J, Panek T, Taborik P, Hradecky J, Margielewski W, Szura C, 2011. Caves in the Flysch Carpathians detected by ERT method. In: J Simmert (Ed.), Proceedings of the 11th Intern. Symp. Pseudokarst. 12–16 May, Saupsdorf – Saxon Switzerland, Germany. Dresden: 132–143.

Vítek J, 1983. Classification of pseudokarst forms in Czechoslovakia. Intern. Journal of Speleology 13, 1–18.

Waga JM, 1993. Genesis of the Komoniecki Cave in the Beskid Mały. Kras i Speleologia 7(XVI): 94–101 (in Polish, English abstract).

Zabuski L, Thiel K, Bober L, 1999. Landslides in the Polish Carpathians Flysch. Geology, modelling, stability calculations. Publ.: IBW PAN, Gdańsk (in Polish, English abstract).

Zawierucha L, 1986. Zarys typologii jaskiń pseudokrasowych Beskidów i Pogórza Karpackiego. In: Inwentarz jaskiń beskidzkich p. V. PTTK, Speleoklub Bielsko-Biała, 16–18 (in Polish).

Zischinsky U, 1966. On the deformation on high slopes. Sitzber, 1 Kongr. Int. Ges. Felsmechanic, 2. Lissboa, 179–185.

Żytko K, Zając R, Gucik S, Ryłko W, Oszczypko N, Garlicka I, Nemčok J, Eliáš M, Menčík E, Stráník Z, 1989. Map of the tectonic elements of the Western Outer Carpathians and their foreland. PIG Warszawa; GUDS Bratislava; UUG Praha.

CAVES IN SANDSTONE DEPOSITS OF THE SOUTHERN ITALIAN APENNINES

Gianni Campanella[1], Mario Parise[2], Angela Rizzi[3], Mariangela Sammarco[4], Antonio Trocino[3]
[1]Gruppo Puglia Grotte, Castellana-Grotte, Italy
[2]CNR, Istituto di Ricerca per la Protezione Idrogeologica, Bari, Italy, m.parise@ba.irpi.cnr.it
[3]Associazione Explora, explora_ndo@hotmail.it
[4]University of Salento, Lecce, Italy

The article describes the main results of cave explorations and field surveys carried out in the territory of Gorgoglione (Basilicata region, southern Italy) and surrounding areas. Due to lithology of outcropping rocks (mainly sandstones belonging to the Gorgoglione Flysch, a turbidite formation of Miocene age), the area is affected by pseudokarst phenomena. Beside several sites showing interesting pseudokarst features, and erosional landforms in the rock mass, five caves have been identified and surveyed near the town and in the valley of the Gorgoglione Fiumara, a left tributary of the Sauro Torrent. The caves can be distinguished based upon their typology in intrastratal caves, gravity-related caves, swallow holes, and caves in vertical rock walls. The variety in the cave typology is an element testifying the need to stimulate further knowledge of this territory, that likely presents others, still undiscovered, caves. Moreover, during the surveys it was possible to appreciate the high relevance of the landscape, which is well integrated to the archaeological and historical characters of the study area.

1. Introduction

In southern Italy, the region Basilicata is probably the area less considered by cavers. The region is, as a matter of fact, surrounded by Campania, Apulia and Calabria, that host, respectively, the most important karst massif of southern Italy (Alburni Mountains; see Del Vecchio et al. 2013), hundreds of caves and karst landforms due to the widespread presence of carbonate rocks in Apulia, and the deepest karst systems in this part of Italy (the Bifurto Abyss in northern Calabria, reaching about 700 m of depth). Notwithstanding the lesser attention by cavers, Basilicata hosts significant karst caves in carbonate rocks: the Vucculi cave, in the territory of Muro Lucano (Parise et al. 2010), and the Castel di Prete system at Marsico Vetere (Bentivoglio and Leoncavallo 1973; Pascali et al. 1996) being the most representatives.

This article illustrates the main pseudokarst features of the territory of Gorgoglione and surrounding areas (Fig. 1), also describing the morphological and caving landforms within the historical and archaeological setting of the area.

Figure 1. Location of the study area.

2. Karst, parakarst, and pseudokarst

In this section we would like to briefly summarize the use of the terms to describe caves in rocks other than limestones, with specific regard to the contribution provided by Italian scientists. The terminology used to describe surface and subsurface features similar to those created by karst processes in classical carbonates and evaporites settings, as a matter of fact, has often been a source of confusion and misunderstandings in the past. In Italy, in 1933, on the occasion of the 1st National Congress of Speleology, Gortani pointed out to the different intensity of karst development, as a function of the solubility of involved rocks, and made a distinction between karstic rocks (that is, those showing high solubility when attacked by meteoric waters) and semi-karstic rocks (Gortani 1933). Such a distinction was not a theoretical one but had definitely a validation when comparing areas with different karst landforms, as regards both intensity and frequency of the produced features.

Some decades later, Franco Anelli particularly felt the need to put order in the chaotic terminology on the matter, by distinguishing karst, parakarst, and pseudokarst phenomena (Anelli 1963, 1964). According to Anelli, karst phenomena consist of the solution of soluble rocks such as carbonates and evaporites. Parakarst, on the other hand, deals with somewhat attenuated processes involving coarse limestones, sandstones with calcareous or siliceous cement, or dolostones showing less solubility. In all these cases, the deriving landforms are less clear and evident than those produced by karst; in particular, the subsurface landforms are very limited in length and depth, due "to the short duration of the evolutive cycle, which generally interests rocks of young age" (Anelli 1963, p. 17). Thus, parakarst phenomena included

subterranean caves produced by subrosion, evolving upward due to regressive erosion, as described by Franc (1953) and by Renault (1953). At the same time, Anelli considered as parakarst landforms also those described by Cvijic (1893) as elements of an imperfect karst (merokarst) as opposed to the complete karst (olokarst).

Again according to Anelli (1963), pseudokarst, eventually, consisted in those processes involving insoluble or low-solubility rocks, derived by the combined action of physical and chemical weathering, with the exclusion of the solution by meteoric waters. Thus, the produced landforms show analogies with the corresponding karst morphologies but are originated as the result of different processes, namely mechanical erosion or frost action. They involve, among the others, clays and crystalline rocks, where tafoni-like morphologies are, for instance, quite common in the Sardinia-Corse massif. Anelli also included in the pseudokarst landforms those acting on volcanic rocks.

However, this attempt in defining different terms by Anelli did not have a great success, both in Italy and at the international level, where the Author presented it during the 3rd International Congress of Speleology, held in Vienna (Anelli 1964). On the other hand, the term pseudokarst began to be used to indicate any morphology, similar to those karstic, involving insoluble or low-solubility rocks (Parker and Higgins 1990). The term pseudokarst, initially attributed to Halliday (1960), who in turn took it from a work by Floridia (1941) on the Sicilian clays, is now ascribed to von Knebel (1906), as reported by Bates and Jackson (1987).

Figure 2. Examples of features produced by pseudokarst processes in deposits of the Gorgoglione Flysch.

2. Geological setting

The study area is characterized by outcrops of rocks belonging to the Gorgoglione Flysch, a turbidite formation of Middle-Lower Miocene age (Boenzi and Ciaranfi 1970; Carbone et al. 1991). From the lithological standpoint, the Gorgoglione Flysch consists of alternating sandstones and marl clays. The sandstones (feldspar and arkose arenites) are gray to yellow on the weathered surfaces, whilst they appear iron gray when unweathered. They are well cemented, and layered in strata with thickness ranging from a few centimeters to some meters. Locally, thicker layers of coarse, less cemented, sandstones and conglomerates in abundant sandy matrix are present. As an effect of the erosional processes, the more resistant layers appear to protrude outward, to create typical features in the rock mass (Fig. 2). As concerns the clays, these are gray in colour, with high marl component, and show thickness of at least some meters.

The Gorgoglione Flysch crops out along the strip extending from the towns of Gorgoglione and Cirigliano toward the SE, in direction of the junction between the Gorgoglione Fiumara and the Sauro Torrent. It is overlain by younger deposits only near the river junction.

Morphologically, the landscape is medium to high hills, with development of deep incisions controlled by tectonics, often with sharp angles the main river courses. The towns are located at the top of the hills (Pedio 1990), in clear situations of topographic control on the surrounding territories, including the main water lines. For instance, Gorgoglione is located on a small ridge (Fig. 3), protected by steep walls on three sides; Cirigliano, on the other hand, stands along a narrow, N-S elongated, ridge between the Fiumara di Gorgoglione and the Fiumara di Fossarolo.

Figure 3. The town of Gorgoglione, located on a ridge bounded by steep slopes.

The presence, within the Gorgoglione Flysch, of different types of rocks, showing variable mechanical characters, and the structural setting characterized by frequent discontinuities within the rock mass, makes this formation highly prone to slope instabilities (Guerricchio and Melidoro 1988). This is especially true as regards the mostly clay facies, severely affected by slope movements of the flow type (Fig. 4), that can be easily observed for long stretches of the State Road leading to Gorgoglione.

The sub-vertical rock faces are, on the other hand, typically characterized by rock falls and, when less steep and in

conditions of favorable bedding, by development of translational slides, which generally start at the passage between a sandstone layer and the underlying clays.

Figure 4. The head scarp of an earthflow in the clay deposits.

3. Archaeology

The main archaeological elements, identified during the surveys, are located at locality Cinto dell'Eremita, and at the margins of the nearby ridge, in locality Scorciabuoi.

Cinto dell'Eremita (Fig. 5) is an isolated and elongated ridge, rising over 30 meters above the surrounding territory. It is located at the junction of three rivers: namely, the Fiumara di Gorgoglione, which is the most important river, coming from the NW; the Fosso dell'Eremita, from the NE; and the Vallone della Foresta, from the N. The vertical walls make the site particularly difficult to be reached, at the same time representing the most significant defensive system; therefore, the site is an important strategic site of control. The morphology itself is clearly indicative of a fortified settlement.

Figure 5. The ridge of Cinto dell'Eremita, seen from NW.

Archaeological researches, carried out at the surface since the year 2004, allowed to reconstruct a complex stratigraphy at the site, dating back to the end of the 5th century B.C. for the most ancient evidence, and lasting until the early Middle Age (De Siena et al. 2006). Among the most important identified elements, it is worth to be mentioned a likely fortified settlement (10th – middle of 11th century), and the Middle Age *castrum*, testifying a further occupation of the site during the 13th–14th century, with erection of a high walls around the settlement.

At the Cinto dell'Eremita, remnants of a significant stone wall, developing at middle slope around the ridge, have been found: the wall is in good state of conservation for long stretches, and is formed by two curtains of local rocks and by a filling of small stone particles. It is in particular well visible at the north-eastern side of the ridge, where it still maintains an height of about 2 meters. Further evidence is located within the area delimited by the walls: a cistern, and other alignments of walls with different directions.

A further area of archaeological interest is located just in front of Cinto dell'Eremita, in locality Scorciabuoi, where the preliminary field surveys carried out for this study has proved the presence of another settlement dating back to the Bronze Age, and possibly occupied with continuity during the Middle Age.

No archaeological remain has been found in the caves described in the following section. However, this should be checked through specific surveys and excavations (not carried out during this study), since the two most significant sites above described are located in the proximity of, respectively, Cinto dell'Eremita Cave and the swallow hole near Masseria Scorciabuoi.

Eventually, bibliographical research, combined with other ancient topography analyses, will allow in the near future to add further elements of knowledge to the history of this area, where several evidence and remnants of high interest seem to be present.

4. Results of cave explorations

As mentioned before, five caves showing variable typologies and origin have been identified in the territory of Gorgoglione. Typology of caves includes: intrastratal caves, with a mostly sub-horizontal pattern, typically developing along the contact between different lithologies; gravity-related caves, originated by detachments of the outer portions of vertical rock cliffs; swallow holes; caves in vertical rock walls, often developing along the fractures of tensional release, bounding the cliffs.

In the following, a brief description of the main explored caves is presented, along with considerations about their origin, evolution, and state of conservation.

4.1. Grotta dei Briganti (Bandits Cave)

The cave is located at the foothills of a 40 m high rock cliff, just below the town of Gorgoglione. It is an intrastratal cave, developed at the contact between the sandstones and the underlying clays, on the left side of Fosso Vallone, a tributary of the Fiumara di Gorgoglione. Along the main direction of development of the cavity, 36 m long, a narrow trench in the deposit was excavated in 1999, to allow access to the inner part of the cave, that showed a maximum height of 2 meters (Campanella et al. 2001). In the inner portion of the cavity, water dripped from the vaults, feeding the growth of stalactites and calcite flowstones and curtains.

The name of the cave takes its origin from the likely use of the site as a refugee for bandits. The toponym is quite common in southern Italy, an area that has historically

experienced several vicissitudes of bandits for a long time before and after the birth of the Kingdom of Italy.

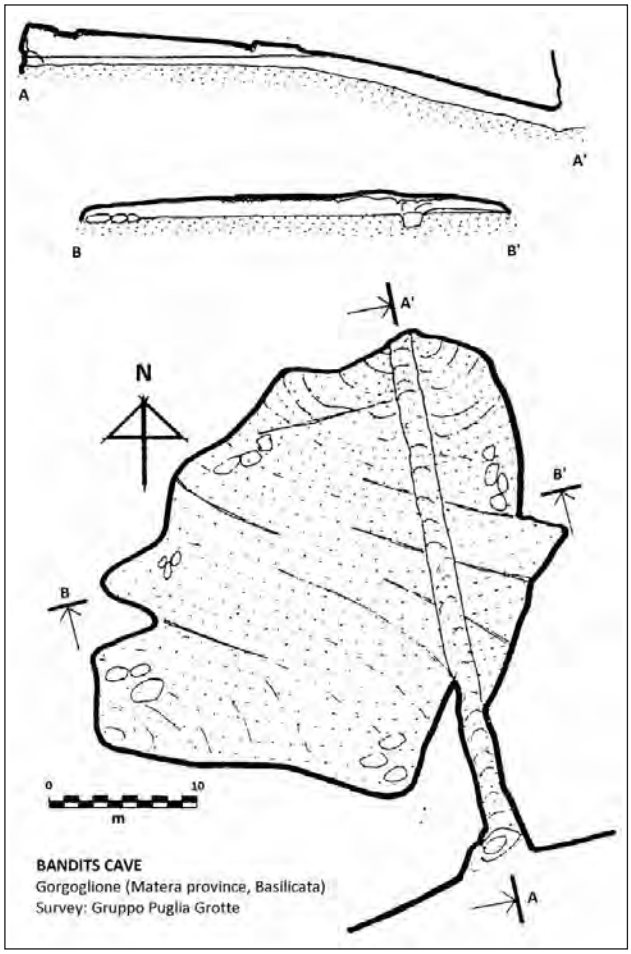

Figure 6. The Bandits Cave.

It can be in fact found at several other sites in Calabria and Basilicata (see, for instance, Parise et al. 2010), as a testimony of the events that were lived soon after the Unification of Italy, when the caves were frequently used as a safe dwelling and hiding place.

In the case of the Bandits Cave at Gorgoglione, location of the site in the proximity of the boundary between the territories of Matera and Potenza, along the watershed of two important catchment basins, makes it a place of peculiar importance for strategical reasons. This same territory was, for instance, the theatre of some of the most bloody fights among the mobs of the bandit Carmine Crocco and the troops of the Kingdom of Italy.

According to a popular tradition, the cave is also thought to be linked through a long tunnel to the subterranea of the Castle of Gorgoglione, originally located at the uppermost part of town. Giving belief to this tradition, some excavation works were carried out by the Municipality of Gorgoglione, in order to look for the hidden passage within the cave, and large amounts of clays were therefore extracted. The cavity so obtained has very few natural elements nowadays, whilst the excavations resulted in no passage being identified.

4.2. Cinto dell'Eremita Cave

The Cinto dell'Eremita cave is located on the NE-facing slope of the Cinto dell'Eremita ridge, along the path leading to the top of the ridge. The origin of the cave has to be looked for in a combination of tectonic and gravitational elements: it is, as a matter of fact, linked to the progressive detachment of the outer portions of rocks, as an effect of the tensional release joints that formed parallel to the rock cliffs. Access to the cave is a triangle-shaped opening, about 1.5 m wide in its lower part, and narrowing upward. It is reached climbing the rock cliff, after passing some stairs hewn in the rock. The cave has an overall length of some 20 m, and is about 16 m deep.

Figure 7. A view from the base of the ridge to the lower entrance of Cinto dell'Eremita Cave.

The lowest part of the cave has a very narrow, and not practicable, passage (Fig. 7), through which the light passes through, to show the foothills of the cliff. In this area, several rock fall deposits are present, with size ranging from small stones to blocks 3.5 m high.

4.3. Swallow hole near Masseria Scorciabuoi

A small swallow hole has been identified in the vicinity of Masseria Scorciabuoi, along the slopes facing the Fiumara di Gorgoglione, in an area showing tectonic lineations of regional importance (Bonini and Sani 2000; Casciello et al. 2000, 2002).

The access, elongated in W-E direction, is at the base of a tree, which roots partly develop at the cave entrance. A 1.5 m drop brings to a small terrace, from where the underlying shaft, 7–8 m deep, is visible (Fig. 8). Following the eastern wall, the first part is about vertical, whilst the lower part is a steep descent over fallen blocks. The whole cave is in fact filled with rock fall deposits, together with stone materials dumped into the cavity from the outside (Fig. 9). Presence of this material makes quite difficult any movement within

the cave, with the danger of further falls of the deposits therein. The western wall is vertical, and shows at the outcrop the sandstone succession, consisting of layers and strata of sandstone, with thickness ranging from 1 m to a few cm. The rock mass is highly fractured, in precarious equilibrium state, and there is high possibility of further detachments of blocks of rock.

Figure 8. Access to the main shaft of the swallow holes at Masseria Scorciabuoi.

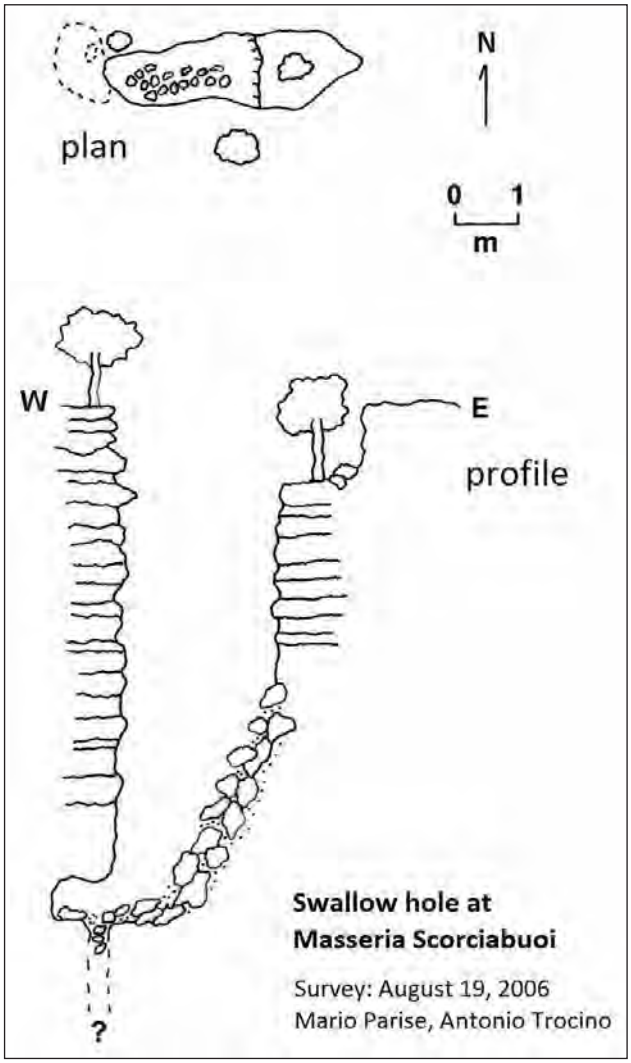

Figure 9. Swallow hole at Masseria Scorciabuoi.

At the base of the shaft, a small room is present on the western side: the limited height (0.7 m) does not allow to stand there. Remains of bones have been found in the room (likely, goat bones), mixed with stones of variable size. At the northern end of the room, another shaft is present, almost entirely filled with debris material. Since a strong air current is coming from this side, an attempt in removing some material was carried out, to check the likely continuation of the cave. However, the difficulty in working in the narrow space, together with the arrival of debris from the main shaft, and the danger of further falls, let to decide to stop the attempt for safety reasons. The final shaft was estimated to be at least 2 meters deep, and some tens of centimeters wide.

4.4. Other caves

Two other caves have been identified and explored during the descent on rope of the over 90 m high rock cliffs on the right-hand side of the Fiumara di Gorgoglione. As in the previously described case of the Cinto dell'Eremita cave, the outer portions of the rock cliffs are affected by several open joints, originated due to the tensional release affecting the cliff. In some cases the opening is wide enough to allow entrance by man. The main feature of these caves is represented by instability of the walls, and the abundant presence of debris. Maximum length observed is on the order of some 10 meters.

5. Conclusions

The field surveys and cave explorations carried out in the territory of Gorgoglione and surrounding areas resulted in appreciating the high potential of this sector of Basilicata, as concerns pseudokarst and speleology, and their link with historical and archaeological sites as well. The different typology of the identified and explored caves represents without any doubt a valuable element to be further examined in the next future. At the same time, it is expected that more detailed and continuous researches may bring to further discoveries of caves, which, even though not reaching high values in terms of depth and development, are very peculiar, due to nature of the outcropping materials.

In particular, the deep and wild valleys, masked by dense vegetation, that bound the main towns in the area, or develop at the sides of the Fiumara di Gorgoglione, should be object of field explorations, since they potentially host several other caves as those described in this article.

A negative element in the area is represented, as unfortunately quite often happens in southern Italy, by the lack of interest and the scarce awareness of the importance of the natural landscape by the local administrators. It is very common to register situations of degradation of the natural environment, that is generally not considered a valuable aspect to safeguard, but rather an obstacle to the development

Figure 10. View of the rock cliffs at the sides of Fiumara di Gorgoglione.

of urban areas. The works realized at the Bandits Cave are quite significant in this sense: they have been carried out without taking into any account the natural condition of the cave, only in the hope to find a passage to reach the inhabited area above, in search of a sort of "hidden treasure". Once again, this was an occasion lost, since the cave, if preserved in its natural state, and due to the vicinity to the urban area, could have been the main goal of a dedicated pathway where to illustrate the many natural and historical features of the area, addressed toward a sustainable tourism, which in our opinion represents the only way to contribute to develop this mountain sectors of inner Basilicata. The natural features and landforms shoud be, at this aim, opportunately combined with the other important elements of the area, as the historical and cultural ones, and linked to the local gastronomy.

References

Anelli F, 1963. Fenomeni carsici, paracarsici e pseudocarsici. Giornale di Geologia, 31, 11–25.

Anelli F, 1964. Fenomeni paracarsici nei calcari grossolani terziari e quaternari delle Murge e del Salento in Puglia. Proc. III Int. Congr. Speleology, Wien, 2, 199–206.

Bates RL, Jackson JA, 1987. Glossary of geology. American Geological Institute, 3rd ed.

Bentivoglio A, Leoncavallo G, 1973 La Grotta di Castel di Lepre – Marsico Nuovo (Potenza). Rass. Speleol. It., 1–4, 136–139.

Boenzi F, Ciaranfi N, 1970 Stratigrafia di dettaglio del "Flysch di Gorgoglione". Mem. Soc. Geol. It., 9, 65–79.

Bonini M, Sani F, 2000. Thrusting, strike-slip faulting and syntectonic deposition in the Potenza-Guardia Perticara area (Basilicata, Southern Apennines, Italy). Mem. Soc. Geol. It., 55, 123–132.

Campanella G, Pace P, Parise M, 2001. La Grotta dei Briganti a Gorgoglione (MT). Puglia Grotte, Castellana-Grotte, Speleoflash, 139–141.

Carbone S, Catalano S, Lazzari S, Lentini F, Monaco wC, 1991. Presentazione della carta geologica del bacino del fiume Agri (Basilicata). Mem. Soc. Geol. It., 47, 129–143.

Casciello E, Pappone G, Zuppetta A, 2002. Structural features of a shear-zone developed in an argillaceous medium: the southern portion of the Scorciabuoi fault (Southern Apennines). Boll. Soc. Geol. It., vol. spec. 1, 659–667.

Casciello E, Cesarano M, Ferranti L, Oldow JS, Pappone G, 2000. Pleistocene non-coaxial fold development in the northern portion of the S. Arcangelo basin (Southern Apennines). Mem. Soc. Geol. It., 55, 133–140.

Cvijic J, 1893. Dar karstphänomen. Geogr. Abh. Von A. Penck, 5, 215–319.

Del Vecchio U, Lo Mastro F., Maurano F, Parise M, Santo A, 2013. The Alburni Massif, the most important karst area of Southern Italy: history of caving explorations, and recent developments. Proceedings 16th International Congress of Speleology, this volume.

De Siena A, De Venuto G, Giannichedda E, Lapadula E, 2006. L'insediamento dell'Eremita (Stigliano, MT) tra Tardoantico e Medioevo. Dati preliminari. Archeologia Medievale, 33, 343–358.

Floridia GB, 1941. Un particolare fenomeno pseudocarsico manifestato da alcune argille. Boll. Soc. Nat. Econ. Palermo, 23.

Franc C, 1953. Sur la formation des gouffres de bas en haut. Atti I Congr. Int. Speleol., Paris, 2, 33–34.

Gortani M, 1933. Per lo studio idrologico e morfologico delle regioni carsiche e semicarsiche italiane. Proc. I Congr. Naz. Speleol., Trieste, 109–115.

Guerricchio A, Melidoro G, 1988. Franosità nei territori comunali di Gorgoglione e Cirigliano (Basilicata). Proc. Conv. "Cartografia e monitoraggio dei movimenti franosi", Bologna, 10–11 november 1988, CNR-GNDCI, 65–85.

Halliday WR, 1960. Pseudokarst in the United States. Natl. Spel. Soc. Bull., 22 (2), 109–113.

Parker GG, Higgins CG, 1990. Piping and pseudokarst in drylands. In CG Higgins & DR Coates (Eds.). Groundwater geomorphology: the role of subsurface water in Earth-surface processes and landforms. Geol. Soc. Am. spec. paper 252, 77–110.

Parise M, Ferrara G, Fuccio M, Gentile CG, Grassi D, Sannicola G, Trocino A, Torres Mirabal LD, Valdes Suarez MV, 2010. "Marmo Platano 2007", la prima spedizione speleologica italo-cubana in Italia. Proceedings 12th Regional Meeting of Speleology "Spelaion 07", Altamura, 7 – 9 December 2007, 231–240.

Pascali E, Lo Mastro F, Inguscio S, 1996 La Grotta di Castel di Lepre. Speleologia, 35, 25–32.

Pedio T, 1990. Centri scomparsi della Basilicata. Venosa.

Renault P, 1953. Caractères generaux des grottes gréseuses du Sahara meridional. Proc. I Congr. Int. Speleol., Paris, 2, 275.

von Knebel W, 1906. Höhlekunde mit berucksichtigung der karst phänomene. Braunschweig, F. Vieweg und Sohn.

KARST DEVELOPED IN SILICICLASTIC ROCKS AT SERRA DO ESPINHAÇO MERIDIONAL, MINAS GERAIS (BRAZIL)

Alessandra Mendes Carvalho Vasconcelos[1,2], Fernanda Cristina Rodrigues de Souza[2], Joel Rodet[1], Cristiane Valéria de Oliveira[2], André Augusto Rodrigues Salgado[2]

[1]Université de Rouen, Laboratory of Geology, Place Emile Blondel, 76821Mont Saint Aignan, France; work in co-supervision with Universidade Federal de Minas Gerais, CAPES granted, alessandravascon@gmail.com, joel.rodet@univ-rouen.fr

[2]Universidade Federal de Minas Gerais, Geography Department, Av. Antônio Carlos, 6627, Belo Horizonte, MG, Brazil, souzageografia@yahoo.com.br, crisval@yahoo.com.br, geosalgado@yahoo.com.br

This study aims to develop a karst synthesis development in siliciclastic rocks and its spatial distribution at Serra do Espinhaço Meridional (SdEM – Southern Espinhaço Ridge), Minas Gerais (MG), from synthetic survey and mapping of the main areas with presence of more common caves and karst morphologies. The methodological procedure consists in a literature review, consulting to the database of Centro Nacional de Pesquisa e Conservação de Cavernas – CECAV (National Center for Research and Conservation of Caves), tabulating the data already surveyed and their respective coordinates, fieldwork and karst prospection. Later, the data were organized for graphing and location maps of the main features and discussion of the results. It is highlighted that most of the features studied in SdEM correspond to caves (88%). The location of the features mapped is inserted, primarily, in the eastern and western edges of SdEM and in the central area of this geomorphological unit. Therefore, it appears that although the entire ridge studied has a potential for development of landforms, the carried studies has a horizontal, conceptual, descriptive, and focused on speleology, nature. In the field, were identified features as pits, shelters, sinkholes, kamenitzas, lapiaz, bee nests, among others, whose morphology is equivalent to those identified in carbonate rocks. It is intended, in this way, to encourage scientific studies development on the other karst features and verticalise issues related to geochronology, morphometry and geochemistry factors of karst formation in this area and siliciclastic rocks.

1. Introduction

The term karst has been used historically to refer to reliefs developed in soluble rocks, primarily of carbonates such as limestone and dolomite, with the main parameter is the lithology. The first studies on karst consider it as an area constituted solely by carbonate rocks, with characteristic shapes, both surface and groundwater. From science evolution, other equally soluble rocks, such as gypsum, came to be regarded in the process of karstification, being capable of developing typical morphological features, as caves, dry valleys, sinks, and others emerged from the dissolution.

As the study progressed, other lithologies have began to be considered for karst formation, relating to its formation particular rocks, soluble, like evaporite, carbonate rocks and quartzite, however this one associated to extremely humid tropical regions. White (1988) relates karst to carbonate, gypsum and other non-specific rocks and describes it as a landscape formed by closed depressions of different sizes, drainage interrupted surface systems, caves and underground drainage formed by dissolving process.

Studies, like Willems (2002) in Equatorial Africa, consider that any rock can produce karst, some more likely to suffer dissolution than others. Some research dismiss (Fénelon 1965, Jennings 1985) the influence of rock and concentrate on the landscape morphological characteristics, considering karst as considering karst as any other area with typical morphological features, independent or from lithology.

Currently, besides lithology and dissolution, other constraints are also being considered in the process of karst formation, such as hydrology, given the importance of water in weathering processes, in the breakdown and in the transportion through the ducts (Ford and Williams 2007). The structural constraints, as cracks and breaks, also play an important role, since they can guide the ducts formation and are among other elements, the gateway to the subsurface water and the karst development. The acidulated water penetrates these cracks by reacting with minerals, regardless of the type of rock, and may produce karstification. If the constraints, tectonic, lithologic, climatic and vegetation are favorable, the greater the variety of karst features generated (Hardt 2011).

Authors like Klimchouk et al. (2000) also does not consider the type of rock as the main element in the karst formation, but other conditions like dissolving and hydrology trait in the karst system, considering the karst as a mass transfer system integrated with soluble rocks, and permeability structural dominated by channels established by the rock material dissolution, being arranged to facilitate the circulation of fluids.

Based on studies performed by the mentioned researchers, then it is understood that the karst can develop from any rock, even from the least soluble, such as sandstone and quartzite. Even though the dissolution process is not predominant, an association among other factors such as tectonics, climate, hydrology, vegetation may extend the conditions for the performance of chemical weathering and generate morphologies typically karstic, forming a karst system. Thus, this study aims to produce a synthesis on karst on Serra do Espinhaço Meridional, Minas Gerais, from the survey and mapping of the main areas with caves, and with the most common morphologies, developed in not carbonate rocks, especially the quartzite.

2. Karstification in siliciclastic rocks

According to Ford and Williams (2007), any type of rock can undergo dissolution depending on environmental conditions, regardless of the type of mineral that composes it.

In the case of silica, the dissolution occurs in the form of silicic acid generated from the hydration of quartz. This acid is much weaker than the carbonic acid. The solubility of silica is not significantly affected at pH lower than 9, continuously decreasing with the pH reduction. This process allows the silica dissolution, but is very time consuming, because it is a very slow reaction.

To Ford and Williams (2007), siliceous rocks can develop karst ways of dissolution, even slowly, from small to intermediate dimensions, because as carbonates and evaporites, they are practically monomineralicos in its composition.

In quartz, under the water action, the silica solubility is too low, but in the case of amorphous silica, such as those found in sandstone cements, the solubility grows. In all forms of silica, solubility increases with water temperatures above 50 °C. However, at higher pH conditions, resulting from hydrolysis, silicon, as well as aluminum, is solubilized and causes the silicate structure breakage, generating fragments of different sizes which are removed by the the action of water, contributing to karstification.

It is common that this reaction occurs in the pH range 5–9. If there are more or less percolation of water soluble components are removed completely or partially, resulting respectively in full or partial hydrolysis.

In quartzites it is common to find karst development along the ridges and cliffs, due to hydraulic gradient these steeper areas, which allows a rapid and efficient flow of the water, removing the accumulated residues. But to the development of the karst morphology on the lithology from the dissolution, there are three basic requirements (Ford and Williams 2007):

- High purity mineral so that grains of insoluble aluminosilicates do not block the underground channels;
- Thick layer of rock with few cleavage planes with intersection fractures with significant and far between.
- Lack of relevant geomorphological processes such as those related to the action of ice or sea, allowing the forms of slow dissolution able to develop.

The discontinuity is another factor that plays a fundamental role in the dissolution process. The secondary porosity, mainly linked to the plans tectonic origin, like fractures and faults, has great influence on the karst forms development, since percolation of water through these plans fractures would cause the gradual dissolution of rock, especially in the discontinuities and its adjacent areas.

From the elements which contribute to the dissolution of siliceous rocks, also stands out the organic material. Karst landscapes developed on siliceous rocks have strong links with plenty of rainfall and vegetation cover over the rock, which makes the water rich in organic acids. These acids are able to erode the rock through the process of chelation by microorganisms, which cause the dissolution of quartz creating alveolar forms (Smith 2004).

Another major factor in the silica dissolution is the presence of ferrous catalysts, which associated with water, favors a more rapid dissolution of quartz (Hardt 2011). In accordance with Silva (2004), the presence of chlorides may also increase dissolution rates due to the increased surface reactivity of the silica, as a function of increasing its ionization potential.

Very often, dissolution in siliceous rocks occurs mainly on the quartzose cement rock, due to amorphous silica and not on quartz grains, yielding a residue of undissolved silica and occupying the void part newly formed. This process was identified by Rodet (1996) and further described by Quinif (2010) and Rodet (2012) as fantomisation or Ghost-rock karst, and may be the process that prevails in forming the siliceous karst (Hardt 2011).

3. The non carbonate karst in Brazil

Brazil has great potential for karstic development in non carbonate rocks, but studies are still recent and the data are incipient. The main studies were developed in quartzite, sandstone and itabirite by Hardt (2009), Auler (2011), Willems et al. (2004), Correa (2012), among others.

As shown in table 1, in Brazil, the largest number of known cavities is developed in carbonate rocks and iron ore. Auler and Piló (2011) emphasize the high Brazilian potential in the development of cavities in quartzite and sandstone, because although the known percentage is small (> 1 %), it is already known that the larger of this type of rock cavities are located in Brazil.

According to Karmann (1979) and Hardt et al. (2009), the main areas with potential for development of non carbonatic karst in Brazil are: Chapada Diamantina – Bahia (quartzite), northwestern Amazon (quartzite and sandstone), south and north-central Minas Gerais (quartzite), Serra das Confusões, and Serra da Capivara, Sete Cidades, in Piaui (sandstone), Tocantins (sandstone), Serra Geral – Minas Gerais and Rio Grande do Sul (sandstone) and Chapada dos Guimarães and Pareci, in Mato Grosso (sandstone).

Karst in itabirite also has a great potential, as in Pará, and in the Iron Quadrangle region in Minas Gerais Gerais, but only in a few studies (Corrêa 2012).

4. Methods

First literature review on karst was performed, focusing especially on the main activities of karst geomorphology developed on Serra do Espinhaço Meridional. Later, we searched the body responsible for caves records in Brazil, Centro Nacional de Pesquisas e Conservação de Cavernas – the National Centre for Research and Conservation of Caves – (CECAV) in order to raise areas with caves in the study region. From then on, field work and karst prospections in certain points previously selected were made. From these data, was organized a database on karst studies already undertaken in the area, as well as some potential areas which do not have scientific studies. Afterwards, the maps of distribution of major karst features identified were generated. It should be noted that this study does not attempt to identify all caves, but to demonstrate

Table 1. Estimation of the speleological potential of Brazil relative to cavities known and development lithology. Source: Auler and Piló (2011a).

Lithology	Nº of cavities known	Cavities Potential unknown	Cavities Known (%)
Carbonates	7,000	> 150,000	< 5%
Quartzite	400	>50,000	< 1%
Sandstone	400	>50,000	< 1%
Iron ore	2,000	>10,000	< 20%
Other Lithology	200	>50,000	< 0,5%

part of the existing potential and encourage the development of further studies in the region.

5. Study area characterization

The Serra do Espinhaço Meridional corresponds to a province that limits the southeastern São Francisco Craton and amalgamates up northeasterly with Araçuaí belt. It extends from the area locally called Serra do Cipó, near Belo Horizonte, to the depressed area of Couto de Magalhães in Minas Gerais, Brazil, forming the band of Precambrian orogenic more extensive and continuous from the Brazilian territory.

It is a mountain range of 1,200 kilometers, formed by Proterozoic metasediments overlying land discordant. It is formed by thick sequences of quartzites which cover a very metamorphosed basement, bounded on the west by São Francisco River Basin, a region of smooth morphology, associated with limestones, sandstones and slates.

To the east, the region is dominated by gneisses, granites and migmatites with intercalations of metasediments, forming rounded reliefs. Geologically, your rocks are part of Espinhaço Range, a term used to denote the set of acidic volcanics and metasedimentary rocks that compose the Espinhaço geomorphic features (Fig. 1) (Almeida Abreu and Renger 2002). Geomorphologically, the SdEM is a set of highlands, best defined as plateau, has general alignment N-S.

The mountain is composed of discontinuous ridge lines, composed by intersection of near directions close to NE-SW and NW-SE. This geomorphological unit represents a hydrograph divider between the basins from the Brazilian east-central and the São Francisco River (Saadi 1995).

Morphologically, the east and west sides have different behavior.The eastern side of the medium SdEM has higher declivity and, theoretically, waterways more aggressive than the western side.

However, the west side presents with more intensity and occurrence the erosional landforms and geochemical data flood record that currently rates of geochemical losses are greater on the western side (Leão et al. 2012).

The weather according to Koppen classification corresponds to CWB (mesothermal), with two distinct seasons, hot and humid summers and cool and dry winters. The average annual rainfall varies from 1,250 to 1,550 mm and the mean annual temperature is equivalent between 18 and 19 ºC.

6. Karst features in Serra do Espinhaço Meridional

The feature that draws more attention when compared to the classic non carbonate karst is the morphology. The featured karst forms are almost always present both in carbonatic lithologies, as well as in non-carbonatic, this one, differing sometimes by a lower degree of development of

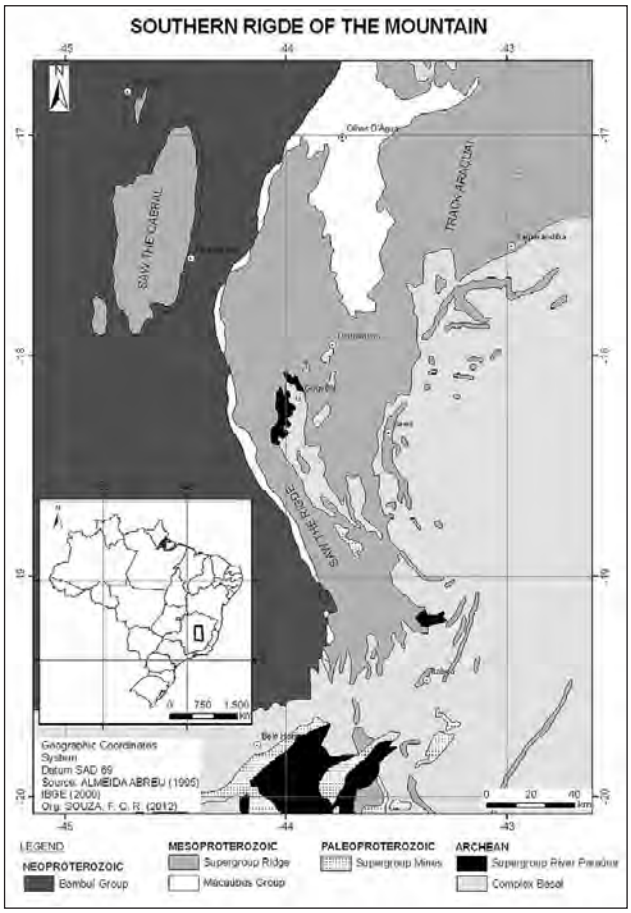

Figure 1. Serra do Espinhaço Meridional, Source: Almeida-Abreu, Edited by F. Souza, 2012.

its forms, since their slower dissolution. From the register of CECAV, satellite images and field inspection analysis were identified and mapped the main the study area features (Fig. 2). It is noteworthy that the major karst features identified and studied so far in SdEM are mainly located at the edges of his geomorphological unit or on the central portion of the Diamantina Plateau.

The main karst features registered in CECAV, which are located in the survey area, correspond: into cavities 88%, 10% shelters, 1% by dolines and 1% resurgences (Fig. 3).

As defined in CECAV, in Brazil under is the feature that has a mouth bigger than the horizontal projection. These data

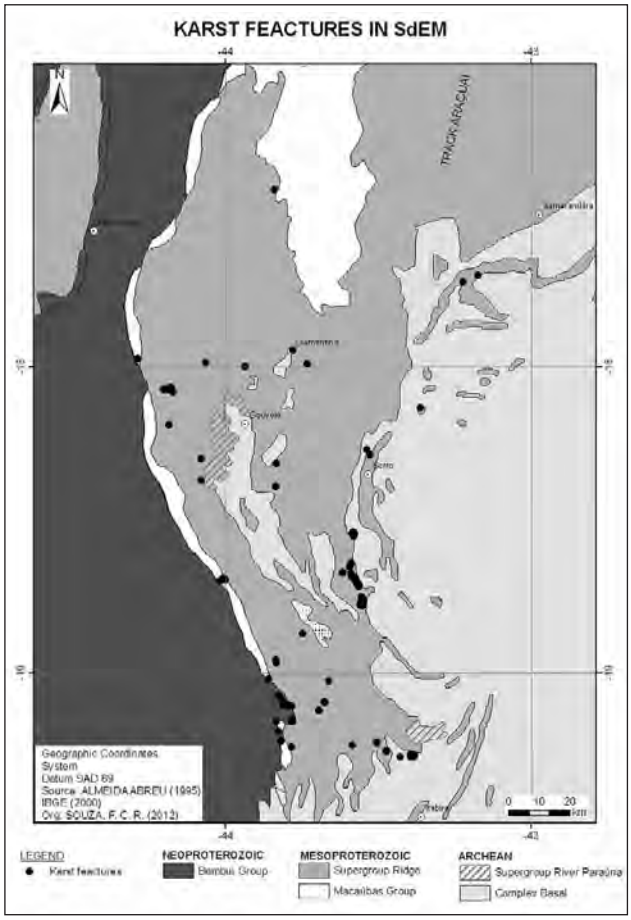

Figure 2. Localization of karst feactures in SdEM, Minas Gerais, Brazil. Source: www.cecav.gov.br (november/2012), organized by Souza, 2012).

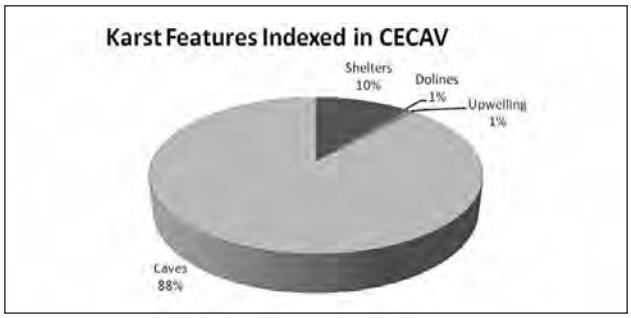

Figure 3. Karst feactures indexed in CECAV in SdEM, Minas Gerais, Brazil. Source: www.cecav.gov.br (november/2012), organized by Souza, 2012.

record the spatial distribution of karst features already identified as well as potential areas for development of these geoforms. It is also observed that records and studies have focused cavities, although there are other recurrence geoforms typical of karst areas, as was verified during the field survey.

The main morphological features found in the area surveyed were cavities, sinkholes, poljés, lapiaz, solid, kamenitzas, and others, and are highlighted below:

Caves (Fig. 4) – were identified caves as Monte Cristo, Salitre and Tromba d'Anta, among others. They have horizontal projection above 30 meters. Altogether have already been studied scientifically more than 111 cavities in SdEM although the speleological potential is higher. Studies cavities are focused mainly on the morphological description, conceptual debates and spatial location and some make

Figure 4. Duct in Monte Cristo Cave – Diamantina region, MG. (Photo by F Souza, 2011).

statistics survey. But there is still no detailed study on morphometry, geochronology or verticalized research.

In these cavities it can be observed the presence of drains and the speleothems have small morphometric dimensions if compared to those developed in carbonate. The main shelters studied in the region of Planalto Diamantina record the presence of paintings, graphics from the Tradition Plateau, as well as archaeological sites and record the occupation in the region. In this context were studied in detail 30 archaeological sites in the region of Diamantina (Linke 2008).

2) Poljes – are large closed depressions which may reach many kilometers long, presenting thick ground cover, where happens the water flow (Ford and Williams 2007). At Serra do Espinhaço occur several areas that indicate the presence of poljes and paleo-poljes (Fig. 5).

3) Dolines – closed depressions, funnel or cylindrical-shaped, variable dimensions and depth, having the dissolution as origin (White 1988). These features may influence the lowering of the rocky surface, penetration of soil, collapse resulted from rebates at the top of the soil or rock cavern (Fig. 6).

At SdEM were identified dolines whose morphometric dimensions are small if compared to the carbonatic ones, but shows typical morphology and functionality of this feature. It was observed that even in the dry season, the centers of the dissolution dolines present themselves wet and with green vegetation.

The dolines location in SdEM was observed mainly in the center of Diamantina Plateau, but we can infer their existence in other geomorphological units.

4) Lapiaz – it is a linear, deep and narrow form, rock dissolution result due to the rainwater movement, which can cause connections between kamenitzas, allowing also feeding of sinks and endokarst. Their size varies from inches to feet deep (Ford and Williams 2007) (Fig. 7). Lapiaz are recurring features in SdEM and can be found in outcrops, solids, cliffs and in different locations.

5) Kamenitzas – small depressions are closed of horizontal end, resulted from the rock peripheral erosion due to the action of surface water (White 1988) (Fig. 8).

The kamenitzas occur mainly associated with lapiaz and are distributed in all contexts of SdEM.

6) Bee nest – a set of wells and drilling coalescent, resulted from the effect of karst rock dissolution (Fig. 9).

Figure 5. Paleo-poljes in Quartéis region, close to Conselheiro Mata, MG. (Photo by A. Vasconcelos, 2011).

Figure 6. Doline close to Conselheiro Mata, MG. (Photo by A. Vasconcelos, 2012).

The karst morphology developed in quartzitic substrate can occur by chemical alteration of rock, especially by hydrolysis, with subsequent mechanical removal, but suffering smaller influence from the rock material dissolution. Anyway, the resulting morphologies are similar to those carbonatic, generating the same type of relief associated to traditional karst (Hardt 2011).

7. Final thoughts

The speleological Brazilian potential on traditional karst is great, since less than 5% of the existing caves were identified. In the case of karst in other lithologies, as in siliciclastic rocks and in Itabirito the potential is even greater, since studies are still very limited. The main studies are targeted to quartzites and sandstones and face more for speleology and less for karst geomorphology.

Therefore, new studies developments in several areas that make up the non carbonate karst will allow better understanding of the dynamics of the Serra do Espinhaço Meridional, which enables to make planning for appropriate use of this region, today Biosphere Reserve of Serra do Espinhaço.

Figure 7. Lapiaz in Curralinho region – MG. (Photo by F. Souza, 2012).

Figure 8. Kamenitza at Diamantina region – MG. (Photo by A. Vasconcelos, 2011).

Figura 9. Bee nest in the Monte Cristo cave outer area, Diamantina region – MG. (Photo by A. Vasconcelos, 2011).

References

Almeida Abreu PA, Renger FE, 2002. Serra do Espinhaço Meridional: um orogêno de colisão do mesoproterozóico. Revista Brasileira de Geociências, 32, 1. 2002-fin, 1–14.

Auler A, Piló LB, 2011. Introdução à Espeleologia. Instituto Chico Mendes de Conservação da Biodiversidade – ICMBio. Centro Nacional de Pesquisa e Conservação de Cavernas – CECAV. Curso de Espeleologia e Licenciamento Ambiental. Brasília.

Corrêa MP, 2012. Aspectos Genéticos e Morfológicos das Cavidades Naturais da Serra da Piedade – Quadrilátero Ferrífero/MG. Dissertação [Manuscrito]. Belo Horizonte: Universidade Federal de Minas Gerais – UFMG. 2012.

Ford D, Williams P, 2007. Karst hydrogeology and geomorphology. John Wiley & Sons Ltd, England, 578.

Hardt R, Pinto SAF, 2009. Carste em litologias não carbonáticas, Revista Brazileira de Geomorfologia, V. 10, no 2, UGB, Brasília, 99–105.

Hardt R, 2011. Da carstificação em arenitos. Aproximação com o suporte de geotecnologias. Tese de doutoramento, Universidade Estadual Paulista – Université de Rouen, Rio Claro, 224.

Klimchouk A B, Ford D C, Palmer A N, Dreybrodt W, 2000 (Eds.). Speleogenesis – Evolution of Karst Aquifers. National Speleological Society, Huntsville/USA, 528.

Leão MR, Rezende E A, Salgado A A R, Nalini Júnior H A, 2012. Erosão, Denudação e Evolução do Relevo da Média Serra do Espinhaço Meridional. Revista Brazileira de Geomorfologia. v. 13. n. 2, 113–124.

Linke V, 2008. Paisagens dos sítios de pinturas rupestres da região de Diamantina – MG. Dissertação [Manuscrito]. Belo Horizonte: Universidade Federal de Minas Gerais – UFMG.

Quinif Y, 2010. Fantômes de roche et fantômisation. Karstologia Mémoires 18, França, 184.

Rodet J, 1996. Une nouvelle organisation geometrique du drainage karstique des craies: Le labyrinthe d'alteration, l'exemple de la grotte de la Mansonniere (Bellou sur Huisne, Orne, France). Comptes Rendus de l'Académie des Sciences de Paris, t. 322 (12), serie II a, 1039–1045.

Rodet J, 2012. Primokarst, inception stages of karstification. Ghost-rock Karst Symposium, Han sur Lesse (Belgium), 07–11 octobre 2012, Booklet: 13, PPT.

Saadi AA, 1995. Geomorfologia da Serra do Espinhaço de Minas Gerais e de suas margens. Geonomos, 3 (1): 41–63.

Silva SM, 2004. Carstificação em rochas siliciclásticas: estudo de caso na Serra do Ibitipoca, Minas Gerais. Dissertação de Mestrado, Universidade Federal de Minas Gerais, Belo Horizonte: 142.

Willems L, 2002. Phénomènes karstiques em roches silicatées non carbonatées – cãs dês grés, dês micaschistes, dês gneiss et dês granites em Afrique sahélienne et équatoriale. Tese, Universite de Liege, France, 259.

Willems L, Rodet J, Pouclet A, Rodet MJ, Hatert F, Compère P, Auler AS, 2004. Carste no quartzito: o Parque Estadual do Rio Preto (São Gonçalo do Rio Preto, Minas Gerais Brazil). I Encontro de Carstologia do Brazil-Carste-2004, Belo Horizonte, 27–31 July, Caderno de Resumos: 86, poster.

White WB, 1988. Geomorphology and Hydrology of Karst Terrains. Oxford University Press, New York, 98.

Session:

Speleogenesis

LAG AND TRANSFER TIME INFERRED FROM MELTING CYCLES RECORD IN THE COULOMP KARST SPRING (ALPES DE HAUTE-PROVENCE, FRANCE)

Philippe Audra[1], Jean-Claude Nobécourt[2]
[1]Polytech Nice, Sophia, University of Nice, Sophia Antipolis, 930 route des Colles, 06903 Sophia-Antipolis, France and Innovative City, IMREDD, Nice, France, audra@unice.fr
[2]CRESPE, Le Hameau de l'Ara, 259 boulevard Reine Jeanne, 06140 VENCE, France, jcnobecourt@free.fr

A 11-days long period of snowmelt cycles was selected from the discharge and temperature data collected at Coulomp spring (Alpes de Haute-Provence, France), which is the largest of French Southern Alps with a discharge of 1 m^3/s. Its catchment is 30–50 km^2-large and mainly composed of marly limestones and poorly permeable covers, responsible of a combined diffuse and concentrated recharge. From Q data we extracted snowmelt discharge (Snowmelt Q = oscillating part of the discharge) and Basal Q. The contribution of Snowmelt Q is 30–50 % of Q. Amplitude of spring temperature (T_{spring}) is about 2 °C due to alternation of cold snowmelt water with low residence time and "warm" phreatic water with longer residence time. The lag between the peak of air temperature (T_{air}) corresponding to the maximum of snow melting and the peaks of Q, corresponding to the transfer time between surface and spring, is less than 10 h. This 10 h transfer time combines about 7 h of vertical transfer through the vadose zone and 3 h of horizontal transfer through the drain.

1. Introduction

Snowmelt recharges karst aquifer through diffuse and slow seepage or through sudden contribution when abrupt melting combines with air warming and huge down pouring. Sudden melting is quickly transferred through high-velocity conduits, with limited storage. On the contrary, part of seepage uses low-velocity routes mainly through tiny fissures and contributes to storage in epikarst, vadose zone, and epiphreatic zone. As a consequence, snowmelt contributes to the deferred runoff during low-water periods at the end of summer, where the amount or scarcity of discharge depends on the thickness of the snow mantle accumulated during winter and on the rhythms of the snowmelt during spring. Otherwise, snowmelt daily cycles give rhythm to the input, which is transformed and transferred at the spring, and which allows making detailed analysis of the transfer function, namely transit routes, transfer time and lag, and storage time and capacity (Vigna and Suozzi 2009).

In this paper, we study the Coulomp spring in Alpes de Haute-Provence (France), which is the largest karst spring of the Southern French Alps. Recharge conditions are complex and are determined by diverse type of rock outcrops in the catchment where diffuse recharge is predominant. The monitoring of the spring, with a record of discharge and temperature during 4 yearly cycles, gives the possibility to focus on different kind of recharge period, namely long recessions, flash floods (Audra and Nobécourt 2012), long flooding periods, or snow melting, which is the topic of this paper. We analyze the recorded data combined with observations of the spring activity. The aim of this study is to understand the snowmelt cycles and their role in the spring activity, and the transfer times in the different karst zones (seepage fissures vs. conduits). Moreover, the understanding of transfer times is an important challenge to allow cave exploration. Indeed, the underground river is the largest of France (average Q = 1 m^3/s), which exploration represents a caving and scientific challenge and the access of the underground system is controlled by 3 sumps at the entrance which require pumping and which can close when flooding occurs.

2. Context and dynamic of the Coulomp spring

The Coulomp spring (commune of Castellet-lès-Sausses, Department of Alpes-de-Haute-Provence, France) pours out at 1,300 m a.s.l. with a scenery 65 m-high waterfall. The underground river has been explored along 1.7 km upstream to the spring (Audra et al. 2009). The spring is fed by a 30–50 km^2-large catchment, which encompasses the Baussebérard and Grand Coyer (2,693 m) Mountains (Fig. 1). The mean annual discharge is 1 m^3/s, making this spring the largest of the Southern French Alps. Most of the seepage occurs through Upper Cretaceous marly limestones, which thickness is several hundreds of meters and which in turn are covered uncomformably by the Nummulitic Trilogy (Nummulitic limestones, Priabonian blue clay, and Annot sandstones). The thickness and extension of these poorly permeable covers makes a particular recharge, which combine both diffuse seepage through marly limestones and concentrated input in sinkholes originating from surface runoff on marls and clays. Extreme discharges (30 m^3/s; 250 L/s) reveal a typical karst dynamic, influenced by fast transfer through conduits and long recessions kept on going by storage in sandstone covers and in the thick marly-limestone infiltration zone.

3. Material and methods

The spring pool level is recorded each 30 mn, and transformed in discharge (Q) through a rating curve, constructed with chemical gauging at different discharge. For the concerned discharges (200–2,000 L/s), the rating curve quality is fair (R^2 = 0.976). We recorded spring temperature (T_{spring}) and air temperature (T_{air}) with the same frequency. T_{air} is overestimated in the middle of the day, since the data logger was exposed to direct solar insulation.

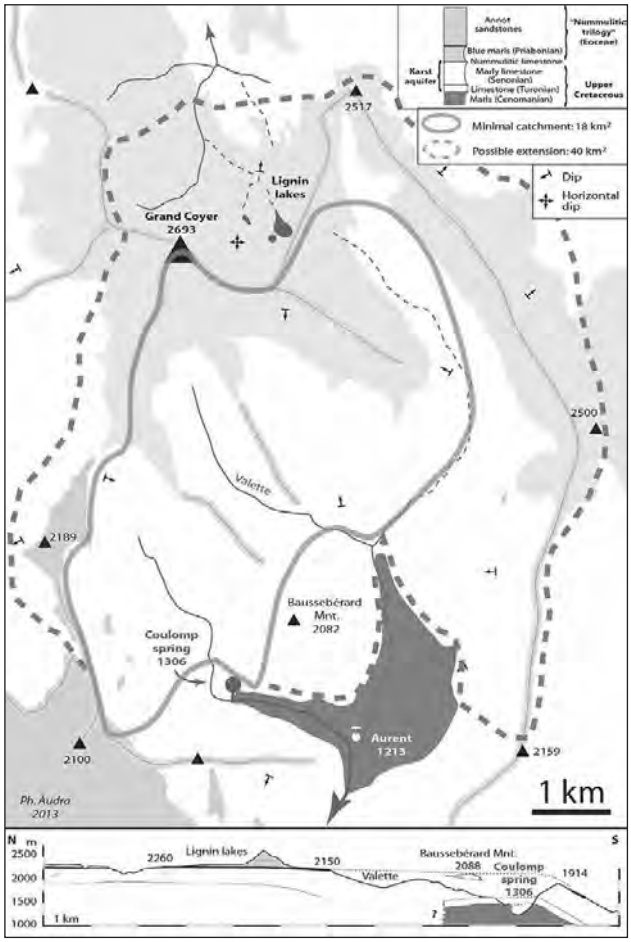

Figure 1. The catchment of the Coulomp spring is about 30–50 km². It stretches from 1,300 m a.s.l. at the spring to 2,693 m a.s.l. at the Grand Coyer. Mainly Cretaceous marly limestones crop out, covered with clay and sandstones.

However, we assume a reasonable validity for the air temperature regarding the relative trend and periods without direct solar heating (i.e. from 4 p.m. to 10 a.m.). Finally, data from the next meteorological station of Méailles (6 km distance, 1,090 m a.s.l.) provide minimal daily temperature and weather.

The chosen study period of 11-days in March 2009 corresponds to a typical stable wintertime "fine weather" (Fig. 2). At that time, most of the snow already melted at the altitude of the spring and up to 2,000 m on the south-exposed slopes of the mountain above the spring, but a thick mantle still remained in northern slopes and in the remote highest parts of the catchment above 2,000 m. At the beginning of the period, snowmelt increases as a consequence of a significant warming: night temperature minima at the spring rise from 0 to 5 °C but remain negative in the high catchment, whereas during the day maxima may overpass 20 °C on the southern slopes. No rain or snow fall occurred during the period, the melting cycle being only influenced by the daily thermal cycles. Weather remains sunny during most of the period, with only 2 partly cloudy days. A cooling with snowfalls ends this period.

The discharge curve (Q) displays daily cycles resulting from snowmelt (Fig. 2). The total discharge corresponds to the combination of a basal discharge (Basal Q) resulting from the slow recharge of the previous days and of snowmelt peak discharge (Snowmelt Q) directly resulting from the melting transfer.

In order to separate the Basal Q and the Snowmelt Q, we made the following treatment: (i) identification of daily discharge minima, (ii) interpolation between each minimum and construction of a curve with 30 mn timing corresponding to Basal Q, (iii) subtraction of Basal Q to Q and extraction of the cyclic Snowmelt Q.

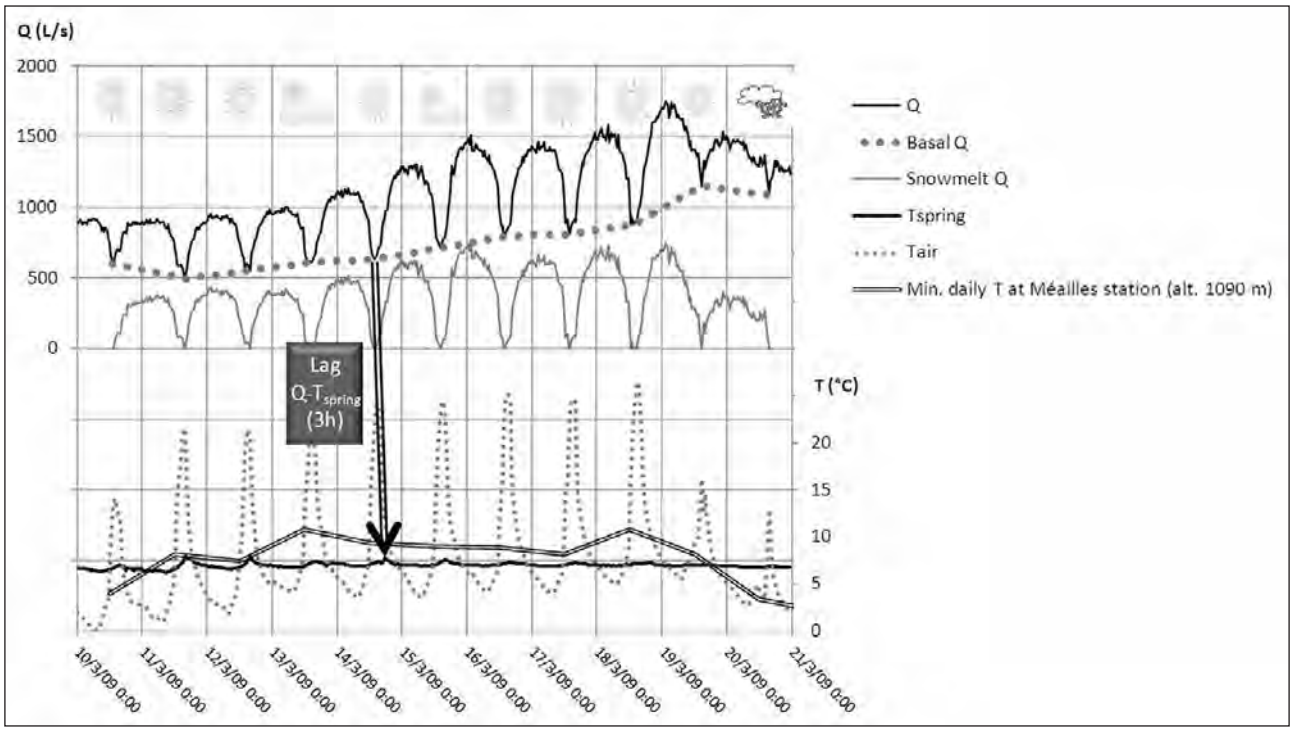

Figure 2. Snowmelt influence on the Coulomp spring in March 2009. The upper curve corresponds to the raw discharge (Q), the middle curve to the basal discharge (Basal Q), and the lower curve to the snowmelt discharge (Snowmelt Q) (see text for explanation). Additionally, the temperature of the spring (T_{spring}) and the temperature minima at the closest meteorological station (Méailles) are shown, with daily weather trend. X axis corresponds to winter time.

4. Results (Tab. 1)

Q: during the period, discharge was about 1m³/s, however with an extreme daily variability due to snowmelt, with constant oscillation between 500–800 L/s and 900–1,700 L/s.

Basal Q and Snowmelt Q: the Basal Q corresponds to the lowest daily discharges corresponding to the cessation of daily snowmelt influence. Through the period, it gradually increases from 600 to 1,200 L/s. The Snowmelt Q strictly corresponds to the daily melting, with a mean value of 400 L/s, oscillation from 0 (snowmelt stop at night) to a maximum of 760 L/s. The relative contribution of Snowmelt Q to the total discharge (Q) evolves from 0 when snowmelt recharges stops at night to a maximum of 50 % of Q, with a mean value of 30 % of Q.

Table 1. Characteristic values of the daily snowmelt cycles at the Coulomp spring in March 2009.

Values	Min.	Aver.	Max.	Date of min.	Date of max.
Q (L/s)	497	1123	1754	11/03/2009 16:00	19/03/2009 01:30
Snowmelt Q (L/s)	0	374	760	N/A	16/03/2009 01:30
Snowmelt Q / Q (%)	0 %	29 %	50 %	N/A	16/03/2009 01:00
Tspring (°C)	6,23	6,94	7,99	11/03/2009 08:30	12/03/2009 16:00
Lag min Tair to min Q (h)	6	7 (±1)	8,5	10/03/2009	20/03/2009
Lag max Tair to max Q (h)	8	12 (±2,3)	16	19/03/2009	10/03/2009

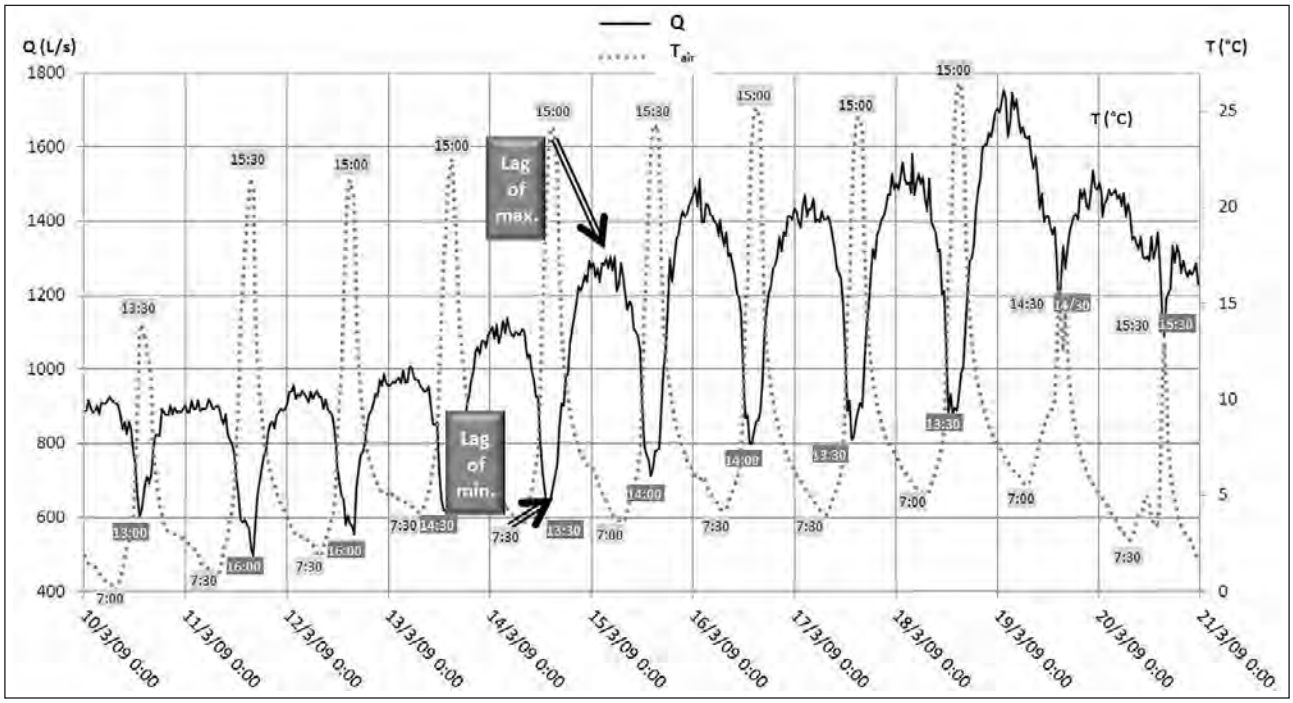

Figure 3. Lag between the air temperature (Tair) and the discharge (Q), for both minima and maxima.

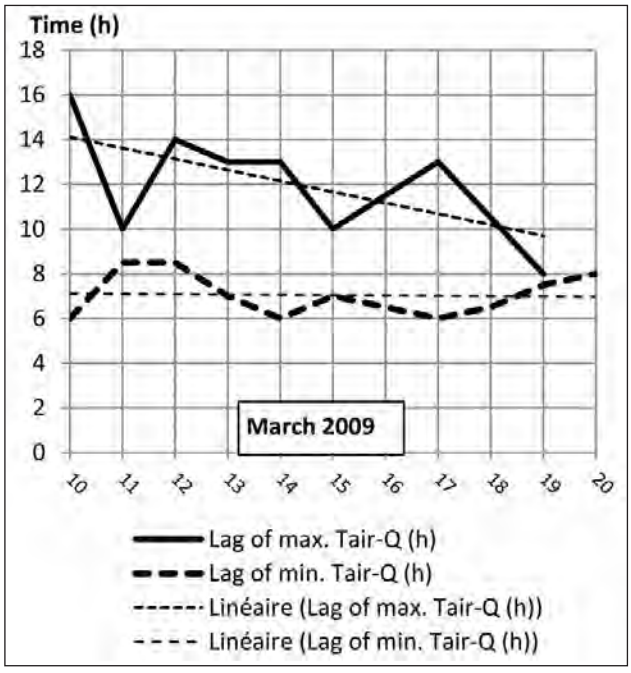

Figure 4. Evolution of the Tair-Q lag for both minima and maxima.

Evolution of Q: Q increase during the period results from the increase of the air temperature and the maintenance of high values during the day, whereas night frost occurring on most part of the catchment stops melting at night. A snowfall occurring at the end of the period stops the cycle.

Min-max Q lag: the daily minimum of Q is at about 14:30, the daily maximum of Q is at about 03:00 (Fig. 3). There is a lag of 7 h between snowmelt start on the surface at sunrise, given by the air temperature minima (T_{air}) and the beginning of restitution of infiltrated meltwater at the spring at the beginning of the afternoon. The lag between the T_{air} maxima and Q maxima (lag of T_{air}-Q maxima) is less defined, because of the presence of several secondary peaks of Q, however it is about 12 h. The lag of T_{air}-Q minima is stable during the period, whereas the lag of T_{air}-Q maxima shortens from 14 to 10 h during the same period (Fig. 4).

T_{spring}: the Q peaks correspond to T_{spring} minima and conversely. T_{spring} and Q are in phase inversion (Fig. 2). The thermal amplitude is up to 1.8°C (extreme T_{spring} are 6.2 and 8 °C). At the daily scale, the thermal amplitude is between 0.3 and 1.5 °C. Largest amplitudes are at the beginning of the period. Amplitudes gradually reduce till a quasi thermal

stability at the end of the period. The lag between Q and Spring T_{spring} is about 3 h.

5. Discussion

Evolution of Basal Q (Fig. 2). The increase of basal Q (500 to 1,100 L/s) results of the infiltration of previous days melting: fast infiltration is transferred within half a day, whereas slow infiltration is spread in the course of the following days and cumulative contributes to the gradual increase of basal Q.

Secondary peaks. Snowmelt cycles are similar throughout the period. However peaks are systematically made of the merging of several secondary peaks (Fig. 3). Several hypotheses are possible: (i) zones of recharge may use different routes, with slightly different velocities. Such a reason would produce rather similar secondary peaks; (ii) the snow stock evolves according to the melting and each zone contribution may evolve through time; (iii) sun exposure may somehow change with the presence of clouds, producing jumps in the melting, with no similitude of secondary peaks across the period. Since secondary peaks do not display any evident similitude, we would favor this last hypothesis.

Snowmelt Q. The gradual increase of daily temperature results in the increase of Snowmelt Q. The instantaneous variations of Snowmelt Q range from 34 L/s in 30 mn in average up to 176 L/s in 30 mn. The highest variations occur during both Q rise and Q lowering. At the end of the period, Snowmelt Q represents halt of the total discharge. The relative lowering of temperature in the middle of the period does not affects snowmelt since day temperatures remain high. On the other hand, the significant temperature increase at the beginning of the period and the 17–18 March provokes a clear and lasting Q increase, for both Q and Snowmelt Q.

Lag. The lag between the snowmelt cycles, directly connected to the air temperature (T_{air}), and the restitution at the spring (Q) gives information about transfer velocity (Fig. 3). The snowmelt water arrives at the spring in 7 h (lag of minima), whereas lag of maxima is 12 h. It does not completely corresponds to water transfer, which is slightly longer, but to the succession of transfer in the vadose zone then to the arriving in the horizontal transfer zone, with both full pipe and open-channel flow, which quickly increases the discharge by piston-flow effect in the phreatic zones (see below). Concerning lags evolution during the period (Fig. 4), the stability of the lags of minima corresponds to the invariant time of infiltration through the vadose zone in recession condition (7 h), whereas the shortening of the lags of maxima reveals the gradual saturation of the vadose zone under the effect of repeated melting cycles and the simultaneous gradual increase of transfer velocity. Such a lag of 7 h, corresponding to the time between the beginning of infiltration and the restitution at the spring is similar to those observed during floods associated to rainy events while the infiltration zone is saturated. However, this lag can be shorter (< 3 h) in case of intense storm producing a preliminary concentration by surface runoff before introduction in sinkholes (Audra and Nobécourt 2012).

Thermal changes at the spring. The 2 °C amplitude of T_{spring} of is significant (Fig. 2). It corresponds to a relative proximity of the recharge zone and to the combination of Basal Q and Snowmelt Q. At the end of the period, T_{spring} amplitude gradually decreases till almost homogenization. It corresponds to the increase of the contribution of water with short residence time, i.e. the "cold" meltwater, which gradually dilutes and replaces the "warm" water having a longer residence time. Together with homogenization, T_{spring} gradually decreases. More precisely, there are 2 successive phases: (i) 10–11 March achieves a cycle of low T_{spring} corresponding to a low contribution of Basal Q; (ii) 11–21 March, strong snowmelt start first expels the "warm" water stored in the phreatic zone, which is gradually replaced by snowmelt water giving a thermal trend of slow decrease and homogenization.

Q-T_{spring} hysteresis curve. Plotting of Q and T_{spring} allows a deeper understanding of the transfer (Fig. 5). The phase

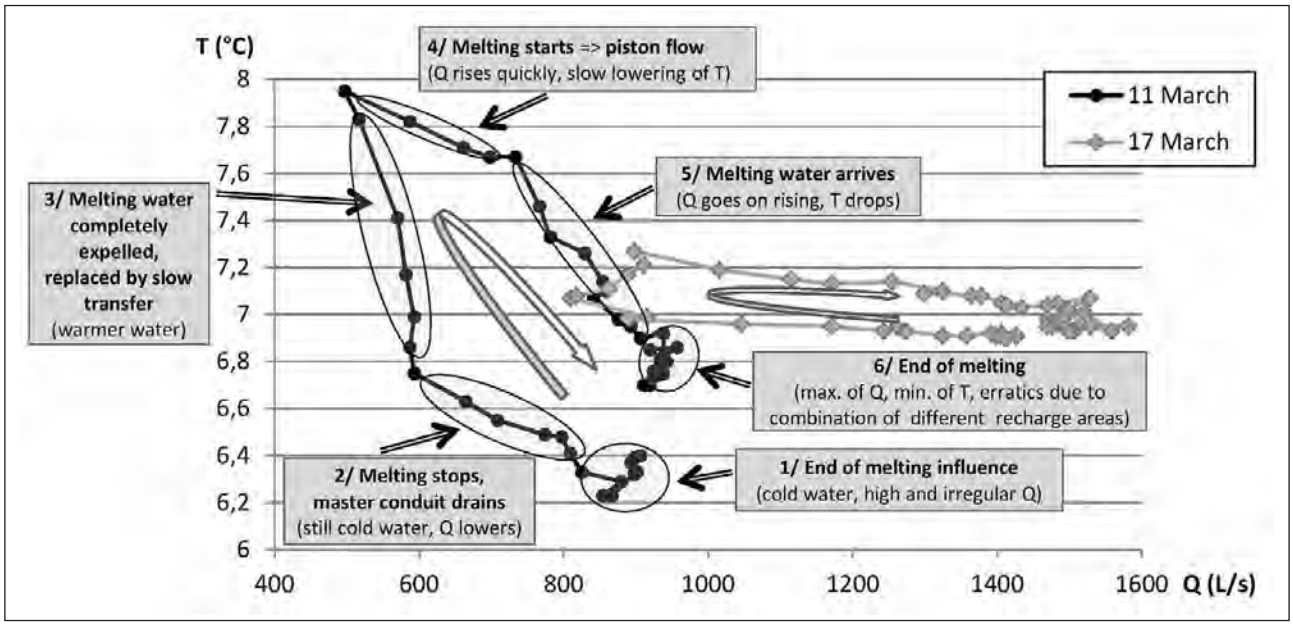

Figure 5. Hysteresis curves characteristic of daily snowmelt cycles (circles correspond to a cycle at the beginning of melting cycles; diamonds to a cycle after several days of intense snowmelt).

inversion between Q and T is easily explained by the contribution of snowmelt water which simultaneously increases Q and lowers T_{spring}. Conversely, during recession without influence of snow melting, contribution of water with longer residence time in the phreatic zone gives warmer T_{spring} and lower Q. The most interesting corresponds to the 3 h lag, where "warm" water is expelled whereas Snowmelt Q starts to rise (Fig. 2). It results from the "piston flow": "warm" water stored in the drain is contributing to the Basal Q, whereas arrival of snowmelt water in the phreatic zone makes a pressure rise, which quickly transfers to the spring. While Snowmelt Q starts to increase, the contributing water is still the "warm" water, progressively expelled of the drain. And conversely, after the end of Snowmelt Q contribution, the draining of the drain still provides cold snowmelt water.

Hysteresis curve represents the pathway of Q and T_{spring} during snowmelt cycles (Fig. 5). It displays 2 significant daily snowmelt cycles at the beginning and at the end of the period. Both pathways are similar even so at the end of the period thermal amplitude is less pronounced. This shows the increasing contribution of meltwater with short residence time, which gradually dilutes and expels the water having longer residence time. This was already visible in the thermal variations of the spring. The Q-T_{spring} 3h-lag corresponds to the transfer time of meltwater in the drain between its arrival in the phreatic zone and the spring (plus the time of transfer of piston-flow, assumed to be short). Or more probably, this time represents the average time of several point contributions of infiltrated water. Let's assume 7 h as the time including the transfer in the vadose zone (plus the transfer of piston-flow) and 3 h in the drain (which also includes the time of transfer of piston-flow). Accordingly, the transfer time from the surface to the spring would be a little less than about 10 h.

6. Conclusion

We studied an 11 days period of snowmelt influence on Coulomp karst spring dynamic. The discharge (Q) regularly oscillates between 500 and 1,700 L/s. The contribution of snowmelt discharge (Snowmelt Q) is 30–50 % of Q. Amplitude of spring temperature (T_{spring}) is about 2 °C due to alternation of cold snowmelt water with low residence time and "warm" phreatic water with longer residence time. The lag between the peak of air temperature (T_{air}) corresponding to the maximum of snow melting and the peaks of Q, corresponding to the transfer time between surface and spring, is less than 10 h. This 10 h transfer time combines about 7 h of vertical transfer through the vadose zone and 3 h of horizontal transfer through the drain. The time of transfer of piston flow is assumed to be short and would not affect significantly the estimation of both vertical and horizontal transfer times. In the future, we will use dye for an assessment of the velocity in the drain, which is know along 1.7 km, including 32 % in siphon (full-pipe flow), 50 % in pools (uniform flow), and 17 % in torrential flow. For similar Q and assuming a 3h time for horizontal transfer, we might obtain an estimation of the average distance of the location of vertical flow arriving in the horizontal transfer zone. Currently, this place, located beyond the upstream sump, remains unknown.

Acknowledgments

To people who kindly help us for the Coulomp Project on either caving or scientific sides. Viviane Bertaina who provides data from the meteorological station of Méailles, Éric Gilli (Univ. Paris 8) who borrowed data loggers, Bruno Arfib (Aix-Marseille Univ.) for improving the text with thorough remarks, and participants to the exploration: cavers and caving associations (CDS 06, CSR Q, FFS, FSE), numerous enterprises, local institutions and people through founding or diverse supports.

References

Audra P, Nobécourt JC, 2012. Flooding in epiphreatic passages. Analysis of the 4–5 Nov. 2011 flood in the Chamois Cave (Alpes-de-Haute-Provence, France). Proceedings of the 13th national Congress of Speleology, Muotathal. Swiss Society of Speleology, 199–205.

Audra P, Mocochain L, Bigot JY, Nobécourt JC, 2009. The Grand Coyer karst, exploration at the Coulomp spring (Alpes-de-Haute-Provence, France). Proceedings of the 15th International Congress of Speleology, Kerrville (TX). International Union of Speleology, 3, 1755–1759.

Vigna B, Suozzi E, 2009. The importance of the nival melting process on the recharging of aquifers, Epitome, vol. 3 (Geoitalia 2009, Rimini), 1.

DISSOLUTION RATES, CARBON DIOXIDE DYNAMICS, AND GEOMORPHOLOGICAL FEEDBACKS IN OPEN CHANNEL CAVE STREAMS

Matthew D. Covington[1,2], Mitja Prelovšek, Franci Gabrovšek[2]
[1]Department of Geosciences, University of Arkansas, Ozark Hall, Fayetteville, AR 72703, USA, mcoving@uark.edu
[2]Karst Research Institute ZRC SAZU, Titov trg 2, Postojna, Slovenia

Extended abstract

A limestone tablet study of dissolution rates in the main stream of Lekinka, a cave in Slovenia, indicated a systematic downstream decrease in dissolution rates with a characteristic length scale of ~250 m over the duration of a 2-year study (Prelovšek 2009). This finding motivated further research to determine the processes responsible for the observed dissolution pattern. Longitudinal changes in rates, like that observed, provide a unique opportunity to constrain the dynamics of, and controls on, processes occurring in cave streams (Covington et al. 2012). In the initial phase of the study, we proposed several potential mechanisms for the observed decrease in rates, including downstream addition of dissolved load due to dissolution within the channel, downstream addition of dissolved load from infeeding streams, and degassing of carbon dioxide (CO_2) along the studied reach.

A theoretical analysis of the expected length scales for each of these processes allowed comparison with the observed length scale of 250 m. Using this test, the first mechanism, saturation due to dissolution in the channel, was deemed implausible. Starting from this theoretical basis, we identified field data that would allow us to test each mechanism. We conducted water chemistry analysis, collected field measurements of water quality parameters, and measured discharges at locations along the cave stream in a variety of seasons and flow conditions. In the latter stages of the study, we modified a non-dispersive infrared (NDIR) CO_2 sensor for direct measurements of dissolved CO_2 using a waterproof breathable membrane. Taken together, the field data confirmed a systematic downstream decrease in dissolved CO_2, and this remained the most likely mechanism to be responsible for the downstream decrease in dissolution rates.

The stream in Lekinka is fed by an allogenic stream that flows across unconsolidated noncarbonate sediments and sinks into the entrance of Lekinka at the limestone contact. The field data indicated that dissolved CO_2 was high in the surface stream and quickly dropped as the stream flowed through the first 100 m of the cave. Since the concentration of CO_2 in cave air is typically higher than that on the surface, this finding could be viewed as surprising. However, the concentration of dissolved CO_2 is controlled by three factors: 1) the pCO_2 of the air, 2) the production rate of CO_2 in the stream and sediment bed, and 3) the gas transfer coefficient for exchange between water and air. While the first factor could not explain the observed decrease of CO_2 in the cave, it remained possible that the other two factors were more important.

Additional field tests were devised to examine these potential mechanisms for the decrease in CO_2. The stream steepens upon entry to the cave, and, consequently, the characteristics of sediment deposited in the channel significantly change. The outside channel is characterized by fine sediments and particulate organic matter, whereas the sediments inside the cave are primarily gravels with little organic debris. Known correlations between CO_2 production rates and the organic content and grain size of sediments (Baker 1986; Hedin 1990) suggest that production rates should be lower within the cave than outside. We conducted CO_2 production experiments using sediments from inside and outside the cave and confirmed that outside sediments produced CO_2 at a much higher rate, suggesting that the shift in sediment type could be responsible for the decrease in dissolved CO_2.

The gas transfer coefficient of a stream is largely determined by the stream depth and degree of turbulence. Therefore, theoretical expectations indicate that the gas transfer coefficient in the steeper, more turbulent reach inside the cave should be higher than the gas transfer coefficient in the more placid surface reach. A high spatial resolution survey of dissolved CO_2 values along the stream using the NDIR sensor indicated that the largest drops in CO_2 were co-located with the steepest portion of the study reach, where the stream pours down a series of short cascades This provides evidence that changes in the gas transfer coefficient also play a role in the downstream decrease in CO_2.

The influence of stream steepness on CO_2 dynamics via biological processes and hydraulics introduces feedback loops that act in the incision process. The stream profile affects the gas transfer coefficient, the sediment type, and the microbial respiration rate, which in turn affect CO_2 concentrations in the stream. CO_2 concentrations in the stream affect dissolution rates, which loop back to the stream profile. The conditions required to produce these feedback mechanisms, a change in steepness and the presence of organic matter or some other source of CO_2, are quite common in cave streams. Therefore, these mechanisms should act in a wide variety of cave settings. Similar feedback mechanisms have been shown to determine the morphology of speleothems, such as rimstone dams (see e.g., Meakin and Jamtveit 2010). However, no current models of speleogenesis consider these feedback mechanisms, and their geomorphological implications are unclear. We argue that more data are needed to constrain the processes driving CO_2 dynamics in cave streams, and that these data should be used to construct improved models of cave stream incision that can be used to explore the long-

term implications of such feedback mechanisms on cave morphology. The details of this study are presented in Covington et al. (in press).

References

Baker J, 1986. Relationship between microbial activity of stream sediments, determined by three different methods, and abiotic variables. Microbial Ecology 12(2), 193–203.

Covington MD, Prelovšek M, Gabrovšek F, in press. Influence of CO2 dynamics on the longitudinal variation of incision rates in soluble bedrock channels: feedback mechanisms. Geomorphology.

Covington MD, Luhmann AJ, Wicks CM, Saar MO, 2012. Process length scales and longitudinal damping in karst. Journal of Geophysical Research – Earth Surface 117(F1), F01025.

Hedin L, 1990. Factors controlling sediment community respriration in woodland stream ecosystems. Oikos 57(1), 94–105.

Meakin P, Jamtveit B, 2010. Geological pattern formation by growth and dissolution in aqueous systems. Proceedings of the Royal Society A: Mathematical, Physical and Engineering Sciences 466(2115), 659–694.

Prelovšek M, 2009. Present-day speleogenetic processes, factors and features in the epiphreatic zone. Ph.D. thesis. University of Nova Gorica, Nova Gorica, Slovenia.

A METHODOLOGY TO ESTIMATE THE AGE OF CAVES IN NORTHERN LATITUDES, USING TOERFJELLHOLA IN NORWAY AS AN EXAMPLE

Trevor Faulkner
Limestone Research Group, Geography, Earth and Environmental Sciences, University of Birmingham, Edgbaston, Birmingham, B15 2TT, UK, trevor@marblecaves.org.uk

The minimum ages of cave passages are commonly reported by dating their chemical or clastic deposits. Few studies have attempted to provide detailed timescales for the evolution of caves without such deposits. This paper addresses this issue for complex caves formed in glaciated regions, especially those in northern latitudes that were covered by extensive icesheets during the Pleistocene. Toerfjellhola in Norway is chosen as an example to illustrate a methodology by which its cave development history can be deduced by considering probable entrenchment and dissolution rates and local geomorphological changes, whilst working backwards in time and upwards in elevation. Such a method suggests that Toerfjellhola initially comprised two separate palaeocaves whose present highest level passages were formed during the Elsterian deglaciation at the transition from MIS12 to MIS11c. The two caves probably became connected by a common flow route during the Eemian Interglacial at MIS5e.

1. Introduction

A universal problem in karst geomorphology is to derive a speleogenetic history for caves in a karst area (Ford and Williams 2007). Although phases of cave development may be deduced from studies of cave surveys and cave elevations, these are commonly correlated with external geological and geomorphological events only if supported by the dating of speleothems and / or other internal deposits. Such deposits can provide minimum existence ages for the containing cave passages, but it is problematic to derive speleogenetic timetables without them. However, the interglacial hydrological flow routes from sinks to risings for caves formed in glaciated valleys can change significantly after rejuvenation caused by each cycle of glacial erosion (e.g., Häuselmann et al. 2007). Glacial cycles had a period of c. 100,000 years during the last one million years. If previous surface flows and underground vadose and phreatic flows can be correlated to glacial events, this should provide an estimated timetable for speleogenesis. This paper considers situations in the repeatedly-glaciated mountainous Caledonides in northern latitudes by using Toerfjellhola in Central Scandinavia as an example of multi-cycle speleogenesis. Large glaciations started the excavation of local U-shaped valleys and fjords from 2.8–2.5 Ma, and full-scale continental glaciations started from 0.9 Ma (Fredin 2002). Toerfjellhola is formed in amphibolite grade marble that was created by intense folding and metamorphism in the Cambrian to Silurian Caledonide orogeny. Hence, any karst structures in its previous sedimentary limestone lithology have been lost. Its tectonic inception is assumed to be derived from open fractures created as late as the Pleistocene by deglacial uplift and seismicity at the culminations of Scandinavian glaciations (Faulkner 2006a). The cave development history for Toerfjellhola is thus likely to be shorter, simpler and easier to derive than the histories of caves in sedimentary limestones that experienced similar glacial environments: inception in those caves may have started soon after diagenesis (Lowe and Gunn 1997).

Central Scandinavia has nearly 1,000 recorded caves between 64°30'N and 66°20'N (Engh and Sjöberg 1981; Faulkner 2005). The caves tend to cluster along marble outcrops and remain within 50 m of the overlying surface or less than one-eighth of the depth of the local glaciated valley (Faulkner 2007a). About a third are "combination" caves (Faulkner 2009a) that contain relict phreatic passages commonly above a single mainly vadose streamway, as in Toerfjellhola. Local cave development probably follows a repeating four-stage process (Faulkner 2005; 2010): *tectonic inception; deglacial speleogenesis* beneath an ice-dammed lake (IDL) or a subglacial reservoir; *interglacial speleogenesis;* and *glacial removal*. These processes lead to an internal Top-Down, Middle-Outwards (TDMO) model of cave development (Faulkner 2007b). The combination caves are mostly "single-cycle" caves that developed their phreatic passages during the Weichselian deglaciation. There are only about 25 that appear to be "multi-cycle" caves that have experienced several Pleistocene glaciations. Of these, Toerfjellhola is one of the most complex, with passages at nine levels. Its sump is c. 50 m below the surface, which is more than the amount of local bedrock removed at each glaciation. It is therefore a good candidate to have developed over several glacial–interglacial cycles. This paper deduces its possible history, despite its lack of datable stalagmite and it having clastic deposits and a few straw stalactites that likely derive from, or were formed after, the last deglaciation.

Toerfjellhola is the longest cave in the Helgeland Nappe Complex (HNC). The marble is well-banded in grey and white colours, commonly with a vertical foliation. The dominant country rock is mica schist, supplemented by outcrops of granite, gneiss and amphibolites, with commonly linear stripe karst marble outcrops (Gustavson 1988). The cave is one of only five known in vertical stripe karst in the HNC that also contain steeply-sloping relict passages. It lies 5 km NE of Tosenfjord on the SW flank of Toerfjell (1,000 m) in Brønnøy commune, Norway (Faulkner and Newton 1995: Fig. 15). The Main Entrance sink is at WGS84 UTM coordinates VN06504927 at an altitude of 485 m a.s.l. The cave has a surveyed length of 1,896 m and a depth of 101 m. It is situated on a bench within an unmapped marble outcrop measuring perhaps 1,000 m by 200 m above the upper, dry, part of

Overengbakkdal (Figure 1). The sides of this valley consist of large areas of jumbled rocks several metres in size and a block stream occupies the valley floor (Figure 2). The cave's catchment area is c. 1.1 km^2, mainly comprising large snowfields on Toerfjell that melt throughout each summer.

Figure 1. Dry Overengbakk canyon beside the limestone bench containing Toerfjellhola. Tosenfjord is in the distance.

The Toerfjellhola stream enters White Water Passage (Figure 3) and passes beneath relict 8 m and 12 m entrance shafts that appear to have been inactive in the Holocene. Beyond here, the passage seems to end where the water sinks in the floor. However, an upward climb leads to the JoKe Exit, probably a relict resurgence. Small holes down also lead to a junction with a small keyhole-shaped tributary inlet at the head of a steeply-entrenched streamway. This passes many powerful waterfalls (Figure 4) before reaching the sump. It lies below several sub-horizontal strike-aligned relict mainly phreatic passages, which interconnect by joint-aligned shafts and rifts. At its lower end, the Ultimate Roof Series leads to the large abandoned Trunk Passage and upwards to the relict Lower Entrance. From the cave survey plan, section and cross-sections, it appears as if much of the early cave development was phreatic, because the Ultimate Roof Series contains the descending parts of several interconnected phreatic loops that are all blocked at boulder chokes beneath surface dry valleys, as is the sump. This is 100 m from the resurgence in Overengbakkdal (Figure 2) and it seems likely that the final 50 m descent to the resurgence is mainly within the valley block stream.

2. Methodology

Karst caves have a "museum" property to preserve evidence of palaeo-environments, from their location, morphology, hydrology, dimensions and contents. By studying these attributes in the more complex caves, it should be possible to explain local speleogenesis, the evolution of the external landscape, and the varying climatic regimes that the caves and their host regions have experienced. Fortunately, the laws of the physics and chemistry of limestone dissolution have now been derived (Palmer 1991). Dissolution rates are almost immeasurably low during the inception phase in sedimentary limestones and in narrow tectonic inception fractures in marbles, prior to reaching the chemical "breakthrough point" (Dreybrodt 1990). The rates only become significant during the later phases of phreatic and any vadose enlargement. They typically reaching a wall retreat rate limit of ~1 mm per year when unsaturated turbulent water at 10 °C flows continuously from a vegetated catchment area, if that raises P_{CO_2} to 1 % (Palmer 1991). Calcite concentrations remained well below saturation in both deglacial and interglacial environments in Central Scandinavia. Hence, most chemical phreatic enlargement took place at rates that were *maximal* for the prevailing conditions. Dissolution can thus be regarded as either "on" or "off" within applicable timescales, depending on the geometry of the flow path. It follows that the diameters of the phreatic passages and the entrenchment depths of vadose passages can commonly be used to represent linear timescales of enlargement, despite these enlargements taking place under varying flow regimes. Even during deglacial conditions at 0 °C and low P_{CO_2}, the chemical wall retreat rate limit remains significant at ~0.35 mm per year, to which can be added high-flow mechanical erosion that might raise the rate to1mm per year (Faulkner 2006b). In the case of Toerfjellhola, it has a present sink to resurgence path length of c. 350 m and a corresponding depth of 150 m, giving a hydraulic ratio (head / length^2) of $1.2\times10^{-3}m^{-1}$. A minimum tectonic fracture aperture of only 2 mm is needed to maintain phreatic dissolution at a maximum rate here (Faulkner 2006a; 2006b: Fig. 3). Earlier, higher, fractures were shorter and therefore even more likely to enlarge at maximum rates from the outset. Thus, slow pre-breakthrough chemical inception probably does not need to be considered here.

Figure 2. Toerfjellhola resurgence below the blockfield at the lower end of the Overengbakk canyon.

In this methodology, caves and local landscapes are discussed by working backwards in time and upwards in elevation, by applying the TDMO model (Faulkner 2007b) in the reverse order. Hence, by raising the floor levels of surface streams and vadose passages by the amounts estimated to have been entrenched during the Holocene interglacial, the local Eemian topography and hydrological drainage systems can be visualised. This assumes that there was little flow of water during the whole of the Weichselian (MIS5d–2), when the Norwegian mountain chain probably remained continuously glaciated. Active vadose streamways are considered first, followed by any relict vadose elements, and phreatic passages are treated upwards in turn, from active to relict. The deglacial IDL that first enlarged the

highest relict phreatic passage then constrains the time when deglacial uplift produced the tectonic fractures that led to the oldest existing passages. An important factor is the glacial and interglacial erosion of the land surface above the cave. Dowdeswell et al. (2010) showed that an average of 230 m of local bedrock was eroded in the last 600 ka, an average of 38 m per glacial cycle. Other data showed that glacial valleys in Norwegian mountains can deepen by >60 m during each 100ka glacial cycle, whilst, at the same time, glacial erosion can be negligible in areas of low relief. Faulkner (2010) deduced that at Tosenfjord at least, the more-recent glacial erosion has been >>20 m per 100 ka glacial cycle. Grønlie (1975) noted that glacial scouring was intense at Durmålstind, only six km from Toerfjellhola. Sollid and Sørbel (1979) suggested from the general absence of heavily weathered summits, rock pinnacles and autochthonous blockfields that much of this area was last-covered by a fast-flowing warm-based icesheet. However, Overengbakkdal is a side valley to the larger Godvassdal, making its glacial erosion less than average. If the maximum 50 m depth of fractures and conduits of the present cave passages remained roughly constant during its development, the total surface lowering to the highest and presumed oldest parts of Toerfjellhola was also equal to 50 m during that period. This is assumed to cover the glaciations at MIS10, 8, 6 and 5d–2. Dates below commonly refer to ^{14}C years Before Present, with conversions to calendar years from Stuiver et al. (1998: Figs. A7 and A8).

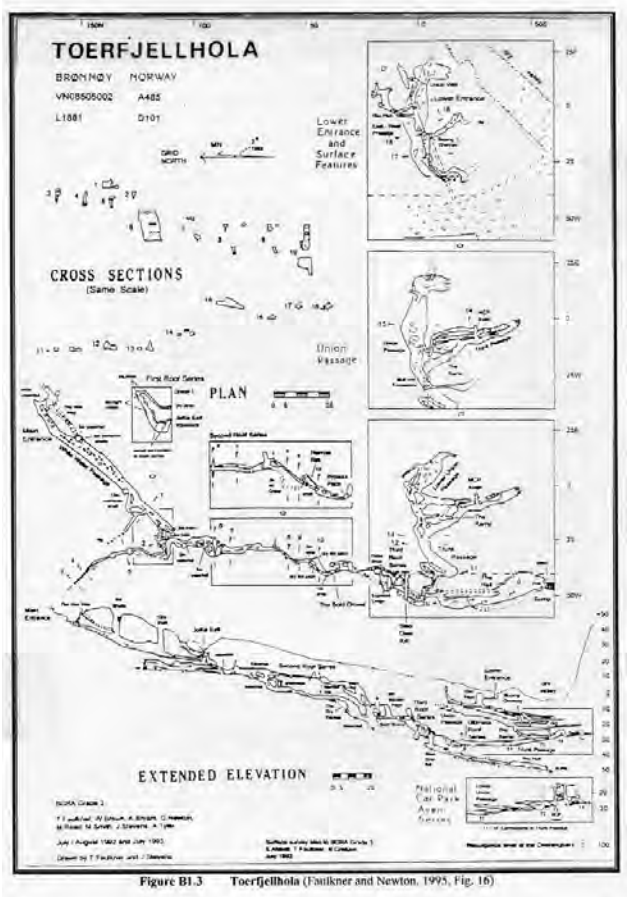

Figure 3. Toerfjellhola This figure is shown at a larger scale by Faulkner and Newton (1995) and Faulkner (2007).

3. Vadose entrenchment

Vadose entrenchment only occurs during interglacial (and possibly interstadial) flow regimes. Hydraulic gradients increased dramatically after the Weichselian valley erosion and deglaciation, promoting the growth of vadose passages by entrenchment of existing phreatic passages or by enlargement of lower inception fractures. The vertical extents of vadose entrenchments and waterfalls below any upper phreatic levels were measured by Faulkner (2009a) from cave surveys for Central Scandinavia: they are nearly all ≤10 m, including in Toerfjellhola. Hence, most local active vadose streamways probably developed within the Holocene, if the continuous rate of limestone dissolution is 1mm per year. None of the cross-sections in Figure 3 have a "double vadose" profile, suggesting that the present streamway and the tributary were not active in any interglacials prior to the Holocene. The Holocene exploitation of inception fractures is shown on Figure 3 by several inaccessible captures along the streamway. Such fractures probably formed neotectonically during the Holocene, giving insufficient time for much enlargement.

Figure 4. Toerfjellhola stream. Photo by M. Smith.

4. Headward recession of waterfalls

Another method to quantify the development timescale of active stream passages is to measure the amount of headward erosion at waterfalls (Faulkner 2009a). Results showed that recessions in most local active caves vary from 2–10 m, again suggesting a Holocene timescale from the

maximum erosion rate of 1.2 mm per year, estimated by White (1990, p170). This also applies to Toerfjellhola, which shows two successive headward erosions of only 5 m each beyond the Dry Pitches (Figure 3). Thus, the main stream appears to be a powerful summer *overfit* (Figure 4), because the entrenchments and recessions along the length of its streamway have dimensions applicable to normal Holocene erosion.

5. Active sump passages

Weichselian deglacial phreatic enlargement likely accounted for passage width increases in the range 1–2 m, when submerged by a flowing IDL that caused chemical and mechanical erosion for up to 1,000 years (Faulkner 2009a). The sump in Toerfjellhola, with a width c. 3 m, is therefore likely to have formed primarily in the Holocene.

6. Relict phreatic and vadose passages

All the relict passages in Toerfjellhola probably drained near the start of the Holocene, and then remained largely unchanged. Those without vadose trenches drained rapidly. The Second Roof Series and East–West Passage (Figure 3: cross-sections 7, 8, 9, 17 and 18) have small, 1 m-scale, relict vadose entrenchments at altitudes from 450–425 m that indicate short-lived vadose flows for a few hundred years. From their elevations, these are unlikely to be caused by present Holocene floods. They probably acted as early Holocene overflow routes before the main streamway was enlarged to its present size. Several relict vadose passages and shafts immediately above the streamway may have been captured earlier in the Holocene, but some are also discussed below as possible Eemian vadose flow routes. Relict possible vadose features in the Ultimate Roof Series may have developed in earlier interglacials, including the wide sloping floors of Union Passage and Lower Union Passage.

7. Early Holocene

Because all the vadose entrenchments, headward erosions and the size of the sump are within expected limits, it is likely that all active parts of the Toerfjellhola system enlarged to their present sizes during the final stages of deglaciation and during the Holocene. The main flow route for the Toerfjellhola stream at the start of the Holocene was probably via the Main Entrance, the Second Roof Series and the Third Roof Series, to a conduit along the roof of The Hall, a route comprising both sumped phreatic and open vadose sections. The present streamway and the inlet passage that joins it near JoKe Exit then existed only as a series of interconnected fractures created by Weichselian deglacial seismicity. As these fractures enlarged, they captured the flows early in the Holocene, which abandoned the higher passages and entrenched the stream passage along its entire length.

8. Weichselian deglaciation speleogenesis

The relict phreatic passages must have enlarged during one or more prior deglaciations or interglacials. Enlargement within a static subglacial lake beneath a warm-based ice sheet over limestone is unlikely, because such a lake would saturate with calcite. However, dissolution within a subglacial waterway leading from a moulin or an IDL to the ice front during deglaciation is also possible. The rather consistent mean diameter of all the local relict phreatic caves is c. 2.0 m, including those at valley floors (Faulkner 2009a). This suggests that these caves, and probably many relict phreatic passages in combination caves, enlarged over similar deglaciation timescales. However, the mean cross-section of Toerfjellhola is 6 m^2, giving an equivalent mean diameter of 2.8 m, suggesting its larger passages pre-date the Weichselian.

The local Weichselian deglaciation was modelled by Faulkner (2005), based on a formula devised by Grønlie (1975). From this model, Toerfjellhola was inundated by a westward-flowing IDL and high pressure subglacial reservoir on the west side of Toerfjell from 10850 BP, when the surface of the icesheet had lowered to the present altitude of 950 m. The Main Entrance at 485 m altitude was submerged to a water depth of 465 m. During the many falls of IDLs on the other (east) side of Toerfjell, their surface levels were controlled by about 17 passes along a 70 km-long, north–south mountain ridge. Pass heights ranged from 950 m down to 810 m, reached at 10400 BP. Nine of these passes have a significant gorge on the western (coastal) side of the ridge, strongly suggestive of a *jökulhlaup* at the change in lake level. The stable lake levels between collapses caused westward flows through these passes into the falling and expanding Toerfjell IDL. A 100 km^2 lake suddenly fell 10 m as the ice collapsed at the 830 m pass-point above a deep canyon at the head of Overengbakkdal. About 1,000 million tonnes of water flowed out before the eastern lake stabilised again. This may account for the valley floor block stream, although glacial erosion and paraglacial processes may also apply.

The final jökulhlaup from the eastern IDL into the Toerfjell IDL flowed through the lowest pass at 700 m altitude at 10200 BP. After that, the eastern IDL had lowered too far to feed the large Toerfjell IDL that still submerged Toerfjellhola and now surrounded the north end of a glacier in Tosenfjord. During these events, the ice margin retreated inland as isostatically-depressed low-lying land became inundated by the sea. The sea finally collapsed the Tosenfjord glacier and the Toerfjell IDL at 9840±90 BP (Faulkner and Hunt, 2009), when the water surface above Toerfjellhola was at the present altitude of 445 m, and the cave suddenly drained. Parts of Toerfjellhola had thus remained submerged by glacial meltwater from 10850 BP until 9840 BP, a duration of 1010 ^{14}C years or c. 1700 cal. years.

Phreatic enlargement by chemical and mechanical erosion is only possible if the water is flowing, and this may not have occurred here below the Plastic Behaviour Limit (Badino 2001). Below this limit, which commonly lies up to 200 m below the ice surface, conduits are unlikely to survive, because they are closed in winter by the pressure of ice. Thus, the passages may only have enlarged in direct

englacial flows to a lower part of the icesheet when within 200 m of the IDL surface. The highest passages in Toerfjellhola could then have enlarged as the ice lowered from 685–485 m, over the period 10300–9900 BP, a duration of 775 cal. years. The lowest passages could only have enlarged as the ice lowered from 584–445 m, over the period 10100–9840 BP, for 500 cal. years. Thus, at a maximum dissolution rate of 1 mma^{-1}, the diameter enlargements could have varied from 1.0–1.6 m in these timescales. These are insufficient to account for the sizes of several passages below the Lower Entrance. Hence, their enlargement probably started prior to the Weichselian deglaciation. Cross-sections 11, 12 and 13 (Figure 3) appear to have "double phreatic" profiles, hinting at enlargements of Trunk Passage at two different times, and there is probable enlargement upwards of relict phreatic elements from The Hall, Trunk Passage / Lower Union Passage to Union Passage, suggesting that higher passages experienced more than one deglaciation. The final (Weichselian) deglacial IDL likely created a phreatic conduit along the roof of the present stream passage that led to Trunk Passage, which grew larger than its pre-Weichselian size. The fact that some of the larger passages were already enlarged before they became drained at the start of the Holocene is shown by the occurrence of unweathered slabs of limestone on their floors, which probably fell there during deglacial seismicity. Moreover, the presence of clay on fallen blocks (presumably deposited in static subglacial lake conditions) suggests that the containing passage already existed before that time.

9. Speleogenesis during the Eemian interglacial

It is assumed that Toerfjellhola was basically unchanged when covered by ice or in periglacial conditions throughout MIS 5d–2. The Eemian interglacial at MIS5e (and the early parts of previous interglacials at MIS9e and MIS11c) probably experienced mid-latitude mean summer temperatures that were warmer than today. There was little, if any, remnant ice, and the mountain summits supported alpine vegetation (Mangerud et al. 1979). Reduced winter precipitation, reduced ablation and increased evapotranspiration probably reduced summer flow rates and durations. Additionally, the relatively high temperatures appear to have lasted for less time during MIS9c, 7e and 5e than in the Holocene, allowing less time for vadose development. This may account for the observed scarcity of relict vadose passages in Central Scandinavia (Faulkner 2009a). In Toerfjellhola, captures of the palaeo-Overengbakk at unknown sinks sent water directly into Union Passage and Lower Union Passage and on via Trunk Passage to an outlet slightly farther down the Overengbakk valley. At least the lower parts of this route were sumped. Most of the passages directly above Union Passage probably remained dry by the end of MIS5e. The main Toerfjellhola stream flowed to Trunk Passage along small passages in the 2nd and 3rd Roof Series, with vadose and phreatic elements.

10. Earlier speleogenesis

The above reasoning can be continued backwards in time to deduce one possible scenario for the cave's history, as summarised in Table 1. Prior to MIS12, two separate palaeocaves existed within the subsequently eroded 50 m of marble bedrock. Deglacial seismicity caused by rapid uplift at the end of this large Elsterian glaciation created fractures at the bases of these caves, whose present manifestations link the 12 m Shaft to JoKe Exit and link an aven above the 10 m Pitch to the Lower Entrance. These fractures enlarged beneath a deglacial IDL, with water emerging via conduits and upper cave systems since removed. During the MIS11, 9 and 7 interglacials, recharges into the two caves were from sinks of the palaeo Toerfjellhola stream and the palaeo Overengbakk, which commonly migrated upstream after each glaciation.

During the MIS11 interglacial, the palaeo Toerfjellhola stream enlarged the 12 m Shaft at the base of the "upper cave" (perhaps partly as a vadose waterfall shaft), with the flow continuing to rise from JoKe Exit. The palaeo Overengbakk enlarged the 10 m Pitch similarly and its water left the known cave via the west end of East–West Passage. The process repeated at the MIS10 deglaciation, with the creation of a longer loop from the 8 m Shaft along the roof of White Water Passage to JoKe Exit and a longer loop via an aven NE of the 10 m Pitch base to the passage below the west end of E–W Passage. The 8m Shaft enlarged during the MIS9 interglacial, and the E–W Passage route enlarged the drop below E–W Passage under a vadose regime, before creating another exit route down the Sloping Chimney to the "dig" passage. The "upper cave" loop was extended back to a fracture at the Main Entrance by the MIS8 deglaciation, and a connection was made in the "lower cave" from E–W Passage via Union View to the roof of Union Passage directly into the "dig" passage. These routes were then enlarged partly under vadose conditions during the MIS 7 interglacial when the floor of Union Passage was widened (cross-section 15). An MIS 6 Late Saalian deglacial IDL flooded and enlarged all the passages then existing and created an exit from the south end of Union Passage. Uplift created new fractures that initiated connections from Union Passage to Trunk Passage via The Ramp and also from Lower Union Passage to Trunk Passage. At the same time, new fractures along the 2nd and 3rd Roof Series connected the two caves.

11. Conclusions

Few cave passages in Central Scandinavia contain multiple phreatic loops in series (Faulkner 2005). Toerfjellhola is distinctive in apparently having one palaeo loop along the roof of White Water Passage that rises into JoKe Exit and another that starts at the adjacent capture point and follows the 2nd and 3rd Roof Series into Trunk Passage, suggesting this cave previously existed as two separate caves. Many local caves also do not consist of fully-symmetrical phreatic loops, but contain instead a tiered series of "incomplete loops", which are choked at their down-valley rising limbs.

These give the appearance of subsequent truncation by removal of upward cave loops by glacial valley deepening and widening. However, another possibility is that such phreatic passages only developed as incomplete half-loops during deglaciation, when the cave hydrology was integrated with that of an ice-dammed lake and the continuing icesheet. For both possibilities, any continuing "passages" are now "virtual", having been removed either by glacial truncation or by the disappearance of englacial conduits with the melting of the ice sheet. For Toerfjellhola, at least, the possibility that complete phreatic loops developed before being removed by glacial erosion seems unlikely, because the limestone outcrop does not seem to continue in the required direction. Also, if the valley floor was much higher than at present, then the lowest level passage formed at a distance greater than 50 m from the surface, which would be exceptional for local caves. Thus, it seems likely that the phreatic half-loop passages developed to their present sizes under one or more Toerfjell IDLs. The common lack of vadose entrenchment at the down-valley ends of phreatic loop passages (Faulkner 2005), as applies in Toerfjellhola, also confirms that a sudden collapse in the level of the IDL was the normal outcome. A gradual lowering would instead have permitted vadose flows through each tiered passage in sequence.

Toerfjellhola is concluded to be a multi-cycle cave developed from two separate palaeocaves since MIS12. It may contain the oldest surviving cave passages in Central Scandinavia, despite Isacsson (1999) suggesting that the complex Swedish cave **Korallgrottan** was fully-formed in the Pliocene. The oldest well-dated speleothem in north Norway appears to be from **Hammernesgrotta** (500 ka: Lauritzen et al. 1994), indicating growth in MIS13. Faulkner (2009b) briefly surmised that **Rågge Javre-Raige** may have passages that have survived for ~1 Ma, and discussed why some caves in northern Scandinavia may be older than those in any other Caledonide terrane. It is argued here that passages in Toerfjellhola commonly developed phreatically *prior* to their vadose entrenchment, giving them "upside-down" morphology, in contrast to that of many cave systems in sedimentary limestones. This methodology has relied only on karst and local geomorphological information to derive a scenario for speleogenesis. It may also apply for the Quaternary history of caves in sedimentary limestones in glaciated regions. If any dating information from internal chemical and clastic deposits becomes available, that should at least confirm the minimum ages of the containing passages.

Table 1. Possible development stages for Toerfjellhola.

MIS Stage	Age ka	Description	Main upper flow route	Main lower flow route	Comments
12 / 11c	427	Elsterian deglaciation	12 m Shaft to JoKe Exit	Aven above 10 m Pitch to Lower Entrance	Two separate caves existed within c. 50 m of removed bedrock, with phreatic dissolution along these lowest fractures.
11c–11a	427–362	Interglacial	12 m Shaft to JoKe Exit	10 m Pitch to E–W Passage end	Two separate caves. Mostly phreatic dissolution.
10 / 9e	336	Early Saalian deglaciation	8 m Shaft to JoKe Exit	Aven NE of 10 m Pitch to upper & lower SW ends	Two separate caves. All phreatic dissolution.
9e–9a	336–303	Interglacial	8 m Shaft to JoKe Exit	Aven and E–W Passage via Sloping Chimney to "dig"	Two separate caves. Upper cave: mostly phreatic dissolution below shafts. Lower cave: vadose and phreatic dissolution.
8 / 7e	243	Mid Saalian deglaciation	Main Entrance to JoKe Exit	Aven and E–W Passage via Union Passage roof to exits	Two separate caves. All phreatic dissolution
7e–7a	243–186	Interglacial	Main Entrance to JoKe Exit	Aven via Union View to passage before "dig"	Two separate caves. Upper cave: mostly phreatic dissolution below shafts. Lower cave: vadose and phreatic dissolution.
6 / 5e	129	Late Saalian deglaciation	Main Entrance to JoKe Exit	Aven via Union View to exit beyond The Ramp	Two separate caves. All phreatic dissolution
5e	129–115	Eemian Interglacial	Main Entrance via 2nd & 3rd Roof Series to an exit from Trunk Passage	Inlets to Union Passage via The Ramp and via Lower Union Passage to an exit from Trunk Passage	The two caves are now connected. Upper part: mainly vadose to the small 2nd and 3rd Roof Series, which vary vadose and phreatic. Lower part: mainly vadose. Trunk Passage: phreatic.
2 / 1	c. 12	Weichselian deglaciation	Most of the whole cave above the present stream route, including an inlet via Lower Union Passage to Trunk Passage		All phreatic dissolution
1	c. 9	Early Holocene Interglacial	Main Entrance and the present tributary via 2nd & 3rd Roof Series and roof of present streamway to a small exit from The Hall		Mixed vadose and phreatic elements
1	0	Late Holocene Interglacial	Main Entrance and the present tributary to the sump		Mainly vadose, with inaccessible partly flooded lower captures

References

Badino G, 2001. Glacial karst phenomenology. Proceedings of the 13th International Speleological Congress. Paper 179, 5.

Dowdeswell JA, Ottesen D, Rise L, 2010. Rate of sediment delivery from the Fennoscandian Ice Sheet through an ice age. Geology, 38 (1), 3–6.

Dreybrodt W, 1990. The role of dissolution kinetics in the development of karst aquifers in limestone: a model simulation of karst evolution. Journal of Geology, 98 (5), 639–655.

Engh R, Sjöberg R, 1981. Svenska Grottor Nr. 4. Karst och Grottor i svenska fjällen, 58.

Faulkner TL, 2005. Cave inception and development in Caledonide metacarbonate rocks. PhD Thesis. University of Huddersfield.

Faulkner T, 2006a. Tectonic inception in Caledonide marbles. Acta Carsologica, 35 (1), 7–21.

Faulkner T, 2006b. Limestone dissolution in phreatic conditions at maximum rates and in pure, cold, water. Cave and Karst Science, 33 (1), 11–20.

Faulkner T, 2007a. The one-eighth relationship that constrains deglacial seismicity and cave development in Caledonide marbles. Acta Carsologica, 36 (2), 195–202.

Faulkner T, 2007b. The top-down, middle-outwards model of cave development in Caledonide marbles. Cave and Karst Science, 34 (1), 3–16.

Faulkner T, 2009a. Relationships between cave dimensions and local catchment areas in Central Scandinavia: implications for speleogenesis. Cave and Karst Science, 36 (1), 11–20.

Faulkner T, 2009b. The general model of cave development in the metalimestones of the Caledonide terranes. Proceedings of the 15th International Speleological Congress, Kerrville, USA. Vol. 2 863–870.

Faulkner T, 2010. An external model of speleogenesis during Quaternary glacial cycles in the marbles of central Scandinavia. Cave and Karst Science, 37 (3), 79–92.

Faulkner TL, Hunt CO, 2009. Holocene deposits from Neptune's Cave, Nordland, Norway: environmental interpretation and relation to the deglacial and emergence history of the Velfjord–Tosenfjord area. Boreas, 38, 691–704.

Faulkner T, Newton G, 1995. Toerfjellhola and Other Caves at Vevelstad and Brønnøy, Norway. Cave and Karst Science, 22 (1), 3–22.

Ford DC, Williams P, 2007. Karst hydrogeology and geomorphology. John Wiley and Sons, 562.

Fredin O, 2002. Glacial inception and quaternary mountain glaciations in Fennoscandia. Quaternary International, 95/96, 99–112.

Grønlie A, 1975. Geologien I Vefsnbygdene. Vefsn Bygdebok 1975, 417–483.

Gustavson M, 1988. Mosjøen. Description of the 1:250,000 bedrock geological map. Norges Geologiske Undersøkelse. Skrifter 87, 47.

Häuselmann P, Granger DE, Jeannin P-Y, Lauritzen S-E, 2007. Abrupt glacial valley incision at 0.8Ma dated from cave deposits in Switzerland. Geology, 35 (2), 143–146.

Isacsson G, 1999. Korallgrottan – ett nyckelhål till historien. Jämtlands Grottförening Årsskrift 1999, 9–11, 18.

Lauritzen, S-E, Haugen, JE, Løvlie, R and Gilje-Nielsen, H. 1994. Geochronological potential of isoleucine epimerization in calcite speleothems. Quaternary Research 41, 52–58.

Lowe DJ, Gunn J, 1997. Carbonate Speleogenesis: An Inception Horizon Hypothesis. Acta Carsologica, 26/2, 38, 457–488.

Mangerud J, Sønstegaard E, Sejrup H-P, 1979. Correlation of the Eemian (interglacial) stage and the deep-sea sea oxygen-isotope stratigraphy. Nature, 277, 189–192.

Palmer AN, 1991. Origin and Morphology of limestone caves. Geological Society of America Bulletin, 103, 1–21.

Sollid JL, Sørbel L, 1979. Deglaciation of western central Norway. Boreas, 8, 233–239.

Stuiver M and 9 authors, 1998. INTCAL 98 radiocarbon age calibration, 24000–0 cal BP. Radiocarbon, 40 (3), 1041–1083.

White WB, 1990. Chapter 7. Surface and near-surface karst landforms. in Higgins CG, Coates DR (Eds.). Groundwater geomorphology: The role of subsurface water in Earth-surface processes and landforms. Geological Society of America Special Paper, 252, 157–175.

HOW DO APERTURE SIZES IN LIMESTONE VARY FOR THE ONSETS OF TURBULENT FLOW AND FIRST-ORDER DISSOLUTION KINETICS?

Trevor Faulkner
Limestone Research Group, Geography, Earth and Environmental Sciences, University of Birmingham, Edgbaston, Birmingham, B15 2TT, UK, trevor@marblecaves.org.uk

It is commonly stated in the literature that the "breakthrough" point at the transition from slow high-order to fast first-order dissolution kinetics in limestone occurs at an exit aperture of about one centimetre, and that this coincides with the transition from a wholly laminar flow to a turbulent flow. These relationships are approximately true for a range of conduit geometries in sub-horizontally bedded strata. However, the exit aperture for the onset of turbulence varies with the hydraulic gradient whereas the exit aperture for the onset of first-order kinetics varies with the hydraulic ratio, which is the hydraulic gradient divided by the path length. These transitions only occur at the same exit aperture for planar fissures and cylindrical tubes of lengths 290 m and 452 m. Breakthrough can occur before or after the onset of turbulence. Aperture sizes for breakthrough and turbulence can be over a metre for long and shallow conduits but sub millimetre for short and steep conduits. This paper analyses these relationships for many conduits in natural and artificial conditions and discusses their relevance to the multitude of possible karst situations, where hydraulic ratios can be considered over 17 orders of magnitude.

1. Introduction

The physics and chemistry of limestone dissolution along planar fissures and cylindrical conduits were derived in two key papers over twenty years ago by Dreybrodt (1990) and Palmer (1991). These built on important earlier works, including those by Weyl (1958), Bögli (1964), White (1977) and Palmer (1981). A later treatise to present detailed (and animated) models of speleogenesis based on the principles of the Palmer / Dreybrodt model is that by Dreybrodt et al. (2005). Palmer (1991: Eq. 6) showed that when water flows past any point in a conduit in natural limestone, the rate of solutional wall retreat (S) is:

$$S = 31.56k_n(1/\rho)(1 - C/C_s)^n \text{ cm per year,}$$

where k_n mg-cm L^{-1} s^{-1} is the appropriate reaction coefficient, ρ gm cm^{-3} is the density of the limestone, C gm cm^{-3} is the point concentration of calcite in solution, C_s gm cm^{-3} is the appropriate saturation concentration of calcite and n is the reaction order. k_n, C and C_s vary with temperature and P_{CO2} levels. $k_{n>1}$ also varies with C/C_s, and C also varies with the geometrical and hydrological parameters of the conduit. Dissolution when the solution is well below saturation occurs at a fast "first-order kinetics" rate, where n = 1. At the beginning of the conduit, C is at a minimum, and may be close to zero for an allogenic stream running from non-carbonate rocks. In this case, dissolution at the entrance is at the appropriate maximum rate of $S_{max} = 31.56k_1/\rho$ cm a^{-1}. The calcite concentration increases downstream from the entry point. If C approaches C_s, the dissolution rate becomes small and the reaction proceeds with "higher-order kinetics" as the flow continues. The change occurs near a point along the conduit that Weyl (1958) called the "penetration length", where $0.6 < C/C_S < 0.9$, dependent on temperature and P_{CO2}. Beyond here, $n \geq 4$, governed by non-calcitic impurities, and "mixing corrosion" (Bögli 1964) can be important if sustained over long geological timescales. The Palmer/Dreybrodt model quantifies the gradual conduit enlargement under slow high-order kinetics as the penetration length slowly increases. When it reaches to the exit of the aperture, there is a "kinetic trigger" (White 1977) and dissolution then occurs at the applicable maximum first-order rate over the whole length of the flow path, to create a conduit with a near-uniform cross-section. This important event in karst evolution is called the "breakthrough point" (Dreybrodt 1990). If limestone comprised pure calcite, the penetration length might not increase and caves would then only form if initial fracture geometries allowed immediate first-order dissolution kinetics, i.e. "tectonic inception" (Faulkner 2006a; 2006b). When C/C_s becomes < c. 60 %, "breakthrough behaviour" dominates and mixing corrosion is unimportant (Romanov et al. 2003). At 10 °C and with the inflowing water containing 1% CO_2, $S_{max} \approx 1$ mm per year (Palmer 1991), although even faster dissolution rates seem possible in water that is extremely unsaturated (e.g., Palmer 1991: Fig. 8). Wall retreat rates may also be increased by mechanical erosion, which is lithology dependent and amplified in turbulent flow. White (1977) pointed out that the kinetic trigger can occur at an exit aperture of 1–10 mm, a range that has been widely quoted. He also stated that this coincides approximately with the size at which wholly laminar flow starts to become turbulent (without there being a causal relationship), and this "coincidence" has also been widely assumed. This paper analyses these relationships and discusses their relevance to the multitude of possible karst situations.

Flow rates, water velocities and the transition to turbulent flow in conduits are controlled by the hydraulic gradient (HG; Head / path length = H/L), among other variables. The main parameters at the chemical breakthrough point are controlled by a geometrical variable called the "hydraulic ratio", which equals the hydraulic gradient divided by the path length (HR; H/L^2; Dreybrodt 1990). The necessity for the extra divisor can be understood, because dissolution always proceeds along the whole path length. Based on the work of Palmer (1991), which itself was based on the Hagen-Poiseuille Equations for laminar flow, these relationships were plotted graphically by Faulkner (2006a: Fig. 3). Those curves illustrated the linear relationships among the logarithms of hydraulic conductivity, water

velocity, flow rate, hydraulic ratio and the exit apertures at the breakthrough point for both wide planar fissures and circular tubes of lengths 1–1,000 m. Also shown were the applicable Reynolds numbers (see below) for each flow regime. Some of these relationships are presented in Table 1 and illustrated in a modified format in Figure 1. This plots the minimum fissure exit aperture or tube radius in centimetres for the establishment of first-order kinetics, plus the minimum conduit size for the onset of turbulent flow, against the hydraulic gradient of the conduit. Logarithmic scales are used in Figure 1, with the axes values chosen to exceed the extreme ranges likely to apply in natural and artificial karst systems. The minimum conduit sizes for the onset of turbulent flow vary with cross-section shape, but are independent of conduit length for uniform conduits. Those for the chemical breakthrough point vary with conduit shape as well, but also vary with length; they are shown for five set lengths from 1–10,000 m.

Table 1. Fissure and tube sizes for the onsets of turbulence and first-order kinetics for various lengths and hydraulic gradients.

Length L	Hydraulic gradient H/L	Aperture $w_t = 0.1663 * HG^{-½}$	Radius $r_t = 0.1153 * HG^{-½}$	Hydraulic Ratio (HR) H/L^2	log w_{fo} = -(4.80 + logHR)/3	Aperture w_{fo}	log r_{fo} = -(5.47 + logHR)/3	Radius r_{fo}
m	HG	cm	cm	m^{-1}		cm		cm
10,000	1.00E-09	166.1907	115.2344	1.00E-13	2.7333	541.1695	2.5100	323.5937
1,000	1.00E-08	77.1448	53.4912	1.00E-11	2.0667	116.5914	1.8433	69.7161
100	1.00E-07	35.8102	24.8303	1.00E-09	1.4000	25.1189	1.1767	15.0199
10	1.00E-06	16.6229	11.5261	1.00E-07	0.7333	5.4117	0.5100	3.2359
1	1.00E-05	7.7163	5.3503	1.00E-05	0.0667	1.1659	-0.1567	0.6972
10,000	1.00E-08	77.1448	53.4912	1.00E-12	2.4000	251.1886	2.1767	150.1989
1,000	1.00E-07	35.8102	24.8303	1.00E-10	1.7333	54.1170	1.5100	32.3594
100	1.00E-06	16.6229	11.5261	1.00E-08	1.0667	11.6591	0.8433	6.9716
10	1.00E-05	7.7163	5.3503	1.00E-06	0.4000	2.5119	0.1767	1.5020
1	1.00E-04	3.5818	2.4836	1.00E-04	-0.2667	0.5412	-0.4900	0.3236
10,000	1.00E-07	35.8102	24.8303	1.00E-11	2.0667	116.5914	1.8433	69.7161
1,000	1.00E-06	16.6229	11.5261	1.00E-09	1.4000	25.1189	1.1767	15.0199
100	1.00E-05	7.7163	5.3503	1.00E-07	0.7333	5.4117	0.5100	3.2359
10	1.00E-04	3.5818	2.4836	1.00E-05	0.0667	1.1659	-0.1567	0.6972
1	1.00E-03	1.6627	1.1529	1.00E-03	-0.6000	0.2512	-0.8233	0.1502
10,000	1.00E-06	16.6229	11.5261	1.00E-10	1.7333	54.1170	1.5100	32.3594
1,000	1.00E-05	7.7163	5.3503	1.00E-08	1.0667	11.6591	0.8433	6.9716
100	1.00E-04	3.5818	2.4836	1.00E-06	0.4000	2.5119	0.1767	1.5020
10	1.00E-03	1.6627	1.1529	1.00E-04	-0.2667	0.5412	-0.4900	0.3236
1	1.00E-02	0.7718	0.5352	1.00E-02	-0.9333	0.1166	-1.1567	0.0697
10,000	1.00E-05	7.7163	5.3503	1.00E-09	1.4000	25.1189	1.1767	15.0199
1,000	1.00E-04	3.5818	2.4836	1.00E-07	0.7333	5.4117	0.5100	3.2359
100	1.00E-03	1.6627	1.1529	1.00E-05	0.0667	1.1659	-0.1567	0.6972
10	1.00E-02	0.7718	0.5352	1.00E-03	-0.6000	0.2512	-0.8233	0.1502
1	1.00E-01	0.3583	0.2484	1.00E-01	-1.2667	0.0541	-1.4900	0.0324
10,000	1.00E-04	3.5818	2.4836	1.00E-08	1.0667	11.6591	0.8433	6.9716
1,000	1.00E-03	1.6627	1.1529	1.00E-06	0.4000	2.5119	0.1767	1.5020
100	1.00E-02	0.7718	0.5352	1.00E-04	-0.2667	0.5412	-0.4900	0.3236
10	1.00E-01	0.3583	0.2484	1.00E-02	-0.9333	0.1166	-1.1567	0.0697
1	1.00E+00	0.1663	0.1153	1.00E+00	-1.6000	0.0251	-1.8233	0.0150
10,000	1.00E-03	1.6627	1.1529	1.00E-07	0.7333	5.4117	0.5100	3.2359
1,000	1.00E-02	0.7718	0.5352	1.00E-05	0.0667	1.1659	-0.1567	0.6972
100	1.00E-01	0.3583	0.2484	1.00E-03	-0.6000	0.2512	-0.8233	0.1502
10	1.00E+00	0.1663	0.1153	1.00E-01	-1.2667	0.0541	-1.4900	0.0324
1	1.00E+01	0.0772	0.0535	1.00E+01	-1.9333	0.0117	-2.1567	0.0070
10,000	1.00E-02	0.7718	0.5352	1.00E-06	0.4000	2.5119	0.1767	1.5020
1,000	1.00E-01	0.3583	0.2484	1.00E-04	-0.2667	0.5412	-0.4900	0.3236
100	1.00E+00	0.1663	0.1153	1.00E-02	-0.9333	0.1166	-1.1567	0.0697
10	1.00E+01	0.0772	0.0535	1.00E+00	-1.6000	0.0251	-1.8233	0.0150
1	1.00E+02	0.0358	0.0248	1.00E+02	-2.2667	0.0054	-2.4900	0.0032
10,000	1.00E-01	0.3583	0.2484	1.00E-05	0.0667	1.1659	-0.1567	0.6972
1,000	1.00E+00	0.1663	0.1153	1.00E-03	-0.6000	0.2512	-0.8233	0.1502
100	1.00E+01	0.0772	0.0535	1.00E-01	-1.2667	0.0541	-1.4900	0.0324
10	1.00E+02	0.0358	0.0248	1.00E+01	-1.9333	0.0117	-2.1567	0.0070
1	1.00E+03	0.0166	0.0115	1.00E+03	-2.6000	0.0025	-2.8233	0.0015
10,000	1.00E+00	0.1663	0.1153	1.00E-04	-0.2667	0.5412	-0.4900	0.3236
1,000	1.00E+01	0.0772	0.0535	1.00E-02	-0.9333	0.1166	-1.1567	0.0697
100	1.00E+02	0.0358	0.0248	1.00E+00	-1.6000	0.0251	-1.8233	0.0150
10	1.00E+03	0.0166	0.0115	1.00E+02	-2.2667	0.0054	-2.4900	0.0032
1	1.00E+04	0.0077	0.0054	1.00E+04	-2.9333	0.0012	-3.1567	0.0007

2. Onset of turbulent flow

By convention, dimensionless Reynolds Numbers (R_e) are used to characterise flow regimes in fissures and pipes. These are commonly defined as: $R_e = w\rho V/\mu$ (fissure) and $R_e = 2r\rho V/\mu$ (tube), where w cm = aperture width of a fissure, r cm = radius of a cylindrical tube, ρ = the density of the water = 1gm cm^{-3}, V cm sec^{-1} = its mean velocity and μ = its dynamic viscosity = 0.01307 gm cm^{-1} sec^{-1} at 10 °C (Ford and Williams 2007: p112).

Laminar flows in fissures and tubes obey the Hagen-Poiseuille Equations: $V = w^2\rho g^*HG/12\mu$ (fissure) and $V = r^2\rho g^*HG/8\mu$ (tube), by re-arrangement of Palmer (1991: Eq. 3), where g = 981 cm sec^{-2} is the gravitational acceleration, HG = Hydraulic Gradient. Normally, $0 \leq HG \leq 1$, which is the normal maximum for vertical flow paths under subaerial conditions. $HG > 1$ is possible for inlets submerged beneath a reservoir or lake.

The above equations can be re-arranged to state the applicable aperture and radius in terms of the Reynolds Number:

$w = [12\mu^2R_e/(\rho^2g^*HG)]^{⅓}$ cm (fissure) and

$r = [4\mu^2R_e/(\rho^2g^*HG)]^{⅓}$ cm (tube).

The value of R_e at which flows in karst conduits start to become turbulent is assumed to be 2,200 (Kaufmann and Braun 1999). Substituting this value and the other given constants into these equations gives: $w_t = 0.1663(HG)^{-⅓}$ cm (fissure) and $r_t = 0.1153(HG)^{-⅓}$ cm (tube), where w_t and r_t are the minimum aperture or radius for the onset of turbulent flow in fissures or tubes in limestone. Two plots in Figure 1 show how these vary from 166 cm or 115 cm at $HG = 10^{-9}$ via 0.018 cm or 0.012 cm at $HG = 10^0$ to 0.008 cm or 0.005 cm at $HG = 10^4$.

3. Onset of first-order kinetics

The approximate fissure aperture (w_{fo}) and tube radius (r_{fo}) at the breakthrough point at 10 °C with 1% P_{CO2} for an unsaturated input stream (i.e. C_0 = 0 gm $CaCO_3$ cm^{-3}) were derived by Faulkner (2006a) from the discussion by Palmer (1991: p8 and Figs. 12a and 12b). These gave: $\log w_{fo} = \log r_{fo} = -(5 + \log HR)/3$, where HR m^{-1} = the hydraulic ratio and the path length L is measured in metres. However, more accurate derivations are: $\log w_{fo} = -(4.80 + \log HR)/3$ and $\log r_{fo} = -(5.47 + \log HR)/3$, which are used to generate five length plots in Figure 1 for both fissures and tubes. These show how the aperture or radius required vary from 541 cm or 324 cm for a 10 km flow route with $HG = 10^{-9}$ and $HR = 10^{-13}$ m^{-1} via 0.12 cm or 0.08 cm for a 100 m length with $HG = 10^0$ and $HR = 10^{-2}$ m^{-1} to 0.0012 cm or 0.0007 cm for a 1 m length with $HG = 10^4$ and $HR = 10^4$ m^{-1}.

4. Coincidence of turbulence and breakthrough

The onsets of turbulent flow and first-order kinetics coincide at the same conduit sizes if: $w_t = w_{fo}$ (fissures) or $r_t = r_{fo}$ (tubes), i.e. if: $\log w_t = \log[0.1663(HG)^{-⅓}] = -(4.80 + \log HR)/3$ or if: $\log r_t = \log[0.1153(HG)^{-⅓}] = -(5.47 + \log HR)/3$.

Noting that HR = HG/L, these relationships simplify at coincidence to L = 290 m (fissures) and L = 452 m (tubes), for any hydraulic gradient and its related conduit size. Because 100 m-long fissures have a similar aperture at breakthrough as the radius of a 100 m-long tube at the onset of turbulence for each HG, and 1,000 m-long fissures have a similar aperture at the onset of turbulence as the radius of a 1,000 m-long tube at breakthrough, these two pairs of curves almost coincide on Figure 1.

5. Discussion

Karst hydrologists state that hydraulic gradients commonly occur in the range 10^{-2} to 10^{-4} for karst aquifers in sub-horizontal sedimentary limestones (e.g., White 1988: p165). From Figure 1, the breakthrough point in a 100 m-long fissure or tube occurs when the aperture or radius reaches 0.54–2.51 cm or 0.32–1.50 cm over this HG range. For 1,000 m- and 10,000 m-long flow routes, the required sizes increase to 1.17–5.41 cm or 0.70–3.24 cm and 2.51–11.66 cm or 1.50–6.97 cm. However, for long flow paths with $HG \leq 10^{-4}$, they can increase up to several metres. For steep flows with $10^{-2} \leq HG \leq 10^0$, they can reduce to < 1 mm. For fissures or tubes that are < 290 m or < 452 m long at any HG, the onset of turbulent flow occurs after their exit widths or radii reach their breakthrough sizes, but will be gained under fast first-order kinetics. For conduits longer than those lengths, turbulence starts before breakthrough is achieved. The Palmer/Dreybrodt analysis applies only for laminar flow. For each conduit size, turbulence reduces the mean velocity and discharge rate. Hence, for these longer conduits, the onset of first-order dissolution is delayed and might only be achieved at larger aperture sizes than shown. Beyond the "central" ranges of HG from 10^{-2} to 10^{-4} and L from 100–1,000 m, Figure 1 illustrates the applicable breakthrough points and onsets of turbulence at the extreme limits of both natural and artificial practical situations, as discussed below.

6. Breakthrough time

Dreybrodt (1990) and Palmer (1991) presented similar equations to represent T_B, the time taken for a planar fissure with an initial aperture of w_0 to achieve breakthrough. A simplified form of Palmer (1991: Eq. 8) is: $T_B = \text{constant}^*w_0^{-3.12}*(HR)^{-1.37}$ years, where the constant varies with temperature and the P_{CO2} of the input stream. Palmer (1991: Fig. 13) plotted T_B against HR for various w_0 from 0.001–0.1 cm for $1{,}000{,}000 \geq T_B \geq 100$ years. For T_B <100 years, the linear relationships on log-log scales breakdown, reaching $T_B = 0$ for conditions at tectonic inception (Faulkner 2006a: Fig. 5). Hence, there is a wide range of breakthrough times in natural karst systems that vary with hydraulic gradient, conduit length and initial aperture.

7. Diagenesis

Limestone is commonly formed by carbonate deposition in shallow tropical or deep marine environments, followed by

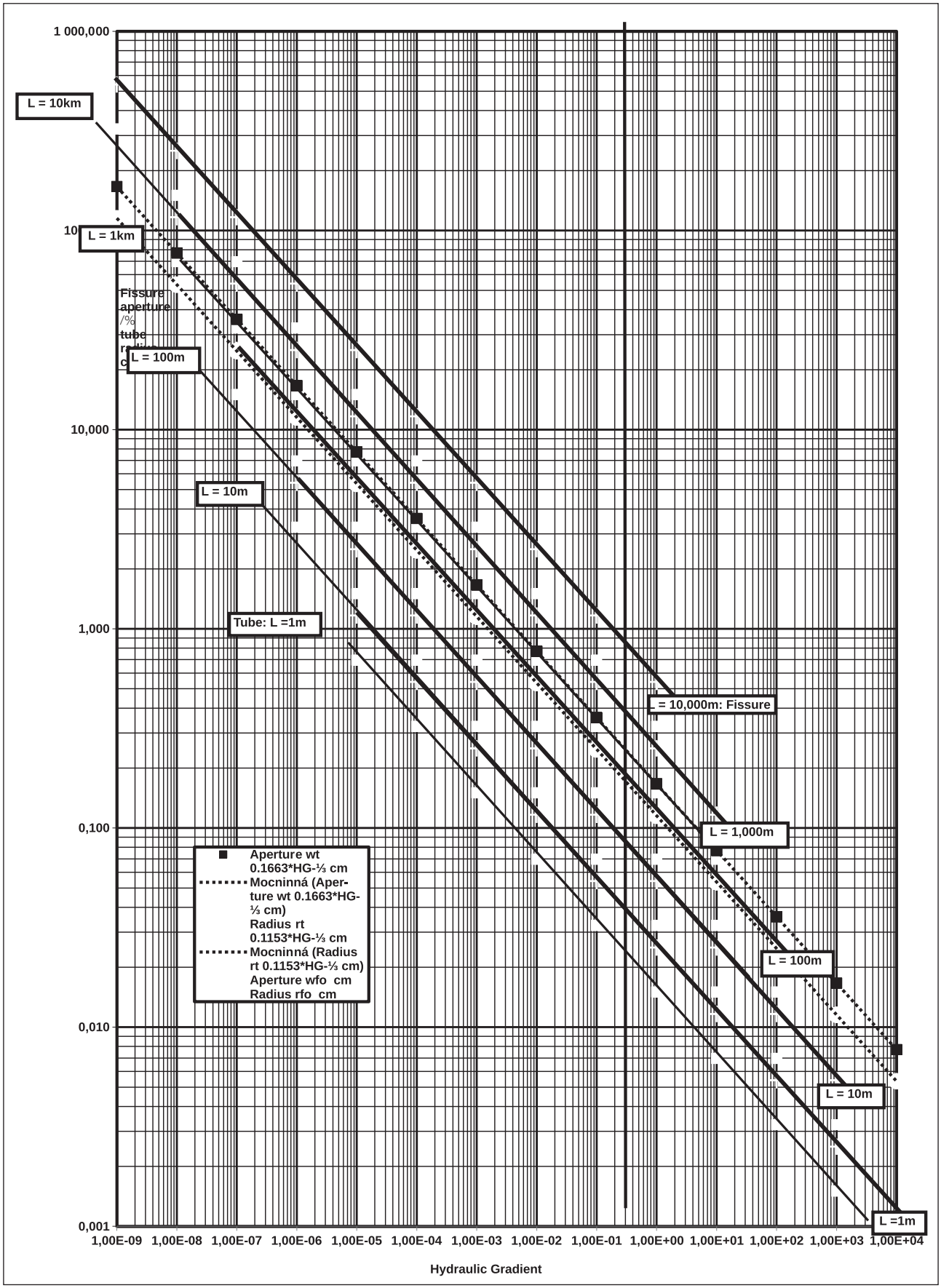

Figure 1. Minimum fissure aperture (wt or wfo) and tube radius (rt or rfo) in cm for the onset of turbulent flow or first order dissolution kinetics at 10 °C and 1% PCO2, plotted against hydraulic gradient (HG). wt (dashed lines) and rt (dotted lines) are independent of path length. wfo and rfo (solid lines) are shown for path lengths of 1 m, 10 m, 100 m, 1,000 m and 10,000 m. The vertical line indicates the maximum HG of 1, for vertical flow paths under normal subaerial conditions. For karst submerged by a reservoir or lake, HG can be >1.

compaction, lithification, and diagenesis in partly meteoric waters. During diagenesis, apertures are at the scale of the pores between crystals, orders of magnitude below values in Figure 1, so that chemical breakthrough does not apply.

8. Long drainage basins

Following exhumation and uplift, initial flows in homogeneous non-fractured limestone would be along inception horizons, perhaps in an adjacent more permeable lithology (Lowe and Gunn 1997). Apertures commonly remain at the pore scale, so that breakthrough is still not possible, even with short vertical flow paths, until high-order dissolution eventually creates conduits with w > 0.001 cm. For example, for long "shallow" karst aquifers, i.e. those ≥ 1 km in length with HG ≤ 10^{-2}, chemical breakthrough does not occur until the conduit reaches over 1 cm in size. From Palmer (1991: Fig. 13), this would take over one million years, if the initial aperture was 0.01 cm.

For long fractured limestone aquifers, the flow route might reach deep below the surface and even pass through non-calcitic lithologies before rising to the resurgence. Because natural fractures tend to reduce in size with depth and the rock temperature increases, the flow would follow a path through apertures of varying initial size at varying temperatures, with the possible addition of strong acid dissolution. The effect on breakthrough times is much more complex. This is the realm of hypogene speleogenesis (Klimchouk 2007), where this new science still requires considerable analysis and quantification (Faulkner 2007a).

9. Shorter drainage routes

The initial apertures of shorter fracture networks probably lie in the range 0.001–0.1 cm. From Figure 1, only those short flow paths with L < 10 m, w > 0.01 cm and HG > 10^{-2} could exhibit breakthrough behaviour. However, fractures in the "common" HG range 10^{-2} – 10^{-4} with 1.0 cm > w > 0.1 cm (which may apply close to the surface) could be at breakthrough for L < 1,000 m.

10. Tall vertical fractures

It is conceivable that limestone cliffs, including any ≥ 1 km high, could have vertical fracture systems that reach from the cliff top to the cliff base. Water percolating down such fractures at HG = 1 would reach the breakthrough point at an aperture of 0.25 cm, if there is enough recharge to keep the fissure filled with water. For shorter cliffs, the required apertures are smaller. This explains the numerous marble cave entrances located near valley shoulders in Central Scandinavia (Faulkner 2005).

11. Epikarst joints and limestone pavements

In the epikarst, water-filled vertical joints ≤ 10 m high that transmit water into a lower vadose zone would need apertures of only 0.05 cm to achieve first-order kinetic dissolution. This is the place where joint openings are naturally the largest, from surface stress relief and other processes. Hence, breakthrough is reached quickly here, or even immediately on the opening of a joint, if it is large enough for tectonic inception. This explains the epikarst phenomenon, where cave entrance passages can be showered with water during heavy rain. Similarly, new dolines can form rapidly in abandoned limestone quarries (Gunn and Gagen 1987). Vertical grikes ≤1 m deep are common in limestone pavements. They achieve fast dissolution with apertures of 0.025 cm, making tectonic inception even more likely here. Smooth pavements under continuous rainfall would lower up to 0.5 mm per year by dissolution, best exemplified by 1.5 m of marble erosion in the Holocene at Madre de Dios, Chile (Faulkner 2009).

12. Speleothem dripwaters

Speleothem deposition occurs when dissolved calcite precipitates by CO_2 vigorously degassing in cave air, where the dripwater flow reaches an open passage roof or wall. If autogenic water at 10 °C seeps through a non-carbonate rock with P_{CO2} of 1% derived from overlying soils, it will contain little dissolved calcite before entering the limestone, but will then reach calcite saturation in closed conditions at 50 mg L^{-1} (Palmer 1991: Fig. 7). Similar autogenic water flowing through calcareous soils with 1% P_{CO2} continuously maintained in open conditions could saturate at 212 mg L^{-1} before entering the lime-stone. The P_{CO2} of cave air does not normally fall below the level of the surface atmospheric, presently 0.04%. Water under such conditions saturates at 12 or 68 mg L^{-1} in closed or open conditions, respectively. Assuming degassing occurs under open conditions, drips may thus become aggress-ive, with no deposition, or deposit a maximum of 144 mg of speleothem from each litre of water. Water flowing from a passage via fissures in its floor that drips into a lower passage may experience "prior calcite precipitation" (Fairchild and Baker, 2012, p. 26). It will then become aggressive or deposit speleothem again, depending on the relative P_{CO2} of the cave air in the two passages.

It seems conceivable that dripwaters could achieve chemical breakthrough and then enlarge bedding planes and joints along their flow path, to create explorable passages and shafts. However, the presence of large and old speleothems in many caves suggests that dripwaters enter the limestone nearly saturated and/or flow in long tiny fissures, remaining near saturation for >> 100,000 years. In the competition between the slow enlargement of the dripwater flow path and the lower P_{CO2} level of cave air, degassing should help retain the chemical regime before the drip exit in a pre-breakthrough condition and prolong deposition.

The geometry of dripwater flow paths is never known, and has rarely, if ever, been modelled. Cave air P_{CO2} can vary from dangerous levels of ~5%, when degassing and deposition are unlikely, to atmospheric levels at cave entrances, where speleothems are commonly located. Nevertheless, dripwaters from cave roofs that follow a vertical path down short joints from a bare limestone surface are more likely to be aggressive and less likely to deposit speleothem, in contrast to those that flow from calcareous soils along longer flow paths with small hydraulic gradients.

Under intermediate conditions, dripwater might become aggressive during floods that raise hydraulic gradients, thereby causing dissolution of speleothem.

During winter, interesting and complex competitions arise among the effects of lower temperature and its consequential reduction of biological activity and therefore of P_{CO2} in dripwaters. Reduced temperature increases the amount of calcite that can be held in solution, thereby increasing penetration lengths and significantly reducing breakthrough times. (However, dissolution rates are significantly reduced after breakthrough). Reduced P_{CO2} levels reduce the calcite saturation level, thereby reducing penetration lengths and increasing breakthrough times (post-breakthrough dissolution rates are also somewhat reduced for applicable ranges of P_{CO2}). Because the temperature change is likely to be damped when the dripwater reaches open cave passage, the change in P_{CO2} is likely to have the major influence. Thus, assuming the dripwater flow always operates with high-order kinetics, i.e. it remains pre-breakthrough, its solute load is reduced and therefore winter precipitation of speleothem should be reduced, at the same flow rate. However, the P_{CO2} of winter cave air may also reduce, increasing precipitation.

13. Speleogenesis below reservoirs and lakes

If the entry to the karst is itself under a head of water, this head needs to be added to the head within the karst to give the applicable hydraulic gradient. Such increased HGs can cause rapid breakthrough by enlargement of karst fractures beneath a reservoir, as studied by Dreybrodt (1996). Thus, a reservoir dam can be bypassed by an underlying conduit, causing significant leakage of the reservoir. Close to the wall of the dam, the HG can exceed unity. For example, from Figure 1, if the leakage is 900 m away and down the valley from a fracture system that leads 100 m below the base of a dam that holds back water 100 m deep, L = 1,000 m and HG = 200/1,000 = 0.2, giving a breakthrough aperture of 0.4 cm. For a 10 m-long sub-horizontal fracture directly beneath the same dam, HG = 10, giving a required aperture of 0.025 cm, so that immediate tectonic inception is likely here. Similar conditions can arise during the deglaciation of continental ice sheets in mountainous areas, if the fractures become submerged by an ice-dammed lake (Faulkner 2005). In this case, the flow path is from the lake and via the fractures back into the lake and then into englacial conduits within the continuing ice sheet, or directly from the fractures into Nye channels at the base of a warm-based ice sheet. Despite the water being at 0 °C, with a P_{CO2} then of only 0.02 %, such situations can also cause tectonic inception and fairly rapid first-order dissolution (Faulkner 2006b).

14. Rejuvenation in alpine situations

Glacial valleys in mountainous areas, including those at high latitudes, were significantly rejuvenated following large-scale erosion during each Pleistocene glaciation. At least the upper and outer parts of palaeocaves may be removed during glacial maxima (Faulkner 2007b). During each ensuing interglacial, sinks may be captured farther upstream and resurgences find lower outlets. Clearly, these effects may make significant changes to hydraulic gradients and hydraulic ratios, depending on the local topography. They provide opportunities for new fractures at lower levels to carry some of the drainage. These may in turn eventually achieve breakthrough and then grow large enough to be explored by diving.

15. Conclusions

The onset of turbulence in a uniform conduit is controlled by two main variables: the aperture (i.e. fissure width or tube radius) and the hydraulic gradient, whereas the onset of first-order kinetics after breakthrough is also controlled by the length of the conduit. Mathematically, hydraulic gradient and length are usefully combined into a single variable, the hydraulic ratio. The two onsets only coincide at the same aperture for planar fissures of length 290 m and for cylindrical tubes of length 452 m, the actual aperture depending on the hydraulic gradient. Thus, breakthrough may occur before or after flow becomes turbulent, depending on conduit length. The time to reach it also depends on three main variables: initial aperture, hydraulic gradient, and conduit length. For many karst aquifers, breakthrough occurs at an aperture of about 1cm for 10 m-long conduits at a hydraulic gradient of 10^{-4} and for longer and steeper conduits up to 1,000 m long at 10^{-2}. However, there are many different karstic situations governed by the same laws. In practice, the breakthrough aperture may vary from the sub-millimetre to several metres and hydraulic ratios can be considered over 17 orders of magnitude.

Acknowledgements

The author is grateful to Art Palmer and Philippe Audra for their suggestions to clarify several points.

References

Bögli A, 1964. Mischungskorrosion – ein Beiträg zur Verkarstungsproblem. Erdkunde, 18, 83–92.

[English translation by Elder E, 1985. Mixture Corrosion – a contribution to the karstification problem. National Speleological Society, Cave Geology, 1 (10), 393–406].

Dreybrodt W, 1990. The role of dissolution kinetics in the development of karst aquifers in limestone: a model simulation of karst evolution. Journal of Geology, 98 (5), 639–655.

Dreybrodt W, 1996. Principles of early development of karst conduits under natural and man-made conditions revealed by mathematical analysis of numerical models. Water Resources Research, 32 (9), 2923–2935.

Dreybrodt W, Gabrovsek F, Romanov D, 2005. Processes of speleogenesis: a modeling approach. Zalozba, ZRC. Postojna – Ljubljana. 376.

Fairchild, IJ, Baker, A, 2012. Speleothem Science. Wiley-Blackwell, 432.

Faulkner TL, 2005. Cave inception and development in Caledonide metacarbonate rocks. PhD Thesis. University of Huddersfield.

Faulkner T, 2006a. Limestone dissolution in phreatic conditions at maximum rates and in pure, cold, water. Cave and Karst Science, 33 (1), 11–20.

Faulkner T, 2006b. Tectonic inception in Caledonide marbles. Acta Carsologica, 35 (1), 7–21.

Faulkner T, 2007a. Book review: Hypogene Speleogenesis: Hydrogeological and morphogenetic perspective by Dr. AB Klimchouk, National Cave and Karst Research Institute Special Paper No. 1, 2007, 106. Cave and Karst Science, 33 (3), 138–141.

Faulkner T, 2007b. The top-down, middle-outwards model of cave development in Caledonide marbles. Cave and Karst Science, 34 (1), 3–16.

Faulkner T, 2009. Limestone erosion rates and rainfall. Cave and Karst Science, 36 (3), 94–95.

Ford DC, Williams P, 2007. Karst hydrogeology and geomorphology, 562. John Wiley and Sons.

Gunn J, Gagen P, 1987. Limestone quarrying and sinkhole development in the English Peak District. in Beck and Wilson (Eds.) Karst hydrogeology, Rotterdam: Balkema, 121–125.

Kaufmann G, Braun J, 1999. Karst aquifer evolution in fractured rocks. Water Resources Research, 35 (11), 3223–3238.

Klimchouk A, 2007. *Hypogene Speleogenesis: Hydrogeological and Morphogenetic Perspective*. National Cave and Karst Research Institute Special Paper No. 1, 106.

Lowe DJ, Gunn J, 1997. Carbonate Speleogenesis: An Inception Horizon Hypothesis. Acta Carsologica, 26/2, 38, 457–488.

Palmer AN, 1981. Hydrochemical factors in the origin of limestone caves. Proceedings of the eighth International Speleological Congress, 120–122.

Palmer AN, 1991. Origin and Morphology of limestone caves. Geological Society of America Bulletin, 103, 1–21, 157–175.

Palmer A, 2007. Cave Geology. Cave Books. Dayton, Ohio. 454.

Romanov D, Gabrovsek F, Dreybrodt W, 2003. The impact of hydrochemical boundary conditions on the evolution of limestone karst aquifers. Journal of Hydrology 276, 240–53.

Weyl PK, 1958. The solution kinetics of calcite. Journal of Geology, 66, 163–176.

White WB, 1977. Role of solution kinetics in the development of karst aquifers. in Tolsen and Doyle (Eds.) International association of Hydrogeologists, Memoirs, 12, 503–517. White WB, 1988. Geomorphology and hydrology of karst terrains. Oxford University Press.

INVESTIGATIONS INTO THE POTENTIAL FOR HYPOGENE SPELEOGENESIS IN THE CUMBERLAND PLATEAU OF SOUTHEAST KENTUCKY, U.S.A.

Lee J. Florea
Department of Geological Sciences, Ball State University, 2000 W. University Ave., Muncie, IN 47306, U.S.A., lflorea@bsu.edu

This manuscript offers preliminary geochemical evidence that investigates the potential for hypogene speleogenesis in the Cumberland Plateau of southeastern Kentucky, U.S.A. The region was traditionally considered a classic example of epigenic karst, but new insights have uncovered tantalizing observations that suggest alternatives to simple carbonic acid speleogenesis. Such first-order observations have included natural petroleum seeps at the surface and in caves, occasional cave morphologies consistent with action of hypogene fluids, and prolific gypsum within cave passages. To this point, geochemical data from caves and springs verify carbonic acid as the primary dissolutional agent; however, these same analyses cannot rule out sulfuric acid as a secondary source of dissolution. In this paper, Principal Component Analysis of ionic data reveals two components that coordinate with parameters associated with "karst water" and shallow brine. In contrast, molar ratios of Ca^{+} and Mg^{+} as compared to HCO_3^{-} and SO_4^{2-} closely follow the reaction pathway stipulated by the carbonate equilibria reactions. Despite these data, the role, if any, of hypogene speleogenesis in the karst of the Cumberland Plateau remains inconclusive. It is very likely that carbonic acid dominates speleogenesis; however, contributions from sulfuric acid may influence our understanding of "inception" and carbon flux within these aquifers.

1. Introduction

The chemistry of groundwater in karst aquifers reflects contributions from the dissolution of carbonate bedrock where the sources of acid come primarily from the reactions between water and dissolved carbon dioxide, which produces carbonic acid, or between dissolved oxygen and sulfide, which produces sulfuric acid. In the case of carbonic acid, the net chemical reaction yields equal contributions of dissolved inorganic carbon (DIC) from both soil/atmosphere and bedrock:

$$H_2CO_{3(aq)} + [(x-1)Ca, xMg]CO_3$$
$$\Leftrightarrow (x-1)Ca^{2+}_{(aq)} + xMg^{2+}_{(aq)} + 2HCO_{3(aq)}$$

Note that the above reaction yields a 1:2 molar ratio of cations to bicarbonate in the products. Contrast this with the case of sulfuric acid, where the net reaction with the carbonate bedrock limestone reveals DIC derived solely from the bedrock:

$$H_2SO_{4(aq)} + 2[(x-1)Ca, xMg]CO_3$$
$$\Leftrightarrow 2(x-1)Ca^{2+}_{(aq)} + 2xMg^{2+}_{(aq)} + SO_{4(aq)} + 2HCO_{3(aq)}$$

In this reaction, note that the molar ratio between the cations and bicarbonate and between the cations and anions in the products is 1:1 and 2:3, respectively.

Finally, if we combine the two reactions above into a net reaction assuming equal contributions from carbonic and sulfuric acids, we arrive at the following:

$$H_2SO_{4(aq)} + H_2CO_{3(aq)} + 3[(x-1)Ca, xMg]CO_3$$
$$\Leftrightarrow 3(x-1)Ca^{2+}_{(aq)} + 3xMg^{2+}_{(aq)} + SO_{4(aq)} + 4HCO_{3(aq)}$$

that reveals a 3:4 molar ratio between the cations in solution and bicarbonate or a 3:5 ratio between the cations and anions in solution. It is important to mention that, when assuming equal contributions from the two acids, only 25% of the DIC will originate from the soil/atmosphere. This testifies to the relative strength of the two acids.

The first of the above equations represents the "carbonic acid speleogenesis", or CAS, model of cave development, where carbon-dioxide-enriched waters from percolating, epigenetic recharge react with the carbonate bedrock (Ford and Williams 2007; White 1988). Caves in southeastern Kentucky, U.S.A. serve in the literature as classic examples of epigenic karst (e.g., Simpson and Florea 2009). In these systems the chemical products of carbonate dissolution, Ca^{2+}, Mg^{2+}, and HCO_3^{-} (and as a result pH) are generally inversely correlated to discharge – as discharge goes up, the concentration of these ions (and therefore specific conductance – SpC) goes down due to, in part, dilution. This notwithstanding pulses of storage water pushed through at the beginning of storm events.

The second equation, in contrast, represents the "sulfuric acid speleogenesis" (Jagnow et al. 2000), or SAS, model of cave development. This model is used to explain, for example, the caves from the Guadalupe Mountains of New Mexico (Hill 1990) where sources of acidity arise from below – a "hypogene" model. Modern examples of SAS have been identified in Cueva de Villa Luz in Mexico (Hose et al. 2000), Grotte di Frasassi in Italy (Galdenzi and Menchetti 1995), the hydrothermal springs and caves in the Cerna River Valley (Wynn et al. 2010; Onac et al. 2011) in Romania, and Lower Kane Cave in Wyoming (Engel et al. 2004), among others. Re-appraisal of hypogenic theories based on hydrogeological definition has been done in Klimchouk (2007). Recent investigations in the Edwards aquifer in central Texas (e.g., Schindel et al. 2008) are an example of a region specific approach to understanding hypogene speleogenesis.

This brief paper explores the relationship between ions in solution and field chemistry in spring water from southeast

Kentucky. These data are analysed using two methods, Principal Component Analysis (PCA) and molar ratios to investigate the reletave importance of the two reaction pathways, CAS and SAS, as they currently contribute to the development of cavernous porosity.

While there can be no doubt, a priori, that CAS dominates the current karst aquifers of southeast Kentucky, closer inspection of caves in these aquifers reveal features noted by Ewers (1985) where he popularized the term "paragenesis", in which the bottom of the cave passage was the inception horizon and the dissolution progressed upward. Recent research on hypogene speleogenesis, in which rising fluids dissolve limestone, raises a question of whether the observed paragenetic features are in fact hypogene features.

For example, Florea et al. (2011a) document passage geometries within caves in southeast Kentucky located near shallow oil reservoirs in Mississippian strata that contain diagnostic features that are concordant with a SAS interpretation, such as rising half-tubes leading toward cupolas, blind passages, and possible bubble tracks (Klimchouk 2007). Some of these caves have identified petroleum seeps and curious passage names such as "sewer room", "gasoline alley", and "oil cave". In fact, "dead oil" is clearly visible within cross-lamina of the Ste. Genevieve limestone of Redmond Creek Cave (Walden et al. 2007).

2. Physical Setting

Data come from the Cumberland Escarpment in southeast Kentucky along the east flank of the Cincinnati Arch, a broad saddle-shaped uplift aligned north-south in north-central Tennessee and south-central Kentucky. Erosion on the structural highs located in the Nashville Dome of Tennessee and the Jessamine Dome of central Kentucky have exposed Ordovician carbonates at the core of those domes. Progressively younger strata are revealed away from the center of those structural highs. The topography of the study area is split equally between uplands of the Cumberland Plateau and deeply incised valleys that drain those uplands. The terrain of the escarpment is rugged, with upper slopes lined with vertical cliffs of Pennsylvanian sandstones and conglomerates of the Lee Formation, a "bench" of gentle slopes marking the exposure of transitional-marine calcareous shale that comprise the upper-Mississippian Paragon Formation, and lower slopes and sinkhole floors underlain by the relatively pure carbonates of the middle-Mississippian Slade Formation (Ettensohn et al. 1984). Relief in the study area exceeds 230 m with ridge tops above 530 m and valley floors below 300 m elevation above sea level.

2.1. Karst Geology and Hydrology

The Slade Formation, regionally divided into the St. Louis, the Ste. Genevieve, and Kidder Limestone members, is significantly modified by solution activity, and karst landscapes dominate the area of carbonate exposure (Simpson and Florea 2009). Less soluble cross-bedded siltstones of the Salem-Warsaw Formations locally act as a base for conduit development below the Slade Formation. Sinkholes and other closed drainage features prevail within incised valleys. Vertical solution shafts occur in stress release fractures along the hillsides (Ferguson 1967) near the contact with overlying siliciclastics and capture allogenic recharge from the plateau surface (Brucker et al. 1972). In the classic epigenic model applied to this region, vadose drainage through caves follows a stair-step pattern through the strata of the plateau margin (Crawford 1984) and coalesces into sinuous base-level conduits that generally parallel the surface valley and topographic contours (Sasowsky and White 1994). Tiers of these horizontal passages formed in response to episodic changes of base level controlled by the advance and retreat of the Laurentide ice sheet (Anthony and Granger 2004). Aquifer storage is concentrated in the rock matrix; however, the low permeability of these carbonates ensures that the communication between the matrix and the cave passages is low. Therefore, springflow hydrographs are "flashy" (White 1988; Florea and Vacher 2006) with most accessible storage lingering within the epikarst.

2.2. Spring Chemistry in Southeast Kentucky

Preliminary geochemical investigations by Dugan et al. (2012) provide a geochemical "snapshot" of water chemistry from fifteen karst springs distributed within the Otter Creek watershed southern Wayne County, Kentucky, USA – a tributary of the Cumberland River that contains sinking streams, sulfur seeps, integrated cave systems, and Kentucky's largest sinkhole. The results cluster into three groups of springs, traditional karst springs, tufa springs, and sulfur seeps, that are in part spatially controlled by the Sunnybrook Anticline (Fig. 1). This anticline has an amplitude of approximately 30 m, is oriented N-NE, and is parallel to the trend of the Cumberland Escarpment.

Tufa springs represent the "most evolved" calcium-bicarbonate water on a geochemical pathway that connects meteoric water, recharge, traditional karst springs, and tufa springs Florea et al. (2011b). Waters at these tufa springs are supersaturated with respect to calcite and where they emerge, calcite precipitates. These springs probably resurge from long, strike-parallel flowpaths on the west flank of the anticline.

Sulfur seeps, with higher average SpC and temperatures (13.3 °C compared to 11.7 °C) are largely concentrated on the east flank of the anticline in the direction of the Appalachian Basin. The presence of these seeps is a manifestation of shallow petroleum reservoirs in lower Mississippian strata, particularly the Stray Sand pay zone, which consists of 3 to 10 m of cherty, geode-bearing limestone near the top of the Fort Payne 50 to 65 m above the Chattanooga shale (McFarlan 1943). These shallow reserves were exploited between the 1880s and the 1920s. Even though initial production in some wells was intense (upwards of 2,000 barrels of oil per day), production was generally short lived.

Sulfate/sulfide concentrations in the seeps are elevated and microbial-mediated sulfur redox is apparent as mats of microbial "slimes" at these seeps. Geologically, this setting is similar to that of Lower Kane Cave in the Mississippian-age Madison Limestone on the east flank of the Little Sheep

Mountain anticline in the Bighorn Basin of north-central Wyoming where sulfide-rich brines from nearby oil reservoirs are oxidized by bacterial-mats to induce SAS (Engle et al. 2004).

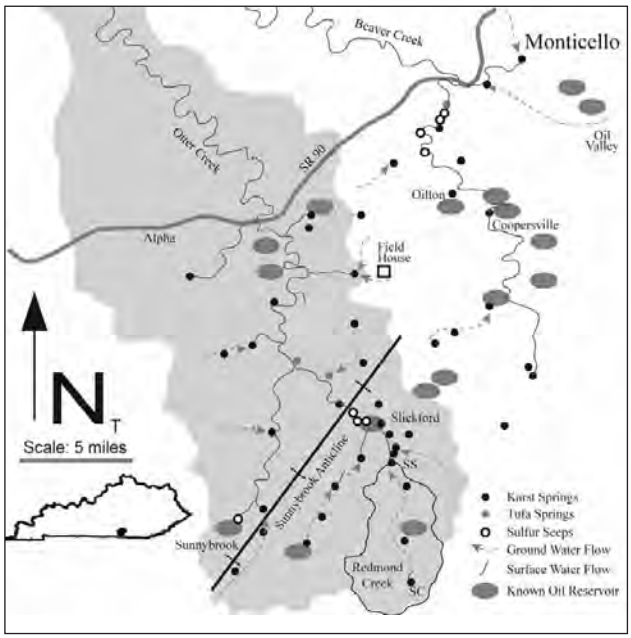

Figure 1. Study areas in Wayne County, KY, U.S.A. Index map of Kentucky illustrates the location of Wayne County. The Field House that serves as a base of operations is shown as an open square. The light gray is the Otter Creek Watershed with the Redmond Creek karst aquifer outlined in black. Sandy Springs and Stream Cave and indicated by SS and SC, respectively. The axis of the Sunnybrook Anticline is indicated as a black line. Principal communities are indicated in text. Groundwater flow paths are inferred by dye tracing and known cave survey. Oil reservoirs in shallow Mississippian-age strata identified by Abbott (1921) are denoted by gray ovals.

3. Methods

Samples come 15 springs in the Otter Creek watershed of southeast Kentucky, U.S.A. Two springs, Stream Cave and Sandy Springs, are one input to and the primary output from the Redmond Creek Karst Aquifer. Remaining sites comprise traditional karst springs, tufa springs, and sulfur seeps. Sixteen sets of bi-montly samples were collected from Stream Cave and Sandy Springs during a detailed investigation in 2010–2011. The remaining sites comprise one or two samples collected between 2010 and 2012. Each sample was collected in two 250-mL HDPE bottles – an un-preserved sample for anions and a sample preserved with 2 mL of 6N HNO_3 for cations. All water samples were refrigerated at 4 °C until the time of analysis. Samples were analysed using Ion Chromatography and Inductively Coupled Plasma-Optical Omission Spectrospcopy at the Waters Lab at Western Kentucky University. All results were reported in mg/L and converterd to molar equivalents.

In the field, values of pH, SpC, Temperature, and Dissolved Oxygen were collected on site using an YSI multiparameter sonde. Alkalinity titrations were conducted onsite using a HACH ditigal titrator and converted to molar equivalents of HCO_3^-. Using the Debye-Hückle relationships the saturation state of the water with respect to calcite (C/C_S) and the partial pressure of carbon dioxide (pCO_2).

All data were compiled in a spreadsheet for analysis including computation of the molar ratios of species in solution. Of specific interest were those ratios outlined in the introduction that reveal the relative magnitudes of reaction pathways consistent with CAS and SAS. Secondarily, the time-series data for each parameter collected at Sandy Springs were input into SPSS software. Factor analysis was applied to these data and resulting eigenvalues were weighted toward each input parameter.

4. Results and Discussion

4.1. Molar Ratios

Figure 2 is a cross plot of the molar concentration of Ca^+ and Mg^+ compared to the molar concentration of HCO_3^-. Two trends are clear. The first is that all data from the traditional karst springs and from tufa springs generally fall along the 1:2 molar ratio line, clearly demonstrating the role of CAS in these systems. Sulfur springs, on the other hand, cluster closer to the 2:1 molar ratio line, which suggests enrichment in Ca^+ and Mg^+ without contemporaneous addition of HCO_3^-. Such a trend is possible with entrainment of shallow brines. A cross plot between the Mg^+/Ca^+ ratio as compared to Mg^+ helps provide further context (Figure 3). In this plot, data from Stream Cave, near the aquifer input and low in Mg^+, have wide range in Mg^+/Ca^+ ratios. Sandy Springs and the tufa springs, have near consistent Mg^+ concentrations and a stable Mg^+/Ca^+ ratio between 0.16 and 0.2. This is consistent with dolomite abundance in the neighborhood of 12 % to 15 %. Sulfur seeps, with influence of shallow brines, have a wider span of Mg^+/Ca^+ ratios and an increasing abundance of Mg^+ in solution.

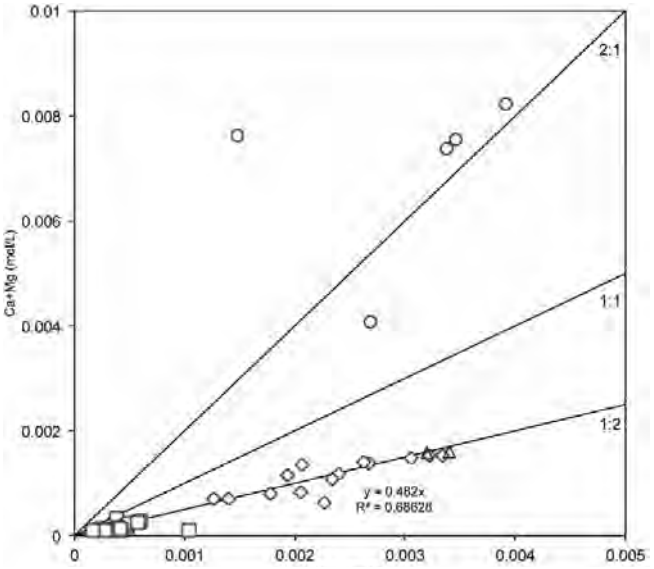

Figure 2. Molar ratios of Ca2+ +Mg2+ as compared against HCO3-. Open squares are from Stream Cave, open diamonds are from Sandy Springs, open triangles are from tufa springs, and open circles are from sulfur seeps. Also shown are linear regressions that demonstrate molar ratios of 1:2, 1:1, and 2:1. The 1:2 and 1:1 linear regressions are an indication of dissolution of carbonate from carbonic acid and sulfuiric acid, respectively.

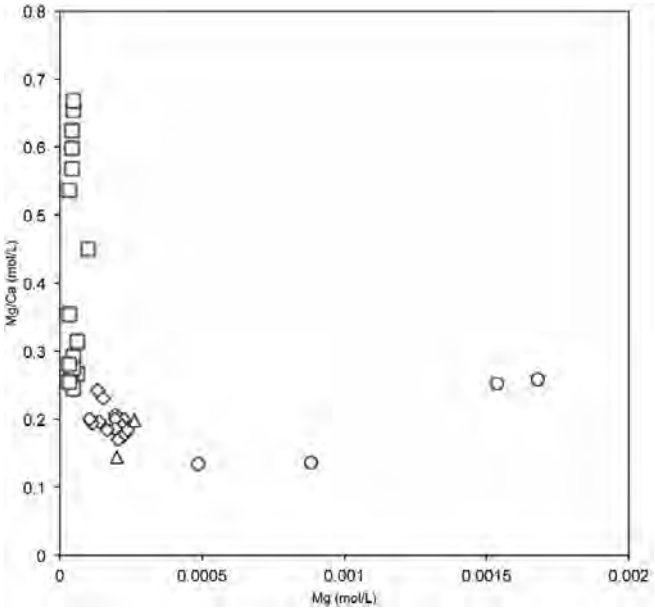

Figure 3. Cross plot of the molar ratio of Mg2+/ Ca2+ as compared against Mg2+. Open squares are from Stream Cave, open diamonds are from Sandy Springs, open triangles are from tufa springs, and open circles are from sulfur seeps.

Figure 4 is a cross plot of the molar concentration of Ca^{+} and Mg^{+} compared to the molar concentration of HCO_3^{-} and SO_4^{2-}. Again, the sulfur springs cluster in a different locus than traditional karst springs or tufa springs, which still lay near the 1:2 molar ratio line, despite the addition of SO_4^{2-}. Interestingly, the data from the sulfur seeps, once corrected for the molar concentration of H_2S, cluster near the 1:1 molar ratio line.

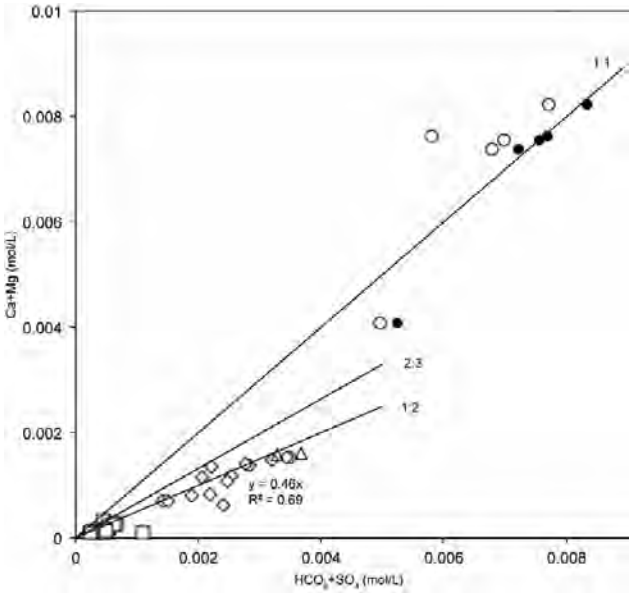

Figure 4. Molar ratios of Ca^{2+} +Mg^{2+} as compared against HCO_3^{-} +SO_4^{2-}. Open squares are from Stream Cave, open diamonds are from Sandy Springs, open triangles are from tufa springs, and open circles are from sulfur seeps. Filled circles are sulfur seeps with the addition of H_2S. Also shown are linear regressions that demonstrate molar ratios of 1:2, 2:3, and 1:1. The 1:2 linear regression is a indication of dissolution of carbonate from carbonic acid. The 2:3 linear regression is the expected molar ratio from dissolution sulfuric acid.

4.2. Principal Component Analysis of Karst Groundwater in Southeast Kentucky

Using PCA, a form of factor analysis in SPSS software, eigenvalues were derived that comprise the maximum amount of data variation (Florea 2012). In contrast to the method of molar ratios, the potential for SAS is revealed using PCA for the time series data of ion chemistry and field data for Sandy Springs. For example, when considering spring discharge (Q), dissolved ion concentrations, and the isotopic composition of DIC and rainwater, one PCA calculates that 48% of the variance can be explained by Q, Ca^{2+}, Mg^{2+}, K^{+}, NO_3^{-}, and HCO_3^{-}. A second component, including Na^{+}, Cl^{-}, SO_4^{2-}, and total organic carbon (TOC) explains 31% of the variance. A final third component, comprising solely the isotopic composition of rainwater includes 10% of the remaining variance.

In a second, more restricted PCA, a first component comprises 48% of the variance and includes Ca^{2+}, Mg^{2+}, the isotopes of DIC, and HCO_3^{-}, and a second component comprises 31% of the variance and includes SO_4^{2-}, the isotopes of DIC, and pH. Finally, a third PCA results in two components: a first incuding HCO_3^{-}, Ca^{2+}, total dissolved solids (TDS) and Q for 53% of the variance, and a second with pH and SO_4^{2-} including 24% of the remaining variance. Component loading diagrams for these three PCA are included in (Figure 5).

Comparing these results to the original time-series data, the first component in each PCA corresponds to parameters that are inversely proportional to discharge; they vary according to interaction time with bedrock, namely limestone dissolution by CAS. In generaly, when discharge goes up, TDS, including NO_3^{-} from agricultural runoff, decreases because of dilution. The second component in these PCA incudes paratmeters generally associated with brines and appears to be somewhat independent of discharge and perhaps directly related to pH. TOC is inversely proportional to these parameters suggesting that these brines have low organic content. The composition of DIC has complex loading on both components, suggesting that the isotopic composition of DIC may result in part from a blend of sources. Finally, the third component includes only the isotopic composition of rainwater, and as such suggests that rainfall composition is modulated external to the aquifer, a subject of a forthcoming publication (Florea, in review).

5. Summary Points

The available data presented in this paper reinforce our scientific understanding of the dominance of carbonic acid in the development of karst in southeast Kentucky, U.S.A. Molar fractions of cations and anions in groundwater samples from karst springs and tufa springs are consistent with the stoichiometry of the carbonate equilibria reactions. Results from PCA consistently reveal an eigenvalue comprised of variables associated with CAS in shallow groundwater that is anit-correlated to discharge. These results are neither revealing nor unexpected. However, the presence of sulfur seeps within caves and along base-level streams combined with morphologic features in caves associated with SAS evokes questions.

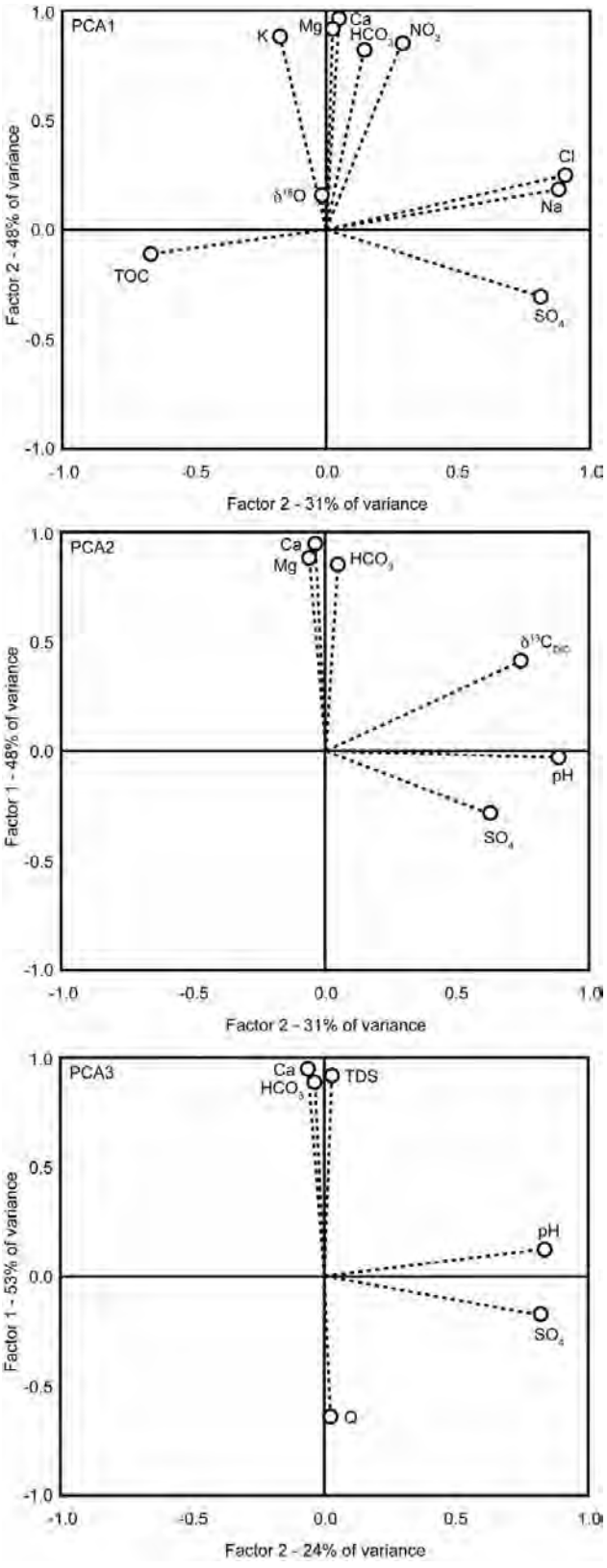

Figure 5. Principal component plots for PCA1, PCA2, and PCA3 showing the eigenvalue weighting of each variable. The percent of variance accounted for by each eigenvalue is given on the axis. Components of sample TDS associtated with shallow groundwater are heavily weighted on eigenvalue 1 and are anti-correlated to discharge. Components of sample TDS associated with shallow brines are heavily weighted on eigenvalue 2 and are anti-correlated to TOC. pH co-varies with the shallow brines. The isotopes of DIC have complex loading.

Molar ratios clearly identify the sulfur seeps are being from shallow brines associated with shallow reservoirs of petroleum. Enriched in H_2S, these sites are likely experiencing SAS. The question remains as to how prevelant this process is (e.g., what is the relative magnitude of CAS and SAS). Such an investigation may influence our understanding of the "inception" period in these karst aquifers – the earliest stages of secondary permeability development – and the magnitude of carbon flux from these aquifers – specifically, the volume of inorganic carbon sequestered from the atmosphere and rhizosphere.

The data from Sandy Springs may lend some additional insight. For example, in each PCA, variables commonly associated with brines co-vary and account for a significant percent of the variance in the data. These data seem to vary independent of discharge and are anti-correlated to TOC. This could be a result of entrainment of shallow brines that are depleted in organic carbon within the karst aquifer. The isotopes of carbon in DIC within these samples exhibit complex loading on each eigenvalue. This suggests that contributions to DIC may come from both shallow groundwater where CAS dominates and from the entrained shallow brines where dissolved sulfides are oxidized creating the conditions for SAS on a limited scope. It is worth noting that at least one small sulfur seep has been identified within the cave that feeds Sandy Springs. Corroded bedrock in the vicinity of this seep is a clear indication of SAS on at least the scale of individual seeps. Recent measurements of isotopes of DIC from sulfur seeps in the Otter Creek watershed (Florea, et al. 2011c) demonstrate an enrichment of lithospheric carbon as would be expected from the stoichiometry of the SAS reaction presented in this manuscript.

Acknowledgments

The author is indebted to the hard work and dedication of fellow caves and colleagues during this study. In particular, thanks go to major contributions by Bill Walden, Chasity Stinson, and Nick Lawhon. The conversations, hospitality, and access provided by landowners Tim Pyles and Kay Koger and cavers Rick Gordon, Deb Moore, Harry Gopel, and Eric Weaver is most welcome. Funding for this work was provided by a WKU Provost Incentive grant, a WKU start-up index, and a Ball State University start-up package.

References

Abbott WR, 1921. Oil Field Map – Wayne and Clinton Counties, Kentucky.

Anthony DM, Granger DE, 2004. A Late Tertiary origin for multilevel caves along the western escarpment of the Cumberland Plateau, Tennessee and Kentucky, established by cosmogenic ^{26}Al and ^{10}Be. Journal of Cave and Karst Studies 66(2), 46–55.

Brucker RW, Hess JW, White WB, 1972. Role of Vertical Shafts in the Movement of Ground Water in Carbonate Aquifers. Ground Water 10(6), 5–13.

Christophersen N Hooper RP, 1992. Multivariate analysis of stream water chemical data: the use of principal components analysis for the end-member mixing problem. Water Resources Research 28, 99–107.

Crawford NC, 1984. Karst landform development along the Cumberland Plateau Escarpment of Tennessee. In: RG LeFleur (ed.). Groundwater as a geomorphic agent. Boston, Allen and Unwin, Inc., 294–338.

Dugan CR Florea LJ, Walden WD, 2012. A Geochemical Investigation of Springs within the Otter Creek watershed: Wayne County, Southeastern Kentucky. Geological Society of America Abstracts with Programs 44(4), 26.

Engel AS, Stern LA, Bennett PC, 2004. Microbial contributions to cave formation: New insights into sulfuric acid speleogenesis. Geology 32(5), 369–372.

Ettensohn FR, Rice CR, Dever GR Jr, Chesnut DR, 1984. Slade and Paragon Formations; New stratigraphic nomenclature for Mississippian rocks along the Cumberland Escarpment in Kentucky. U.S. Geological Survey Bulletin 1605-B, 37.

Ewers RO, 1985. Patterns of cave development along the Cumberland Escarpment. In: PH Dougherty (ed.). Caves and karst of Kentucky. Kentucky Geological Survey Special Publication, 63–77.

Ferguson HF, 1967. Valley stress release in the Allegheny Plateau. Bulletin of the Association of Engineering Geologists 4, 63–71.

Florea LJ, In revision. Selective recharge and isotopic composition of shallow groundwater within temperate, epigenic carbonate aquifers. Journal of Hydrology.

Florea LJ, 2012. Principal Component Analysis of Geochemical Data from a Karst Aquifer in Southeast Kentucky. Geological Society of America Abstracts with Programs 44(4), 26.

Florea, L.J.; Stinson, C.L.; Weaver, E.; Lawhon, N.; Wynn, J. 2011a. Finding holes in a theory or finding a theory in holes – the potential role of hypogene speleogenesis for caves of the Cumberland Plateau in southeastern Kentucky. Geological Society of America Abstracts with Programs 43(5), 19.

Florea LJ, Lawhon N, Stinson CL, 2011b. William D. Walden. Geochemical Characterization of the Redmond Creek Karst Aquifer, Southeast Kentucky. 2011 National Speleological Society Convention Program Guide, 32–33.

Florea LJ, Wynn J, Lawhon N, Stinson CL, Walden W, 2011c. Variation of $\delta^{13}C$ in the Carbonate Aquifers of the Cumberland Plateau of Southeast Kentucky. Geological Society of America Abstracts with Programs 43(5), 342.

Florea, LJ, Vacher, HL, 2006. Springflow Hydrographs: Eogenetic versus Telogenetic Karst. Ground Water 44(3), 352–361.

Ford DC, Williams P, 2007. Karst Hydrogeology and Geomorphology. John Wiley & Sons, 562.

Galdenzi S, Menichetti M, 1995. Occurrence of hypogenic caves in a karst region: Examples from central Italy. Environmental Geology 26, 39–47.

Hill CA, 1990. Sulfuric acid speleogenesis of Carlsbad Cavern and its relationship to hydrocarbons, Delaware Basin, New Mexico and Texas. American Association of Petroleum Geologists Bulletin 74(11), 1685–1694.

Hose LD, Palmer AN, Palmer MV, Northup DE, Boston PJ, DuChene HR, 2000. Microbiology and geochemistry in a hydrogen sulphide rich karst environment. Chemical Geology 169, 399–423.

Jagnow DH, Hill CA, Davis DG, DuChene HR, Cunningham KI, Northup DE, Queen JM, 2000. History of the sulfuric acid theory of speleogenesis in the Guadalupe Mountains, New Mexico, Journal of Cave and Karst Studies 62(2), 54–59.

Klimchouk AB, 2007. Hypogene speleogenesis: Hydrogeological and Morphogenetic perspective. National Cave and Karst Research Institute Special Paper 1, 106.

McFarlan AC, 1943. Geology of Kentucky. University of Kentucky, 531.

Onac BP, Wynn JG, Sumrall JB, 2011. Tracing the sources of cave sulfates: a unique case from Cerna Valley, Romania. Chemical Geology 288, 105–114.

Sasowsky ID, White WB, 1994. The role of stress release fracturing in the development of cavernous porosity in carbonate aquifers. Water Resources Research 30(12), 3523–3530.

Schindel, GM, Johnson S, Alexander CE, 2008. Hypogene Processes in the Edwards Aquifer in South-Central Texas, a New Conceptual Model to Explain Aquifer Dynamics. AAPG Annual Convention, San Antonio, TX.

Simpson LC, Florea LJ, 2009. The Cumberland Plateau of Eastern Kentucky. In: AN Palmer and MV Palmer (eds.). Caves and Karst of America. National Speleological Society, 70–79.

Walden WD, Walden KM, Florea LJ, 2007. The Caves and Karst of Redmond Creek, Wayne County, Kentucky. 2007 National Speleological Society Convention Program Guide, 107.

White WB, 1988. Geomorphology and Hydrology of Karst Terrains. New York, Oxford University Press, 464.

Wynn JG, Sumrall JB, Onac BP, 2010. Sulfur isotopic composition and the source of dissolved sulfur species in the thermo-mineral springs of the Cerna Valley, Romania. Chemical Geology 271, 31–43.

THE ROLE OF BASE LEVEL INCISION AND TRANSIENT RECHARGE IN VERTICAL ORGANISATION OF KARST NETWORK

Franci Gabrovšek[1], Philipp Häuselmann[2], Philippe Audra[3]
[1]*Karst Research Institute ZRC SAZU, Titov trg 2, Postojna, Slovenia, gabrovsek@zrc-sazu.si*
[2]*Swiss Institute for Speleology and Karstology SISKA, Box 818, 2300 La Chaux-de-Fonds, Switzerland, praezis@speleo.ch*
[3]*Polytech Nice – Sophia, University of Nice – Sophia Antipolis, 930 route des Colles, 06410 BIOT, France & Innovative City – IMREDD, Nice, France, audra@unice.fr*

Vertical organization of karst network or "speleogenesis in the dimension of length and depth" has been in research focus for more than a century. Different models have been proposed, each focusing the speleogenesis to: a) the vadose zone, where the solution is most aggressive b) the water table, where the density of flow is highest and c) to the phreatic zone, referring to the deep Darcyan flow paths.

Different models were unified into a single concept, the four state model of Ford and Ewers (1978). The model relates geometry of caves to the frequency of penetrable fissures. It has been successfully applied to numerous speleogenetic settings.

In the last decade these conceptual models have been also verified with the numerical ones. Gabrovšek and Dreybrodt (2001) modelled 2D unconfined fracture network in constant boundary conditions. The model showed the importance of flow focusing at the water table which is dropping in time due to the increasing permeability. Most simulations resulted in the formation of a water table cave at the base level. Deeper phreatic loops were more an exception than a rule, limited to the cases with the absence of flow paths in the vicinity of the base level. Similar results were obtained by Kaufmann (2003) who modelled a vertical fracture network embedded in a porous matrix. Base level changes have been also considered (Dreybrodt et al. 2005), demonstrating that valley incision and back filling can result in deep phreatic loops.

Carbonate massifs of young orogenes are normally heavily fractured due to the intense tectonic activity. According to the four state model, one would expect that water table caves would be common, but several studies reveal that they are more an exception than a rule. The *looping caves* with soutirages connecting different cave levels, are more common than the water table caves (Jeannin et al. 2000).

Speleogenesis in Alpine environments is influenced by high uplift and valley incision rate and irregular recharge.

Several works have stressed the potential importance of recharge variation in vertical development of karst network (e.g., Häuselmann et al. 2003) based on field observations. In this work we adopt some of these conceptual approaches and translate them into a simple mathematical model based on basic principles of flow, dissolution and transport. The full paper described in this extended abstract has been submitted to publication (Häuselmann et al. 2012).

The conceptual model is fairly simple: Initially we assume a master conduit discharging part of the karst massif to a spring at the base level. The incision of the base level starts and triggers the evolution of new pathways along some deeper levels below the master conduit. While master conduit also incises into an underground canyon, the deep pathways evolve toward maturity and capture increasing portion of flow. The question arises what will happen first: a) an underground – water table cave connecting both levels or b) all the flow will be diverted along the lower pathway.

The incision of the master conduit is a result of a combination of chemical and mechanical erosion. We make a rather crude (but reasonable for the purpose) assumption that it is constant in time.

The development of deep pathway is treated with the approach given in detail in several sources (Dreybrodt et al. 2005). The model couples flow and dissolution along a pathway (single fracture) through mass balance assuming that within each segment of the fracture, the dissolved mass contributes to the saturation ratio of the solution. Analytical solution is based on the approximation that the entire pathway is widened uniformly, defined by minimum dissolution rates at the exit (Gabrovšek and Dreybrodt 2000). This way dissolution and widening rates of the fracture is calculated. When the head difference between both ends of the pathway is constant, such coupling results in increasing flow rate, which in turn enhances dissolution rates and vice versa. The feedback mechanism ends with an abrupt increase of both, flow and dissolution rates, called *the breakthrough*. After the breakthrough, the dissolution rate along the pathway is constant and maximal and the flow rate increases at the maximal rate. Soon the pathway can capture all available flow.

In our model the evolution of deep pathway is driven by a variable hydraulic head. It initially increases in time as the valley incises faster than the master conduit. When valley passes the elevation of deep pathway, the head is maximal, latter the head drops with incision of the an underground.

The analytical solution for the evolution of a pathway under varying hydraulic head as given above, divides the parameter space into a region where the breakthrough of the lower pathway is possible (formation of a loop) and a region where the master conduit develops into a an underground.

We introduce the Loop-to-Canyon-Ratio (LCR), a parameter predicting which of the two outcomes is more likely to occur in certain settings.

Generally an initial master conduit is not straight, but undulates in both planes. One can also assume several sub-

vertical fractures (proto soutirages) connecting the level of the master conduit and the deep pathway. In case of a transient recharge, composed of floods and dry periods, the event water is stored in the depression of the (undulating) master conduit after the flood recession. This water seeps along the proto soutirages towards the deep pathway and enlarges them. Therefore, deep pathways evolve also when the master conduit does not. This mechanism considerably increases the LCR. Therefore, the loops evolve more likely in transient recharge conditions.

Although the model includes several approximations, it presents a step forward by assessing the relative importance of some basic parameters related to specific speleogenetic settings.

References

Audra Ph, Palmer AN (in press). The vertical dimension of karst – Controls of vertical cave pattern. In: J Shroder and A Frumkin (Eds.). Treatise on Geomorphology, vol. 6. Academic Press, San Diego.

Dreybrodt W, Gabrovsek F, 2000. Dynamics of the evolution of a single karst conduit. In: A. Klimchouk, DC Ford, AN Palmer and W Dreybrodt (Eds.). Speleogenesis: Evolution of Karst Aquifers. NSS, Huntsville, 184–193.

Dreybrodt W, Gabrovsek F, Romanov D, 2005. Processes of speleogenesis: a modeling approach. Zalozba ZRC, Ljubljana.

Ford DC, Ewers RO, 1978. The development of limestone cave systems in the dimensions of length and depth. Can J Earth Sci, 15, 1783–1798.

Gabrovsek F, Dreybrodt W, 2001. A model of the early evolution of karst aquifers in limestone in the dimensions of length and depth. Journal of Hydrology, 240(3–4), 206–224.

Häuselmann Ph, Gabrovšek F, Audra Ph, 2012. “Looping caves” versus “watertable caves”: The role of base level changes and recharge variations in the dimensions of length and depth. Submitted to GSA.

Häuselmann Ph, Jeannin P-Y, Monbaron M, 2003. Role of epiphreatic flow and soutirages in conduit morphogenesis: the Bärenschacht example (BE, Switzerland). Zeitschrift für Geomorphologie, 47(2), 171–190.

Jeannin PY, Bitterli T, Häuselmann Ph, 2000. Genesis of a large cave system: the case study of the North of Lake Thun system (Canton Bern, Switzerland). In: A. Klimchouk, DC Ford, AN Palmer and W Dreybrodt (Eds.). Speleogenesis: Evolution of Karst Aquifers. NSS, Huntsville, 338–347.

Kaufmann G, 2003. Modelling unsaturated flow in an evolving karst aquifer. Journal of Hydrology, 276(1–4), 53–70.

Palmer AN, 1991. Origin and morphology of limestone caves. Geological Society of America Bulletin, 103, 1–21.

HYPOGENIC SPELEOGENESIS IN THE CRIMEAN FORE-MOUNTAINS (THE BLACK SEA REGION, SOUTH UKRAINE) AND ITS ROLE IN THE REGIONAL GEOMORPHOLOGY

Alexander B. Klimchouk, Gennadiy N. Amelichev, Elizaveta I. Tymokhina, Sergiy V. Tokarev
Ukrainian Institute of Speleology and Karstology, 4 Vernadsky Prospect, Simferopol, Ukraine, klim@speleogenesis.info

The leading role in the geomorphic development of the Crimean fore-mountain region is played by the processes of dismemberment of "shielding" limestone layers of the monoclinal stratified structure through valley entrenchment, and by further retreat of vertical rocky outcrops via block-toppling mechanism. These processes are guided by the presense of hypogene karst structures, whose formation preceded the modern relief. Karstified fracture-karst zones, 100 to 400 m wide, in the Cretaceous-Paleogene strata controlled the entrenchment of valleys in the limestone layers. The basic elements of hypogenic karst structures, which form their spatial framework, are sub-vertical fracture-karst conduits (karst "rifts"). Denudational opening of vertical fracture-karst rift conduits in limestone layers set the cliff-like shape of valleys slopes, and presence of such rift conduits in the rear of cliffs of already incised valleys determines the block-toppling mechanisms of slope retreat. This maintains the verticality of cliff segments in the cuesta ridge and controls their position.

Hypogenic sculptural morphology is extensively displayed in the exposed walls of cliffs (former conduit walls), which determines the originality and nomenclature of morphology of limestone cliffs of the Inner Ridge. In those areas of slopes where position of cliffs has stabilized for considerable time due to absence of new lines of block detachment in the rear, weathering becomes a significant process in the morphogenesis of surfaces. The abundance, outstanding expression, preservation and accessibility of relict hypogene karst features in the extensive cuesta cliffs of the Inner Ridge makes the region the foremost one for studying regularities of hypogene solution porosity development, the process currently ongoing in the adjacent artesian basin of the Plain Crimea.

The Crimean Mountains in the south of the Crimean Peninsula (the Black Sea region, south Ukraine), with its Main Ridge composed by Jurassic limestones, are a part of the Alpine fold-thrust belt. Adjacent to north, lays the Prichernomorsky artesian basin resting on the basement of the Scythian Plate within the Crimea Peninsula (Figure 1).

The Crimean fore-mountain region stretches as an arch along the tectonic suture junction zone between the above two structures. It is composed by two cuesta-like ridges (the Outer Ridge and Inner Ridge) whose structural slopes are formed by limestone beds of Paleocene and Eocene (the Inner Ridge), and of Neogene (the Outer Ridge).

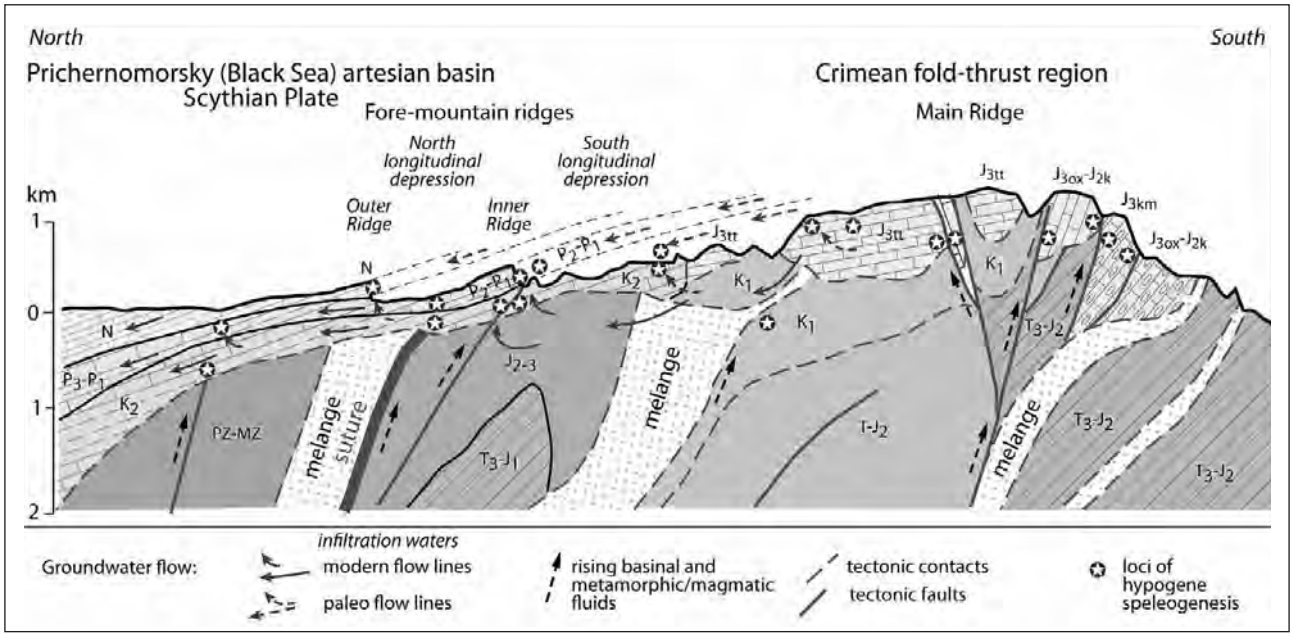

Figure 1. Schematic geological cross-section across the Crimean fold-thrust region and its junction with the Scythian Plate (simplification based on Yudin 2011), showing modern and paleo flow systems and localization of hypogene speleogenesis.

In the south-east-faced cuesta cliffs of the Inner Ridge, as well as in the canyon-like transverse valleys that cut the ridge, extensive vertical outcrops of the Upper Cretaceous marls and Paleocene and Eocene limestones display a rich array of features indicative of wide-spread hypogenic karst development in the region, which occurred before the monoclinal layered structure had been dissected by erosion. Upwelling of deep fluids across the layered aquifer system of the monoclinal slope was likely linked with the geodynamic activity along the suture zone (Figure 1).

Erosional valleys that transected the area and formed cuesta main escarps followed a linear pattern of hypogenic karst structures developed along fault zones and fracture corridors. The basic elements of these structures, which formed their spatial framework, are sub-vertical rift-like conduits (Figure 2). Elements of such karstified corridors are still present along the edges of massifs, in the rear parts of cliffs, causing the dominant block-toppling mechanism of the slope retreat processes (Figure 3). This maintains the verticality of limestone escarps and exposes "fresh" hypogenic karst morphology of former rift-like conduits. The suit of hypogenic karst features displayed in exposed walls includes variously sculptured surfaces, honeycomb, boxwork and spongework surfaces, metasomatic alteration halo, and a rich array of forms composing a cavernous "fringe" of the principal rift-like conduits. The features of the "fringe" are now displayed in the exposed walls as grottoes, niches, large vugs, and zones of smaller vuggy porosity. Caves in the region are fracture-controlled, linear, or crude mazes (the longest one is 500 m long), demonstrating the complete suite of speleogens indicative of the hypogenic origin. Caves are, in fact, those "branches" of former karst systems that are oriented normal or oblique to the present escarps, and hence retain their integrity, in contrast to those former caves that had been utilized by valleys. U/Th dating of phreatic calcite (rising spring "facies"; 260–350 ka) and stalagmite bases (ca. 130 ka) permitted to establish age constrains for the period of termination of the hypogenic development of karst systems in the south-west sector of the range, geomorphologic expression of the modern Paleocene segment of the cuesta in the relief, and respective transition to vadose conditions.

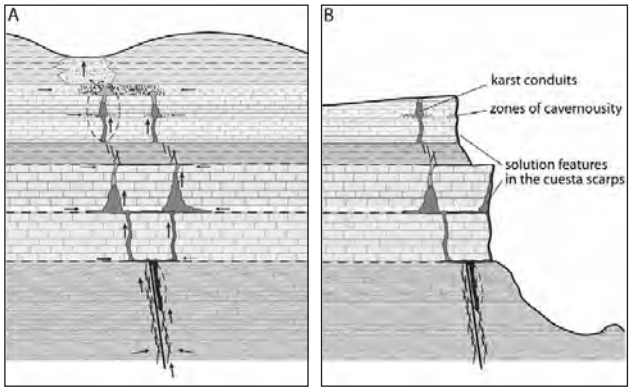

Figure 2. Conditions of the formation (A) and the current geomorphic situation (B) of caves and other karst features in the Inner Ridge of the Crimean fore-mountains.

The main speleogenetic process, clearly discerned from hydrostratigraphic/structural relations and morphology of caves and features at cliffs, is the renewal of aggressiveness due to mixing of deep rising flow (along cross-formational fracture conduits) and shallow stratiform flow in the layered aquifer system (Figure 1). Dissolution by rising thermal waters and by sulfuric acid (due to oxidation of H_2S) is also likely to play a role, at least locally.

We conclude that hypogenic karst was one of the primary factors of regional geomorphic development, as it determined locations and specific morphology of valleys and cuesta cliffs, as well as further landform development in the adjacent areas of the structural surfaces (blind valleys). The abundance, outstanding expression, preservation and accessibility of relict hypogene karst features in the extensive cuesta exposures of the Inner Ridge makes it the foremost region for studying regularities of hypogene solution porosity development, the process currently ongoing in the adjacent artesian basin of the Plain Crimea.

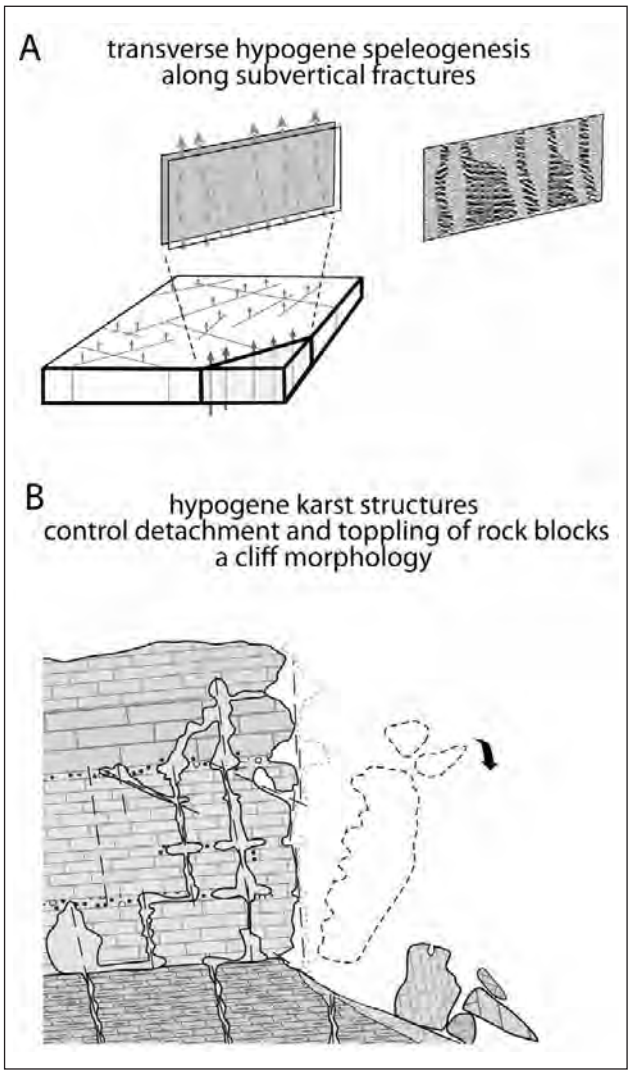

Figure 3. Cartoons illustrating transverse hypogene speleogenesis (A) and its control over slope processes in the Inner Ridge of the Crimean fore-mountains.

References

Yudin VV, 2011. Geodynamics of Crimea. Diaypi, Simferopol.

PARAGENESIS: THE "ROYAL MARK" OF SUBGLACIAL SPELEOGENESIS

Stein-Erik Lauritzen
Department of Earth Science, Bergen University, Allegaten 41, N-5007 Bergen, Norway, Stein.lauritzen@geo.uib.no

Paragenesis results in characteristic speleogens that are found in caves developed under most climatic regimes. However, being a result of sediment excess in the karst conveyor system, it is also a characteristic of the glacier ice-contact (i.e. subglacial) regime. In this case, paragenetic galleries and passage half-tubes may be regarded as a continuation of subglacial esker systems. A unique feature of subglacial speleogenesis – and subglacial paragenesis – is topographically reversed flow from englacial hydraulic gradients superimposed onto adjacent karst.

1. Introduction

Paragensesis (Renault 1968), or antigravitative erosion (Pasini 1975; Pasini 2009), is a speleogenetic mode that occurs in cases where there is a sediment excess in the karst transport system (Farrant and Smart, 2011, Farrant, 2004). Sedimentation in phreatic passages causes corrosion to be directed vertically, or sometimes sideways, onto soluble surfaces not covered in sediment (Lauritzen and Lundberg 2000), Figure 1. The result is either inverted canyons of a similar dimension as the host passage (Ford and Ewers 1978), incised halftubes of a distinctly smaller dimension than the host passage, or a pattern of anastomosing half-tubes leaving a pattern of "rock pendants" between them (Bretz 1942). This process can be simulated on small-scale analogue plaster models (Lauritzen, 1981b) where half-tubes and pendants only form when cave walls and ceiling are in contact with a sediment fill, se also Slabe (1995). Half-tubes and pendant fields are strong indicators of previous sediment fills, and of phreatic or epi-phreatic conditions. The ambiguity of inverted canyons versus normal vadose incisions in relation to the water-table can be solved uniquely (Lauritzen and Lauritsen 1995), thus providing a valuable tool for speleogenetic analysis.

2. Morphological characteristics

A characteristic of paragenetic evolution is asymmetric development around a gently dipping guiding fracture that has identical litology on either side, Figure 1a. In extreme cases, a perfectly circular or elliptical conduit may have formed entirely above its guiding fracture. In principle, first-order proto-conduits may be regarded as paragenetic, as insoluble clay may occupy the floor during the laminar, inception regime, resulting in an asymmetric development around the guiding fracture or bedding plane. Paragenesis may occur through several phases or "stages" as revealed in passage cross-sections where half-tubes and channels are superimposed into each other, Figure 1c. Therefore, a system of *passage order* may be a useful nomenclature in distinguishing and keeping track of the various stages of passage development (Lauritzen 2010). This is somewhat similar to the nomenclature of "channel order" in the Hortonian system. A primary conduit (proto-conduit) is then a *first order conduit*, and may remain so if it continues to develop symmetrically through its entire post-breakthrough stage. However, any change in the cross-sectional profile is of one higher order than the speleogen it is superimposed into. A vadose canyon incised from a first order tube is then second order. Paragenetic half-tubes, canyons and pendant fields are related in the same way, see Figure 2.

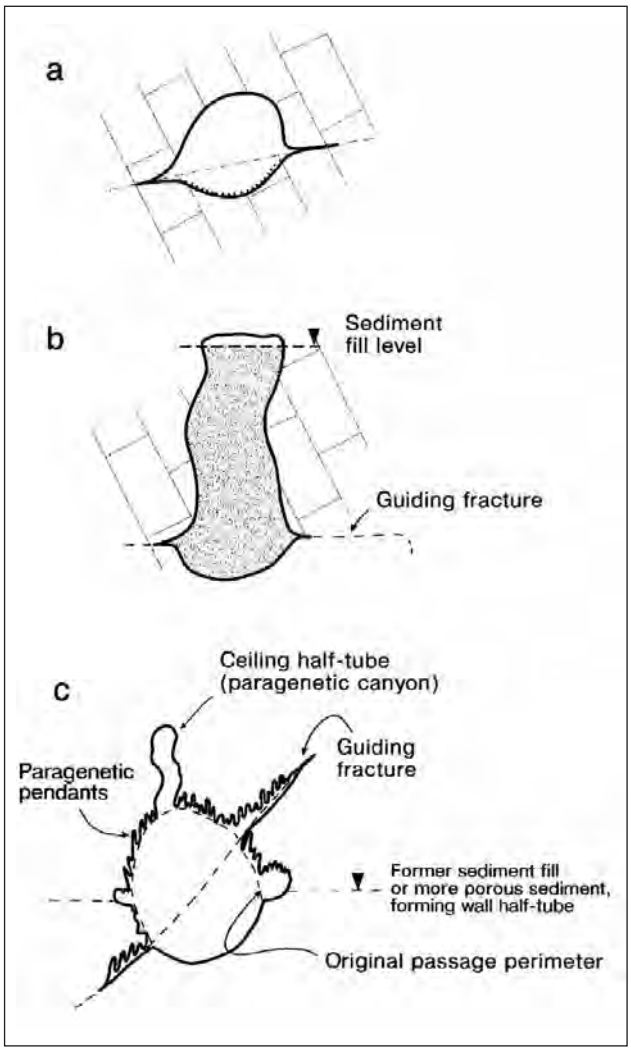

Figure 1. Various expressions of paragenetic passasge cross-sections. From Lauritzen & Lundberg (2000).

3. The sub-glacial regime

In the sub-glacial environment, eskers and sub-glacial tunnels are, in essence, paragenetic, where an ice conduit, or R-channel (Hooke et al. 1990), is maintained above a phreatic streambed of gravel and boulders. Eskers display sinuous "meandering" and are often found in elevated positions relative to the valley floor. In this situation, paragenetic development of caves adjacent to wet-based

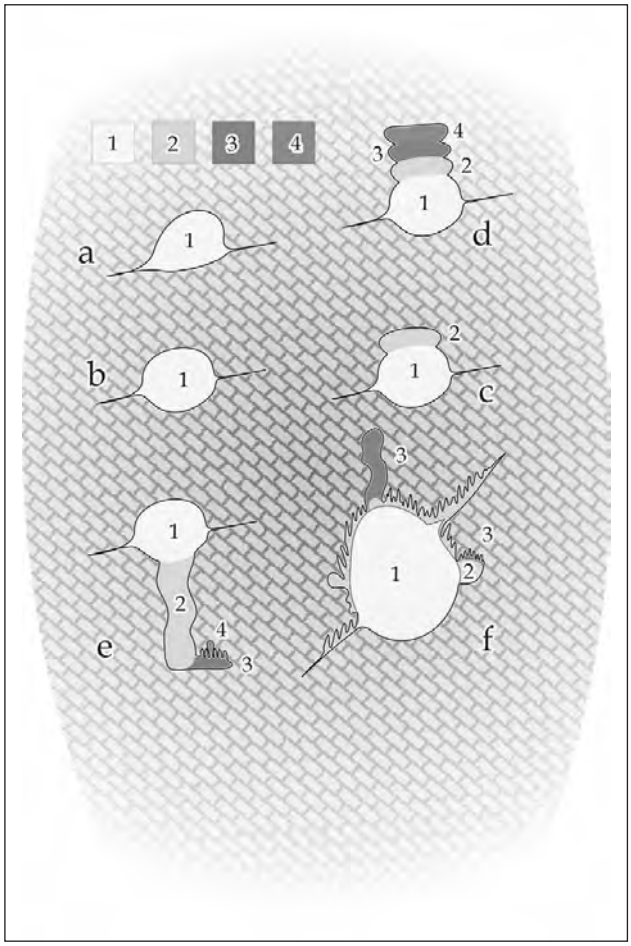

Figure 2. Speleogen order as expressed in passage cross-sections. Numbers, 1, 2, … are speleogen order, a….f are various examples of superposition. From Lauritzen (2010).

glaciers may be regarded as a continuation of its esker systems into the karst. Examples of large amplitude, inverted canyons as well as systems of half-tube and pendant development will be discussed in the presentation. Subglacial water flow is dictated by the glacier surface and may override local topography. In fortuous cases, this effect is preserved in some phreatic caves where scallop flow direction reveal reversed flow, i.e. "up-hill", relative to the present topography (Lauritzen 1981a, 1981b, 1984, 1983). Often, such reversed flow is associated with paragenetic half-tubes and rock pendants. Although not unique to the sub-glacial ice-contact regime, paragensesis appears to be a characteristic feature of it and a valuable resource in speleogenetic analysis.

References

Bretz JH, 1942. Vadose and phreatic features of limestone caverns. Journal of Geology, 50, 675–811.

Farrant AR, 2004. Paragenesis. In Gunn, J. (ed.) Encyclopedia of caves and Karst Science. Fitzroy Dearborn, London.

Farrant AR, Smart PL, 2011. Role of sediment in speleogenesis; sedimentation and paragenesis. Geomorphology, 134, 79–93.

Ford DC, Ewers RO, 1978. The development of limestone cave systems in the dimensions of length and breadth. Canadian Journal of Earth Sciences, 15, 1783–1798.

Hooke RL, Laumann T, Kohler J, 1990. Subglacial Water Pressures and the Shape of Subglacial Conduits. Journal of Glaciology, 36, 67–71.

Lauritzen SE, 1981a. Glaciated karst in Norway. Proceedings, 8th International Speleological Congress. Bowling Green, 8, 410–411.

Lauritzen SE, 1981b. Simulation of rock pendants – small scale experiments on plaster models. Proceedings, 8th International Speleological Congress. Bowling Green, Ky USA, 8, 407–409.

Lauritzen SE, 1983. Arctic and Alpine karst symposium, August 1–15. 1983. Program and Field guide, Department of Chemistry, University of Oslo, Oslo.

Lauritzen SE, 1984. Evidence of subglacial karstification in Glomdal, Svartisen, Norway. Norsk Geografisk Tidsskrift, 38, 169–170.

Lauritzen SE, 2010. Litt Om Paragenese eller antigravitativ korrosjon; klassifikasjon av former (Paragenesis, or antigravitative corrosion, a classification system). Acta Spelæologica Norvegica, 1&2, 94–104.

Lauritzen SE, Lauritsen Å, 1995. Differential diagnosis of paragenetic and vadose canyons. Cave and Karst Science, 21, 55–59.

Lauritzen SE, Lundberg J, 2000. Meso- and Micromorphology of Caves: Solutional and erosional morphology. In Klimchouk, A., Ford, D. C. & Palmer, A. N. (eds.) Speleogenesis: Evolution of Karst Aquifers. National Speleological Society, Huntsville, Ala.

Pasini G, 1975. Sulli'importanza speleogenetica dell' "erosione antigravitativa". Le Grotte d'Italia, 4, 297–326.

Pasini G, 2009. A terminological matter: paragenesis, antigravitative erosion or antigravitationla erosion? International Journal of Speleology, 38, 129–138.

Renault P, 1968. Contribution a l'étude des actions mécaniques et sédimentologiques dans la spéléogenŠse. Les facteurs sédimentologiques. Annales de Spéléologie, 23, 529–593.

Slabe T, 1995. Cave Rocky Relief and its Speleological Significance, Znanstvenoraziskovalni Center Sazu, Ljubliana.

GLACIER ICE-CONTACT SPELEOGENESIS

Stein-Erik Lauritzen[1], Rannveig Øvrevik Skoglund[2]
[1]Department of Earth Science, Bergen University, Allegaten 41, N-5007 Bergen, Norway, Stein.lauritzen@geo.uib.no
[2]Department of Geography, University of Bergen, Fosswinckelsgt. 6, N-5007, Bergen, Norway, rannveig.skoglund@geog.uib.no

The classic hypothesis of G. Horn's (1935) subglacial speleogenesis as an explanation of the relatively small diameter cave conduits in the Scandinavian marble stripe karst is reviewed. Recent work, including accurate cave mapping and morphological analysis, radiometric dating of cave deposits, chemical kinetics experiments and computer simulations have challenged the old theory. Scandinavia has relatively small caves that often have surprisingly high ages, going beyond the limit of Th/U dating. The high ages are apparently compensated by correspondingly slow wall retreat rates in the ice-contact regime, and longer periods when the caves were inactive. Ice-contact speleogenesis varied in time and space, in pace with waxing and waning of wet-based ice. Maze or labyrinth morphology appears as a characteristic feature of caves ascribed to these processes.

1. Subglacial speleogenesis

Between WW1 and WW2, the Norwegian geologist and speleologist *Gunnar Horn* (1894–1946) studied caves in the marble karst of North Norway. Horn published his results in German and Norwegian periodicals (Horn 1935, 1937, 1945, 1947). These ideas were new and radical for their time, resulting from a remarkable train of original observations and thoughts. Horn's main thesis was that phreatic speleogenesis under subglacial conditions was a simple and feasible explanation for the formation of numerous relict and truncated phreatic caves that are located in hanging position within the walls of glacially sculptured valleys. In modern terminology, the ice-contact regime beneath wet-based glaciers and ice-sheets was a sufficient speleogenetic agent. Presently, more than 2,000 karst caves have been recorded in the country, with maximum lengths and depths of 25 km and 580 m, respectively. However, most of them are relatively small (passage diameter) compared to caves in other countries, and – from the viewpoint that size is a measure of (active growth) age – one may infer that the caves are relatively young. Horn suggested that the last glacial cycle would have been sufficient to account for the development of these relatively small cave passages. Horn was also the first to name the characteristic *stripe-karst* morphology (Horn 1937; Lauritzen 2001) in the marble-mica schist setting.

2. Chronology

Our investigations, since the mid-1970'ies, have focussed on morphological analysis, studies of cave sediments and radiometric dating of speleothems which made it possible to test Horn's hypothesis. First, we have shown that many caves, also relatively small ones, consist of labyrinths or mazes, either horizontally or vertically, depending on the attitude of the host rock in the marble stripes. Second, many caves, even quite small ones, contain speleothems that date beyond the last glacial cycle, some also exceed the present limit of the method (Th/U: 750,000 yr.). These caves may, in principle, even be older than the Quaternary ice-ages, although direct proof of pre-glacial deposits in them has yet to be found.

3. Flow regimes and labyrinth morphology

Through accurate cave mapping and scallop morphometry, we have been able to demonstrate that the corrosive flow that caused wall retreat was quite slow, corresponding to average groundwater velocities in non-glacial karst (Lauritzen et al. 2011), and that "levels" or tiers in vertical maze caves did not operate independently, but were part of a flow network that involved the whole (known) cave (Lauritzen 1982). Many relict labyrinths which slope into the hillside, like the Grønli system (Lauritzen et al. 2005) and the Nonshaugen system (Skoglund Øvrevik and Lauritzen 2011) were effluent (discharge areas) when active. Other caves display terrain-reversed phreatic flow (Lauritzen 1984). These features are best explained by ice-contact under hydraulic gradients superimposed from a surrounding glacier or ice-sheet. Modelling experiments suggest that when in contact with a wet-based glacier, karst aquifers tend to develop maze or labyrinth morphology (Skoglund et al., 2010).

4. Subglacial wall retreat rates

Due to the chemical conditions in subglacial waters and the general high content of alkaline rock flour with a large specific area, speleogenetic wall retreat rates are up to 50 times less effective under subglacial conditions than under non-glacial (interglacial) conditions. All these effects, and field observations, provides a good explanation why we have relatively small caves of a comparably high age (Lauritzen and Skoglund 2013).

5. The "car-wash" analogy

Speleothem (stalagmite) dates represent periods when the cave was inactive (drained). Likewise, the periods of formation for calcareous concretions (*Höhlenkrapfen, Kyrle (1923), "doles" in French)*, reveal periods when the cave was filled with sediments having pore-water that was super-saturated with respect to carbonate, which by inference mean that speleogenesis was stagnant. Many *Höhlenkrapfen* which we to-day find cemented onto clean-

washed passages date beyond the last glacial maximum, yet they *do not* stay proud of the surrounding marble wall. Hence, *no effective wall retreat has occurred since the concretion was formed*, even during the deglaciation, when water availability and presumably chemical aggressiveness was optimal. If we plot all available data of speleothems and *Höhlenkrapfen* ages in the same diagram, together with the time-distance diagram of glacial cover during the last glacial-interglacial cycle, an interesting picture appears (Figure 1). If all these observations came from the same cave (they do not), there would hardly be any time-windows available for wall retreat (active speleogenesis). Since we also have positive evidence that speleogenesis did occur during this period, for instance through the *Kvithola Mechanism*, i.e. phreatic ice-contact speleogenesis under thin ice cover (Lauritzen 1986) and through interglacial speleothems that have become part of a scalloped wall, we must conclude that ice-contact speleogenesis was relatively slow, and sporadic in time and space, in pace with waxing and waning of wet-based ice in the local topography. Therefore, the so-called "car-wash analogy" (Lauritzen 2010) offers a feasible concept of this process, Figure 2. In this situation, we consider two caves, 1) and 2) situated in valley floor and wall, respectively. According to the position of the ice-sheet/glacier front at any time, the two caves are either activated or stagnant. Scenario a) represents a continental, mainly dry-based ice-sheet with the margin on the continental edge. At b) the ice front is closer, so that both caves are within the ablation area and can receive supraglacial and subglacial water. At c) the ice front is at the caves, which both experience maximum hydraulic gradient, water flow and CO_2 supply. At d) the glacier front is proximal to the caves and only the valley floor cave can receive water.

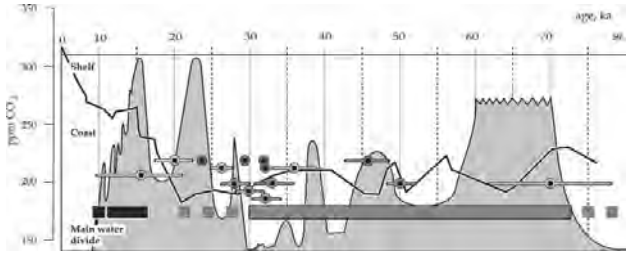

Figure 1. Time-distance diagram for glaciations on the Norwegian mainland during the last 80 kyr (purple areas). The black curve represents atmospheric CO_2 content based on Antarctic ice. Dots with error bars: radiometrically dated speleothems and Höhlenkrapfen. Horisontal bars: periods with paleomagnetically dated cave sedimentation. From Lauritzen & Skoglund (2013).

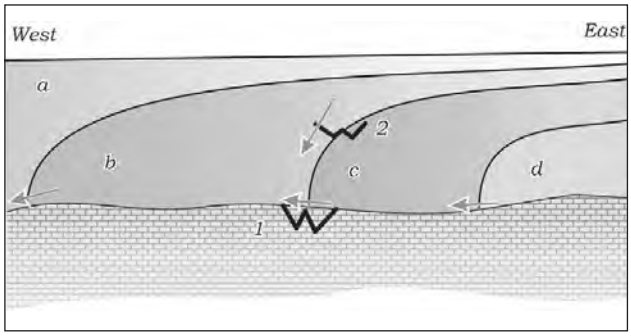

Figure 2. The car-wash analogy of speleogenesis, where glacier contact may be likened to a car-wash moving through the landscape with stationary caves. From Lauritzen (2010).

References

Horn G, 1935. Űber die Bildung von Karsthöhlen unter einem Gletcher. Norsk Geografisk Tidsskrift, 5, 494–498.

Horn G, 1937. Űber einige Karsthöhlen in Norwegen. Mitteilungen für Höhlen und Karstforschung, 1–15.

Horn G, 1945. Om Dannelsen av de Nordlandske Karsthuler. Norsk Geologisk Tidsskrift, 25, 180–182.

Horn G, 1947. Karsthuler i Nordland. Norges Geologiske Undersøkelse, 165, 1–77.

Kyrle G, 1923. Grundriss der theoretischen speläologie.

Lauritzen SE, 1982. The paleocurrents and morphology of Pikhåggrottene, Svartisen, North Norway. Norsk Geografisk Tidsskrift, 36, 183–209.

Lauritzen SE, 1984. Evidence of subglacial karstification in Glomdal, Svartisen, Norway. Norsk Geografisk Tidsskrift, 38, 169–170.

Lauritzen SE, 1986. Kvithola at Fauske; Northern Norway: an example of ice-contact speleogenesis. Norsk Geologisk Tidsskrift, 66, 153–161.

Lauritzen SE, 2001. Marble Stripe karst of the Scandinavian Caledonides: An end-member in the contact karst spectrum. Acta Carsologica, 30, 47–79.

Lauritzen SE, 2010. Grotter. Norges ukjente underverden. (Caves. Norway's unknown underground), Tun Forlag, Oslo.

Lauritzen SE, Hestangen H, Skutlaberg S, Øvrevik R, 2005. The Grønli-Seter cave research project, Rana, North Norway. Proceedings of the 14th International Congress of Speleology, Athen-Kalamos, August 2005, Paper P-22, 1–6.

Lauritzen SE, Skoglund Øvrevik R, 2013. kap. 6.15: Glacier ice-contact speleogenesis in marble stripe karst. In Frumkin, A. (ed.) Treatise of Geomorphology, Vol. 6: Karst Geomorphology. Elsevier, London.

Lauritzen SE, Skoglund Øvrevik R, Skutlaberg S, Lauritsen Å, Worthington SRH, 2011. What can scallops tell us about ice-contact speleogenesis in Scandinavia? In Heldal, T. (ed.) Winter Conference 2011, Norwegian Geological Society. Norwegian Geological Survey, Stavanger.

Skoglund Øvrevik R, Lauritzen S-E, Gabrovsek F, 2010. The impact of glacier ice-contact and subglacial hydrochemistry on evolution of maze caves: A modelling approach. Journal of Hydrology, 388, 157–172.

Skoglund Øvrevik R, Lauritzen SE, 2011. Subglacial maze origin in low-dip marble stripe karst: examples from Norway. Journal of Cave and Karst Studies, 73, 31–43.

GROUNDWATER / SURFACE WATER MIXING IN THE UNDERGROUND HYDROLOGIC SYSTEM OF THE DEMÄNOVSKÁ DOLINA VALLEY (SLOVAKIA)

Peter Malík[1], Dagmar Haviarová[2], Jaromír Švasta[1], Miloš Gregor[1], Anton Auxt[3]
[1]Štátny geologický ústav Dionýza Štúra – Geological Survey of Slovak Republic, Mlynská dolina 1, SK-817 04 Bratislava 11, Slovakia, peter.malik@geology.sk, jaromir.svasta@geology.sk, milos.gregor@geology.sk
[2]Slovak Cave Administration – ŠOP SR, Správa slovenských jaskýň, Liptovský Mikuláš, Slovakia, haviarova@ssj.sk
[3]HES-COMGEO spol. s r. o., Kostiviarska cesta 4, SK-974 01 Banská Bystrica, Slovakia, anton.auxt@hescomgeo.sk

In the Demänovská dolina Cave system (Slovakia) and its vicinity, discharge of water courses on the surface and in the underground hydrologic system on 49 places were measured by current meter in 7 series of discharge measurements. These measurements included discharges of the surface streams, waters of the underground hydrological system as well as the springs in the vicinity of streams. Together with discharge measurements, water temperature and specific electric conductivity (EC) records were taken on the same place. EC values of the surface streams waters, running from the northern slopes of the Nízke Tatry Mts., formed by crystalline rocks, allochtonous to the underground hydrological system (~30 to 80 $\mu S \cdot cm^{-1}$), substantially differ from the EC values of the autochtonous surface water streams (formed in the cave system or within the side valleys of the main karstic canyon; ~270 to 350 $\mu S \cdot cm^{-1}$). Water temperature of the surface streams is quite variable throughout the year (~0.0 to 15.0 °C), while that of underground streams is pretty stable (~5.0 to 7.0 °C). Discharge measurements, performed both on the surface and in the cave system enabled the estimation of hidden surpluses or discharge losses between measurement points in different hydrologic situation (high / low water stages). Using the mixing equation with known hidden surplus, we could also calculate the supposed water temperature and EC value of the "new" water entering the system. Its EC value and seasonally-dependent (or independent) temperature helped us to decide on its connection to the surface water input from the crystalline slopes or its affinity to waters recharged directly through the karstic structure. Results of the seven series of measurements had revealed that only autochonous water is recharging the upper part of the Demänovská dolina Cave system, and water losses of the surface stream of Demänovka have no direct connection to the underground cave river unless it reaches its lowest few hundred meters near its terminating point of "Vyvieranie".

1. Introduction

Demänovský Cave System is up to now the longest speleologically interconnected karst system in Slovakia. Its position is within the northern slopes of the Nízke Tatry Mts. (northern part of Central Slovakia), just beneath the highest peaks of this range (directly 5.8 km north from Chopok with 2,024.0 m a.s.l., and 8.5 km NW from the Ďumbier Mt. of 2,043.4 m a.s.l.). Two show caves are opened in the system, with position of their entrances of N48.998135°/E19.585230° (Demänovská jaskyňa Slobody / Cave of Liberty) and N49.016383°/E19.580893° (Demänovská ľadová jaskyňa / Demänovská Ice Cave).

The length of the system is 35,358 km, the system was formed by the Demänovka River under the eastern slopes (right side) of the Demänovská dolina Valley in the Middle Triassic dark-grey Guttenstein limestones of the Fatricum tectonic unit (Krížna nappe; Biely et al. 1997). It represents a large and complicated complex of cave passages, domes and abysses developed in 9 evolution levels with an active allochthonous stream. Altogether 10 speleologically interconnected caves form the system as known today – the most important are: Demänovská jaskyňa Slobody / Cave of Liberty (8,336 m) and Demänovská ľadová jaskyňa / Demänovská Ice Cave (2,445 m), which are open to the public. The other ones are Demänovská jaskyňa mieru / Cave of Peace (16,174 m), Vyvieranie Cave (1,437 m), Demänovská medvedia jaskyňa / Bear Cave (1,447 m), Pustá Cave (4,663 m) and another five smaller caves (Údolná Cave, Cave Pod útesom, Pavúčia Cave, Jaskyňa trosiek Cave and Cave No. 15).

Figure 1. Position of the Demänovský Cave System (Nízke Tatry Mts., Slovakia, Europe).

Other interesting caves, present within the Demänovská dolina valley like Štefanová Cave (10,047 m), Okno Cave (2,570 m), and Suchá Cave (780 m) are genetically related (Bella et al. 2007). We can expect speleological connection of these caves with the system in the future, but also further discoveries. Hydrologic system in the central part of the Demänovská dolina valley can be divided into its surface part (surface stream of Demänovka) and underground part flowing through the cave system (underground stream of Demänovka).

2. Natural settings of the Demänovská jaskyňa Slobody / Cave of Liberty

Demänovská jaskyňa Slobody / Cave of Liberty is considered to be the most beautiful cave in the system, as it represents morphologically the most variegated part of the Demänovský Cave System, developed in six levels by the ancient ponor inflows of Demänovka River and its side hanging ponor tributaries. The length is reported to be 8,336 m with elevation distance of 120 m. The underground part of the Demänovka water-course flows through the lowest floor of the Cave of Liberty. Demänovka River springs in the non-karstic granitic territory of the main ridge of the Nízke Tatry Mts., and on its northward flow it partly sinks into underground in the area of Lúčky. The underground part of the river reappears again on the ground surface in the form of a massive karst stemming point, called Vyvieranie / Springing, through the Vyvieranie Cave northerly from the Cave of Liberty. Air temperature here ranges from 6.1 to 7.0 °C, relative humidity is between 94 and 99 %. Apart from running water, several lakes are found within the system – with the most interesting Veľké jazero "Těsnohlídko" / Great Lake of "Těsnohlídko" is 52 m long, 5 to 12 m wide and more than 7 m deep. Demänovská jaskyňa Slobody / Cave of Liberty is unique with quantity and variety of stalactite formations of all types (Droppa 1957). Apart from white stalactites, we can find here also yellow, pink, red and even purple stalactites, and sometimes grey, dark-green up to black coloration. In addition to the Veľké jazero "Těsnohlídko", several little sinter lakes with various stalactite and stalagmite formations are found at the bottom (lakes of Zlaté / Golden, Koralové / Atoll, Leknové / Water Lily, Perlové / Pearl's, Hroznové / Grape's). Cave pearls in the form of pea balls in the Veľký dóm / Big Dome, frost stalactites, Stony Sun in Klenotnica / Treasury House and water lily lakes with rococo style dolls in the Ružový dóm / Pink Dome are considered as the cave's rarity. All stalactite and stalagmite formations are still growing, with high gloss in comparison to other caves of the system.

Discovered by A. Král and A. Mišura in the dry period of 1921 through the swallow hole, lead the Demänovská jaskyňa Slobody / Cave of Liberty was opened for the public in 1927, after pathways and electric lights were completed. Later, current entrance was digged in 1930. It is situated in the western slope of the Točište hill at the altitude of 870 m a.s.l. (50 m above the bottom of the valley). Attractive for domestic and foreign visitors, with 100,000–180,000 visits annually, it is the most visited cave in Slovakia and deserves relevant degree of its protection. However, the surrounding area, known as popular ski resort of Jasná, is developing quickly thus creating a constant environmental threat (not only) to the whole underground karst system.

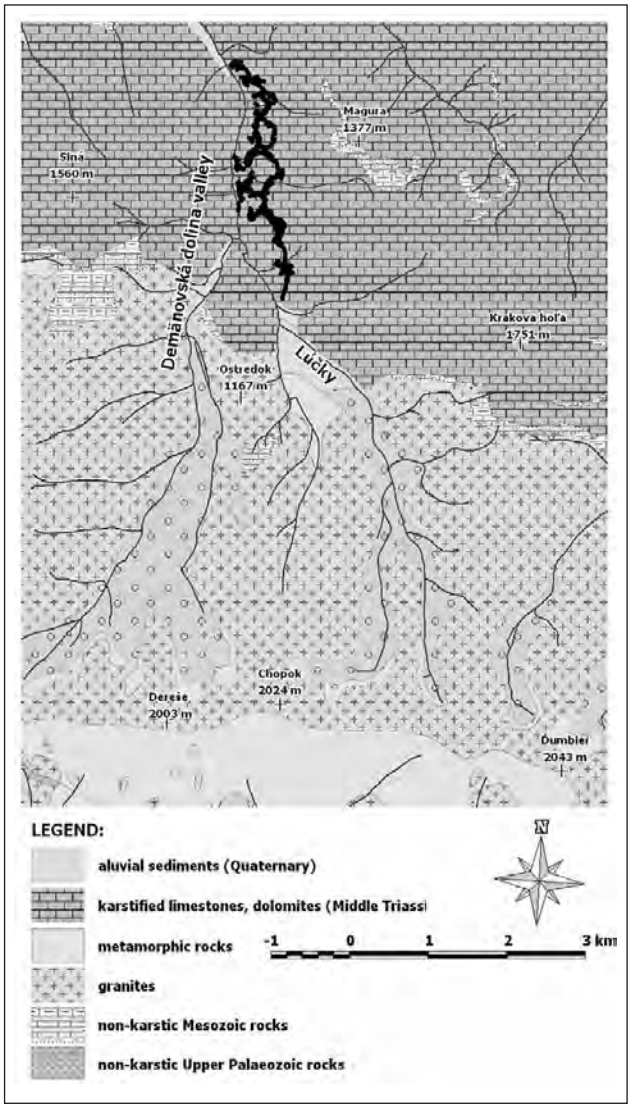

Figure 2. Geological settings of the Demänovský Cave System (in black) surroundings (after Biely et al. 1992).

3. Methods

To extend existing knowledge on hydrogeological and hydrological settings of the Demänovský Cave System, which seem to play key role for its protection, and that should serve as technical arguments for management measures aimed at maintaining favourable status of the site in professional positions of the Slovak Cave's Administration in planning and building procedures associated with this site, a large project of hydrogeological prospection started here in 2009 (Haviarová et al. 2011).

Several specific hydrogeological activities were planned and realized within the framework of this project. They include geophysical measurements – magnetometry and geoelectric methods in symmetrical modifications of resistance profiling and vertical electrical soundings in the area of Lúčky (a contact zone between crystalline rocks and karstified Mesozoic carbonates) from where the development of the Demänovský Cave System begins. Hydrogeological settings of this part of the Demänovská dolina valley have not been thoroughly investigated yet. Therefore, in this part also drilling of 3 boreholes and

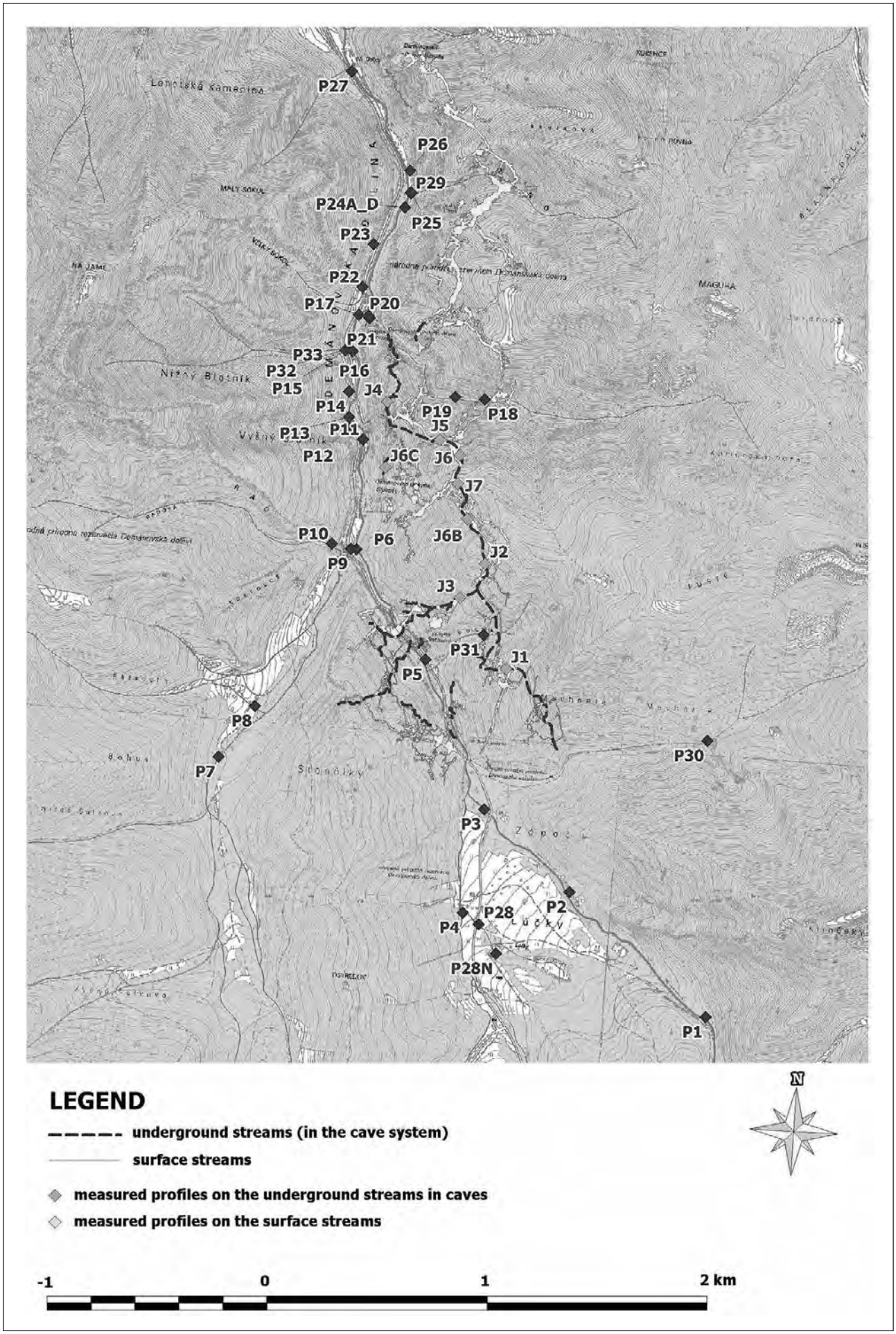

Figure 3. Position of the discharge measurement points on the surface streams and on the underground streams.

following hydrodynamic tests was performed and subsequent groundwater level gauging was set here. In addition, a monitoring network of so-called environmental isotopes ($\delta^{18}O$; $\delta^{2}H$ and tritium) counting 32 sampling places for regular observation (in 2-months interval) of in water was established. This type of analysis – in contrast to the relatively large number of classical analyzes, providing the basic physicochemical parameters of water – in Demänovská dolina valley has not been realized. Within the project, also 12 tracer tests using a biological tracer were realized in the whole Demänovský Cave System. Discharge gauging started since the beginning of November 2009 on 5 profiles of the Demänovka river or its tributaries on the ground surface, and long-term monitoring of discharges in its underground part was set up in the same time. Finally, continuous discharge measurements on these gauging objects were supplemented by denser network of current meter measurements in seven different climatic periods. These were performed mainly in these parts of water courses, where the existence of active river sinks was proven. To identify directions of groundwater flow, hidden karstic flow connection and possible interaction between low mineralized surface water and groundwater with 3–4 times higher TDS content.

Discharge of water courses on the surface and in the underground hydrologic system on 49 places were measured by current meter in 7 series of discharge measurements. These measurements included discharges of the surface streams, waters of the underground hydrological system as well as the springs in the vicinity of streams. Together with discharge measurements, water temperature and specific electric conductivity (EC) records were taken on the same place. EC values of the surface streams waters, running from the northern slopes of the Nízke Tatry Mts., formed by crystalline rocks, allochtonous to the underground hydrological system (~30 to 80 $\mu S \cdot cm^{-1}$), substantially differ from the EC values of the autochtonous surface water streams (formed in the cave system or within the side valleys of the main karstic canyon; ~270 to 350 $\mu S \cdot cm^{-1}$). Water temperature of the surface streams is quite variable throughout the year (~0.0 to 15.0 °C), while that of underground streams is pretty stable (~5.0 to 7.0 °C). Discharge measurements, performed both on the surface and in the cave system enabled the estimation of hidden surpluses or discharge losses between measurement points in different hydrologic situation (high / low water stages).

Discharge measurements were performed mostly by current meter (OTT, C2 type), and sometimes when possible – in the case of smaller streams or streams – method of dish & stop watch was applied. Measurements of discharge in the Demänovka watershed were repeatedly performed during field work campaigns in 2011–2012 in various water stages to enable respective comparison of different water exchange. These were performed in the days of 20.–22. 01. 2011 (series 1); 03.–05. 03. 2011 (series 2); 05.–07. 05. 2011 (series 3); 27.–29. 06. 2011 (series 4); 08.–09. 09. 2011 (series 5); 01.–03. 12. 2011 (series 6); and 10.–12. 05. 2012 (series 7). Measurements were concentrated on the surface part of the Demänovka stream and its tributaries between the sites of Lúčky and Kamenná chata, and underground Demänovka between Achátový dóm Dome in the Pustá Cave and its terminating point on the karstic spring of Vyvieranie (Figure 3).

Table 1. Algorithms used for calculation of the hidden surpluses or hidden losses of discharge between the measured profiles.

Reference profile	Profiles of the stream interval	Algorithm of hidden surplus / water loss calculation
Surface stream of Demänovka		
P2	P2 / P1	P2 - P1
P3	P3 / P2	P3 - P2
P5	P5 / P3	P5 - P4 - P28 - P3
P6	P6 / P5	P6 - P5
P11	P11 / P6	P11 - P9 - Z6 - P6
P13*	P13 / P11	P13 - P12 - P11
P17	P17 / P13	P17 - (P14 + P15 + P16 + P32ABCDE) - P13"
P25	P25 / P17	P25 - (P21_P + P22 + P23 + P24ABC) - P17"
P27	P27 / P25	P27 - P29 - P26 - P25
Underground stream of Demänovka		
J2	J2 / J1	J2 - J3 - J1
J7	J7 / J2	J7 - J6B - J2
J6	J6 / J7	J6 - J7
J5	J5 / J6	J5 - J6
J4	J4 / J5	J4 - J6C + (P13 - P12 - P11)* - J5
P21	P21 / J4	P21 - P20 - J4 + VZ**
Stream in the Zadná voda side valley		
P9	P9 / P7	P9 - P10 - P8 - P7
Stream in the Vyvieranie side valley		
P20	P20 / P18	P20 - P19 - P18
Stream in the Okno side valley		
P29	P29 / P33	P29 - P33

Notes:
** visible surplus through the original "Discovery swallow hole"*
*** water abstraction by waterworks (Vyvieranie source)*

Together with discharge measurements, water temperature and specific electric conductivity (EC) records were taken on the same place using the WTW tools (LF 215 and Cond 3310).

Typical EC and water temperature properties of both basic water types (allochtonous and autochnonous) can be applied in the search for origin of unknown waters in the system, even if they can be considered as a mixture of both types. Here, a mixing equation is used for determining of EC and water temperature of a hidden surplus of discharge. Specific electric conductivity EC_1 of the discharge Q_1 can be changed when mixed with additional discharge Q_2 with specific electric conductivity EC_2 to final specific electric conductivity EC of discharge Q. If $Q = Q_1 + Q_2$ (and both mixing discharges are known), then $Q_1 \cdot EC_1 + Q_2 \cdot EC_2 = Q \cdot EC$, and eventually unknown value of specific electric conductivity EC_2 of the known hidden discharge surplus Q_2 can be calculated as $EC_2 = (Q \cdot EC - Q_1 \cdot EC_1) / Q_2$. If between the two measured profiles of the main (evaluated) stream also other registered water side inputs are measured and their discharges are known (Q3, Q4…Qn) as well as their EC values of EC_3, EC_4…EC_n, we can add more members to the mixing equation and unknown value of EC_2 can be calculated as $EC_2 = (Q \cdot EC - Q_1 \cdot EC_1 - Q_3 \cdot EC_3 - Q_4 \cdot EC_4 - \ldots - Q_n \cdot EC_n) / Q_2$, if $Q = Q_1 + Q_2 + Q_3 + Q_4 + \ldots + Q_n$. The same procedure can be applied to water temperatures. Main sources of error here can be found in changes of water chemistry by mixing and by the use of differently adjusted

Table 3. Average and median values of hidden discharge surpluses (+) or losses (-) in l·s-1; EC (in μS·cm-1) and water temperature (°C) average and median values calculated by mixing equations from 7 series of measurement. If discharge surplus was identified, also water temperature and EC are conventionally marked by (+); for water temperature and EC of discharge losses conventional marking of (-) was applied.

Reference profile	number of measurements	hidden surplus (+) or discharge loss (-)		calculated water temp. of hidden surplus (+) or discharge loss (-)		calculated EC of hidden surplus (+) or discharge loss (-)	
		average	median	average	median	average	median
Surface stream of Demänovka							
P2	7	+ 13.1	- 8.1	(+) 1.7	(-) 0.8	(-) 2	(-) 34
P3	7	- 25.4	- 14.7	(-) 4.0	(-) 3.0	(-) 40	(-) 42
P5	7	- 22.6	- 22.9	(-) 4.5	(-) 3.2	(-) 54	(-) 47
P6	7	- 30.2	- 31.0	(-) 4.1	(-) 2.9	(-) 36	(-) 43
P11	7	- 203.7	- 131.3	(-) 4.0	(-) 5.0	(-) 39	(-) 44
P13	7	- 11.9	- 4.6	(+) 1.4	0.0	(-) 28	(-) 44
P17	7	- 75.4	- 54.7	(-) 4.1	(-) 3.6	(-) 47	(-) 47
P25	7	+ 93.4	+ 58.7	(+) 16.3	(+) 8.5	(+) 261	(+) 234
P27	7	+ 47.6	+ 50.8	(-) 9.5	(+) 2.9	(+) 274	(+) 183
Underground stream of Demänovka							
J2	7	+ 41.3	+ 47.3	(+) 7.4	(+) 6.4	(+) 465	(+) 355
J7	7	- 24.5	- 21.1	(-) 5.7	(-) 5.6	(-) 253	(-) 262
J6	7	+ 97.6	+ 85.8	(+) 5.6	(+) 5.6	(+) 251	(+) 259
J5	7	- 18.8	+ 1.4	(+) 5.2	(+) 5.3	(+) 57	(+) 259
J4	7	+ 71.9	+ 70.4	(+) 4.7	(+) 6.2	(+) 178	(+) 81
P21 rep.	4	- 163.4	- 159.5	(-) 4.9	(-) 4.2	(-) 200	(-) 213
P21	7	- 128.9	- 123.4	(-) 5.3	(-) 4.8	(-) 200	(-) 201
Stream in the Zadná voda side valley							
P9	7	- 47.0	- 41.0	(-) 1.6	(-) 1.9	(-) 31	(-) 42
P9 rep.	3	- 49.2	- 46.8	(-) 2.0	(-) 1.5	(-) 59	(-) 65
Stream in the Vyvieranie side valley							
P20	7	- 11.1	- 11.1	(-) 4.4	(-) 4.5	(-) 276	(-) 322
Stream in the Okno side valley							
P29	7	- 0.8	- 0.8	(-) 4.9	(-) 4.0	(-) 343	(-) 345

measuring devices at different places. However, existing extremely contrast of both characteristics in local conditions of the Demänovská dolina valley prevails over the aforementioned influences.

4. Results

Results of all the discharge, water temperature and specific electric conductivity (EC) measurements on 49 profiles in 7 different series are shown in the Table 2. Repeated measurements that were performed at some of the profiles are also shown here; in lines bellow the "main" measurements. Repeated measurements were mostly taken on the other day after the "main" measurement, in the same filed work campaign, to confirm the previous day results for the next day and to understand the current hydrologic situation (raising or falling water stage). For calculation of the hidden surpluses or hidden losses of discharge between the measured profiles on the surface and underground Demänovka stream, algorithms shown in Table 1 were used. For calculation of the unknown values of EC and water temperature of water appearing in the hidden surpluses of discharge, the data from the same points were applied. The discharge, specific electric conductivity and water temperature results are referenced to the lowermost profile (measuring point), appearing in the first column of the Table 1. Position of the profiles (measuring points) is clear from the Figure 3.

In the case when a loss of water amount was identified by discharge measurement, its properties (water temperature and specific electric conductivity) were linked to those which were measured on the upper profile delineating the considered stream interval. Finally, in Table 3, average and median values of calculated hidden discharge surpluses or losses, calculated EC and water temperature values (mixing equations) are found.

5. Discussion and Conclusions

Typical properties of the two basic water types in the area of the Demänovská dolina valley (allochtonous water typical for the surface streams running from the upper crystalline slopes of the mountain range and autochtonous waters recharged directly in the karstified carbonate rock masses) were used in the discussion on the origin of unknown hidden water surpluses in the Demänovský Cave System (based on the knowledge of their specific electric conductivity, water temperature and known discharge of the supposed water mixture). By knowing the discharge of supposed mixture, supposed EC or water temperature value were determined by mixing equation as other end members were known. Typical values of the specific electric conductivity for allochtonous (crystalline) waters were found between 30 to 80 $\mu S \cdot cm^{-1}$ (waters running in the surface streams of Demänovka and its tributaries of Zadná voda and Priečny potok streams above the level of the site of Lúčky), while autochtonous waters (e.g., smaller tributaries of surface stream Demänovka from the valleys of Machnaté, Pustá, Vyvieranie, Okno or groundwater of springs from the Triassic carbonates of the fatricum tectonic unit) have their EC values in the interval from 270 to 350 $\mu S \cdot cm^{-1}$.

Because in the upper part of the surface Demänovka watershed mostly discharge losses were identified (with very few exceptions), we can link water quality of these hidden losses to the properties of the feeding surface stream ($\approx$ 30 to 80 $\mu S \cdot cm^{-1}$). In the stream interval of P25 / P17 the hydrologic situation changes, as here an intensive drainage

function is evident (gaining river), and autochtonous waters (waters of the Demänovská dolina underground hydrologic system) are feeding the surface stream in this part. Average EC value of the hidden surpluses that were calculated by the mixing equation was 261 $\mu S \cdot cm^{-1}$ and its median value was 234 $\mu S \cdot cm^{-1}$ (hidden surpluses average was 93.4 $l \cdot s^{-1}$, and their median was 58.7 $l \cdot s^{-1}$). Similar situation was found on the last stream interval of the surface Demänovka (P27 / P25; hidden surpluses in average of 47.6 $l \cdot s^{-1}$ and median of 50.8 $l \cdot s^{-1}$). Average value of the calculated specific electric conductivity according to the mixing equation should be of 274 $\mu S \cdot cm^{-1}$ and EC median from the seven series of measurements was 183 $\mu S \cdot cm^{-1}$. The lowermost tested stream interval – according to wider range of calculated values – is probably characterised by mixing of different water types with variable EC value, probably more connected to the same or other (i.e. tributaries of Demänovka) surface streams.

In the underground hydrologic system of the Demänovská dolina valley, between the profiles of J1 (Achátový dóm Dome of the Pustá jaskyňa Cave) and J2 (Pekelný dóm Dome of the Demänovská jaskyňa slobody Cave) an average EC value of hidden water surplus according to the mixing equation was found as 465 $\mu S \cdot cm^{-1}$ and median value of 7 series of measurements was 355 $\mu S \cdot cm^{-1}$. Similarly calculated average value of the supposed water temperature was 7.4 °C (median of 6.4 °C). This means that in the area between those two profiles apart from the tributary stream from the Jazerný dóm Dome of the Štefanová Cave (registered on the J3 profile) also another surplus of water of several tens of $l \cdot s^{-1}$ of autochtonous origin, i. e. waters circulating vôd within the hydrogeologic structure of Triassic carbonates of the fatricum tectonic unit (with average of 41.3 $l \cdot s^{-1}$ and median of 47.3 $l \cdot s^{-1}$).

More important hidden water surpluses to the underground Demänovka stream, confirmed by all seven series of measurements between the profiles of J7 / J6 (reaching values from 43.0 $l \cdot s^{-1}$ to 195.3 $l \cdot s^{-1}$, with an average of 97.6 $l \cdot s^{-1}$, and median of 85.8 $l \cdot s^{-1}$), showed average value of the calculated EC of about 251 $\mu S \cdot cm^{-1}$ and their median was 259 $\mu S \cdot cm^{-1}$. Average of calculated water temperatures of the hidden discharge surplus was 5.6 °C and median of these values calculated by mixing equations was also 5.6 °C. Calculated water temperatures were found within the range of 4.6–6.8 °C. Also in this case, it is evident that autochnous waters, recharged and circulating within the Triassic limestones and dolomites of the Demänovská dolina fatricum unit hydrogeological structure are participating on feeding of the underground stream here.

Acknowledgments

Discharge measurements were covered by the project "Improving the care of the Ramsar site – caves in the Demänovská dolina Valley", proposed by the Slovak Caves Administration to the call of the Operational Program Environment (call number OPZP-PO5-09-1) for the program period of 2007–2013, co-financed by the European Fund of Regional Development and the Ministry of Environment of Slovak Republic. All these institutions are deeply acknowledged.

References

Bella P, Hlaváčová I, Holúbek P (eds.), 2007. Zoznam jaskýň Slovenskej republiky. Slovenské múzeum ochrany prírody a jaskyniarstva, Správa slovenských jaskýň, Slovenská speleologická spoločnosť, Liptovský Mikuláš (in Slovak).

Biely A (ed.), Beňuška P, Bezák V, Bujnovský A, Halouzka R, Ivanička J, Kohút M, Klinec A, Lukáčik E, Maglay J, Miko O, Pulec M, Putiš M, Vozár J 1992. Geologická mapa Nízkych Tatier 1: 50,000, GÚDŠ, Bratislava, map (in Slovak).

Biely A, Bezák V (eds.), Bujnovský A, Vozárová A, Klinec A, Miko O, Halouzka R, Vozár J, Beňuška P, Hanzel V, Kubeš P, Liščák P, Lukáčik E, Maglay J, Molák B, Pulec M, Putiš M & Slavkay M 1997. Vysvetlivky ku geologickej mape Nízkych Tatier 1: 50 000, GÚDŠ, Bratislava (in Slovak).

Droppa, A. 1957: Demänovské jaskyne. Krasové zjavy Demänovskej doliny (in Slovak). SAV, Bratislava (in Slovak).

Haviarová D, Malík P, Grolmusová Z, Veis P, Michalko J, 2011. Predbežné výsledky monitorovania izotopového zloženia vôd v Demänovskej doline a jej podzemnom hydrologickom systéme (in Slovak). Aragonit 16(1–2), 69–70 (in Slovak).

KARST PROCESSES AND CARBON FLUX IN THE FRASASSI CAVES, ITALY

Marco Menichetti
Earth, Life and Environmental Department, Urbino University, Campus Scientifico, 61029 Urbino, Italy
National Center of Speleology, 06021, Costacciaro, Italy, marco.menichetti@uniurb.it

Hypogean speleogenesis is the main cave formation process in the Frasassi area. The carbon flux represents an important proxy for the evalution of the different speleogenetic processes. The main sources of CO_2 in the underground karst system are related to endogenic fluid emissions due to crustal regional degassing. Another important CO_2 source is hydrogen sulfide oxidation. A small amount of CO_2 is also contributed by visitors to the parts of the cave open to the public.

1. Introduction

The Frasassi area is located in the eastern side of the Apennines chain of Central Italy and consists of a 500 m-deep gorge formed by the West-East running Sentino River (Fig. 1). More than 100 caves with karst passages that occupy a volume of over 2 million cubic meters stretch over a distance of tens of kilometres at different altitudes in both banks of the gorge.

The main karst system in the area is the Grotta del Fiume-Grotta Grande del Vento that develops over more than 20 km, about 1 km of which is open to the public and is visited by about 200,000 tourists each year. The caves are hosted in Jurassic carbonate banks with a well developed syngenetic porosity. The groundwater drainage is controlled by N-S trending fault systems and a network of conjugate joint sets distribuited in the NE-SW and NW-SE directions.

The caves consist of a maze system of solutional passages, and are developed over at least four main altimetric levels, related to the evolution of an external hydrographic network. The lowest parts of the caves reach the phreatic zone where H_2S-sodium-chloride mineralized groundwaters combine with CO_2-rich meteoric circulation (Fig. 1). The carbonate waters originate from the infiltration and seepage from the surface and have total dissolved solids (TDS) contents of 500 mg/L. Mineralized waters with a temperature of about 14 °C and more than 1,500 mg/L TDS rise from depth into a complex regional underground drainage system. Here, the H_2S can reach concentrations of up to 0.5 mmol/L and the endogenic CO_2 in the water can have values close to 100 mg/L.

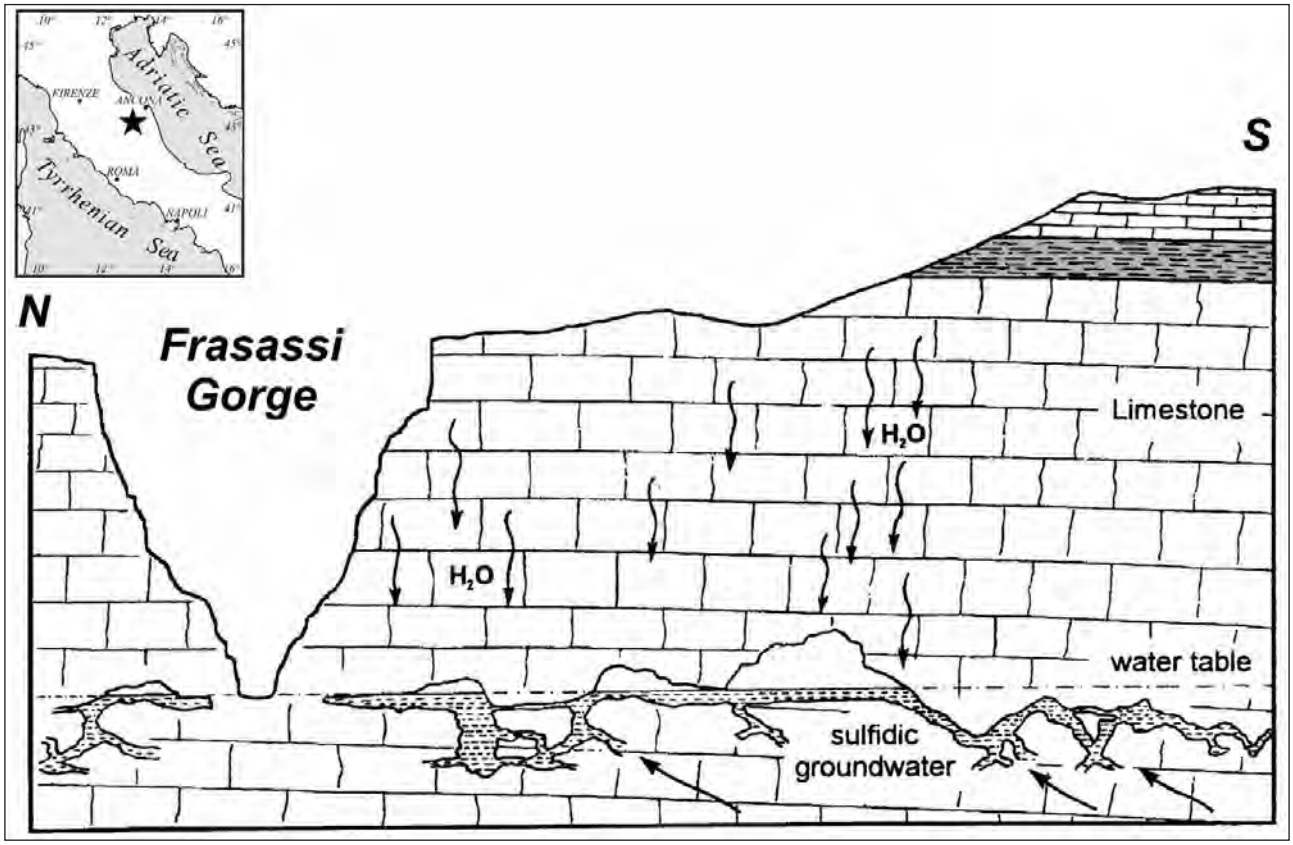

Figure 1. Schematic geological cross-section through the Frasassi Gorge showing the groundwater pathways.

The Frasassi karst system is mainly horizontal and has a ramiform pattern; several big rooms with wide ceilings end abruptly in narrow passages or fissures; phreatic passages (1–10 m size), often anastomotic, also spread over large parts of the cave where they form some network zones. The

prevailing underground morphology is 3D-mazes with cupolas, bubble trails, roof pendants, and knife edges also rather common.

Various types of gypsum deposits fill the cave passages. At present, gypsum formation only occurs on the cave walls above the watertable, owing to H_2S oxidation (Menichetti et al., 2008).

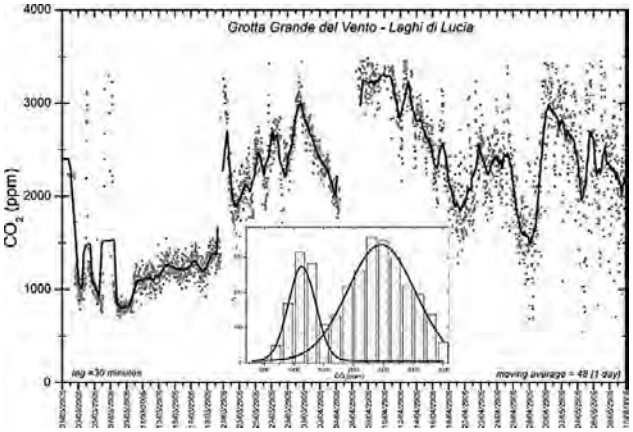

Figure 2. A record of the CO_2 air values near the sulfuric lake from March 1st through May 10th, 2005. The CO_2 values are corrected for altitude. The thick line is the moving average. In the inset graph shows the CO_2 bimodal frequency distribution.

2. Karst processes

The hypogenic origin of the Frasassi cave, as well as other karst systems in the Central Italy, is well known and studied (Menichetti 2009). Hypogean speleogenesis is related to the circulation of hydrogen sulfide rich groundwater through lower Jurassic limestone (Galdenzi and Menichetti 1989, 1995; Menichetti et al. 2008). The same speleogenic mechanisms were also suggested for caves with similar morphologies in other parts of the world (Egemeier 1981; Ford and Williams 2007; Palmer 2007).

The main karst processes in Frasassi occur close the water table where most of the H_2S-rich groundwater is circulated. The oxidation of hydrogen sulfide to sulfate [1] happens in the upper phreatic zone, near the watertable, in the presence of oxygen from dripping waters and from the cave atmosphere. Limestone dissolution [2] takes place both in phreatic and vadose conditions.

[1] $H_2S + 2O_2 \leftrightarrow 2H^+ + SO_4^{2-}$

[2] $2H^+ + SO_4^{2-} + CaCO_3 + H_2O \leftrightarrow CaSO_4.\ 2\ H_2O + CO_2$

Carbonate corrosion produces sulfate ions in the phreatic zone and replacement of limestone in the walls of the vadose sectors of the caves with gypsum (Menichetti et al. 2008).

The cave's sulfuric streams contain much floating organic matter. Sulfur-oxidizing bacterial communities that use H_2S as an energy source and are part of a chemoautotropic aphotic ecosystem supporting invertebrate life are known in the Frasassi caves (Sarbu et al. 2001). The role played by this organic matter in limestone corrosion has not been well defined. The chemical process described in [2] releases fresh CO_2 into the upper portion of the groundwater, as well as into the cave atmosphere, augmenting the aggressivity of the environment toward carbonates. Endogenic CO_2 sources resulting from the significant groundwater flow through carbonate rocks found in correlation with several travertine outcrops are well known in Central Italy (Menichetti, 2009). In the study region, groundwater P_{CO_2} values range from 0.03 to 0.1 atm.

The rate of sulfuric acid speleogenesis was tested over a five year period using calibrated limestone tablets located in the deep sulfidic branch of the Grotta del Fiume containing a fast flowing sulfidic stream. The tablet surfaces where replaced with gypsum at a limestone corrosion rate of about 0.05mm/y. The weight loss was strongly influenced by the location of each tablet within the cave chamber and by the concentration of hydrogen sulfide in the cave atmosphere (Menichetti et al. 2008).

Calcium carbonate deposition occurs in many parts of the caves, and the experimental values obtained are especially important for the cave branch open to the public, where in the vicinity of the underground tourist pathway coins and dust are incorporated into the thin carbonate flowstones.

3. Carbon flux

Measurements of CO_2 in the air were carried out over many years using various techniques, with both spot and automated sample aquisition. The measurement density is higher close to the branch of the cave open to the public where electric power is available; measurements were also taken close to the sulfuric lakes and streams. Spot measurements were acquired using vials through wich a calibrated air sample was drawn with a pump. Continuos measurements were recorded with infrared sensors (accuracy of ± 5ppm) connected to a datalogger. The carbon dioxide concentration in the deep branch of the cave varies from 600 to 4000 ppm and is related to the discharge of rising sulfidic water and to the seasonal biological cycles (Fig. 2).

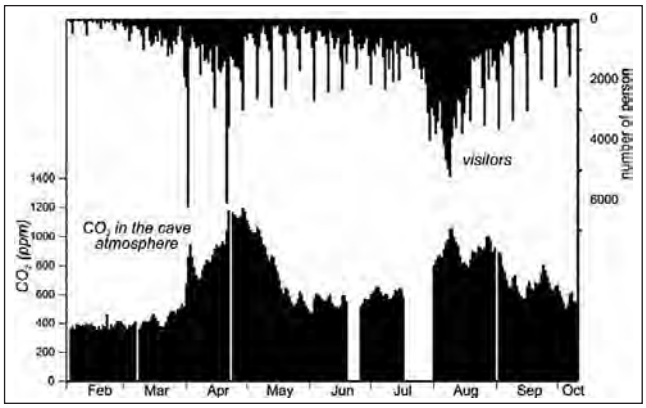

Figure 3. A record of the CO_2 air values in the branch of the Grotta Grande del Vento open to the public. A total of 250,000 visitors entered the cave from February 1st through October 15th, 1993. The CO_2 values are corrected for altitude.

In the part of the cave open to the public, the natural background CO_2 concentration in the air is augmented by an anthropogenic component. Tourists' breath, as well the opening of the air-tight doors, contributes significantly to the variations in carbon dioxide concentration in the cave atmosphere. The carbon dioxide levels recorded close to the tourist pathway in 1993 show seasonal variations with a summer maximum that exceeds 1,000 ppm and a winter minimum of about 400 ppm. Daily and hourly fluctuations of up to 1,100 ppm can be correlated to the number of

visitors (Fig. 3). In the summer, the drop of the CO_2 concentrations back to background values may take a few days, especially after a severe increase caused by a combination of natural and anthropogenic factors (Menichetti et al. 1994). The CO_2 records close the cave entrance in the Frasassi Gorge show a variation between 350 and 450 ppm that can be related to weather conditions and seasonal vegetation production (Fig. 4).

From July to November of 1997 the CO_2 record above the sulfidic lake shows different cycles that can be correlated with the tectonic activity affecting the area (Fig. 4). CO_2 values reaching 1,400 ppm in August are most likely due to seasonal cycles, while the lower values in September may be related to seismic activity with the occurance of a few earthquakes of M > 5 and epicenters at a distance of 40 km from Frasassi. A frequency distribution diagram of the CO_2 concentrations in the underground sulfuric stream shows an asymmetric distribution (Fig. 4a), while the distribution of epigenic CO_2 concentrations is much more symmetrical. Removing the seasonal trend places the endogenic CO_2 release, which could be related to pre/co-seismic crustal

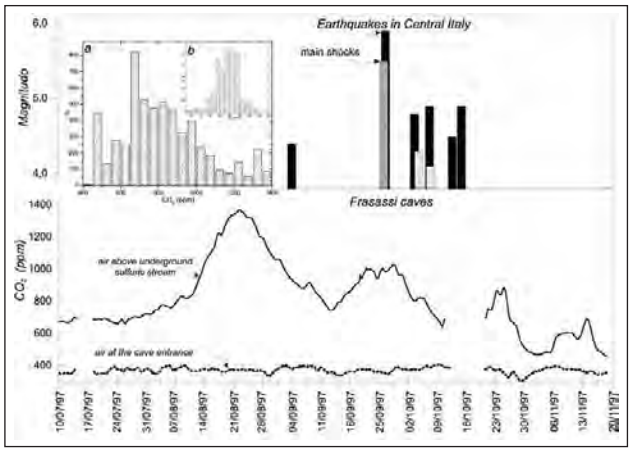

Figure 4. A correlation of the CO2 air concentrations above the sulfuric lake from July 1997 through November 1997, with the regional seismic activity. The inset graphs show the CO2 the frequency distribution in the caves (a) and on the surface (b).

degassing, in evidence (Daddomo et al., 2012).

The carbonate ions in the infiltration water represent 95% of the TDS with an average concentration of 1.5 meq/L. while in the mineralised groundwater, with concentrations reaching 4 meq/L, they represent only 15% of the dissolved geochemical species. The CO_2 concentration in the rising mineralised water is 50 mg/L and varies from 15 to 30 mg/L in the dripping water (Fig. 5). Bicarbonate in the sulfidic waters in the Frasassi region is isotopically light with respect to carbon, ranging between $\delta^{13}C$ = -7.5‰ and -9‰. Microbial mats, consisting of sulfur oxidizing bacteria, collected in the cave's sulfidic stream had average $\delta^{13}C$ values of -35‰ indicating a fractionation of approximately -20‰. This is consistent with carbon stable isotope fractionation values known for chemoautotrophic sulfur oxidizing microorganisms (Serban et al., 2001).

The main CO_2 source in the Frasassi area can, therefore, be related to the endogenic CO_2 flux due to regional crustal degassing. An additional CO_2 source is connected to hydrogen sulfide oxidation reactions.

The antropogenic contribution is important in the branch of the cave open to the public but is minor at the scale of the entire karst system.

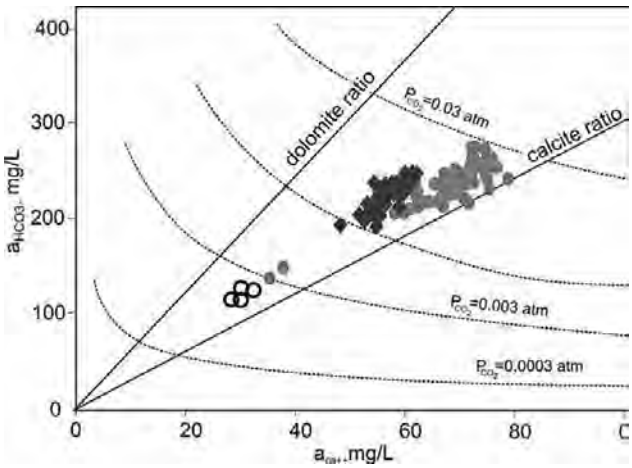

Figure 5. $[HCO_3]$ vs. $[Ca^{++}]$ (mg / L) binary diagram for the Frasassi waters. Solid line represents the $[HCO_3^-]/[Ca2+]$ values expected for calcite and dolomite dissolution based on a heterogeneous equilibrium: $CaMg(CO_3)_2 + 2CO_2 + 2H_2O = Ca^{++} + Mg^{++} + 4HCO_3$. Dashed curves represent equilibrium conditions at different P_{CO2}. Open circles: runoff waters; fill circles: mineralized waters; fill diamonds: dripping waters (from Menichetti et al., 2008).

References

Dadomo A, Lemmi M, Martinelli G, Menichetti M, Telesca L, 2012. Springwater continuous monitoring in the L'Aquila area in concomitance with the April 2009. Chem. Geol., doi:10.1016/j.chemgeo.2012.07.011.

Egemeier SJ, 1981. Cavern development by thermal waters. National Speleological Society Bulletin, 43: 31–51.

Galdenzi S, Menichetti M, 1989. Space time evolution of underground karst system in the Umbria-Marche Apennines in Central Italy. Xth Cong Int Speleol Budapest 3: 745–747.

Galdenzi S, Menichetti M, 1995. Occurrence of hypogenic caves in a karst region: examples from Central Italy. Environmental Geology, 26: 39–47.

Ford DC, Williams P, 2007. Karst geomorphology and hydrology. Wiley London, 562.

Menichetti M, Cigna AA, Galdenzi S, Marinelli G, 1994. Relazione tra flusso turistico e condizioni ambientali nella Grotta Grande del Vento a Frasassi (AN). Atti XVII, Congresso Nazionale di Speleologia, 209–224.

Menichetti M, Chirenco MI, Onac B, Bottrell S, 2008. Depositi di gesso nelle grotte del M.Cucco e della Gola di Frasassi, Considerazioni sulla speleogenesi. – Mem. Ist. Ital.Speleol., II, XXI, 308–325.

Menichetti M, 2009. Speleogenesis of the hypogenic caves in Central Italy. Proceedings of the 15th Int. Cong.of Speleology, 909–915, Kerville.

Menichetti M, 2011. Hypogenic caves in Western Umbria (Central Italy). Acta Carsologica 40/1, 129–145.

Palmer AN, 2007. Cave Geology. – Cave book Ed., Dayton, OH USA, 453.

Sarbu SM, Galdenzi S, Menichetti M, Gentile G, 2001. Geology and biology of the Frasassi Caves in Central Italy, an ecological multi-disciplinary study of a hypogenic underground ecosystem. In: H Wilkens, et al. (Eds.): Ecosystems of the world, Elsevier, New York, 359–378.

MIOCENE – PLIOCENE AGE OF CAVE SNEŽNA JAMA NA RADUHI, SOUTHERN ALPS, SLOVENIA

Andrej Mihevc[1], Ivan Horáček[2], Petr Pruner[3], Nadja Zupan Hajna[1], Stanislav Čermák[3], Jan Wagner[3], Pavel Bosák[1, 3]

[1]Karst Research Institute ZRC SAZU, Titov trg 2, Postojna, Slovenia, mihevc@zrc-sazu.si

[2]Department of Zoology, Faculty of Science, Charles University, Viničná 4, 128 43 Praha 2, Czech Republic, horacek@natur.cuni.cz

[3]Institute of Geology of the Academy of Sciences of the Czech Republic, v. v. i., Rozvojová 269, 165 00 Praha 6, Czech Republic, pruner@gli.cas.cz

Snežna jama cave is 1,600 m long horizontal cave at about 1,500 m a.s.l. in Raduha Massif (Kamnik-Savinja Alps) rich in cave deposits (both allogenic sediments and massive flowstones). The cave size, shape and deposits show (1) formation of the cave in different conditions, and (2) its substantial age. A 4.8 m deep pit was excavated in allogenic sediments. Samples were taken both for palaeomagnetic analysis and palaeontological screening. Sediments consist of rhythmically arranged layers deposited in phreatic conditions. Fragments of rodent teeth and a well-preserved molar of genus Baranomys were identified. Fossil remains indicate mammalian zone MN 16 and MN 14. A high-resolution palaeomagnetic analysis revealed total of 3 principal normal polarized and 2 principal reverse polarized magnetozones. If we accept the palaeontologic calibration, the deposition took place within Gauss and Gilbert chrons, from about 2.6 to more than 5 Ma. Long sedimentation period is in concordance with the cave rocky relief that shows phreatic and epiphreatic morphology and predates the main uplift of the area for about 900 m.

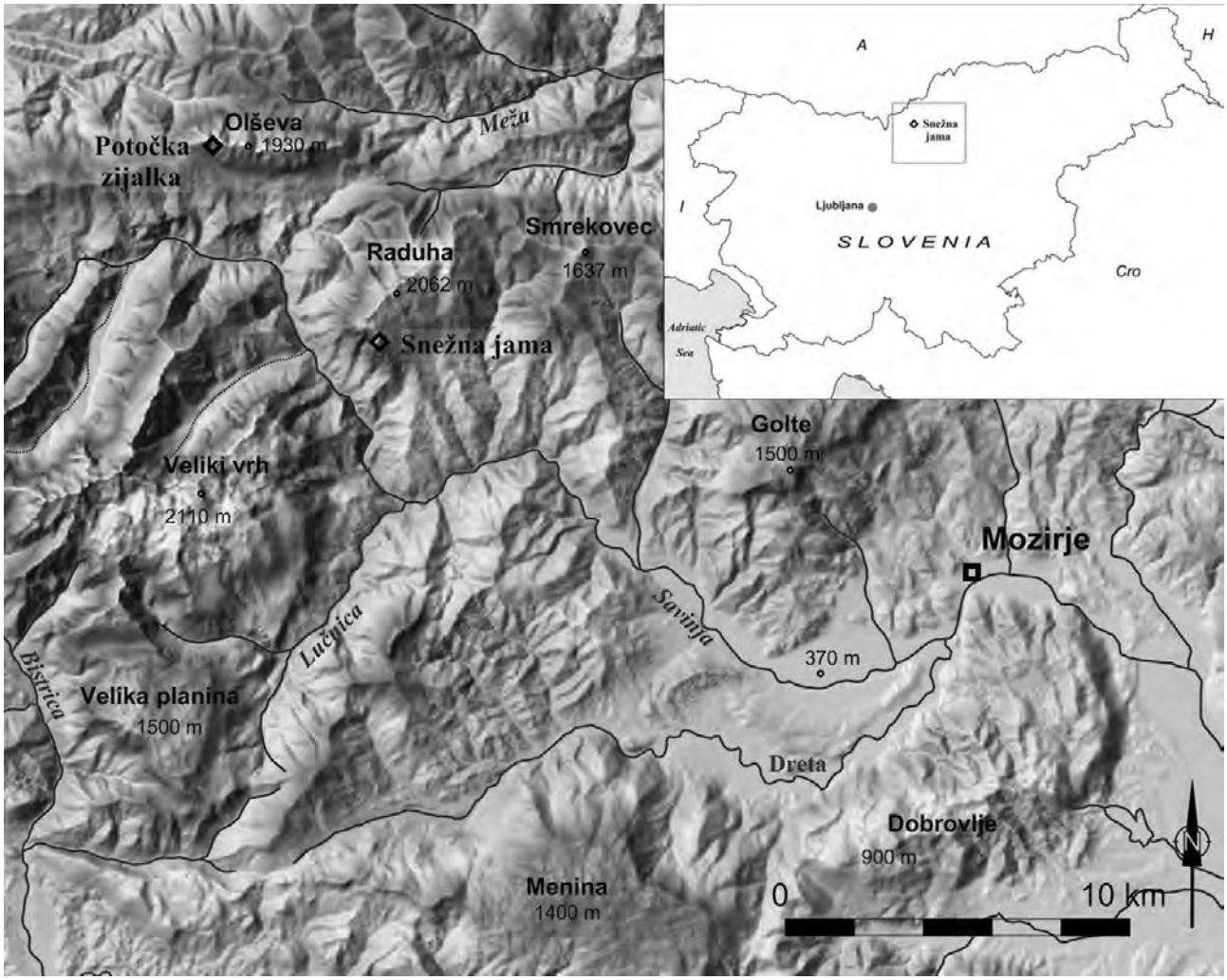

Figure 1. Kamnik-Savinja Alps and location (red dot) of the cave on Raduha Mountain. Potočka zijalka cave on the Olševa Mountain is also marked.

1. Introduction

The Kamnik-Savinja Alps are up to 2,500 m high mountain group in N-central part of Slovenia (Fig. 1), which belongs to Southern Calcareous Alps. Most of the mountains consist of Triassic and Jurassic well-karstified limestones and dolomites in which caves with mostly narrow passages and vadose shafts prevail. In the eastern part of the mountain group, on the Raduha Massif, there are some caves which differ from the rest by large horizontal passages, allogenic sediments and massive flowstone deposits. The size, sediments and especially massive flowstone deposits in these caves show different conditions and older age of the cave formation. The largest of them is the cave Snežna jama.

Snežna jama was explored by cavers after 1980, when the ice blocking the entrance melted (Naraglav and Ramšak 1990). From the morphology and position of the cave, cave sediments and relation to the cave Potočka zijalka on the Olševa Massif, Mihevc (2001) presumed, that the cave predates the uplift of that part of the Alps and that it can serve well for palaeogeographic reconstruction of the area. Paleontological research of samples (Sigé et al. 2003), collected in shallow depth of sediments gave no good results, since the faunal remains of bats and rodents found were sub-Recent. Detailed study of the sediments that followed in the Snežna jama (Bosák et al. 2002; Zupan Hajna et al. 2008) gave some minimum ages of the sediment. Th/U ages of seven analysed speleothems were all over the limit of the method (i.e. >350 ka), but the uranium isotopic equilibrium indicated age of samples over 1.2 Ma. Magnetostratigraphic analyses of the 2.4 m high flowstone profile showed the minimum age 1.77 Ma, but indicated possible correlation with the Gauss and Gilbert Chrons (about 2.6 to 5 Ma; Bosák et al. 2002).

The cave entrance is situated in steep southern slopes of the Raduha (46°23'55.94"N; 14°44'29.78"E) at 1,556 m a.s.l. about 900 m above the Savinja river bed (Fig 2). The cave was formed in massive and thick-bedded limestone (Mioć and Žnidarčič 1983).

The main part of the cave consists of a large and mostly horizontal gallery at 1,470 to 1,520 m a.s.l., some narrow side passages and shafts (Fig. 3). Main passage is about 10 m wide and in some places over 15 m high. On several places, wall notches and large scallops indicate formation in epiphreatic, phreatic and paragenetic conditions.

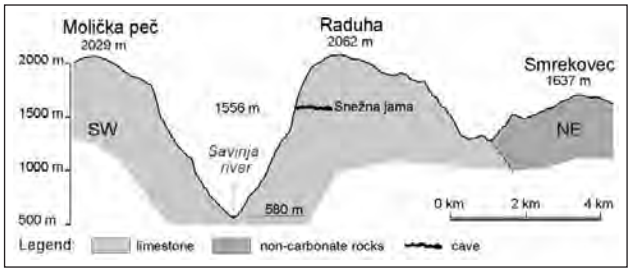

Figure 2. Schematic cross-section of the Savinja river valley and Raduha Massif with the cave.

In some places more than 10 m thick allogenic fluvial sediments have filled the main gallery of the cave. Sediments vary from clayey to pebbly, with particles up to 30 cm. Pebbles of Upper Oligocene andesite tuffs prevail, while poorly-rounded autochthonous limestone pebbles are less frequent.

Speleothems and flowstones deposited over the allogenic sediments and covered large part of the cave floor. At present climatic conditions, there is no deposition of flowstone in this or in other caves located at the same altitude in the region.

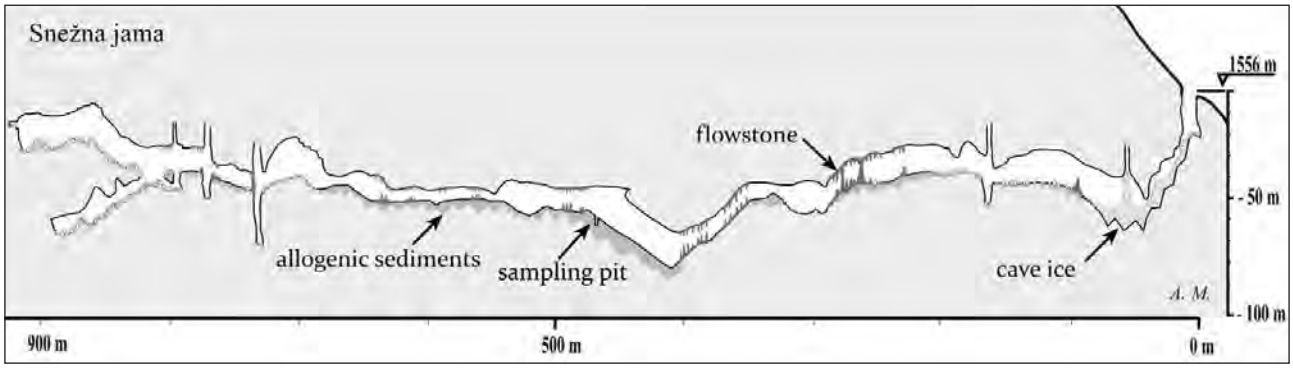

Figure 3. Schematic cross section of the cave Snežna jama. After Naraglav and Ramšak (1990).

2. Geology, position and morphology of the cave

The Raduha Massif (2,062 m a.s.l.) is built of Triassic limestone. It is separated from the main massif of the Kamnik-Savinja Alps by the deeply incised valley of the Savinja River and its tributaries. Towards east and southeast, it is surrounded by Oligocene volcanic and volcanoclastic rocks of Smrekovec Mountain (1,637 m a.s.l.), and by noncarbonate Carboniferous and Permian rocks on the north. At present relief, noncarbonate rocks form lower relief level than the Raduha Massif and the Snežna jama.

The main cave passage is penetrated by four large invasion vadose shafts. Their morphology is comparable to vadose shafts in this part of the Southern Alps. One of them was transformed into the entrance to the Snežna jama. Between the entrance and one of the shafts that brings cold air into the cave permanent ice exists. In the freezing zone all speleothems are broken away and together with other sediments displaced by cryoturbation. Today in the inner part of the cave temperature is 4 to 5 °C all year round. Cryogenic damage on speleothems and cave walls indicates that there existed a period, when two cave entrances permitted air movements and freezing of the whole cave.

Figure 4. Sampling in 4.8 m deep excavated pit in allogenic fluvial sediments in Snežna jama in year 2010.

3. Methods and results

Two profiles were excavated into sediment in a central part of the main passage named Jedilnica about 460 m from the entrance. Main passage here is 8 to 15 m wide and about 15 m high. Passage rises towards NW for about 20 m in the distance of 50 m. The present passage bottom is on sedimentary fill. Gravel interbeds occur in the lower part of the slope, while finer siliciclastic sediments prevail in the upper part of the slope. Wall notches in the passage dip parallel to sediment floor and indicate phreatic conditions during sediment deposition (probably sump) in this part of the cave.

Lower profile (natural outcrop) at the slope foot is 2 m high. It is attached to cave wall and consists of disturbed sediments. The upper profile was excavated near the top of rather steep slope. Following the 5 deep hand drill, which did not reached the cave bottom, we excavated 4.8 m deep pit (Fig. 4). Profile was documented by usual sedimentological methods. Samples for palaeontological analysis were taken in intervals of 30 cm, 20 to 25 kg each. Totally 89 samples for the palaeomagnetic analyses were taken as well.

Excavated profile consists of two sequences separated by erosion horizon. Both sequences are composed of redeposited weathered Upper Oligocene volcanic and volcaniclastic rocks deposited in the cave by a sinking river with the chatchment area inside the Smrekovec (1,637 m) to the E of cave.

Sediment profile generally consists of 2 to 4 cm thick layers of rhythmically arranged clays and silts with medium-to coarse-grained sandy admixture. Cross-bedded sets occur locally. The content of clay component increases in upper parts of rhythms (flyshoid style of sequences). The strata dip is uniform from 38° to 42°. The strata inclination is synsedimentary feature reflecting the deposition in a sump pool.

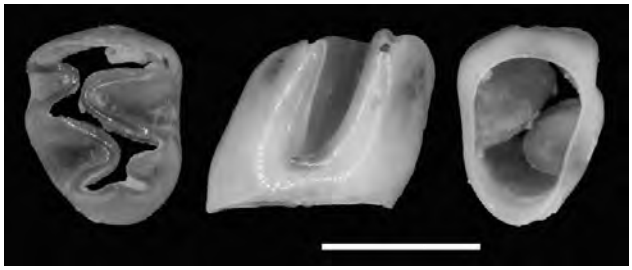

Figure 5. Well preserved enamel of molar of Lower Pliocene rodent that corresponds to genus Baranomys.

A well-preserved rodent molar was found in lower part of the profile. It corresponds to the genus Baranomys (Fig. 5), which presents an index genus of the Lower Pliocene. Several fragments of enamel from incissors and molars of small rodents were also found in poor state of preservation not allowing precise identification. Besides mammalian fossils, several rests of teeth of cf. Chondrichthyes fish were found in several layers most likely represent re-deposited fossils from Upper Oligocene source rocks.

A complex high-resolution palaeomagnetic analysis revealed total of 3 principal normal polarized and 2 principal reverse polarized zones. All magnetozones contain one or more short magnetozones of opposite npolarities (Fig. 6). The matching of obtained magmetostratigraphy with the GPTS (Cande and Kent 1992) is calibrated by the fauna remains (especially of the Baranomyinae). Fauna indicate age of mammalian zones MN 16 to MN 14. If we accept the most probable age corresponding to the MN 16 zone, magnetostratigraphy can be easily correlated with the Gauss and Gilbert Chrons, i.e. from about 2.6 to more than 5 Ma.

4. Discussion and Conclusions

The study of new sediment profile brought new information on the age of allogenic sediments and especially about the duration of their deposition. The data correspond to the geomorphology of the cave and the adjacent karst regions.

Fluvial sediments were deposited in the cave by a sinking river, which eroded highly weathered Upper Oligocene submarine volcanics and volcaniclastics of the Smrekovec area. They were also the source of marine fauna rests (shark teeth) found in cave sediments (Bosák et al. 2012).

The main part of the known cave was formed as an epiphreatic cave containing some phreatic elements. Both the dimensions and shape of the main cave gallery indicate the stabilization of the karst water level for a prolonged time period which caused slow sedimentation and paragenetic re-shaping of the cave. This stable period, dated by fauna and magnetostratigraphy, lasted from about 6 Ma to 2.6 Ma. This period was probably even longer, since the studied profile didn't reach the bottom of sediment fill. This results

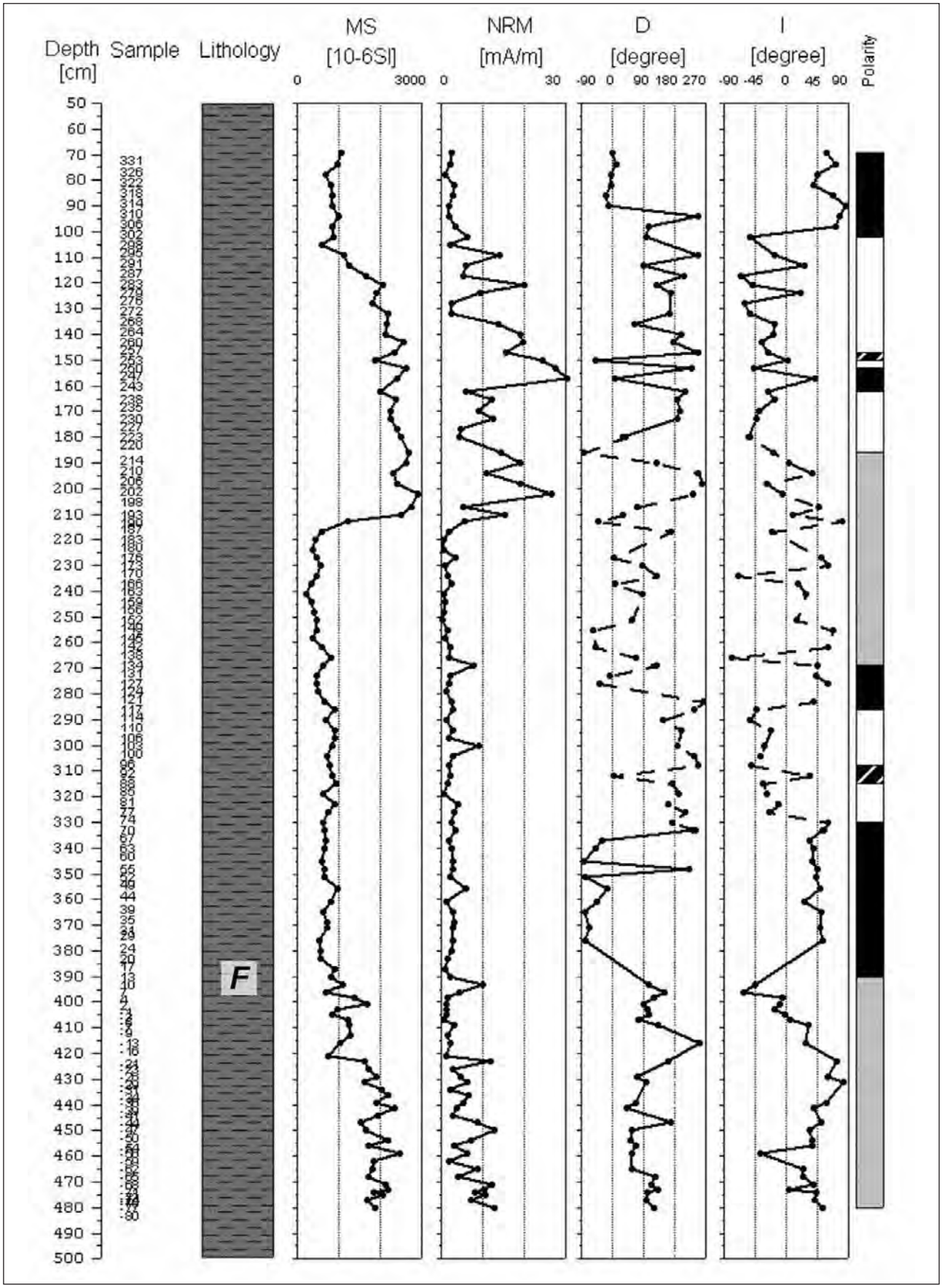

Figure 6. Basic magnetic and paleomagnetic properties of sediment profile from Snežna jama; preliminary results. Polarity scale: black = normal, white = reverse, grey = transient. F = location of the fossil tooth in the profile.

are concordant with the age determined by cosmogenic Al/Be nuclides on quartz pebbles from the same sediment fill by P. Häuselmann, A. Mihevc, D. Sahy and M. Fiebig (in preparation).

The termination of sedimentation in a cave at about 2.6 Ma, was related to mountain uplift causing the river entrenchment and cut off the subterranean karst drainage.

The deposition of flowstone started in passages abandoned by subterranean river. Massive speleothems indicate warm and wet climate, and a low altitude position of the cave. The

massive speleothem deposition later ceased due to climate change following the mountain uplift. During the Upper Pleistocene, the denudation of mountain slopes uncovered the cave and created, most probably, two entrances. Cold Pleistocene climates or simply two entrances with strong air circulation caused freezing throughout the entire cave. Recently these processes have been limited to the entrance part only.

The altitude differences of the relief at the time of cave formation at Miocene/Pliocene boundary can be estimated to 600 m at least, but the hydraulic head in the karst was small. There were several sinking rivers flowing from noncarbonate rocks, sinking and creating caves penetrating limestone ridges and plateaus. Allogenic sediments and Miocene limestone pebbles, fragments of Turitella shells and pebbles of metamorphic rocks and are mixed with local Triassic limestone gravel in cave Potočka zijalka (located at the similar altitude and only about 10 km to the north of the Raduha Massif with the Snežna jama). The possibility that both caves were formed in the same prolonged stable period is great. But the catchment areas of sinking rivers were different. Potočka zijalka received sediments from the north and Snežna jama from the east. They were both discharging to Savinja River, which had only shallow valley at that time (Mihevc 2001; Mihevc et al. 2010).

The evolution of karst surfaces is comparable with the Northern Calcareous Alps where the main phase of subterranean flow connected with the last stage of origin of huge horizontal cave systems is believed to be at the end of Miocene and in Pliocene (Frisch et al. 2000, 2001) and that many main cave systems about 900 m above the modern local base levels of erosion (Zötl 1989).

Following the tectonic uplift, the Savinja River was slowly cutting down for about 900 m. It created deep valleys which now separate high mountains ridges of Olševa, Raduha and karst plateaus like Velika planina, Menina and Dobrovlje. It also created conditions favourable for deep vertical karst drainage and origin of vadose shafts. This palaeogeographic change is well-recorded in the palaeomagnetic properties of sediments preserved in Snežna jama, which is apparently older than the present mountain relief itself.

Acknowledgments

We are grateful to Mrs. L. Strahovnik from Institute of the Republic of Slovenia for Nature Conservation, Reg. unit Celje and Mr. M. Simić from Environmental Agency RS for issuing permissions for the sampling in cave and for field assistance of Mr. D. Naraglav and Mr. S. Ramšak and caving society Jamarsko društvo Črni galeb Prebold. Explorations were performed through Czech Republic – Slovenia bilateral program KONTAKT Nos. 2001/009 (Evolution of karst and caves based on study of cave fills, Slovenia), and MEB 090908 (Karst sediments: tools for the reconstruction of tectonic and geomorphic evolution of karst regions; exemplified on karst territories of Slovenia). Work in the Czech Republic was done within the Program of Advancements in Scientific Research of the Academy of Sciences of the Czech Republic No. K3046108, Research Plans of the Institute of Geology AS CR Nos. CEZ A09/98 Z3-013-912 and AV0Z30130516, and Grants of the Grant Agency of the Academy of Sciences of the Czech Republic Nos. IAA3013201 (Magnetomineralogical and magnetostratigraphic research of cave and fluvial sediments in the Central European region), and IAA30013001 (Palaeomagnetic research of karst sediments: palaeotectonic and geomorphological implications). Research in Slovenia was financed by research programs of the Ministry of Science of Slovenia and Slovenian Research Agency Nos. P6–0119–0618 and P0–0119 (Karst Research), and projects Nos. J6–3035–0618–01 (Origin and development of karst caves) and J6–6345–0618–04 (Development and function of caves in different speleological settings).

References

Bosák P, Hercman H, Mihevc A, Pruner P, 2002. High resolution magnetostratigraphy of speleothems from Snežna Jama, Kamniške–Savinja Alps, Slovenia. Acta Carsologica, 31(3), 1, 15–32.

Bosák P, Pruner P, Zupan Hajna N, Mihevc A, 2012. Karst sediments: tools for the reconstruction of tectonic and geomorphic evolution of karst regions (exemplified on karst territories of Slovenia). Research Reports 2010. Institute of Geology AS CR, v. v. i.: 14–17. Praha.

Cande SC, & Kent D V, 1995. Revised calibration of the geomagnetic polarity timescale for the Late Cretaceous and Cenozoic. – Journal of Geophysical Research, 100, B4, 6093–6095.

Frisch W, Szekely B, Kuhlemann J, Dunkl I, 2000. Geomorphological evolution of the Eastern Alps in response to Miocene tectonics. Zeitschrift für Geomorphologie, 44(1), 103–138.

Frisch W, Kuhlemann J, Dunkl I, Szekely B, 2001. The Dachstein paleosurface and the Augenstein Formation in the Northern Calcareous Alps – a mosaic stone in the geomorphological evolution of the Eastern Alps. International Journal of Earth Sciences, 90(3), 500–518.

Mihevc A, 2001. Jamski fluvialni sedimenti v Snežni jami na Raduhi in v Potočki zijalki. Geološki zbornik, 16, 60–63.

Mihevc A, Horáček I, Pruner P, Zupan Hajna N, Čermák S, Wagner J, Bosak P, 2010. Mio-pliocenska starost jamskih aluvialnih sedimentov v Snežni jami na Raduhi. – In: Košir A., Horvat A., Zupan Hajna N., Otoničar B. (Eds.): 3. slovenski geološki kongres, Bovec, 16.–18. september 2010. Abstracts and field trips, 34–35.

Mioć P, Žnidarčič M, 1983. Osnovna geološka karta SFRJ, list Ravne, 1: 100,000. Zvezni geološki zavod, Beograd.

Naraglav D, Ramšak S, 1990. Snežna jama na Raduhi. Naše jame, 32, 88–92.

Sigé B, Mihevc A, Aguilar JP, 2003. Les chiroptères actuel et fossiles (Pléistocène supérieur d'une grotte d'altitude des Alpes de Slovénie, témoins d'une détérioration climatique = Recent and Late Pleistocene bats in a mountain cave of Slovenia: evidence of a climatic drop. Coloq. paleontol., 2003, 1, 637–645.

Zötl J, 1989. Paleokarst as an important hydrogeological factor. In: Bosák P, Ford DC, Głazek J & Horáček I (Eds) Paleokarst. A systematic and regional review. Academia-Elsevier, Praha–Amsterdam, 483–509.

Zupan Hajna N, Mihevc A, Pruner P, Bosák P, 2008. Palaeomagnetism and Magnetostratigraphy of Karst Sediments in Slovenia. Carsologica 8, Založba ZRC, Ljubljana.

SEDIMENTARY STUDY AND U-TH DATATIONS CONTRIBUTION TO THE MORPHODYNAMIC RECONSTITUTION OF THE JUNCTION CHAMBER (KASSARAT CAVE, NABAY, LEBANON): A GEOMORPHOLOGICAL APPROACH FOR PALAEOHYDROLOGICAL RECORDS ANALYSIS

Nehme C.[1,2,3], Delannoy J.-J.[1,3], Jaillet S.[1], Adjizian-Gerard J.[2,3], John Hellstrom[4], Comaty T.[3], Arzouni M.[3], Matta P.[3]
[1]EDYTEM UMR 5204-CNRS, Université de Savoie, le Bourget du Lac, France, carole.nehme@univ-savoie.fr
[2]Département de géographie, Université Saint-Joseph de Beyrouth, Liban
[3]Association Libanaise d'Etudes Spéléologique (ALES), Mansourieh, Liban, ales.liban@gmail.com
[4]Earth science department, University of Melbourne, Australia

Several studies on karst systems and geomorphology has been initiated in Lebanon recently by EDYTEM laboratory UMR 5204-CNRS, France in collaboration with Saint Joseph University of Beirut and the Association Libanaise d'études spéléologiques (ALES). One of these researches aims at reconstituting: i) speleogenic evolution based on geomorphologic indicators, ii) karstogenesis reconstitution related with the downcutting of the Mediterranean hydrographic network (Antelias and Kelb river), iii) paleogeographical reconstitution of these tow valleys.
Two caves have been chosen in each valley and a morphogenic analysis has been completed in each cave with a geomorphological approach. One of the main caves studied, downstream Antelias valley, is Kessarat cave with its underground river and its 4.6 km gallery development. A 6.45 m height section has been studied in the Junction gallery to reconstitute the deposition process of the sector in response to a collapse process. Stratigraphy observations as well as grain size and morphoscopic analysis on sand layers have helped us to reconstitute the deposit dynamics and the paleoflows of the underground river such as velocity variations and flows directions. Four reconstitution stages are suggested to describe the river deviation. U-Th datations on two stalagmites Kt12011 and Kt22011 suggest upper Pleistocene age to the collapse and the deposition episode in the Junction Chamber. Both collapse and deposition processes are set in the recent stage of Kessarat cave speleogenesis.

1. Introduction

In the framework of a PhD research study, Antelias valley was chosen as a main study site to reconstitute paleogeographical phases of the landscape based on speleogenesis and sedimentary analysis conducted on caves networks and sediments. One of the main caves studied is Kessarat cave (Nabay) with its underground river, situated in the downstream section of the Antelias valley. A morphogenic analysis has been completed by using a speleogenetic approach. Six speleogenetic stages have been identified in Kassarat cave (Nehme et al. 2012):

- The first speleogenetic stage embraces initial development of the cave. Phreatic forms (tubular galleries, semi tubular channel and anastomosis ceiling, notches and dissolution pockets) located along the canyon ceiling and in the upper galleries of Kassarat cave were formed in the phreatic zone of the Antelias karst system during a period of high position of the base level.
- The second and third stages are the result of a water table migration downstream of the valley. The Kassarat Underground River entrenched a canyon below the initial phreatic level.
- The fourth stage is a second erosion level characterized by formation of a semi-phreatic tube at the base of the Kassarat underground canyon. This indicates a probable second erosional level with a long-term stabilization of the water table level at the base of the canyon.
- The fifth and the sixth stage resume processes occurred in the vadose zone of the Antelias Karst after the water level migration downstream: collapse of the canyon ceiling initiated local hydrodynamic readjustments of the underground river regime.

To better understand recent hydrodynamic modifications of Kassarat Underground River in respond to a ceiling collapse, the Junction Chamber was chosen for its morphology aspects and for its well-preserved sediments. The chamber contains a wide range of fluvial sediments (pebble, sand, clay) up to 10 m height. This sector functioned as a sediment trap due to the collapse. A sedimentary study was conducted on these deposits. Stratigraphy analyses as well as grain-size and morphoscopic analysis on sand layers helped us to reconstitute the deposition dynamics of this site during and after the collapse phenomena.

2. Geography and geology settings

Located in the central part of Mount-Lebanon chain, 10 km north of Beirut city, Antelias area is mostly formed by middle Jurassic dolomitic limestone (J4-J5) (Dubertret 1951; Walley 1998). This well karstified area is known for its high concentration of caves (Abdul-Nour 2004) and karstic networks (e.g., Kassarat, Nabaa el-Chataouieh, 22 April, Bear, el-Dahr, Kanaan) (Figure 3). The tectonic setting (Hakim 1988; Walley 1998; Gédéon 1999) of Antelias region indicates local and regional faults with a NNE-SSW and E-W orientation.

Antelias River has 20.4 km^2 of catchment area and drains directly to the Mediterranean Sea (Figure 1). Feeding the Antelias river all over the year, the Fouar Antelias spring catchment area is ten times greater (208 km^2) than the Antelias River catchment area (Hakim 1985; Labaky 2005)

Kessarat cave is one of the largest subsurface networks with 4.6 km passages (Karanouh et al, 2004; Metni et al. 2005). Two siphons, the northern and the main siphon, feed the Kassarat Underground River (Figure 2). Dye coloration campaigns (Hakim and Karakabi 1988; Labaky 2005) showed hydrogeological connection between Kassarat river and Fouar Antelias spring. The cave water is partially collected by the National Water Office of Beirut and Mount-Lebanon to supply Beirut area with drinking water.

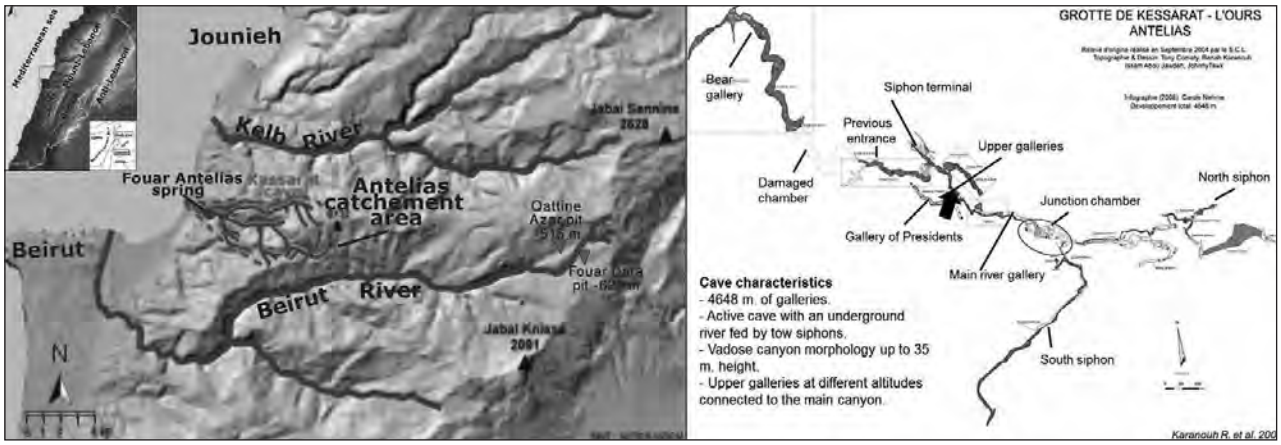

Figure 1. Localization of Antelias river catchment area and the Kassarat map – Nabay (right) and its morphological aspects (left).

3. Methods

A geomorphological map and six detailed sections were produced to identify the main morphogenesis scenario of the Junction Chamber by using a relative chronology approach (Nehme et al. 2012). A sediment section CSJK-I of a 6.45 m in height is studied in the Junction chamber. In the first stage, 50 samples are extracted to characterize each layer. Grain size analyses were conducted using MASTER SIZER S 2.19. In the second stage, 11 U-Channels from the upper part (1.25 m) of the sedimentary unit were extracted and grain-size measurements were completed on 190 samples.

Figure 2. The Junction gallery and the sand deposit showed on the left. Tow conduits are related to the junction Chamber. The first on the left is the upper siphon and on the right, the southern siphon (Photo by S. Jaillet).

4. Results and discussion

4.1. Stratigraphy observation

Observations on layers structure and texture show three sedimentary units (Nehme et al. 2011): Mostly sandy layers with disturbed structure constitute the lower unit. The middle unit is composed by pebbles conglomerate. Sandy and clayey layers with a conserved sub-horizontal structure mostly compose the third unit. Grain-size analysis shows sedimentation processes related to a high-energy flood in the lower unit. The middle unit composed by consolidated pebbles shows a dramatic modification in flow velocity related probably to an external environmental change. The upper unit is formed by nearly flatted bed layers structure. The alternating sand/clay composition of levels is related probably to a low energy flood.

4.2. Grain-size analysis

Grain-size analysis identified some aspects of the flow dynamics during deposition. The analyses of first 50 samples showed mainly two units with different flow dynamic regime (Figure 3):

The lower unit is composed mostly by sandy deposits with well sorted particles. The asymmetry index is positive and

Figure 3. Grain-size analysis on the 50 samples extracted from the lower and the upper unit of the Junction Chamber CSJK-I unit.

tends generally to medium particles. Lower unit deposits are related to regular flows marked by flows with high velocity rates. The upper unit of sequence shows different aspects of the flow regime: variations in the composition of deposits are much more significant in the upper levels of the sequence. We observe well sorted particles in the silt and clay levels and poorly sorted particles in the sand levels. This alternation in the sorting index is in good agreement with the modification of the mean size particles as well as with the stratigraphy observation. The significant and rapid modifications in grain size, sand/clay composition ratio and sorting index indicate fluctuations in the hydrological dynamics between regular flow regime and over flow circulation. These water flows generate poorly sorted particles due to reduction of the flow area, caused initially by the collapse and the progressive deposition process in the Junction chamber. Therefore, stratigraphy and grain-size analyses identified some aspects of the site effect on the sedimentation process in the Junction chamber, especially in the upper unit.

The grain-size analysis of the upper unit, made in 1 cm intervals, helped us to better identify the karst system effect on the sedimentation process. The Figure 4 shows a general decrease of the mean size of particles, despite the composition of fine sand or silt particles. This tendency indicates a hydrodynamic process related to a general decline in the flow velocity. This process can occur in sedimentary traps environments due to an obstruction of a river passage or can be related to a low water discharge in the cave system.

4.3. Discussion

The grain-size and stratigraphy analysis combined with the speleogenetic observations of the sector identify four hydrodynamic stages (Figure 5). Each stage explains the hydrodynamic reorganization of Kassarat river flow in the Junction Chamber:

1) The ceiling collapse obstructed the normal passage of the underground river. Fluvial deposits fill in the Junction gallery as well as a part of the upper and southern siphon conduits. Sediments deposition reaches up to 12 m height and obstructs this part of the cave. Rivers flows circulate in the upper part on the Junction Chamber and form conduits at the same level of the river flow (*Drain annexe* formed in the same direction of the southern siphon conduit and filled with fine deposits).

2) The second stage is related to two major events: flows coming from both siphons were separated due to the sediment deposition in the Junction chamber. The southern siphon flows form a new passage (Capture) to evacuate most of the underground water and join the main river gallery, downstream of Kassarat cave.

Similarly, the upper siphon flows excavated a passage through the Junction deposits. A temporary evacuation of the flows occurred in the narrow tubular conduit. However, the conduit diameter (capture and the tubular passage) is not wide enough to drain all the flows during floods. A flooding process occurs in this area.

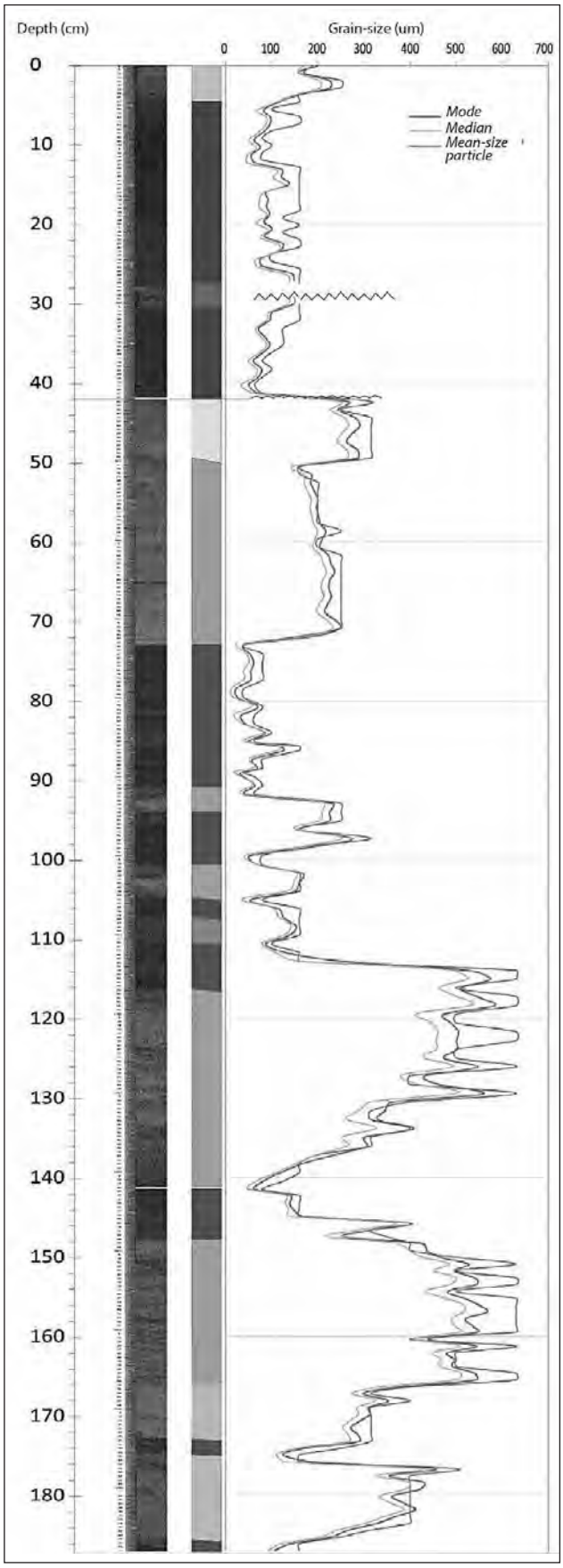

Figure 4. Grain-size analysis on the upper unit of the Junction sediment CSJK-I unit.

3) The third stage describes the regularization of the capture conduit diameter: the flooding process is still active in the area because of the small size of the capture conduit. Therefore, clay and silt sediments are progressively deposited on the upper part of the sedimentary unit CSJK-I. When the size of the capture conduit became wide enough, the southern siphon flows were totally evacuated during each flood episode. During flood season, the southern siphon flows evacuated what left of the deposits blocking the southern siphon passage. This evacuation process causes a local lowering of the water level. The southern siphon water level becomes lower than both of the upper siphon flow and the tubular conduit levels.

4) The last stage shows that the capture controls the local water level on this area in Kassarat cave. The upper siphon flows are then diverted from the initial direction (NW) and joined the southern siphon flows (SE). The tubular conduit becomes inactive and both southern and upper siphon flow are evacuated from the capture conduit.

4.4. Contribution of the U/Th datations

In order to constrain the sedimentary episodes of the Junction Chamber in the general speleogenesis history of Kassarat cave, an age should be suggested for both collapse and fluvial deposition process. Collapsed blocks and fluvial sediments are actually covered by flowstone and speleothems. Two stalagmites were chosen in order to date separately the collapse and the deposition process. The first one is located at the top of the fluvial deposits. The second was extracted from the collapse sector. Calcite sample were extracted from the base of the stalagmites and dated by the uranium/thorium method in the Geochemistry laboratory, Earth Science department, University of Melbourne, Australia (Table 1).

Stalagmite Kt2-2011 located in the collapse zone showed an age around 33.921 ± 1.09 ka. The stalagmite Kt1-2011, located at the top of the fluvial deposits, showed an age around 37.590 ± 0.82 ka. Although 4ka difference is observed between both stalagmites, we suggest that stalagmite growth was set after the collapse and the deposition process in the Junction Chamber. We could not suggest an exact age for each process separately. However both processes were completed prior to the late upper Pleistocene epoch. The calcite deposition phase was long enough after the disconnection of the Junction Chamber from the active network of Kassarat cave. The development of speleothems in this sector suggests wetter climate conditions during the late upper Pleistocene.

U/Th dating records show that the ceiling collapse is set in the upper Pleistocene epoch causing an important fluvial deposition in the Junction Chamber. The final speleogenetic stage (stage 5 and 6) of Kassarat cave is set during the upper Pleistocene, while all other stages (e.g., Introduction: Stage 1 to 4) were prior to that age.

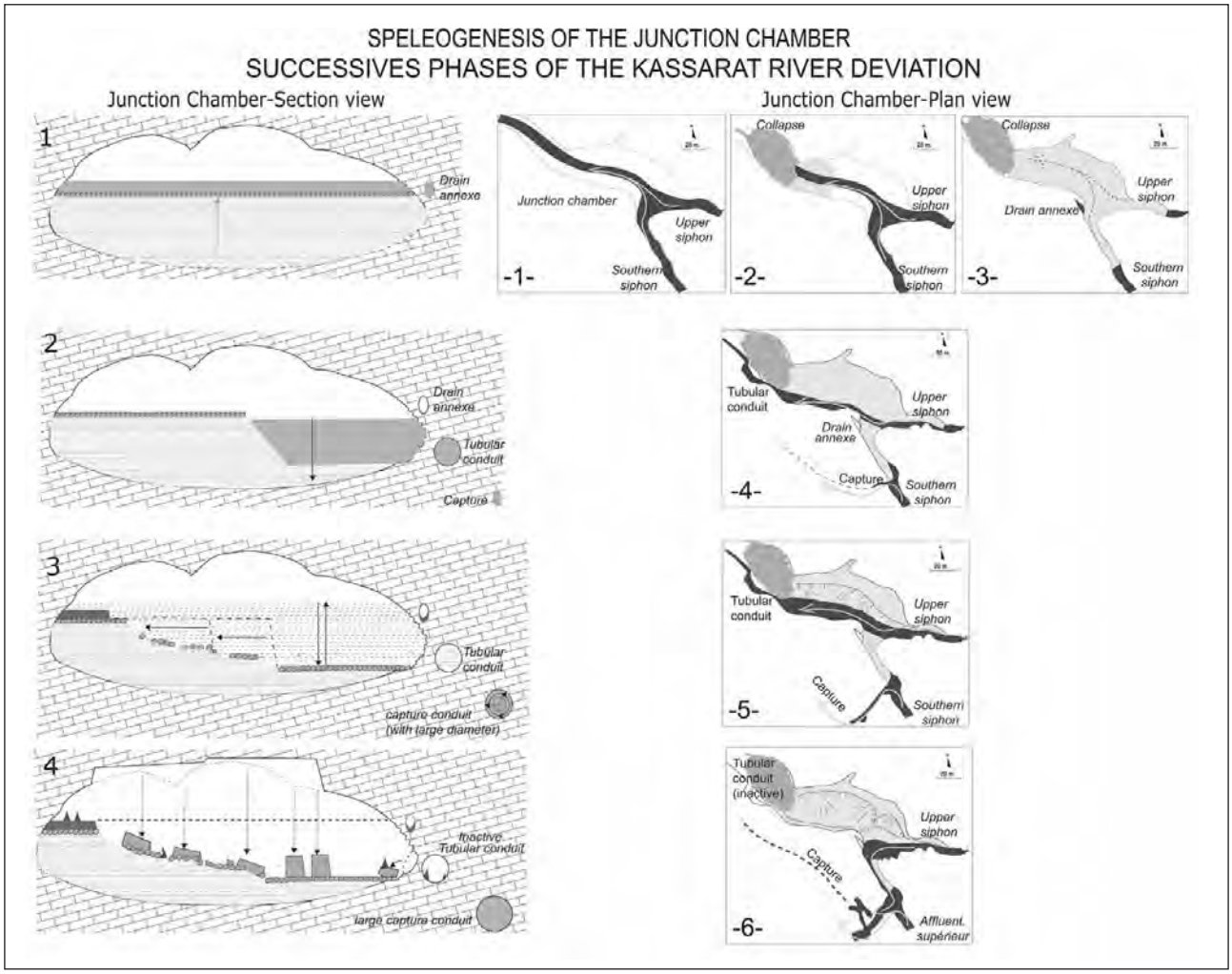

Figure 5. Speleogenesis of the Junction Chamber: successive phases of the Kassarat river deviation.

5. Conclusions

These results helped us to identify some aspects of the geomorphological environments of the Junction chamber and to understand the hydrology dynamic of the sediment trap in respond to a collapse event. Both speleogenesis and sediment analysis resume the history of the Junction Chamber in three phases:

Phase 1: During the upper Pleistocene epoch, the collapse of the ceiling blocked the river channel. Fluvial sediments were deposited in the Junction Chamber leading eventually to filling in almost all the area. The river flow circulates at the upper part of the Junction Chamber.

Phase 2: The river flow level rejoins the initial flow level before the deposition process in the phase 1. Two flow adjustments process occurs simultaneously at the upper and major siphons: The flow coming from the upper siphon excavates a new passage in the deposits. The flows are mostly evacuated through a new tubular conduit. Similarly, a new conduit is formed at the southern siphon. The capture is not wide enough to evacuate the entire flow during flood seasons. Overflow process occurs in the junction Chamber and silt and clayey sediments are deposited in the upper unit.

It is only when the size of the capture becomes large enough to evacuate all flow from the southern siphon; the deposits obstructing the southern siphon are then gradually evacuated. Therefore, the level of flow becomes lower than the upper siphon. The upper siphon flows are then diverted to the capture conduit that controls the flow of both upper and south siphons.

Phase 3: During the late upper Pleistocene epoch, the Junction chamber became no longer active and was disconnected from the active network of Kassarat cave system. Ceiling collapse occurs in the Junction Chamber and stalagmite growth took place on collapsed block as well as on the fluvial deposits.

Table 1. Corrected ages of calcite extracted from stalagmites Kt12011 and Kt22011.

Sample Name	Lab Number	Mass/g	$^{230}U/^{238}U$	$^{234}Th/^{238}U$	$^{232}U/^{238}U$	$^{230}Th/^{232}Th$	Age (a)
Kt12011	UMD120325-213	0.0958	0.2471	0.8469	0.002581	95.7	37.590 ± 0.82
Kt22011	UMD120325-214	0.0939	0.2961	1.0838	0.005027	58.9	33.921 ± 1.09

Acknowledgments

We aknowledge ANR-LIBRIS for providing financial support for the U/Th datations. Many thanks to B.T.D. (Bureau Technique et Développement) for providing hydrological data on Antelias spring. Finally, we're thankful to Pierre-Charles Gérard and A.L.E.S. cavers-Association Libanaise d'Etudes Spéléologiques for providing technical support to complete sampling during field trips.

References

Abdul-Nour H, 2004. Les cavités de l'endokarst du Liban-Spéléorient, (4), 116–128.

Dubertret L, 1951. Carte géologique du Liban: Feuille de Beyrouth 1/50000e. Carte géologique et notice, Ministère des travaux publics, Beirut, Lebanon.

Gedeon M, 1999. Structural analysis of latitudinal fault in the Mount-Lebanon north of Beirut: their kinematics and their role in the tectonic evolution of Lebanon. Master thesis, American University of Beirut, Lebanon.

Hakim B, Karkabi S, 1988. Coloration du gouffre de Faouar Dara et de la grotte des Kessarat. Al-Ouate-Ouate, (3), 18–31.

Karanouh R, Bou jawdeh I, Comaty A, Tawk J, 2004. Mgharet el Kessarat cave system. Al-Ouate-Ouate, (13), map appendix.

Labaky W, 2005. A semi quantitative description of a dye tracing Experiment in the fouar Antelias drainage Basin. Al-Ouat-Ouat, (13), 28–35.

Metni M, Nader FH, Mgharet el-Kessarat, 2005. History, Morphology and Speleogenesis. Al-Ouate-Ouate, (13), 8–13.

Nehme C, Delannoy J-J, Adjizian-Gerard J, 2011. Reconstitution of the groundwater palaeoflow of Kessarat cave, Antelias valley, Lebanon: A geomorphological approach in palaeohydrological records analysis. Poster abstract ID 1893, XVIII INQUA Congress, Bern, Switzerland, 2011.

Nehme C, Delannoy J-J, Adjizian-Gerard J, Hellstrom J, 2012. Late Pleistocene evolution of Antelias valley (Lebanon): speleogenic approach applied on Kassarat cave system with implication of U/Th datations records. Fianl Proc. 20th Int. karst school, Karst Research Institute, Postojna, Slovenia, 66–67.

A GENETIC CLASSIFICATION OF CAVES IN LOWER AUSTRIA

Pauline Oberender, Lukas Plan
Karst and Cave Research Group, Natural History Museum Vienna, Museumsplatz 1/10, A-1070 Vienna, Austria, paulob06@uni-bonn.de, lukas.plan@nhm-wien.at

Caves evolve due to various geomorphological processes which can be used to develop a classification scheme. We adapted existing genetic classifications and focused on the main genetic process which we defined as the one that was responsible for most of the cave volume. This scheme was applied to the 4,849 known caves of Lower Austria and some neighbouring areas. It turned out that more than half of the caves have developed due to weathering and erosion and only 45 % are karstic ones.

1. Introduction

Besides the majority of karstic ones, caves can develop due to various processes. Surprisingly there are only a few comprehensive schemes to classify caves according to their genesis like Trimmel (1968), White (2005), and Striebel (2005). It is even more surprising that, to our knowledge, these classifications have not been applied to extensive data sets of caves yet.

As the classifications mentioned above all have their pros and cons we combined them into a new classification. It is based on the dominant genetic process of a cave. In order to enable the classification of a huge number of caves it was necessary that it is applicable by means of existing cave maps, topographic maps, photographs and reports.

In the present paper we applied this classification to 4849 caves in Lower Austria which have been registered up today.

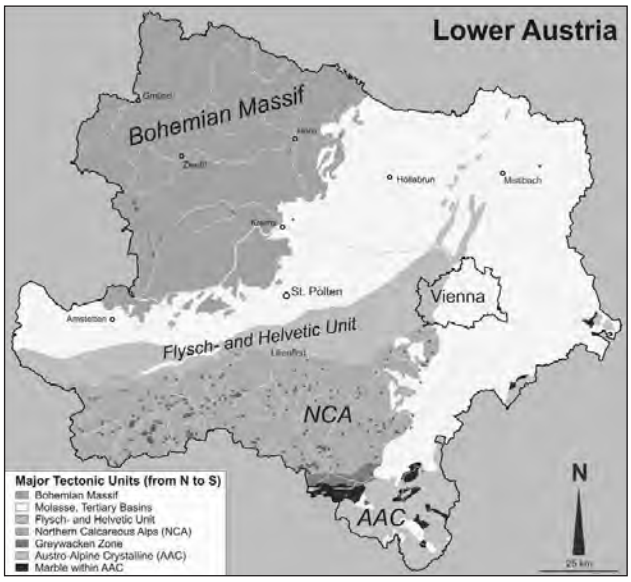

Figure 1. Major tectonic units of Lower Austria and caves longer than 50 m (dots).

2. Study Area

The area of investigation includes the Austrian province of Lower Austria and some neighbouring areas in Upper Austria, Styria, Burgenland, and Vienna (ca. 23,000 km²). The caves of this area are registered in the cadastre of the Spelaeologic Society of Vienna and Lower Austria.

This area comprises most major tectonic units of the Eastern Alps (Fig. 1). These are from north to south:

- Bohemian Massive
- Flysch and Helvetic Unit
- Northern Calcareous Alps
- Grauwackenzone
- Austro-Alpine Crystalline (including Lower Austro-Alpine)
- Molassezone and Vienna Basin

This results in a highly diverse landscape ranging from high alpine karst plateaus (up to 2,079 m a.s.l.), low mountains and hills to extended lowlands (e.g., Schnabel et al 2002).

By April 2012 a total of 4,849 caves longer than 5 m were registered in the study area (Fig. 2). Even though the longest system is 27 km long and the deepest is 756 m deep, most of the caves are rather small. 50 % of the caves are only 5 to 11 m long and only 486 caves are longer than 50 m.

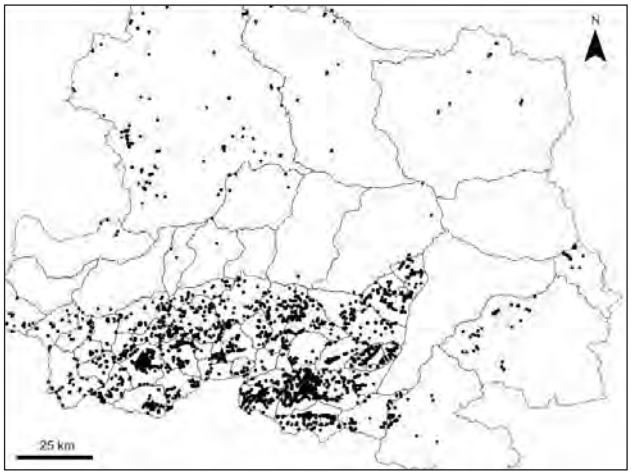

Figure 2. Spatial distribution of the caves in the study area. Obviously the concentration of caves is very diverse as a function of the geological and geomorphological settings. The highest cave density is found in the Northern Calcareous Alps.

3. Methods

3.1. The classification scheme

As some genetic processes are missing in the classification schemes published by White (2005) and Striebel (2005) they were combined and adopted to a new scheme. Further we restricted it to the genetic processes that are active in the caves of the area of investigation (Fig. 3).

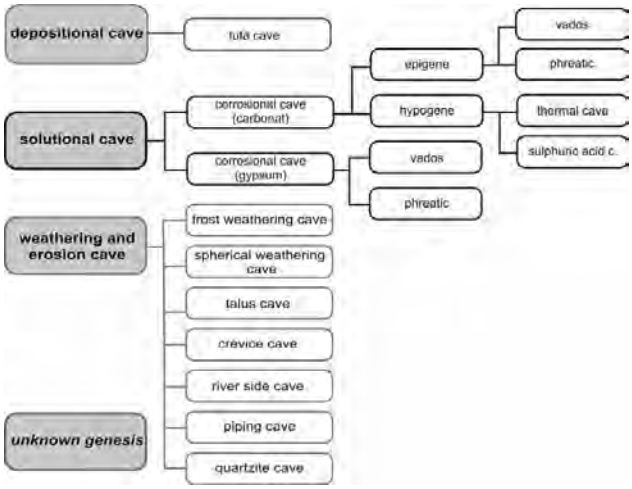

Figure 3. Classification scheme based on the dominant genetic process. The left column (grey) shows four main types, which are differentiated into several sub types due to different processes.

3.2. Classification of caves

Even though it is clear that each cave is polygenetic and a couple of processes have been active to form the present shape it was necessary to keep it simple in order to perform static analyses. Therefore we classified according to the most dominant process i.e. the process that was responsible for the biggest gain in volume.

In geomorphology it is a common approach to reconstruct the process from morphologic observations (Dikau 2006). Therefore we set up a key of characteristic attributes for each cave type considering overall cave morphology and pattern, micro morphologic features (scallops etc.), cave sediments, and the relation of the cave to the surface and to hydrology. Besides some direct field observations (some hundred caves) these attributes were deduced from cave maps, descriptions, photographs, topographic maps (including a high resolution laser scan; NÖ-Atlas, 2012), and discussion with speleologists.

To enable more sophisticated statistical analyses each cave was allocated (1) one of the four main types and (2) a sub type specifying the main type (Fig. 3). In the following we will present only the results of the main cave types.

4. Results

4,849 caves were analysed. For 7 % of these caves the key was not applicable as there was not enough data. This was mainly the case for very small caves which results in missing characteristic data on the cave maps. For 93 % of the caves a classification was possible but for 15 % of them classification is somewhat uncertain.

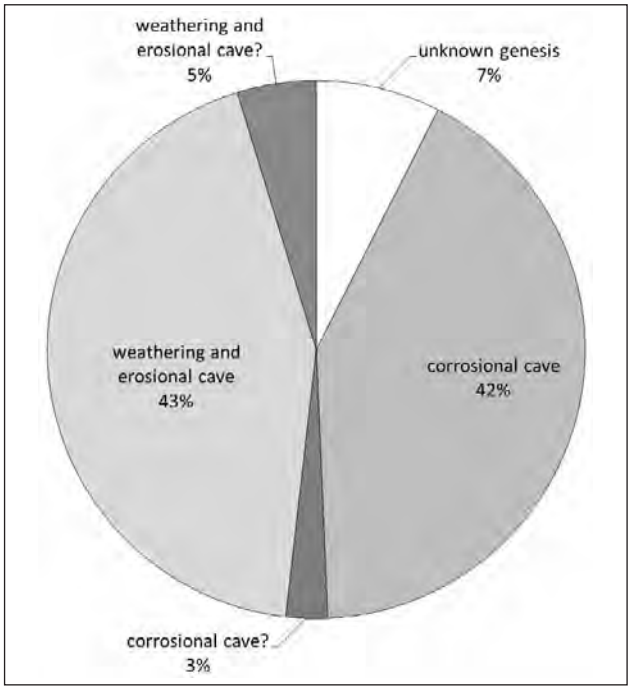

Figure 4. Distribution of the main cave types in Lower Austria and neighbouring areas. The dispositional caves are not labelled because they are represented with much less than 1%.

The most surprising result of the classification was that the majority of the classifiable caves (48 %) are not karstic caves but have been formed by weathering and erosion processes.

However, if only caves bigger that 50 m (10 % of the dataset) are considered 83 % are karstic caves and all caves longer than 500 m are karstic ones.

5. Discussion and Conclusions

The advantage of the presented classification scheme is that it is well structured and based only on the main genetic process. Overall the classification was easily applicable even for that big amount of caves within a few weeks. This was only possible because all the data were available in a well-structured cave cadastre, in paper form as well as from an online database.

During the classification it turned out that especially for small caves (< 10 m) there are very few morphological indicators that allow a clear distinction of the processes. A further problem was the heterogeneous quality of the cave maps and other documents used, which made a classification impossible.

Another difficulty for small caves was that the dominant process responsible for most of volume is hard to determine. For example especially in very small caves frost weathering is active over the whole length. So if the cave has a karstic origin but is blocked after a few meters by sediments frost weathering will be responsible for more cave volume than dissolution.

As expected, in tectonic units that are not dominated by carbonate rocks like the Bohemian Massive or the Flyschzone and Molasse Basins, the caves are mainly formed by weathering and erosion processes. Surprisingly also in the Northern Calcareous Alps which are dominated

by limestone and dolomite half of the caves have been developed by karstification and the other half by weathering and erosion processes.

Acknowledgments

The work was supported in the frame of a project (NÖHÖKAT) with the Federal Government of Lower Austria. The Speleological Society of Vienna and Lower Austria provided all the collected information on caves.

References

Dikau R, 2006. Oberflächenprozesse – ein altes oder ein neues Thema? Geographica Helvetica, 61 (3), 170–180.

Striebel T, 2005. Höhlenbildung in “nicht verkarstungsfähigen” Gesteinen: welche Formen sind Karstformen? Laichinger Höhlenfreund, 40, 31–52.

Trimmel H, 1968. Höhlenkunde. Friedrich Vieweg & Sohn, Braunschweig.

White W B & Culver D C, 2005. Defintion of Cave. In: White W B & Culver D C (Eds). Encyclopedia of Caves. Elsevier, Amsterdam, 81–85.

NÖ-Atlas, 2012. Geländehöhe (Laserscan). http://atlas.noe.gv.at

EFFECTS OF CO_2-DEPLETED VADOSE SEEPAGE IN KARST

Arthur N. Palmer[1], Margaret V. Palmer[2]
[1]Department of Earth and Atmospheric Sciences, State University of New York, Oneonta, NY 13820-4015, USA
[2]619 Winney Hill Road, Oneonta, NY 13820
[1,2]palmeran@oneonta.edu

Where infiltration takes place into porous, non-carbonate rock (e.g., sandstone), and then encounters carbonate rock below, carbonate dissolution takes place in a system nearly closed to CO_2. The water approaches saturation at very low PCO_2 and carbonate content, and high pH. When it seeps into a cave, it rapidly absorbs CO_2 from the cave air, causing wall corrosion or white microcrystalline weathering rinds. Elsewhere it can cause gypsum replacement of carbonate in cave walls and deposition of silica. Most of these effects are quantitatively small; but in ideal conditions, mixing that includes such low-CO_2 water can be responsible for considerable cave enlargement.

L'infiltration à travers les rochers qui sont poreux et insolubles (par exemple, le grès), peut dissoudre le calcaire sous-jacent, mais ne peut plus absorber le CO_2 du sol. Le système chimique est pratiquement fermée, et quand l'eau approche de la saturation avec du calcaire, la teneur en carbonate et 3 sera très faible, et le pH devient très élevée. Lorsque cette eau s'infiltre dans les grottes, il absorbe rapidement beaucoup de CO_2 de leurs atmosphères. Cela provoque la corrosion des parois, ou des croûtes microcristallines blanches. De plus, elle peut permettre de remplacer le calcaire avec le gypse, ou de déposer de petites quantités de silice. La plupart de ces effets sont faibles, mais dans des conditions idéales, lorsque l'eau avec du CO_2 faible est capable de se mélanger avec l'eau qui a des niveaux typiques de CO_2, un élargissement considérable de grottes peuvent se produire.

1. Introduction

Vadose seepage through carbonate rock generally retains most of its soil-derived CO_2 as it descends. Most carbonate dissolution takes place in the sub-soil epikarst where the PCO_2 is near equilibrium with that in the soil. When the water emerges into a cave, where the PCO_2 is usually far smaller, much of the CO_2 degasses into the cave atmosphere, driving the water to supersaturation and producing speleothems.

However, if non-calcareous rock (e.g., quartz sandstone) underlies the soil and overlies carbonate rock, water that infiltrates through the sequence will dissolve the carbonate rock while more or less closed to CO_2. Downward diffusion of CO_2 is limited and cannot keep pace with the rate of water flow. As a result, the amount of carbonate rock that can be dissolved is very small, and the water approaches equilibrium at high pH and very low PCO_2. The flow system is outlined in Figure 1.

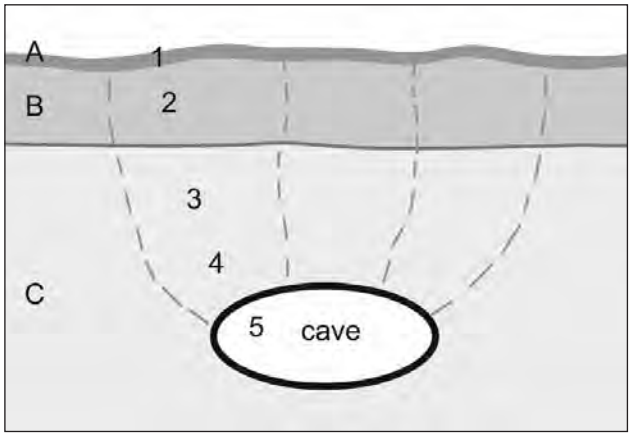

Figure 1. Sketch of closed-system vadose seepage into a cave. A = soil; B = porous insoluble rock; C = carbonate rock. The chemistry evolves as follows: (1) Infiltrating water absorbs high CO_2 from soil. (2) It passes through insoluble rock. (3) In the carbonate rock, dissolution consumes most of the CO_2. The soil cannot replenish it. (4) Water drains into the cave by gravity and/or capillarity. (5) The water absorbs CO_2 from the cave air and becomes aggressive.

To simulate this reaction, add powdered calcite to a flask of distilled water, then insert a pH probe and seal the opening. The pH will soon rise above 9 or 10.

When this water emerges into a cave, it rapidly absorbs CO_2 from the cave air and becomes solutionally aggressive toward limestone and dolomite. Visible effects are usually small and subtle, but widespread. They are most recognizable as zones of deeply etched carbonate rock and weathered zones in cave walls. In their greatest expression they can account for major cave features, and even significant (but rare) examples of cave origin.

2. Field evidence

We first recognized closed-system vadose flow in Mammoth Cave, Kentucky (USA) and surrounding regions. The majority of these caves are overlain by sandstone-capped plateaus. Most infiltration to the caves takes place along the eroded plateau margins, and carbonate speleothems are concentrated in those areas. However, beneath a thin overlying sandstone cap-rock there are places where small quantities of capillary water seep intermittently from narrow fissures. Most of these fissures are very narrow, less than the thickness of a sheet of paper, and have undergone almost no solutional enlargement; but the walls around and below them have been sharply etched by dissolution to depths of 1–3 cm (Figure 2). It is evident that the water is rapidly absorbing CO_2 from the cave air. Oddly, the CO_2 of the cave air is some of the lowest ever documented – less than 0.0008 atm (A Palmer and M Palmer, 1995), and it is odd to see it absorbed so readily by vadose water. The sandy

Figure 2. Renewed aggressiveness of capillary water emerging in a wall in Mammoth Cave after infiltration through a sandstone cap-rock. The shadow at top obscures some of the narrow input fissure. Pen for scale.

soil above the cave has a PCO_2 only slightly higher, averaging 0.001 atm (from *in situ* measurements by Miotke, 1973). Before the water emerges into the cave, its dissolved CO_2 must be depleted by carbonate dissolution in a nearly closed system. This process (or even its existence) is very difficult to measure without disturbing the closed conditions. It is easier to model the evolution of the water chemistry with the appropriate chemical equilibria.

3. Chemical modeling

In a closed vadose system of this kind, dissolution of carbonate rock consumes much of the available CO_2, so the amount of dissolution is diminished. Calculating the equilibria is simple (overview in Garrels and Christ, 1965, p. 86–88), but convergence requires multiple successive approximations by computer. Professional software is available, but the chemistry is easily programmed by hand to offer personal insight. All relevant equilibria need to be observed, along with the charge balance (electroneutrality), and – since this is a closed system – the total mass of carbon must remain equal to that from the initial CO_2 in addition to all dissolved carbonates. Concentrations are low enough that the simple Debye-Hückel equation is sufficient to evaluate activity coefficients.

For this exercise, equilibrium constants were those recommended by Plummer and Busenburg (1982). Other equilibrium constants were calculated from thermodynamic data in Faure (1998). The simplest routine is to scan the full range of pH values back and forth at decreasing intervals until all equations balance with an insignificant error. Reconstructing the complex interactions between water and gas is beyond the scope of this paper.

Figure 3 shows the result for the system described here for Mammoth Cave. Note the sharp decrease in PCO_2 and rise of pH as calcite dissolves. The low PCO_2 accounts for the rapid uptake of CO_2 from the cave air, even in Mammoth Cave, where the CO_2 level is so low. Table 1 shows the effect of initial (soil) PCO_2. A value of 0.005 atm is more typical of soil moisture in the Mammoth Cave area (Miotke, 1973); and in nearby regions where soil directly overlies limestone, PCO_2 averages 0.012 atm. These calculations assume perfectly closed systems, which are unlikely in the field; but the rapid uptake of CO_2 observed in Mammoth Cave validates the overall process.

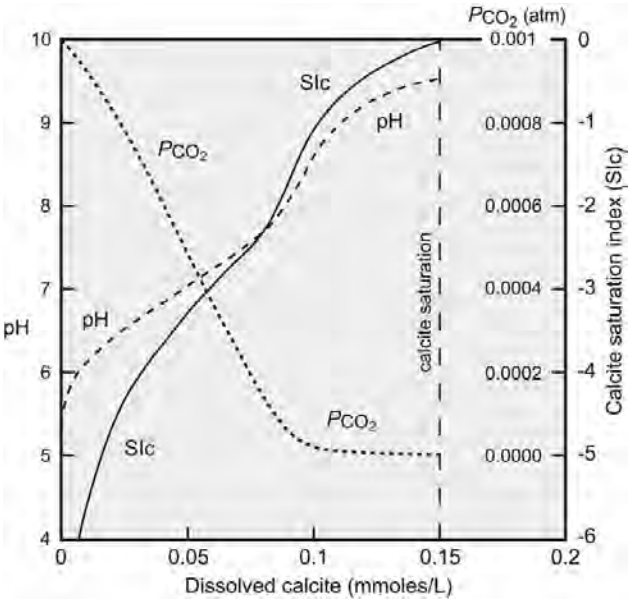

Figure 3. Chemical evolution of infiltrating water in limestone after isolation from soil CO_2, for initial PCO_2 of 0.001 atm at 15 °C. SIc =calcite saturation index = log [$(Ca^{2+})(CO_3^{2-})/Kc$], where Kc = calcite equilibrium constant. Saturation is reached at SIc = 0.The odd curvatures of pH and SIc are caused by the complex equilibria of dissolved carbonate species.

Table 1. Final values for PCO_2 and pH for closed-system dissolution at various values of initial soil PCO_2. In the field, the final PCO_2 is likely to be larger, and pH smaller. At low initial PCO_2, a 10 °C difference in temperature causes a roughly 40% difference (higher temperatures causing lower final PCO_2 and higher final pH), but the effect diminishes to less than 10% at high initial PCO_2.

Initial PCO_2 (atm)	Final PCO_2 (atm)	Final pH	$CaCO_3$ at saturation (mmoles/L)
0.001	$<10^{-5}$	9.55	0.15
0.005	0.00018	8.46	0.48
0.01	0.0010	7.96	2.63
0.05	0.023	7.08	3.80
0.1	0.061	6.80	3.11

4. Applications of concepts

4.1. Localized corrosion of carbonate rock

The example in Figure 2 is most significant because it is so close to proof of closed-system vadose dissolution. The rough, abrasive texture of the rock is common in many caves. But quantitatively this is one of the least significant results of the process.

4.2. Weathering rinds on cave walls

Much more extensive in the Mammoth Cave region, and in similar geologic settings elsewhere, are white weathering rinds on limestone cave walls (Figure 4). These can have a variety of origins, but where they are uniform, widespread, and in favorable geologic settings, the following origin is most probable:

Figure 4. Weathering rind in a collapse block of granular Carboniferous limestone in Mammoth Cave, located 4 m below a thin sandstone cap. Pencil for scale.

Closed-system seepage can also take place within the intergranular pores of a carbonate rock. As the moisture approaches a relatively dry cave wall, CO2 from the cave air will be absorbed even before the water emerges from the rock. The moisture becomes slightly aggressive toward calcite or dolomite, and their grains are etched by dissolution to produce an opaque white, microcrystalline rind. Microscopic examination shows no other cause for the white appearance. Isotopic values in the weathering rind show a decrease in $\delta^{18}O$ and $\delta^{13}C$ of about –1‰ from those in the unaltered bedrock (M Palmer and A Palmer, 2012). The O shift is apparently caused by the reaction between oxygen in the local bedrock (high $\delta^{18}O$) and that in the meteoric water (low $\delta^{18}O$). The low water/rock oxygen ratio limits the amount of shift. Likewise, the slight decrease in $\delta^{13}C$ is caused by the reaction between carbon in the bedrock and that in the absorbed CO_2 from the cave air (mainly biogenic, with lower $\delta^{13}C$). Corrosion and isotopic shifts can also be caused by condensation of moisture on rock surfaces from rising evaporative water, but only in areas of large vertical air circulation. The example in Figure 4 is near the floor of a low crawlway and unlikely to be affected by condensation. This is another example of a process with little quantitative impact, but which helps to explain cave features.

4.3. Gypsum replacement of carbonate rock in caves

Gypsum growth in dry caves is often produced by oxidation of pyrite. In some carbonate rocks, the gypsum is carried in solution from residual evaporite beds. Less commonly, the outer edges of exposed cave walls are replaced by gypsum (Figure 5). Palmer (1986) proposed that this process can be facilitated by absorption of cave air by infiltrating water in which much of the dissolved CO_2 has been depleted by closed-system vadose dissolution. Conversion of calcite to gypsum can take place by the reaction

$$CaCO_3 + SO_4^{2-} + 2H_2O \rightarrow CaSO_4{\cdot}2H_2O + CO_3^{2-}$$

but only if the solution is supersaturated with gypsum, and, at 15 °C, if $(SO_4^{2-}) / (CO_3^{2-})$ in the solution is greater than about 4900 (determined with free-energy and enthalpy data; see Faure, 1998). Consider the following example, which is appropriate for sandstone-capped cavernous plateaus like those at Mammoth Cave:

1. Water at 15 °C and PCO_2 = 0.005 atm (with resulting pH ~5.03) infiltrates through sandstone and stays closed to CO_2 as it enters the underlying limestone. Calcite dissolves toward saturation while PCO_2 drops to ~0.00018 atm and pH rises to ~8.5.

2. Water encounters gypsum sometime during stage 1. As it dissolves, it decreases the solubility of calcite by the commonion effect and may force some calcite to precipitate. At 15 °C, the saturation concentration of gypsum is 0.014 mole/L (0.014 M). Calcite solubility is ~0.00048 M, but in combination with gypsum saturation it is limited to ~0.0016 M. If both reach saturation, SO_4^{2-}/CO_3^{2-} rises to ~6,700 at pH = 7.9. Calcite commonly reaches saturation, but gypsum, if sparse, may not.

3. The moisture emerges into a relatively dry cave and rapidly absorbs CO_2 from the cave air. PCO_2 rises to ~0.0008 atm, while pH drops to ~7.3. This causes an abrupt decrease in CO_3^{2-}, because most of these ions convert to HCO_3^- as H^+ increases. The SO_4^{2-}/CO_3^{2-} ratio zooms to more than 10^5 but drops rapidly, but at decreasing rates, as calcite dissolves toward equilibrium with the cave PCO_2.

4. As calcite dissolves, the SO_4^{2-}/CO_3^{2-} ratio remains higher than the critical value of 4,900 as long as gypsum is more than 75% saturated. If gypsum is supersaturated, it can replace calcite. Otherwise, evaporation at the cave wall can drive gypsum to supersaturation at SO_4^{2-}/CO_3^{2-} >6,700, which may allow it to replace calcite.

The validity of this model has been questioned by White and White (2003), because the sulfate/carbonate ratios at equilibrium do not seem high enough. Calculating carbonate activity solely from carbonate equilibria can be a source of the problem, because to maintain the charge balance, the abundant dissolved sulfate must be considered as well. On the other hand, the conclusions of Palmer (1986) were unrealistically optimistic by not accounting for the instability of the equilibria as the reactions took place. However, the conclusions in this section address that fault and show that the calcite-replacement process is valid. Gypsum replacement of dolomite is also feasible, but the reactions are more complex. Recognition of gypsum replacement in samples generally requires microscopic analysis.

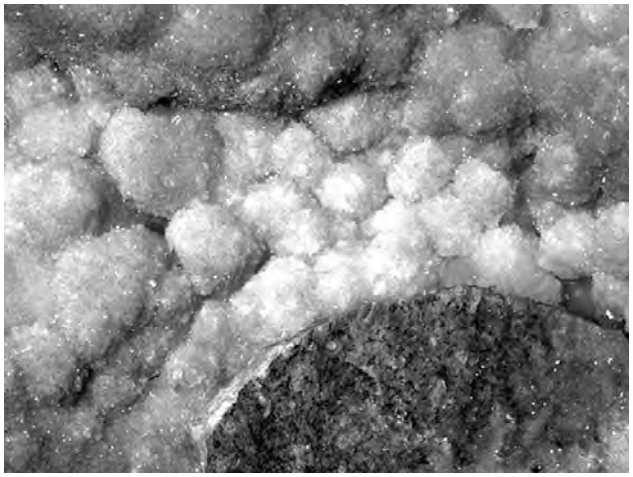

Figure 5. Partial replacement of limestone by gypsum in Mammoth Cave (most visible in lower right). Elsewhere in the photo the gypsum consists mainly of evaporative overgrowths. Width of frame is roughly 12 cm.r.

4.4. Deposition of silica at cave walls

In rare situations, small amounts of quartz or amorphous SiO_2 (for example, chalcedony) can precipitate at and just within cave walls. Identification usually requires laboratory analysis.

Silica (e.g., SiO_2) maintains a nearly uniform solubility across most of the pH range; but above pH 8.5 its solubility increases rapidly (Faure, 1998). The main form of dissolved silica is silicic acid (H_4SiO_4), but this is such a weak acid that it can dissociate only at high pH, where H^+ migrates away to leave $H_3SiO_4^-$, $H_2SiO_4^{2-}$, etc. The combination of the three or more Si-bearing ions raises the total silica in solution.

Up to pH 8.5 the solubility of crystalline quartz is only about 5 ppm at 15 °C (greater as temperature rises), but at pH = 12 it is about 1,000 ppm. The solubility of amorphous silica is considerably greater but follows the same trend. (This pattern can be disrupted by organic complexes, etc.)

As carbonate rock dissolves in a closed system with a low initial PCO_2, the water can reach a pH as high as 10, at which the solubility of silica has climbed to about twice its low-pH value. When this water emerges into a cave and equilibrates with the cave air, the pH abruptly drops, usually to between 7 and 8, where silica solubility is much lower. This process can account for small deposits of silica on cave walls or in weathering crusts. The setting of Figure 4 is a fertile place to search for these deposits. Laboratory analysis at high magnification is usually needed to distinguish between true SiO_2 precipitates and siliceous detrital grains.

4.5. Contribution of closed-system dissolution to mixing-zone speleogenesis

In contrast to the subtle small-scale processes described here, closed-system vadose dissolution may have speleogenetic consequences that operate at a much larger scale. Caves of the Black Hills, South Dakota, USA, provide a good example. Wind Cave and Jewel Cave (Figure 6) are the two largest and are open to the public under National Park Service management. They are located in the confined Carboniferous Madison aquifer along zones of mid-Carboniferous paleokarst (M Palmer and A Palmer, 1989). The Madison and related strata dip away from the high mountains in the center of the Black Hills.

It appears that the present extent of the caves is the result of mid-Cenozoic enlargement of paleokarst voids. The caves are not undergoing active enlargement today. Their origin is a topic of lively debate. Several water sources have been present throughout most of the Cenozoic, but none shows a clear relationship to cave origin (A. Palmer et al., 2009).

Most researchers consider the caves to have a thermal origin, with water rising from depth and cooling as it approaches the surface, to provide solutionally aggressive recharge (e.g., Bakalowicz et al., 1987; Ford, 1989). Evidence includes thick calcite wall crusts with thermal isotopic signatures; high-temperature minerals (e.g., large euhedral quartz crystals, etc.; White and Deike, 1962); network pattern, irregular profiles with solution cupolas in the ceilings, little relation to overlying topography, etc.

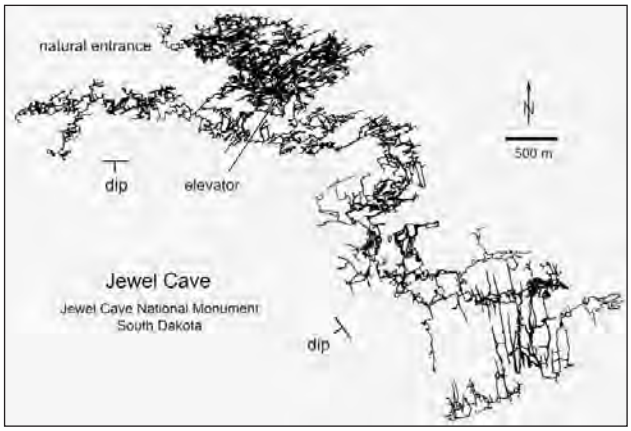

Figure 6. Map of Jewel Cave, Black Hills, South Dakota, USA (courtesy of National Park Service).

The Madison is one of the most productive confined aquifers in the USA, so cave origin as a result of artesian confinement has also been suggested (e.g., Tullis and Gries, 1938; Deal, 1962, 1965; Howard, 1964). It is capped by the thick Minnelusa Formation (mainly late Carboni-ferous), which is composed mainly of quartz sandstone with interbeds of carbonates and sulfates. An origin by infiltration of water through the Minnelusa has also been proposed (Wiles, 2005). Finally, the caves may simply be the surviving relics of paleokarst.

During our own study we have supported all of these ideas at various times, but have concluded that none by itself is sufficient (A Palmer and M Palmer, 1989). The caves are clustered beneath the thin up-dip edge of the Minnelusa, which suggests a genetic relationship (Figure 7). However, the caves do not extend up to the Minnelusa contact, except in a few places, so infiltration through the cap-rock is unlikely to be the only source. Although the Madison is 135 m thick at Jewel Cave and 90 m thick at Wind Cave, each cave occupies a range of only 70 m near the top.

Only a few small, scattered passages extend up-dip beyond the eroded edge of the Minnelusa, so aggressive recharge directly into the Madison carbonates seems out of the question. The caves also do not extend far down-dip.

Figure 7. Geologic profile through Wind Cave (A. Palmer & M. Palmer, 1988). The main entrance is located in a small window in the Minnelusa and is not related to the cave origin.

Wind Cave reaches the water table only in a few places and apparently does not extend far below it. Jewel does not reach the water table at all. The caves terminate down-dip approximately where the overlying Minnelusa cap exceeds about half its maximum thickness.

It is only along the strike of the limestone beds that the caves extend without obvious limits. Along that trend the caves maintain a rather constant hydrogeologic setting. Also, to some extent, the caves appear to be constrained to areas of paleokarst voids and breccias (Wind Cave more so than Jewel).

Possible paths for aggressive groundwater recharge are shown in Figure 8. But how could the water have formed caves that do not emanate from obvious points of recharge? Generation of acidity within the Madison itself is possible by oxidation of sulfides, but except for some surviving clues in the paleokarst, there is no evidence for that process in the caves.

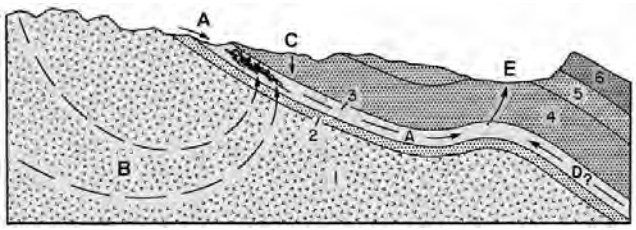

Figure 8. Potential paths for groundwater that formed the Black Hills caves. 1 = Precambrian metamorphic and igneous rocks. 2 = Deadwood Sandstone and other strata (mainly Cambrian). 3 = Madison Limestone (lower Car-boniferous, Mississippian). 4 = Minnelusa Formation (upper Carboniferous, Pennsylvanian – lower Permian). 5, 6 = overlying strata, mainly shales and sandstones (Triassic–Cretaceous). A = water entering the outcrop area of the limestone (autogenic seepage, allogenic streams). B = rising water, possibly thermal, recharged from the higher hills. C = diffuse recharge through the lower beds of the Minnelusa Formation (mainly sand-stone, but with carbonate and sulfate interbeds). D = up-dip flow from surrounding lowlands (unlikely, because it would appear to be against the hydraulic gradient). E = major springs around the perimeter of the Black Hills, where confined water in the Madison passes upward along faults and breccia in the upper Minnelusa and overlying strata. (A Palmer & M Palmer, 2008).

Extensive calcite wall crusts that overlie weathered bedrock show that the caves were drained before they were filled with supersaturated water. U/Pb dating of the calcite in Jewel Cave by V. Polyak gives ages of 26–14.7 Ma (A Palmer et al., 2009). These dates correlate with extensive continental sandstone, shale, and volcanic strata that buried the lower half of the Black Hills. Most of these sediments have been removed by erosion since then, exposing a presediment landscape that has seen only a little change little since the early Oligocene.

The caves therefore formed near the end of the Eocene or beginning of the Oligocene. Earlier dates are not feasible, because the close association between the caves and present topography would not have existed.

So it is probable that the caves formed by the mixing of waters from two or more sources. These most likely included recharge from the eroded edge of the limestone (the most abundant and continuous source), combined with seepage through the sandstone beds of the lower Minnelusa (which accounts for the close association between those strata and the underlying cave).

According to the topics discussed in the previous pages, much of the diffuse infiltration would have been approximately closed to CO_2. Carbonate beds in the Minnelusa and at the top of the Madison would have dissolved only slightly in this water, while the pH rose and PCO_2 dropped to low values. This water would regain its aggressiveness when it mixed with the more abundant water from the Madison outcrop area, which preferentially followed Carboniferous paleokarst voids and breccias. Dissolution would have been most intense where mixing took place between the high-CO_2 water from the limestone outcrop and the very low-CO_2 vertical seepage (see Figure 9). That is why the caves are not concentrated at the Madison-Minnelusa contact.

The lack of evidence for great allogenic flow into the limestone (A in Figure 8) seems odd. But the Madison has always been an inefficient aquifer because it drains upward through insoluble beds. High flows in surface streams would simply fill all available solutional openings in the limestone, overflowing at the surface and bypassing the caves. The pattern of present and former drainage lines supports this idea.

All of the geomorphic characteristics of the caves are compatible with this origin except for the thermal evidence. That is explained by high-temperature deposits in paleokarst voids during deep burial, and by moderately

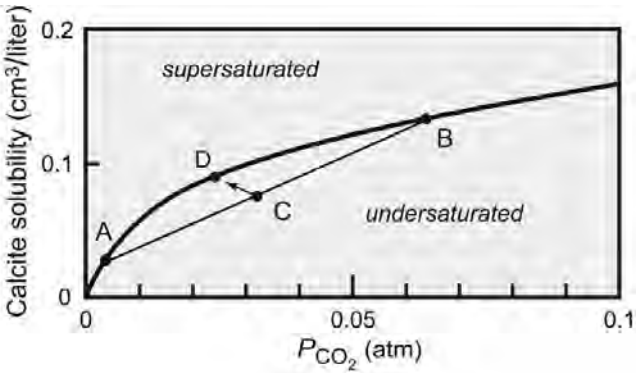

Figure 9. Solubility of calcite vs. PCO_2 at 15 °C. The shape of the curve allows a mixture of two calcite-saturated waters at different PCO_2 to become under-saturated (cf. Bögli, 1964). A mixture of equal amounts of solutions A and B (both at calcite saturation) would produce mixture C, which falls below the saturation curve and is undersaturated with calcite. Mixing would take place in a closed system, so as further dissolution took place, the solution would migrate to D along the sloping line (each mole of calcite dissolution is balanced by a loss of one mole of CO_2). Note that the effect is greatest where one water source has a very low PCO_2.

warm-water calcite accumulating in the caves when they were buried by the mid-to-late Cenozoic deposits.

The present climate is semi-arid, and a reliable source of recharge through the Minnelusa is hard to imagine. However, in the mid-Cenozoic the climate was much more humid. One indication of that is the rapid erosional removal of 1–2 km of rocks in the central Black Hills during the Paleocene-Eocene, during the major period of mountain uplift.

Even today, however, a moderate amount of infiltration takes place through the lower Minnelusa (Wiles, 1992). This is equivalent to about 10^4 $m^3/yr/km^2$, which would be enough to enlarge the caves to their present size in about 10^6 years (A Palmer and M Palmer, 2008). Conditions were probably more favorable during the mid-Cenozoic.

5. Conclusions

Dissolution of carbonate rocks in systems closed to CO_2 exchange is common in phreatic water, but it is relatively rare in the vadose zone, where there is normally an efficient CO_2 exchange between infiltrating water and the overlying soil, via open fissures, conduits, and pores. The role of insoluble beds in limiting this exchange, described in Sections 1–3, has not been widely recognized in the past because field evidence is so sparse.

The effects on the caves – such as enhanced corrosion, bedrock weathering, silica deposition, and replacement of carbonate by gypsum – are common in these geologic settings, but they are subtle and quantitatively small. In contrast, this type of water can have a large impact on cave enlargement where the mixing of waters of greatly contrasting CO_2 content is the only significant agent of speleogenesis.

These phenomena help to explain cave and karst features that are often overlooked, but which can provide clues to cryptic or ancient geochemical environments. They also reveal an aspect of infiltrating water that is very difficult to measure in the field without disrupting the closed conditions.

Acknowledgments

Many thanks to Rick Olson (National Park Service) for discussions about closed-system dissolution in Mammoth Cave; to Richard Zopf (Yellow Springs, Ohio) for helping to sample weathered crusts in Mammoth Cave; to Dwight Deal (Aurora, Colorado), Rod Horrocks, Mike Wiles, and Marc Ohms (National Park Service), and Victor Polyak (Univ. of New Mexico), for discussions of the geology of Black Hills caves. Isotopic analyses were supported by the Research Foundation of the State University of New York.

References

Bakalowicz M, Ford D, Miller T, Palmer A, and Palmer M, 1987. Thermal genesis of dissolution caves in the Black Hills, South Dakota. Geological Society of America Bulletin, 99, 729−738.

Bögli A, 1964. Mischungskorrosion, ein Beitrag zur Verkarstungsproblem. Erdkunde 18, 83−92.

Deal D, 1962. Geology of Jewel Cave National Monument, Custer County, South Dakota. M.A. Thesis, University of Wyoming, Laramie, Wyoming, USA.

Deal D, 1965. Origin and secondary mineralization of caves in the Black Hills of South Dakota, USA. Proc. 4th Int. Congr. of Speleology, Ljubljana, 67–70.

Faure G, 1998. Principles and applications of geochemistry (2nd ed.). Prentice-Hall, Upper Saddle River, N.J.

Ford D, 1989. Features of the genesis of Jewel Cave and Wind Cave, Black Hills, South Dakota. National Speleological Society Bulletin, 51(2), 100−110.

Howard A, 1964. Model for cavern development under artesian ground water flow, with special reference to the Black Hills. National Speleological Society Bulletin, 26(1), 7−16.

Miotke F-D, 1973. Der Karst im zentralen Kentucky bei Mammoth Cave. Arbeiten aus dem Geographischen Institut der Technischen Universitat Hannover, Jahrbuch.

Palmer A, 1986. Gypsum replacement of limestone by alternating open and closed systems in the vadose zone, Mammoth Cave, Kentucky. Cave Research Foundation, 1986 Annual Report.

Palmer A, Palmer M, 1995. Geochemistry of capillary seepage in Mammoth Cave. Mammoth Cave National Park, Proceedings of 4th Science Conference, 119–133.

Palmer, A., Palmer, M., 1989. Geologic history of the Black Hills caves, South Dakota: National Speleological Society Bulletin, 51(2), 72–99.

Palmer A, Palmer M, 2008. Field guide to the paleokarst of the Black Hills. In: I Sasowsky, C Feazel, J Mylroie, A Palmer, and M Palmer (Eds.), Karst from recent to reservoirs. Karst Waters Institute, Special Publication 14, 189–230.

Palmer A, Palmer M, Polyak V, and Asmerom Y, 2009. Genetic evolution of the Black Hills caves, South Dakota, USA. Proc. 15th Int. Congr. Speleology, Kerrville Texas, 2, 946–951.

Palmer A, Palmer M, 1989. Paleokarst of the United States. In: P Bosak, (Ed.), Paleokarst. Acdemia/Elsevier, Prague, 337–363.

Palmer M, Palmer A, 2012. Petrographic and isotopic evidence for late-stage processes in sulfuric acid caves of the Guadalupe Mountains, New Mexico, USA. International Journal of Speleology, 41(2), 231–250.

Plummer N, Busenberg E, 1982. The solubilities of calcite, aragonite, and vaterite in CO_2–H_2O solutions between 0 and 90°C and an evaluation of the aqueous model for the system $CaCO_3$–CO_2–H_2O. Geochimica et Cosmochimica Acta 46, 1011–1040.

Tullis E, Gries J, 1938. Black Hills caves. The Black Hills Engineer, 24(4), 233–271.

White W, Deike G, 1962. Secondary mineralization in Wind Cave, South Dakota. National Speleological Society Bulletin, 24, 74–87.

White W, White E, 2003. Gypsum wedging and cavern breakdown: Studies in the Mammoth Cave System, Kentucky. Journal of Cave and Karst Studies, 65(1), 43–52.

Wiles M, 1992. Infiltration at Wind and Jewel Caves, Black Hills, South Dakota. M.S. Thesis, South Dakota School of Mines and Technology, Rapid City, S.D., USA.

Wiles M, 2005. Mapping surface geology to protect cave and karst resources of the Jewel Cave System (abstract). Proceedings of 17th National Cave and Karst Management Symposium, Albany, NY, 165.

DETAILED MORPHOLOGIC ANALYSIS OF PALAEOTRAUN GALLERY USING A TERRESTRIAL LASER SCAN (DACHSTEIN-MAMMUTHÖHLE, UPPER AUSTRIA)

Lukas Plan[1], Andreas Roncat[2], Gregor Marx[2]

[1]Natural History Museum Vienna, Dep. for Geology and Palaeontology, Cave and Karst Group, Museumsplatz 1/10, Vienna, Austria, lukas.plan@nhm-wien.at

[2]Vienna University of Technology, Department of Geodesy and Geoinformation, Research Groups Photogrammetry and Remote Sensing, Gußhausstraße 27-29, 1040 Vienna, ar@ipf.tuwien.ac.at; gregor.marx@chello.at

Having a length of currently 67 km the Dachstein-Mammuthöhle is one of the major cave systems in the Northern Calcareous Alps. The genesis of its partly huge galleries has been discussed controversially almost since its discovery ca. 100 years ago. Special focus was always given to a 200 m long gallery named Paläotraun. To study the morphology of this more than 10 m high tunnel in detail a terrestrial laser scan was performed. The method proved to be successful and confirmed that the Paläotraun is a paragenetic channel.

1. Introduction

Dachstein-Mammuthöhle cave is the fourth longest cave in the Eastern Alps and in Austria. Currently it has a length of 67 km and a vertical range of 1.2 km (Pfarr et al. 2012). A very small portion of the cave is developed as a show cave. It includes a huge 200 m long gallery with up to 100 m² cross sectional area that was named *Paläotraun* (Fig. 1).

Since the discovery of the cave at the beginning of the 20th century, its speleogenesis has been discussed controversially. Hermann Bock proposed his *Höhlenflusstheorie* (*cave river hypothesis*), well-known in the German-speaking area, stating that an enormous underground river with a discharge of 1,500 to 3,000 m³/s that had its catchment area in the Austro-Alpine Crystalline crossed the Northern Calcareous Alps in the Tertiary (Bock et al. 1913). The showpiece of his model was the *Paläotraun*, the origin of which was mainly attributed to mechanical erosion by the palaeo Traun River. His hypothesis formed the core of a long-standing and ongoing scientific dispute among speleologists and other scientists in Austria about the origin of the Dachstein-Mammuthöhle in general and the "Paläotraun" in particular (for details see Plan and Herrmann 2010 and Trimmel 2012).

Other theories were for example that the Paläotraun formed mainly by seepage water and collapse (e.g., Trimmel 1949) or is purely of tectonic origin (e.g., Arnberger 1953). Already in 1961 Bauer concluded from the flow direction deduced from scallops that Paläotraun is a rising phreatic channel and that the floor was covered by a growing pile of sediments and the ceiling only could evolve upward. Detailed morphological mapping and the application of modern speleogenetic models could confirm the paragenetic origin proposed by Bauer (Plan and Xaver 2010).

However, with conventional methods in the up to 15 m high *Paläotraun* morphometric measurements were restricted to the lower 2 m. Therefore a high resolution terrestrial laser scan (TLS) was conducted to enable detailed morphologic studies over the whole cross section.

Figure 1. Performing the terrestrial laser scan in Paläotraun.

2. Geography and geology

The Dachstein-Mammuthöhle is located at the northern margin of the Dachstein plateau (Dachstein-Summit: 2,995 m a.s.l.) reaching below the local summit of Krippenstein (being 2,108 m a.s.l.). Up today 21 entrances are known to the polygenetic cave system that consists of (1a) epiphreatic horizontal galleries with up to 100 m² cross sectional area, (1b) inclined mazes that are controlled by bedding planes and (1c) (epi?)phreatic pits with up to 90 m depth. Younger vadose parts are (2a) series of canyons and complex canyon systems that reach up to 200 m height and (2b) vadose pits of up to 100 m depth.

The entire cave developed in well bedded Upper Triassic limestone (partly dolomitic) of the Dachstein Formation and generally the strata dip with 20 to 40° to the northeast.

The geometry of the cave and several small-scale features (e.g., scallops, karren, ceiling meanders), which date back to the early history of the cave formation, allow the following interpretation: old phreatic parts (galleries, mazes, and some pits) developed under epiphreatic conditions during flood events, followed by younger, vadose canyon-shaft-systems. Scallops and sedimentary structures indicate a general westward flow direction.

Sediments played an important role during the formation of the profiles, i.e. the profiles expanded upward (paragenesis) because the floor of the galleries was sealed by sediments, and only part of the cross section, as it can be seen today after removal of these sediments, was occupied by water (Plan and Xaver 2010).

3. Methods

The laser scanning measurements in Paläotraun took place on May 7th, 2011. The instrument used for this purpose was a Z+F Imager 5006i phase-shift scanner, capable of recording 3D point clouds in distances from 0.4 m to 79 m. The scanner's field of view is 360° horizontally and 310° vertically (for details see: Zoller+Fröhlich 2012). Paläotraun was scanned from 14 positions; four of them in the scan mode "super high" (angular resolution of 0.018° which corresponds to a point spacing of 3 mm in a distance of 10 m) for a detailed recording of the scallops. Two scans were done in the "high" mode (resolution: 0.036° and 6 mm@10 m, resp.) and 8 scans in "middle" mode (resolution: 0.072° and 13 mm @10 m, resp.), resulting in an overall 3D point cloud of approx. 860 million points. The single 3D point clouds were accompanied by panoramic images acquired with an integrated camera on the scanner platform, enabling a better visual interpretation of the data and the derivation of a textured 3D model of Paläotraun.

For the calculation of this 3D model, the point clouds of the single scans were first approximately aligned relative to each other using coded targets (as visible in Fig. 1, lower right corner). For a precise alignment, also referred to as "co-registration", the point clouds underwent a special filtering, and the calculation was done automatically using an ICP (iterative closest point) algorithm (cf. Nothegger and Dorninger 2009). After the co-registration, the overall point cloud was filtered again with special emphasis on keeping small features while removing redundant information in locally planar areas where a high point density is not needed. The resulting model is a three-dimensional triangulation of this filtered point cloud (Roncat et al, 2011).

Using the software package GoCAD and ArcGIS the structures were analysed and morphometric measurements on scallops were performed. A movie of a virtual flight through the gallery along defined points was rendered using the software Pointools (Fig. 2).

Figure 2. Screenshot of the flight through the Paläotraun.

5. Results and Conclusions

The conducted study showed that a TLS is a powerful tool to investigate the morphology of large cave passages in detail. However a high – higher than expected – resolution is necessary if very small scale features like cm-sized scallops shall be investigated.

The Laser Scan shows many morphologic details of the cave walls and the ceiling including: faults, bedding planes, scallops, paragenetic dissolution ramps, and paragenetic ceiling cannels.

In general the hypothesis that Paläotraun is a huge paragenetic Channel proposed by Bauer (1961) and in more detail by Plan and Xaver (2010) could be confirmed.

Indicators for a paragenetic origin of the main portion of the profile are paragenetic dissolution ramps and ceiling channels that developed above a single bedding plane at the basis of the profile. It is the only spelaeogenetically relevant bedding plan as it shows small tubes and anastomoses, which is not the case for other bedding planes that are visible in upper parts of the profile. Further, the average length of groups of scallops differs with the height of the profile which can only be interpreted by a paragenetic origin: At different sediment fill levels different flow velocities have caused these differences (Fig. 3).

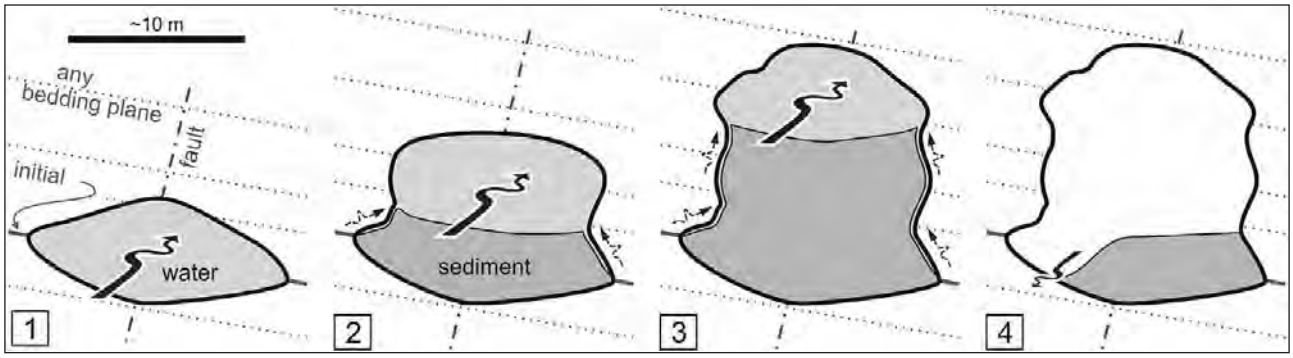

Figure 3. Schematic evolution of the paragenetic profile of Paläotraun gallery: (1) at the junction of a bedding plane and a fault an (epi)phreatic elliptical profile develops. (2) Sediments at the floor enable only an upward evolution of the profile. Water rinsing between the sediment and the cave wall forms paragenetic ceiling channels at the overhanging parts. Further bedding planes play no role for the development of the profile. (3) Further upward development of the profile above a growing pile of sediments. (4) Erosion of the sediment – most probably by vadose waters – exposes the whole profile as it is visible today.

Acknowledgments

Michael Behm and Agelika Xaver helped in the field. The management of the Dachstein show caves enabled access to the cave and provided the infrastructure (electricity, powerful spotlights) for the scan. The Austrian Spelaeologic Association covered the costs for accommodation at Schnöbergalpe for the time of the fieldwork.

References

Arnberger E, 1953. Neue Ergebnisse morphotektonischer Untersuchungen in der Dachstein-Mammuthöhle. Mitteilungen der Höhlenkommission, 1953, 68–79.

Bauer F, 1961. Sedimentation und Konvakuationserweiterung in aufsteigenden Siphonstrecken. – Atti Symp. Internaz. Speleol., Varenna (Como), Rassegna Speleologica Italiana, 5(1), 171–175.

Bock H, 1913. Alte Höhlenstromläufe im Inneren des Mittagskogels. In: Bock H, Lahner G & Gaunersdorfer G (Eds.). Höhlen im Dachstein. Graz, Verein f. Höhlenkunde in Österreich, 72–88.

Nothegger C, Dorninger P, 2009. 3D Filtering of High-Resolution Terrestrial Laser Scanner Point Clouds for Cultural Heritage Documentation. Photogrammetrie, Fernerkundung, Geoinformation 2009 (1), 53–63. doi: 10.1127/0935-1221/2009/0006.

Pfarr T, Seebacher R, Plan L, 2012. Longest and deepest caves of Austria. www.hoehle.org/long&deep.php

Plan L, Herrmann E, 2010. Paläotraun – Der Wissenschaftsdisput um die Entstehung der Dachstein-Mammuthöhle. Die Höhle, 61, 3–17.

Plan L, Xaver A, 2010. Geomorphologische Untersuchung und genetische Interpretation der Dachstein-Mammuthöhle (Österreich). Die Höhle, 61, 18–38.

Roncat A, Dublyansky Y, Spötl C, Dorninger P, 2011. Full-3D Surveying of Caves: A Case Study of Märchenhöhle (Austria). IAMG Conference Salzburg 2011 – Mathematical Geosciences at the Crossroads of Theory and Practice. 11pp. doi: 10.5242/iamg.2011.0074.

Trimmel H, 1949. Gab es Riesenhöhlenflüsse? – Natur und Technik, 3 (6), 166–168.

Trimmel H, 2012. Zur Erforschungsgeschichte der Paläotraun (Dachstein). Die Höhle 63, 43–62.

Zoller+Fröhlich, 2012. Homepage of the company Zoller+Fröhlich GmbH, www.zf-laser.com

INFLUENCE OF THE PLIO-PLEISTOCENE TECTONICS ON THE EVOLUTION OF THE PURGATORIO POLJE (NORTH-WESTERN SICILY)

Rosario Ruggieri[1], Giuseppe Napoli [2], Pietro Renda[2]
[1]Centro Ibleo di Ricerche Speleo-Idrogeologiche, Via Carducci 165, Ragusa, Italy, info@cirs-ragusa.org
University of Nova Gorica, Vipavska 13, p.p. 301, Rožna dolina, Nova Gorica, Slovenia
[2]Dipartimento di Scienze della Terra e del Mare (DiSTeM), Università degli Studi di Palermo, via Archirafi, 22, Palermo, Italy, giuseppe.napoli@unipa.it

The evolution of large landforms such as polje are related in most cases to geological events affecting a specific areal context and / or to climatic events which, in combination with the tectonics, affect the karst base level, in a more or less pronounced manner depending on the proximity of limestone karst mountains to the coastline. The genesis of these aforementioned forms depends primarily on structural and lithological factors, their evolution is instead controlled by tectonic and climatic-eustatic factors in the reliefs close to the coast. In the inland, due to the distance from the coast, the effects of the latter factors on the karstification process could be less, or very bland, in respect to the predominant tectonic movements. In this context, the Purgatorio polje, in the north-west of Sicily, activated in the Middle Pleistocene and regressed to a relict form at the end of the Upper Pleistocene – Holocene, can be seen as a result of the tectonic events that have lifted, and still lift, the Monti di Capo San Vito in differential blocks, with a consequent lowering of the erosion base level.

1. Introduction

The area of the Monti di Capo San Vito, in the north-west of Sicily, is characterized by a series of Meso-Cenozoic carbonate reliefs on which the karst processes, triggered at the end of the Miocene with the first uprisings, have generated a large series of morphologies both in the surface and in the underground (Ruggieri 1994, 2002). The landscape, mainly formed by ridges and landlocked depressed areas, surrounded, more or less, by extensive coastal plains, presents some morphological features typical of the karst areas, with a wide variety of karren and complex forms such as doline, fluviokarst gorges and polje.

In this framework lie the landforms "Polje of Purgatorio – Muciara dry valley – Bufara doline – Cipollazzo gorge", constituting a related set, whose genesis and subsequent evolution, influenced by the tectonics that affected the area of the Monti di San Vito Lo Capo in the Plio-Pleistocene, is described in this paper.

2. Geographic and geological context

The area, situated in the eastern part of the territory of Custonaci in theTrapani Province (Figs. 12), is constituted by a plain edged towards west by cliffs (Rumena and Scurati), towards north and south by ridges. The cliffs delimit the plain from the Cornino coastal strip, while the ridges, trending NW-SE, delimit the area with the Castelluzzo plain at north and with the Forgia river plain at south. The west part of the area has elevations ranging from 180 m to 240 m a.s.l. (Piano Zubbia sector), which increase towards the east sector of the Purgatorio plain from 240 to 290 m a.s.l. The reliefs delimiting the Purgatorio plain show maximal elevation of 1,108 m a.s.l. in the Mt. Sparagio ridge and 595 m a.s.l. in the Mt. Palatimone-Mt. Giovanni ridge (Fig. 2). The study area falls within the orographic context of the Monti di Capo San Vito, which, along with the mountains of Trapani, are the westernmost portions of

Figure 1. Location of the study area.

the Sicilian orogenic chain.

The reliefs are formed by a group of east and southeast verging tectonic units stacked between the Middle-lower Miocene and Lower Pliocene with stepped, ramp-flat and duplex geometries, during the building of the Appenninic-Maghrebian Orogen. Later in the Lower Pliocene-Upper Pleistocene these units were segmented into blocks as a result of a wrench tectonics (Giunta and Liguori 1972, 1973; Abate et al. 1998).

Several authors (Nigro et al. 2000; Renda et al. 2000; Gueguen et al. 2002; Giunta et al. 2004; Tondi et al. 2006) frame the most recent tectonic structures in the northwestern Sicily as a high-angle fault system constituted by right strike slip structures mostly E-W oriented and left strike slips structures N-S oriented. In the whole area of the Monti di Capo San Vito minor tectonic structures are also widespread related to the cited main features (Abate et al. 1998; Giunta et al. 2004) that on the basis of geometric and

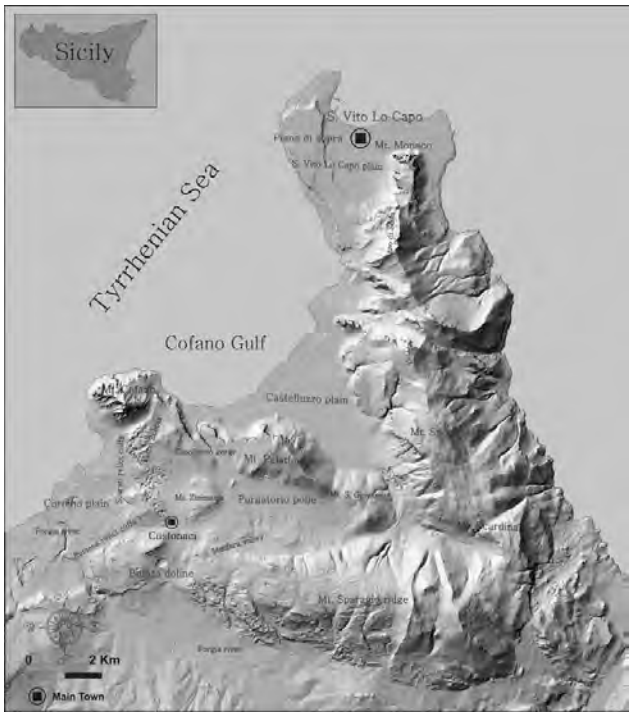

Figure 2. Location of the polje in the geographic contest of the Monti di Capo San Vito.

kinematic characteristics can be grouped in four main sets: a set oriented from ESE-WNW to E-W with mostly right kinematic character, a set NW-SE also characterized by predominantly right movements, a N-S set with left wrench kinematic, and a NE-SW set mainly characterized by left wrench movements. Some of these high angle faults also affect the Pliocene and Pleistocene deposits showing evidence of recent movements (Tondi et al. 2006) (Fig. 3).

3. The "Polje of Purgatorio – Bufara doline – Cipollazzo gorge"

The karst macro landforms are present in the studied area described below.

3.1. The Bufara doline

The Bufara doline, located in the south-west sector in respect to the Polje, is elliptical in form, has a major axis of 300 m, a minor one of 230 m and a depth of 58 m. This depression of collapsing could probably link also with intersection of old paleokarstic features (Fig. 4).

3.2. The Gorge of Cipolazzo

This fluviokarst gorge of Cipollazzo is located in the north-west sector of Mt. Palatimone ridge. This morphology is an example of a karst gorge constituted by a deep narrow gash of a few meters wide, which runs for about 550 m along a NW-SE trending tectonic discontinuity.

Along its course there are various erosive and corrosive morphologies such as: giant potholes, which form large deep pools of various dimensions at the foot of the high vertical walls; swallow holes, vertical caves and various karst corrosion morphologies on the walls (Fig. 5).

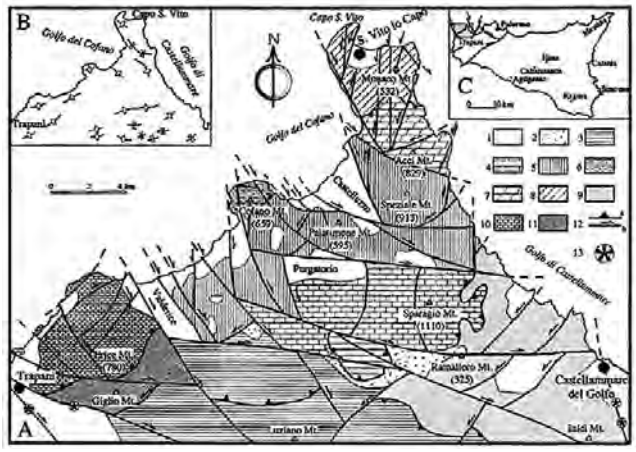

Fig. 3. Tectonic sketch of the Trapani Mts. 1) Plio-Pleistocene deposits; 2) Tortonian-Messinian deposits; 3) Monte Luziano Unit (Upper Cretaceous-Upper Miocene); 4) Sparagio Mt. Unit (Upper Triassic-Middle Tortonian); 5) Speziale-Palatimone Mts. Unit (Upper Triassic-Middle Tortonian); 6) Cofano Mt. Unit (Upper Triassic-Middle Tortonian); 7) Acci Mt. Unit (Upper Triassic-Middle Tortonian); 8) Monaco Mt. Unit (Upper Triassic-Middle Tortonian); 9) Ramalloro Mt. Unit (Upper Triassic-Middle Tortonian); 10) Mt. Erice Unit (Upper Triassic-Middle Tortonian); 11) Giglio Mt. Unit (Upper Triassic-Middle Tortonian); 12a) main thrusts; 12b) main strike-slip faults; 13) thermal springs. B. Plio-Pleistocene axial fold trends (Abate et al. 1998).

Figure 4. Bufara doline.

3.3. The Purgatorio polje

The Purgatorio plain because of its morphological, structural and karst characteristics forms a polje, that extends in an E-W direction for about 5,5 km^2 (Fig. 6).

This flat surface depression is bordered on the north by the slope of the Mt. Palatimone-Mt. San Giovanni ridge, on the south by the Mt. Sparagio ridge, on the west by the relief of Mt. Zimmaria and Mt. Bufara and closed on the east side (Fig. 7).

From a structural point of view, evidence of faults can be recognised on the northern and western side, while on the southern side an overthrusting limit has been identified by Abate et al. (1991) or a reverse fault by Catalano et al. (2011). As far as the lithological profile is concerned the following terrains outcrop in this landform: Norian-Liassic dolomites and Tithonian-Lower Cretaceous calcirudites, breccias and calcarenites, which form an 300–500 m wide belt on the northern side, morphologically constituting a pediment formed by the retreat of Mt. Palatimone's slopes; Upper Serravallian – Lower Tortonian marly clay, sands and

Figure 5. Giant pothole in the Cipollazzo fluviokarst gorge.

arenites outcropping in the southern sector right up to the boundary with the slopes of the Mt. Sparagio ridge; Lower Pliocene biocalcarenites which outcrop in the central sector of the plain, passing into eluvial and colluvial silts and sands towards the north-west and south sector.

As far as the surface hydrology is concerned the Polje shows two shallow incisions that originate on the slopes of Mt. Sparagio and run south-north, the waters from both being captured by swallow holes. The deep fluviokarst *Gole di Cipollazzo*, which constitutes the only outlet for the runoff which forms in the Purgatorio plain, is located on the north-west border.

Relict fluviokarst morphologies attributable to a past drainage condition with an outlet in the Muciara area are recognizable in the south-west sector of the polje.

The most markedly karst character of the Purgatorio polje, however, is to be found in the north sector where there are Upper Triassic dolomites outcropping and a various series of both surface and subterranean morphologies.

Particularly significant concerning the evolution of the polje is the series of swallow holes, along a belt close to the presumed fault line between the Lower Pliocene biocalcarenites and the Triassic dolomites that capture the running water of the plain. In the general morphological context of the polje the isolated relief of Cozzo Catarucci is singular, and constitutes relict morphologies Hum type of the previous relief worn away by the processes of karst corrosion (Fig. 8).

Finally in the underground area of the polje there are numerous vertical caves, some of them of considerable depth (Purgatorio Abyss, Cipollazzo Abyss) (Ruggieri 1994, 2002; Ruggieri and Messina Panfalone 2011).

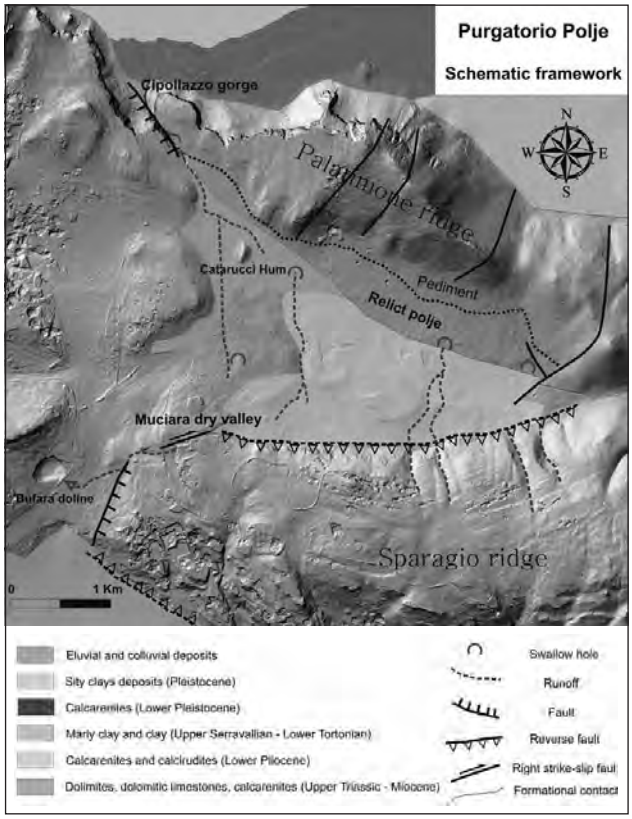

Figure 7. Map of Purgatorio polje and karst landforms.

Figure 8. Cozzo Catarucci Hum.

Figure 6. Polje of Purgatori and Mt. Palatimone ridge.

4. Structural Analysis

Structural data are collected to be useful to constrain the genesis of the Bufara doline to the karst system of the Purgatorio Polje.

Currently these two landforms are not in connection being separated by a structural high, located in the area of Muciara.

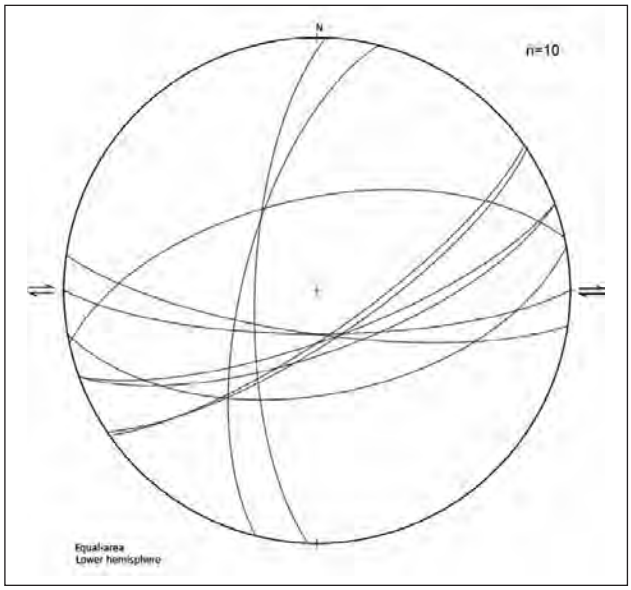

Figure 9. Stereonet of the structures surveyed in the Muciara site.

The data were collected in different outcrops around the "Purgatorio polje – Bufara doline – Cipollazzo gorge" in correspondence with some areas characterized by the presence of numerous caves. Several structural reliefs were carried out on calcarenite and calcirudite of the Lower Cretaceous – Titonian (Bufara doline) and on dolomite and dolomitic limestones of the Upper Triassic – Liassic (Monte Palatimone, Monte Sparagio, Muciara) outcroppings on the walls of several quarries.

The collected structural data projected on Schmidt diagrams show that in three of the four studied sites, despite a dispersion of the measures, there are always two sets of structures trending approximately NW-SE and NE-SW.

The site called "Muciara", extreme south-western sector of the polje (Fig. 7), is instead interested by a set of structures trending from E-W to ENE-WSW (Fig. 9).

The study of abutting and crosscutting relationships (Fig. 10A) and kinematic indicators present on the shear planes (Fig. 10B) has allowed reconstructing for this set of structures a right strike-slip movement.

The presence of these set of structures in the studied area is also documented by several authors (Abate et al. 1998; Renda et al. 2000; Tondi 2007). These authors attribute to these three set predominantly strike-slip kinematics. The W-E and NW-SE sets are characterized by right-lateral movement and the N-S and NE-SW by left-lateral (Abate et al. 1998; Tondi et al. 2006). The authors, also frames the genesis of these structures in a Plio-Pleistocene right shear system of regional transtension that involves the southern Tyrrhenian Sea and the northern portion of the Sicily island (Renda et al. 2000) (Fig. 11).

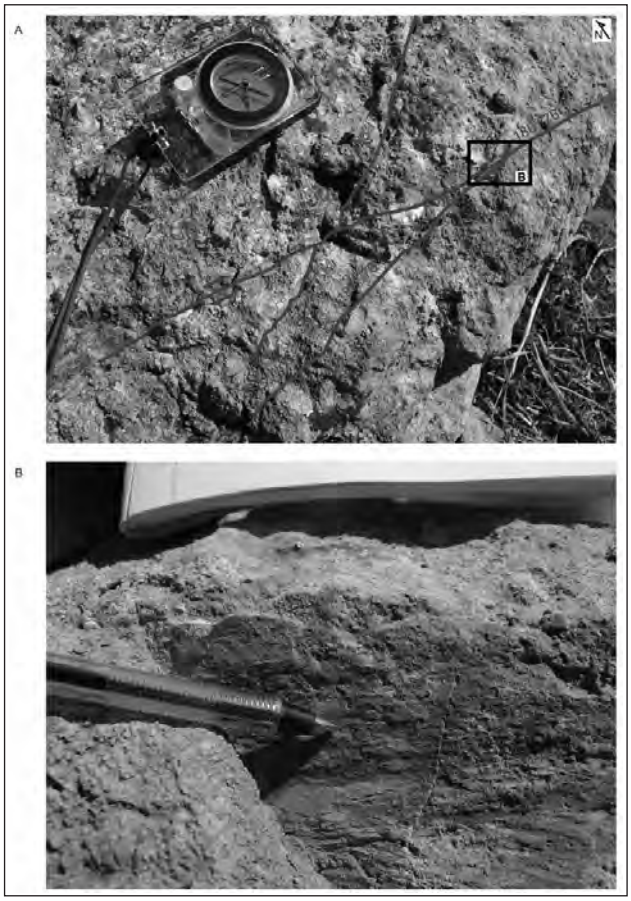

Figure 10. E-W trending right-lateral small fault (the measures indicate dip direction/inclination). A) crosscutting relationship between the South dipping structure and SE dipping structure; B) striae and calcite fibers on the fault plane.

In fact, as shown in Figure 11a, the most abundant features exposed in the studied area may be interpreted as minor structures related to a roughly east-west-striking fault driven by a NW-oriented compression (Tondi et al. 2006).

Also in the different studied sites, we have been detected NW-SE and E-W trending surfaces with evidence of right strike-slip kinematic and NE-SW trending structures with left-lateral strike-slip kinematics.

Abate et al. (1998) and Tondi et al. (2006) testify in the whole area of Monti di Capo San Vito the presence of positive flower structure at both the right and left strike-slip lineaments. The high structural of Muciara, which currently forms a barrier that separates the Polje of Purgatorio from the dolina of Bufara, is located in an area affected by some large strike-slip lineaments having the same directions of the three sets encountered in the above mentioned structural stations.

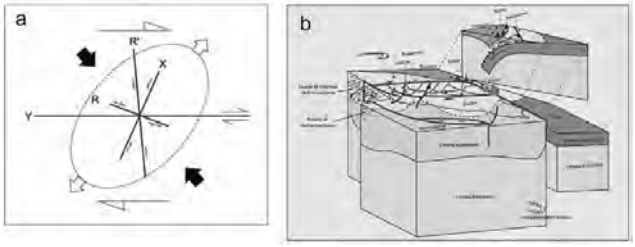

Figure 11. a) Two-dimensional geometry of the stress field acting in northwestern Sicily, and structural interpretation of the structures mapped in the studied area. b) 3D model of the sicilian area shows the most important neotectonic fault system, the chain sectors and the undeformed areas.

5. Discussion and conclusion

Based on the morphological and structural elements surveyed with the present study, the evolution of the Polje of Purgatorio is hereafter formulated, in relation to the influence of the Plio-Pleistocene tectonic events, occurred in the Monti di Capo San Vito.

The polje probably begins to delineate in the late Miocene and early Pliocene with an extensional tectonic phase governed mainly by NW-SE trending structures that displace the Mesozoic carbonate formations in a sequence of structural high and low (Nigro and Renda 2005). In this way, the opening of the plain of Cornino and the depression of Purgatorio is outlined. With the progress of the uplifting in the Lower Pleistocene, started at the end of the Pliocene, the morphology and paleogeography of the depression is redrawn, characterized by a western sector of peninsulas, of islands and of landlocked submerged areas, where the Lower Pleistocene calcarenite sediments, and by an emerged central-eastern sector subject to planation due to karst corrosion.

At the end of Lower Pleistocene – early Middle Pleistocene the paleogeographic context had to be an emerged area bounded on the west by sea-cliffs, constituted by the Piano Zubbia eastwards adjacent to the plain of Purgatorio, bounded by the lifting ridges of Mt. Palatimone and Mt. Sparagio.

The cave karst processes, in this late lower Pleistocene phase, involve NE-SW structures both in the Piano Zubbia area and in the depression of Purgatorio.

Figure 12. Muciara dry fluviokarst valley.

With the beginnings of the Middle Pleistocene the depression of Purgatorio starts to assume, to all effects, the aspect and the hydrological functions of a Polje characterized, as a whole, by an absorbent area with autigenic recharge bordered on the northern side by the ridge of the Mt. Palatimone, and in its southern part by a clay belt bordered by the Mt. Sparagio ridge.

The phases of absorption-capture, through swallow holes, and flooding contribute to the planation of the karstified sector of the depression and to the contextual retreat of the southern slope of Mt. Palatimone-San Giovanni ridge.

In this phase of activity, characterized by periods of concentrated absorption through swallow holes, and periods of overflow, two karst landforms, in particular, could have had a certain importance for the evolution of the polje: the sink cave “Abyss of Purgatorio” and the dry fluviokarst valley of Muciara (Figs. 7,12). The former due to its function of capturing the waters of the eastern part of the polje, the latter for its function of collecting and draining, outside the depression, the overflow of the central-western part of the area.

To this drainage would, therefore, be attributed the genesis of the actual Muciara dry paleo-valley and most likely the formation of the collapse doline of Bufara to which the waters were directed. This assumption is supported by the presence of a relict form of tributary valley which from the Muciara area is directed towards the Bufara doline (Fig. 7).

To a Medium Pleistocene strike-slip tectonic phase (Abate et al. 1998) could be ascribed the progressive closure of the drainage way of the fluviokarst valley of Muciara (Fig. 10), due to the formation of high positive flower structures, surveyed with the present study.

It is conceivable, therefore, that this area, once crossed by a valley which allowed the water drainage from the Polje area to the doline of Bufara, has been tectonically raised during the Plio-Pleistocene due to the strike-slip movements generated on the outlines NW-SE, NE-SW and E-W structures in response to the right strike-slip system that controls the recent development of the southern margin of the Tyrrhenian Sea (Giunta et al 2000 b; Renda et al. 2000; Napoli et al. 2012) and generates the neotectonic lineaments affecting the northern area of Sicily (Fig. 11).

The above mentioned closure should affect the consequent reorganization of the hydrology of the waterproof south-western sector of the polje that begins to transfer the meteoric recharge and runoff in the northern areas towards the Cipollazzo fluviokarst gorges which, due to this reason, start to take shape. Regarding this, the following development of the gorge could explain its characteristic of a hanging valley 50 m higher in respect to the Castelluzzo plain below (Fig. 13).

Acknowledgments

Field work at Custonaci was made comfortable thanks to Davide Vito Messina Panfalone and Vito Santoro.

References

Abate B, Di Maggio C, Incandela A, Renda P, 1991. Nuovi dati sulla geologia della penisola di Capo San Vito (Sicilia nord-occidentale. Mem. Soc. Geol. It., 47(1991), 15–25 (in Italian).

Abate B, Incandela A, Nigro F, Renda P, 1998. Plio-Pleistocene strikeslip tectonics in the Trapani Mts. (NW Sicilia). Bollettino della Società Geologica Italiana 117, 555–567.

Catalano F, Agate M, Basilone L, Di Maggio C, Mancuso M, Sulli A, 2011. Note illustrative della carta geologica D’Italia alla scala 1:50,000, Castellammare del Golfo. Regione Siciliana Ass. Territorio Ambiente (in Italian).

Boccaletti M, Conedera C, Dainelli P, Gocev P, 1982. The recent (Miocene-Quaternary) rhegmatic system of western Mediterranean region. A new model of ensialic geodynamic evolution in a context of plastic/rigid deformation. Journal of Petroleum Geology, 5, 31–49.

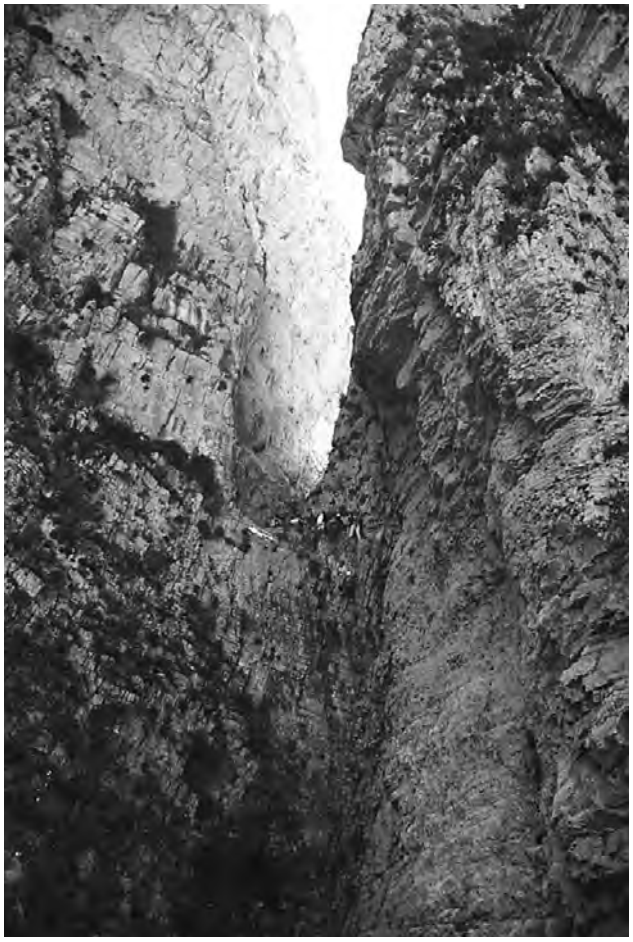

Figure 13. The outlet of the Cipollazzo gorge 50 m higher than the Castelluzzo plain below.

Finetti I, Del Ben A, 1986. Geophysical study of the Tyrrhenian opening. Boll. Geof. Teor. Appl., 28, 75–155.

Ghisetti F, Vezzani L, 1984. Thin-skinned deformation in Western Sicily. Bollettino della Società Geologica Italiana, 103, 129–157.

Giunta G, Liguori V, 1972. Geologia della estremità nord-occidentale della Sicilia. Riv. Min. Sic., 136–138, 156–226 (in Italian).

Giunta G, Liguori V, 1973. Evoluzione paleotettonica della Sicilia nord-occidentale. Boll. Soc. Geol. It., 138, 903–924 (in Italian).

Giunta G, Luzio D, Tondi E, De Luca L, Giorgianni A, D'Anna G, Renda P, Cello G, Nigro F, Vitale M, 2004. The Palermo (Sicily) seismic cluster of September 2002, in the seismotectonic framework of the Tyrrenian Sea-Sicily border area. Annals of Geophysics 47/6, 1755–1770.

Giunta G, Nigro F, Renda P, Giorgianni A, 2000. The Sicilian-Maghrebides Tyrrhenian Margin: a neotectonic evolutionary model. Bollettino della Società Geologica Italiana, 119, 553–565.

Gueguen E, Tavarnelli E, Renda P, Tramutoli M, 2002. The geodynamics of the southern Tyrrhenian Sea margin as revealed by integrated geological, geophysical and geodetic data. Bollettino della Societa' Geologica Italiana. Volume Speciale 1, 77–85.

Napoli G, Nigro F, Renda P, 2012. The interation of compressional and extensional tectonics during the Sicily Chain building. Rend. Online Soc. Geol. It., 21, 178–180.

Nigro F, Renda P, Arisco G, 2000. Tettonica recente nella Sicilia nordoccidentale e nelle Isole Egadi. Bollettino della Società Geologica Italiana, 119, 307–319 (in Italian).

Nigro F, Renda P, 2005. Transtensional/extensional fault activity from Mesozoic rifting to Tertiary chain building in Northen Sicily (Central Mediterranean). Geologica Carpathica, June 2005. 56, 3, 255–271.

Renda P, Tavarnelli E, Tramutoli M, Gueguen E, 2000. Neogene deformations of Northern Sicily, and their implications for the geodynamics of the Southern Tyrrenian Sea margin. Memorie della Societa` Geologica Italiana, 55, 53–59.

Ruggieri R., 1994. Primo resoconto della campagna di ricerca speleologica realizzata dal C.I.R.S. a Custonaci (Tp). Boll. Acc. Gioenia Sc. Nat., 27 (38): 525–545 (in Italian).

Ruggieri R, 2002. Peculiarità geomorfologiche e speleologiche dell'area carsica di Custonaci (Tp). Speleologia Iblea, 10, 197–203 (in Italian).

Ruggieri R, Messina Panfalone D, 2011. Dentro e fuori la Montagna. Priulla, Palermo (in Italian).

Tondi E, 2007. Nucleation, development and petrophysical properties of faults in carbonate grainstones: Evidence from the San Vito Lo Capo peninsula (Sicily, Italy) Jour. Str. Geol., 29, 614–628.

Tondi E, Zampieri D, Alessandroni M, Giunta G, Renda P, Unti M, Giorgianni A, Cello G, 2006. Active faults and inferred seismic sources in the San Vito lo Capo peninsula, north-western Sicily, Italy. Geological Society, London, Special Publications, 262, 365–377.

SPELEOGENESIS OF A 3D-MAZE CAVE (HERMANNSHÖHLE, LOWER AUSTRIA)

Andrea Schober[1], Lukas Plan[2], Denis Scholz[3], Christoph Spötl[4]
[1]University of Vienna, Althanstraße 14, Vienna, Austria, andreaschober@gmx.at
[2]Natural History Museum, Museumsplatz 1/10, Vienna, Austria, lukas.plan@nhm-wien.at
[3]Johannes Gutenberg-University Mainz, J.-J.-Becher-Weg 21, Mainz, Germany, scholzd@uni-mainz.de
[4]University of Innsbruck, Innrain 52, Innsbruck, Austria, christoph.spoetl@uibk.ac.at

The 4.4 km-long Hermannshöhle is one of the largest caves in the Lower Austroalpine Unit. The cave is unusual in two respects: its dense network of corridors is arranged in a three-dimensional maze and the most outstanding macro- and micromorphologic features were caused by paragenesis. The aim of this study was to enlighten the origin of this cave using morphological and sedimentological observations as well as U/Th dating of speleothems. First results show that the palaeo-environment of the Hermannshöhle was drastically different from today. Highly corrosive water sourced from nearby non-karstic gneisses and schists gave rise to well-developed contact karst features. A distinct system of paragenetic canyons developed following pulses of clastic sediment input creating the unique maze character of the cave. Preliminary U/Th results suggest that speleothems from the middle level of the cave are already older than ca. 600 ka.

1. Introduction

Hermannshöhle located near *Kirchberg am Wechsel* (Lower Austria) is one of the biggest caves in the Lower Austroalpine tectonic unit (Pfarr et al. 2012). It developed in an isolated block of weakly metamorphic banded marble. Within only 140 × 160 m ground area and 73 m of elevation difference a total of 4.4 km of corridors formed in a three-dimensional maze. There are three more caves nearby (Mäanderhöhle, Antonshöhle and Rauchspalten) and it is presumed that all four are genetically related (Hartmann et al. 1997) giwving a length of almost 5 km.

Due to the labyrinthic array and the geological features (e.g., the extensive sediment fill and the fact that one part of the cave developed below the local base level but still is dry) the cave is special and its genesis – especially the extremely labyrinthic character (cf. Palmer 1975, 2011) – has remained unexplained.

Comprehensive studies including cave biology, mineralogy, geology, meteorology and other fields culminated in a monograph by Hartmann et al. (1997). Despite attempts to describe the evolution of the Hermannshöhle (Mrkos 1997), the mechanisms driving its formation are not fully understood, as modern concepts of speleogenesis (e.g., Klimchouk et al. 2000) have not been considered. Speleothem dating was also performed using ^{14}C in comparison with alpha-spectrometric U/Th but the results were inconclusive (Seemann et al. 1997).

The focus of this study is to understand the origin of the extreme maze structure and the almost omnipresent paragenetic features in Hermannshöhle. Using state-of-the-art MC-ICP-MS U/Th dating of well-selected speleothems we are striving to constrain the chronology of speleogenesis in this cave and its connection to the evolution of the adjacent Kirchberg Basin.

2. Geographic and geologic implications

Hermannshöhle is located in the *Eulenberg* hill near the village *Kirchberg am Wechsel* in the South of the province of Lower Austria. The host rock are Middle Triassic carbonates which are part of the Lower Austroalpine unit, bordered by a Palaeozoic gneiss-and-schist-complex in the North. In the South the area is covered by Neogene and Quaternary sediments of the Kirchberg Basin (580 m a.s.l.), which was formed during the last phase of the alpidic orogeny due to lateral extrusion (Ebner 1991; Faupl 2003; Figure 1). The basin is linked to branches of one of the largest strike-slip fault in Austria, the SEMP (Salzachtal-Ennstal-Mariazell-Puchberg-Fault) and the Mur-Mürz-Fault, respectively (Decker et al. 1994).

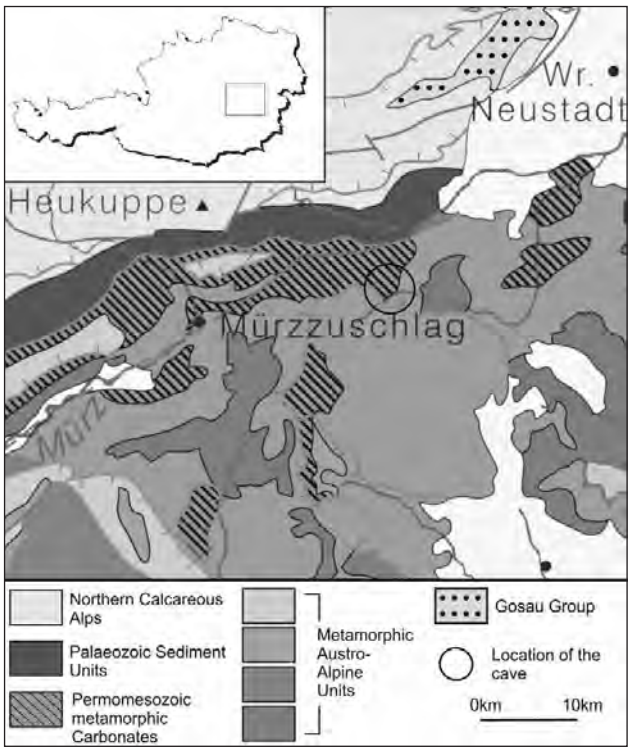

Figure 1. Geological overview of the Eastern Lower Austroalpine tectonic unit (modified after Egger et al. 1999) and the location of the investigated area hosting Hermannshöhle.

The rather isolated carbonate block hosting the cave system consists of a foliated, weakly metamorphic calcite marble

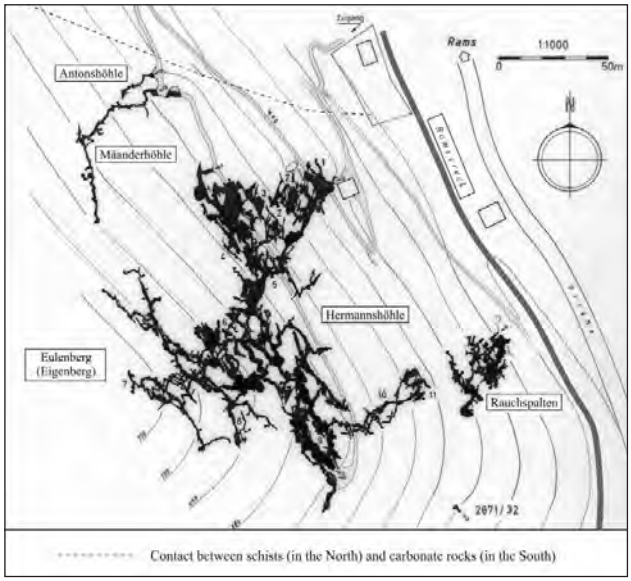

Figure 2. Topographic overview map of the cave and its surroundings (edited after Hermann 1989). Note the border between karstifiable carbonate and non-karstifiable crystalline rocks.

that is part of the Lower Austroalpine Semmering-Wechsel-System. This system consists of the tectonically overlying Semmering-Unit built up of Permo-Mesozoic sedimentary rocks above a series of coarse-crystalline gneisses. The Wechsel-Unit marks the lowest level of the Austroalpine and is exposed in tectonic windows. At the northern margin of the largest of these tectonic windows the Kirchberg Basin developed during the Neogene. On its eastern margin Permo-Triassic metamorphic carbonates of the Eulenberg are exposed, forming a karst system that was and probably is still fed by the Rams brook. This brook originates in the nearby gneisses and schists and therefore contains corrosive water (Hartmann et al. 1997; Figure 2).

Due to its strong faulting and probably also its foliation the marble provides good conditions for the formation of caves.

The internal morphology of the cave is quite baffling. On a very small area of only 140 × 160 × 73 m a 3D-maze developed that is unique not only in the Lower Austroalpine caves but also in the entire Eastern Alps. The cave ranges from about 600 m to 680 m a.s.l. Although the overall volume of passages is roughly only 17,000 m³ (1% of the neighbouring host rock) the cumulative length and density of corridors are remarkable. The corridors developed along prominent fault directions and NW-SE striking corridors are the most abundant. Most are sub-horizontal with almost no inclination and some are inclined between 40 and 60° but only very few are subvertical. The second main strike direction is NE-SW, which is nearly perpendicular to the first one with more or less horizontal corridors.

Speleothems are abundant throughout the cave comprising flowstones, dripstones, helictites, popcorn, calcite rafts, a shield, and moonmilk.

Besides some vadose dripwater the cave is dry today. A conspicuous feature is the lack of a single water path and instead a maze with multiple flow paths formed. This maze extends in all three spatial directions with corridor sizes of all scales from non-passable up to 10 m in diameter (*Fürstenhalle*) and 16 m of height (*Great Dome*).

Another interesting feature is that one part of the cave developed below the level of the Rams brook but is still dry. There are small ponors reported from the Rams brook (which were observed during river regulation) indicating an actively draining karst system, which is not yet explored (Mrkos 1997).

Figure 2 shows the Hermannshöhle and three nearby caves. The eastern one (Rauchspalten) was proven to be related to the Hermannshöhle via an aerated connection by a smoke test. The other two (Mäanderhöhle and Antonshöhle) have no known connection to Hermannshöhle but it is assumed that they are genetically related (Hartmann et al. 1997).

3. Methods

3.1. 3D-vizualisation of the cave using Spelix

For the 3D visualisation of the cave Spelix was used, a software which is part of the Austrian online cave data. A 3D-vrml-model was generated using the data of the survey traverse (length, inclination and azimuth) as well as the extensions about the height and the width at each survey station.

3.2. Morphological and sedimentological observations

A detailed geological and morphological field mapping of the cave and its surrounding was performed focussing on the contact between the karstic and non-karstic rocks. This knowledge is essential to understand the tectonic implications of the formation of the Kirchberg basin and the cave itself.

In addition to sediment analyses undertaken by Seemann (1997), who investigated the mineralogical composition including heavy minerals, a couple of representative samples were taken in order to study grain size and shape.

3.3. Dating of flowstone

To constrain the minimum age of the cave (levels) and of certain sedimentation events speleothems were sampled using drilling as well as using a hammer and a chisel and processed for U/Th-dating (e.g., Scholz 2008).

4. Results

4.1. Morphology

Even though most passages are canyon-shaped, the cave shows exclusively phreatic features, and no indication of vadose speleogenesis was found as well as of epiphreatic conditions like karren or solution pockets.

Paragenesis on all scales is clearly the dominant morphological factor in this cave: almost all profiles are paragenetic canyons and most of the overhanging parts show well-developed paragenetic ceiling channels. Paragenetic dissolution ramps are abundant as well as paragenetic bypass tubes. In most passages the floor is covered by thick layers of sediment and many passages are clogged by sediment.

Scallops are abundant especially in the lower parts of the cave and were used to detect the palaeo-flow directions. Surprisingly, the overall flow direction is not parallel to the Rams brook but rather directed to the West, which is towards the centre of the marble outcrop. Clear cross-cutting relationships between the scallops and the paragenesis could be observed that show that the paragenesis is younger (Fig. 3).

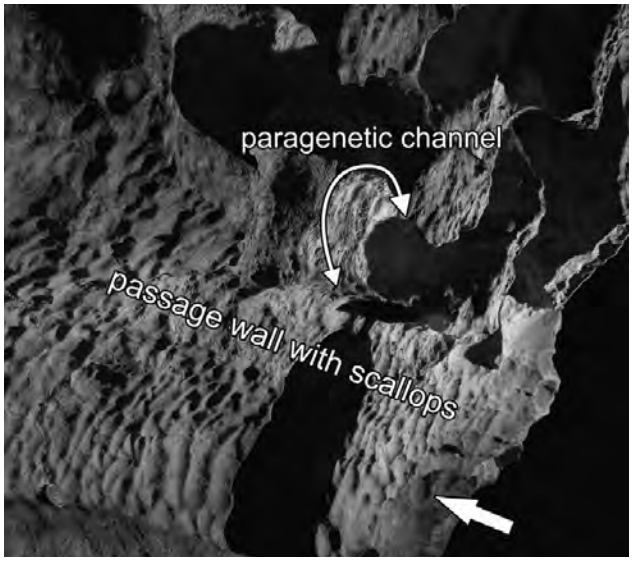

Figure 3. Cave wall with scallops (arrow indicates flow direction from SE to NW). The paragenetic ceiling half tubes do not show scallops and are clearly a younger feature. Note the 1 € coin at lower left for scale.

4.2. Clastic sediments

Sediment fills are abundant, mostly covering the floor of passages to an unknown depth. Partly cemented relics of former sediment fills including sandstones and conglomerates can be observed up to the ceiling of some passages. The sediment contains mainly allochthonous material, i.e. schists and gneisses from the area north of the Eulenberg as studied by Seemann (1997). The grain size ranges from rocks with up to 30 cm diameter to clay. Little autochthonous sediment is observed, consisting mainly of local rock debris. Only a few poorly rounded marble cobbles were observed.

4.3. Speleothem dating

So far nine speleothem samples were dated by the U/Th method. Except for one recent flowstone (ca. 1 ka), all samples are rather old, ranging from 100 to ca. 500 ka. Two of the samples are out of range and are probably older than 600 ka. Surprisingly, these old ages were found in the middle niveau of the cave which is 45 and 60 m, respectively, above the Kirchberg Basin, which forms the base level of the karst system and only 25 and 40 m above Rams brook, which potentially fed the system in former times.

5. Discussion and Conclusions

Hermannshöhle represents a nice example of contact karst where undersaturated surface water sourced from schists and gneisses infiltrate into marble karst. A high sediment load in former times resulted in various forms of paragenesis (cf. Farrant and Smith 2011).

For a modern karst system the most likely emergence would be on the south-eastern side of the carbonates at the confluence of the Rams brook into the Kirchberg Basin. However, the palaeo-flow indicators in the cave point to the West and the overall palaeo-flow direction beyond the cave remains enigmatic. Therefore it is likely that the palaeo-surface drainage was quite different from the modern setting which has implication for the age of the cave formation.

Two main processes are considered regarding the formation of the 3D-maze pattern: (a) a rather short flow distance through the soluble rock, and (b) a high discharge along many alternative routes during flooding events as discussed by Palmer (2007: 197). Furthermore, paragenesis created bypass tubes which enhanced the maze characteristics. A hypogenic origin of the cave was also considered, but apart from very few cupolas (e.g., at the upper entrance) there is no supporting evidence.

Preliminary speleothem dating results suggest that the cave is at least ca. 600 ka old. As these old speleothems were found in the middle level of the cave system it can be assumed that the upper parts, that are located 60 m higher are even older. Further datings are needed to validate these first results and to shed more light on the history of the cave system in comparison to the surface drainage system.

Acknowledgments

We would like to thank the Ministry of Traffic, Innovation and Technology for the financial support granted in the course of the FEmtec working experience program. Further acknowledgements go to the Hermannshöhlen Research- and Protection Association. We would like to thank Harald Bauer, Mathias Bichler, Kathi Bürger, Thomas Exel, Heinz Morenbesser, Pauline Oberender, and Doris Rupprecht for their support during the field and laboratory work.

References

Decker K, Peresson H, Faupl P, 1994. Die miozäne Tektonik der östlichen Kalkalpen: Kinematik, Paläospannungen und Deformationsaufteilung während der “lateralen ‘Extrusion’” der Zentralalpen. Jb. Geol. B.-A., 137, 5–18 (in German).

Ebner F, Sachsenhofer RF, Schwendt A, 1991. Das Tertiär von Kirchberg am Wechsel. Mitt. naturwiss. Ver. Steiermark 121, 119–127 (in German).

Egger H, Krenmayr H-G, Mandl GW, Martura A, Nowotny A, Pascher G, Pestal G, Pistotnik J, Rockenschaub M, Schnabel W, 1999. Geological Map of Austria 1:2,000,000. Geological Survey of Austria, Vienna.

Farrant AR, Smart PL, 2011. Role of sediment in speleogenesis; sedimentation and paragenesis. Geomorphology, 134, 79–93.

Faupl P, 2003. Historische Geologie. – Wien: Facultas Universitätsverlag (in German).

Mrkos H, 1997. Zur Entstehung der Herrmannhöhle, In: Hartmann H, Hartmann W & Mkros H (Eds.), Die Herrmannshöhle. Die Höhle, Supplement 50. Hermannshöhlen-Forschungs- und Erhaltungsverein, Wien (in German).

Hartmann H, Hartmann W, Mrkos H, 1997. Die Herrmannshöhle. Die Höhle, Supplement 50. Hermannshöhlen-Forschungs- und Erhaltungsverein, Wien (in German).

Herrmann P, Mandl GW, Matura A, Neubauer F, Riedmüller G & Tollmann A, 1992. Geologische Karte der Republik Österreich 1:50,000: Blatt 105 Neunkirchen. – Geologische Bundesanstalt, Wien (in German).

Klimchouk AB, Ford DC, Palmer, AN, Dreybrodt W, 2000. Speleogenesis: Evolution of Karst Aquifers. – NSS, Huntsville, Alabama (USA).

Palmer AN, 1975. The origin of maze caves. Natl. Speleol. Soc. Bull. 37, 56–76.

Palmer AN, 2007. Cave Geology. Cave Books, Dayton.

Palmer AN, 2011. Distinction between epigenic and hypogenic maze caves. Geomorphology, 134, 9–22.

Pfarr T, Seebacher R, Plan L, 2012. Longest and deepest caves of Austria. www.hoehle.org/long&deep.php

Scholz D, Hofmann D, 2008. ^{230}Th/U-dating of fossil corals and speleothems. Quaternary Science Journal, 57 (1–2), 52–76.

Seemann R, 1997. Sediment- und Mineralinhalt der Hermannshöhle, In: Hartmann H, Hartmann W & Mkros H (Eds.), Die Herrmannshöhle. Die Höhle, Supplement 50. Hermannshöhlen-Forschungs- und Erhaltungsverein, Wien (in German).

Seemann R, Geyh MA, Franke HW, 1997. Altersbestimmung an Sinter- und Tropfsteinformationen der Herrmannhöhle, In: Hartmann H, Hartmann W, Mrkos H (Eds.), Die Herrmannshöhle. Die Höhle, Supplement 50. Hermannshöhlen-Forschungs- und Erhaltungsverein, Wien (in German).

EVOLUTION OF CAVE PROVALATA: REMARKABLE EXAMPLE OF HYPOGENIC THERMAL CARBONIC AND SULFURIC ACID SPELEOGENESIS

Marjan Temovski[1], Philippe Audra[2]
[1]Vlado Stojanoski 37, MK-7500 Prilep, Macedonia, temovski_m@yahoo.com
[2]Polytech'Nice-Sophia, Engineering School of Nice – Sophia Antipolis University, 1645 route des Lucioles, FR-06410 Biot, France, audra@unice.fr

Cave Provalata (Mariovo, southern part of Republic of Macedonia) is a small but remarkable hypogenic cave with abundant gypsum deposits, mostly covering thick corroded calcite crust, with cupolas, ceiling and wall channels, feeders and replacement pockets as some of the most characteristic morphological features. Morphological and mineralogical analyses suggest hypogenic origin in two phases: the first by thermal CO_2 rich waters, the second by sulfuric acid dissolution, separated by complete infilling of cave passages with clays. In the first phase cave passages were formed by dissolution along fractures due to cooling of rising carbonated thermal waters. They were later covered with thick calcite crust, deposited after shifting to shallower environment. The cave was completely filled with clays in Early Pleistocene, due to deposition of pyroclastic rocks and travertine deposits in lacustrine environment in Mariovo Basin. After draining of Mariovo Lake and establishing fluvial drainage, Buturica River incised first in the lacustrine deposits, then in Cambrian marbles, creating its superimposed valley, which lowered the water table and allowed washing of the clay deposits. The second phase started after introduction of H_2S in the thermal waters, which produced sulfuric acid at or near water table, rapidly dissolving the calcite crust and marble host rock. Most of the dissolution happened above water table due to condensation corrosion which produced abundant gypsum deposits as replacement gypsum crust, that later detached and pilled as gypsum blocks. At the contact of sulfuric acid with the clay deposits, alunite, jarosite and natroalunite were formed. $^{40}Ar/^{39}Ar$ dating gave maximum age of 1.6 Ma (alunite) and 1.46 Ma (jarosite). The cave continued to evolve downwards due to lowering of the water table as Buturica River incised its valley.

1. Introduction

Two major classes of hypogenic caves form due to dissolution of carbonate rocks by CO_2 and H_2S rich thermal waters (Palmer 1991; Dublyansky 2000a).

Rising thermal carbonic waters cool down along their flow path, increasing their aggressiveness due to inverse relationship between solubility and temperature, which leads to progressive increase in $CaCO_3$ solubility, and also drastic drop of solubility near water table due to loss of CO_2. As a result geochemical zone of carbonate dissolution and zone of carbonate precipitation appear (Dublyansky 2000a). Where H_2S rich waters mix with shallower oxygen rich waters, sulfuric acid forms at or near water table, which rapidly dissolves the carbonate rocks (Egemeier 1981). This process is known as sulfuric acid speleogenesis (SAS) and have been recognized as a significant cave forming process in many caves around the world, such as Carlsbad and Lechuguilla Caves in New Mexico (Hill 2000), Frasassi caves in Italy (Galdenzi and Menichetti 1995), la Cueva de Villa Luz in Mexico (Hose and Pisarowicz, 1999), Le Chat cave in France (Audra 2007), Krausholle in Austria (Plan et al. 2012). Above the water table H_2S escapes in the cave air and redissolves in water condensation droplets on cave walls, where oxidizes to sulfuric acid which attacks the carbonate rock and converts it to gypsum by forming replacement gypsum crusts on cave walls an ceiling. Replacement gypsum crusts may detach and deposit on the floor as mounds or blocks of massive gypsum (Egemeier 1981; Galdenzi and Maruoka 2003). In contact with alumino-silicates, sulfuric acid produces characteristic suit of minerals such as alunite, jarosite, natroalunite, hydrated halloysite (Polyak and Provencio 2001). Such K rich minerals formed in the same time as the cave allow dating of the age of the cave forming process (Polyak and Provencio 2001).

This paper presents the results of a morphological study, combined with X-ray and stable isotope analyses of cave sediments, in order to determine the origin and evolution of Cave Provalata, a small cave in the southern part of Republic of Macedonia (Fig. 1), formed on the edge of a coal bearing Neogene basin. The cave was first explored by caving clubs Peoni and Ursus Speleos from Skopje, and first published in scientific literature (as Cave Gulabinka) by Kolčakovski et al. (2004). They noted the presence of gypsum in the cave and suggested that the origin of the cave

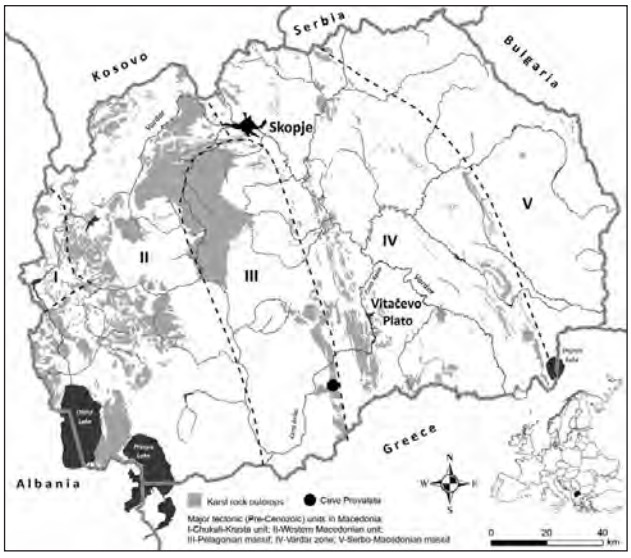

Figure 1. Location of Cave Provalata in Macedonia.

is connected with dissolution of marble by hydrothermal waters enriched with H_2S, although concluded that the cave is a fossil ponor cave.

Our results suggest origin in two recognizable speleogenetic phases, thermal carbonic phase responsible for thick calcite crust and sulfuric acid phase creating abundant gypsum deposits.

2. Location and geological setting

Cave Provalata is located near Melnica and Vitolište villages in Mariovo, southern part of Republic of Macedonia, on the eastern edge of a Neogene tectonic basin (Mariovo Basin), at the top of the southern slope of the superimposed valley of Buturica river (Fig. 2). In a wider tectonic sense this area is part of the Pelagonian massif, a pre-Cenozoic major tectonic unit which consists of Precambrian gneiss and schist rocks, covered by thick section of dolomitic and calcitic marble in the upper part, and with abundant granitic plutons (Dumurdžanov et al. 2005).

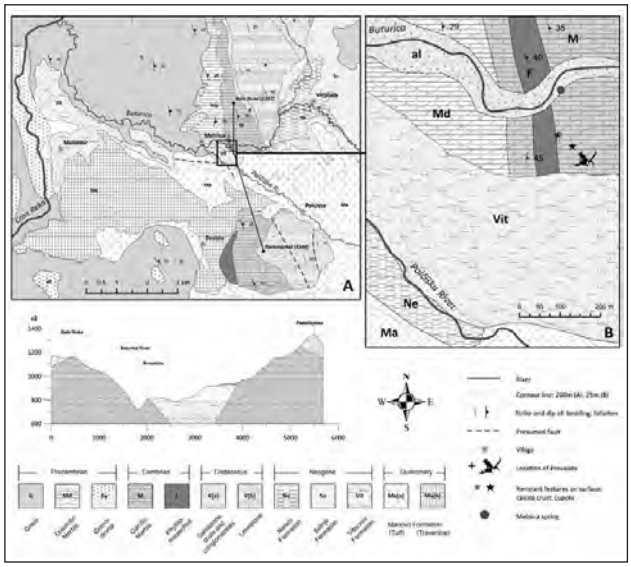

Figure 2. Geological setting of the cave.

The cave is mostly formed in Cambrian marbles with some (mostly upper) parts formed in marble breccia (paleokarst), which together with the underlying Precambrian dolomitic marbles are part of a Veprcani Monocline that has NNW-SSE direction and dips to ENE by 25 to 50°. In the northern parts this Cambrian marbles have lenses of Phyllite-micaschists, and to the south they lay directly over Cambrian Phyllito-micaschists (Dumurdžanov et al. 1976). One such lense is located just west of the cave (the cave is formed near the contact of marbles and Phyllito-micaschists).

To the south and east, this Pre-Cenozoic rocks are covered by Neogene and Quaternary lacustrine and pyroclastic sediments of Mariovo graben (Dumurdžanov et al. 2004):

- Nerezi formation (Upper Miocene) – gravel and sandstone; siltstone and silty claystone that grades upward into claystone and coal; and siltstone and sandstone followed by a hiatus.
- Solnje Formation (Pliocene) – poorly stratified gravel and sandstone, continuing to:
- Vitačevo formation (Pliocene) – stratified tuff overlaid by sandstone and gravel interbedded with beds of diatomite, tuff, and sandy claystone; travertine deposits, tuff-agglomerate and sandstone.
- Mariovo formation (Pleistocene) – pyroclastic rocks with nine travertine layers and a 20-m-thick travertine deposit on top.

Dumurdžanov et al. (2004, 2005) interpret the evolution of the Neogene basins in Macedonia in 5 cycles, with Mariovo basin forming in cycle II (late Miocene: late Sarmatian-Meotian), with total hiatus at the end of cycle III (Pontian). Then a transgression occurs in Pliocene – cycle IV (Solnje formation), accompanied with volcanic activity in Kožuf and Kozjak Mts (Vitačevo formation), which continued through Early Pleistocene (Mariovo formation). With the draining of the lake system in central Macedonia as a result of subsidence in the Aegean sea (which started probably as late as Middle Pleistocene; Dumurdžanov et al. 2005), Mariovo lake also drained, thus Crna Reka established its fluvial basin, including the super-imposed valley of Buturica River in which Provalata Cave has formed.

3. Methods

We made a detail survey of the cave, combined with morphological analyses in order to determine the presence of characteristic hypogenic morphology.

Characteristic cave sediments were sampled for X-Ray analyses. This includes samples from gypsum, grey clay, yellow sand, pinkish clay, pale yellow sand and dark crust under the gypsum crust. X-ray analyses were carried at the CEREGE – CNRS, France. X-ray powder diffraction (XRD) patterns were recorded on a Philips diffractometer using Cobalt radiation (λ = 1.79 Å) with a secondary graphite monochromator. The diffractometer optic used to record all samples was a front fixed slit of 1°, a scattered radiation slit of 1° after the sample, and a 0.2 mm detector slit. The X-ray tube operating conditions were 40 kV and

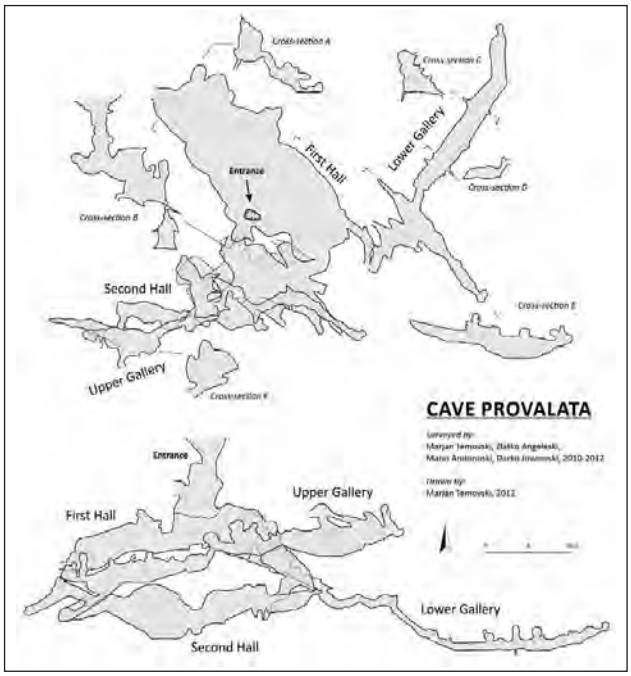

Figure 3. Map of Cave Provalata.

40 mA and the step-scan data were continuously collected over the range 3.5 to 78° 2θ using a step interval of 0.05° 2θ and a counting time of 2.5 s.

Calcite crust, with presumed thermal origin, was sampled for stable isotope analyses ($\delta^{13}C$, $\delta^{18}O$). The sample was collected from the ceiling of a small channel emerging from the north part of the First Chamber. The $\delta^{13}C$ and $\delta^{18}O$ stable isotope ratios were measured at the Stable Isotope Laboratory at Saint Louis University (Department of Earth and Atmospheric Sciences), Missouri, USA. The isotopic ratio is given in per mill (‰), according to VPDB international standard. Standard deviations for oxygen isotopes were between 0.06‰ and 0.09‰ (5 tests), and for carbon isotopes between 0.03‰ and 0.11‰ (5 tests).

Sulfur isotope ratio of cave gypsum was analyzed at the Institute of Mineralogy and Geochemistry of the University of Lausanne using a Carlo Erba 1108 elemental analyzer (EA) connected to a Thermo Fisher (Bremen, Germany) Delta V isotope ratio mass spectrometer (IRMS) that was operated in the continuous helium flow mode via a Conflo III split interface (EA-IRMS). The stable isotope composition of sulfur is reported in the delta (δ) notation as the per mil (‰) deviation of the isotope ratio relative to known standards: $\delta = [(R_{sample} - R_{standard})/R_{standard}] \times 1000$, where R is the ratio of the heavy to light isotopes ($^{34}S/^{32}S$). The sulfur standard is the Vienna Cañon Diablo Troilite (VCDT). The reference SO_2 gas was calibrated against the IAEA-S-1 sulfur isotope reference standard (Ag_2S) with $\delta^{34}S$ value of -0.3‰. The overall analytical reproducibility of the EA-IRMS analyses, assessed by replicate analyses of three laboratory standards (barium sulfate, with a working $\delta^{34}S$ value of +12.5‰; pyrite Ch, +6.1‰; pyrite E, –7.0‰) is better than ±0.2‰ (1 SD). The accuracy of the $\delta^{34}S$ analyses was checked periodically by analyses of the international reference materials IAEA-S-1 and IAEA-S-2 silver sulfides (0.3‰ and +22.7±0.2‰, respectively, values from IAEA-Catalogue and Documents) and NBS-123 sphalerite (+17.09±0.31‰, value from NIST-Catalogue and Documents).

Samples of alunite and jarosite (pale yellow sand) were dated by $^{40}Ar/^{39}Ar$ method at the New Mexico Geochronology Research Laboratory in Socorro, New Mexico, USA. They were analyzed twice, once routinely and once wrapped in Ag with a platinum crimp. The second analysis was not a complete degassing. Results were similar for both the alunite and jarosite, but some higher step ages were apparent at the end of degassing, indicating minor to trace amounts of contamination from another older phase. Because of this, the results are considered maximum ages and could be younger.

4. Results

4.1. Morphology

Provalata is a small cave with total length of about 230 m and total depth of 24 m. There are two major rooms (First and Second) with more or less vague (due to collapse) form, and two main passages (Lower and Upper) with more distinct (fracture guided) morphology.

The most representative and common morphological features of the cave are cupolas and solution pockets (Fig. 4: A, D). Cupolas vary in form and size, often combining several cupolas overlaid on another. They are most abundant in the Lower Passage as well as in the Upper Passage, but the highest ones (up to 7 m) are in the First Room, in marble breccias, as well as the entrance shaft which is a cupola formed in marble breccias opened to the surface by collapse. Two generations of cupolas and solution pockets can be clearly separated in the cave: one formed in marbles (or marble breccia) and covered with calcite crust, and the other formed in the calcite crust covering the first cupolas, or completely cutting trough the calcite crust to the first generation cupola, and creating secondary cupola or solution pocket. Half tube wall channels are best presented in the Lower Passage, starting from feeders and leading to ceiling channels and cupolas (Fig. 4: C, D, E, F). Replacement pockets can also be found in Upper Passage, with gypsum deposits already emptied (Fig. 4: A, B).

4.2. Sediments

Calcite crust, black to transparent, up to 0.5 m thick and highly corroded, is covering walls and ceiling throughout the cave, at places completely dissolved (Fig. 5: E).

It is covering various channel features with phreatic morphology, such as cupolas, wall and ceiling channels, solution pockets. The morphology and thickness suggest formation by carbonic degassing in shallow thermal waters (Palmer 1991; Dublyansky 2000b; Audra 2009) that precedes the clay infilling and sulfuric acid phase.

Five samples from a ~20 cm cut through the calcite crust and marble host rock were collected for $\delta^{13}C$ and $\delta^{18}O$ analyses, two of which were from the weathered marble host rock (C1, C2) and three from the calcite crust (C3, C4, C5). All of the five sample have light $\delta^{18}O$ ratio (-12.69 to -10.39‰), but quite heavy $\delta^{13}C$ ratio (2.78 to 7.16‰). The values of $\delta^{18}O$ are within the typical range for thermal calcite (Dublyansky 2000b), and also suggest some thermal alteration of the marble, but the values for $\delta^{13}C$ are quite

Table 1. Mineralogical composition of clays from Cave Provalata and caves in the nearby Vitačevo Karst.

Cave	Sediment (sample)	Mineralogical composition
Provalata	Grey clay (PR04)	montmorillonite, kaolinite, sanidine, albite, muscovite, quartz
Provalata	Pink clay (PR08)	natroalunite, halloysite, muscovite, quartz
Provalata	Pale yellow sand (PR10)	alunite, jarosite, muscovite, quartz
Dragoželska Propast	Dark brown clay (DR01)	montmorillonite, halloysite, illite, quartz
AramiskaPeštera	pale brown clay (AR01)	montmorillonite, kaolinite, sanidine, fluorapatite, muscovite, quartz
Čulejca	reddish-brown clay (CH)	montmorillonite, halloysite, kaolinite, calcite, muscovite, quartz

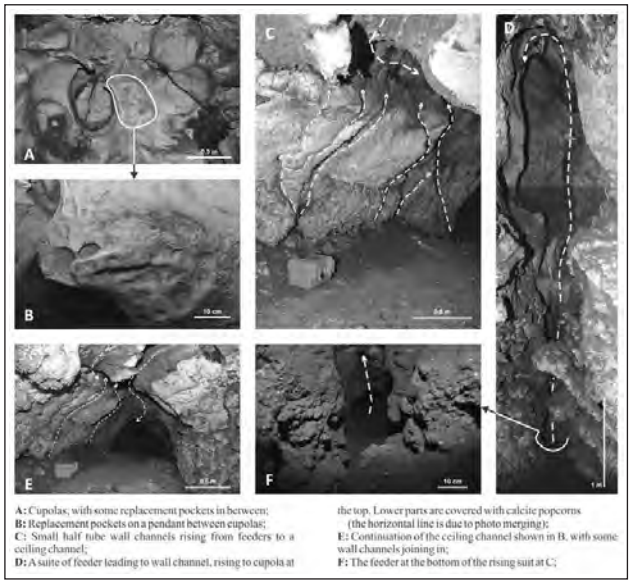

Figure 4. Morphological features in Cave Provalata.

high for the calcite. The heavy carbon isotope ratio might be as a result of deep-seated origin of CO_2 (Bakalovicz et al. 1987), connected to the nearby Kozjak volcanic area.

Grey clays (Fig. 5: B) are covering the lower parts of cave passages, but small patches of grey clay can be found filling parts of cupolas in the Upper Passage, suggesting complete infilling of the cave at some time, and later washing. X-ray analyses confirmed composition of sanidine, kaolinite, montmorillonite, albite, muscovite and quartz. Considering the composition, its origin is likely related to the overlaying pyroclastic sediments (tuff) of the Mariovo formation. This is also suggested by results of X-Ray analyses of clays from caves (Aramiska Peštera, Dragoželska Propast, Čulejca) of the nearby Vitačevo Plato (Fig.1), formed in limestones covered by similar pyroclastic sediments (Tab.1).

Fine grained pale yellow sands can be found in the First Room, covering walls and ceiling, and filling fractures (Fig. 5: C). X-ray analyses of sample from the wall in the SE end of the First Room confirmed presence of alunite, jarosite, quartz and muscovite. $^{40}Ar/^{39}Ar$ dating of alunite and jarosite gave maximum age of 1.6 Ma and 1.46 Ma, respectably

Pink clay was found on the wall at the entrance part of the Lower Channel (Fig. 5: D). X-ray analyses confirmed composition of halloysite, natroalunite, muscovite and quartz minerals. It has white to pale pink color and it is dehydrated, with waxy texture.

Gypsum deposits are the most characteristic cave sediments. They are found in every part of the cave, except some places which have periodic vadose percolation, where gypsum most likely was dissolved. Gypsum deposits are present as replacement crusts up to 40 cm thick (Fig. 5: F), or detached replacement gypsum crust (Fig. 5: G) that pilled in gypsum blocks (Fig. 6: H).

Stable isotopes analyses of sulfur from cave gypsum (2 samples) gave $\delta^{34}S$ values of -2.3 to -1.9 ‰. The negative $\delta^{34}S$ values of gypsum indicate formation from oxidation of H_2S which derived from reduction of sulfates.

Sulfur isotope ratio of gypsum and vitrinite from the coals in Mariovo Basin, sampled nearby Vitoliste village, has positive $\delta^{34}S$ values: +8.5 to +17.3‰ for gypsum in coal seams and +5.4 to +13.2 for vitrinite (Lerouge et al., 2007). Considering the location of the cave to the coal deposits in Mariovo Basin, the origin of H_2S responsible for gypsum formation, might be attributed to sulfate reduction in the nearby coal basin.

Calcite popcorns are covering the corroded calcite crust at various places. Also small flowstone deposits are developing in few places in the cave as a result of late vadose percolation, but the cave is clearly not very well connected with the overlaying surface (except the entrance collapse shaft), which is also confirmed by the well preserved large amount of gypsum deposits.

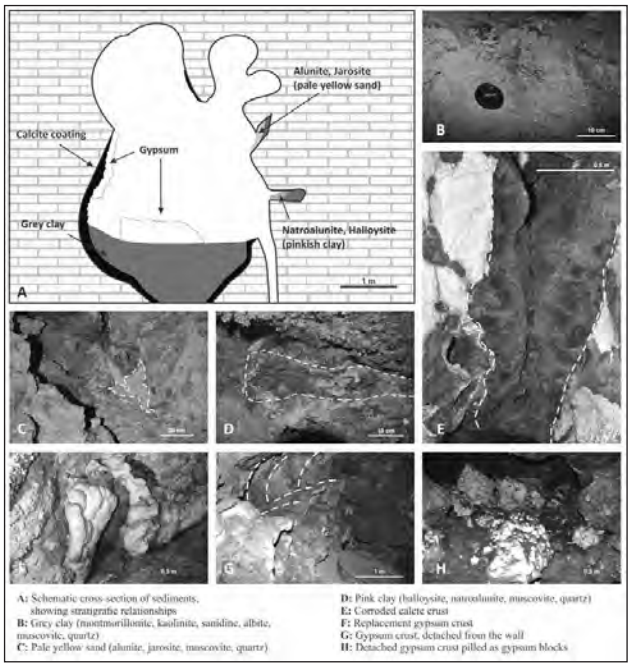

Figure 5. Characteristic sediments in Cave Provalata.

5. Discussion

The thickness, distribution, morphology and stable isotopes ratios (Oxygen, Carbon) of the calcite crust, clearly suggest calcite deposition in a low temperature thermal environment, at or near the water table. The calcite deposits filled passages and convectional features (cupolas, pockets), which were formed in a previos phase in deeper parts of the thermal system due to cooling effect of carbonated thermal waters.

The cave was later completely filled with clay deposits, originating from weathering of pyroclastic sediments most likely from Mariovo formation, which were deposited in a lacustrine environment in Early Pleistocene (Dumurdžanov et al. 2004).

Presece of alunite, jarosite, natroalunite in altered clay deposits, combined with large deposits of gypsum found as replacement crusts or gypsum blocks, and morphological features such as feeders leading to wall and ceiling (half tube) channels and cupolas, which cut first trough the calcite crust, then the marble host rock, as well as the highly corroded calcite crust remnants, clearly point towards sulfuric acid speleogenesis. H_2S oxydized to sulfuric acid at or near water table, rapidly dissolving the calcite crust and marble, but most of the cave void formation happened

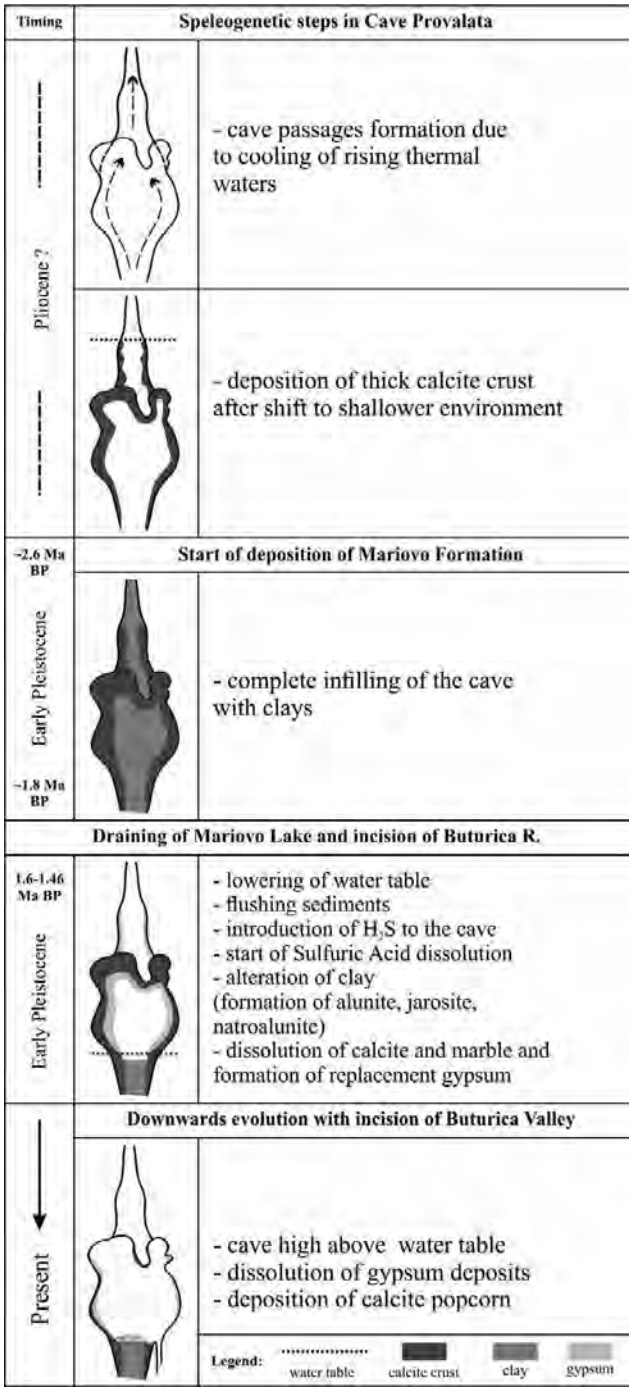

Figure 6. Speleogenetic evolution of Cave Provalata.

above water table by condensation corrosion and replacement of carbonate rock with gypsum. This first started by dissolving the calcite crust and creating second generation cupolas and pockets, which gradualy evolved towards the marble host rock, and at places ended in completely dissolving the calcite crust. $^{40}Ar/^{39}Ar$ dating of alunite and jarosite from the First Room gave maximum age of 1.6 and 1.46 Ma.

Considering the necessary environment for the sulfurc acid speleogenesis (position of the water table near the location of the cave passages), this sulfuric acid phase started after the draining of Mariovo Lake and incision of the valley of Buturica River.

Since last layers of tephra can be found in the travertine layers deposited in lacustrine environment as endpart of Mariovo formation, and the volcanic activity in Kozjak Mt. was dated from 4.0 ± 0.2 to 1.8 ± 0.1 Ma (Kolios et al. 1999), we can place the draining of Mariovo Lake somewhere between 1.8 and 1.6 Ma.

Consequently the calcite crust and the cave features covered by it which represent the first thermal carbonic phase, formed before deposition of Mariovo Formation and are probably from Pliocene age.

The cave then evolved downwards with lowering of water table due to the incision of Buturica Valley, with remnant features (cupolas, pockets, calcite crust) found on surface on the slope of the valley, and a small low temperature (21 °C) thermal spring (Melnica Spring) now located in the alluvial deposits of the river bed of Buturica River.

6. Summary

Cave Provalata is a small (~230 m) cave in the southern parts of Republic of Macedonia, which formed in two phases by thermal waters due to carbonic and sulfuric acid dissolution, which were separated by complete infilling with pyroclastic-derived clay deposits. In the first phase (Pliocene?), cave passages formed by dissolution of marbles due to cooling of thermal carbonated waters, and were later covered with thick calcite crust deposits due to shift in shallower phreatic environment. These passages were then completely filled with clay deposits, originating from weathering of pyroclastic sediments of Mariovo Formation which were deposited in lacustrine environment (Early Pleistocene). Sometime between 1.8 and 1.6 Ma BP, Mariovo Lake drained and Buturica River incised first in deposits of Mariovo Formation, then forming superimposed valley and cutting trough the Cambrian marbles. This lowered the water table, and allowed washing of clay deposits. Then due to introduction of H_2S in the thermal waters (formed probably by reduction of sulfates in the nearby coal basin), sulfuric acid formed at or near water table, rapidly dissolving first calcite crust, then marble host rock, with most of the cave void formation above water table due to condensation corrosion which resulted with replacement of carbonate rock with gypsum. At contact of sulfuric acid with clay deposits, alunite, jarosite and natroalunite were formed, given maximum age of 1.6 Ma (alunite) and 1.46 Ma (jarosite) by $^{40}Ar/^{39}Ar$ dating. As Buturica River incised, tha water table lowered and the sulfuric acid dissolution shifted downward. Today Cave Provalata is 100 m above the riverbed of Buturica River, where a small low temperature thermal spring (Melnica Spring) is located.

Aknowledgement

V. Polyak separated alunite and jarosite from the pale yellow sand sample. Z. Angeleski, M. Andonoski, D. Jovanoski, D. Nedanoski and M. Dameski helped in surveying the cave and collecting samples.

References

Audra P, 2007. Karst et spéléogenèse épigènes, hypogènes, recherches appliquées et valorisation (Epigene and hypogene karst and speleogenesis. Operative research and valorisation). Habilitation Thesis, University of Nice Sophia-Antipolis, 278.

Audta P, 2009. The association between bubble trails and folia: a morphological and sedimentary indicator of hypogenic speleogenesis by degassing, example from Adaouste Cave (Provence, France). International Journal of Speleology, 38(2), 93–102.

Bakalowicz MJ, Ford DC, Miller TE, Palmer AN, Palmer MV, 1987. Thermal genesis of dissolution caves in the Black Hills, South Dakota. Geological Society of America Bulletin, 99, 729–738.

Dublyansky YV, 2000a. Dissolution of carbonates by geothermal waters. In: Klimchouk AB, Ford DC, Palmer AN, Dreybrodt W, (Eds). Speleogenesis: Evolution of karst aquifers: Huntsville, Ala. National Speleological Society, 158–159.

Dublyansky YV, 2000b. Hydrothermal speleogenesis – its settings and peculiar features. Klimchouk AB, Ford DC, Palmer AN, Dreybrodt W, (Eds). Speleogenesis: Evolution of karst aquifers: Huntsville, Ala. National Speleological Society, 292–297.

Dumurdžanov N, Hristov S, Pavlovski B, Ivanova V, 1976. Explanatory notes for the General Geological map of Vitolište and Kajmakčalan. Federal Geological Survey, Beograd, 1–61 (in Macedonian).

Dumurdžanov N, Serafimovski T, Burchfiel, BC, 2004. Evolution of the Neogene-Pleistocene Basins of Macedonia. Geological Society of America, Digital Map and Chart Series 1, 1–20.

Dumurdžanov N, Serafimovski T, Burchfiel BC, 2005. Cenozoic tectonics of Macedonia and its relation to the South Balkan extensional regime. Geological Society of America, Geosphere, 1(1), 1–22.

Egemeier SJ, 1981. Cavern development by thermal waters. NSS Bulletin 43, 31–51.

Galdenzi S, Maruoka T, 2003. Gypsum deposits in the Frasassi caves, Central Italy. Journal of Cave and Karst Studies, 65, 111–125.

Galdenzi S, Menichetti M, 1995. Occurrence of hypogenic caves in a karst region: examples from central Italy. Environmental Geology 26, 39–47.

Hill CA, 2000. Overview of geological history of cave development in the Guadalupe Mountains, New Mexico, Journal of Cave and Karst Studies, 62(2), 60–71.

Hose LD, Pisarowicz JA, 1999. Cueva de Villa Luz, Tabasco, Mexico: reconnaissance study of an active sulfur spring cave and ecosystem. Journal of Cave and Karst Studies 61, 13–21.

Kolios N, Innocenti F, Maneti P, Poccerilo O, Guiliani O, 1980. The Pliocene Volcanism of the Voras Mts (Central Maceodonia, Greece). Bull. Volcanol., 43(3), 553–568.

Kolčakovski D, Boev B, Hristovski S, Petreska B, 2004. Cave Gulabinka – Mariovo, preliminary speleological exploration. Bulletin for Physical Geography, Institute of Geography – PMF, Skopje, 1, 35–43 (in Macedonian).

Lerouge C, Gouin J, Deschamps Y, Widory D, Laggoun-Defarge F, Tasev G, Serafimovski T, Yossifova M, 2007. Characterization of coal from the Mariovo basin, Macedonia – Insights from organic geochemical and sulphur isotopic data. In: Andrew CJ, et al (Eds.). Digging Deeper, 9th Biennial SGA Meeting, August 20–23, 2007, Dublin, Ireland, vol. II, 901–904.

Palmer AN, 1991. Origin and morphology of limestone caves. Geological Society of America Bulletin, 103 (1), 1–21.

Plan L, Tschegg C, De Waelle J, Spötl C, 2012. Corrosion morphology and cave wall alteration in an Alpine sulfuric acid cave (Kraushöhle, Austria), Geomorphology 169–170, 45–54.

Polyak VJ, Provencio P. 2001. By-product materials related to H_2S-H_2SO_4 influenced speleogenesis of Carlsbad, Lechuguilla, and other caves of the Guadalupe Mountains, New Mexico. Journal of Caves and Karst Science, 63(1), 23–32.

FLANK MARGIN CAVES ON A PASSIVE CONTINENTAL MARGIN: NARACOORTE AND OTHER SOUTHERN AUSTRALIAN EXAMPLES

Susan White
[1]*Environmental Geoscience Latrobe University Bundoora Victoria Australia*
[2]*Australian Speleological Federation Inc., susanqwhite@netspace.net.au*

Flank margin caves (FMC) have been predominantly described on carbonate islands such as in the Bahamas or the Marianas, using the Island Karst Model. This model has been used to explain karst development on young carbonate islands with poorly cemented eolianites, which differ substantially from continental karst, formed in well cemented limestones. Karst on continental margins especially the southern Australian coast, are not in well cemented telogenic rocks but in highly porous, highly permeable marine and eolian calcarenites. The gradual uplift over the past 50 Ma of the southern edge of the continent has resulted in Flank Margin Caves which formed in a coastal setting, being positioned significantly further inland and reflect the neotectonics of the Southern Australian passive continental margin rather than solely the Pleistocene glacio/eustatic sealevel fluctuations. The inter-relationship of tectonic setting, the distinctive characteristics of FMC and the speleogenesis of coastal karst assists in the understanding of the karst landscape evolution of significant karst areas of southern Australia.

1. The Characteristics of Flank Margin Caves

Flank Margin Caves form along the margins of the freshwater lenses just beneath the flanks of the enclosing land mass (Mylroie and Carew 1995, Mylroie et al. 2004) (Figure 1). This is where aggressive solution occurs as the result of mixing corrosion (Bogli 1980) and either the saline halocline or the meteoric water/watertable. They have predominantly been described in island environments, partly because island fresh water lenses are more intensively studied that the equivalent on continental margins. The cave development is primarily related to the geometry of the freshwater lens.

These caves have a distinctive passage shape and configuration due to their development as isolated entrance-less chambers (or groups of chambers) often described as "beads on a string" (Mylroie et al. 2001). These chambers are breached as surface erosion occurs. The complex cave perimeters show dissolutional wall morphologies such as bell holes and very large scallops. As the chambers were sealed and with ~100 % humidity, dense crystalline calcite spelothems are common. Solution has cut across carbonate facies disregarding differences in porosity and grain size and primary structures such as bedding planes.

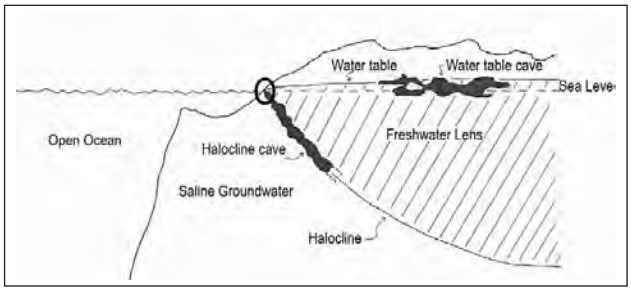

Figure 1. Superposition of the vadose/phreatic and fresh/marine mixing zones at the lens margin means cave development is favored at the lens margin, under the flank of the land; hence the name "Flank Margin Cave" (after Mylroie and Carew).

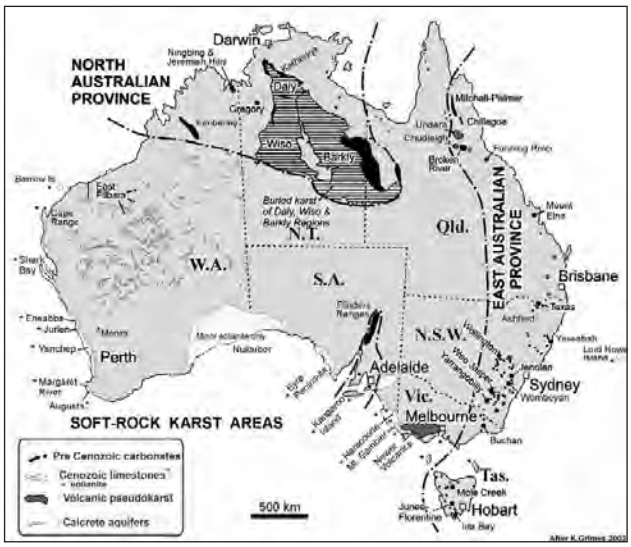

Figure 2. Australian Karst areas (after K.G. Grimes).

2. Southern Australian coastal karst

Across southern Australia highly porous and permeable carbonates occur in a coastal setting. These carbonates are either Oligocene to Pliocene cool water marine limestones or Pleistocene aeolian calcarenites derived from them (Figure 2).

The tectonic setting is a passive continental margin, which has been developing since the Late Mesozoic when the break up of the Gondwanan super continent occurred. The active spreading centre, the Southeast Indian Ridge, separates the Antarctic Plate from the Australian Plate and is some 2,500–3,000 km to the south. The structure of southern Australian continent is largely inherited from the pre-existing Cretaceous extensional faulting.

The Australian continent is generally considered a "stable" intra-plate region despite having high levels of seismicity (Blewett et al. 2012). Its passive margin, where the transition from oceanic to continental crust occurs, exists along the south coast. However the plate is moving generally northwards at a rate of ~7 cm pa; the fastest moving plate on Earth.

Australia also has significant neotectonic activity especially

across the southern coastal area. There are kink folds in ~125 ka old cemented aeolianite at Cape Liptrap (Sandiford, 2003). The Eucla Basin has been tilted, expressed as a west-side up, east-side down tilting of ~100–200 m during the Neogene; a broader north-downsouthwest-up dynamic topographic tilting of the Australian continent associated with relatively fast (6–7 cm/yr) northward plate motion since fast spreading commenced in the Southern Ocean at ~43 Ma (Hou et al. 2008). Similarly there is significant uplift across southeast Australia where a significant Late Miocene uplift caused a regional angular unconformity, at around the Miocene-Pliocene boundary onshore (Dickinson et al. 2002, Dickinson et al. 2001). This event occurred across and coincided with a change in the dynamics of the Australian plate to the current compressional regime. A second, but less significant, uplift occurred in the Late Pliocene to Early Pleistocene (Dickinson et al. 2002, Dickinson et al. 2001, Paine et al. 2004). During the Pleistocene, as the sea regressed, bioclastic carbonate beach, barrier and sub-parallel calcareous and karstic dune complexes (Bridgewater Formation eolianites) were deposited over extensive areas of the western Otway Basin in a high-energy coastal environment with barrier dunes and associated lagoons. Dune building occurred from at least 1.3 Ma through to present times, and continues today on the coast where suitable conditions of sediment supply are available. The gradual uplift of the coastal plain (~0.07 mm/year) west and south of the Kanawinka Fault resulted in a well dated, punctuated, time-transgressive aeolianite sequence associated with sea-level high stands spanning most of the Pleistocene (Belperio et al. 1995). Uplift is a factor in the preservation of these dunes and their karst.

3. Charactersitics of the karst

Distinctive characteristics of the karst on calcareous dunes include a range of features that are distinctively associated with Flank Margin Caves. These include shallow caprock caves, irregular horizontal mazes, caves that are either dominated by collapse domes or “inclined fissures”, with little or none of the original solutional passage remaining. Many of these features are also found in the caves in the poorly consolidated marine cool water carbonates, although these have a stronger linear orientation in the larger caves. The caves in both lithologies have been modified by extensive collapse, solution pipes, bell hole development, and speleothem deposition, especially moonmilk, can be extensive.

Wall morphologies indicate phreatic dissolution without turbulent (conduit) flow as is typical for FMC conditions. Four main solutional features found are horizontal grooves (notches), speleogens, spongework and large non-directional scallops. In addition, ceilings with avens and bell holes are found in many caves.

Bell holes or ceiling pockets are cylindrical cavities with vertical long axes, varying between 0.3 to 1 m in diameter and 0.5 to 1.0 m deep, tapering upwards and are present in the ceilings of many caves. These have not been extensively reported in the literature in temperate climates but are common in the poorly consolidated limestones in southern Australia indicating that they are not necessarily restricted to tropical and subtropical climates. The most spectacular are in the roof of Wet Cave (U 10), where over 50 densely spaced, narrow vertical cones of up to I m depth and 0.5 to 0.8 m diameter are found (Figure 3). As a feature of ceilings rather than walls, and not associated with jointing in the cave ceilings, bell holes show that these large chambers were primarily formed by solution, and these chambers generally lack collapse debris.

Figure 3. Bell holes and speleogens Wet Cave (U10) Naracoorte Photo N. White.

4. Speleogenesis

Karst phreatic caves formed in coastal environments on an upwarping continental margin, where specific localised conditions created enhanced solutional conditions over relatively short time periods. Subsequent modification of the karst was controlled by the combination of continuing neotectonic uplift combined with falling sea levels throughout the rest of the Pleistocene. The position of the dated dunes in the western Otway Basin e.g., Naracoorte, mean that we have a well documented sequence of host rocks over the past ~1 M years.

When deposition of the East Naracoorte Range occurred in the Early Pleistocene, the coastline lay approximately along the Kanawinka Fault, about 70 m above present sea level. Thus cave development was probably influenced by the halocline mixing zone at the base of the fresh water lens,

enhancing aggressiveness. The groundwater mixing zone geometry is controlled by sea level and the water table in high permeability limestones such as the Miocene cool water Gambier Limestone. Additionally the watertable would have been generally very flat at Naracoorte. The caves show many characteristic features of FMC. The main area of cave development lay probably between 400 m to 500 m inland from the high water mark when sea level was at 70 m above present conditions. If the water table were between 1 and 2 m above sea level in this area (assuming a similar very low gradient of 1:250 to that inland from the present coastline), the fresh/seawater zone would have been at least 40 m below sea level. This appears to be below the depth at which most caves at Naracoorte have developed (~61 m a.s.l. and 25 to 30 m below present surface. However, if the area was an estuarine or back swamp environment similar to the present coastal areas, e.g., Glenelg River estuary, the water table would have been lower, e.g., at 0.75 m above sea level or less. The halocline would then be at ~30 m depth and halocline enhanced formation is possible.

Similar development and features can be seen on the Nullarbor (Burnett et al. in review) and on Kangaroo Island (Mylroie and Mylroie 2009). However in all cases the length of time of the landscape development means that significant landscape lowering has occurred and the caves may now be closer to the present land surface than when they formed.

In the case of Kangaroo Island, Mylroie and Mylroie (2009) have argued for the presence of FMC but have over emphasised the role of the Pleistocene eustatic sea level fluctuations and under estimated the role of neotectonics which has overprinted the global sea level fluctuations on the southern Australian continental margin.

5. Conclusions

Limestone dissolution is enhanced at the vadose/phreatic and fresh-water/saltwater interfaces due to mixing effects and oxidation of organic matter at these density interfaces. The position of the fresh-water lens has fluctuated through a vertical range of over 100 m, due to Quaternary glacio-eustasy, but local tectonics can overprint glacio-eustatic events, adding to the complexity of the record. The karst is eogenetic, having been formed in eogenetic rocks, which are rocks that never underwent burial beyond the range of meteoric diagenesis.

The karst landscape development on the Cenozoic cool water marine limestones and eolianites along the southern Australian margin are related to the coastal conditions when the main karstification has occurred. This much more extensive than previously thought and helps explain the complex speleogenesis. The uplift of the land coupled with the fluctuating Pleistocene sea levels has resulted in a much more complex scenario than previously thought and explains the relatively sparse karst areas interspersed with very intense karstification.

Acknowledgements

Thanks to John Webb and Nicholas White for their assistance.

References

Belperio AP (Compiler), 1995. Quaternary. In: JF Drexel and WV Preiss (Eds.), The Geology of South Australia. South Australia Geological Survey Bulletin 54. Adelaide, 219–280.

Blewett RS, Kennett BLN, Huston DL, 2012. Australia in Time and Space. In: Shaping a Nation: A Geology of Australia, Blewett RS (ed.),Geoscience Australia and ANU E Press, Canberra, 332–379.

Bögli A, 1980. Karst hydrology and physical speleology: Springer-Verlag, Berlin, 270.

Burnett S, Webb JA, White S, in review. Shallow Caves and Blowholes on the Nullarbor Plain, Australia – Flank Margin Caves on a Low Gradient Limestone Platform.

Carew JL, Mylroie JE, 1995. Quaternary tectonic stability of the Bahamian Archipelago: Evidence from fossil coral reefs and flank margin caves: Quaternary Science Reviews, 14, 144–153.

Dickinson JA, Wallace MW, Holdgate GR, Daniels J, Gallagher SJ, Thomas L, 2001. Neogene Tectonics in SE Australia: implications for petroleum systems. Australian Petroleum Exploration Association Journal (2001): 37–52.

Dickinson JA, Wallace MW, Holdgate G, Gallagher SJ, Thomas L, 2002. Origin and timing of the Miocene Pliocene unconformity in southeast Australia. Journal of Sedimentary Research, 72(2), 288–303.

Hou B, Frakes LA, Sandiford M, Worrall L, Keeling J., Alley NF, 2008. Cenozoic Eucla Basin and associated palaeovalleys, southern Australia – climatic and tectonic influences on landscape evolution, sedimentation and heavy mineral accumulation. Sedimentary Geology 203, 112–130.

Mylroie JE, Jenson JW, Mylroie JR, Carew JL 2004. Epikarst on Eogenetic Rocks In Karst Waters Institute Special Publication 9. 132–134.

Mylroie JE, Mylroie JR, 2009. Caves as sea level and uplift indicators, Kangaroo Island, South Australia. Journal of Cave and Karst Studies, 71 (1), 32–47.

Mylroie JE, Jenson JW, Taborosi D, Jocson JMU, Vann DT, Wexel C, 2001. Karst features of Guam in terms of a general model of carbonate island karst: Journal of Cave and Karst Studies, 63(1), 9–22.

Paine MD, Bennetts DA, Webb JA, Morand VJ, 2004. Nature and extent of Pliocene strandlines in southwestern Victoria and their application to Late Neogene tectonics. Australian Journal of Earth Sciences, 51(3), 407–422.

Sandiford M, 2003. Neotectonics of southeastern Australia: linking the Quaternary faulting record with seismicity and in situ stress, In: RR Hillis and D Muller (Eds.). Evolution and dynamics of the Australian Plate. Geological Society of Australia, Special Publication, 22, 101–113.

TRITIUM AND H, O AND C STABLE ISOTOPES AS A TOOL FOR TRACKING OF WATER CIRCULATION IN THE NIEDŹWIEDZIA CAVE SYSTEM (SUDETES, POLAND)

Michał Gąsiorowski, Helena Hercman
Institute of Geological Sciences PAS, Twarda 51/55, PL-00818, Warszawa, Poland, mgasior@twarda.pan.pl

Water circulation in Niedźwiedzia Cave system is complicated. The system is fed by direct infiltration of precipitation, infiltration from the surface stream and, possibly, by rising flow from deep sources. The cave is drained by system of karst springs in the Kleśnica stream valley, but some part of water flows across border ridge and occurs in Morava stream valley, Czech Republic (Ciężkowski et al. 2009). We tried to use tritium and stable isotopes to describe hydrology of the cave system and analyzed 155 water samples for stable isotopes and 38 water samples for tritium content. The Niedźwiedzia Cave system is composed of three levels of halls and galleries. In the upper level, stable isotope composition in drip water plots close to the local meteoritic water line (LMWL) on the $\delta^{18}O$ vs δD diagram. It varies during the year similar to stable isotope composition of precipitation (i.e. low $\delta^{18}O$ values during winters and higher $\delta^{18}O$ during summers). The delay between isotopic signal in precipitation and drip water is ~10–14 days and this can be interpreted as a time of infiltration from the surface to the cave upper level. The correlation between isotopic composition of precipitation and drip water is not observed in the lower level of the cave system. There isotopic composition of drip water is more stable during the year. We use tritium dating method to estimate the age of this water. It has shown that infiltration time to the lower level is 1.4±0.3 year. The "oldest" water was found in karst spring draining the cave system. The estimated transit time is 3–4 years and suggest admixture of some "old" water that was not sampled in the cave.

Acknowledgments

The authors thank Artur Sawicki from the "Niedźwiedzia Cave" authority for his support during the field work. Jerzy Bieroński gave us many useful hydrological information and guys from the speleological club "Sekcja Grotołazów Wrocław" gave us strong support during collection of water samples. This study is funded by the National Science Center grant no. N N306 131038 and IGS PAS internal project "Tryt".

References

Ciężkowski W, Buczyński S, Rzonca B, Marszałek H, Wąsik M, Staśko S, 2009. Groundwater of karst terrain in the Sudetes. In: K. Stefaniak, A. Tyc and P. Socha (Eds). Karst of the Częstochowa Upland and of the Eastern Sudetes. Studies of the Faculty of Earth Sciences University of Silesia, Sosnowiec-Wrocław, 371–384.

Session:

Cave Mineralogy

HYPOGENE SULFURIC ACID SPELEOGENESIS AND RARE SULFATE MINERALS (FIBROFERRITE, JAROSITE SUBGROUP) BAUME GALINIERE CAVE (ALPES-DE-HAUTE-PROVENCE, FRANCE)

Philippe Audra[1], Fernando Gázquez[2], Fernando Rull[3], Jean-Yves Bigot[4], Hubert Camus[5]

[1]Polytech Nice – Sophia, University of Nice – Sophia Antipolis, 930 route des Colles, 06903 Sophia-Antipolis, France & Innovative City – IMREDD, Nice, France, audra@unice.fr

[2]Water Resources and Environmental Geology Research Group, Dept. of Hydrogeology and Analytical Chemistry – University of Almería, Crta. Sacramento s/n, 04120 La Cañada de San Urbano, Almería, Spain, f.gazquez@ual.es

[3]Unidad Asociada UVA-CSIC al Centro de Astrobiología, University of Valladolid. Parque tecnológico Boecillo, 47151 Valladolid, Spain, rull@fmc.uva.es

[4]Association française de karstologie (AFK), 21 rue des Hospices, 34090 Montpellier, France, catherine.arnoux@clubinternet.fr

[5]CENOTE, 1 chemin de Valdegour, 30900 Nîmes, France, camus.hubert@laposte.net

The oxidation of sulfide sources (H_2S gas, pyrite, hydrocarbons) produces sulfuric acid that strongly reacts with bedrock, causing limestone dissolution and complex interactions with other minerals. This type of cave development, known as sulfuric acid speleogenesis, is a subcategory of hypogenic speleogenesis, where aggressive water rises from depth. It also produces uncommon minerals, mainly sulfates. Baume Galinière is located in Southern France, in the Vaucluse spring watershed. This small maze cave displays characteristic features such as corrosion notches, calcite dikes and iron crusts, and sulfate minerals. Thirteen minerals were identified, including elemental sulfur, calcite, quartz, pyrite, goethite, gypsum, fibroferrite, plus all of the six members of the jarosite subgroup (jarosite, argentojarosite, ammoniojarosite, hydroniumjarosite, natrojarosite, plumbojarosite). The Baume Galinière deposits are the first documented cave occurrence of argentojarosite and the second known occurrence of plumbojarosite, hydronium jarosite, ammoniojarosite, and fibroferrite. Together with other hypogenic caves in the Vaucluse watershed, Baume Galinière Cave owes its origin in buried conditions to deep water rising along major faults, mixing with meteoric water at the contact of the karst aquifer and overlying impervious cover, and causing pyrite deposition. Sulfuric acid speleogenesis occurred later after base level drop, when the cave arrived in shallow phreatic then in vadose zone, with oxidation of pyrites involving sulfidic gases. Attenuated oxidation is still occurring through condensation of incoming air from outside. Baume Galinière Cave records the position of the paleo-cover and documents its retreat in relationship to valley incision caused by uplift and tilting of the Vaucluse block during Neogene.

1. Introduction

Sulfuric acid speleogenesis involves the dissolution of limestone by sulfuric acid derived from H_2S that degasses from hypogenic water fed by deep sources (Egemeir 1983). The source of acidity may be hydrocarbons, sulfides or sulfates, or may be a result of volcanism. Cave development is due to strong acid corrosion, which also resulted in production of secondary sulfate minerals and development of microbial activity evidenced by the presence of poolfingers (Melim et al. 2001). These minerals are mainly gypsum and rare sulfate minerals, depending on the composition of the hypogenic water and the host carbonate rock. Sulfuric acid caves develop near the water table, where mixing of meteoric water and hypogenic water allows oxidation processes. Such caves record position of the water table contemporaneous with their development and are good markers of geomorphological evolution. Baume Galinière is a cave located at the edge of the Vaucluse Plateau, close to the margin of impervious beds that overlie the karst aquifer. The cave contains masses of pyrite that are of hypogenic origin. The speleogenetic history of the cave points toward the oxidation of these pyrite masses during a vadose phase as a result of meteoric water seepage. Oxidation is ongoing under the influence of air convection between the surface atmosphere and the cave, which results in seasonal condensation and evaporation. Beside the classical products of sulfide oxidation, such as gypsum and iron oxihydroxides, some unusual sulfates are present. These minerals occur as colorful crusts or foam-like silky masses. Mineral analyses have been performed, using XRD, Raman, SEM imaging, and stable isotopes. In this paper, we present details of mineralogy of Baume Galinière. Discussion focuses on mineral genesis and on cave genesis in relation to the geomorphological evolution of the region. In addition to the presence of rare sulfate cave minerals, Baume Galinière also records successive stages of regional geomorphological evolution. The area is an important place to study the evolution of the Vaucluse area landscape.

2. A sulfuric cave at the border of the Vaucluse Plateau

Baume Galinière Cave is located in Provence (South-East France), at the foot of Ventoux Plateau, which roughly corresponds to the Vaucluse spring catchment (Fig. 1).

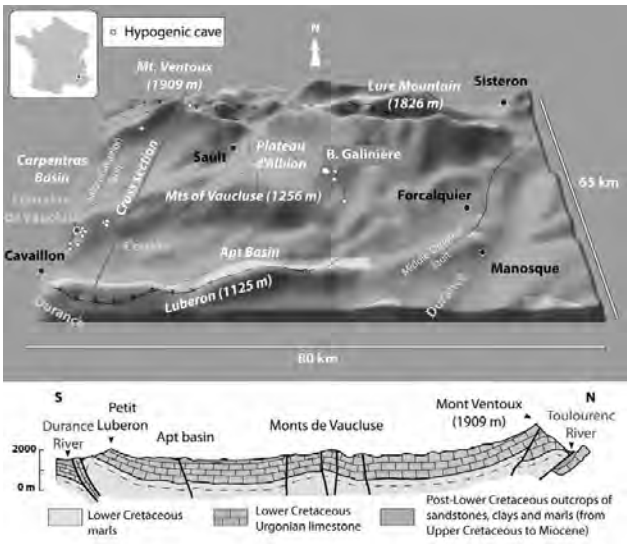

Figure 1. Structural characteristics of the Vaucluse plateau (geology after Blavoux 2010). The block is composed of thick Lower Cretaceous Urgonian Limestone. It is gently undulant and bounded to the north and south by overthrusts resulting from alpine crustal shortening. Hypogenic caves are located on the periphery of the plateau along primary fault lines (Audra et al. 2013).

To the north, the Lure crest rises to 1,826 m. Elevation decreases to the south toward the Durance River at about 300 m above sea level. Topographic relief is caused by an Urgonian (Barremian-Bedoulian) monocline containing. 1,000 m thick limestone that has been carved by karst processes that formed poljes, gorges, dolines, and some avens. To the north, the Lure crest corresponds to a north-verging overthrust. To the south, the limestone monocline gradually plunges under a thick cover of clastic formations ranging from Upper Cretaceous to Oligocene (successively Gargasian marls, Albian sandstone, Cenomanian sand, then Eocene-Oligocene clay, marls and marly limestone; Blanc et al. 1973). The boundary of this cover follows an irregular line caused by erosional retreat that exposed Urgonian limestone and allowed the development of surface karst features. Additionally, the plateau is cut by several N-S faults that form horsts and grabens, such as the Oppedette graben, which is still filled with Cenozoic cover and is surrounded by higher karst surfaces.

Baume Galinière Cave is at the top of the northern slope of a 200 m deep valley, in the uppermost part of the Urgonian limestone. The entrance is a few meters below Albian sandstone cover, close to a local fault. Baume Galinière is a horizontal maze cave less than 200 m long (Fig. 2). Passages are commonly between 0.5 and 2 m high and wide, with two main routes forming a loop around the entrance chamber. Two chimneys rise above the maze, the highest reaching overlying sandstone cap rock. Vadose flow features and sediments are absent, except at one spot corresponding to a small collapse undermining the overlying cover. Typical sulfuric acid corrosion features and mineral byproducts are present (Audra 2007; Audra et al. 2009). Walls are deeply etched or weathered. The floor, which is devoid of sediment, displays smooth surfaces and deeply entrenched rills caused by corrosive laminar or concentrated flow. Numerous niches, pockets, and bell holes result from the intense corrosion. A horizontal notch records the position of a pool once filled with corrosive water. Above, some odd-shaped voids may be replacement pockets. Feeder channels occur as narrow fissures where aggressive water rose from depth, whereas blind chimneys were upper outlets truncated at the contact with the overlying sandstone caprock.

Several minerals are present and have a specific distribution in the cave. A fissure rising along the chimney to the sandstone caprock is filled with iron oxihydroxides and calcite spar. Iron occurs as dikes and crusts, with centimeter-long pool fingers in some places. Calcite spar lining the fissure is mostly scalenohedral.

Pyrite bodies are present, surrounded by gypsum crusts and iron oxihydroxides. The inner and dryer parts of the cave are partly covered by evaporitic sulfate minerals, mostly gypsum, displayed as saccharoid crusts on ceilings and grey to yellow minute crystals on walls. Foam-like masses of a green color, silky appearance and a ribbon-like texture correspond to an uncommon mineral, fibroferrite. Additionally, some iron oxihydroxide stalactites are present. Currently, the cave is entirely dry, due to its perched position at the top of the limestone, to the presence of the sandstone caprock, and to the absence of connections to the

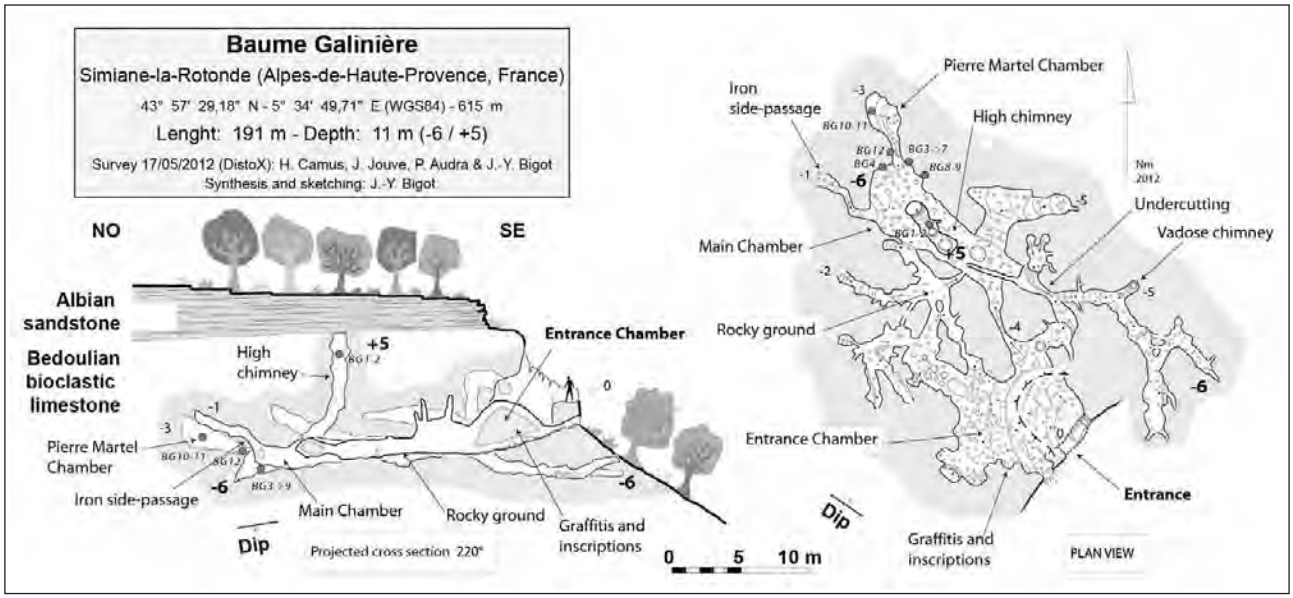

Figure 2. Baume Galinière Cave survey. Red dots indicate sampling locations.

surface. Consequently, the atmosphere is extremely dry and under the influence of thermobarometric exchange with the outer atmosphere. Since the cave is horizontal, we suppose that convection drives the cave climate: cold air entering in winter mainly favors evaporation whereas cooling of warm summer air favors condensation.

3. Methods

In May 2012, the cave survey was completed, documented with pictures, and 13 samples were taken for mineralogical analysis (Fig. 3; the locations of the sampling sites are shown on Fig. 2). Samples are labeled BG1 through BG13.

(i) **Calcite-iron oxihydroxides association**: ferruginous pool fingers hanging under ghosts of calcite scalenohedra (BG1); calcite scalenoedra covered with iron oxihydroxides (BG2); calcite scalenohedra (BG11). (ii) **Sulfidic deposit with oxidized aureole**: mass of pyrite (BG3a) with a white to yellow gypsum crust (BG3b); core of greyish-blue mass (BG5) with an inner yellow-white aureole of gypsum (BG6) and an outer red aureole of iron oxihydroxides (BG7). (iii) **Gypsum crystals associated with colored crusts:** yellow gypsum crystals (BG4); grey gypsum crust (BG10); large grey gypsum crystal (BG12). (iiii) **Foam-like mass** (BG8), located on gypsum crust with yellow surface (BG9).

Mineral identification was carried out using X-ray powder diffraction (XRD) and micro-Raman spectroscopy. The spectra obtained were compared with those reported by Frost et al. (2006) from natural jarosites and our database. Oxygen and hydrogen isotopes were measured on calcite scalenohedra (details in Dublyansky and Spötl 2009). Scanning Electron Microscopy (SEM) was use to observe microbial traces on ferruginous pool fingers.

4. Results

Analytical results of the samples (mineralogy, stable isotopes) are presented in Fig. 3. Thirteen minerals were identified: one native element (sulfur), one carbonate (calcite), one silicate (quartz), one sulfide (pyrite), one hydroxide (goethite), eight sulfates (gypsum, fibroferrite plus six members of the jarosite subgroup (jarosite, argentojarosite, ammoniojarosite, hydronium jarosite, natrojarosite and plumbojarosite). The mineralogical analysis by micro-Raman spectroscopy revealed the presence of up to five different minerals of the jarosite subgroup in the samples (Tab. 1). For space reasons, the Raman spectra are not displayed here and will be discussed in a future paper.

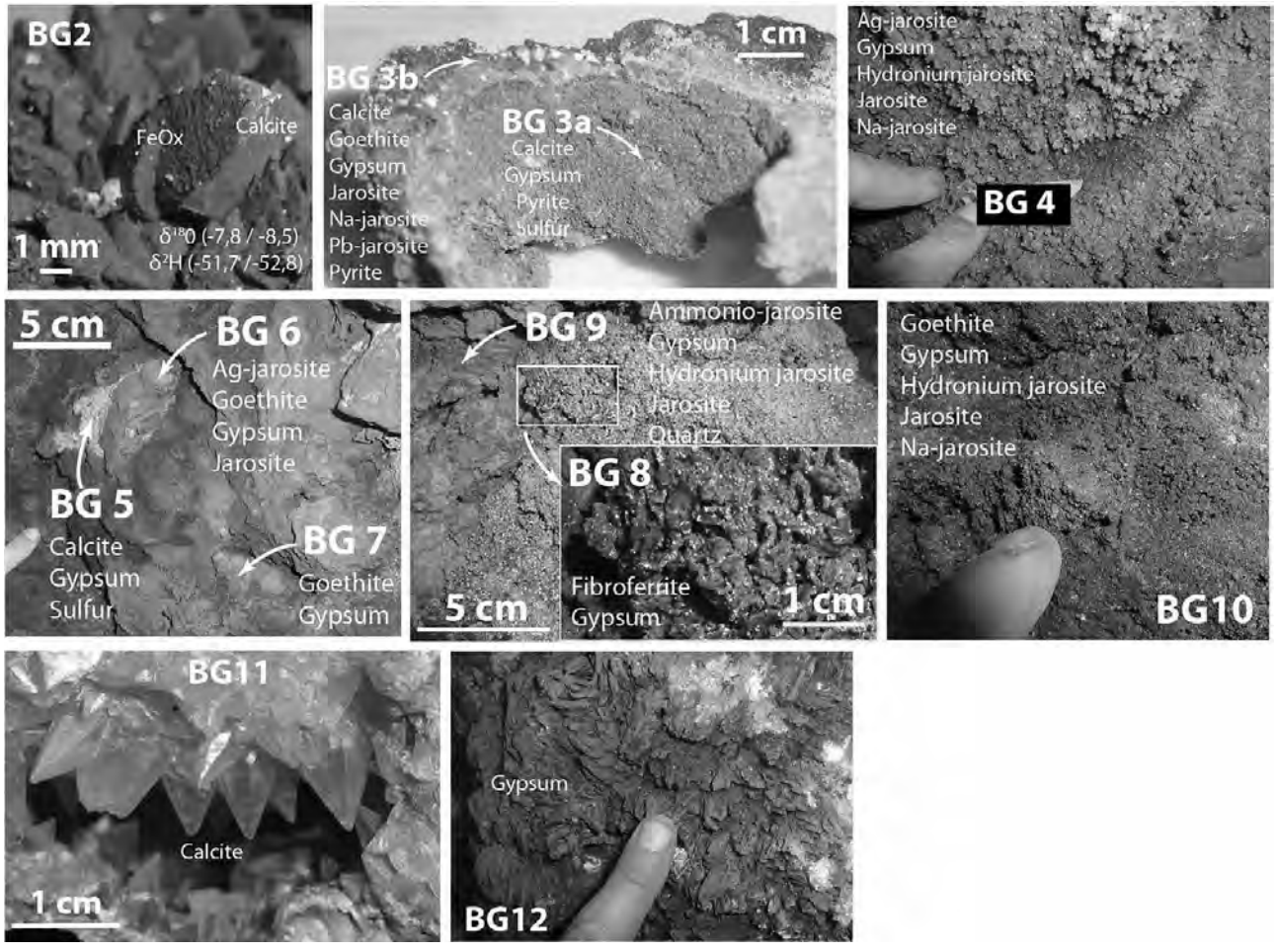

Figure 3. General results of the mineralogical analysis (XRD, micro-Raman spectroscopy), and stable isotopes. Thirteen minerals were identified: One native element (sulfur), one carbonate (calcite), one silicate (quartz), one sulfide (pyrite), one hydroxide (goethite), eight sulfates (gypsum, fibroferrite, and six members of the jarosite subgroup (jarosite, argentojarosite, ammoniojarosite, hydronium jarosite, natrojarosite, plumbojarosite).

Table 1. Results of the mineralogical analysis by micro-Raman spectroscopy. Percentages represent the occurrence of each mineral in each sample regarding the total number of spots analyzed (n).

Sample No.	Number (n) of analyzed spots	Jarosite	Hydronium jarosite	Argento-jarosite	Plumbo-jarosite	Natro-jarosite
BG3b	11	36%	–	–	54%	10%
BG4	10	10%	20%	50%	–	20%
BG6	7	14%	–	86%	–	–
BG9	9	–	100%	–	–	–
BG10	10	40%	20%	–	–	40%

Oxidation of sulfide produces suites of variably soluble efflorescent sulfate salts (Hammarstrom et al. 2005). In Baume Galinière, sulfide is present as **pyrite** [FeS_2], and is the original sulfide deposit. It is displayed in decimetric masses of small pyrite crystals (< 1 mm). It may not be considered as a true cave mineral, since it was deposited by hydrothermal solution in vugs before the cave developed. **Calcite** [$CaCO_3$] is found as detrital grains of limestone host rock inside sulfide deposits or in the weathering aureole. Other minerals result from reactions between the pyrite, the surrounding limestone, and the clays where sulfuric acid from the oxidation of pyrite is responsible for a strong acidic environment.

Native **sulfur** [S°] is present inside the pyrite deposit and probably results from the oxidation of pyrite. **Goethite** [FeO(OH)] is typically displayed as red crusts surrounding oxidized pyrite masses. **Gypsum** [$CaSO_4{\cdot}2H_20$] is displayed in two forms according to its location. On ceilings, the high parts of walls, and around pyrite masses it occurs as saccharoid white crusts. On the lower parts of walls it occurs as macrocrystals which are always tinted yellow, grey or brown.

Jarosite sub-group minerals and **fibroferrite** are present around the pyrite masses in the oxidation aureole. The **Jarosite subgroup** is composed of six sulfate minerals, with the following common composition [$MFe_3(SO_4)_2(OH)_6$], where M = K^+ (jarosite), Ag^+ (argentojarosite), NH_4^+ (ammoniojarosite), Na^+ (natrojarosite), Pb (plumbojarosite), H_3O (hydronium jarosite). Such minerals are commonly found in mines in the oxidized zones of sulfide deposits, formed by sulfuric acid derived from the oxidation of pyrite reacting with clay from the wall rock. **Jarosite** [$KFe^{3+}{}_3(SO_4)_2(OH)_6$] is named after the type locality, Barranco Jaroso in Southern Spain. It is usually displayed as yellow, amber, or brown crusts. It is not soluble in water, and rather common in sulfuric caves (Fiume – Vento, Italy; Cottonwood, New Mexico, USA). It also occurs in volcanic caves, or in caves in metamorphic rocks where sulfidic ores are present (Hill and Forti 1997). Jarosite may also precipitate subaqueously in shallow, low-pH pools (Hammarstrom et al. 2005). **Ammoniojarosite** [$(NH_4)Fe^{3+}{}_3(SO_4)_2(OH)_6$] is named from the ammonium ion (NH_4^+) and displays as light yellow to nearly colorless crusts. It has been mentioned only once before, in Cueva Alfredo Jahn, Venezuela, where it brought into the cave by flooding, and the mineral, displayed as light blue spots, forms by evaporation during the dry season (Forti et al. 1998). **Argentojarosite** [$AgFe^{3+}{}_3(SO_4)_2(OH)_6$] is named from silver (Ag) and displays as pale yellow, yellow, yellow-brown to brown crusts. It is mentioned here for the first time as a cave mineral. **Hydronium jarosite** [$(H_30)Fe^{3+}{}_3(SO_4)_2(OH)_6$] is named from the hydronium ion (H_30^+) and displays as ochrous, amber to dark brown granular masses or crystalline to earthy crusts. It has been mentioned as a cave mineral only once, in Iza Cave, Romania, where *"goethite and hydronium jarosite formed through the action of percolating water over pyrite that is present as accessory mineral in the crystalline schists"* (Tămaş and Ghergari 2003). **Natrojarosite** [$NaFe^{3+}{}_3(SO_4)_2(OH)_6$] is named from sodium (natrium) and displays as yellow, golden brown, red-brown crusts. It has been mentioned as a cave mineral only once, in Jungle Pot Cave, South Africa, originating from the oxidation of pyrite from shales combined with Na from a diabase sill (Martini 1984). **Plumbojarosite** [$Pb_{0.5}Fe^{3+}{}_3(SO_4)_2(OH)_6$] is named from lead (Pb) and displays as golden brown to dark brown crusts or masses. It has been mentioned only from Naica Cave, Mexico, originating from neoformation after the dewatering of the famous geode (Forti 2010). **Fibroferrite** [$Fe^{3+}SO_4(OH){\cdot}5H_2O$] is a hydrated iron sulfate. It displays as fibrous mushroom-like masses of minute acicular crystals. Coalescent needles form ribbons folded by extrusion. The color ranges from pale yellow, yellowish green, greenish gray, nearly white, to translucent, with a typical silky luster. It is soluble in water and forms by evaporation. Consequently it is most stable in arid regions, rarely as volcanic sublimate (Anthony et al. 2003). It has been mentioned only from Grotta Ferrata, Italy, originating from pyrite oxidation and growing over mud associated with goethite and gypsum. Its stability requires strong acid environment (pH < 2). When pH increases due to the buffering effect of limestone reacting with sulfuric acid, fibroferrite becomes unstable and forms iron oxihydroxides (Forti and Salvatori 1988).

Stable isotopes of fluid inclusions ($\delta^{18}O$, δ^2H) were made on tips and bottoms of calcite scalenohedra (BG2). The released water amount (0.39 and 0.54 µL, respectively) provided valuable results. The ratios of $\delta^{18}O$ and δ^2H for tips and bottoms (-7.8/-51.7 and -8.5/-52.8) plot close to the meteoric water line (MWL) (Craig 1961).

SEM imaging of iron pool fingers clearly shows the presence of microbial communities, mainly as filaments growing onto the iron oxihydroxides (Fig. 4). The largest filaments (diam. 5µm, length > 100 µm) must be fungi. Smaller filaments (diam. 2 µm, length 50 µm) and cell-like individuals could be bacteria (H. Barton pers. comm.).

5. Discussion (mineralogenesis and sulfuric acid speleogenesis)

The identification of minerals in the framework of geological and geomorphological context helps understand the genesis of this mineralized cave. Mineralization took place in at least three main phases (Fig. 5).

Early phreatic fissure phase. The initial mineralization phase occurred at depth, below the water table and under the cover of thick marls and sandstones. Chemically reduced water rising from depth along faults carried metallic ions (Fe^{2+}, Pb^{2+}, Ag^+) and sulfur. At shallow depths,

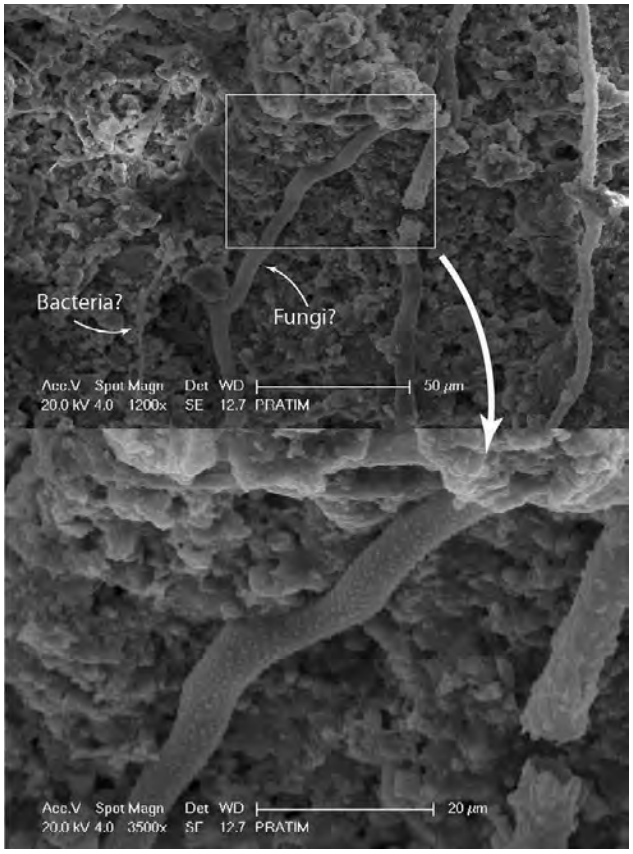

Figure 4. BSE imaging of iron pool fingers. Microbial filaments are developing on iron oxyhydroxides. Largest filaments (diam. 5 µm, length > 100 µm) must be fungi. Smaller filaments (diam. 2 µm, length 50 µm) could be bacteria.

mixing of reduced water with oxygenated meteoric water, probably carried along the sandstone acting as aquifer, changed pH and Eh conditions and led to the deposition of sulfide minerals, mainly pyrite [FeS_2] with traces of Pb and Ag, as masses or sills along fractures. The contact between reduced flow and fresh water from the sandstone aquifer could explain the sulfidic deposits localization where mineralization is concentrated at the top of the limestone just below the sandstone cover. Eventually, calcite with scalenohedral habit was precipitated. This type of calcite is generally associated with a warmer environment than common trigonal rhombohedral calcite spar (Dublyansky and Smirnov 2005). Isotopic ratios ($\delta^{18}O$, $\delta^{2}H$) close to MWL indicate a contribution from surface water. At that time, no cave was present and the corresponding voids were limited to tiny fissures and vugs.

Main vadose phase. Valley entrenchment combined with erosional retreat of the overlying caprock dramatically changed conditions. The water table fell below the sulfidic deposits resulting in vadose conditions and associated oxygenated meteoric seepage. Thinning of the caprock allowed development of soils and vegetation just above the cave. Oxidation of the pyrite masses produced sulfuric acid that dissolved the limestone host rock, resulting in sulfuric acid speleogenetic processes. The earliest sulfuric acid speleogenesis may have occurred in a shallow phreatic environment at the onset of the fall of the water table, when meteoric water was able to flow and be replenished. However, the most active processes occurred in atmospheric conditions after the cave was drained, when seepage water oxidized pyrite masses and produced concentrated sulfuric acid. Most of the cave volume probably developed during this phase, associated with typical sulfuric acid features such as notches along acidic pools, corrosion trenches, *etc*., and sulfate mineral byproducts. Saccharoid gypsum crusts formed on some ceiling and upper wall surfaces where condensation was limited. Otherwise, ceilings and upper walls were etched by condensation corrosion and sulfates in solution were precipitated downwards through evaporation as centimetric gypsum crystals. This sulfuric process produced a low pH environment, and secondary ions combined with iron sulfates to form jarosite subgroup minerals. Hydronium jarosite is produced by seepage on pyrite. Trace amounts of Pb and Ag produced argento- and plumbojarosite, respectively. Weathering of the Albian green sandstone caprock, which contains glauconite group minerals [$(Ka,Na)(Fe^{3+},Al,Mg)_2(Si,Al)_4O_{10}(OH)_2$], may have provided K^+ and Na^+ ions, which in turn produced jarosite and natrojarosite, respectively. Biological activity produced the ammonium ion (NH_4^+), which combined to form ammoniojarosite. Meantime, oxidation of pyrite is boosted by ferro-oxidant bacteria taking energy from oxidation of ferrous ion Fe^{2+} to ferric ion Fe^{3+}, resulting in iron oxihydroxides, mainly goethite. Ferruginous material occurs as massive coatings on calcite spars, as pool fingers, or as powdery masses mixed with gypsum surrounding pyrite masses (Fig. 3).

Still-active seasonal sulfuric mineralogenesis. Currently, the cave is open to the surface allowing convective air exchange. In summer, cooling of air entering the cave favors condensation and thus slow pyrite oxidation and the formation of the associated suite of sulfuric byproducts (gypsum, sulfates ion and iron oxihydroxides). In winter, warming of entering air causes evaporation that concentrates acidic solutions around pyrites and favors evaporitic sulfate development, namely fibroferrite.

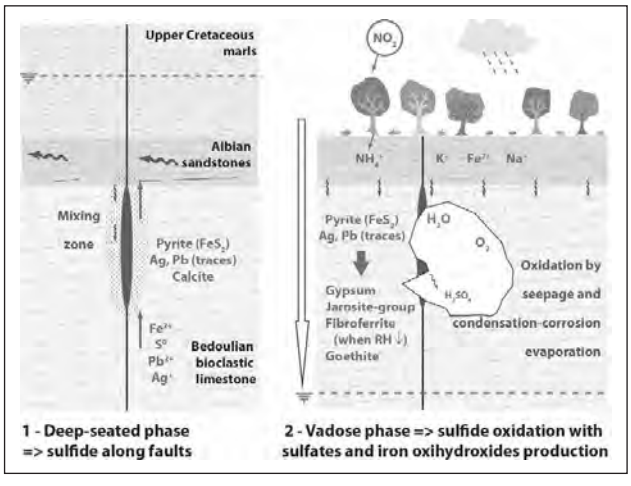

Figure 5. Genesis of minerals in Baume Galinière. First phase in deep-seated conditions, where mixing of hypogenic flow and fresh water produces sulfide deposits (pyrite) along fault below the sandstone aquifer. After a base level drop, vadose seepage oxidizes the sulfide deposits, making sulfuric speleogenesis, with cave development and secondary minerals (sulfates and iron oxihydroxides). Jarosite subgroup minerals appear thanks to the presence of accessories ions originating from traces in the sulfide deposits (Pb, Ag), from sandstone minerals weathering (glauconite), or from biogenic production (ammonium ion). Seasonal changes between condensation and evaporation allow developing of fibroferrite.

Although we did not observe it during our visits, we suspect that fibroferrite follows seasonal cycles of relative humidity (RH), dissolving when wet and regrowing when dry. Evaporation in the vicinity of oxidizing pyrite may be responsible for the deposition of native sulfur, which requires high H_2S concentration in the surrounding atmosphere.

The progression of speleogenesis can be traced at the regional scale. Comprehensive data are still missing, but main phases can be traced and assigned to periods when physical conditions were permissive (Fig. 6). Phase 1 of hypogenic rising flow requires a hydraulic gradient and the presence of impervious caprock. Such conditions could have occurred after the first phases of orogenic uplift at the beginning of Miocene. During Phase 2, which corresponds to the main sulfuric acid speleogenetic event, vadose conditions gradually phased in. This occurred after the erosional retreat of the marly caprock and the onset of valley incision. Erosion and caprock retreat caused the water table to fall to depths below the cave. During Phase 3, the cave is open to the surface allowing air exchange in response to seasonal changes in RH. Phase 3 is currently active.

6. Conclusions

Baume Galinière sulfate mineralization resulted from sulfuric acid speleogenesis in successive phases. The first phase of sulfide deposition (pyrite masses) occurred in deep-seated conditions, where hypogene water rising along a fault mixed with meteoric water flowing within an overlying sandstone aquifer. At that time, probably at the beginning of Miocene, the onset of orogenic uplift allowed water to move in a deep loop through the karst aquifer. Impervious caprock cover was present, keeping the karst aquifer in anoxic conditions. Locally there were local, discrete zones where anoxic hypogene water could mix with meteoric water at the contact between the karst aquifer and the overlying sandstone aquifer. Hypogenic flow was probably warm, as shown by the scalenohedral habit of calcite crystals.

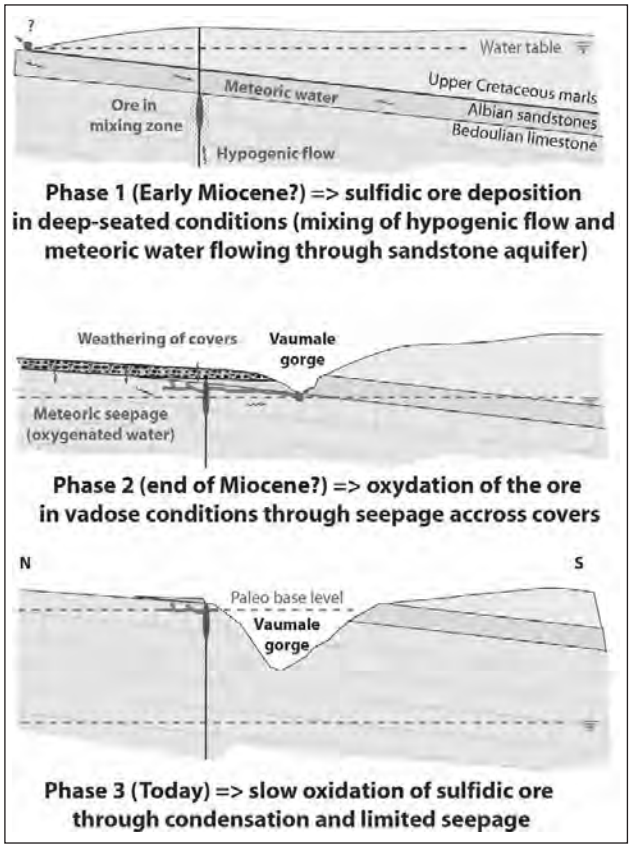

Figure 6. Evolution of Baume Galinière from Miocene. Successive phases, from deep-seated to vadose conditions are related to the retreat and stripping of covering strata related to valley incision.

The second phase of sulfuric speleogenesis corresponds to vadose conditions that were coeval with valley incision. The water table was shallow, and meteoric seepage water reacted with pyrite. Sulfur oxidation released sulfuric acid, which reacted with the carbonate host rock. Typical sulfuric corrosion features developed, with enlargement of voids, including pockets, bell holes, pool notches and entrenchments. Sulfate minerals, mainly gypsum, covered walls as saccharoid crust on ceilings and recrystallized macro-crystals on the lower passage walls. Oxidation of pyrite also produced iron oxihydroxide crusts, masses, and pool fingers on walls around pyrite masses. The oxihydroxides mixed with and tinted the sulfates. Microbial and fungal activity (fungi and probably ferro-oxidant bacteria) developed and is preserved as filaments in the pool fingers. Beside gypsum, rare sulfates crystallized, including all members of the jarosite subgroup. Precipitation of jarosite is mainly due to the weathering of glauconite in the overlying sandstone, which delivered ions by seepage.

The present phase corresponds to the deep entrenchment of the valley and the opening of the cave allowing air exchange corresponding to seasonal changes of RH. Cooling results in condensation that maintains pyrite oxidation and sulfate production. Warming causes evaporation and development of fibroferrite. The development of this cave records the gradual incision of valley and correspondent retreat of impervious caprock, an important milestone for the reconstruction of paleolandscapes. As with similar caves (Audra et al. 2013), Baume Galinière is located at the topographic intersection of a regional fault and the edge of the caprock covering the karst aquifer. The chronology of speleogenesis probably starts at Early Miocene and continues to the present. Dating of successive speleogenetic stages could provide a better understanding of the geomorphological evolution of the Vaucluse region.

Acknowledgments

I thank Y. Dublyansky (Univ. of Innsbruck) for helping with the stable isotopes, D. Borschneck and R. Notonier (Aix Marseille University) for XRD and SEM, respectively. H. Barton (Univ. of Akron) made useful comments on SEM images of microbial filaments. B.P. Onac and P. Forti are thanked for discussions during the identification of minerals. We are also grateful to two anonymous reviewers who greatly improved the text and A. Sanz, the technician who performed the Raman analyses. Financial support was made available through Project “RLS Exomars Science” (AYA2011-30291-C02-02; Ministry of Science and Innovation, Spain and FEDER funds of EU).

References

Anthony JW, Bideaux RA, Bladh KW, Nichols MC, (Eds.) 2003. Handbook of Mineralogy, 1, 588p. Mineralogical Society of America, Chantilly. http://www.handbookofmineralogy.org/

Audra P, 2007. Karst et spéléogenèse épigènes, hypogènes, recherches appliquées et valorisation. Habilitation Thesis, Univ. of Nice Sophia-Antipolis, France.

Audra P, Mocochain L, Bigot JY, Nobécourt JC, 2009. Morphological indicators of hypogenic speleogenesis. In: Klimchouk A and Ford D (Eds.). Hypogene Speleogenesis and Karst Hydrogeology of Artesian Basins, Special Paper, 1. Ukrainian Institute of Speleology and Karstology, Kiev, 23–32.

Audra P, Bigot JY, Camus H, Gauchon C, Wienin M, 2013. La grotte-mine du Piei (Lagnes, Vaucluse), paléokarst hypogène à remplissage de minerai de fer oxydé (The Piei mine-cave (Lagnes, Vaucluse, France), a hypogene iron-ore paleokarst). Karstologia (accepted).

Blanc JJ, Weydert P, Masse JP, Roux M, Peyronnet P de, Rouire J. 1973. Carte géologique de la France à 1/50,000 “Sault-de-Vaucluse”. BRGM, Orléans.

Craig H, 1961. Isotopic variations in meteoric waters source. Science, 133(3,465), 1702–1703.

Dublyansky YV, Spötl C, 2009. Hydrogen and oxygen isotopes of water from inclusions in minerals: design of a new crushing system and on-line continuous-flow isotope ratio mass spectrometric analysis. Rapid Commun. Mass Spectrom, 23, 2605–2613.

Dublyansky YV, Smirnov S, 2005. Cavity-based secondary mineralization in volcanic tuffs of Yucca Mountain, Nevada: a new type of the polymineral vadose speleothem, or a hydrothermal deposit? International Journal of Speleology, 34(1–2), 25–44.

Egemeier SJ, 1981. Cavern development by thermal waters. NSS Bulletin, 43(2), 31–51.

Forti P, 2010. Genesis and evolution of the caves in the Naica Mine (Chihuahua, Mexico). Zeitschrift für Geomorphologie, 54(2), 115–135.

Forti P, Salvatori S, 1988. Nuovi minerali di grotta: la fibroferrite di Grotta Ferrata. Riv. Mineral. Italiana, 4, 219–226.

Forti P., Urbani F, Rossi A, 1998. Minerales secundarios de las cuevas del Indio y Alfredo Jahn, estado Miranda, Venezuela. Boletín de la Sociedad Venezolana de Espeleología, 32.

Frost RL, Will RA, Weir ML, Martens W, Mills S, 2006. A Rama spectroscopy study of selected natural jarosites. Spectrochimica Acta, Part A., 63, 1–8.

Hammarstrom JM, Seal II RR, Meier AL, Kornfeld JM, 2005. Secondary sulfate minerals associated with acid drainage in the eastern US: recycling of metals and acidity in surficial environments. Chemical Geology, 215, 407–431.

Hill C, Forti P, 1997. Cave mineral of the world. National Speleological Society, Huntsville.

Martini J, 1984. Jungle Pot. South Africa speleol. Assoc. Bull, 22, 5.

Melim LA, Shinglman KM, Boston PJ, Northup DE, Spilde MN, Queen JM 2001. Evidence for Microbial Involvement in Pool Finger Precipitation, Hidden Cave, New Mexico. Geomicrobiology Journal, 18(3), 311–329.

Tămaş T, Ghergari L, 2003. Hydronium jarosite from Iza Cave (Rodnei Mts., Romania). Acta Mineralogica-Petrographica, Abstract Series, 1, 102.

RARE SULFATES (MIRABILITE, EUGSTERITE) IN THE DRY MICROCLIMATE OF CHAMOIS CAVE (ALPES-DE-HAUTE-PROVENCE, FRANCE)

Philippe Audra[1], Jean-Claude Nobécourt[2]
[1]Polytech Nice – Sophia, University of Nice – Sophia Antipolis, 930 route des Colles, 06903 Sophia-Antipolis, France & Innovative City – IMREDD, Nice, France, audra@unice.fr
[2]CRESPE, Le Hameau de l'Ara, 259 boulevard Reine Jeanne, 06140 VENCE, France, jcnobecourt@smb.mc

The Chamois Cave (Alpes-de-Haute-Provence, France) opens at 1,360 m asl. above the Coulomp spring, which is fed by the Grand Coyer massif (2,693 m). The cave develops 10 km and gives access to the Underground Coulomp, one of the largest underground rivers in France. As any mountain cave, the air is cold, between 4 °C (highest part receiving air breathed in at 2,000 m altitude) and 8.5 °C (lowest confined part) where the river temperature is 6 °C. In this low part of the cave, a tributary (Thenardier Gallery) displays a fossil level covered with various decorations. On the ceiling, calcite helictites [$CaCO_3$] are surrounded with hydromagnesite [$Mg_5(CO_3)_4(OH)_2 \cdot 4H_2O$]. The lower part of the walls and the fine sediment on the ground are covered with sulfates: gypsum [$CaSO_4 \cdot 2H_2O$], mirabilite [$Na_2SO_4 \cdot 10H_2O$], and eugsterite [$Na_4Ca(SO_4)_3 \cdot 2H_2O$]. The two last minerals are common in salars depressions, lava tube and in cave developing under semi-arid condition, and not so frequent in temperate caves. Their presence in Chamois Cave is explained by the microclimate (RH 88 %, T = 8.5 °C). The lowest part of the cave is under dry conditions because of the air subsidence that causes warming without moisture renewal since percolation are rare. Moreover, the Thenardier Gallery is confined between a sump upstream and a temporary sump downstream. Such a low RH allows developing of these minerals under evaporation effect. S comes from the weathering of pyrites that are present in limestone and Na from the weathering of sandstones in sediments. These evaporative conditions makes the Chamois cave an exceptional one, since mirabilite is not frequent in temperate caves and eugsterite is mentioned only for the second time in cave.

1. Introduction

Caves are well known for their decorations, where calcite is the dominant mineral precipitated by CO_2 degassing. Some minerals, such as sulfates, are due to evaporation process. Gypsum is a common species; however some sulfate minerals are more rarely encountered, especially in temperate and wet caves. Several mineralogical species in caves are partly or entirely due to evaporation processes. If calcite [$CaCO_3$] generally precipitates through CO_2 degassing, precipitation can be boosted by evaporation allowing supersaturation. When evaporation continues, the Ca/Mg ratio lowers, allowing the successive deposition of aragonite, huntite [$CaMg_3(CO_3)_4$], then hydromagnesite [$Mg_5(CO_3)_4(OH)_2 \cdot 4H_2O$]. Such gradation is typical in confined or ventilated parts of caves where strong evaporation occurs, making calcite stalactites covered with aragonite frostwork generally developing on wind side, and hydromagnesite cotton ball growing at the tip of aragonite needles where the solution reaches the highest saturation. Sulfates are frequent and highly soluble minerals, which consequently can develop only in dry conditions. Gypsum [$CaSO_4 \cdot 2H_2O$] is the most frequent. In especially dry conditions, magnesium sulfates such as epsomite [$MgSO_4 \cdot 7H_2O$] or sodium sulfates, such as mirabilite [$Na_2SO_4 \cdot 10H_2O$] and thenardite [Na_2SO_4] can develop with decreasing level of hydration. Eugsterite [$Na_4Ca(SO_4)_3 \cdot 2H_2O$] was only once identified in a cave, in Turner Avenue, Mammoth Cave (Benington 1959; visible in White 2005, photo. 2B, p. 290), but the name was later given from another locality. It occurs as acicular crystals inside a water-clear mirabilite stalactite (White oral comm.).

The evaporation gradient pumps out the solutions present inside the rock toward the cave wall. Sulfates crystals grow by extrusion (Hill and Forti 1997). In cold caves, percolations can only be saturated with respect to calcite and aragonite. Consequently, other mineral forms depend on processes other than degassing, i.e. concentration of the solution by evaporation (Harmon et al. 1983).

The stability of extremely soluble sulfates is closely dependent on cave climate conditions. Consequently, they grow seasonally when cave air is dry and re-dissolve when moisture increases. Epsomite melts under the breath or the heat of carbide lamp (Hill and Forti 1997). Below 70 % of relative humidity (RH), mirabilite spontaneously dehydrates to thenardite (Onac 2012), which in turn is stable at 5–40 % RH. Phase diagram (T – RH) of sodium sulfates are available from Flatt (2002), and discussed by Rodriguez-Navarro et al. (2000) for non-equilibrium conditions.

Cave sulfate minerals can have several origins (White 2005): interstratal evaporites in limestone rock (gypsum, anhydrite), oxidation of pyrite present in the limestone or in the caprock (e.g., sandstone at Mammoth Cave, Kentucky), oxidation of hypogenic H_2S corroding and replacing the limestone (Lechuguilla Cave, New-Mexico; Polyak and Provencio 2001), or brines such as in the Naica mine geodes (Mexico; Forti 2010). The geochemistry of the solution shall contain the elements necessary for Na-Ca-sulfate salt precipitation, i.e. Na, sulfate ion, etc. Studies on soil and salt pans evidenced the need of Na/Ca ratio > 4, pH > 5, and rapidly changing local environments and variations in redox, pH, and rates of availability of S and other elements (Fitzpatrick et al. 2005). In caves, percolation through limestone containing pyrites and strong evaporation could mimic such conditions.

Gypsum forms bulk crystals (on soil, dentate gypsum, gypsum

needles), crusts (granular or fibrous), and fibers (gypsum flowers, angel hairs, cotton) (White 2005). The highly soluble sulfates have habitus similar to gypsum, but different crystal structures; epsomite and mirabilite form crusts and in the driest conditions flowers may be present (White 2005). On the field, highly soluble minerals can be easily distinguished from gypsum, since they display ice-clear crystals and salty taste. However, their visual identification is difficult, even if epsomite has a bitter taste only, whereas mirabilite taste is bitter and salty (Hill and Forti 1997).

The highly soluble sulfates are generally found in extremely dry environments, such as salar depressions. In cave, they are mostly encountered in young volcanic caves still influenced by fumaroles and residual heat, and in warm and dry limestone caves (Guadalupe Mountains caves in New-Mexico, Cup-Coutunn Cave in Turkmenistan, Bahamas islands) (Hill and Forti 1997). However, they are also found in limestone and gypsum caves in which the temperature is below 20 °C. The first occurrence of thenardite, growing together with mirabilite, was in an Italian cave with temperature below 15 °C (Bertolani 1958). Thenardite (or mirabilite?) is present in "alpine" caves such Picos de Europa (Spain) (Hill and Forti 1997), and mirabilite occurs in a similar environment in Gamslöcher-Kolowrathöhle**,** Salzburg Alps (Bieniok et al. 2011). In even colder caves, they are present in Norway (Onac and Lauritzen unpubl.) and in the Canadian Rockies: in Castleguard Cave, during winter, outside air entering the cave abruptly warms to about 25 °C, at the origin of an 83% RH. The seasonal reversing of the draught considerably changes the moisture conditions of both extremities of the cave, so that dry conditions are only permanent in the central part of the cave where sulfates are present, such as mirabilite and epsomite (Harmon et al. 1983). The wide range of temperatures, from volcanic to arctic settings, shows that RH is the key-factor. Sulfated solution submitted to strong evaporation alone can form highly soluble sulfate minerals.

In this paper, we present the Chamois cave in Southern French Alps, where sulfate minerals have been identified by X-rays, including gypsum, mirabilite, and eugsterite, together with hydromagnesite associated to calcite. We discuss the conditions of their occurrence, originating from the composition of the host rock and of the allogenic sediments, from the low rate of percolation, and mainly from the microclimatic conditions with low RH allowing strong evaporation.

2. Cave and context

The Chamois Cave (Castellet-lès-Sausses, Alpes de Haute-Provence, France) opens at 1,360 m asl. in Grand Coyer, between the upper segments of the Var and Verdon valleys (Audra et al. 2009). The Chamois cave develops more than 10 km for a depth of 326 m (+284/-42) (Fig. 1). It gives access to a 1 km segment of the Underground Coulomp, the largest underground river in France (1 m^3/s). This underground river gives origin to the Coulomp spring, the largest in the Southern Alps, which pours out below the cave in a scenery waterfall. A sequence of thick marly limestone from Upper Cretaceous (Turonian-Coniacian-Santonian) begins with thick bedded limestones, where the cave develops, at the top of black marls. This sequence is covered in unconformity by the Cenozoic "nummulitic trilogy" (nummulitic limestone, Priabonian blue marls, and Annot sandstones). Decorations are abundant especially in the dry fossil passages: flowstones, aragonite bushes on wall exposed to the draft, gypsum crosses and needles on black marls.

3. Sampling and methodology

The Thénardier Gallery is the lower segment of the Hormones gallery, from which it is isolated by a sump. Access is from Underground Coulomp, through a temporary sump that only opens after a long dry period. As a consequence, this gallery is confined most of the year. A dry and well-decorated level develops 15 m above the temporary course of the active level. Spots of calcite helictites ringed by hydromagnesite develop on bare walls (Fig. 2). Gypsum of different fabrics (Fig. 3) and other sulfate minerals (Fig. 2) cover some parts of the walls and of the soil, which is covered with fluvial sediments made of pebbles, gravels and fine dusty sands. The sulfate minerals other than gypsum are distinguished by ice-clear crystals and a salty taste. All crystals have been sampled in hermetic bottles (numbered from 0 to 9), in order to keep them in dry condition. To preserve this exceptional site we only sampled broken small fragments from each given mineral.

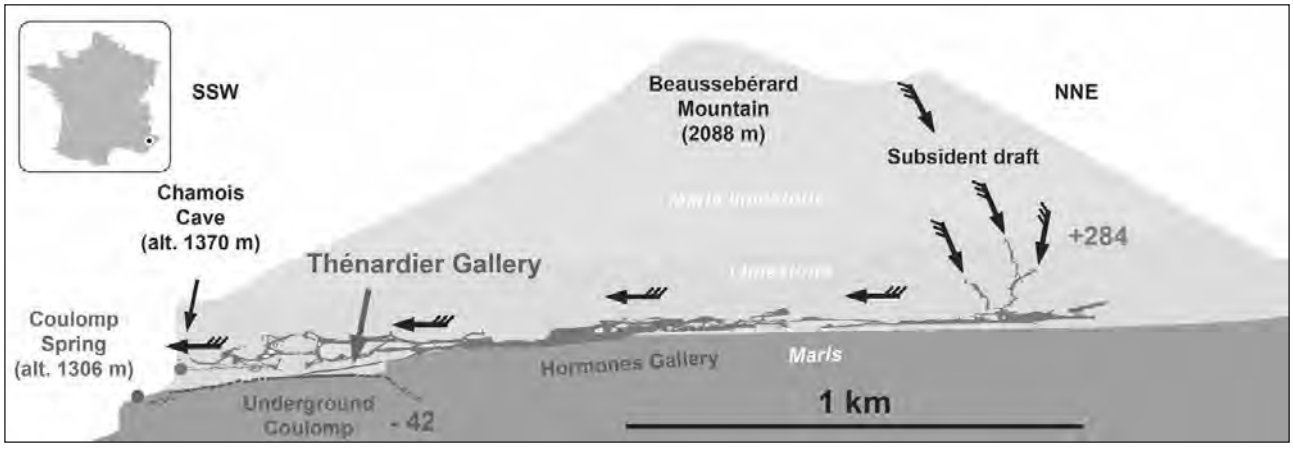

Figure 1. Cross section of the Chamois Cave, showing its development below a narrow ridge, at the contact of a marly basement and in a limestone covered with a thick sequence or marly limestones. Strong draft entering at high altitude crosses the cave system towards the cave entrance. The Thénardier gallery is a tributary of the river, the Underground Coulomp, which is most of the time confined between sumps.

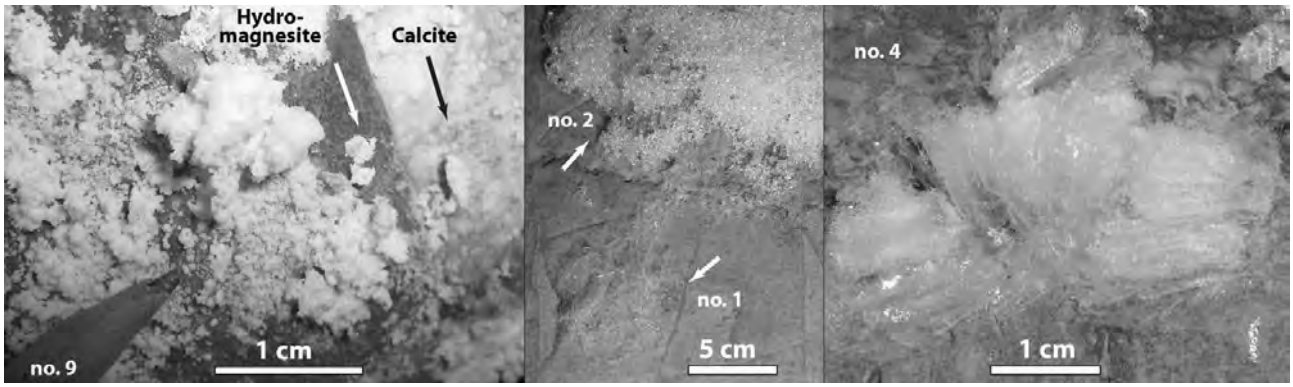

Figure 2. Left picture: calcite spot occurring as wall coating originating from small percolation along a fissure, ringed by hydromagnesite cotton-like bundles [sample no. 9]. Central and right pictures: diverse mirabilite crystal fabrics. Candy floss-like filaments [sample no. 1]; melting snow-like isometric crystals [sample no. 2]; ice clear blades forming a flower [sample no. 4].

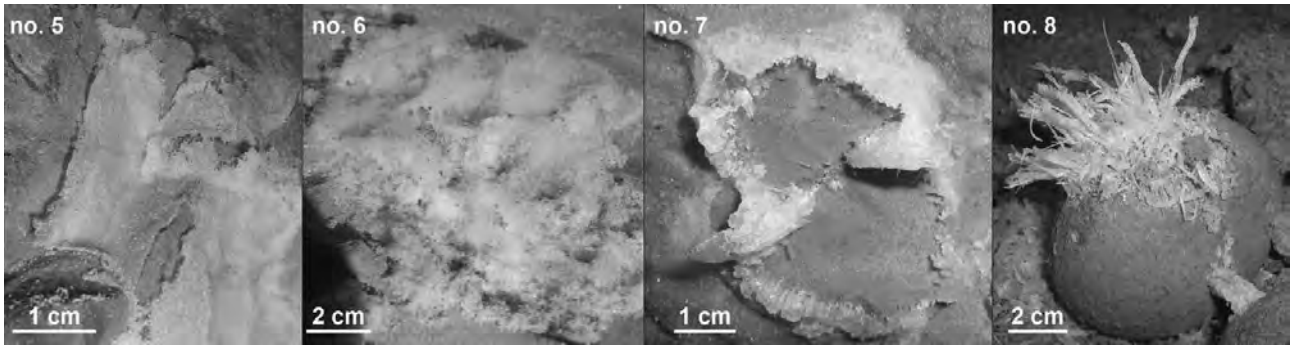

Figure 3. Diverse fabrics of gypsum crystals: wall crust [sample no. 5]; saltpeter-like fibers growing on dry silts [sample no. 6]; gypsum flower ringed by transparent crust [sample no. 7]; gypsum crosses on sandstone pebble [sample no. 8].

X-ray powder diffraction (XRD) patterns were recorded on a Philips diffractometer using Cobalt radiation ($\lambda = 1.79$ Å) with a secondary graphite monochromator. The diffractometer optic used to record all samples was a front fixed slit of 1°, a scattered radiation slit of 1° after the sample, and a 0.2 mm detector slit. The X-ray tube operating conditions were 40 kV and 40 mA and the step-scan data were continuously collected over the range 3.5 to 78° 2θ using a step interval of 0.05° 2θ and a counting time of 2.5 s. Patterns were matched with reference bibliotheca to identify minerals. Since Na-sulfates are highly instable at normal Temperature (T) and relative humidity (RH) conditions (involving hydration or dehydration resulting in mineral change), we assessed a possible influence of the RH change during X-ray analysis. Some grains of sample no. 2 were exposed to an atmosphere close to vapor saturation during several days, being put in a small beaker, which was placed in a water-filled crystallizer, itself covered with a second beaker. X-ray analysis was immediately done while putting grains directly on the silicon mount. Then a second analysis was done after 50 min. of exposition to drier laboratory atmosphere (45–55 % RH).

While sampling on the field site, T and RH were measured with a Brannan Compact Sling Psychrometer, where temperature is read on a dry bulb thermometer and % RH is later calculated from dry and wet bulb T using a table. Reading precision of T values is expected to be ±0.5 °C and calculated RH about ±5 %. Additionally, a TFA-Dostmann 30.3015 thermo-hygrometer with data logger was settled to record T and RH for the coming year. Precision is 1 °C for T and ±3 % for RH from 35 to 75 % RH, otherwise ±5 %.

4. Results

X-ray analysis showed the presence of quartz and calcite in several sample, together with hydromagnesite, gypsum, thenardite, and eugsterite. Table 1 and Fig. 4 resumes the presence of the minerals found in each sample. The hydration-dehydration experiment on sample no. 2 shows mirabilite after exposure to wet atmosphere then thenardite after 50 min. in the drier atmosphere of the laboratory.

Microclimatic values in Thénardier Gallery at the sampling moment were 8.5 °C and 88 % RH.

Table 1. The minerals identified with X-rays.
(*): see below for discussion about dehydration.

Minerals	Sample No.									
	0	1	2	3	4	5	6	7	8	9
Quartz	x	x	x	x			x	x		
Calcite	x	x	x	x			x			
Hydromagnesite										x
Gypsum		x	x	x		x	x	x	x	
Thenardite	x	x	x(*)	x	x					
Mirabilite			x(*)							
Eugsterite	x									

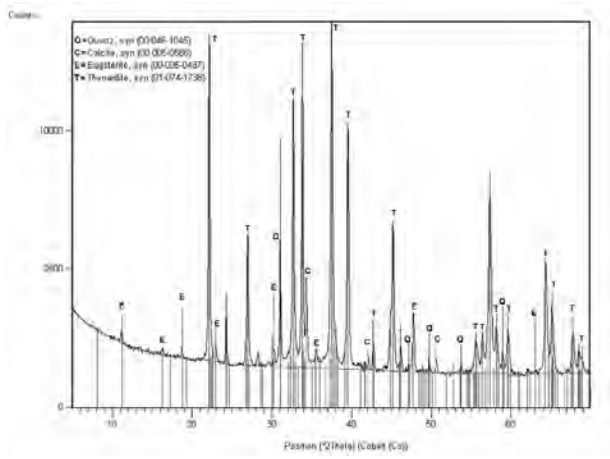

Figure 4. Pattern example for the no. 0 sample.

5. Discussion

Slow percolation from wall fissures makes calcite spots that are ringed by distinct aureoles of powder aggregates, which is composed of pure hydromagnesite (Fig. 2). The evaporation of the slow percolation makes the calcite to precipitate first. As evaporation proceeds, the decrease of Ca/Mg ratio progressively brings the residual fluid into the field of hydromagnesite (Harmon et al. 1983). The calcite spot close to the percolation feeder is relatively wet. Centrifuge capillarity strength brings the increasingly saturated solution toward the dry walls where hydromagnesite deposits as a distinct aureole. In Castleguard Cave, Harmon et al. (1983, Fig. 5, p. 506) evidenced that between both end-products (calcite and hydromagnesite), the calcite core also contains transitional mineral species (aragonite, huntite) originating from progressive evaporation and concentration of the solution.

Solutions of carbonates, sulfates, and sodium sulfates account to several origins. Hydromagnesite is mainly present on the walls, i.e. originating from vertical percolations across the limestone vadose zone. Mg is likely to come from slow dissolution of the above Turonian-Coniacian limestone. Sulfates are likely coming from the oxidation of pyrites, present in both Turonian-Coniacian limestone and in Turonian marly basement. The Thenardier gallery develops in massive limestone, but the marly basement crops out less than 200 m upstream. Consequently, sulfates may come both from pyrite in surrounding limestone or from the weathering of fluvial sediments containing marly pebbles that veneer the soil of the gallery. Sulfur isotopes data may precise this relationship with pyrites. For both mirabilite and eugsterite, the Na source is likely to be the fluvial sediments that contain sand and pebbles from Annot sandstones, in which sodium plagioclases (albite) and secondarily perthites are present (Stanley 1961). The weathering of these endogenous minerals would provide the Na present in eugsterite and mirabilite.

The identification of thenardite as cave mineral is a confusing question, since this mineral is unstable outside of the cave atmosphere, which makes it instantaneously evolve to mirabilite, its hydrated form. We made an experience on sample no. 2, where analysis first gave thenardite (conditions in the diffractometer chamber were measured at 29 °C and 30–35 % RH). Then, it was exposed several days to a moist atmosphere, and immediately analyzed, giving mirabilite alone. After 50 min. of exposure to the dry laboratory atmosphere (24 °C and 45–55 % RH), the renewed analysis gave thenardite alone. This strongly suggests that the thenardite result is a laboratory artifact and that the mineral present in the cave was mirabilite. A same interpretation arises from other studies base on similar protocol (Bieniok et al. 2011) or without such a control (Harmon et al. 1983). We suspect that the thenardite identified in Picos de Europa (ref. quoted in Hill and Forti 1997) is most probably mirabilite.

The phase diagram of sodium sulfates (Fig. 5, Flatt 2002) also shows that mirabilite is in the field of these caves climates, whereas thenardite can only occur in much warmer and drier environments, such as a laboratory chamber or caves in arid climate. However, in case of strong supersaturation and very low RH (i.e. non-equilibrium conditions possibly encountered in field "reality"), presence of both species is possible during hydration in the stability field of mirabilite (Rodriguez-Navarro et al. 2000).

Since highly soluble sulfates are present in a wide range of temperature, the key-factor for their growth is the dryness of the air, at least seasonally. The Chamois Cave has a special climate due to its topographic and geological setting and to the cave structure. Firstly, most of the cave develops below a narrow crest in a thick sequence of marly limestones dipping perpendicularly to the main passages. As a consequence, most of the infiltration above the cave is guided toward west, and a high cliff to the east (i.e. no catchment) prevents any contribution of the cave itself.

Percolations are small and not frequent; the cave owes its origin to allogenic input and to a remote recharge. Secondly, most of the year, a strong draft enters at high altitude and crosses the main passages towards the entrance. During its

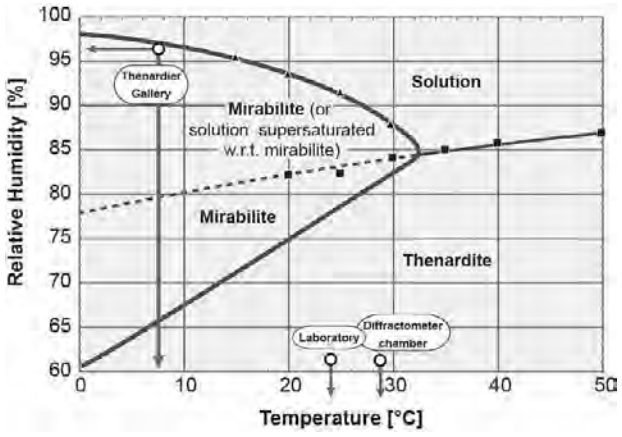

Figure 5. Phase diagram for sodium sulfates. The continuous lines indicate the boundaries of the stable phases. Triangles and squares are experimental data for mirabilite and thenardite, respectively. The discontinuous line corresponds to a solution in metastable equilibrium with respect to thenardite and supersaturated with respect to mirabilite (figure extracted from Flatt 2002 experiments, redrawn). Note that the phase diagram of Hill & Forti (1997, p. 192) displays the mirabilite-thenardite boundary line, constructed from one field case, in a slightly lower position (i.e. with drier conditions). We plotted the T – RH conditions of the Chamois Cave and of the Laboratory were X-ray analyses have been done, which clearly show that they are in the stability field of mirabilite and thenardite, respectively.

subsidence, it warms up (from 4.3 to 7.1 °C) and dries out (93 to 92 % RH), both by compression and by contact with the passage wall which are warmed by geothermic flux since cooling by percolation is very limited [see paper about the Chamois Cave temperature in these Proceedings]. Moreover the Thénardier Gallery has even a more pronounced microclimate (8.5 °C, 88 % RH). There is no percolation in the upper dry gallery where sulfates occur. It is confined by sumps most of the year, and especially during wet season. Very similar conditions occur in Gamslöcher-Kolowrathöhle, qualified as "aridity" in the gallery where sulfates are present (Bieniok et al. 2011) and Castelguard Cave (Harmon et al. 1983). Regarding Chamois Cave, we might have expected a strong ventilation to account for the evaporative conditions, but surprisingly Thénardier gallery is a confined passage isolated by sumps during long periods, with at the maximum only slight convection air movements due to local temperature differences.

6. Conclusion

The Chamois Cave (Alpes-de-Haute-Provence, France) harbors unusual highly soluble sulfate minerals, usually found in caves from arid areas or in volcanic caves still under heat influence, but less common in such cold limestone caves (here 8.5 °C). X-ray analyses allow identifying, beside carbonate mineral (calcite and hydromagnesite), calcium sulfate (gypsum), together with highly soluble sodium sulfates, mirabilite and eugsterite. To our knowledge, it is only the second mention of eugsterite as cave mineral. Thenardite also appeared on X-rays, but it is likely an artifact due to dehydration of the cave mineral mirabilite during the analytical process. The origin of sulfate is likely the oxidation of pyrite from the host rock, and the sodium probably comes from the weathering of sodium plagioclases (albite), one of the components of the alluvial deposits coming from Annot sandstones erosion. The main reason for the presence of these sodium sulfates is the dry atmosphere of the Thénardier Gallery, with low RH (88 %). Such microclimatic specificities are the result of conditions present in the whole cave (topographic and geologic conditions responsible of scarce percolations, subsiding draft through the cave that warms and dries up thanks to a strong geothermal gradient) and to local conditions of the Thénardier gallery (long isolation periods by temporary sumps). All in all, the main factor for sodium sulfates growth relies on these strong evaporation conditions that are not so frequent in such cold-temperate limestone caves.

Finally, due to the presence of a seasonal sump, we cannot figure of possible period of growth and dissolution of the sodium sulfates. However, a dive project will allow us to observe the site during confinement period and a data logger left last year is currently recording the temperature and humidity cycles. Isotopes analysis could confirm the relationship between pyrites and sulfates.

Acknowledgments

B. P. Onac, P. Forti, and W. White for the fruitful discussion and additional information. D. Borschneck for X-ray analyses at CEREGE (Univ. Aix-Marseille) and for conclusive experiments on hydration-dehydration.

References

Audra P, Mocochain L, Bigot J-Y, Nobécourt J-Cl, 2009. The Grand Coyer karst, exploration at the Coulomp spring (Alpes-de-Haute-Provence, France). Proceedings of the 15th International Congress of Speleology, Kerrville (TX), 3, 1755–1759.

Benington F, 1959. Preliminary identification of crystalline phases in a transparent stalactite. Science, 129 (3357), p. 1227.

Bieniok A, Zagler G, Brendel U, Neubauer F, 2011. Speleothems in the dry parts of the Gamslöcher-Kolowrat Cave, Untersberg near Salzburg (Austria). International Journal of Speleology, 40 (2), 117–124.

Bertolani M, 1958. Particolare ambiente minerogenetico in una grotta delle argille scagliose emiliane. Proc. 2nd Intern. Cong. Speleol., Bari, 1, 220–225.

Fitzpatrick RW, Baker AKM, Raven M, Rogers S, Degens B, George R, Kirby J, 2005. Mineralogy, biogeochemistry, hydro-pedology and risks of sediments, salt efflorescences and soils in open drains in the wheatbelt of Western Australia. In: IC Roach (Ed.). Regolith 2005 – Ten Years of CRC LEME. Cooperative Research Centre for Landscape Environments and Mineral Exploration, Symonston. pp. 97–101.

Flatt RJ, 2002. Salt damage in porous materials: how high supersaturations are generated. Journal of Crystal Growth, 242, 435–454.

Forti P, 2010. Genesis and evolution of the caves in the Naica Mine (Chihuahua, Mexico). Zeitschrift für Geomorphologie, 54 (2), 285–306.

Harmon RS, Atkinson TC, Atkinson JL, 1983. The Mineralogy of Castleguard Cave, Columbia Icefields, Alberta, Canada. Arctic and Alpine Research, 15(4), 503–516.

Hill CA, Forti P, 1997. Cave mineral of the world. National Speleological Society, Huntsville.

Onac BP, 2012. Minerals. In: WB White and DC Culver (Eds.). Encyclopedia of Caves, Academic Press, Chennai, pp. 499–508.

Polyak VJ, Provencio P, 2001. By-product materials related to H_2S-H_2SO_4 influenced speleogenesis of Carlsbad, Lechuguilla, and other caves of the Guadalupe Mountains, New Mexico. Journal of Caves and Karst Science, 63(1), 23–32.

Rodriguez-Navarro C, Doehne E, Sebastian E, 2000. How does sodium sulfate crystallize? Implication for the decay and testing of building material. Cement and Concrete Research, 30, 1527–1534.

Stanley D-J, 1961. Étude sédimentologiques des grès d'Annot et de leurs équivalents latéraux [Sedimentological study of Annot sandstones and their lateral equivalent]. Ph.D. Thesis, Univ. Grenoble, France.

White WB, 2005. Gypsum flowers and related speleothems. In: DC Culver and WB White (Eds.). Encyclopedia of Caves, Elsevier, pp. 288–291.

MINERALOGY AND SPELEOGENESIS OF THE CORONA 'E SA CRABA QUARTZITE CAVE (SOUTHWEST SARDINIA)

Eleonora Baldoni[1], Jo De Waele[1], Ermanno Galli[2], Mauro Messina[3], Bogdan P. Onac[4], Laura Sanna[5], Francesco Sauro[1], Mauro Villani[6]

[1]Department of Biological, Geological and Environmental Sciences, Bologna University, Via Zamboni 67, 40126 Bologna, Italy, eleonb@hotmail.it; jo.dewaele@unibo.it; cescosauro@gmail.com

[2]Department of Earth Sciences, University of Modena and Reggio Emilia, Largo S. Eufemia 19, 41121 Modena, Italy, gallier@unimore.it

[3]Speleo Club Domusnovas, Domusnovas, Italy

[4]Department of Geology, University of South Florida, 4202 E. Fowler Ave., SCA 528, Tampa, FL 33620, USA, bonac@usf.edu

[5]Department of Natural Sciences and Land, Sassari University, Via Piandanna 4, 07100 Sassari, Italy, speleokikers@tiscali.it

[6]Gruppo Ricerche Speleologiche E.A. Martel Carbonia, Italy

Sa Corona 'e sa Craba (Barbusi, Carbonia, Southwest Sardinia) is a natural cave almost entirely developed within a quartzite vein. Its natural entrance, enlarged during mining operations, opens at 260 m asl. The cave is composed of an over 200 m long and 20 m wide gallery developed in a NW-SE direction.

During our surveys we collected over 50 small samples of crusts, coatings and spars from all over the cave, on which we performed X-ray diffraction analysis in order to understand the speleogenetic pathways. These samples ranged in color from yellow to red, purple, brownish, grey, white, pinkish, bluish and black. Beside the already known minerals, the following have been discovered for the first time within this cavity: *sulfide*: cinnabar; *sulfates*: alunite, natroalunite, basaluminite, walthierite and gypsum; *phosphates*: taranakite, spheniscidite, robertsite, Al-rich strengite, hydroxylapatite, vashegyite and an unnamed Pb-Mo oxide phosphate; *silicates*: halloysite, lizardite and clay minerals of the illite and smectite group; oxyhydroxides: hematite, goethite, pyrolusite and todorokite.

1. Introduction

Presently, more than 350 minerals are known to form in a variety of cave settings (Onac and Forti 2011). In general, the precipitation of most cave minerals has no relationship with the cave's genesis itself. According to Hill and Forti (1997) *"a cave mineral is a secondary deposit precipitated inside a human-sized natural cavity"*, in other words, a secondary mineral derived from a primary mineral existing in the bedrock or other cave deposit through a physico-chemical reaction. Caves can be very special environments and in some cases the study of cave minerals can clarify the genesis of the void itself (Hill and Forti 1997). This is especially true for sulfuric acid caves, where the presence of unusual sulfates or other "exotic" minerals typical for extremely acid environments help us understand the processes responsible for the creation of the voids (Sulfuric Acid Speleogenesis – SAS, Morehouse 1968; Onac et al. 2009).

Corona 'e sa Craba Cave qualifies as a special environment because it is carved in quartzites (mainly) and dolostones.

The cave hosts a wide variety of minerals created by the interaction between host rock, guano deposits, H_2S derived from oxidation of sulfides, rising hydrothermal solutions and seeping water. Despite over 20 years of high interest for mineral collectors in this cave, only five minerals were previously known from this locality: barite (in gorgeous crystals turning bluish when exposed to light), calcite, quartz, dolomite, and aragonite. This paper describes the morphology of the cave, its mineralogy, and proposes a preliminary interpretation of its peculiar speleogenesis.

2. The Corona 'e Sa Craba Cave

Corona 'e sa Craba Cave opens at an altitude of 260 m asl, immediately East of the small settlement of Barbusi (Carbonia, SW Sardinia, Italy) (Fig. 1). Its small entrance has been enlarged by mining excavations at the base of an important quartzite ridge in the early 1970s. The Corona 'e sa Craba area, in fact, was explored for Pb, Zn and Ba ores in the early 1930s, and economic exploitation went on for a little more than 30 years after 1950. Cavers became aware of the existence of the cave through mineral collectors, who exploited a natural void for its beautiful bluish barite crystals. In 1971, the Gruppo Ricerche Speleologiche E.A. Martel of Carbonia explored the cave too late, unfortunately, to try and protect this beautiful and meaningful mineralogical site. A complete survey of the cave was carried out some years later by the Speleo Club Cagliari and the same caving association of Carbonia.

The cave is composed of a series of rooms, almost entirely developed in quartzite (Fig. 2). The hostrock is dark grey to brownish, and there are no speleothems typical of carbonate caves. The cave floor is scattered with rock fragments, especially along the first 50 meters, probably the result of the excavations carried out by the mineral collectors. The entrance room has a semi-circular plan shape and is separated from the rest of the cave by a large and dangerous rockfall. Once passing behind the rockfall, the cave becomes very large. A 20 m wide and 20 m high gallery develops for over 80 m in a SE direction (Fig. 2).

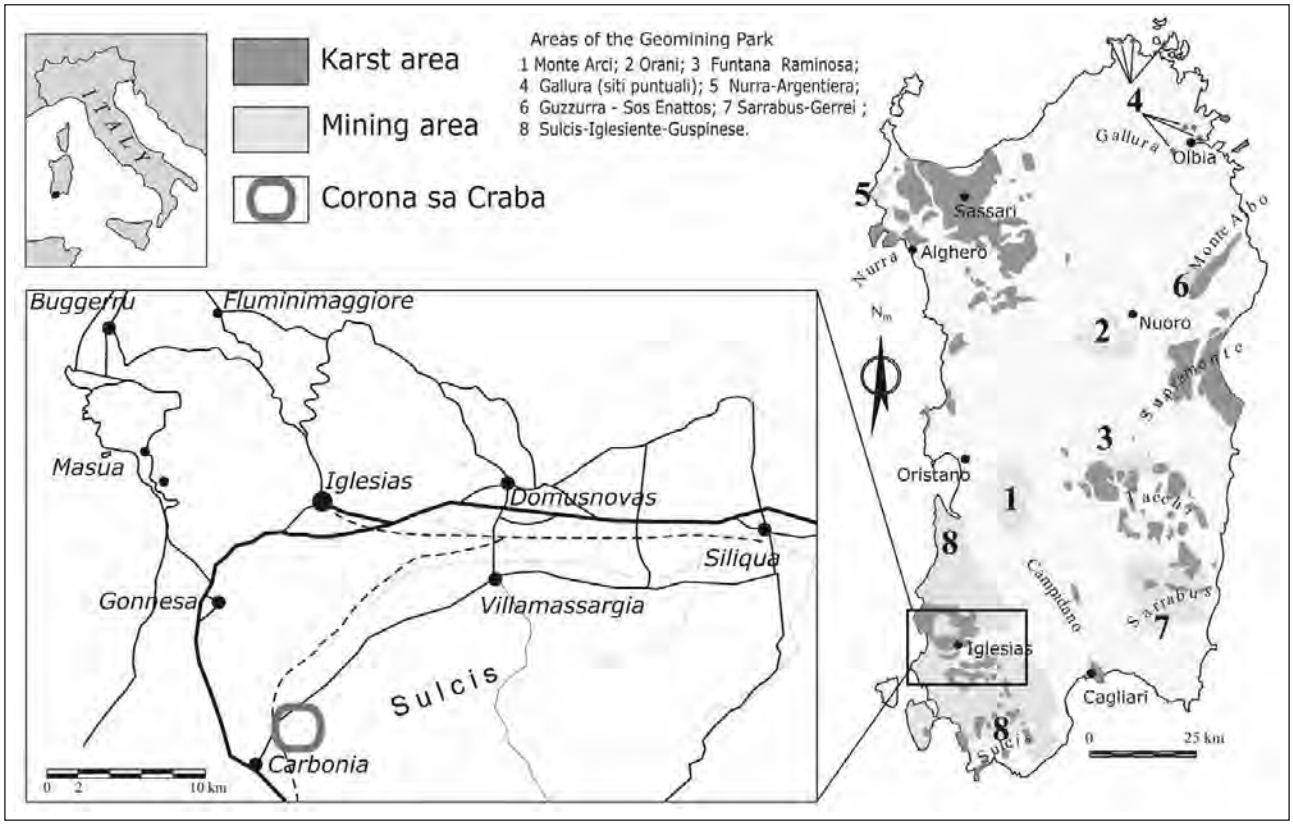

Figure 1. Location of the study area. To the right: Sardinia, its karst areas (blue) and the areas of the Geomining, Historical and Environmental Park of Sardinia (in grey). Corona 'e Sa Craba Cave is located in the main of these old mining areas, Sulcis-Iglesiente, with many important abandoned Pb-Zn mines in a range of less than 10 km.

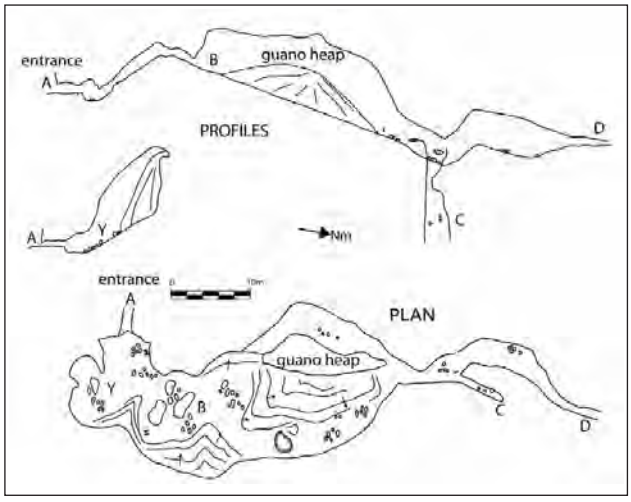

Figure 2. Map of the Corona 'e sa Craba Cave.

The center of this gallery hosts an important guano deposit generated by a large bat colony inhabiting the cave during spring-early summer. In the lowest part of this elongated room the cave continues as an 8 m wide and 20 m high passage, probably developed along a fracture. Forty meters further, the cave becomes too narrow for humans to pass, bringing the total development to 250 m.

Of special interest are the corrosion forms present along the walls of the cave (Fig. 3). In several places mm-thick dark brown quartz veins (boxwork) protrude out of the host rock wall by several decimetres or even up to a metre. The rock wall is composed of microcrystalline quartz, whereas the veins are made up of larger quartz crystals. In between the veins there is a wet and fine-grained black or very dark brown material composed of poorly crystallized Mn and Fe oxides.

3. Methods

Mineral samples were collected by means of a steel spoon or a geological hammer (normally by scratching secondary minerals crusts or coatings), and a few grams of material were placed in small plastic containers or sampling bags. The various mineralogical phases were separated using a stereoscopic microscope in the laboratory. Single phases were analyzed by an X-ray diffractometer (Philips PW 1050/25) or in a Gandolfi camera (Ø: 114.6 mm, exposition: 24/48 hrs) (experimental conditions 40 kV and 20 mA tube, CuKα Ni filtered radiation λ = 1.5418 Å) at Modena and Reggio Emilia University.

Additional mineralogical analyses were performed on the University of South Florida's Bruker Analytical X-Ray System, Inc. D8 Endeavor X-Ray diffractometer (XRD). Samples were scanned from 5° to 75° 2θ with a step increment of 0.02°, a scan speed of 0.5 s/step (analytical

Figure 3. Boxwork of quartz veins protruding out of the quartzite bedrock by over half a metre (Photo by R. De Luca).

conditions: 50 kV, 40 mA, Cu Kα radiation, line source filtered with a Ni foil). Mineral identification and abundance was evaluated semi-quantitatively by determining peak intensities (peak height) of the X-ray diffraction results with the DIFFRAC^{Plus} EVA V.8.0 software. Qualitative chemical analyses were carried out on a Philips XL40 environmental scanning electron microscope (ESEM) equipped with an energy dispersive spectrometer (EDS-EDAX 9900) at the C.I.G.S. (Centro Interdipartimentale Grandi Strumenti) of the Modena and Reggio Emilia University.

4. Mineralogy

Aside from the previously 5 known mineral species (barite, calcite, aragonite, dolomite, and quartz), 19 new minerals for this cave have been revealed during this study. Of these, spheniscidite has never been reported from a cave environment, making it a new cave mineral, whereas lizardite, and robertsite are very rare in caves and have previously been reported only from the Cupp-Couttun Cave in Turkmenistan and St. Paul's Underground River cave system in Palawan, respectively (Maltsev 1997; Billi et al. 2012). Berlinite might be present, but further analyses are necessary to confirm the presence of this high temperature mineral. Table 1 reports the list of all minerals known from Corona 'e Sa Craba.

4.1. Sulfides

Galena and sphalerite were mined from the nearby ore deposits, but were never identified in the present cave. This is because the hostrock sample in which these sulfides are scattered was never collected. The only sulfide mineral positively documented is cinnabar. It occurs as submillimetric bright red powdery coatings on the lower part of the cave walls, especially on the overhanging ledges of both rock walls and fallen boulders (Fig. 4A). The origin of this mineral seems to be related to either vapors or hydrothermal fluids ascending from below. Further investigations are needed to confirm this "hypogenic" or "volcanic" origin.

4.2. Oxides and Hydroxides

Four oxides and hydroxides have been found: hematite, pyrolusite, goethite, and todorokite. They mostly occur as dark colored coatings and crusts on the cave walls. These are common cave minerals, related to oxidation of sulfides occurring in nearby ores or within the cave hostrock.

4.3. Carbonates

Calcite and aragonite are also common minerals found in caves, whereas dolomite is rather uncommon unless the bedrock is a dolostone (Onac 2012). In this case, however, the carbonates are late stage deposits precipitated from low-temperature seeping waters that percolated through the nearby or overlying Cambrian limestones and dolostones. In Corona 'e sa Craba, these minerals do not form typical speleothems (e.g., stalactites), but are found as crusts or minor powdery coatings.

4.4. Sulfates

These are the most important minerals found in Corona 'e sa Craba Cave. Besides barite, occurring as beautiful big bluish, reddish, and yellowish crystals, gypsum, alunite (Fig. 4J), basaluminite (Fig. 4D-E), natroalunite, and walthierite were also identified. Walthierite is a rather rare Ba-Al sulfate that is associated with alunite. It normally forms by the interaction of hydrothermal acid sulfate fluids with barite (Li et al. 1992). The other 4 sulfates are typical for sulfuric acid weathered Al-rich minerals. They are often found in SAS caves (Polyak and Güven 1996).

4.5. Phosphates

The phosphate group is widely represented in Corona 'e sa Craba Cave, with 6–7 different species. Taranakite and hydroxylapatite are rather common cave minerals, whereas the Al-rich variety of strengite and vashegyite are far more rare (Onac et al. 1995, 2006; Forti et al. 2000). Robertsite is a very rare cave phosphate, recently discovered in the Lion's Cave in the St. Paul's Underground River National Park in Palawan (Billi et al. 2012). Spheniscidite (Fig. 4F–H) is a hydrated phosphate that belongs to the

Table 1. List of minerals discovered in the Corona 'e Sa Craba quartzite cave.

Mineral	Formula	Mineral	Formula
Cinnabar	HgS	Walthierite	$Ba_{0.5}Al_3(SO_4)(OH)_6$
Hematite	Fe_2O_3	Gypsum	$CaSO_4{\cdot}2H_2O$
Pyrolusite	MnO_2	Spheniscidite	$(NH_4,K)(Fe,Al)_2(PO_4)_2(OH){\cdot}2H_2O$
Goethite	FeO(OH)	Taranakite	$H_6K_3Al_5(PO_4)_8{\cdot}18\ H_2O$
Todorokite	$(Na,Ca,K,Ba,Sr)_{1-x}(Mn,Mg,Al)_6O_{12}{\cdot}3\text{-}4H_2O$	Robertsite	$Ca_2Mn_3(PO_4)_3O_2{\cdot}3H_2O$
Calcite	$CaCO_3$	Strengite	$Fe^{3+}PO_4{\cdot}2H_2O$
Aragonite	$CaCO_3$	Hydroxylapatite	$Ca_5(PO_4)_3(OH)$
Dolomite	$CaMg(CO_3)_2$	Vashegyite	$Al_{11}(PO_4)_9(OH)_6{\cdot}38(H_2O)$
Barite	$BaSO_4$	Berlinite (?)	$AlPO_4$
Basaluminite	$Al_4SO_4(OH)_{10}{\cdot}5H_2O$	Quartz	SiO_2
Alunite	$K_2Al_6(SO_4)_4(OH)_{12}$	Lizardite	$Mg_3Si_2O_5(OH)_4$
Natroalunite	$NaAl_3(SO_4)_2(OH)_6$	Halloysite	$Al_2Si_2O_5(OH)_4$

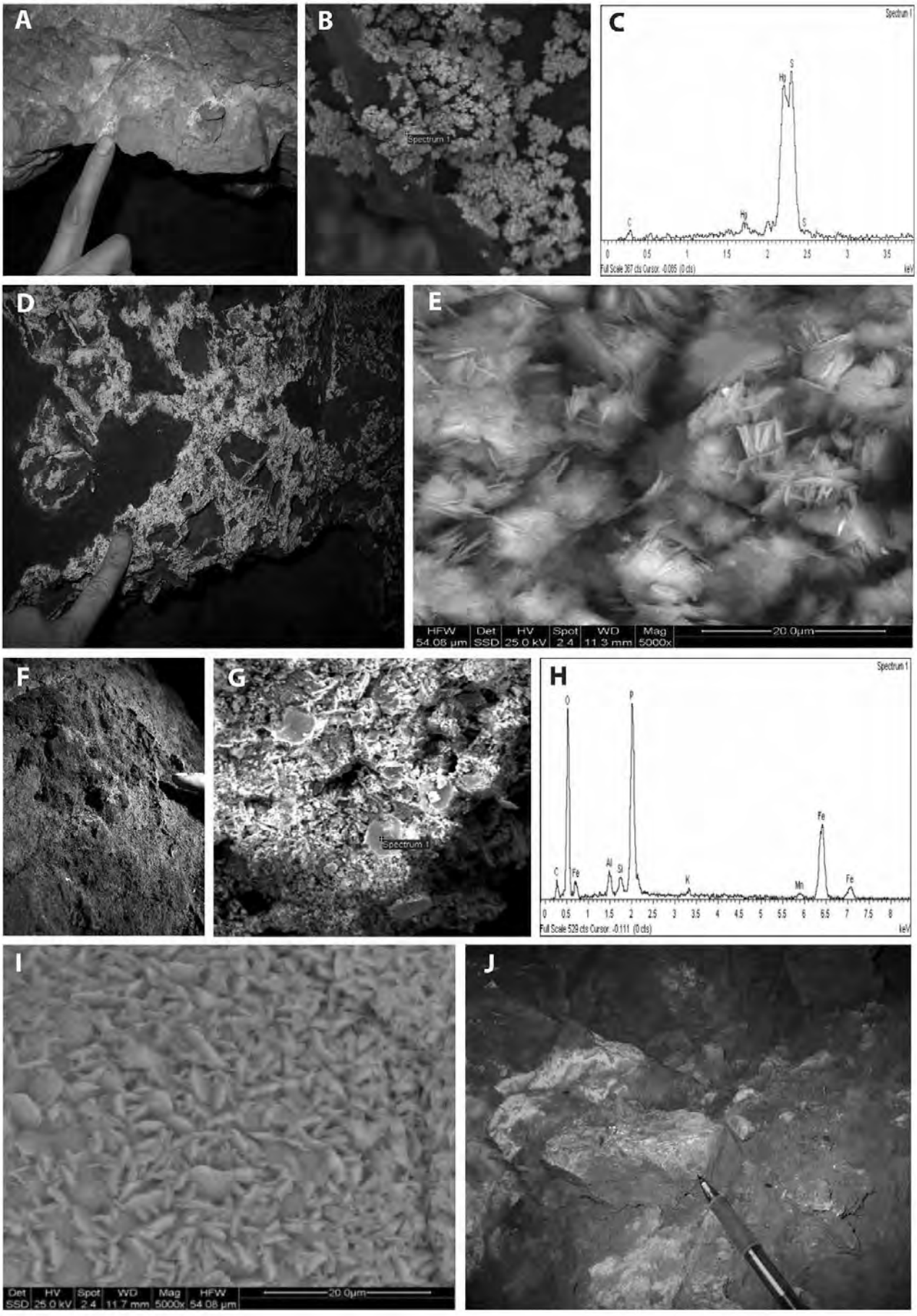

Figure 4. In situ pictures, electron microscope images and diffractograms of some minerals from Corona 'e Sa Craba Cave: A-B-C. Cinnabar; D-E. Basaluminite; F-G-H. Spheniscidite; I. Lizardite; J. Alunite.

leucophosphite group along with tinsleyite and leucophosphite. Except for the latter mineral, which has been reported from several caves, tinsleyite is known from only one other cave location (Marincea et al. 2002), whereas for spheniscidite this is the first reported cave environment occurrence. Its origin most likely relates to the reaction between the phosphoric acid leaching from underneath ammonium-rich fresh guano and the bedrock. Berlinite might also be present in the cave, as some of the diagnostic XRD patterns reported by Onac and White (2003) are present in our sample too. This mineral, however, requires very high temperatures (Onac and Effenberger 2007), conditions that might not have existed in this cave. Further investigations are necessary to confirm the presence of this rare phosphate. During our analyses we also found an unknown Pb-Mo phosphate oxide, still under study.

4.6. Silicates

Besides quartz and some expected clay minerals of the smectite and illite group, two other silicates are worth discussing. Halloysite is a mineral typical for a hydrothermal and highly acid environment (Polyak and Guven 1996; Perruchot et al. 1997; Melka et al. 2000; De Waele et al. 2008). Lizardite (Fig. 4I) is a mineral that usually forms by hydrothermal alteration (serpentinitisation) of Mg-rich minerals such as olivine. Prior to our finding it was reported only from the Cupp Couttun Cave in Turkmenistan (Maltsev 1997).

5. Minerogenesis and speleogenesis

The mineralogical association found in Corona ‘e sa Craba Cave is typical for two different minerogenetic environments: the sulfuric acid speleogenesis (SAS) and the guano environments. In our case, the sulfuric acid may have two different origins: oxidation of sulfides in nearby ores, or diffused in the quartzite hostrock and above lying carbonate formations (Mississippi Valley type mineralization), and deep seated (volcanic) hypogenic rising of fluids (Onac et al. 2011). Stable S isotopes will be carried out in the near future to correctly distinguish between the two processes.

The origin of the guano-related minerals is much easier to explain, although the presence of spheniscidite, robertsite, vashegyite, and possibly berlinite shows the cave environment underwent rather significant changes (relative humidity, pH, and temperature). Along with these parameters, it is the composition of the bedrock that controlled the precipitation of this unique suite of phosphate minerals.

The large array of minerals typical of a very acid environment indicates that aggressive fluids having a low pH dissolved the cave. The extremely well-developed boxworks, on the other hand, suggest the dissolution occurred in subaerial conditions, by airflow and condensation-corrosion processes. These processes are no longer active. The presence of cinnabar exclusively in the lower parts of the cave could be an indication of rising steam or hot fluids from depth. Such conditions might have been present, particularly during the Oligo-Miocene volcanic activity that characterized this part of Sardinia for several millions of years. The cinnabar coatings, however, appear to be formed quite recently. Stable isotope studies on S might throw light on its origin.

6. Conclusions

Corona ‘e Sa Craba has turned out to be a very special cave, not only because it is carved in quartzite, but also for its extremely rich mineral association. The secondary minerals indicate the cave might have formed by highly acidic vapors (steam?) in a subaerial environment. Despite the fresh appearance of the wall morphologies, the origin of the cave might possibly be ascribed to the Oligo-Miocene volcanic activities that occurred in the region between 32 and 12 million years ago.

Detailed petrographical studies on the hostrock and on its weathering might confirm that Corona ‘e sa Craba cave has been formed by acid dissolution of the quartzite. This would be the first case of speleogenesis in siliceous rocks occurred under subaerial conditions at very low pH, on the contrary to what happens in other areas around the world (e.g., Tepui caves in Venezuela, South Africa or Brazil; Corrêa Neto 2000; Martini 2000), where quartzite caves are formed in basic conditions by large underground water drainages.

Acknowledgments

SEM images and X-ray diffractograms have been acquired at the Laboratorio Grandi Strumenti of Modena and Reggio Emilia University. Many thanks to Paolo Forti and an anonymous reviewer for their useful comments.

References

Billi S, Forti P, Galli E, Rossi A, 2012. Robertsite: un nuovo fosfato scoperto nella Tagusan Cave (Palawan – Filippine). Atti del XXI Congresso Nazionale di Speleologia, Trieste, pp. 196–199.

Corrêa Neto AV, 2000. Speleogenesis in quartzite in Southeastern Minas Gerais, Brazil. In Speleogenesis. Evolution of Karst Aquifers (Klimchouk et al.), National Speleological Society, Huntsville, 452–457.

De Waele J, Frau F, Muntoni A, Cannas C, 2008. Ritrovamento di Halloysite nella Grotta Eraldo (Barega, Iglesias, Sardegna sud-occidentale). Atti del XX Congresso Nazionale di Speleologia, Iglesias, pp. 245–254.

Forti P, Galli E, Rossi A. 2000. Minerali geneticamente correlati al guano in una grotta naturale dell’Albania. Primo contributo. Le Grotte d’Italia, 1, 45–59.

Hill C, Forti P, 1997. Cave minerals of the world, second edition, National Speleological Society, Huntsville.

Li G, Peacor DR, Esene EJ, Brosnahan DR, Beane RE, 1992. Walthierite, $Ba_{0.5}X_{0.5}Al_3(SO_4)_2(OH)_6$, and Huangite, $Ca_{0.5}X_{0.5}Al_3(SO_4)_2)(OH)_6$, two new minerals of the alunite group from the Coquimbo region, Chile. American Mineralogist, 77, 1275–1284.

Maltsev V, 1997. Cupp-Coutunn Cave, Turkmenistan. In Cave minerals of the world (Hill CA & Forti P, eds.), Huntsville, National Speleological Society: 323–328.

Marincea S, Dumitras D, Gibert R, 2002. Tinsleyite in the "dry" Cioclovina Cave (Sureanu Mountains, Romania): the second occurence. European Journal of Mineralogy, 14, 157–164.

Martini JEJ, 2000. Quartzite caves in southern Africa. In Speleogenesis. Evolution of Karst Aquifers (Klimchouk et al.), National Speleological Society, Huntsville, 458–461.

Melka K, Suchy V, Zeman A, Bosak P, Langrovà A, 2000. Halloysite from karst sediments of the Koneprusy area: evidence for acid hydrothermal speleogenesis in the Bohemian karst, Czech Republic. Acta Universitatis Carolinae, Geologica, 44(2–4), 117–124.

Morehouse DF, 1968. Cave development via the sulfuric acid reaction. National Speleological Society Bulletin, 30(1), 1–10.

Onac BP, 2012. Minerals. In Encyclopedia of Caves (White WB & Culver DC, eds.), Chennai: Academic Press, 499–508.

Onac BP, Effenberger HS, 2007. Re-examination of berlinite ($AlPO_4$) from the Cioclovina Cave (Romania). American Mineralogist, 92, 1998–2001.

Onac BP, Forti P, 2011. Minerogenetic mechanisms occurring in the cave environment, an overview. International Journal of Speleology, 40 (2), 1–20.

Onac BP, White WB, 2003. First reported sedimentary occurrence of berlinite ($AlPO_4$) in the phosphate bearing sediments from Cioclovina Cave (Romania). American Mineralogist, 88, 1395–1397.

Onac BP, Bengeanu M, Botez M, Zih J, 1995. Preliminary report on the mineralogy of Pestera din Valea Rea (Bihor Mountains, Romania). Theoretical and Applied Karstology, 8, 75–79.

Onac BP, Zaharia L, Kearns J, Veress D, 2006. Vashegyite from Gaura cu Muscă Cave (Locvei Mountains, Romania): a new and rare phosphate occurrence. International Journal of Speleology, 35(2), 67–73

Onac BP, Sumrall J, Tămaş T, Povară I, Kearns J, Dârmiceanu V, Vereş D, Lascu C, 2009. The relationship between cave minerals and H_2S-rich thermal waters along the Cerna Valley (SW Romania). Acta Carsologica, 38(1), 27–39.

Onac BP, Wynn JG, Sumrall JB., 2011. Tracing the sources of cave sulfates: a unique case from Cerna Valley, Romania. Chemical Geology, 288, 105–114.

Perruchot A, Dupuis C, Brouard E, Nicaise D, Ertus ETR, 1997. L'halloysites karstique: comparaison des gisements types de Wallonie (Belgique) et du Perigord (France). Clay Minerals, 32(2), 271–287.

Polyak VJ, Güven N, 1996. Alunite, natroalunite and hydrated halloysite in Carlsbad Cavern and Lechuguilla Cave, New Mexico. Clays and Clay Minerals, 44(6), 843–850.

GENESIS AND EVOLUTION OF CALCITE BUBBLES IN GYPSUM CAVES

Massimo Ercolani[1], Katia Poletti[2], Paolo Forti[3]
[1]Federazione Speleologica dell'Emilia Romagna, massimoercolani@filtcgil.it
[2]Gruppo speleologico Faentino, kapoletti@gmail.com
[3]Istituto Italiano di Speleologia, via Zamboni 67, 40126 Bologna, Italy, paolo.forti@unibo.it

Recently in two different gypsum caves of Emilia Romagna (Italy) a peculiar type of calcite bubbles have been found for the first time in the world. Its genesis is controlled by strict boundary conditions, among which the presence of organic mats is fundamental. Their evolution is controlled by a complex multistage process, which makes extremely rare their genesis. Moreover calcite bubbles are a classical ephemeral formation and their life hardly exceeds a few weeks: this explains why they were never seen before. Their discovery shows that gypsum caves, even if explored and studied for a century may be still considered interesting places where searching for new spleothems.

1. Introduction

Cave bubbles are a rare hollow, often floating, calcareous speleothem developing at the water-air boundary (Hill and Forti, 1997). They consist of a very thin (<0.2 mm thick) crust of calcite (or, more rarely, aragonite) always developed over a long lasting air bubbles in a quiet shallow pool setting associated cave rafts.

Practically all but one the know location for cave bubbles are in limestone caves and their genesis is induced by the preferential diffusion of CO_2 in the cavern atmosphere occurring from the thin water film of the bubble. This genetic mechanism explains why the thickness of the cave bubbles never exceeds 0.2 mm: in fact as soon as the bubble wall is thicker it inhibits the diffusion process.

The inner surface of the bubbles is always smooth while the outside is more crystalline: this is also a consequence of the genetic mechanisms. Each single calcite grain develop over the outer part of the water film which therefore controls the shape of the inner surface of the speleothem, while the outer part can develop without in the free atmosphere without any boundary conditions.

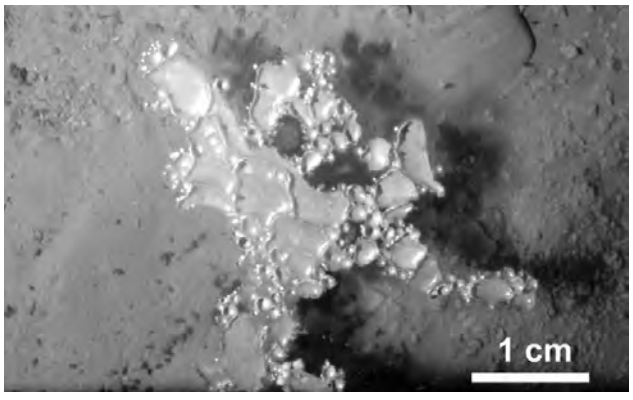

Figure 1. Half-bubbles floating in the underground river of Grave Grubbo gypsum cave (Photo by Mauro Chiesi).

Cave bubbles are extremely delicate thus normally are ephemeral, lasting only during the dry season and being destroyed when a flood increase the energy of the pool.

Only one occurrence of cave bubbles was reported from a gypsum cave (Forti and Chiesi, 1995, Forti and Lombardo, 1998), and the described speleothems are really peculiar being in reality "half bubbles" floating on the surface of an highly polluted gour of the Grave Grubbo karst system (Calabria, Italy) (Fig. 1).

The genesis of these formations was completely different from that of the "normal" calcite bubbles: their development was induced by the oxidation of the organic matter in an environment saturated with gypsum. In the first step of its oxidation, the organic mat gave rise to long lasting foam, which, in turn supported the genesis of the calcite half-bubbles. In fact, their thin film enhanced the diffusion of O_2 from the cave atmosphere into the solution, increasing the process of oxidation of the organic matter. Thus the reaction between the produced carbon dioxide and the high concentration of calcium present in the solution was faster. The produced cave rafts moved along the foam film to sink by gravity and to consolidate in the lower part of the film until the breaking of the foam bubbles gave rise to the half bubbles (Fig. 2).

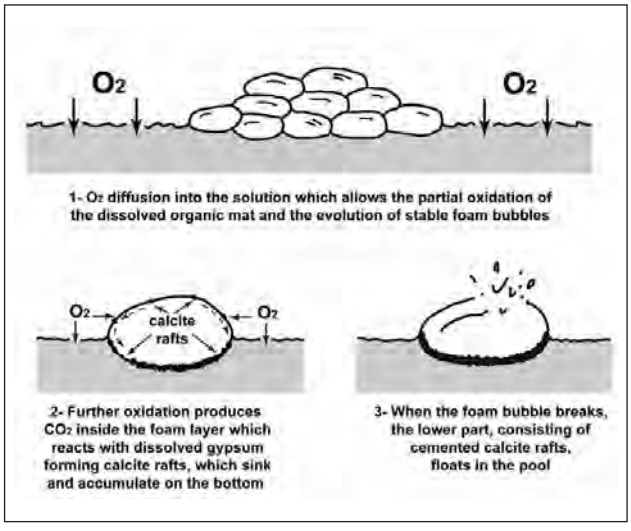

Figure 2. Genetic steps for the calcite half-bubbles of Grave Grubbo (after Hill & Forti 1997, modified).

Recently a new occurrence of calcite bubbles has been reported from the "Vena del Gesso Romagnola", Emilia-Romagna Region, Italy) (Fig. 3).

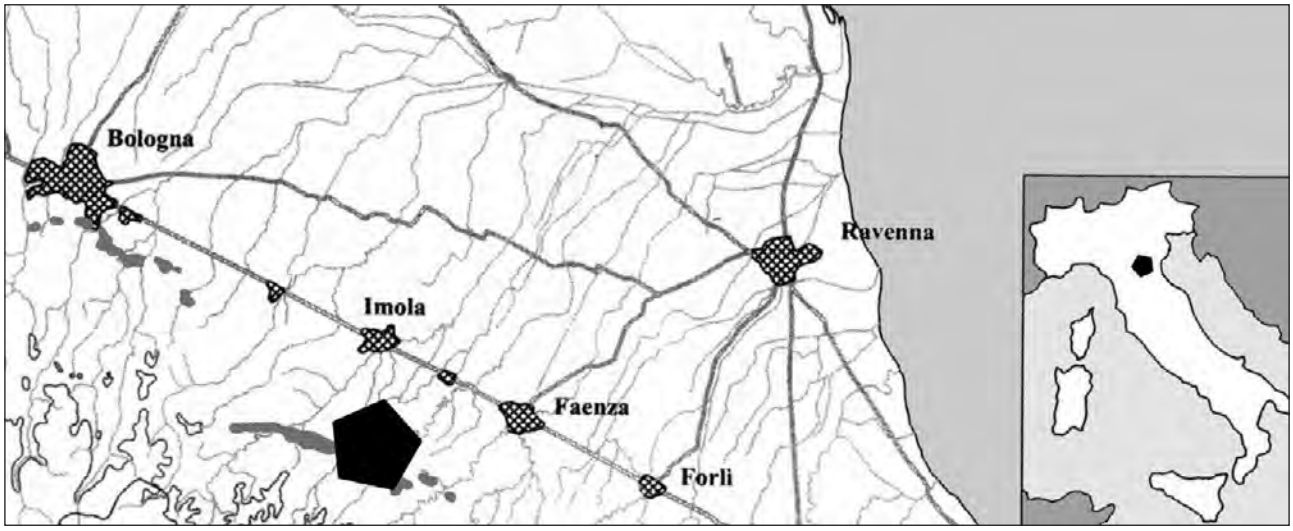

Figure 3. Location map: the larger of grey areas represent the "Vena del Gesso Romagnola" and the black polygon correspond to the two caves in which the calcite bubbles have been found.

In this occurrence several tens of perfect bubbles from 2 mm to over 1 cm in diameter with an average thickness of 0.1 mm developed over strongly dissolved gypsum rocks (Figs. 4, 5).

In the present paper the mechanism and boundary conditions, which allowed the evolution of these rare speleothems, are discussed.

Figure 4. Morning Abyss: the gypsum boulder, in the middle of riverbed of the underground river, on which the calcite bubbles developed (photo by Davide Dal Borgo, Gruppo Speleologico Faentino).

2. The calcite bubbles of the Abisso Morning

The first place where the calcite bubbles were observed and photographed is the Abisso Morning (near Brisighella). The bubbles were over a gypsum boulder, partially covered by a thin yellowish crust, lying in the underground riverbed: the boulder was taken to allow the study of these peculiar speleothems.

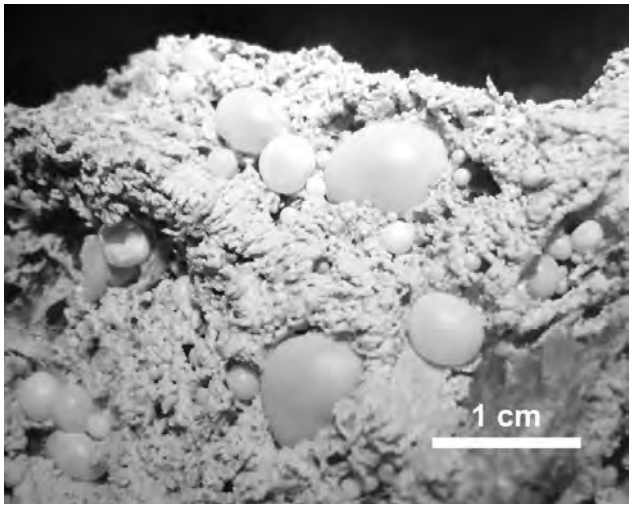

Figure 5. Morning Abyss: a close view of a group of unbroken calcite bubbles; around them the thin layer of calcified mud is evident (Photo by Davide Dal Borgo, Gruppo Speleologico Faentino).

Few weeks later the Gruppo Speleologico GAM of Mezzano observed the same formations inside the Grotta Grande dei Crivellari (near Riolo Terme): their setting was practically the same as those in Abisso Morning. Unfortunately no pictures were taken and a few days later a flood destroyed all the bubbles, leaving the boulder covered by a thin film of mud. This fact demonstrated that calcite bubbles in a gypsum environment are ephemeral speleothems growing and lasting only in the interval between floods.

On the basis of the observation made in both the caves and of the analyses performed over the sample taken in the Abisso Morning, it was possible to define the boundary conditions and the steps in the development of calcite bubbles (Figs. 6, 7).

Boundary conditions seem to be the following:

1. A gypsum substratum is required: in fact no bubble is present over a thick mud layer or over calcite flowstone.
2. The gypsum surface must be normally out of the water flow, and dripping water is unable to develop calcite bubbles, which are in reality destroyed by such phenomena.
3. A thin layer of organic rich mud must cover most of the gypsum surface.
4. The gypsum surface must host lot of small depressions in which water may be stored

The first boundary condition is useful to define the genetic mechanism allowing for the development of calcite. As it is well known (Forti and Rabbi 1981), calcite deposition in a gypsum environment is normally produced by the reaction between dissolved CO_2 within the soil by seeping water and the Ca^{2+} coming from gypsum dissolution.

It is therefore evident that this reaction may proceed only on a gypsum surface. The presence of a thick mud layer surface will hinder the reaction practically stopping the process of calcite deposition beyond a given thickness.

Organic material over a calcite formation will only result in corroding the speleothem' surface.

The second boundary condition is required because, when the gypsum surface is disturbed by turbulent flow, the calcite bubbles are immediately destroyed (as seen inside the Grotta Grande dei Crivellari). Moreover if only pure water is in contact with gypsum, no deposition at all will occur because the fast diffusion of CO_2 from the dripping water will prevent a reaction with gypsum due to the low concentration of dissolved carbon dioxide.

The third boundary condition is the presence of organic matter that, in aerated environment, oxidizes, thus supplying CO_2 to the system. The evidence of this process is given by the fact that the gypsum boulder is almost completely covered by a thin film of calcified mud. But this process alone will not last long enough to allow the development of even small calcite bubbles: the fast evaporation of the scarce water trapped in the organic film will stop the process in a couple of days or so.

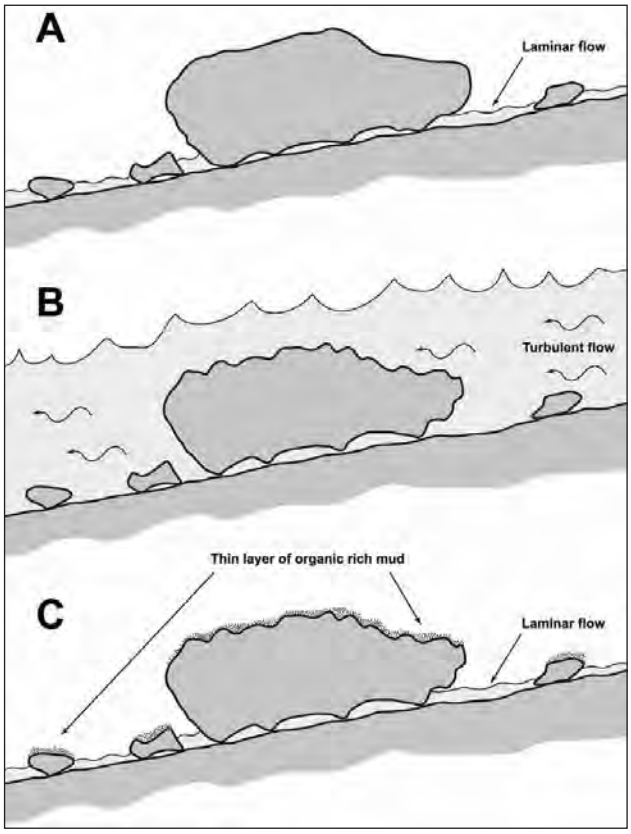

Figure 6. The alternation of dry periods with laminar flow far below the boulder surface (A & C) and floods with turbulent flow submerging the boulder (B) causes the deposition of thin layer of organic rich mud over the upper surface of the boulder.

The forth boundary condition is the presence of enough water to induce the deposition process until calcite bubbles becomes completely formed. The mechanism, which leads to the evolution of the small cups over the boulder surface, is a classical feedback process. In fact the first time the gypsum surface is exposed to turbulent flow the erosion-dissolution processes creates small depressions. These depressions will be filled by under saturated water during the following events, thus allowing faster deepening of these depressions in the gypsum upper surface.

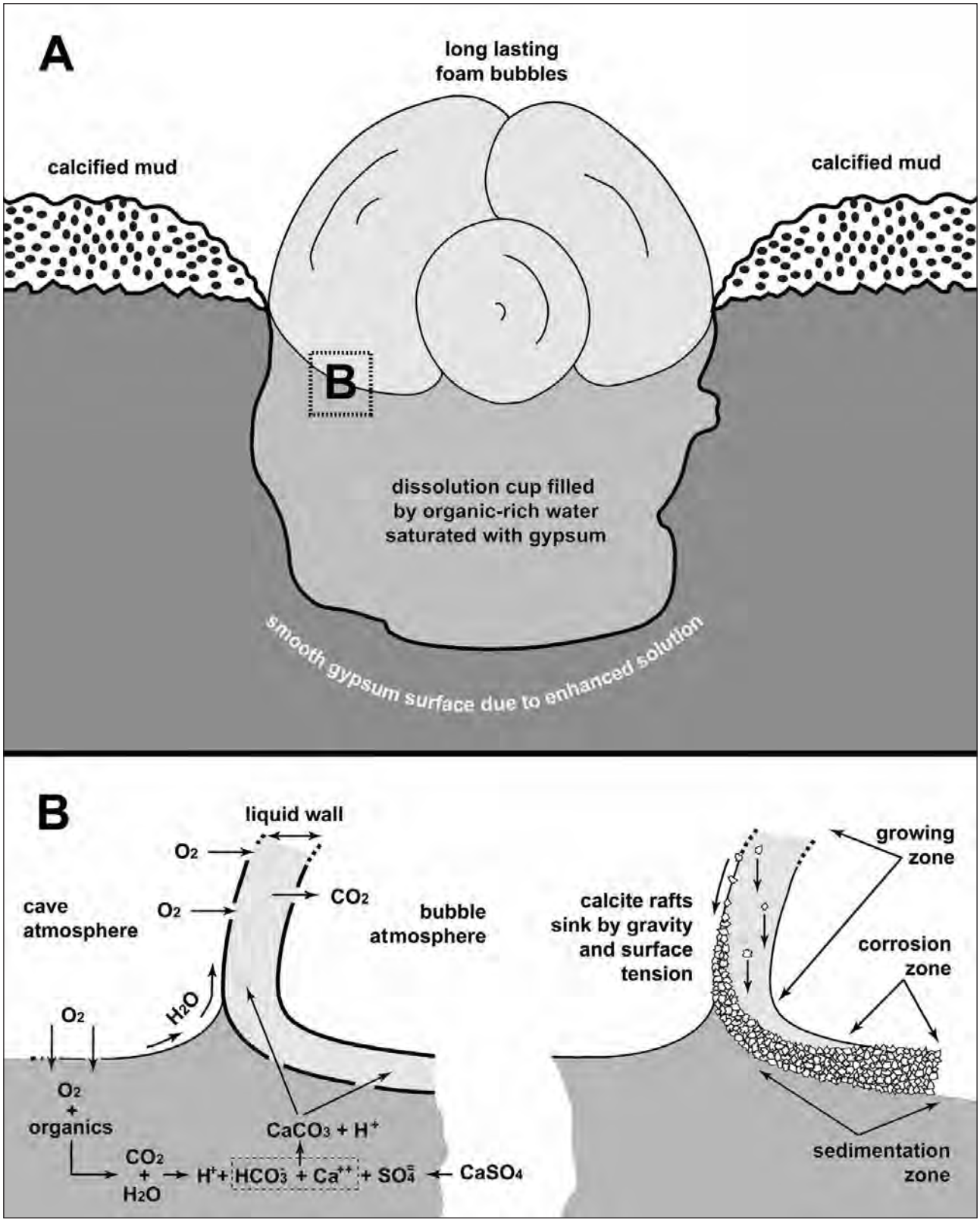

Figure 7. A: Sketch of a dissolution cup filled by water and covered by foam bubbles: note that due to the strong dissolution inside the cup the calcified mud is present only outside it. B: Close up view of the contact between the cup water and a foam bubble: on the left the physico-chemical active processes and on the right the evolution of a calcite bubble.

Finally this process is magnified by the presence of "steady water" inside the depression, which induces corrosion of the gypsum bottom of the cup due to the oxidation process of the organic matter. Evidence of the efficiency of the dissolution mechanisms within the cups is given by the fact that none of the cup bottoms is covered by calcified mud and they always consist of clearly strongly dissolved gypsum (Fig. 6).

In the case of the Morning Abys it was also possible to make a rough evaluation of the time needed to form the dissolution cups: in fact it is well known when the boulder arrived on the riverbed. This event corresponds to the artificial widening of a squeeze just few metres above the riverbed, which was performed by the Gruppo Speleologico Faentino in 2004. It is evident that, at the time of its fall,

the bypsum boulde was abosolutely flat, coming from a compact gypsum layer, and thus all the dissolution cups on its surface must have developed in less than 8 years.

Finally it is necessary to explain why the genesis of such strange speleothems is so rare. This is explained by the complexity of the subsequent steps by which the process must develop, which makes the sequence extremely difficult to be fulfilled.

The 10 steps in the development of the calcite bubbles may be summarized as follow:

1. The process starts with a gypsum boulder being located along the main flow of a subterranean river, with its upper part always dry except for short and rare periods of the highest floods. The fast erosion and dissolution of gypsum exposed to turbulent water flow makes practically impossible to the gypsum riverbed to be in such a condition. Moreover this occurrence is short lasting also for a fallen and/or transported gypsum boulders.
2. During rare foods the gypsum boulder is submerged by water and its upper surface is partially eroded and dissolved by the under saturated water thus creating several small “dissolution cup” on its surface. Any subsequent flood will enlarge and deepen these cups. In case the food occurs when calcite bubbles where already developed (step 10), all of them will be broken and/or washed away.
3. At the end of each flood a thin film of mud and clay is deposited over the gypsum boulder and a small quantity of water is also stored in each “dissolution cup”. If organic content of the mud and of the water is low the development of the calcite bubbles cannot start: in fact no foam can be produced and no CO_2 will be available to react with gypsum and produce calcium carbonate. In this case nothing will happen except for evaporation of all the water from the gypsum surface until a new flood occurs (step 2).
4. If the concentration of organic mats is high, the development of the calcite bubbles may start. Oxygen diffuses from the cave atmosphere into the wet mud layer and into the water in the dissolution cups. Thus the organic mat is oxidized and the produced CO_2 corrodes the underlying gypsum with simultaneous deposition of calcite which gives rise to the thin crust composed by calcified mud over the corroded gypsum surface.
5. In a very short time (a few days) the oxidation stops because all the water trapped within the mud layer evaporates. The only places in which oxidation may last much longer is within the “dissolution cups”, which act as accumulation traps and, in the mean time, avoid fast evaporation due to their scarce surface contact with the cave atmosphere.
6. Oxidation within the cups allow for the development of long lasting foam bubbles, which in turn act as preferential places for diffusion of the atmospheric oxygen into the solution saturated by gypsum, thus becoming places of enhanced calcite deposition.
7. The dimension of the “cups” controls the maximum size of the foam bubbles (i.e. of the calcite bubbles) even if in the same cup different independent bubbles may develop.
8. The calcite deposition over the foam causes a progressive hindering of the diffusion of the atmospheric O_2 into the solution, which brings to complete stop the process when the calcite films reaches a thickness of about 0.1 mm, which is in fact the same for all the bubbles no matter their dimensions.
9. After calcite deposition ceases, over the bubbles the process still going on is the slow capillary upwelling of water from the cup to the free surface, where evaporation lasts until water is available. During this period, the drying out of the calcite bubbles may cause cracks in their surface and also the breakdown of those not perfectly developed.
10. When all the water and mud left by the flood is died up no further evolution of the speleothems (calcified mud and bubbles) is possible. From this moment on the cave bubbles are “frozen” until a new flood destroys them and new bubbles evolve (from step 2).

The complexity of the boundary conditions, and of the process leading to the development of the calcite bubbles in a gypsum cave, can explain why these speleothem are so rare. Maybe these formation are fairly more common, but their fragility avoid them from being seen even few weeks after their growth.

In our opinion the condensation-corrosion is the main agent for the demolition of the cave bubbles. In fact condensation water, carrying CO_2 (due to the diffusion from the cavern atmosphere) and no $CaCO_3$ at all, is always aggressive toward calcite.

Condensation over the bubbles brings aggressive water in contact with the very thin film of calcite, which is rapidly corroded causing the collapse of the whole bubble.

3. Final Remarks

The recently discovered calcite bubbles of the Grotta Grande dei Crivellari and Abisso Fantini are a clear example of the complexity of the physico-chemical processes that can be active within a gypsum cave.

The main reason why they were never observed before is because they tend to be destroyed few days or weeks after their development.

Until now it was commonly accepted that the few speleothems growing in the gypsum environment were well known and there was no chance to find a new one.

The newly discovered cave bubbles show that gypsum caves, even those explored and studied for a least a century, may still be very interesting places to search for new speleothems.

References

Forti P, Chiesi M, 1995. A proposito di un particolare tipo di calcite flottante osservato nella Grotta Grave Grubbo – CB 258 (Verzino, Calabria). Atti e Mem. Comm. Boegan 32, 43–53.

Forti P, Lombardo N, 1998. I depositi chimici del sistema carsico Grave Grubbo – Risorgente di Vallone Cufalo (Verzino, Calabria). Memorie dell'Istituto Italiano di Speleologia s. 2, 10, 83–92.

Forti P, Rabbi E, 1981. The role of CO_2 in gypsum speleogenesis: I° contribution. Int. J. of Speleol. 11, 207–218.

Hill CA, Forti P, 1997. Cave Minerals of the World. National Speleological Society, Huntsville.

STRONTIANITE FROM SERIZJAN CAVE (IRAN): A NEW OCCURRENCE OF THIS RARE CAVE MINERAL WITH A DISCUSSION ON ITS GENESIS

José Maria Calaforra[1], Jo De Waele[2], Paolo Forti[2], Ermanno Galli[3], Masoud Ebadi[4]

[1]Water Resources and Environmental Geology Research Group, Department of Hydrogeology and Analytical Chemistry, University of Almería, Crta. Sacramento s/n, 04120 La Cañada de San Urbano, Almería, Spain, jmcalaforra@ual.es

[2]Italian Institute of Speleology, Department of Biological, Geological and Environmental Sciences, University of Bologna, Via Zamboni, 67, 40126 Bologna, Italy, paolo.forti@unibo.it; jo.dewaele@unibo.it

[3]Department of Earth Sciences, University of Modena and Reggio Emilia, Largo S. Eufemia 19, 41121 Modena, Italy, gallier@unimore.it

[4]Basic Researches on Water Resources, Fars Regional Water Authority, Eram street, Shiraz, Iran, masoudebadi2011@gmail.com

Strontianite is a very rare cave mineral, up to now found in only two caves respectively in Spain and in the USA. The discovery of dissolution pockets and fractures filled with almost pure strontianite in a small cave in Iran has allowed us to investigate in detail the minerogenetic mechanisms that have brought to its formation in a carbonate karst environment.

1. Introduction

So far only two strontium minerals are known from the cave environment (Hill and Forti 1997; Onac and Forti 2011): celestite ($SrSO_4$) and strontianite ($SrCO_3$). The sulphate of strontium (celestite) is rather common in caves, and its genesis is often related to the presence of upwelling hydrothermal fluids (García-Guinea et al. 2002), the transformation of anhydrite into gypsum (García Ruiz et al. 2007; Panieri et al. 2008), and/or aragonite into calcite (Helz and Holland 1965). The carbonate of strontium (strontianite) is very rare in the carbonate cave environment, being reported from only two caves in the world: Sima de las Fumarolas, Granada, Spain (Fernandez Rubio et al. 1975), and in a small nameless cave in the Terrace Mountains in the United States of America (Hill and Forti 1987). In the American case all we know is that strontianite occurs in euhedral crystals on the cave walls, but nothing is known about its genesis. In the Spanish case a detailed description is given: strontianite occurs together with gypsum and celestite, but in pure aggregates. Its genesis in this case was attributed to the rising of thermal fluids that dissolved gypsum and celestite, both of thermal origin, and the reaction with fluids rich in carbonates, calcium and strontium.

Recently strontianite has been discovered in a small cave close to the village and dam site of Tangab, in Iran. This new occurrence has allowed for a better description of a possible genesis of this mineral in a carbonate karst environment.

2. The Serizjan Cave

The study area is a typical anticline of the Zagros Mountain range (the Podenow anticline), located approximately 80 km southeast of Shiraz and 15 km north of Firoozabad (central-southern Iran) (Fig. 1). The Podenow anticline is cut by the Firoozabad River forming the Tangab Gorge, in which narrowest part a dam is under construction (Karimi et al. 2005; Mohammadi and Raeisi 2007). The core of the anticline is composed of Oligo-Miocene limestones of the Asmari Formation, confined between the less permeable Pabdeh Gurpi (Paleocene-Oligocene marls, shales and marly limestones) and Razak (Lower Miocene silty marls and limestones with gypsum beds) Formations. The contact with the Razak Formation is transitional and can show appreciable pemeability.

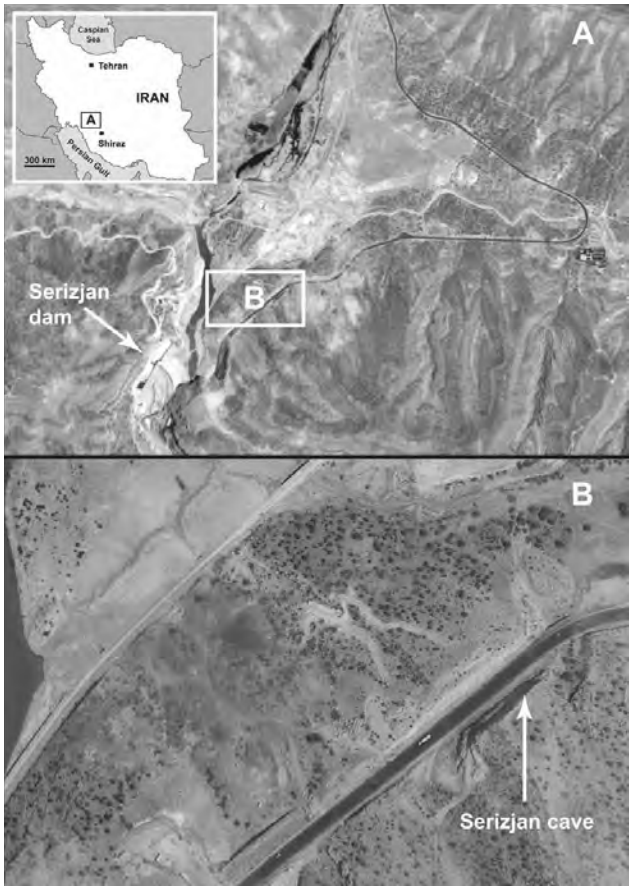

Figure 1. Index map for Serizjan Cave: A: the area of the Serizjan Dam, B: the location of the Serizian Cave.

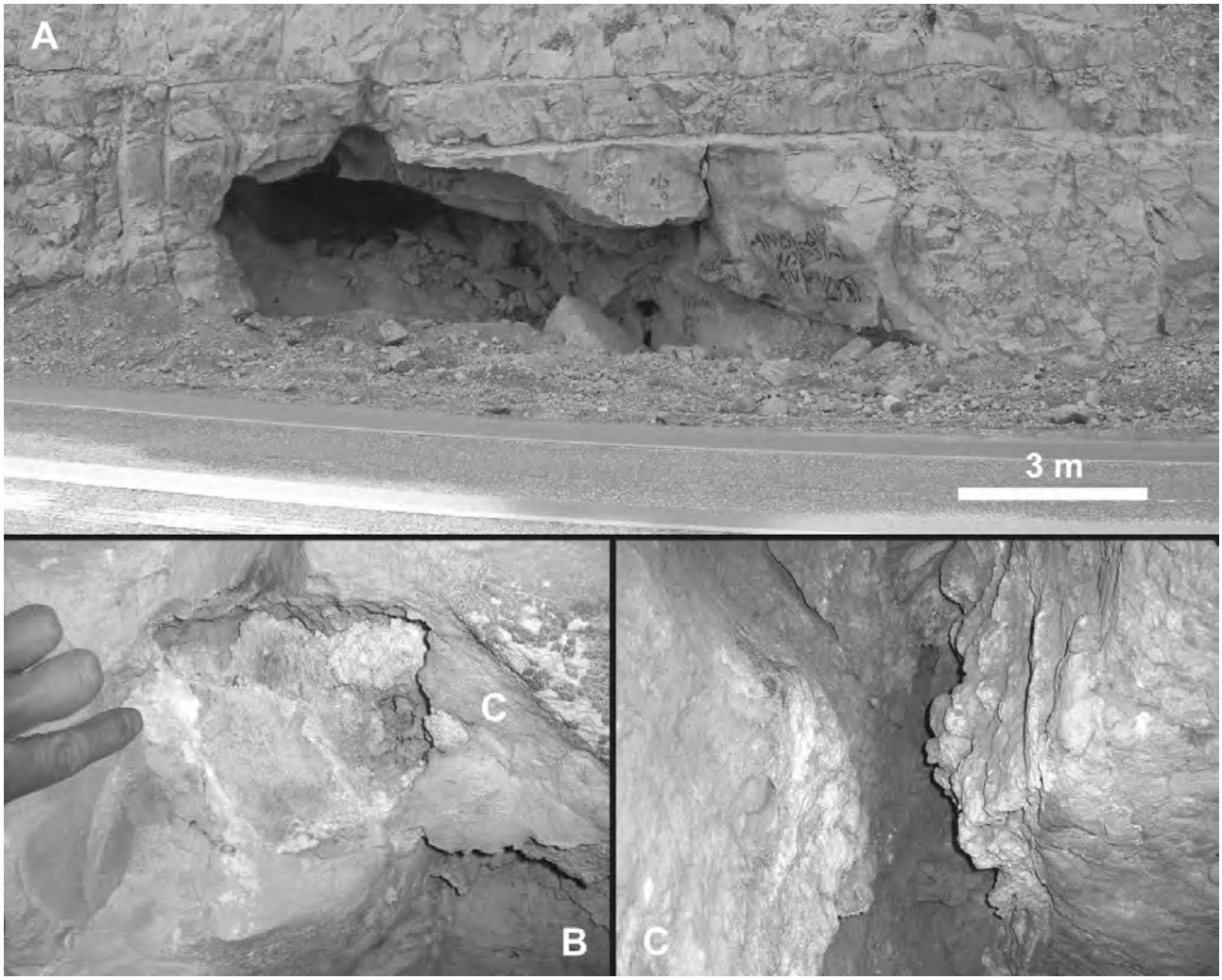

Figure 2. A: The entrance of the Serizjan Cave has been partially widened by the road construction; B: a corrosion pocket in the wall partially filled by strontianite; C: strontianite linings over a vertical partially widened fracture.

There are two caves on the northern flank of the Podenow anticline, both carved in Asmari limestone: Homouk and Serizjan (or Sarizijhon). Both caves are located on the left bank of the Firoozabad River respectively 100 and 500 m upstream of the gorge (Karimi et al. 2005). Serizjan Cave is the most important of the two, having a development of 180 m (Raeisi and Laumanns 2003). It is composed of a 15 m wide and 4–5 m high room, opened by the road cut (Fig. 2A), entering the flank of the mountain for about 15 meters. To the right some narrow shafts have been explored by Iranian cavers (Karimi 1998; Karimi et al. 2000).

During a short visit in 2012 – on the right walls of the first room, some pockets filled with a white powderish material (Fig. 2B) and some harder 2–3 cm thick white crusts covering the walls of a fracture clearly enlarged by dissolution (Fig. 2C) were discovered and sampled. Nowhere in the visited parts of the cave were calcium carbonate speleothems seen. The analysis of this material by XRD diffraction at the "Laboratorio Grandi Strumenti" of University of Modena and Reggio Emilia have confirmed it to be totally composed of strontianite.

A further analysis of the peaks from different XRD diffractions proved that the chemical composition of the strontianite of Serizjan Cave varies from crystal to crystal, always being a solid solution where the Ca^{2+} ion substitutes for the Sr^{2+} ion, with a Ca/Sr ratio ranging from 9.7 to 16.2%.

Scanning Electron Microscope analysis performed in the same laboratories has shown this mineral to be composed by small aggregates of acicular crystals (Fig. 3A, B), a few of which have an hollow structure (Fig. 3C), while most are characterized by hopper-like structures on their external surfaces (Fig. 3D).

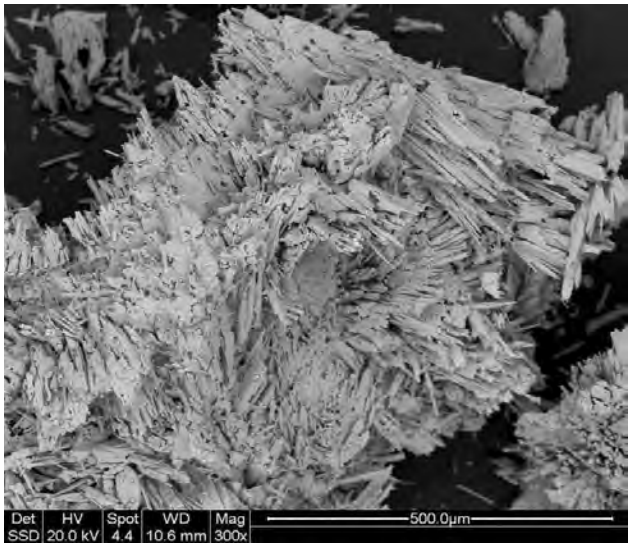

Figure 3A. SEM image of an aggregate of strontianite.

Figure 3B. A group of strontianite crystals.

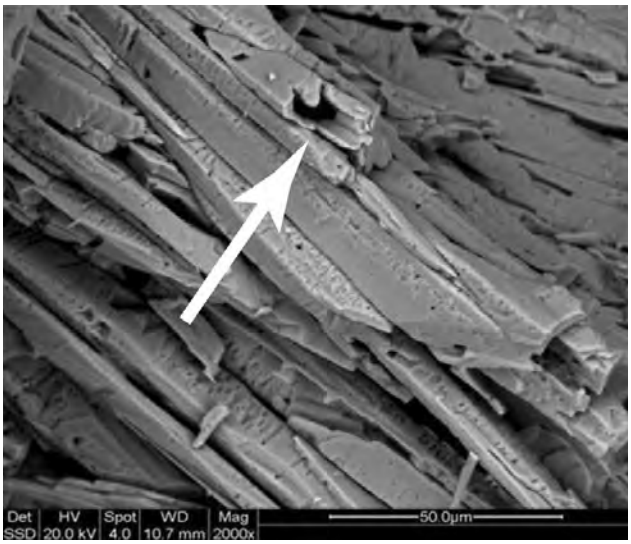

Figure 3C. A hollow crystal of strontianite.

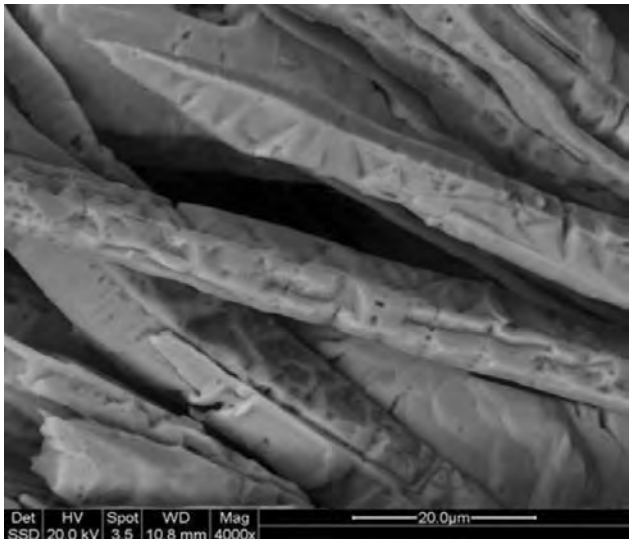

Figure 3D. The hopper-like surfaces of the strontianite crystals.

3. How and when may strontianite develop as a cave mineral?

The presence of the cation Sr^{2+} in waters circulating in the carbonate karst environment is rather common, leading to the widespread formation of celestite in caves (Hill and Forti 1997). Sr^{2+} is easily found as a trace element in both carbonate and evaporite rocks, substituting Ca^{2+} in gypsum and calcite. Recently the presence of Sr^{2+} in water has been studied in relationship to the diagenesis of minerals involving the transformation of a mineral able to host certain quantities of Sr^{2+} into other minerals whose crystalline lattice can hold far less Sr^{2+}. Examples of such transformations are anhydrite in gypsum and aragonite in calcite (Helz and Holland 1965; García Guinea et al. 2002; García Ruiz et al. 2007).

Despite the availability of Sr^{2+} in cave waters, why does celestite precipitate in almost all cases, while only very rarely does strontianite form? From a chemical point of view strontianite is far less soluble in pure water (solubility product $K_{sp} = 10^{-9}$) than celestite ($K_{ps} = 10^{-6.5}$), so in theory strontianite should precipitate much earlier than celestite. In practice, however, strontianite is a carbonate, thus its solubility in nature, similar to what happens with $CaCO_3$, is strongly related to the presence of CO_2 according to the well-known equation:

$$SrCO_3 + CO_2 + H_2O = Sr^{2+} + 2HCO_3^-$$

So in waters in contact with the atmosphere (with a partial pressure of CO_2 of around 350×10^{-6} atm), the solubility of strontianite reaches around 0.011 g L^{-1}, only about ten times less than that of celestine (0.13 g L^{-1}) (Fig. 4).

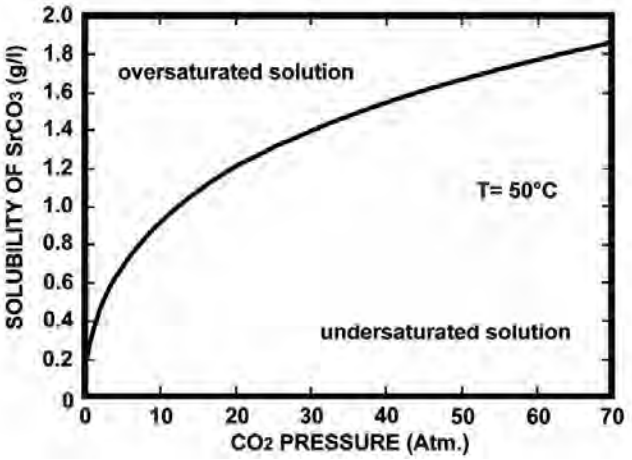

Figure 4. Strontianite solubility (after Helz & Holland 1965).

But the average concentration of dissolved CO_2 in karst waters is often much higher than that of the air, and can reach values of 10^{-2} to 10 atm in thermal waters (Capasso and Inguaggiato 1998). Consequently, in nature, the real solubility of strontianite is almost always higher than that of celestite. Additionally, the solubility of strontianite varies considerably with the temperature of the water, reaching in hot waters in contact with the atmosphere values of 0.65 g L^{-1} (Busenberg et al. 1984) while that of celestite remains substantially the same (0.14 g L^{-1}). So in thermal environments, that are also the richest in Sr^{2+}, the formation of strontianite becomes even more difficult to explain.

It is also obvious that in an environment rich in SO_4^{2-}, such as in evaporitic sequences, strontianite has no chance to form, since the precipitation of celestite will be advantaged. Also in a carbonate environment, if SO_4^{2-} anions are present, celestite will precipitate immediately. And in nature SO_4^{2-} is a common constituent of waters circulating in carbonate karst areas, deriving from different sources such as:

1 – oxidation of sulfides (e.g., pyrite) in the rock; 2 – dissolution of nearby evaporite rocks; 3 – oxidation of H_2S in the O_2-rich cave environment in (thermal or connate) waters rising from depth; and 4 – mineralization of guano or other organic material (Hill and Forti, 1997).

But if SO_4^{2-} is present in very small concentrations or if it is absent, the formation of strontianite remains very difficult. To allow the precipitation of strontianite the ratio between the concentration in solution of Sr^{2+} and Ca^{2+} (m_{Sr}/m_{Ca}) has to be higher than that observed in nature (Helz and Holland 1965).

So the deposition of strontianite in a cave is an extremely rare event that requires a combination of absolutely special and unusual conditions. One of the conditions that can allow for the genesis of strontianite is the transformation of celestite in an alkaline hydrothermal environment (Suárez-Orduña et al. 2007), but these conditions are extremely difficult to achieve in a carbonate cave.

In limestone caves three conditions have to be met to allow for the formation of strontianite: 1) enrichment of karst waters in Sr^{2+}, 2) absence of SO_4^{2-}, and 3) establishment of a high Sr/Ca ratio.

The first condition is easily met thanks to one of the Sr-enriching mechanisms explained earlier. However, this contemporarily enrichment causes a direct (dissolution of celestite) or indirect (oxidation of metal sulfides) increase in SO_4^{2-} in the solution, inhibiting the formation of strontianite. It is thus necessary that this enrichment of Sr^{2+} in solution be accompanied by the simultaneous or slightly delayed removal of SO_4^{2-} from the solution. This can happen in two ways: 1) formation of minerals that are less soluble than celestite, or 2) reduction of sulfate into sulfide. The first mechanism is easily encountered in nature when cations such as Ba can cause the precipitation of insoluble barite, while reduction can be triggered by the presence of organic material that – oxidizing in an O_2-depleted environment – reduce sulfate into sulfide. Both reactions can occur in carbonate karst environments, but their concurrent action is very rare, so most of the time celestite is deposited.

It is important to underline that in the case of Sima de las Fumarolas strontianite, although prevalent in many samples, is not the only phase, and is most of the time associated with gypsum and celestite (Fernandez Rubio et al. 1975). This demonstrates that the removal of SO_4^{2-} from the solution has not always been complete, and the final products have first been gypsum and celestite, bringing SO_4^{2-} concentration to zero, and only later strontianite that can also have formed by the transformation of the earlier-formed celestite. In Serizjan Cave the strontianite is relatively pure, so the removal of SO_4^{2-} appears to have been complete before the deposition of strontianite from solution.

If the first two conditions are satisfied, then a third condition has to be reached before strontianite can form in a carbonate environment. The ratio of Sr/Ca has to be greater than 0.1 at 25 °C (Helz and Holland 1965), a condition at which both calcite and strontianite are saturated.

From the chemical point of view there are two ways to reach this high Sr/Ca ratio: 1) a cooling of the solution saturated in calcite and strontianite or 2) a drastic decrease in Ca in the solution accompanied by an important increase in Sr.

The first case is the one that normally allows the deposition of strontianite in a hydrothermal environment. The cooling of the fluid influences the solubility of calcite and strontianite in an opposite way increasing that of calcite and lowering that of strontianite. If no other processes take place, a solution saturated in both minerals at 150 °C, cooled down to 25 °C in a carbonate environment, causes a slight dissolution of the limestone and a great deposition of strontianite, since the Sr/Ca ratio changes from 0.6 (equilibrium value at 150 °C) to 0.1 at 25 °C (Helz and Holland 1965).

The other mechanism does not require the presence of thermal waters, although their presence would boost the efficiency in the case that the waters are initially undersaturated with respect to strontianite. When karst waters arrive close to the epiphreatic or vadose zone, the CO_2 is released from solution to the cave atmosphere, thus causing calcium carbonate to precipitate. This leaves only strontium carbonate in solution, and if continuous release of CO_2 occurs, the solution can reach supersaturation. The precipitation of strontianite at this point will cause a further decrease in CO_2 in solution, thus slowing down the process. To efficiently cause the formation of strontianite there is the need of another important process: evaporation.

However, if this last mechanism is the one causing the precipitation of strontianite, it would be logical to find this mineral covering calcium carbonate speleothems. In Serizjan Cave strontianite is deposited directly upon the calcite bedrock, and nowhere has calcite or aragonite speleothems been observed. It is thus necessary to conclude that the precipitation of calcite and/or aragonite has taken place in a different place respect to where strontianite formed. This fact can be explained by considering that calcium carbonate previously formed in the epiphreatic zone, and that the place where strontianite was deposited is only occasionally reached by flood waters supersaturated only in strontianite, and containing no calcite nor aragonite. Even though this mechanism of formation of strontianite cannot be completely rejected for the case of Serizjan Cave, these extremely restricted conditions make the formation of strontianite in a non-thermal environment extremely improbable. The fact that there are some corrosion forms that seem to indicate slightly thermal conditions in the cave (e.g., solution pockets) makes it more credible to link the formation of strontianite to the final cooling phases of a thermal fluid. The relatively scarce imprint of very clear thermal morphologies in the cave can be related to the fact that the thermal waters, at the time of their circulation in this part of Serizjan Cave, was only characterized by convective motion and did not leave the cave. These waters, already cool and supersaturated with respect to strontianite, were saturated (or only slightly aggressive) towards calcite, thus they had no possibility to develop clear corrosion forms.

4. Final remarks

The presence of pure strontianite inside some solution pockets or an enlarged fracture in the walls of Serizjan Cave, a carbonate cave in SW Iran, can only be explained by the circulation of low temperature thermal waters. Under these conditions the thermal fluids – initially saturated in calcite and undersaturated in strontianite – cooled and turned corrosive towards the limestone, thus becoming supersaturated respect to strontium carbonate. To definitively verify this genetical hypothesis, further analyses and more detailed observations are required – not only inside Serizjan Cave, but also in the Sima de las Fumaroles and in the cave in the Terrace Mountains.

Acknowledgments

Many thanks to Dr. Mohammed Gohari, director of the Karst Research Institute in Shiraz, who helped us with many logistical problems in Iran. The authors thank Bogdan P. Onac and Carol A. Hill for their careful revision of the manuscript.

References

Ashjari J, Raeisi E, 2006. Influences of anticlinal structure on regional flow, Zagros, Iran. Journal of Cave and Karst Studies, 68(3), 118–129.

Busenberg E, Plummer LN, Parker VB, 1984. The solubility of strontianite ($SrCO_3$) in CO_2-H_2O solutions between 2 and 91 °C, the association constants of $SrHCO_3^+$ (aq) and $SrCO_3^0$ (aq) between 5 and 80 °C, and an evaluation of the thermodynamic properties of Sr^{2+} (aq) and $SrCO_3$ (cr) at 25 °C and 1 atm total pressure. Geochimica et Cosmochimica Acta, 48(10), 2021–2035.

Capasso G, Inguaggiato S, 1998. A simple method for the determination of dissolved gases in natural waters. An application to thermal waters from Vulcano Island. Applied Geochemistry, 13(5), 631–642.

Forti P, Menichetti M, Rossi A, 1989. Speleothems and speleogenesis of the Faggeto Tondo cave (Umbria, Italy). Proc. 10th Int. Congr. Speleol., Budapest, 1, 74–76.

Fernandez Rubio R, Eraso Romero A, Ortega Huertas M, Arana Castillo R, Rojas Pacheco E, 1975. Estudio de la Sima termal de las Fumarolas (Montevives, Granada, España). Annales de Spéléologie, 30(2), 287–302.

García Guinea J, Morales S, Delgado A, Recio C, Calaforra JM, 2002. Formation of gigantic gypsum crystals. Journal of the Geological Society, 159, 347–350.

García Ruiz JM, Villasuso R, Ayora C, Canal A, Otalora F, 2007. Formation of natural gypsum megacrystals in Naica, Mexico. Geology, 35(4), 327–330.

Helz GR, Holland HD, 1965. The solubility and geologic occurrence of strontianite. Geochimica et Cosmochimica Acta, 29(12), 1303–1315.

Karimi H, 1998. Hydrogeological and hydrochemical evaluation of springs and piezometers of Podenow anticline, Firoozabad. University of Shiraz, M.Sc. thesis, 527.

Karimi H, Raeisi E, Zare M, 2000. Hydrogeological investigation and formation mechanism of Serizjan cave, Firoozabad. Abstract, 4th Conference of Geological Society of Iran, Shiraz.

Karimi H, Raeisi E, Zare M, 2005. Physicochemical time series of karst springs as a tool to differentiate the source of spring water. Carbonates and Evaporites, 20(2), 138–147.

Mohammadi Z, Raeisi E, 2007. Hydrogeological uncertainties in delineation of leakage at karst dam sites, the Zagros Region, Iran. Journal of Cave and Karst Studies, 69(3), 305–317.

Onac BP, Forti P, 2011. State of the art and challenges in cave minerals studies. Studia UBB Geologia, 56, 33–42.

Panieri G, Forti P, Gasparotto G, Soliani L, 2008. Studio delle inclusioni solide presenti nei cristalli di gesso della Grotta delle Spade (Naica, Messico). Congresso Nazionale di Speleologia, Iglesias 2007, Memorie dell'Istituto Italiano di Speleologia, II(21), 150–158.

Raeisi E, 2004. Iran cave and karst. In Encyclopedia of Cave and Karst (Gunn J, ed.), New York, Fitzroy Dearborn: 460–461.

Raeisi E, Laumanns M, 2003. Cave directory of Iran, 2nd edition. Berlin, Berliner Hohlenkundliche Berichte, 37, 1–101.

Suárez-Orduña R, Rendón-Angeles JC, Yanagisawa K, 2007. Kinetic study of the conversion of mineral celestite to strontianite under alkaline hydrothermal conditions International Journal of Mineral Processing, 83(1–2), 12–18.

SKELETON CRYSTALS OF CRYOGENIC GYPSUM FROM KUNGUR ICE CAVE, URAL MOUNTAINS, RUSSIA

Olga Kadebskaya, Ilya Tchaikovsky
Mining Institute of Ural Branch of Russian Academy of Sciences – Sibirskaya78a – 614007 Perm, Russia; icecave@bk.ru

Investigation of new cryogenic formations from the Kungur Ice Cave allowed identifying, for the first time, unusually large individual crystals of gypsum, some reaching 5 mm or more. The main influencing factor in the formation of the new gypsum crystals is the microclimate of karst cavity. The cave is being the laboratory where the processes of modern formation of minerals (cryogenic among them) can be observed. The variety of forms existence of water (liquid, ice, vapor), the character of air moving and thermal regime are defined by diversity of microclimatic zones and geochemical barriers. All these conditions specify such a wide variation of crystallomorphological features of newly formed cryogenic gypsum. The mineral component was filtered from the liquid water and studied (morphology and chemical composition) with a scanning electronic microscope (SEM) VEGA 3 LMH with a system of the x-ray energy-dispersive microanalysis INCA Energy 350/X-max 20. It was found that most of the subindividuals within aggregates are twins with a complex skeleton structure. The skeleton structure of gypsum individuals is determined by presence of internal partitions, oriented according to the faces of two or three pinacoids ({010}, {100}, {001}) and two prisms ({120} {111}), that is, parallel to the faces defining crystal shape. Such formations of mineral objects have not been observed before and this paper discusses the most possible mechanisms responsible for their formation.

1. Introduction

The Kungur Ice Cave is located in Eastern Europe on the outskirts of the old Russian town of Kungur. In physiography terms, the region surrounding the cave area lies in the Eastern part of the Russian (East European) plain and is limited to the juncture of two geographical areas – the High Trans-Volga (Zavolzhye) and the Ufa plateau. The region is often called Pre-Urals due to its proximity (about 100 km) to the Ural Mountains.

The cave is widely known in Russia and abroad as the most interesting speleological tourism attraction, as a kind of "visiting card" of the Perm Krai. Over 5 million tourists have visited the cave since the early XXth century. In the last 5 years, annual attendance is on average 90,000 people, but in the mid-1980s the number of tourists amounted to 200,000 people a year.

The cave has attracted keen interest of naturalists for about 300 years. It has been reviewed in about 100 popular and over 500 scientific publications. Detailed stationary geological, speleological, biological and other observations have been made there for the last 50 years.

2. Geography and geology

The Kungur Ice Cave has been developed in the interfluvial gypsum-carbonate massif, cut from the south by the major river Sylva and from the north by the Shakva River. The water regime, both in the past and in the present, is closely related to the Sylva River. The "Ledyanaya Gora" massif is a plateau-like, strongly karstified elevation, rising at 90–96 m above the river valley beds. The massif slopes are steep, with fragments of fractured terraces. The karst relief of the interfluvial plateau is notable for its morphological diversity. Density of karst forms on the Ledyanaya Gora ranges from 150–200 units in the watershed part of the plateau to 200–300 units in the slope and over 500 units per square kilometer in the selvedge of the massif (including the cave).

The massif and the cave act in all respects as a model of conjugated evolution of surface and subsurface forms of carbonate and sulphate karst. Unlike well-known gypsum caves of Europe (Germany, Spain, Italy, Poland and Ukraine) formed in the Trias and Miocene gypsum, the Kungur cave developped in the much older sulphate strata – those of the lower Permian section. Air circulation characteristics, cave morphology as well as regional climate are conducive to the formation and accumulation of different ice forms in the cave, including perennial ice (underground ice mounds). Due to more severe climatic conditions in the region and peculiarities of the cave air exchange with environment, underground ice persists in the cave year-round despite low hypsometric marks of the terrain (120 m above sea level) – in contrast to East European ice caves, located from 969 m (Dobshinskaya Ice cave) to over 1,100 m above sea level (e.g., Eiseriesenwelt, Scărișoara and others).

The cave constitutes a fairly special environment for mineral formation, which is characterized by:

- mainly sulphate, less so carbonate, lithologic background of the cave host rocks (gypsum, anhydrite, dolomite, limestone, and clay);
- abundant moisture (infiltration of rain, surface snow melt and groundwater, underground lakes, periodic floodwater with suspension, condensation moisture, etc.);
- in general cool (0 to +4 °C) and cold (below 0 °C) air temperatures;
- microclimatic inhomogeneity manifested in the air temperature zonality, seasonal migration of microclimatic zones, and vertical stratification of the air column;

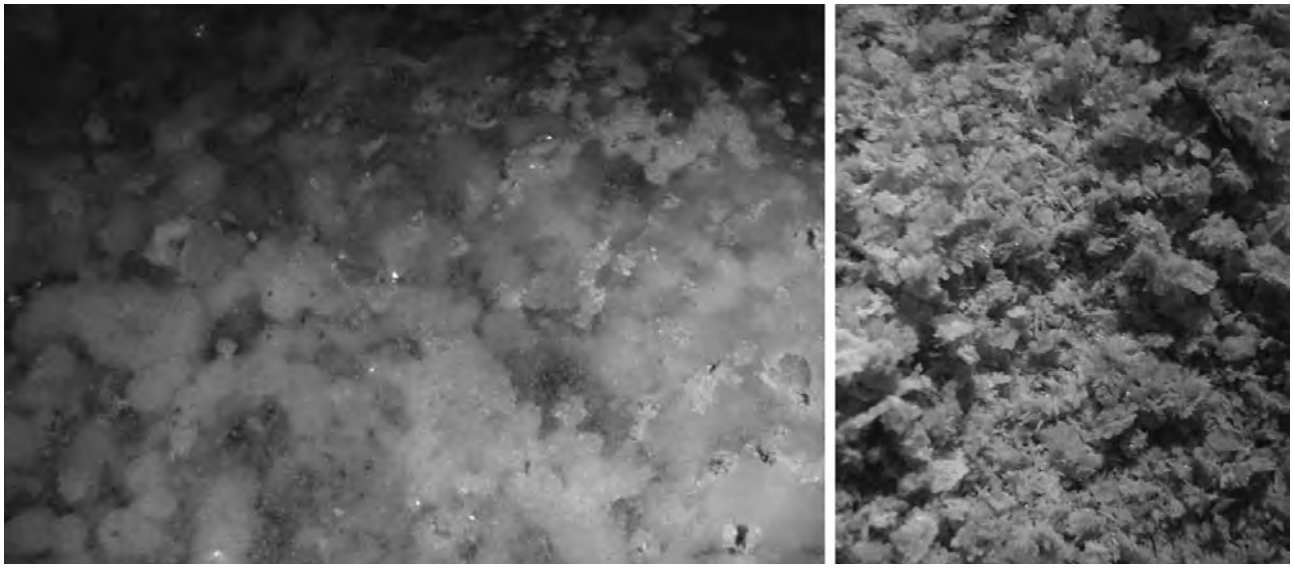

Figure 1. Cryogenic gypsum from the Grotto Pervy, frozen in the ice in summer and released by sublimation of ice during winter.

- considerable amounts of underground ice, especially in the winter-spring time, and thermal instability of climatic conditions, particularly in off-season time (spring and autumn), which brings about changes in the phase state of water;
- penetration (from the surface – through the sinks) of clastic, argillaceous and soil materials containing fair quantity of organic matter.

The above conditions in the cave predetermine considerable variety of conditions and factors of mineral formation, the most important and interesting of which seems to be the cold setting favorable to the formation of cryogenic mineral formation.

3. Methods

The mineral component was filtered from the liquid water and examined (morphology and chemical composition) with a scanning electronic microscope VEGA 3 LMH with a system of the x-ray energy-dispersive microanalysis INCA Energy 350/X-max 20.

4. Results and discussion

The first cryogenic gypsum in karst cavities was decribed by Polyakov (1880) and Fedorov (1884) as "gypsum flour" on the surface of ice in the Kungur Ice Cave.

Recent studies of the cave (Andreychuk and Galuskin 2001) showed that "flour", sampled between the Brilliantovy and the Polarny grottoes, consists of two morphological types of gypsum aggregates. The first one is represented by individual crystals and their parallel intergrowths, up to 300–400 μm large. The presence of case-like individuals was interpreted as the result of an interrelated formation of gypsum and ice crystals. The second type of aggregates (size 50–100 μm) – crystalline crusts (with signs of spherulitic growth) – is predominantly perpendicular to the ice surface. Formation of gypsum was associated with the crystallization in thin layer of water on the ice surface, and the accumulation of "flour" – with its release during ice evaporation.

Investigation of cryogenic formations from the Grotto Pervy allowed identifying unusually large crystal individuals of gypsum, some reaching 5 mm or more, which has never been noted before. Their formation was associated (Tchaikovsky and Kadebskaya 2009) with multi-seasonal temperature fluctuations, followed by

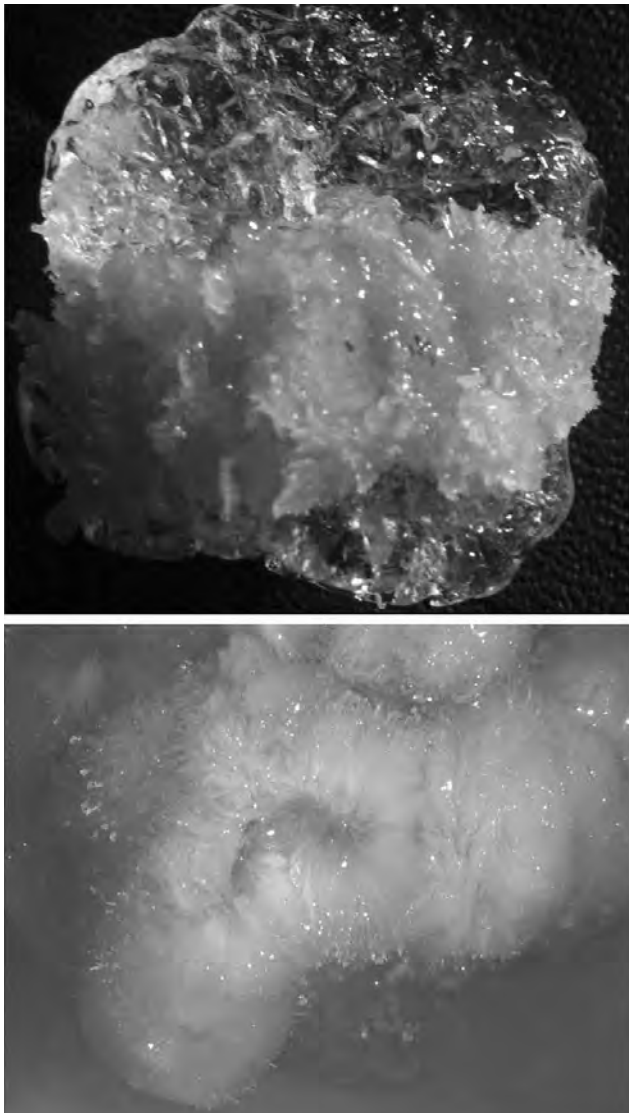

Figure 2. Interlayer enriched with aggregates (2–5 mm) and spherulites (3–6 mm) of gypsum in ice.

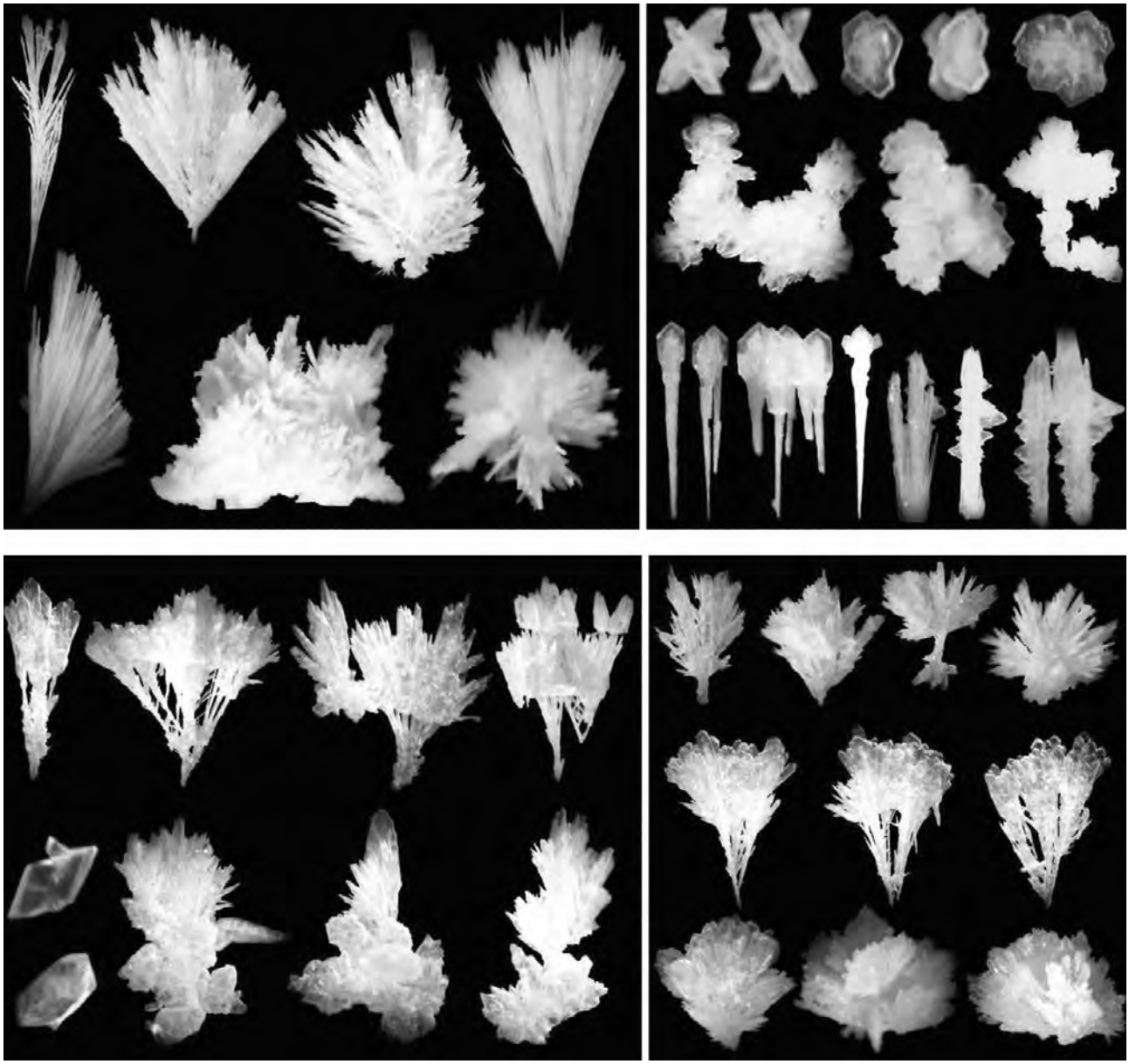

Figure 3. Aggregates (2–5 mm) consisting of needle and fan-shaped subindividuals, single crystals of gypsum and their aggregates from the Grotto Pervy.

recrystallization of both ice and gypsum material, according to the mechanism proposed by Dorofeev (1966). He believed that the large "flakes" are connected with recrystallization of wet microcrystals ("flour"). The specificity of the Grotto Pervy, in contrast to the other parts of the cave, is in the cold temperatures maintained throughout the year, rapid freezing of the infiltration and floodwater coming in the Grotto during spring and summer, and intensive evaporation in winter, due to the high velocity of the air coming through the entrance tunnel and the old entrance.

Thus, cryogenic gypsum hides under a layer of ice by late summer and accumulates again on its surface by spring.

The cryogenic gypsum morphology study under a binocular microscope has found that its aggregates are composed of needle subindividuals that form three-dimensional or flat formations, similar to a fan (Fig. 3). Conventional tabular microcrystals (size 0.2–0.5 mm) of gypsum were observed as separate individuals, as well as intergrown with split aggregates. It was noted that the microcrystals could both grow on aggregates and serve as seeds for the latter. These relationships suggest alternating normal smooth face growth with the split one, related to strong supersaturations, what comports with the concept of repeated recrystallization of gypsum material. Registered were both relatively simple aggregates and zonal ones, formed by three (annual) generations.

Fundamentally new information was obtained by the investigation of these structures with a scanning electron microscope VEGA 3 LMH with the X-ray energy dispersive microanalysis INCA Energy 350/X-max 20. It was found that most of subindividuals within aggregates are twins with a complex skeleton structure (Fig. 4).

The skeleton structure of gypsum individuals is determined by the presence of internal partitions, oriented according to the faces of two or three pinacoids ({010}, {100}, {001}) and two prisms ({120} {111}), that is, parallel to the faces defining crystal shape.

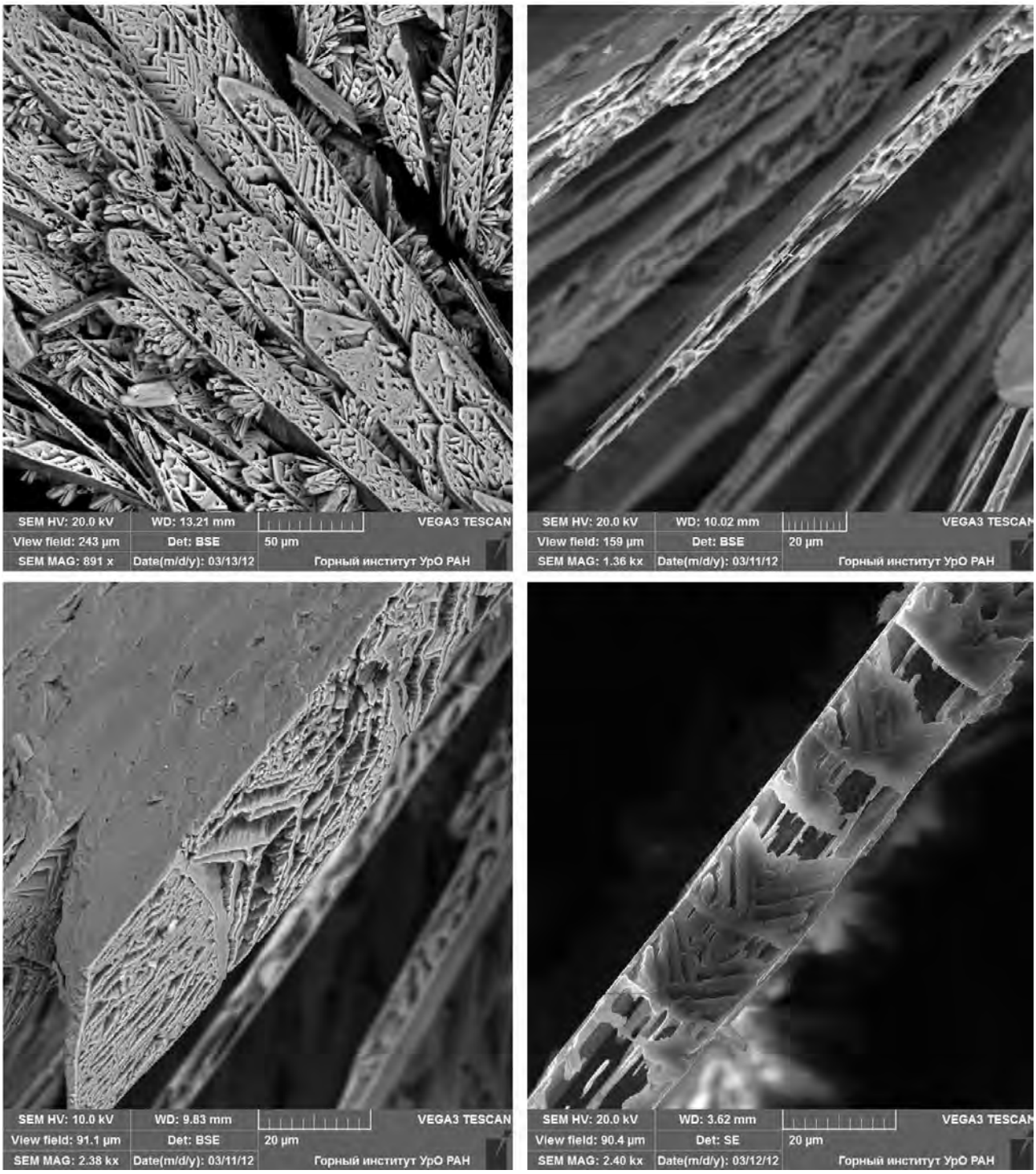

Figure 4. The internal skeleton structure of crystals caused by the presence of partitions oriented parallel to the faces.

5. Conclusions

Unusually large cryogenic formations of gypsum, some reaching 5 mm or more, were found in the Grotto Pervy of the Kungur Ice Cave. Their examination found that most of subindividuals are twins with a complex skeleton structure, determined by internal partitions, oriented according to the faces. Such formations of mineral objects have not been observed before. Several mechanisms may be suggested to explain their nature.

1. It is known (Wallace 1946) that gypsum dissolution, in the absence of sodium chloride, is proceeded with release of heat and, therefore, the growing gypsum individual has to create a zone of supercooling around itself during crystallization. This effect should be particularly strong on the fast-growing faces of the prism. Perhaps, it is this phenomenon that causes the growth of a certain portion of ice, which blocks normal growth for a certain time. That is, the skeleton crystal is the result of the alternating growth of gypsum and ice.
2. Most skeleton individuals are twins. Under rapid supersaturations, there might be an accelerated growth along the most energetically favorable twin seams and a delayed growth along other faces, which creates chamber structure of crystals.
3. The most unlikely formation scenario for such individuals is the disintegration of the solid solution of

calcium sulphate which contains more than two molecules of water. However, chemists or mineralogists have not yet known such a compound.

Identification of the reasons for such individuals formation may hold the key to create the innovative construction materials through the use of cold.

References

Andreychuk V, Galuskin E, 2001. Cryogenic mineral formations of the Kungur Ice Cave. Caves: Univ. Perm, 27–28, 108–116.

Dorofeyev E, 1966. Calcite films and crystals of gypsum in the Kungur Ice Cave. Caves: Perm. Univ. Perm, 6 (7), 39–47.

Tchaikovsky II, Kadebskaya OI, 2009. Cryogenic gypsum of Kungur Ice Cave. Problems of Mineralogy, Petrology and Metallogeny. Col. of articles. Perm. Univ. Perm, 12, 85–90.

Polyakov IS, 1880. Anthropological trips to Central and Eastern Russia. Notes of the Anthropological Society. St-Petersburg, Encl. to vol. 37, 12 p.

Fedorov YeS, 1884. Observations in Kungur Ice cave. Notes of the Mineralogical Society. The 2nd series, 19, 191 pp.

Wallace WE, 1946. Heats of Solution and Dilution of Calcium Sulfate Dihydrate in Aqueous, Sodium Chloride Solutions. J. Phys. Chem., 50 (2), 152–168.

ALLOPHANE MOONMILK FROM A GRANITE-GNEISS CAVE IN NORWAY: A BIOGENIC INTERMEDIATE IN DEEP WEATEHRING?

Stein-Erik Lauritzen
Department of Earth Science, Bergen University, Allegaten 41, N-5007 Bergen, Norway, Stein.lauritzen@geo.uib.no

The first occurrence of allophane as a speleothem-forming cave mineral in Norway is reported. It occurs in a fissure cave developed in granitic gneiss and appears to be formed by CO_2 degassing (or microbiological action) from acidic seepage water originating from humic ponds and small bogs on the surface above the cave.

1. Introduction

Previous studies of cave minerals in Norway have revealed calcite as a moonmilk-forming mineral (Onac and Lauritzen 1995). Recently, we have initiated a geobiological investigation of moonmilk deposits in karst caves in the country, including the classic location of Høeg (1946) where cyanobacteria were first detected in moonmilk. In this communication, a deviant example of non-carbonaceous moonmilk from a non-karstic location is presented, where allophane is a probable candidate.

2. Observations

During a mapping project of fissure and marine abrasion caves in the Brønnøy area, Northern Norway (Fig. 1), a massive moonmilk deposit was located in a pseudokarst cave. The fissure (*"Svarthola2"*) is developed in granitic gneiss (Lauritzen et al. 2011) along vertical fissures. The caves display features of chemical weathering (tafoni) as well as marine abrasion (polished rocks and allogenic rounded boulders). Fine-grained, sticky clays of pale pink to light brown colors are found inside tight terminations of the guiding fractures. In a side-passage, where wall morphology is dominated by mechanical breakdown (frost or tectonic stress?) a large deposit of a soft, moonmilk-like mass is found covering both walls and ceiling of the vertical fissure. In contrast to the rest of the cave, which is essentially dry under normal weather, there is considerable seepage over the deposit (Fig. 2). It covers several square meters of the cave walls. On the sloping wall, it has micro-gour and runnel morphology; on the hanging walls, stalactitic morphology is found. Everywhere the mass appears wet and "fresh", no patches of hardened or dried-up material could be seen.

The material was sampled and investigated by scanning electron microscopy, EDX analysis of elemental composition, X-ray diffraction, and simple chemical tests. Upon acid treatment, there is no evolution of gas (CO_2), the material dissolves slowly in HCl to an opaque solution. Under SEM magnification, the material displays aggregates of rounded flakes, approximately 1–2 µm diameter (Fig. 3). The elemental composition suggests Si: Al approximately 1:2. There is a variable signal from carbon, but since there is no gas evolution by acid treatment, we suspect it stems from the conductive tape used in the mount or from organics within the material. The above-mentioned clay which appears to be derived from wallrock feldspar, displays a similar composition as the moonmilk (Si: Al = 1:2), but has a more crystalline appearance under SEM. Both materials lack the potassium present in the intact wallrock feldspar (Fig. 4). The XRD pattern shows no crystalline peaks.

Figure 1. Location of the Brønnøy area, North Norway.

3. Discussion

The situation in a "granite cave", macroscopic and microscopic appearance, elemental composition and amorphous nature from XRD analysis, suggests allophane as a likely candidate (Ramdohr and Strunz 1967). Allophane is well known from caves as a speleothem-forming mineral (Hill and Forti 1997), including moonmilk. It is also reported from non-karstic (granite) caves (Webb and Finlayson 1984, 1985; Finlayson and Webb 1985). The site has been subject to microbiological sampling and genome analysis. Results are pending.

Figure 2. The moonmilk deposit.

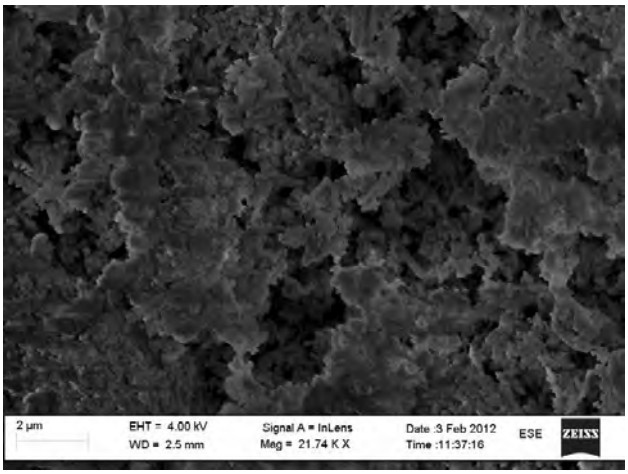

Figure 3. SEM image of the moonmilk. Aggregates of rounded flakes, approximately 1–2 µm diameter.

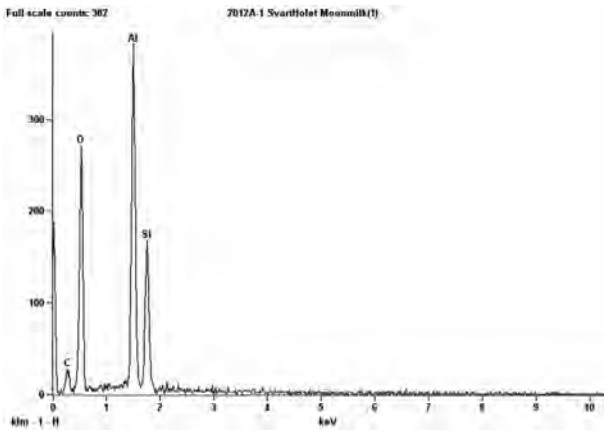

Figure 4. EDX analysis of the moonmilk-forming mineral.

4. Conclusions and future aspects

This is the first observation of allophane as a cave mineral in Norway and also as a moonmilk-forming material. It appears to be linked to and derived from the seepage water, which is originating from peat-rich ponds and small bogs on the surface above the cave. This may support the previously suggested formation mechanism of Webb and Finlayson (1984), where allophane is precipitated by CO_2 degassing from dissolved or colloidal alumina species, in part mediated by humic acids.

If mediated by microbiological processes, the formation of allophane might represent an intermediate stage in deepweathering of feldspar- and quartz-rich rocks, like the present granitic gneisses, where perhaps crystalline clays, like kaolinite, may be the end-product. A microbiological sampling program at the site was initiated in May 2012 to further investigate these possibilities.

References

Finlayson B, Webb BW, 1985. Amorphous speleothems. Cave Science, 12, 3–8.

Hill CA, Forti P, 1997. Cave Minerals of the World, 2nd ed. National Speleological Society, Huntsville, AL.

Høeg OA, 1946. Cyanophyceae and bacteria in calcareous sediments in the interior of limestone caves in Nord-Rana, Norway. Nyt Magasin for Naturvi-denskaperne, 85, 99–104.

Lauritzen SE, Nielsen JO, Stav BA, 2011. Kartlegginger i Torghatten, Brønnøy kommune: Torghatthullet og Svartholene. (Mapping in Torghatthullet and adjacent caves, Brønnøy, noth Norway). Acta Spelæologica Norvegica, 3, 57–76.

Onac PB, Lauritzen SE, 1995. On some cave minerals from Northern Norway. International Journal of Speleology, 24, 67–75.

Ramdohr P, Strunz H, 1967. Klockmann's Lehrbuch der Mineralogie, Ferdinand Enke Verlag, Stuttgart.

Webb BW, Finlayson B, 1984. Allophane and opal from granite caves in south-east Queensland. Australian Journal of Earth Sciences, 31, 341–349.

Webb BW, Finlayson B, 1985. Allophane Flowstone from newton Cave, western Washington state. National Speleological Society Bulletin, 47, 47–50.

CALCITE SPELEOTHEMS IN PSEUDOKARST TJUV-ANTES GROTTA, NORTHERN SWEDEN

Johannes E. K. Lundberg[1], Magnus Ivarsson[1], Therese Sallstedt[1,2], Rabbe Sjöberg[3], Juan Ramón Vidal Romaní[4], Love Dalén[1], Stina Höglund[5]

[1]Swedish Museum of Natural History, P.O. Box 50007, SE-104 05 Stockholm, Sweden, johannes.lundberg@nrm.se, magnus.ivarsson@nrm.se, therese.sallstedt@nrm.se, love.dalen@nrm.se

[2]Biologisk Institut, Syddansk Universitet, Campusvej 55, DK-5230 Odense M, Denmark

[3]Bodviksvägen 14, SE-913 42 Obbola, Sweden, rabbe.sjoberg@telia.com

[4]Instituto Universitario de Xeoloxia Isidro Parga Pondal, ES-15071 A Coruña, Spain, juan.vidal.romani@udc.es

[5]Stockholm University, Wenner-Gren Institute, SE-106 91 Stockholm, stina.hoglund@wgi.su.se

Tjuv-Antes grotta (Tjuv-Ante's Cave) is a 30 m long round-abraded sea cave ("tunnel cave") formed along a dolerite dyke in granite gneiss. The cave was formed during a relatively short period about 7 ka ago. In the inner part, on the dolerite ceiling and walls, are several coralloid and crust forming speleothems. The main speleothem forming mineral was identified as calcite, and later research has focused on the role of the microorganisms (in particular fungi and bacteria) in the precipitation and erosion of the speleothem. DNA has successfully been extracted from young and old (ca. 1 ka) speleothem and preliminary results show a dominance of Actinobacteria and Proteobacteria. Actinobacteria (actinomycetes) seems to play an important role in the formation of speleothem while a fungal community plays both a constructive role, as they stimulate calcite precipitation, and are being incorporated in the speleothem, and a destructive role as they actively bore and dissolve the calcite.

1. Introduction

Although often not as spectacular as their karstic counterparts, speleothems in granitic caves are fairly common (Vidal Romaní et al. 2010). The most common mineral is opal-A (Vidal Romaní and Vaqueir 2007), a non-crystalline, amorphous and hydrated form of silica, while calcite so far has not been reported as speleothem forming mineral from granitic caves. Tjuv-Antes grotta (Tjuv-Ante's Cave) in Västerbotten County, northern Sweden, is a round-abraded sea cave ("tunnel cave" sensu Sjöberg 1986). It is located in Storrisberget's Nature Reserve (N63°35.6' E19°22.8', 90 m a.s.l.), and the about 30 m long cave is formed along a dolerite dyke in granite gneiss (Sjöberg 1982). Its formation took place during a relatively short time about 7 ka ago at a time when the post-glacial rebound exposed the dolerite dyke for the plucking and polishing effects from the high-energy waves and the pebbles and cobbles it carried (Sjöberg 1982). In the inner part of the cave one of us (RS) observed speleothems already in the late 1960's. Samples were recently sent to JVR who concluded that the speleothems are mainly composed of calcite with an associated microflora. The presence of calcite speleothems in a basically granitic cave thus prompted a more detailed investigation.

2. Material and Methods

Tjuv-Antes Grotta lies in the cold temperate zone, but near the subarctic, with a climate characterized by large temperature variations. The January mean temperature is about -10 °C, while the July mean temperature is around +15 °C; the annual mean temperature is close to +5 °C. The mean precipitation is 700 mm/year, with about 35 % of the precipitation falling as snow (SMHI 2012).

Samples from four locations in the cave were collected in early May 2011. During the sampling, we made sure not to handle the specimens with ungloved hands. The specimens were wrapped in aluminum foil, and stored on ice during the transportation to the Swedish Museum of Natural History (NRM), Stockholm, and transferred to freezer (-20 °C) where they were stored until analysis. Samples of nearby non-mineralized biofilms (colonies) were collected in glass tubes and also stored on ice until transfer to freezer. A subset of the samples was sent to JVR in A Coruña, Spain, where they were analyzed using Scanning Electron Microscopy (SEM) coupled with Energy Dispersive Spectrometry (EDS). At NRM, they were analyzed with Environmental Scanning Electron Microscopy (ESEM) coupled with EDS. $\delta^{13}C$ analysis were also performed on two speleothem samples, using a Carlo Erbas NC2500 analyzer connected to a Finnigan MAT Delta V mass spectrometer. One sample was radiocarbon dated. Samples of the biofilms were stained using the dye DyLight 488 NHS ester and analyzed under fluorescent microscopy. At the Ancient DNA laboratory at NRM, one speleothem was sampled for DNA extraction and sequencing.

3. Results

The speleothems were exclusively found on dolerite in the innermost part of Tjuv-Antes Grotta (Fig. 1). We observed three morpho-types of speleothems in Tjuv-Antes Grotta (Fig. 2). Type 1 is coral-like speleothems consisting of globular calcite cemented into 1–4 cm long, elongated finger-shaped coralloids (Fig. 2A). They were apparently actively growing on the cave wall and ceiling, and often covered in a brown-black biofilm. Type 2 includes popcorn-like smooth and rounded speleothems, resembling the coralloid fabrics to some extent (Fig. 2B). Type 3 are smooth calcite crusts that often exhibits small evenly polished protrusions, and resembling a highly eroded

version of the coralloids (Type 1); this type is often covered in dark biofilms, and is more moist than the other two types (Fig. 2C).

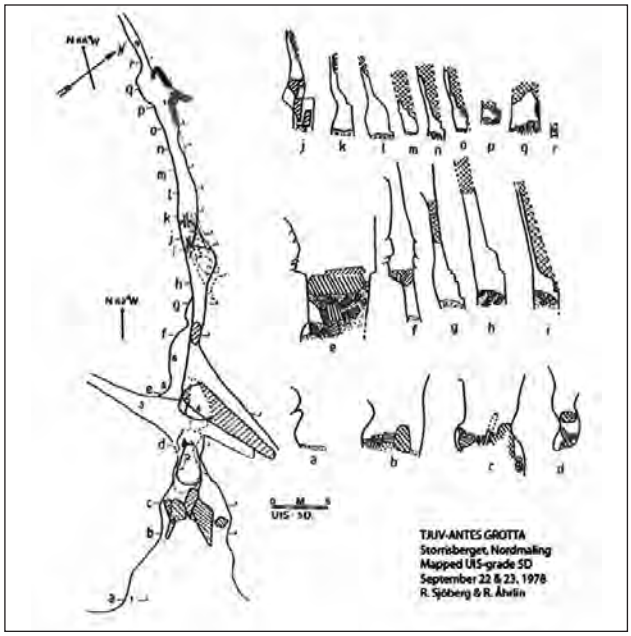

Figure 1. Map of Tjuv-Antes Grotta, Västerbotten, northern Sweden. The location of the speleothems is indicated in dark grey, and the location of the living biofilms in light grey (modified from Sjöberg 1982).

A microfabric analysis of vertical profiles reveals that the speleothems have accreted in cycles (Fig. 2D), with alternating dark and lighter layers. These layers can be distinguished in elemental composition; the light layers consist of almost pure calcite, while the silica content is high in the dark layers. There are also elevated levels of Mg and C in the dark layers. The C14-dating gave an age of 1259±30 years B.P. The $\delta^{13}C$ measurements of the calcium carbonate range between 9.0 and 11.0‰, suggesting an inorganic source for the carbon.

There are mainly two distinct types of biofilms associated with the speleothems: a recent mycelium-like community around the top of the coralloids (Fig. 2E), and a biofilm dominated by small filaments (Fig. 2F) associated with spore-like coccoids (Fig. 2G). The filaments, about 1µm in diameter, are partly incorporated, partly protruding from the matrix, and septated and branching. The mycelium-like filaments are larger, 10–20 µm in diameter, and differ in coloration, and are mostly associated with micro-erosional forms on the speleothem, but also show incrustations with calcite (Fig. 2E).

The non-mineralized biofilms were located to fractures in the dolerite on the innermost wall (Fig. 3A). The biofilm is dominated by filaments, only a few µm in thickness and with coccoidal structures, imbedded in a matrix of extracellular polymeric substances (EPS) that also

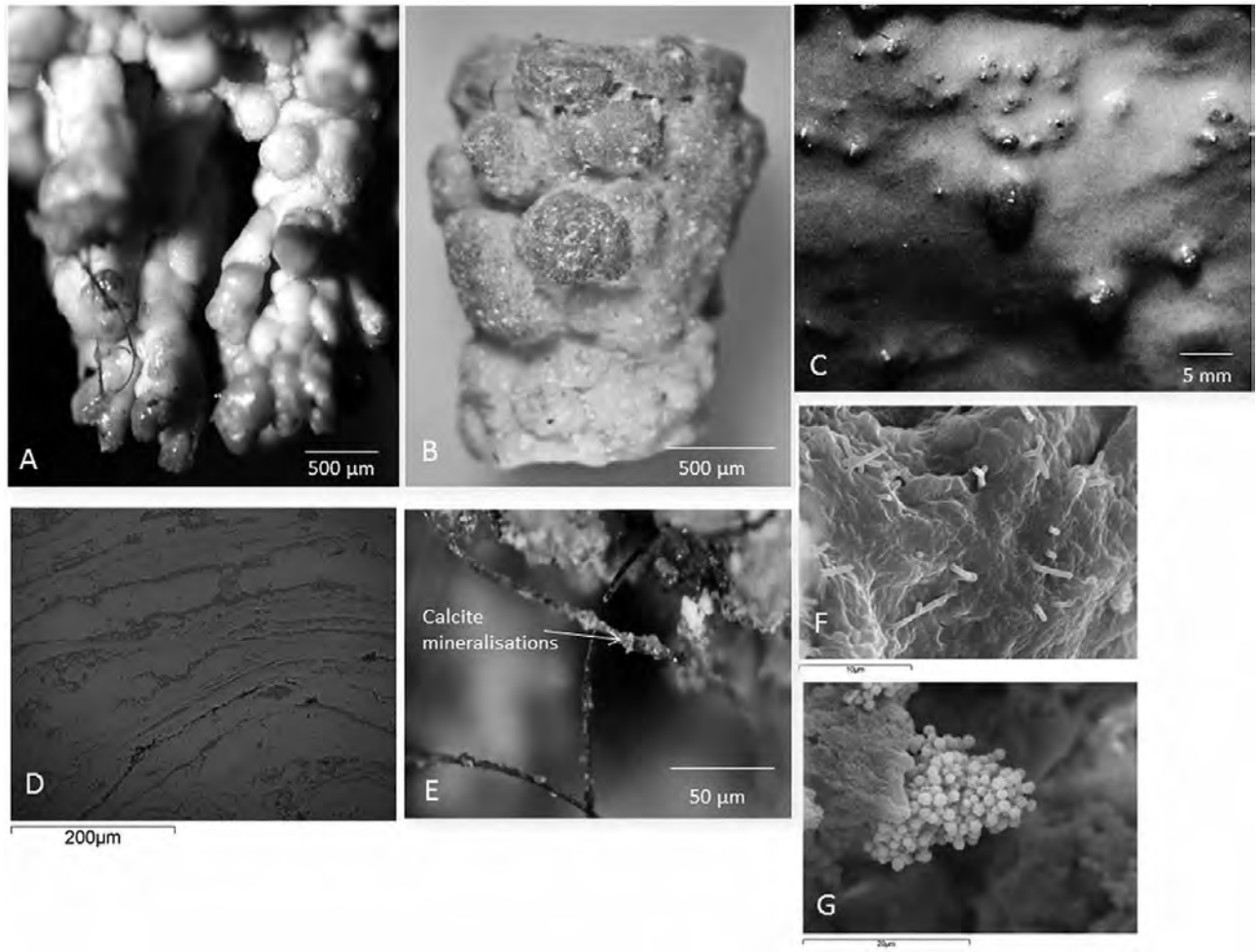

Figure 2. Microphotographs by optical microscopy, ESEM images and SEM images. A: Type 1, coral-like speleothems. B: Type 2, popcorn-like speleothems. C: Type 3, smooth calcite crust speleothems. D: Profiles of a speleothem with alternating dark and lighter layers due to cyclic accretion. E: Recent mycelium-like community usually found around the top of the coralloids. F: Biofilm dominated by small, protruding filaments. G: Spore-like coccoids associated with the biofilm.

incorporates mineral fragments (Fig. 3B, C). These mineral fragments are dominated by carbonates that appear to be precipitated in the biofilm, but also fragments of the dolerite (composed of Fe, Si, Al, S, Mg, K, Mn, and Ti) are frequent. The fluorescence microscopy revealed that the coccoidal structures are sacs containing smaller, spore-like structures (Fig. 3D).

The DNA is still under analysis, but preliminary results show that large amounts of DNA were extracted, and that they represent several distinct phylogenetic lineages.

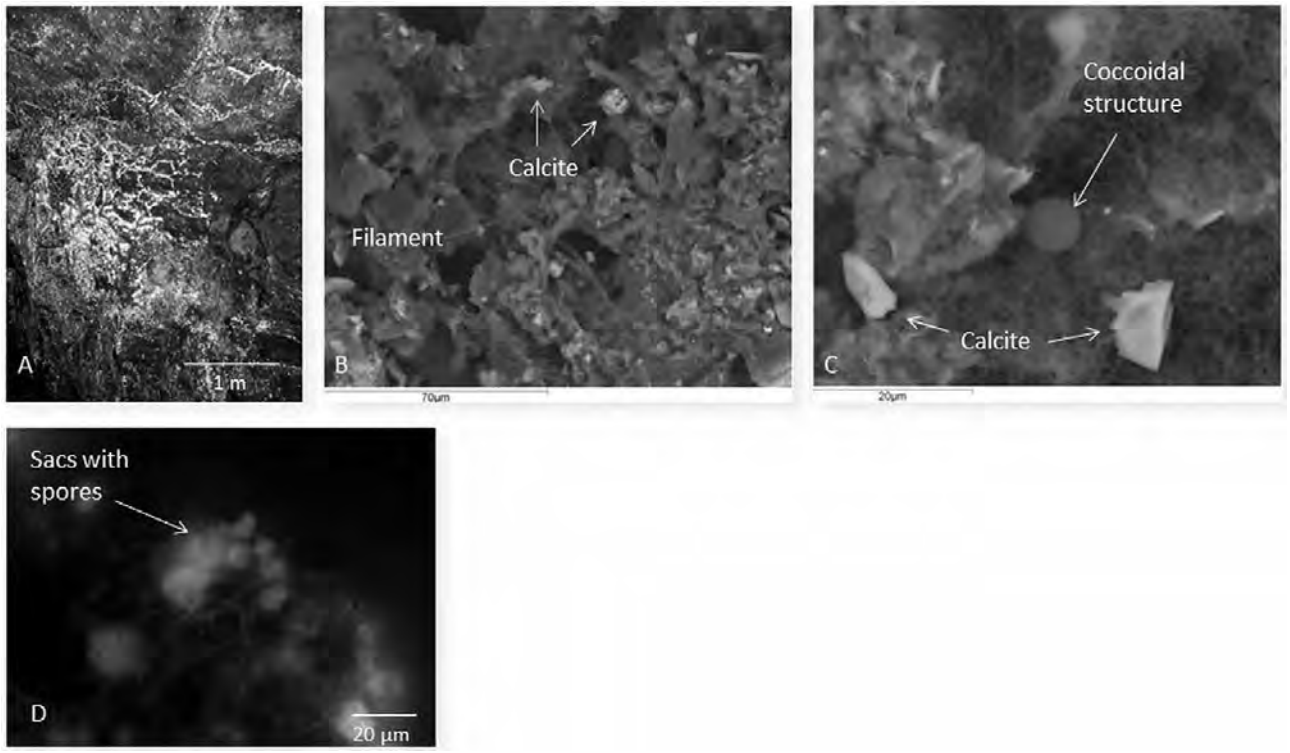

Figure 3. A: Photograph of the modern, non-mineralized biofilms located to fractures in the dolerite on the innermost wall. B, C: ESEM images of the biofilm with filaments and coccoidal structures imbedded in a matrix of extracellular polymeric substances (EPS) that also incorporates mineral fragments. D: Samples of the biofilms stained using the dye DyLight 488 NHS ester and analyzed under fluorescent microscopy, which revealed that the coccoidal structures are sacs containing smaller, spore-like structures.

4. Discussion

4.1. Biofilms

From the morphology, the thinner filaments found both in the non-mineralized wall biofilms and on the growing speleothems, can be attributed to the bacterial order Actinomycetales (Miyadoh et al. 1997). This is a diverse and large group of bacteria with a global distribution in particular in soils but also from various types of caves including karst, lava tunnels and granitic caves (Groth et al. 1999; Jones 2009; Northup et al. 2011; Porca et al. 2012). It is however likely that the biofilms do not consist of actinomycetes exclusively but of various bacterial communities, which will be characterized in future molecular studies, even if the actinmycetes appear to be the dominating group of bacteria in Tjuv-Antes Grotta. The dominance of actinomycetes in the cave is expected: both the low temperature and the relatively high humidity are factors that promote growth of actinomycetes in caves (Groth and Saiz-Jimenez 1999). The thicker filaments are consistent with fungal hyphae. The microbial populations in Tjuv-Antes Grotta thus seem to consist of heterotrophs, probably living of organic matter transported from the surface by percolating fluids and/or on the bacterial communities. It is not known if there are any chemoautotrophs in the dolerite that can act as a carbon source for the heterotrophic communities on the cave walls.

4.2. Mineralogy

Both the speleothem and the active biofilms are concentrated to the dolerite; no speleothems are found on the granite. This makes Tjuv-Antes Grotta most related to volcanic (basalt) caves with respect to secondary mineralizations. The calcium content is high in dolerite compared to granite, due to the presence of anorthite, a calcium-rich plagioclase. This readily explains the presence of calcite speleothems in many volcanic caves (White 2012), and also in Tjuv-Antes Grotta. The mechanism of calcite speleothem formation in volcanic caves is the same as in limestone caves, where meteoric water supersaturated with calcium precipitates calcite in the cave environment. The difference between limestone caves and caves in mafic rocks (e.g., volcanic caves and dolerite caves) is the source of calcium. In the mafic rocks calcium is likely to be derived from the breakdown of anorthite and not from calcium carbonates as in limestone. Even if anorthite is the least stable of the common mafic minerals, its breakdown is normally much slower than the dissolution of limestone, explaining the less developed speleothems in mafic caves, together with the much younger age of many volcanic caves.

4.3. Life cycle of the speleothems

The speleothems in Tjuv-Antes Grotta seem to be highly influenced by the microbial presence. The actinomycete-dominated biofilms cover most of the surface of the growing speleothems, and seem to be incorporated in the darker layers of the speleothems. There are also apparently abiotic growths of the speleothems (as deduced from the $\delta^{13}C$ analysis), resulting in the light colored bands. It is still possible that microbial activity have indirect influences also on this phase of the growth by altering the microenvironment to facilitate precipitation of calcite (Castanier et al. 1999).

The fungal presence seems to have a dual role in the life cycle of the speleothems. There are evidence for a constructional role by precipitation of calcite (encrusted hyphae), but also for an erosion dominated phase, that may be responsible, at least in part, for the Type 3 speleothems.

We are still awaiting the results from the molecular analysis of the microbial communities in the speleothems. We would also like to characterize the different phases in the speleothem life cycle, and the different contributions from the microbial communities.

Acknowledgment

The speleothems were collected in a Nature Reserve and Natura 2000 Site, with permission from the County Government Länsstyrelsen Västerbotten (permission 521-6864-2010), and we want to thank the Länsstyrelsen for the permission. Some of the analyses (ESEM/EDS, fluorescent microscopy and stable isotope analysis) were conducted at Stockholm University; in particular we would like to thank Marianne Ahlbom at the Department of Geological Sciences for assistance during the ESEM. Many thanks also to Dr. Bogdan P. Onac (University of South Florida) and one anonymous reviewer for valuable comments on an earlier draft of the manuscript.

References

Castanier S, Le Metayer-Levrel G, Perthuisot J-P, 1999. Ca-carbonates precipitation and limestone genesis: the microbiogeologists point of view. Sedimentary Geology, 126, 9–23.

Groth I, Siaz-Jimenez C, 1999. Actinomycetes in hypogean environments. Geomicrobiology Journal, 16, 1–8.

Groth I, Vettermann R, Schuetze B, Schumann P, Saiz-Jimenez C, 1999. Actinomycetes in karstic caves of northern Spain (Altamira and Tito Bustillo). Journal of Microbiological Methods, 36, 115–122.

Jones B, 2009. Phosphatic precipitates associated with actinomycetes in speleothems from Grand Cayman, British West Indies. Sedimentary Geology, 219, 302–317.

Miyadoh S, Tsuchizaki N, Ishikawa J, Hotta K, 1997. Digital Atlas of Actinomycetes. Society for Actinomycetes Japan and Akasura publishing, Tokyo.

Northup DE, Melim LA, Spilde MN, Hathaway JJM, Garcia MG, Moya M, Stone FD, Boston PJ, Dapkevicius MLNE, Riquelme C, 2011. Lava cave microbial communities within mats and secondary mineral deposits: implications for life detection on other plantes. Astrobiology, 11, 601–618.

Porca E, Jurado V, Žgur-Bertok D, Saiz-Jimenez C, Pašic L, 2012. Comparative analysis of yellow microbial communities growing on the walls of geographically distinct caves indicates a common core of microorganisms involved in their formation. FEMS Microbiology Ecology, 81, 255–266.

Sjöberg R, 1982. Tunnelgrottor i södra Västerbotten: morfologiska och morfogenetiska studier. Gerum Rapport, A31.

Sjöberg R, 1986. Tunnelgrottor i Norden: geomorfologiska studier. Gerum Naturgeografi 3. Umeå University, Umeå.

SMHI 2012. Klimatdata, http://www.smhi.se/klimatdata (visited 2012-12-13).

White WB, 2012. Secondary mineral in volcanic caves: data from Hawai'i. Journal of Cave and Karst Studies, 72, 75–85.

Vidal Romaní JR, Vaqueiro M, 2007. Types of granite caves and associated speleothems: genesis and evolution. Nature Constervation, 63, 41–46.

Vidal Romaní JR, Sanjurjo Sánchez J, Vaqueiro M, Fernández Mosquera D, 2010. Speleothems of granite caves. Communicações Geológicas, 97, 71–80.

DATING DIAGENISED ARAGONITE SPELEOTHEMS

Rebeca Martín-García[1], Ana M. Alonso-Zarza[1], Silvia Frisia[2]
[1]Department of Petrology and Geochemistry, Faculty of Geology-Institute of Geosciences, Universidad Complutense de Madrid-CSIC 28040, Madrid, Spain, rmarting@ucm.es
[2]Environmental and Climate Change Research Group, School of Environmental and Life Sciences, The University of Newcastle, Callaghan 2308 NSW, Australia, Silvia.Frisia@newcastle.edu.au

The U-series method is widely used to date cave carbonates. Generally, in stalagmites, every layer is cover by a younger one, but locally the U/Th analysis reveals that some speleothem layers display a different age than expected given their relative stratigraphic position. These results are omitted very often in palaeoclimate studies and considered just as "anomalies". Two samples of speleothems with anomalies from Castañar Cave (Spain) have been studied in detail in order to decipher the causes involved in these processes of age modification. A stalagmite sampled at -20 m from the surface displays an older than expected age and does not follow the stratigraphic order. This anomaly can be explained due to enrichment in the daughter isotope, ^{230}Th, or a leaching of the parent isotope, ^{238}U. A pool rim sampled at -26 m displays a younger age in the inner part of the speleothem than in the outer part. This anomaly can be explained due to enrichment in the parent isotope ^{238}U, or due to leaching of the daughter isotope ^{230}Th. The exposure of the samples to continuous natural dripping and the diagenetic processes observed, caused an alteration of the original age. The presence of these diagenetic processes is only detectable through detailed petrographic analysis of the speleothems.

1. Introduction

Speleothem-based chronology studies are fundamental to understand past climate events, timing speleogenesis processes and the rates at which they occur (St Pierre et al., 2009). The U-series analytical method is well-known for dating (Frank et al. 2000; Hellstrom 2003; van Calsteren and Thomas 2006). This dating method is based on the disequilibrium between U and Th and among other uses, it has application to the Quaternary carbonate materials and speleothems. ^{230}Th/^{234}U radioactive isotopes begin with an activity ratio equal to 0, that over time approaches 1 by the decay of ^{234}U to ^{230}Th. Knowing the value of this relationship and the decay constants is possible to calculate the age of the samples (Hellstrom 2003). This method has been widely used in rocks, which, in combination with the analysis of ^{13}C and ^{18}O isotopes, are used to obtain palaeoclimate curves (Kaufman 1998; Fairchild et al. 2006; Spötl et al. 2008).

The U and Th isotopes are in secular equilibrium with the host rock, which usually is at least several million years old. However, percolation waters are well away from this balance due to the different geochemical behavior of both isotopes. Th is insoluble and therefore the ratio ^{230}Th/^{238}U in drip water is 0; this is one of the bases of this dating technique. By contrast, the U concentration in the drip waters is well above the equilibrium because ^{234}U is very soluble (Scholz and Hoffmann, 2008). The initial ^{234}U/^{238}U in drip waters can vary greatly depending on the age of the host rock and the time of residence of water in the rock. In any case this does not affect the application of the U/Th-series dating technique because the initial ^{234}U/^{238}U ratio is not necessary for the calculations (Scholz and Hoffmann 2008).

However, sometimes the U/Th analysis reveals speleothem layers with inverted ages. When this occurs, these anomalous results are simply omitted without a genetic explanation. The origin of these anomalies is important to know because of the obvious consequences for speleothem dating and paleoclimate implications (Muñoz-García et al. 2007). The most important criterion for deciding if an age is correct or not is that it should follow a logical stratigraphic order, with the oldest age at the base and youngest towards the tip (Kaufmann 2003; Romanov et al. 2008a).

The basic characteristics for an ideal-for-dating speleothem are, according to Borsato et al. (2003), 1. that it contains sufficient amounts of U, 2. that it is not contaminated with detrital Th particles, and 3. that it behaves as a closed system in which no remobilization or input of U or its decay products, especially ^{230}Th, has occurred (Cherdyntsev 1971; Gascoyne et al. 1978; Ford and Williams 2007). According to Scholz and Hoffmann (2008) the breach of any of these criteria along with errors during analysis or sample preparation can generate anomalous ages.

In this work we try to analyze the reasons for the presence of anomalous dating in the speleothems of Castañar Cave. In this cave, most of the speleothems were originally aragonitic in mineralogy. Aragonite, being an unstable mineral, undergoes diagenetic processes that cause problems in dating which are sometimes difficult to detect. Errors during the preparation and analysis of the samples are discarded as long as the anomalous results were repeated.

2. Castañar Cave

Castañar Cave is located in the village of Castañar de Ibor, in Cáceres, Spain. Geologically is located in the eastern Iberian Massif (west-central sector of the Iberian Peninsula), specifically in the Ibor Anticline which forms part of a sector named Domain of Vertical Folds (Díez-Balda et al. 1990). This domain is characterized by the presence of broad antiforms of NW-SE direction (Fig. 1a). The rocks of the area can be divided into two large stratigraphic units, the Domo Extremeño Group and Ibor Group (Álvarez Nava et al. 1988), separated by an

unconformity. Both units are mainly composed of shales and greywackes, but the Ibor Group includes carbonate beds close to the Neoproterozoic–Cambrian boundary.

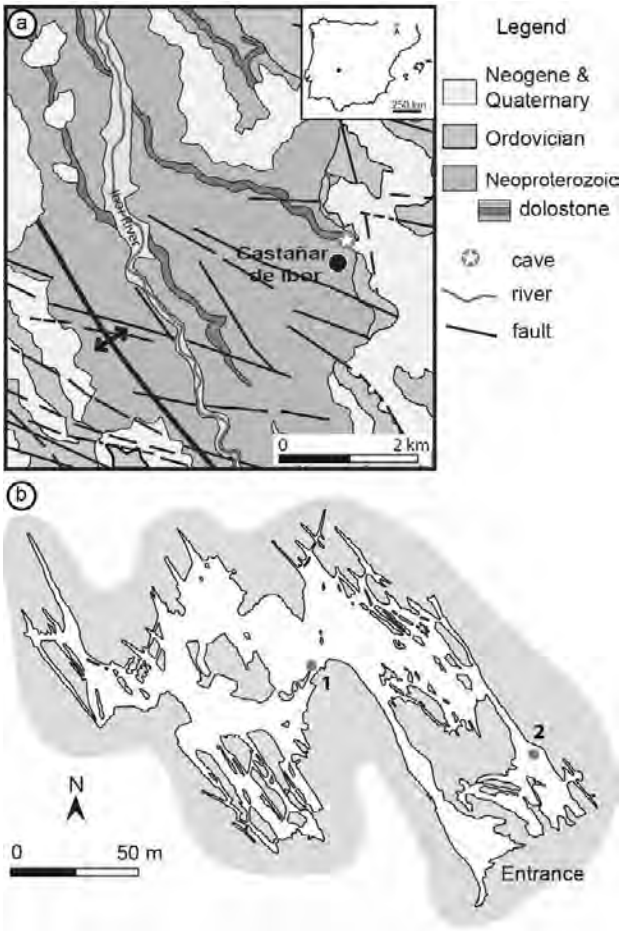

Figure 1. a) Simplified geological map of the studied area. b) Map of Castañar Cave. 1 and 2 correspond to the location of the samples.

The climate of the area is mild continental with Mediterranean influence. Mean annual temperature in the area is about 16 ºC, and annual thermal oscillation is in the order of 20 ºC. Precipitation shows strong interannual and seasonal variability, with a mean annual rainfall amount of 750 mm mainly concentrated in winter (Ninyerola et al. 2005).

Castañar Cave is a maze cave consisting of a network of galleries few meters wide and about 2 m high. The entrance of the cave is located at 590 m above sea level. It is a subhorizontal cave in which the deepest point is found at -35 m below the surface. The cave galleries follow the N150°E orientation (Fig. 1b) and the morphology of the main structures of the area (Alonso-Zarza et al. 2011). The cave was formed by dissolution of the carbonate levels of the host rock and the subsequence collapse of the siliciclastic beds. Some parts of the cave are covered by red clays sourced from the partial weathering of the host rock to clays. The red coating contrasts with the white speleothems. No sand or other detrital material has been found to indicate transportation inside the cave.

The composition of the cave waters is stable throughout the year being rich in Mg^{2+}, Ca^{2+} and HCO_3^{2-}, with a mean pH of 7.8. At present there is no flowing water in the cave, although there are small pools and drip and capillary seepage water occur in all the rooms. The temperature is 16.94 ºC with an annual variation of 0.09 ºC. The CO_2 values in the cave atmosphere are 3,680 ppm with an annual oscillation of 1,120 ppm (Sánchez-Moral et al. 2006). The relative humidity is higher than 99.5 %, close to saturation (Fernández-Cortés et al. 2010).

3. Materials and methods

The speleothems used for this study are a stalagmite sampled at -20 m from the surface (Sample 1) and a pool rim sampled at -26 m (Sample 2) (Fig. 1b). Both samples are formed by aragonite and calcite.

Thin sections of the speleothems were examined by petrographic microscopy. Due to their fragility, the speleothem samples were embedded in a resin containing Epofer EX 401 and Epofer E 432 in a vacuum system. Mineralogical characterization was done by X-ray diffraction using a Philips PW-1710 XRD system operating at 40 kV and 30 mÅ, at 2º/min, with monochromated CuKα radiation. XRD spectra were obtained from 2 to 66º 2θ.

U/Th dating was undertaken on samples between 5 and 100 mg cut from the speleothems by dental drill using the procedure described by Hellstrom (2003). Radiometric analysis used a Nu Instruments multi-collector ICP-MS at the School of Earth Sciences of the University of Melbourne. ($^{230}Th/^{238}U$) and ($^{234}U/^{238}U$) were determined using a ^{229}Th–^{233}U mixed spike calibrated against a Harwell uraninite (HU–1) solution. Age was calculated assuming an initial $^{230}Th/^{232}Th$ activity ratio of 1.5 ±1.5 using equation 1 of Hellstrom (2006), although the effect of initial ^{230}Th is negligible in this case. ($^{234}U/^{238}U$) is calculated using ($^{234}U/^{238}U$) and the corrected age.

4. Results and interpretation

4.1. Petrography

Castañar Cave contains a large variety of speleothems including frostwork, anthodites, helictites, stalactites, stalagmites, columns, draperies, flowstones, coralloids, crusts, gours, pool deposits and moonmilk. Most of the speleothems are composed or contain high amounts of aragonite. The other common mineral in the cave is calcite.

These speleothems of Castañar Cave are affected by different diagenetic processes. These processes have been described in detail by Alonso-Zarza and Martín-Pérez (2008), Martín-García et al. (2009), Martín-García et al. (2011) and Martín-Pérez et al. (2012). The samples used in this work have undergone aragonite-to-calcite transformation and micritization. The aragonite-to-calcite transformation is a process in which the unstable polymorph (aragonite) transforms into the stable one (calcite) in the presence of water, also known as neomorphism (Folk, 1965). Micritization is a process of destruction of the original structure of a carbonate by the formation of microcrystalline textures (Reid and Macintyre 1998). In caves it can be related to the phenomenon of condensation corrosion (Sarbu and Lascu, 1997; Tarhule-Lips and Ford, 1998; Martín-García et al. 2011).

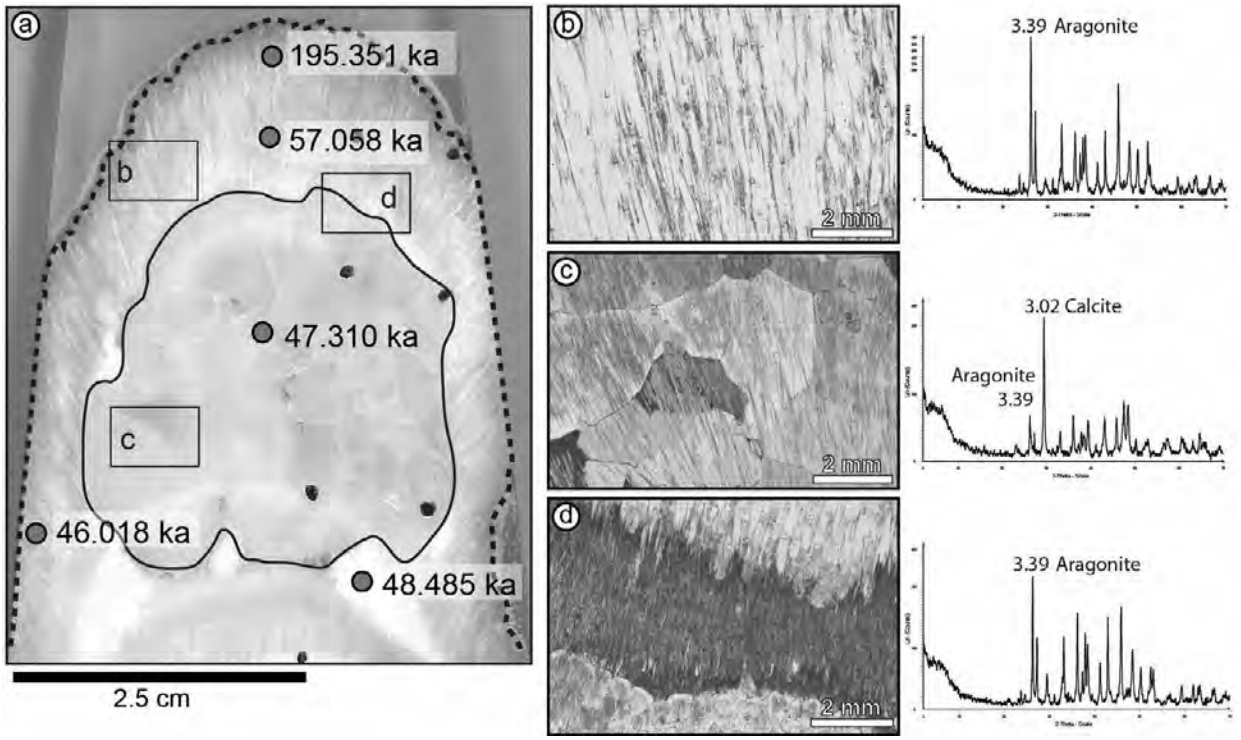

Figure 2. a) Polished hand sample. The dating points (grey) and the ages are indicated. b) Microphotography of the aragonite fibers of the rim. Plain-polarized light. c) Calcite mosaic with aragonite relics. Cross-polarized light. d) Aragonite micrite. Plain-polarized light.

After the systematic dating of the speleothems, two of them were found to have anomalous ages and thus were selected for this study. These speleothems show different textures and mineralogies.

Sample 1 (Fig. 2a) is a stalagmite constituted of aragonite and calcite, with three different textures: 1 – large crystals (2 cm) of acicular aragonite form the rim and some inner areas (Fig. 2b); 2 – a large mosaic of crystals of calcite (≈ 5 mm) with aragonite relics that cross the calcite crystals along the entire speleothem (Fig. 2c); 3 – in the areas of contact between the two previous textures, an irregular zone formed by a powdery white material which corresponds to aragonitic micrite is commonly found (Fig. 2d). Petrographic observations indicate that the sample has undergone several stages of aragonite growth followed by aragonite-to-calcite transformation of the inner parts.

Sample 2 (Fig. 3) is a pool rim. The nucleus over which the sample grew is a fragment of shale from the host rock. Macroscopically are two different areas, one of them is homogeneous and compact (Fig. 3b) and the other one is darker and fibrous with high porosity (Fig. 3c). Under the microscope these areas correspond to two different textures. The first of these, the innermost part of the sample surrounding the host rock is constituted by a mixture of aragonite fans of about 2 mm in length and a mosaic of small calcite crystals (~ 0.25 mm) (Fig. 3c). The texture of the outer zone constitutes the majority of the sample and consists of a mosaic of calcite crystals with feather morphology which have neither aragonite nor relic textures, thus it has been considered primary calcite. (Fig. 3b). The most probable diagenetic history of Sample 2 is the crystallization of a layer of aragonite over the substrate. Subsequently, the growth of a calcite phase formed the second layer, which can be also the responsible for the transformation of the inner aragonitic layer, resulting in the mixed texture found today.

4.2. Dating

Sample 1: To determine the duration of the aragonite-to-calcite transformation process, four samples were prepared for dating. The samples were taken along the central axis sampling all types of textures (Fig. 2a). The results obtained were anomalous as the age of the outermost rim consisting of aragonite was much older than the inner area composed of a mosaic of calcite with aragonite relics. This could indicate that the transformation of aragonite to calcite occurred long after its formation, and so the younger age of the aragonite transformed to calcite is not the age of the formation of the primary mineral, but the age of aragonite to calcite transformation

The aragonite of the outer rim was sampled in two points, one at the tip and other at the base of the rim. The points are separated by 6 mm with an age difference of 138 ka (57 and 195 ka). To check if the entire rim was the same age, a third point from the lateral of the speleothem was dated. This point gave an age of 46 ka, within the age range expected.

Sample 2: Both textures were dated; the first near the host rock corresponds to the mixing zone of aragonite and calcite (Fig. 3a). The second is in the outermost zone, where the mineralogy is calcite. The results obtained show that the inner part is about 231 ka old, while the outer part is older and has about 241 ka.

5. Discussion

The anomalies detected in Sample 1, in which the anomalous age is older than expected and do not follow the stratigraphic order of the rest of the dates of the stalactite, can be explained due to an enrichment in the daughter isotope, ^{230}Th, or a leaching of the parent isotope, ^{238}U. The

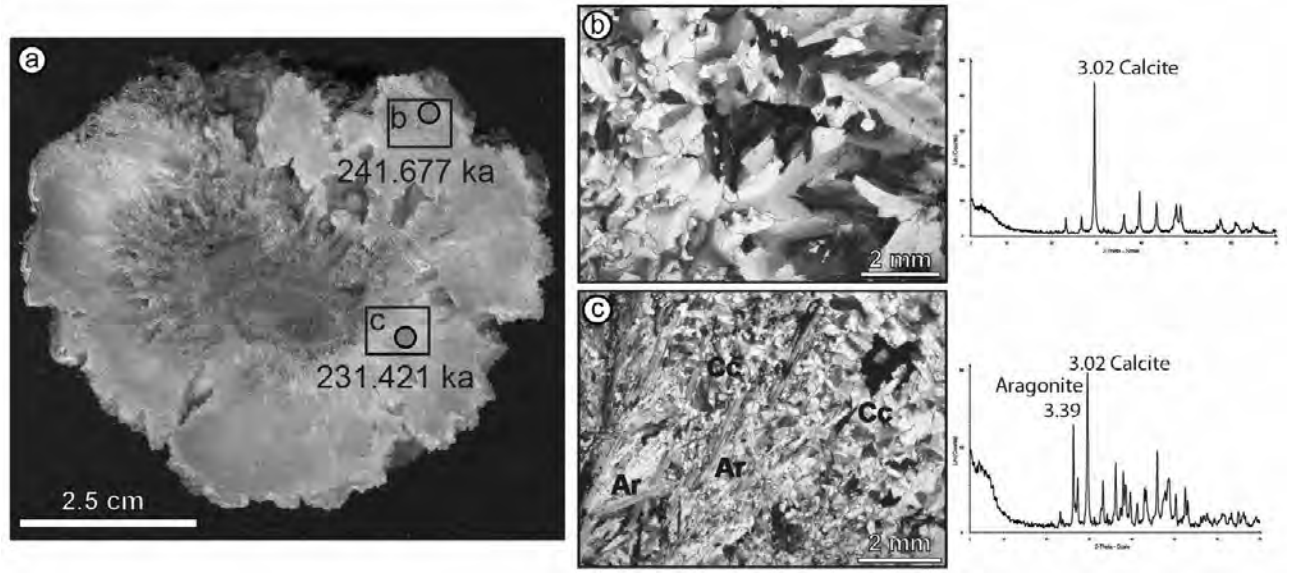

Figure 3 a) Polished hand sample. The dating points (grey) and the ages are indicated. b) Microphotography of the calcite crystals. Cross-polarized light. c) Aragonite fibers (Ar) surrounded by calcite equant mosaic (Cc). Cross-polarized light.

enrichment of Th occurs when Th-bearing waters enter the system and this detrital Th stays between the crystals forming the speleothem (Borsato et al. 2003), thus the amount of Th is higher with respect to the initial U, and ages become older. On the other hand, U-leaching is produced because of the high solubility of this isotope in the presence of water. Water can leach the U leaving Th and making the U/Th relation lower, thus the age seems older. Both processes lead to a false enrichment in Th, thus the dating gives older ages and do not fit the stratigraphy of the sample.

The petrographic observations and X-ray diffraction of Sample 1 prove that there is no detrital contamination. The age that corresponds to the outermost dated point has a higher anomaly than the one that is immediately below since that is more exposed to dripping. Dabous et al. (2000) described U-leaching in speleothems of Waddi Sannur Cave, Egypt, recognizing two periods of leaching related to well-known stages of high rainfall in the Western Desert.

In the case of Sample 2, the age founded in the inner part of the speleothem is younger than in the outer part. The anomaly can be explained due to enrichment in the parent isotope ^{238}U, or leaching of the daughter isotope ^{230}Th. The diagenetic processes such as dissolution-reprecipitation and recrystallization cause an alteration in the original age, causing the ages to become younger because of the addition of U to the system (Muñoz-García et al. 2007). These processes take place when cave waters percolate the speleothems through the porosity causing dissolution and reprecipitating new minerals (Frisia et al. 2000, 2002).

The petrographic and XRD studies show the coexistence of aragonite and calcite in a 70/30 (Fig. 3c) proportion in the inner part of the speleothem, where the anomaly is found. Therefore precipitation of calcite in the porosity between the aragonite fibers is responsible for the entry of uranium into the system causing the anomalous age of 231 ka. However, since there is still original aragonite, it is not possible to conclude that the age corresponds to calcite, but that it would be the result of mixing the U/Th ratios of the new calcite and the aragonite that is still preserved. Therefore, the age of the inner part does not correspond to the deposition moment, but neither matches the time of aragonite-to-calcite transformation.

6. Conclusions

Our results indicate that the data obtained through U/Th dating may give anomalous ages especially if the initial mineral is aragonite. The possible causes of the anomalies are variable: U-leaching, U input or Th input.

Sample 1 show an anomaly that causes an older than expected age. This is presumably caused by the leaching of the U. Th detrital enrichment would cause the same result, but it has been discarded since no traces of detrital particles were found throughout the sample. This leachate only affects the speleothem tip, in this case a stalagmite, since that is where it receives the dripping.

The anomaly found in Sample 2 causes a younger than expected age. This is due to an U input in the system. Th leaching is unlikely since it is insoluble in water. The petrological studies allowed distinguishing aragonite-to-calcite transformation features in the area in which the anomaly is found. Not being completly transformed the aragonite to calcite, there is coexistence of both minerals, therefore the obtained age does not represent the original or the mineral transformation ages, but is a mixture of both.

Acknowledgments

This work received financial support from the Junta de Extremadura through FEOGA-RIENTACION-FEDER funds, Projects CGL-2008-05584-C02-02 and CGL-2011-27826-C02-01 from the MCINN and UCM-910404 from UCM-CAM. R. M-G was supported by a JAEPredoc-CSIC grant. We are grateful to Dr. J. Hellstrom for the age analyses.

References

Alonso-Zarza AM, Martín-Pérez A, 2008. Dolomite in caves: recent dolomite formation in oxic, non-sulfate environments. Castañar Cave, Spain. Sedimentary Geology, 205, 160–164.

Alonso-Zarza AM, Martín-Pérez A, Martín-García R, Gil-Peña I, Meléndez A, Martínez-Flores E, Hellstrom J, Muñoz-Barco P, 2011. Structural and host rock controls on the distribution, morphology and mineralogy of speleothems in the Castañar Cave (Spain). Geological Magazine, 148, 211–225.

Álvarez Nava H, García Casquero JL, Gil A, Hernández Urroz JLorenzo S, López Díaz F, Mira M, Monteserín V, Nozal F, Pardo MV, Picart J, Robles R, Santamaría J, Solé J, 1988. Unidades litoestratigráficas de los materiales precámbrico-cámbricos de la mitad suroriental de la Zona Centro-Ibérica. In: II Congreso Geológico de España. 19–22.

Borsato A, Quinif Y, Bini A, Dublyansky Y, 2003. Open-system alpine speleothems: implications for U-series dating and paleoclimate reconstructions. Studi Trentini di Scienze Naturali: Acta Geologica, 80, 71–83.

Dabous A, Osmond J, 2000. U/Th isotopic study of speleothems from the Wadi Sannur Cavern, Eastern Desert of Egypt. Carbonates and Evaporites, 15, 1–6.

Díez-Balda MA, Vegas R, González-Lodeiro F, 1990. Central-Iberian Zone. Autochthonous Sequences: Structure. In: R.D. Dallmeyer and E. Martínez-García (Eds.). Pre-Mesozoic Geology of Iberia. Springer-Verlag, Berlin, 172–188.

Fairchild IJ, Smith CL, Baker A, Fuller L, Spötl C, Mattey D, McDermott F, EIMF, 2006. Modification and preservation of environmental signals in speleothems. Earth-Science Reviews, 75, 105–153.

Fernández-Cortés A, Sánchez-Moral S, Cañavera JC, Cuevas-González J, Cuezva S, Andreu JM, 2010. Variations in seepage water geochemistry induced by natural and anthropogenic microclimatic changes: Implications for speleothem growth conditions. Geodinamica Acta, 23, 1–13.

Folk RL, 1965. Some aspects of recrystallization in ancient limestones. In: L.C. Pray and R.C. Murray (Eds.) Dolomitization and Limestone Diagenesis. A Symposium. SEMP Special Paper, Tulsa, Oklahoma, 14–48.

Ford DC, Williams PW, 2007. Karst geomorphology and hydrology. Wiley, Chichester.

Frank N, Braum M, Hambach U, Mangini A, Wagner G, 2000. Warm Period Growth of Travertine during the Last Interglaciation in Southern Germany. Quaternary Research, 38–48.

Frisia S, Borsato A, Fairchild IJ, McDermott F, 2000. Calcite fabrics, growth mechanisms, and environments of formation in speleothems from the Italian Alps and Southwestern Ireland. Journal of Sedimentary Research, 70, 1183–1196.

Frisia S, Borsato A, Fairchild IJ, McDermott F, Selmo EM, 2002. Aragonite-Calcite relationships in speleothems (Grotte de Clamouse, France): environment, fabrics, and carbonate geochemistry. Journal of Sedimentary Research, 72, 687–699.

Gascoyne M, Ford DC, Schwarcz HP, 1978. Uranium series dating and stable isotope studies of speleothems. Part 1: Theory and techinques, In: Transactions. British Cave Research Association, Buxton, 91–112.

Hellstrom J, 2003. Rapid and accurate U/Th dating using parallel ion-counting multi-collector ICP-MS. Journal of Analytical Atomic Spectrometry, 18, 1346–1351.

Hellstrom J, 2006. U-Th dating of speleothems with high initial ^{230}Th using stratigraphical constraint. Quaternary Geochronology, 1, 289–295.

Cherdyntsev VV, 1971. Uranium 234. Israel Programme for Scientific Translations, Jerusalem.

Kaufman A, Wasserburg GJ, Porcelli D, Bar-Matthews M, Ayalon A, Halicz L, 1998. U-Th isotope systematics from the Soreq cave, Israel and climatic correlations. Earth and Planetary Science Letters, 156, 141–155.

Kaufmann G, 2003. Stalagmite growth and palaeo-climate: the numerical perspective. Earth and Planetary Science Letters, 214, 251–266.

Martín-García R, Alonso-Zarza AM, Martín-Pérez A, 2009. Loss of primary texture and geochemical signatures in speleothems due to diagenesis: Evidences from Castañar Cave, Spain. Sedimentary Geology, 221, 141–149.

Martín-García R, Martín-Pérez A, Alonso-Zarza AM, 2011. Weathering of host rock and corrosion over speleothems in Castañar cave, Spain: an example of a complex meteoric environment. Carbonates and Evaporites, 26, 83–94.

Martín-Pérez A, Martín-García R, Alonso-Zarza AM, 2012. Diagenesis of a drapery speleothem from Castañar Cave: from dissolution to dolomitization. International Journal of Speleology, 42, 251–266.

Muñoz-García MB, Martín-Chivelet J, Rossi C, Ford DC, Schwarcz HP, 2007. Chronology of Termination II and the Last Interglacial Period in North Spain based on stable isotope records of stalagmites from Cueva del Cobre (Palencia). Journal of Iberian Geology, 33, 17–30.

Ninyerola M, Pons X, Roure JM, 2005. Atlas Climatico Digital de la Peninsula Iberica. Metodologia y aplicaciones en bioclimatologia y geobotanica. Universidad Autonoma de Barcelona, Bellaterra.

Reid RP, Macintyre IG, 1998. Carbonate recrystallization in shallow marine environments: A widespread diagenetic process forming micritized grains. Journal of Sedimentary Research, 68, 928–946 Part A.

Romanov D, Kaufmann G, Dreybrodt W, 2008. Modeling stalagmite growth by first principles of chemistry and physics of calcite precipitation. Geochimica et Cosmochimica Acta, 72, 423–437.

Sarbu SM, Lascu C, 1997. Condensation corrosion in Movile Cave, Romania. Journal of Cave and Karst Studies, 59, 99–102.

Sánchez-Moral S, Cuezva S, Lario J, Taborda-Duarte M, 2006. Hydrochemistry of karstic waters in a low-energy cave (Castañar de Ibor, Spain). In: J.J. Durán, B. Andreo and F. Carrasco (Eds.). Karst, cambio climático y aguas subterráneas. IGME, Madrid, 339–347.

Scholz D, Hoffmann D, 2008. ^{230}Th/U-dating of fossil corals and speleothems. Eiszeitalter und Gegenwart. Quaternary Science Journal, 57, 52–76.

Spötl C, Scholz D, Mangini A, 2008. A terrestrial U/Th-dated stable isotope record of the Penultimate Interglacial. Earth and Planetary Science Letters, 276, 283–292.

St Pierre E, Zhao J, Reed E, 2009. Expanding the utility of Uranium-series dating of speleothems for archaeological and palaeontological applications. Journal of Archaeological Science, 36, 1416–1423.

Tarhule-Lips RFA, Ford DC, 1998. Condensation corrosion in caves of Cayman Brac and Isla de Mona. Journal of Cave and Karst Studies, 60, 84–9.

van Calsteren P, Thomas L, 2006. Uranium-series dating in natural enviroment science. Earth-Science Reviews, 75, 155–175.

THE HYPOGENE ORIGIN OF DIANA CAVE (ROMANIA) AND ITS SULFURIC ACID WEATHERING ENVIRONMENT

Bogdan P. Onac[1,2], Cristina M. Pușcaș[1], Herta S. Effenberger[3], Ioan Povară[4], Jonathan G. Wynn[1]
[1]University of South Florida, Department of Geology, 4202 E. Fowler Ave., SCA 528, Tampa, FL 33620 USA, bonac@usf.edu
[2]Babes-Bolyai University, Department of Geology & Emil Racoviță Institute of Speleology, Clinicilor 5, 400006 Cluj-Napoca, Romania
[3]Institute of Mineralogy and Crystallography, University of Wien, Geozentrum, Althanstraße 14, 1090 Wien, Austria
[4] Emil Racoviță Institute of Speleology, Frumoasă 31, 010986 Bucharest, Romania

The Diana Cave in SW Romania develops along a fault line at the contact between Late Jurassic limestones and Early Cretaceous marls. It formed through corrosion of bedrock (limestone and marls) by sulphuric acid-rich steam condensate resulted after oxidation/hydrolysis of H_2S escaping from the thermo-mineral water emerging from depth in the cave. The sulfuric acid causes a strong acid sulfate weathering of the bedrock generating a sulfate-dominated secondary cave-mineral assemblage that includes gypsum, anhydrite, bassanite, epsomite, alunite, and halotrichite group minerals. Closely associated with these minerals are two rare sulfate species, namely rapidcreekite and tamarugite that represent new occurrences in limestone caves. Traditional X-ray diffraction and single crystal analyses were used along with scanning electron microscope (SEM), stable isotope, and electron microprobe investigations to fully characterize the primary and secondary speleogenetic by-products of Diana Cave.

1. Introduction

Sulfates are the largest group among cave minerals with 89 species which form in a variety of settings (Hill and Forti 1997; Onac and Forti 2011a, b). Of these, only gypsum, epsomite, and mirabilite may be considered common for the cave environments, with gypsum perhaps the second most frequent cave mineral after calcite (Onac 2012). The majority of the other sulfates only occur under very particular settings, such as in caves located nearby ore deposits or thermo-mineral water sources and in areas with abundant post-volcanic activities.

This paper provides an overview of the mineralogy of Diana Cave, an active sulfide-rich thermal water geochemical system. The study emphasizes the sulfuric acid origin of this cavity and the rich mineral assemblage precipitated in its steam-condensate environment.

2. Geology and cave settings

The geology of the Cerna Valley is complicated by the occurrence of several nappe complexes, such as Getic, Danubian, etc (Balintoni et al. 2010). Diana Cave develops at the contact between nodular limestones (Late Jurassic; J_3) and dark grey Iuta marls (Late Cretaceous; K_1), both part of the sedimentary cover of the Danubian nappe (Năstăseanu 1980) (Fig. 1). The major clay minerals within the Iuta marls (forming the floor and lower part of the cave walls) are illite, kaolinite, and chlorite (Diaconu and Medeșan 1973). Their importance resides in the ions released to the cave geochemical system upon reacting with the H_2SO_4 that condenses on cave walls. Relevant to this paper is that the cave passage formed along the Diana Fault (Fig. 2), which brings in contact the Late Jurassic limestones with the gray marls of Iuta strata (Năstăseanu 1980).

The regional hydrogeology of the region is rather complex; its relationship with the karst of the Cerna Valley has been described in details elsewhere (Povară et al. 2008; Wynn et al. 2010).

The Diana Cave is located in the lower section of the Cerna Valley (SW Romania), in the old center of Băile Herculane, a famous thermal spa known for over 2000 years (Fig. 1). It opens on the right bank of the Cerna River and consists of a 22 m long cave passage at the far end of which the Diana thermal springs emerge (Povară et al. 1972).

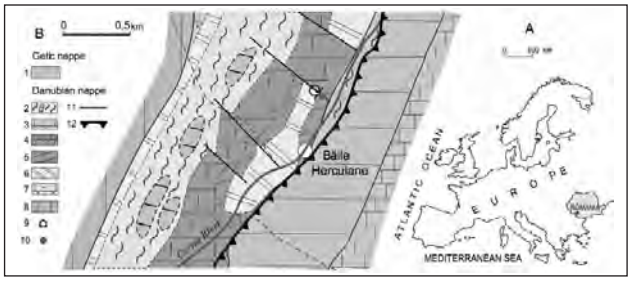

Figure 1. Location of Diana Cave and the geology of the lower Cerna Valley (from Pușcaș et al. 2013). 1. crystalline schists; 2. wildflysch with olistoliths (K_2); 3 Urgonian limestones (K_1); 4. Iuta strata (K_1); 5. bedded limestones (K_1); 6. nodular limestones (J_3); 7. conglomerates (J_1); 8. crystalline basement (PreЄ); 9. Diana Cave; 10. Diana 1 and 2 springs; 11. normal fault; 12. thrust fault (Cerna fault).

Diana Cave hosts two thermal springs (referred to as Diana 1 and 2, respectively; Povară et al. 2008). The waters are of sodium-chloride-calcium type, contain on average 1,392.5 mg/L Na^+, 725 mg/L Ca^{2+}, 3,370 mg/L Cl^-, and abundant H_2S degasses into the cave atmosphere. The thermo-mineral water has a nearly neutral pH (~6.5), the total dissolved solids amount ~5,760 mg/L, and its total sulfide and sulfate concentration 37 and 92 mg/L, respectively (Marin 1984; Wynn et al. 2010). In the early 70's, the narrow cave passage heading SE (Fig. 2) was enlarged to drain the thermal water outside in a retention basin for further therapeutic uses. During this work, the entrance cave

passage was also enlarged and the walls, especially where the marl outcrops, were reinforced using concrete. Therefore, the original cave morphology was heavily altered, but since this happened, the strong acid sulfate weathered the concrete and the cave walls are now exposed on restricted areas allowing for sample collection.

Corroborating the regional hydrogeology with springs hydrochemistry, temperature, and sulfur isotopic composition, Povară et al. (2008) and Onac et al. (2011) concluded that the thermal waters around Băile Herculane Spa (including the Diana Springs) represent deeply circulating meteoric waters that are upwelling along stratigraphic boundaries or faults.

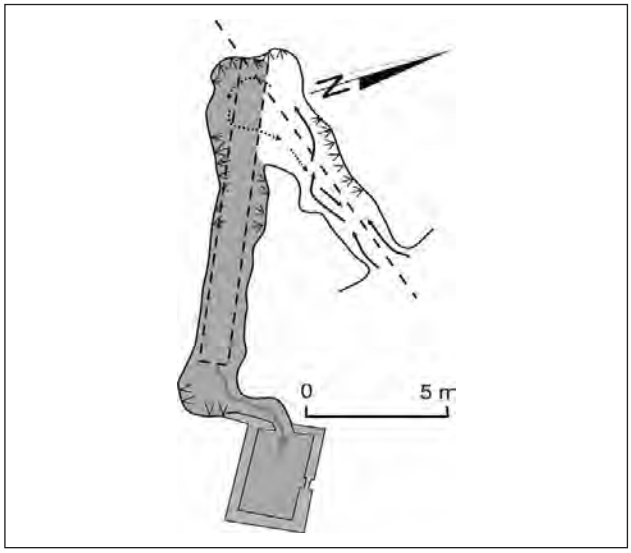

Figure 2. Map of the Diana Cave and the location of samples (∨,∀); dashed line = Diana Fault; arrows = air circulation pattern (modified from Povară et al. 1972).

The water in the cave is milky due to suspended elemental sulfur and sub-millimeter thin gypsum rafts precipitating at its surface. The abundant sulfidic steam released by the hot waters emerging from the Diana Springs condenses on the colder bedrock surface. Subsequent oxidation/hydrolysis of sulfides creates a sulfuric acid solution (pH between 2 and 4.5), which reacts with the bedrocks to form a variety of sulfates and controls the resulting cave steam-condensed weathering environment of the Diana Cave.

3. Methods

Chemical analyses were performed using a JEOL 8900R Superprobe electron microprobe (EMPA) instrument at the Department of Earth Sciences, Florida International University. The SEM investigations were carried out on a JEOL 6490 LV operated in low vacuum mode and equipped with an EDS analytical system in the Lisa Muma Weitz Imaging Core Laboratories (University of South Florida). Sulfur and oxygen isotopic composition of SO_4^{2-} in bulk sulfates and in specific minerals (hand picked under the microscope) was measured in the Stable Isotope Laboratory of the Department of Geology (USF) on a Delta V Isotope Ratio Mass Spectrometer (IRMS) using a Costech Elemental Analyzer. Analytical conditions and methods for all these methods are available in Wynn et al. (2010), Onac et al. (2009, 2011, 2013), Pușcaș et al. (2013).

4. Results

Using the methods listed in the previous chapter, we positively identified 14 minerals that belongs to the group of native elements, halogenides, carbonates, and sulfates (Table 1).

Sulfur was first mentioned in this cave by Povară et al. (1972) covering the halotrichite earthy aggregates. Later, it has been documented as tiny aggregates suspended in the upper part of the water column and as earthy masses associated with other halotrichite-group minerals (Pușcaș et al. 2013). The elemental sulfur forms when the sulphides mobilized from deep anoxic reservoirs are rapidly oxidised in the oxic section of the cave (see reactions below).

$$HS^- + ½O_2 + H^+ \rightarrow S^0 + H_2O$$

$$2H_2S + O_2 \rightarrow 2S^0 + 2H_2O$$

Halite occurs as sub-millimeter crystals intermixed with tamarugite (Pușcaș et al. 2013). Its origin is most likely related to the reaction between the Na^+ in the Iuta marls and the cave chloro-sodic thermal water (Diaconu 1974).

Calcite and *aragonite* are the only minerals in this cave that are not related to the H_2S-rich environment, being precipitated by the percolating waters entering the cave.

Table 1. Minerals identified in the Diana Cave, type of speleothems they form, and abundance (C: common; R: rare; VR: very rare).

Mineral name	Chemical composition	Speleothem type and frequency
Sulfur	S	earthy aggregates, C
Halite	NaCl	crystals, R
Calcite	$CaCO_3$	crusts; C
Aragonite	$CaCO_3$	crystals, R
Alunite	$KAl_3(SO_4)(OH)_6$	efflorescences; R
Anhydrite	$CaSO_4$	crystals; R
Apjohnite	$Mn^{2+}Al_2(SO_4)_4 \cdot 22H_2O$	efflorescences; C
Bassanite	$CaSO_4 \cdot 0.5H_2O$	crystals, R
Epsomite	$MgSO_4 \cdot 7H_2O$	crystals; R
Gypsum	$CaSO_4 \cdot 2H_2O$	crusts, rafts, flowers; C
Halotrichite	$Fe^{2+}Al_2(SO_4)_4 \cdot 22H_2O$	efflorescences; C
Pickeringite	$MgAl_2(SO_4)_4 \cdot 22H_2O$	efflorescences; C
Rapidcreekite	$Ca_2(SO_4)(CO_3) \cdot 4H_2O$	crystals; VR
Tamarugite	$NaAl(SO_4)_2 \cdot 6H_2O$	earthy aggregates, R

The first reported presence of *anhydrite* as a cave mineral came from Diana Cave (Diaconu 1974), where it occurs as acicular and prismatic crystals closely associated with *gypsum*. Responsible for its precipitation seems to be the presence in the $CaSO_4$ solutions of high amounts of sodium and magnesium. Gypsum is the primary speleogentic by-product in Diana Cave and it occurs as crusts, crystals, anthodites, moonmilk, and delicate rafts (Fig. 3a).

Halotrichite was one of the minerals identified and reported by Povară et al. (1972). However, a year later Diaconu and Medeșan (1973) published a more detailed study of the yellowish-greenish efflorescences occurring on the Iuta marls suggesting that the mineral is in fact *pickeringite*. The

Figure 3. Diana Cave. Gypsum rafts (a); halotrichite-group minerals (b); SEM image of rapidcreekite (c).

site was resampled in 2007 and 2008 and X-ray analyses not only confirmed the presence of halotrichite and pickeringite, but also identified the Mn^{2+} end-member of this group, *apjohnite* (Onac et al. 2009) (Fig. 3b). On three of the X-ray spectrum peaks for *alunite* were also identified. All these minerals formed in the acid-condensate micro-environment on the expanse of the clay minerals from Iuta marls.

Both *bassanite* and *epsomite* appear as fibrous micrometer size crystals in patchy white efflorescence covering the cave walls. The precipitation of epsomite is favored by the presence of magnesium in the thermal water and limestone bedrock, which combines with the sulfate-rich solutions condensing on the walls. Bassanite likely resulted through the partial dehydration of gypsum during winter seasons when cold, drier air enters the cave and evaporation occurs.

Tamarugite forms dull white earthy aggregates that under SEM reveal tabular subhedral crystals smaller than 15 µm in length. The sulfuric acid alteration of marls (which contributes Al^{3+} and Na^{+}; see reaction below) seems to be responsible for this unique occurrence of tamarugite (Pușcaș et al. 2013).

$$Al_2[(OH)_4|Si_2O_5]\ (\text{kaolinite}) + 2Na^+ + 4SO_4^{2-} + 6H^+ +$$

$$11H_2O \rightarrow 2\ NaAl(SO_4)_2{\cdot}6H_2O\ (\text{tamarugite}) + 2H_4SiO_4$$

This is the first time when this minerals forms in a typical limestone cavity that has no relationship to any past or present volcanic activity.

The sulfate-dominated primary and secondary cave-mineral assemblage also includes *rapidcreekite*, intimately associated with gypsum and halotrichite group minerals. Rapidcreekite forms bundles of colorless tabular rhombic crystals elongated along [001] and reaching up to 1.5 mm in length (Fig. 3c). The reaction suggested by Onac et al. (2013) to lead to rapidcreekite deposition is:

$$3Ca^{2+} + 2HCO_3^- + SO_4^{2-} + 3H_2O \rightarrow Ca_2(SO_4)(CO_3){\cdot}4H_2O + CaCO_3$$

For a confident identification of rapidcreekite from a karst cave, a precision single-crystal study was performed at the University of Vienna (Onac et al. 2013). The crystal structure was refined starting from the atomic coordinates given by Cooper and Hawthorne (1996). The increased accuracy is mainly based on the larger number of observed reflections due to the use of an area detector, which allowed establishing the location of the H atoms in a difference Fourier summation and the refinement of their atomic coordinates. Rapidcreekite unit-cell parameters are: *a* 15.524(2), *b* 19.218(3), *c* 6.161(1) Å; *V* 1838.1 Å^3, *Z*=8, space group *Pcnb*. Chemical composition (wt.%): CaO 35.65, SO_3 24.97, CO_2 13.7, H_2O 23.9, Na_2O 0.291, MgO 0.173, Al_2O_3 0.07, total 98.75%. The empirical formula based on 11 oxygen atoms per formula unit is: $Ca_{1.98}Na_{0.029}Mg_{0.013}Al_{0.004}(S_{0.971}O_4)(C_{0.97}O_3){\cdot}4.13H_2O$, very close to the ideal chemical formula.

The isotopic composition ($\delta^{34}S$ and $\delta^{18}O$) of rapidcreekite, gypsum, and bulk sulfate minerals occurring as crusts and efflorescences is homogeneous, showing ^{34}S-enriched $\delta^{34}S$ values (18 to 19.5 ‰ CDT) whereas the $\delta^{18}O$ values (in the sulfate site) range from -9.7 to -7.8 ‰ VSMOW.

5. Conclusions

Considering that Diana Cave's passages were heavily impacted by the mining activities described earlier, it is impossible to recognize any diagnostic features (cupolas, feeders, etc.) of sulfuric acid speleogenesis. However, the cave is an active sulfuric acid environment generated by the oxidation/hydrolysis of the H_2S in the hot thermal water and cave atmosphere:

$$H_2S + 2O_2 \rightarrow SO_4^{2-} + 2H^+$$

Due to the presence of abundant H^+ in the system (both in the water and steam), limestone weathers according to the reaction below:

$$CaCO_3 + 2H^+ \rightarrow Ca^{2+} + H_2O + CO_2$$

This very efficient aggressive weathering of the carbonate bedrock (Polyak and Provencio 2001; Palmer 2007) extends from below the water table up to the ceiling of the cave, being responsible for the development and further enlargement of its passages. In addition, the H_2S-rich steam condensate favors the development of an acid-sulfate weathering environment that is conducive to the precipitation of the primary and secondary speleogentic minerals described above.

The $\delta^{34}S$ values of the sulfate samples from the Diana Cave indicate an almost complete, sulfate-limited thermo-sulfate reduction (high H_2S/SO_4^{2-}) under anoxic conditions; they are consistent with an oxidation of dissolved sulfide in springs of the lower Cerna Valley described by Wynn et al. (2010). This suggests that S in the investigated sulfate minerals is derived from dissolution of primary evaporites from marine limestone followed by reduction in the thermal

aquifer and re-oxidation in the cave atmosphere. The $\delta^{18}O$ values of the sulfate minerals indicate an abundant ^{18}O exchange with $H_2O_{(l)}$ during hydration and near complete exclusion of oxygen derived from $O_{2(aq)}$ in sulfate minerals from the Diana Cave (Onac et al. 2011).

The results reported in this note provide further evidence that apart from expected speleogentic primary by-product minerals such are gypsum and alunite, other rarer phases (i.e. tamarugite and rapidcreekite) precipitate in the sulfide-rich steam condensate environment of Diana Cave if optimal pH, geochemical ingredients, and relative humidity conditions are met. These settings, however, are essentially different from other non-carbonate caves or terrestrial records previously documented for the last two minerals.

Acknowledgments

The Domogled-Valea Cernei National Park granted approval to collect samples for analysis. Dr. C. Marin from the "Emil Racoviţă" Institute of Speleology and G. Ponta (PELA) offered many insights into Cerna Valley hydrochemistry; S.C. Hercules S.A. Vera Dârmiceanu, Lucian Nicoliţă, S. Bucur, E. Primejdie, Z. Puşcaş, C. Stremţan, Daniel Vereş, and C. Cizmaş assisted us during the field campaigns. M. Pușcaș acknowledges the financial support through POSDRU 6/1.5/S/3–"Doctoral studies: through science towards society". The Romanian National University Research Council (grant ID_544 to Onac) contributed funds for this research.

References

Balintoni I, Balica C, Ducea MN, Hann HP, Şabliovschi V, 2010. The anatomy of a Gondwanan terrane: The Neoproterozoic-Ordovician basement of the pre-Alpine Sebeş-Lotru composite terrane (South Carpathians, Romania). Gond. Res., 17, 561–572.

Cooper MA, Hawthorne FC, 1996. The crystal structure of rapidcreekite, $Ca_2(SO_4)(CO_3)(H_2O)_4$, and its relation to the structure of gypsum. Can. Mineral., 34, 99–106.

Diaconu G, 1974. Quelques considérations sur la présence de l'anhydrite dans la grotte "Pestera Diana" (Băile Herculane-Roumanie). Trav. Inst. Spéol. "E. Racovitza", XIII, 191–194.

Diaconu G, Medeşan A, 1973. Sur la présence de pickeringite dans la grotte Diana (Băile Herculane, Roumanie). Trav. Inst. Spéol. "E. Racovitza", XII, 303–309.

Hill CA, Forti P, 1997. Cave minerals of the world. National Speleological Society, Huntsville, Alabama.

Marin C, 1984. Hydrochemical considerations in the lower Cerna river basin. Theor. Appl. Karstol., 1, 173–182.

Năstăseanu SV, 1980. Géologie des Monts Cerna. Anuarul Institutului de Geologie şi Geofizică, LIV, 153–280.

Onac BP, 2012. Minerals. In: WB White and DC Culver (Eds.). Encyclopedia of Caves, Academic Press, Chennai, pp. 499–508.

Onac BP, Forti P, 2011a. Minerogenetic mechanisms occurring in the cave environment: an overview. Int. J. Speleol., 40, 79–98.

Onac BP, Forti P, 2011b. State of the art and challenges in cave minerals studies. Studia UBB Geologia, 56, 33–42.

Onac BP, Puşcaş CM, Effenberger HS, Wynn JG, Povară I, 2013. Rapidcreekite in the sulfuric acid weathering environment of Diana Cave, Romania. Am. Mineral., accepted.

Onac BP, Sumrall J, Tămaş T, Povară I, Kearns J, Dârmiceanu V, Vereş D, Lascu C, 2009. The relationship between cave minerals and hypogene activity along the Cerna Valley (SW Romania). Acta Carsologica, 38, 67–79.

Onac BP, Wynn JG, Sumrall JB, 2011. Tracing the sources of cave sulfates: a unique case from Cerna Valley, Romania. Chem. Geol., 288, 105–114.

Palmer AN, 2007. Cave Geology. Cave Books, Dayton.

Polyak VJ, Provencio P, 2001. By-product materials related to H_2S-H_2SO_4 influenced speleogenesis of Carlsbad, Lechuguilla, and other caves of the Guadalupe Mountains, New Mexico. Journal of Cave and Karst Studies, 63(1), 23–32.

Povară I, Diaconu G, Goran C, 1972. Observations préliminaires sur les grottes influencées par les eaux thermo-minérales de la zone Băile-Herculane. Trav. Inst. Spéol. "Emile Racovitza", XI, 355–365.

Povară I, Simion G, Marin M, 2008. Thermo-mineral waters from the Cerna Valley Basin (Romania). Studia UBB, Geologia, 53, 41–54.

Puşcaş CM, Onac BP, Effenberger HS, Povară I, 2013. Acid-sulphate alteration origin of tamarugite in a typical karst setting: Diana Cave, Romania. Eur. J. Mineral., DOI: 10.1127/0935-1221/2013/0025-2294.

Wynn JG, Sumrall JG, Onac BP, 2010. Sulfur isotopic composition and the source of dissolved sulfur species in thermo-mineral springs of the Cerna Valley, Romania. Chem. Geol., 271, 31–43.

THE LIFE CYCLE OF SPELEOTHEMS, WITH POSSIBLE IMPLICATIONS FOR RADIOMETRIC DATING

Charles Self
University of Bristol Spelaeological Society, UK, self@globalnet.co.uk

All speleothems have a natural life cycle, which begins with their initiation as a crystal embryo (crystallite). As a crystallite grows and becomes a crystal, it now needs to compete with other crystals for growth space and the supply of new material. Some crystals are competitively successful and continue their development, while others are not and their growth ceases. This process is known as selection. The successful crystal *individuals* have a distinct pattern of boundaries with neighbouring crystals (called texture) and the combined mineral body is now an *aggregate*. Most speleothems are mineral aggregates.

There are four main factors which control the growth of a speleothem: the chemistry of the supply solution generally determines the mineral species; supersaturation determines the size and structure of the mineral individuals from which it is constructed; characteristic (Curie) symmetry controls texture and therefore what type of aggregate is formed; geometry of supply determines the speleothem's morphology. As a speleothem ages it may undergo alteration, either by replacement (with another mineral species) or by recrystallization. The ultimate fate of any speleothem is disintegration, either by solution or mechanical erosion.

Diagenesis poses a serious problem for palaeo-environmental studies. Partial dissolution of speleothems causes micritization within crystals, with selective dissolution based on trace element chemistry. During recrystallization, the cave water may introduce new material, or leach away trace elements such as uranium. The destruction of structure as crystal boundaries are erased can bring sedimentary impurities such as thorium within the body of the new crystal. In this way uranium and its daughter fission products become separated and the homogeneity of the sample is lost. Petrographic and geochemical screening may be necessary before attempting radiometric dating of old speleothems.

1. Introduction

The study of the origin and evolution of mineral bodies is termed *genetic mineralogy* and includes nucleation, initiation on a growth surface, development, alteration and disintegration (Grigor'ev 1961). Genetic mineralogy has two branches: phylogeny is the study of mineral species and their paragenesis (i.e. their contemporary growth with other mineral species); ontogeny is the study of individual crystals (mineral *individuals*), how these combine as *aggregates*, and their development as physical bodies. Ontogeny can only be applied to *minor mineral bodies*, i.e. those that have a "through" structure and/or texture (defined below) and are a product of synchronous crystallization or recrystallization in some geometrically defined space. Most speleothems are minor mineral bodies and so can be studied by mineralogic techniques such as ontogeny; only spelothems that have gone through more than one cycle of growth need be studied by petrographic techniques.

It is possible to recognise four levels of organisation of minor mineral bodies. At the first level are *individuals* which grow from a single crystal nucleus during one phase of crystallization and which have a continuous crystallographic structure. At the second level are *aggregates* made from several (often many) of these individuals; most single speleothems are aggregates. At the third level the Russian term *kora* (meaning "crust") is used to link similar aggregates growing at the same time in the same crystallization space; an example is the stalactite/stalagmite kora, which is such a familiar feature of the cave landscape. An *ensemble* is the fourth hierarchy level and is necessary because each cycle of growth begins wet and becomes steadily drier (Stepanov 1999); in this way stalactites of the gravitational water environment become overgrown by corallites of the capillary film environment. Some old speleothems have gone through two or more cycles of growth; for these mineral bodies, each cycle must be considered separately.

The terms structure and texture have very precise meanings in ontogeny. Structure describes the physical nature of crystal individuals and their bonding, while texture describes the geometric aspects of construction of aggregates made from these individuals. "Through" structure therefore means that an aggregate is made from individuals that have a similar structure. "Through" texture means that a kora describes aggregates with a similar texture that are growing independently and near to each other. In this way, the rules governing the growth of individuals and aggregates also apply to the higher hierarchy levels. This introduction is intended as a brief overview of the main terms and concepts of ontogeny. For a detailed report, see Self and Hill (2003); for a more concise version, see Self (2004) or Self and Hill (2005a). For a modern crystallographic assessment of ontogeny, see White (2012).

2. The life cycle of speleothems

2.1. Nucleation and initiation

Nucleation (in free space) and initiation (on a growth surface) are alternative beginnings for a minor mineral body. For homogeneous nucleation, forming directly from the liquid, there is an energy barrier that needs to be overcome to create a solid/liquid interface; this requires a

significantly supersaturated solution (White 2012). Initiation (heterogeneous nucleation) proceeds much more easily, since there is already a growth surface to provide a scaffold on which the crystal can build itself. For these reasons, mineral deposition in ore veins and speleothem deposition in caves is likely to be by initiation.

There are some cave situations which mimic nucleation. Cave rafts form on the surfaces of pools that are supersaturated with respect to calcite; the "growth surface" on which they initiate is a grain of dust that has fallen from the cave air. Similarly a cave pearl initiates on and overgrows a grain of sand at the bottom of a shallow pool.

Both moonmilk and tufaceous speleothems appear to nucleate within gravitational water streams. Moonmilk is a coagulation of disordered acicular individuals of microcrystalline to nanocrystalline size, which coats the walls or floor of a cave passage. Tufaceous mineral bodies are built from disordered microcrystals and form some of the most massive stalactites, stalagmites and flowstones seen in caves. Both types of deposit have been associated with bacteria or algal cells, which provide both a substrate and also an organically induced microclimate for their initiation and development. Moonmilk and tufaceous speleothems can also be of purely mineral composition, growing in turbulent, highly supersaturated gravitational water streams (Stepanov 1998). It has been suggested that crystals are initiated on cavitation bubbles within the feeding solution, later to be deposited as a disordered sediment (Self and Hill 2003).

2.2 Growth and development

Calcite, aragonite and gypsum are the most common mineral species in typical karst caves, but these minerals can grow in a wide variety of speleothem forms. There are four main factors which control the growth of speleothems: chemistry of the supply solution, supersaturation, characteristic symmetry, and geometry of supply. Chemistry determines the mineral species which is deposited, though temperature and humidity are contributing factors for some mineral species. Chemical impurities adsorbed on or incorporated into the lattice can change the deposition of calcite to its calcium carbonate polymorph aragonite (White 2012).

Supersaturation determines the size and structure of the mineral individuals which form aggregates such as speleothems (Stepanov 1998). If a solution is only just supersaturated, there will be few opportunities for initiation and mineral growth will be slow and without defects; with only a few individuals competing for material, the crystals can grow very large. Very high supersaturation leads to the rapid initiation of many small crystals, as in the case of moonmilk and tufaceous speleothems. High levels of supersaturation cause rapid growth of individuals, which often lead to growth defects; these may accumulate and result in crystal splitting. This is common in carbonate cave minerals such as calcite and aragonite, where high levels of supersaturation are created by a combination of evaporation and carbon dioxide degassing. Aragonite in caves often occurs as acicular visibly split crystals.

The component crystals of an aggregate do not simply grow together; they compete for growth space and the supply of new material. This competition leads to a reduction in the number of competing individuals, a process called selection. *Geometric selection* is the most important of the selection processes as it allows the individuals that are best aligned for mass transfer with their environment to continue to grow; individuals of other orientations are "selected out". Competition and selection cause a specific pattern of crystal boundaries to form in an aggregate, which is termed *texture*.

The various *aggregate types* are defined by their different textures, and the underlying control of texture is the Curie Universal Symmetry Principle. This states that the *characteristic symmetry* (or dissymmetry) of an object or medium must be found in the causes that generated that object or medium (Curie 1894). For cave minerals, there are three symmetry groups: spherical, cylindrical and conical. For spherical symmetry, all directions from any point are equivalent; in a supersaturated cave pool, crystal embryos (crystallites) initiate on all available surfaces and are randomly oriented during the first stage of growth. The distinctive feature of cylindrical symmetry is growth along one axis, with neighbouring crystals parallel to each other; the classic example is a helictite. Conical symmetry has neighbouring crystals diverging from each other; this is typical for corallite speleothems growing in the capillary film environment.

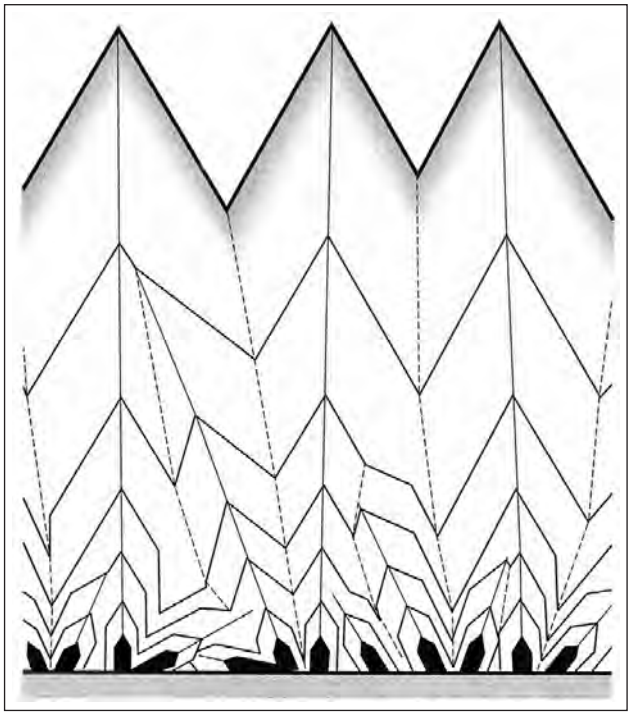

Figure 1. A parallel-columnar aggregate (cylindrical symmetry) is produced when randomly oriented crystallites (spherical symmetry) undergo geometric selection.

Dissymmetry may be regarded as the symmetry element which is missing, thus changing the characteristic symmetry of a phenomenon. Unidirectional forces such as gravitation and geometric selection are dissymmetries. In the case of spar crystals growing in a cave pool, the randomly oriented crystallites all grow at the same rate until competition begins; geometric selection then reduces the number of crystals forming the aggregate, with only those oriented

perpendicular to the substrate continuing to grow (a parallel-columnar aggregate). At the local level, this aggregate has cylindrical symmetry; the original spherical symmetry survives in the uniform thickness of the spar crystals in all parts of the pool (Fig. 1).

The various *speleothem types* were named by cavers, not mineralogists, so generally these names are based on the physical appearance (morphology) of the speleothem. Morphology depends on the geometry of the supply scheme (i.e. the supply of solute and/or loss of solvent). *Bulk* supply is typically subaqueous (pool spar deposits) but also applies to gravitational water streams (flowstone); in both settings similar simple crystals form on all available surfaces. *Area* supply is a two dimensional feeding scheme that applies to capillary thin films; these are very sensitive to variations in air flow and to surface irregularities, which cause considerable variation in the morphology of the corallites that grow in this environment (Fig. 2). *Linear* supply is where a solution gathers into linear streams (from which draperies form) or issues from fracture openings (producing shields). *Axial* supply is a one dimensional feeding scheme that applies to solutions that move through the middle of a speleothem (such as a helictite) and to the "point source" solutions that cause stalactites and stalagmites to grow out into the cave void. Note that flowstones, draperies, stalactites and stalagmites are all the same (parallel-columnar) type of aggregate; their different morphologies lie in their different supply schemes.

Figure 2. A stalactite (parallel-columnar aggregate, axial supply) has been overgrown by crystallictites(corallites built from faced crystals, branching aggregate, area supply). This minor mineral body is therefore an ensemble.

For a more detailed explanation of speleothem growth and development, see Self and Hill (2005b) or Self (2009).

2.3 Alteration and recrystallization

For cave minerals, there are two significant types of alteration: replacement (of one mineral species by another) and recrystallization. In palaeokarst settings, high temperature and pressure forms of diagenesis should also be considered.

Replacement is rather rare in caves with one exception: calcite pseudomorphs after aragonite. The original morphology of the aragonite crystal is retained, often with structural relicts, but the mineral species changes to calcite. Since these two species have the same chemical composition but different crystallographic structure, this is sometimes called a polymorphic transformation (or paramorphism). Solid state transformation at cave temperatures is very slow (White 2012), but in the presence of cave waters another process applies. Metastable aragonite dissolves while stable (and less soluble) calcite is precipitated. This commonly leaves relict fibres of aragonite surrounded by new calcite growth (Martín-Garcia et al. 2009); the terms neomorphism and inversion may be used to describe this process.

Calcite is the only thermodynamically stable form of calcium carbonate at room temperature and pressure (Kawano et al. 2009). However, aragonite grows in preference to calcite in the presence of the trace elements magnesium (which locally depresses the calcite supersaturation) and strontium (which has the aragonite structure and acts as a template). Aragonite then inverts to calcite over a period of thousands of years; the trace element strontium appears to delay this process (White 2012).

Moonmilk deposits are composed of very tiny crystals which are thermodynamically unstable; this allows a much quicker transformation. Onac and Ghergari (1993) have identified calcite paramorphs after aragonite and vaterite (another structural form of calcium carbonate), and calcite pseudomorphs after monohydrocalcite in moonmilk samples from caves in Norway and Romania.

Another form of replacement takes place continuously during the growth stage of one relatively common type of corallite, which forms when magnesium is present in the feeding solution. A multi-corallite has at its base a calcite "popcorn" coralloid speleothem; from this grows aragonite needles tipped with a ball of a more soluble mineral such as hydromagnesite. The hydromagnesite remains on the needle tip as the speleothem grows, but with regard to any fixed point it is being replaced by aragonite (otherwise it would be incorporated within the needle).

Recrystallization is where there is a redistribution of the constituents of a crystal or crystalline aggregate so that a new crystal is formed. This usually involves the destruction of structure and the growth of a new much larger crystal. The aim is a reduction in the free energy, which is tied up in the crystal surfaces (Gibbs function), a single large crystal having greater thermodynamic stability than many smaller ones. This can happen during the growth of a mineral body in a subaqueous environment if the level of

supersaturation is very low. The solution remains supersaturated with respect to large crystals, but becomes undersaturated with respect to small ones (because the ratio of mass/surface energy is a function of size). Small crystals dissolve while large ones continue to grow, thus minimizing the stored energy (Grigor'ev 1961). This is particularly relevant to the growth of readily soluble minerals such as gypsum.

Recrystallization during growth is a feature of conical stalactites: skeleton crystals are formed at the growth tip during disconnection of each drip; these later recrystallize into the central monocrystalline tube which is always present in crystalline stalactites.

Recrystallization of older calcite speleothems is very common in caves, though most stalactites, stalagmites and flowstones retain their structures for hundreds of thousands of years. When recrystallization begins, this is sometimes visible on the surface of the speleothem, which develops highly reflective, plate-like facets. One side effect of recrystallization is that the speleothem develops a simpler texture, which greatly reduces its shear and tensile strengths; as a result, it is weaker and much more prone to destruction.

2.4 Destruction and disintegration

There are occasions where the processes of destruction and disintegration of a mineral body are incomplete. In a country prone to earthquakes, broken stalactites and stalagmites may litter the floor of a cave; this is destruction, but not disintegration. New stalagmites may grow on the tilted remains of the old, the cave environmental conditions not having changed. Both the old and the new speleothems are still part of the same stalactite/stalagmite kora, having the same structural and textural regularities, but now organized in a more complex manner.

Crystallization environments in caves evolve, becoming successively drier until a new wet phase marks the start of a new growth cycle (Stepanov 1999). These cycles are not always complete, but the sequence remains the same. At the end of one cycle of growth, a new one may begin with further deposition of material rather than partial or complete dissolution of the earlier mineral body. In this way, more complex mineral bodies may form.

Partial dissolution is a very important diagenetic process that can affect the rock surfaces of a cave (Zupan Hajna 2003) and also its speleothems (Martín-Garcia et al. 2009). This process is also known as micritization, from the size of the particles left behind. For aragonite speleothems, there appears to be preferential dissolution of crystals (or zones within crystals) with a high Sr content; for calcite speleothems, it is zones with a high Mg content. There may also be a change in the stable isotope signatures of carbon and oxygen in the remaining micrite, as lighter isotopes have a greater mobility (Martín-Garcia et al. 2009).

The ultimate fate of any minor mineral body is disintegration, whether by solution or mechanical erosion. It may take many millions of years, or (in the case of ice frostwork) it can happen overnight.

3. Radiometric dating of speleothems

The primary assumption for all radiometric dating of speleothems is that the material being tested is homogeneous. The feeding solutions that form carbonate speleothems have traces of uranium in solution which is incorporated into the crystal lattice. Small sedimentary inclusions containing the element thorium, which is not water soluble, are also sometimes incorporated into the growing crystal. ^{234}Uranium decays to ^{230}Thorium at a fixed rate, so the proportion of the two elements in a speleothem sample gives its age. Sedimentary thorium contains a mixture of isotopes, including ^{230}Thorium but, provided the quantity of impurity is small, it is possible to calculate the proportion that formed within the sample by radioactive decay. On this basis, the sample can be considered homogeneous and the calculated age reliable.

Diagenesis changes everything. During partial dissolution, the trace element and stable isotope chemistry of a speleothem can change, making the sample unsuitable for palaeo-environmental studies. During replacement and recrystallization, the cave water may introduce new material with a different chemistry. The destruction of structure means that crystal boundaries, where insoluble impurities might be expected, may become incorporated into a new and larger crystal. Some parts of the new crystal will appear "clean", while other parts will be full of impurities. Over longer periods of time, the new crystal lattice actively tries to eject material that does not conform: this is known as *collecting recrystallization* and is very obvious in mineral veins, where dark metallic and pale gangue minerals are clearly separated (Stepanov 1998).

The problem for radiometric studies is that sedimentary and radiogenic thorium will collect together as recrystallization progresses. Uranium is more mobile and may be leached from the calcite lattice structure. This means that the uranium and its daughter fission products become separated, and homogeneity of the sample is lost. Where there is a suspicion that recrystallization has taken place, petrographic and geochemical screening should be used to determine if a sample is of primary origin (Bruce Railsback et al. 2002). Coarse clear columnar calcite and wide ranges of uranium concentration in the same specimen are useful warning signs.

This conclusion applies to other uranium series dating techniques, such as uranium-lead, since thorium is a link in the chain of radioactive decay. The great age that the U/Pb technique is able to measure means that many of the speleothems being tested are likely to have recrystallized. The trend towards smaller sample sizes means that local inhomogeneities should be more clearly apparent, but only if there are multiple tests of the same sample. This subject warrants further investigation.

References

Bruce Railsback L, Dabous AA, Osmond JK, Fleisher CJ, 2002. Petrographic and geochemical screening of speleothems for U-series dating: an example from recrystallized speleothems from Wadi Sannur Cavern, Egypt. Journal of Cave and Karst Studies, 64, 108–116.

Curie P, 1894. Sur la symetrie dans les phenomenes physiques, symetrie d'un champ electrique et d'un champ magnitique. Journal de Physics, 3, 3, 395–415 (In French).

Grigor'ev DP, 1961, Ontogeny of minerals. Lvov, Izdatel'stvo L'vovskogo Univ. (In Russian). English translation 1965, Israel Program for Scientific Translations.

Kawano J, Shimobayashi N, Miyake A, Kitamura M, 2009. Precipitation diagram of calcium carbonate polymorphs: its construction and significance. Journal of Physics: Condensed Matter, 21, 1–6.

Martín-Garcia R, Alonso-Zarza A, Martín-Pérez A, 2009. Loss of primary texture and geochemical signatures in speleothems due to diagenesis: Evidences from Castañar Cave, Spain. Sedimentary Geology, 221, 141–149.

Onac BP, Ghergari L, 1993. Moonmilk mineralogy in some Romanian and Norwegian caves. Cave Science, 20, 107–111.

Self CA, 2004. The internal organization of speleothems. Acta Carsologica, 33, 245–255.

Self CA, 2009. Which features of the cave environment control the growth of speleothems? Proc. 15th ICS, Kerrville, Texas, USA, pp. 332–337.

Self CA, Hill CA, 2003. How speleothems grow: An introduction to the ontogeny of cave minerals. Journal of Cave and Karst Studies, 65, 130–151.

Self CA, Hill CA, 2005a. An introduction to genetic mineralogy and the concept of "ontogeny of cave minerals". Proc. 14th ICS, Athens, Greece, pp 125–129.

Self CA, Hill CA, 2005b. How geometric factors determine which type of speleothem will grow in a cave environment. Proc. 14th ICS, Athens, Greece, pp. 318–321.

Stepanov VI, 1998. Notes on mineral growth from the archive of V. I. Stepanov (1924–1988). Proceedings of the University of Bristol Spelaeological Society, 21, 25–42.

Stepanov VI, 1999. Periodicity of crystallization processes in karst caves. Cave Geology, 2, 209–220.

White WB, 2012. Speleothem microstructure/speleothem ontogeny: a review of Western contributions. International Journal of Speleology, 41, 329–358.

Zupan Hajna N, 2003. Incomplete solution: weathering of cave walls and the production, transport and deposition of carbonate fines. ZRC SAZU, Postojna-Ljubljana.

SPELEOTHEMS IN CAVITIES DEVELOPED IN MAGMATIC ROCKS

Juan Ramón Vidal-Romaní, Jorge Sanjurjo-Sánchez, Marcos Vaqueiro-Rodríguez, Laura González-López, María José López-Galindo[1]

[1]University Institute of Geology, Campus de Elviña s/n 15071, Coruña, Spain, juan.vidal.romani@udc.es

Four types of natural cavities in magmatic rocks are known: (1) developed along fracture planes, (2) associated with residual block fields, (3) tafone, and (4) lava tube. These openings are the only access for the runoff toward inside the rocky massif. The water flows always of low velocity (trickles) weather the rock forming small fissural regoliths that are moved by the water and then deposited, giving rise to granular detrital accumulations (primary speleothems) of openwork texture. The porous system of these sediments is the temporal refuge for different microorganisms (bacteria, algae, fungi, testate amoebae, spores, diatoms, collembola and mites, etc.), which inhabit the cavity during the humid stage. Their organic activity provides the water with metabolic compounds able to solubilise ions, mainly Si, of the rock without changes in pH which in the dry stage will precipitate by oversaturation as opal-A and other authigenic minerals that will not only contribute to cement the primary speleothems but also to form the secondary speleothems. The shape of the speleothems, either cylindrical or planar, is mainly defined by the way of the water circulation at low velocity by dripping, capillarity, foam-drops like textures or by laminar flow. The relationship between the microbiological activity and the processes of weathering, dissolution and sedimentation justifies their name as biospeleothems.

1. Introduction

The speleothems studied in this paper are formed during the water circulation at low velocity (trickles) through the fissural system of massifs of igneous rocks. In the water/rock contact the physical weathering produces a heterometric detrital aggregate of mineral grains which are first moved by the water as a hydro-suspension (slurry) and then deposited on the walls, floor or ceiling of the cave. These types of speleothems may be considered as residual materials because they derive from the rocky substratum of the cavity, but other authigenic species are associated with them, i.e. generated in the same cave at room temperature as amorphous opal, evansite, bolivarite, struvite, pigotite, taranakite, allophane, hematite, goethite. The most common mineral species among these is the amorphous opal (called coralloid in the old works (Caldcleugh 1829; Swarzlow and Keller 1937), though here the term opal-A is used (Vidal Romaní et al. 2010). An additional feature of the silica hydrogel from which the opal-A speleothems are formed is that it may be the base for the formation of new authigenic mineral species called whiskers (Twidale and Vidal Romaní 2005). Whiskers twined crystalline aggregates of mineral species such as halite, gypsum, siderite, cerussite, plumbean aragonite, malachite, etc., though this list is growing every day more. However, in the caves developed in basic igneous rocks (gabbros, diorites, peridotites, basalts), the amorphous opal speleothems are not very frequent, other minerals, also authigenic, as the carbonates of Ca, Mg, Fe, Pb, etc. being habitual. All these minerals were described in caves of very different rock types and varied geographic-climatic environments: temperate humid, arid to cold regions (Spain, Portugal, Azof speleothems in cavities in magmatic rocksores Islands, United Kingdom, Germany, Poland, Czech Republic, Sweden, Finland, Corea), tropical (Brazil, Venezuela, Madagascar), arid (South Australia, Argentina, Nigeria, Botswana, Mexico, U.S.A., etc) (Willems et al. 1998, 2002; Twidale and Vidal Romaní 2005; Vidal Romaní et al. 2010).

2. Morphological features of the speleothems

Speleothems are not only differentiated by their mineralogical composition but also by their morphology. For example, carbonates or whiskers associated with the amorphous opal speleothems are always presented as crystals of high idiomorphy in spite of their small size. On the contrary, the amorphous mineral species are adapted to the relief of the surface on which they deposit, and their morphology is related to the features of the dynamics of the fluid, which originates the speleothem.

The following types of speleothems in cavities in magmatic rocks are distinguished:

2.1. Cylindrical speleothems

They are associated with water movement either by dripping or capillarity. There are different types as follows:

Stalactites *s.s.*: they are formed on the upper part of rock fissures (the ceiling or eaves of cavities) when the weight of the drop overcomes the superficial stress (then dripping is produced).

Grass-shaped speleothems: multiple associations of very thin (maximum 1 mm) cylindrical forms and associated with the ceiling, walls or floor of cavities. These speleothems grow by deposition associated with capillary movements of the water through the agglomerate mass of clastic accumulations of angular grains soaked with water.

Anti-stalactites: These individual speleothems (Vidal Romaní and Vilaplana 1984) grow by capillary movements of the water from a clast grain mineral agglomerate soaked in water. They are usually thicker (up to 4 mm of diameter) and reach longitudinal developments between 4 and 10 mm.

Stalagmites *s.s.*: these speleothems are infrequent in the igneous rock caves. They are formed by the precipitation of the substances dissolved or dragged by the water which fall from the stalactites *s.s.*

Club-like stromatolites s.l.: they are formed by the growth of biofilms of blue-green algae while there is humidity inside the cave. When the environment dries, the algae transform into the substratum of the new generation of algae that will grow in the following humid stage.

2.2. Planar speleothems

They may normally appear associated on any flat, low relief surface (either ceiling or floor) but even in subvertical surfaces as far as they do not overpass the threshold of dripping, which is given by the stress adherence of the water to the cave rocky surfaces. Different types of planar speleothems are distinguished:

Flowstone, rimstones and microgours: they are continuous covers of the cave rocky surface with variable thicknesses and may also hide the rock micro rugosity. They are disordered accumulations of mineral clasts pushed by the water layer during the humid phases marked by lineal accumulations with sinuous shape behind the ones that may even hold water temporarily. Flowstones, rimstones and associated pool (microgour) are associated with flat (either ceiling or floor), gentle-sloped and inclined or even subvertical surfaces when the flow speed does not overpass the threshold of water-rock superficial adherence in the trickles.

Water drop structures: they are similar to the foam-like structures formed on the upper part of the beach when an advance front of the water layer is individualized into small drops. They are associated with the ceiling of the cavity where the water is divided into small drops, which, by superficial stress, attract a thin coat of clasts of minerals that the water evaporation will cement as opal-A allowing the conservation of the morphology of the drop.

3. Methods

Different analytical techniques have been used to study these speleothems: ICP Mass Spectroscopy, XRD, XRF, and mainly SEM; all of them, but the last, are destructive analytical methods. Though SEM gives morphological information (texture, structure, morphometry of grains), it also gives data of elemental composition with the backscattered X-R. From the first works (Caldcleugh 1829) these speleothems were considered to be formed by water dripping ignoring the existence of other types of speleothems. In this work, the information obtained by Stereoscopic Microscopy is included, allowing to establishing the complete sequence of formation of speleothems.

4. Results and discussion

The following stages are distinguished in the formation of speleothems: (1) accumulation of the granular material coming from the fissure regolith and transported by water; (2) first colonisation by microorganisms as bacteria, algae, fungi, amoebae, collembola and mites; (3) formation, dissolution and precipitation of amorphous opal; and (4) formation of whiskers from the silica hydrogel. The activity of these microorganisms promotes the dissolution of Si, mainly, (Ehrlich 1996) providing with low molecular weight organic acids (mainly oxalates) with chelant ability without pH changes (McMahon and Chapelle 1991; Barker et al. 1997). Later, the dissolved Si precipitates as amorphous opal $SiO_2 \cdot 15(H_2O)$, 100 times more soluble in water converting the generation of speleothems into a continuous process always depending on the water circulation through the fissure system. Each time it rains again, the re-circulation of water through the fissural system of the rocky massif produces the re-dissolution of the amorphous opal and its later re-precipitation. This phase in the evolution of the speleothem is favourable for the growth of authigenic minerals of small size, whiskers, which are located on the points where water accumulates; for the cylindrical speleothems on their final edge and for the planar speleothems or flowstone in the places where the water accumulates in the microgour or pool. The mineralogy of these whiskers is very varied: gypsum, carbonates, halides, though the most common is gypsum ($CaSO_4 \cdot 2H_2O$). In some cases, whiskers appear as isolated individuals except for gypsum which always gives nice twinned crystalline associations in physical continuity, with deposits of opal-A. Some authors attribute the presence of S necessary for the formation of gypsum to the activity of microorganisms (Franklin et al. 1994; Welch and Ulllman 1996) which are able to produce sulphate oxides from oxidation of organic matter, this latter invariably associated with the zones where the speleothems are observed (Vidal Romaní et al. 2003). Some authors (García Ruíz and Migues 1982) achieved to reproduce the process in laboratory using a silica hydrogel base to obtain the growth of crystals of different substances in very low concentrations. In the cavities of igneous rocks, gypsum whiskers are normally found, but also, in accordance with our own observations, whiskers of calcite, aragonite, plumboaragonite and phosphates are also formed. Some authors (Van Rosmalen and Marcheé 1976) explain the diverse morphology of the gypsum whiskers formed from silica hydrogel by the presence of different additives or impurities. The lowest abundance of opal-A speleothems is symptomatic in cavities (e.g., lava tube) (Woo et al. 2008) developed in basic igneous rocks (syenites, granodiorites, diabases, etc.) and their physical association with calcite crystals obviously formed (Beinlich and Austrheim 2012) by combination of CO_2 dissolved in water with brucite or other carbonates existing in the rock. At pressure and room temperature, Si does not form stable crystalline structures but minerals of low temperature (opal-A) slowly evolve toward more stable polymorphs of silica as opal-CT (Bustillo 1995). Notwithstanding, the first essays to date opal-A speleothems by OSL (Sanjurjo and Vidal Romaní 2011) seem to indicate that at least in some climatic environments the transition Opal-A to Opal-CT may be delayed many thousands of years.

These types of microenvironments developed in the porous system of the speleothems either cylindrical or flowstones with their small gours where water is kept temporarily are a very suitable environment for the development of microorganisms which develop their vital cycle while water remains. Their disappearance by evaporation during the dry stages causes the precipitation of amorphous opal dissolved

in it fossilizing the microorganisms or their remains that are immediately coated by opal-A. Each time the rain provides the fissural system with water, life regenerates, at least partially, in the speleothem producing the germination of the latent or resistance forms developed in diatoms, spores, algae, testate amoebae, etc, which live and develop in the micro speleological system. At the same time, other organisms (mites and collembola) use the speleothem as physical support to move and feed on organic matter. The growth processes of the speleothems are superposed to the ones of the development of microorganisms in these cavities causing subtle differences between life and sedimentation, justifying the name of biospeleothems given to these deposits.

5. Conclusions

The partially open fissure systems of granitic massifs through which water circulates at very slow speed (trickles) are natural environments with which different types of neomineralizations are associated: opal-A, gypsum, the most frequent minerals. These biominerals or biospeleothems are formed indirectly due to microbiological processes (as a consequence of reactions produced by the metabolic products derived from the organic activity). Si and Al are the most abundant elements in the granitic rocks and thus mainly prevail in the infiltration water. The oversaturation by water evaporation or/and the pH changes cause the precipitation of the elements and solubilised compounds originating the speleothems of granite systems. Opal-A (Si) is the most important type of speleothem quantitatively and the most diversified morphologically. The organisms (bacteria, algae, fungi) that live and are developed in these speleothems are active while the speleothem is wet. When water flow diminishes or evaporates, the organisms react developing resistance spores staying until the next humid period when they germinate again. Mites and collembola also have activity in the speleothem using the content in organic matter of the same speleothem for their subsistence. The last stage in the speleothem development is where S of organic origin is combined with the Ca of the plagioclases, and using the substratum of amorphous silica (silica gel) gypsum crystals develop with an excellent idiomorphy and are present widely in the opal-A.

Acknowledgments

This paper is a contribution to the Research Project BTE-CGL-2006-08996 of the Ministry of Education and Science of Spain. We thanks Ana Martelli for the translation and help to eliminate many errors and inconsistencies.

References

Barker WW, Welch SA, Banfield JF, 1997. Biogeochemical weathering of silicate minerals. In: Geomicrobiology: interactions between microbes and minerals (Banfield, J. F. and Nealson KH, eds.). Washington: Mineralogical Society of America, 391–428.

Beinlich A, Håkon Austrheim H, 2012. In situ sequestration of atmospheric CO_2 at low temperature and surface cracking of serpentinized peridotite in mine shafts. Chemical Geology, 332–333, 32–44.

Bennett PC, 1991. Quartz dissolution in an organic-rich aqueous system. Geochimica et Cosmochimica Acta, 55, 1781–1797.

Blyth AJ, Baker A, Collins MJ, Penkman KEH, Gilmour MA, Moss J S, Genty D, Drysdale RN, 2008. Molecular organic matter in speleothems and its potential as an environmental proxy. Quaternary Science Reviews, 27, 905–921.

Brady PV, Walther JV, 1990. Kinetics of quartz dissolution at low temperatures. Chemical Geology, 82, 253–264.

Bustillo MA, 1995. Una nueva ultraestructura de ópalo CT en silcretas. Posible indicador de influencia bacteriana. Estudios Geológicos, 51, 3–8.

Caldcleugh A, 1829. On the geology of Rio de Janeiro. Transactions of the Geological Society, 2, 69–72.

Cañaveras JC, Sánchez-Moral S, Soler V, Saiz-Jiménez C, 2001. Microorganisms and microbially induced fabrics in cave walls. Geomicrobiology Journal, 18, 223–240.

Ehrlich HL, 1996. Geomicrobiology. 3rd ed. Marcel Dekker, Inc., New York, 719.

Franklin SP, Ajas AJr, Dewers, TA, Tieh T.T, 1994. The role of carboxilic acids in albite and quartz dissolution: An experimental study under diagenetic conditions. Geochimica et Cosmochimica Acta, 58(20), 4259–4279.

García-Ruíz JM, Migues F, 1982. Condiciones de formación del primer precipitado en la técnica del gel de sílice. Estudios Geológicos, 38, 3–14.

Kröger N, Deutzmann R, Sumper M, 1999. Polycationic peptides from diatom biosilica that direct silica nanosphere formation. Science, 286, 1129–1131.

McMahon PB, Chapelle FH, 1991. Microbial production of organic acids in aquitard sediments and its role in aquifer geochemistry. Nature, 349, 233–235.

Sanjurjo Sánchez, J, Vidal Romaní JR, 2011. Luminescence dating of pseudokarst speleothems: a first approach. 2nd Conference on Micro-raman and luminescence studies in the Earth and Planetary Sciences (CORALS II). May 18–21, Madrid, Spain.

Swarzlow CI, Keller WD, 1937. Coralloid Opal. Journal of Geology, 45, 101–108.

Twidale CR, Vidal Romaní JR, 2005. Landforms and geology of granite terrains. Balkema, London, 351.

Van Rosmalen GM, Marcheé WGH, 1976. A comparison of gypsum crystals grown in silica gel and agar in the presence of additives. Journal of Crystal Growth, 35, 169–176.

Vidal Romani J.R, Vilaplana JM, 1984. Datos preliminares para el estudios de espeleotemas en cavidades graníticas. Cadernos do Laboratorio Xeolóxico de Laxe, 7, 35–324.

Vidal Romaní JR, Bourne, J A, Twidale CR, Campbell EM, 2003. Siliceous cylindrical speleothems in granitoids in warm semiarid and humid climates. Zeitschrift für Geomorphologie, 47(4), 417–437.

Vidal Romaní JR, Sanjurjo J, Vaqueiro, M, Fernández Mosquera D, 2010. Speleothem development and biological activity in granite cavities. Geomorphologie: relief, processus, environment, 4, 337–346.

Welch SA, Ullman WJ, 1996. Feldspar dissolution in acidic and organic solutions: Compositional and pH dependence of dissolution rate. Geochimica et Cosmochimica Acta, 60(16), 2939–2948.

Willems L, Compere P, Sponholz B, 1998. Study of siliceous karst genesis in eastern Niger: microscopy and X-ray microanalysis of speleothems. Zeitschrift für Geomorphologie, 42(2), 129–142.

Willems L, Compère P, Hatert F, Pouclet A, Vicat JP, Ek C, Boulvain F, 2002. Karst in granitic rocks, South Camerun: cave genesis and silica and taranakite speleothems. Terra Nova, 14, 355–362.

Woo KS, Choi DW, Lee KC, 2008. Silicification of cave corals from some lava tube caves in the Jeju Island, Korea: Implications for speleogenesis and a proxy for paleoenvironmental change during the Late Quaternary. Quaternary International, 176–177, 82–95.

EVOLUTION OF GUANO UNDER DIFFERENT ENVIRONMENTAL CONDITIONS: A MINERALOGICAL APPROACH

Alexandra M. Giurgiu[1,2], Bogdan P. Onac[2,3], Tudor Tămaş[1,2], Joan J. Fornós[4]

[1]Emil Racoviţă Institute of Speleology, Clinicilor 5, 400006 Cluj-Napoca, Romania, alexandra.giurgiu@iser-cluj.org

[2]Department of Geology, "Babeş-Bolyai" University, Kogălniceanu 1, 400084 Cluj Napoca, Romania

[3]Department of Geology, University of South Florida, 4202 E. Fowler Ave., SCA 528, Tampa, FL 33620 USA

[4]Departament de Ciències de la Terra, Universitat de les Illes Balears, Ctra. Valldemossa km 7.5, 07122 Palma de Mallorca, Spain

The phosphate minerals from three Romanian caves that host bat guano deposits have been investigated. The XRD and SEM analyses have revealed the presence of seven phosphates (brushite, francoanellite, hydroxylapatite, leucophosphite, taranakite, vashegyite and variscite) along with the more common gypsum, calcite and various allochthonous clay minerals. The occurrence of these phosphate minerals highlights the decomposition and various reactions that take place between the phosphate-rich solutions leaching out from the guano and different cave sediments and/or bedrock. The variation of the environmental conditions in the vicinity and within the guano accumulations is responsible for the type of mineral that is being precipitated. The abundance of specific phosphates indicates changes of the pH (from acidic to alkaline) and moisture (both wet and dry conditions) in all the three caves.

1. Introduction

Phosphates represent the second largest group among cave minerals (after sulfates), 55 out of over 300 being found in different cave settings (Hill and Forti 1997; Onac 2012). The most abundant phosphate minerals are hydroxylapatite, brushite, ardealite, taranakite and variscite, whereas the rest are rare and form only if particular conditions are present. The occurrence of phosphate minerals is related to the accumulation of significant bat guano or bone accumulations. The clay minerals from detrital sediments in caves are a source for aluminum, silica, potassium, and sodium, which, when combined with the phosphoric acid will increase the chances for precipitation of rare phosphate minerals (Hill and Forti 1997).

The present study provides data on some phosphate minerals identified in three Romanian caves (Zidită [Walled], Gaura cu Muscă, and Gaura Haiducească; Fig. 1) that host important guano deposits. The aim of the paper is to emphasize that the phosphate solutions leaching from underneath the guano have reacted with the bedrock and other cave sediments under different environmental conditions precipitating a variety of phosphate minerals.

Figure 1. Gaura cu Muscă (GM), Gaura Haiducească (GH), and Zidită (PZ) caves on the Romanian karst map.

2. Cave settings

The Gaura cu Muscă is a 254 m long active cave developed in Upper Jurassic limestones and opens in the left bank of the Danube near the village of Moldova Nouă (Caraş-Severin county, SW Romania). The guano deposits in this cave are related to the presence of large bat colonies (*Myotis myotis* and *Rhinolophus ferrumequinum*) (Negrea and Negrea 1979). The samples collected for this study were taken from the Bats Passage, a short fossil gallery that shortcuts the Water Passage (Fig. 2a) and consist of ochre to dark brown earthy material interbedded within horizons of fossil guano deposits.

The second cave, Gaura Haiducească, is developed in the Lower Cretaceous (Barremian-Aptian) limestones of the Locvei Mountains and is located north from the town of Moldova Nouă. The cave, explored and mapped on 714 m until 1976 (Bleahu et al. 1976) is presently a hydrological traverse 1,370 m long and consists of three well individualized sectors: a large entrance room (Great Hall, 180 m long, 60 m large and 25 m high) in its upstream part, a small median passage, temporary active but which sometimes may get completely flooded, and a larger downstream active passage leading to the "spring" entrance (Iurkiewicz et al. 1996). The phosphate samples were collected from the slopes on the southern side of the Great Hall (Fig. 2b), where they occur as white to yellowish-brown nodules, lenses, and earthy aggregates within a significant guano accumulation.

Zidită Cave (also known as Dacilor) is an old cave fortress in the Metaliferi Mountains (SE part of the Western Carpathians) developed in Upper Jurassic limestones. The cave is a fossil maze with a total length of 547 m (Fig. 2c) and has several guano accumulations. The largest of them, possibly belonging to a *Rhinolophus* colony, is a 1.5 m guano deposit located in Bat Room, near the end of the cave

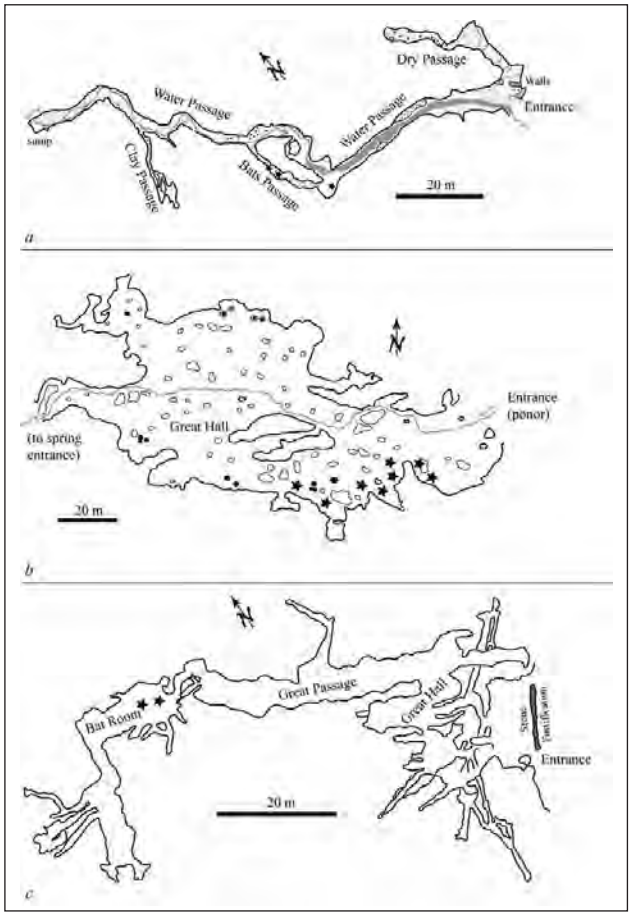

Figure 2. Maps of the studied caves with location of samples (stars): a. Gaura cu Muscă (simplified from Bleahu et al. 1976); b. The Great Hall from Gaura Haiducească (simplified from Bleahu et al. 1976); c. Zidită Cave (map by Proteus Hunedoara Caving Club, used with permission).

(Fig. 2c). All the samples taken from this cave were collected from the vicinity of this large deposit and consist of crusts formed on limestone blocks and on clay deposits from the room floor.

3. Methods

The X-ray diffractions were performed using a Siemens D5000 diffractometer operated at 40 kV and 30 mA. The instrument employs Cu*Kα* radiation. The step-scan data were continuously collected over the range of 5° to 75° 2θ, using a step interval of 0.05° 2θ. Counting time was 1 second per step. The scanning electron microscopy was performed on a Hitachi S-3400N equipped with a Bruker Energy Dispersive Spectroscopy (EDS) microanalyzer system. All analyses were carried out using instruments at the Serveis Cintificotècnics (Universitat des les Illes Balears, Palma de Mallorca, Spain).

4. Results

Brushite [$Ca(PO_3OH)\cdot 2H_2O$] occurs only in Zidită Cave as a white-ivory paste-like material. It is a common cave mineral, which is isostructural with gypsum and is stable under acidic (pH < 6) and damp conditions (Hill and Forti 1997). It results from the reaction of carbonate bedrock or calcite/aragonite speleothems with the phosphoric acid derived from guano deposits (Fiore and Laviano 1991).

Francoanellite [$K_3Al_5(PO_3OH)(PO_4)_2\cdot 12H_2O$] was identified in Gaura cu Muscă and Gaura Haiducească along with taranakite and illite-group minerals (Nickel and Nichols 2009). The likely process that leads to the formation of francoanellite is the mechanism proposed by Hill and Forti (1997), which suggests dehydration of taranakite formed by the reaction between the clay-rich sediments and guano solutions under acidic conditions.

The EDS spectrum of sample 1563 (Gaura Haiducească) shows characteristic peaks for O, P, and Zn suggesting the possibility that hopeite or another Zn-rich phosphate may occur in this cave. More investigations are needed to fully confirm the presence of any Zn-phosphate.

Hydroxylapatite $Ca_5(PO_4)(OH)$, was identified in Gaura cu Muscă and Zidită caves as light- to dark-brown or even black thin crusts, which overlay the limestone bedrock. It most occurrences is closely associated with gypsum. The presence of hydroxylapatite indicates a slightly alkaline environment as this mineral generally forms through the reaction of phosphatic solutions derived from guano with limestone when the pH is above 6 (Fiore and Laviano 1991; Dumitraş and Marincea 2008).

Taranakite [$K_3Al_5(PO_3OH)_6(PO_4)_2\cdot 18H_2O$] forms 3–7 cm thick earthy white masses in Gaura cu Muscă and Gaura Haiducească caves. Under ESEM, taranakite appears as platy, pseudohexagonal crystals (Fig. 3). The interaction between bat guano and clay (which provide the Al ions) in acidic conditions is at the origin of taranakite.

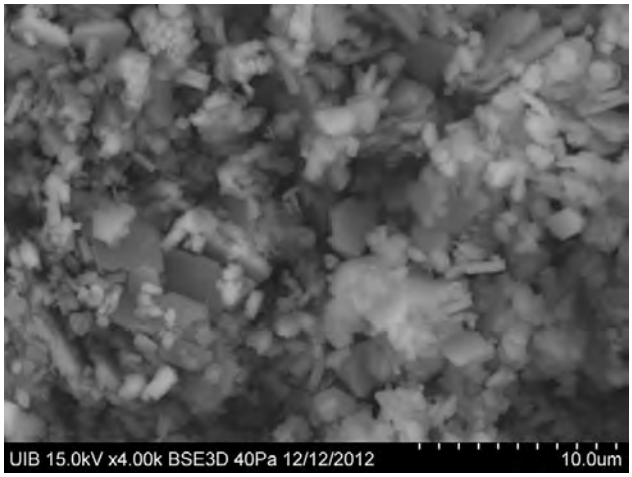

Figure 3. ESEM microphotograph of taranakite crystals (sample 1563; Gaura Haiducească).

Variscite [$AlPO_4\cdot 2H_2O$] was found in Gaura cu Muscă in an interbedded guano/clay sequence. We attribute the formation of variscite to the reaction between the phosphate-rich leachates derived from guano and the underlying clay sediments (Onac et al. 2004). Another mineral earlier described from this cave is *vashegyite* (Onac et al. 2006). It occurs as dull white nodules within a highly phosphatized clay horizon interbedded and covered by guano. The underground stream regularly floods the entire deposit, thus permanent damp conditions prevail most of the time.

Leucophosphite [$K(Fe^{3+})_2(PO_4)_2(OH)\cdot 2H_2O$] is a rare phosphate mineral and forms through the reaction between H_3PO_4 (derived from leached guano) and clay minerals in the presence of iron hydroxides. The XRD, SEM, and EDS

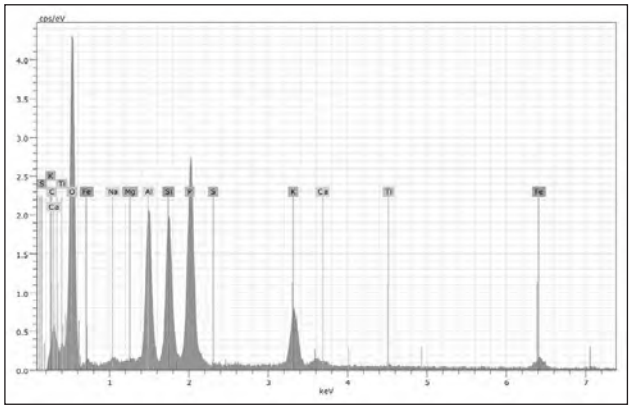

Figure 4. The EDS analysis of leucophosphite (sample 1569; Gaura cu Muscă Cave).

analyses of the sample 1569 reveal the presence of this phosphate in Gaura cu Muscă. Illite-group minerals and iron-rich phases provide the K and Fe ions, respectively. These elements were documented by EDS microanalyses (Fig. 4).

5. Conclusions

Bat guano deposits and the related minerals from three Romanian caves were studied and the analyses have revealed the presence of seven phosphates along with calcite, gypsum, and illite-group minerals. The occurrence of phosphate minerals highlights the decomposition of bat guano in time and the variation of the environmental conditions (mainly changes in pH and moist vs dry) in the vicinity and within the accumulation.

The results suggest diverse interactions between the solutions from bat guano and the limestones and clay sediments from the cave. The reaction with limestone is responsible for the formation of Ca-rich phosphates whereas the precipitation of taranakite, variscite, or leucophosphite normally suggests the existence of a clay mineral precursor (Dumitraş et al. 2002). Francoanellite has formed by the partial dehydration of taranakite. The occurrence of Ca-rich phosphates indicates variations of the pH and moisture within and below the guano deposit as well as an increase in Ca/P ratio towards apatites (Onac and Vereş 2003) in all three caves.

The described phosphate minerals provide information about the environment in which they have formed. In Zidită Cave brushite is the most common phosphate mineral suggesting an overall acidic and damp depositional environment. In Gaura Haiducească the same acidic environmental conditions but much wetter are inferred from the abundance of taranakite. Phosphate minerals from Gaura cu Muscă show different abundances, with taranakite, variscite, vashegyite, and francoanellite indicating a wet, acidic environment (in the proximity of the guano deposits). The hydroxylapatite occurs mainly at distant locations from the large guano accumulations in sections of the cave where only small-size colonies are hibernating (Negrea and Negrea 1979). Its presence indicates slightly alkaline and drier conditions.

Acknowledgments

The authors would like to thank Ferran Hierro and Joan Cifre from the Serveis Científicotècnics at the Universitat de les Illes Balears in Palma (Spain) for their support while conducting the analyses. T. Brad and I. Vişan are thanked for helping during the field work activities. R. Breban (Proteus Caving Club, Hunedoara) kindly provided the map of Zidită Cave. Financial support from the Romanian National Authority for Scientific Research (grant PCE-2011-3-0588 to BPO and TT) is gratefully appreciated.

References

Bleahu M, Decu, V, Negrea Ş, Pleşa C, Povară I, Viehmann I, 1976. Peşteri din România. Bucureşti, 415 (in Romanian).

Dumitraş D, Marincea Ş, 2008. Apatite-(CaOH) in the fossil bat guano deposit from the "Dry" Cioclovina Cave, Şureanu Mountains, Romania. Canadian Mineralogist, 46, 431–445.

Dumitraş D, Marincea Ş, Diaconu G, 2002. Leucophosphite and taranakite in the bat-guano deposit from Lazului Cave (Mehedinţi Mountains). Romanian Journal of Mineral Deposits, 80, 23–25.

Fiore S, Laviano R, 1991. Brushite, hydroxylapatite, and taranakite from Apulian caves (southern ltaly): New mineralogical data. American Mineralogist, 76, 1722–1727.

Hill C, Forti P, 1997. Cave minerals of the world. National Speleological Society, Huntsville, Alabama.

Iurkiewicz A, Constantin S, Bădescu B, 1996. Sisteme carstice majore din zona Reşiţa – Moldova Nouă. A.S. Exploratorii Reşiţa, 70 (in Romanian).

Negrea A, Negrea Ş, 1979. Peşterile din Defileul Dunării şi fauna terestră. In: Orghidan T. & Negrea Ş. (Eds.) – Speologia, Bucureşti: Editura Academiei RSR: 30–75 (in Romanian).

Nickel EH, Nichols MC, 2009. IMA/CNMNC list of mineral names. http://www.MaterialsData.com

Onac BP, 2012. Minerals. In: William B. White and David C. Culver, (Eds.), Encyclopedia of Caves. Academic Press.

Onac BP, Vereş DS, 2003. Sequence of secondary phosphates deposition in a karst environment: evidence from Măgurici Cave (Romania). European Journal of Mineralogy, 15, 741–745.

Onac BP, Kearns J, Breban R, Cîntă Pânzaru S, 2004. Variscite ($AlPO_4 \cdot 2H_2O$) from Cioclovina Cave (Şureanu Mountains, Romania): A tale of a missing phosphate. Studia UBB Geologia, 49 (1), 3–14.

Onac BP, Zaharia L, Kearns J, Vereş D, 2006. Vashegyite from Gaura cu Muscă Cave. International Journal of Speleology, 35 (2), 67–73.

A CONTRIBUTION TO THE MINERALOGY OF MONTE GUISI CAVE (SW SARDINIA, ITALY)

Cristian Moldovan[1], Monica I. Călugăr[1], Bogdan P. Onac[2,3], Jo de Waele[4], Angelo Naseddu[5], Joan J. Fornós[3]
[1]Department of Geology, Babeș-Bolyai University, Kogălniceanu 1, 400084 Cluj Napoca, Romania
[2]Department of Geology, University of South Florida, 4202 E. Fowler Ave., Tampa, FL 33620, USA (bonac@usf.edu)
[3]Departament de Ciències de la Terra, Universitat de les Illes Balears, Ctra. Valldemossa km 7.5, 07122 Palma de Mallorca, Spain
[4]Italian Institute of Speleology, University of Bologna, via Zamboni 67, 40126 Bologna, Italy
[5]Speleo Club Domusnovas, Federazione Speleologica Sarda, Ex Direzione Miniera San Giovanni, Regione San Giovanni, 09016 Iglesias, Italy

This note presents a preliminary mineralogical study of the skarn-hosted Monte Guisi Cave in SW Sardinia (Italy).

X-ray diffraction (XRD) and environmental scanning electron microscope (including energy dispersive X-ray spectroscopy microanalysis; EDS) analyses allowed us to identify some uncommon cave minerals such as: cerussite $PbCO_3$, rosasite $(Cu,Zn)_2(CO_3)(OH)_2$, dundasite $PbAl_2(CO_3)_2(OH)_4 \cdot H_2O$), brochantite $Cu_4SO_4(OH)_6$, cuprite Cu_2O, hemimorphite $Zn_4Si_2O_7(OH)_2 \cdot H_2O$, chrysocolla $(Cu,Al)_2H_2Si_2O_5(OH)_4 \cdot nH_2O$, shattuckite $Cu_5(SiO_3)_4(OH)_2$, and plancheite $Cu_8(Si_4O_{11})_2(OH)_4 \cdot H_2O$. Dundasite and plancheite are for the first time reported as cave minerals. All these species appear to represent oxidation/hydrolysis products of the primarily Pb-Zn and Cu-rich ore mineralization that impregnates the carbonate bedrock.

1. Introduction

Caves are natural underground laboratories where the precipitation of minerals can be directly monitored. The caves carved in carbonate rocks (limestone, dolomite, marble) normally display a monotonous mineralogy, with calcite, aragonite, and gypsum being the most common species (Onac 2012). If caves are active/fossil H_2S systems (e.g., Frasassi, Diana, Carlsbad, etc.) or host massive accumulations of guano (Cioclovina, Rastoci, etc.), rich association of sulfates and phosphates will normally be encountered (Galdenzi and Menichetti, 1995; Polyak and Provencio 2001; Onac et al. 2002, 2009). The mineralogical situation changes dramatically when caves are located nearby ore deposits or sometimes within them. Such settings guarantee very diverse and unique assemblages of secondary cave minerals (Maltsev 1997; Onac et al. 2002, 2007; Audra and Hofmann 2004; de Waele and Forti 2005; Forti et al. 2006). These are formed by oxidation/hydrolysis, acid/base, and redox processes (White 1997; Onac and Forti 2011a). The recent focus and more thorough investigations conducted in these last types of caves added a significant number of new minerals (Hill and Forti 1997; Onac and Forti 2011b).

Over the past years, Sardinia, with its countless caves discovered during mining activities, became a focal point for mineralogical research (Naseddu 1993; Forti et al. 2005; Boldoni et al. 2013). This paper reports on the cave minerals precipitated in the unique environment of the Monte Guisi Cave (SW Sardinia), from where all samples were collected (not from mine passages).

2. Local geology and mining activities

Paleozoic sedimentary rocks dominate the geology of Sardinia, but igneous and metamorphic rocks are also common. The Variscan deformation phase is responsible for low-grade metamorphism and several phases of magmatic intrusion, some of which produced at the contact with the carbonate rocks skarn deposits (Boni 2001). The Iglesiente-Sulcis region in the SW Sardinia, Italy (Fig. 1) is one of the oldest mining districts in the world, with ore exploitation since Phoenicians times. In the early stages, the mining activities focused on recovering silver, lead, and copper, and later, zinc and barium deposits (Boni 2001). Most of the ores are hosted in the Lower Cambrian carbonate formations of Gonnesa Group. In mining areas such as Monteponi, San Giovanni, or Barega, very spectacular and important (mineralogically speaking) cavities were discovered during the exploration and in the process of extracting the ore. Most of these caves develop in the Lower Cambrian limestones, with some (e.g., Monte Guisi Cave) carved in calcic skarns in which rich Pb-Zn (±Ba) mineralizations of Mississippi-type valley deposits (MVT) occur as veins, breccia cements, void-filling, and diagenetic replacements. The most common ore minerals are sphalerite, galena, and barite with variable amounts of pyrite. Near the surface these minerals oxidize/hydrolyze to form smithsonite, hydrozincite, and cerussite (Aversa et al. 2002).

Figure 1. Location of the investigated cave in the Iglesiente-Sulcis region, SW Sardinia (Italy). Map from the National Geological Service of Sardinia.

3. Methods

The mineral samples collected in the Monte Guisi Cave, were identified by means of a Siemens D5000 diffractometer with a monochromated (CuKα) diffracted-beam operated at 40 kV and 30 mA. Digitally recorded patterns were collected between 5° and 75° 2θ (step size of 0.05° 2θ and count rate of 2 to 4 second/step) and compared against the PDF2 mineral database using EVA software (version 8.0). Silicon (NBS 640b) served as internal standard. A Hitachi S-3400N environmental electron scanning microscope (ESEM; operation parameters: 15 kV, 5 to 10 nA, defocussed electron-beam diameter of 30 µm) equipped with a QUANTAX microanalysis system (Bruker AXS Flash 4010) was used to observe freshly fractured mineral fragments or hand-picked aggregates.

4. Results and discussion

The ongoing mineralogical study of the Monte Guisi Cave highlighted, besides relatively common cave minerals (e.g., calcite, aragonite, malachite, azurite, goethite, lepidocrocite, hematite, pyrolusite), a few others that are rather uncommon in ordinary cave environments. Among these we identified the following carbonates (rosasite $(Cu,Zn)_2(CO_3)(OH)_2$, cerussite $PbCO_3$, dundasite $PbAl_2(CO_3)_2(OH)_4 \cdot H_2O$), sulfates (brochantite $Cu_4SO_4(OH)_6$, anglesite $PbSO_4$), silicates (plancheite $Cu_8(Si_4O_{11})_2(OH)_4 \cdot H_2O$, shattuckite $Cu_5(SiO_3)_4(OH)_2$, hemimorphite $Zn_4Si_2O_7(OH)_2 \cdot H_2O$, chrysocolla $(Cu,Al)_2H_2Si_2O_5(OH)_4 \cdot nH_2O$), and one oxide (cuprite, Cu_2O). Below is an overview of the most abundant species. A more thorough study on the new cave minerals discovered in Monte Guisi Cave will make the topic of a forthcoming paper.

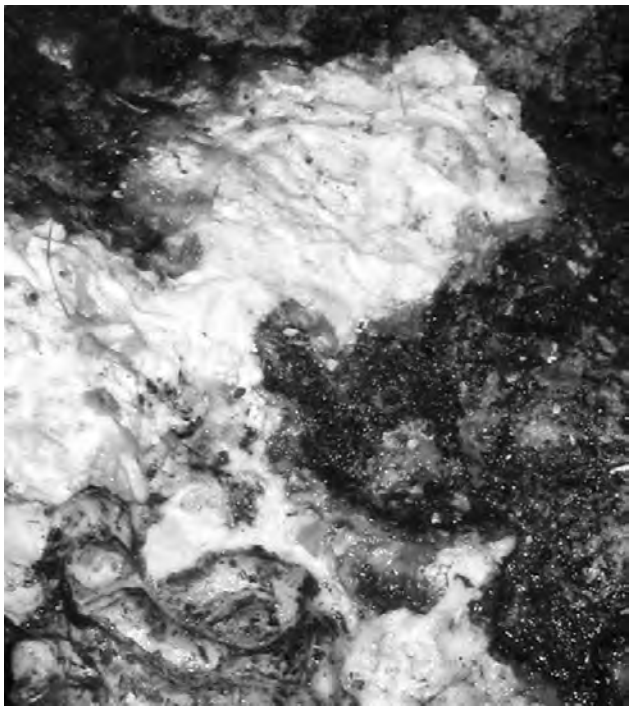

Figure 2. Deposits of cerussite in the Monte Guisi Cave (field of view: 50 cm).

Cerussite occurs as creamy white-bluish deposits (up to 1 cm in thickness) on the walls and floor of the cave (Fig. 2). In one section, it forms delicate saw teeth-type seeping speleothems. The blue tint is likely due to the presence of Cu-carbonates and sulfates. Cerussite is an oxidation product of sphalerite, which is the main ore mineral in the cave region.

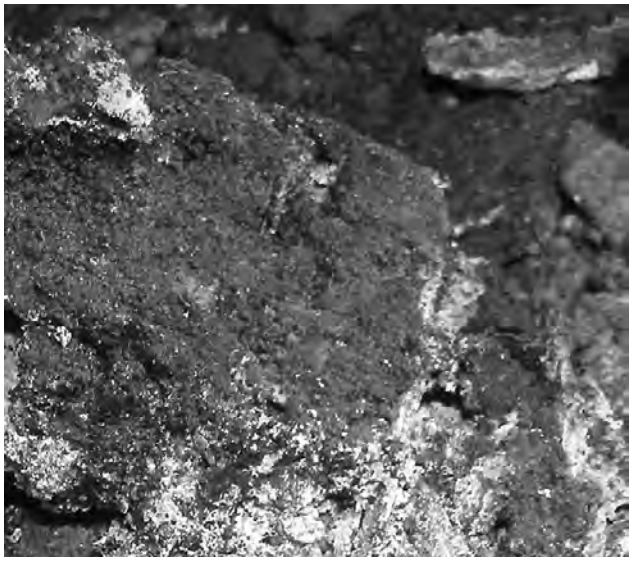

Figure 3. Crusts of hemimorphite and brochantite (fieldview 30 cm across).

Hemimorphite is the most important Zn ore mineral in the region. As a cave mineral it has been already documented from a number of mine-intercepted caves in SW Sardinia. Probably the best mineral specimens are found in Crovassa Quarziti (San Giovanni Mine; De Waele et al. 2013). In Monte Guisi Cave this mineral is closely associated with **brochantite** and forms millimeter-size crusts that cover the walls over large areas. Hemimorphite forms brownish sub-millimeter crystals, whereas the majority of the brochantite occurs as patchy green microcrystalline aggregates covering hemimorphite crusts (Fig. 3).

Apart from the occurrences documented from this karst region, brochantite is a rare cave mineral identified in very few other locations (Hill and Forti 1997).

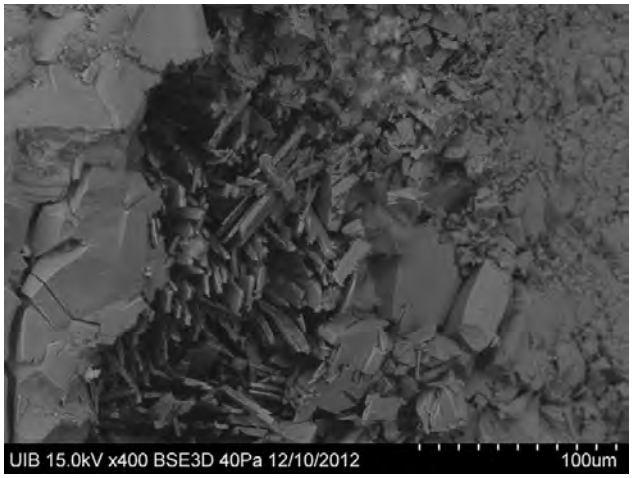

Figure 4. The ESEM microphotograph of massive hemimorphite (1) and platy tabular crystals of brochantite(2).

The distinct morphology of each of these two minerals is recognizable when observed under ESEM. Hemimorphite builds up blocky, euhedral or/and subhedral crystals, whereas brochantite is prismatic (Fig. 4). Both minerals show their characteristic peaks on the X-ray diffraction spectrum obtained on sample #1918 (Fig. 5).

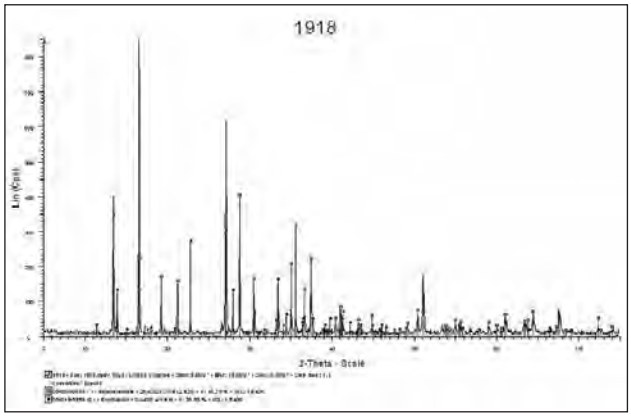

Figure 5. The XRD spectrum of hemimorphite and brochantite (sample 1918).

Crusts of **cuprite** and goethite appear in the upper section of the cave. A close inspection of the crusts reveals that the minerals are precipitated as paper-thin botryoids covering highly weathered ochre clay-looking material (Fig. 6).

Cuprite was first identified in a cave in the Bisbee copper mine (Arizona, USA; Graeme 1981) and more recently in the Shopov cave system (Bulgaria; Shopov 1993).

Chrysocolla was identified by means of XRD analysis and further documented by ESEM/EDS (Fig. 7). It forms dark blue crusts directly overlying the cave walls along the main passage. Under binocular, chrysocolla display botryoidal aggregates, intimately mixed with some other Cu and Pb secondary mineral species that are not discussed in the present note. To our knowledge this is the second cave occurrence of this mineral (Hill and Forti 1997; Onac and Forti 2011b).

Figure 7. The ESEM microphotograph of the globular chrysocolla aggregates and their EDS spectrum (upper right inset).

5. Conclusions

The mining activities in the SW Sardinia, especially around the city of Iglesias, led to the discovery of significant number of mine caves. Given the particular geological setting of this region (highly mineralized carbonate rocks), most of the caves contain very rich mineral assemblages.

In Monte Guisi Cave, the secondary Pb, Cu, Zn, and Fe minerals identified so far appear to represent oxidation and/or hydrolysis products of primarily ore deposit minerals

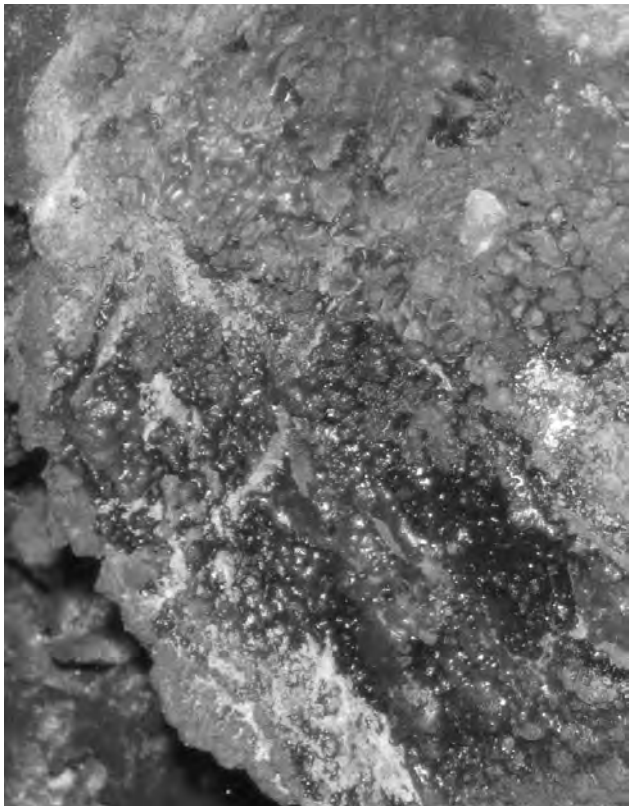

Figure 6. Botryoidal crusts composed of cuprite (dark red) and goethite (light red) in the Monte Guisi Cave (fieldview 0.5 m across).

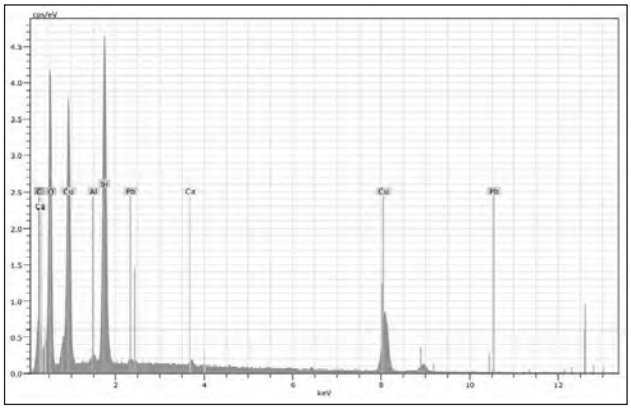

(sphalerite, galena, and chalcopyrite). Two of the minerals mentioned in the present report (dundasite and plancheite) are new for the cave environment; however, additional studies are needed before making clear statements regarding their origin and significance in the mineral association documented in the Monte Guisi Cave.

Thorough investigations, including single crystal X-ray, electron microprobe, and stable isotope analyses on such exotic minerals may provide important insight into the chemical and physical conditions existing in the cave environments at various times during the mineral formation.

Acknowledgements

The authors would like to thank Drs. Tudor Tămaș (Babeș-Bolyai University, Cluj, Romania), Ferran Hierro, and Joan Cifre (Serveis Científicotècnics, Universitat de les Illes Balears in Palma, Spain) for their support while conducting the analyses, and also to Prof. J.M. Calaforra and an

anonymous reviewer for improving our contribution. Alexandra Giurgiu is thanked for running the X-ray investigations for part of the samples.

References

Audra P, Hofmann BA, 2004. Les cavités hypogènes associées aux dépôts de sulfures métalliques (MVT). Le Grotte d'Italia, 5, 35–56.

Aversa G, Balassone G, Boni M, Amalfitano C, 2002.The mineralogy of the "Calamine" ores in SW Sardinia (Italy): preliminary results. Periodico di Mineralogia, 71, 201–218.

Boldoni E, De Waele J, Galli E, Messina M, Onac BP, Sanna L, Sauro F, Villani M, 2013. Mineralogy and speleogenesis of the Corona 'E Sa Craba quartzite cave (southwest Sardinia). *This volume*.

Boni M, 2001. The Iglesiente former mining district (SW Sardinia): an itinerary in the Iglesias valley and along the Western Coast. Rendiconti Seminario Facoltà Scienze Università Cagliari, 71, 77–90.

De Waele J, Forti P, 2005. Mineralogy of mine caves in Sardinia. Proceedings of the 14th International Congress of Speleology, Kalamos, Greece, 306–311.

De Waele J, Forti P, Naseddu A, 2013. Speleogenesis of an exhumed hydrothermal sulphuric acid karst in Cambrian carbonates. Earth Surface Processes and Landforms, doi: 10.1002/esp.3375.

Forti P, Galli E, Rossi A, 2006. Peculiar minerogenetic cave environments of Mexico: the Cuatro Ciénegas area. Acta Carsologica, 35, 79–98.

Forti P, Pagliara A, Galli E, Rossi A, De Waele J, Naseddu A, Papinuto S, 2005. Studio morfologico e mineralogico di dettaglio del concrezionamento del sistema carsico di Santa Barbara (Miniera di San Giovanni, Iglesias). Memorie dell'Istituto Italiano di Speleologia, 17, 57–68.

Galdenzi S, Menichetti M, 1995. Occurrence of hypogenic caves in a karst region: Examples from central Italy. Environmental Geology, 26, 39–47.

Graeme RW, 1981. Famous mineral localities; Bisbee, Arizona. Mineral Record, 12 (5), 287–291.

Hill CA, Forti P, 1997. Cave minerals of the world, Huntsville, AL, National Speleological Society, 463.

Maltsev V, 1997. Cupp-Coutunn Cave, Turkmenistan, *in* Hill CA, Forti P, (Eds.). Cave minerals of the world (2nd ed.), Huntsville AL, National Speleological Society, 323–328.

Naseddu A, 1993. Grotte in miniera. Sardegna Speleologica, 3, 8–14.

Onac BP, 2002. Caves formed within Upper Cretaceous skarns at Baita (Bihor county): mineral deposition and speleogenesis. Canadian Mineralogist, 40 (6), 1551–1561.

Onac BP, Forti P, 2011a. Minerogenetic mechanisms occurring in the cave environment: an overview. International Journal of Speleology, 40, 79–98.

Onac BP, Forti P, 2011b. State of the art and challenges in cave minerals studies. Studia UBB Geologia, 56, 33–42.

Onac BP, Hess JW, White WB, 2007. The relationship between the mineral composition of speleothems and mineralization of breccia pipes: evidence from Corkscrew Cave, Arizona, USA. Canadian Mineralogist, 45, 1177–1188.

Onac BP, Breban R, Kearns J, Tămaș T, 2002. Unusual minerals related to phosphate deposits in Cioclovina Cave, Sureanu Mts. (Romania). Theoretical and Applied Karstology, 15, 27–34.

Onac BP, Sumrall JG, Tămaș T, Povară I, Kearns J, Dărmiceanu V, Vereș D, Lascu C, 2009. The relationship between cave minerals and H_2S-rich thermal waters along the Cerna Valley (SW Romania). Acta Carsologica, 38, 67–79.

Onac BP, 2012. Minerals. *in*: White WB, Culver DC, (Eds.). Encyclopedia of Caves. Academic Press, Chennai, 499–508.

Polyak JV, Provencio P, 2001. By-product materials related to H_2S-H_2SO_4 influenced speleogenesis of Carlsbad, Lechuguilla, and other caves of the Guadalupe Mountains, New Mexico. Journal of Cave and Karst Studies, 63, 23–32.

Shopov YY, 1993. Genetic classification of cave minerals. Proceedings of the 10th International Congress of Speleology, Beijing, China, 101–105.

White WB, 1997. Thermodynamic equilibrium, kinetics, activation barriers, and reaction mechanisms for chemical reactions in karst terrains. Environmental Geology, 30, 46–58.

NEW LOCALITIES OF COARSELY CRYSTALLINE CRYOGENIC CAVE CARBONATES IN SLOVAKIA

Monika Orvošová[1], Lukáš Vlček[2], Karel Žák[3]
[1]Slovak Museum of the Nature Protection and Speleology, Školská 4, SK-031 01 Liptovský Mikuláš, Slovak Republic; orvosova@smopaj.sk
[2]Slovak Speleological Society, Hodžova 11, SK-031 01 Liptovský Mikuláš, Slovak Republic; lukasvlcek@yahoo.com
[3] Institute of Geology AS CR, v. v. i., Rozvojová 269, CZ-165 00 Prague 6, Czech Republic; zak@gli.cas.cz

Three new localities of coarsely crystalline cryogenic cave carbonates (CCC_{coarse}) have been recently discovered in the Western Carpathians, Slovakia. CCC_{coarse} are secondary mineral formations in the cave and belong to speleothems. They occur in the form of loose accumulations of calcite crystals and crystal aggregates freely deposited on the bottom of the cavities. Their genesis is interpreted as related to slow karst-water freezing in pools inside the caves, in relation to the existence of a permafrost zone during Quaternary glacials. The newly discovered CCC_{coarse} localities in Četníkova svadba Cave, Demänovská j. mieru Cave and Zlomísk Cave are characterized by description and photodocumentation of the present crystal forms, by preliminary C and O isotope data, and by their U-series ages. The ages of the cryogenic crystals are in the range between 47 and 12 ka BP, corresponding to the latter half of the Last Glacial. Any new locality of CCC_{coarse} formed during the Last Glacial represents an important source of information about paleoclimatic conditions of adjacent areas. The U-series ages of the new localities support the earlier conclusion that the formation of CCC_{coarse} is related to transitions from cold to warm climate periods within the Last Glacial.

1. Introduction

New evidence on the past glaciation in caves of Central Europe was obtained during last several years based on finds of a specific type of speleothems – cryogenic cave carbonates (abbreviated CCC, Žák et al. 2004, 2008). Generally, the CCC form in caves in two modes of occurrence: fine-grained precipitates in areas of rapid freezing of usually thin water films on the surface of ice (CCC_{fine}), and coarsely crystalline precipitates (CCC_{coarse}) formed by slow water freezing in pools (Žák et al. 2008, Luetscher et al. 2013). This contribution is focused only on the CCC_{coarse}. The published models suppose crystallization of CCC_{coarse} during complete, very slow freezing of water cave pools. These carbonates typically occur in caves or cave sections of moderate to low ventilation, usually far from cave entrances. Such cavities can be cooled to freezing temperature mainly in relation to a former permafrost existence, their cooling exclusively by airflow is impossible. Therefore, the caves hosting CCC_{coarse} are not of the cold-air trap type.

The presented models (Richter and Riechelmann 2008, Richter et al. 2010, Žák et al. 2012) indicate that the infiltration into these cavities was restricted during permafrost formation. In contrast, during permafrost destruction related to a surface warming (permafrost "thawing", both from above and below), karst water penetrates into a cavity which is still within relic permafrost zone, and first forms a water pool here. The water pool slowly freezes. Formation of water surface ice cover and freezing from the pool bottom can proceed simultaneously. Depending on the climate, the process can be repeated several times, with new water pools formed on the surface of earlier cave ice fill.

The size of CCC_{coarse} crystal aggregates usually ranges from 1 mm to approximately 35 mm. The crystals and crystal aggregates show highly variable morphologies. Their morphologies and C and O isotopic compositions reflect progressive water freezing, accompanied by an increasing content of the dissolved compounds in the residual, as yet unfrozen water (Žák et al. 2004). With respect to elevated U content, which is typically higher than in usual speleothems of the same cave, the CCC_{coarse} can be precisely dated by the U-series disequilibrium method. They represent an important source of information about the paleoclimatic conditions during the Last Glacial, especially about the thickness of the permafrost zone and periods of its existence (Žák et al. 2012). Under present-day conditions all samples contain calcite as the main mineral. Unstable carbonate phases like ikaite could have been primarily formed as well (cf. Onac et al. 2011), being later, under warmer Holocene climates, all converted to calcite.

During the earlier systematic study of CCC_{coarse} in Central Europe several localities were discovered and studied also in the Western Carpathians in the territory of Slovakia. First information about the presence of these carbonate types was published by Tulis and Novotný (1989) from the Stratenská Cave (without interpretation of their origin), the same locality was later studied by Žák et al. (2004). A locality from the Studeného vetra Cave (Cold Wind Cave) was described by Žák et al. (2009). Šmída (2010) described a locality in the Hačova Cave in the Lesser Carpathians (the most south-located locality). Another locality of CCC_{coarse} was recently reported from the Mesačný tieň Cave (Moon Shadow Cave) by Šmída in Žák et al. (2011), another one from the Verných Cave (Faithfull People Cave) and V Záskočí Cave by Orvošová and Vlček (2012). The number of known caves with published occurrences of CCC_{coarse} in Slovakia reached 6.

Owing to the increasing number of amateur speleologists and scientists searching for CCC, the number of localities known in Slovakia is still increasing. The authors of this contribution checked tens of caves in Slovakia, mainly situated at higher altitudes. These caves frequently show morphological indications of former frost and ice action (Orvošová et al., in press). Three new localities of CCC_{coarse} are presented here, with preliminary results of their geochemical study.

2. New CCC sites in Slovakia

The three new sites with the occurrence of CCC are located in the Četníkova svadba Cave situated in the Strážovské Hills, and in two caves situated in the Nízke Tatry Mts. – Demänovská j. mieru Cave and Zlomísk Cave. For the location of all caves known to host the CCCs in the territory of Slovakia see Figure 1.

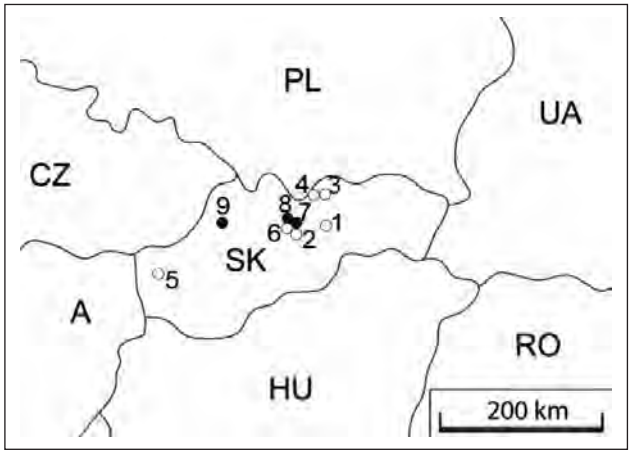

Figure 1. A map showing the positions of caves hosting CCC_{coarse} in Slovakia (full circles are new localities described in this paper). 1 – Stratenská Cave, Slovak Paradise (main cave entrance at 991 m a.s.l.); 2 – Studeného vetra Cave, Nízke Tatry Mts. (main cave entrance at 1,678 m a.s.l.); 3 – Verných Cave, Vysoké Tatry Mts. (cave entrance at 1,522 m a.s.l.); 4 – Mesačný tieň Cave, Vysoké Tatry Mts. (cave entrance at 1,767 m a.s.l.); 5 – Hačova Cave, Malé Karpaty Mts. (cave entrance at 690 m a.s.l.); 6 – V Záskočí Cave, Nízke Tatry Mts. (cave entrance at 1,332 m a.s.l.); 7 – Zlomísk Cave, Nízke Tatry Mts. (cave entrance at 854 m a.s.l); 8 – Demänovská j. mieru Cave, Nízke Tatry Mts. (main entrance at 812 m a.s.l.); 9 – Četníkova svadba Cave, Strážovské Hills (cave entrance at 1,075 m a.s.l.).

2.1. Četníkova svadba Cave

The cave is a part of the cave system located in the Strážov Hills in the NW part of Slovakia (the highest peak has an elevation of 1,213 m a.s.l.). The cave is 1,276 m long and 78 m deep (Kortman 2012). It is developed along a system of faults and fissures in Triassic limestone and dolomite. The cave entrance is located at an altitude of 1,075 m a.s.l.

The only occurrence of CCC_{coarse} in the cave was found in a flat hall 4 m high and 10 m × 5 m in area (Fig. 2). Crystalline aggregates consist of semi-transparent calcite scalenohedrons, yellow in color, forming radially-arranged aggregates several mm to about 20 mm in size (Fig. 10J). They form loose accumulation, together with fragments of limestone, on the thin muddy layer coating the surface of limestone blocks covering the bottom of the hall (Fig. 3). Some aggregates were found fallen down into the gaps between these blocks. Two up-sloping, fissure-controlled corridors lead from this hall in the direction to the surface. The cave has now a moderate ventilation (semi-dynamic cave, with several small and partly restricted entrances, enlarged by excavations) with temperatures slightly oscillating around a yearly average of ca. 5 °C.

Figure 2. A general view of the central part of the Braňové ozveny Hall, Četníková svadba Cave, with the occurrence of CCC. Photo by M. Orvošová.

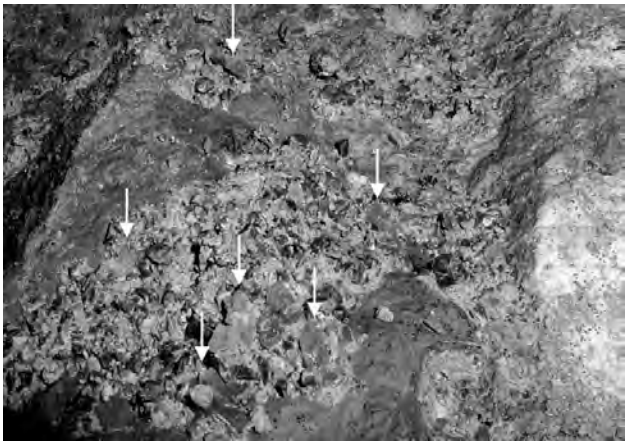

Figure 3. A detailed view of CCC (indicated by arrows) mixed with limestone fragments, freely deposited on the thin muddy layer covering the limestone blocks. Četníková svadba Cave. The photo width is about 20 cm. Photo by M. Orvošová.

2.2. Demänovská j. mieru Cave

The Demänovská j. mieru Cave is an extensive sector of the much larger Demänová Cave System developed in the right (eastern) side of the Demänová Valley. The whole Demänová Cave System is 35,358 m long, developed at altitudes between 771 and 966 m a.s.l., which gives an elevation difference of 195 m. The Demänovská j. mieru Cave itself consists of large or smaller domes interconnected by wide horizontal corridors, inclined corridors and vertical shafts, including numerous chimneys connecting the cave levels. The cave is hosted by Triassic limestones and dolomites, mainly by the Gutenstein Limestone. The cave sections hosting three sites of CCC_{coarse} show limited ventilation and their yearly average cave temperature is stable at ca. 6 °C. The cave has no large open entrance.

The first site is located in the Dukelský pomník Hall, just few hundred meters from the artificial cave entrance in the Vyvieranie Valley (800 m a.s.l.). The CCC concentrate in gaps between limestone boulders or on theirs surfaces (Figs. 4, 5). The second site is located in the Waterfall Hall at the same altitude. The CCC_{coarse} occur in layers up to 20 cm thick around a large, cryogenically damaged stalagmite.

Figure 4. Small accumulation of CCC on the collapse block (arrows) on the bottom of the Dukelský pomník Hall, Demänovská j. mieru Cave. Photo by L. Vlček.

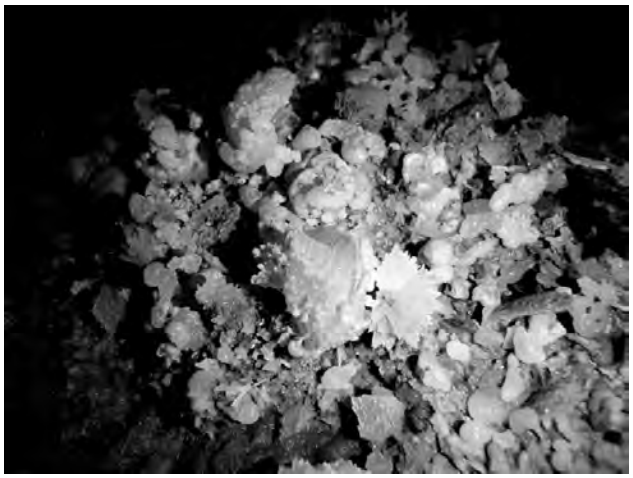

Figure 5. A close-up view of crystals and aggregates of CCC in the Dukelský pomník Hall, Demänovská j. mieru Cave. The width of the photographed area is 15 cm. Photo by L. Vlček.

Figure 6. A photomicrograph of mainly skeleton-shaped, occasionally spherical aggregates of CCC from the Waterfall Hall, Demänovská j. mieru Cave. The width of the photographed area is 2 cm. Photo by M. Orvošová.

Both skeletal aggregates and spherical forms are present (Fig. 6). The third site is located at the highest cave level (848–860 m a.s.l.). Crystalline forms occurring in a small accumulation (30 × 40 cm) are similar to those at the previous site. Indicators of former freezing and ice action are present as well.

2.3. Zlomísk Cave

The cave is located in the Triassic Gutenstein Limestone in the left (western) side of St. Ján Valley. An extensive maze cave is developed at several levels. The cave is 11,036 m long and 147 m deep. The meandering galleries are intersected by larger halls with break-downs. The main course of the cave is parallel to the S–N course of the valley. Most passages are located at the elevation of 800 to 835 m a.s.l. At the same cave level, four CCC sites are located, consisting of 15 smaller CCC accumulations. The morphology of the halls is widely affected by freezing: abundant stony debris is present and walls are broken. The former ice-fill presence is documented by CCC finds. The CCC crystals and crystal aggregates are located mostly in the debris or among the boulders on the bottoms of passages and halls (Fig. 7). The sites are mostly small, several tens of cm across. Crystals and crystal aggregates are less than 1 mm to 20 mm in size, variously shaped, with common spherical forms and their intergrowths, locally resembling expanded polystyrene beads (Fig. 8); they can be also radial, hemispherical or cauliflower-shaped. The cave has a moderate ventilation. The average annual temperature is 5.8 °C (Hochmuth and Holúbek 2001).

Figure 7. Typical CCC accumulation ("coarse sand") in debris on the bottom of halls (Sieň večných priekov Hall) in Zlomísk Cave. The camera cap is 5 cm across. Photo by M. Orvošová.

Figure 8. A close-up view of another aggregate type (resembling expanded polystyrene beads) from the CCC site in the Pilierová sieň Hall, Zlomísk Cave. The camera cap is 5 cm across. Photo by M. Orvošová.

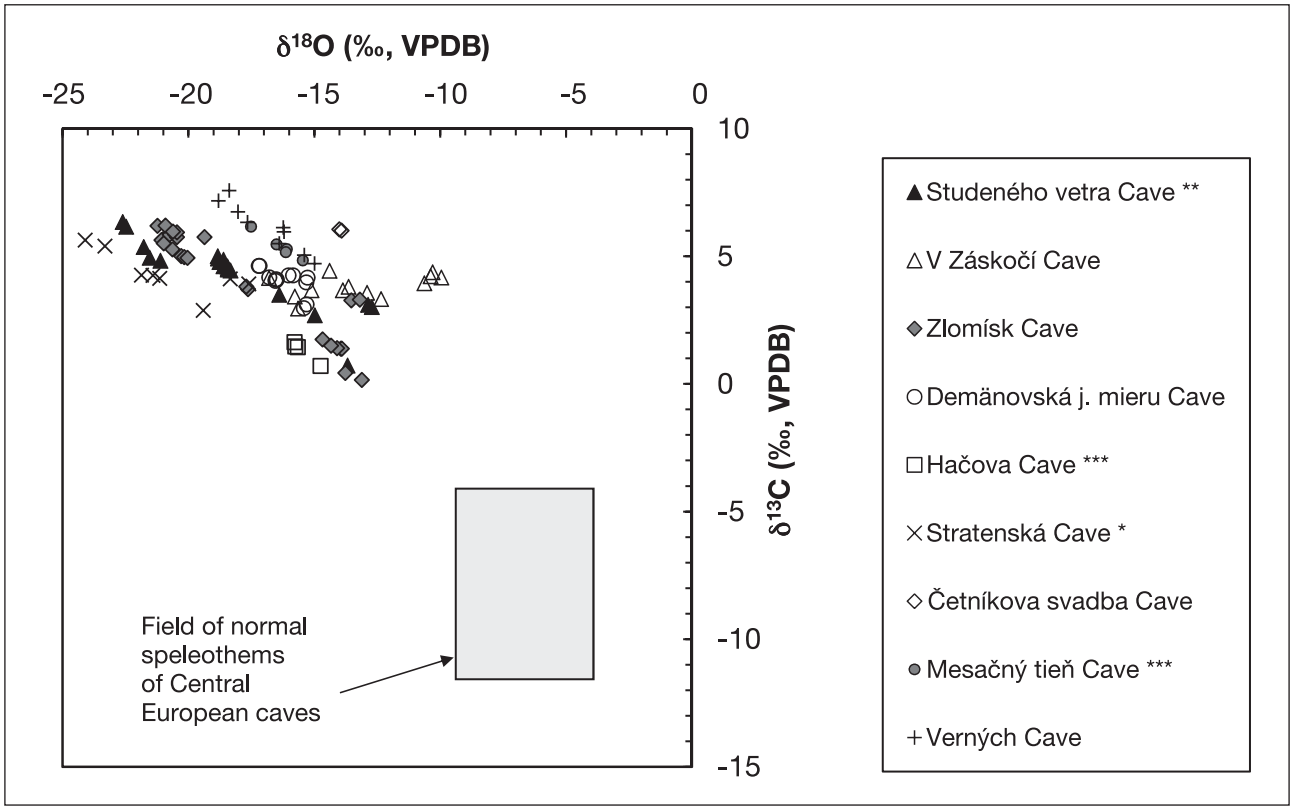

*Figure 9. Stable isotope data of CCC_{coarse} for all Slovak localities. Asterisks indicate previously published data: * data from Žák et al. (2004); ** data from Žák et al. (2009); *** data from Žák et al. (2011). See text for further explanation.*

3. Discussion and conclusions

Besides the typical morphology and typical mode of occurrence, another method useful for the confirmation of the cryogenic origin of the studied crystals and crystal aggregates is their carbon and oxygen stable isotope geochemistry. The published model of formation (e.g., Žák et al. 2012) explains C and O isotope data as a result of equilibrium isotope fractionation between ice, water and carbonate during slow water freezing. Ice incorporates preferentially the heavier ^{18}O isotope, which results in a decrease in $\delta^{18}O$ values of the unfrozen portion of the solution. Since the oxygen isotope exchange between dissolved carbonate and water is slow (Scholz et al. 2009), freezing of the water pool must have been also very slow, otherwise the decrease in $\delta^{18}O$ of the solution would not be reflected in the carbonate data.

Preliminary C and O isotope data for the new localities exhibit typical negatively-sloped trends in the $\delta^{13}C$ vs. $\delta^{18}O$ diagram, reaching to very low $\delta^{18}O$ values. Carbonate data are shifted towards extremely low $\delta^{18}O$ values and slightly elevated $\delta^{13}C$ values as the slow water freezing and carbonate precipitation proceeds (Fig. 9). Water freezing and carbonate precipitation occurred under isotope equilibrium between ice, residual water and carbonate.

The U-series ages of the new sites (13 samples, Orvošová et al., submitted) lie in the range from 47.3 to 12.08 ka BP. Seven of the dated samples were formed during a more restricted age interval between 17.2 and 12.08 ka BP. This Late Glacial age interval is characterized by variable climates after the Last Glacial Maximum, with abrupt climatic changes (Blockley et al. 2012). Rapid climatic changes, probably also accompanied by changes in the precipitation quantity and permafrost depth oscillation, seem to be optimum conditions for the CCC formation.

The caves hosting CCC localities today show temperatures similar to the mean annual air temperature of the outside atmosphere. Their ventilation is low to moderate. None of the described caves is of a cold-air trap type. Therefore, they could not have been cooled to a freezing temperature by trapping of cold dense winter air.

The only probable process which can cool the cavities down to freezing temperatures was cooling of the limestone massif itself and thus the existence of permafrost. The depths of the sites can therefore indicate the minimum permafrost depth of the Last Glacial. The CCC sites in the Jaskyňa Zlomísk Cave lie mostly at depths between 50 m and 110 m under the surface. One site is located only 25 m under the surface. The described CCC site in the Četníkova svadba Cave is located at a depth of only 10 to 20 m under the surface. The three sites of the Demänovská jaskyňa mieru Cave are located 80 m to 180 m from the nearest surface.

The caves seem to be the unique underground environment with suitable conditions for the preservation of former permafrost markers. The finds of CCC show that the Last Glacial subsurface freezing and permafrost occurrence in Slovakia was not a domain of the high mountains only. It occurred also in lower mountains and hills. Correlations of CCC formation and surface climatic changes are not straightforward, since the subsurface climatic changes in low ventilation caves can be significantly delayed with respect to surface climates.

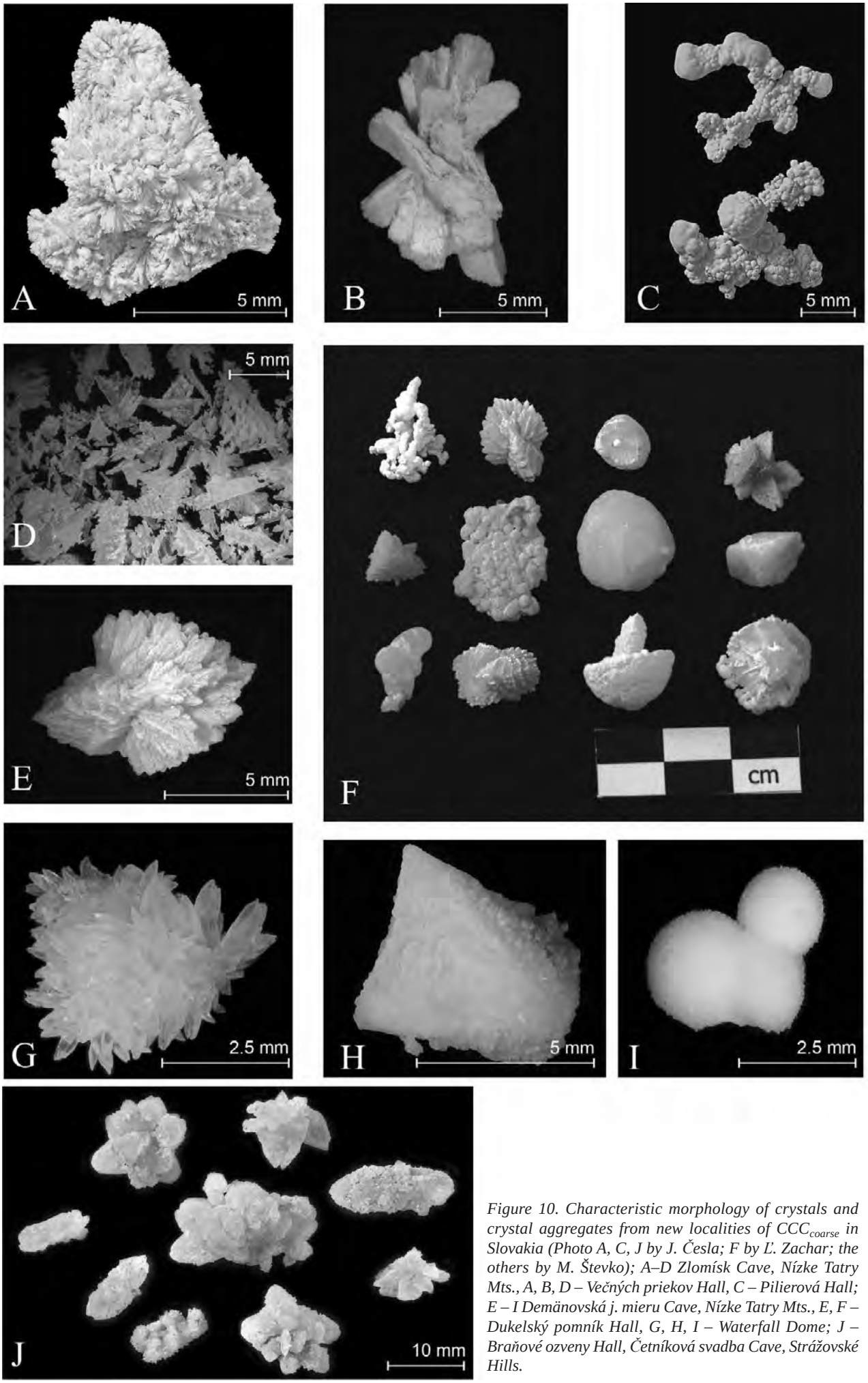

Figure 10. Characteristic morphology of crystals and crystal aggregates from new localities of CCC_{coarse} in Slovakia (Photo A, C, J by J. Česla; F by Ľ. Zachar; the others by M. Števko); A–D Zlomísk Cave, Nízke Tatry Mts., A, B, D – Večných priekov Hall, C – Pilierová Hall; E – I Demänovská j. mieru Cave, Nízke Tatry Mts., E, F – Dukelský pomník Hall, G, H, I – Waterfall Dome; J – Braňové ozveny Hall, Četníková svadba Cave, Strážovské Hills.

The high morphological variability of CCC crystals and aggregates and their causes are the the subject of current continuous research (Fig. 10). Regional mapping of CCC sites, their morphology, ages, and geographic distribution should provide important information about the distribution of Glacial temperatures and help in the study of terrestrial paleoclimates of the Western Carpathians.

Nowadays, there are 9 CCC localities known in the caves of Western Carpathians, Slovakia. The last three – the Četníkova svadba Cave in the Strážovské Hills, the Demänovská j. mieru Cave and Zlomísk Cave in the Nízke Tatry Mts. – are newly introduced in this paper.

Acknowledgments

This study was supported by Operational Program Research and Development through the project "Centre of excellence for integrated research of Earth's geosphere" No. ITMS-26220120064 co-financed by ERDF. Participation of K. Žák was supported by RVO67985831 Program. For the possibility to work in the caves, technical help, and important field-data we wish to thank the members of the Slovak Speleological Society, the Strážovské vrchy Speleoclub, the Demänovská dolina Speleoclub and the Nicolaus Speleoclub, especially Bohuslav Kortman, Ján Kasák, Milo Lisý, Pavel Herich, Michal Danko and Peter Holúbek.

References

Blockley SPE, Lane CS, Hardiman M, Rasmussen SO, Seierstad IK, Steffensen JP, Svensson A, Lotter AF, Turney CSM, Ramsey CB, INTIMATE members, 2012. Synchronisation of palaeoenvironmental records over the last 60,000 years, and extended INTIMATE event stratigraphy to 48,000 b2k. Quaternary Science Reviews, 36, 2–10.

Hochmuth Z, Holúbek P, 2001. Geomorfologické pomery a topografia novoobjavených častí Jaskyne zlomísk v Jánskej doline v Nízkych Tatrách. Slovenský kras, 36, 59–80.

Kortman B, 2012. "Zbojnícky systém" na Strážove realitou? Spravodaj Slovenskej speleologickej spoločnosti, 3, 48–49.

Luetscher M, Borreguero M, Moseley GE, Spötl C, Edwards RL, 2013. Alpine permafrost thawing during the Medieval Warm Period identified from cryogenic cave carbonates. The Cryosphere Discuss, 7, 419–440.

Onac BP, Wynn JG, Citterio M, 2011. Ikaite in the Scarisoara Ice Cave (Romania): origin and significance. Geophysical Research Abstracts, 13, EGU2011–5188.

Orvošová M, Vlček L, 2012. Nové nálezy kryogénnych jaskynných agregátov – čudesných kryštálikov z doby ľadovej. Spravodaj SSS, 1, 76–82.

Orvošová M, Vlček L, Holúbek P, Orvoš P, in press. Frost and cave ice action as a cause of speleothem destruction during the Glacial: examples from selected caves of Slovakia. Acta Carsologica Slovaca.

Orvošová M, Žák K, Deininger M, Milovský R, under review. Detection of permafrost depth penetration and permafrost duration in caves: Methodology based on cryogenic cave carbonate and a case study of the Last Permafrost Maximum in Western Carpathians, Slovakia. Boreas, submitted.

Richter DK, Riechelmann DFC, 2008. Late Pleistocene cryogenic calcite spherolites from the Malachitdom Cave (NE Rhenish Slate Mountains, Germany): origin, unusual internal structure and stable C-O isotope composition. International Journal of Speleology, 37, 2, 119–129.

Richter DK, Meissner A, Immenhauser U, Schulte U, Dorsten I, 2010. Cryogenic and non-cryogenic pool calcites indicating permafrost and non-permafrost periods: a case study from the Herbstlabyrinth-Advent Cave system (Germany). The Cryosphere, 4, 501–509.

Scholz D, Mühlinghaus C, Mangini A, 2009. Modelling $\delta^{13}C$ and $\delta^{18}O$ in the solution layer on stalagmite surfaces, Geochimica et Cosmochimica Acta, 73, 2592–2602.

Šmída B, 2010. Geomorfológia a genéza Plaveckého krasu ako modelového územia tzv. konktaktného krasu Západných Karpát s nižšou energiou reliéfotvorby, Ph.D. Thesis, Faculty of Natural Sciences, Comenius University in Bratislava, 220.

Tulis J, Novotný L. 1989. System of Stratenská Cave, Osveta Publishers, Martin, 464.

Žák K, Urban J, Cílek V, Hercman H, 2004. Cryogenic cave calcite from several Central European caves: age, carbon and oxygen isotopes and a genetic model. Chemical Geology, 206, 119–136.

Žák K, Onac BP, Perşoiu A, 2008. Cryogenic carbonates in cave environments: A review. Quaternary International, 187, 84–96.

Žák K, Hercman H, Orvošová M, Jačková I, 2009. Cryogenic cave carbonates from the Cold Wind Cave, Nízke Tatry Mountains, Slovakia: Extending the age range of cryogenic cave carbonate formation to the Saalian. International Journal of Speleology, 38, 2, 139–152.

Žák K, Šmída B, Filippi M, Živor R, Komaško A, Vybíral S, 2011. Nové lokality kryogénneho karbonátu v České republice a na Slovensku. Speleofórum, 30, 103–110.

Žák K, Richter DK, Fillipi M, Živor R, Deininger M, Mangini A, Scholz D, 2012. Cryogenic cave carbonate – a new tool for estimation of the Last Glacial permafrost depth of the Central Europe. Climate of the Past, 8, 1–17.

Partners of the 16th ICS

We thank all partners for their kind support of the 16th International Congress of Speleology!

Ministry of the Environment of the Czech Republic

South Moravian Region

City of Brno

Czech Convention Bureau

CzechTourism

Administration of the Moravian Karst Protected Landscape Area

Moravian Museum

Cave Administration of the Czech Republic

Czech Geological Survey

Town of Blansko

Institute of Geology, Academy of Sciences of the Czech Republic

Agency for the Nature Conservation and Landscape Protection of the Czech Republic

Village of Rudice

Association for Country Development – Moravian Karst

Sponsors of the 16th ICS

We thank all sponsors for their kind support of the 16th International Congress of Speleology!

Mediform spol. s r.o.

Czech Lime Association

Society for the Moravian Karst

Planteko

Starobrno

Esri

Wine of Pazderka's Clan

Scurion

Beal

Trade Fairs Brno

Authors Index

Czech Republic, Brno

July 21–28, 2013

www.speleo.cz

ISBN 978-80-87857-09-0